



Flanders
State of
the Art

13_131_L1
WL rapporten

Integraal Plan Bovenzeescheide

Subreport 1 – SCALDIS: a 3D Hydrodynamic Model
for the Scheldt Estuary

DEPARTMENT
**MOBILITY &
PUBLIC
WORKS**

www.flandershydraulicsresearch.be



Integraal Plan Bovenzeeschelde

Subreport 1 – SCALDIS: a 3D Hydrodynamic Model for the Scheldt Estuary

Smolders, S.; Maximova, T.; Vanlede, J.; Plancke, Y.; Verwaest, T.; Mostaert, F.

August 2016

WL2016R13_131_1

This publication must be cited as follows:

Smolders, S.; Maximova, T.; Vanlede, J.; Plancke, Y.; Verwaest, T.; Mostaert, F. (2016). Integraal Plan Bovenzeeschede: Subreport 1 – SCALDIS: a 3D Hydrodynamic Model for the Scheldt Estuary. Version 5.0. WL Rapporten, 13_131. Flanders Hydraulics Research: Antwerp, Belgium.

**Flanders
Hydraulics Research**







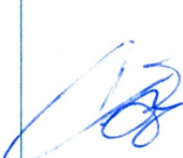


Flanders
State of the Art

Nothing from this publication may be duplicated and/or published by means of print, photocopy, microfilm or otherwise, without the written consent of the publisher.

Document identification

Title:	Integraal Plan Bovenzeeschelde: Subreport 1 – SCALDIS: a 3D Hydrodynamic Model for the Scheldt Estuary		
Customer:	Waterwegen en Zeekanaal NV Afdeling Zeeschelde	Ref.:	WL2016R13_131_1
Keywords (3-5):	Numerical model, Telemac, Scaldis, Scheldt estuary		
Text (p.):	246	Appendices (p.):	228
Confidentiality:	<input type="checkbox"/> Yes	Exceptions:	<input type="checkbox"/> Customer
			<input type="checkbox"/> Internal
			<input type="checkbox"/> Flemish government
		Released as from: September 2016	
	<input checked="" type="checkbox"/> No	<input checked="" type="checkbox"/> Available online	

Approval

Author	Reviser	Project Leader	Research & Consulting Manager	Head of Division
Maximova, T. 	Vanlede, J. 	Vanlede, J. 	Verwaest, T. 	Mostaert, F. 
Smolders, S. 	Plancke, Y. 			

Revisions

Nr.	Date	Definition	Author(s)
1.0	17/09/2015	Concept version	Maximova, T.; Smolders, S.
2.0	08/12/2015	Substantive revision	Vanlede, J.; Plancke, Y.
3.0	15/03/2015	External revision chapter 6	Prof. De Mulder, T.
4.0	09/05/2016	Revision customer	Depreiter, D.
5.0	31/08/2016	Final version	Smolders, S.; Vanlede, J.

Abstract

In the framework of the projects 'Integrated plan for the Upper Sea Scheldt' and 'Agenda for the Future', it was necessary to develop a hydrodynamics and sediment transport model that covers the entire tidally influenced zone of the Scheldt Estuary and the mouth area, and that has sufficient resolution in the upstream part.

Existing models lack a high resolution in the Upper Sea Scheldt, Durme, Rupel and Nete. For this reason, the SCALDIS model, a new unstructured high resolution model of the Scheldt Estuary is developed in TELEMAC 3D for the entire estuary, but with special attention to the upstream parts. The use of an unstructured grid allows to combine a large model extent with a high resolution upstream. The calibrated model will be used to analyse the effects of several scenarios (different morphology of the Scheldt with different ranges of boundary conditions).

This report describes the model development, calibration and validation of the hydrodynamics. The model is calibrated for one spring-neap tidal cycle in 2013 against field data: water levels, velocities (in deep and shallow zones) and discharges.

Contents

1	Introduction.....	1
2	Units and reference plane	2
3	List of abbreviations.....	3
4	Available measurement data	4
4.1.	Water levels	4
4.2.	Velocities	6
4.2.1.	Sailed ADCP measurements	6
4.2.2.	Stationary velocity measurements in deep areas	9
4.2.3.	Stationary velocity measurements in shallow areas	9
4.3.	Discharges	11
4.4.	Wind data	13
4.5.	Salinity.....	14
5	The numerical model	16
5.1.	Software	16
5.2.	Model grid	16
5.2.1.	Grid dimensions	16
5.2.2.	Vertical Schematisation.....	20
5.2.3.	The grid and the sigmaplan areas.....	21
5.2.4.	Grid quality.....	23
5.3.	Bathymetry	25
5.3.1.	Coastal zone and mouth of the Western Scheldt.....	25
5.3.2.	Eastern Scheldt and Western Scheldt	26
5.3.3.	Lower Sea Scheldt.....	27
5.3.4.	Upper Sea Scheldt.....	27
5.3.5.	Rupel basin	28
5.4.	Boundary conditions.....	29
5.5.	Salinity.....	30
5.5.1.	Boundary conditions and correction.....	30
5.5.2.	Simulation period and initial condition.....	32
5.6.	Time step	34
5.7.	Computational time	34
5.7.1.	Number of output variables : tracers	34
5.7.2.	Number of culverts	34
5.7.3.	Number of processors.....	35
5.8.	Model settings	36
5.9.	Simulation period	37
5.10.	Turbulence implementation in the model.....	37
5.10.1.	Vertical turbulence model	38
5.10.2.	Horizontal turbulence model.....	38
5.10.3.	Velocity near bottom.....	39
5.11.	Numerical diffusion	39
6	Culvert functionality	40
6.1.	Field of application	40
6.2.	Flow through a culvert: theoretical background	40
6.3.	Culvert simulation in existing codes	47

6.3.1.	TELEMAC-2D	47
6.3.2.	DELFT 3D	48
6.3.3.	MIKE 11	50
6.4.	Proposed implementation in TELEMAC-3D	55
6.4.1.	Culvert function	55
6.4.2.	Transport of tracers through culverts	60
6.4.3.	Telemac-3D input files (.cas file and .txt file) and the implemented code	61
6.5.	Testcase 1: Simplified model	62
6.5.1.	Model setup.....	62
6.5.2.	Results reference run.....	64
6.5.3.	Small scale parameter testing.....	67
6.5.4.	Transport of tracers.....	72
6.6.	Test case: Lippenbroek	75
6.6.1.	Lippenbroek area	75
6.6.2.	Lippenbroek model setup.....	76
6.6.3.	Lippenbroek Results	78
6.7.	Test case Bergenmeersen	82
6.7.1.	CRT Bergenmeersen	82
6.7.2.	Bergenmeersen model setup.....	84
6.7.3.	Results	85
6.8.	Concluding remarks	89
6.9.	With or without culverts: full scale model results.....	90
6.9.1.	Water levels	90
6.9.2.	Flow velocities.....	92
7	Sensitivity analysis	93
7.1.	Discharge at Melle	93
7.2.	Bed roughness of the intertidal areas	97
7.3.	Diffusivity	100
7.4.	Number of vertical layers	103
7.5.	Bathymetry	117
7.5.1.	Durme	117
7.5.2.	Tidal branch Gentbrugge	121
7.6.	Turbulence model	124
7.6.1.	k-Epsilon vs. Smagorinski model	124
7.6.2.	Constant viscosity vs. Smagorinski model.....	132
7.6.3.	Eddy patterns in the harbour of Zeebrugge	140
7.7.	Mass lumping on diffusion.....	145
7.8.	Implication for velocities	148
7.9.	Coriolis coefficient	151
7.10.	Coefficient of wind influence.....	155
7.11.	Grid adaptation	157
7.12.	Effect of salinity on water levels	160
7.13.	Conclusions	163
8	Model calibration	164
8.1.	Methodology.....	164
8.2.	Cost function	164

8.3.	Calibration results	166
9	Quality of the calibrated model	172
9.1.	Water levels	172
9.1.1.	Analysis of the high and low waters and time series.....	172
9.1.2.	Harmonic analysis.....	172
9.2.	ADCP velocities	175
9.2.1.	Analysis of the complete transects	175
9.2.2.	Estimation of error in the intertidal zones.....	176
9.3.	Discharges	176
9.4.	Stationary velocities	177
9.4.1.	Deep areas.....	177
9.4.2.	Shallow areas.....	177
9.5.	Salinity.....	178
9.5.1.	Salinity in run Scaldis_039_2.....	178
9.5.2.	Effect of diffusion on the salinity distribution	181
10	Model performance during storm	183
10.1.	North sea and Scheldt estuary	183
10.1.1.	Analysis of high and low waters and time series	183
10.1.2.	Harmonic analysis	183
10.2.	Flood areas.....	183
11	Smoothing of the roughness field for sediment analysis	185
12	Model validation	188
13	Tracer calculations for dispersion coefficients	189
13.1.	Introduction	189
13.2.	Deliverables	190
13.3.	Approach	190
13.4.	Polygons.....	191
13.5.	Find mesh elements in polygon	192
13.6.	Assigning a tracer concentration	193
13.7.	Surface area of triangles in polygon	194
13.8.	Volume within polygon.....	194
13.9.	Tracer concentration results	197
13.10.	Tracer conservation	209
14	Conclusions	211
15	List of references	212
16	Tables	214
17	Figures	223
Appendix 1. Results of the model calibration		A1
Water levels		A1
ADCP velocities		A62
Discharges		A104
Stationary velocities		A108
Salinity		A136
Appendix 2. Model performance during storm.....		A153
Scheldt estuary		A153
Flood areas		A202

Appendix 3. Results of the model validation.....	A207
Appendix 4. Tidal coefficients	A216
Appendix 5. Statistical parameters	A217
Appendix 6. Fortran code culvert functionality for Telemac 3D	A222

List of tables

Table 1. Water level stations	4
Table 2. Water level measurements during the Sinterklaasstorm	5
Table 3. Available ADCP measurements	6
Table 4. Stationary velocity measurements in deep areas	9
Table 5. Stationary velocity measurements in shallow areas	10
Table 6. Available discharge measurements	12
Table 7. Available salinity measurements	15
Table 8. List of all Sigma areas, their future function and if they are included in the Scaldis 3D model	22
Table 9. Correction of harmonic components	30
Table 10. Applied model settings	36
Table 11. Simulation period	37
Table 12. Conditions for each type of flow defined by <i>Bodhaine</i> (1968).	45
Table 13. Conditions for each type of flow used in DELFT 3D	50
Table 14. Conditions for each type of flow used in TELEMAC-3D	56
Table 15. Different parameters for each type of flow to calculate the hydraulic radius in TELEMAC-3D	59
Table 16. Values for the head loss coefficient depending on the opening of a gate valve	59
Table 17. Geometric features of the inlet and outlet sluices	63
Table 18. Chosen values for the reference run	64
Table 19. Mass balance for water	64
Table 20. Mass balance for water	74
Table 21. Mass balance for tracers	74
Table 22. Characteristics of the inlet and outlet sluices of FCA/CRT in Lippenbroek	75
Table 23. Input .txt file for the culvert subroutine in TELEMAC-3D to model the Lippenbroek FCA/CRT	78
Table 24. Normalized root mean square error for the mean water level (MWL_error), outlet discharge (Q_{out_error}) and inlet discharge (Q_{in_error})	80
Table 25. Characteristics of the new inlet and outlet culverts of the new FCA/CRT in Bergenmeersen.	83
Table 26. Input .txt file for the culvert subroutine in TELEMAC-3D to model the Bergenmeersen FCA/CRT	85
Table 27. Normalized root mean square error for the mean water level (MWL_error), outlet discharge (Q_{out_error}) and inlet discharge (Q_{in_error}) in Bergenmeersen test case	88
Table 28. Model runs used for the sensitivity analysis to the upstream discharge	93
Table 29. Model runs used for the sensitivity analysis to the bed roughness	97
Table 30. Measured and modeled velocity for one of the transects at Schoonaarde in runs with different roughness of the intertidal areas	98
Table 31. Measured and modeled velocity for one of the transects at Boom in runs with different roughness of the intertidal areas	99
Table 32. Model runs used for the sensitivity analysis to the diffusivity	100
Table 33. Measured and modeled velocity at Schellebelle in runs with different diffusivity	101
Table 34. Model runs used for the sensitivity analysis to the number of vertical layers	103
Table 35. Model runs used for the sensitivity analysis to the bathymetry of Durme	118

Table 36. Model runs used for the sensitivity analysis to the bathymetry of the tidal branch Gentbrugge ..	121
Table 37. Model runs with different turbulence models (Smagorinski and k-Epsilon)	124
Table 38. Measured and modeled velocity profiles in runs with different turbulence model (Smagorinski vs. k-Epsilon model)	125
Table 39. Model runs with different turbulence models	132
Table 40. Measured and modeled velocity profiles in runs with different turbulence models (Smagorinski vs. Constant viscosity model)	133
Table 41. Model runs used for the sensitivity analysis to the mass lumping.	145
Table 42. Measured and modeled velocity profiles in runs with and without mass lumping	146
Table 43. Model runs used for the sensitivity analysis to the implication for velocities	148
Table 44. Measured and modeled velocity profiles in runs with different implication for velocities	148
Table 45. Model runs used for the sensitivity analysis to the Coriolis coefficient	151
Table 46. Measured and modeled velocity profiles in runs with and without Coriolis coefficient	152
Table 47. Model runs used for the sensitivity analysis to the wind influence	155
Table 48. Model runs used for the sensitivity analysis to the grid	157
Table 49. Weights and thresholds used in the cost function	165
Table 50. Weights and thresholds used in the cost function for the Upper Sea Scheldt	166
Table 51. Velocity profiles calculated in Scaldis_028_0 and Scaldis_039_0 in the upstream part of the estuary	167
Table 52. Statistical parameters for the time series of salinity (run Scaldis_039_2 vs. measurement)	179
Table 53. Statistical parameters for the filtered time series of salinity (run Scaldis_039_2 vs. measurement)	179
Table 54. Comparison of salinity in Scaldis_028_2 and Scaldis_039_2	181
Table 55. Salinity range in runs Scaldis_028_2 and Scaldis_039_2	182
Table 56. Comparable tides for the ADCP measurements used for the calibration	214
Table 57. Comparable tides for the ADCP measurements used for the validation	215
Table 58. Comparable tides for the discharge measurements	215
Table 59. Statistical parameters for the water level time series (Scaldis_028_Q2 vs. Scaldis_028_Q1) ...	216
Table 60. Statistical parameters for high waters (Scaldis_028_Q2 vs. Scaldis_028_Q1)	217
Table 61. Statistical parameters for low waters (Scaldis_028_Q2 vs. Scaldis_028_Q1)	217
Table 62. Measured and modeled velocity at Kruikebe, Dendermonde and Schoonaarde in runs with different diffusivity	218
Table 63. Statistical parameters for the water level time series (North sea and Western Scheldt)	A1
Table 64. Statistical parameters for the water level time series (Eastern Scheldt)	A2
Table 65. Statistical parameters for the water level time series (Lower Sea Scheldt)	A2
Table 66. Statistical parameters for the water level time series (Upper Sea Scheldt)	A3
Table 67. Statistical parameters for the water level time series (Rupel basin and Durme)	A3
Table 68. Statistical parameters for high waters (North sea and Western Scheldt)	A4
Table 69. Statistical parameters for high waters (Eastern Scheldt)	A4
Table 70. Statistical parameters for high waters (Lower Sea Scheldt)	A5

Table 71. Statistical parameters for high waters (Upper Sea Scheldt)	A5
Table 72. Statistical parameters for high waters (Rupel basin and Durme)	A5
Table 73. Statistical parameters for low waters (North sea and Western Scheldt).....	A6
Table 74. Statistical parameters for low waters (Eastern Scheldt)	A6
Table 75. Statistical parameters for low waters (Lower Sea Scheldt)	A7
Table 76. Statistical parameters for low waters (Upper Sea Scheldt)	A7
Table 77. Statistical parameters for low waters (Rupel basin and Durme).....	A7
Table 78. Harmonic analysis: Amplitude M2 (North sea and Western Scheldt).....	A8
Table 79. Harmonic analysis: Amplitude M2 (Eastern Scheldt)	A8
Table 80. Harmonic analysis: Amplitude M2 (Lower Sea Scheldt).....	A9
Table 81. Harmonic analysis: Amplitude M2 (Upper Sea Scheldt).....	A9
Table 82. Harmonic analysis: Amplitude M2 (Rupel basin).....	A9
Table 83. Harmonic analysis: Phase M2 (North sea and Western Scheldt).....	A10
Table 84. Harmonic analysis: Phase M2 (Eastern Scheldt)	A10
Table 85. Harmonic analysis: Phase M2 (Lower Sea Scheldt)	A11
Table 86. Harmonic analysis: Phase M2 (Upper Sea Scheldt)	A11
Table 87. Harmonic analysis: Phase M2 (Rupel basin).....	A11
Table 88. Harmonic analysis: Amplitude M4 (North sea and Western Scheldt).....	A12
Table 89. Harmonic analysis: Amplitude M4 (Eastern Scheldt)	A12
Table 90. Harmonic analysis: Amplitude M4 (Lower Sea Scheldt).....	A13
Table 91. Harmonic analysis: Amplitude M4 (Upper Sea Scheldt).....	A13
Table 92. Harmonic analysis: Amplitude M4 (Rupel basin).....	A13
Table 93. Harmonic analysis: Phase M4 (North sea and Western Scheldt).....	A14
Table 94. Harmonic analysis: Phase M4 (Eastern Scheldt)	A14
Table 95. Harmonic analysis: Phase M4 (Lower Sea Scheldt)	A15
Table 96. Harmonic analysis: Phase M4 (Upper Sea Scheldt)	A15
Table 97. Harmonic analysis: Phase M4 (Rupel basin).....	A15
Table 98. Harmonic analysis: Amplitude M6 (North sea and Western Scheldt).....	A16
Table 99. Harmonic analysis: Amplitude M6 (Eastern Scheldt)	A16
Table 100. Harmonic analysis: Amplitude M6 (Lower Sea Scheldt).....	A17
Table 101. Harmonic analysis: Amplitude M6 (Upper Sea Scheldt).....	A17
Table 102. Harmonic analysis: Amplitude M6 (Rupel basin).....	A17
Table 103. Harmonic analysis: Phase M6 (North sea and Western Scheldt).....	A18
Table 104. Harmonic analysis: Phase M6 (Eastern Scheldt)	A18
Table 105. Harmonic analysis: Phase M6 (Lower Sea Scheldt).....	A19
Table 106. Harmonic analysis: Phase M6 (Upper Sea Scheldt).....	A19
Table 107. Harmonic analysis: Phase M6 (Rupel basin).....	A19
Table 108. Harmonic analysis: Amplitude S2 (North sea and Western Scheldt).....	A20
Table 109. Harmonic analysis: Amplitude S2 (Eastern Scheldt)	A20

Table 110. Harmonic analysis: Amplitude S2 (Lower Sea Scheldt)	A21
Table 111. Harmonic analysis: Amplitude S2 (Upper Sea Scheldt)	A21
Table 112. Harmonic analysis: Amplitude S2 (Rupel basin).....	A21
Table 113. Harmonic analysis: Phase S2 (North sea and Western Scheldt)	A22
Table 114. Harmonic analysis: Phase S2 (Eastern Scheldt).....	A22
Table 115. Harmonic analysis: Phase S2 (Lower Sea Scheldt)	A23
Table 116. Harmonic analysis: Phase S2 (Upper Sea Scheldt)	A23
Table 117. Harmonic analysis: Phase S2 (Rupel basin)	A23
Table 118. Harmonic analysis: Amplitude K1 (North sea and Western Scheldt).....	A24
Table 119. Harmonic analysis: Amplitude K1 (Eastern Scheldt)	A24
Table 120. Harmonic analysis: Amplitude K1 (Lower Sea Scheldt)	A25
Table 121. Harmonic analysis: Amplitude K1 (Upper Sea Scheldt)	A25
Table 122. Harmonic analysis: Amplitude K1 (Rupel basin).....	A25
Table 123. Harmonic analysis: Phase K1 (North sea and Western Scheldt)	A26
Table 124. Harmonic analysis: Phase K1 (Eastern Scheldt).....	A26
Table 125. Harmonic analysis: Phase K1 (Lower Sea Scheldt)	A27
Table 126. Harmonic analysis: Phase K1 (Upper Sea Scheldt)	A27
Table 127. Harmonic analysis: Phase K1 (Rupel basin)	A27
Table 128. Harmonic analysis: Amplitude O1 (North sea and Western Scheldt)	A28
Table 129. Harmonic analysis: Amplitude O1 (Eastern Scheldt).....	A28
Table 130. Harmonic analysis: Amplitude O1 (Lower Sea Scheldt).....	A29
Table 131. Harmonic analysis: Amplitude O1 (Upper Sea Scheldt).....	A29
Table 132. Harmonic analysis: Amplitude O1 (Rupel basin)	A29
Table 133. Harmonic analysis: Phase O1 (North sea and Western Scheldt).....	A30
Table 134. Harmonic analysis: Phase O1 (Eastern Scheldt).....	A30
Table 135. Harmonic analysis: Phase O1 (Lower Sea Scheldt).....	A31
Table 136. Harmonic analysis: Phase O1 (Upper Sea Scheldt).....	A31
Table 137. Harmonic analysis: Phase O1 (Rupel basin).....	A31
Table 138. Harmonic analysis : Z0 (North sea and Western Scheldt).....	A32
Table 139. Harmonic analysis : Z0 (Eastern Scheldt)	A32
Table 140. Harmonic analysis : Z0 (Lower Sea Scheldt).....	A33
Table 141. Harmonic analysis : Z0 (Upper Sea Scheldt).....	A33
Table 142. Harmonic analysis : Z0 (Rupel basin).....	A33
Table 143. Vector differences of model results vs. measurements (North sea and Western Scheldt)	A34
Table 144. Vector differences of model results vs. measurements (Eastern Scheldt)	A34
Table 145. Vector differences of model results vs. measurements (Lower Sea Scheldt)	A35
Table 146. Vector differences of model results vs. measurements (Upper Sea Scheldt)	A35
Table 147. Vector differences of model results vs. measurements (Rupel basin)	A36
Table 148. Comparison of the model results and ADCP velocities for transverse transects.....	A62

Table 149. Comparison of the model results and ADCP velocities for longitudinal transects	A63
Table 150. RMSE of velocity magnitude in the intertidal areas	A87
Table 151. Statistical parameters for discharges (model vs. measurement) in the Western Scheldt	A104
Table 152. Statistical parameters for discharges (model vs. measurement) in the Lower Sea Scheldt.....	A105
Table 153. Statistical parameters for discharges (model vs. measurement) in the Upper Sea Scheldt.....	A105
Table 154. Statistical parameters for discharges (model vs. measurement) in the Rupel basin.....	A105
Table 155. Statistical parameters for the stationary velocities in deep zones	A108
Table 156. RMSE for the stationary velocities in shallow zones at INBO locations	A112
Table 157. RMSE for the stationary depth average velocities in shallow zones in the Western Scheldt ..	A113
Table 158. RMSE for the stationary depth average velocities at Hooze Platen Noord	A114
Table 159. RMSE for the stationary depth average velocities at Hooze Platen West.....	A116
Table 160. RMSE for the stationary depth average velocities at Plaat van Walsoorden	A118
Table 161. Statistical parameters for the water level time series during storm (North sea and Western Scheldt).....	A153
Table 162. Statistical parameters for the water level time series during storm (Eastern Scheldt).....	A154
Table 163. Statistical parameters for the water level time series during storm (Lower Sea Scheldt).....	A154
Table 164. Statistical parameters for the water level time series during storm (Upper Sea Scheldt).....	A155
Table 165. Statistical parameters for the water level time series during storm (Rupel basin and Durme) ..	A155
Table 166. Statistical parameters for high waters during storm (North sea and Western Scheldt)	A156
Table 167. Statistical parameters for high waters during storm (Eastern Scheldt).....	A156
Table 168. Statistical parameters for high waters during storm (Lower Sea Scheldt)	A157
Table 169. Statistical parameters for high waters during storm (Upper Sea Scheldt)	A157
Table 170. Statistical parameters for high waters during storm (Rupel basin and Durme)	A157
Table 171. Statistical parameters for low waters during storm (North sea and Western Scheldt).....	A158
Table 172. Statistical parameters for low waters during storm (Eastern Scheldt)	A158
Table 173. Statistical parameters for low waters during storm (Lower Sea Scheldt)	A158
Table 174. Statistical parameters for low waters during storm (Upper Sea Scheldt)	A159
Table 175. Statistical parameters for low waters during storm (Rupel basin and Durme).....	A159
Table 176. Harmonic analysis: Amplitude M2 during storm (North sea and Western Scheldt).....	A160
Table 177. Harmonic analysis: Amplitude M2 during storm (Eastern Scheldt)	A160
Table 178. Harmonic analysis: Amplitude M2 during storm (Lower Sea Scheldt).....	A161
Table 179. Harmonic analysis: Amplitude M2 during storm (Upper Sea Scheldt).....	A161
Table 180. Harmonic analysis: Amplitude M2 during storm (Rupel basin).....	A161
Table 181. Harmonic analysis: Phase M2 during storm (North sea and Western Scheldt).....	A162
Table 182. Harmonic analysis: Phase M2 during storm (Eastern Scheldt)	A162
Table 183. Harmonic analysis: Phase M2 during storm (Lower Sea Scheldt).....	A163
Table 184. Harmonic analysis: Phase M2 during storm (Upper Sea Scheldt)	A163
Table 185. Harmonic analysis: Phase M2 during storm (Rupel basin).....	A163
Table 186. Harmonic analysis: Amplitude M4 during storm (North sea and Western Scheldt).....	A164

Table 187. Harmonic analysis: Amplitude M4 during storm (Eastern Scheldt)	A164
Table 188. Harmonic analysis: Amplitude M4 during storm (Lower Sea Scheldt).....	A165
Table 189. Harmonic analysis: Amplitude M4 during storm (Upper Sea Scheldt).....	A165
Table 190. Harmonic analysis: Amplitude M4 during storm (Rupel basin).....	A165
Table 191. Harmonic analysis: Phase M4 during storm (North sea and Western Scheldt).....	A166
Table 192. Harmonic analysis: Phase M4 during storm (Eastern Scheldt)	A166
Table 193. Harmonic analysis: Phase M4 during storm (Lower Sea Scheldt).....	A167
Table 194. Harmonic analysis: Phase M4 during storm (Upper Sea Scheldt)	A167
Table 195. Harmonic analysis: Phase M4 during storm (Rupel basin).....	A167
Table 196. Harmonic analysis: Amplitude M6 during storm (North sea and Western Scheldt).....	A168
Table 197. Harmonic analysis: Amplitude M6 during storm (Eastern Scheldt)	A168
Table 198. Harmonic analysis: Amplitude M6 during storm (Lower Sea Scheldt).....	A169
Table 199. Harmonic analysis: Amplitude M6 during storm (Upper Sea Scheldt).....	A169
Table 200. Harmonic analysis: Amplitude M6 during storm (Rupel basin).....	A169
Table 201. Harmonic analysis: Phase M6 during storm (North sea and Western Scheldt).....	A170
Table 202. Harmonic analysis: Phase M6 during storm (Eastern Scheldt)	A170
Table 203. Harmonic analysis: Phase M6 during storm (Lower Sea Scheldt).....	A171
Table 204. Harmonic analysis: Phase M6 during storm (Upper Sea Scheldt)	A171
Table 205. Harmonic analysis: Phase M6 during storm (Rupel basin).....	A171
Table 206. Harmonic analysis: Amplitude K1 during storm (North sea and Western Scheldt).....	A172
Table 207. Harmonic analysis: Amplitude K1 during storm (Eastern Scheldt)	A172
Table 208. Harmonic analysis: Amplitude K1 during storm (Lower Sea Scheldt)	A173
Table 209. Harmonic analysis: Amplitude K1 during storm (Upper Sea Scheldt)	A173
Table 210. Harmonic analysis: Amplitude K1 during storm (Rupel basin).....	A173
Table 211. Harmonic analysis: Phase K1 during storm (North sea and Western Scheldt)	A174
Table 212. Harmonic analysis: Phase K1 during storm (Eastern Scheldt).....	A174
Table 213. Harmonic analysis: Phase K1 during storm (Lower Sea Scheldt)	A175
Table 214. Harmonic analysis: Phase K1 during storm (Upper Sea Scheldt)	A175
Table 215. Harmonic analysis: Phase K1 during storm (Rupel basin)	A175
Table 216. Harmonic analysis: Z0 during storm (North sea and Western Scheldt).....	A176
Table 217. Harmonic analysis: Z0 during storm (Eastern Scheldt)	A176
Table 218. Harmonic analysis: Z0 during storm (Lower Sea Scheldt).....	A177
Table 219. Harmonic analysis: Z0 during storm (Upper Sea Scheldt).....	A177
Table 220. Harmonic analysis: Z0 during storm (Rupel basin).....	A177
Table 221. Vector differences of model results vs. measurements during storm (North sea and Western Scheldt).....	A178
Table 222. Vector differences of model results vs. measurements during storm (Eastern Scheldt)	A178
Table 223. Vector differences of model results vs. measurements during storm (Lower Sea Scheldt)	A179
Table 224. Vector differences of model results vs. measurements during storm (Upper Sea Scheldt)	A179

Table 225. Vector differences of model results vs. measurements during storm (Rupel basin)	A179
Table 226. Comparison of the model results and ADCP velocities for the model validation	A207
Table 227. Typical values of the tidal coefficients for neap, average and spring tides	A216
Table 228. Model qualification based on (<i>Sutherland et al.</i> , 2003)	A219

List of figures

Figure 1 - Measured velocity at Doel.....	11
Figure 2 - Wind at Vlakte van de Raan during the calibration period	13
Figure 3 - Wind at Vlakte van de Raan during the Sinterklaas storm.....	14
Figure 4 - Potential flow around a cylinder	17
Figure 5 - Original (black) and projected (red) coordinate system	19
Figure 6 - Tidal excursion length based on the M2 component near the port of Zeebrugge.....	20
Figure 7 - Representations of the 5 sigma levels in Scaldis and their z* distribution. Small insert in right bottom corner: connection of the levels to form stacked prisms.....	21
Figure 8 - Map showing edge growth ratio (EGR) in coastal zone, Western Scheldt and Eastern Scheldt of Scaldis.	24
Figure 9 - Map showing edge growth ratio (EGR) in Sea Scheldt and tributaries of Scaldis.....	24
Figure 10 - Model bathymetry (m TAW)	25
Figure 11 - Overview of the bathymetric data for the coastal zone : blue colour – greater North sea bathymetry ; orange colour – Belgian continental shelf and coastal zone ; green colour – measurements for the Dutch coast.....	26
Figure 12 - Bathymetry lower Sea Scheldt. Beneden Zeeschelde. The purple coloured zone is part of a topo-bathymetric dataset from 2011. The grey area is the back is part of the DHM Vlaanderen dataset from 2007.....	27
Figure 13 - Datasets of bathymetry/topography of Upper Sea Scheldt: black color = DHM Vlaanderen for most upper part of the Durme. Blue color = topobathymetry from 2011. Orange color = topobathymetry from 2014. Red color = bathymetry for Durme from 2012. Green color = bathymetry for Durme from 2013. Yellow areas = topography of flood control areas from 2013.....	28
Figure 14 - Rupel basin: blue = topo-bathymetry from 2013-2014 from MT; orange = topography from total Sea Scheldt basin from 2007, given by MT; red = bathymetry Zenne = cross sections from 2001. Data from IMDC; black = bathymetry from 2010-2013 coming from W&Z; grey = cross sections from 2001 coming from IMDC; yellow = bathymetry coming from W&Z dating from 2010-2013; green = cross sections from 2001 from IMDC data.	29
Figure 15 - Nesting of Scaldis model in ZUNO. Scaldis boundary nodes given in red.....	31
Figure 16 - Comparison of modelled salinity in ZUNO and measured salinity for Vlakte van de Raan station.	32
Figure 17 - Salinity values at 17/09/2013 00:00 extracted from ZUNO (orange dots) and location of the stations that measure salinity in the Scheldt Estuary (red dots). These stations are named (from downstream to upstream) Vlakte van de Raan, Overloop van Hansweert, Baalhoek, Prosperpolder, Liefkenshoek, Boei 84, Hemiksem and Driegoten.....	33
Figure 18 - Initial salinity field for start simulation at “17/09/2013 00:00”	33
Figure 19 - The calibrated roughness field (Manning $m^{-1/3}$ s) of the Scaldis model.....	37
Figure 20 - Water movements between the FCA and river without CRT (on the left) and with CRT (on the middle and right pannels). (Source: <i>De Mulder et al. (2013)</i>).....	40
Figure 21 - Sketch of general flow through a culvert (<i>Bodhaine, 1968</i>)	41
Figure 22 – Schematization of the 6 different types of flow that occur through culverts according to <i>Bodhaine (1968)</i> . The red line represents the critical water depth.	42
Figure 23 - Criterion for classifying flow types 5 and 6 in concrete box or pipe culverts with square, rounded, or bevelled entrances, either with or without wingwalls (<i>Bodhaine, 1968</i>)	46

Figure 24 - Representation of the different variables used to calculate the discharges for each type of flow	47
Figure 25 - Summary of the equations used in TELEMAC-2D, Delft 3D and MIKE 11 to deal with culverts	54
Figure 26 - Representation of the different variables used to calculate the discharges for each type of flow	56
Figure 27 - Local loss coefficient for a sudden contraction as a function of diameter ratio between the diameter after the contraction (D_1) and before the contraction D_u (<i>Bruce et al.</i> , 2000)	57
Figure 28 - Discharge coefficient (Alfa) due to the presence of open valves for each type of flow (source: IMDC Report 613_9_1)	60
Figure 29 - 2D computational grid used for the simplified model	63
Figure 30 - Flow patterns when the free surface level (m) is higher in the upper part than the lower part of the domain at time $t=4h$ (on the left side) and the opposite case at $t=8h$ (on the right side)	65
Figure 31 - Mean water levels (MWL) modelled by TELEMAC-3D in the river (blue line) and in the Flood Control Area (FCA) (red line)	66
Figure 32 - Evolution in time of the inlet sluice discharge	66
Figure 33 - Outlet culvert discharges with two locations for the inlet sluices (Ref Run)	67
Figure 34 - Influence of the correction coefficient for flow type 5 (C15) on the inlet discharges	68
Figure 35 - Comparison of modelled mean water levels (upper panel) and outlet discharges (lower panel) between the reference run ($C_v=0$) and a different simulation with $C_v=17$	69
Figure 36 - Measurement of the opening angle of the non-return-valve of the outlet culverts of CRT Bergenmeersen. The measurement was done in the framework of projects 15_034 at a 13 hour measurement on the 3 rd of September 2015.	70
Figure 37 - Comparison of modelled mean water levels (upper panel) and outlet discharges (lower panel) between the reference run ($C_T=0$) and a simulation with $C_T=1.4$	71
Figure 38 - Evolution of tracer concentration in time in the river (red line) and in the FCA (blue line) for Run 1.	72
Figure 39 - Evolution of tracer concentration in the river (red line) and in the FCA (blue line). Run 2.	73
Figure 40 - Evolution of tracer concentration in time in the river (red line) and in the FCA (blue line). Run 3.	73
Figure 41 - Configuration of the inlet and outlet sluices (on the left) and detail of the weir structures in the inlet sluices (on the right) in Lippenbroek area (source: <i>De Mulder et al.</i> (2013))	75
Figure 42 - Outlet entrance (on the left) and exit (on the right) in Lippenbroek (Patrimoniumdatabank W&Z)	76
Figure 43 - Planview of the computational grid to model the FCA/CRT Lippenbroek. The colour scale represents the bottom values in m NAP.	77
Figure 44 - Comparison of water level (m NAP) in the polder: numerical results versus measurements	78
Figure 45 - Comparison between numerical results and measurements for outlet culvert discharges	79
Figure 46 - Comparison between empirical formula and numerical results for inlet culvert discharges	79
Figure 47 - Output of numerical results when the water level in the river is higher than in the FCA. The arrows represent the velocity vectors	80
Figure 48 - Output of numerical results when the water level in the river is lower than in the FCA. The arrows represent the velocity vectors	81
Figure 49 - Mean water levels modelled by TELEMAC-3D in the river (blue line) and in the FCA (red line) (left axis) and the corresponding flow types that occur during the time series (right axis). Flow through inlet sluice (type 2-6) and through outlet sluice (type 12-16)	81

Figure 50 - Detail of the side view of the construction of the new inlet and outlet culverts in Bergenmeersen.	82
Figure 51 - Inlet and outlet culvert configuration on the river side (construction phase) (Patrimoniumdatabank W&Z)	83
Figure 52 - View on the inlet culverts from the river side and inlet and outlet culverts from the FCA side	83
Figure 53 - Planview of the computational domain to model the FCA/CRT in Bergenmeersen. The colour scale represents the bathymetry (m TAW).	84
Figure 54 - Comparison of the mean water level time evolution in the river between numerical results and measurements	86
Figure 55 - Comparison of the mean water level time evolution in the polder between numerical results and measurements	87
Figure 56 - Comparison of outlet culvert discharges time evolution between numerical results and measurements	87
Figure 57 - Comparison of inlet culvert discharges time evolution between numerical results and measurements	88
Figure 58 - Mean water levels modelled by TELEMAC-3D in the river (blue line) and in the FCA (red line) and the corresponding flow types that occur during the time series. Flow through inlet culvert (type 2 - 6) and through outlet culvert (type 12 - 16)	89
Figure 59 - Scaldis 3D model showing 1km interval sampled thalweg (=white dots).	90
Figure 60 - Detail of Figure 59 showing upper Sea Scheldt in Scaldis 3D model with the 1km interval sampled thalweg. Samples are numbered. These numbers represent the number of km in the estuary starting from Vlissingen.	91
Figure 61 - High water levels along thalweg of Scheldt Estuary in Scaldis 3D model with focus on Upper Sea Scheldt. The insertion gives the tidal curve in Vlissingen (km 1) in black line and at Bergenmeersen (km 152) in blue line.	91
Figure 62 - Differences in flow velocities of two points near Bergenmeersen: one just downstream the FCA/CRT and one just upstream. Water level is given as reference to associate differences in flow velocities.	92
Figure 63 - Measured discharge at Merelbeke	94
Figure 64 - Water level at Schoonaarde in Scaldis_028_Q1 and Scaldis_028_Q2	95
Figure 65 - Water level at Wetteren in Scaldis_028_Q1 and Scaldis_028_Q2	96
Figure 66 - Water level at Melle in Scaldis_028_Q1 and Scaldis_028_Q2	97
Figure 67 - M2 amplitude in runs with different roughness of the intertidal areas (Western Scheldt and Sea Scheldt)	100
Figure 68 - Velocity profiles at Vlakte van de Raan	103
Figure 69 - Velocity profiles at Westkapelle	104
Figure 70 - Velocity profiles at Cadzand	104
Figure 71 - Velocity profiles at Kramp (sharp river bend)	104
Figure 72 - Velocity profiles at Schoonaarde	105
Figure 73 - Velocity profiles at Melle	105
Figure 74 - M2 amplitude in SA1b and SA13 (North sea)	106
Figure 75 - M2 amplitude in SA1b and SA13 (Western Scheldt and Sea Scheldt)	106
Figure 76 - Profiles of horizontal viscosity NUX at Vlakte van de Raan	107
Figure 77 - Profiles of horizontal viscosity NUX at Westkapelle	107

Figure 78 - Profiles of horizontal viscosity NUX at Cadzand	108
Figure 79 - Profiles of horizontal viscosity NUX at Kramp	108
Figure 80 - Profiles of horizontal viscosity NUX at Schoonaarde	108
Figure 81 - Profiles of horizontal viscosity NUX at Melle	109
Figure 82 - Profiles of vertical viscosity NUZ at Vlake van de Raan.....	109
Figure 83 - Profiles of vertical viscosity NUZ at Westkapelle	109
Figure 84 - Profiles of vertical viscosity NUZ at Cadzand.....	110
Figure 85 - Profiles of vertical viscosity NUZ at Kramp	110
Figure 86 - Profiles of vertical viscosity NUZ at Schoonaarde.....	110
Figure 87 - Profiles of vertical viscosity NUZ at Melle	111
Figure 88 - Map of the depth average horizontal viscosity in the North sea in runs SA1b and SA13	112
Figure 89 - Map of the depth average horizontal viscosity in the Western Scheldt in runs SA1b and SA13	113
Figure 90 - Map of the depth average horizontal viscosity in the Sea Scheldt in runs SA1b and SA13	114
Figure 91 - Map of the depth average vertical viscosity in the North sea in runs SA1b and SA13	115
Figure 92 - Map of the depth average vertical viscosity in the Western Scheldt in runs SA1b and SA13.....	116
Figure 93 - Map of the depth average vertical viscosity in the Sea Scheldt in runs SA1b and SA13.....	117
Figure 94 - M2 amplitude in runs SA1 and SA15 (North sea)	118
Figure 95 - M2 amplitude in runs SA1 and SA15 (Western Scheldt and Sea Scheldt)	119
Figure 96 - M2 amplitude in runs SA1 and SA15 (zoom to the zone with changes in water levels)	119
Figure 97 - Bias of high water (SA15 – SA1).....	120
Figure 98 - Bias of low water (SA15 – SA1)	120
Figure 99 - Water level at Tielrode in SA1 and SA15.....	121
Figure 100 - M2 amplitude in runs SA1 and SA16 (North sea)	122
Figure 101 - M2 amplitude in runs SA1 and SA16 (Western Scheldt and Sea Scheldt)	122
Figure 102 - Bias of high water (SA16 – SA1).....	123
Figure 103 - Bias of low water (SA16 – SA1)	123
Figure 104 - Water level at Melle in SA1 and SA16	124
Figure 105 - M2 amplitude in runs SA8a and SA14a (North sea)	127
Figure 106 - M2 amplitude in runs SA8a and SA14a (Western Scheldt and Sea Scheldt)	127
Figure 107 - Viscosity calculated in SA8a (20/09/2013 02:00) (m ² /s)	129
Figure 108 - Viscosity calculated in SA14a (20/09/2013 02:00) (m ² /s)	129
Figure 109 - Viscosity calculated in SA8a in the Western Scheldt (20/09/2013 02:00) (m ² /s)	130
Figure 110 - Viscosity calculated in SA14a in the Western Scheldt (20/09/2013 02:00) (m ² /s)	130
Figure 111 - Viscosity calculated in SA8a in the Sea Scheldt (20/09/2013 02:00) (m ² /s)	131
Figure 112 - Viscosity calculated in SA14a in the Sea Scheldt (20/09/2013 02:00) (m ² /s)	131
Figure 113 - Discharge at R6 Middelgat (SA19, SA30 and measurement).....	135
Figure 114 - Discharge at Kruibeke (SA19, SA30 and measurement).....	135
Figure 115 - Discharge at Schoonaarde (SA19, SA30 and measurement).....	136

Figure 116 - M2 amplitude in runs SA19 and SA30 (North sea)	136
Figure 117 - M2 amplitude in runs SA19 and SA30 (Western Scheldt and Sea Scheldt)	137
Figure 118 - Viscosity calculated in SA19 (20/09/2013 02:00) (m ² /s)	138
Figure 119 - Viscosity calculated in SA30 (20/09/2013 02:00) (m ² /s)	138
Figure 120 - Viscosity calculated in SA19 in the Western Scheldt (20/09/2013 02:00) (m ² /s)	139
Figure 121 - Viscosity calculated in SA30 in the Western Scheldt (20/09/2013 02:00) (m ² /s)	139
Figure 122 - Viscosity calculated in SA19 in the Sea Scheldt (20/09/2013 02:00) (m ² /s)	140
Figure 123 - Viscosity calculated in SA30 in the Sea Scheldt (20/09/2013 02:00) (m ² /s)	140
Figure 124 - Flow velocities in Zeebrugge in SA_8a 1 hour before high water	141
Figure 125 - Flow velocities in Zeebrugge in SA_14a 1 hour before high water	141
Figure 126 - Flow velocities in Zeebrugge in SA_19 1 hour before high water	142
Figure 127 - Flow velocities in Zeebrugge in SA_30 1 hour before high water	142
Figure 128 - Flow velocities in Zeebrugge in SA_8a around high water	143
Figure 129 - Flow velocities in Zeebrugge in SA_14a around high water	143
Figure 130 - Flow velocities in Zeebrugge in SA_19 around high water	144
Figure 131 - Flow velocities in Zeebrugge in SA_30 around high water	144
Figure 132 - M2 amplitude in runs SA1 and SA12 (North Sea).....	147
Figure 133 - M2 amplitude in runs SA1 and SA12 (Western Scheldt and Sea Scheldt).....	147
Figure 134 - M2 amplitude in runs SA1 and SA11 (North sea)	149
Figure 135 - M2 amplitude in runs SA1 and SA11 (Western Scheldt and Sea Scheldt).....	150
Figure 136 - Measured and calculated water level at Wetteren (runs SA1, SA11)	150
Figure 137 - Measured and calculated water level at Melle (runs SA1, SA11)	151
Figure 138 - M2 amplitude in runs SA3 and SA4 (North sea)	154
Figure 139 - M2 amplitude in runs SA3 and SA4 (Western Scheldt and Sea Scheldt)	154
Figure 140 - Water level calculated in runs SA1 and SA10 at Vlakte van de Raan	155
Figure 141 - Water level calculated in runs SA1 and SA10 at Schoonaarde	156
Figure 142 - M2 amplitude in runs SA2 and SA3 (North sea)	156
Figure 143 - M2 amplitude in runs SA2 and SA3 (Western Scheldt and Sea Scheldt)	157
Figure 144 - Difference in high water (SA27 – SA25)	158
Figure 145 - Difference in low water (SA27 – SA25).....	158
Figure 146 - M2 amplitude in runs SA25 and SA27 (North sea)	159
Figure 147 - M2 amplitude in runs SA25 and SA27 (Western Scheldt and Sea Scheldt)	159
Figure 148 - Schematic view on the effect of salt water on the average water level.....	160
Figure 149 - Difference in water level at the estuary mouth caused by presence of salinity in the model. .	161
Figure 150 - Difference in water level near Bath caused by presence of salinity in the model.	161
Figure 151 - Difference in water level near Antwerp caused by presence of salinity in the model.....	162
Figure 152 - Showing the differences in water levels between a simulation with and without density effects for salinity. Water level differences are shown for Vlissingen (black line), Bath (blue line) and Antwerp (red line).	162

Figure 153 - Cost function for the entire Scheldt estuary (Scaldis_016_0 is reference)	169
Figure 154 - Cost function for the Upper Sea Scheldt (Scaldis_016_0 is reference)	170
Figure 155 - Cost function for the entire Scheldt estuary (Scaldis_028_0 is reference)	170
Figure 156 - Cost function for the Upper Sea Scheldt (Scaldis_028_0 is reference)	171
Figure 157 - M2 amplitude in the North sea (Scaldis_039_0 and measurement)	173
Figure 158 - M2 amplitude in the Scheldt estuary (Scaldis_039_0 and measurement)	173
Figure 159 - M2 phase in the North sea (Scaldis_039_0 and measurement)	174
Figure 160 - M2 phase in the Scheldt estuary (Scaldis_039_0 and measurement)	174
Figure 161 - Measured and modeled salinity at Prosperpolder	180
Figure 162 - Measured and modeled salinity minus moving average at Prosperpolder	180
Figure 163 - Roughness field near Antwerp in Scaldis_039_0 (Manning $m^{-1/3}s$)	185
Figure 164 - Roughness field near Antwerp in Scaldis_039_BFS (Manning $m^{-1/3}s$)	185
Figure 165 - M2 amplitude in the North sea in runs Scaldis_039_0 and Scaldis_039_BFS	186
Figure 166 - M2 amplitude in the Western Scheldt and Sea Scheldt in runs Scaldis_039_0 and Scaldis_039_BFS	186
Figure 167 - M2 amplitude in the Eastern Scheldt in runs Scaldis_039_0 and Scaldis_039_BFS	187
Figure 168 - M2 amplitude in the Rupel basin and Durme in runs Scaldis_039_0 and Scaldis_039_BFS	187
Figure 169 - Polygon numbering in Western Scheldt	191
Figure 170 - Polygon numbering in Sea Scheldt	192
Figure 171 - assigning mesh elements to polygons based on the location of their center of mass	193
Figure 172 - Polygons representing the Scheldt estuary and some filled with a passive tracer (red color)	193
Figure 173 - Calculating surface area of an irregular triangle using Heron's formula	194
Figure 174 - Volume of irregular prism under surface triangle	195
Figure 175 - Volume calculation of irregular shape under a triangle	195
Figure 176 - Volume irregular triangular pyramid	196
Figure 177 - Movement of average salinity concentrations in polygons over 73 time steps of one hour	197
Figure 178 - Movement of tracer 2 concentrations in polygons over 73 time steps of one hour.	198
Figure 179 - Movement of tracer 3 concentrations in polygons over 73 time steps of one hour.	198
Figure 180 - Movement of tracer 4 concentrations in polygons over 73 time steps of one hour.	199
Figure 181 - Movement of tracer 5 concentrations in polygons over 73 time steps of one hour.	199
Figure 182 - Movement of tracer 6 concentrations in polygons over 73 time steps of one hour.	200
Figure 183 - Movement of tracer 7 concentrations in polygons over 73 time steps of one hour.	200
Figure 184 - tracer 7 remaining in some parts of the estuary	201
Figure 185 - Movement of tracer 8 concentrations in polygons over 73 time steps of one hour.	202
Figure 186 - Movement of tracer 9 concentrations in polygons over 73 time steps of one hour.	202
Figure 187 - Movement of tracer 10 concentrations in polygons over 73 time steps of one hour.	203
Figure 188 - Movement of tracer 11 concentrations in polygons over 73 time steps of one hour.	204
Figure 189 - Movement of tracer 12 concentrations in polygons over 73 time steps of one hour.	204
Figure 190 - Movement of tracer 13 concentrations in polygons over 73 time steps of one hour.	205

Figure 191 - Movement of tracer 14 concentrations in polygons over 73 time steps of one hour.	205
Figure 192 - Movement of tracer 15 concentrations in polygons over 73 time steps of one hour.	206
Figure 193 - Movement of tracer 16 concentrations in polygons over 73 time steps of one hour.	207
Figure 194 - Movement of tracer 17 concentrations in polygons over 73 time steps of one hour.	207
Figure 195 - Movement of tracer 18 concentrations in polygons over 73 time steps of one hour.	208
Figure 196 - Movement of tracer 19 concentrations in polygons over 73 time steps of one hour.	208
Figure 197 - Movement of tracer 20 concentrations in polygons over 73 time steps of one hour.	209
Figure 198 - Water level stations	223
Figure 199 - Location of the available measurements for the Sinterklaasstorm.....	224
Figure 200 Measurement locations at Tielrode	224
Figure 201 - Measurement location at Waasmunster.....	225
Figure 202 - Measurement locations at Bergenmeersen	225
Figure 203 - Measurement location at Walem.....	226
Figure 204 - Measurement locations at Lier	226
Figure 205. Available ADCP measurements in the Western Scheldt.....	227
Figure 206 - Available ADCP measurements in the Lower Sea Scheldt.....	228
Figure 207 - Available ADCP measurements in the Upper Sea Scheldt and Rupel	229
Figure 208 - Stationary velocity measurements in deep areas	230
Figure 209 - Location of stationary velocity measurements in shallow areas.....	230
Figure 210 - Stationary velocity measurements Hooge Platen West and Hooge Platen Noord.....	231
Figure 211 - Stationary velocity measurements Plaat van Walsoorden	231
Figure 212 - Discharge cross sections in the Western Scheldt	232
Figure 213 - Location of salinity measurements	233
Figure 214 - Scaldis_v17_035 versus Sigma contour 04/2015: Grensgebied, Hedwigepolder en Doelpolder	234
Figure 215 - Scaldis_v17_035 versus Sigma contour 04/2015: Potpolder van lillo en Fort Filip.....	234
Figure 216 - Scaldis_v17_035 versus Sigma contour 04/2015: Burchtse Weel en KBR	235
Figure 217 - Scaldis_v17_035 versus Sigma contour 04/2015: Oudbroekpolder, Schellandpolder, Hingene Broekpolder, Spierbroekpolder, Groot Schoor, Stort Hingene, Stort Ballooi en Schouselbroek	235
Figure 218 - Scaldis_v17_035 versus Sigma contour 04/2015: Tielrodebroek en De Bunt	236
Figure 219 - Scaldis_v17_035 versus Sigma contour 04/2015: Klein Broek en Groot Broek	236
Figure 220 - Scaldis_v17_035 versus Sigma contour 04/2015: Potpolder I en Polder van Waasmunster ..	237
Figure 221 - Scaldis_v17_035 versus Sigma contour 04/2015: Potpolder IV	237
Figure 222 - Scaldis_v17_035 versus Sigma contour 04/2015: Lippenbroek	238
Figure 223 - Scaldis_v17_035 versus Sigma contour 04/2015: Blankaart, Zwijn, Grote Wal en Kleine Wal	239
Figure 224 - Scaldis_v17_035 versus Sigma contour 04/2015: Uiterdijk, Vlassenbroek I en Vlassenbroek II	239
Figure 225 - Scaldis_v17_035 versus Sigma contour 04/2015: Scheldebroek	240
Figure 226 - Scaldis_v17_035 versus Sigma contour 04/2015: Paardeweide en Bergenmeersen	240

Figure 227 - Scaldis_v17_035 versus Sigma contour 04/2015: Wijmeers I en Wijmeers II	241
Figure 228 - Scaldis_v17_035 versus Sigma contour 04/2015: Bastenakkers en Ham.....	241
Figure 229 - Scaldis_v17_035 versus Sigma contour 04/2015: Zandput Melle en Heusden	242
Figure 230 - Stort De Naeyer.....	242
Figure 231 - Scaldis_v17_035 versus Sigma contour 04/2015: Bovenzanden	243
Figure 232 - Scaldis_v17_035 versus Sigma contour 04/2015: Heindonk Tien Vierendelen I en Heindonk Tien Vierendelen II	243
Figure 233 - Scaldis_v17_035 versus Sigma contour 04/2015: Grote Vijver I, Grote Vijver II en Battenbroek	244
Figure 234 - Scaldis_v17_035 versus Sigma contour 04/2015: Zennegat.....	244
Figure 235 - Scaldis_v17_035 versus Sigma contour 04/2015: Schoneberg.....	245
Figure 236 - Scaldis_v17_035 versus Sigma contour 04/2015: Rijmenam	245
Figure 237 - Scaldis_v17_035 versus Sigma contour 04/2015: Hollaken-Hoogdonk	246
Figure 238 - Scaldis_v17_035 versus Sigma contour 04/2015: Polder van Lier, Anderstadt I en Anderstadt II	246
Figure 239 - Bias of high water magnitude (model – measurement) in the North sea and Western Scheldt	36
Figure 240 - Bias of high water magnitude (model – measurement) in the Eastern Scheldt	A37
Figure 241 - Bias of high water magnitude (model – measurement) in the Lower Sea Scheldt.....	A37
Figure 242 - Bias of high water magnitude (model – measurement) in the Upper Sea Scheldt.....	A38
Figure 243 - Bias of low water magnitude (model – measurement) in the North sea and Western Scheldt	A38
Figure 244 - Bias of low water magnitude (model – measurement) in the Eastern Scheldt.....	A39
Figure 245 - Bias of low water magnitude (model – measurement) in the Lower Sea Scheldt	A39
Figure 246 - Bias of low water magnitude (model – measurement) in the Upper Sea Scheldt	A40
Figure 247 - RMSE of high water magnitude (model vs. measurement) in the North sea and Western Scheldt.....	A40
Figure 248 - RMSE of high water magnitude (model vs. measurement) in the Eastern Scheldt.....	A41
Figure 249 - RMSE of high water magnitude (model vs. measurement) in the Lower Sea Scheldt.....	A41
Figure 250 - RMSE of high water magnitude (model vs. measurement) in the Upper Sea Scheldt.....	A42
Figure 251 - RMSE of low water magnitude (model vs. measurement) in the North sea and Western Scheldt	A42
Figure 252 - RMSE of low water magnitude (model vs. measurement) in the Eastern Scheldt.....	A43
Figure 253 - RMSE of low water magnitude (model vs. measurement) in the Lower Sea Scheldt	A43
Figure 254 - RMSE of low water magnitude (model vs. measurement) in the Upper Sea Scheldt	A44
Figure 255 - Bias of the water level time series in the North sea and Western Scheldt.....	A44
Figure 256 - Bias of the water level time series in the Eastern Scheldt	A45
Figure 257 - Bias of the water level time series in the Lower Sea Scheldt.....	A45
Figure 258 - Bias of the water level time series in the Upper Sea Scheldt.....	A46
Figure 259 - RMSE of the water level time series in the North sea and Western Scheldt	A46
Figure 260 - RMSE of the water level time series in the Eastern Scheldt.....	A47
Figure 261 - RMSE of the water level time series in the Lower Sea Scheldt	A47

Figure 262 - RMSE of the water level time series in the Upper Sea Scheldt	A48
Figure 263 - M2 amplitude in the North sea and Western Scheldt.....	A48
Figure 264 - M2 amplitude in the Eastern Scheldt	A49
Figure 265 - M2 amplitude in the Lower Sea Scheldt.....	A49
Figure 266 - M2 amplitude in the Upper Sea Scheldt.....	A50
Figure 267 - M2 phase in the North sea and Western Scheldt.....	A50
Figure 268 - M2 phase in the Eastern Scheldt	A51
Figure 269 - M2 phase in the Lower Sea Scheldt	A51
Figure 270 - M2 phase in the Upper Sea Scheldt	A52
Figure 271 - S2 amplitude in the North sea and Western Scheldt	A52
Figure 272 - S2 amplitude in the Eastern Scheldt.....	A53
Figure 273 - S2 amplitude in the Lower Sea Scheldt	A53
Figure 274 - S2 amplitude in the Upper Sea Scheldt	A54
Figure 275 - S2 phase in the North sea and Western Scheldt	A54
Figure 276 - S2 phase in the Eastern Scheldt.....	A55
Figure 277 - S2 phase in the Lower Sea Scheldt.....	A55
Figure 278 - S2 phase in the Upper Sea Scheldt.....	A56
Figure 279 - Calculated and measured water levels at Vlakte van de Raan	A56
Figure 280 - Calculated and measured water levels at Oosterschelde 14	A57
Figure 281 - Calculated and measured water levels at Sluis Kats	A57
Figure 282 - Calculated and measured water levels at Hansweert	A58
Figure 283 - Calculated and measured water levels at Antwerpen	A58
Figure 284 - Calculated and measured water levels at Schelle.....	A59
Figure 285 - Calculated and measured water levels at Sint Amands	A59
Figure 286 - Calculated and measured water levels at Schoonaarde	A60
Figure 287 - Calculated and measured water levels at Melle.....	A60
Figure 288 - Calculated and measured water levels at Boom.....	A61
Figure 289 - Time series of the measured and modeled velocity magnitude and direction at 20110705 Everingen	A63
Figure 290 - Time series of the measured and modeled velocity magnitude and direction at 20110706 R7 Terneuzen	A64
Figure 291 - Time series of the measured and modeled velocity magnitude and direction at 20120508 R6 Middelgat	A64
Figure 292 - Time series of the measured and modeled velocity magnitude and direction at 20120509 R6 GatVanOssenissee.....	A65
Figure 293 - Time series of the measured and modeled velocity magnitude and direction at 20080407 dwarsraai Ossenissee	A65
Figure 294 - Time series of the measured and modeled velocity magnitude and direction at 20060323 Waarde.....	A66
Figure 295 - Time series of the measured and modeled velocity magnitude and direction at 20130424 R5 SchaarVanWaarde	A66

Figure 296 - Time series of the measured and modeled velocity magnitude and direction at 20130425 R5 Zuidergat.....	A67
Figure 297 - Time series of the measured and modeled velocity magnitude and direction at 20060912 Schaar van Ouden Doel	A67
Figure 298 - Time series of the measured and modeled velocity magnitude and direction at 20050217 Zandvliet	A68
Figure 299 - Time series of the measured and modeled velocity magnitude and direction at 20110902 Galgenschoor	A68
Figure 300 - Time series of the measured and modeled velocity magnitude and direction at 20100318 langsraai O	A69
Figure 301 - Time series of the measured and modeled velocity magnitude and direction at 20060323 DGD K	A69
Figure 302 - Time series of the measured and modeled velocity magnitude and direction at 20080311 DGD K	A70
Figure 303 - Time series of the measured and modeled velocity magnitude and direction at 20050217 Liefkenshoek	A70
Figure 304 - Time series of the measured and modeled velocity magnitude and direction at 20130625 Liefkenshoek	A71
Figure 305 - Time series of the measured and modeled velocity magnitude and direction at 20140514 Liefkenshoek	A71
Figure 306 - Time series of the measured and modeled velocity magnitude and direction at 20050218 Kallo	A72
Figure 307 - Time series of the measured and modeled velocity magnitude and direction at 20090529 Oosterweel.....	A72
Figure 308 - Time series of the measured and modeled velocity magnitude and direction at 20130627 Oosterweel.....	A73
Figure 309 - Time series of the measured and modeled velocity magnitude and direction at 20140516 Oosterweel.....	A73
Figure 310 - Time series of the measured and modeled velocity magnitude and direction at 20100414 Kruikeke.....	A74
Figure 311 - Time series of the measured and modeled velocity magnitude and direction at 20130530 Kruikeke.....	A74
Figure 312 - Time series of the measured and modeled velocity magnitude and direction at 20140702 Kruikeke.....	A75
Figure 313 - Time series of the measured and modeled velocity magnitude and direction at 20060323 Schelle.....	A75
Figure 314 - Time series of the measured and modeled velocity magnitude and direction at 20060928 Schelle.....	A76
Figure 315 - Time series of the measured and modeled velocity magnitude and direction at 20130213 Wintam.....	A76
Figure 316 - Time series of the measured and modeled velocity magnitude and direction at 20090610 Ballooi dwars	A77
Figure 317 - Time series of the measured and modeled velocity magnitude and direction at 20090610 Notelaer langs	A77
Figure 318 - Time series of the measured and modeled velocity magnitude and direction at 20130612 Driegoten	A78

Figure 319 - Time series of the measured and modeled velocity magnitude and direction at 20140617 Driegoten	A78
Figure 320 - Time series of the measured and modeled velocity magnitude and direction at 20110804 Branst	A79
Figure 321 - Time series of the measured and modeled velocity magnitude and direction at 20110218 Kramp ebb	A79
Figure 322 - Time series of the measured and modeled velocity magnitude and direction at 20110218 Kramp flood	A80
Figure 323 - Time series of the measured and modeled velocity magnitude and direction at 20140417 Dendermonde	A80
Figure 324 - Time series of the measured and modeled velocity magnitude and direction at 20110801 Appels downstream	A81
Figure 325 - Time series of the measured and modeled velocity magnitude and direction at 20130527 Schoonaarde	A81
Figure 326 - Time series of the measured and modeled velocity magnitude and direction at 20140703 Schoonaarde	A82
Figure 327 - Time series of the measured and modeled velocity magnitude and direction at 20140415 Schellebelle	A82
Figure 328 - Time series of the measured and modeled velocity magnitude and direction at 20100427 Boom	A83
Figure 329 - Time series of the measured and modeled velocity magnitude and direction at 20130529 Terhagen	A83
Figure 330 - Time series of the measured and modeled velocity magnitude and direction at 20140630 Terhagen	A84
Figure 331 - Example of the modeled and measured velocity magnitude and direction for one of the transects at Ossensisse (transverse profile)*	A85
Figure 332 - Example of the modeled and measured velocity magnitude and direction for one of the transects at Wintam*	A86
Figure 333 - Time series of the measured and modeled velocity magnitude and direction in the intertidal area at 20110706 R7 Terneuzen	A88
Figure 334 - Time series of the measured and modeled velocity magnitude and direction in the intertidal area at 20120508 R6 Middelgat	A89
Figure 335 - Time series of the measured and modeled velocity magnitude and direction in the intertidal area at 20120509 R6 GatVanOssensisse	A89
Figure 336 - Time series of the measured and modeled velocity magnitude and direction in the intertidal area at 20130424 R5 SchaarVanWaarde	A90
Figure 337 - Time series of the measured and modeled velocity magnitude and direction in the intertidal area at 20130425 R5 Zuidergat	A90
Figure 338 - Time series of the measured and modeled velocity magnitude and direction in the intertidal area at 20050217 Zandvliet	A91
Figure 339 - Time series of the measured and modeled velocity magnitude and direction in the intertidal area at 20060323 DGD K	A91
Figure 340 - Time series of the measured and modeled velocity magnitude and direction in the intertidal area at 20080311 DGD K	A92
Figure 341 - Time series of the measured and modeled velocity magnitude and direction in the intertidal area at 20050217 Liefkenshoek	A92

Figure 342 - Time series of the measured and modeled velocity magnitude and direction in the intertidal area at 20130625 Liefkenshoek	A93
Figure 343 - Time series of the measured and modeled velocity magnitude and direction in the intertidal area at 20140514 Liefkenshoek	A93
Figure 344 - Time series of the measured and modeled velocity magnitude and direction in the intertidal area at 20090529 Oosterweel	A94
Figure 345 - Time series of the measured and modeled velocity magnitude and direction in the intertidal area at 20100414 Kruibeke	A94
Figure 346 - Time series of the measured and modeled velocity magnitude and direction in the intertidal area at 20130530 Kruibeke	A95
Figure 347 - Time series of the measured and modeled velocity magnitude and direction in the intertidal area at 20140702 Kruibeke	A95
Figure 348 - Time series of the measured and modeled velocity magnitude and direction in the intertidal area at 20060323 Schelle.....	A96
Figure 349 - Time series of the measured and modeled velocity magnitude and direction in the intertidal area at 20060928 Schelle.....	A96
Figure 350 - Time series of the measured and modeled velocity magnitude and direction in the intertidal area at 20090610 Ballooi dwars	A97
Figure 351 - Time series of the measured and modeled velocity magnitude and direction in the intertidal area at 20130612 Driegoten	A97
Figure 352 - Time series of the measured and modeled velocity magnitude and direction in the intertidal area at 20140617 Driegoten	A98
Figure 353 - Time series of the measured and modeled velocity magnitude and direction in the intertidal area at 20140417 Dendermonde.....	A98
Figure 354 - Time series of the measured and modeled velocity magnitude and direction in the intertidal area at 20130527 Schoonaarde	A99
Figure 355 - Time series of the measured and modeled velocity magnitude and direction in the intertidal area at 20140703 Schoonaarde	A99
Figure 356 - Time series of the measured and modeled velocity magnitude and direction in the intertidal area at 20140415 Schellebelle	100
Figure 357 - Time series of the measured and modeled velocity magnitude and direction in the intertidal area at 20100427 Boom	A100
Figure 358 - Time series of the measured and modeled velocity magnitude and direction in the intertidal area at 20130529 Terhagen	A101
Figure 359 - Time series of the measured and modeled velocity magnitude and direction in the intertidal area at 20140630 Terhagen	A101
Figure 360 - Time series of the measured and modeled velocity magnitude and direction in the intertidal area at 20110902 Galgenschoor	A102
Figure 361 - Time series of the measured and modeled velocity magnitude and direction in the intertidal area at 20090610 Notelaer langs	A102
Figure 362 - Time series of the measured and modeled velocity magnitude and direction in the intertidal area at 20110804 Branst.....	A103
Figure 363 - Time series of the measured and modeled velocity magnitude and direction in the intertidal area at 20110801 Appels downstream	A103
Figure 364 - Calculated and measured discharges at R12 Wielingen	A106
Figure 365 - Calculated and measured discharges at R5 Schaar van Waarde	A106

Figure 366 - Calculated and measured discharges at Liefkenshoek.....	A107
Figure 367 - Calculated and measured discharges at Driegoten	A107
Figure 368 - Calculated and measured discharges at Schoonaarde	A108
Figure 369 - Measured and modeled velocities at Buoy 84 (bottom)	A109
Figure 370 - Measured and modeled velocities at Buoy 84 (top)	A109
Figure 371 - Measured and modeled velocities at Oosterweel (bottom)	A110
Figure 372 - Measured and modeled velocities at Oosterweel (top)	A110
Figure 373 - Measured and modeled velocities at Driegoten (real).....	A111
Figure 374 - Measured and modeled velocities at Driegoten (proxy1).....	A111
Figure 375 - Location of the measurement location Driegoten.....	A112
Figure 376 - Measured and modeled velocity at HPW_MP0311 (1.3 m above the bottom).....	A121
Figure 377 - Measured and modeled velocity at HPW_MP0311a (1.3 m above the bottom).....	A121
Figure 378 - Measured and modeled velocity at HPW_MP0311 (2.3 m above the bottom).....	A122
Figure 379 - Measured and modeled velocity at HPW_MP0311a (2.3 m above the bottom).....	A122
Figure 380 - Measured and modeled velocity at HPN_MP0310 (0.3 m above the bottom)	A123
Figure 381 - Measured and modeled velocity at HPN_MP0310a (0.3 m above the bottom)	A123
Figure 382 - Measured and modeled velocity at Paardenschor 0.05 m above the bottom (spring tide) ...	A124
Figure 383 - Measured and modeled velocity at Doel Kerncentrale 0.05 m above the bottom (spring tide)	A124
Figure 384 - Measured and modeled velocity at Lillo polder 0.05 m above the bottom (spring tide)	A125
Figure 385 - Measured and modeled velocity at Ballooi 0.05 m above the bottom (spring tide).....	A125
Figure 386 - Measured and modeled velocity at Notelaer 0.05 m above the bottom (spring tide)	A126
Figure 387 - Measured and modeled velocity at Branst 0.05 m above the bottom (spring tide)	A126
Figure 388 - Measured and modeled velocity at Plaat Driegoten 0.05 m above the bottom (spring tide).A127	
Figure 389 - Measured and modeled velocity at Dendermonde 0.05 m above the bottom (spring tide)...A127	
Figure 390 - Measured and modeled velocity at Nieuw schor van Appels 0.05 m above the bottom (average tide).....	A128
Figure 391 - Measured and modeled velocity at Brede Schooren 0.05 m above the bottom (spring tide).	A128
Figure 392 - Measured and modeled velocity at Bergenmeersen 0.05 m above the bottom (spring tide)	A129
Figure 393 - Measured and modeled velocity at Heusden 0.05 m above the bottom (spring tide)	A129
Figure 394 - Measured and modeled depth average velocity at Hooge Platen Noord MP0102 (average tide)	A130
Figure 395 - Measured and modeled velocity at Hooge Platen Noord MP0102 1.8 m above the bottom (spring tide).....	A130
Figure 396 - Measured and modeled depth average velocity at Hooge Platen Noord MP0206 (average tide)	A131
Figure 397 - Measured and modeled depth average velocity at Hooge Platen Noord MP0104 (spring tide)	A131
Figure 398 - Measured and modeled depth average velocity at Hooge Platen West MP0102 (spring tide)....	A132

Figure 399 - Measured and modeled velocity at Hooge Platen West MP0102 0.8 m above the bottom (spring tide).....	A132
Figure 400 - Measured and modeled depth average velocity at Hooge Platen West MP0310 (spring tide)	A133
Figure 401 - Measured and modeled depth average velocity at Hooge Platen West MP0312 (spring tide)	A133
Figure 402 - Measured and modeled depth average velocity at Plaat van Walsoorden MP0101 (neap tide)	A134
Figure 403 - Measured and modeled velocity at Plaat van Walsoorden MP0101 at 3.79 m above the bottom (average tide).....	A134
Figure 404 - Measured and modeled depth average velocity at Plaat van Walsoorden MP0309a (spring tide).....	A135
Figure 405 - Measured and modeled depth average velocity at Plaat van Walsoorden MP0518 (spring tide)	A135
Figure 406 - Measured and modeled salinity at Vlake van de Raan in Scaldis_039_2.....	A136
Figure 407 - Measured and modeled salinity at Overloop van Hansweert in Scaldis_039_2	A136
Figure 408 - Measured and modeled salinity at Baalhoek in Scaldis_039_2	A137
Figure 409 - Measured and modeled salinity at Prosperpolder in Scaldis_039_2	A137
Figure 410 - Measured and modeled salinity at Buoy 84 in Scaldis_039_2.....	A138
Figure 411 - Measured and modeled salinity at Liefkenshoek in Scaldis_039_2.....	A139
Figure 412 - Measured and modeled salinity at Oosterweel in Scaldis_039_2.....	A140
Figure 413 - Measured and modeled salinity at Hemiksem in Scaldis_039_2	A141
Figure 414 - Measured and modeled salinity at Driegoten in Scaldis_039_2	A141
Figure 415 - Measured and modeled salinity at Vlake van de Raan in Scaldis_028_2 and Scaldis_039_2	A142
Figure 416 - Measured and modeled salinity at Overloop van Hansweert in Scaldis_028_2 and Scaldis_039_2	A143
Figure 417 - Measured and modeled salinity at Baalhoek in Scaldis_028_2 and Scaldis_039_2	A144
Figure 418 - Measured and modeled salinity at Prosperpolder in Scaldis_028_2 and Scaldis_039_2.....	A145
Figure 419 - Measured and modeled salinity at buoy 84 'top' in Scaldis_028_2 and Scaldis_039_2 (measurement at top vs 2D model result)	A146
Figure 420 - Measured and modeled salinity at buoy 84 'bottom' in Scaldis_028_2 and Scaldis_039_2 (measurement at bottom vs 2D model result)	A147
Figure 421 - Measured and modeled salinity at Liefkenshoek in Scaldis_028_2 and Scaldis_039_2	A148
Figure 422 - Measured and modeled salinity at Oosterweel 'top' in Scaldis_028_2 and Scaldis_039_2 (measurement at top vs 2D model result)	A149
Figure 423 - Measured and modeled salinity at Oosterweel 'bottom' in Scaldis_028_2 and Scaldis_039_2 (measurement at bottom vs 2D model result)	A150
Figure 424 - Measured and modeled salinity at Hemiksem in Scaldis_028_2 and Scaldis_039_2	A151
Figure 425 - Measured and modeled salinity at Driegoten in Scaldis_028_2 and Scaldis_039_2	A152
Figure 426 - Bias of high water magnitude (model – measurement) during storm in the North sea and Western Scheldt	A180
Figure 427 - Bias of high water magnitude (model – measurement) during storm in the Eastern Scheldt	A180

Figure 428 - Bias of high water magnitude (model – measurement) during storm in the Lower Sea Scheldt	A181
Figure 429 - Bias of high water magnitude (model – measurement) during storm in the Upper Sea Scheldt	A181
Figure 430 - Bias of low water magnitude (model – measurement) during storm in the North sea and Western Scheldt	A182
Figure 431 - Bias of low water magnitude (model – measurement) during storm in the Eastern Scheldt	A182
Figure 432 - Bias of low water magnitude (model – measurement) during storm in the Lower Sea Scheldt	A183
Figure 433 - Bias of low water magnitude (model – measurement) during storm in the Upper Sea Scheldt	A183
Figure 434 - RMSE of high water magnitude (model vs. measurement) during storm in the North sea and Western Scheldt	A184
Figure 435 - RMSE of high water magnitude (model vs. measurement) during storm in the Eastern Scheldt	A184
Figure 436 - RMSE of high water magnitude (model vs. measurement) during storm in the Lower Sea Scheldt	A185
Figure 437 - RMSE of high water magnitude (model vs. measurement) during storm in the Upper Sea Scheldt	A185
Figure 438 - RMSE of low water magnitude (model vs. measurement) during storm in the North sea and Western Scheldt	A186
Figure 439 - RMSE of low water magnitude (model vs. measurement) during storm in the Eastern Scheldt	A186
Figure 440 - RMSE of low water magnitude (model vs. measurement) during storm in the Lower Sea Scheldt	A187
Figure 441 - RMSE of low water magnitude (model vs. measurement) during storm in the Upper Sea Scheldt	A187
Figure 442 - Bias of the water level time series during storm in the North sea and Western Scheldt	A188
Figure 443 - Bias of the water level time series during storm in the Eastern Scheldt	A188
Figure 444 - Bias of the water level time series during storm in the Lower Sea Scheldt	A189
Figure 445 - Bias of the water level time series during storm in the Upper Sea Scheldt	A189
Figure 446 - RMSE of the water level time series during storm in the North sea and Western Scheldt	A190
Figure 447 - RMSE of the water level time series during storm in the Eastern Scheldt	A190
Figure 448 - RMSE of the water level time series during storm in the Lower Sea Scheldt	A191
Figure 449 - RMSE of the water level time series during storm in the Upper Sea Scheldt	A191
Figure 450 - M2 amplitude during storm in the North sea and Western Scheldt	A192
Figure 451 - M2 amplitude during storm in the Eastern Scheldt	A192
Figure 452 - M2 amplitude during storm in the Lower Sea Scheldt	A193
Figure 453 - M2 amplitude during storm in the Upper Sea Scheldt	A193
Figure 454 - M2 phase during storm in the North sea and Western Scheldt	A194
Figure 455 - M2 phase during storm in the Eastern Scheldt	A194
Figure 456 - M2 phase during storm in the Lower Sea Scheldt	A195
Figure 457 - M2 phase during storm in the Upper Sea Scheldt	A195

Figure 458 - Calculated and measured water levels at Vlake van de Raan during storm.....	A196
Figure 459 - Calculated and measured water levels at Zeebrugge during storm.....	A196
Figure 460 - Calculated and measured water levels at Vlissingen during storm.....	A197
Figure 461 - Calculated and measured water levels at Oosterschelde 14 during storm.....	A197
Figure 462 - Calculated and measured water levels at Sluis Kats during storm.....	A198
Figure 463 - Calculated and measured water levels at Hansweert during storm.....	A198
Figure 464 - Calculated and measured water levels at Antwerpen during storm.....	A199
Figure 465 - Calculated and measured water levels at Schelle during storm.....	A199
Figure 466 - Calculated and measured water levels at Sint Amands during storm.....	A200
Figure 467 - Calculated and measured water levels at Schoonaarde during storm.....	A200
Figure 468 - Calculated and measured water levels at Melle during storm.....	A201
Figure 469 - Calculated and measured water levels at Boom during storm.....	A201
Figure 470 - Calculated and measured water levels at Bergenmeersen CRT.....	A202
Figure 471 - Calculated and measured water levels at Bergenmeersen (Scheldt).....	A202
Figure 472 - Calculated and measured water levels at Bergenmeersen CRT2 (Scheldt).....	A203
Figure 473 - Calculated and measured water levels at Polder van Lier 1.....	A203
Figure 474 - Calculated and measured water levels at Polder van Lier 2.....	A204
Figure 475 - Calculated and measured water levels at Polder van Lier 3.....	A204
Figure 476 - Calculated and measured water levels at Tielrode 1.....	A205
Figure 477 - Calculated and measured water levels at Tielrode 2.....	A205
Figure 478 - Calculated and measured water levels at Waasmunster 2.....	A206
Figure 479 - Calculated and measured water levels at Walem.....	A206
Figure 480 - Time series of the measured and modeled velocity magnitude and direction at 20080604 Everingen.....	A207
Figure 481 - Time series of the measured and modeled velocity magnitude and direction at 20080407 Ossenisse langsraai.....	A208
Figure 482 - Time series of the measured and modeled velocity magnitude and direction at 20060928 Waarde.....	A208
Figure 483 - Time series of the measured and modeled velocity magnitude and direction at 20100319 dwarsraaiD.....	A209
Figure 484 - Time series of the measured and modeled velocity magnitude and direction at 20060322 DGD K.....	A209
Figure 485 - Time series of the measured and modeled velocity magnitude and direction at 20060927 DGD K.....	A210
Figure 486 - Time series of the measured and modeled velocity magnitude and direction at 20060322 Liefkenshoek.....	A210
Figure 487 - Time series of the measured and modeled velocity magnitude and direction at 20100430 Liefkenshoek.....	A211
Figure 488 - Time series of the measured and modeled velocity magnitude and direction at 20100429 Oosterweel.....	A211
Figure 489 - Time series of the measured and modeled velocity magnitude and direction at 20090526 Kruibeke.....	A212

Figure 490 - Time series of the measured and modeled velocity magnitude and direction at 20050217 Schelle	A212
Figure 491 - Time series of the measured and modeled velocity magnitude and direction at 20090611 Notelaer dwars.....	A213
Figure 492 - Time series of the measured and modeled velocity magnitude and direction at 20100415 Driegoten	A213
Figure 493 - Time series of the measured and modeled velocity magnitude and direction at 20110805 Branst	A214
Figure 494 - Time series of the measured and modeled velocity magnitude and direction at 20110801 Appels upstream.....	A214
Figure 495 - Time series of the measured and modeled velocity magnitude and direction at 20100414 Schoonaarde	A215
Figure 496 - Time series of the measured and modeled velocity magnitude and direction at 20090622 Boom	A215
Figure 497 - Definition of straight and oblique setup (after <i>Adema</i> , 2006).	A217

1 Introduction

In the framework of the projects 'Integrated plan for the Upper Sea Scheldt' and 'Agenda for the Future', it was necessary to develop a hydrodynamics and sediment transport model that covers the entire tidally influenced zone of the Scheldt Estuary and the mouth area, and that has sufficient resolution in the upstream part.

Existing models lack a high resolution in the Upper Sea Scheldt, Durme, Rupel and Nete. For this reason, the SCALDIS model, a new unstructured high resolution model of the (tidal) Scheldt Estuary is developed in TELEMAC 3D for the entire estuary, but with special attention to the upstream parts. The use of an unstructured grid allows to combine a large model extent with a high resolution upstream. The calibrated model will be used to analyse the effects of several scenarios (different morphology of the Scheldt with different ranges of boundary conditions).

This report describes the model development, calibration and validation of the hydrodynamics. The model is calibrated for one spring-neap tidal cycle in 2013 against field data: water levels, velocities (in deep and shallow zones) and discharges.

2 Units and reference plane

Time is expressed in CET (Central European Time).

Depth, height and water levels are expressed in meter TAW (Tweede Algemene Waterpassing).

Bathymetry and water levels are positive above the reference plane.

The horizontal coordinate system is RD Parijs.

3 List of abbreviations

ADCP	Acoustic Doppler Current Profiler
CET	Central European Time
CRT	Controlled Reduced Tide
DHM	Digital Height Model
FCA	Flood Control Areas
HIC	Hydrological Information Centre
HMCZ	Hydro Meteo Centrum Zeeland
INBO	Instituut voor Natuur-en Bosonderzoek (Institute for Nature and Forest Research)
LAT	Lowest Astronomical Tide
MAE	Mean Absolute Error
NAP	Normaal Amsterdams Peil (Normal Amsterdam Level)
PSU	Practical Salinity Unit
RMAE	Relative Mean Absolute Error
RMSE	Root Mean Square Error
TAW	Tweede Algemene Waterpassing (Second General Level)
UTC	Coordinated Universal Time
WGS84	World Geodetic System 1984

4 Available measurement data

4.1. Water levels

Water level measurements for the year 2013 are available from different sources. Table 1 shows the list of the stations for which validated measured water levels are available for the simulation period (described in chapter 5.9). Figure 198 shows the location of the measurement stations.

10 minute interval time series of the water level measurements (m NAP, CET) were retrieved from the Hydro Meteo Centrum Zeeland database (HMCZ, www.hmcz.nl) for the stations located in the Netherlands and some Belgian stations. Measured water levels for the coastal Belgian stations were available from the Meetnet Vlaamse banken (www.kustdata.be) for Zeebrugge, Oostende and Nieuwpoort. For other Belgian coastal stations the data were received from the Afdeling Kust. For the Belgian stations in the Sea Scheldt and Rupel the data (m TAW, UTC) were available from Hydrologisch Informatie Centrum (HIC).

Table 1. Water level stations

	Station	Data source
North Sea		
1	MP0 Wandelaar	Afdeling Kust
2	MP1 A2B boei	
3	MP2 Appelzak	
4	MP3 Bol van Heist	
5	MP4 Scheur Wielingen	
6	MP6 Radar toren	
7	Nieuwpoort	www.kustdata.be
8	Oostende	
9	Zeebrugge	
10	Vlakte van de Raan	HMCZ
Western Scheldt		
11	Westkapelle	HMCZ
12	Cadzand	
13	Vlissingen	
14	Breskens	
15	Borssele	
16	Terneuzen	
17	Overloop van Hansweert	
18	Hansweert	
19	Walsoorden	
20	Baalhoek	
21	Schaar van de Noord	
22	Bath	
Eastern Scheldt		
23	Oosterschelde 4	HMCZ
24	Oosterschelde 11	
25	Oosterschelde 14	
26	Roompot buiten	
27	Roompot binnnen	
28	Sluis Kats	

29	Krammersluis	
30	Stavenisse	
31	Yerseke	
32	Bergsediepsluis	
33	Marollegat	
Sea Scheldt		
34	Zandvliet	HIC
35	Prosperpolder	HMCZ, HIC
36	Liefkenshoek	
37	Kallo lock	
38	Antwerp	
39	Hemiksem	HIC
40	Schelle	
41	Temse	
42	Tielrode	
43	Sint Amands	
44	Dendermonde	
45	Schoonaarde	
46	Wetteren	
47	Melle	
Rupel and tributaries		
48	Boom	HIC
49	Walem	
50	Duffel	
51	Lier Molbrug	
52	Lier Maasfort	
53	Emblem	
54	Kessel	
55	Mechelen lock	
56	Hombeek	
Durme		
57	Waasmunster	HIC

During the Sinterklaas storm (Xaver) of 5 and 6 December 2013 water levels were measured in some Flood Control Areas (FCA) and Controlled Reduced Tide (CRT) systems in the Scheldt estuary (Table 2). The location of the available measurements is shown in Figure 199 to Figure 204.

Table 2. Water level measurements during the Sinterklaasstorm

	Station name
1	Bergenmeersen CRT
2	Bergenmeersen CRT2
3	Bergenmeersen Scheldt
4	Polder van Lier 1
5	Polder van Lier 2
6	Polder van Lier 3
7	Tielrode 1 Sluis
8	Tielrode 2
9	Waasmunster 2
10	Walem

4.2. Velocities

4.2.1. Sailed ADCP measurements

Available ADCP measurements located in the model domain are described in Table 3. Figure 205 to Figure 207 show the location of the ADCP transects.

A tidal coefficient is calculated as a ratio of the tidal amplitude during the analyzed period to the amplitude of the average tide for the period from 1991 to 2000. The amplitude of the average tide for this period is given in the tidal tables provided by Coastal department, Flemish Hydrography. More information about the tidal coefficients k is given in Appendix 4.

Table 3. Available ADCP measurements

Location	Date and time (MET)	Tide (k coefficient)	Project	Used for (C: calibration; V: validation)
Western Scheldt				
R7 Everingen	04/06/2008 5:58 – 19:01	1.16 (spring)	MONEOS	V
R7 Everingen	05/07/2011 5:05 – 17:55	1.12 (spring)	MONEOS	C
R7 Terneuzen	06/07/2011 5:34 – 18:14	1.09 (spring)	MONEOS	C
R6 Middelgat	08/05/2012 05:58 – 18:55	1.23 (spring)	MONEOS	C
R6 Gat van Ossensisse	09/05/2012 04:57 – 17:50	1.17 (spring)	MONEOS	C
Ossensisse (dwarsraai)	07/04/2008 13:01 – 17:17	1.22 (spring)	753_07_Ossensisse 2008	C
Ossensisse (langsraai)	07/04/2008 12:52 – 17:04	1.22 (spring)	753_07_Ossensisse 2008	V
Waarde	23/03/2006 9:07 – 20:55	0.83 (neap)	HCBS IMDC 2006 March	C
Waarde	28/09/2006 6:52 – 19:53	0.97 (average)	HCBS IMDC 2006 September	V
R5 Schaar van Waarde	24/04/2013 05:35 – 18:28	1.09 (spring)	MONEOS	C
R5 Zuidergat	25/04/2013 06:18 – 19:12	1.14 (spring)	MONEOS	C

Lower Sea Scheldt				
Schaar van Ouden Doel	12/09/2006 07:03 – 19:00	1.10 (spring)	GGG Doelpolder	C
Zandvliet	17/02/2005 05:23 – 17:32	0.86 (neap)	HCBS IMDC 2005	C
Galgenschoor	02/09/2011 07:17 – 19:58	1.15 (spring)	00_028 Habitatmapping	V
Langsraai O	18/03/2010 13:08 – 19:45	1.10 (spring)	837 Mona Lisa	C
Dwarsraai D	19/03/2010 07:25 – 19:49	1.13 (spring)	837 Mona Lisa	V
DGD (K raai)	11/03/2008 07:07 – 19:41	1.15 (spring)	596_04 LDM DGD	C
DGD (K raai)	27/09/2006 06:16 – 19:04	1.01 (average)	HCBS IMDC 2006 September	V
DGD (K raai)	22/03/2006 08:42 – 21:03	0.90 (neap)	HCBS IMDC 2006 March	V
DGD (K raai)	23/03/2006 09:09 – 22:01	0.83 (neap)	HCBS IMDC 2006 March	C
Liefkenshoek	17/02/2005 04:32 – 17:36	0.86 (neap)	HCBS IMDC 2005	C
Liefkenshoek	22/03/2006 08:31 – 20:59	0.90 (neap)	HCBS IMDC 2006 March	V
Liefkenshoek	30/04/2010 04:54 – 17:57	1.15 (spring)	MONEOS	V
Liefkenshoek	25/06/2013 06:26 – 19:18	1.18 (spring)	MONEOS	C
Liefkenshoek	14/05/2014 07:33 – 19:25	1.15 (spring)	MONEOS	C
Kallo	18/02/2005 06:03 – 18:13	0.73 (neap)	HCBS IMDC 2005	C
Oosterweel	29/05/2009 07:37 – 20:29	1.05 (average)	MONEOS	C
Oosterweel	29/04/2010 05:07 – 17:50	1.20 (spring)	MONEOS	V
Oosterweel	27/06/2013 06:24 – 19:06	1.11 (spring)	MONEOS	C
Oosterweel	16/05/2014 06:49 – 19:44	1.17 (spring)	MONEOS	C
Kruikeke	26/05/2009 05:27 – 18:19	1.14 (spring)	MONEOS	V
Kruikeke	14/04/2010 04:40 – 17:20	1.13 (spring)	MONEOS	C

Kruibeke	30/05/2013 06:10 – 19:06	1.05 (average)	MONEOS	C
Kruibeke	02/07/2014 08:03 – 20:01	1.00 (average)	MONEOS	C
Schelle	17/02/2005 05:25 – 12:28	0.86 (neap)	HCBS IMDC 2005	V
Schelle	23/03/2006 08:55 – 21:45	0.83 (neap)	HCBS IMDC 2006 March	C
Schelle	28/09/2006 06:34 – 19:32	0.97 (average)	HCBS IMDC 2006 Sept	C
Upper Sea Scheldt				
Wintam	13/02/2013 07:25 – 20:39	1.21 (spring)	12_101 Stroomatlas Wintam	C
Ballooi (dwars)	10/06/2009 06:42 – 19:22	1.02 (average)	713_21 Notelaer and Ballooi	C
Notelaer (dwars)	11/06/2009 07:15 – 19:53	0.99 (average)	713_21 Notelaer and Ballooi	V
Notelaer (langs)	10/06/2009 07:00 – 19:42	1.02 (average)	713_21 Notelaer and Ballooi	C
Driegoten	15/04/2010 05:33 – 18:27	1.14 (spring)	MONEOS	V
Driegoten	12/06/2013 06:52 – 19:15	1.02 (average)	MONEOS	C
Driegoten	17/06/2014 06:28 – 19:31	1.12 (spring)	MONEOS	C
Branst1 (right bank)	04/08/2011 08:46 – 19:47	1.13 (spring)	00_028 Habitatmapping	C
Branst2 (left bank)	05/08/2011 07:19 – 20:17	1.07 (spring)	00_028 Habitatmapping	V
Kramp	18/02/2011 7:47 – 11:55 (ebb) 18/02/2011 14:30 – 17:42 (flood)	1.18 (spring)	753_15 Kramp	C
Dendermonde	17/04/2014 07:31 – 19:51	1.17 (spring)	13_131 Integraal plan	C
Appels	01/08/2011 07:12 – 19:12 (downstream) 01/08/2011 07:03 – 18:02 (upstream)	1.14 (spring)	00_028 Habitatmapping	C V
Schoonaarde	14/04/2010 06:43 – 19:00	1.12 (spring)	MONEOS	V

Schoonaarde	27/05/2013 08:17 – 20:05	1.17 (spring)	MONEOS	C
Schoonaarde	03/07/2014 08:17 – 20:55	0.95 (average)	MONEOS	C
Schellebelle	15/04/2014 07:28 – 19:32	1.15 (spring)	13_131 Integraal plan	C
Rupel				
Boom	22/06/2009 06:58 – 19:44	1.09 (spring)	MONEOS	V
Boom	27/04/2010 08:52 – 18:50	1.16 (spring)	MONEOS	C
Terhagen	29/05/2013 07:11 – 19:34	1.10 (spring)	MONEOS	C
Terhagen	30/06/2014 07:44 – 20:19	1.03 (average)	MONEOS	C

4.2.2. Stationary velocity measurements in deep areas

Stationary velocity measurements from 2013 are available in three locations in deep zones (Table 4, Figure 208).

Table 4. Stationary velocity measurements in deep areas

Location	Height
Buoy 84 top	3.3 m above the bottom
Buoy 84 bottom	0.8 m above the bottom
Oosterweel top	4.5 m above the bottom
Oosterweel bottom	1 m above the bottom
Driegoten	3 m below the water surface

4.2.3. Stationary velocity measurements in shallow areas

Stationary velocity measurements used for the model calibration are described in Table 5. The location of the measurements is shown in Figure 209 to Figure 211.

Table 5. Stationary velocity measurements in shallow areas

Location	Available from	Date
Hooge Platen West	HMCZ	08 – 09/2013
Hooge Platen Noord		03 - 04/2013
Plaat van Walsoorden		11 - 12/2013
Paardenschor	INBO	17 – 21/01/2014
Doel kerncentrale		16 – 20/02/2014
Lillo polder		17 – 21/03/2014
Ballooi		12 – 13/06/2013 14 – 18/04/2014
Notelaer		14 – 18/05/2014
Branst		19 – 23/09/2013
Plaat Driegoten		18 – 22/10/2013
Nieuw schor van Appels		15 – 19/12/2013
Dendermonde		11 – 16/07/2014
Bergenmeersen		27/06 – 01/07/2014
Brede Schoore		13 – 17/06/2014
Heusden		11 – 14/08/2014
Weert	FHR	22/01 – 19/02/2014

The velocity measurements provided by INBO are 1 second time series. They were averaged to get 1 minute data of velocities. Then 10 minute time series were generated by selecting every 10th value. As a result some peak velocities present in the original 1 second time series were lost (Figure 1).

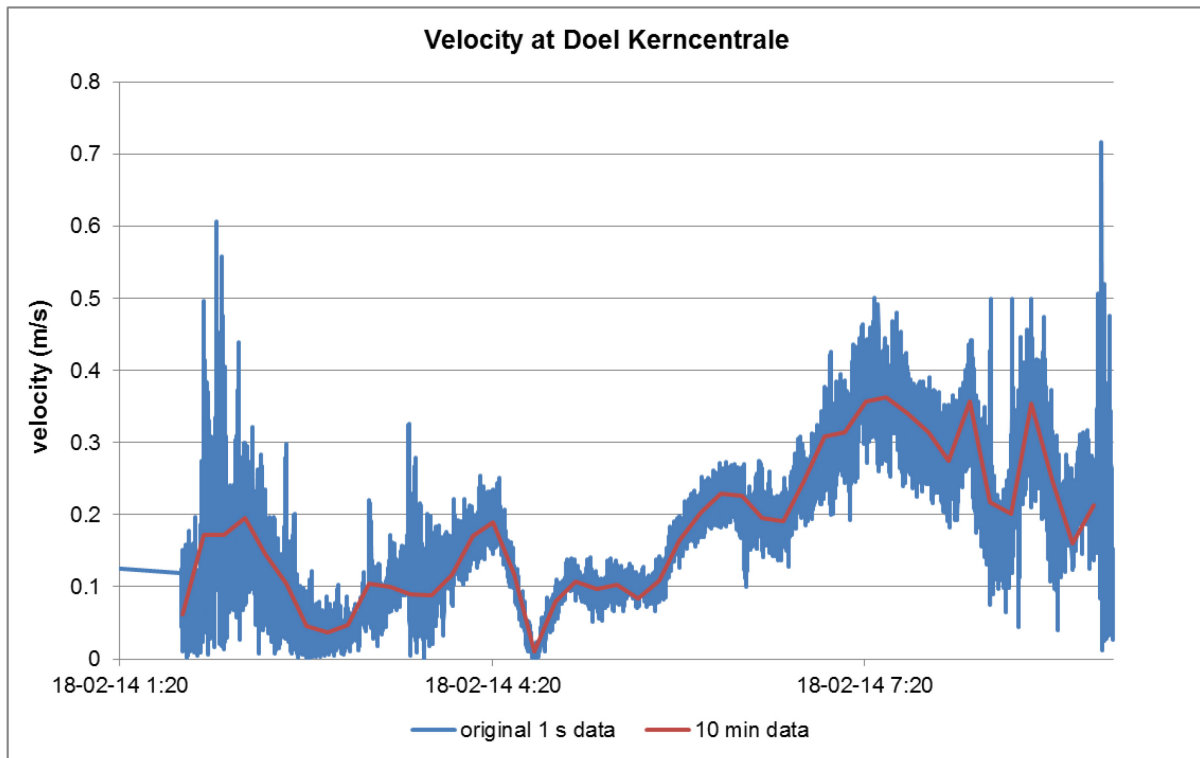


Figure 1 - Measured velocity at Doel

4.3. Discharges

Table 6 gives an overview of the discharge measurements that can be used for the model calibration. The location of the cross sections in the Western Scheldt is presented in Figure 211. The location of the cross sections in the Sea Scheldt and Rupel is shown in Figure 205 and Figure 206.

Table 6. Available discharge measurements

Name of cross section	Date
Western Scheldt	
R1 Vaarwater boven Bath	25/10/2006; 30/03/2010
R1 Ballastplaat	01/04/2010
R2 Nauw van Bath	28/10/2004
R2 Schaar van de Noord	28/10/2004
R2 Total	11/04/2012
R3 Overloop van Valkenisse	14/08/2007
R3 Zimmermangeul	15/08/2007
R5 Schaar van Waarde	01/12/2005
R5 Zuidergat	30/11/2005
R6 Gat van Ossenisse	13/10/2004
R6 Middelgat	13/10/2004
R7 Everingen	04/06/2008
R7 Pas van Terneuzen	05/06/2008
R9 Honte Schaar van Spijkerplaat	12/09/2006
R9 Vaarwater langs Hoofdplaat	13/09/2006
R10 Honte Schaar van Spijkerplaat	10/10/2007
R10 Vaarwater langs Hoofdplaat	11/10/2007
R11 Sardijngeul	16/05/2006
R11 Wielingen	17/05/2006
R12 Deurloo	03/07/2007
R12 Oostgat	18/06/2007
R12 Wielingen	19/06/2007
Lower Sea Scheldt	
Liefkenshoek	27/05/2009 30/04/2010 25/06/2013
Oosterweel	29/05/2009 29/04/2010

	27/06/2013
Kruikeke	26/05/2009 14/04/2010 30/05/2013
Upper Sea Scheldt	
Driegoten	23/06/2009 15/04/2010 12/06/2013
Schoonaarde	25/06/2009 14/04/2010 27/05/2013
Rupel	
Boom	22/06/2009 27/04/2010
Terhagen	29/05/2013

4.4. Wind data

Wind is acting upon the coastal zone area only. A time series measured at Vlakte van de Raan is used for the X and Y directions (Figure 2, Figure 3).

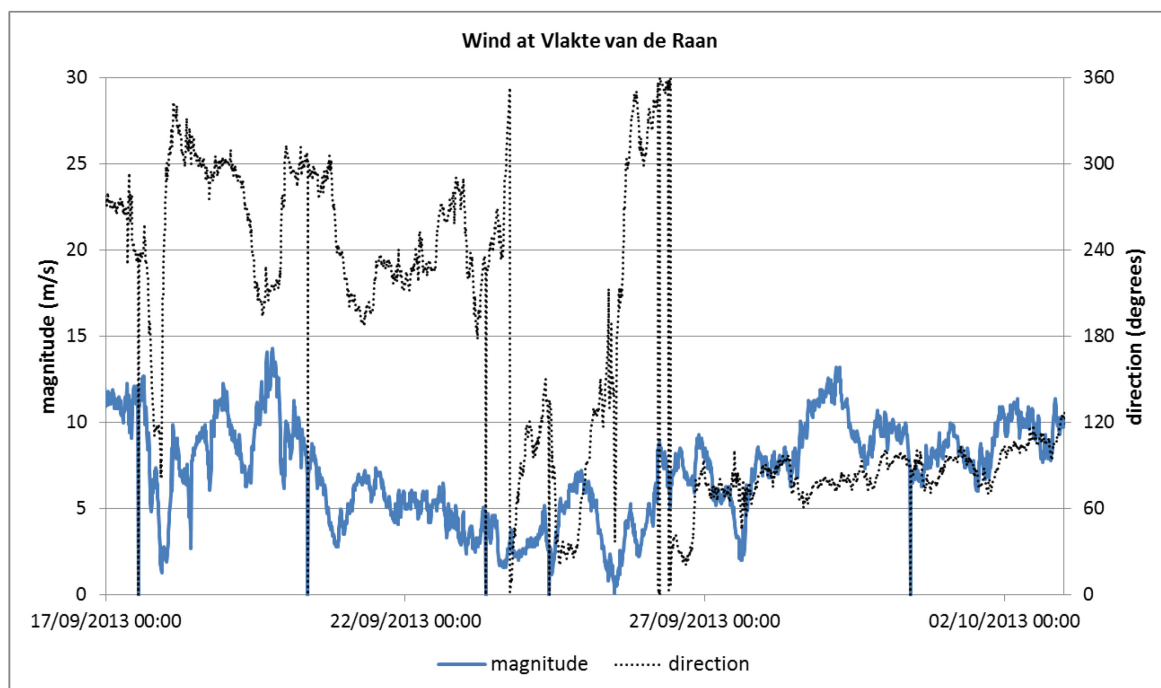


Figure 2 - Wind at Vlakte van de Raan during the calibration period

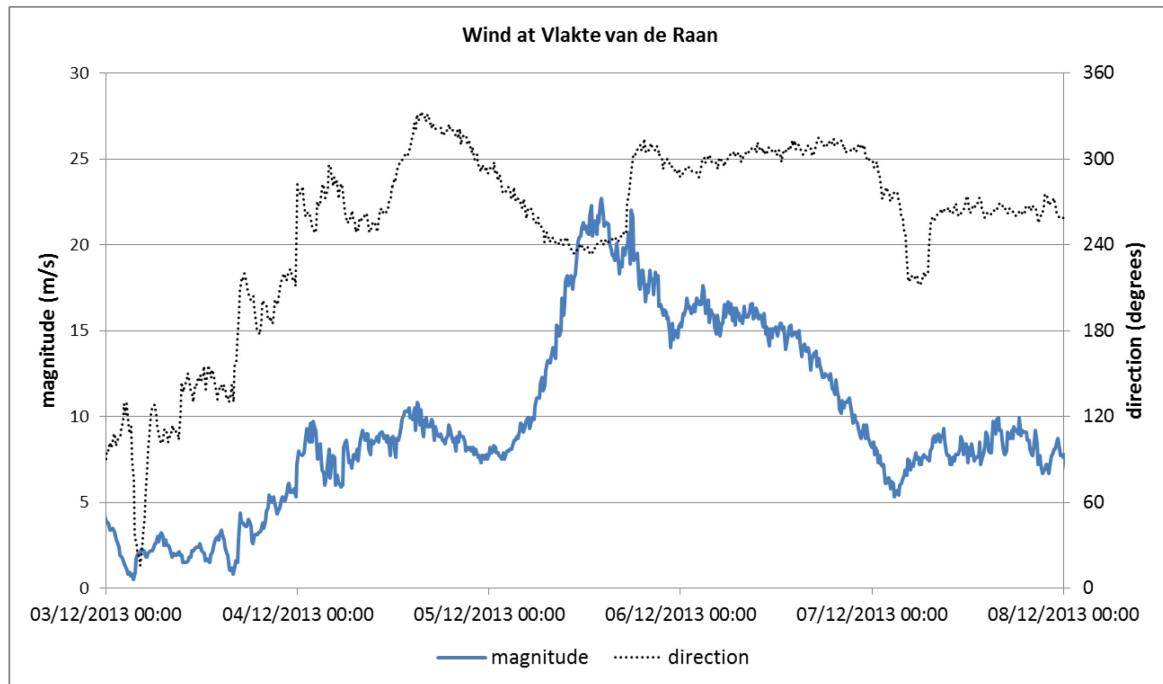


Figure 3 - Wind at Vlakte van de Raan during the Sinterklaas storm

4.5. Salinity

Salinity data are available in the Western Scheldt from HMCZ and in the Sea Scheldt from HIC (Table 7). The location of salinity measurements is shown in Figure 212.

Salinity used in this project for the Sea Scheldt (in psu) is calculated by HIC based on the conductivity and temperature (converted with the UNESCO formule) (*De Boeck et al.*, 2014). The calculation of the salinity for the Western Scheldt is done by HMCZ with the same formule.

Table 7. Available salinity measurements

	Station	Data source
Western Scheldt		
1	Vlakte van de Raan	HMCZ
2	Hoofdplaat (no data in 2013)	
3	Overloop van Hansweert	
4	Baalhoek	
Sea Scheldt		
5	Prosperpolder	HIC
6	Buoy 84 (top and bottom)	
7	Liefkenshoek	
8	Oosterweel (top and bottom)	
9	Hemiksem	
10	Driegoten	

5 The numerical model

5.1. Software

The model for this project is developed in the TELEMAC software V6P3, which is based on the finite element method. The model domain is discretised into an unstructured grid of triangular elements and it can be locally refined in the study area. Therefore, the complex geometry of the study area can be taken into account. Parallel computing is used to decrease the computational time.

5.2. Model grid

5.2.1. Grid dimensions

The computational grid inside the estuary is constrained by the dikes along the estuary. For the coastal zone it was crucial for future scenario computations that the mouth area of the Scheldt estuary was included. For possible future scenarios of morphological changes along the Belgian coastline the entire Belgian coastline was included in the model. The boundaries of the model in the coastal zone were placed at a certain distance from the Belgian coastal zone in order not to have an influence on flow around possible future morphological changes. We don't want the morphological changes to influence the model's boundaries too much. The distance that the boundaries of the model need to have from potential morphological changes is calculated using the potential flow around a cylinder. We approximate the effect of a morphological change on the flow pattern by the potential flow around a cylinder as shown in Figure 4. The theory about potential flow is explained in more detail in Janna (2010). We assume a two dimensional, incompressible, nonviscous fluid.

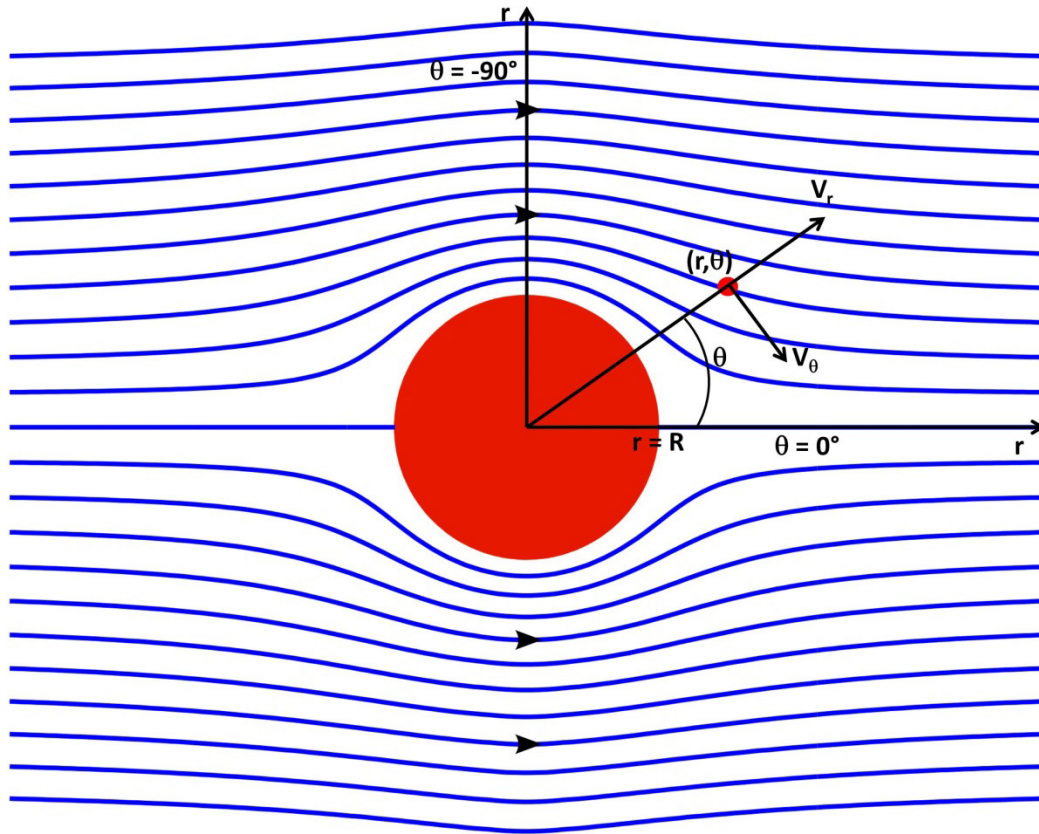


Figure 4 - Potential flow around a cylinder

Potential flow around a circle: theory

The velocity potential ϕ is function of x and y and is defined in terms of flow velocities as:

$$V_x = \frac{\partial \phi}{\partial x} \quad \text{and} \quad V_y = \frac{\partial \phi}{\partial y}$$

The continuity equation is given by:

$$\frac{\partial V_x}{\partial x} + \frac{\partial V_y}{\partial y} = 0$$

Combining the two equations above gives:

$$\frac{\partial}{\partial x} \left(\frac{\partial \phi}{\partial x} \right) + \frac{\partial}{\partial y} \left(\frac{\partial \phi}{\partial y} \right) = 0 \quad \text{or} \quad \frac{\partial^2 \phi}{\partial x^2} + \frac{\partial^2 \phi}{\partial y^2} = 0 \quad \text{or} \quad \nabla^2 \phi = 0$$

Replacing the cartesian coordinates with polar coordinates ($x = r \cos \theta$ and $y = r \sin \theta$) gives the following equation:

$$\frac{1}{r} \frac{\partial}{\partial r} \left(r \frac{\partial \phi}{\partial r} \right) + \frac{1}{r^2} \frac{\partial^2 \phi}{\partial \theta^2} = 0$$

where r is the distance from the middle of the cylinder and θ is the angle with the X-axis (θ is positive in clockwise direction).

The solution for this equation, i.e. the velocity potential (ϕ), for a cylinder with radius R in two dimensions is then given by (Janna, 2010):

$$\phi(r, \theta) = U \left(r + \frac{R^2}{r} \right) \cos \theta$$

where U is the flow without the cylinder (solution of the Laplace equation).

The velocity components in polar coordinates are:

$$V_r = \frac{\partial \varphi}{\partial r} = U \left(1 - \frac{R^2}{r^2}\right) \cos \theta$$

$$V_\theta = \frac{1}{r} \frac{\partial \varphi}{\partial \theta} = -U \left(1 + \frac{R^2}{r^2}\right) \sin \theta$$

For $\theta = 0$ this gives:

$$V_r = U \left(1 - \frac{R^2}{r^2}\right), \quad V_\theta = 0$$

and for $\theta = -90^\circ$ (θ is positive in clockwise direction):

$$V_r = 0, \quad V_\theta = U \left(1 + \frac{R^2}{r^2}\right)$$

Longshore current

Let's assume we want a maximum difference in flow velocity (between a simulation with and without a morphological change in the coastal zone) at our model boundary of 0.01 m/s (Δ). We assume a longshore flow with maximal amplitude of $U = 1$ m/s.

We suppose that our coastline direction is equal to $\theta = 0^\circ$. We want to know at which distance, r , from the morphological change, the difference in flow velocity is equal or less than 0.01 m/s and this in the direction along the shore ($\theta = 0^\circ$) and perpendicular ($\theta = -90^\circ$) to the shore. We want to find a relation between the size of the morphological change ($= R$, half the diameter of the circular morphological change) and the distance r at which the difference in flow velocity will be equal or less than 0.01 m/s.

For the flow velocity along the shore ($\theta = 0^\circ$) we can calculate the difference as follows and extract r in function of R :

$$\Delta = U - U \left(1 - \frac{R^2}{r^2}\right) \xrightarrow{\text{yields}} r = \frac{R}{\sqrt{\Delta/U}}$$

$$r = R / \sqrt{\frac{0.01 \text{ m/s}}{1 \text{ m/s}}} = 10R$$

For the flow velocity along the shore but at a distance r perpendicular to the shore ($\theta = -90^\circ$) we can calculate the difference as follows and extract r in function of R :

$$\Delta = U - U \left(1 - \frac{R^2}{r^2}\right) \xrightarrow{\text{yields}} r = \frac{R}{\sqrt{\Delta/U}}$$

$$r = R / \sqrt{\frac{0.01 \text{ m/s}}{1 \text{ m/s}}} = 10R$$

This gives exactly the same relationship between r and R , which is to be expected from a potential flow around a cylinder. We can do the same for the offshore current.

Offshore current

For the offshore current the direction of the flow as seen in Figure 4 will change and will flow in the direction of $\theta = -90^\circ$. Since both extremes ($\theta = -90^\circ$ and $\theta = 0^\circ$) give the same relationship between r and R and if we assume a maximal offshore current of 0.2 m/s we get the following relationship:

$$\Delta = U - U \left(1 + \frac{R^2}{r^2}\right) \xrightarrow{\text{yields}} r = \frac{R}{\sqrt{-\Delta/U}}$$

$$r = R / \sqrt{\frac{0.01 \text{ m/s}}{0.2 \text{ m/s}}} = 4.47R$$

for both $\theta = -90^\circ$ and $\theta = 0^\circ$.

A smaller current offshore will lead to a smaller distance of influence of the morphological change. For the boundaries of the model we will continue with the $r = 10 R$ relationship.

If we choose 3 km as the radius R of the maximum change (comparable with the size of the port of Zeebrugge) then it means that we should stay about 30 km away from the interest area along the coast and 30 km away offshore. The real flow will be different from a potential flow as friction will lower the affected area. Therefore we will take these distances (= 30 km) from the Belgian shoreline.

Tidal Excursion Length

For the sediment transport model we want to stay 4 'Tidal Excursion Lengths' or TEL from the area of interest. 1 TEL is the distance that a suspended particle can travel in a certain direction during one tidal ellipse. This is the maximum distance a particle travels within one cycle and not the integrated distance over one tidal cycle. The distance a particle in suspension can travel is divided in a long shore component and a component perpendicular on the coast. The measured velocities are therefore projected in a counterclockwise rotating coordinate system which is turned 30° counterclockwise to mimic the position of the Belgian coastline (Figure 5). This exercise was done in a previous project for the port of Zeebrugge and is described in *Leyssen et al.* (2012). The analysis was based on four BMM tripod measurement campaigns of 2009. The X component of the flow velocity in the projected coordinate system proved to be approximately 3 orders larger than the Y component.

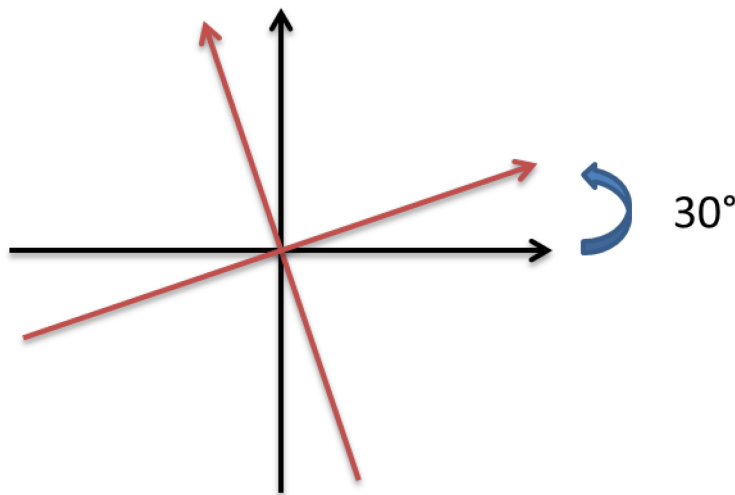


Figure 5 - Original (black) and projected (red) coordinate system

A harmonic analysis of the X and Y components is performed by the harmonic analysis software *t_tide* (*Pawlowicz et al.*, 2002). The maximal M2 amplitude is used as estimator of the tidal excursion length. The integral of the velocity over half a tidal period gives the M2 tidal excursion:

$$Tidal\ excursion = \int_0^{T/2} A * \sin\left(\frac{2\pi}{T}t\right)dt = A * \frac{T}{2\pi} \left[-\cos\left(\frac{2\pi}{T}t\right)\right]_0^{T/2}$$

With $A=0.55\text{m/s}$ and $T=12.42\text{h}$ this results in a M2 tidal extrusion length of 7.9km in the along shore direction and 2.4km in the offshore direction (Figure 6). Four times these distances means that we should keep the model boundary 32 km away from the area of interest, in our case the Belgian coastal zone, along the coast line and 10 km offshore.



Figure 6 - Tidal excursion length based on the M2 component near the port of Zeebrugge

Keeping in mind the above recommendations for the coastal zone, The TELEMAC model developed in the framework of this project covers a large part of the North Sea (from Duinkerke in France to Goeree in the Netherlands, and the entire Scheldt estuary (until the tidal border), including Eastern Scheldt. Further, the flood control areas (FCA's) with or without a controlled reduced tide (CRT) are included in the model grid as they are important for the storm scenarios. The model domain is shown in Figure 10. The model covers an area in the coastal zone of 150 km along the coastline, reaching almost Calais (France) in the southwest and Renesse (The Netherlands) in the Northeast. It stretches 30 km offshore. The Eastern Scheldt is also included. The ports of Nieuwpoort, Oostende, Blankenberge and Zeebrugge are present in the model. The grid covers a total area of 5.321.127.607 m² of which 4.540.149.969 m² is coastal zone, i.e. the area outside the Eastern Scheldt barrier and outside the Vlissingen-Breskens transect. An overview of the Sigmaplan areas is given in Table 8.

5.2.2. Vertical Schematisation

The model grid consists of 459,692 nodes in 2D mesh and 873,419 elements. The 3D mesh consists of prisms eventually cut into tetrahedrons and is automatically constructed from the 2D mesh. This construction is done in the subroutine CALCOT based on the information given by the user in subroutine CONDIM. The keyword NUMBER OF HORIZONTAL LEVELS, of which the default value is two, will define the number of stacked prisms = # levels - 1. TELEMAC-3D uses a change of variables in order to freeze the mesh on a time step. Without such a change, the mesh dimensions z vary in accordance with the free surface evolution. In the Scaldis model the method of change of variables is the sigma transformation which consists in shifting from the $z(x,y,t)$ co-ordinate to the $z^*(x,y)$ co-ordinate. The user should enter the z^* co-ordinates in the CONDIM subroutine. The normalized co-ordinates will then range from 0 (the bottom) to 1 (the surface). In the Scaldis model we use 5 levels (and thus 4 stacked prisms) with the following z^* values (specified in the CONDIM subroutine):

```
ZSTAR%R(1)=0.D0
ZSTAR%R(2)=0.12D0
ZSTAR%R(3)=0.30D0
ZSTAR%R(4)=0.60D0
ZSTAR%R(5)=1.D0
```

With these 5 levels our Scaldis 3D model has 2,298,460 nodes in total. These 5 levels and their z^* distribution is shown in Figure 7. Increased number of levels did not add extra information to the model. For sensitivity of the number of layers on the model results, we refer to section 7.4.

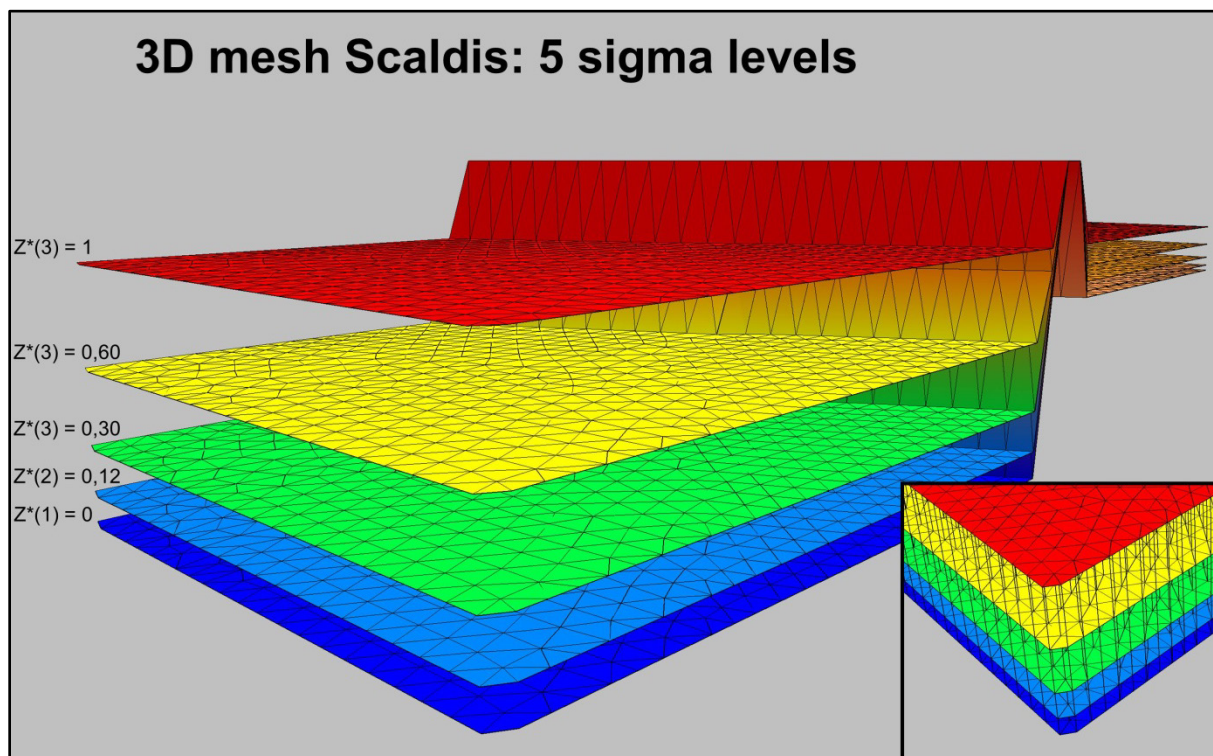


Figure 7 - Representations of the 5 sigma levels in Scaldis and their z^* distribution.
Small insert in right bottom corner: connection of the levels to form stacked prisms.

The horizontal resolution varies from 500 m to 3 m. In the coastal area the resolution varies from 500 to 200 m depending on the depth. The resolution in the Eastern Scheldt is 200 m. In the Western Scheldt the resolution is 120 m. In the Sea Scheldt this resolution is increasing slowly towards 30m near Antwerp, further increasing towards 8 m in the Upper Sea Scheldt. In the upstream tributaries the resolution can reach 3m. In upstream tributaries the mesh is sometimes stretched along the channel axis. Triangles can be stretched in this direction if the flow in this section is considered in the along channel direction. In these small tributaries, where otherwise the mesh resolution needed to be very high to accurately represent the local bathymetry, the technique reduces the number of grid nodes, and thus calculation time. For the flood control areas the overflow dike needs to be very accurate in the model. The areas themselves don't need a high resolution because only the storage function of an FCA, and not its internal hydrodynamics, is important for the hydrodynamics in the river. Trying to represent all creeks and ditches of a FCA would also make this model too big and no longer practically manageable. The mesh resolution for these areas was set between 50 and 80 m.

5.2.3. The grid and the sigmaplan areas

All flood control areas (that are currently active, planned or decided) have to be included in the Scaldis model. A shapefile with the Sigma contour lines (version april 2015) was used. Areas assigned as wetlands are not included in the Scaldis model as they lay outside the Sigma dikes.

FCA's planned in the future are included in the Scaldis model except the areas that were assigned to be reserve areas (=Blankaart, Hingene Broekpolder, Spierbroekpolder, Heindonk Tien Vierendelen II, and Battenbroek).

Table 8 gives a list of all areas with their function and if they are included in the model. Figure 214 to Figure 238 give a detailed view on all areas separately.

Table 8. List of all Sigma areas, their future function and if they are included in the Scaldis 3D model

Area	Function	In the model?
Grensgebied	addition	yes
N-Prosperpolder	de-embankment	yes
Doelpolder Noord en Midden	CRT	ja
Potpolder van Lillo	soil remediation	yes
Fort Filip	de-embankment	yes
Burchtse weel	addition	yes
Kruikeke Bazel Rupelmonde	FCA/CRT	yes
Oud Broekpolder	FCA	yes
Schellandpolder	FCA	yes
Hingene Broekpolder	FCA (reserve)	no
Spierbroekpolder	FCA (reserve)	no
Groot Schoor (Bornem)	de-embankment	yes
Stort van Hingene	de-embankment	yes
Stort Ballooi	soil remediation	yes
Schousselbroek	FCA/CRT	yes
Tielrode Broek	FCA/CRT	yes
De Bunt	FCA/CRT	yes
Klein Broek	de-embankment	yes
Groot Broek	de-embankment	yes
Potpolder I	de-embankment	yes
Weijmeerbroek en Oude Durme	wetland	no
Polder van Waasmunster	de-embankment	yes
Bulbierbroek	wetland	no
Hof ten Rijen	wetland	no
Zuidelijke vijver Hof ten Rijen	wetland	no
Potpolder IV	FCA/wetland	yes
Potpolder V	wetland	no
Nonnengoed	wetland	no
Putten van Ham	wetland	no
Hagemeersen	wetland	no
Lippenbroek	FCA/CRT	yes
Blankaart	FCA (reserve)	no
Zwijn	FCA	yes
Groot Schoor (Hamme)	de-embankment	yes
Grote Wal – Kleine Wal	FCA	yes
Vlassenbroekse polder 1	FCA/CRT	yes
Vlassenbroekse polder 2	FCA	yes
Uiterdijk	de-embankment	yes
Scheldebroek	FCA	yes
Paardebroek	wetland	no
Paardeweide	FCA/wetland	yes
Bergenmeersen	FCA/CRT	yes
Wijmeers 1	FCA	yes

Area	Function	In the model?
Wijmeers 2	de-embankment	yes
Kalkense Meersen	wetland	no
Ham	FCA/CRT	yes
Bastenakkers	FCA	yes
Zandput Melle	de-embankment	yes
Heusden	de-embankment	yes
Stort de Naeyer	Afgraven	yes
Bovenzanden	FCA/CRT	yes
Heindonk – Tien Vierendelen (deel1)	FCA	yes
Heindonk – Tien vierendelen (deel 2)	FCA (reserve)	no
Zennegat – Oude Dijlearm	FCA/CRT	yes
Grote Vijver 1+2	FCA/CRT/addition	yes
Battenbroek	FCA (reserve)	no
Schonenberg	dike allocation	yes
Rijmenam	FCA	Yes
Pikhaken	wetland	no
Hollaken – Hoogdonk deel 1	FCA	yes
Hollaken – Hoogdonk deel 2	FCA	yes
Anderstadt 1	de-embankment	yes
Anderstadt 2	FCA	yes
Anderstadt 3	wetland	no
Vijvers Hof van Lachenen	wetland	no
Polder van Lier	FCA	yes
Mondingsgebied Grote Nete	wetland	no
Varenheuvel - Abroek	wetland	no
Herinrichting Grote Nete	dike allocation	no
Dorent	wetland	no

5.2.4. Grid quality

An ideal unstructured triangular mesh with optimal quality consists of only equilateral triangles off which all angles are equal to 60°. The outline of our model area and the change in mesh resolution makes these triangles deviate from their ideal shape. In some parts upstream where we stretched the triangles to save computation nodes, this deviation is on purpose. In other parts this deviation is the result of the unstructured mash adapting to the geometry of the local area and the change in mesh resolution. To guard the qualtiy of the mesh the edge growth ratio is controlled at the mesh construction. This edge growth ratio is the ratio between the edge length of one element and the edge length of the next elemant. Constructing the mesh this ratio is set to not exceed 8% for the channels and 20% for the flood control areas. For the final mesh, the ratio between the minimum and maximum edge length at each node was calculated. This is shown in Figure 8 and Figure 9. This ratio should be minimal for optimal qualtiy.

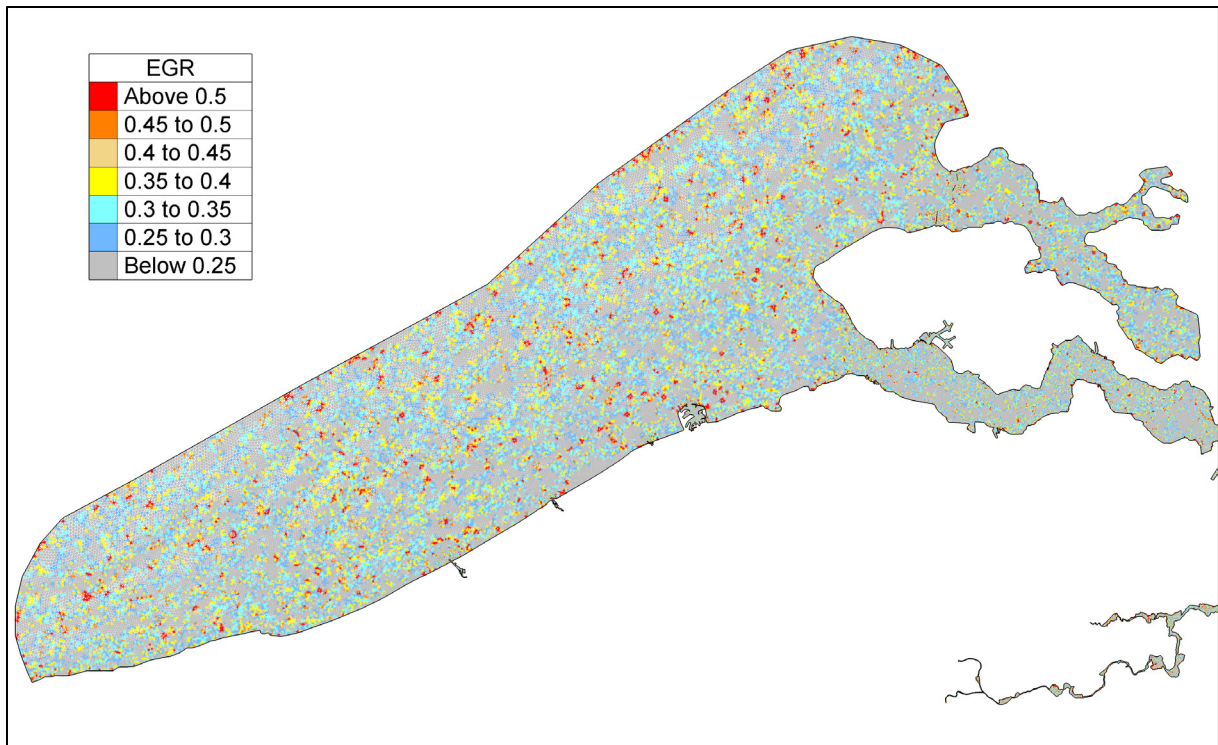


Figure 8 - Map showing edge growth ratio (EGR) in coastal zone, Western Scheldt and Eastern Scheldt of Scaldis.

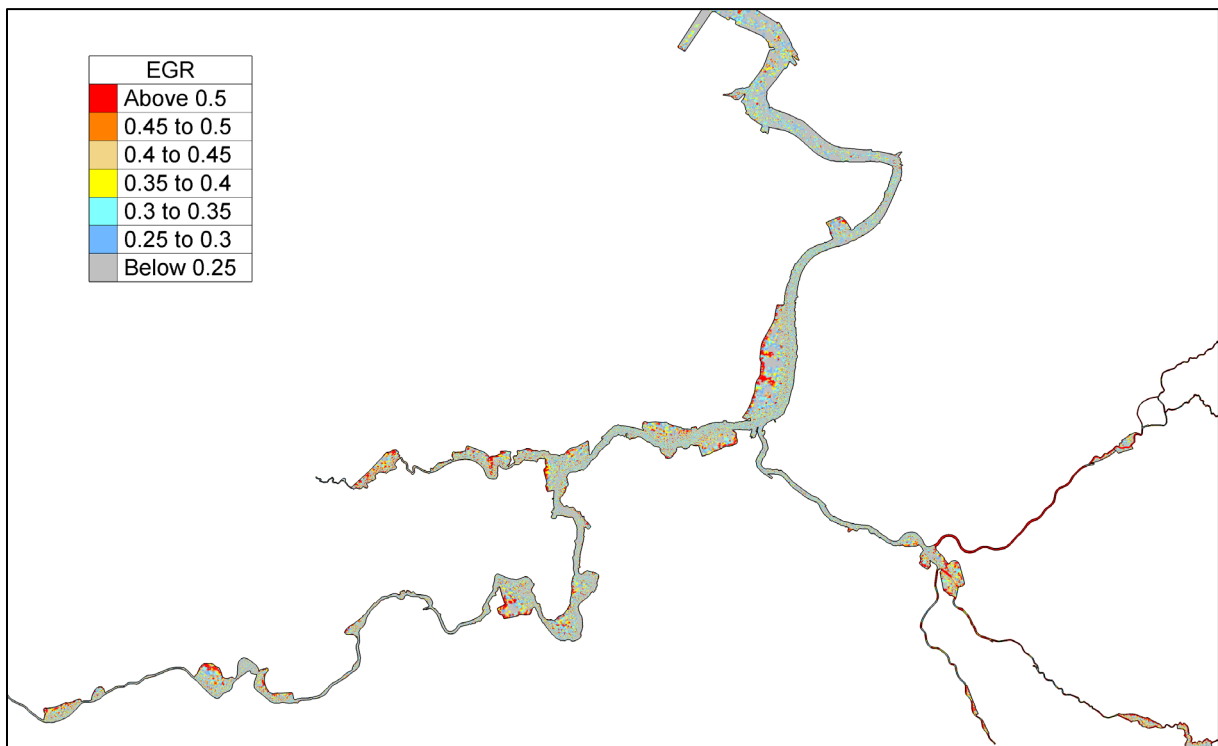


Figure 9 - Map showing edge growth ratio (EGR) in Sea Scheldt and tributaries of Scaldis

A second quality measure are the angles within each element. A large deviation from the ideal 60° can truncate the simulation results. Because we used a channel mesher, i.e. we stretched the triangles along the axis of the upstream tributaries, this will negatively influence our over all overview of the angles of this mesh (while as long as the flow direction is also along the channel axis,

this will give no truncated results). Therefore we give the results with and without these stretched elements in the mesh :

with : 11911 elements with an angle between 90° – 131° or 1% of all elements
 843284 elements with an angle between 30°- 90° or 97% of all elements
 18224 elements with an angle between 10°-30° or 2% of all elements
without : 2765 elements with an angle between 90°-131°
 359 elements with an angle between 10°-30°

We can conclude that the larger part of the elements with deviating angles are elements we stretched on purpose and will have no or minor negative influence on the results.

Finally we limit the number of neighbours of the nodes to be maximum eight.

5.3. Bathymetry

The model bathymetry is presented in Figure 10. For this large model domain several different bathymetry datasets were used and pasted together from different sources and in different coordinate systems. All coordinate conversions were done with the Open earth Toolbox in Matlab. The coordinate systems of all data were converted to RD Paris. In this paragraph, an overview of the different datasets to build this large model domain is given.

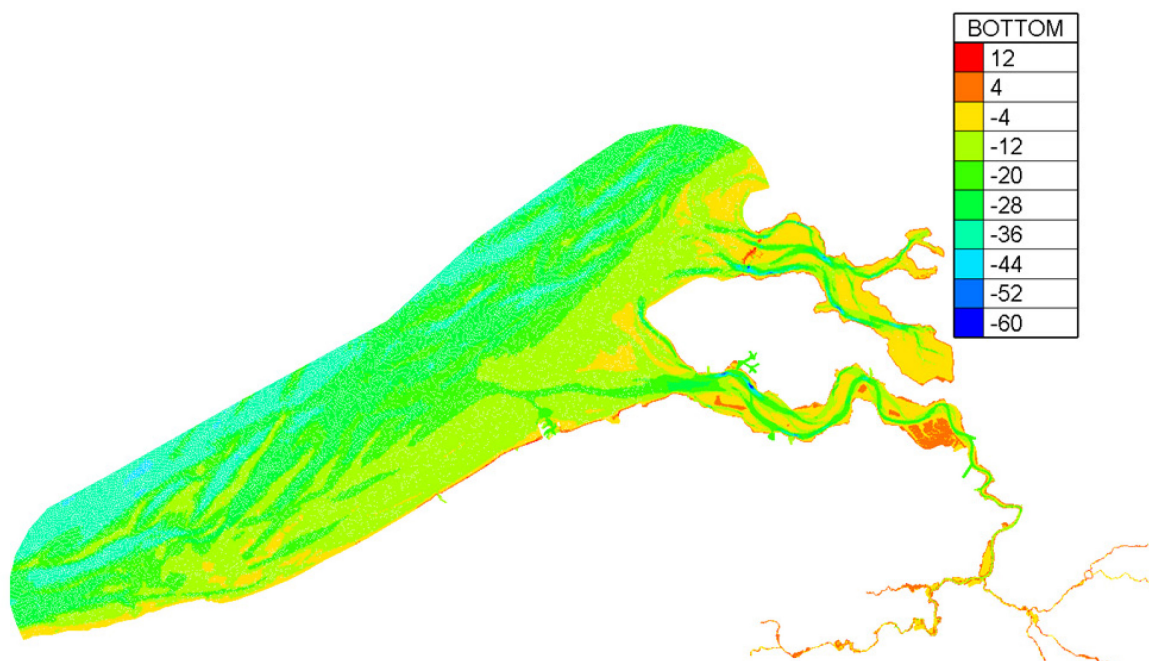


Figure 10 - Model bathymetry (m TAW)

5.3.1. Coastal zone and mouth of the Western Scheldt

Greater North sea bathymetry is available from EMODnet.eu database. The year of measurement is unknown. Original data were in WGS84 and LAT (blue colour in Figure 11).

The bathymetry of the Belgian continental shelf and coast comes from MDK coastal department. The data for the beaches are measured in 2010. The coastal zone (shoreface) is measured in 2009. The offshore part is measured in 2007. The original data were in WGS84 UTM31N and m TAW (orange colour in Figure 11).

The measurements for the Dutch coast were downloaded from the Open Earth database. The original data are in RD Parijs and m NAP (green colour in Figure 11). It was measured from 2007 to 2012 (different parts in different years).

For the port of Zeebrugge the bathymetry was measured in 2014. The original data was given in ETRS89 UTM31 and m TAW. The data was copied from the aMT GIS database (\\wm162458\Data\GISdata\frame\bth\frame_bth_kub_etr89utm31n.gdb).

For the port of Nieuwpoort a bathymetry from VHO from 2014-2015 was used. The original data were in ETRS89 UTM31 and LAT. LAT conversion to TAW was done by adding 0,65 m to all datapoints.

For the port of Oostende a bathymetry of VHO from 2014 was used. The original data were given in ETRS89 UTM31 and LAT. LAT conversion to TAW was done by adding 0,50 m to all datapoints.

For the port of Blankenberge a bathymetry of VHO from 2015 was used. The data were originally in ETRS89 UTM31 and LAT. LAT conversion to TAW was done by adding 0,32 m to all datapoints.

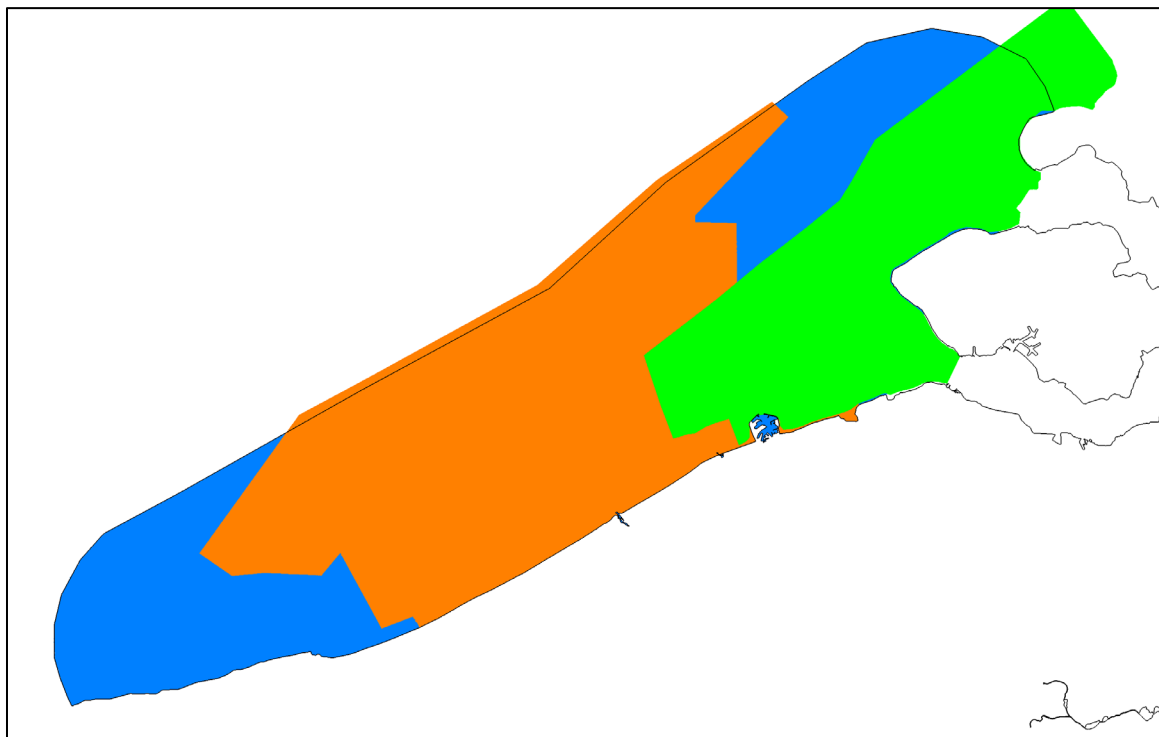


Figure 11 - Overview of the bathymetric data for the coastal zone : blue colour – greater North sea bathymetry ; orange colour – Belgian continental shelf and coastal zone ; green colour – measurements for the Dutch coast

5.3.2. Eastern Scheldt and Western Scheldt

The bathymetry of the Western Scheldt was delivered by RWS. We started from data from 2013 in ETRS89 UTM31 and LAT. The data was collected from aMT GIS database. Conversion to TAW was done by a conversion grid LAT-to-TAW.

The bathymetry of the Eastern Scheldt was measured in 2010 and is delivered by RWS. This dataset was in RD Parijs and m NAP.

5.3.3. Lower Sea Scheldt

The topographic data for the channel banks are taken from the Mercator databank as a Digital Height Model (DHM) with a resolution of 5x5 m (Lambert 72). The data originates from 2007.

A topo-bathymetric data set from Maritime Access is used for the Lower Sea Scheldt. These data originate from 2011, and were in RD Paris and m TAW (purple colour in Figure 12).



Figure 12 - Bathymetry lower Sea Scheldt. Beneden Zeeschelde. The purple coloured zone is part of a topo-bathymetric dataset from 2011. The grey area is the back is part of the DHM Vlaanderen dataset from 2007.

5.3.4. Upper Sea Scheldt

The Upper Sea Scheldt region topo-bathymetry consists of several datasets put together. The most recent data are always on top of older data.

For the Upper Sea Scheldt a topo-bathymetry from 2011 is used (RD Parijs, m TAW). (=blue colour in Figure 13). Maritime Access Division (MT) delivered the data.

The data from the Mercator database (DHM with a resolution of 5x5 m, Lambert 72) is used to fill up the missing topography/bathymetry of the upper part of Durme. (= black colour in Figure 13) This part of the Durme is not continuously filled with water. Therefore the topography will suffice.

A topo-bathymetry from 2013-2014 is used in the Upper Sea Scheldt and Rupel (resolution 1x1 m, Lambert 72, m TAW). (= Orange colour in Figure 13). The data was delivered by Maritime Access.

For the Durme between Waasmunster and Lokeren a bathymetry from 2012 was available (from W&Z in Lambert 72 and m TAW with 1x1 m resolution ; red colour in Figure 13). For the Durme from mouth to Waasmunster a bathymetry of 2013 was available (from W&Z in Lambert 72 and m TAW with a 1x1 m resolution; green colour in Figure 13).

For the tidal branch from Merelbeke to Zwijnaarde, measured cross sections were available from MT. The original data was given in WGS84UTM31 and m TAW and dates from 2003. (not shown in Figure 13).

Additional datasets for the flood control areas were available for Bergenmeersen, Paardeweide, Uiterdijk, Potpolder I, Potpolder IV, Tielrodebroek, Klein Broek, Groot Broek, Lippenbroek, Bovenzanden, Polder van Lier, Grote Wal and Scheldebroek. Topography data was from 2013 provided by W&Z. The data were originally given in Lambert 72 and m TAW with a 1x1 m resolution. (= yellow areas in Figure 13).

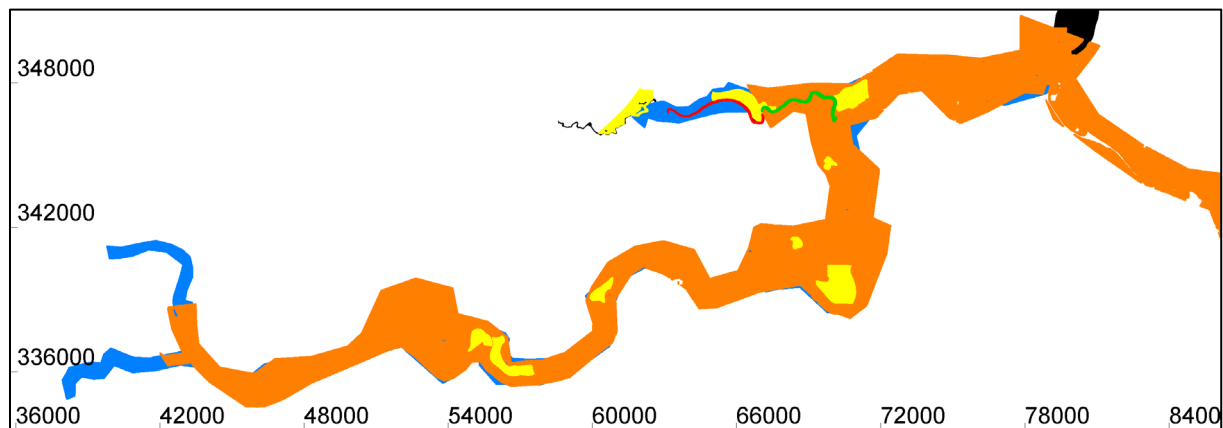


Figure 13 - Datasets of bathymetry/topography of Upper Sea Scheldt: black color = DHM Vlaanderen for most upper part of the Durme. Blue color = topobathymetry from 2011. Orange color = topobathymetry from 2014. Red color = bathymetry for Durme from 2012. Green color = bathymetry for Durme from 2013. Yellow areas = topography of flood control areas from 2013.

5.3.5. Rupel basin

The topo-bathymetry for the Rupel is taken from the dataset Sea Scheldt Topo-bathymetry 2013 – 2014 (m TAW, RD Parijs) from Maritime Access (= blue colour in Figure 14).

A part of the topographic data set from 2007 (from Maritime Access Division, m TAW, RD Parijs) was used for the tributaries of the Rupel (orange colour in Figure 14). For the Zenne, cross sections from 2001 were also used (from IMDC, RD Parijs, mTAW ; red colour in Figure 14). For the Dijle (grey colour in Figure 14) and Nete (green colour in Figure 14) the bathymetry from 2010 – 2013 (from W&Z, RD Parijs, m TAW) and cross sections from 2001 (from IMDC) were used.

The bathymetry of the flood areas was defined based on the topographic data. The areas outside this topographic data were filled with the data from the Mercator database, DHM Flanders.

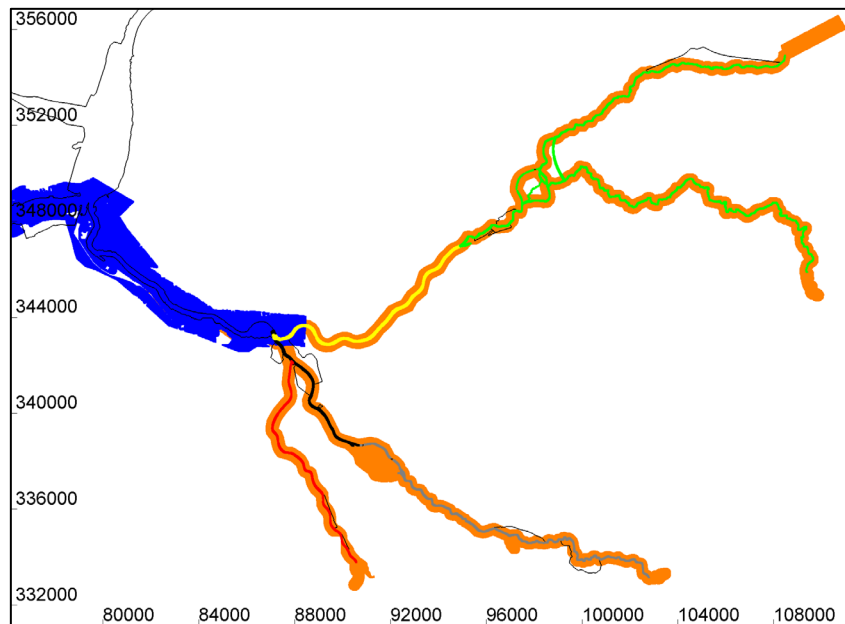


Figure 14 - Rupel basin: blue = topo-bathymetry from 2013-2014 from MT; orange = topography from total Sea Scheldt basin from 2007, given by MT; red = bathymetry Zenne = cross sections from 2001. Data from IMDC; black = bathymetry from 2010-2013 coming from W&Z; grey = cross sections from 2001 coming from IMDC; yellow = bathymetry coming from W&Z dating from 2010-2013; green = cross sections from 2001 from IMDC data.

5.4. Boundary conditions

The downstream model boundary is located in the North sea. The SCALDIS model is nested in the regional ZUNO model of the southern North Sea. The 10 minute time series of the water level calculated in ZUNO are defined at the downstream boundary of SCALDIS (after correction of the harmonic components). The subroutine bord3d.f was modified to allocate a water level and a salinity value for each boundary node separately.

A correction of the harmonic components is calculated based on the comparison of the harmonic components of the ZUNO results and measurements for a period of 1 year (*Maximova et al.*, 2015). Differences in harmonic components (ZUNO vs. measurements) are found for stations in the Belgian and Dutch Coastal zone for the M2, M4, S2 phases and the Z0 component (Table 9). Z0 component was corrected first by -16 cm (this value was obtained from the comparison of the ZUNO results and measurements for a period of 1 year). However, the comparison of the TELEMAC results and measurements showed that this component should be corrected by -21 cm.

For the modeling of the storm period no Z0 correction was implemented.

In the next step, the timeseries of the boundary conditions of the SCALDIS model are “harmonically corrected” with the obtained correction terms in Table 9. This means that the timeseries at the boundary locations of SCALDIS that are obtained out of ZUNO, are decomposed in harmonic components and a residual term. The harmonic components are corrected, and the signal is re-synthesised. Applying these corrected boundary conditions in SCALDIS makes that the hydrodynamics in SCALDIS does not have the systematic bias in harmonic components that is present in ZUNO.

Table 9. Correction of harmonic components

Harmonic component	Correction
Phase M2	+4°
Phase M4	-6°
Phase S2	+7°
Z0	-21 cm

There are 8 upstream boundaries with prescribed discharge and free tracer. The measured daily average discharges are defined as upstream boundary conditions at the Upper Sea Scheldt for Merelbeke, Dender, Zenne, Dijle, Kleine Nete, Grote Nete, channel Ghent – Terneuzen. For the values of the channel Ghent-Terneuzen a proxy was taken downstream the weir of Evergem. These daily averaged discharge data were used. For the channel of Bath hourly discharge measurements were available. In this time series the small negative values were set to zero for stability reasons. All the other daily averaged discharge values for the other upstream discharge boundaries were then hourly interpolated. So all discharge boundaries have hourly discharge values.

Wind is applied on the coastal zone through the subroutine meteo.f.

5.5. Salinity

5.5.1. Boundary conditions and correction

The salinity boundary conditions are generated by nesting the SCALDIS in the CSM-ZUNO model train (Figure 15). Model results for salinity are highly influenced by values imposed at the boundaries. Therefore, it is very important to have accurate salinity boundary conditions. Salinity boundary values in the SCALDIS model were corrected based on the comparison of the simulated and measured salinity time series at Vlakte van de Raan (located in the North sea; red dot in Figure 17 in the larger mouth area of the Scheldt Estuary).

The modeled and measured salinity at Vlakte van de Raan are shown in Figure 16. Thicker lines show the daily averaged curves. The missing values in the daily averaged measured salinity were filled by a linear interpolation. The ZUNO model underestimates the salinity values in the area of interest. Therefore, a salinity correction at the boundaries was necessary.

The correction, the difference between the daily averaged measured and modelled values was added to the boundary point values of the Scaldis model (*Maximova et al.*, 2015). Salinity is the only active tracer in the Scaldis model.

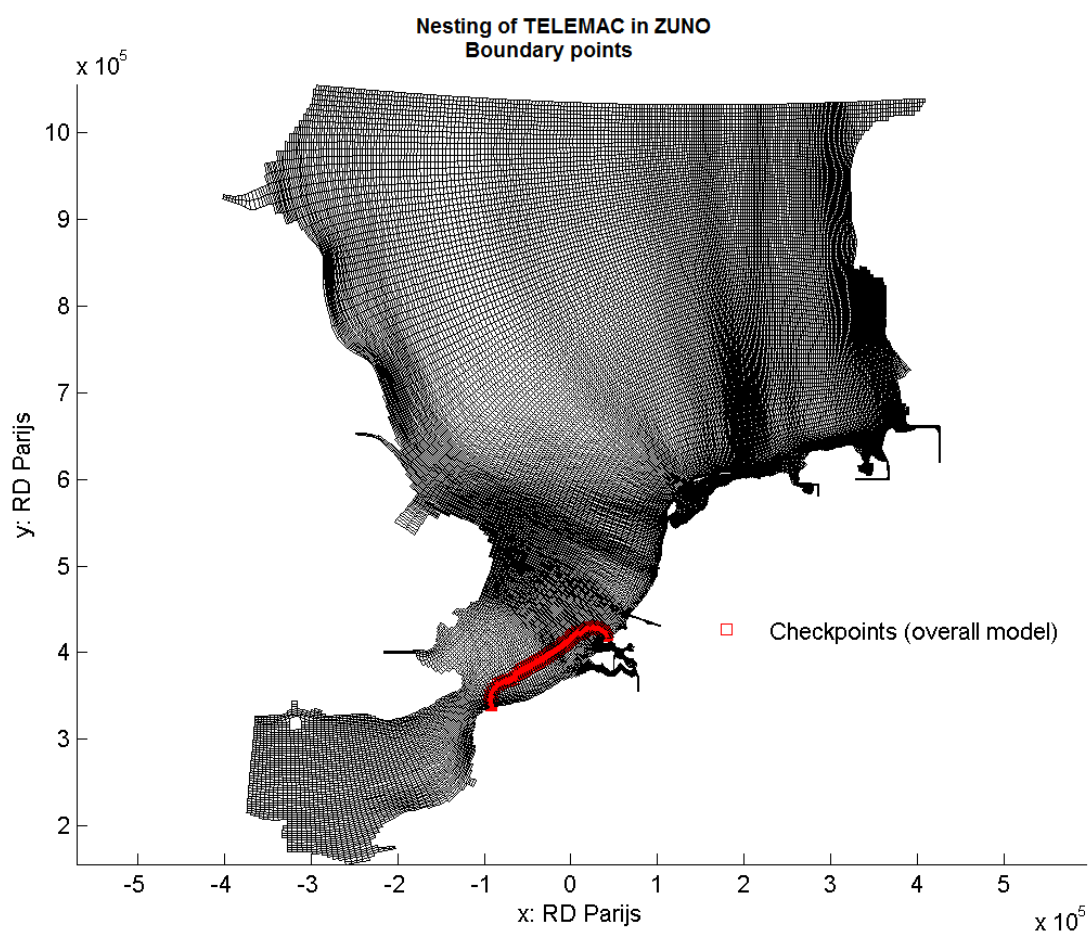


Figure 15 - Nesting of Scaldis model in ZUNO. Scaldis boundary nodes given in red.

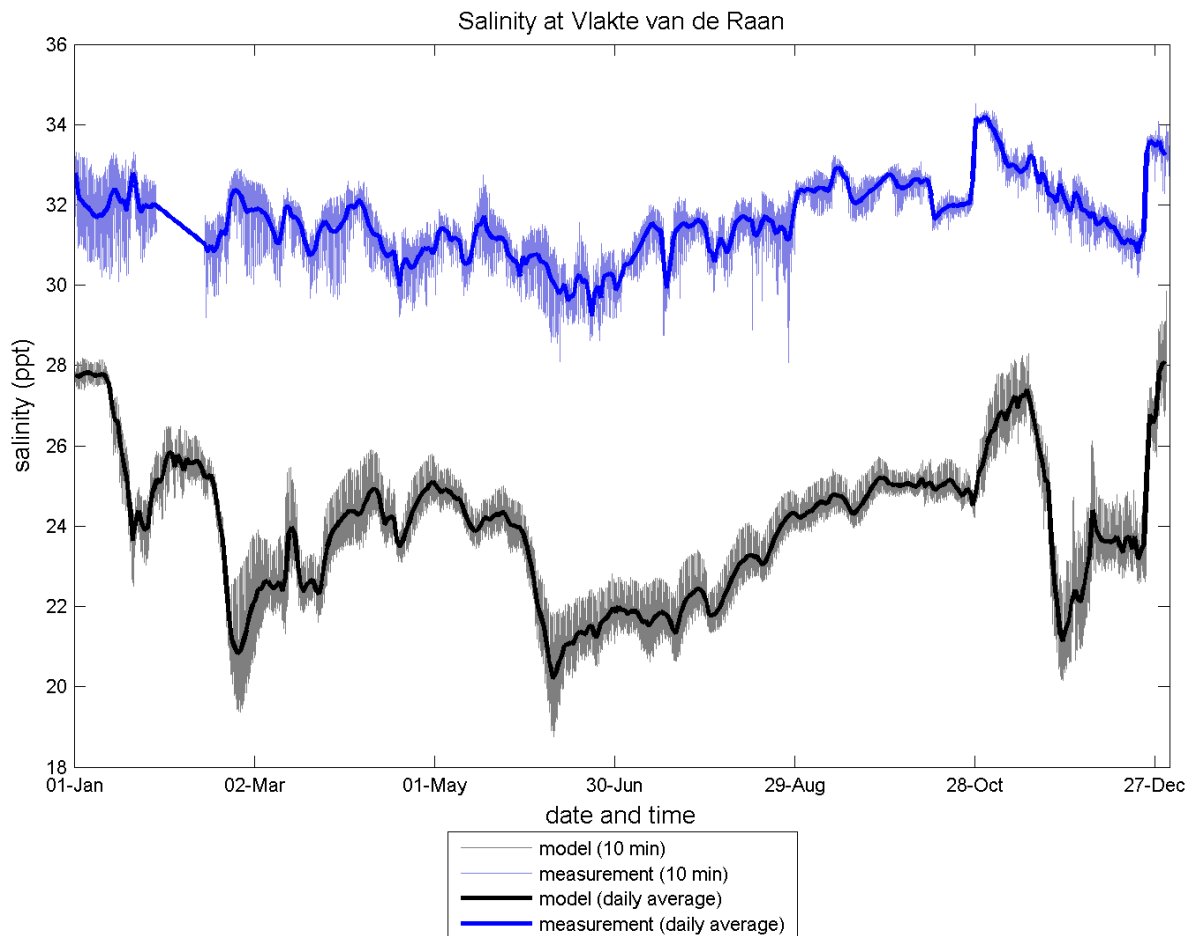


Figure 16 - Comparison of modelled salinity in ZUNO and measured salinity for Vlake van de Raan station.

5.5.2. Simulation period and initial condition

Salinity simulations are done in a three month simulation. The model starts from a previous computation file (a short simulation to start up the tidal motion in the model). The model runs from 17/09/2013 00:00 to 20/12/2013 00:00.

To start with a salinity distribution in the estuary that corresponds more or less with the measurements, the model starts from an initial salinity field: a map is made based on a combination of salinity measurements and corrected model results from ZUNO. Figure 17 shows the outline of the model. The dots in the North Sea and Eastern Scheldt are extracted from the ZUNO model from the start date for the new simulation. All these point values are first corrected in the same way as the boundary conditions. The red dots in Figure 17 give the location of stations where salinity is measured. The measured values at 17/09/2013 00:00 were interpolated using inverse distance method together with the corrected model values from ZUNO to give an initial salinity map (Figure 18) that is read by a modified subroutine fonstr.f in TELEMAC-3D. The values of the 2D map are copied to the other four layers in the model.

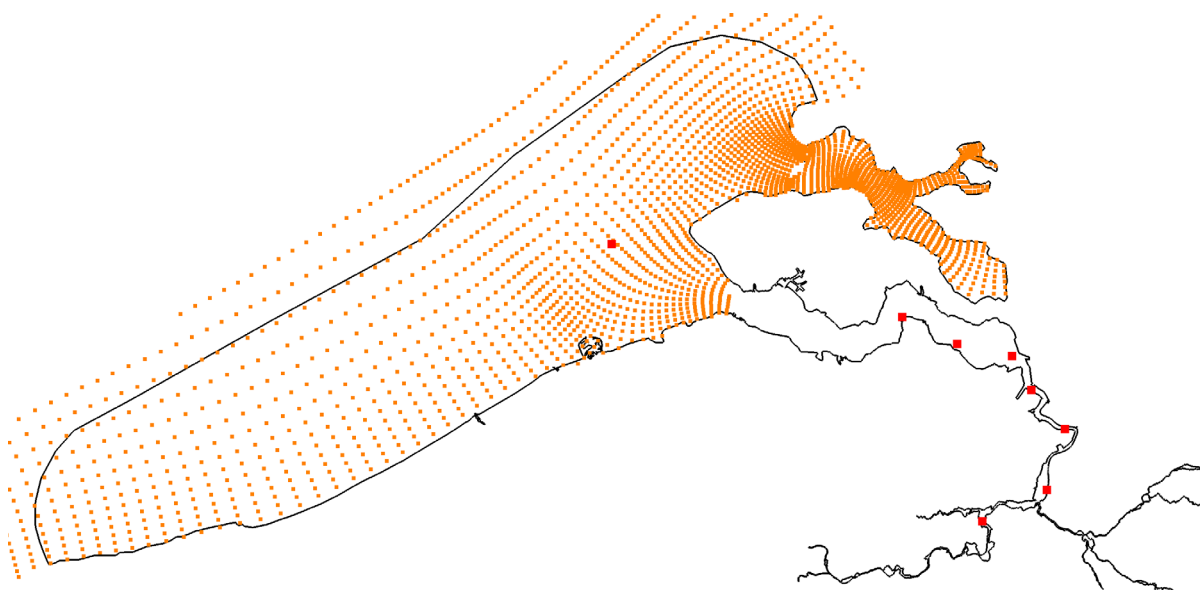


Figure 17 - Salinity values at 17/09/2013 00:00 extracted from ZUNO (orange dots) and location of the stations that measure salinity in the Scheldt Estuary (red dots). These stations are named (from downstream to upstream) Vlake van de Raan, Overloop van Hansweert, Baalhoek, Prosperpolder, Liefkenshoek, Boei 84, Hemiksem and Driegoten.

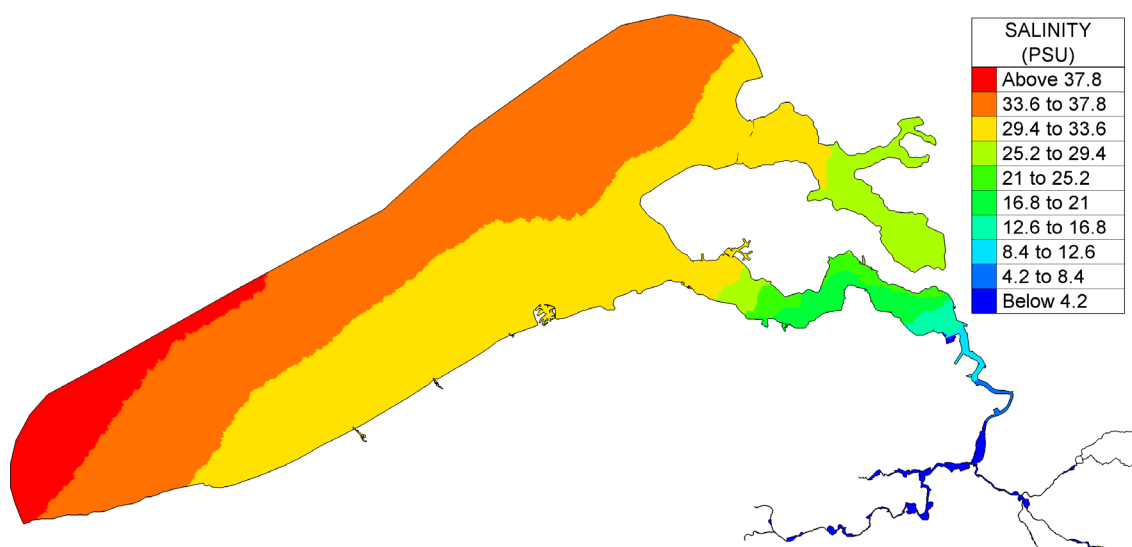


Figure 18 - Initial salinity field for start simulation at "17/09/2013 00:00"

5.6. Time step

The relationship between the time step and the grid size has an effect on the model accuracy and stability. The time step used for the model simulations is 4 s. It was chosen based on the sensitivity analysis which showed that this time step is the optimum for computational speed and still keep a stable computation. More information is given by Smolders (2014 a).

5.7. Computational time

For a numerical model the computation time depends on the one hand on parameters intrinsic to the model itself and on the other hand on parameters of the device that executes the computation. Examples of intrinsic model parameters are the number of nodes in the grid, the number of output variables, the time step, the turbulence model, numerical parameters that simplify the calculation of the RANS equations. For the Scaldis model we will discuss only two of these parameters : the number of output variables (tracers) and the number of culverts (sink and source structure). After those we briefly discuss the optimum number of processors to be used for the simulations.

5.7.1. Number of output variables : tracers

More output variables means more variables that have to be calculated at each time step. In this project we will have to run some tracer simulations, where 19 extra tracers (above tracer1 = salinity) are added to specific parts of the estuary. All other parameters of the model stay the same and we give here two examples of computation time :

- 19 extra tracers added (=20 in total). 2.300.000 nodes. Time step = 4s. Simulation period = 3 days. Calculated on 60 Stevin processors on our Linux cluster.
simulated in 134 hours → speed up of 0,5
- only salinity as tracer. 2.300.000 nodes. Time step = 4s. simulation period = 4 days. Calculated on 60 Stevin processors on our Linux cluster.
simulated in 26 hours → speed up of 3,7

The example shows that the difference in computation time is huge when adding extra output variables.

5.7.2. Number of culverts

A culvert in TELEMAC is the combination of a sink and a source term. They are two nodes communicating with each other. In the TELEMAC release v6p3 the discharge coming from a sink and going to a source is calculated based on the culvert equations we implemented (cfr. chapter 6). The discharge is calculated based on the water level of the node and its neighboring nodes. This approach demands a lot of computation time, especially when the number of sinks and sources is increasing. In the next release of the Telemac suite (v7p1) for sinks and sources there is an option to choose for the so called “Dirac” sources. These type of sources do not take neighboring nodes into account when calculating discharges. This approach also don’t consumes a lot of computational power. From the moment this will be operational this approach will be chosen in the calculations. Here below we give an example of the effect of extra culverts on the computation time.

We have ran the same simulation three times on the KUL cluster “Thinking” on 180 processors (=9 nodes with 20 processors)

- 0 culverts active: 24 hours simulated in 2h09min44s → speed up of 11,2
- 45 culverts active: 24 hours simulated in 2h49min25s → speed up of 8,5
- 256 culverts active: 24 hours simulated in 9h05min31s → speed up of 2,6

These examples show the high computational cost of using sink and sources without the “Dirac” option.

5.7.3. Number of processors

In general the more processors used, the faster the computation will be... up to a point when the communication between all these processors is demanding more time than the actual calculation itself. There should be an optimum in this: the maximum number of processors with still an acceptable communication cost. In reality we see that on large linux cluster the speed of a computation is not only influenced by its own number of processors used, but also by the number of jobs running on that cluster at that time. When the cluster is filled with jobs, we noticed that our computation times drop and thus there is some spread in efficiency.

For example: one of the calibration runs for Scaldis (=20 days; 45 culverts) was done on our Reynolds cluster on 96 processors (6x16) and took 4 days (speed up time of 5). The same simulation for a different calibration step on the same number of processors took only 2 days and 20 hours (a speed up of 7). For the linux cluster at the lab the fastest computation is however every time with the maximum of processors available (max = 128). For the KUL cluster “Thinking” we found an optimum around 180 processors. The upscaling capabilities of TELEMAC are good. Using however even more processors slowed down the total computation time. We noticed also that using the same amount of processors on a “busy” cluster also gave higher computation times, which made us assume that not the number of processors, but the communication between processor nodes is the limiting factor to speed up large simulations. This assumption was also made by Moulinec et al. (2011) where they name the same reason as limitation in further speed up. The variability in computation time makes it very difficult to estimate the exact computation time of a specific simulation.

In Delft3D there is a possibility to manually assign specific neighbouring subdomains to one cluster node and hence decreasing the interprocessor communication. This decreased significantly the total computation time. Such a feature is however not yet available in TELEMAC.

5.8. Model settings

The most important model settings are described in Table 10.

Table 10. Applied model settings

Parameter	Value
Time step	4 s
Initial condition	constant elevation and start with smoothing time (calibration run) or from the restart file (salinity run)
Number of layers in the vertical	5 (3D model)
Version TELEMAC	TELEMAC Balloonfish (Linux) (= local branch of TELEMAC V6P3 to include culverts in 3D)
Salt transport	On
Wind	On
Roughness formula	Manning
Bed roughness value	varying roughness field (Figure 19)
Option for the treatment of tidal flats	1: equations solved everywhere with correction on tidal flats
Treatment of negative depths	2: flux control
Free surface gradient compatibility	0.9
Vertical turbulence model	2: mixing length
Mixing length model	3: Nezu and Nakagawa
Horizontal turbulence model	4: Smagorinski
Scheme for advection of velocities	1: characteristics
Scheme for advection of depth	5: conservative scheme
Scheme for advection of tracers	13: Leo Postma for tidal flats
Scheme for diffusion of velocities	1: implicit (1 is default; 0 cancels the diffusion)
Scheme for diffusion of tracers	1: implicit
Solver	7: GMRES

The free surface gradient compatibility was set to 0.9 (it is a recommended value) to avoid free surface wiggles (for example in areas with strong bathymetry gradient). The main consequence is a slightly altered compatibility between depth and velocity in the continuity equation (*EDF-R&D*, 2010).

GMRES solver (Generalised Minimum RESidual method) is used for the calculations. The analysis in *Smolders et al.*, (2015, in preparation) showed that this solver produces good results. The model runs are stable.

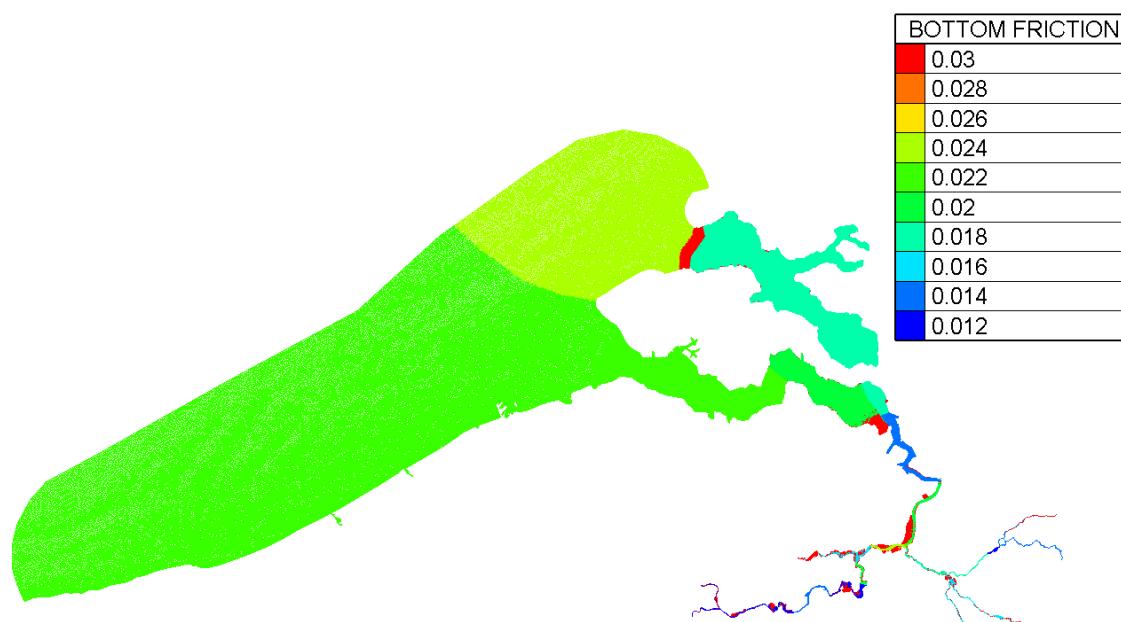


Figure 19 - The calibrated roughness field (Manning $m^{-1/3}s$) of the Scaldis model

5.9. Simulation period

The simulation periods used for different runs are described in Table 11. The period for the model calibration is chosen based on the analysis of the comparable tides for the available ADCP measurements.

The simulation period for the storm run is chosen from 03/12/2013 00:00 to 09/12/2013 00:00. It includes the Sinterklaas storm (Xaver) of 5 and 6 December 2013. The Flood Control Areas (FCA) and a Controlled Reduced Tide (CRT) systems implemented in the model (see chapter 6) are active during this period.

A simulation period of 3 months is chosen for the analysis of salinity.

Table 11. Simulation period

Run		Simulation period	
Scaldis_039_0	calibration	13/09/2013 00:00 - 03/10/2013 00:00 (results are analyzed from 17/09 00:00 to 03/10/2013 00:00)	20 days
Scaldis_039_1	storm period	03/12/2013 00:00 - 09/12/2013 00:00	5 days
Scaldis_039_2	analysis of salinity	17/09/2013 00:00 - 18/12/2013 00:00	3 months

5.10. Turbulence implementation in the model

The vertical and horizontal turbulence scales are separated in TELEMAC because they behave differently in shallow water applications. That involves defining two models of horizontal and vertical turbulence and defining separate additional horizontal and vertical viscosities in the input file, rather than a single viscosity (EDF-R&D, 2013).

Different types of turbulent models were tested during the sensitivity analysis (chapter 7.6). The vertical and horizontal turbulence models used in the calibrated model are described here.

5.10.1. Vertical turbulence model

Mixing length is used as the vertical turbulence model. The vertical diffusivity of velocities is automatically computed by TELEMAC-3D by means of the selected mixing length model taking or not taking the effects of density into account. The mixing length model expresses the turbulent viscosity (or diffusion coefficient) as a function of the mean velocity gradient and the mixing length (Prandtl's theory) (EDF-R&D, 2013). Nezu and Nakagawa mixing length model is selected.

Nezu and Nakagawa model takes into account that turbulent viscosity decreases to zero towards the free surface (assuming the absence of wind). This model is very useful for representing diffusion along the vertical (Hervouet, 2007).

$$v_t = ku^*z(1 - \frac{z}{h})$$

v_t - turbulent viscosity;

k – von Karman parameter (equal to 0.41);

u^* - the shear velocity;

z – the distance from the bed;

h – water depth.

The turbulent viscosity calculated in the mixing length model of Nezu and Nakagawa is added to the laminar viscosity which the coefficient for vertical diffusion of velocities that is specified in .cas file (*personal communication with Hervouet J.-M., Telemac forum*).

5.10.2. Horizontal turbulence model

The Smagorinsky horizontal turbulence model is used. The Smagorinsky scheme is recommended, in particular, in the presence of a highly non-linear flow (EDF-R&D, 2013). The Smagorinsky model belongs to the category of sub-grid turbulence models. The principle is as follows: turbulence is the solution of the Navier-Stokes equations. It would naturally appear in the numerical solutions if the size of finite elements allowed the reproduction of all mechanisms including the viscous dissipation of very small vortices. Only in the formation of smaller vortices, where turbulence is inhibited by the mesh, does modelling take place in a numerical simulation. Smagorinsky's idea is to add to the molecular viscosity a turbulent viscosity deduced from a mixing length model. This mixing length corresponds to the size of the vortices smaller than that of the mesh size (Hervouet, 2007).

$$v_t = C_s^2 \Delta^2 \sqrt{2D_{ij}D_{ij}}$$

v_t - turbulent viscosity;

C_s – a dimensionless coefficient;

Δ – the mesh size derived in 2D or 3D from the surface or from the volume of the elements;

D - the strain rate tensor, which involves velocity gradients.

$$D_{ij} = \frac{1}{2} \left(\frac{\partial \bar{U}_i}{\partial x_j} + \frac{\partial \bar{U}_j}{\partial x_i} \right)$$

C_s coefficient is hard coded in the Telemac routines. The turbulent viscosity calculated in the Smagorinskiy formula is added to the laminar viscosity which is the coefficient for horizontal diffusion of velocities specified in the .cas file (*personal communication with Hervouet J.-M., Telemac forum*).

5.10.3. Velocity near bottom

A default boundary condition on the bottom is used: an impermeable slip boundary (Neumann condition of the same type as vertical conditions). Velocities at the bottom are not zero.

In Telemac bottom velocities can be set to zero by using value 2 of the keyword BOUNDARY CONDITION ON THE BOTTOM. This option is valid only if the vertical mesh is refined at bottom level (EDF-R&D, 2013). It was not used in the model in this study.

5.11. Numerical diffusion

Numerical diffusion is an "uncontrolled" diffusion that is automatically introduced in the calculation and which is due to several reasons (mesh more/less coarse, numerical schemes more/less diffusive etc.). The numerical diffusion depends on the mesh size. It can be estimated in a 1Dh model by $U \cdot \Delta x / 2$. This formula gives an order of magnitude for a 3D case (*Hervouet J.-M., Telemac forum*).

Numerical diffusion can have a significant effect on the model results. It is important to keep this in mind while choosing the model parameters and during the sensitivity analysis (chapter 7.3).

6 Culvert functionality

6.1. Field of application

Flood Control Areas (FCA) together with a Controlled Reduced Tide (CRT) system are implemented in the Scheldt estuary to reduce the risk of flooding. The former is defined by an area specifically located in the regions where the bottom elevation is lower than the mean tide elevation. This area is surrounded by a outer higher dyke (ring dyke) and in the interface with the river, it has a lower dyke (overflow dyke) that allows the flow to overtop the structure during storm surges. The CRT is based on the construction of inlet and outlet sluices that control the flow between the river and the polder depending on the water levels on both sides (Figure 20) (Teles, 2014).

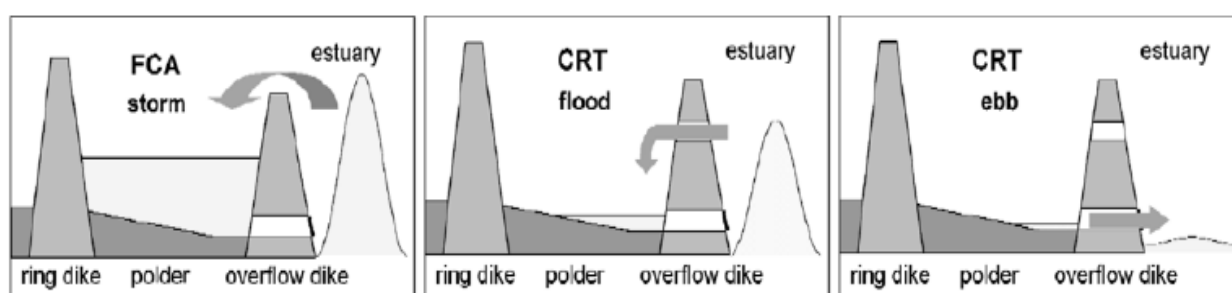


Figure 20 - Water movements between the FCA and river without CRT (on the left) and with CRT (on the middle and right panels). (Source: De Mulder et al. (2013))

The incorporation of these structures in numerical models is essential to better predict and describe the flow hydrodynamics going to and coming from these areas. Inlet and outlet sluices are no standard structures in TELEMAC 3D, so the sinks and sources subroutine was modified to fulfil our needs. The inlet and outlet sluices act like a weir when they are not fully submerged and when water levels rise above the inlet ceiling pressurised flow formulas are used. The calibration of the head loss coefficients for the inlet and outlet sluices was done comparing model results with measured water levels and discharges of one specific CFA/CRT, called Lippenbroek. Later these values were validated using the measurements from the CFA/CRT Bergenmeersen. The coefficients found in this calibration/validation exercise are used for all the other inlet and outlet sluices for the other FCA, FCA/CRT areas in the 3D model.

6.2. Flow through a culvert: theoretical background

A number of studies regarding the description of flows through the culverts refer to the work of Bodhaine (1968). Bodhaine categorized the flow through a culvert into six types, and for each type the discharge is calculated in a different way. The equations are deduced from the continuity and energy equations between the approach section (see Figure 21) and the exit (downstream) section of the culvert. The type of flow depends on whether the culvert flows full and whether the flow is controlled by the entrance or exit part of the culvert. Figure 21 shows a sketch for culvert flow definition.

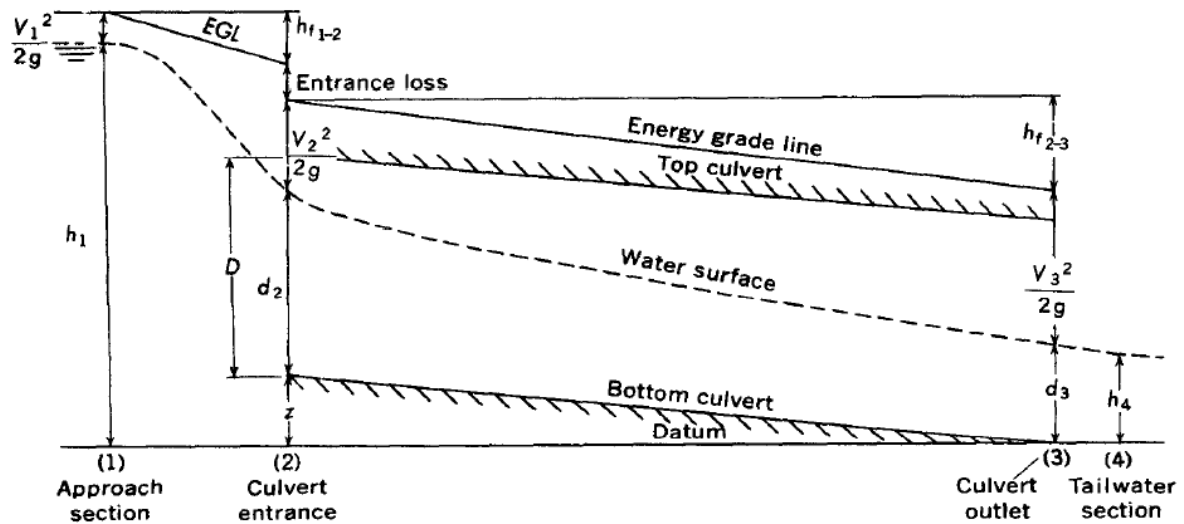


Figure 21 - Sketch of general flow through a culvert (*Bodhaine, 1968*)

Z gives the elevation of the culvert entrance relative to the datum through the culvert exit. The gravitational constant is given by g and h_{f12} is the head loss due to friction from the approach section to the culvert entrance; h_{f23} is the head loss due to friction inside the culvert; d_2 and d_3 are the water depths at the culvert entrance and exit, respectively; V_1 , V_2 and V_3 are the velocities at the approach section, culvert entrance and culvert exit, respectively; D is the culvert height; and h_1 and h_4 are the water depths upstream and downstream of the culvert structure.

The six types of flow classified by *Bodhaine* (1968) depend on the water depths upstream and downstream of the culvert. Figure 22 gives a schematization of the different flow types made according to the equation for each type of flow. The different equations are presented below.

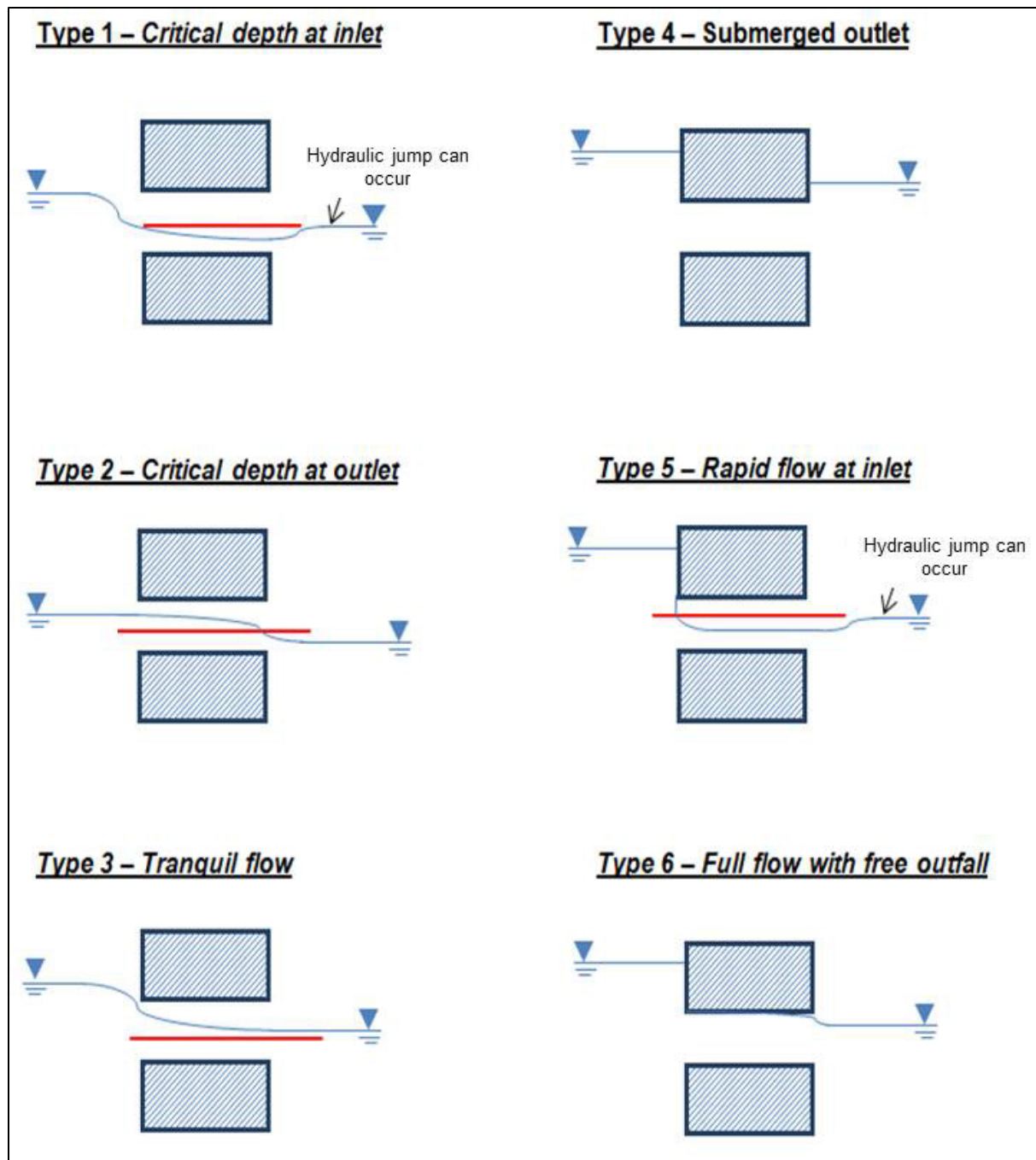


Figure 22 – Schematization of the 6 different types of flow that occur through culverts according to Bodhaine (1968). The red line represents the critical water depth.

Type 1 – Critical depth at inlet- supercritical flow inside the culvert

In flow type 1 the critical depth occurs at the entrance of the culvert and the flow is supercritical inside the culvert. The culvert slope (S_0) has to be greater than the critical slope (S_c) and the culvert flows partially full. For the Froude number $Fr=1$ (which is the case at the entrance section for a flow of type 1), the discharge coefficient is typically $C_D=0,95$. The discharge is then calculated according to the following formula:

$$Q = C_D A_c \sqrt{2g \left(h_1 - z - h_c - h_{f12} + \alpha \frac{V_1^2}{2g} \right)} \quad (5.1)$$

with: C_D the discharge coefficient
 A_c flow area at critical water depth
 g the gravitational constant
 h_1 upstream water depth
 z elevation of the culvert entrance
 h_c critical water depth
 h_{f12} head loss due to friction from the approach section to the culvert entrance
 α kinetic energy correction coefficient for the approach section¹
 V_1 average flow velocity at the approach section of the culvert

Type 2 – Critical depth at outlet – subcritical flow inside the culvert

In flow type 2 the flow is tranquil (i.e. subcritical) inside the culvert. The critical depth is located at the culvert outlet. The culvert flows partially full. Here the culvert slope S_0 has to be smaller than the critical slope S_c . The discharge coefficient is similar to flow type 1. The discharge is then calculated according to the following formula:

$$Q = C_D A_c \sqrt{2g * \left(h_1 - h_c - h_{f12} - h_{f23} + \alpha \frac{V_1^2}{2g} \right)} \quad (5.2)$$

with: h_{f23} head loss due to friction inside the culvert

Type 3 – Tranquil flow – subcritical flow throughout the culvert

In flow type 3 the flow is subcritical throughout the culvert. There is no critical depth. The culvert flows partially full. Like flow types 1 and 2, the discharge coefficient varies in function of the Froude number, being typically between $C_D=0.82 - 0.95$. The discharge is calculated according to the following formula:

$$Q = C_D A_3 \sqrt{2g \left(h_1 - d_3 - h_{f12} - h_{f23} + \alpha \frac{V_1^2}{2g} \right)} \quad (5.3)$$

with: A_3 flow area at the culvert outlet
 d_3 water depth at the culvert outlet

¹ In hydraulic literature there is still some debate whether the momentum correction coefficient beta should not appear here instead of alpha.

Type 4 – Submerged inlet and outlet

In flow type 4 the culvert inlet and outlet are submerged. The culvert flows full. The discharge coefficient varies in function of the culvert geometry, ranging typically between $C_D=0.75$ and $C_D=0.95$. The discharge is calculated according to the following formula:

$$Q = C_D A_0 \sqrt{\frac{2g(h_1 - h_4)}{1 + 29C_D^2 n^2 L / R^{4/3}}} \quad (5.4)$$

with: A_0 flow area at the culvert entrance
 h_4 downstream water depth
 n Manning coefficient
 L length of the culvert
 R hydraulic radius

! Bodhaine (1968) uses Anglo-Saxon units. As a consequence, we must be careful when presenting the equations in this report that is written in SI units. In equation 5.4 here above the factor 29 is an artefact of the Anglo-Saxon units.

Type 5 – Rapid flow at inlet

In flow type 5, the flow is supercritical at the inlet to the culvert. The culvert flows partially full. Type 5 flow does not usually occur. When it does, the discharge coefficient is in general lower than the other types.

$$Q = C_D A_0 \sqrt{2g(h_1 - z)} \quad (5.5)$$

Type 6 – Full flow with free outfall

In flow type 6 the culvert flows full. The discharge coefficient is similar to the one obtained for the flow type 4. The discharge is calculated according to the following formula:

$$Q = C_D A_0 \sqrt{2g(h_1 - d_3 - h_{f23})} \quad (5.6)$$

The indices of the different variables might seem a bit confusing, but it was chosen to take the formulas from Bodhaine as they were and not to make any changes to them. Bodhaine differentiated between these six flow type based on conditions given in the Table 12.

Table 12. Conditions for each type of flow defined by *Bodhaine* (1968).

Type 1	$\frac{h_1 - z}{D} < 1.5$	$\frac{h_4}{h_c} < 1.0$	$S_0 > S_c$
Type 2	$\frac{h_1 - z}{D} < 1.5$	$\frac{h_4}{h_c} < 1.0$	$S_0 < S_c$
Type 3	$\frac{h_1 - z}{D} < 1.5$	$\frac{h_4}{D} \leq 1.0$	
Type 4	$\frac{h_1 - z}{D} > 1.0$	$\frac{h_4}{D} > 1.0$	
Type 5	$\frac{h_1 - z}{D} \geq 1.5$	$\frac{h_4}{D} \leq 1.0$	
Type 6	$\frac{h_1 - z}{D} \geq 1.5$	$\frac{h_4}{D} \leq 1.0$	

All the different culvert geometric features will affect the presence of culvert flow type 5 or 6. To differentiate the two types, *Bodhaine* (1968) suggests to use the relations given in Figure 23, in which r denotes the radius of curvature of a rounded entrance and w is the measure of a chamfered entrance. First a curve corresponding to r/D , w/D is chosen. Then a point is set using the value for the culvert slope and for the ratio between the culvert length and height. If the point lies to the right of the chosen curve, the flow is type 6, if it lies to the left of the curve, the flow is type 5.

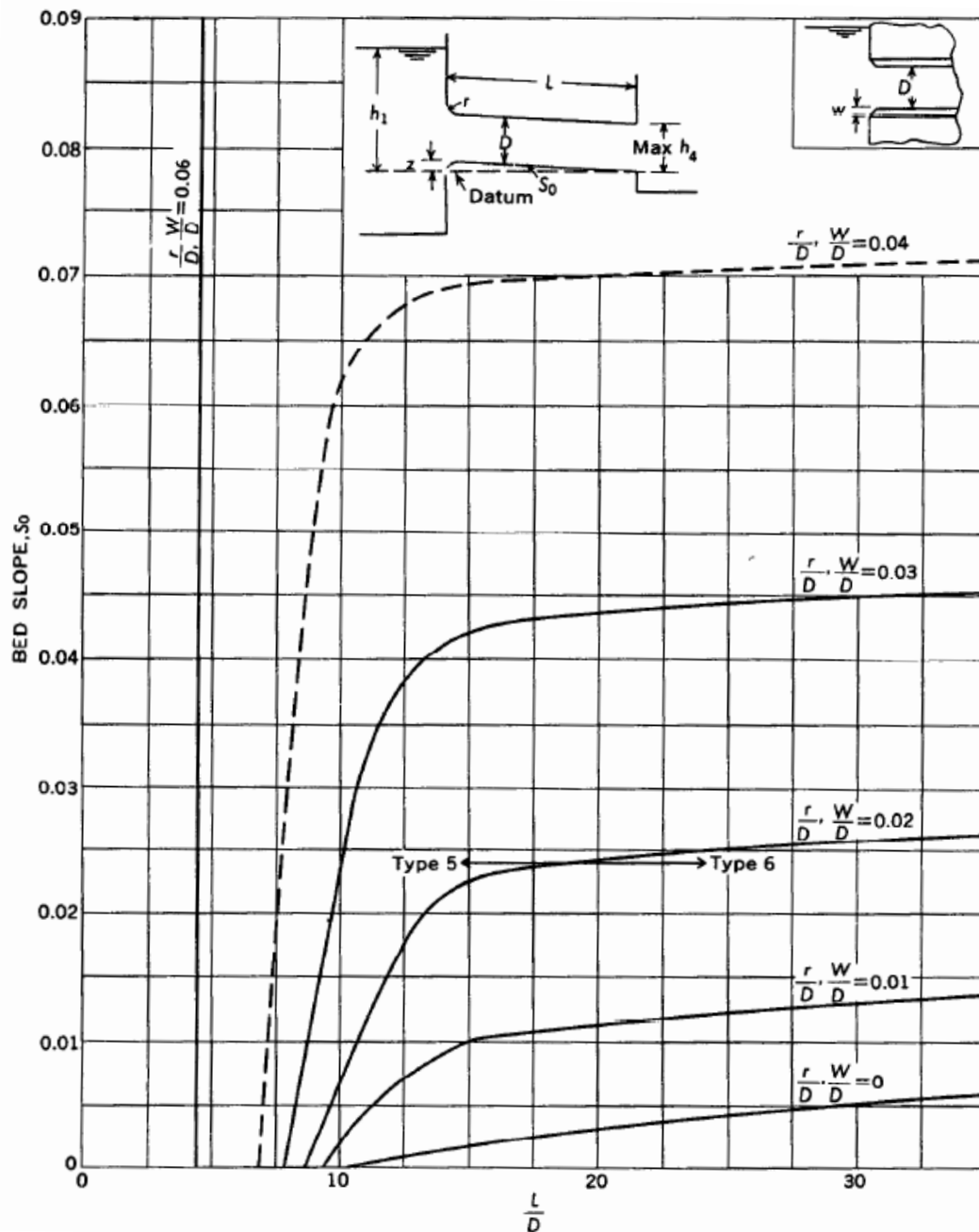


Figure 23 - Criterion for classifying flow types 5 and 6 in concrete box or pipe culverts with square, rounded, or bevelled entrances, either with or without wingwalls (Bodhaine, 1968)

The head loss coefficients are subject of different studies made in laboratory experiments. A number of authors have arrived to different values or empirical relationships for the head loss coefficients. For instance, Bodhaine (1968) suggests different values for the discharge coefficient (C_D) for each type of flow and depending on a number of geomtric features from the culvert. The discharge coefficients can vary from 0.39 to 0.98. another example is Carlier (1972) who proposes a non-dimensional coefficient μ , also refereed to as a discharge coefficient, that for hydraulic structures made of only one culvert can be written as follows:

$$\mu = \frac{1}{\sqrt{C_1 + C_2 + C_3}} \quad (5.7)$$

with: C_1 head loss coefficient at the entrance of the hydraulic structure
 C_2 head loss coefficient in the hydraulic structure
 C_3 head loss coefficient at the exit of the hydraulic structure

If the general expression for the discharge $Q = \mu A \sqrt{2g\Delta H}$ proposed by *Carlier* (1972) is compared with the formulas given by *Bodhaine* (1968), it can be seen that the non-dimensional discharge coefficient (μ), incorporates both the effect of the discharge coefficient (C_D) and the continuous and local head losses. ΔH is the head for each type of flow.

6.3. Culvert simulation in existing codes

6.3.1. TELEMAT-2D

TELEMAT-2D is a two dimensional hydrodynamic model that solves the depth-integrated shallow water equations. It makes part of the TELEMAT-MASCARET numerical platform. In the latest release of TELEMAT-MASCARET model (version v6p3), TELEMAT-2D gives the possibility of modelling hydraulic structures, such as bridges, discharges under a dike or tubes in which free-surface or pressurized flows may occur during the total simulation time. This is done by a couple of points between which flow may occur in function of the water levels in the river and in the polder. Here, a subroutine to model this kind of structures is called and four different flow conditions are taken into account.

Each kind of flow has its own type of discharge calculation. The different equations implemented in TELEMAT-2D to code the calculated discharges are dependent on the flow regime and follow *Carlier* (1972). From the discharges, velocities are deduced and subsequently taken into account as source terms both in the continuity and momentum equations.

The critical water depth (h_c) is approximated as $h_c \approx 2/3 h_1$ (*Carlier*, 1972). Figure 24 presents the different variables used to calculate the discharges. S_1 and S_2 are the upstream and downstream water elevations, respectively, z_1 and z_2 the downstream and upstream culvert bottom elevations, D the culvert height and $h_1 = S_1 - z_1$ and $h_2 = S_2 - z_2$ the upstream and downstream water depths, respectively.

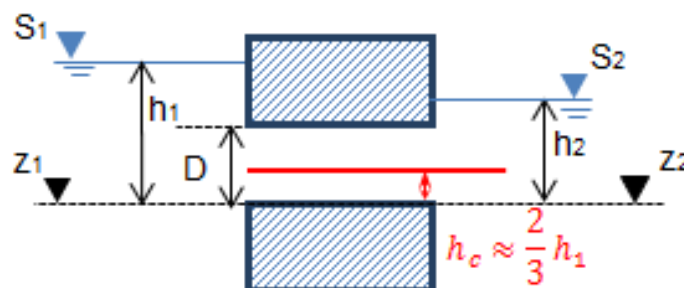


Figure 24 - Representation of the different variables used to calculate the discharges for each type of flow

The equations coded in TELEMAC-2D are described below. Between brackets the corresponding flow type according to *Bodhaine* (1968) is given.

- Free surface flow equations:
 - o Submerged weir (Bodhaine type 3)

$$Q = \mu(S_2 - z_2)W\sqrt{2g(S_1 - S_2)} = (S_2 - z_2)W\sqrt{\frac{2g(S_1 - S_2)}{C_1 + C_2 + C_3}} \quad (5.8)$$

- o Unsubmerged weir (Bodhaine type 2)

$$Q = 0.385W\sqrt{2g}(S_1 - z_1)^{3/2} \quad (5.9)$$

- Pressurised flow equations:

- o Submerged orifice law (Bodhaine type 4)

$$Q = \mu DW\sqrt{2g(S_1 - S_2)} = DW\sqrt{\frac{2g(S_1 - S_2)}{C_1 + C_2 + C_3}} \quad (5.10)$$

- o Unsubmerged orifice law

$$Q = \mu DW\sqrt{2g(S_1 - S_2)} = DW\sqrt{\frac{2g(S_1 - S_2)}{C_1 + C_2}} \quad (5.11)$$

TELEMAC-2D gives the user the possibility of assigning different values for C_1 , C_2 and C_3 . The flow direction is imposed, e.g., the user can specify if the flow is going in only one direction or in both directions and in which direction. The keyword CLP specifies this behaviour.

CLP=0, flow is allowed in both directions;

CLP=1, flow is only allowed from section 1 to section 2

CLP=2, flow is only allowed from section 2 to section 1

CLP=3, no flow allowed.

A relaxation parameter (θ) is introduced such that the discharge is calculated in an explicit, implicit, or semi-implicit way. If $\theta = 1$ the calculation of the discharge is explicit while if $\theta = 0$ the discharge calculation is implicit:

$$Q^n = \theta Q^n + (1 - \theta)Q^{n-1} \quad (5.12)$$

Relaxation gives slower convergence speed to get the final solution but smooths some instabilities. If the solution does not converge because of instabilities, the coefficient can be lowered.

6.3.2. DELFT 3D

The three-dimensional hydrodynamic model DELFT 3D has also implemented the culvert functionality through inlet/outlet couplings. The equations are based on the work presented by *Bodhaine* (1968) and are the following:

Type 2 – Critical depth at outlet

$$Q = \mu h_c W \sqrt{2g * ((S_1 - z) + h_c)} \quad (5.13)$$

with:

$$\mu = C_{D1} / \sqrt{1 + \left\{ \frac{2gLn^2}{R^{4/3}} + C_v \right\} (C_{D1})^2 \left(\frac{h_c}{h_s} \right)^2}; \quad (5.14)$$

$$h_s = 0.5h_c + 0.5(S_1 - z); \quad (5.15)$$

$$R = \frac{h_s W}{2h_s + W} \quad (5.16)$$

Type 3 – Tranquil flow

$$Q = \mu(S_2 - z_2)W\sqrt{2g(S_1 - S_2)} \quad (5.17)$$

with:

$$\mu = C_{D1} / \sqrt{1 + \left\{ \frac{2gLn^2}{R^{4/3}} + C_v \right\} (C_{D1})^2 \left(\frac{(S_2 - z_2)}{h_s} \right)^2}; \quad (5.18)$$

$$h_s = 0.5(S_1 - z) + 0.5(S_2 - z); \quad (5.19)$$

$$R = \frac{h_s W}{2h_s + W} \quad (5.20)$$

Type 4 – Submerged outlet

$$Q = \mu DW\sqrt{2g(S_1 - S_2)} \quad (5.21)$$

with:

$$\mu = C_{D2} / \sqrt{1 + \left\{ \frac{2gLn^2}{R^{4/3}} + C_v \right\} C_{D2}^2}; \quad (5.22)$$

$$h_s = D; \quad (5.23)$$

$$R = \frac{h_s W}{2h_s + 2W} \quad (5.24)$$

Type 5 – Rapid flow at inlet

$$Q = \mu DW\sqrt{2gh_1} \quad (5.25)$$

with:

$$\mu = C_{D3}; \quad (5.26)$$

$$h_s = D; \quad (5.27)$$

$$R = \frac{h_s W}{2h_s + 2W} \quad (5.28)$$

Type 6 – Full flow with free outfall

$$Q = \mu DW \sqrt{2g(S_1 - (z_2 + D))} \quad (5.29)$$

with:

$$\mu = C_{D2} / \sqrt{1 + \left\{ \frac{2gLn^2}{R^{4/3}} + C_v \right\} C_{D2}^2}; \quad (5.30)$$

$$h_s = D; \quad (5.31)$$

$$R = \frac{h_s W}{2h_s + 2W} \quad (5.32)$$

The head loss coefficient expressions were obtained from experimental studies made at Flanders Hydraulics Research.

The discharge coefficient, C_D , is dependent of each type of flow, being the same for types (1,) 2 and 3 (C_{D1}), then for types 4 and 6 (C_{D2}) and finally for type 5 (C_{D3}). The conditions at which a certain type of flow occurs, are presented in Table 13.

Table 13. Conditions for each type of flow used in DELFT 3D

	$\frac{h_1}{D}$	$\frac{h_2}{D}$	h_2
Type 2	<1.5		$\leq h_c$
Type 3	<1.5	≤ 1.0	$> h_c$
Type 4	>1.0	> 1.0	
Type 5	≥ 1.5	≤ 1.0	$\leq h_c$
Type 6	≥ 1.5	≤ 1.0	$\geq h_c$

Note that in DELFT 3D, only culverts with a horizontal bottom are considered. As a consequence, only type 2 (mild slope) can occur and type 1 (steep slope) is not implemented.

6.3.3. MIKE 11

The one-dimensional Mike 11 model also takes the different types of flow through culverts into account. Nevertheless the solution technique differs from the one used in TELEMAC-2D and DELFT 3D, especially for downstream controlled flows (flow types 3 and 4).

Here some preliminary calculations are made based on relations between the discharge (Q) and water depths (h) established on the different characteristics of the culvert and flow type. The solution technique used in Mike 11 is obtained by replacing the momentum equation with an Q - h relationship or a Q assignment. The general momentum equation is given as follows:

$$\alpha_j h_{j-1}^{n+1} + \beta_j Q_j^{n+1} + \gamma_j h_{j+1}^{n+1} = \delta_j \quad (5.33)$$

where, α , β and γ depend on Q and h at time level n and Q on time level $n+1/2$.

When a zero flow condition is present, the momentum equation coefficients at the culvert are:

$$\alpha = 0, \quad \beta = 1, \quad \gamma = 0, \quad \delta = 0$$

When the flow is controlled by the downstream end, the discharge is a function of both downstream and upstream culvert water depths and therefore the Q - h cannot be *a priori* tabulated, and the calculations take place during a simulation. Below a list of the downstream controlled flows modelled by Mike 11 is given. The flow types that correspond to *Bodhaine* (1968) classification are referred to in bold.

The types of flow modelled are:

- Partially full inflow and outflow (**type 3**);
- Submerged inflow and partially full outflow
- Partially full inflow and submerged outflow;
- Fully submerged (**type 4**)

The coefficients for the momentum equations are calculated such that:

$$C_a = \frac{C_1}{A_{s1}^2} + \frac{C_2+C_b}{A_s^2} + \frac{C_3}{A_{s2}^2} - \frac{1}{A_1^2} + \frac{1}{A_2^2}; \quad (5.34)$$

$$\text{with:} \quad C_b = h_1 - h_2; \quad (5.35)$$

$$C_c = \text{sign}(C_a) \sqrt{\frac{2g}{|C_a|C_b}} \quad (5.36)$$

A_1 and A_2 are the inflow and outflow river cross-section areas, A_{s1} and A_{s2} are the culvert inflow and outflow cross-section areas and A_s is the average between the A_{s1} and A_{s2} . The matrix coefficients at the culvert become:

$$\alpha = -C_c, \quad \beta = 1, \quad \gamma = C_c, \quad \delta = 0$$

To calculate the head loss coefficients the following expressions are used:

$$C_1 = C_{in} \left(1 - \frac{A_{s1}}{A_1}\right) \quad (5.37)$$

$$C_3 = C_{out} \left(1 - \frac{A_{s2}}{A_2}\right)^2 \quad (5.38)$$

$$C_2 = \frac{2gLn^2}{R^{4/3}} \quad (5.39)$$

$$\Delta H_{loss} = \frac{Q^2}{2g} \left(\frac{C_1}{A_{s1}^2} + \frac{C_2+C_b}{A_s^2} + \frac{C_3}{A_{s2}^2} \right) \quad (5.40)$$

A_s is the mean cross-section area along the length of the culvert, A_{s2} the culvert outflow cross-section area, A_2 the outflow river cross-section area, A_{s1} culvert inflow cross-section area and A_1 the inflow river cross-section area. Typically $C_{in} = 0.5$ and $C_{out} = 1$. C_b is the bend head loss coefficient.

For partially full inflow and outflow (**type 3**), an iteration procedure is used to determine the inflow and outflow water levels in the culvert (h_{s1} , h_{s2}) and the hydraulic radius (R).

$$h_{s1} = S_1 - \frac{(1+C_1)(S_1-S_2)}{C_{as}A_{s1}^2} \quad (5.41)$$

$$h_{s2} = S_2 - \frac{(1-C_3)(S_1-S_2)}{C_{as}A_{s2}^2} \quad (5.42)$$

$$C_{as} = \frac{C_1}{A_{s1}^2} + \frac{C_2+C_b}{A_s^2} + \frac{C_3}{A_{s2}^2} \quad (5.43)$$

For submerged flow (**type 4**), A_s is calculated in the following way:

$$A_s = \frac{L_{full}}{L} A_{full} + \left(1 - \frac{L_{full}}{L}\right) + \frac{A_{full} + A_{s2}}{2} \quad (5.44)$$

L_{full} is the length of the culvert which is flowing full and $= L$, the total length.

When the flow is controlled by the upstream end, the flow is only dependent on the river side of the culvert. In order to reduce the computational cost a priori tabulated Q - h relationships are used to replace the momentum equations.

The types of flow modelled here are:

- Critical inflow (**type 1**);
- Partially full inflow and critical outflow (**type 2**)
- Submerged inflow and critical outflow (**type 5**)
- Orifice flow at inflow with free outflow (**type 6**)

For critical outflow the critical depth is assumed at the outflow and then a backwater analysis is made to find h_1 . The upstream water level is calculated based on the inflow water depth using the iteration procedure, Q - h relationship calculations.

When the flow is critical inflow or outflow (**type 1 and type 2**):

$$Q_c = \alpha_c A_c \sqrt{g \frac{A_c}{T}} \quad (5.45)$$

T is the flow width at the water surface and α_c a critical flow correction factor.

When the critical flow no longer occurs, the flow condition is either orifice flow or full culvert flow. The Q - h relationship continues to be constructed by calculating the discharge for increasing values of h_1 . Iteration procedures are also made for the orifice flow and the primed flow. For orifice flow at inflow (**type 5**), the discharge is calculated through:

$$Q = \alpha_c C_d DW \sqrt{2g(S_1 - z_1)} \quad (5.46)$$

For full culvert flow with free outflow (**type 6**) the discharge is given by:

$$Q = DW \sqrt{\frac{2g(S_1 - (z_2 + D))}{C_1 + C_2 + C_b + 1}} \quad (5.47)$$

To conclude this section Figure 25 gives a summary of the implementation of the culvert equation in the three different software packages: TELEMAC-2D, DELFT 3D and MIKE 11. The main difference between the new culvert functionality in TELEMAC-3D and the one already included in DELFT 3D is the way how the head loss coefficient is calculated. While in TELEMAC-3D, the *Carlier* (1972) reference was followed, in DELFT 3D they refer to experiments executed by Flanders Hydraulic Research. It is also clear that MIKE 11 uses a different approach to calculate for instance discharges for flow types 3 and 4.

TELEMAC-3D vs DELFT3D vs MIKE11

Type of flow	TELEMAC-3D	DELFT 3D	MIKE 11
Flow type 2	$Q = \mu h_c W \sqrt{2g * (S_1 - (z_2 + h_c))}$ $\mu = \frac{1}{\sqrt{C_1 + C_2 + C_3 + C_v + C_r}}$	$Q = \mu h_c W \sqrt{2g * (S_1 - (z_2 + h_c))}$ $\mu = C_{D1} / \sqrt{1 + \left\{ \frac{2gLn^2}{R^{4/3}} + C_v \right\} (C_{D1})^2 \left(\frac{h_c}{h_s} \right)^2}$	$Q_c = \alpha_c A_c \sqrt{\frac{A_c}{gT}}$
Flow type 3	$Q = \mu (S_2 - z_2) W \sqrt{2g(S_1 - S_2)}$ $\mu = \frac{1}{\sqrt{C_1 + C_2 + C_3 + C_v + C_r}}$	$Q = \mu (S_2 - z_2) W \sqrt{2g(S_1 - S_2)}$ $\mu = C_{D1} / \sqrt{1 + \left\{ \frac{2gLn^2}{R^{4/3}} + C_v \right\} (C_{D1})^2 \left(\frac{S_2 - z_2}{h_s} \right)^2}$	$\alpha_j h_j^{n+1} + \beta_j Q_j^{n+1} + \gamma_j h_j^{n+1} = \delta_j$ $\alpha = -C_c, \quad \beta = 1, \quad \gamma = C_c, \quad \delta = 0$
Flow type 4	$Q = \mu DW \sqrt{2g(S_1 - S_2)}$ $\mu = \frac{1}{\sqrt{C_1 + C_2 + C_3 + C_v + C_r}}$	$Q = \mu DW \sqrt{2g(S_1 - S_2)}$ $\mu = C_{D2} / \sqrt{1 + \left\{ \frac{2gLn^2}{R^{4/3}} + C_v \right\} C_{D2}^2}$	$\alpha_j h_j^{n+1} + \beta_j Q_j^{n+1} + \gamma_j h_j^{n+1} = \delta_j$ $\alpha = -C_c, \quad \beta = 1, \quad \gamma = C_c, \quad \delta = 0$
Flow type 5	$Q = \mu DW \sqrt{2g(S_1 - z_1)}$ $\mu = \frac{1}{\sqrt{\alpha_1^5 C_1 + \alpha_v^5 C_v + C_r}}$	$Q = \mu DW \sqrt{2g(S_1 - z_1)}$ $\mu = C_{D3}$	$Q = \mu DW \sqrt{2g(S_1 - z_1)}$ $\mu = \alpha_c C_D$
Flow type 6	$Q = \mu DW \sqrt{2g(S_1 - (z_2 + D))}$ $\mu = \frac{1}{\sqrt{C_1 + C_2 + C_3 + C_v + C_r}}$	$Q = \mu DW \sqrt{2g(S_1 - (z_2 + D))}$ $\mu = C_{D2} / \sqrt{1 + \left\{ \frac{2gLn^2}{R^{4/3}} + C_v \right\} C_{D2}^2}$	$Q = \mu DW \sqrt{2g(S_1 - (z_2 + D))}$ $\mu = \frac{1}{\sqrt{C_1 + C_2 + C_v + 1}}$

Figure 25 - Summary of the equations used in TELEMAC-2D, Delft 3D and MIKE 11 to deal with culverts

6.4. Proposed implementation in TELEMAC-3D

6.4.1. Culvert function

TELEMAC-3D solves the three-dimensional RANS equations. In the latest release of TELEMAC-3D (v6p3), hydraulic structures such as culverts or tubes were not included in the code and therefore it was needed to implement this feature in the hydrodynamic model.

Assuming the hydrostatic hypothesis, TELEMAC-3D solves the following equations:

$$\frac{\partial U}{\partial x} + \frac{\partial V}{\partial y} + \frac{\partial W}{\partial z} = 0 \quad (5.48)$$

$$\frac{\partial U}{\partial t} + U \frac{\partial U}{\partial x} + V \frac{\partial U}{\partial y} + W \frac{\partial U}{\partial z} = -g \frac{\partial \eta}{\partial x} + \nu \Delta(U) + F_x \quad (5.49)$$

$$\frac{\partial V}{\partial t} + U \frac{\partial V}{\partial x} + V \frac{\partial V}{\partial y} + W \frac{\partial V}{\partial z} = -g \frac{\partial \eta}{\partial y} + \nu \Delta(V) + F_y \quad (5.50)$$

$$\frac{\partial h}{\partial t} + \frac{\partial(uh)}{\partial x} + \frac{\partial(vh)}{\partial y} = 0 \quad (5.51)$$

(U, V, W) are the three components of the flow velocity, (u,v) are the depth integrated flow velocities, ν is the (horizontal eddy) viscosity coefficient and (F_x , F_y) represent the source and sink terms of the momentum equations.

The capability of the model to impose source/sink terms in the domain was useful to implement a culvert function. The inflow and outflow of a culvert then act as a couple of source/sink points (in the code, new terms are added to the righthand side of the depth integrated continuity equation (5.51)). For instance, when the flow is going from the river to the polder side, a source term is added on the side of the polder, i.e., a discharge is imposed on that point, and at the same time a sink term is put in the river with the symmetric value of that discharge (e.g. $Q_{\text{river}} = -Q_{\text{polder}}$). Following this method we make an important assumption: it is considered that the discharge occurs at the same time in the river and polder. This is in reality not true, but with output time steps of 10 minutes, this assumption is very reasonable.

New equations were then incorporated in the code in order to cover a wider range (relatively to what is currently implemented in TELEMAC-2D) of the flow conditions that exist through a culvert. The following equations, corresponding to each type of flow presented above, were implemented in TELEMAC-3D. They are based on the equations proposed in *Bodhaine* (1968) and similar to the ones incorporated in DELFT 3D model. The flow type 1 conditions were not incorporated since they only occur when the culvert slope is larger than the critical flow slope. This only happens in very rare occasions if the culvert slope is very steep.

Type 2 – Critical depth at outlet: $Q = \mu h_c W \sqrt{2g * (S_1 - (z_2 + h_c))} \quad (5.52)$

Type 3 – Tranquil flow: $Q = \mu (S_2 - z_2) W \sqrt{2g(S_1 - S_2)} \quad (5.53)$

Type 4 – Submerged outlet: $Q = \mu D W \sqrt{2g(S_1 - S_2)} \quad (5.54)$

Type 5 – Rapid flow at inlet: $Q = \mu D W \sqrt{2gh_1} \quad (5.55)$

Type 6 – Full flow with free outfall: $Q = \mu D W \sqrt{2g(S_1 - (z_2 + D))} \quad (5.56)$

The conditions for which each type of flow occurs are summarized in Table 14. To distinguish flow type 5 from flow type 6 a constant c is defined that is dependent on the culvert slope and the ratio w/D . Using Figure 23, the curve (w/D) is chosen and the point for which the value of the slope (S_0) encounters the curve will have as abscissa the value c . Then if $L/D < c$, flow type 5 occurs, otherwise it is flow type 6 that is used (Bodhaine, 1968).

Table 14. Conditions for each type of flow used in TELEMAC-3D

	$\frac{S_1 - z_1}{D}$	$\frac{S_2 - z_2}{D}$	$S_2 - z_2$	L/D
Type 2	< 1.5		$< h_c$	
Type 3	< 1.5	≤ 1.0	$> h_c$	
Type 4	> 1.0	> 1.0		
Type 5	≥ 1.5	≤ 1.0		$< c$
Type 6	≥ 1.5	≤ 1.0		$\geq c$

The equations presented above are written to describe flow conditions through a culvert system with a single pipe. Nevertheless, additional features are sometimes incorporated in the hydraulic structures, such as weirs in the vicinity of the culvert entrance or exit. Such combined structures have to be taken into account. Then the geometric features of the culvert presented in Figure 24 are modified (Figure 26). We assume that an equivalent culvert bottom elevation should be used, which replaces both the bottom elevations z_1 and z_2 in the formulas described above. The equivalent bottom culvert elevation is taken equal to the mean between z_1 and z_2 . The diameter used in the equations will be the one corresponding to the entrance of the culvert, i.e., regarding Figure 26, if the flow goes from left to the right D will be replaced by D_1 and on the opposite direction, the value D_2 will be used. For the start of the watering into the flooding area we still use the z_1 and z_2 bottom elevations so that the start and end of watering through the culverts remains as close as possible to reality. By applying our assumptions as mentioned above, we are aware that that we overestimate the culverts frictional head losses and we do not account for the local head losses due to the presence of the weir exactly. These kind of complicated structures are difficult to model and we wanted to keep it as simple as possible. The user can tune the calculated discharges with many coefficients and we assume this will give us enough room to take into account the above mentioned considerations.

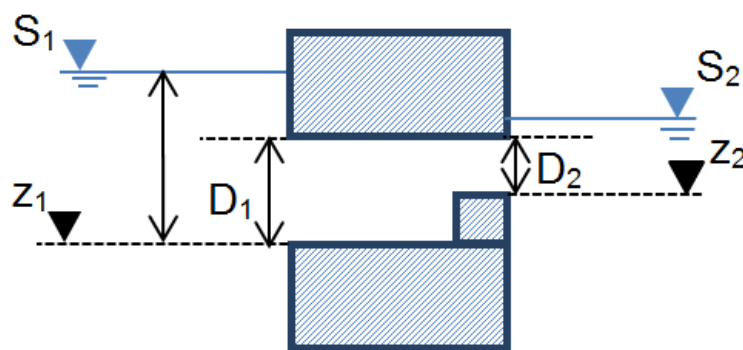


Figure 26 - Representation of the different variables used to calculate the discharges for each type of flow

The head loss coefficient (μ) was adapted from the one calculated in TELEMAC-2D, based on *Carlier* (1972) and is used as main head loss coefficient. Structures that caused additional head loss, like valves, grilles (trash screens) or pillars were added in the calculation of this main coefficient. In this way these additional features that can be present in culvert structures of different geometric configurations are taken into account and contribute to the flexibility of the implementation of many types of culvert structures.

The head loss due to singularities can be obtained by the general relation (*Lencastre*, 1961 and *Carlier*, 1972):

$$\Delta H = C \frac{U^2}{2g} \text{ or } U = \mu \sqrt{2g\Delta H} \quad (5.57)$$

with: $\mu = \frac{1}{\sqrt{C}}$ (5.58)

The coefficient C represents the sum of the different contributions for the head loss due to singularities:

$$C = C_1 + C_p + C_2 + C_3 + C_v + C_T \quad (5.59)$$

The different contributions to this head loss coefficient C will be discussed separately and in detail here below.

C_1

C_1 represents the head loss due to the contraction of the flow at the entrance of the hydraulic structure. Usually it is equal to 0.5 (Figure 27). Usually, there is an abrupt contraction at the culvert entrance that will cause a head loss due to the deceleration of the flow immediately after the vena contracta.

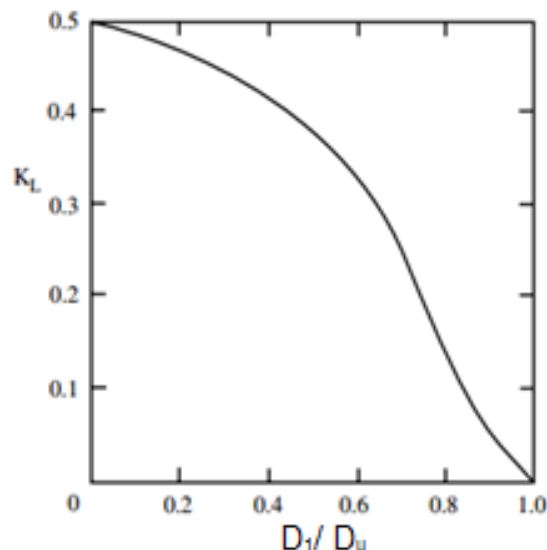


Figure 27 - Local loss coefficient for a sudden contraction as a function of diameter ratio between the diameter after the contraction (D_1) and before the contraction D_u (*Bruce et al.*, 2000)

Already in the past, *Bodhaine* (1968) noticed that the discharge coefficient (C_D) for type 5 flow had to be lowered comparatively with the other flow types. It seems that the calculated discharge tends to be overestimated when the default equation is applied. In order to take into account that effect, a correction coefficient (α_1^5) is applied to C_1 when type 5 flow occurs, such that:

$$\Delta H_{1,5} = \alpha_{1,5} C_1 \frac{U^2}{2g} \quad (5.60)$$

Comparing with the values proposed by *Bodhaine* (1968), $4 \leq \alpha_{1,5} \leq 10$.

C_p

Sometimes at the entrance of culverts the flow is divided into two sections caused by two entrance boxes instead of one but then the flow converges into a single culvert pipe. In other words a kind of pillar is dividing the flow at the entrance. This causes additional head loss and is taken into account. Following *Carlier* (1972) the head loss through parallel pillars is given by:

$$\Delta H_p = C_p \frac{U^2}{2g} \quad (5.61)$$

where $C_p = \beta \left(\frac{L_p}{b}\right)^{4/3} \sin \theta$ represents the head loss coefficient due to the presence of pillars. L_p is the thickness of the pillars, b the distance between two consecutive pillars and β a coefficient dependent on cross-sectional area of the pillar. According to *Carlier* (1972) β will be 2,42 for rectangular pillars and 1,67 for rounded pillars. Theta stands for the angle of the pillar with the horizontal plane. In most cases this will be 90° and sin theta will be equal to 1.

C_2

C_2 represents the head loss coefficient due to the friction in the structure and is expressed by (*Lencastre*, 1972):

$$\Delta H_2 = C_2 \frac{U^2}{2g} = \frac{2gLn^2}{R^{4/3}} \frac{U^2}{2g} \quad (5.62)$$

where L is the length of the structure, n the Manning Strickler coefficient of the structure and R the wet cross-sectional area in the structure calculated in the code for each type of flow. Table 15 presents the expressions for the calculation of R , following what was done in the DELFT 3D model. Here an assumption is made when calculating the hydraulic radius since the code does not make any kind of backwater analysis to get the precise water depths that occur in the culvert (like Mike 11 does).

Table 15. Different parameters for each type of flow to calculate the hydraulic radius in TELEMAC-3D

Type of flow	h_s	R
Type 2	$0.5h_c + 0.5(S_1 - z)$	$R = \frac{h_s W}{2h_s + W}$
Type 3	$0.5(S_1 - z_1) + 0.5(S_2 - z_2)$	
Type 4	D	$R = \frac{h_s W}{2h_s + 2W}$
Type 5		
Type 6		

C_3

C_3 is the head loss coefficient due to expansion of the flow exiting the culvert. It can be given by (Lencastre, 1961):

$$\Delta H_3 = \left(1 - \frac{A_s}{A_{s2}}\right)^2 \frac{U^2}{2g} = C_3 \frac{U^2}{2g} \quad (5.63)$$

where A_s and A_{s2} are the sections in and at the downstream part of the structure. Usually C_3 is equal to unity for a sudden enlargement.

C_v

C_v is the head loss coefficient due to the presence of a valve. The head loss due to valves (ΔH_v) can also be estimated:

$$\Delta H_v = C_v \frac{U^2}{2g} \quad (5.64)$$

where C_v depends on the type of valve and the degree of opening. For a flap gate valve (rotating around to hinges at its upper edge), some values were obtained experimentally, and they depend on the opening of the valve (Bruce *et al.*, 2000):

Table 16. Values for the head loss coefficient depending on the opening of a gate valve

	C_v
Wide open	0.2
$\frac{3}{4}$ open	1.
$\frac{1}{2}$ open	5.6
$\frac{1}{4}$ open	17

Again, a correction coefficient ($\alpha_{v,5}$) is applied to the head loss coefficient due to a valve in order to take into account the increase of the head loss when type 5 flow occurs (Eq. 4.12). Through a number of laboratory experiences at Flanders Hydraulics Research (IMDC Report 613_9_1), it can be seen that when type 5 flow occurs, there is a greater influence of having a valve: the associated head loss coefficient is in general much higher than for the other types of flow. Please note that the variable *Alfa* in Figure 28 it is not the same as $\alpha_{v,5}$. Figure 28 is given here just to show the influence of the valve in the different types of flow.

$$\Delta H_{v,5} = \alpha_{v,5} C_v \frac{U^2}{2g} \quad (5.65)$$

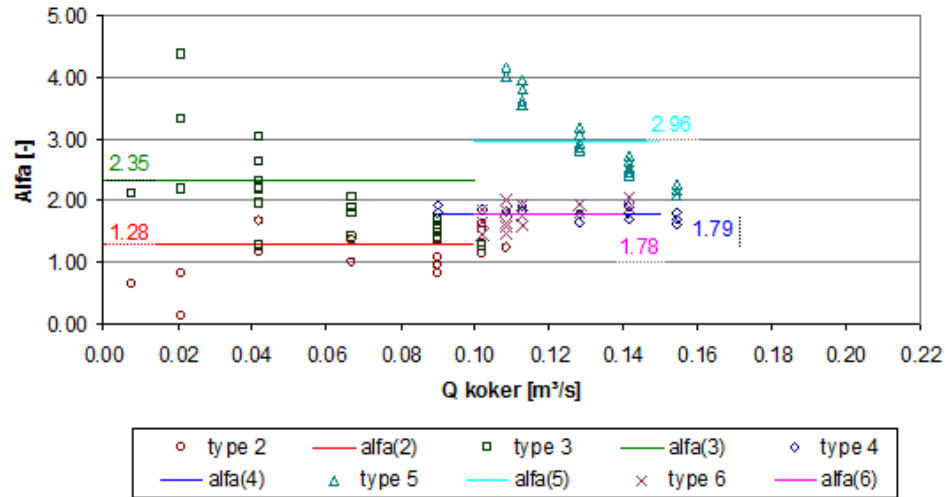


Figure 28 - Discharge coefficient (Alfa) due to the presence of open valves for each type of flow (source: IMDC Report 613_9_1)

C_T

Trash screens are usually present at the inlet of culverts to prevent garbage from entering or blocking the culvert. The head loss due to trash screens (ΔH_t) can be estimated by its relationship with the velocity head through the net flow area. A number of expressions were obtained in the past by several authors. We use the expression given by the U.S. Bureau of Reclamation (1987):

$$\Delta H_t = (1.45 - 0.45A_t - A_t^2) \frac{U^2}{2g} = C_t \frac{U^2}{2g} \quad (5.66)$$

where $A_t = \frac{A_{net}}{A_{gross}}$ gives the ratio of net flow area to gross rack area. U is the net flow velocity. The value for C_t can vary between $C_t = 0$ (for $A_t = 1$, equivalent to not having any trash screens) to approximately $C_t = 1.4$ (for $A_t = 0$, for which the net flow area is negligible small compared to the gross rack area).

6.4.2. Transport of tracers through culverts

TELEMAC-3D gives the possibility of taking into account passive or active tracers in the model domain. The following equation describing the evolution of tracer concentration (T) is solved:

$$\frac{\partial T}{\partial t} + U \frac{\partial T}{\partial x} + V \frac{\partial T}{\partial y} + W \frac{\partial T}{\partial z} = v_t \Delta(T) + Q' \quad (5.67)$$

The tracer diffusion coefficient is given by ν_t and Q' represents the source terms for tracers.

With the implementation of the culvert functionality, some modifications had to be done in the code such that it would be possible to model the passage of the tracer through the culvert structure. Following the same idea implemented to model the flow through culverts, the concentration of the tracer in the model domain is assigned to source and sink terms for tracers (Q'). When the flow goes from the river to the polder side, there is a source point in the polder with a tracer concentration equal to the one in the river. At the same time in the river there is a sink term with the same tracer concentration. The opposite happens when the flow goes from the polder to the river. Please note that it is the tracer concentration (kg/m^3) that is assigned to Q' and not the tracer concentration per second. In its structure, Telemac-3D deals with that concentration and associates it to the discharge and volume of fluid at the source terms.

In order to take into account the transport of tracers in the model the user has only to specify in the steering file the keywords relative to the tracers.

6.4.3. Telemac-3D input files (.cas file and .txt file) and the implemented code

In order to take culverts into account in TELEMAC-3D, the user has to define in the steering file two new keywords:

CULVERT

CULVERT DATA FILE

The number of culverts has to be assigned to the keyword CULVERT (please note that is the number of culverts and not the number of sources/sink terms: one culvert has two sink/source terms). The keyword CULVERT DATA FILE refers to a text file where the geometric characteristics and all head loss coefficients are given to be used by the code. The text file has to follow a strict structure of the input parameters in order for the software to read the right values for the right parameter. Here below an example is given:

X1 Y1 Z1 X2 Y2 Z2 CE1 CE2 CS1 CS2 CV C56 CV5 C5 CT W D1 D2 N L CLP

data culvert 1 ...

data culvert 2 ...

...

The index number 1 refers to the river side and the index 2 refers to the polder side. X, Y and Z correspond to the coordinates of the source/sink terms in the river side and in the polder that represent the beginning and end of the culvert. CE1, CE2 and CS1, CS2 are the head loss coefficients for the inlet and outlet sluice entrance (C_1) and exit (C_3), respectively. CV refers to the head loss coefficient due to the presence of a valve (C_v) and CT is the head loss coefficient due to the presence of trash screens (C_t). C56 (c) is the constant used to differentiate flow types 5 and 6. C5 and CV5 represent correction coefficients to C1 and to CV coefficients due to the occurrence of the type 5 flow. W is the width of the sluice, D1 and D2 the height of the culvert at the river and polder side, N is the Manning Strickler's coefficient and L the length of the culvert. Following what was done in TELEMAC-2D, the flow direction is also imposed through the keyword CLP and a relaxation parameter (keyword RELAXB) is incorporated in the code. This relaxation parameter will give a weight for the calculation of a weighted average between the discharge calculated at the current time step and the discharge calculated in the previous time step. The relaxation parameters gives the weight to the current time step (value between 0 and 1).

With respect to the code, the following changes were made:

- A new sub-routine was created: **t3d_culvert.f** (full code in Appendix 6) where the discharge for the different kinds of flows is calculated.
- The main subroutine **telemac3d.f** had to be changed in order to call **t3d_culvert.f** and take into account the transport of tracers through the culvert.
- **lecdon_telemac3d.f** and **telemac3d.dico** were also changed to include the new keywords (CULVERT and CULVERT DATA FILE)

The subroutines shown in the appendix correspond to the version installed in the branch balloonfish (revision **#5484**).

IMPORTANT: Please note that if the culvert functionality is used, it is not possible to impose external sources/sink terms. This will be possible from version TELEMAC V7P1, in the subversion balloonfish.

6.5. Testcase 1: Simplified model

6.5.1. Model setup

In this simplified model we want to check and test how the different parameters in the culvert subroutine influence the discharges through the culverts. Therefore we use a simple computational grid, with dimensions of 145 m x 400 m, with a resolution of 10 m both in x and y directions (Figure 29). Five horizontal layers were used in the vertical direction. On the river side (upper part of the domain) the elevation was set to -2.5 m and on the polder side (lower part) the elevation was set to 0 m. In the limit of the river side, where boundary conditions are imposed, a lower bottom elevation (-12 m TAW, i.e. the blue area in Figure 29) was used in order to avoid high velocities and make it more stable. A dyke separates the river from the FCA.

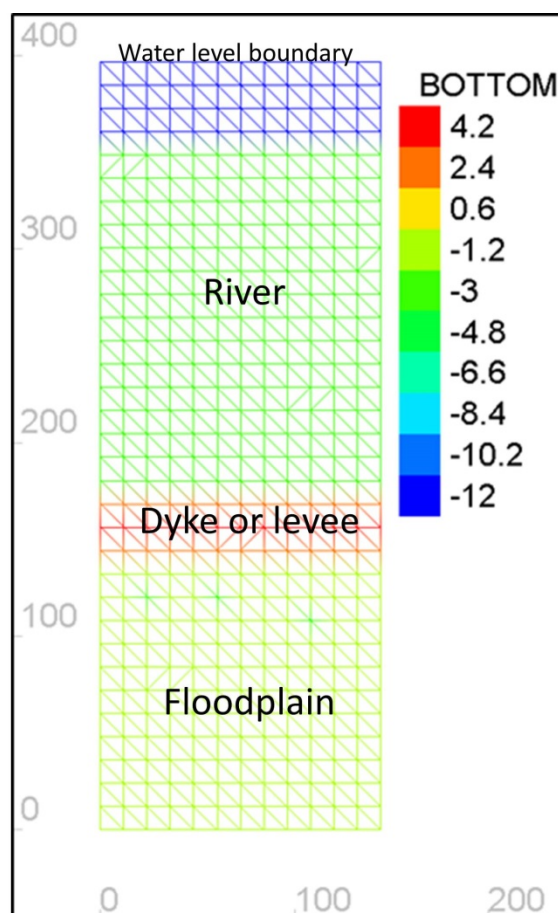


Figure 29 - 2D computational grid used for the simplified model

Two inlet and one outlet culverts were imposed in the model domain. The first inlet sluice is located at $(x=24\text{ m}, y=193\text{ m})$ and $(x=24\text{ m}, y=120\text{ m})$ while the second inlet sluice is located at $(x=60\text{ m}, y=180\text{ m})$ and $(x=60\text{ m}, y=120\text{ m})$. The outlet sluice is defined by the two points $(x=108\text{ m}, y=180\text{ m})$ and $(x=108\text{ m}, y=120\text{ m})$. The geometric characteristics of the culverts are presented in Table 17.

Table 17. Geometric features of the inlet and outlet sluices

	Inlet sluice	Outlet sluice
Number of culverts	2	1
Culvert width (m)	1	1.5
Culvert height (m)	1	1
Culvert length (m)	13	40
Level of culvert floor (m TAW)	0.5	0.1

At the upper side of the domain, water levels were imposed as boundary condition during a 13 h period. The time step was set to 1 second. The input file given to the hydrodynamic model to take into account the culverts is presented on Table 18. Regarding the head loss coefficients at the entrance and exit of the inlet and outlet sluices typical values, found in the literature (Lencastre, 1961) were imposed ($CE1=CE2=0.5$; $CS1=CS2=1$). It is considered that for the reference run (Ref Run) there are no valves or trash screens in the structure ($CV=0$; $CT=0$). The coefficient $C56$,

used to differentiate flow types 5 and 6 is set to $C56=10$, since it is considered that the culvert barrel slope is zero and that $w/D=0$. A correction coefficient has to be applied for flow type 5: $C5=6$, to obtain, approximately, the same value that Bohdaine (1968) suggests for the discharge coefficient.

Based on values found in the literature (Bodhaine, 1968), a value of $n = 0.015$ (typical value for concrete in smooth conditions) was assigned for the Manning Strickler parameter inside the culvert.

Table 18. Chosen values for the reference run

	CE1	CE2	CS1	CS2	CV	CT	C56	CV5	C5	W	D1	D2	N	L	CLP
Inlet1	0.5	0.5	1	1	0	0	10	0	6	1	1	1	0.015	13	1
Inlet2	0.5	0.5	1	1	0	0	10	0	6	1	1	1	0.015	13	1
Outlet	0.5	0.5	1	1	0	0	10	0	6	1.5	1	1	0.015	40	2

6.5.2. Results reference run

A first simulation (Run1) was made with the setup described above. When analysing the mass balance at the end of the calculation, it could be seen that there was a big mass loss in the domain. The mass conservation was found to be problematic everytime the water depth for the sink and source nodes was close to zero. This is probably related to the fact of assigning sources in the bottom of the domain (first horizontal level of the mesh). They should be assigned at least at the second horizontal plane. Therefore the bottom elevation of the sources/sinks nodes was lowered so these points would always have a positive water depth (kind of swimming pools) (We found later that sinks and sources take their water not only from the assigned node but also from the neighbouring nodes of this node). In reality these structures have also at the outlet of the culverts a lowered bottom elevation due to the intense scour of the water leaving the culverts. A new simulation was run and was kept as the reference run (Ref Run).

In Table 19 the values of the mass balance obtained by the model are displayed for the two different runs. It can be seen that there is a great improvement in the mass conservation when it is ensured that the nodes, where the sources are imposed, always have an amount of water (Ref Run). The mass loss is defined as the initial mass minus the final mass minus the mass leaving the domain.

Table 19. Mass balance for water

WATER (m³)	Run1	Ref Run
INITIAL MASS	138003.30	139305.30
FINAL MASS	126979.50	128714.10
MASS LEAVING THE DOMAIN	-10937.20	10591.14
MASS LOSS	86.6	-0.1261480E-04

The general flow patterns in the computational domain for two different time steps are given in Figure 30. When the water level in the river is higher than in the polder (left side of Figure 30), the two inlet culverts start to work (it can be observed that the flow arrows are directed outwards in the polder side). On the other hand, when the water level in the river is lower than the water level in the polder (right panel), the outlet culvert becomes active (here the velocity arrows are converging into the outlet culvert; right side of Figure 30).

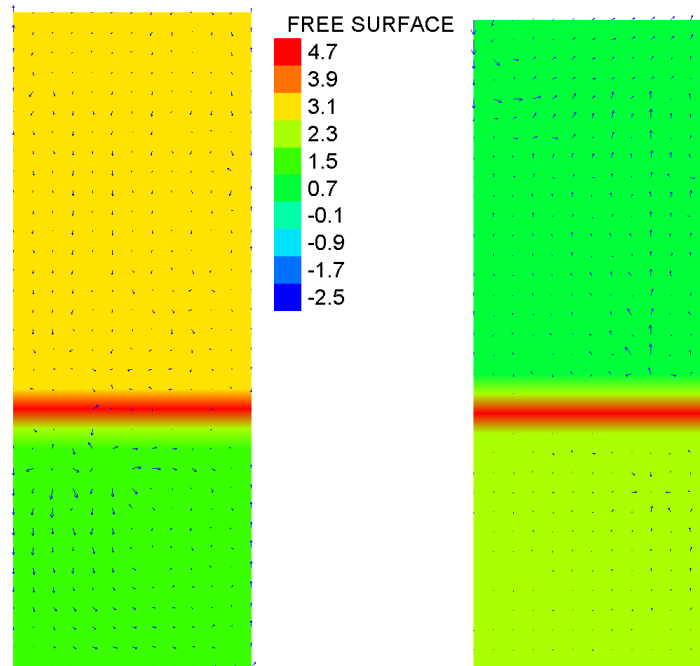


Figure 30 - Flow patterns when the free surface level (m) is higher in the upper part than the lower part of the domain at time t=4h (on the left side) and the opposite case at t=8h (on the right side)

In Figure 31, from the modelled water level at the river side (blue line), there is a flood tide period of 5h followed by a ebb tide period. In response to that, the mean water level in the polder (red line) increases just after the peak of the high tide and then starts to decrease when the tide is lower.

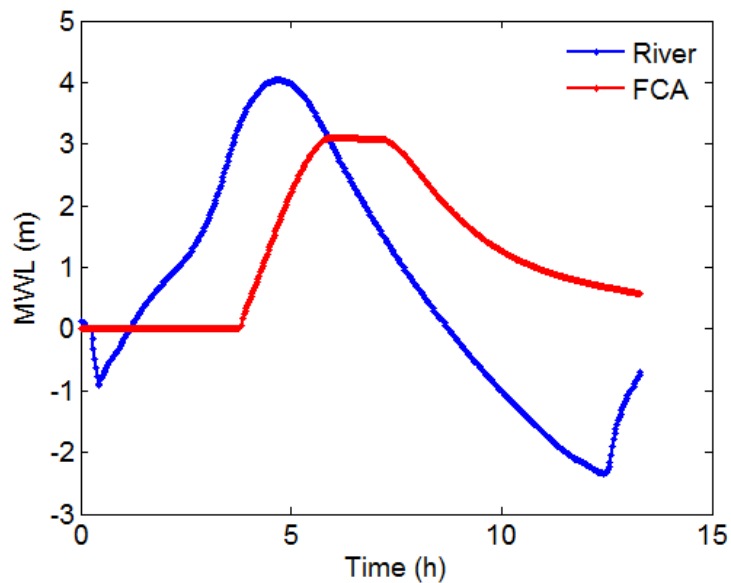


Figure 31 - Mean water levels (MWL) modelled by TELEMAC-3D in the river (blue line) and in the Flood Control Area (FCA) (red line)

Figure 32 shows that the inlet sluice starts to work around $t = 2$ h, which is the time at which the mean water level in the river (Figure 31) reaches the level of the inlet sluice ($z = 0.5$ m). For these inlet culverts no flow was allowed from the polder back towards the river (by setting the keyword $CLP=1$) and therefore no negative discharge values are present. In reality these kind of inlet culverts can transport a part of the water back to the river if the water level in the polder reaches the appropriate level.

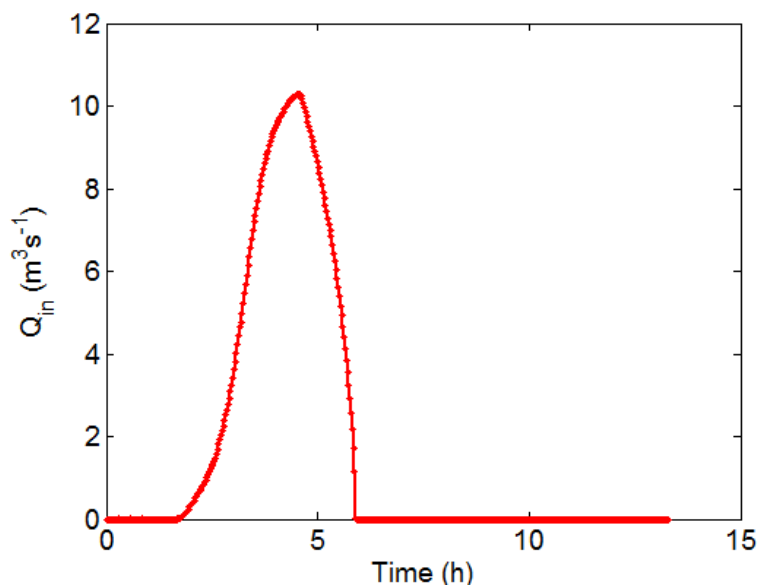


Figure 32 - Evolution in time of the inlet sluice discharge

Figure 33 shows that the outlet sluice becomes active around time $t = 7$ h, corresponding to the moment that the water level in the river drops below the water level in the polder.

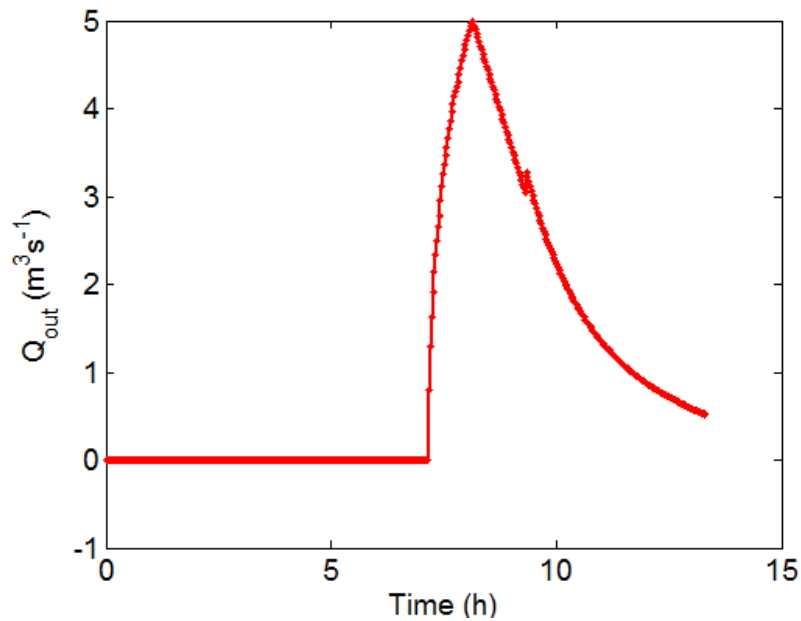


Figure 33 - Outlet culvert discharges with two locations for the inlet sluices (Ref Run)

6.5.3. Small scale parameter testing

A first test showed that for this simple test case it didn't matter if both inlet culverts were set on the same nodes in the model or were given separate nodes. The discharge results and thus water levels in the polder were very similar.

A second test was done to see the difference in discharges when flow type 5 is present or not and the effect of the correction coefficient for flow type five (C_5). Figure 34 shows the results of the comparison between the Reference run (Ref Run) in which the inlet sluice length is 13 m and therefore there is no flow type 5 and another simulation in which the length of the inlet sluice was decreased to 9 m inducing flow type 5. When $C_5 = 1$, i.e., the correction coefficient is not taken into account, there is a discontinuity of the inlet discharge when flow type 5 occurs (pink line in Figure 34). When $C_5=6$ (blue line in Figure 34) the evolution of the inlet discharge is smoother.

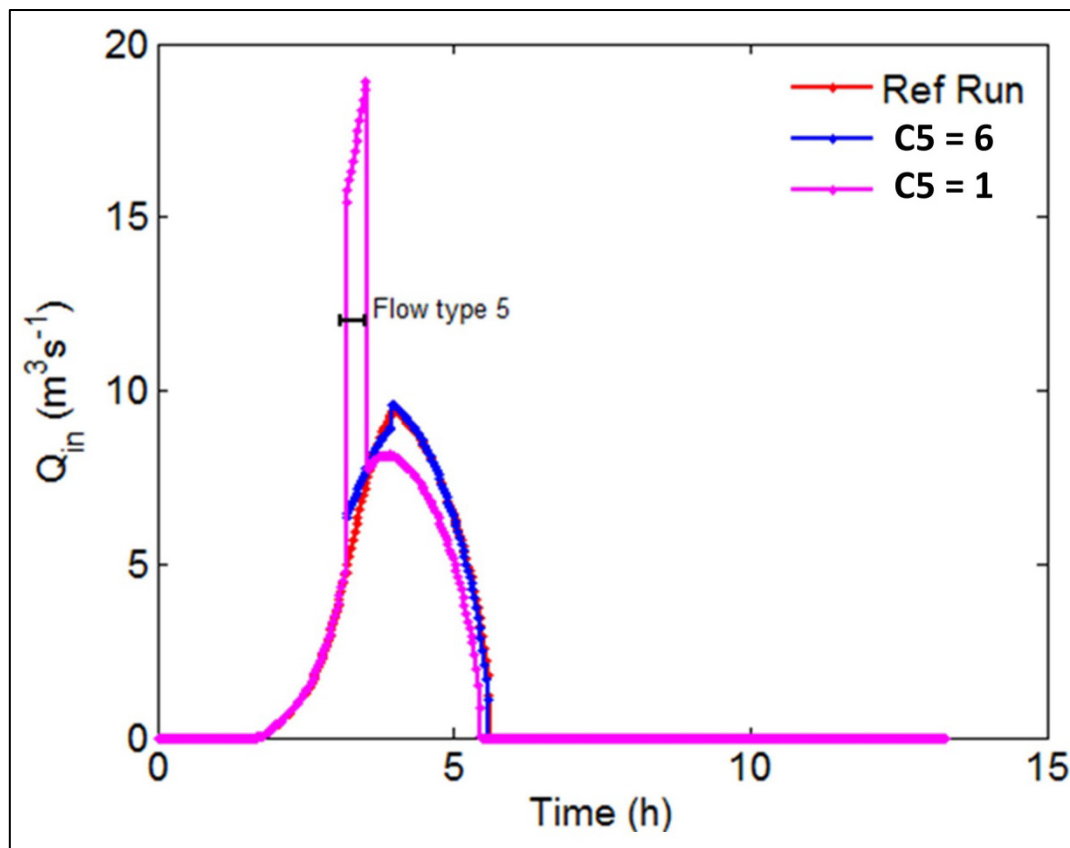


Figure 34 – Influence of the correction coefficient for flow type 5 (C15) on the inlet discharges

A third test was done to see the effect of the presence of a non-return-valve. The valve was assumed to be present at the outlet of the outlet culvert (like it would be in reality). Different values for the keyword C_v can be given, being dependent on the degree of valve opening (Table 16). Furthermore, when a valve is considered, a correction coefficient has to be applied when flow type 5 occurs. For this correction coefficient the value of $CV5=1.5$ was chosen to take into account the 50% increase, approximately, that occurs when this type of flow is present. Figure 35 shows the model results for water levels and outlet culvert discharges when no valve is present (red line = Ref Run) and when the valve only opens $\frac{1}{4}$. As expected if the head loss coefficient due to the valve increases, the outlet discharge will decrease (lower panel). As a consequence, the mean water level in the FCA will decrease much slower (upper panel).

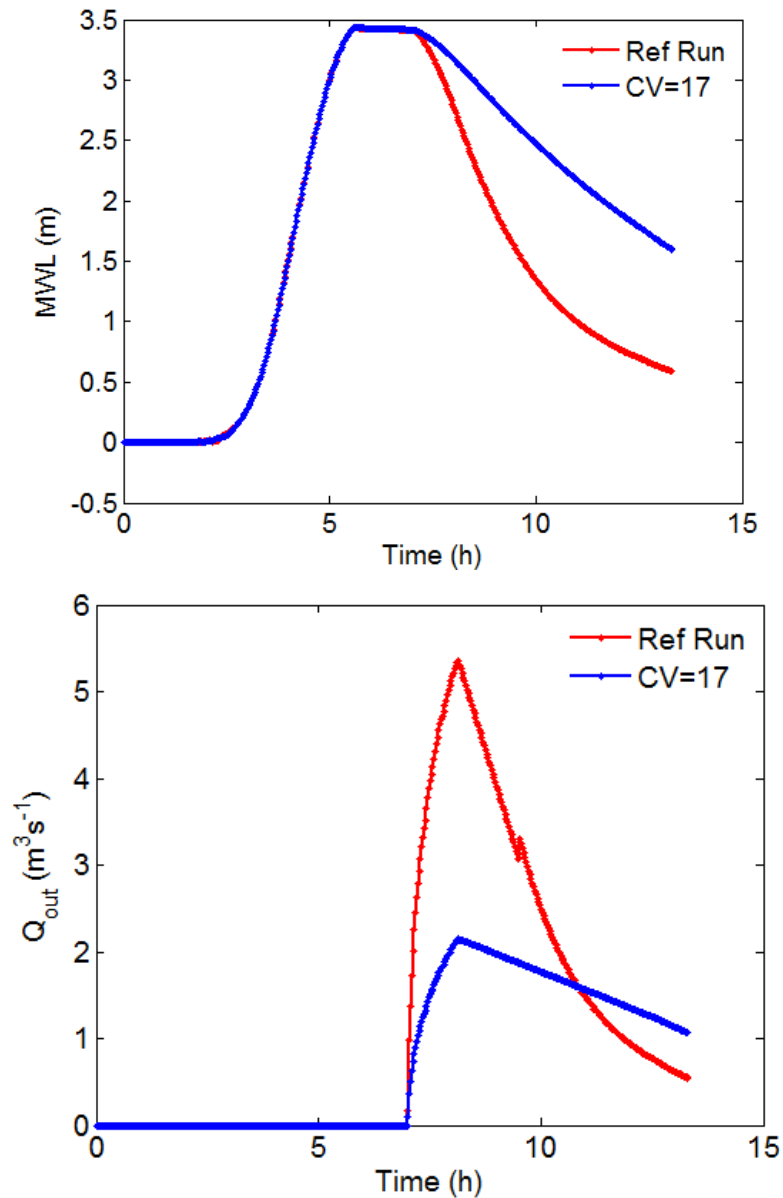


Figure 35 - Comparison of modelled mean water levels (upper panel) and outlet discharges (lower panel) between the reference run ($C_v=0$) and a different simulation with $C_v=17$

For test cases like Lippenbroek and Bergenmeersen the value for the head loss coefficient for the valve will be chosen $C_v=1$, according to Table 16. In the framework of project 15_034 Bergenmeersen, the opening angle of the non return valve of Bergenmeersen was measured for a 13 hour period. From the results (given in Figure 36) we can conclude that the valve opens easily $\frac{3}{4}$ confirming our choice for $C_v=1$ according to Table 16.

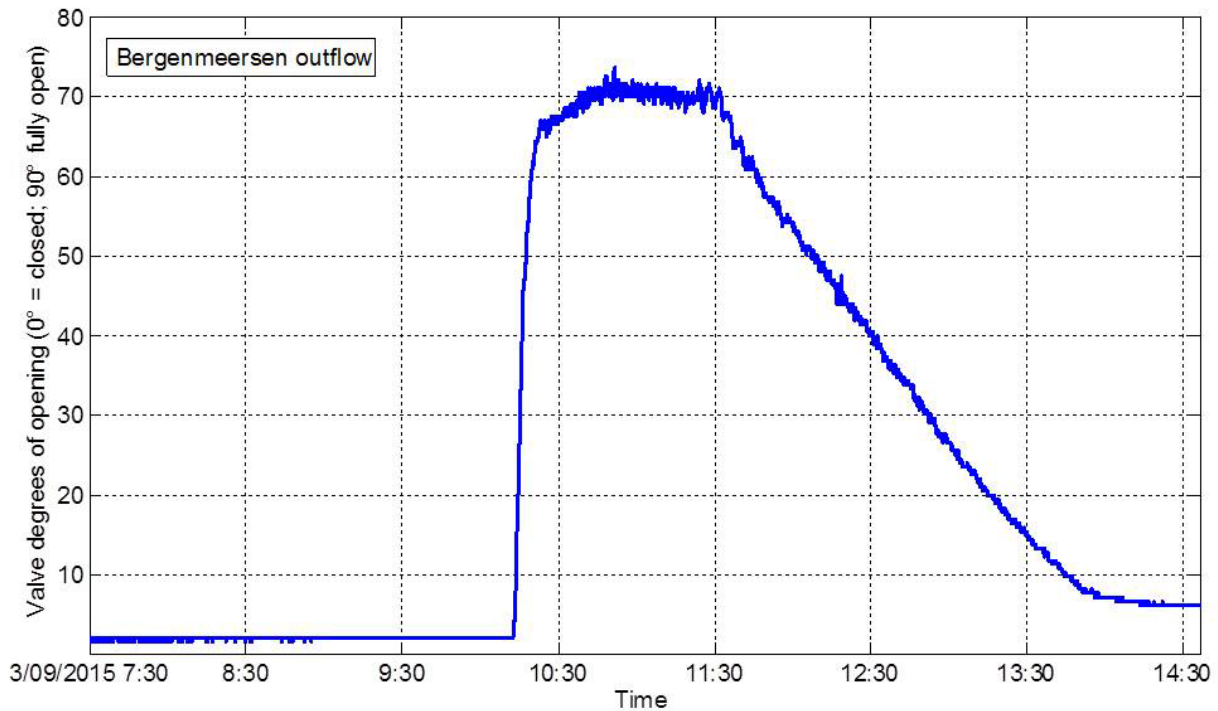


Figure 36 – Measurement of the opening angle of the non-return-valve of the outlet culverts of CRT Bergenmeersen. The measurement was done in the framework of projects 15_034 at a 13 hour measurement on the 3rd of September 2015.

A final test included trash screens or grilles in front of the inlet and outlet culvert. The head loss coefficient that has to be taken into account for this kind of structure can be calculated using expression (5.66). Figure 37 shows that when considering the trash screens the head loss coefficient is higher and therefore the outlet and inlet discharges lower. Increasing the ratio between the net flow area and the gross rack area, the head loss coefficient is decreased.

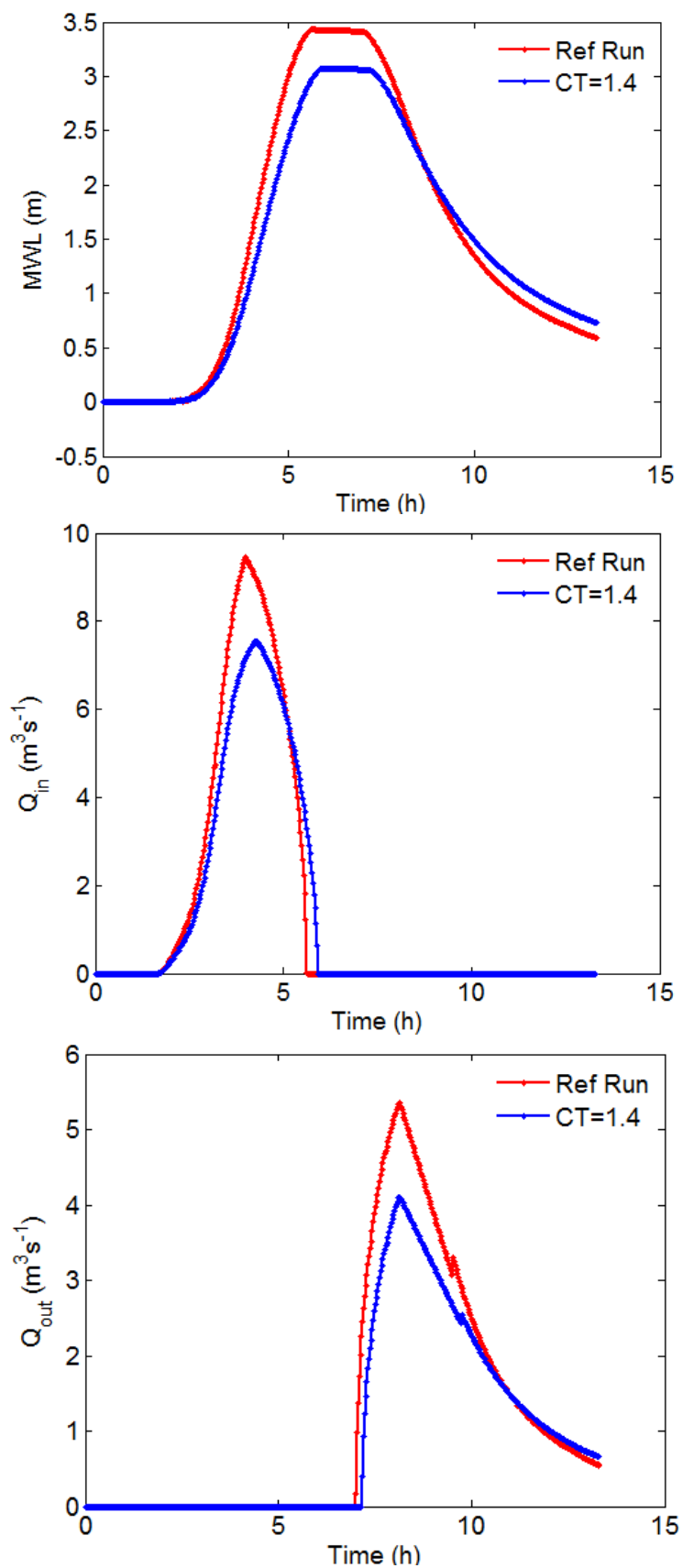


Figure 37 - Comparison of modelled mean water levels (upper panel) and outlet discharges (lower panel) between the reference run ($C_T=0$) and a simulation with $C_T=1.4$

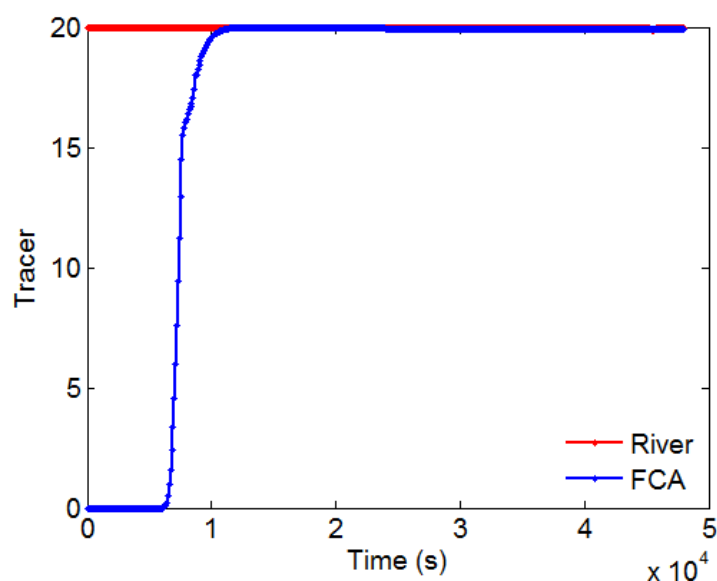


Figure 39 - Evolution of tracer concentration in the river (red line) and in the FCA (blue line). Run 2.

As the computational cost is an important parameter, an explicit scheme + MURD PSI scheme was tried since this scheme does not require the special treatment of negative water depths (Run 3). However, it required a much smaller time step for the model to run stable. Figure 40 shows the evolution of tracer concentration in time for this simulation (Run 3)

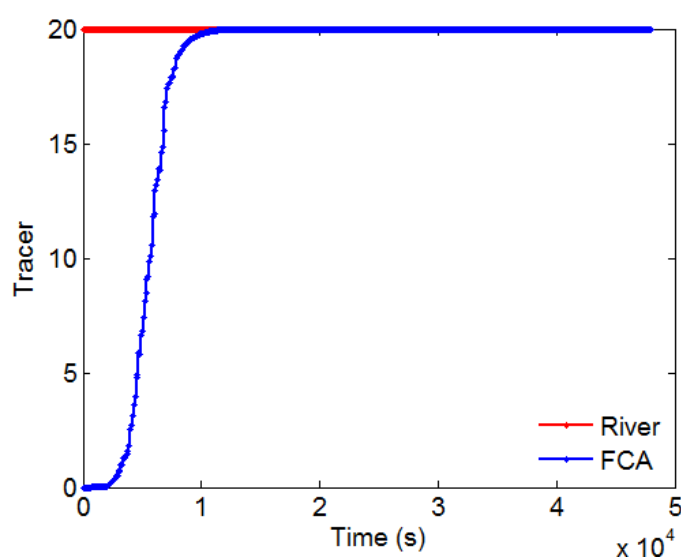


Figure 40 - Evolution of tracer concentration in time in the river (red line) and in the FCA (blue line). Run 3.

The mass balance at the end of each simulation gives us an idea about the conservation of mass of the water and the tracer. The mass balance of water is given in Table 20 for Run1 to 3. The mass balance of tracer is given in Table 21 for Run 1 to 3. From the mass conservation of water point of view Run 2 and 3 perform much better than Run 1. For the conservation of tracers Run 2 has the better results. Therefore we decided to use the parameters setting of Run 2 when simulating tracers while using culverts in the model. However these settings of Run 2 (i.e. an explicit scheme plus MURD (Multidimensional Upwind Residual Distribution) N scheme,

particularly created to deal with tidal flats and a special treatment of negative water depths) do not work properly in parallel. Therefore we inserted one line of code that will eliminate negative depths by clipping them. This has an effect on the conservation of mass of water, but this effect is rather small.

Table 20. Mass balance for water

WATER (m³)	Run1	Run2	Run3
INITIAL MASS	139305.30	139305.30	139305.30
FINAL MASS	126657.20	127088.90	125663.60
MASS LEAVING THE DOMAIN	12648.11	12216.33	13641.63
MASS LOSS	-0.1861179E-03	-0.7312337E-09	-0.4365575E-10

Table 21. Mass balance for tracers

TRACER (tracer unit*m³)	Run1	Run2	Run3
INITIAL MASS	2760067.	2760067.	2760067.
FINAL MASS	2053645.	2535572.	2501004.
MASS LEAVING THE DOMAIN	-271169.3	224487.1	263141.3
MASS LOSS	977591.1	8.268102	-4077.894

Below we show the numerical parameters (Keywords of the telemac steering file) common to all the runs:

```

SUPG OPTION = 0;0;0
IMPLICITATION FOR DEPTH          = 1.0
IMPLICITATION FOR VELOCITIES     = 1.0
IMPLICITATION FOR DIFFUSION      = 1.0
MASS-LUMPING FOR DEPTH           = 1
MASS-LUMPING FOR VELOCITIES      = 1
MASS-LUMPING FOR DIFFUSION       = 1
FREE SURFACE GRADIENT COMPATIBILITY = 1
SOLVER FOR DIFFUSION OF VELOCITIES = 7
SOLVER FOR DIFFUSION OF TRACERS = 7
SOLVER FOR PROPAGATION = 7
OPTION OF SOLVER FOR DIFFUSION OF VELOCITIES = 7
OPTION OF SOLVER FOR DIFFUSION OF TRACERS = 7
OPTION OF SOLVER FOR PROPAGATION = 7
MAXIMUM NUMBER OF ITERATIONS FOR DIFFUSION OF VELOCITIES = 100
MAXIMUM NUMBER OF ITERATIONS FOR DIFFUSION OF TRACERS = 5000
MAXIMUM NUMBER OF ITERATIONS FOR PROPAGATION = 500
ACCURACY FOR DIFFUSION OF VELOCITIES = 1.0E-08
ACCURACY FOR DIFFUSION OF TRACERS = 1.E-08
ACCURACY FOR PROPAGATION = 1.0E-08
MATRIX STORAGE                   = 3

```

6.6. Test case: Lippenbroek

6.6.1. Lippenbroek area

Lippenbroek is a pilot project of a flood protection area (FCA) with controlled reduced tide (CRT) entering this area to create tidal nature inside the FCA. The area is enclosed within so called Sigma dikes, which are dikes with a crest level of 8,35 m TAW according to Sigmaplan to guarantee safety against flooding. The polder is situated in the fresh water part of the river. A smaller dike separates the river from the polder and this one is 450 m long, in which 40 m were lowered (6.8 m TAW). This lower part of the dike allows a storm tide to flow over the dike, filling the polder and storing storm water at a crucial moment: extracting water from the river and this water will not propagate further upstream with the storm tide (This is the FCA function of the polder)

To create the CRT function three inlet sluices were built at a distance of 50 m from the outlet sluice, already existent in the area. Both in the river and in the polder sides, the inlet and outlet sluices are connected to the river and FCA respectively, by a creek. The characteristics of both inlet and outlet sluices are given in Table 22 and in Figure 41. The configuration of the inlet and outlet sluices as well the wooden weirs, that are located at the exit of the inlet sluices, are shown. Figure 42 shows the outlet entrance and exit in more detail. For further detailed information about the geometry of these structures and their functioning we refer to *De Mulder et al. (2013)*.

Table 22. Characteristics of the inlet and outlet sluices of FCA/CRT in Lippenbroek

	Inlet sluice	Outlet sluice
Number of culverts	3	1
Culvert width (m)	1	1.5
Culvert height (m)	1.9	1.5
Culvert length (m)	13	40
Level of culvert floor (m TAW)	4.0	1.5
Crest level of stop weirs (m TAW)	5.30 / 5.00 / 4.70	

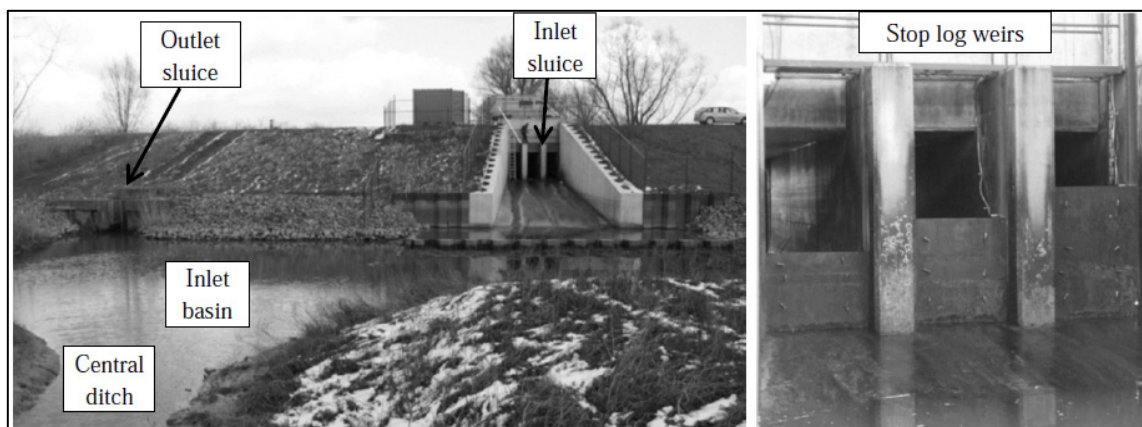


Figure 41 - Configuration of the inlet and outlet sluices (on the left) and detail of the weir structures in the inlet sluices (on the right) in Lippenbroek area (source: *De Mulder et al. (2013)*)



Figure 42 - Outlet entrance (on the left) and exit (on the right) in Lippebroek (Patrimoniumdatabank W&Z)

6.6.2. Lippebroek model setup

A mesh of the computational domain was built with a resolution of about 20 m in the Scheldt river and 10 m in the polder (Figure 43). In the vertical dimension, five sigma layers were imposed in the model (like the full scale Scaldis model). For this small test case this mesh resolution was sufficient. The bathymetry dated from 2010 and was delivered by the University of Antwerp. Bathymetry plays an important role in the obtained water levels in the polder.

Water levels obtained in the Tielrode station were imposed in the downstream part of the river as a boundary condition. The time period was chosen as such that it would coincide with measured water levels at and in Lippebroek. Four days in the beginning of April 2010 (1st to 4th April) was the simulation period.

Measurements were available for water levels in the polder and discharges in the outlet culvert of Lippebroek. The inlet discharges were estimated based on the measured water levels according to the following formula (Kindsvater & Carter, 1975):

$$Q_i = C_{e,i} \frac{2}{3} \sqrt{2g} W h_i^{1.5} \quad (5.68)$$

with the effective discharge coefficient according to Bos (1989):

$$C_{e,i} = 0.02 + 0.075 \frac{h_i}{p_i} \quad (5.69)$$

h_i is the water level above the spillway sill and p_i is the height of the spillway sill (m).

The time step was set to 6 seconds. The bottom friction was taken into account in the model through the Manning Strickler's parameter n . It was given a value of $n=0.02 \text{ s/m}^{1/3}$ to the river part and $n=0.07 \text{ s/m}^{1/3}$ to the polder area. These are typical values found in the literature for natural channels and floodplains (French, 1987). The model stability is usually sensitive to the choice of the horizontal viscosity. Here, it was set to $1 \text{ m}^2\text{s}^{-1}$ since the model was stable with this value. For the vertical turbulence viscosity, the choice is more subjective, being this value usually set between 10^{-3} and 10^{-1} . We chose a value of $0.01 \text{ m}^2\text{s}^{-1}$.

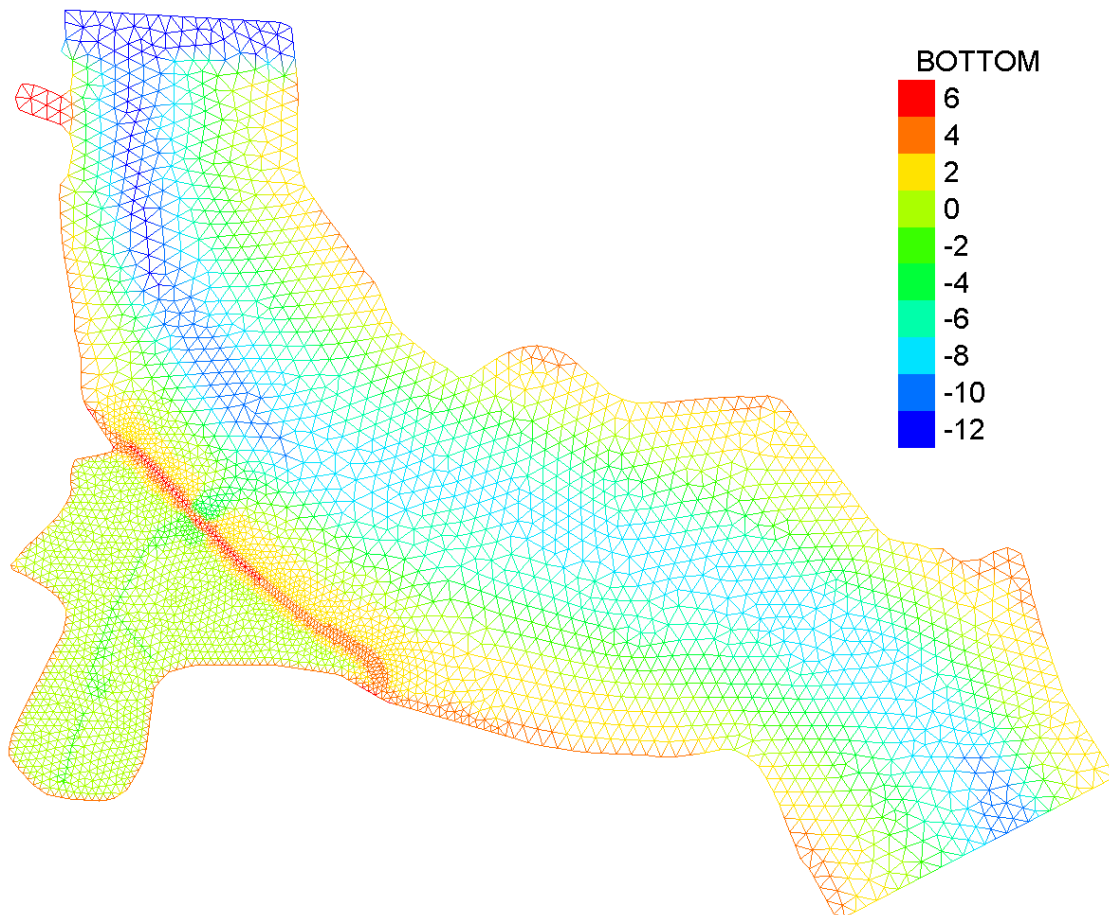


Figure 43 - Planview of the computational grid to model the FCA/CRT Lippenbroek.
The colour scale represents de bottom values in m NAP.

Table 23 presents the different parameters used to model the FCA with CRT in Lippenbroek. The different geometric features for the inlet and outlet sluices have to be given and the direction of the flow through the culvert has to be indicated. An outlet sluice only allows the flow to go from the polder to the river (CLP= 2) because it has a one-way valve, and an inlet sluice allows the flow to go in both directions (CLP=0), but water leaving the FCA through an inlet sluice will only occur when the FCA was completely filled in a storm situation.

The different head loss coefficients were assigned and some of them were used to calibrate the model based on experimental data. Regarding the head loss coefficients at the entrance and exit of the inlet and outlet sluices typical values, found in the literature (*Lencastre, 1961*) were imposed. It was considered that the valve at the outlet culvert was $\frac{3}{4}$ opened when flow was going out, which corresponds to a value of CV=1 (*Bruce et al., 2000*) and this value was confirmed by measurements on a valve in Bergenmeersen CRT (see previous simple test case). Trash screen coefficients were also considered, since these structures were present at the inlet and outlet culverts in Lippenbroek. Tree branches and leaves may hamper the free flow through these trash screens, explaining the need for this parameter.

Based on values found in the literature (*Bodhaine, 1968*), a value of $n=0.015 \text{ s/m}^{1/3}$ (typical value for concrete in smooth conditions) was assigned to the Manning Strickler parameter inside the culvert.

Table 23. Input .txt file for the culvert subroutine in TELEMAC-3D to model the Lippenbroek FCA/CRT

	CE1	CE2	CS1	CS2	CV	CT	C56	CV5	C5	W	D1	D2	N	L	CLP
Inlet1	0.5	0.5	1	1	0	0.8	10	0	6	1	1.9	0.6	0.015	13	0
Inlet2	0.5	0.5	1	1	0	0.8	10	0	6	1	1.9	0.9	0.015	13	0
Inlet3	0.5	0.5	1	1	0	0.8	10	0	6	1	1.9	1.2	0.015	13	0
Outlet	0.5	0.5	1	1	1	0.1	10	1.5	6	1.5	1.5	1.5	0.015	40	2

6.6.3. Lippenbroek Results

With the chosen head loss coefficients we can say that the model can reproduce the measured water levels inside Lippenbroek very well (Figure 44). Only the low water levels are not matching the measurements. The model water levels decrease further than the measured levels and the first phase of water entering the polder is slower in the model than in the measurements (Figure 44). It is however unclear if the difference in low water levels between model and measurements are caused by the head loss coefficients or by a bad representation of the bathymetry.

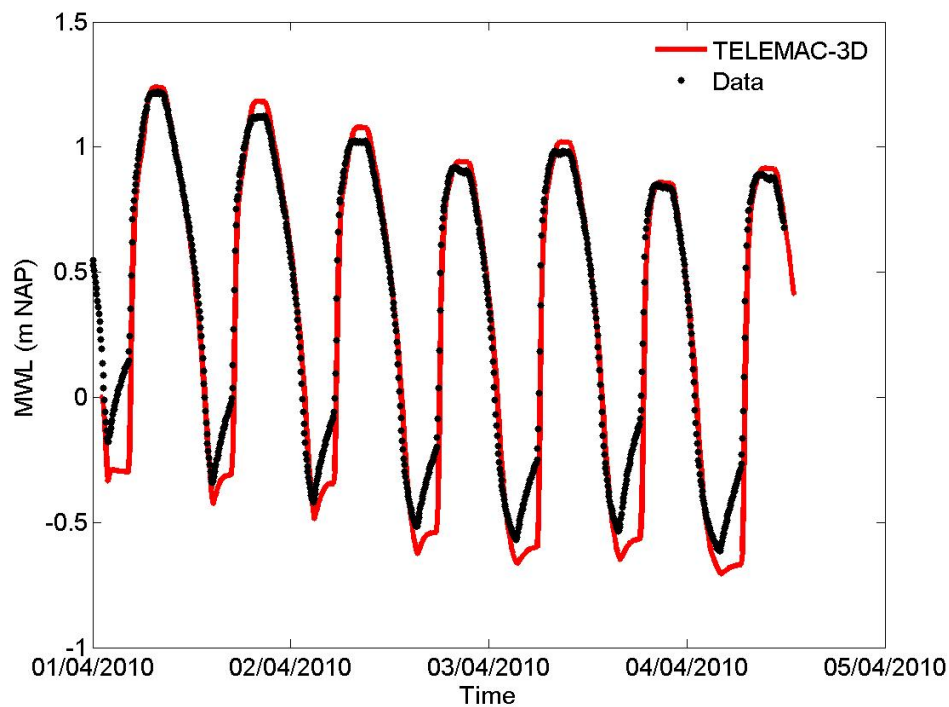


Figure 44 - Comparison of water level (m NAP) in the polder: numerical results versus measurements

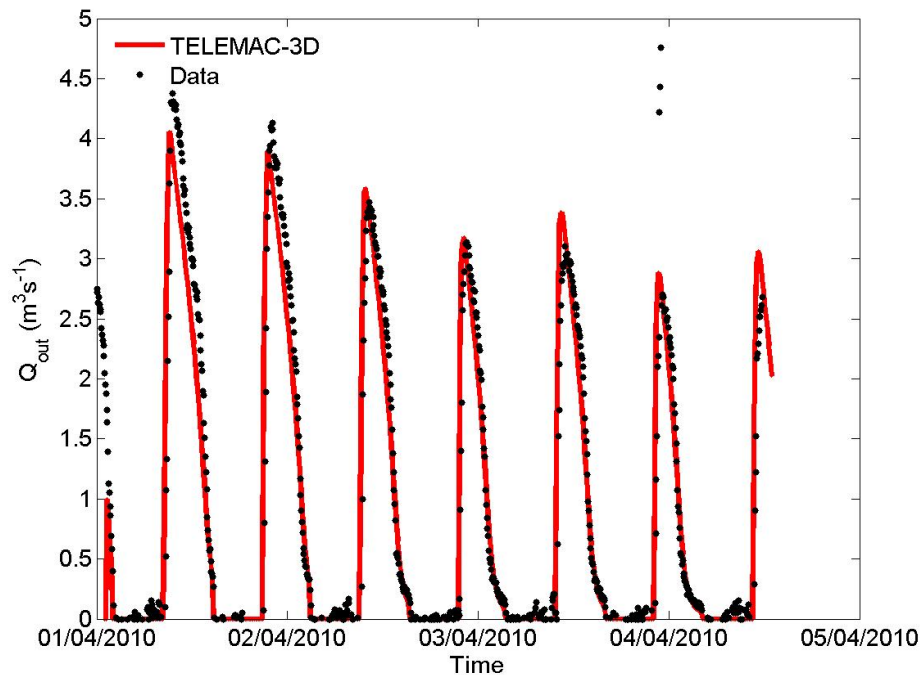


Figure 45 - Comparison between numerical results and measurements for outlet culvert discharges

The outlet discharges produced by the model coincide very well with the measured values (Figure 45). The inlet discharges were not measured, but calculated using an empirical formula (Eq. 5.68). Figure 46 compares these calculated discharges with the modeled ones. The model succeeds very well in reproducing the calculated discharges for the inlet culverts.

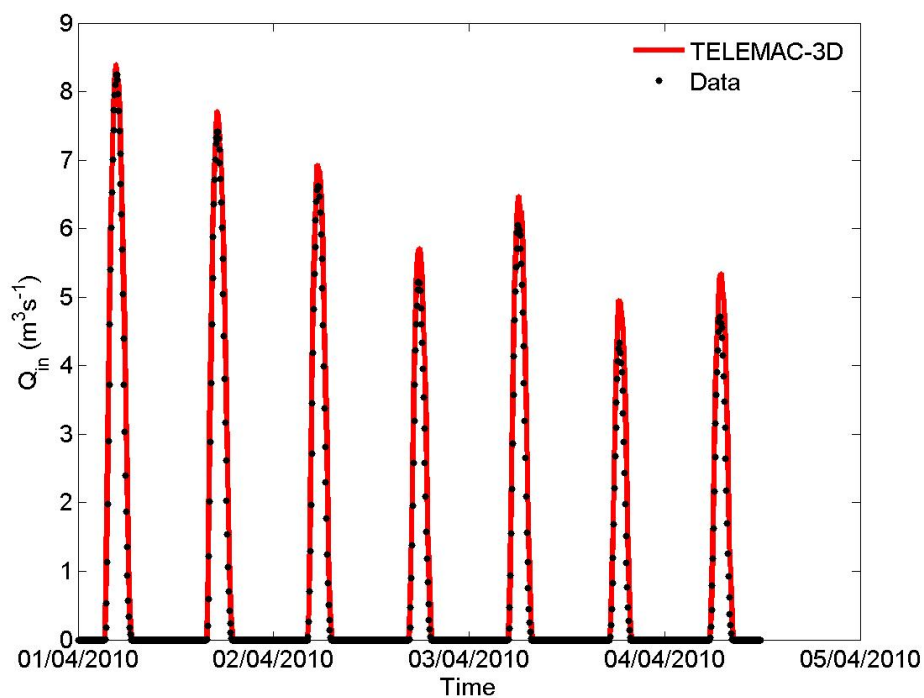


Figure 46 - Comparison between empirical formula and numerical results for inlet culvert discharges

In order to have a more quantitative analysis for the differences between numerical results and measured data, the normalized root mean square error value (Eq. 5.70) was applied to the different variables (Table 24).

$$\varphi_i = \sqrt{\frac{\sum_{i=1}^n (d_i - m_i)^2}{\sum_{i=1}^n d_i^2}} \quad (5.70)$$

The variable d_j represents the predicted values and m_j the measured values.

Table 24. Normalized root mean square error for the mean water level (MWL_error), outlet discharge (Q_{out_error}) and inlet discharge (Q_{in_error})

MWL_error	0.199
Q_{out_error}	0.287
Q_{in_error}	0.139

Figure 47 shows the model domain where the water level in the river is higher than in the polder and thus water is flowing over the crest of the dike in Lippenbroek. Figure 48 shows a lower water level in the river than in the FCA and thus water is flowing out. Flow velocity is represented by arrows in both figures. Higher flow velocities are found inside the creeks and lower flow velocities are found on the floodplain itself.

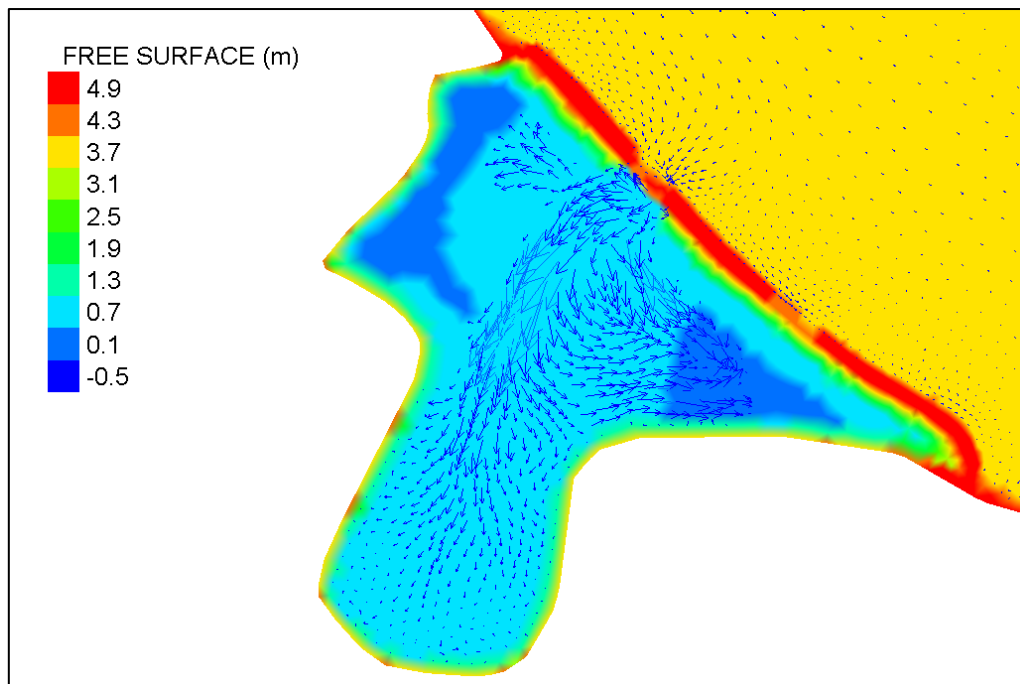


Figure 47 - Output of numerical results when the water level in the river is higher than in the FCA.
The arrows represent the velocity vectors

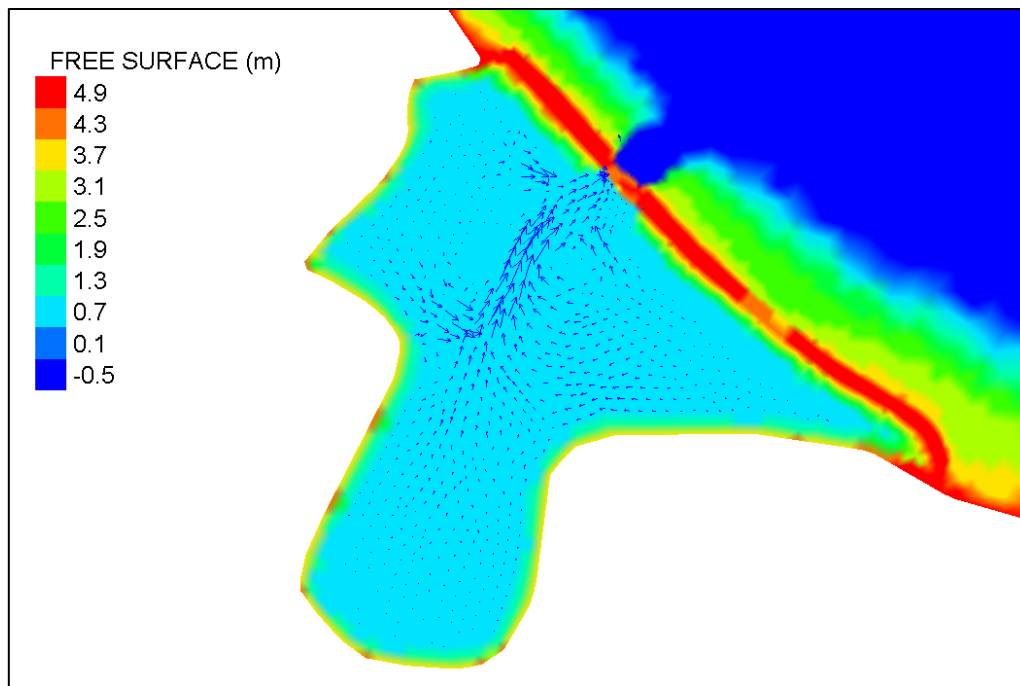


Figure 48 - Output of numerical results when the water level in the river is lower than in the FCA.
The arrows represent the velocity vectors

Figure 49 shows which type of flows occur the most through the culvert. It can be seen that through the inlet sluices (variation between flow type 2 to 6), flow types 2, 4 and 6 are predominant, while for the outlet sluices flow (variation between flow type (1)2 to (1)6) types 2, 3 and 4 are the ones that occur the most.

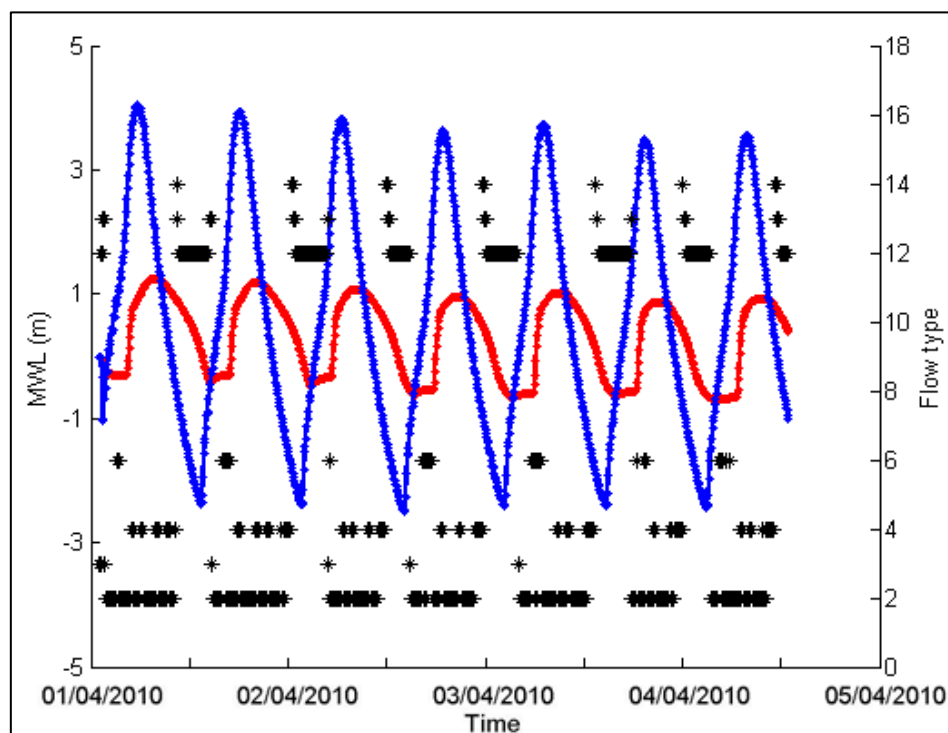


Figure 49 - Mean water levels modelled by TELEMAC-3D in the river (blue line) and in the FCA (red line) (left axis) and the corresponding flow types that occur during the time series (right axis).
Flow through inlet sluice (type 2-6) and through outlet sluice (type 12-16)

6.7. Test case Bergenmeersen

6.7.1. CRT Bergenmeersen

Another recent (2013) example of the implementation of a flood control area with a controlled reduced tide system is located in Bergenmeersen. The ring dike that surrounds the FCA has a crest level of 8 m TAW and the overflow dike has a crest level of 6.8 m TAW.

Here the configuration used for the inlet and outlet culverts (see Figure 50) is quite different from the one used in Lippenbroek. To test the new culvert functionality implemented in TELEMAC-3D this new configuration of in- and outlet culverts was also tested. For this area water level and discharge measurements were also available.

Three outlet culverts were built to add to other older three outlet culverts that existed in the area. Above the new outlet culverts, six new inlet culverts were built and at their entrance weirs (i.e. a stack of stop logs) with different heights were added (Figure 50 and Figure 51). At each inlet and outlet culvert the flow is separated into two parts at the entrance of the culvert by a kind of pillar and then converges again right after this pillar. Figure 52 shows an example of the trash screens that are present. Table 25 gives an overview of the characteristics of these new inlet and outlet culverts.

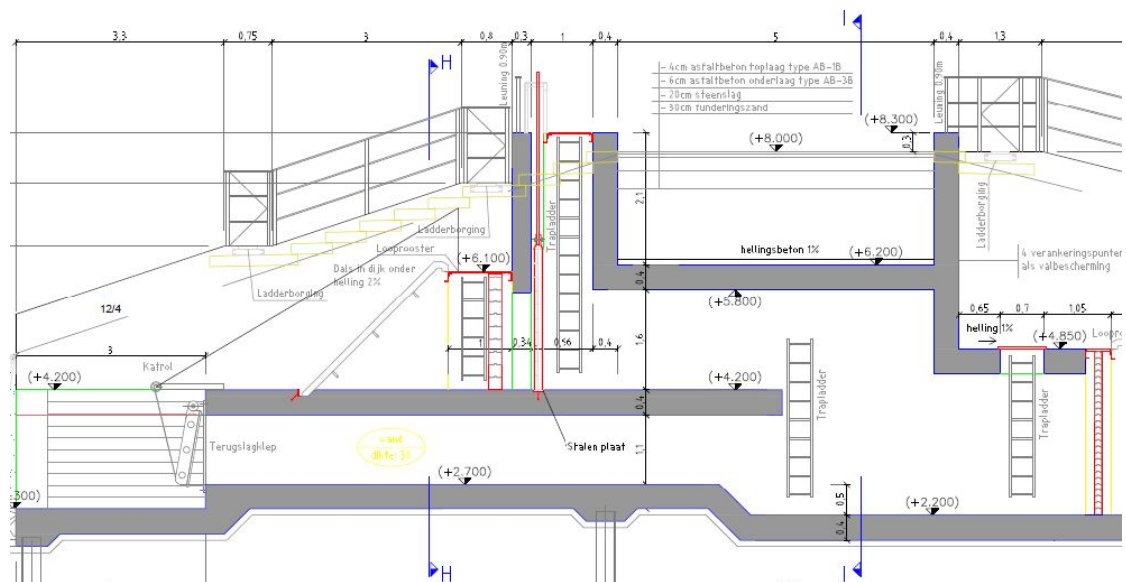


Figure 50 - Detail of the side view of the construction of the new inlet and outlet culverts in Bergenmeersen.



Figure 51 - Inlet and outlet culvert configuration on the river side (construction phase)
(Patrimoniumdatabank W&Z)



Figure 52 - View on the inlet culverts from the river side and inlet and outlet culverts from the FCA side

Table 25. Characteristics of the new inlet and outlet culverts of the new FCA/CRT in Bergenmeersen.

	Inlet (Scheldt side)	Inlet (FCA side)	Outlet (Scheldt side)	Outlet (FCA side)
Number of culverts	6		3	
Culvert width (m)	2.7		3	
Culvert length (m)	9.5		18	
Culvert height (m)	1.6	2.25	1.1	2.25
Level of culvert floor (m TAW)	4.2	2.2	2.7	2.2
Crest level of weirs (m TAW)	4.2/ 4.2/ 4.2/ 4.35/ 4.5 / 4.5			

6.7.2. Bergenmeersen model setup

The mesh of the computational domain is shown in Figure 53. The mesh was cut out of an early version of the Scaldis model. It has a resolution of about 8 m in the river side, and 10 m in the polder. Five horizontal layers were uniformly imposed in the model. Detailed bathymetric/topographic data from 2013 was available and used for this model.

The water levels in the Scheldt river were obtained at the Wetteren tidal station. These values were used as the downstream boundary condition for the hydrodynamic model. Upstream a discharge boundary condition was imposed.

The simulation time was about one day (10th September) corresponding to the time period for which measurements of mean water levels were available. The time step was set to 4 seconds, providing, together with the chosen mesh resolution, a stable simulation.

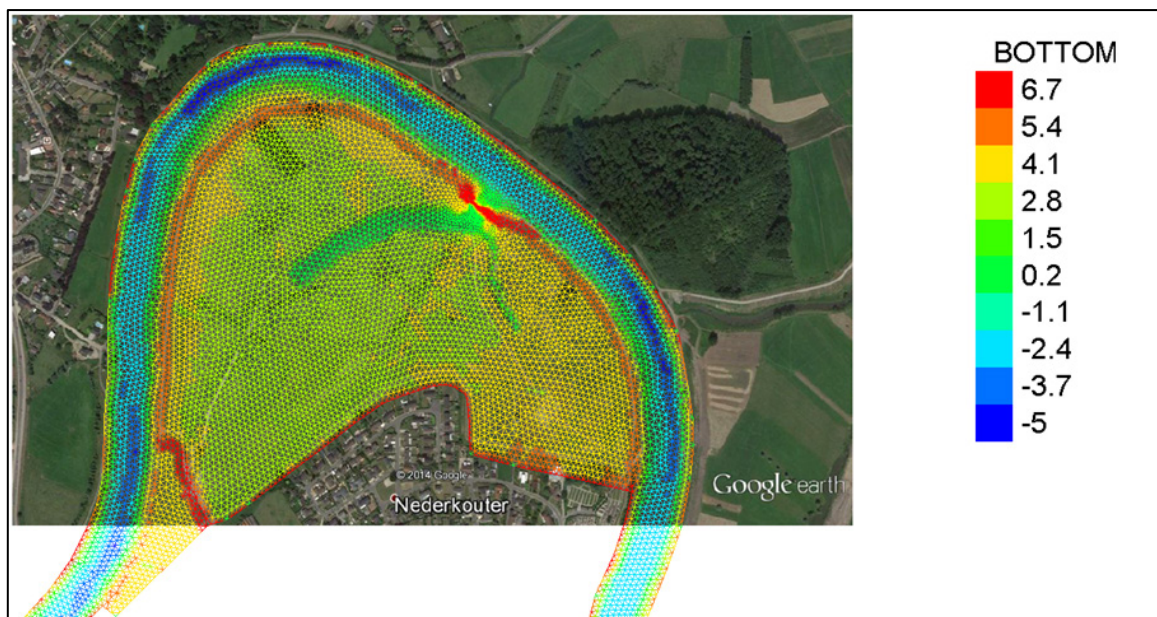


Figure 53 - Planview of the computational domain to model the FCA/CRT in Bergenmeersen.
The colour scale represents the bathymetry (m TAW).

The bottom friction was taken into account in the model through the Manning Strickler's parameter n . Like in the Lippenbroek test case it was set to $n=0.02 \text{ s/m}^{1/3}$ for the river part and $n=0.07 \text{ s/m}^{1/3}$ to the polder. The horizontal and vertical turbulence viscosity coefficients were set to $1 \text{ m}^2\text{s}^{-1}$ and $0.01 \text{ m}^2\text{s}^{-1}$, respectively.

Table 26 shows the file that the user has to give to TELEMAC-3D in order to take into account the culverts for this FCA with CRT in the Bergenmeersen test case. Besides this new structure there were already in the area three outlet sluices also represented in the input text file as outlet 3 to outlet 6 (information for these outlet sluices was obtained from the Patrimoniumdatabank W&Z)

Once again the different head loss coefficients were used to calibrate the model with the experimental data. Most of the parameters were maintained comparatively with the Lippenbroek test case. But there are some exceptions, given the fact that the inlet and outlet culvert configurations are also different. For instance the head loss coefficients at the entrance of the inlet were increased in order to take into account the effect of the flow being split into two parts by a pillar. Following the expression given by *Carlier* (1972), the head loss due to the presence of pillars is about $C_p \approx 0.4$ and therefore $CE1$ becomes $CE1=C_1+C_p$.

There was also at the exit of the outlet sluices the separation of the flow into two parts. This effect was taken into account in the head loss due to a valve, increasing the value for C_v . Also during the measurement campaign, the trash screens at the inlet sluices were not cleaned and therefore this coefficient was increased both for the inlet and outlet sluices.

Table 26. Input .txt file for the culvert subroutine in TELEMAC-3D to model the Bergenmeersen FCA/CRT

	CE1	CE2	CS1	CS2	CV	CT	C56	C5	CV5	W	D1	D2	N	L	CP
Inlet1	0.9	0.5	1	1	0	1	10	6	0	2.7	1.45	2.25	0.015	9.5	0
Inlet2	0.9	0.5	1	1	0	1	10	6	0	2.7	1.3	2.25	0.015	9.5	0
Inlet3	0.9	0.5	1	1	0	1	10	6	0	2.7	1.3	2.25	0.015	9.5	0
Inlet4	0.9	0.5	1	1	0	1	10	6	0	2.7	1.6	2.25	0.015	9.5	0
Inlet5	0.9	0.5	1	1	0	1	10	6	0	2.7	1.6	2.25	0.015	9.5	0
Inlet6	0.9	0.5	1	1	0	1	10	6	0	2.7	1.6	2.25	0.015	9.5	0
Outlet1	0.5	0.5	1	1	12	1	10	6	1.5	3	1.1	2.25	0.015	18.5	2
Outlet2	0.5	0.5	1	1	12	1	10	6	1.5	3	1.1	2.25	0.015	18.5	2
Outlet3	0.5	0.5	1	1	12	1	10	6	1.5	3	1.1	2.25	0.015	18.5	2
Outlet4	0.5	0.5	1	1	12	1	10	6	1.5	1.5	1.8	2.55	0.015	20	2
Outlet5	0.5	0.5	1	1	12	1	10	6	1.5	1.5	1.8	2.6	0.015	20	2
Outlet6	0.5	0.5	1	1	12	1	10	6	1.5	1.5	1.8	2.55	0.015	20	2

6.7.3. Results

Measurements were performed by Flanders Hydraulic Research in Bergenmeersen within a 13 hour campaign during the 10th September, 2013. They obtained water levels in front of the culverts in the Scheldt and in the polder sides and discharges for the inlet and outlet culverts.

The model results for this period will be compared with the measurements. Figure 54 shows the differences in water level in the river in front of the in- and outlet construction of Bergenmeersen. This Figure shows that it is difficult to get the water levels in this model correct. The downstream water level boundary of this small model is not located at the same location as the Wetteren tidal measurement station, but more upstream. Keeping this in mind Figure 55 shows the difference between measured and modeled water levels in the polder. The water level in the model follows a similar path as the measured water level. Given the complicated construction (in terms of translating this to an equation for discharge) of the in- and outlet structure, these results are a good approximation of reality.

In Figure 56 we see that the outlet discharge computed by the model fits fairly well the experimental data even if the numerical results overestimate the measurements around 12h. Regarding the inlet discharge, Figure 57 shows that the computed discharges are overestimated by the model, resulting on the overestimation seen in the mean water level in the FCA. A possible explanation for the discrepancies is that the inlet sluices have gates incorporated and in this test case it was considered that these gates were completely opened. We have heard that in reality this is not the case and that the opening of these gates is changed several times over the last two years. The purpose of these gates is to close the area and prevent water from entering prior to a predicted storm surge. There was no information on the openings of these gates at the time of this 13 hour measurement campaign.

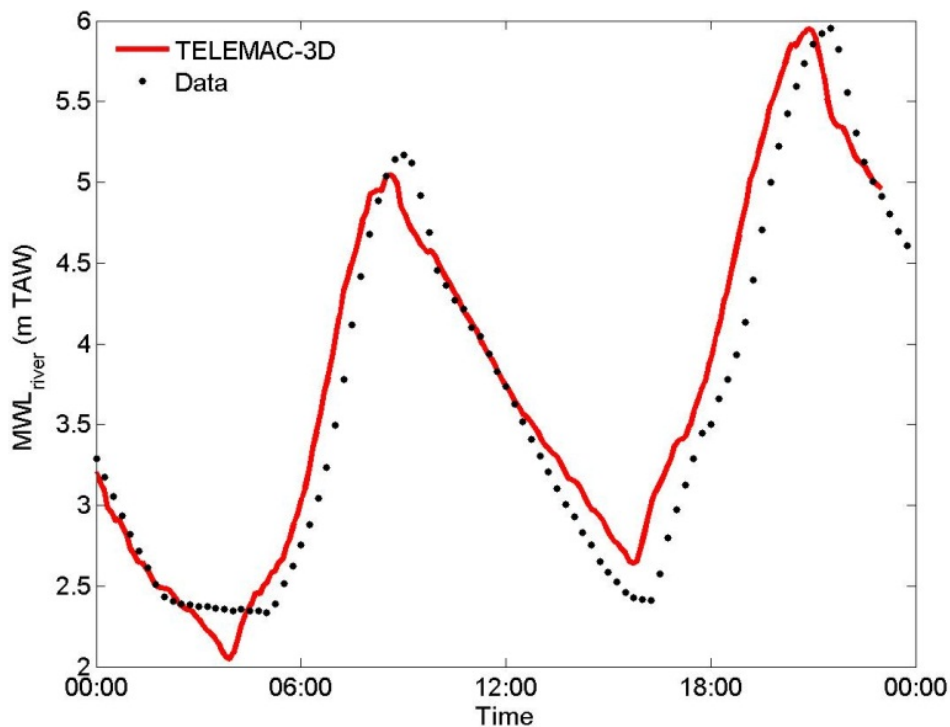


Figure 54 - Comparison of the mean water level time evolution in the river between numerical results and measurements

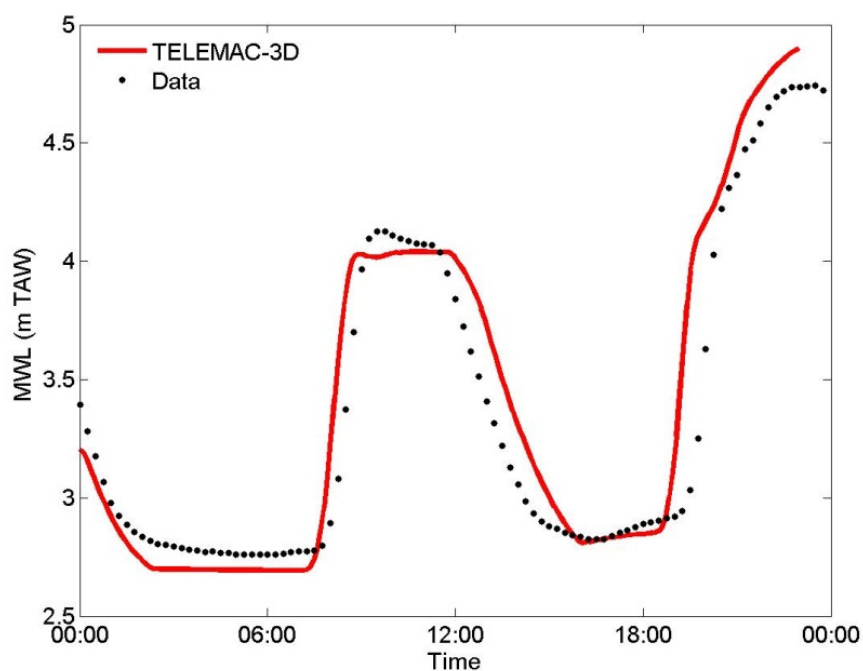


Figure 55 - Comparison of the mean water level time evolution in the polder between numerical results and measurements

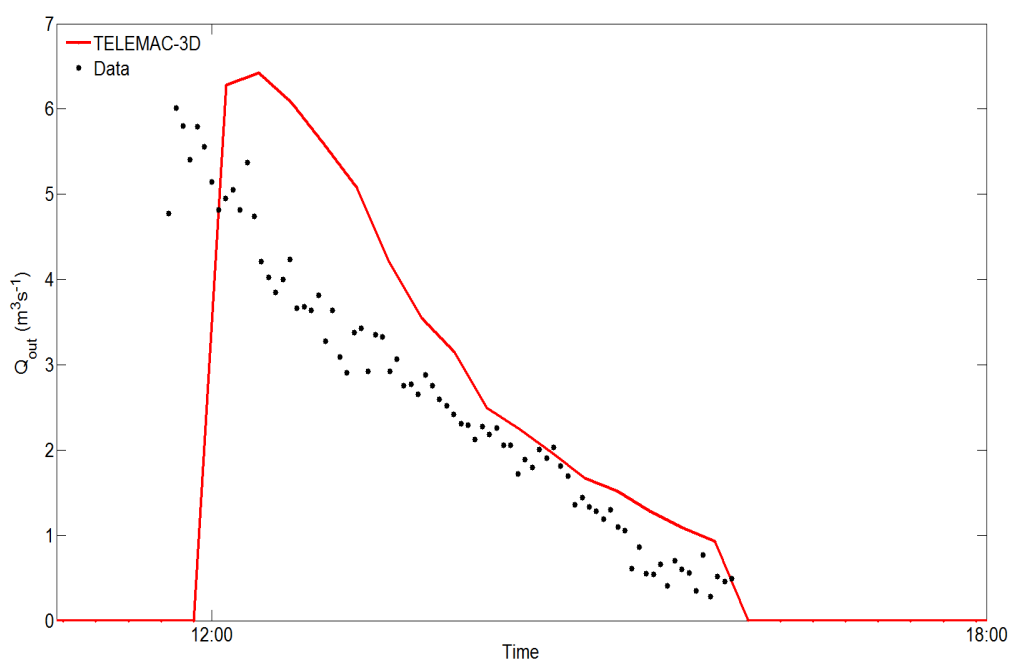


Figure 56 - Comparison of outlet culvert discharges time evolution between numerical results and measurements

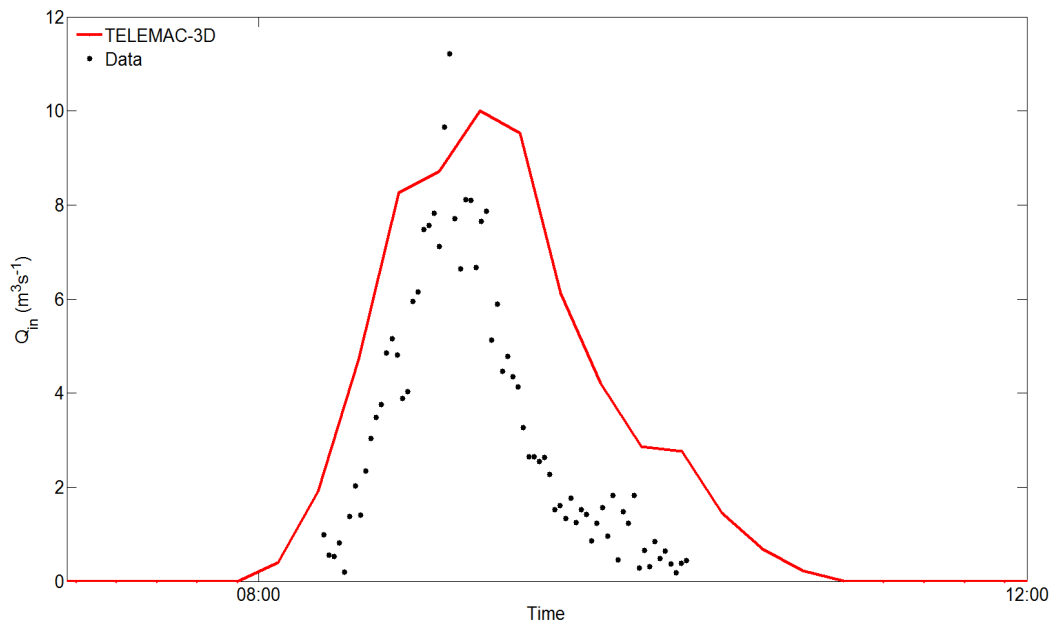


Figure 57 - Comparison of inlet culvert discharges time evolution between numerical results and measurements

Like the Lippenbroek test case, the normalized root mean square error was calculated for the mean water levels, outlet and inlet discharges (Table 27).

Table 27. Normalized root mean square error for the mean water level (MWL_error), outlet discharge (Q_{out_error}) and inlet discharge (Q_{in_error}) in Bergenmeersen test case

MWL_error	0.275
Q_{out_error}	0.453
Q_{in_error}	0.538

In Figure 58, the type of flows that predominate through the inlet and outlet culverts are presented. While for the former, flow types 2, 3 and 4 predominate (though also type 6 is present), for the latter flow types 2 and 3 are the ones that occur the most (though also type 4 is present).

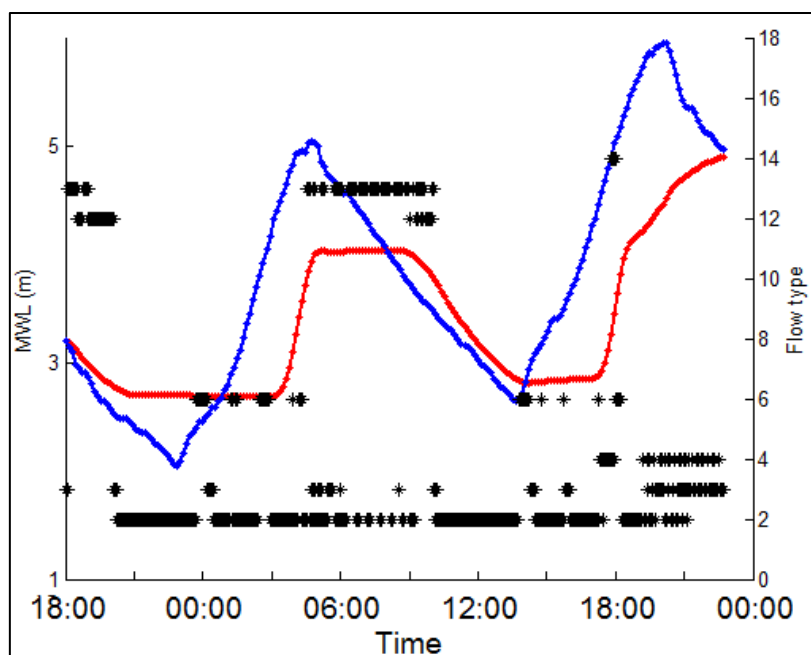


Figure 58 - Mean water levels modelled by TELEMAC-3D in the river (blue line) and in the FCA (red line) and the corresponding flow types that occur during the time series. Flow through inlet culvert (type 2 - 6) and through outlet culvert (type 12 - 16)

6.8. Concluding remarks

The main aim of the work in this chapter was to implement a new culvert functionality in the three-dimensional hydrodynamic model TELEMAC-3D. For that purpose, a literature review about the description of the different kind of flows that occur through culverts was done first. Then, different models, such as TELEMAC-2D, DELFT-3D and MIKE 11, that take already into account the culvert functionality were analysed and compared, regarding the different equations that each one uses to describe the flow through culverts. In general the equations coded in the models are quite similar, with exception on the way the head losses are taken into account.

The new culvert functionality was implemented in TELEMAC-3D. A culvert works as a couple of source and sink terms between which the discharges are calculated depending on the water levels in the source/sink terms, i.e., on the water levels in the flood control area and in the river. The theoretical framework was based on the work of *Bodhaine* (1968) together with *Lencastre* (1961). The model presents some limitations, such as the fact of making approximations on the calculation of water levels inside the culvert and not making a backwater analysis to know exactly the water levels at the entrance, inside and at the exit of the culvert (as MIKE 11 model does).

Some parameter analyses was made in order to test the new functionality. For that purpose a simplified model was generated in order to observe how the model behaves with inlet and outlet culverts in the domain and how some of the different “free” parameters (that the user has to assign) interfere in model results.

Finally, in order to calibrate and/or verify model results, two test cases were applied. While the first test case is applied to the flood control area with controlled reduced tide system built in Lippenbroek, which became a pilot project to study the CRT function of such an area, the second one is built in Bergenmeersen where recently a new FCA with CRT was implemented.

In both areas, there were measurements of the mean water levels inside the flood control area as well as measurements of outlet discharges available. In the Bergenmeersen test case, there were also measurements of inlet discharges and mean water levels at the river side available.

After a calibration process, it was concluded that, given some uncertainty like the representation of ditches and creeks in the topo-bathymetry of the model or the complexity of the in- and outlet structure, numerical results fit fairly well with data, both for the mean water levels and inlet and outlet discharges.

6.9. With or without culverts: full scale model results

Two model runs (full domain) were started to simulate 2 days. The first simulation had no culvert functionality and the second had 40 culverts active. All other parameters were kept the same. The time step was 5 seconds. Both simulations were run on the same nodes and the same amount of processors (=60) on the Linux Cluster of Flanders Hydraulics Research. Without culverts, the speed-up time was 8.75 and with 40 culverts active the speed-up decreased to 3.25.

6.9.1. Water levels

The high water levels of a spring tide were sampled along the thalweg (see white dots in Figure 59) of the estuary in the Scaldis 3D model for both the run with and without culverts active. The results are given in Figure 61. We see that only in the most upstream part the flood control area (FCA) with controlled reduced tide (CRT) has a small influence on the water levels (< 0.04 m). Reference of km notation in Figure 61 is given in Figure 60.

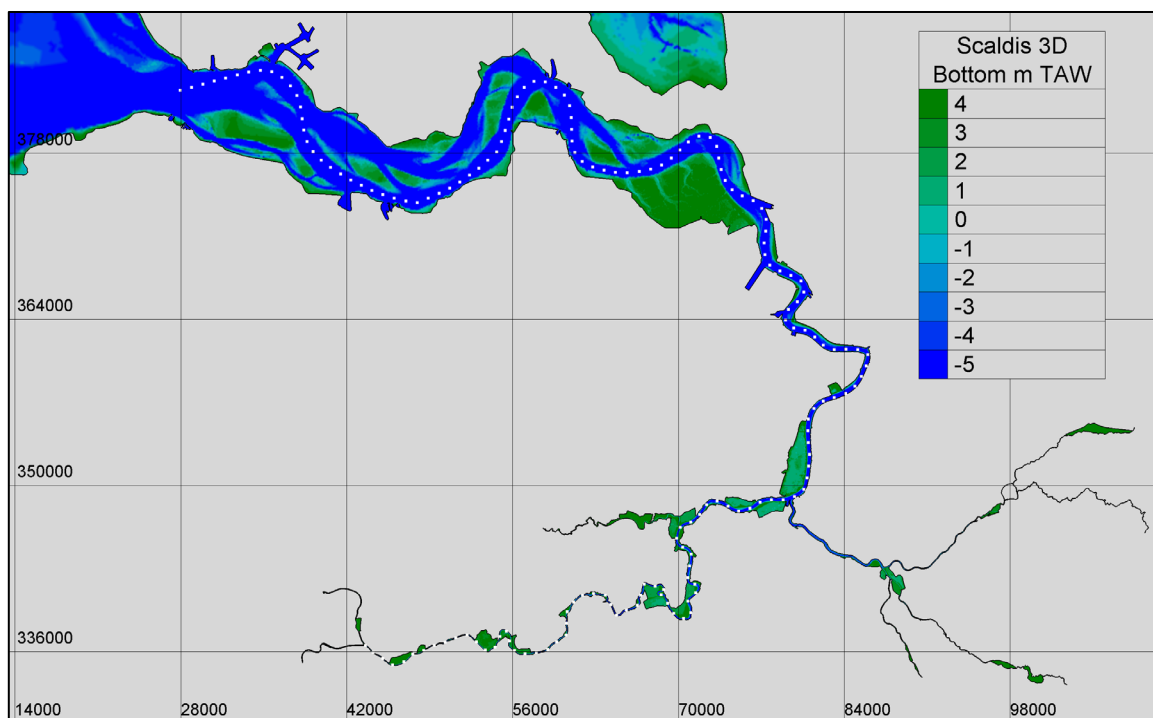


Figure 59 - Scaldis 3D model showing 1km interval sampled thalweg (=white dots).

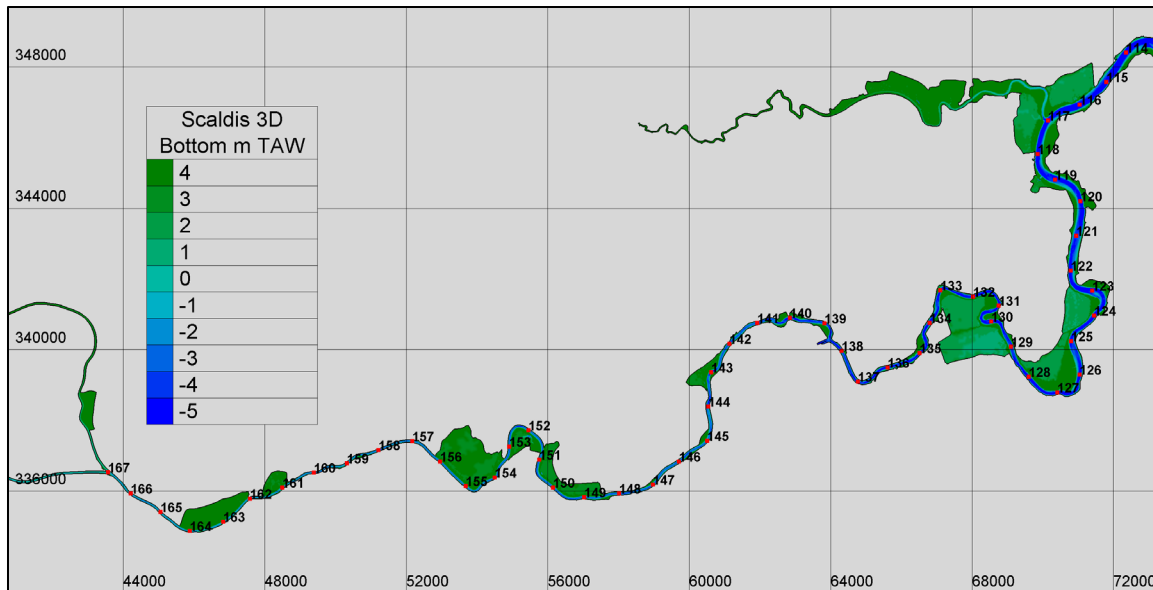


Figure 60 - Detail of Figure 59 showing upper Sea Scheldt in Scaldis 3D model with the 1km interval sampled thalweg. Samples are numbered. These numbers represent the number of km in the estuary starting from Vlissingen.

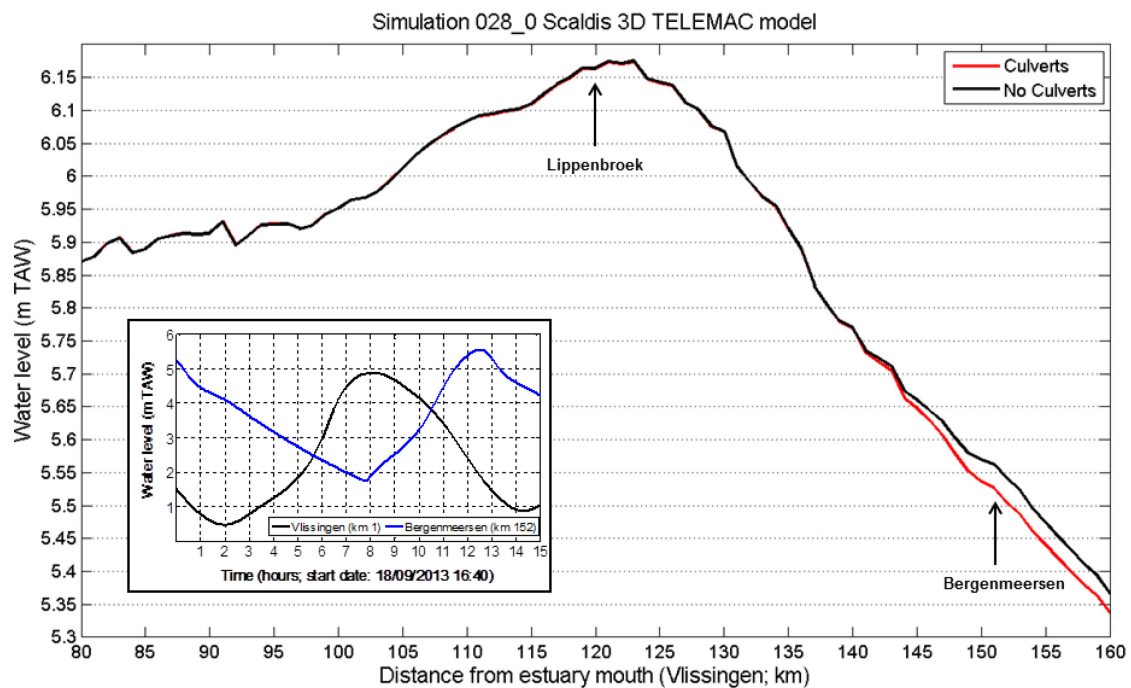


Figure 61 - High water levels along thalweg of Scheldt Estuary in Scaldis 3D model with focus on Upper Sea Scheldt. The insertion gives the tidal curve in Vlissingen (km 1) in black line and at Bergenmeersen (km 152) in blue line.

6.9.2. Flow velocities

At two points, one just downstream and one just upstream Bergenmeersen FCA/CRT, velocities were compared between the model run with and without culvert activity.

Point downstream: For maximum flood flow local velocity dropped with less than 1% (e.g. from 0.99 m/s (with culverts) to 0.98 m/s (without culverts)). For maximum ebb flow local velocities dropped with less than 3% (e.g. they change from 0.73 m/s (with culverts) to 0.71 m/s (without culverts)).

Point upstream: For flood and ebb flow the velocity differences were smaller than 1%, but here the simulation without culverts gave the highest velocities.

The difference in flow velocity between the simulation without and with culverts is graphically shown in Figure 62. Water level is given as a reference to associate differences in flow velocities.

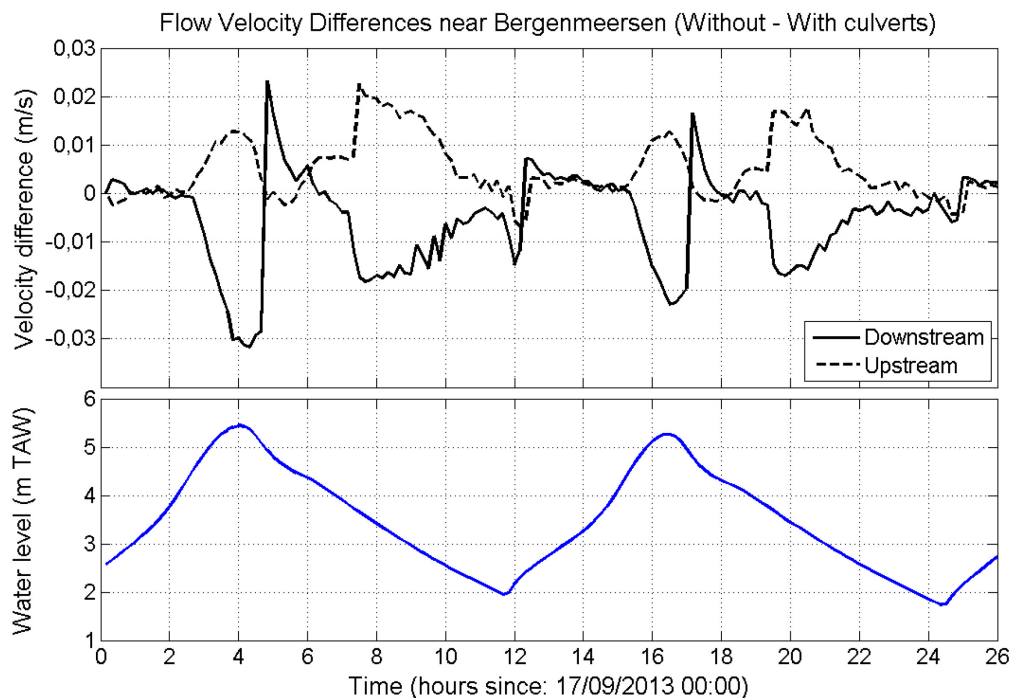


Figure 62 - Differences in flow velocities of two points near Bergenmeersen: one just downstream the FCA/CRT and one just upstream. Water level is given as reference to associate differences in flow velocities.

7 Sensitivity analysis

7.1. Discharge at Melle

The discharge at Merelbeke is the largest fresh water discharge coming to the Scheldt estuary. Thus, it has the most significant effect on the model output. Therefore, it is very important to have an accurate and detailed time series of discharge for this location. For 2013 measured discharges at Merelbeke are not available. Daily time series of the discharge at Melle are specified at the upstream boundary. In this chapter the model sensitivity to the upstream discharge is tested.

The data series of the discharge at Merelbeke (measured by IMDC) are available as 5 min values for a period from 19/06/2002 12:30 to 17/07/2002 7:56. The data from 30/06/2002 00:00 to 16/07/2002 00:00 was used for the sensitivity runs (Figure 63). There were gaps in data for the periods from 02/07/2002 14:35 to 02/07/2002 17:22, 09/07/2002 09:57 to 09/07/2002 15:11 and from 12/07/2002 08:11 to 12/07/2002 08:21. They were filled by the linear interpolation.

Daily time series were made based on the 5 min time series (Figure 63). The model runs used for the sensitivity analysis are described in Table 28.

Table 28. Model runs used for the sensitivity analysis to the upstream discharge

Model run	Upstream discharge at Melle	Upstream discharges Nete, Zenne, Dijle, etc.	Downstream boundary
Scaldis_028_Q1	5 min	constant	id. calibration runs
Scaldis_028_Q2	daily	constant	id. calibration runs

The same downstream boundary conditions were defined in these runs as in the calibration runs (from 17/09/2013 00:00 to 03/10/2013 00:00). The available discharge at Merelbeke is from another period but it does not matter for the sensitivity analysis. The results of the two sensitivity runs are compared to each other to see the influence of the upstream discharge on the modeled water levels.

Constant discharges were defined at Terneuzen (30 m³/s), Dender (15 m³/s), Zenne (10 m³/s), Dijle (19 m³/s), Grote Nete (5 m³/s), Kleine Nete (7 m³/s) and Bath (24 m³/s).

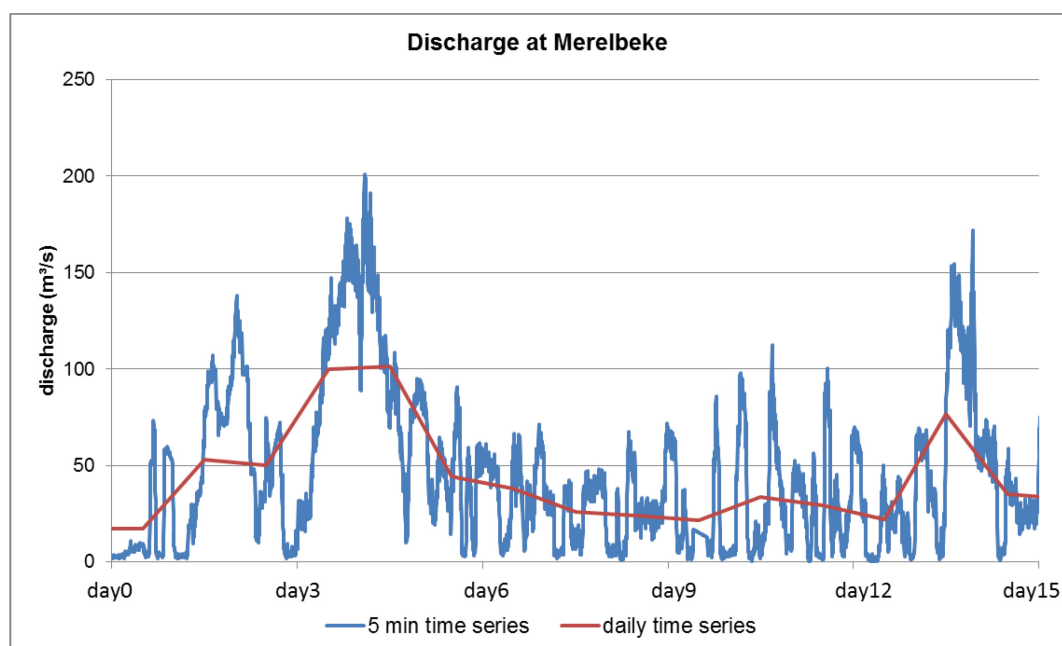


Figure 63 - Measured discharge at Merelbeke

In the Western Scheldt and Eastern Scheldt there is no influence of the upstream discharge at Melle. The water levels stay the same in Scaldis_028_Q1 and Scaldis_028_Q2.

In the Lower Sea Scheldt there is a very small influence at Hemiksem (only 1 cm difference). In the Rupel the differences are very small too.

The biggest differences are calculated in the Upper Sea Scheldt (Table 59 to Table 61). RMSE of the water level time series varies between 1 cm at Schelle to 23 cm at Melle. The RMSE of high waters changes from 1 cm to 14 cm and RMSE of low waters is from 1 cm at Schelle to 32 cm at Melle. The average bias is significantly lower than RMSE because some high and low waters are higher in Scaldis_028_Q2 than in Scaldis_028_Q1 and some are lower. The average difference for the analyzed period becomes zero.

The difference in some low waters at Melle can reach 80 cm.

It is necessary to have an accurate and detailed time series of the discharge at Merelbeke to get an accurate model output at the upstream stations in the Scheldt estuary. The use of the daily time series can result in big differences between the modeled and measured water levels.

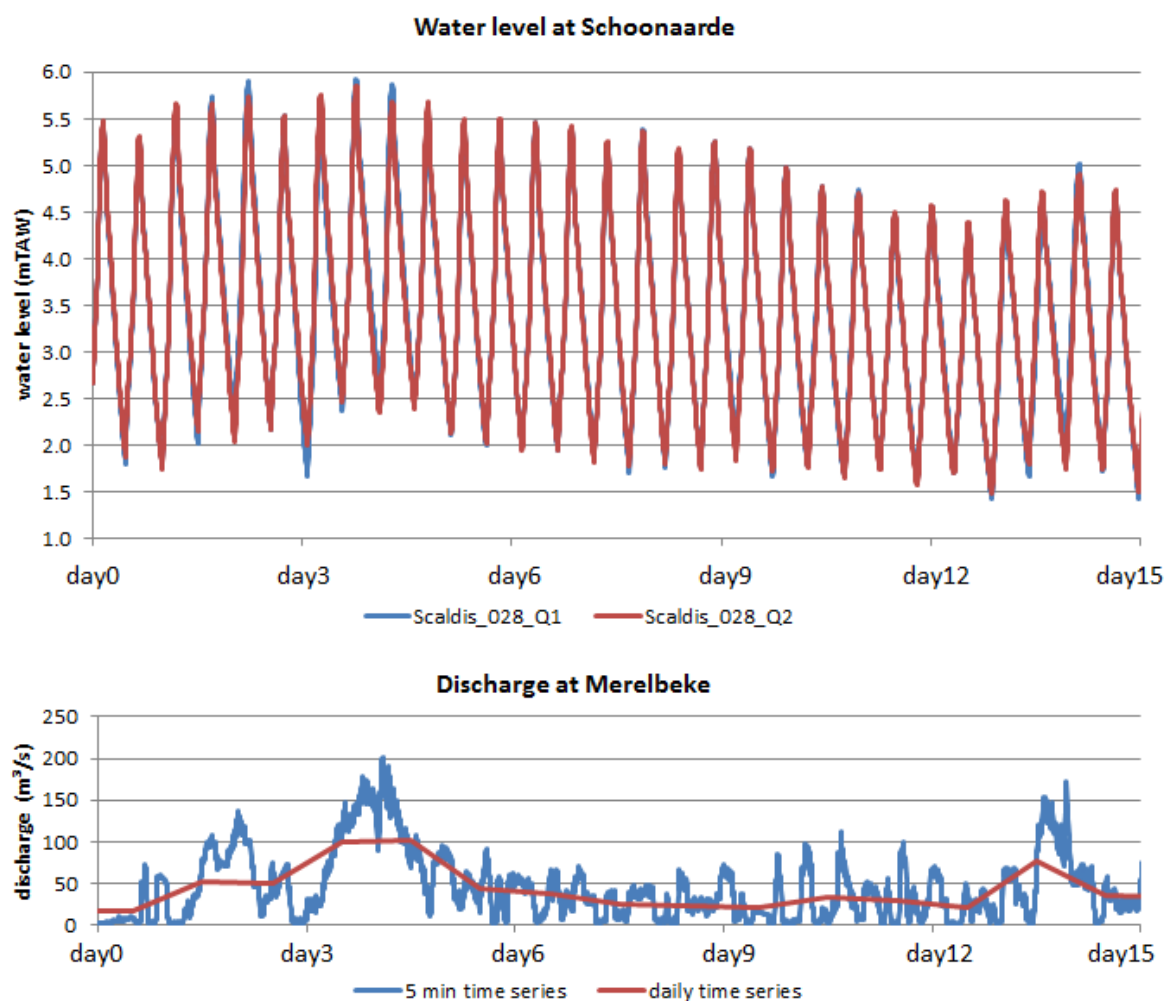


Figure 64 - Water level at Schoonaarde in Scaldis_028_Q1 and Scaldis_028_Q2

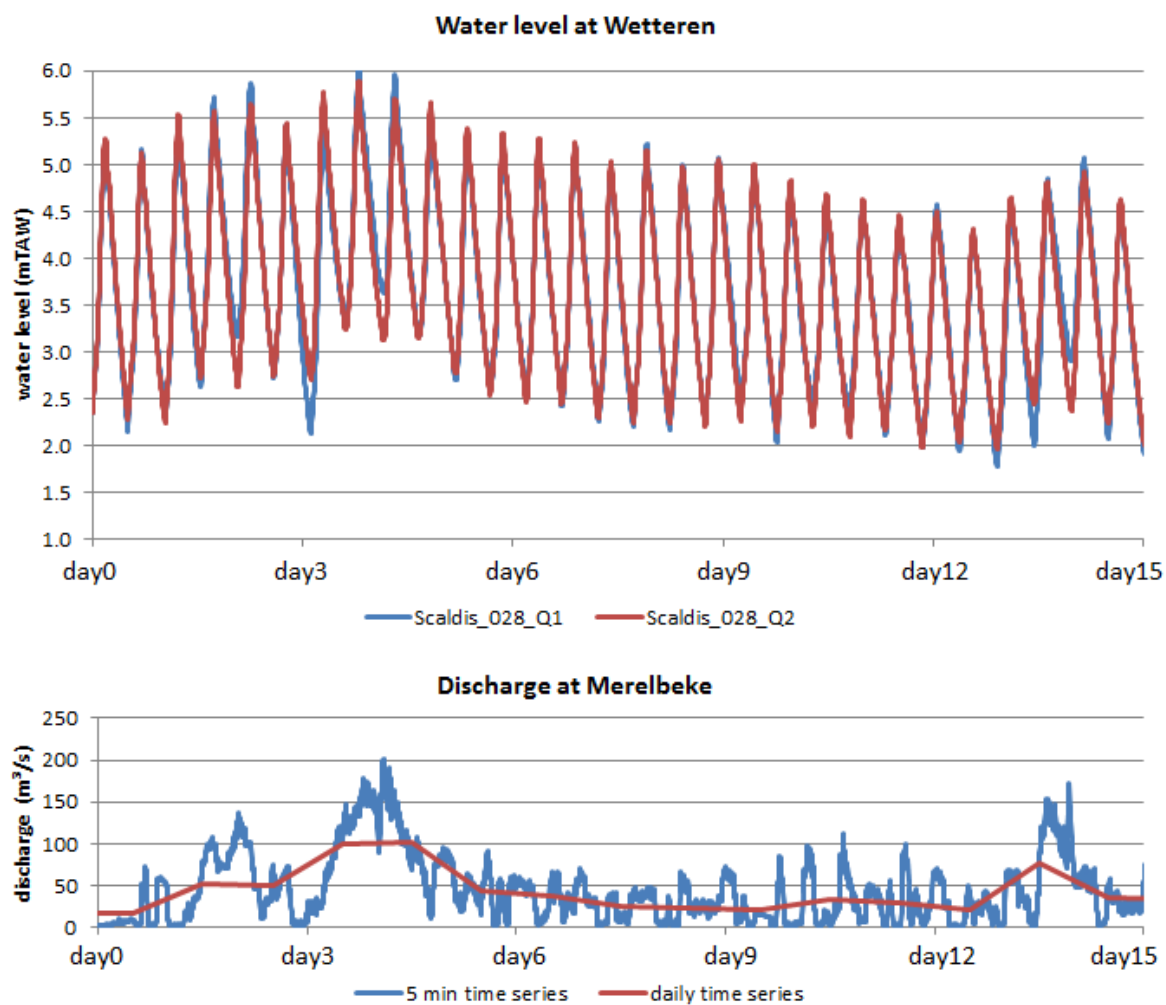


Figure 65 - Water level at Wetteren in Scaldis_028_Q1 and Scaldis_028_Q2

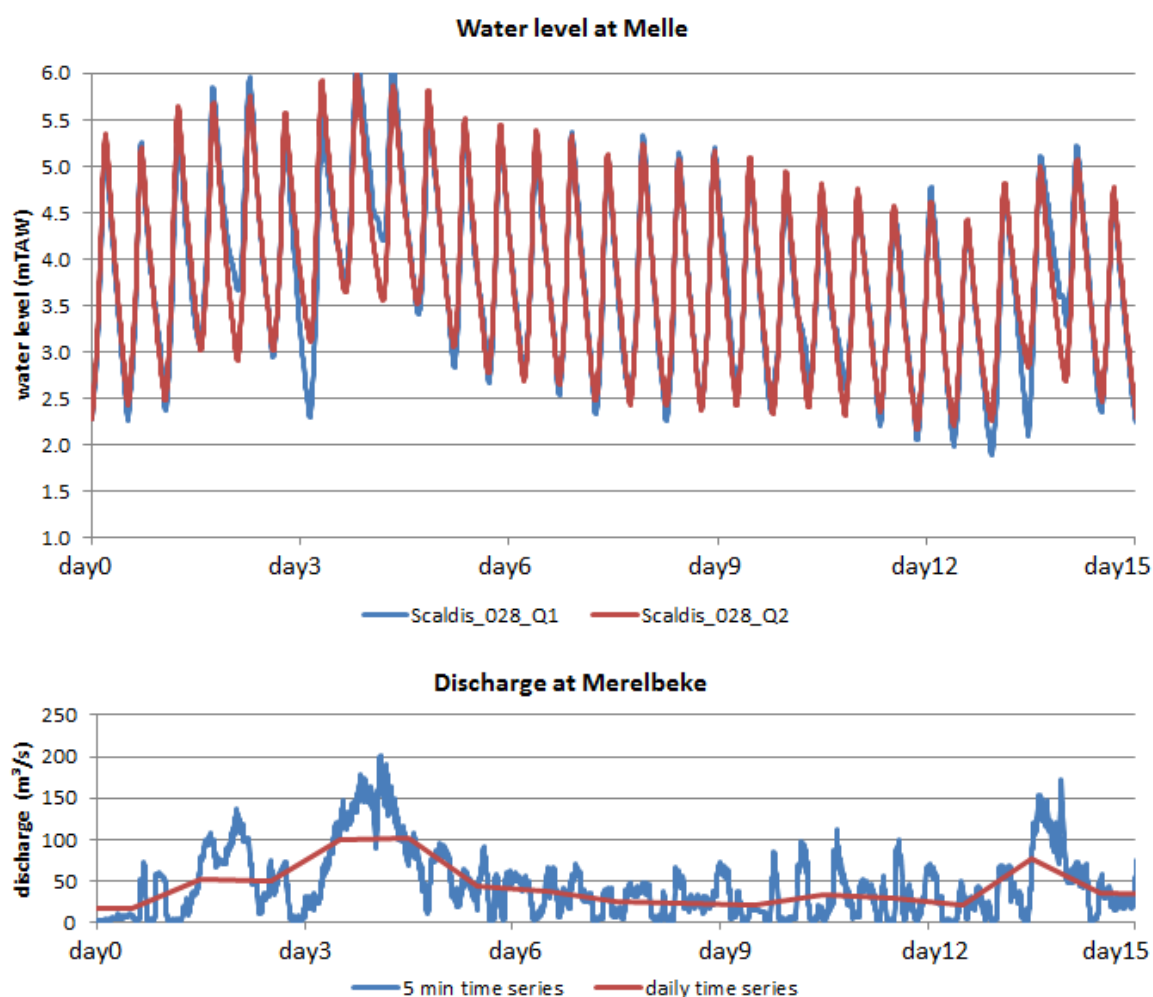


Figure 66 - Water level at Melle in Scaldis_028_Q1 and Scaldis_028_Q2

7.2. Bed roughness of the intertidal areas

Model sensitivity to the roughness change of the intertidal areas was tested. The model runs used for the analysis are described in Table 29.

Table 29. Model runs used for the sensitivity analysis to the bed roughness

Model run	Roughness of the intertidal areas ($\text{m}^{-1/3}\text{s}$)
Scaldis_027_rgh0	rgh of intertidal areas = rgh of deep zones
Scaldis_027_rgh1	rgh of intertidal areas = rgh of deep zones + 0.003
Scaldis_027_rgh2	rgh of intertidal areas = rgh of deep zones + 0.006
Scaldis_027_rgh3	rgh of intertidal areas = rgh of deep zones + 0.1
Scaldis_027_rgh4	rgh of intertidal areas = rgh of deep zones + 0.05

The roughness change in runs Scaldis_027_rgh1 and Scaldis_027_rgh2 has almost no effect on the modeled velocities. The increase of the roughness of the intertidal areas in runs Scaldis_027_rgh3 and Scaldis_027_rgh4 results in a decrease of the flow velocities there. This helps to improve the velocity profile for some transects for some moments of tide. For example, velocities improve at Boom in the end of flood (Table 31). Velocities decrease and improve in the intertidal zones for some transects at Dendermonde and Terhagen. However, the modeled velocities at Boom during ebb become worse in Scaldis_027_rgh4 (Table 31). Velocities in deeper part of the river become too low at Dendermonde and Terhagen.

At most upstream locations (Schoonaarde, Schellebelle) the increase of the roughness results in a decrease of the velocities everywhere along the transect (even in a deeper zone). The model accuracy worsens (Table 30). Furthermore, the roughness adaptation of the intertidal areas affects the water levels. High waters decrease, low waters increase, M2 amplitude becomes too low (Figure 67).

Table 30. Measured and modeled velocity for one of the transects at Schoonaarde in runs with different roughness of the intertidal areas

20130527_Schoonaarde			
Run	Roughness	Ebb	Flood
Scaldis_027_rgh0	rgb of intertidal areas = rgh of deep zones		
Scaldis_027_rgh4	rgb of intertidal areas = rgh of deep zones + 0.05		

Table 31. Measured and modeled velocity for one of the transects at Boom in runs with different roughness of the intertidal areas

20100427_Boom			
Run	Roughness	Ebb	Flood
Scaldis_027_rgh0	rgb of intertidal areas = rgh of deep zones		
Scaldis_027_rgh4	rgb of intertidal areas = rgh of deep zones + 0.05		

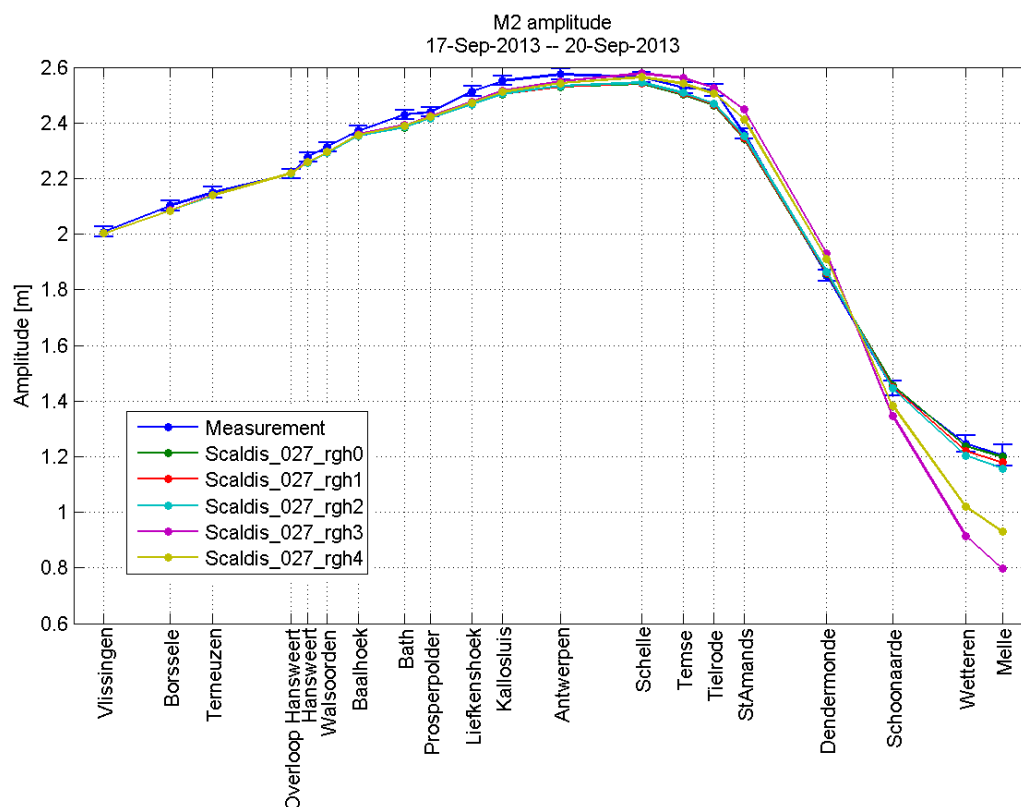


Figure 67 - M2 amplitude in runs with different roughness of the intertidal areas (Western Scheldt and Sea Scheldt)

7.3. Diffusivity

For the sensitivity analysis to the diffusivity the coefficient for horizontal diffusion of velocities was changed in the model. Simulations used for the sensitivity analysis are described in Table 32.

Table 32. Model runs used for the sensitivity analysis to the diffusivity

Model run	Coefficient for horizontal diffusion of velocities (m ² /s)
SA8	10 ⁻⁶
SA19	0.01
SA20	0.1
SA1	1
SA10	10

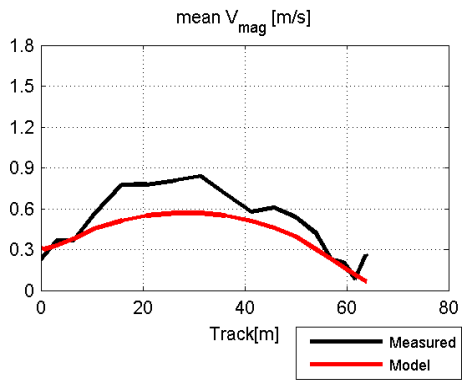
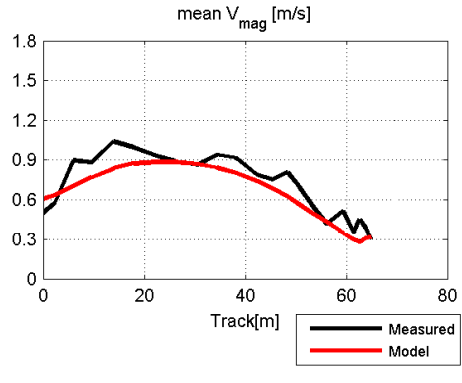
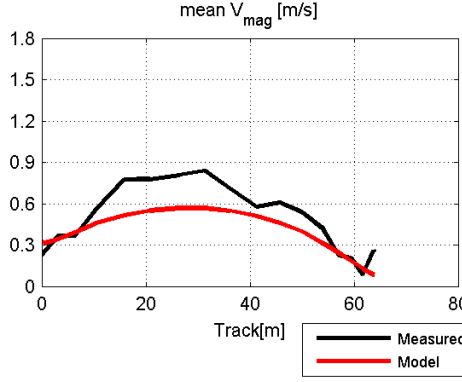
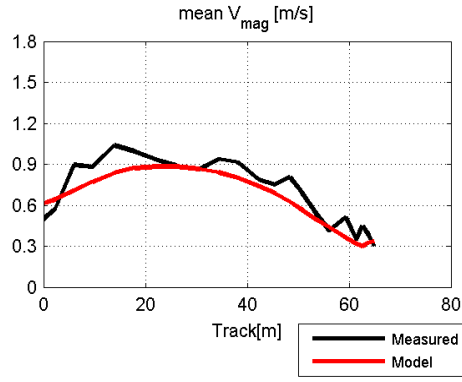
A change of the diffusivity (viscosity) affects the velocity profile along the cross section. When viscosity decreases, the velocity profile becomes more convex and the horizontal velocity gradients increase. This results in a decrease of the flow velocities in the intertidal areas and an increase of velocities in a deeper part of the river.

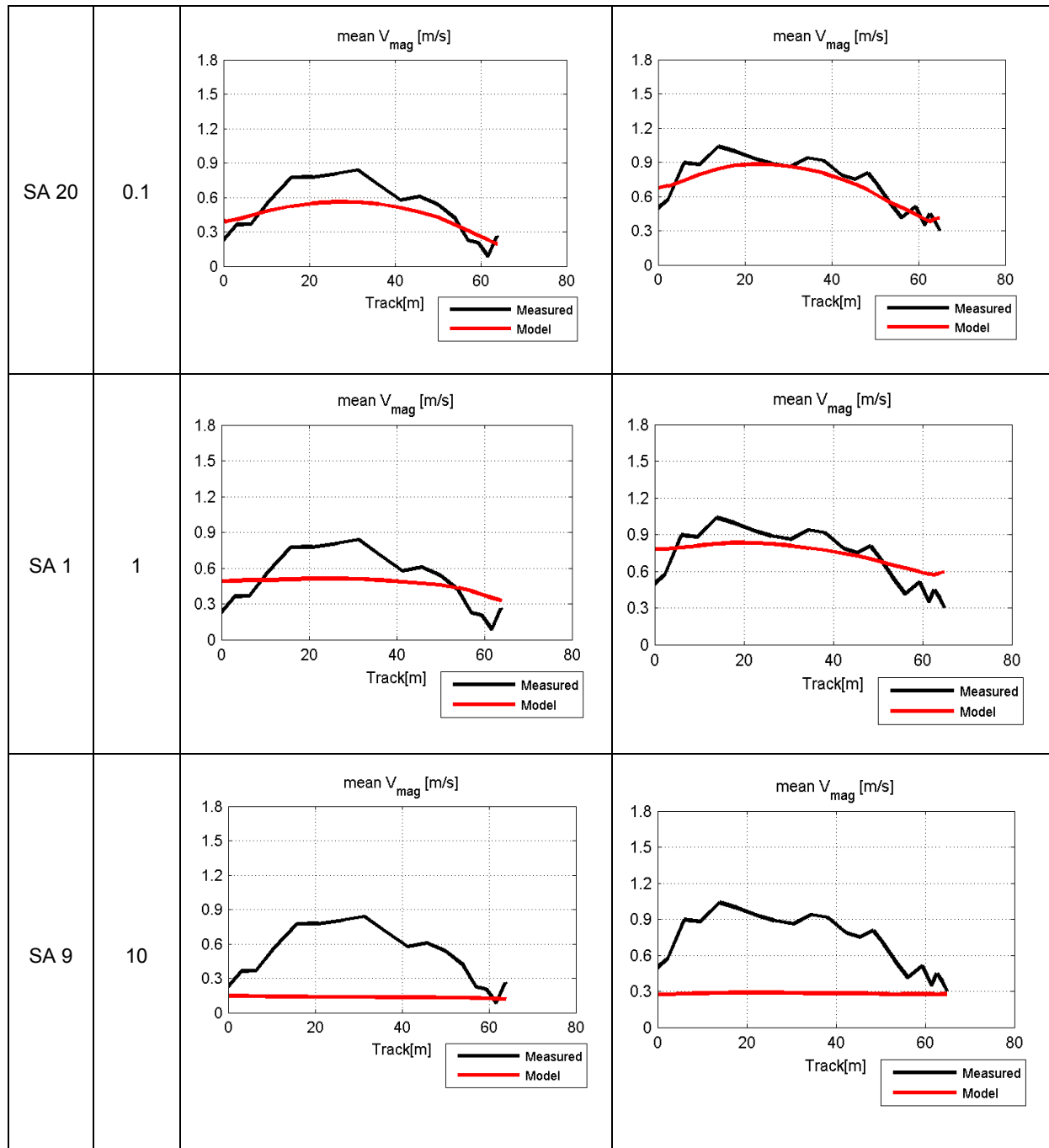
The diffusivity change has an effect on the flow velocities only in the upstream part of the estuary (upstream Antwerp). In the downstream part the grid size is bigger and the diffusivity change does not have any effect on the model results because of a higher numerical diffusion (see chapter 5.11).

An example of the velocity profiles in the runs with different diffusivity is given in Table 33 for Schellebelle. Plots of the velocity profiles at Kruibeke, Dendermonde and Schoonaarde are given in Table 62 in the end of the report.

The velocity profiles in runs SA8 and SA19 (diffusivity is 10^{-6} and $0.01 \text{ m}^2/\text{s}$ respectively) are very similar. A further increase of the diffusivity in runs SA20, SA1 and SA9 results in flattening of the velocity profiles. In run SA9 (diffusivity is $10 \text{ m}^2/\text{s}$) the velocity profile is almost a straight line.

Table 33. Measured and modeled velocity at Schellebelle in runs with different diffusivity

20140415_Schellebelle			
Run	Diffusivity (m^2/s)	Max ebb	Max flood
SA 8	10^{-6}		
SA 19	0.01		



7.4. Number of vertical layers

For the analysis of the model sensitivity to the number of vertical layers the results of two simulations were compared (Table 34).

Table 34. Model runs used for the sensitivity analysis to the number of vertical layers

Model run	Number of vertical layers	Distribution of sigma layers
SA01b	5	0D, 0.12D, 0.30D, 0.60D, 1D
SA13	15	0D, 0.03D, 0.09D, 0.15D, 0.20D, 0.25D, 0.30D, 0.37D, 0.44D, 0.52D, 0.60D, 0.69D, 0.80D, 0.90D, 1D

The differences in vertical velocity profiles calculated in SA1b and SA13 are negligible (smaller than 1 cm/s) (Figure 68 to Figure 73). There are also no significant differences in the calculated velocities at Kramp (a sharp river bend in the Upper Sea Scheldt) (Figure 71). The differences in high and low waters and M2 amplitude calculated in these runs are smaller than 1 cm (Figure 74, Figure 75). It means that the model with 5 layers represents the hydrodynamics well and an increase of vertical resolution is not necessary.

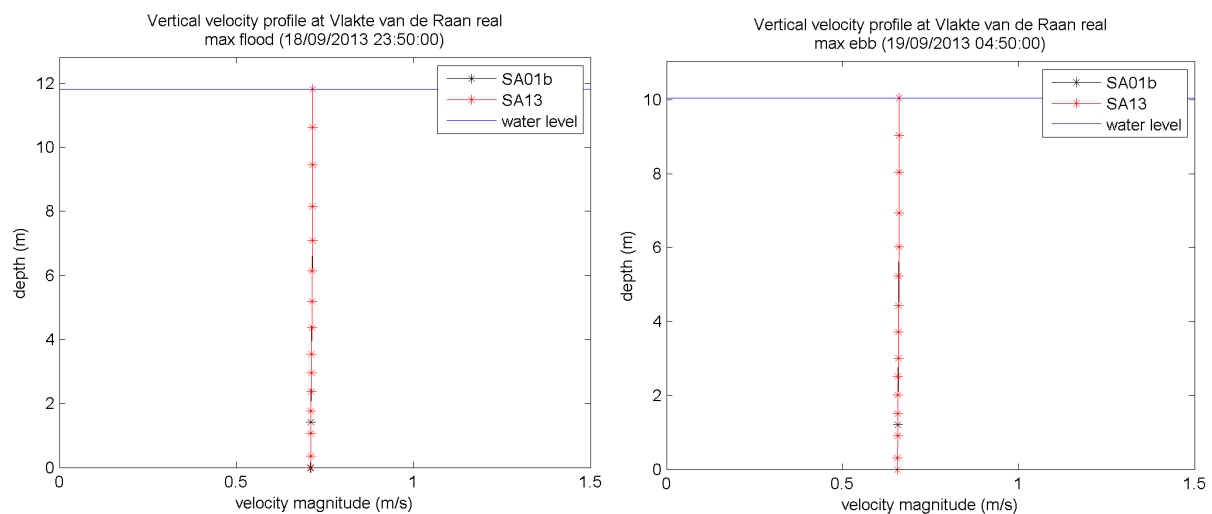


Figure 68 - Velocity profiles at Vlake van de Raan

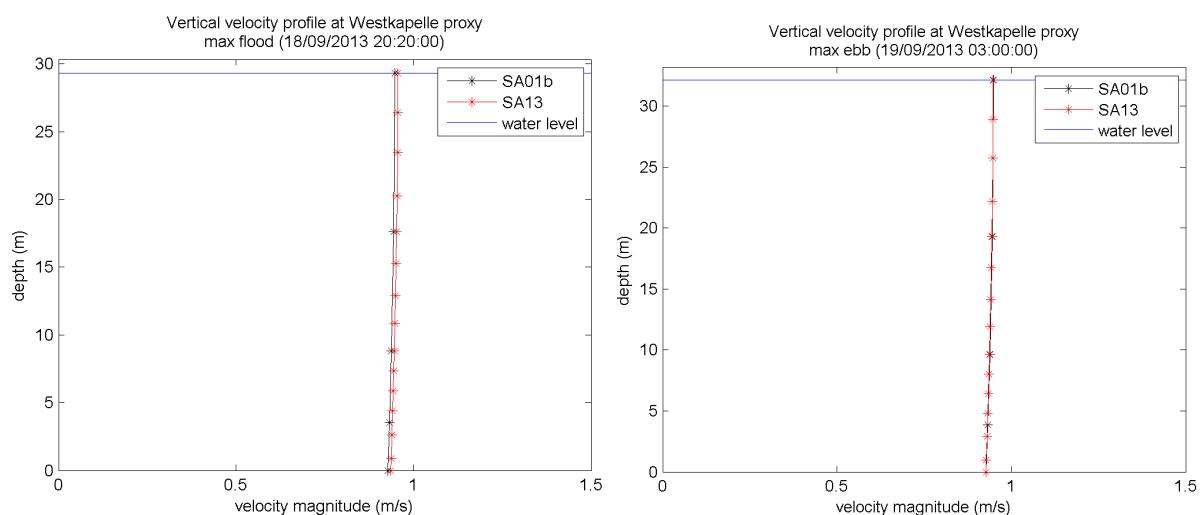


Figure 69 - Velocity profiles at Westkapelle

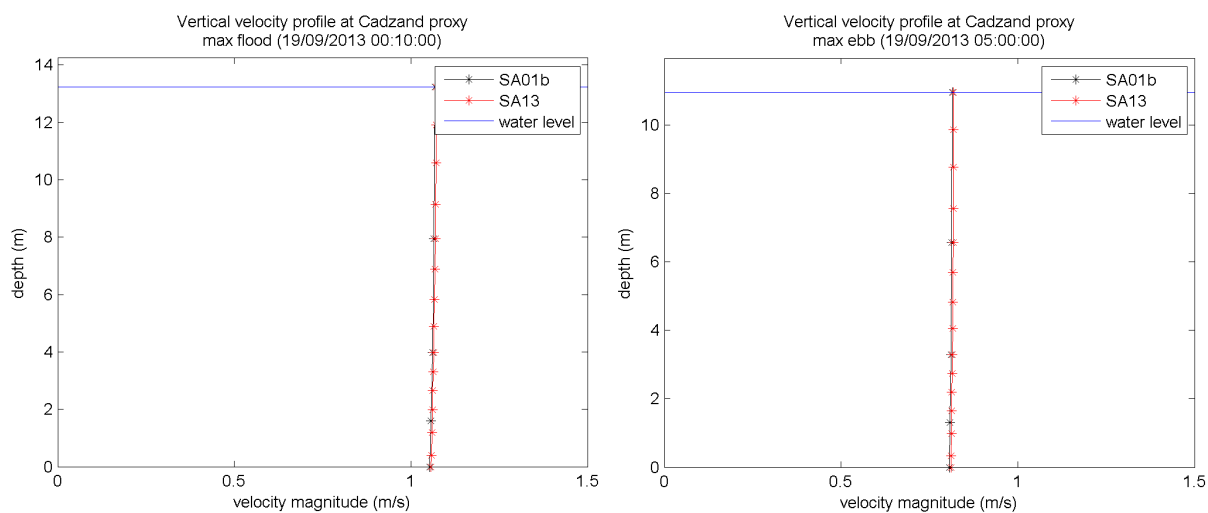


Figure 70 - Velocity profiles at Cadzand

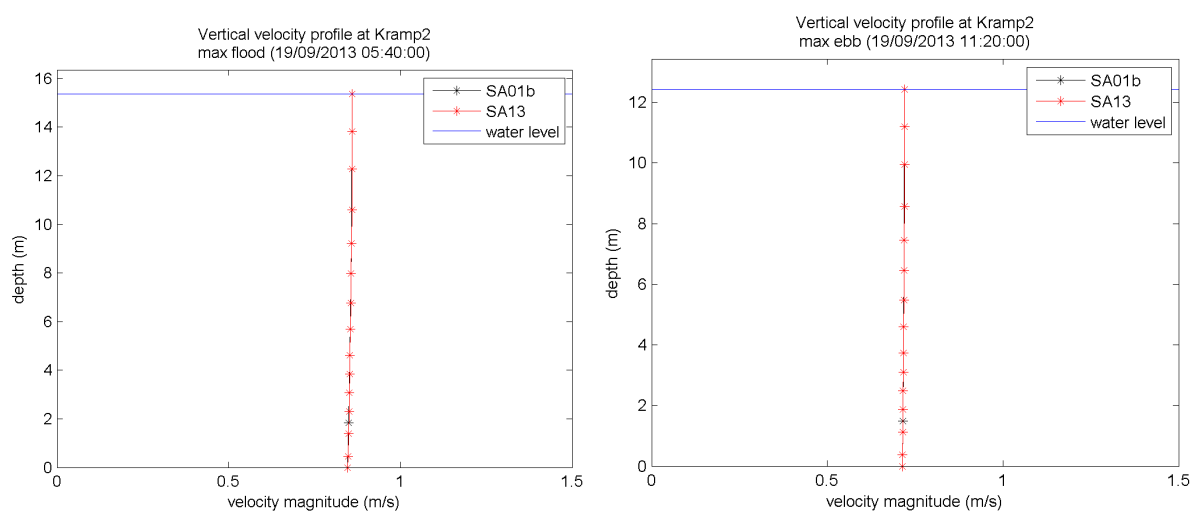


Figure 71 - Velocity profiles at Kramp (sharp river bend)

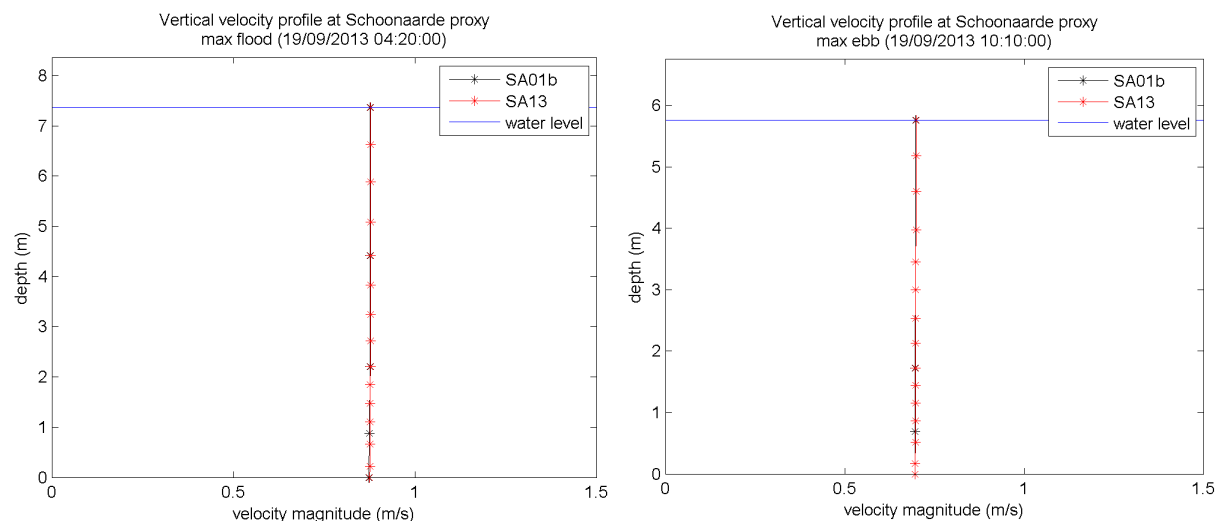


Figure 72 - Velocity profiles at Schoonaarde

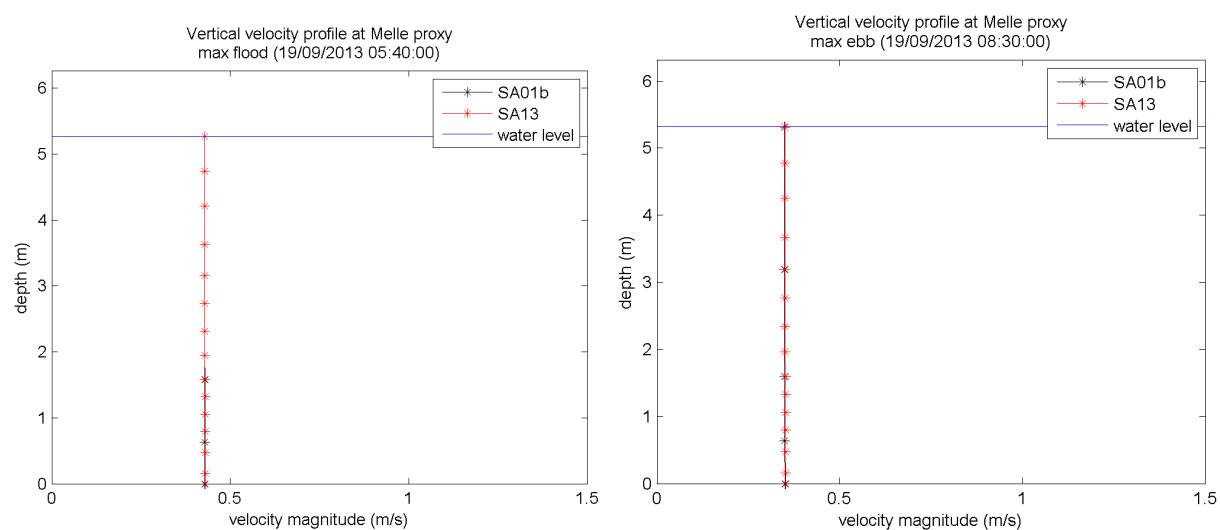


Figure 73 - Velocity profiles at Melle

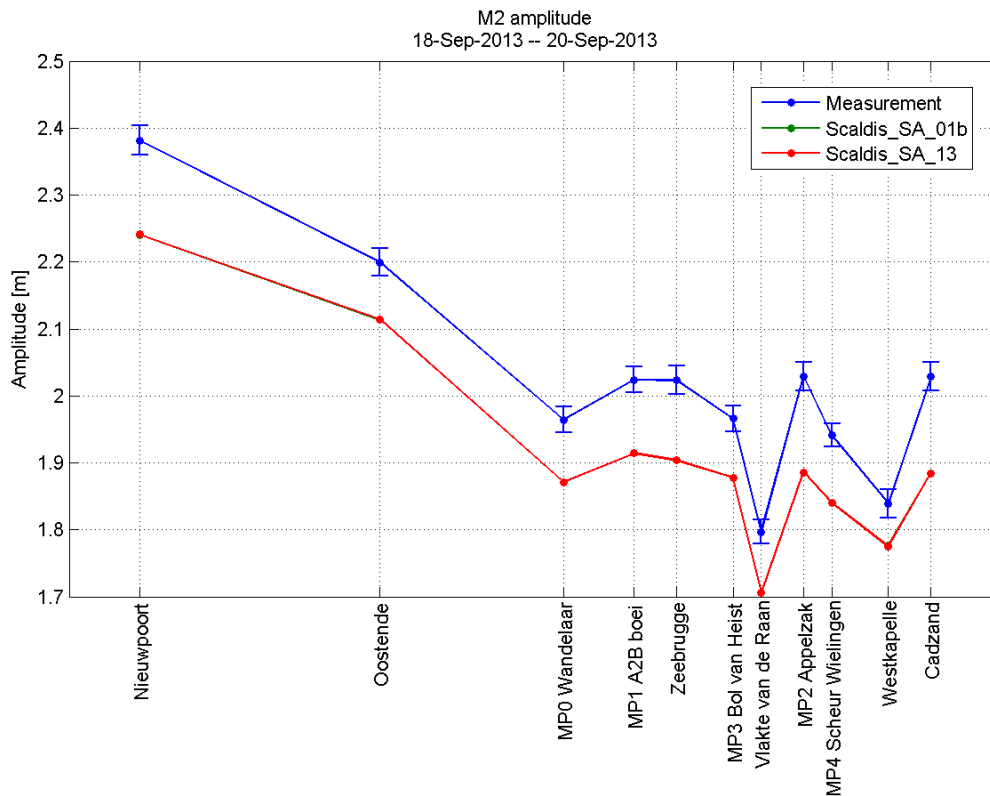


Figure 74 - M2 amplitude in SA1b and SA13 (North sea)

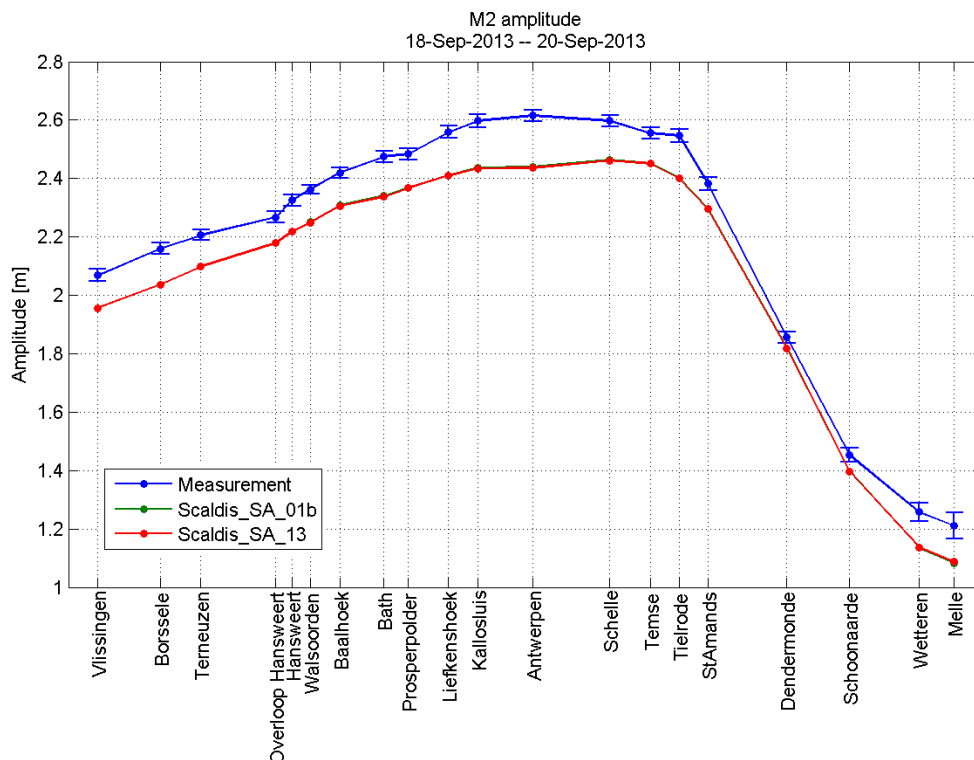


Figure 75 - M2 amplitude in SA1b and SA13 (Western Scheldt and Sea Scheldt)

The calculated viscosity for U and V along x, y and z axis (m^2/s) was written in the Telemac output file (the name of the variables are NUX, NUY and NUZ). Viscosities in X and Y direction are the same. In the following figures only the viscosities in X direction (Figure 76 to Figure 81) and Z direction (Figure 82 to Figure 87) are presented.

There are differences in horizontal viscosity (NUX) calculated in runs SA01b and SA13 in the North sea and the mouth area (Figure 88). For example, Westkapelle (Figure 77) is located in the northern part of the mouth area near the shore (where differences in viscosity are high). When Smagorinski turbulence model is used, the model is supposed to give the turbulent viscosity that occurs at sub grid level, so it depends on the mesh size (*personal communication with Hervouet J.-M., Telemac forum*). However, these differences in viscosity do not have any significant impact on the calculated velocities. This is probably because the numerical diffusion in the downstream part of the estuary is higher than the calculated viscosity. More upstream the differences in calculated horizontal viscosity are very small (Figure 90).

The calculated vertical viscosity (NUZ) is the same in both runs (Figure 91 to Figure 93).

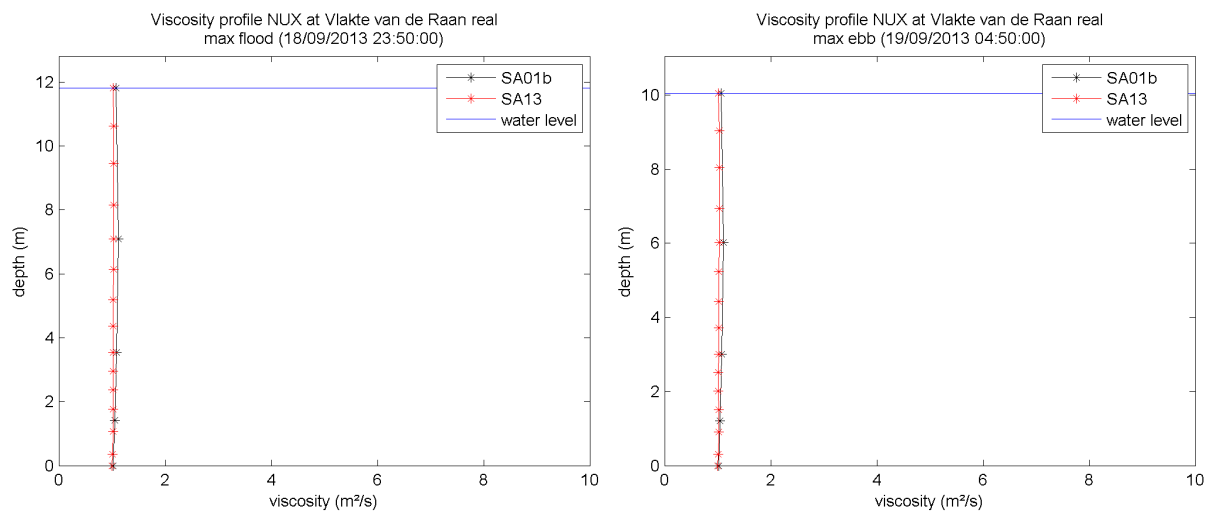


Figure 76 - Profiles of horizontal viscosity NUX at Vlakte van de Raan

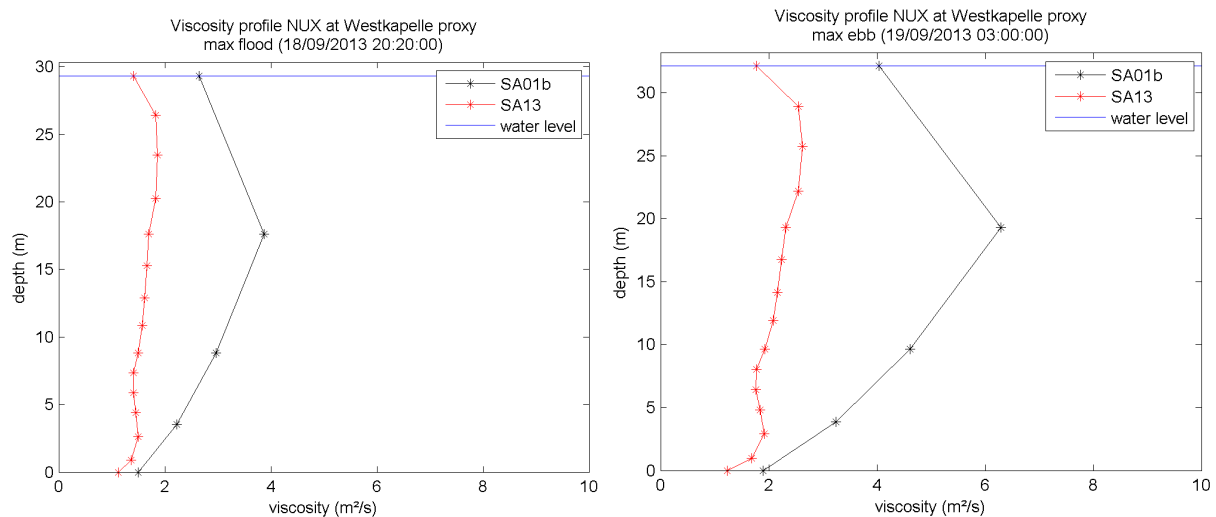


Figure 77 - Profiles of horizontal viscosity NUX at Westkapelle

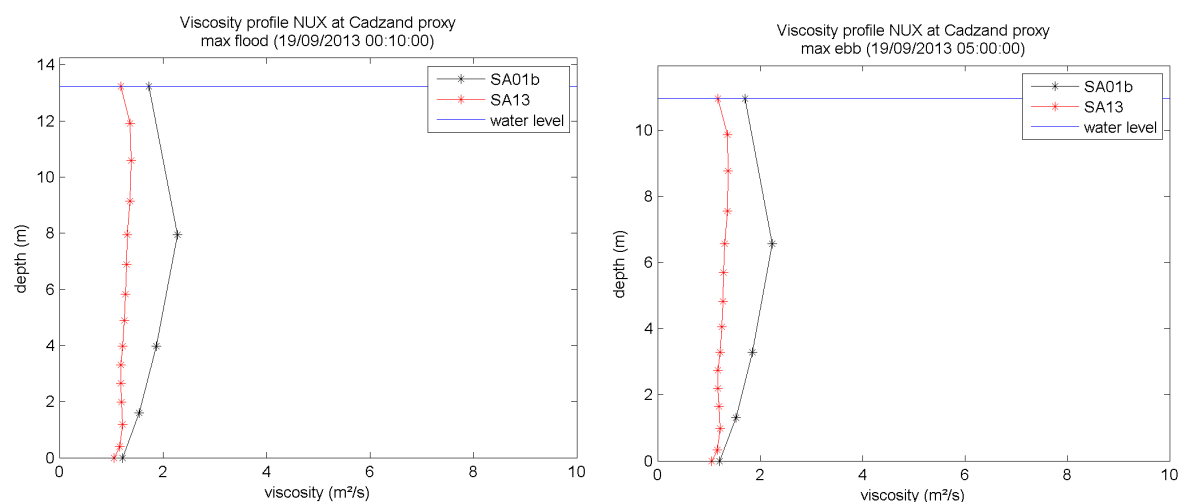


Figure 78 - Profiles of horizontal viscosity NUX at Cadzand

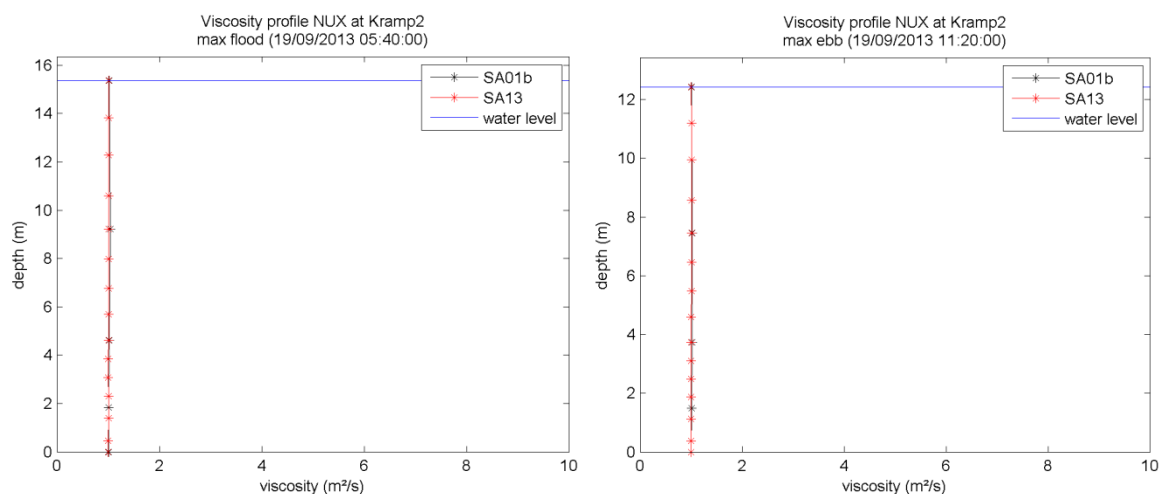


Figure 79 - Profiles of horizontal viscosity NUX at Kramp

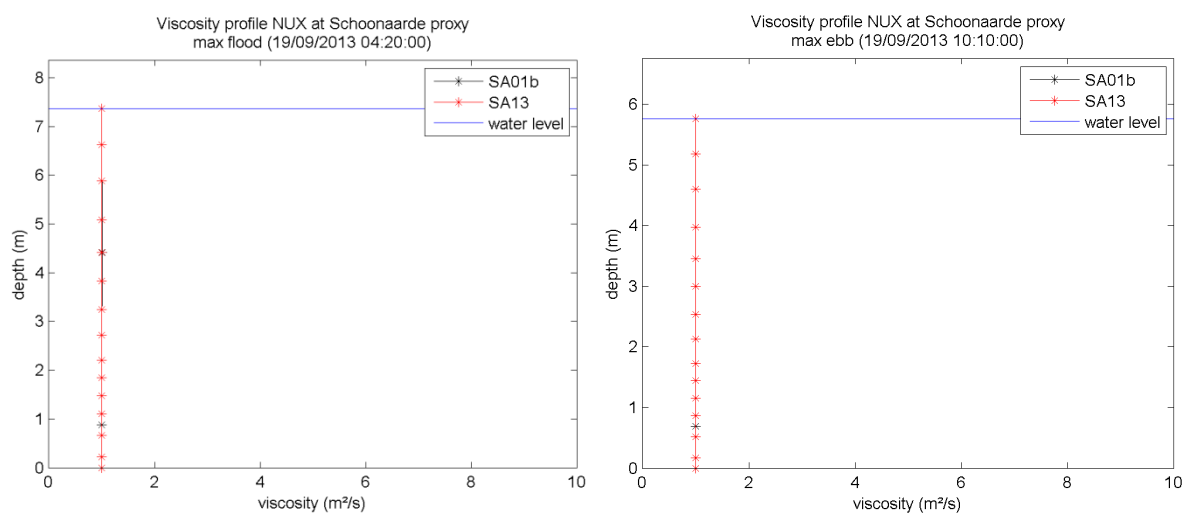


Figure 80 - Profiles of horizontal viscosity NUX at Schoonaarde

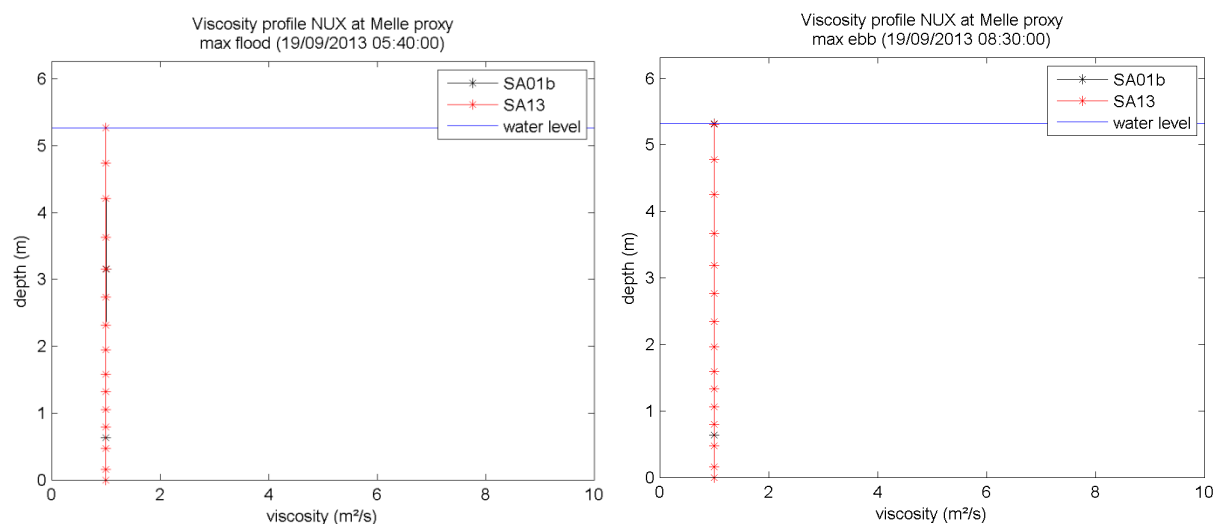


Figure 81 - Profiles of horizontal viscosity NUX at Melle

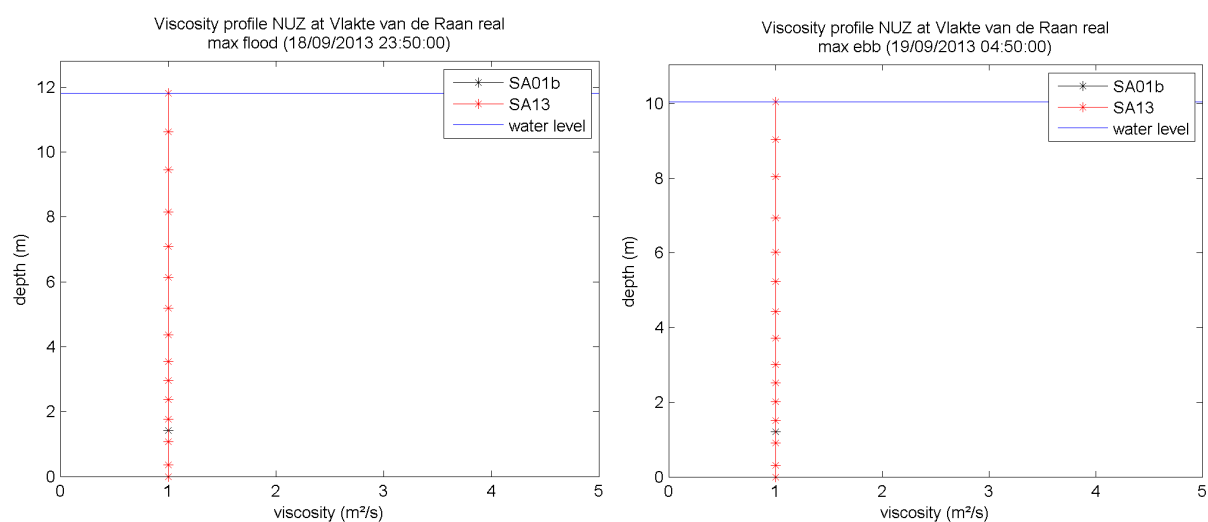


Figure 82 - Profiles of vertical viscosity NUZ at Vlakte van de Raan

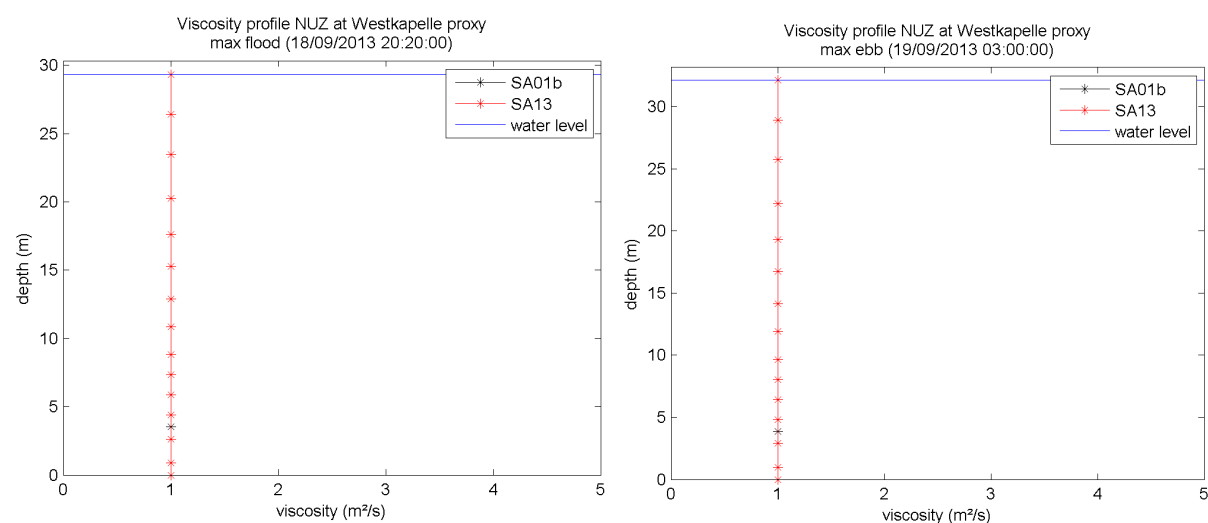


Figure 83 - Profiles of vertical viscosity NUZ at Westkapelle

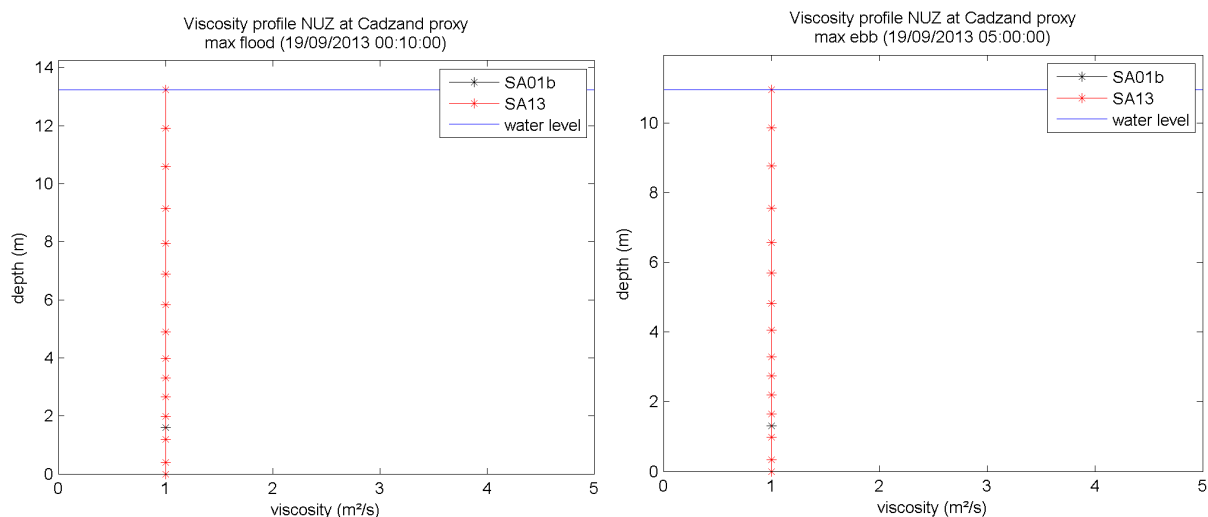


Figure 84 - Profiles of vertical viscosity NUZ at Cadzand

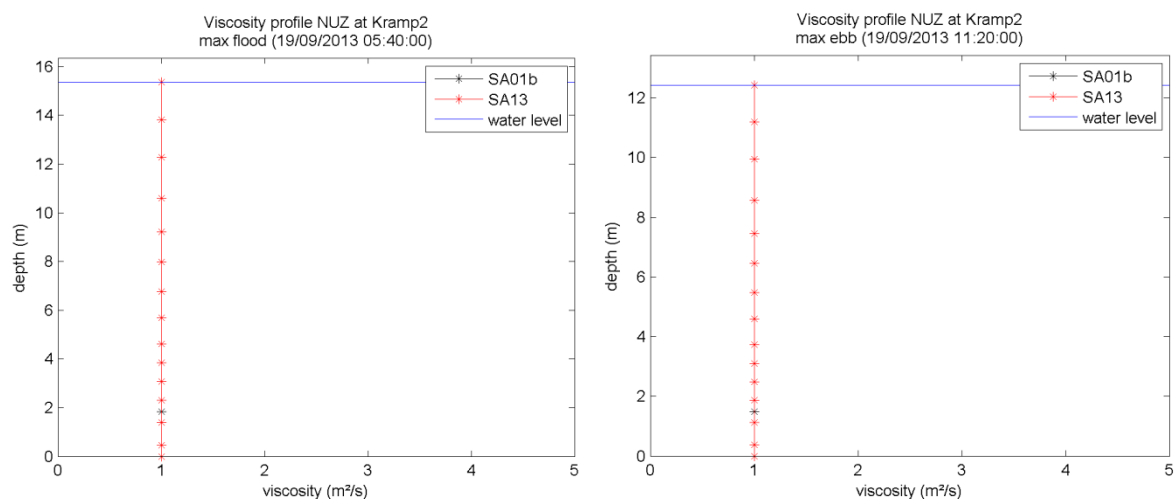


Figure 85 - Profiles of vertical viscosity NUZ at Kramp

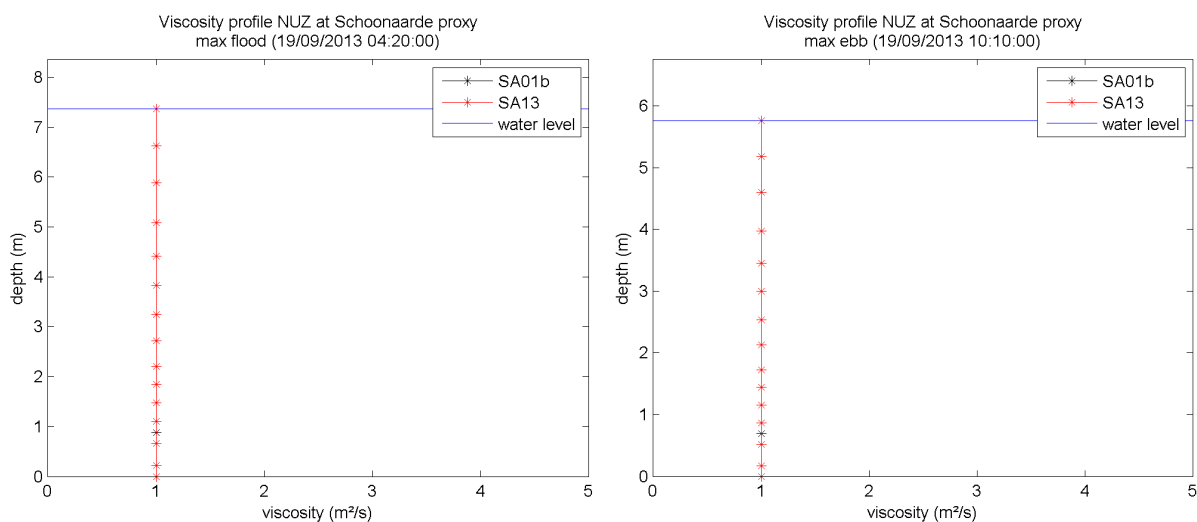


Figure 86 - Profiles of vertical viscosity NUZ at Schoonaarde

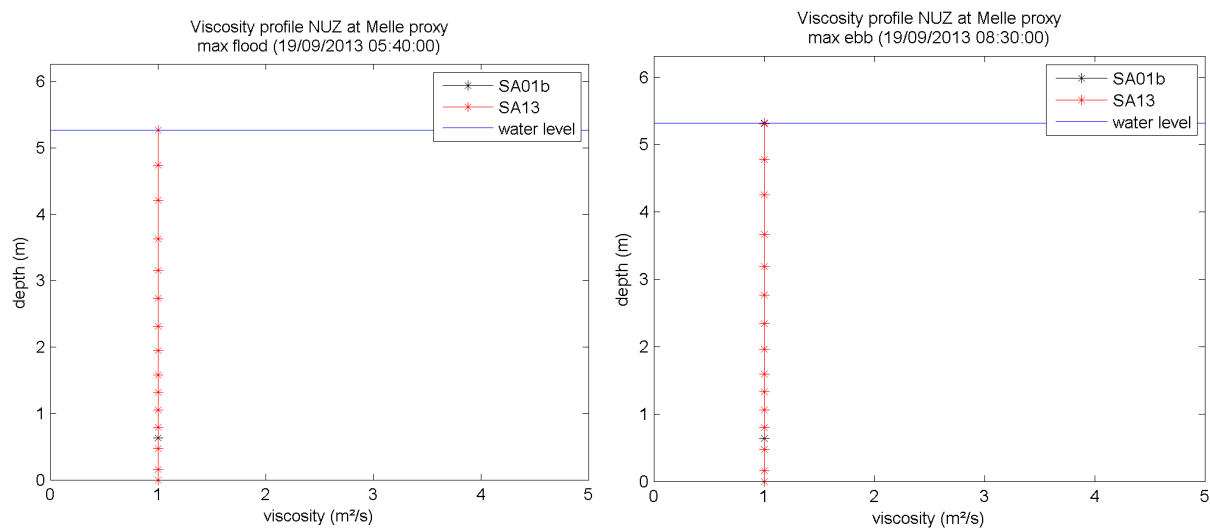


Figure 87 - Profiles of vertical viscosity NUZ at Melle

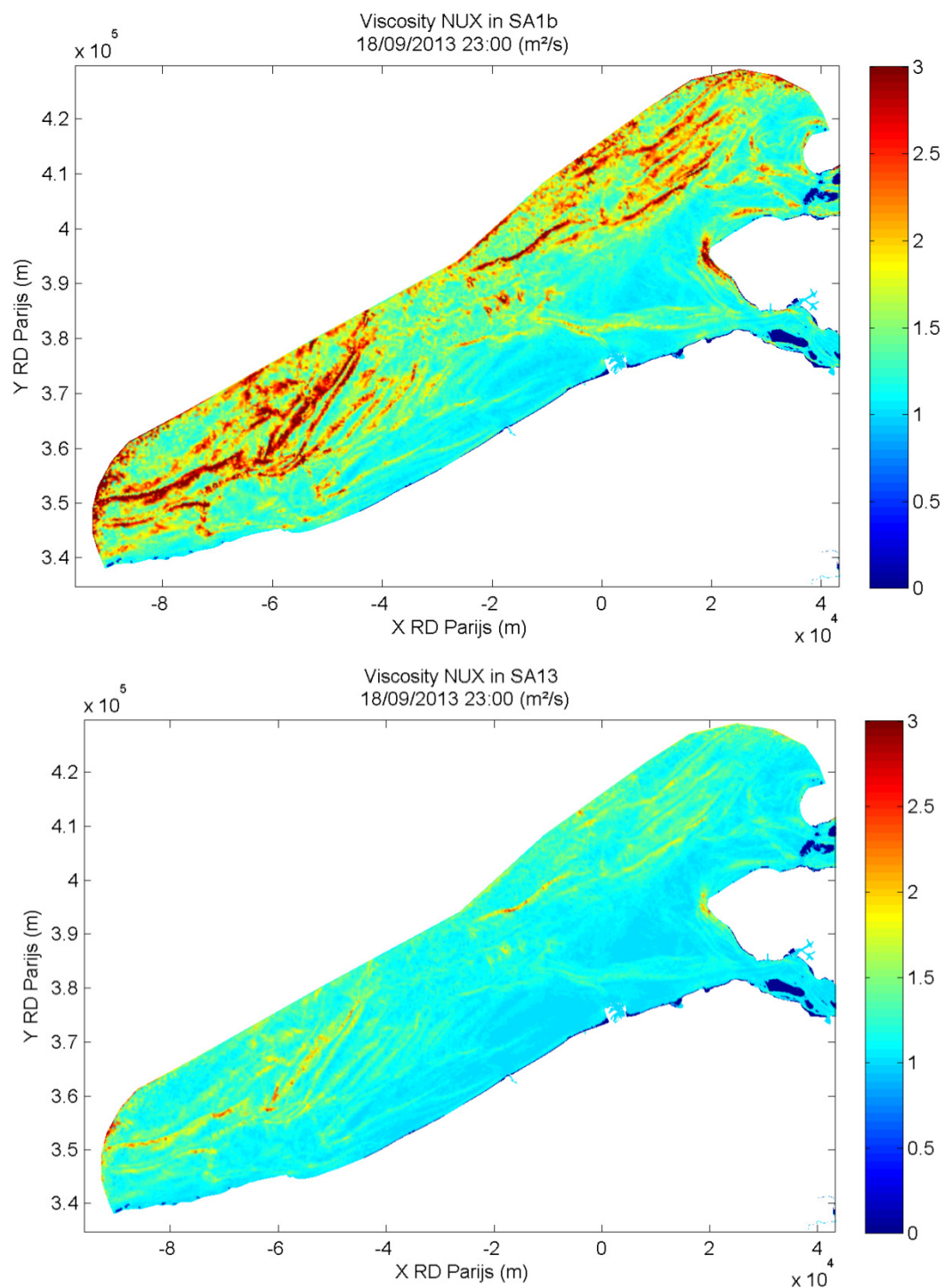


Figure 88 - Map of the depth average horizontal viscosity in the North sea in runs SA1b and SA13

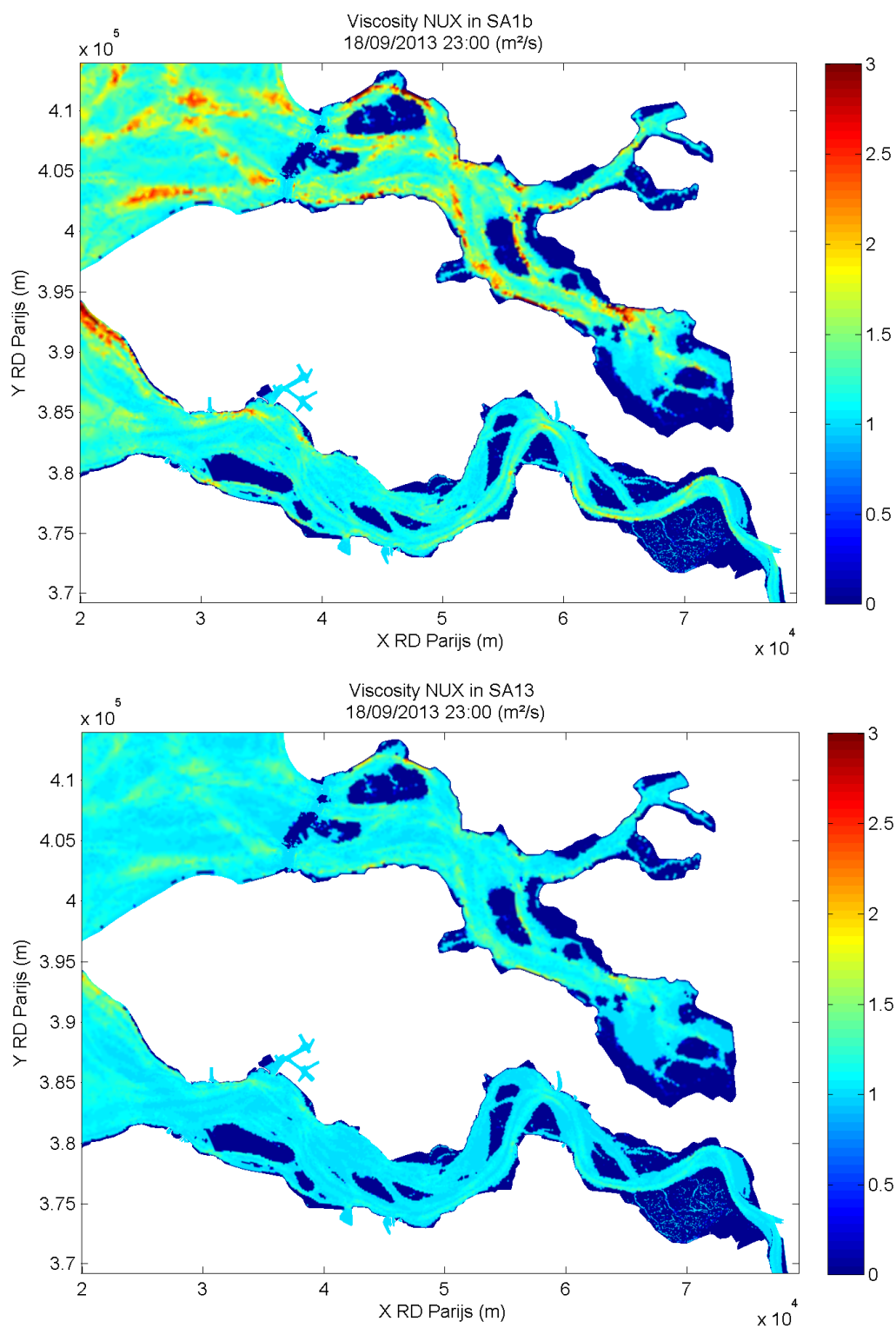


Figure 89 - Map of the depth average horizontal viscosity in the Western Scheldt in runs SA1b and SA13

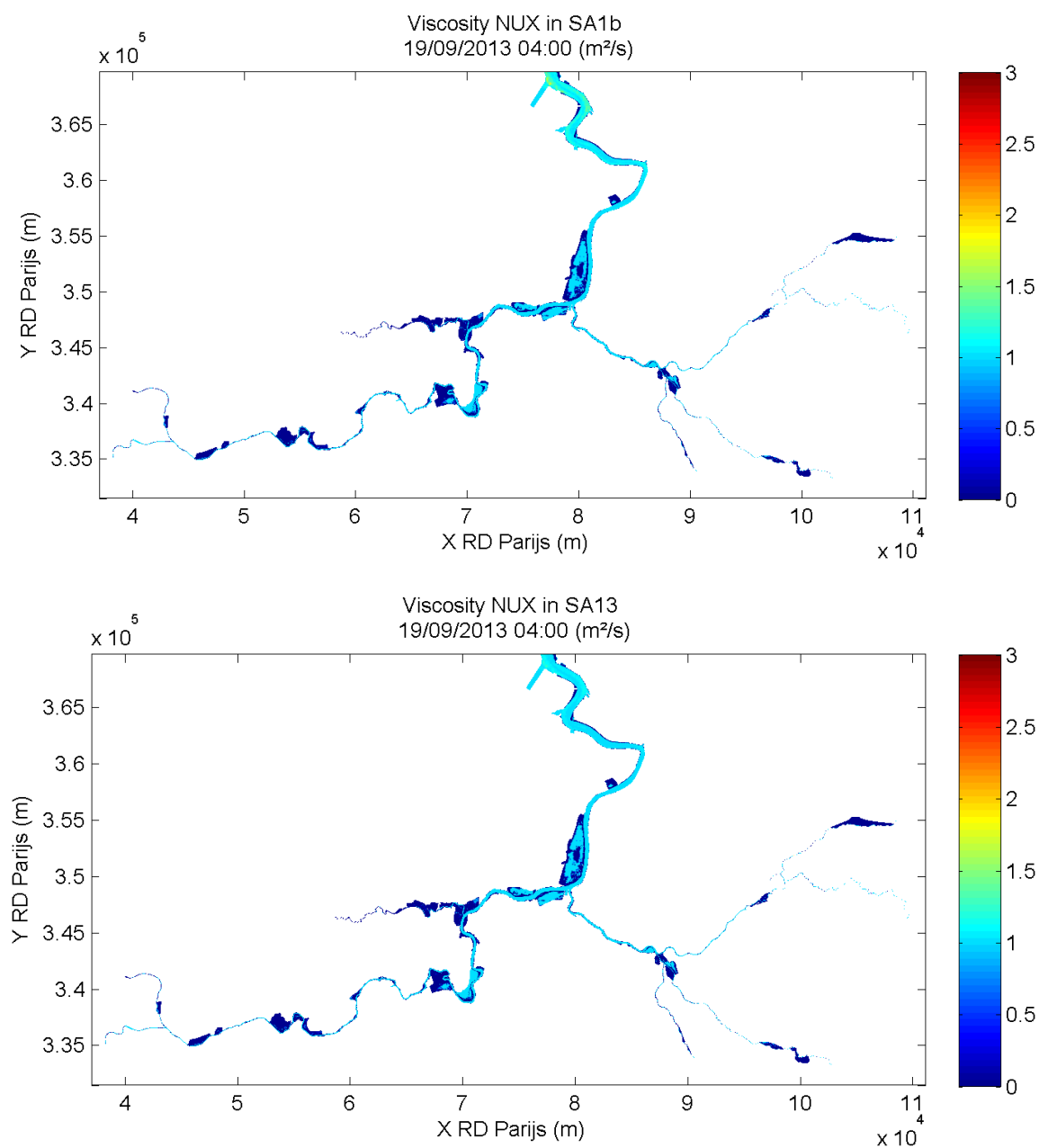


Figure 90 - Map of the depth average horizontal viscosity in the Sea Scheldt in runs SA1b and SA13

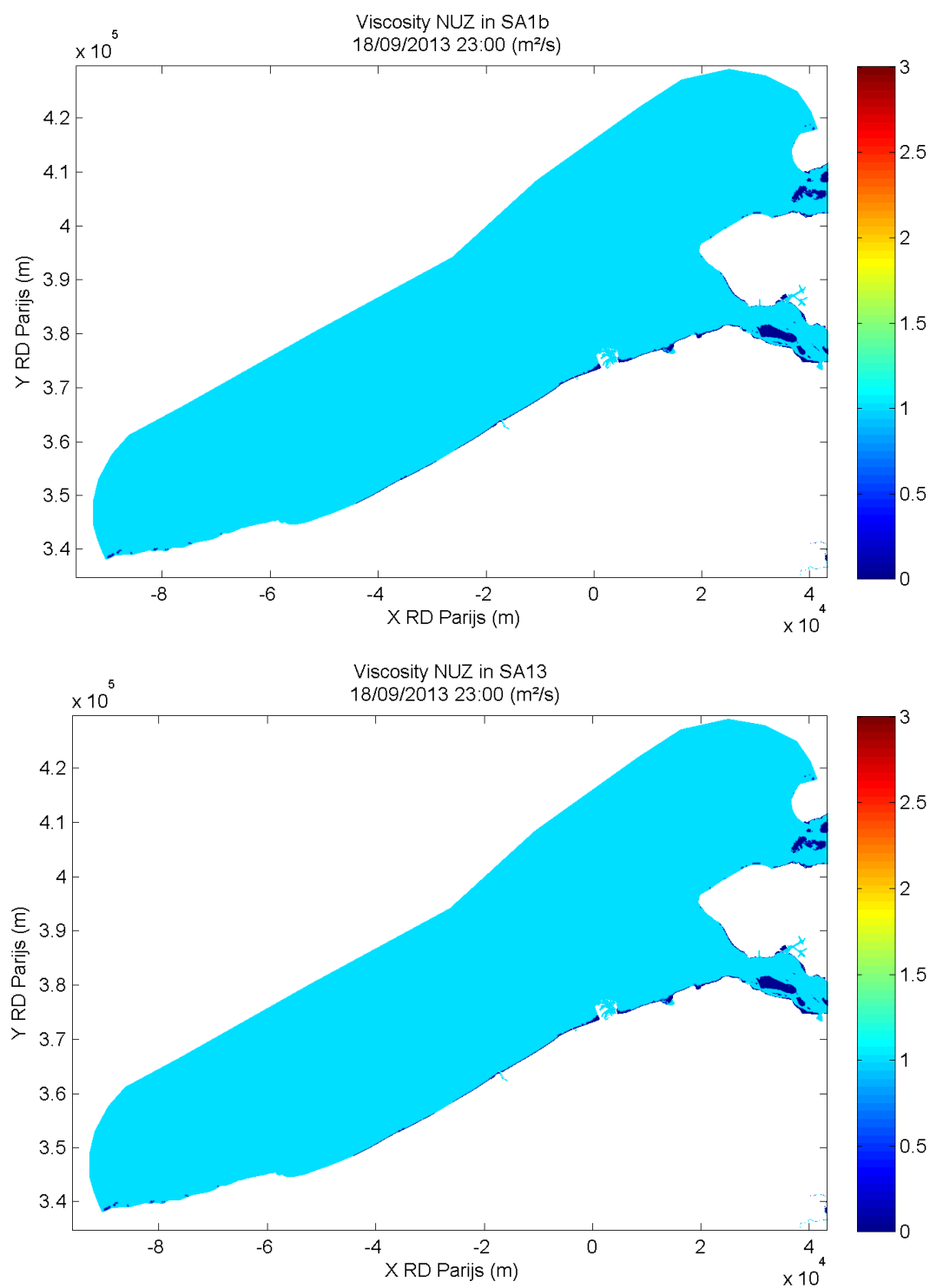


Figure 91 - Map of the depth average vertical viscosity in the North sea in runs SA1b and SA13

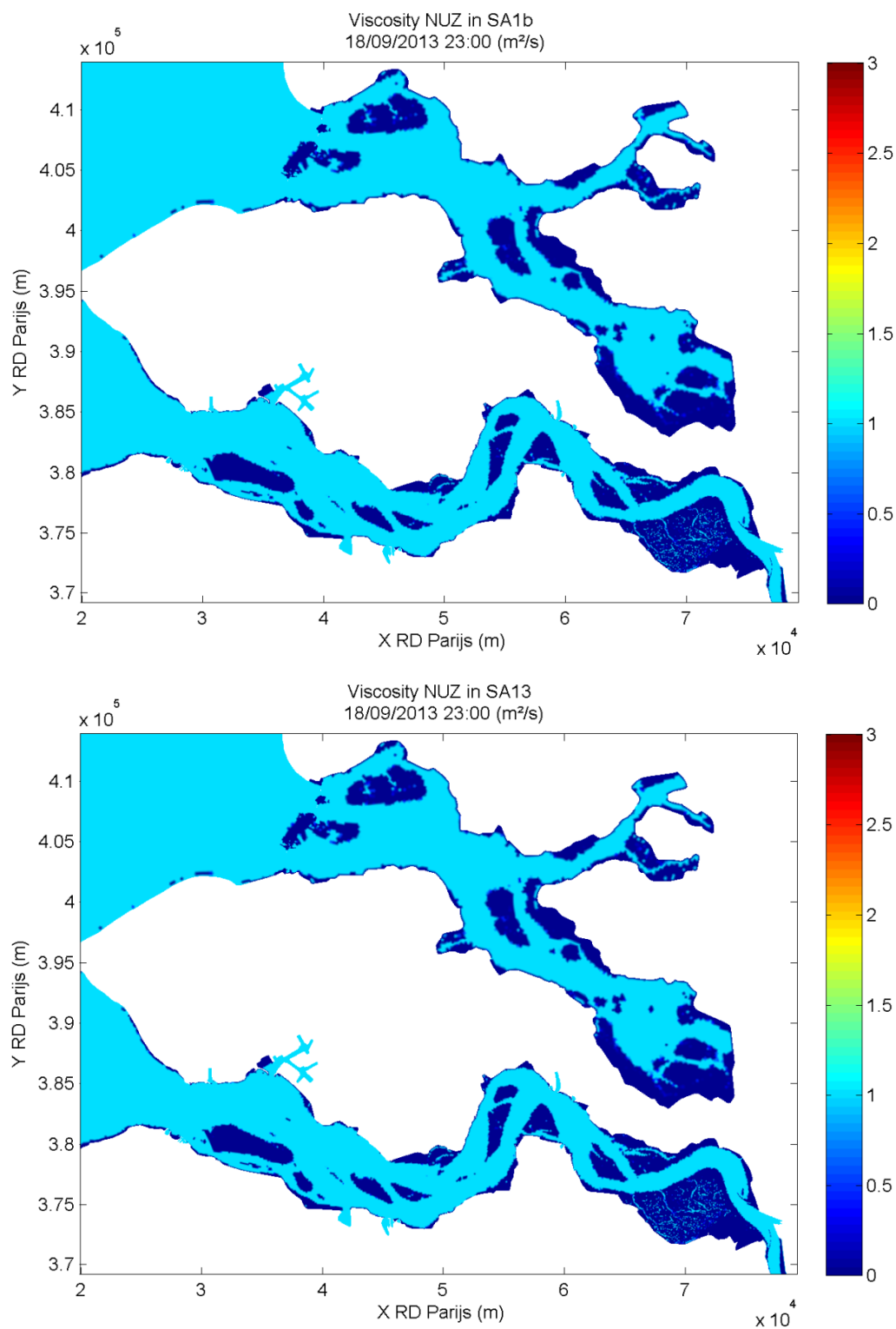


Figure 92 - Map of the depth average vertical viscosity in the Western Scheldt in runs SA1b and SA13

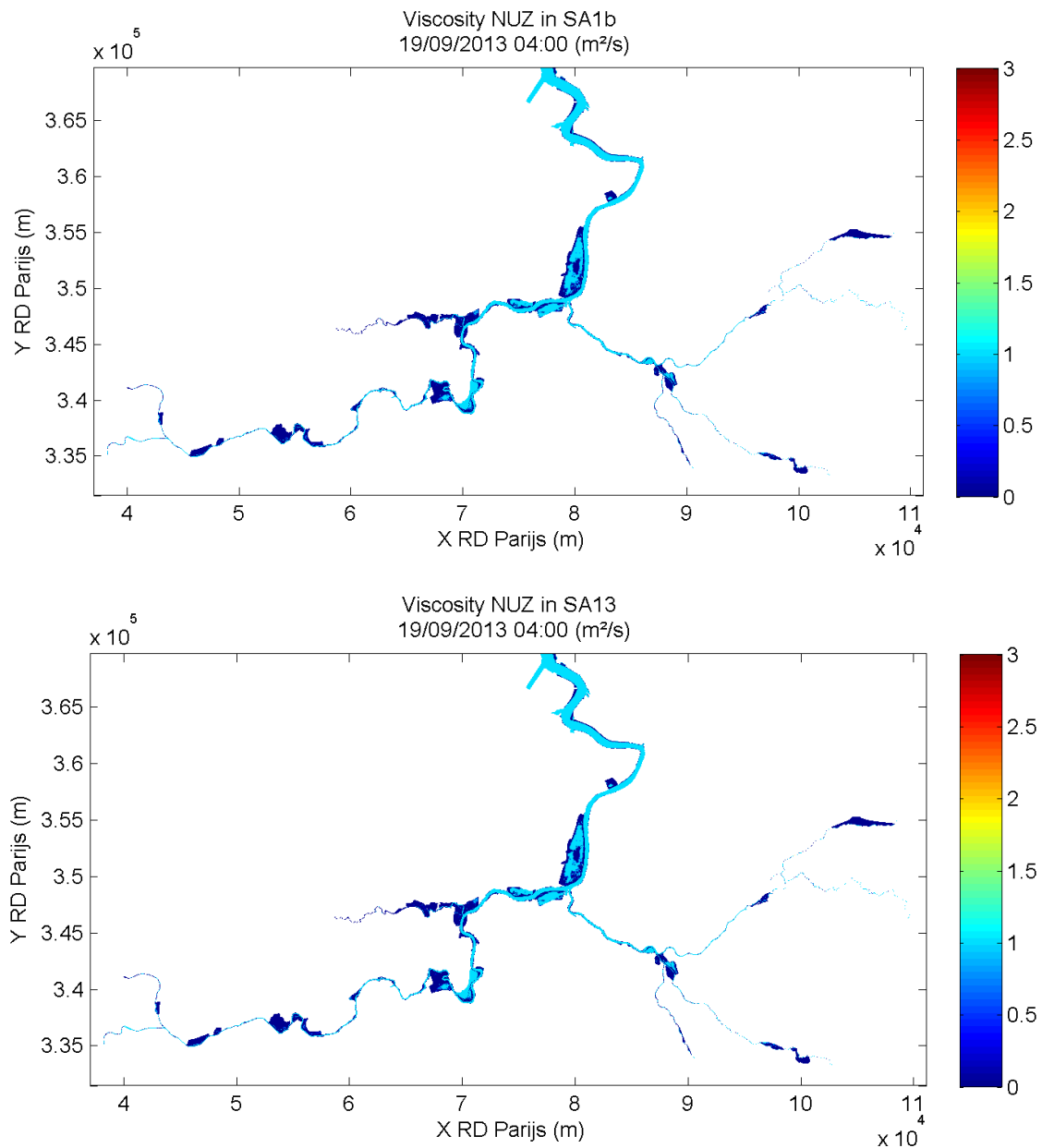


Figure 93 - Map of the depth average vertical viscosity in the Sea Scheldt in runs SA1b and SA13

7.5. Bathymetry

7.5.1. Durme

From the calibration simulations we noticed that the error on the water levels in the Durme is much larger than in the Scheldt. Modifying the bottom roughness coefficient is not sufficient to correct the water levels. Here we try to modify the bathymetry of the Durme to see what kind of effect this has on the modeled water levels. Bathymetry of the Durme river is decreased by 1 m in run SA15. The output of this run is compared to simulation SA1 (original bathymetry).

Table 35. Model runs used for the sensitivity analysis to the bathymetry of Durme

Model run	Bathymetry of Durme
SA1	original
SA15	original bathymetry – 1m

The M2 amplitude calculated in runs SA1 and SA15 is presented in Figure 94 to Figure 96. The differences between the calculated high and low waters are shown in Figure 97 and Figure 98. The bathymetry of Durme has effect on water levels upstream Antwerp. The biggest differences are calculated at Tielrode (Figure 99).

M2 amplitude decreases in SA15 by 1 cm from Antwerp to Schoonaarde (2 cm at Temse); it increases by 1 cm at Tielrode. High waters decrease everywhere upstream Hemiksem by 2 to 4 cm. Low waters decrease at Tielrode by about 6 cm.

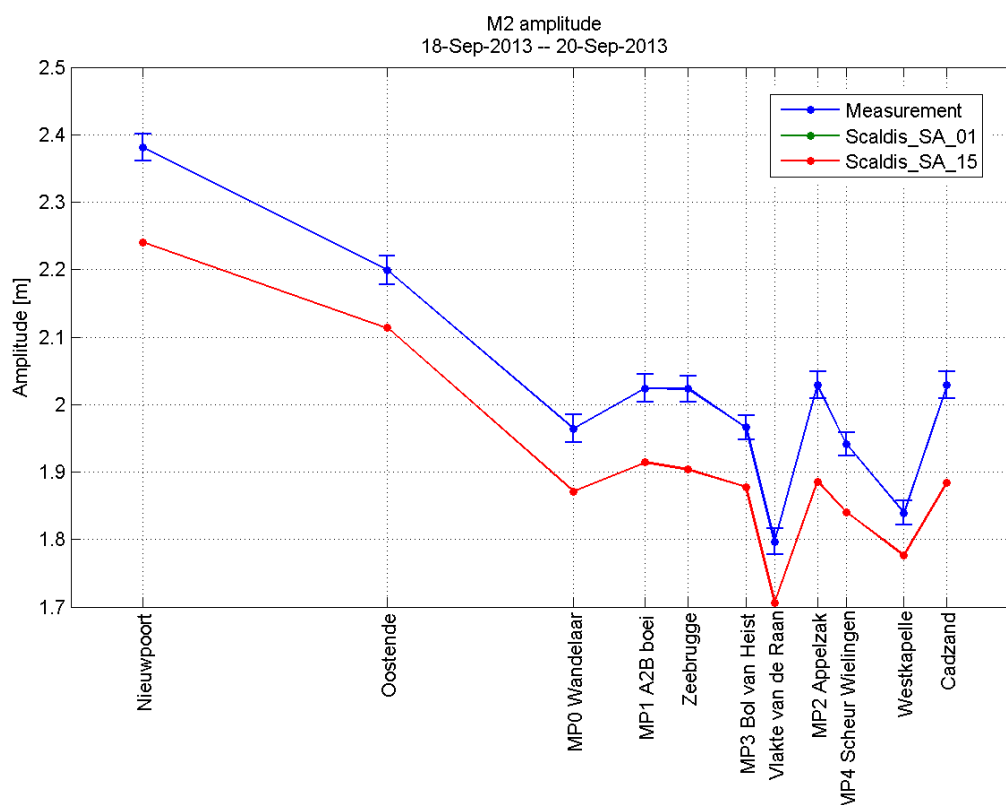


Figure 94 - M2 amplitude in runs SA1 and SA15 (North sea)

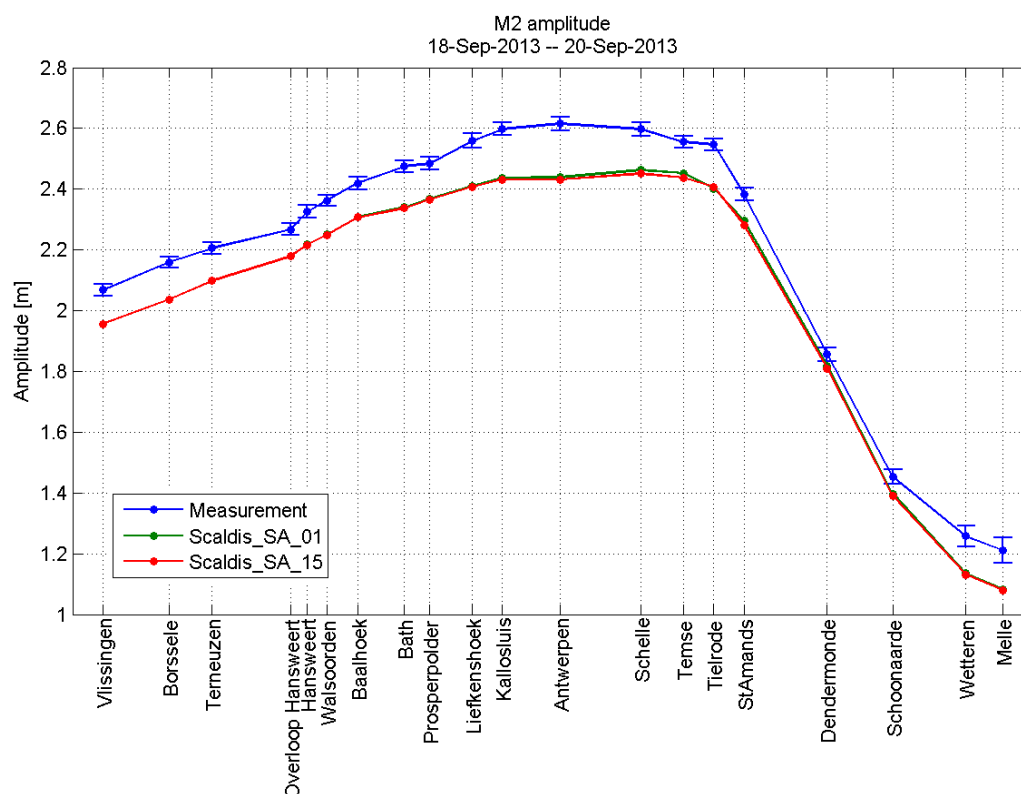


Figure 95 - M2 amplitude in runs SA1 and SA15 (Western Scheldt and Sea Scheldt)

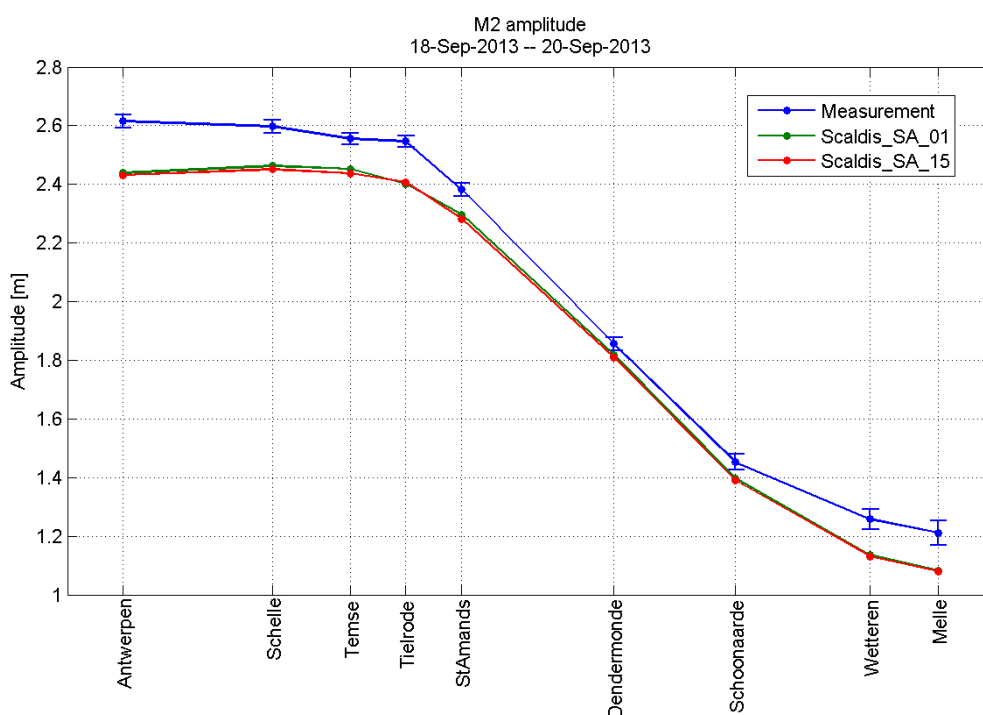


Figure 96 - M2 amplitude in runs SA1 and SA15 (zoom to the zone with changes in water levels)

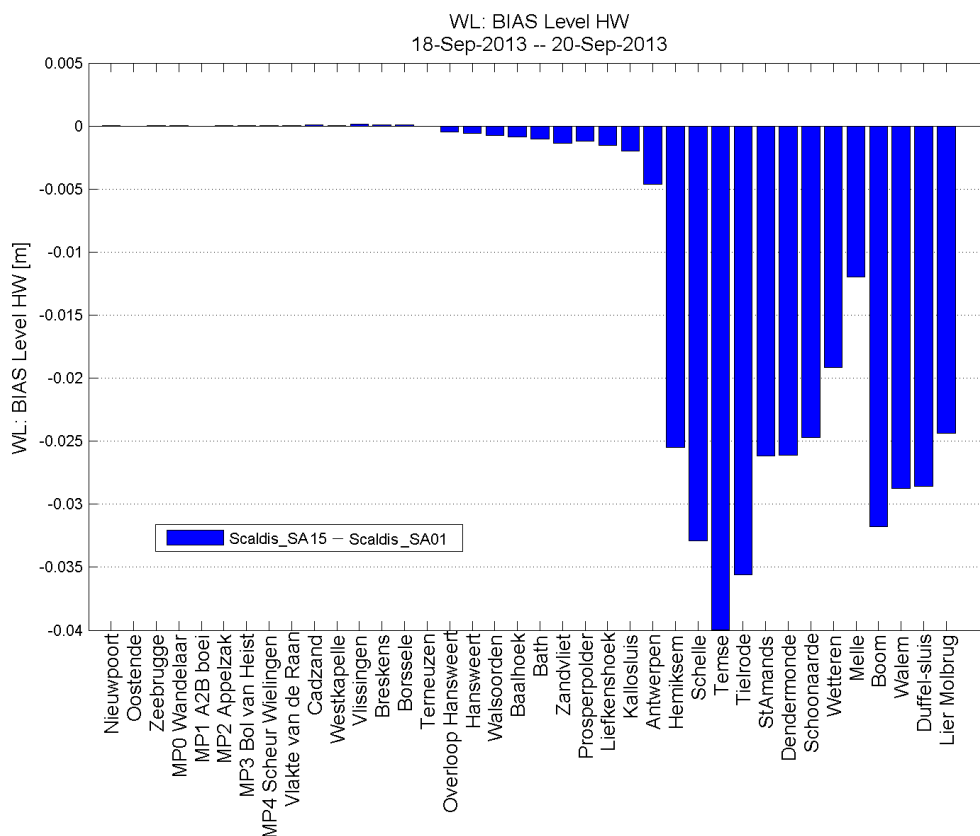


Figure 97 - Bias of high water (SA15 – SA1)

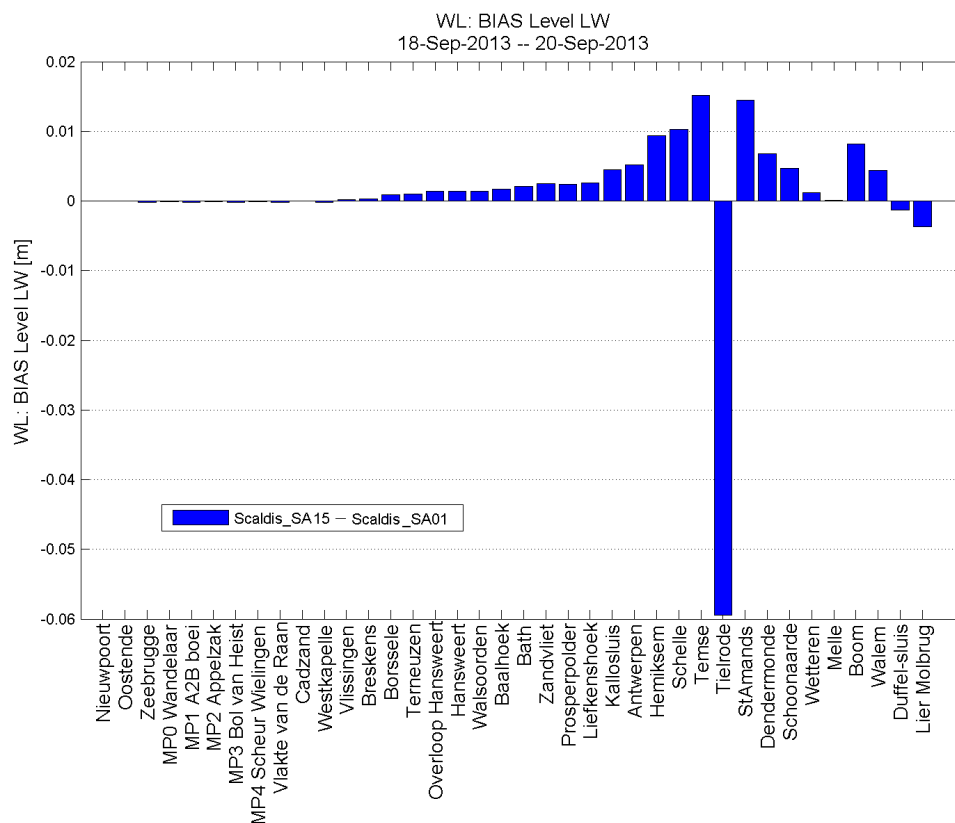


Figure 98 - Bias of low water (SA15 – SA1)

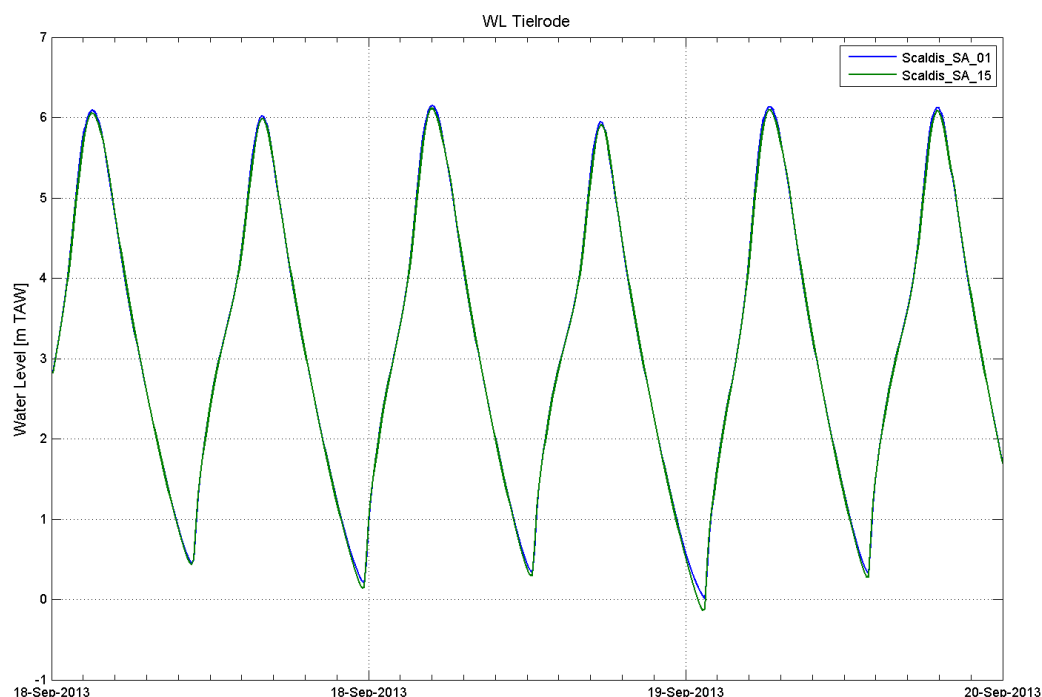


Figure 99 - Water level at Tielrode in SA1 and SA15

7.5.2. Tidal branch Gentbrugge

Bathymetry of the tidal branch Gentbrugge is decreased by 1m in run SA16. The output of this run is compared to simulation SA1 (original bathymetry).

Table 36. Model runs used for the sensitivity analysis to the bathymetry of the tidal branch Gentbrugge

Model run	Bathymetry of tidal branch Gentbrugge
SA1	original
SA16	original bathymetry – 1m

The M2 amplitude calculated in runs SA1 and SA16 is presented in Figure 100 and Figure 101. The differences between the calculated high and low waters are shown in Figure 102 and Figure 103. The bathymetry of the tidal branch Gentbrugge has effect on water levels at Schoonaarde, Wetteren and Melle.

High waters decrease by 8 cm at Wetteren and 19 cm at Melle. Low waters increase at Schoonaarde, Wetteren and Melle by 4, 10 and 12 cm respectively.

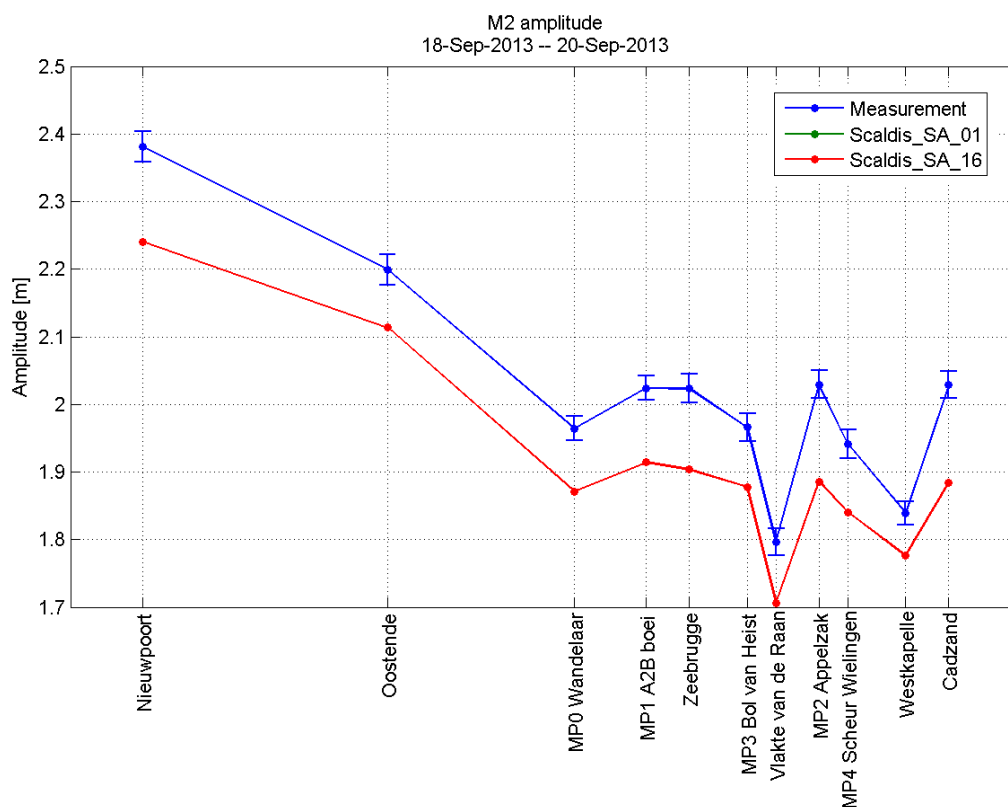


Figure 100 - M2 amplitude in runs SA1 and SA16 (North sea)

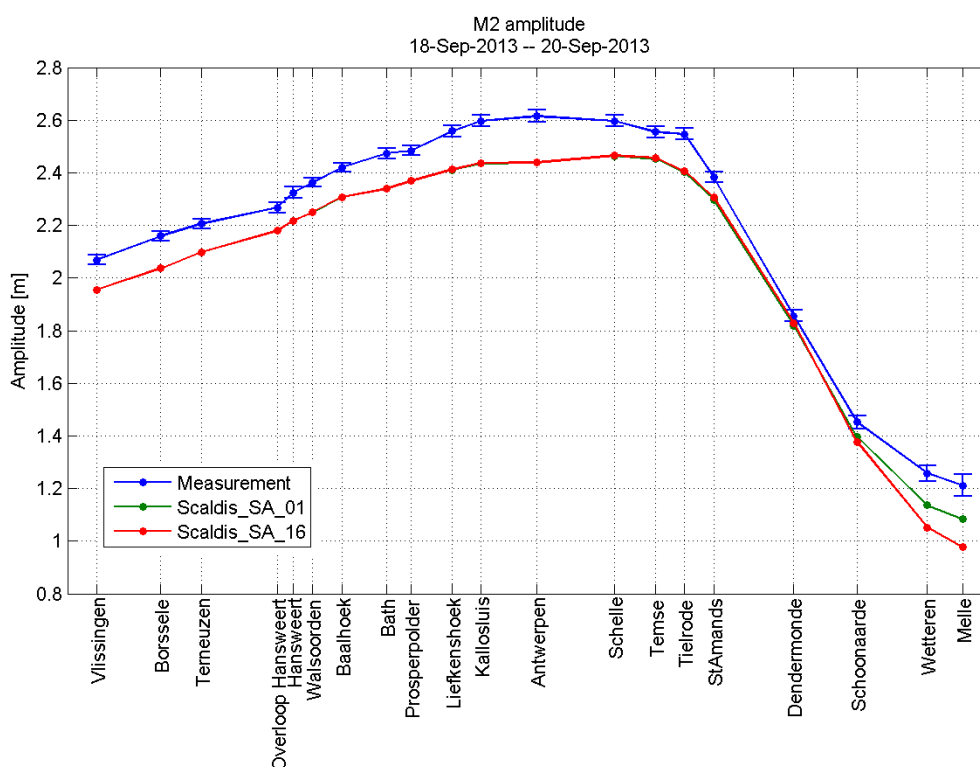


Figure 101 - M2 amplitude in runs SA1 and SA16 (Western Scheldt and Sea Scheldt)

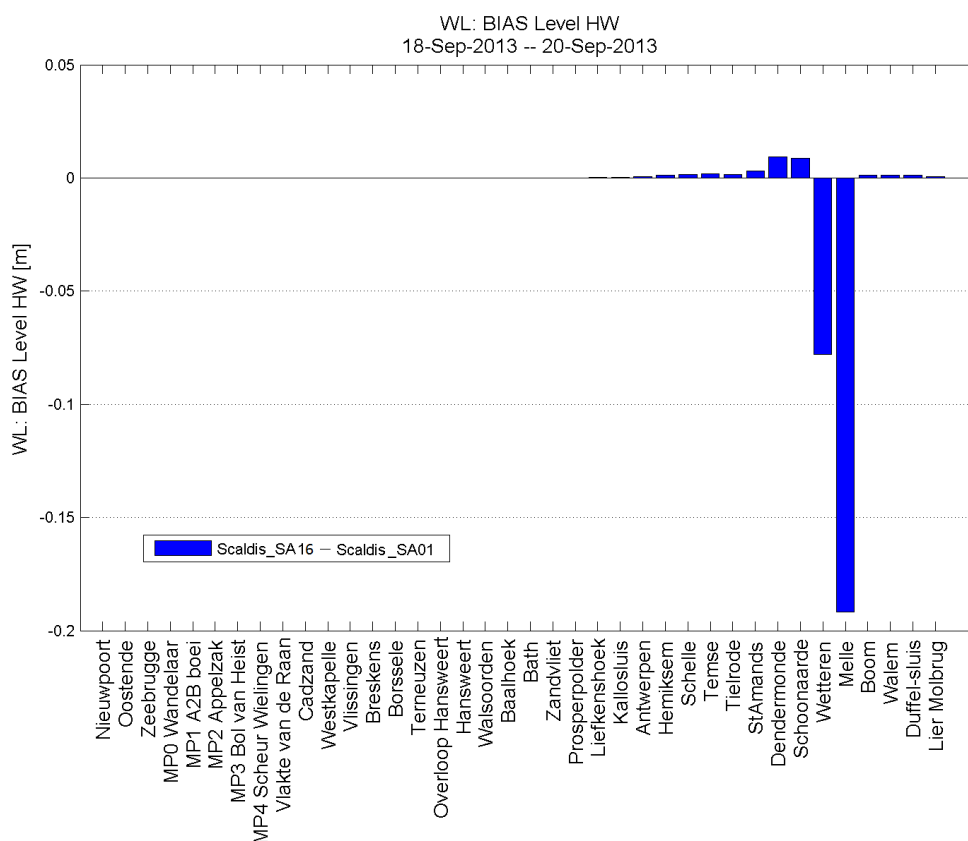


Figure 102 - Bias of high water (SA16 – SA1)

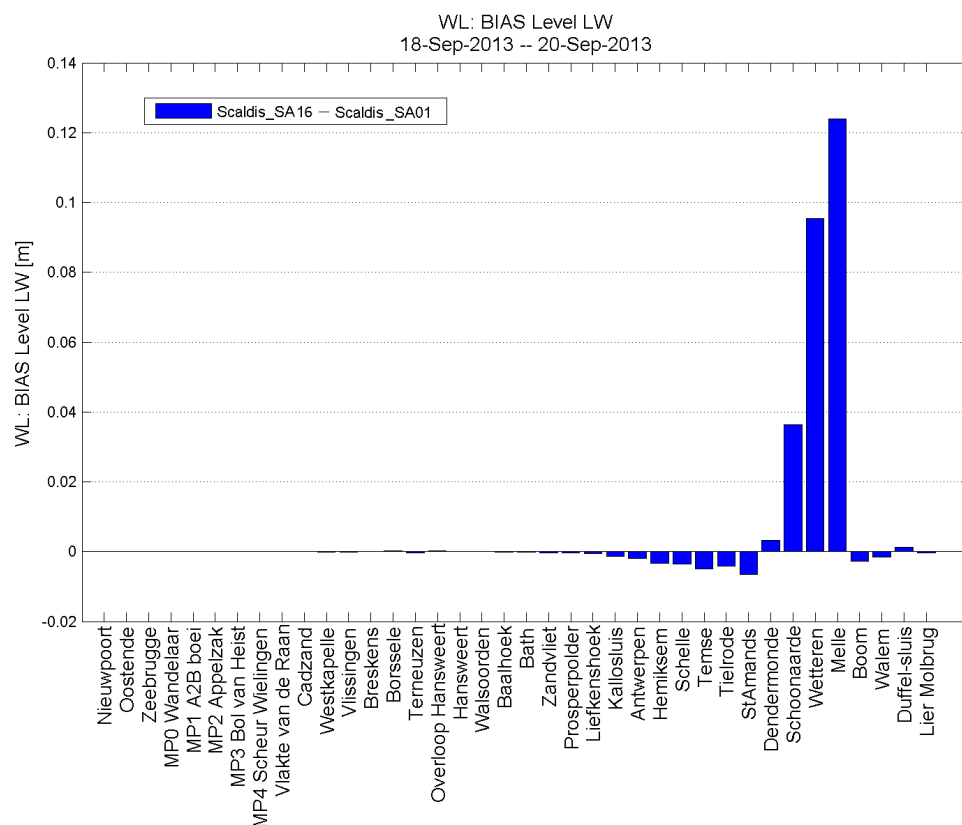


Figure 103 - Bias of low water (SA16 – SA1)

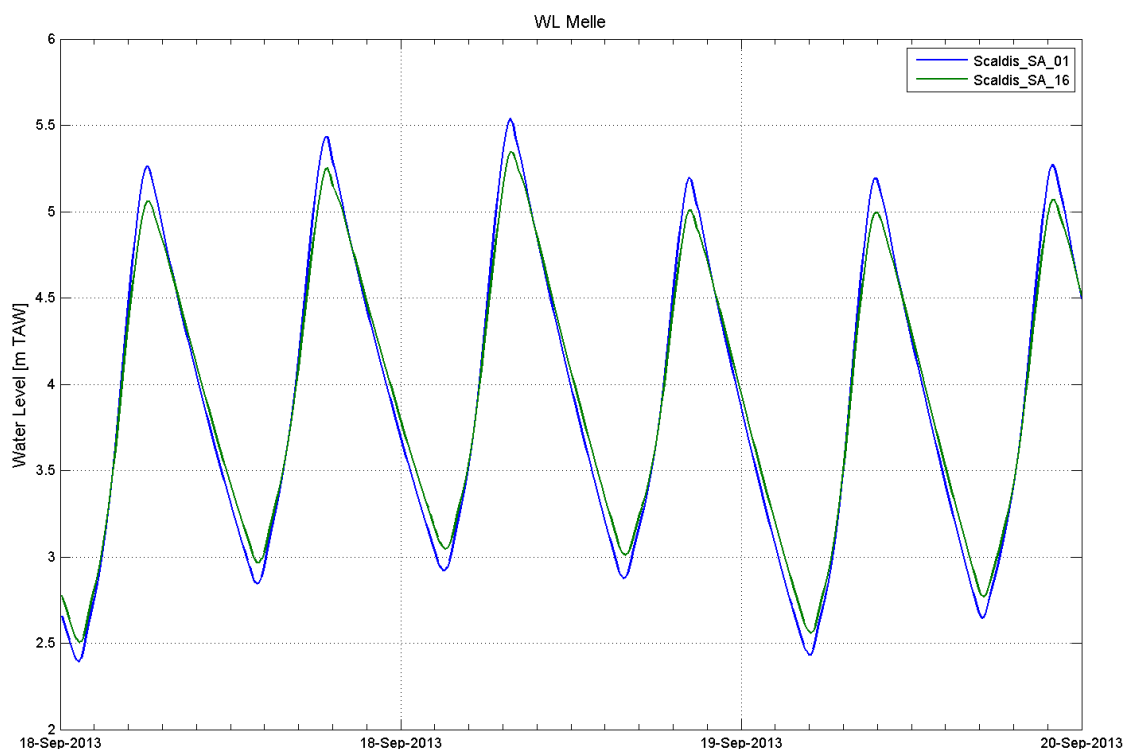


Figure 104 - Water level at Melle in SA1 and SA16

7.6. Turbulence model

7.6.1. k-Epsilon vs. Smagorinski model

Runs with k-Epsilon and Smagorinski turbulence models are described in Table 37.

Table 37. Model runs with different turbulence models (Smagorinski and k-Epsilon)

Model run	Horizontal turbulence model	Coefficient for horizontal diffusion of velocities (m ² /s)	Vertical turbulence model	Coefficient for vertical diffusion of velocities (m ² /s)
SA8a	Smagorinski model	10 ⁻⁶	mixing length model Nezu and Nakagawa	10 ⁻⁶
SA14a	k-Epsilon model*	10 ⁻⁶	k-Epsilon model*	10 ⁻⁶

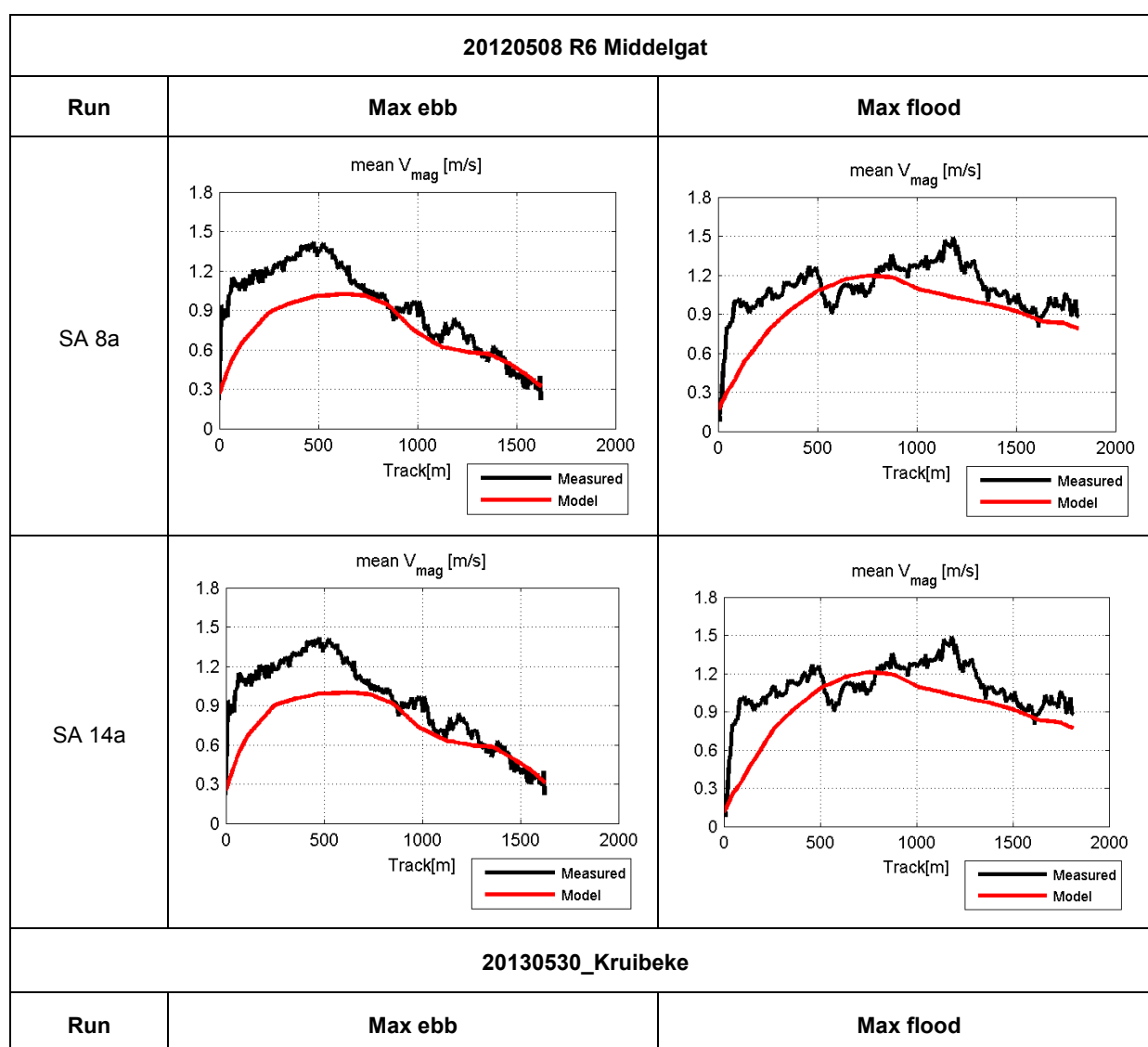
* when k-Epsilon model is used, the parameter COEFFICIENT FOR HORIZONTAL (or VERTICAL) DIFFUSION OF VELOCITIES must get its real physical value (10⁻⁶ for molecular diffusivity of water), as this is used as such by the turbulence model (EDF-R&D, 2013)

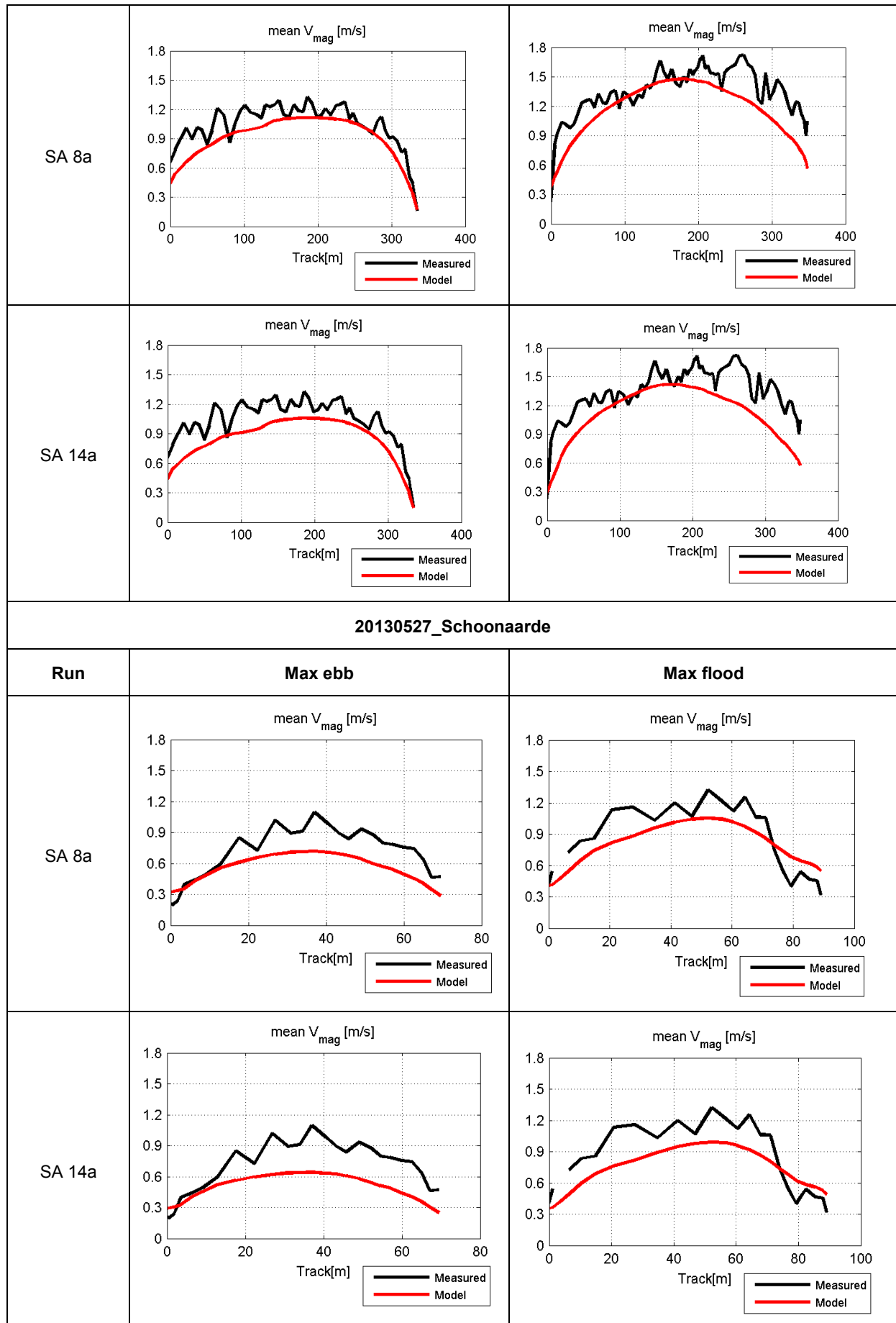
The results of SA_8a (Smagorinski and mixing length models) are compared with the output of SA_14a (k-Epsilon model). The same coefficients for horizontal and vertical diffusion of velocities are used in these runs. The k-Epsilon model comprises a couple of equations solving the balance equation for k (turbulent energy) and ϵ (turbulent dissipation). The Smagorinski turbulence model is described in chapter 5.10.2.

The implementation of the k-Epsilon turbulence model results in a decrease of the flow velocities in the upstream part of the estuary (see Kruijbeke and Schoonaarde in Table 38). In the downstream part the changes in velocities between these runs are not significant (see Middelgat in Table 38).

M2 amplitude increases downstream Antwerp in run SA_14a and it decreases upstream Sint Amands (Figure 105, Figure 106).

Table 38. Measured and modeled velocity profiles in runs with different turbulence model (Smagorinski vs. k-Epsilon model)





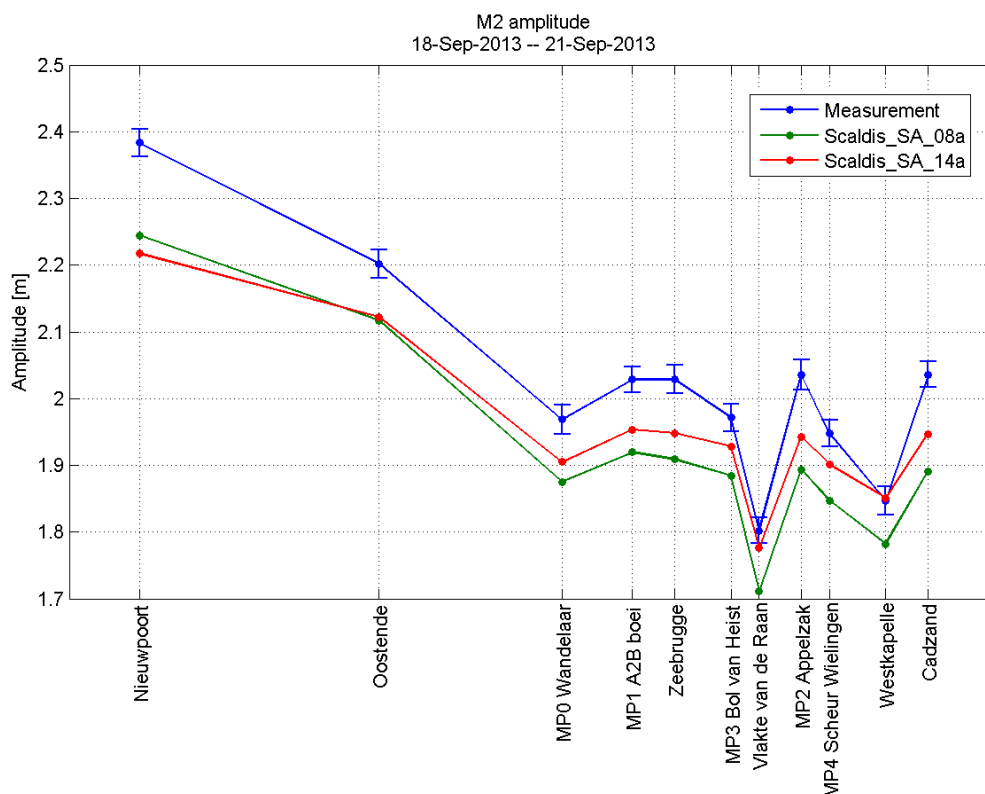


Figure 105 - M2 amplitude in runs SA8a and SA14a (North sea)

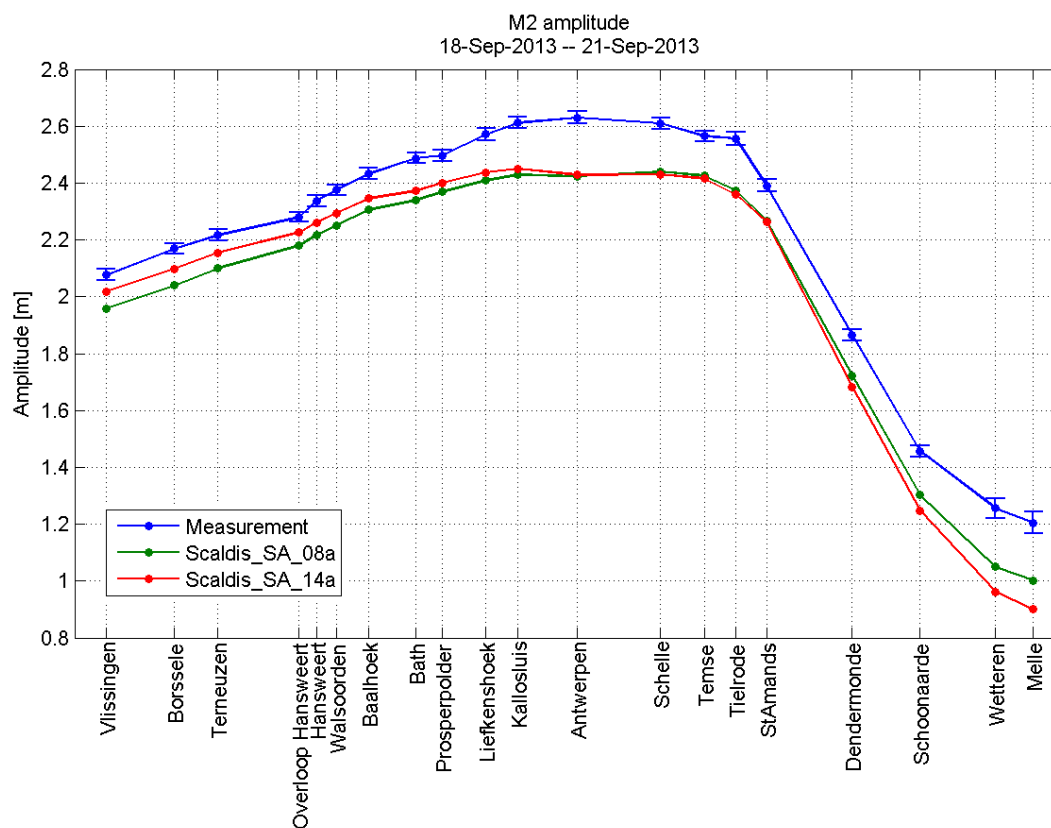


Figure 106 - M2 amplitude in runs SA8a and SA14a (Western Scheldt and Sea Scheldt)

The calculated viscosity for U and V along x, y and z axis (m^2/s) can be written in the Telemac output file (the name of the variables are NUX, NUY and NUZ). Viscosities in X and Y direction are the same. In the following figures only the viscosity in X direction is presented. The calculated viscosity in the North sea and Western Scheldt is higher than in the Sea Scheldt. Different scales are used for the figures.

In the run with the k-Epsilon model the calculated viscosity is below $1 \text{ m}^2/\text{s}$ in the entire model domain.

A higher viscosity is calculated in the run with the Smagorinski turbulence model. It is higher than $3 \text{ m}^2/\text{s}$ in some locations in the North sea, Western and Eastern Scheldt. In this area the turbulence is inhibited by the mesh (due to a bigger grid size). Smagorinsky's idea is to add to the molecular viscosity a turbulent viscosity deduced from a mixing length model. This mixing length corresponds to the size of the vortices smaller than that of the mesh size (*Hervouet, 2007*). The viscosity becomes lower in the upstream part of the estuary where the grid is finer (and allows the reproduction of the viscous dissipation of smaller vortices).

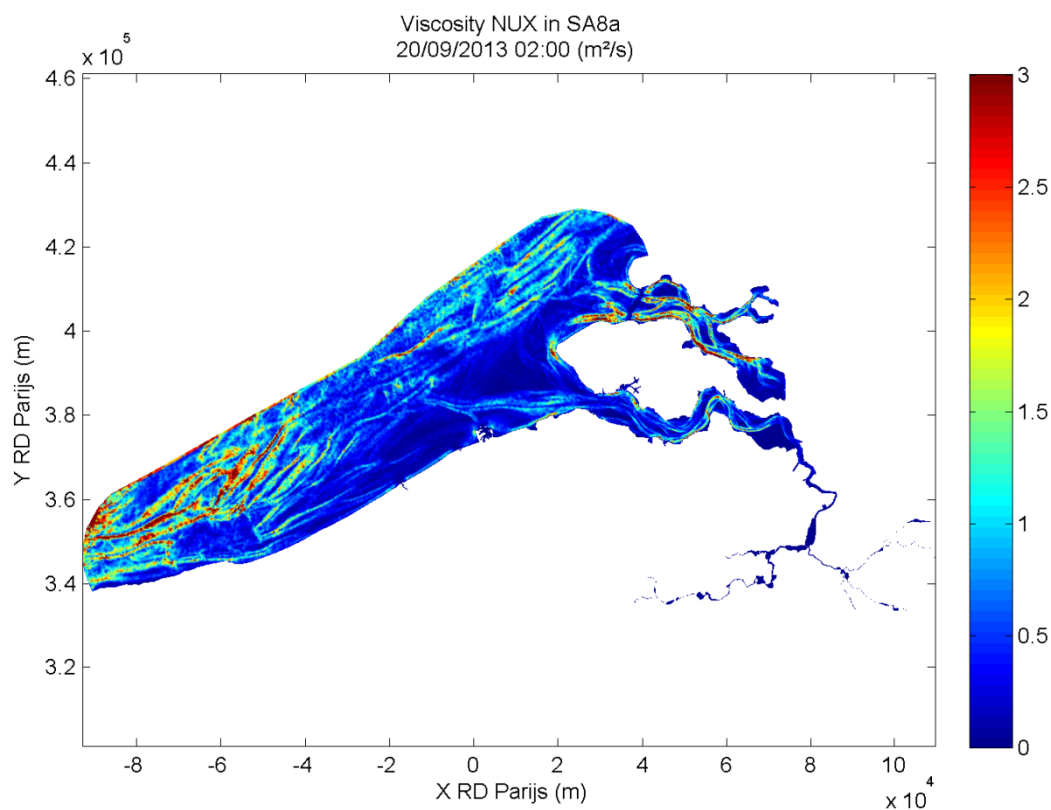


Figure 107 - Viscosity calculated in SA8a (20/09/2013 02:00) (m^2/s)

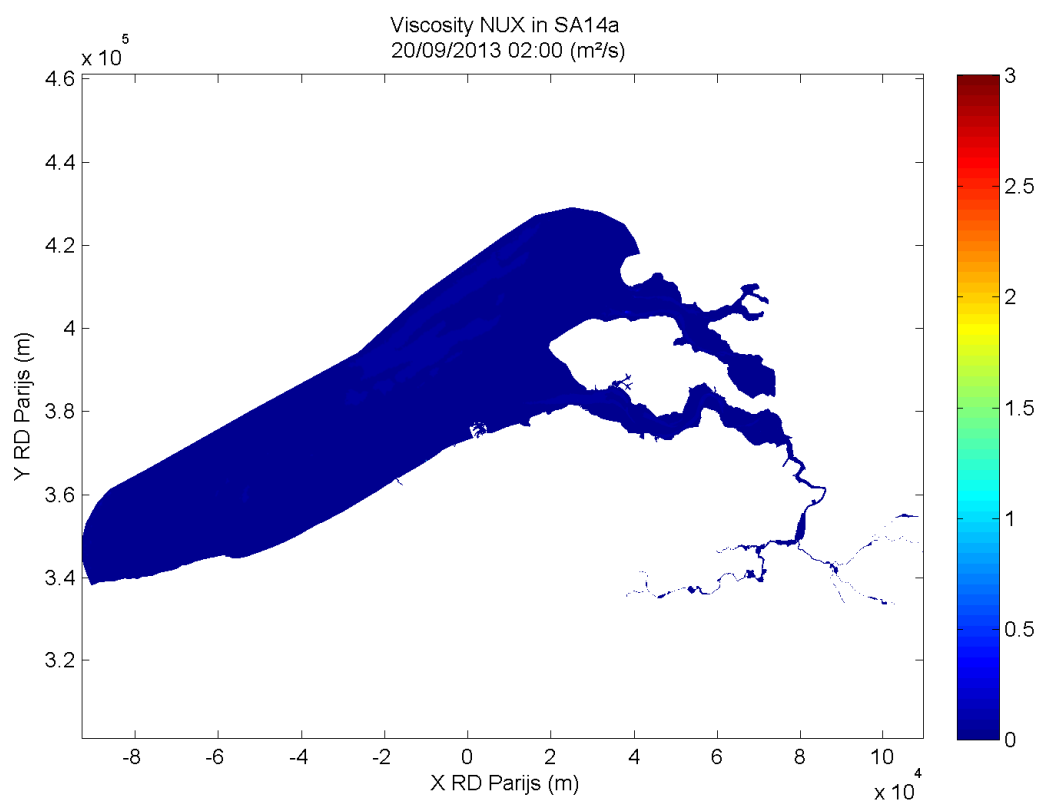


Figure 108 - Viscosity calculated in SA14a (20/09/2013 02:00) (m^2/s)

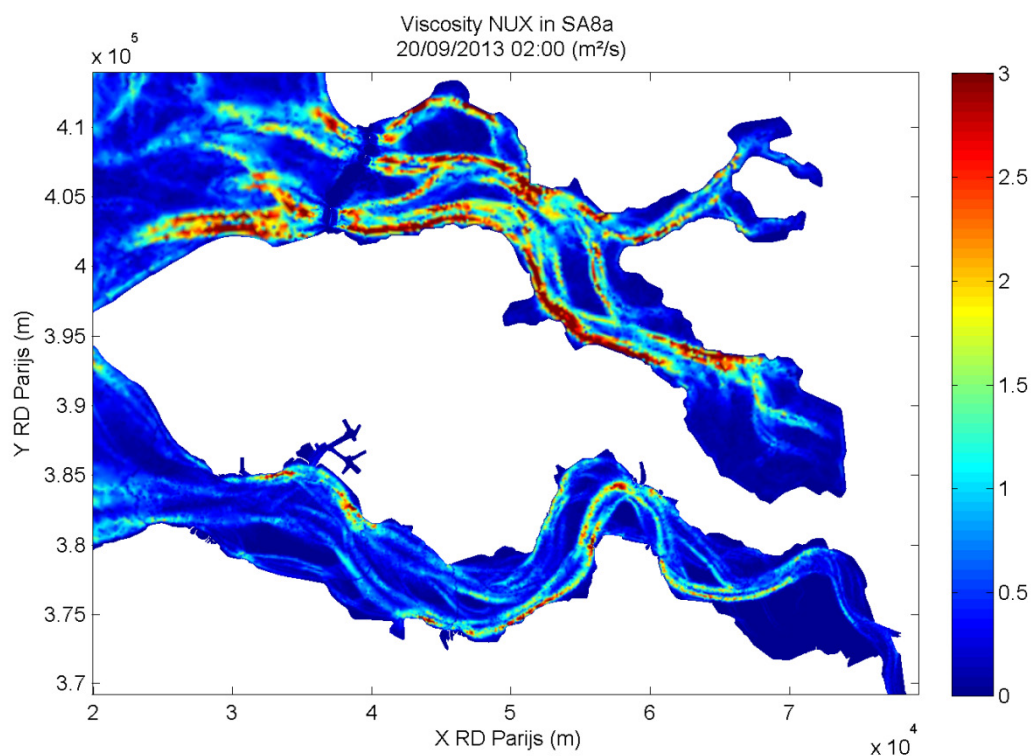


Figure 109 - Viscosity calculated in SA8a in the Western Scheldt (20/09/2013 02:00) (m^2/s)

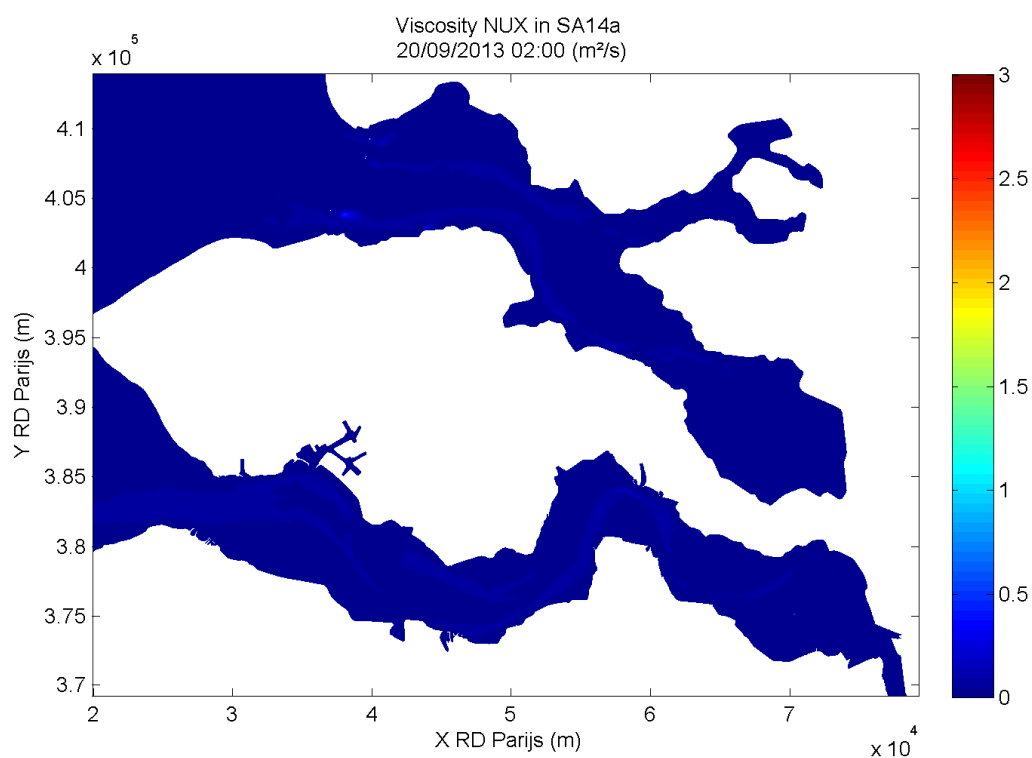


Figure 110 - Viscosity calculated in SA14a in the Western Scheldt (20/09/2013 02:00) (m^2/s)

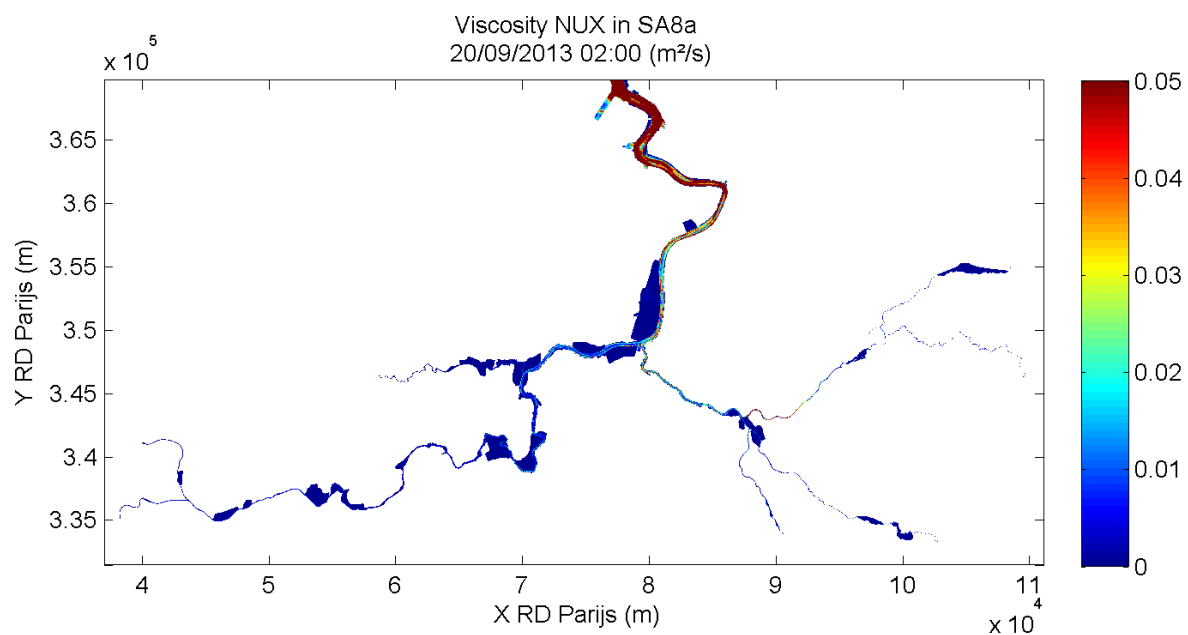


Figure 111 - Viscosity calculated in SA8a in the Sea Scheldt (20/09/2013 02:00) (m^2/s)

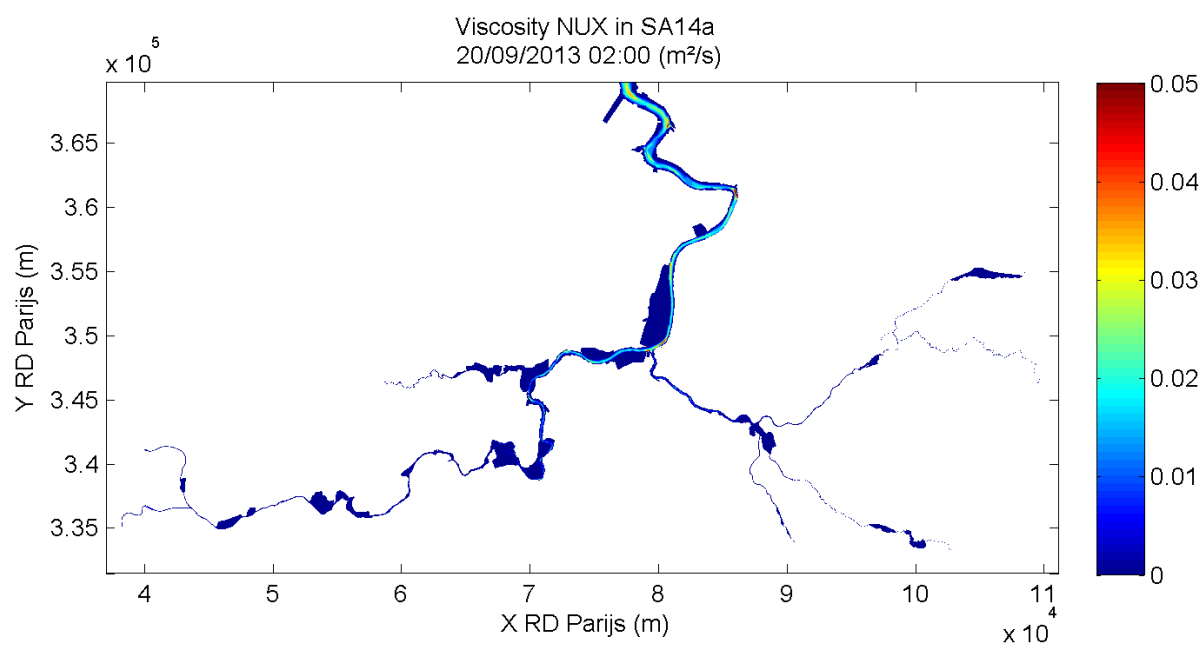


Figure 112 - Viscosity calculated in SA14a in the Sea Scheldt (20/09/2013 02:00) (m^2/s)

7.6.2. Constant viscosity vs. Smagorinski model

Constant viscosity and Smagorinski turbulence models are used in runs SA19 and SA30 (Table 39).

Table 39. Model runs with different turbulence models

Model run	Horizontal turbulence model	Coefficient for horizontal diffusion of velocities (m^2/s)	Vertical turbulence model	Coefficient for vertical diffusion of velocities (m^2/s)
SA19	Smagorinski model	0.01	mixing length model Nezu and Nakagawa	1
SA30	Constant viscosity	0.01	mixing length model Nezu and Nakagawa	1

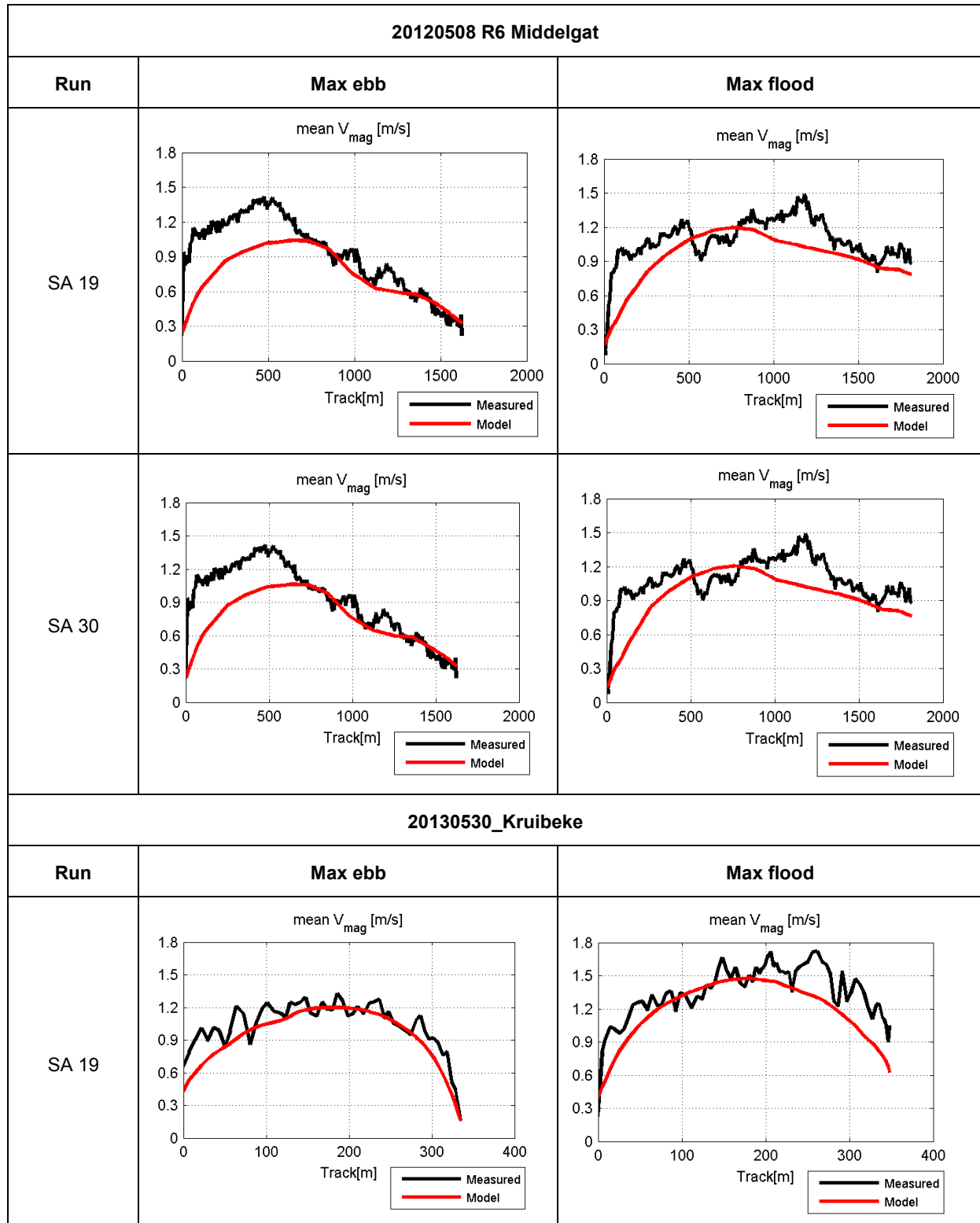
The constant viscosity horizontal turbulence model is compared to the Smagorinski model in runs SA_19 and SA_30.

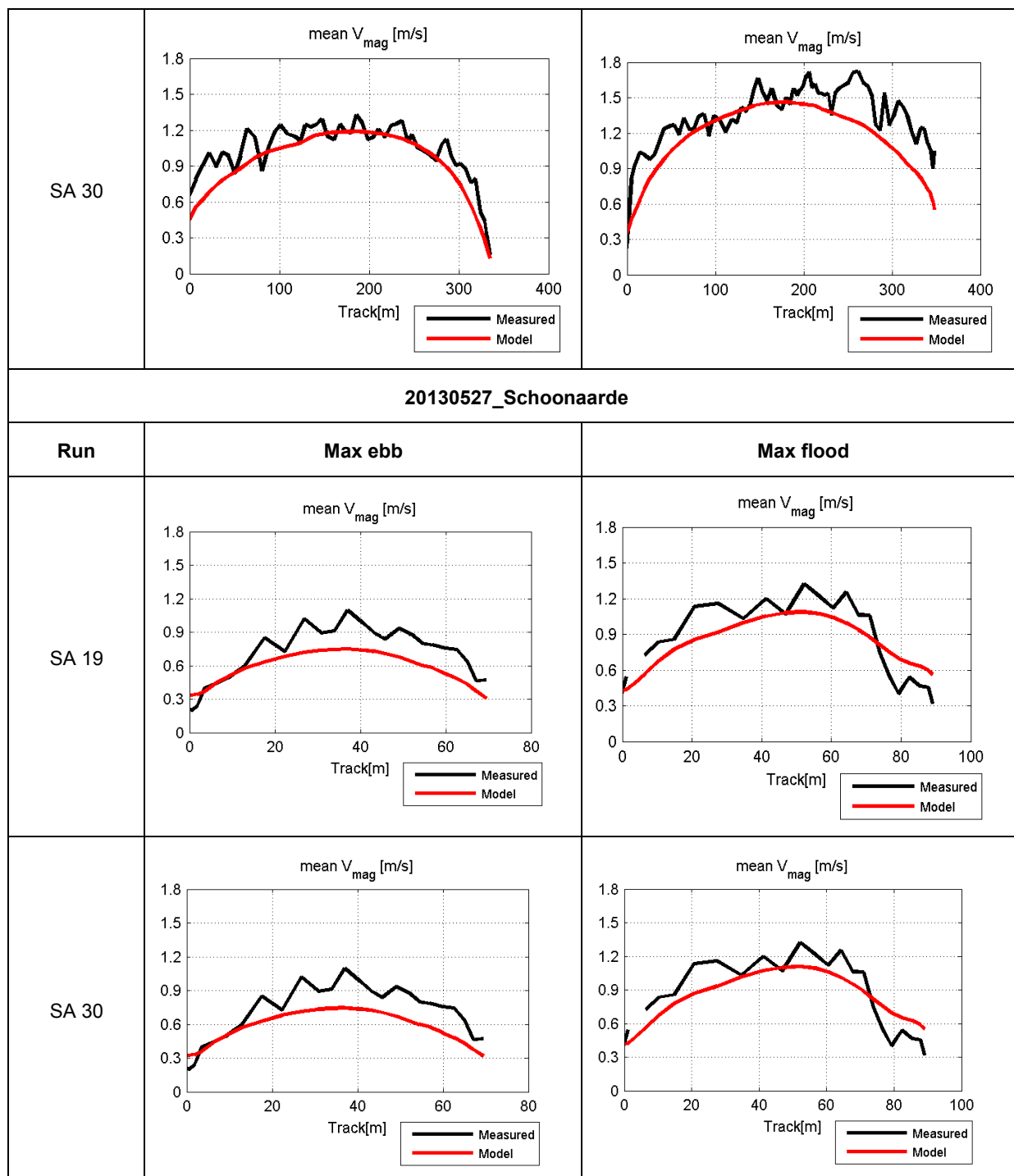
The constant viscosity model uses a constant viscosity coefficient that includes the effects of molecular viscosity and dispersion. The turbulent viscosities are then constant throughout the domain. The global (molecular + turbulent) viscosity coefficients are provided by the user (*EDF-R&D*, 2013). The Smagorinski turbulence model is described in chapter 5.10.2.

The M2 amplitude calculated in the run with the constant viscosity turbulence model is higher than in run with the Smagorinski turbulence model downstream Sint Amands (Figure 116, Figure 117). There is no significant change of the velocity profiles (Table 40). Figure 113 to Figure 115 show discharges calculated at the locations where velocity profiles are analyzed. The differences in maximum flood and ebb discharges calculated in SA19 and SA30 are very small. There is a phase difference between the runs.

At most stations high waters increase in run SA30 by 1 to 3 cm, low waters decrease by 1 to 4 cm. The RMSE of the complete water level time series varies from 8 downstream to 19 cm at Temse (run SA30 vs run SA19). More upstream it decreases again to 10 cm at Melle.

Table 40. Measured and modeled velocity profiles in runs with different turbulence models
(Smagorinski vs. Constant viscosity model)





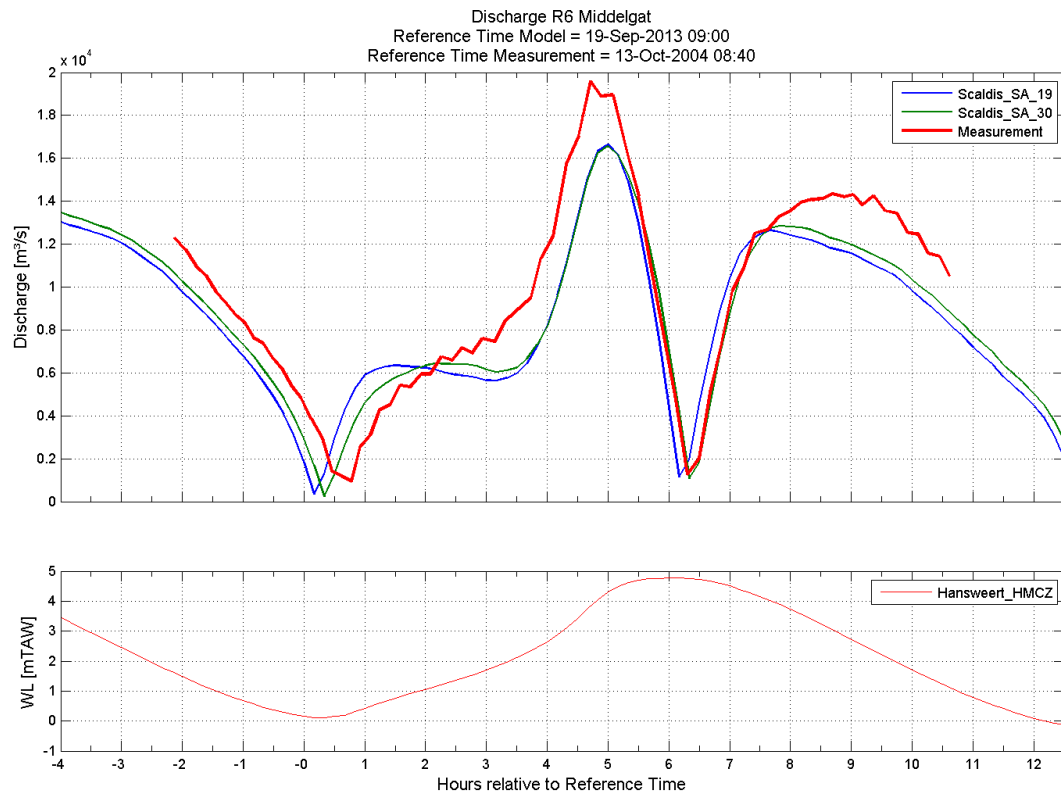


Figure 113 - Discharge at R6 Middelgat (SA19, SA30 and measurement)

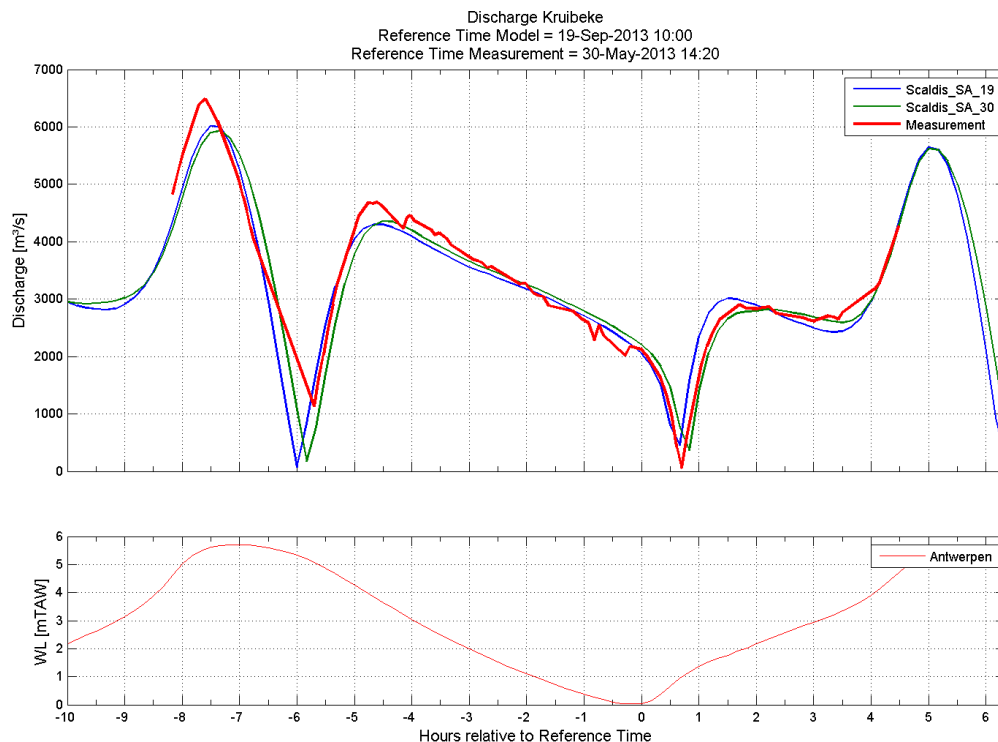


Figure 114 - Discharge at Kruibeke (SA19, SA30 and measurement)

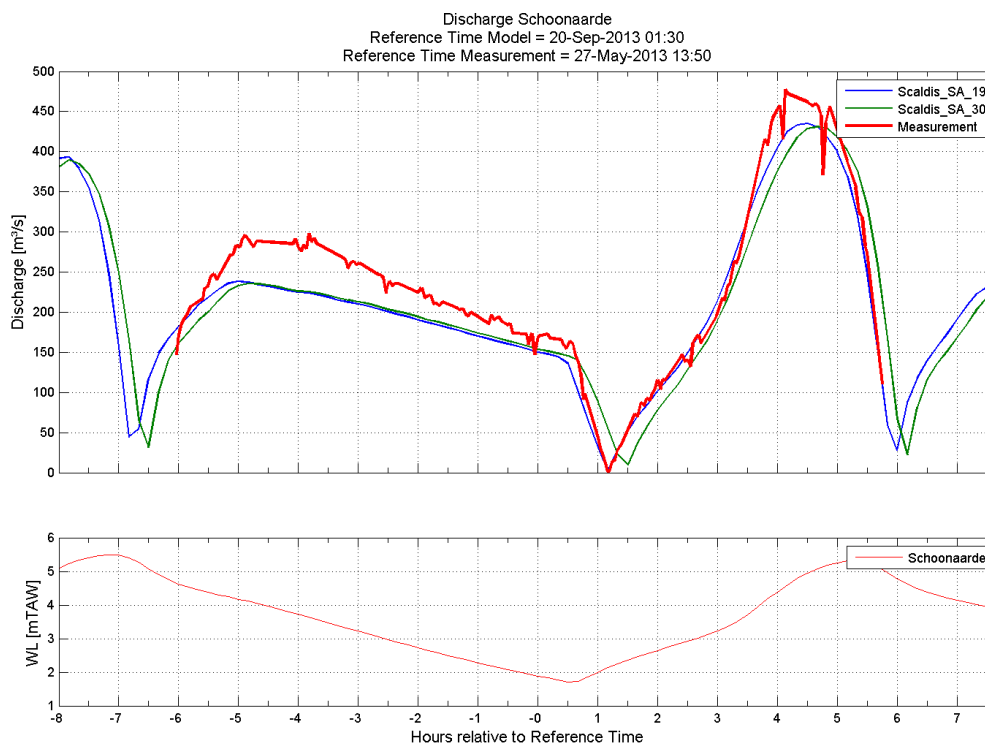


Figure 115 - Discharge at Schoonaarde (SA19, SA30 and measurement)

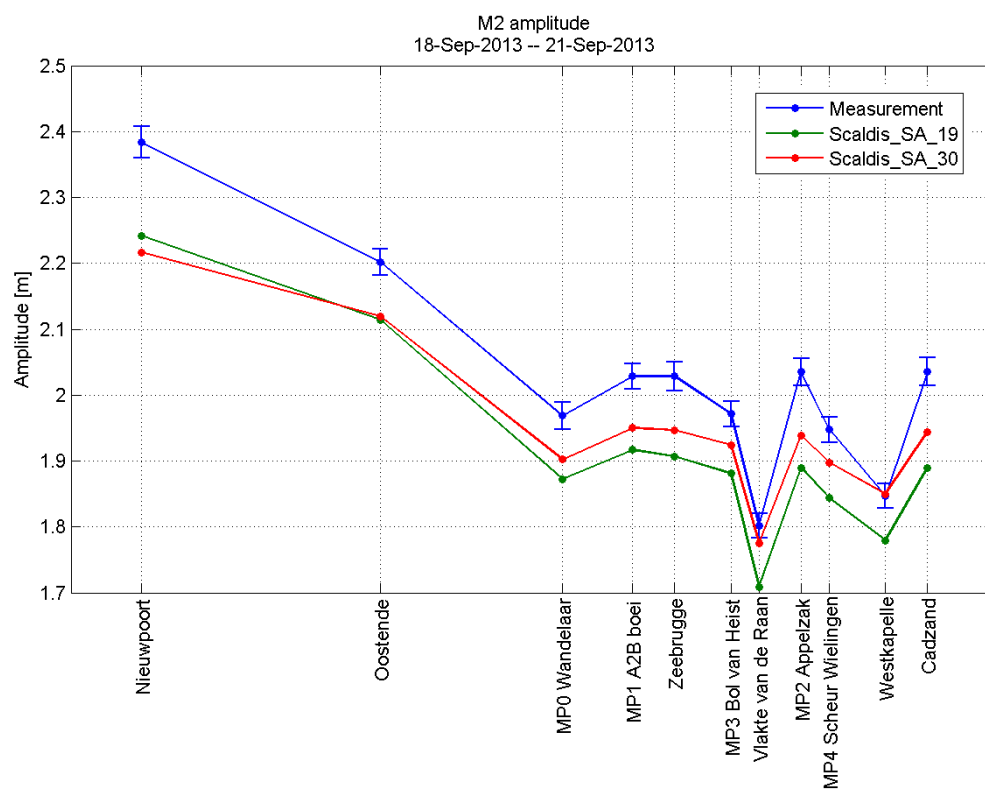


Figure 116 - M2 amplitude in runs SA19 and SA30 (North sea)

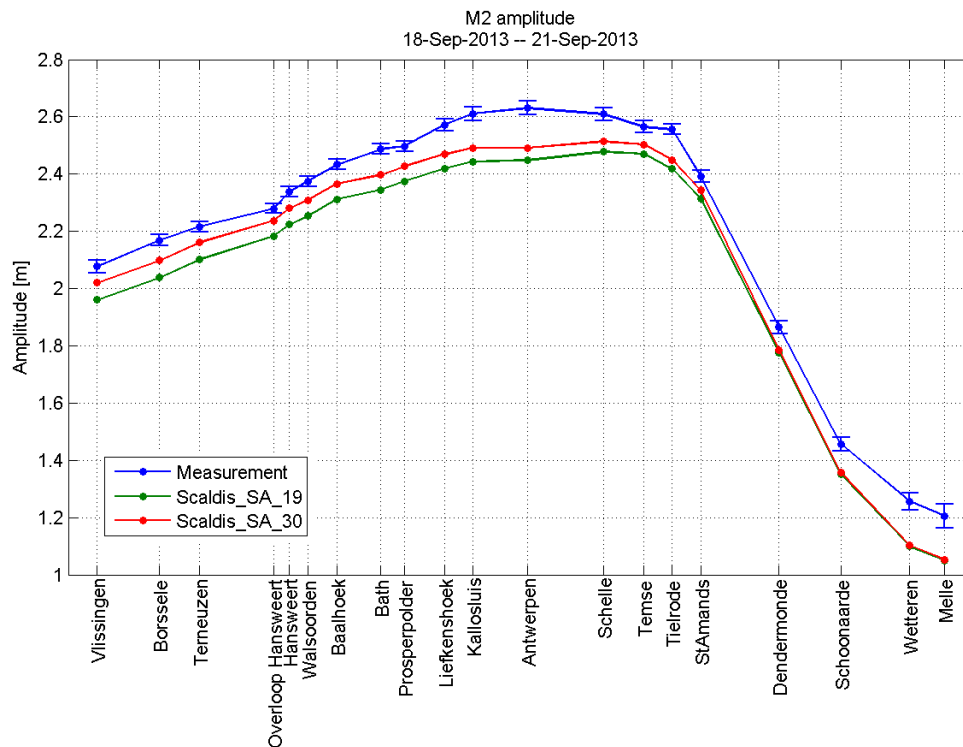
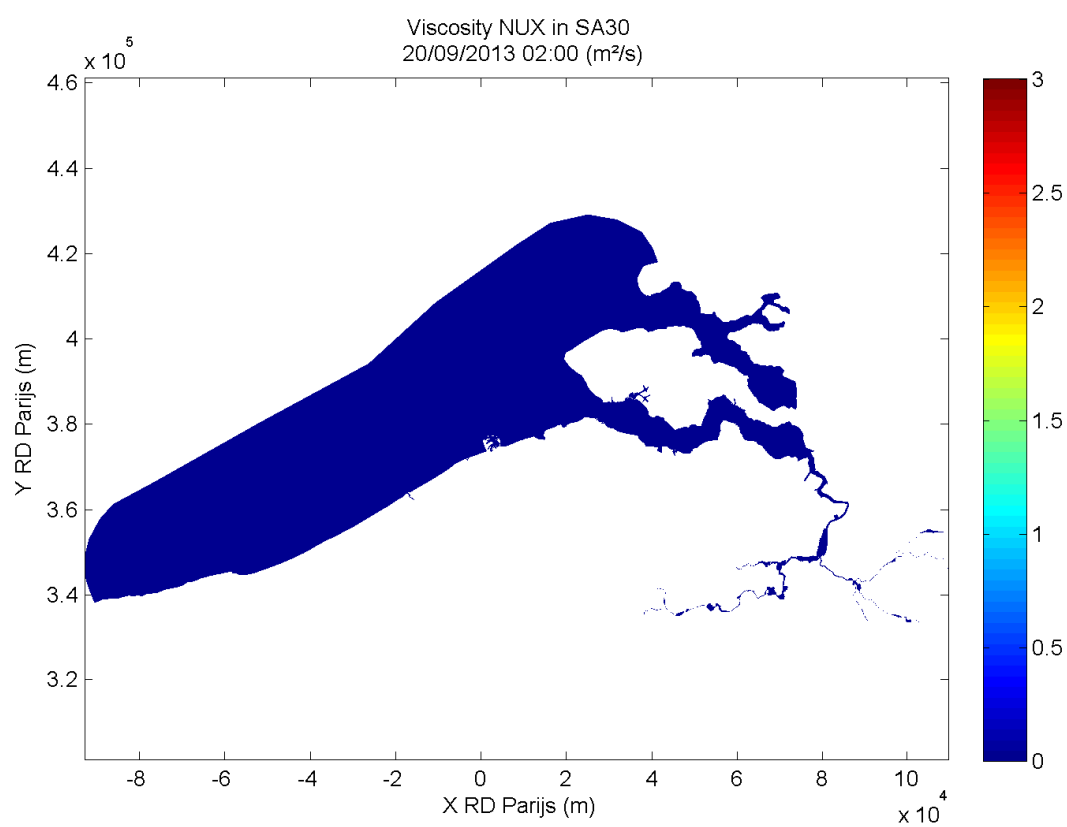
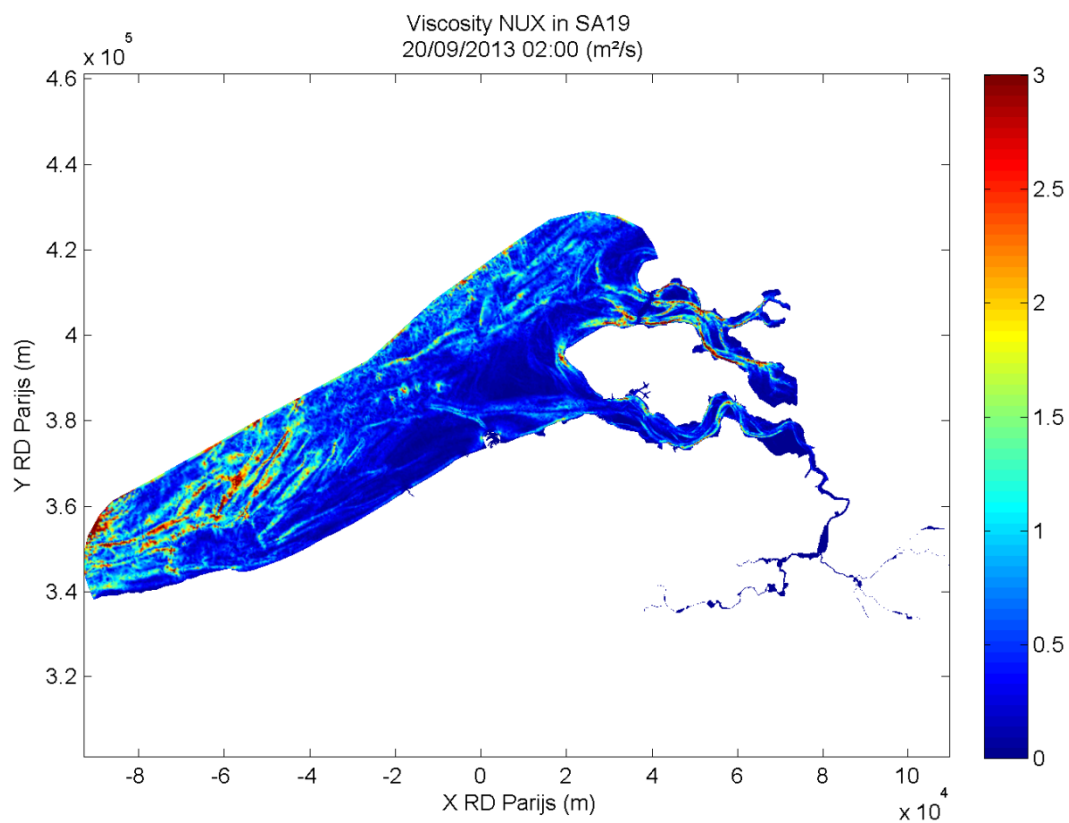


Figure 117 - M2 amplitude in runs SA19 and SA30 (Western Scheldt and Sea Scheldt)

Viscosity fields calculated in the two simulations are very different from each other. A constant viscosity of $0.01 \text{ m}^2/\text{s}$ (horizontal) is used in SA_30 (Figure 119, Figure 121 and Figure 123). (The colour is not constant in Figure 123 because some areas in the model are dry). In the model run with the Smagorinski turbulence model the viscosity is higher than $3 \text{ m}^2/\text{s}$ in some areas in the North sea, Western and Eastern Scheldt. It is higher than $0.05 \text{ m}^2/\text{s}$ in some zones in the Sea Scheldt. More explanation about Smagorinski model is given in chapter 5.10.2.



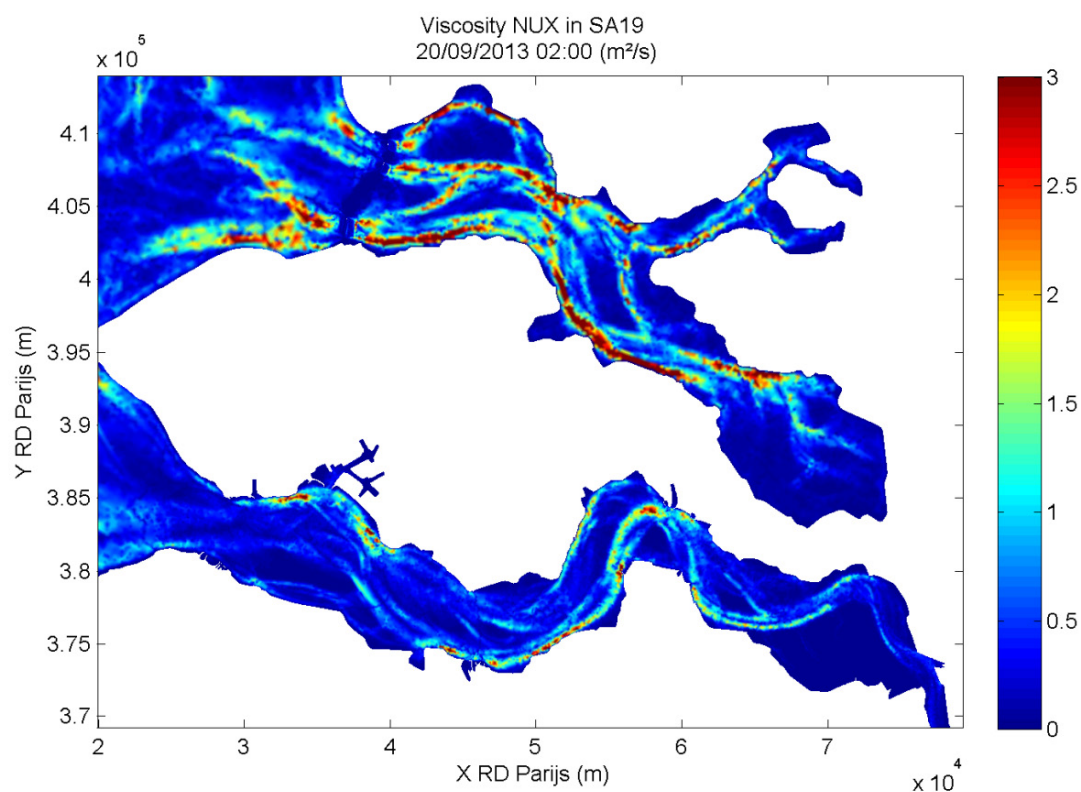


Figure 120 - Viscosity calculated in SA19 in the Western Scheldt (20/09/2013 02:00) (m^2/s)

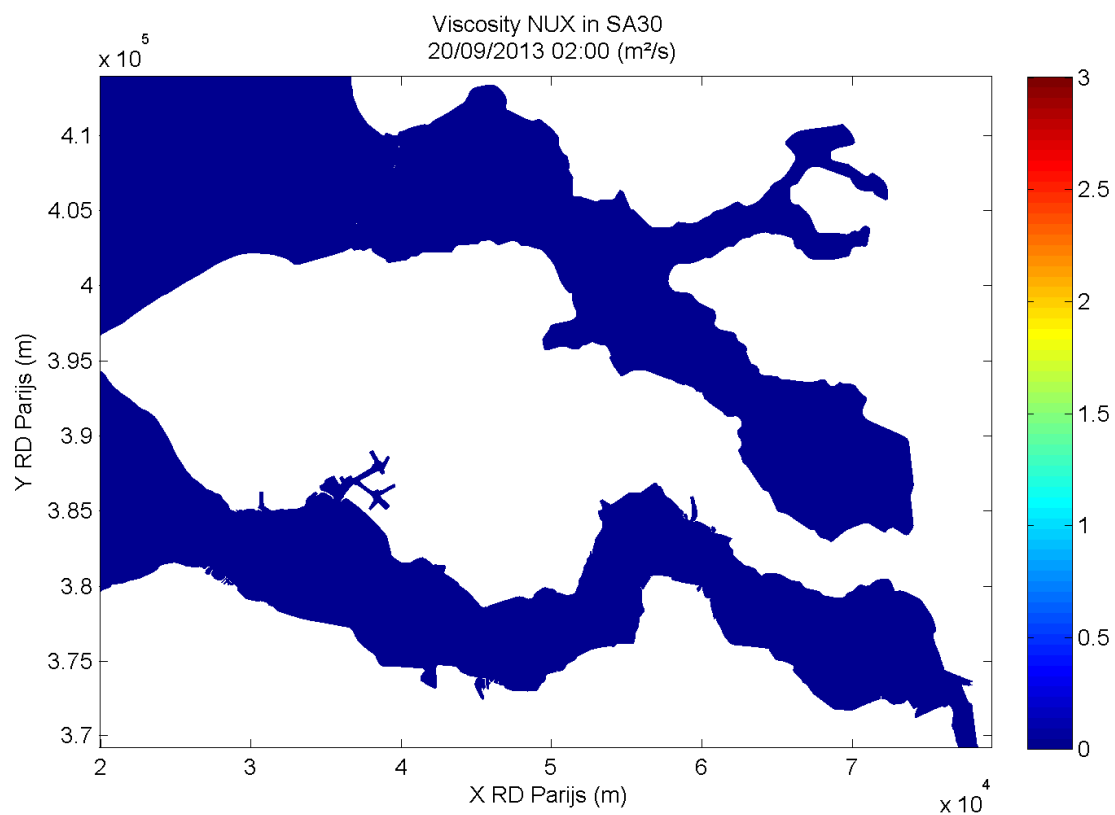


Figure 121 - Viscosity calculated in SA30 in the Western Scheldt (20/09/2013 02:00) (m^2/s)

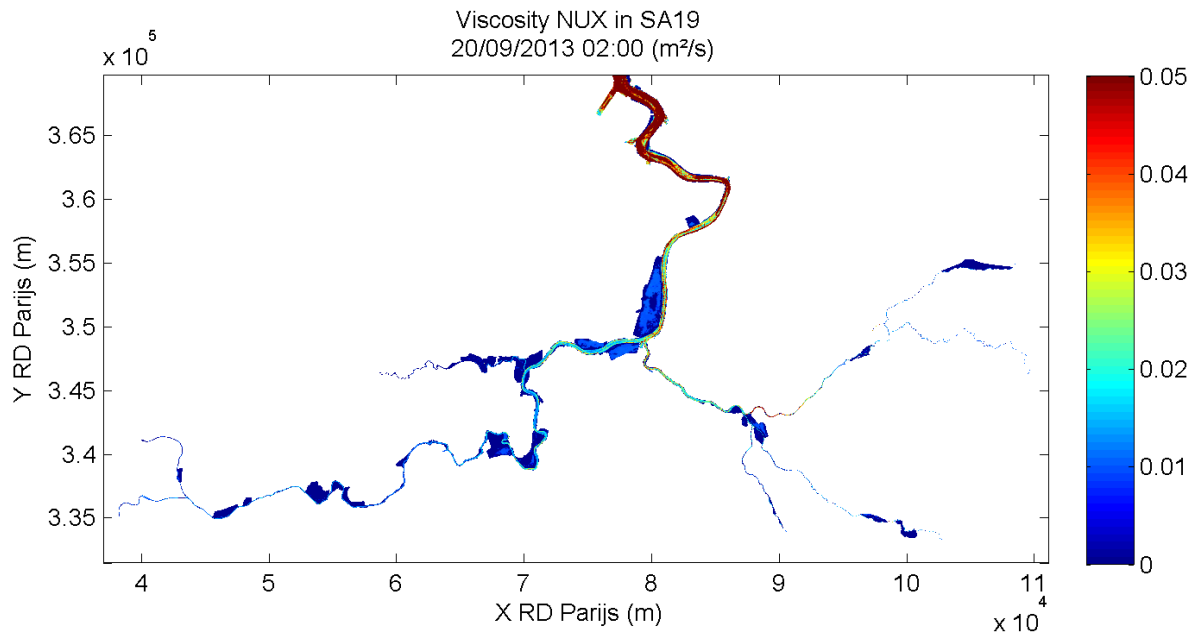


Figure 122 - Viscosity calculated in SA19 in the Sea Scheldt (20/09/2013 02:00) (m^2/s)

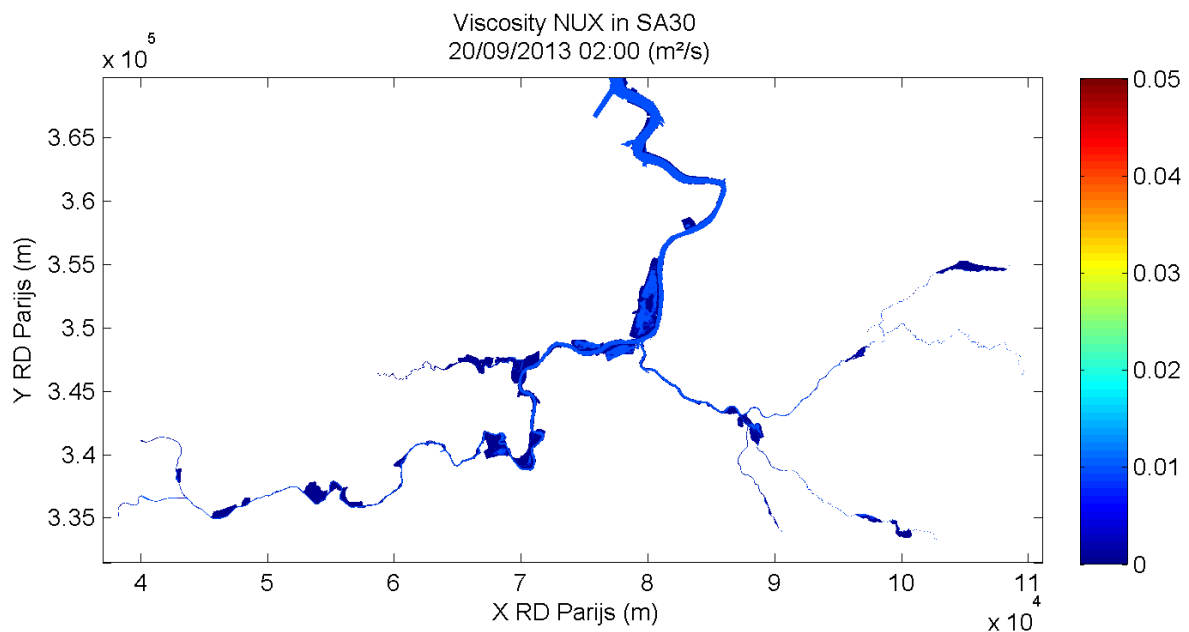


Figure 123 - Viscosity calculated in SA30 in the Sea Scheldt (20/09/2013 02:00) (m^2/s)

7.6.3. Eddy patterns in the harbour of Zeebrugge

Complex eddy flow patterns are observed in the harbor of Zeebrugge. These patterns were studied by IMDC using Telemac 3D. A sensitivity analysis showed that the model results are very sensitive to the choice of different parameters in the model (*Breugem et al., 2013*). The harbor of Zeebrugge is outside of the area of interest of our project. However, in this chapter we analyze if the direction of eddies in Zeebrugge is represented well in the model.

Around high water two eddies are formed at the entrance to the harbor of Zeebrugge. The primary eddy is directed in clockwise direction. A smaller secondary eddy rotates counter clockwise.

Figure 124 to Figure 131 present the plots of flow velocities in the harbour around high water. Red arrows are modeled velocity vectors, white arrows are ADCP measurements. Measurements are plotted in the figures just to indicate the direction of the measured velocities. The agreement between the calculated and measured tides is not sufficient for the comparison of the velocity magnitudes. Only a short period is analyzed in the sensitivity runs. It is not possible to find a better comparable tide during this period.

Similar eddy patterns are calculated in all four simulations. The primary and secondary eddies are observed in the model results.

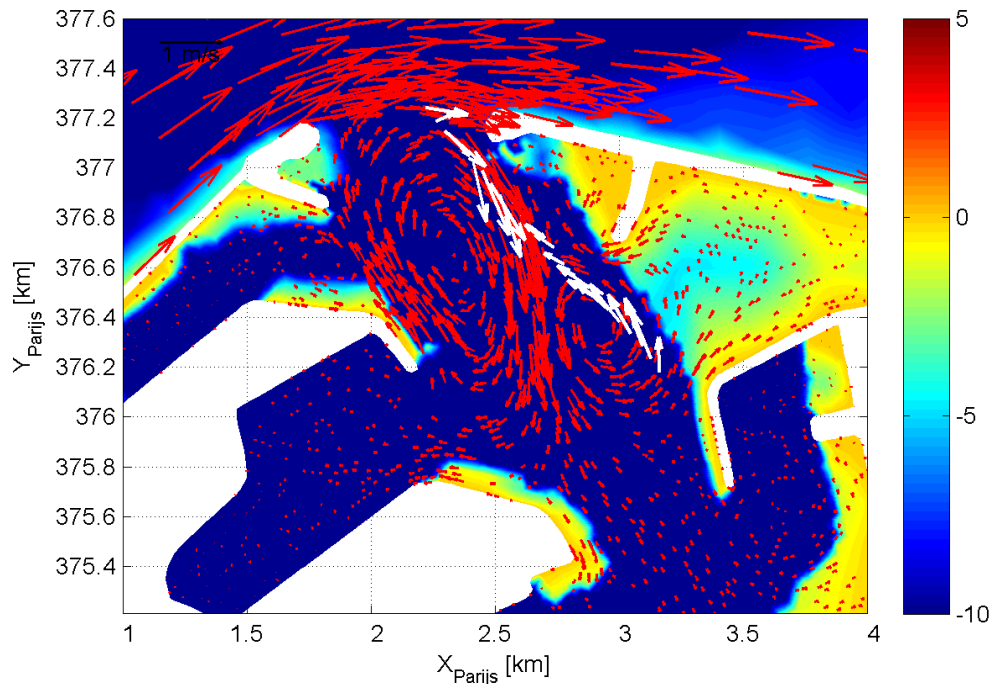


Figure 124 - Flow velocities in Zeebrugge in SA_8a 1 hour before high water

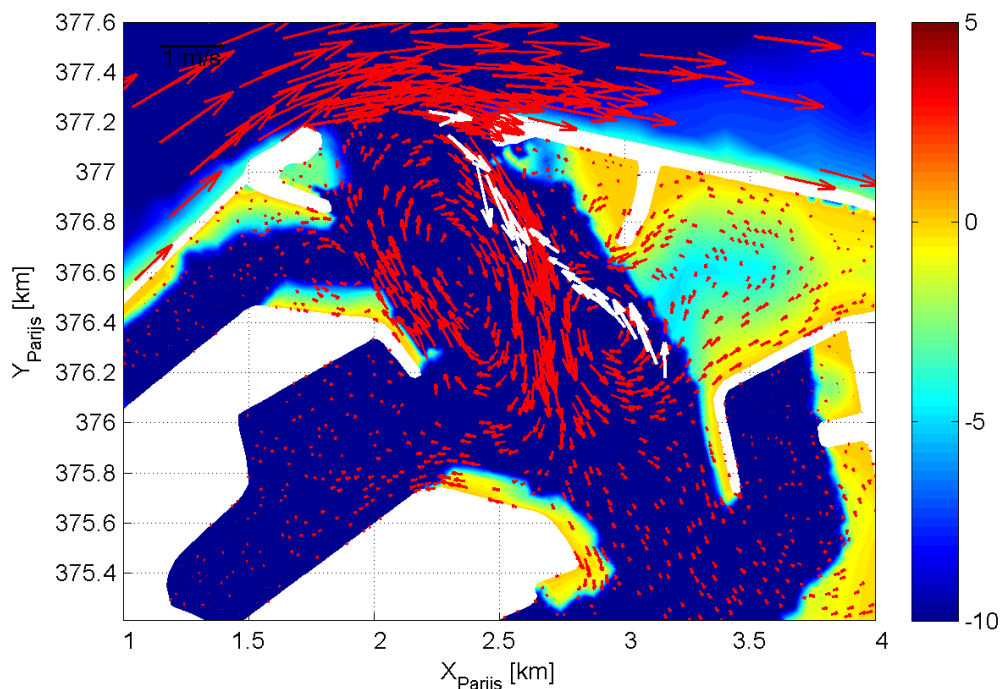


Figure 125 - Flow velocities in Zeebrugge in SA_14a 1 hour before high water

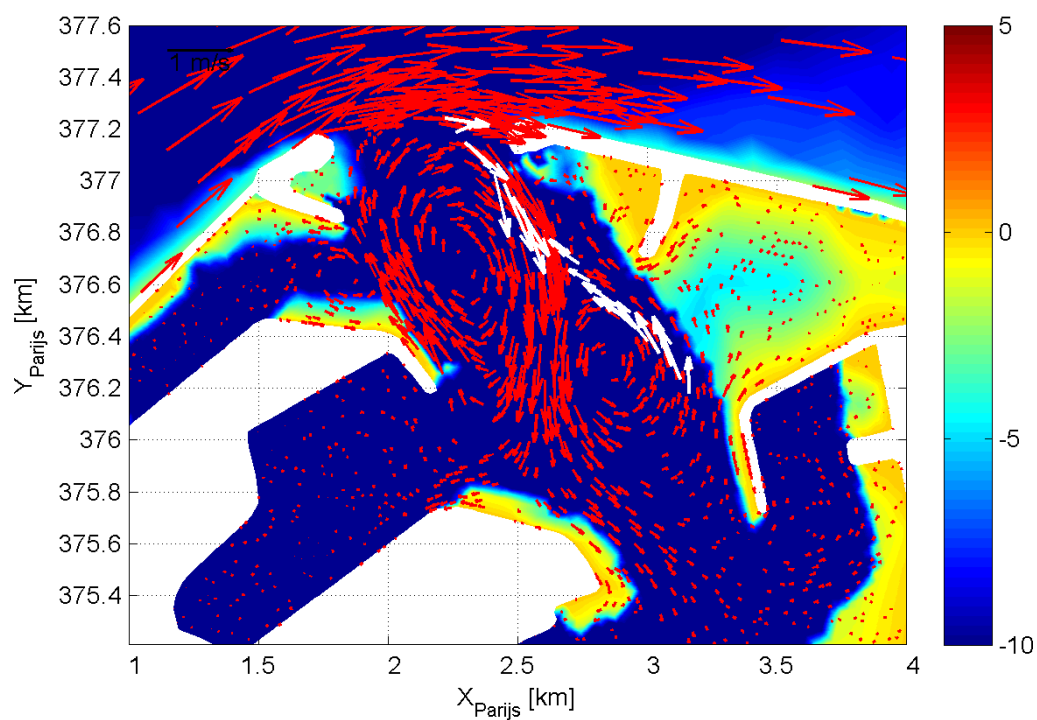


Figure 126 - Flow velocities in Zeebrugge in SA_19 1 hour before high water

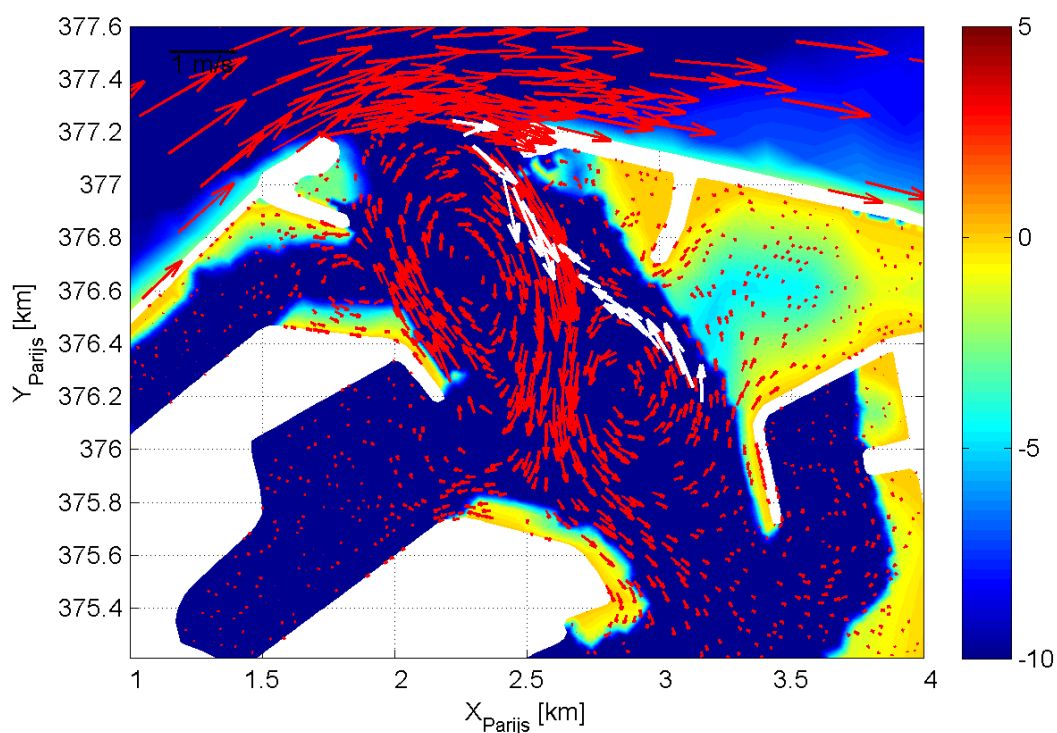


Figure 127 - Flow velocities in Zeebrugge in SA_30 1 hour before high water

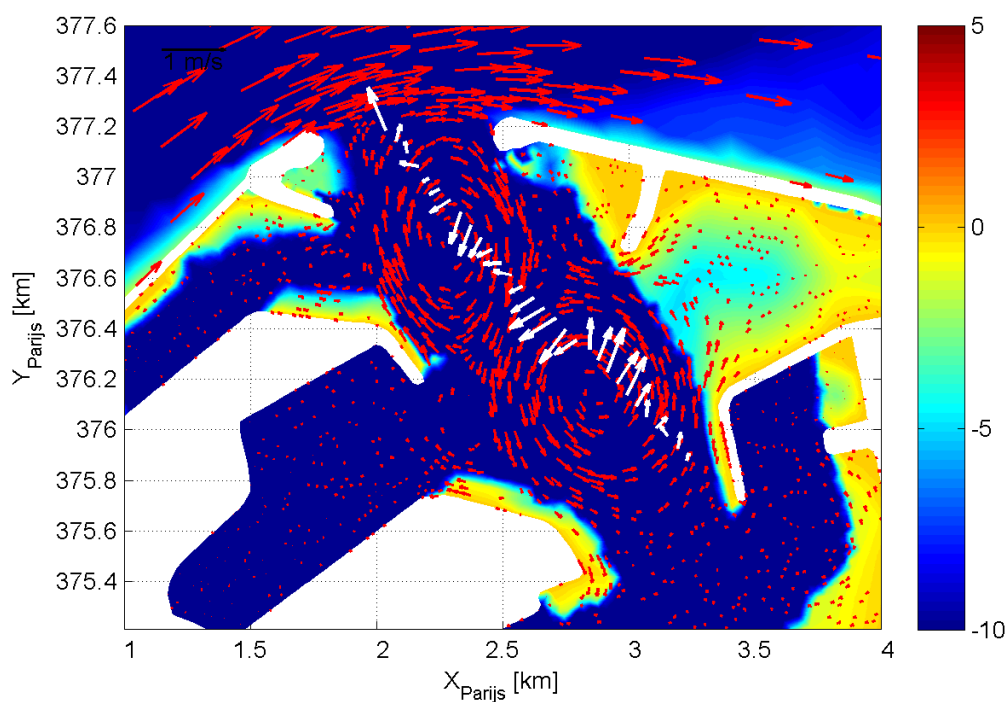


Figure 128 - Flow velocities in Zeebrugge in SA_8a around high water

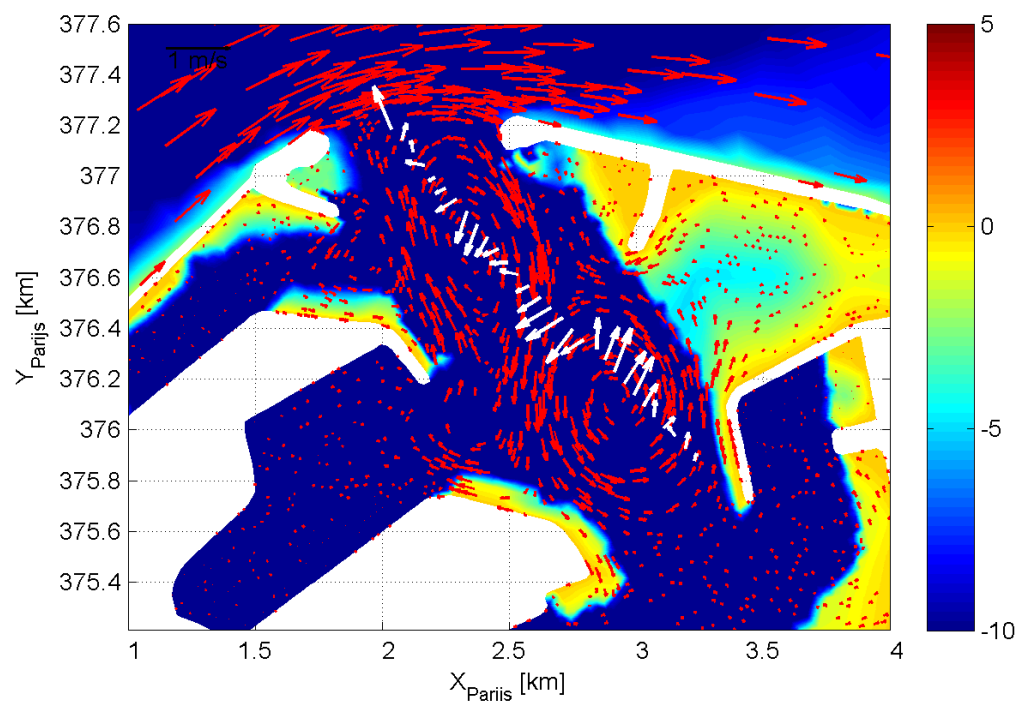


Figure 129 - Flow velocities in Zeebrugge in SA_14a around high water

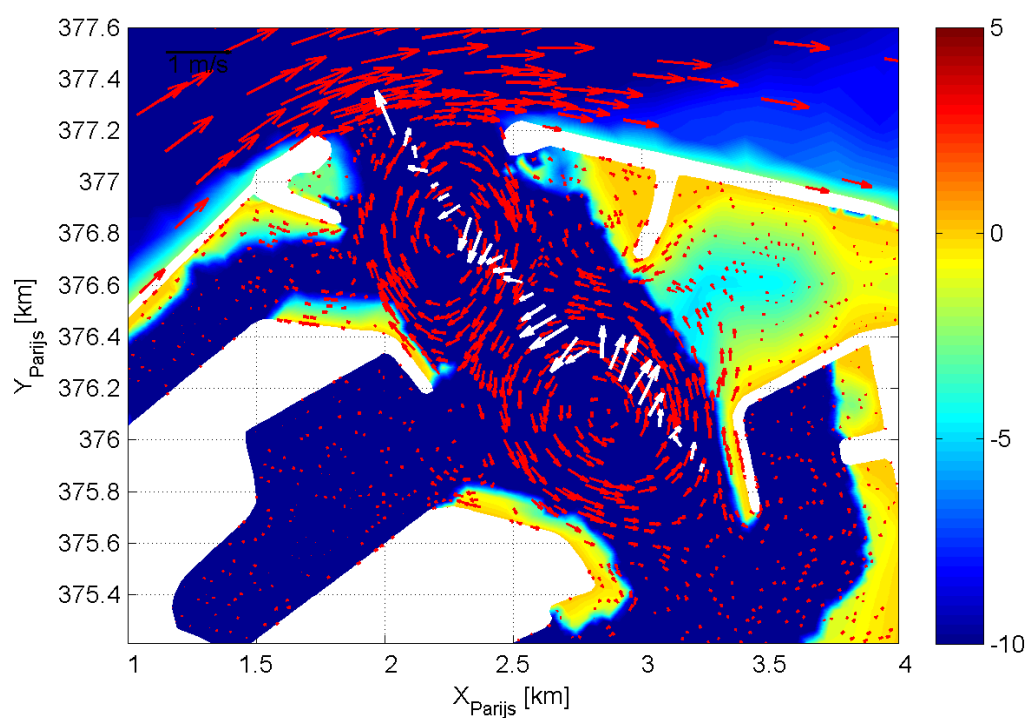


Figure 130 - Flow velocities in Zeebrugge in SA_19 around high water

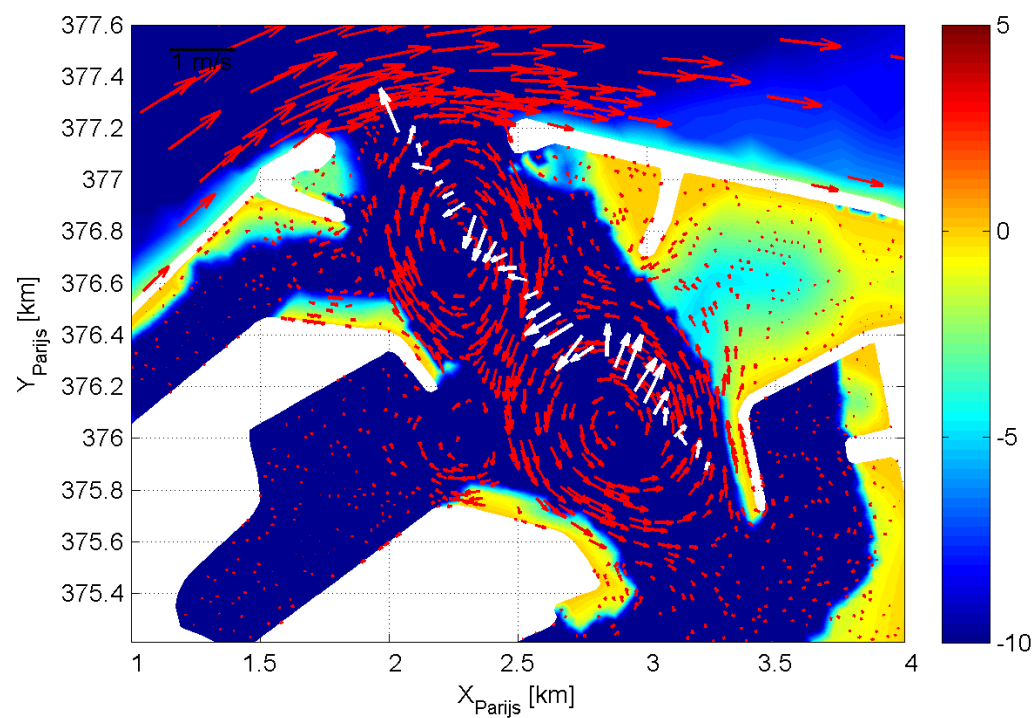


Figure 131 - Flow velocities in Zeebrugge in SA_30 around high water

7.7. Mass lumping on diffusion

An increase of the mass lumping parameter results in more diagonal result matrix and faster computation. However, the obtained solution is smoothed. The value 1 indicates maximum mass-lumping (the mass matrices are diagonal) and the value 0 corresponds to normal processing without mass-lumping.

The mass lumping for depth has to be 1.

The model sensitivity to the mass lumping was tested in runs SA1 and SA12 (Table 41).

Table 41. Model runs used for the sensitivity analysis to the mass lumping.

Model run	Mass lumping		
	for depth	for velocities	for diffusion
SA1	1	1	1
SA12	1	0	0

There are no differences between the results of model runs with and without mass lumping (Table 42, Figure 132, Figure 133).

Table 42. Measured and modeled velocity profiles in runs with and without mass lumping

20130530_Kruiabeke		
Run	Max ebb	Max flood
SA 1		
SA 12		
20130527_Schoonaarde		
Run	Max ebb	Max flood
SA 1		
SA 12		

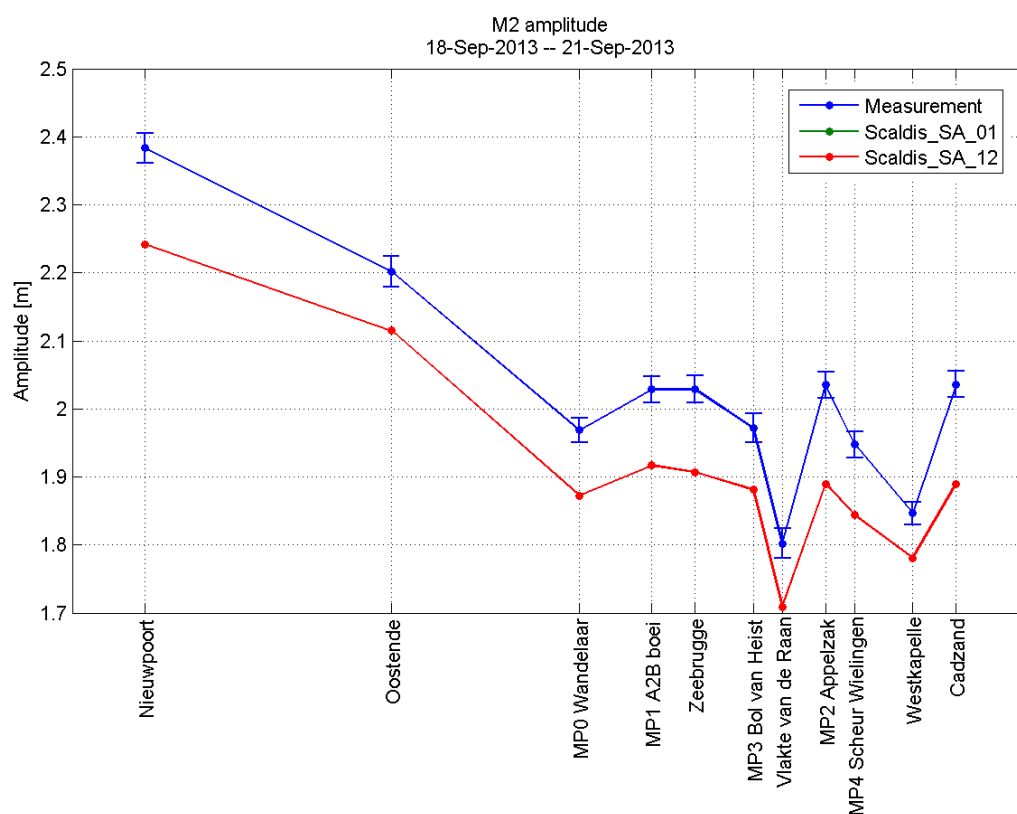


Figure 132 - M2 amplitude in runs SA1 and SA12 (North Sea)

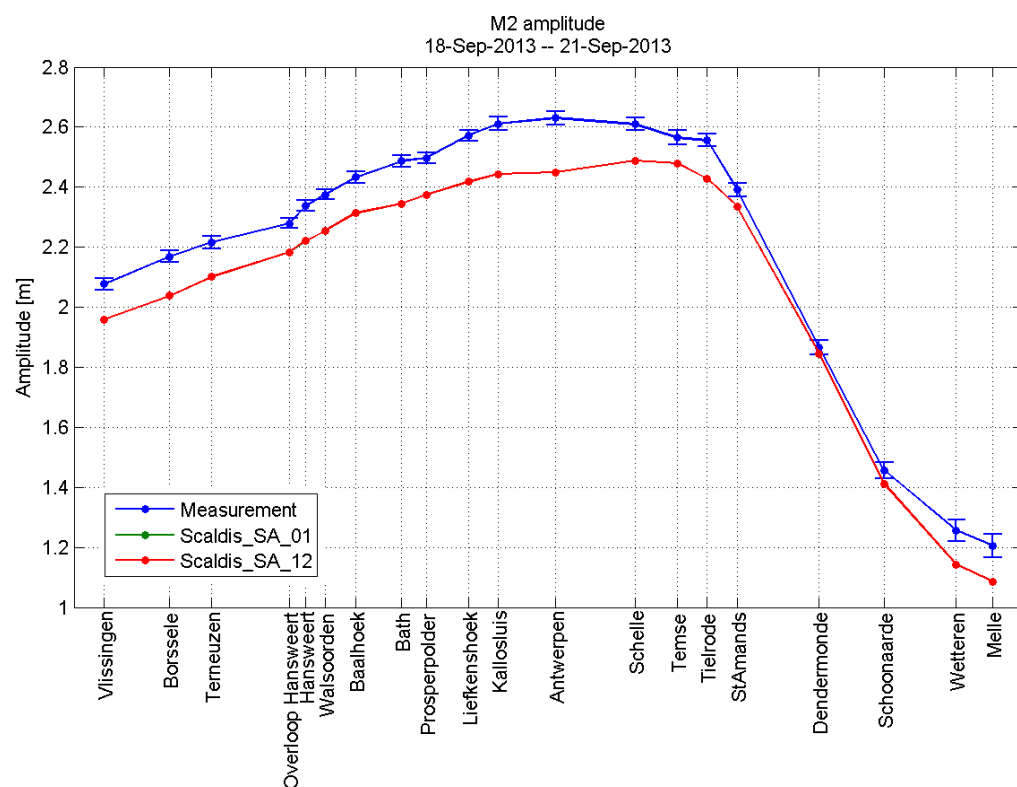


Figure 133 - M2 amplitude in runs SA1 and SA12 (Western Scheldt and Sea Scheldt)

7.8. Implicitation for velocities

The model sensitivity to the implicitation for velocities was analyzed in runs SA1 and SA11 (Table 43).

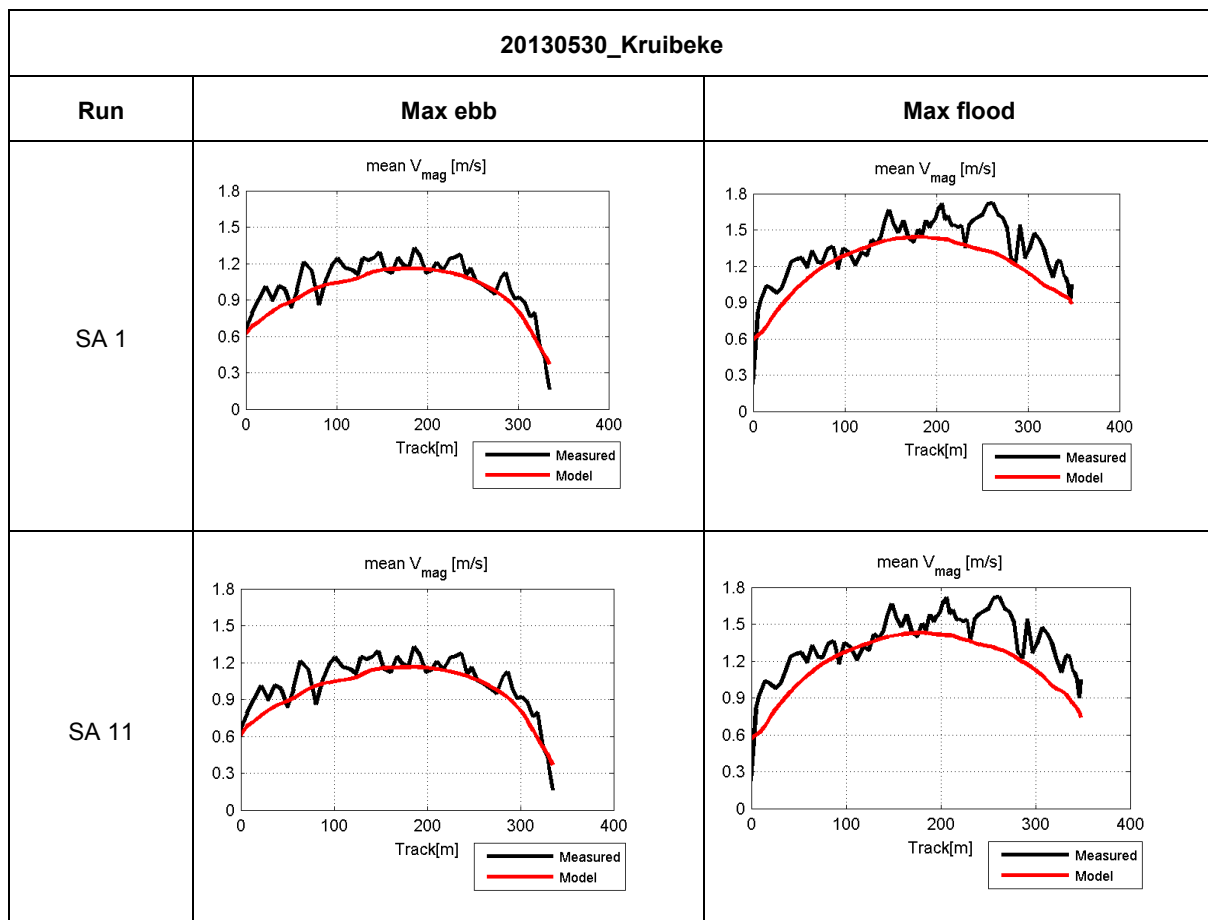
Table 43. Model runs used for the sensitivity analysis to the implicitation for velocities

Model run	Implicitation for velocities
SA1	1
SA11	0.6

There are no big differences in velocity profiles calculated in runs SA1 and SA11. The maximum flood velocities slightly decrease (along the entire cross section) in the upstream part of the estuary in SA11 (Schoonaarde in Table 44).

The water levels in the upstream part of the estuary become unstable in the run with a decreased parameter for the implicitation for velocities (Figure 136, Figure 137).

Table 44. Measured and modeled velocity profiles in runs with different implicitation for velocities



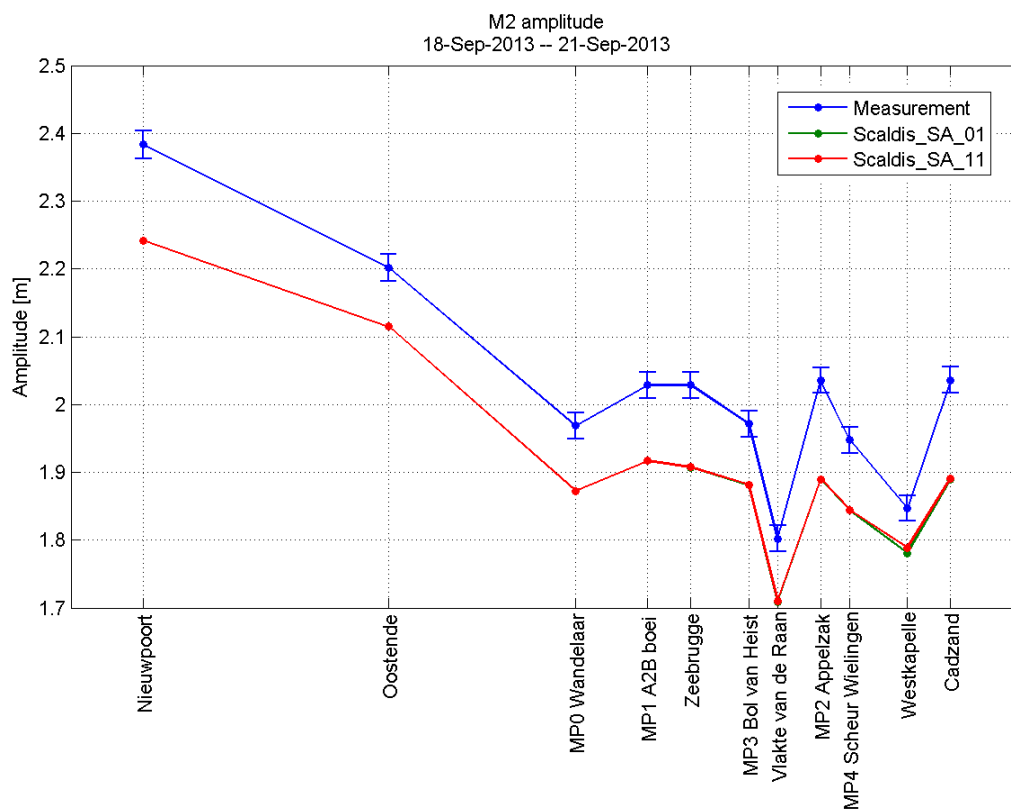
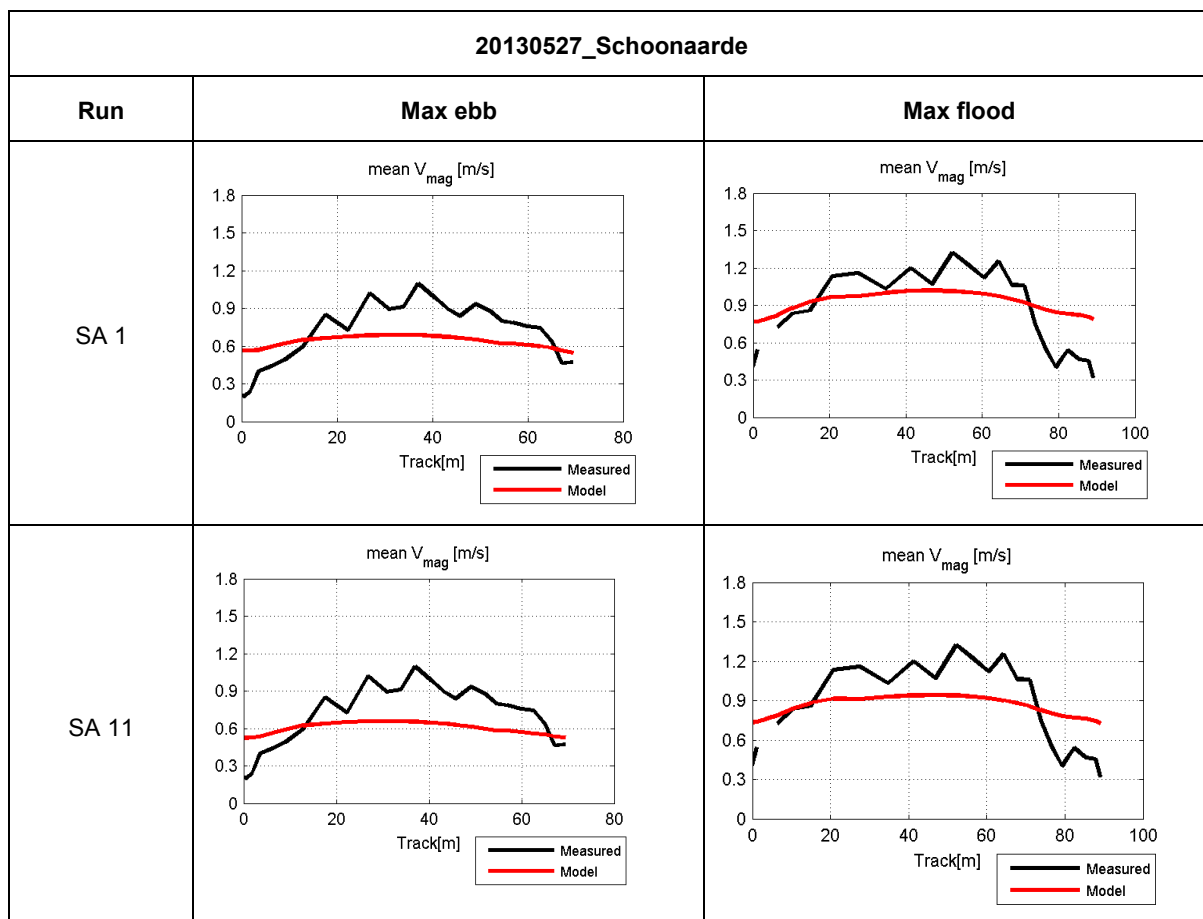


Figure 134 - M2 amplitude in runs SA1 and SA11 (North sea)

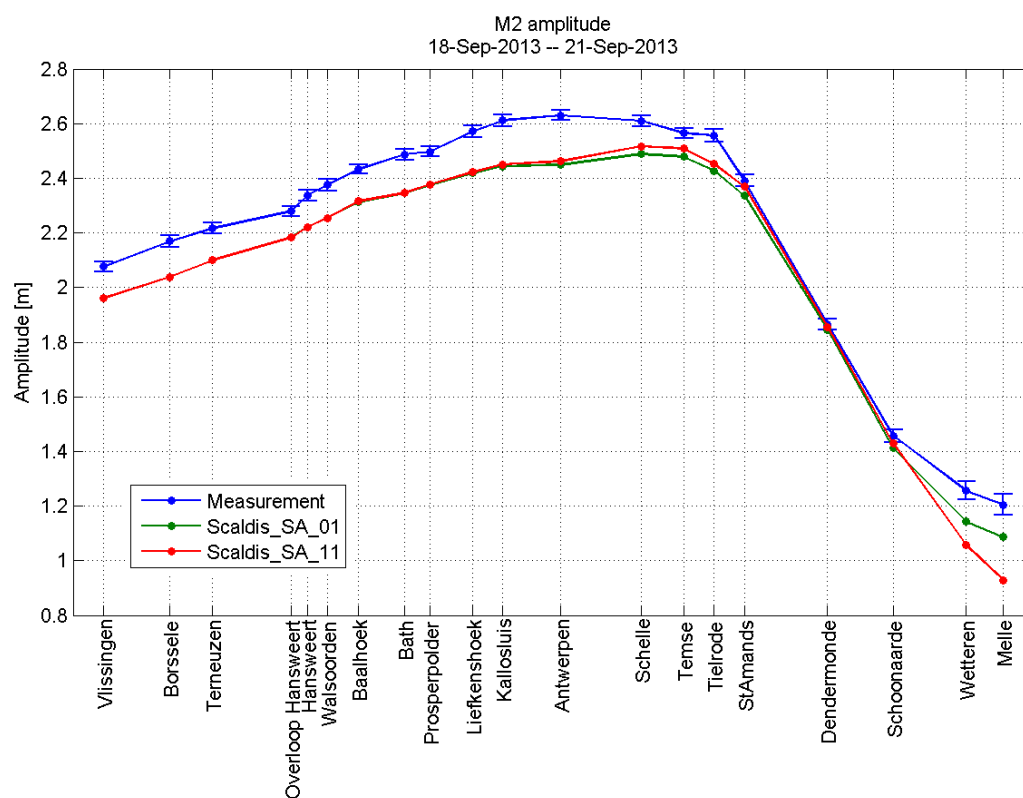


Figure 135 - M2 amplitude in runs SA1 and SA11 (Western Scheldt and Sea Scheldt)

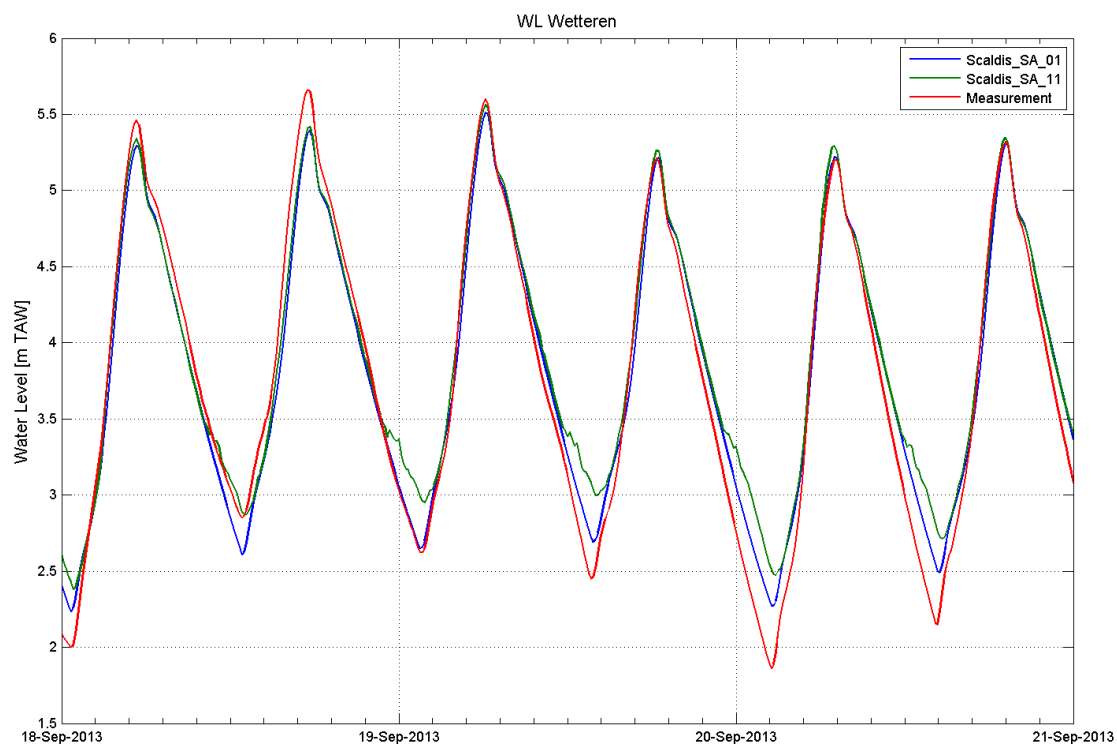


Figure 136 - Measured and calculated water level at Wetteren (runs SA1, SA11)

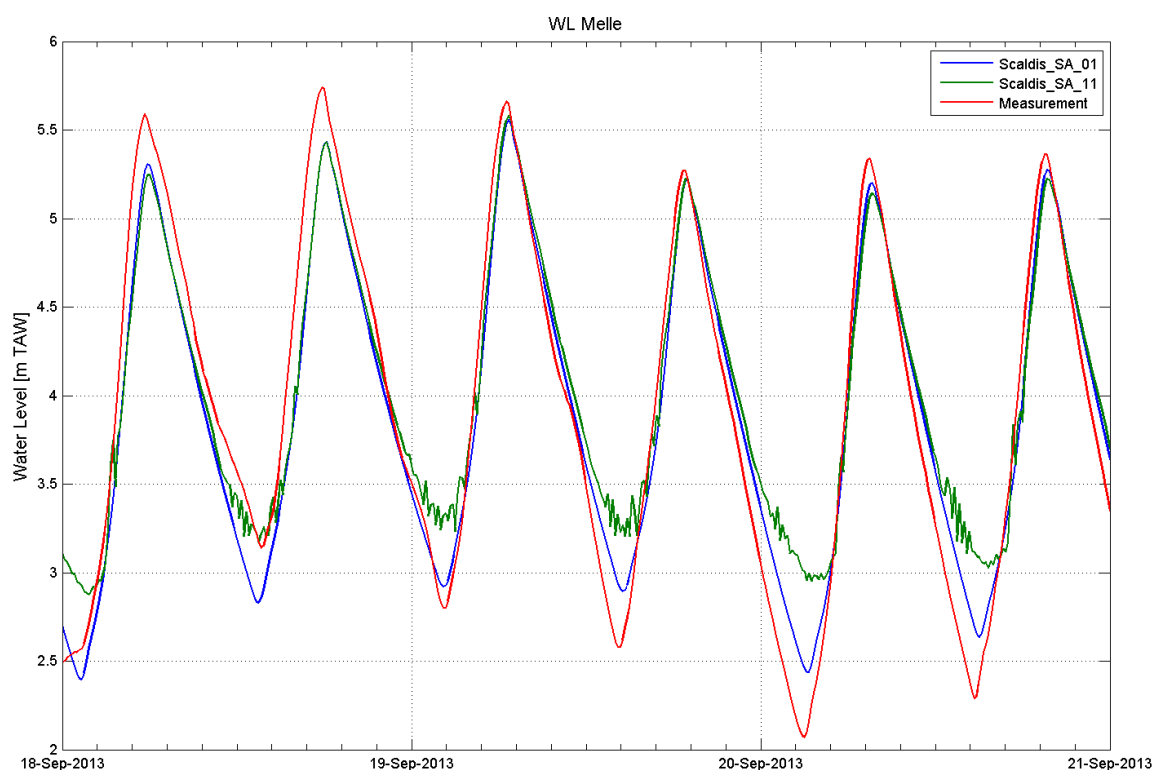


Figure 137 - Measured and calculated water level at Melle (runs SA1, SA11)

7.9. Coriolis coefficient

Two model runs are used to analyze the model sensitivity to the Coriolis coefficient. The Coriolis force is not taken into account in run SA4.

Table 45. Model runs used for the sensitivity analysis to the Coriolis coefficient

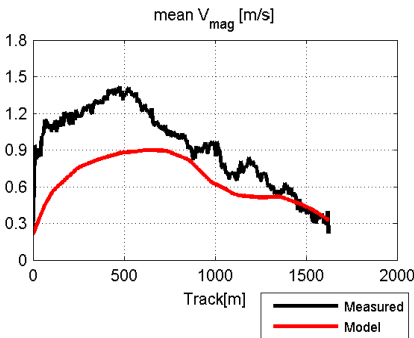
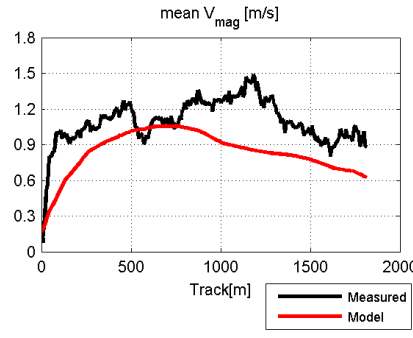
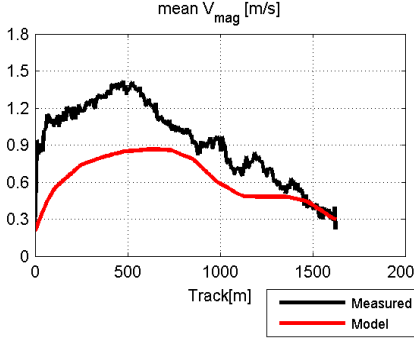
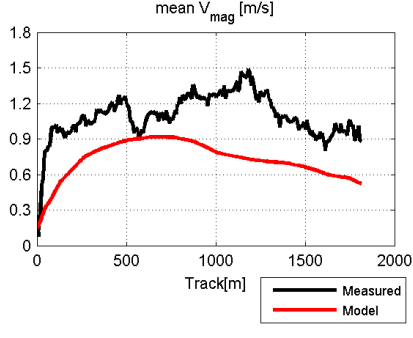
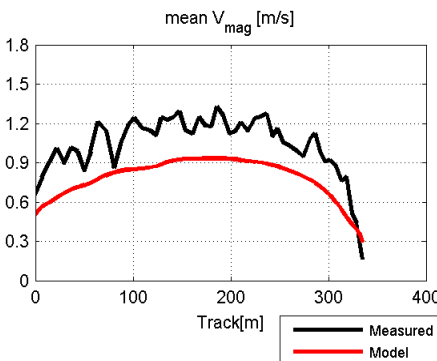
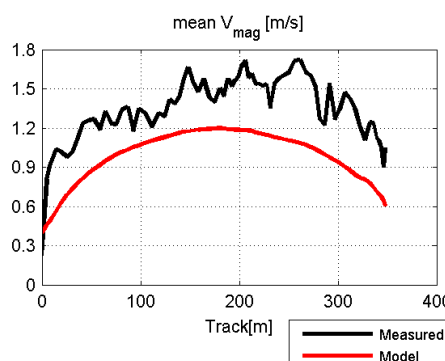
Model run	Coriolis coefficient
SA3	1.13522E-04
SA4	no

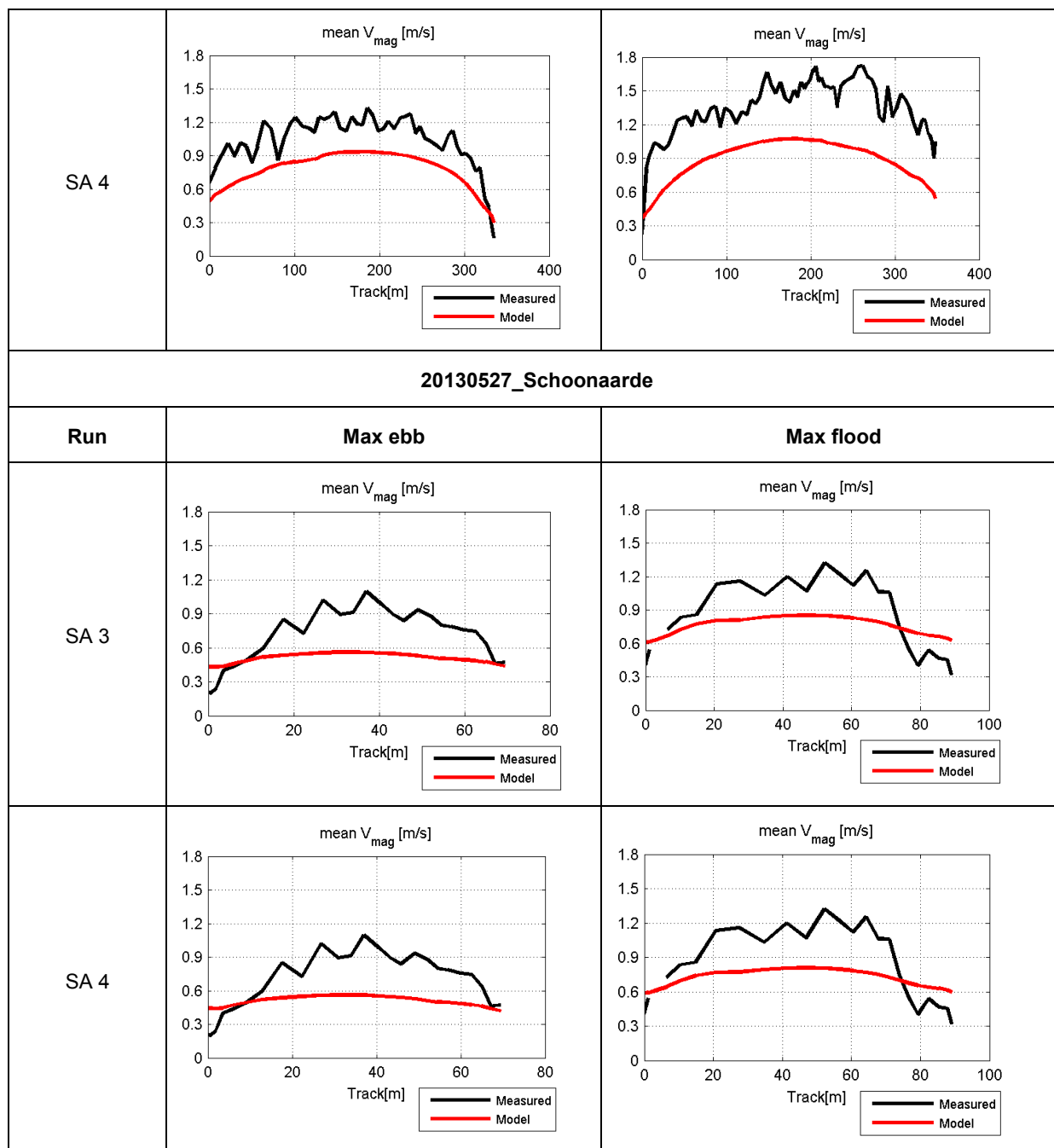
The Coriolis force has a strong effect on the modeled water levels and velocities. The M2 amplitude decreases in the run without Coriolis force by 15 to 23 cm in the North sea and Western Scheldt, 12 to 16 cm in the Lower Sea Scheldt and only 2 to 11 cm in the Upper Sea Scheldt (Figure 138, Figure 139).

High waters decrease at all stations in run SA4, low waters increase (the changes in low waters are smaller than the changes in high waters). The RMSE of high waters (run SA4 vs run SA3) varies between 31 cm downstream and 5 cm upstream. The RMSE of low waters is 20 to 1 cm. RMSE of complete time series changes from 19 cm downstream to 8 cm upstream.

The effect of the Coriolis force on velocities decreases in the upstream part of the estuary. Maximum flood velocity decreases in SA4 (Table 46).

Table 46. Measured and modeled velocity profiles in runs with and without Coriolis coefficient

20120508 R6 Middelgat		
Run	Max ebb	Max flood
SA 3		
SA 4		
20130530_Kruikeke		
Run	Max ebb	Max flood
SA 3		



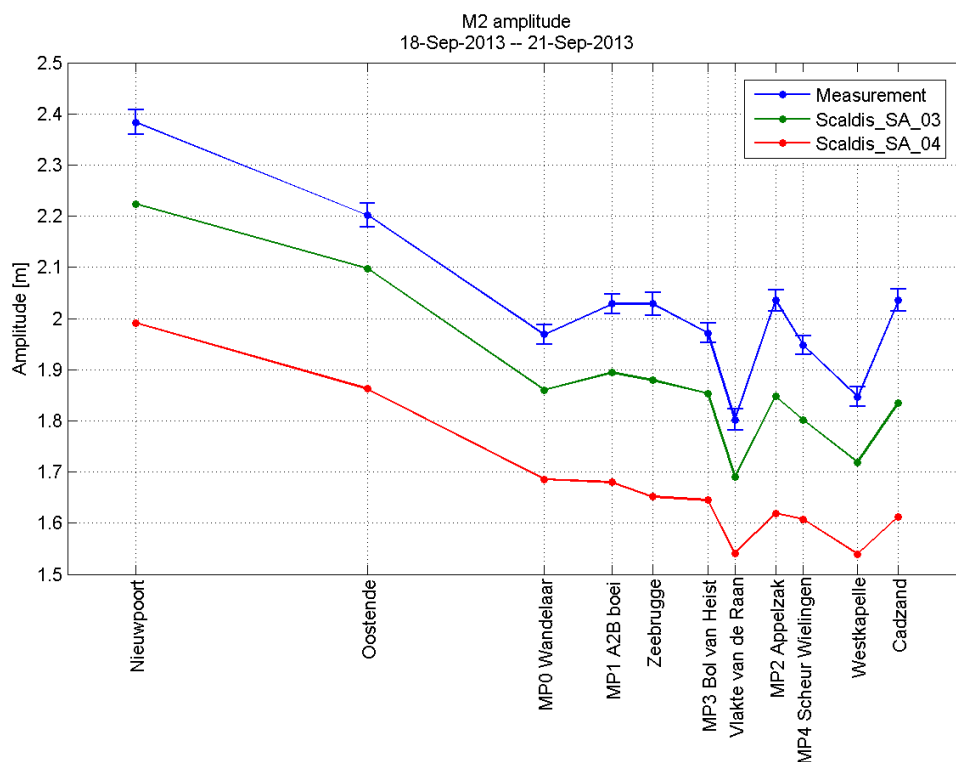


Figure 138 - M2 amplitude in runs SA3 and SA4 (North sea)

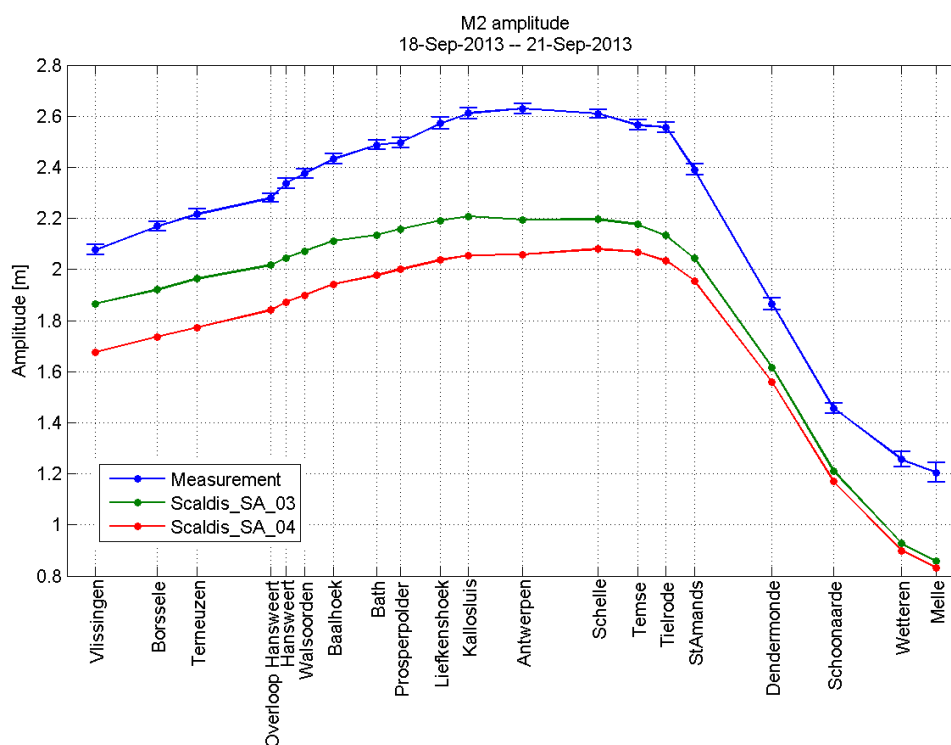


Figure 139 - M2 amplitude in runs SA3 and SA4 (Western Scheldt and Sea Scheldt)

7.10. Coefficient of wind influence

Model runs used for the analysis of the model sensitivity to wind influence are described in Table 47. The results of SA1 are compared with the output of SA10; SA3 is compared with SA2 because the same roughness formula is used in these simulations.

Table 47. Model runs used for the sensitivity analysis to the wind influence

Model run	Coefficient of wind influence	Roughness
SA1	0.565E-6	Manning
SA10	1.E-4	Manning
SA3	0.565E-6	Nikuradse
SA2	no wind	Nikuradse

The use of a large wind coefficient in SA10 results in unstable model results (Figure 140, Figure 141).

The differences between runs SA2 and SA3 are very small (Figure 142, Figure 143). This means that in our simulation period wind has no effect on the model results. Simulation SA10 however shows that wind can play a role in the model domain and that the source terms of wind are taken into account in our TELEMAC-3D model.

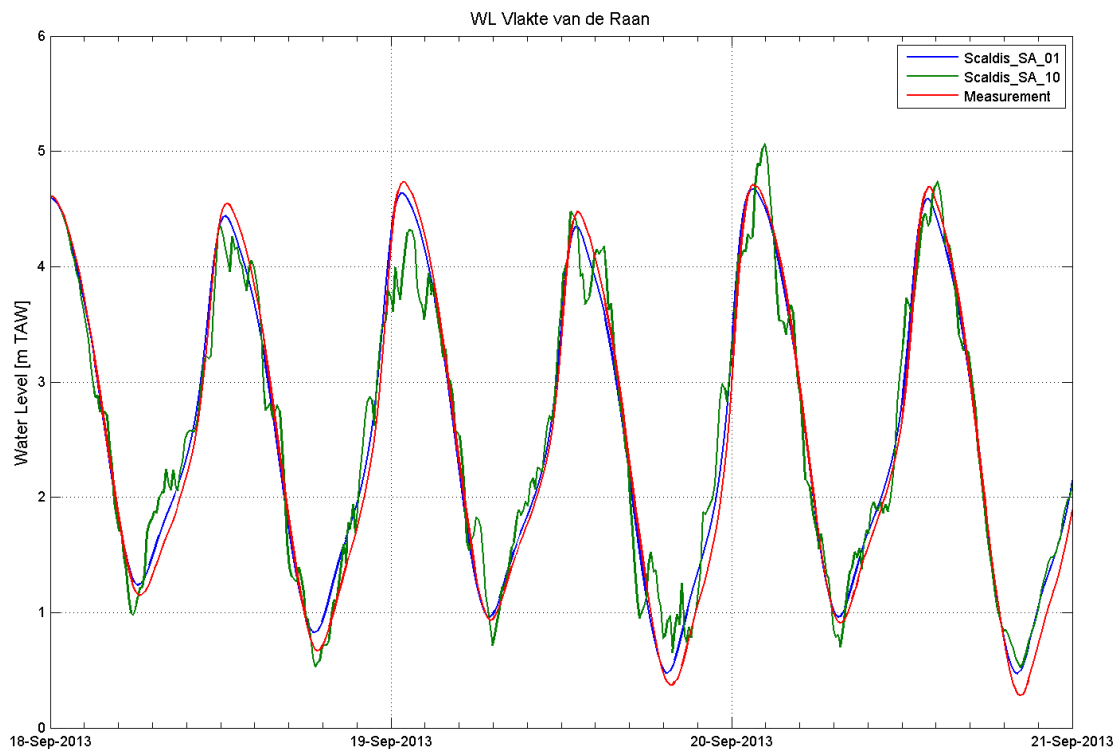


Figure 140 - Water level calculated in runs SA1 and SA10 at Vlake van de Raan

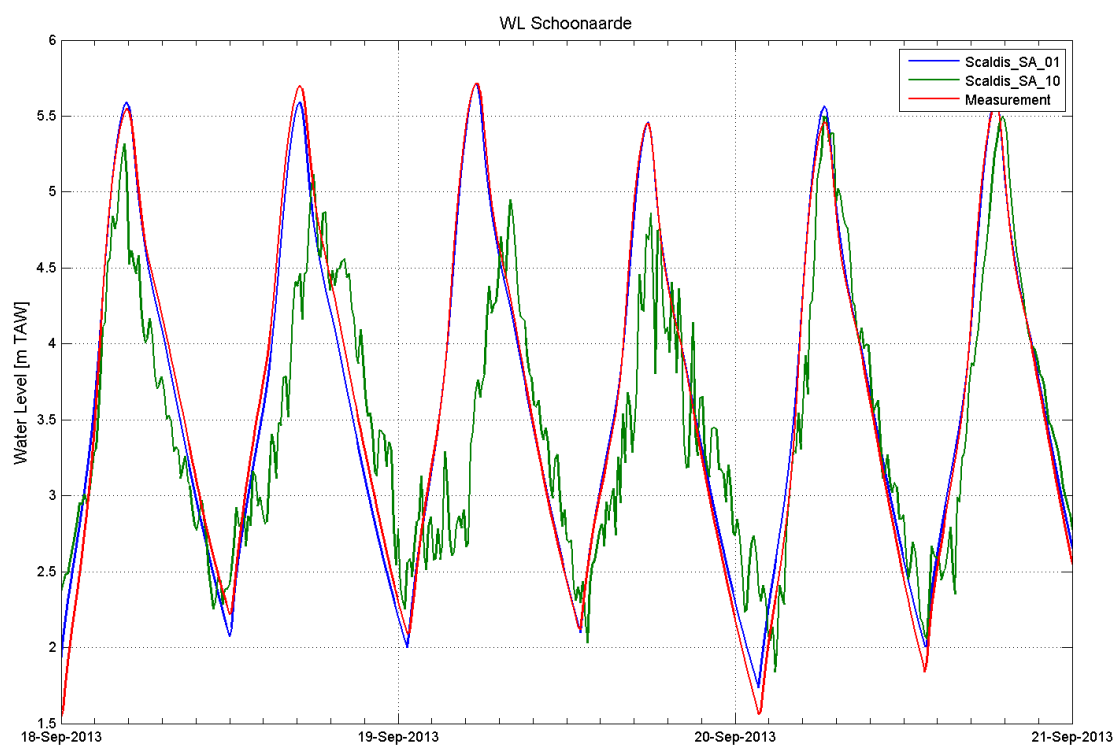


Figure 141 - Water level calculated in runs SA1 and SA10 at Schoonaarde

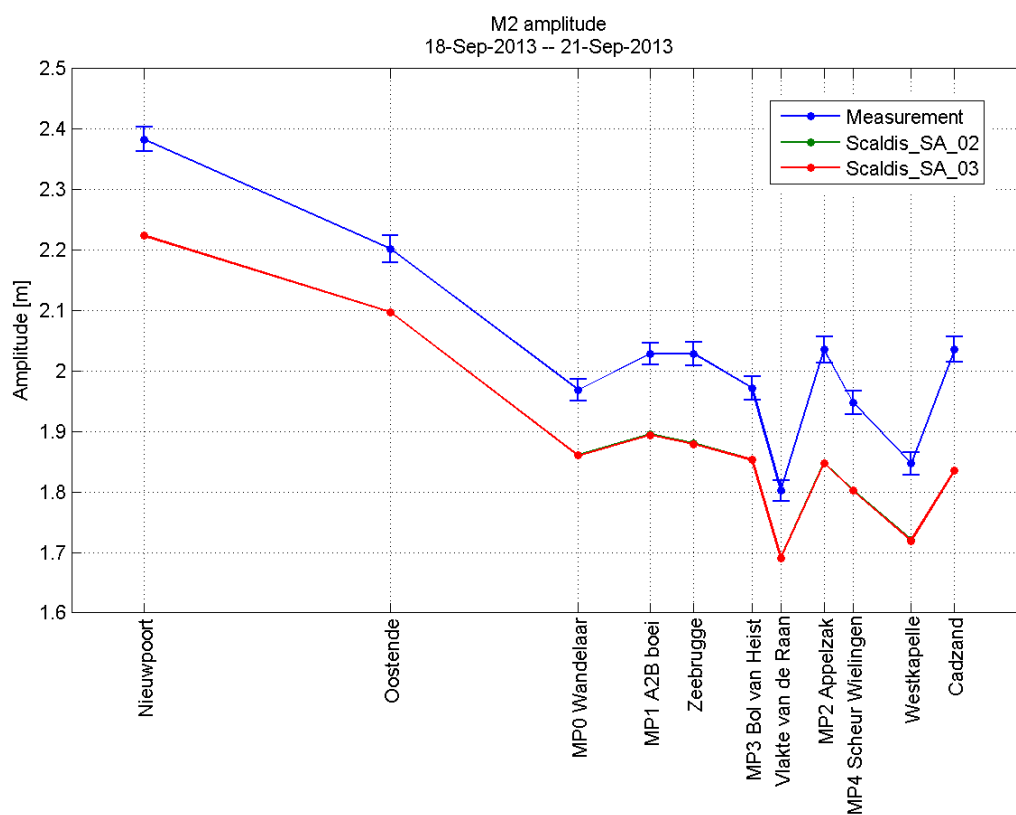


Figure 142 - M2 amplitude in runs SA2 and SA3 (North sea)

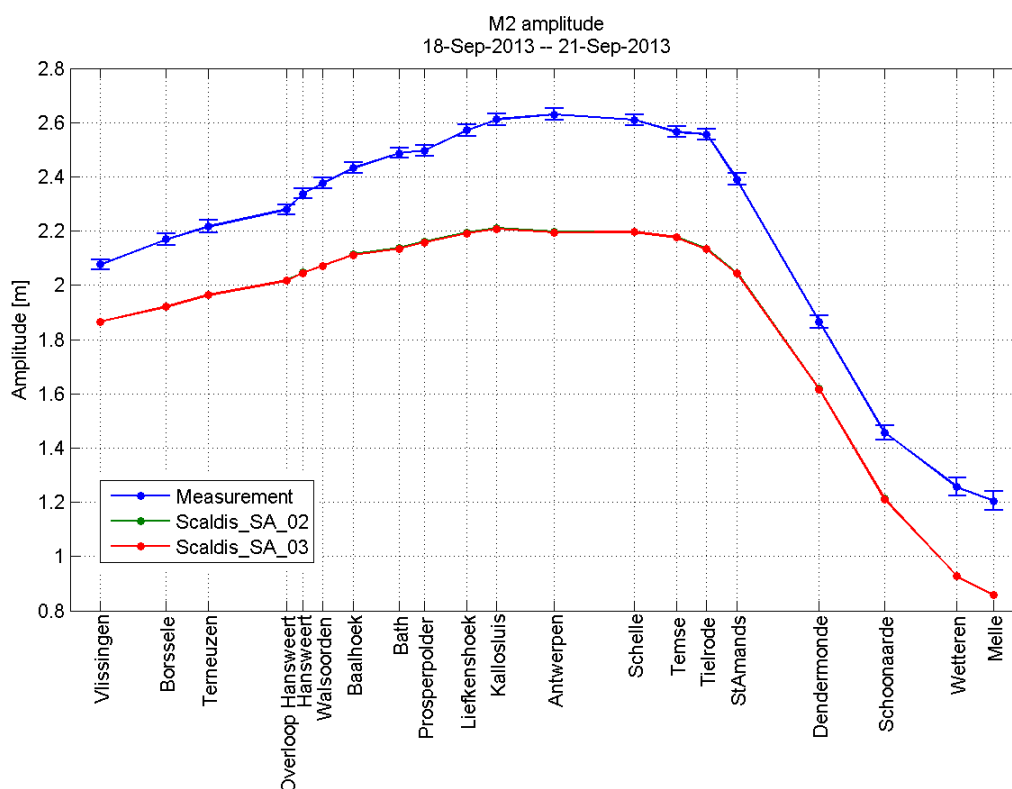


Figure 143 - M2 amplitude in runs SA2 and SA3 (Western Scheldt and Sea Scheldt)

7.11. Grid adaptation

The model sensitivity to the grid adaptation was tested in runs SA25 and SA27. The same bathymetric samples were interpolated to different grids in these runs.

Table 48. Model runs used for the sensitivity analysis to the grid

Model run	Grid	Bathymetry
SA25	geo_v16_034_0.slf	before the update (v16_034)
SA27	geo_v17_035_bathyv16_034.slf	before the update (v16_034)

The model grid is updated in run SA27 based on the most recent Sigma contour. The grid is extended to include the areas outside the dikes. The same bathymetric samples are used in SA25 and SA27. These samples are interpolated to the model grid in Blue Kenue. No effect on the water levels was expected because the adaptation of the model grid was done only for the areas that stay dry in these simulations.

However, high waters change by up to 1.5 cm at all stations. The effect on low waters is about 1 cm at most stations and 3.5 to 4 cm at Melle and Wetteren (Figure 144, Figure 145). M2 amplitude changes by 1 to 2 cm (Figure 146, Figure 147). This is probably related to the differences in interpolation of the bathymetric samples to the grids in Blue Kenue.

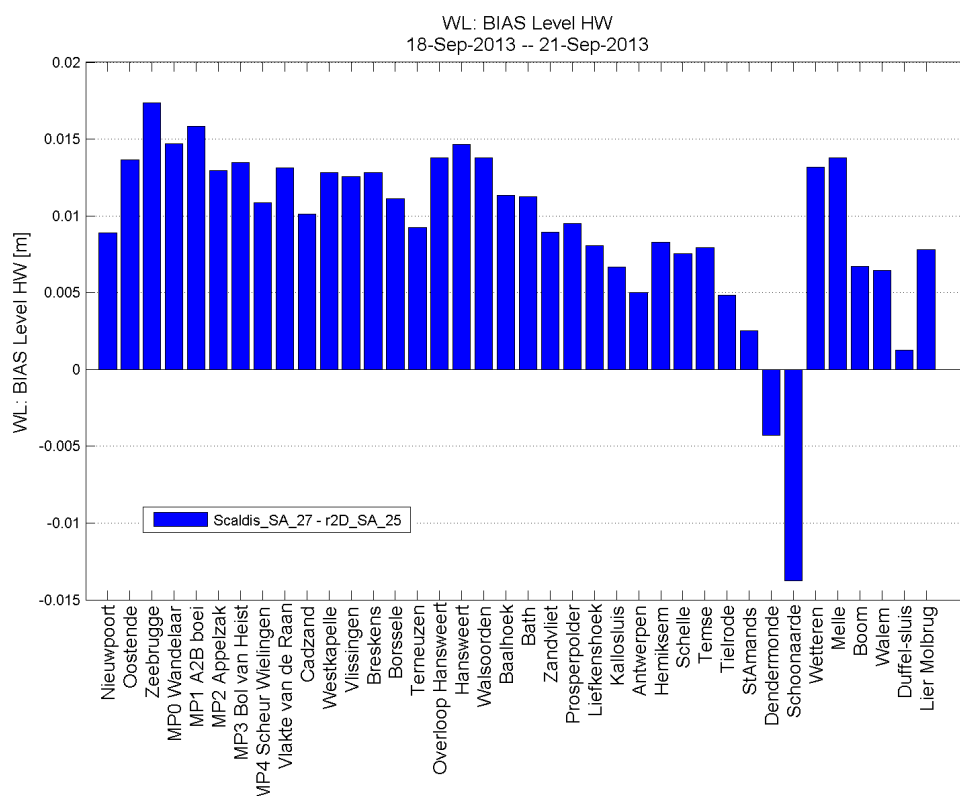


Figure 144 - Difference in high water (SA27 – SA25)

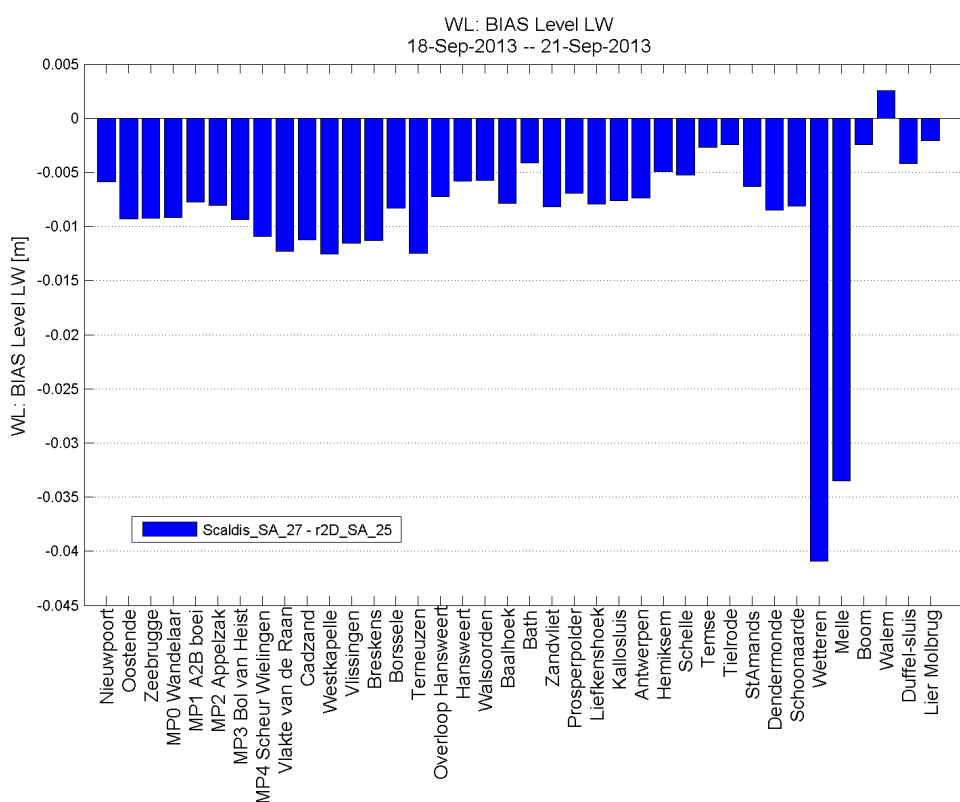


Figure 145 - Difference in low water (SA27 – SA25)

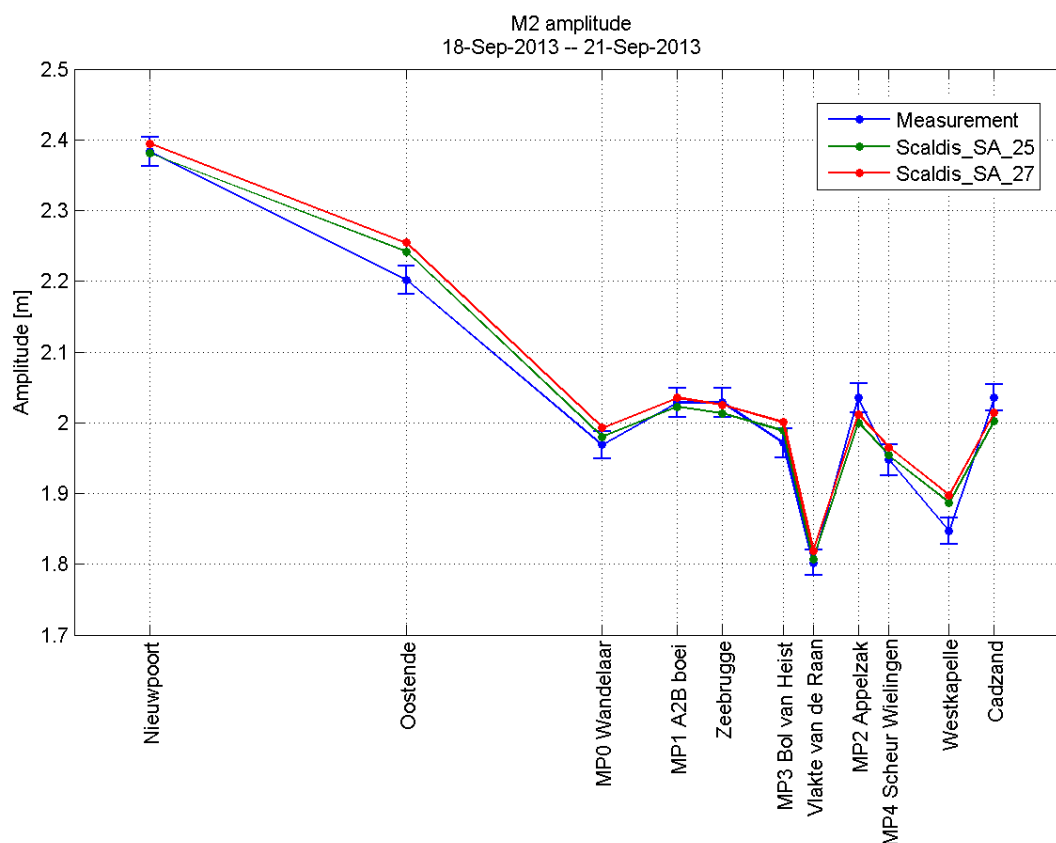


Figure 146 - M2 amplitude in runs SA25 and SA27 (North sea)

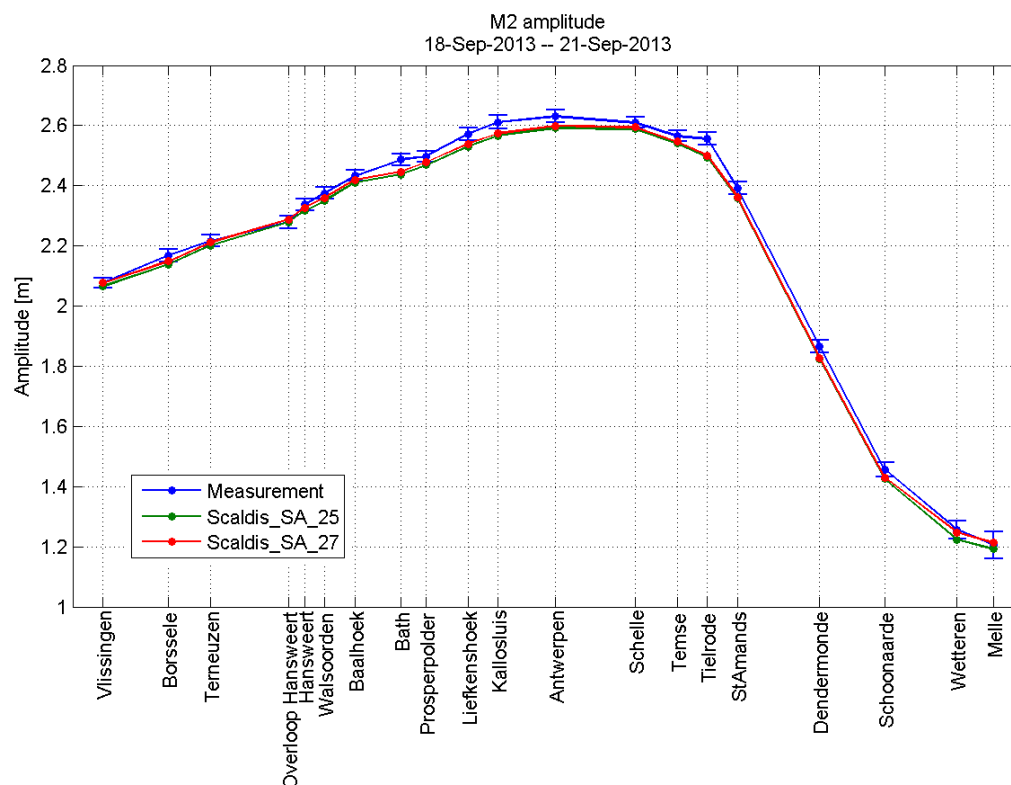


Figure 147 - M2 amplitude in runs SA25 and SA27 (Western Scheldt and Sea Scheldt)

7.12. Effect of salinity on water levels

Salinity in Scaldis is added as a tracer. Tracers in TELEMAC can be passive or active. Passive means they don't affect the hydrodynamics. Salinity as an active tracer will invoke density effects. This was tested with two identical simulations where in the second simulation salinity was considered as a passive tracer. All other parameter remained unchanged.

Beforehand we can estimate the effect of salt water on the simulation by considering a static force balance (represented in Figure 148):

$$\frac{1}{2} \rho_{\text{sea}} g h_{\text{sea}}^2 = \frac{1}{2} \rho_{\text{river}} g h_{\text{river}}^2$$

Where: ρ_{sea} = density of sea water (1023 kg/m³)
 ρ_{river} = density of river water (1000 kg/m³)
 h_{sea} = water level sea
 h_{river} = water level river

If we extract h_{river} from this static force balance we get:

$$h_{\text{river}} = h_{\text{sea}} \sqrt{\rho_{\text{sea}}/\rho_{\text{river}}}$$

If we take $h_{\text{sea}} = 10$ m we get a difference of 11 cm in the water level ($h_{\text{river}} = 10,11$ m) caused by the presence of a salinity gradient.

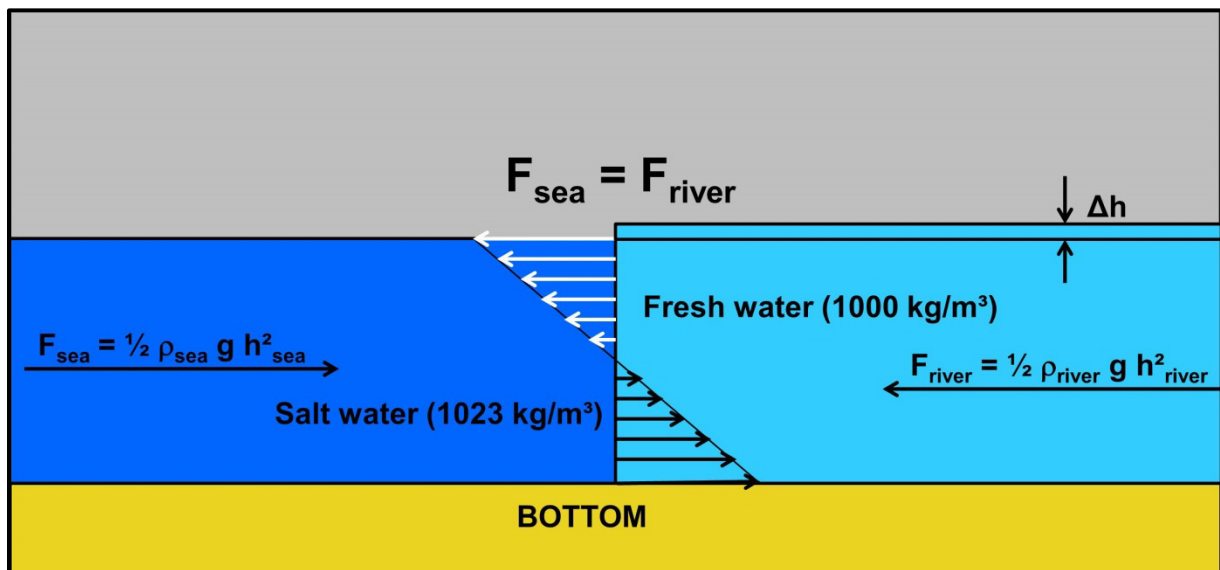


Figure 148 - Schematic view on the effect of salt water on the average water level

The difference we calculated above returns also in the simulation results. When salinity is present as a passive tracer water levels inside the estuary are lower compared when salinity is an active tracer. This is shown for water levels at the estuary mouth (Figure 149), water levels near Bath (Figure 150) and water levels near Antwerp (Figure 151). The exact differences are shown in Figure 152 for Vlissingen, Bath and Antwerp. The largest differences in the beginning of the simulation are due to the start-up of the model. The differences we see lie within the expectations like the example we calculated above.

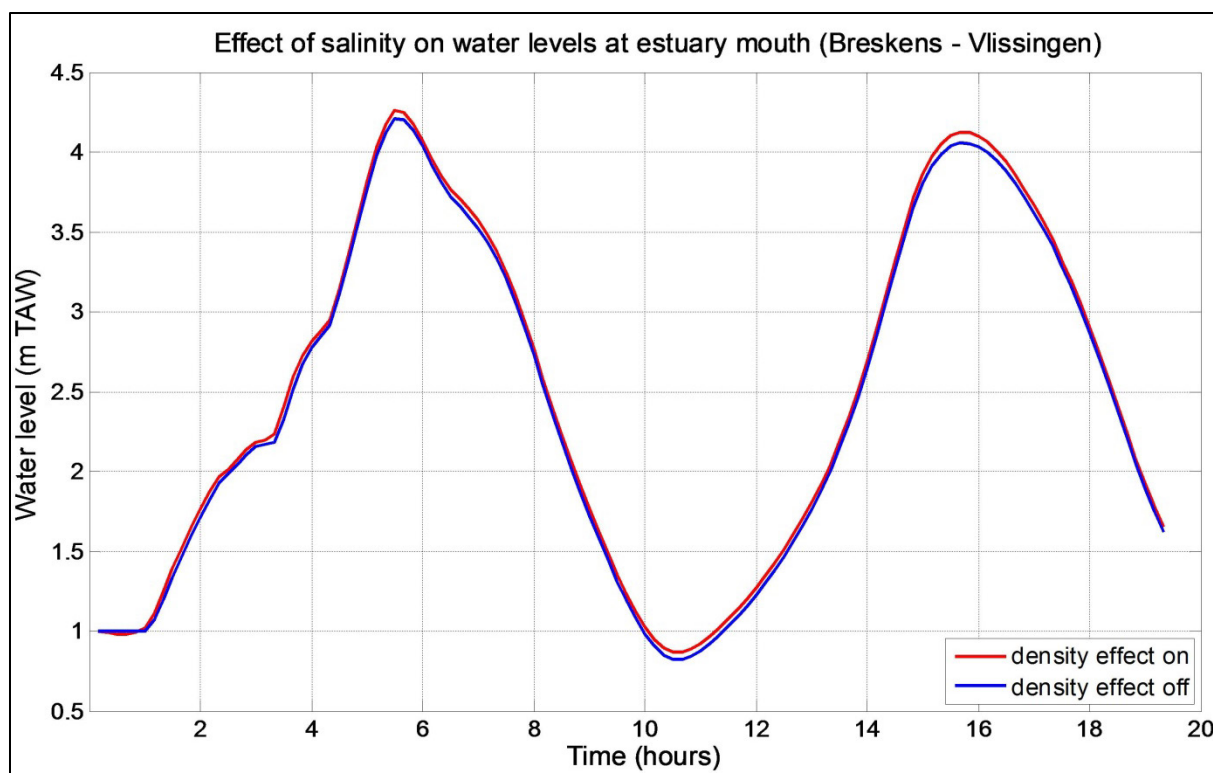


Figure 149 - Difference in water level at the estuary mouth caused by presence of salinity in the model.

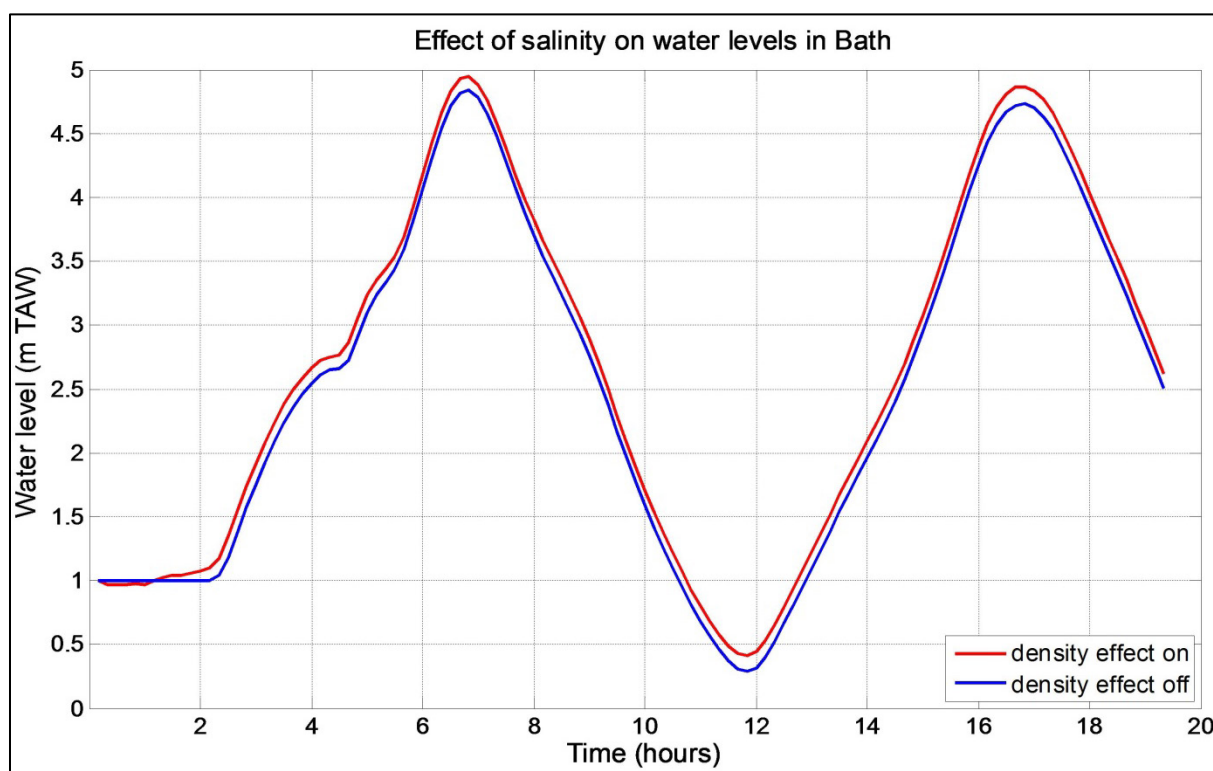


Figure 150 - Difference in water level near Bath caused by presence of salinity in the model.

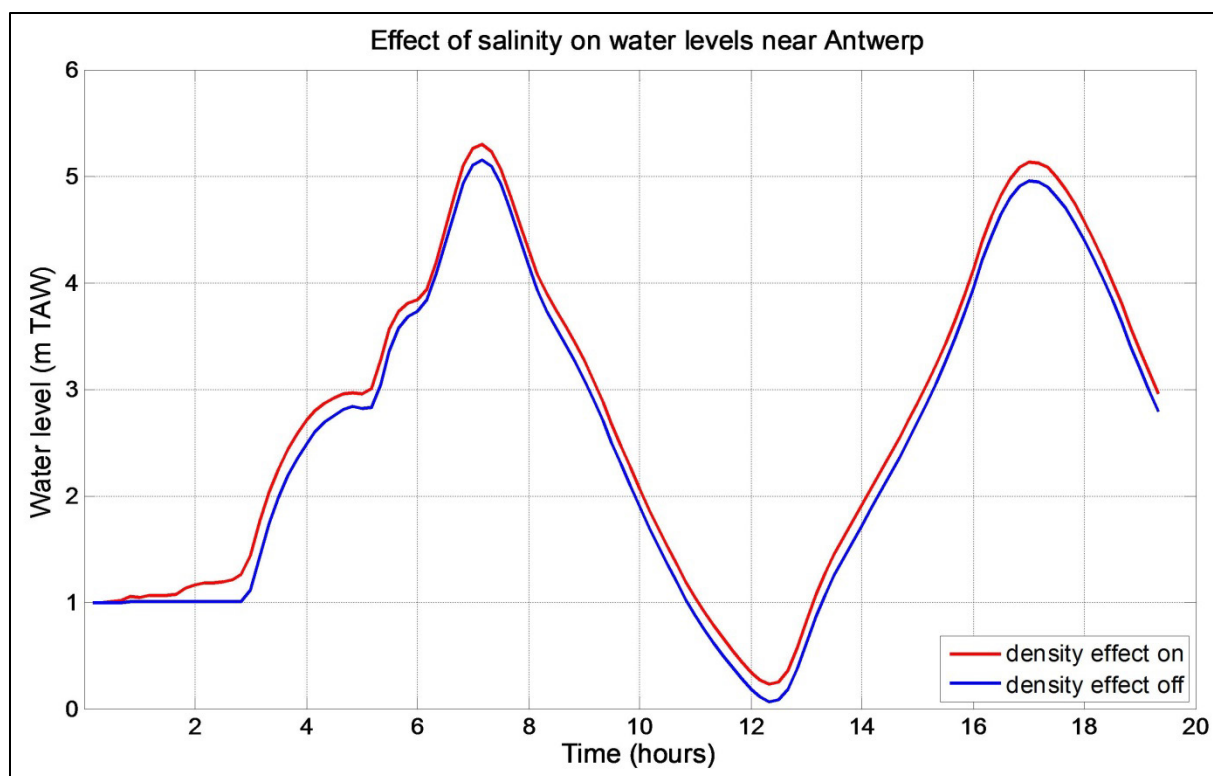


Figure 151 - Difference in water level near Antwerp caused by presence of salinity in the model.

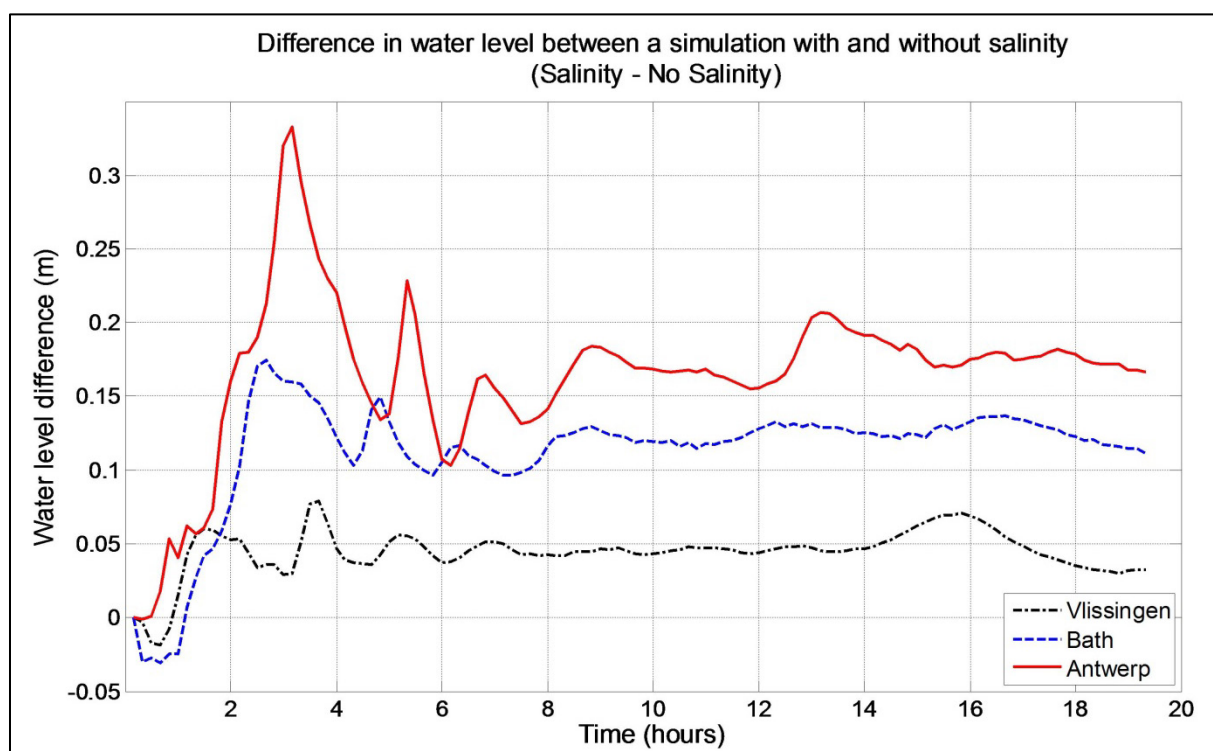


Figure 152 - Showing the differences in water levels between a simulation with and without density effects for salinity. Water level differences are shown for Vlissingen (black line), Bath (blue line) and Antwerp (red line).

7.13. Conclusions

The model sensitivity to different parameters was tested. The sensitivity analysis showed that it is necessary to have an accurate and detailed time series of the discharge at Merelbeke to get an accurate model output at the upstream stations in the Scheldt estuary. The use of the daily time series can result in big differences between the modeled and measured water levels.

An effect of the bed roughness increase was analyzed for the intertidal areas. At the upstream locations (Schoonaarde, Schellebelle) the increase of the roughness results in a decrease of the velocities everywhere along the transect (even in a deeper zone). The model accuracy worsens. Furthermore, the roughness adaptation of the intertidal areas results in the worsening of the water levels. Therefore, it was decided not to increase the bed roughness of the intertidal areas.

The diffusivity change has an effect on the flow velocities only in the upstream part of the estuary (upstream Antwerp). In the downstream part the grid size is bigger and the diffusivity change does not have any effect on the model results because of a higher numerical diffusion. The coefficients for horizontal and vertical diffusion of velocities will be chosen during the calibration process.

The sensitivity to the number of vertical layers was tested. The model with 5 layers represents the hydrodynamics well and an increase of vertical resolution is not necessary.

It is important to have an accurate bathymetry for Durme and Gentbrugge. The bathymetry of Durme has an effect on water levels upstream Antwerp. The bathymetry of the tidal branch Gentbrugge has an effect on water levels at Schoonaarde, Wetteren and Melle.

Different turbulence models were analyzed. Mixing length (Nezu and Nakagawa) vertical turbulence model and Smagorinski horizontal turbulence model will be used for the model calibration.

There are no differences between the results of model runs with and without mass lumping. A mass lumping of 1 will be used for depth, velocities and diffusion.

The water levels in the upstream part of the estuary become unstable in the run with a decreased parameter for the implicitation for velocities. This parameter will be set to 1 for the model calibration.

The Coriolis force has a strong effect on the modeled water levels and velocities in the downstream part of the estuary. This force is taken into account in the model.

Wind can play an important role in the model domain. Therefore, the source terms of wind are taken into account in the model.

The model grid was adapted to include the areas outside the dikes. No effect on the water levels was expected because the adaptation of the model grid was done only for the areas that stay dry in the simulations. However, small changes in high and low waters were observed. This is probably related to the differences in interpolation of the bathymetric samples to the grids in Blue Kenue.

Salinity as an active tracer invokes density effects. This was tested with two identical simulations where in the second simulation salinity was considered as a passive tracer. All other parameter remained unchanged. When salinity is present as a passive tracer water levels inside the estuary are lower compared to the run where salinity is an active tracer.

8 Model calibration

8.1. Methodology

The main objective of the model calibration is to improve the model performance in the upstream part of the estuary. Bed roughness is used as a calibration parameter. The model is calibrated for deep zones by comparison of the model results and measured water levels, discharges, ADCP velocities and stationary velocity measurements in deep areas. The analysis for shallow zones is done by comparison of the model results and velocity measurements (ADCP and stationary) in the intertidal areas.

Comparison between modeled and measured water levels is done by comparing the time series, the high and low waters, and the harmonic components obtained from a harmonic analysis.

For ADCP measurements and discharge data, comparison with the model results is done for a selected modeled tide that is comparable to the tidal conditions during the measurements (Table 56 to Table 58). This allows us to use ADCP and discharge data from different periods for the comparison with the model results. Bigger differences between the calculated and measured velocities and discharges are expected when the agreement between the measured and modeled tides is not sufficient. Differences between the model bathymetry and the actual bathymetry during the measurements can be another reason for the differences in discharges.

The magnitude and direction of the stationary velocities in deep zones are analyzed. Also an analysis of the components of the currents is performed based on *Sutherland et al.*, 2003 (Appendix 5). This results in a MAE (mean absolute error), combining magnitude and direction and RMAE (relative mean absolute error).

Stationary velocity measurements in shallow zones are usually available for a long period which is different from the modeled period. In order to compare these measurements with the model results separate tidal cycles were assembled based on concurrent water level data and given tidal amplitude boundaries.

8.2. Cost function

In order to select the best calibration run, a cost function is calculated for each simulation. The cost function is defined to get one objective factor that represents improvement or deterioration of the model performance. The cost function is expressed in function of the reference run, so a value lower than 1 indicates an improvement (*Vanlede et al.*, 2015, in preparation).

$$Cost = \sum \frac{\max(Factor_i, Threshold_i)}{\max(Factor_{i,ref}, Threshold_i)} * Weight_i$$

Several parameters are selected as factors for the calculation of the cost function (Table 49):

- RMSE of the water level time series, RMSE of high waters, vector difference (that shows the accuracy of harmonic components in the model);
- RMAE for each location with the available ADCP measurements. The RMAE gives information about the model accuracy for both velocity magnitude and direction;
- RMSE of discharges.

An expected observation error (a threshold for different parameters), needs to be taken into account to assess the accuracy of the model reference in relation to the pre-defined modelling objective (Vos *et al.*, 2000). For example, the threshold for the M2 amplitude is 2 cm. It means that if the error in M2 amplitude in both runs is smaller than 2 cm, the cost of this parameter will remain the same. This methodology helps to avoid giving too much weight to a very small improvement or deterioration of a parameter.

The threshold for the M2 amplitude was obtained from the VIMM output for harmonic components. The threshold for the RMSE of water levels is 3 cm (*personal communication with Elin Vanlierde*). The threshold for the RMSE of discharges was calculated as 2% of RMS discharge in a certain area (Western Scheldt, Eastern Scheldt, Lower Sea Scheldt and Upper Sea Scheldt) (*a range of measurement uncertainties for discharges was given by Styn Claey's (depending on the flow velocities); we take here the smallest value of 2% for the analysis*).

In the cost function more weight is given to the Upper Sea Scheldt because the main objective of the calibration is to improve the model accuracy there.

A small weight is given to the RMAE of sailed ADCP in shallow zones. In shallow areas a small inaccuracy in bathymetry (due to the interpolation to the grid with a certain resolution) has a big effect on the water depth, and therefore it has a big impact on the velocities. Therefore, a limited resolution of the model grid can result in significant differences between the model results and sailed ADCP measurements in shallow zones.

The cost function is calculated for the entire Scheldt estuary and for the Upper Sea Scheldt separately.

Table 49. Weights and thresholds used in the cost function

	Zone	Factor	Weights [%]			Threshold
Vertical Tide (water levels)	Western Scheldt	RMSE water level time series (m)	3.50	14.00	50	0.03
		RMSE high water level (m)	3.50			0.03
		Vector difference	3.50			0
		delta M2 amplitude (m)	3.50			0.02
	Eastern Scheldt	RMSE water level time series (m)	1.25	5.00		0.03
		RMSE high water level (m)	1.25			0.03
		Vector difference	1.25			0
		delta M2 amplitude (m)	1.25			0.02
	Lower Sea Scheldt	RMSE water level time series (m)	3.50	14.00		0.03
		RMSE high water level (m)	3.50			0.03
		Vector difference	3.50			0
		delta M2 amplitude (m)	3.50			0.02
	Upper Sea Scheldt	RMSE water level time series (m)	4.25	17.00		0.03
		RMSE high water level (m)	4.25			0.03
		Vector difference	4.25			0
		delta M2 amplitude (m)	4.25			0.02
Horizontal Tide (velocities and fluxes)	Western Scheldt	RMAE of sailed ADCP deep zone	10.00	13.33	50	0
		RMSE of discharges (m³/s)	3.33			738
	Lower Sea Scheldt	RMAE of sailed ADCP deep zone	10.00	15.83		0
		RMAE of sailed ADCP shallow zone	2.50			0
	Upper Sea Scheldt	RMSE of discharges (m³/s)	3.33	20.83		87
		RMAE of sailed ADCP deep zone	15.00			0
		RMAE of sailed ADCP shallow zone	2.50			0
		RMSE of discharges (m³/s)	3.33			13
Sum			100	100	100	

Table 50. Weights and thresholds used in the cost function for the Upper Sea Scheldt

	Zone	Factor	Weights [%]		Threshold
Vertical Tide (water levels)	Upper Sea Scheldt	RMSE water level time series (m)	12.5	50.0	0.03
		RMSE high water level (m)	12.5		0.03
		Vector difference	12.5		0
		delta M2 amplitude (m)	12.5		0.02
Horizontal Tide (velocities and fluxes)	Upper Sea Scheldt	RMAE of sailed ADCP deep zone	35.0	50.0	0
		RMAE of sailed ADCP shallow zone	5.0		0
		RMSE of discharges (m³/s)	10.0		13
Sum			100	100	

8.3. Calibration results

In order to improve the representation of water levels, a harmonic correction of the boundary conditions was done. M2, M4, S2 and Z0 components were corrected (see chapter 5.4). The model was further calibrated by varying the roughness parameter. The adaptation of the bed roughness resulted in an improvement of the M2 amplitude.

As explained in chapter 8.2, a cost function was used to give an objective estimation of the model performance. The model run with the best accuracy has the lowest score. Figure 153 and Figure 154 show the scores of the model runs for the entire Scheldt estuary and for the Upper Sea Scheldt if run Scaldis_016_0 is used as reference. Figure 155 and Figure 156 show the cost functions if run Scaldis_028_0 is used as a reference run.

In run **Scaldis_028_0** the coefficients for horizontal and vertical diffusion of velocities were set to 1 m²/s. The model accuracy for harmonic components and water levels is good in this simulation. However, the velocity profiles in the upstream part of the estuary are too flat in this run (Table 51). It was necessary to make them more convex.

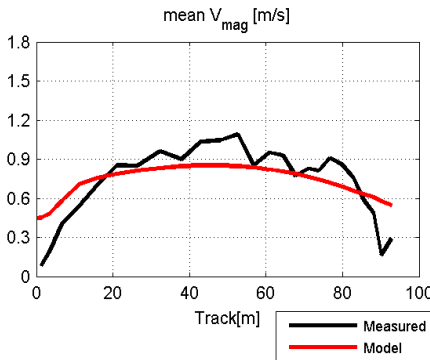
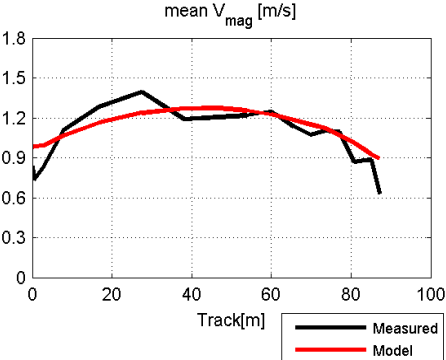
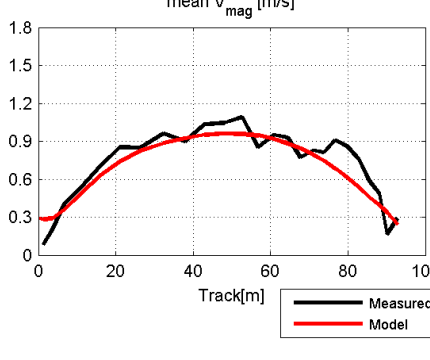
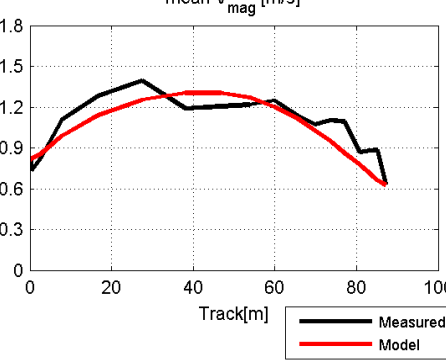
An attempt was made to improve the model accuracy in shallow zones by increasing the roughness of the intertidal areas (chapter 7.2). This helped to improve the velocity profiles for some transects. However, this change of roughness resulted in too low M2 amplitude in the upstream part of the estuary and in a decrease of the flow velocities everywhere along the transect (even in a deeper zone). Therefore, it was decided not to decrease the roughness of the intertidal areas.

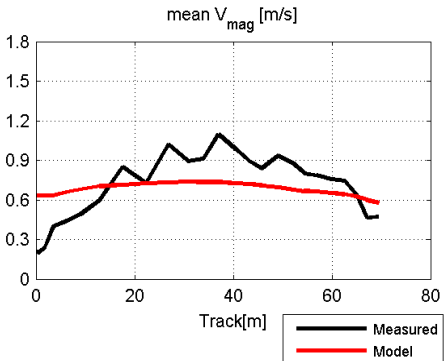
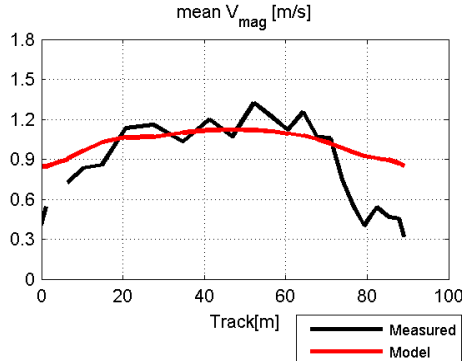
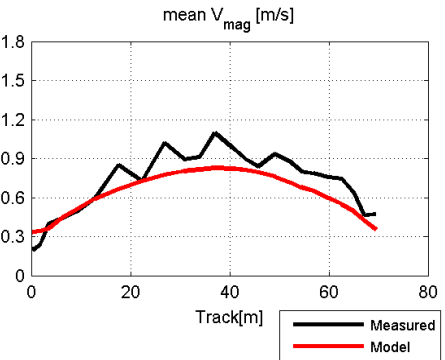
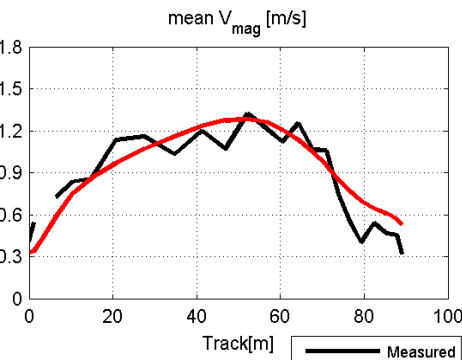
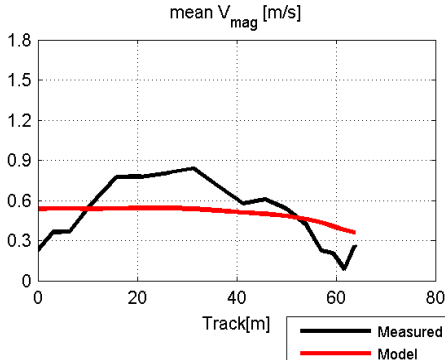
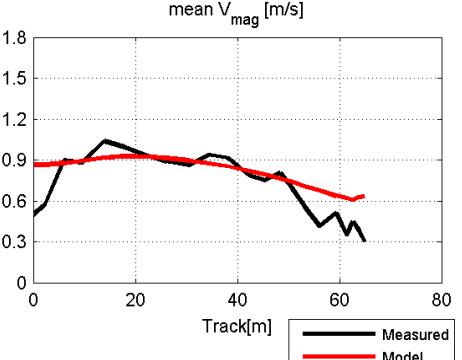
The coefficients for horizontal and vertical diffusion of velocities were decreased from 1 to 0.01 m²/s in **Scaldis_029_0**. This resulted in a decrease of the flow velocities in the intertidal areas and an increase of the velocities in deeper parts of the channel in the upstream part of the estuary. The velocity profiles became more convex. The cost function increased because the bed roughness field had to be adapted again to ensure a better accuracy of the model with a lower diffusivity. After the adaptation of the bed roughness the modeled velocities and water levels improved in the Upper Sea Scheldt (**Scaldis_034_0**).

More recent bathymetry and Sigma contour of the flood areas became available and had to be implemented in the model (**Scaldis_035_0**). A new model grid was generated in Blue Kenue and bathymetry was interpolated to the new grid. This had an effect on the model results. As explained in chapter 7.11, adaptation of the model grid can have an effect on the modeled water levels (1.5 cm for most stations, up to 4 cm upstream). This is probably related to the differences in interpolation of the bathymetric samples to the grids in Blue Kenue. The cost function increased in Scaldis_035_0 in comparison to Scaldis_034_0.

The bed roughness was adapted in runs Scaldis_036_0 to Scaldis_040_0. From these runs **Scaldis_039_0** produces the best results. The cost function of this simulation is slightly higher than the one of Scaldis_034_0. However, the differences between the results of these runs are very small. The quality of the calibrated model Scaldis_039_0 is described in chapter 9 for the calibration period. The model performance during storm is described in chapter 10. The comparison of velocity profiles at several upstream locations is presented in Table 51 for Scaldis_039_0 and Scaldis_028_0.

Table 51. Velocity profiles calculated in Scaldis_028_0 and Scaldis_039_0 in the upstream part of the estuary

20140417_Dendermonde			
Run	Diffusivity (m ² /s)	Max ebb	Max flood
Scaldis_028_0	1		
Scaldis_039_0	0.01		

20130527_Schoonaarde			
Run	Diffusivity (m ² /s)	Max ebb	Max flood
Scaldis_028_0	1		
Scaldis_039_0	0.01		
20140415_Schellebelle			
Run	Diffusivity (m ² /s)	Max ebb	Max flood
Scaldis_028_0	1		

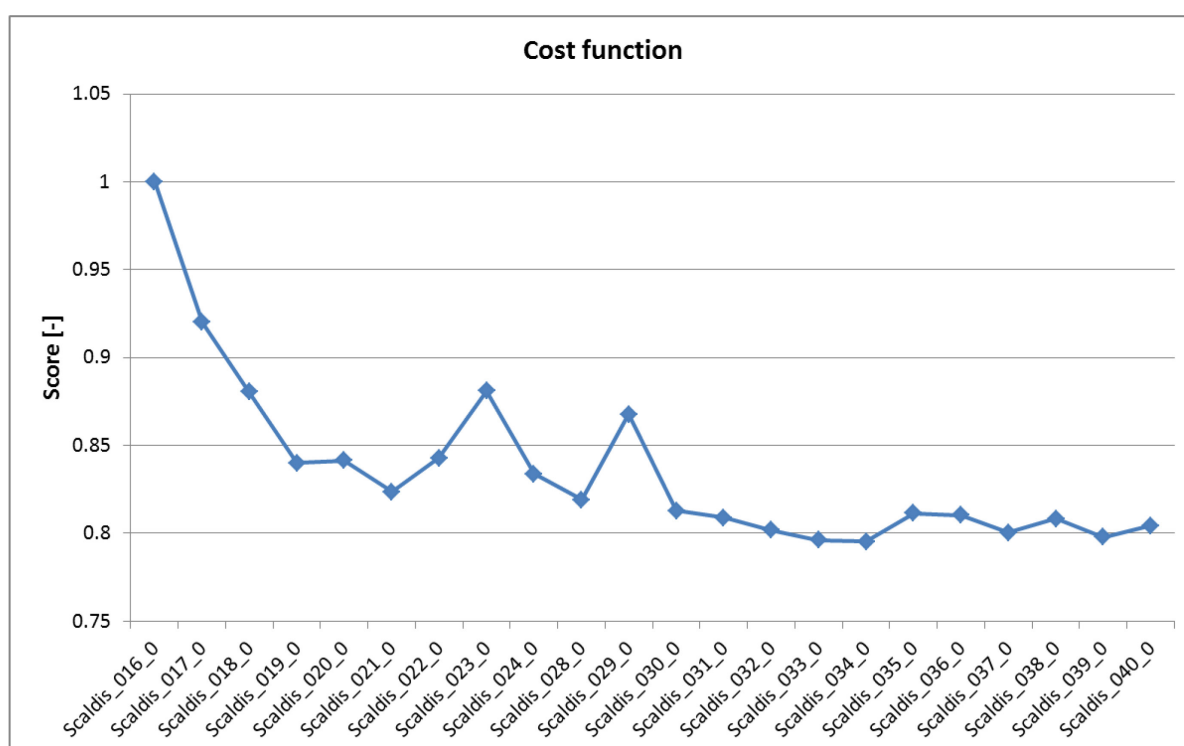
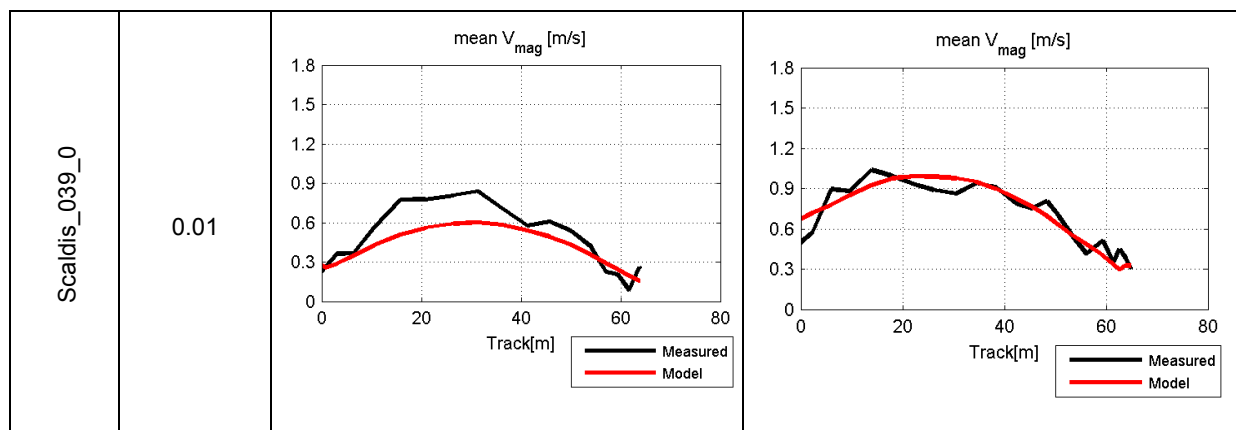


Figure 153 - Cost function for the entire Scheldt estuary (Scaldis_016_0 is reference)

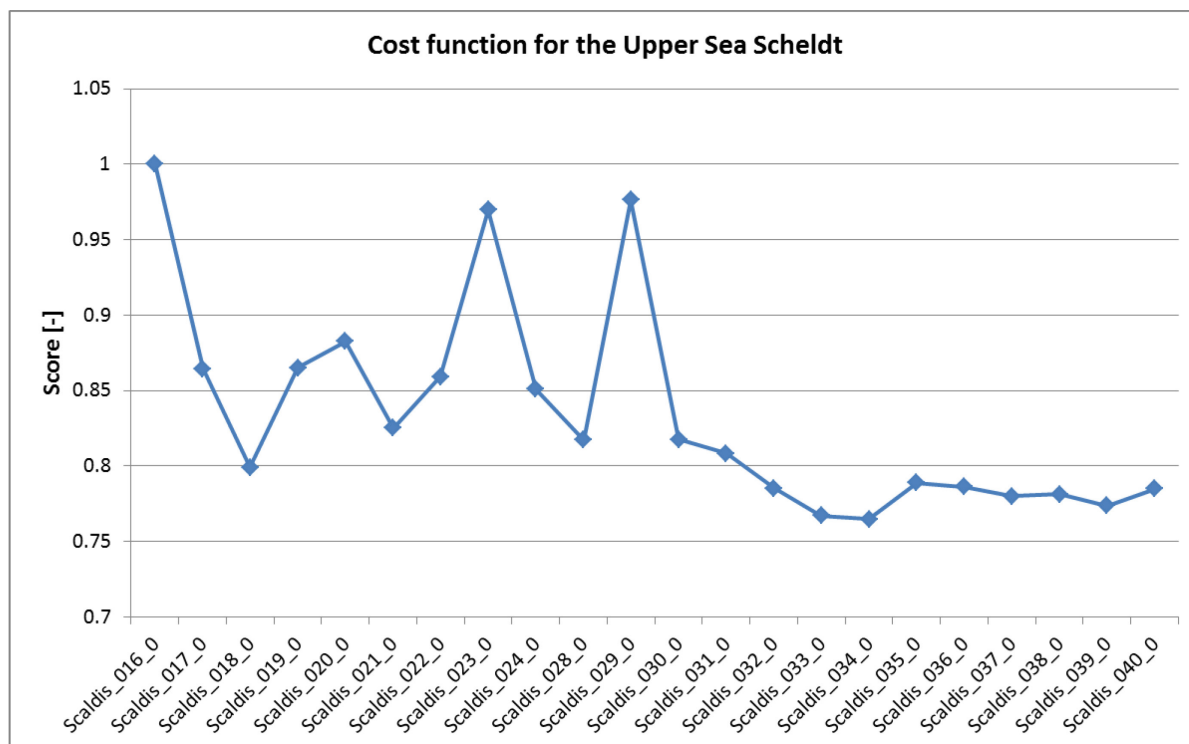


Figure 154 - Cost function for the Upper Sea Scheldt (Scaldis_016_0 is reference)

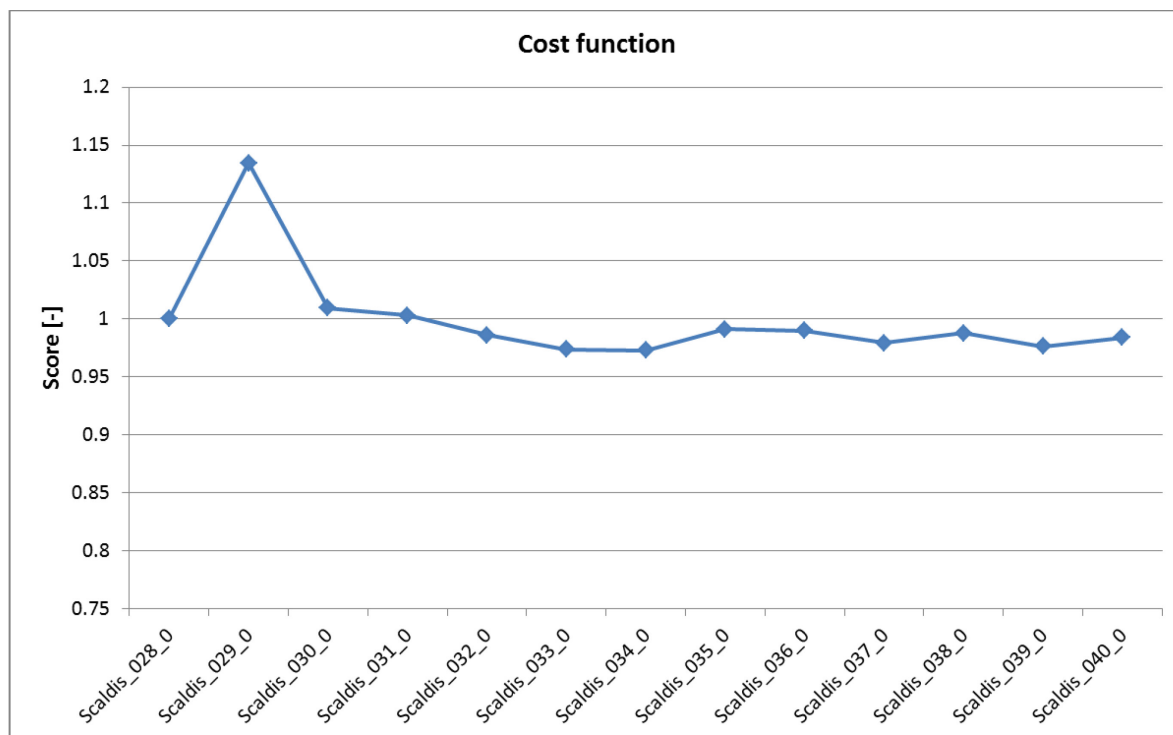


Figure 155 - Cost function for the entire Scheldt estuary (Scaldis_028_0 is reference)

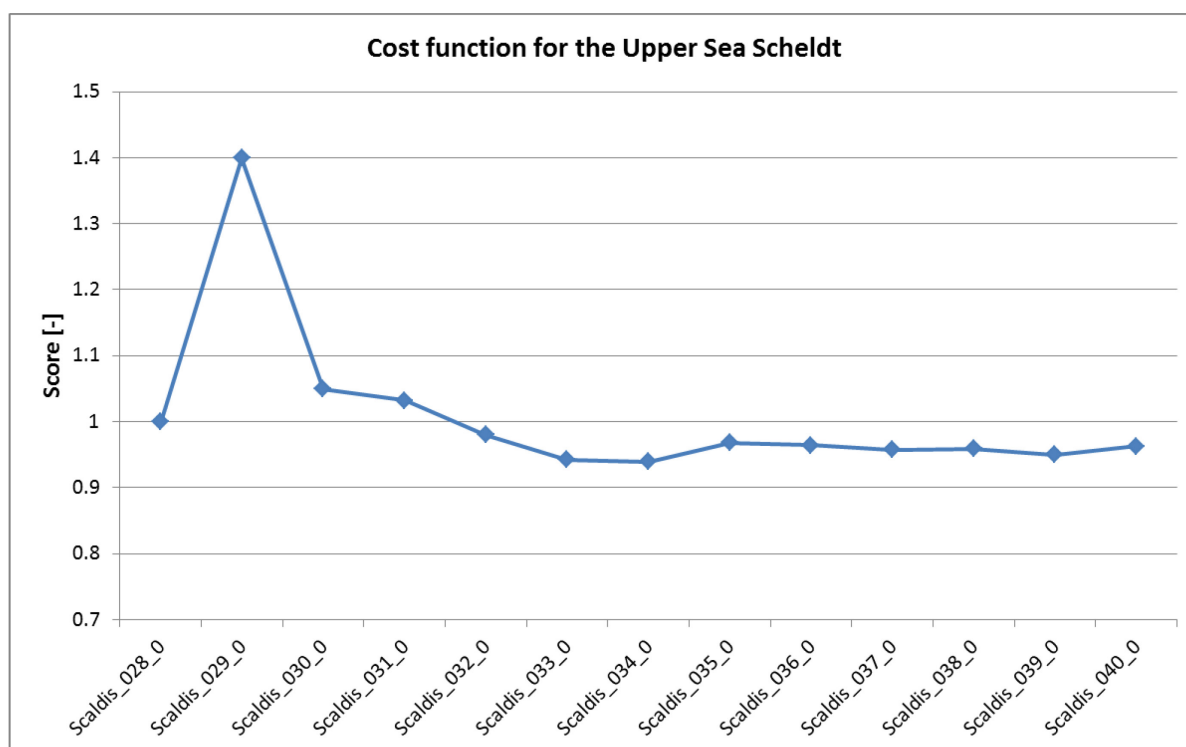


Figure 156 - Cost function for the Upper Sea Scheldt (Scaldis_028_0 is reference)

9 Quality of the calibrated model

9.1. Water levels

9.1.1. Analysis of the high and low waters and time series

Figure 239 to Figure 261 show the plots of the statistical parameters for high and low waters and for the complete time series. The values of the statistical parameters are given in Table 63 to Table 77. The history plots of water levels for some stations are presented in Figure 279 to Figure 288.

The total RMSE of high, low waters and complete water level time series is 7 to 10 cm in the North Sea and Western Scheldt, around 10 cm in the Eastern Scheldt, 9 to 14 cm in the Lower Sea Scheldt and 12 to 14 cm in the Upper Sea Scheldt. The absolute value of the bias of water levels is smaller than 10 cm at most stations. The differences between the modeled and measured water levels are higher at the upstream stations (Wetteren, Melle). This is related to the use of the daily discharge time series at the upstream model boundary in the Upper Sea Scheldt (see chapter 7.1). More detailed discharge time series are necessary to improve the model results at these stations.

The calculated water levels in the Durme and the Rupel basin are less accurate than in the Sea Scheldt. This can be related to the uncertainties in bathymetry of these rivers. The sensitivity analysis showed that the bathymetry has a significant impact on the modeled water levels (chapter 7.5).

9.1.2. Harmonic analysis

The harmonic analysis of the water levels is presented in Table 78 to Table 145. The amplitude and phase of different harmonic components (M2, M4, M6, S2, K1 and O1) are calculated for different stations along the estuary using T-TIDE. T-TIDE is a function that computes the harmonic analysis of a time series. A description of the theoretical basis of the analysis and some implementation details can be found in *Pawlowicz et al., 2002*.

The M2 harmonic component has the highest amplitude in the zone of interest, implying that the tidal amplitude will depend to a large extent on the amplitude of M2. M2 amplitude and phase for all the analysed stations are presented in Appendix 1 in Figure 263 to Figure 269. Figure 157 to Figure 160 show the results for the North sea, Western Scheldt and Sea Scheldt. In the North sea and Western Scheldt the difference in M2 amplitude is -2 to 5 cm; it is smaller than 2 cm at most stations. The difference is -1 to 2 cm in the Eastern Scheldt, -2 to 1 cm in the Lower Sea Scheldt and Upper Sea Scheldt. The difference in M2 phase is not significant at most stations (-3 to 3 degrees).

The S2 amplitude and phase are shown in Figure 271 to Figure 277. The difference in S2 amplitude is smaller than 3 cm and the difference in S2 phase is smaller than 3 degrees at most stations. At Wetteren and Melle the difference is 5 and 4 degrees respectively.

M4, M6, K1 and O1 components are presented in Table 88 to Table 135. They are less important for the model calibration than M2 and S2.

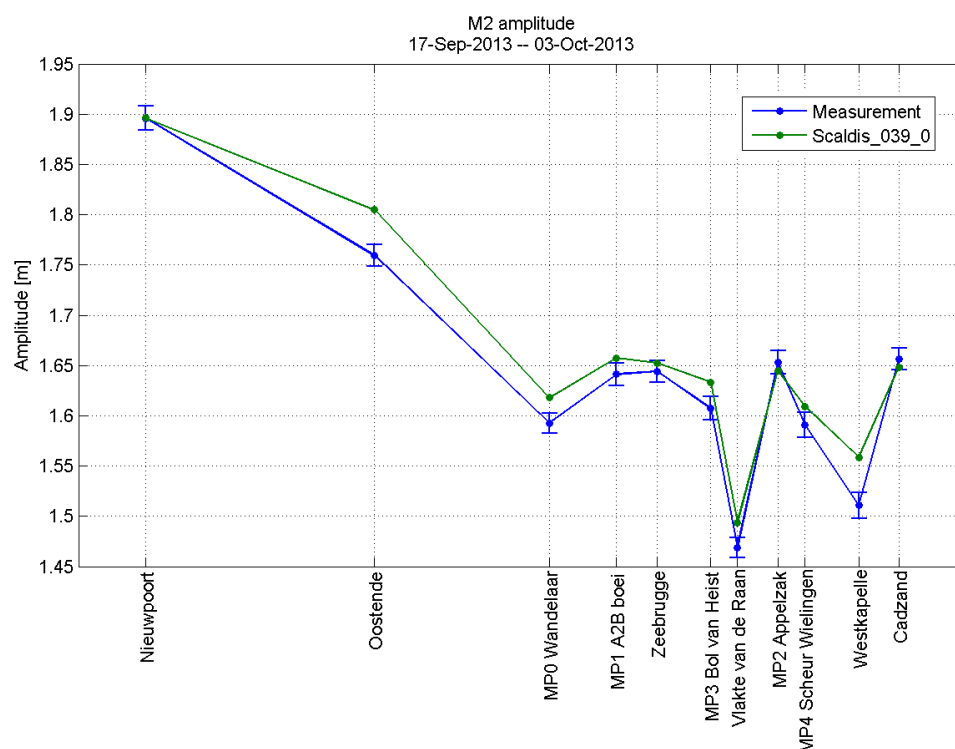


Figure 157 - M2 amplitude in the North sea (Scaldis_039_0 and measurement)

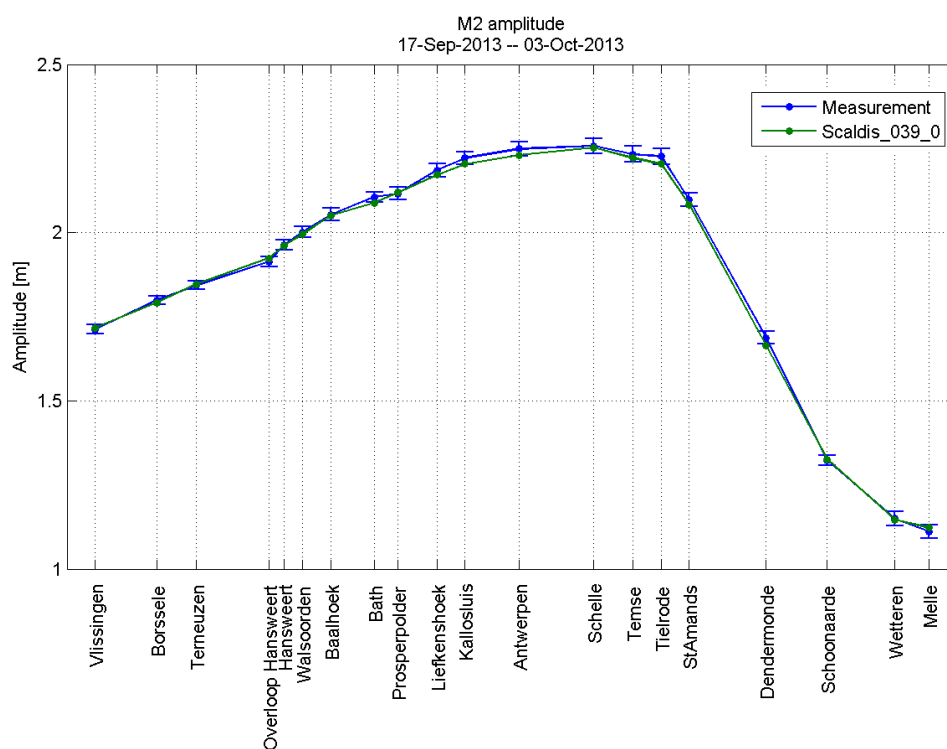


Figure 158 - M2 amplitude in the Scheldt estuary (Scaldis_039_0 and measurement)

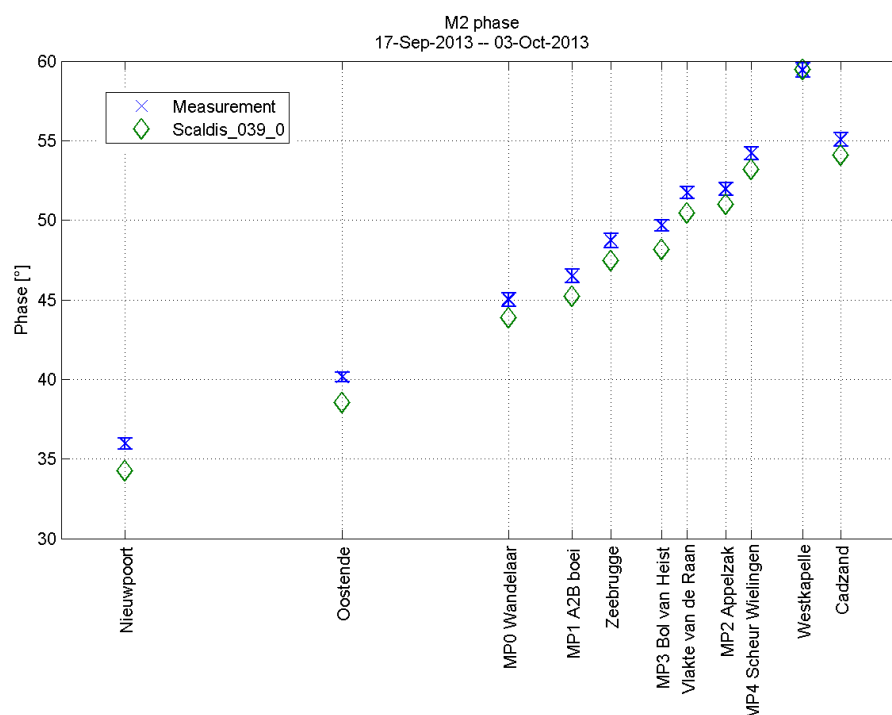


Figure 159 - M2 phase in the North sea (Scaldis_039_0 and measurement)

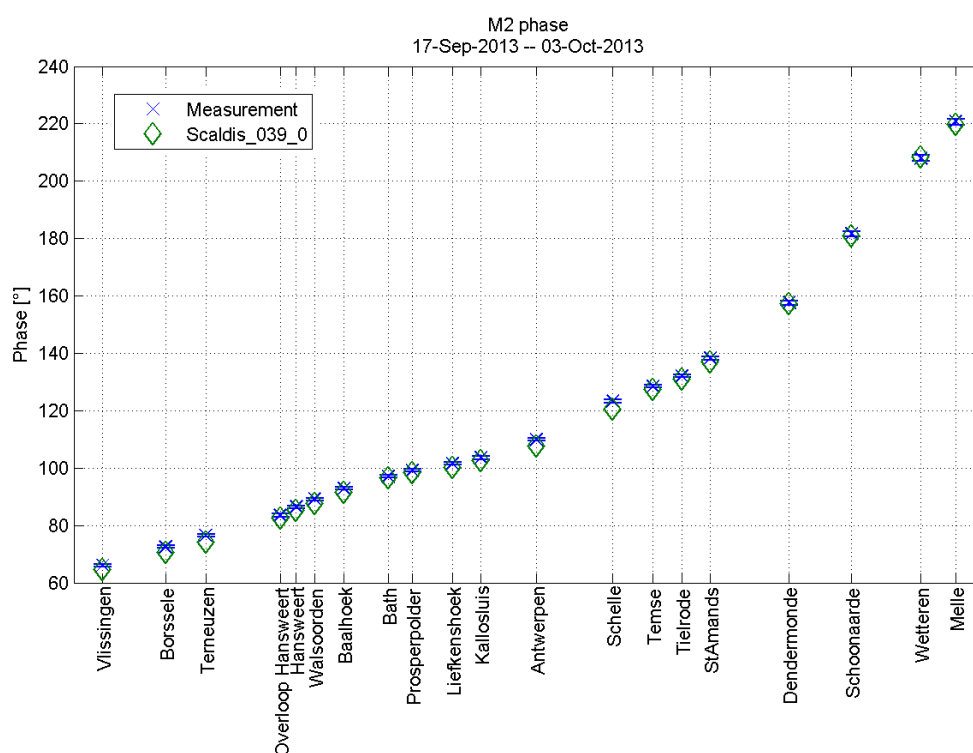


Figure 160 - M2 phase in the Scheldt estuary (Scaldis_039_0 and measurement)

9.2. ADCP velocities

ADCP measurements at 37 locations in deep zones (from Terneuzen in the Western Scheldt to Schellebelle in the Upper Sea Scheldt) and 5 transects in shallow zones along the estuary were used for the model calibration. Bias and RMSE of velocity magnitude and direction are calculated for each location with available ADCP measurements. Furthermore, a relative mean absolute error (RMAE) is derived to identify the order of magnitude of the error compared to the observed velocities. This parameter shows the accuracy of both magnitude and direction.

9.2.1. Analysis of the complete transects

Table 148 to Table 149 show the values of statistical parameters for different ADCP transects. The plots of the time series of the measured and modeled velocities are shown in Figure 289 to Figure 330. Each point on the plots of statistical parameters represents an average bias or RMSE for a certain transect. Each point on the time series plots of the measured and modeled velocities represents an average velocity for a certain transect measured with ADCP or calculated in the model. Some transects are measured only in a deeper part of the river. This results in a higher average velocity for a transect (peak in the plot). If there are more data in the shallow areas, a lower average velocity is calculated for a transect. Since in the model we analyze velocities for the same extent as the measurements, peaks in the measured and modeled velocities are observed at the same moments on the plots.

Average velocity magnitude and direction for each transect are calculated as the magnitude and direction of the average vector (based on the average U and V components), (average means the combination of the depth average and average over the transect). This means that both magnitude and direction of velocities are taken into account. The bias of magnitude and direction is calculated as the difference between the calculated and measured average velocity magnitude and direction (see more information in the end of Appendix 5).

The RMSE of velocity magnitude and direction is calculated based on the depth average velocity magnitude and direction for each point along the transect. Magnitude is not taken into account for the calculation of the RMSE of velocity direction and vice-versa. Therefore, the RMSE plots show more variation between the model and measurements than the plots of average velocity magnitude and direction for all transects.

The RMSE of velocity magnitude varies between 12 cm/s and 21 cm/s for the locations with transverse ADCP measurements. For most transects it is smaller than 20 cm/s. The average RMSE of velocity magnitude for all the analysed transects in the Western Scheldt is 16 cm/s (excluding the transverse measurements at Ossensisse). In the Lower Sea Scheldt, Upper Sea Scheldt and Rupel the average RMSE of velocity magnitude is the same : 16 cm/s. At transverse profile Ossensisse the RMSE is 46 cm/s. The velocities in the small channel are not accurately represented in the model (Figure 331). The bathymetry of this area may be poorly represented in the model because of the small scale of the channel. Therefore, it is not unexpected that this small-scale area produces a worse than average result.

The RMSE of velocity magnitude of the longitudinal transects varies between 15 and 25 cm/s. The longitudinal transects are sailed in shallow areas where a limited resolution of the model grid can result in significant differences between the model results and ADCP measurements (due to the differences in bathymetry).

The RMSE of velocity direction is 16 to 43 degrees. The RMSE of velocity direction is very high (72 degrees) at Wintam. The model accuracy for the velocity direction is good when the velocity magnitude is high. It worsens in the areas where velocity magnitude is very small (for example, near the entrance of the Wintam lock (Figure 332)). This results in an increase of the RMSE value of the entire transect.

The RMAE varies between 0.16 and about 0.35 for most transverse transects. It means that model has a good quality. The model qualification for different RMAE values is described in Table 228 in Appendix 5 based on *Sutherland et al.*, (2003). The RMAE is higher for the transects where velocity direction is not well defined (e.g. longitudinal profiles at Branst and Appels).

9.2.2. Estimation of error in the intertidal zones

From all available transects only ADCP measurements in the intertidal areas are selected for the comparison with the model results. The border of the intertidal areas is defined as the average low water at a certain location during spring tide for a period from 2001 to 2010. The model results and measurements in the locations with the bathymetry deeper than the low water of spring tide are excluded from the analysis.

The velocity direction is not well defined in the areas where velocity magnitude is small. Therefore, in the intertidal zones only the model accuracy for the velocity magnitude is analyzed.

It is important to keep in mind that in shallow areas a small inaccuracy in bathymetry (due to the interpolation to the grid with a certain resolution) has a big effect on the water depth, and therefore it has a big impact on the velocities. Therefore, a limited resolution of the model grid can result in significant differences between the model results and sailed ADCP measurements in shallow zones.

The RMSE's of velocity magnitude are presented in Table 150. The time series of the modeled and measured velocities in shallow zones are shown in Figure 333 to Figure 363. The RMSE varies between 11 and 20 cm/s for most transects. The model accuracy is worse (RMSE more than 30 cm/s) at some transects where the grid resolution is not fine enough in the intertidal area. The calculated velocities are lower than the measurements at some transects in the Western Scheldt and Lower Sea Scheldt. For example, Terneuzen (during ebb), Middelgat, Gat van Ossensisse, Zandvliet, Galgenschoor, Schelle (some moments of the tide) and Ballooi. The agreement between the model results and measurements is better at Schellebelle, Kruikebeke, Boom (during flood), Notelaer (flood), Terhagen (ebb and some moments during flood).

The differences in the Western Scheldt can be related to the grid resolution. The analyzed ADCP transects include shallow areas on the sides of the channel where the grid resolution is not refined.

9.3. Discharges

Table 151 to Table 152 show the statistical parameters (bias, RMSE and RRMSE) calculated for discharges. The comparison of the measured and modeled discharges for some locations is presented in Figure 364 to Figure 368.

The model results and measurements are analyzed for comparable tides. The shape of the discharges is well represented in the model for most cross sections. The RMSE of the discharge time series is 3 to 16% of the maximum discharge at a certain location.

The RRMSE (RMSE relative to the measurement) was calculated for every cross section. It varies between 0.08 and more than 0.30 (at Zimmermangeul and Ballastplaat, where discharges are small in comparison to the total discharges through the entire cross section) in the Western Scheldt. It is 0.06 to 0.22 in the Sea Scheldt. The model results and measurements are analyzed for comparable tides. Differences between the calculations and measurements are expected when the agreement between the measured and modeled tides is not sufficient.

9.4. Stationary velocities

9.4.1. Deep areas

3D modeled velocities were compared with the stationary velocity measurements at Buoy 84, Oosterweel and Driegoten at corresponding heights above the bottom. History plots were made and statistical parameters (MAE and RMAE of the velocity vector, bias and RMSE of the velocity magnitude and direction) were calculated to evaluate the model accuracy (Table 155, Figure 369 to Figure 373).

At Buoy 84 and Oosterweel the bias of velocity magnitude is -7 to 5 cm/s. The RMSE of velocity magnitude is 10 to 15 cm/s. The RMAE is 0.21 to 0.29. Accordingly to *Sutherland et al.*, (2003) the model performance at these locations is good (see Appendix 5). There is less variation in the modeled velocities at different levels (at Buoy 84 and Oosterweel) than in the measurements. The vertical velocity profile calculated in TELEMAC has less variation than the real profile.

The differences at Driegoten are higher than at other stations. The point with the real coordinates of the measurement becomes dry in the model in the second half of ebb (Figure 373). If we analyze the flow velocities in a deeper point (Driegoten proxy) close to the location of the real point, velocities are overestimated in the model (Figure 374). The differences between the calculated and measured velocity can be related to the inaccuracies in the bathymetry implemented in the model or to the location of the point (in the river bend) (Figure 375).

The discharge at Driegoten is modeled accurately (Figure 367). Maximum flood discharge is higher than the maximum ebb discharge. This corresponds to the calculated velocities: the maximum flood velocity is higher than the maximum ebb velocity. The measured velocities are different: the maximum flood velocity is significantly lower. These differences between the model results and measurements can be related to the location of the measurement point.

9.4.2. Shallow areas

The model results are compared with the stationary velocity measurements described in Table 5 and Figure 209 to Figure 210. At Hooge Platen Noord, Hooge Platen West and Plaat van Walsoorden measurements are available at different levels. The model results at corresponding levels are compared with these measurements. Also depth average model results are compared with the depth average velocity measurements at these locations.

Measured and modeled velocity ensembles for several points are presented in Figure 382 to Figure 403. Black and green lines in the figures represent the model result and measurement respectively. Grey and green shaded bars show the modeled and measured standard deviation.

RMSE's are calculated for each analyzed location for neap, average and spring tides (in case if measurements are available for these tides). Also total RMSE's are calculated (Table 156).

For the analysis of flow velocities in shallow zones it is very important that the measurement point and the analyzed point in the model have similar depths. It was not always possible to find a model node with a similar depth close to the measurement location. This may have resulted in differences between the calculated and measured velocities. At some locations the output in different points was tested. The points with the real coordinates of the measurement locations have names 'real'. The bathymetry in these points in the model is sometimes very different from the real bathymetry in these locations. The points with a more similar bathymetry (located close to the real points but not in exactly the same location) have names 'a', 'b', etc.

In many locations the model results in 'real' points are similar to the output in the alternative points or slightly better (Table 156). In several locations there are some differences. For example, in HPW_0311a the model results improved at some levels compared to HPW_0311_real (Figure 376 to Figure 379). There are still significant differences between the measured and modeled velocities in point HPN_MP_0310a. However, the velocity profile in this point is shorter and more similar to the measurement than the results in point HPN_MP_0310_real (because of more similar bathymetry) (Figure 380, Figure 381). At some locations (for example, Doel Kerncentrale, Plaat Driegoten, Heusden, HPN_MP_0416, PVW_MP0101, PVW_MP0310) it is not possible to find a model node with the bathymetry similar to the measured bathymetry. It is important to keep this in mind while analysing the model results.

The comparison of the modeled and measured velocities at the INBO locations is presented in Figure 382 to Figure 393. The RMSE's are shown in Table 156. They vary between 5 and 21 cm/s. The differences between the model results and velocities provided by INBO can be related to the location of the measurements. The flow velocities in these points are measured at 5 cm above the bottom. The model is not suitable for the analysis so close to the bottom. At most INBO locations the model overestimates the velocities. The best results are calculated at the Lillo polder, Notelaer, Dendermonde and Heusden.

Big differences are calculated between the model results and measurements at Weert (measurements from the project 'Habitatmapping') (Table 156). The measured bathymetry in these points is unknown. Differences between the bathymetry in the model and measurement can result in significant differences in velocities.

The differences between the modeled and measured velocities in shallow zones are smaller at most locations in the Western Scheldt. Some examples are given in Figure 394 to Figure 405. The RMSE of velocity magnitude in all the analyzed points is presented in Table 157 for the depth average velocities and in Table 158 to Table 160 for the velocities at different levels.

The modeled velocities in most points are very similar to the measurements (examples for Hooge Platen Noord are shown in Figure 394 to Figure 396, for Hooge Platen West in Figure 398 to Figure 400 and for Plaat van Walsoorden in Figure 402 to Figure 404). However, the model accuracy in some other points is worse (for example, Figure 397, Figure 401 and Figure 405). The RMSE of velocity magnitude at Hooge Platen Noord varies between 5 and 20 cm/s. At Hooge Platen West it is 5 to 15 cm/s. At Plaat van Walsoorden the RMSE of velocity magnitude is 5 to 10 cm/s. When velocities at different levels are analyzed the RMSE is higher than 20 cm/s at some levels. It may be related to the limited amount of data at these levels (e.g., when measurements are available only around high water).

9.5. Salinity

9.5.1. Salinity in run Scaldis_039_2

The Scaldis model was run for a period of 3 months to analyse the salinity distribution (run Scaldis_039_2 in Table 11). The comparison of the modeled and measured salinity time series is presented in Figure 406 to Figure 414. Salinity is well represented in the model. The differences between the calculated and measured salinity are smaller than 2 psu for all the analyzed stations. The RMSE varies between 0.4 psu in the upstream part of the estuary and 2.4 psu more downstream (Table 52).

Table 52. Statistical parameters for the time series of salinity (run Scaldis_039_2 vs. measurement)

Stationname	Scaldis_039_2 vs. Measurement	
	bias (psu)	RMSE (psu)
Vlakte van de Raan	0.82	1.49
Overloop van Hansweert	1.28	1.93
Baalhoek	1.96	2.41
Prosperpolder	1.07	1.28
Boei 84*	0.54	0.84
Liefkenshoek	0.63	0.88
Oosterweel*	-0.04	0.50
Hemiksem	-0.36	0.44
Driegoten	-0.41	0.42

*at Boei 84 and Oosterweel measurements are available at the top and bottom levels. Since the differences between these measurements are not big, they are averaged and compared with 2D model output.

The measured and modeled time series of salinity are transformed by subtracting the moving average (calculated by function `moving_average_centered.m`). A filter of 24 hours is used for this calculation. An example of plot for Prosperpolder is presented in Figure 161 (real time series) and Figure 162 (transformed time series).

The RMSE and bias are calculated for the filtered time series (Table 53). The bias is negligible, the RMSE is smaller than 1 psu for all the analyzed stations.

Table 53. Statistical parameters for the filtered time series of salinity (run Scaldis_039_2 vs. measurement)

Stationname	Scaldis_039_2 vs. Measurement	
	bias (psu)	RMSE (psu)
Vlakte van de Raan	0.00	0.67
Overloop van Hansweert	0.00	0.82
Baalhoek	0.00	0.84
Prosperpolder	0.00	0.49
Boei 84	0.00	0.51
Liefkenshoek	0.00	0.50
Oosterweel	0.00	0.37
Hemiksem	0.00	0.16
Driegoten	0.00	0.03

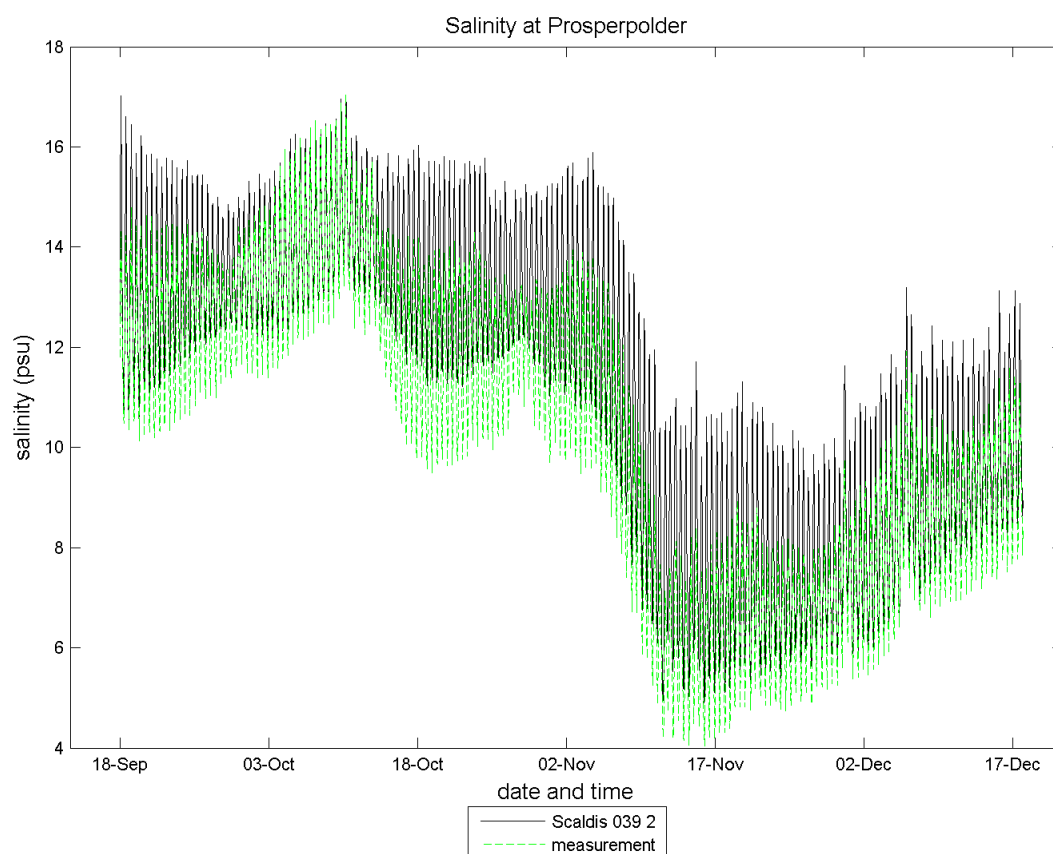


Figure 161 - Measured and modeled salinity at Prosperpolder

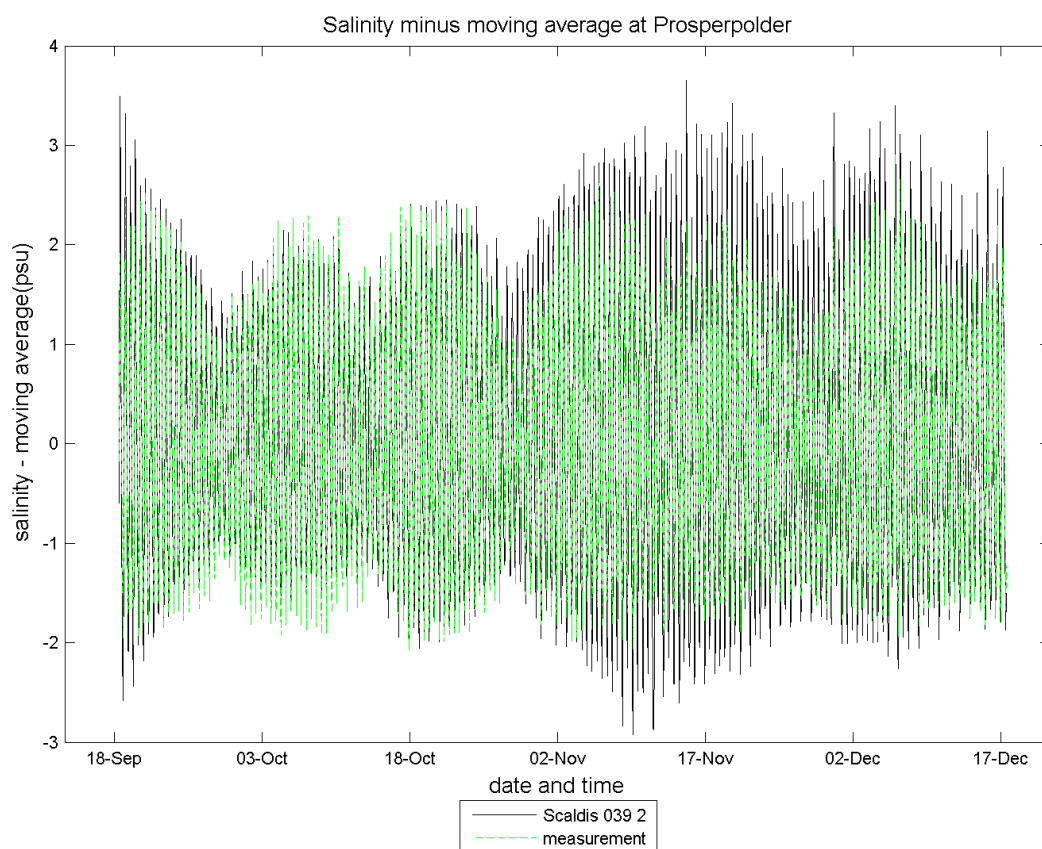


Figure 162 - Measured and modeled salinity minus moving average at Prosperpolder

9.5.2. Effect of diffusion on the salinity distribution

In run Scaldis_028_2 the coefficients for horizontal and vertical diffusion of velocities were set to 1 m²/s. The velocity profiles in the upstream part of the estuary are too flat in this simulation and it is necessary to make them more convex (see chapter 8.3).

The coefficients for horizontal and vertical diffusion of velocities are decreased from 1 to 0.01 m²/s in Scaldis_039_2. This results in a decrease of the flow velocities in the intertidal areas and an increase of the velocities in deeper parts of the channel in the upstream part of the estuary. The velocity profiles become more convex.

Salinities calculated in runs Scaldis_028_2 and Scaldis_039_2 are compared in Figure 415 to Figure 425 for different stations. Table 54 presents the RMSE's and maximum differences (Scaldis_028_2 vs Scaldis_039_2) calculated for different stations.

The RMSE of salinity (run vs. run) varies between 0.08 and 1.4 psu. It is smaller than 1 psu for most stations. The RMSE relative to the average salinity at a certain location varies between 1 and 11% in the Western Scheldt and 14 to 33% at Liefkenshoek and Oosterweel in the Lower Sea Scheldt. At Hemiksem and Driegoten the average salinity is lower than 1 psu. Therefore, a very small difference in salinity results in a very big relative RMSE.

The salinity range calculated in both runs is presented in Table 55. The difference in salinity range between runs Scaldis_028_2 and Scaldis_039_2 varies from 0.1 to 1.5 psu.

Table 54. Comparison of salinity in Scaldis_028_2 and Scaldis_039_2

Station	Average salinity (psu)	Scaldis_028_2 vs Scaldis_039_2		
		RMSE (psu)	RMSE relative to average salinity	Max difference (psu)
Vlakte van de Raan	33.24	0.57	0.02	2.65
Overloop Hansweert	21.58	0.22	0.01	1.29
Baalhoek	16.71	0.29	0.02	0.86
Prosperpolder	11.28	0.91	0.08	2.01
Boei 84	9.58	1.08	0.11	2.25
Liefkenshoek	8.64	1.25	0.14	2.49
Oosterweel	4.16	1.38	0.33	2.88
Hemiksem	0.59	0.40	0.68	1.68
Driegoten	0.05	0.08	1.43	0.54

Table 55. Salinity range in runs Scaldis_028_2 and Scaldis_039_2

Scaldis_039_2			Scaldis_028_2			Difference in salinity range (psu)
Minimum salinity (psu)	Maximum salinity (psu)	Salinity range (psu)	Minimum salinity (psu)	Maximum salinity (psu)	Salinity range (psu)	
29.01	37.45	8.44	28.82	36.25	7.43	-1.01
18.38	25.39	7.01	18.10	25.43	7.33	0.32
10.01	21.61	11.60	9.53	21.58	12.05	0.45
4.90	17.02	12.13	3.67	17.34	13.66	1.54
1.98	15.21	13.23	0.69	14.95	14.26	1.02
0.95	14.59	13.64	0.19	14.31	14.12	0.48
0.00	12.20	12.20	0.00	11.42	11.42	-0.79
0.00	6.52	6.52	0.00	5.11	5.11	-1.41
0.00	0.81	0.81	0.00	0.72	0.72	-0.09

10 Model performance during storm

10.1. North sea and Scheldt estuary

10.1.1. Analysis of high and low waters and time series

The model performance is analyzed for the storm period of 5 and 6 December 2013 (Sinterklaas storm). Table 161 to Table 175 present the statistical parameters calculated for high and low waters and for the water level time series. Plots of the statistical parameters are shown in Figure 426 to Figure 448. Figure 458 to Figure 469 present the time series of the calculated and measured water levels at some stations.

The Sinterklaas storm is represented in the model at the correct moment, there is no time shift. The highest high water during the storm is represented well in the model at most stations. The RMSE of time series varies between 17 and 24 cm in the Western Scheldt, 23 to 27 cm in the Lower Sea Scheldt, 17 to 25 cm in the Upper Sea Scheldt and 14 to 27 cm in the Rupel basin.

In the Eastern Scheldt the RMSE of time series is 21 to 23 cm downstream the barrier. High water in the Eastern Scheldt upstream Roompot_buiten is overestimated in the model during the Sinterklaas storm because the barrier was closed in reality while in the model it stayed open. This results in big differences between the model results and measurements for the stations behind the barrier (for example, Figure 462).

The average bias of high waters is -2 to 11 cm in the North Sea and -7 to 1 cm in the Western Scheldt. Most high waters are slightly overestimated in the North Sea in the model and slightly underestimated in the Western Scheldt. The bias of high waters is -2 to 3 cm in the Lower Sea Scheldt and -8 to 0 cm in the Upper Sea Scheldt. The total RMSE of high waters is 13 cm in the North sea and Western Scheldt, 18 cm in the Lower Sea Scheldt and 15 cm in the Upper Sea Scheldt.

The bias of low waters is 19 to 30 cm in the North sea, 12 to 22 cm in the Western Scheldt, 12 to 19 cm in the Lower Sea Scheldt and -5 to 16 cm in the Upper Sea Scheldt. The total RMSE of low waters is 26 cm in the North sea and Western Scheldt, 23 cm in the Lower Sea Scheldt and 15 cm in the Upper Sea Scheldt.

10.1.2. Harmonic analysis

The calculated and measured harmonic components are presented in Table 176 to Table 223. Plots of the M2 amplitude and phase are shown in Figure 450 to Figure 456.

The calculated M2 amplitude is lower than the measurement at most stations. The difference is -10 to 0 cm in the North sea and Western Scheldt, -9 to -5 cm in the Lower Sea Scheldt and it is -7 to 3 cm in the Upper Sea Scheldt.

The difference in M2 phase is -2 to 2 degrees in the North sea, Western Scheldt and Lower Sea Scheldt and it is -5 to -2 degrees in the Upper Sea Scheldt.

10.2. Flood areas

During the Sinterklaasstorm water levels were measured in some Flood Control Areas (FCA) and Controlled Reduced Tide (CRT) systems in the Scheldt estuary. These data are compared with the model results to evaluate the model accuracy in the flood areas.

The history plots of the measured and modeled water levels are shown in Figure 470 to Figure 479. The flow enters in the flood areas in the model. The peak high water is represented accurately at Bergenmeersen CRT, Bergenmeersen Scheldt, Bergenmeersen CRT2 and Walem. It is overestimated in Polder van Lier and flood areas at Tielrode and Waasmunster. The timing of the highest high water during the storm is accurate at all the analysed locations.

The differences between the model results and measurements can be related to the differences between the modeled and measured bathymetry of the FCA's. For the analysis of water levels in flood areas it is very important that the measurement point and the analyzed point in the model have a similar depth. It was not always possible to find a model node with a similar depth close to the measurement location. This resulted in differences between the calculated and measured water levels.

11 Smoothing of the roughness field for sediment analysis

The roughness field shown in Figure 19 is smoothed in simulation Scaldis_039_BFS because it is important for the sediment transport calculations. An example of the changes in the roughness (for the area around Antwerp) is shown in Figure 163 and Figure 164.

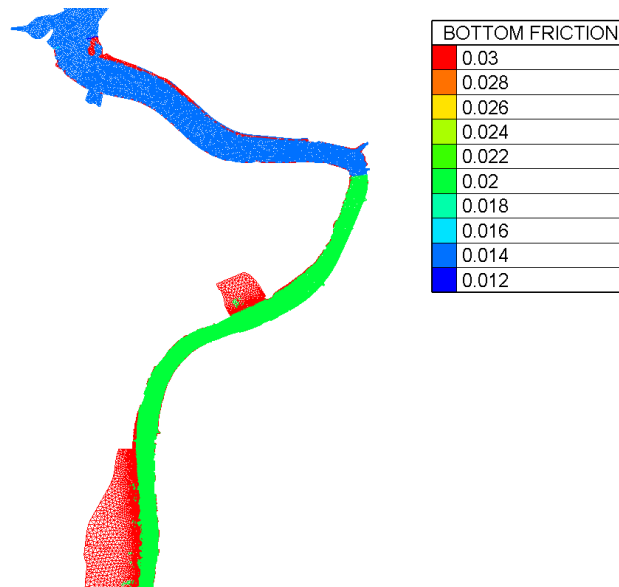


Figure 163 - Roughness field near Antwerp in Scaldis_039_0 (Manning $m^{-1/3}s$)

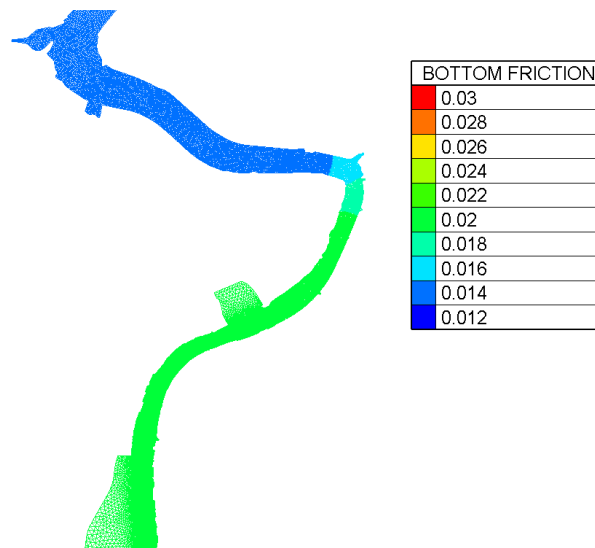


Figure 164 - Roughness field near Antwerp in Scaldis_039_BFS (Manning $m^{-1/3}s$)

This adaptation of the bed roughness did not result in big changes in the model results. The M2 amplitude calculated in runs Scaldis_039_0 and Scaldis_039_BFS is presented in Figure 165 to Figure 168. The differences between two runs are very small. The M2 amplitude between Temse and Sint Amands improved slightly in Scaldis_039_BFS.

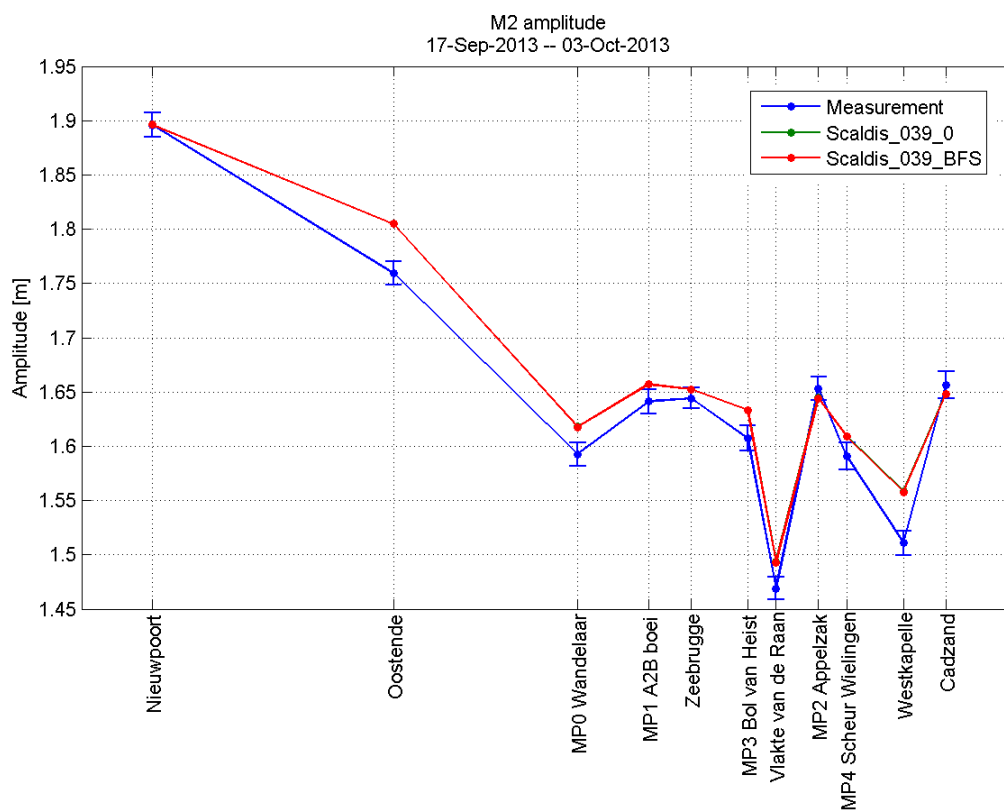


Figure 165 - M2 amplitude in the North sea in runs Scaldis_039_0 and Scaldis_039_BFS

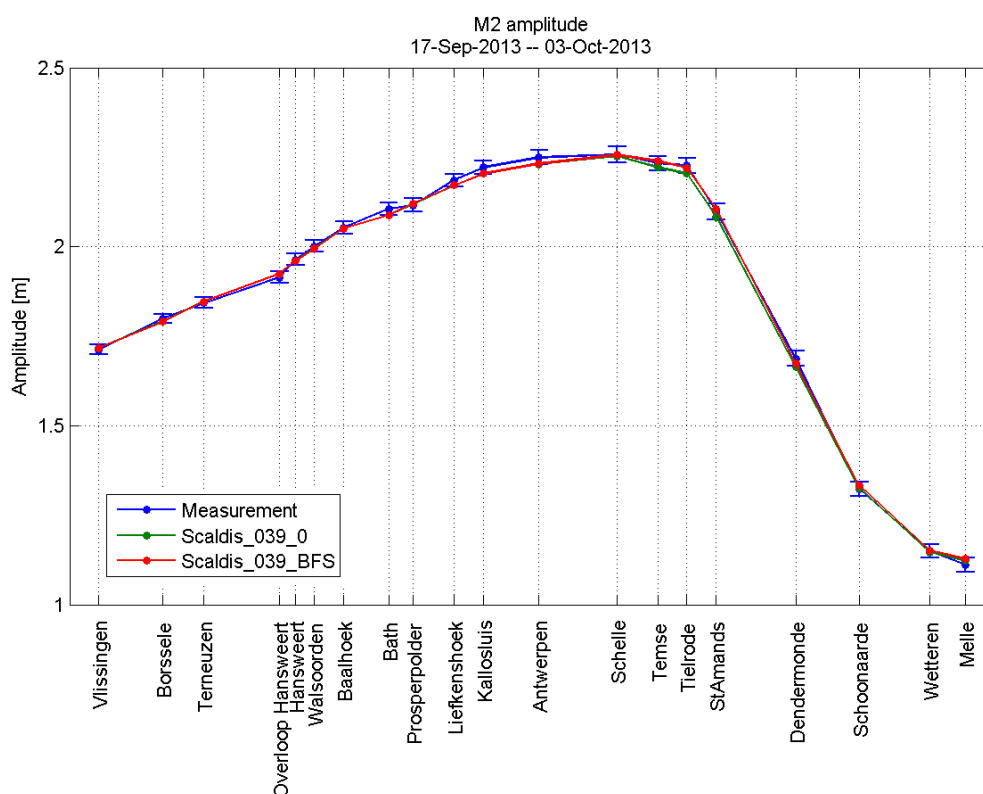


Figure 166 - M2 amplitude in the Western Scheldt and Sea Scheldt in runs Scaldis_039_0 and Scaldis_039_BFS

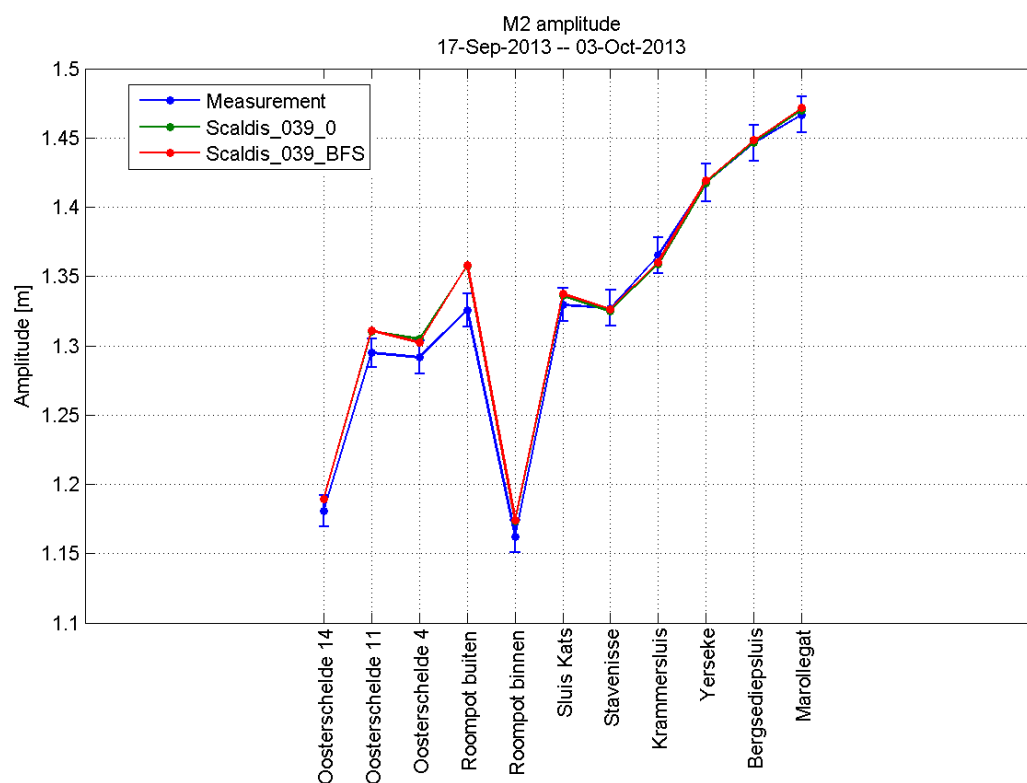


Figure 167 - M2 amplitude in the Eastern Scheldt in runs Scaldis_039_0 and Scaldis_039_BFS

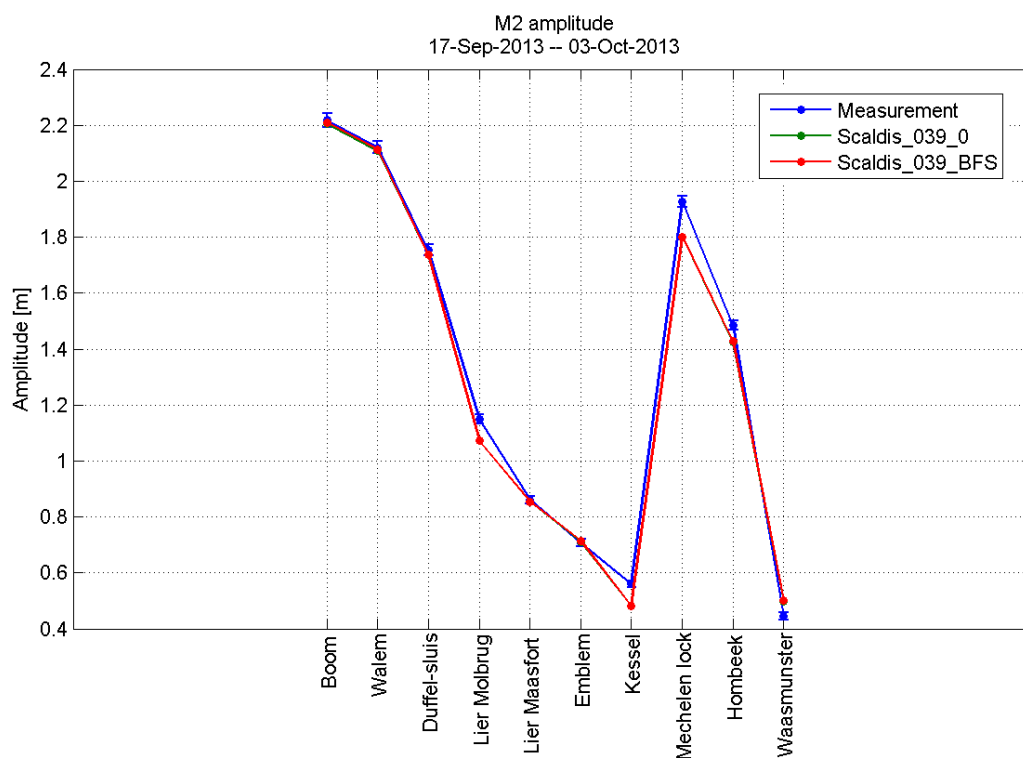


Figure 168 - M2 amplitude in the Rupel basin and Durme in runs Scaldis_039_0 and Scaldis_039_BFS

12 Model validation

For verification purposes, an independent set of ADCP measurements was used for the model validation (see Table 3). The plots of the time series of the measured and modeled velocities are shown in Figure 480 to Figure 496. The statistical parameters are presented in Table 226.

The model performance during the validation period is comparable with the performance during the calibration. The RMSE of velocity magnitude is smaller than 20 cm/s for most transects; the RMSE of velocity direction is 20 to 60 degrees (it worsens in the locations with a low velocity magnitude).

13 Tracer calculations for dispersion coefficients

13.1. Introduction

For the FHR project 13_131 Integrated Plan Upper Sea Scheldt the partners IMDC, UA, INBO and WL work together and share data to use as input for different models. For the 1D ecosystems model of UA, Flanders Hydraulics delivers tracer calculations with their 3D Scaldis model to calibrate dispersion coefficients in the 1D ecosystems model.

Special tracer calculations are ran with the Scaldis model of Flanders Hydraulics including 19 passive tracers. These tracers will enable the calibration of the dispersion coefficients of the 1D ecosystem model to predict salinity (as a conservative tracer in the 1D model) values or a salinity distribution in the Scheldt estuary. These predictions are done for specific scenarios and will deliver an initial salinity gradient for the Scaldis model in which these scenarios will be simulated.

In the 1D ecosystems model of UA the volumetric transport consists of a unidirectional advective component and a diffusive/dispersive component, and is based on equation (3.16) in *Soetaert and Herman (2009)*:

$$\frac{\delta C}{\delta t} = -\frac{1}{A} \cdot \frac{\delta(Q \cdot C)}{\delta x} + \frac{1}{A} \cdot (A \cdot E \frac{\delta C}{\delta x})$$

with C the tracer concentration, A the surface area of the box interfaces, Q the discharge, and E a diffusion coefficient.

If this formula is discretized for a series of boxes, and we assume that

$$V_i = A_i \cdot x_i$$

the formula becomes:

$$\frac{dC_i}{dt} = -\frac{\Delta_i(Q \cdot C)}{\Delta V_i} + \frac{(A_i \cdot E \frac{\Delta C_i}{\Delta x_i})}{V_i}$$

Following this formula the dispersion (second) term can be calibrated using a set of box/interface-specific dispersion coefficients D_i with:

$$D_i = \frac{E \cdot A_i}{\Delta x_i}$$

This approach allows a good fine-tuning of the model, but requires a substantial computational effort and (passive tracer) data to calibrate. These tracer data will be provided by Flanders Hydraulics as part of their 3D model output and how this is done is subject of this memo. The advective part of the mass fluxes is modelled as the product of a discharge and concentration value.

13.2. Deliverables

Data from the 3D Scaldis model to the 1D ecosystems model:

1. For every hour the tracer concentration, water volume and water surface are calculated in every polygon.
2. Bathymetric info per polygon: the volume of every polygon in the Scaldis model is given in function of the water level starting from -60 m TAW to 10 m TAW with a 1 meter interval.
3. A tide average (over a neap spring tidal cycle) water level in every polygon.

13.3. Approach

Every box in the 1D model (see Figure 169 and Figure 170) is represented by a polygon. Data is extracted from the Scaldis model based on these polygons.

Telemac is coded to use up to 20 tracers. One tracer is already in use as an active tracer to represent salinity. 19 tracers are left to use for determining dispersion coefficients for the 1D ecosystems model.

In Matlab the polygons are imported and initial conditions for these 19 tracers are made to create an initial selafin file including the bathymetry (BOTTOM), bottom friction coefficients (BOTTOM FRICTION), the initial salinity field (SALINITY) and then 19 maps with in each map one tracer in one polygon (TR2 – TR20). There are 86 polygons from which 73 are on the Scheldt itself (others include FCA/CRT areas, tributaries and the North Sea). The 19 tracers are distributed over 19 of these 73 polygons. An initial concentration of 1000 kg/m³ is given.

The simulation is started from a previous computation file. This means that the model does not need time for a startup but that hydrodynamics just continue where they stopped in the previous computation. On top of this, the tracers values are initialized. The model simulates 3 days and output is written to a results file with an interval of 1 hour.

Post processing is done again in Matlab. For every polygon, the elements of the mesh that lie within it are determined. Based on every element, the volume, surface and tracer concentration is calculated and integrated over the entire polygon and this for every polygon and for every time step.

For the bathymetric info, a fictitious water surface was imposed on the model, starting from -60 m TAW to 10 m TAW with a 1 meter interval. For every polygon the volume and water surface area was calculated.

For the spring-neap tidal cycle run of the calibrated Scaldis model for every time step (= 10 minutes) per polygon the average free water surface height was calculated. These values were averaged per polygon for the entire spring-neap tidal cycle and give then the tide average water level in each polygon.

All these steps are described in more detail in the next sections.

13.4. Polygons

The polygons start at the boundary Vlissingen-Breskens. The length along the estuary axis is 5 km gradually refined upstream to 1,5 km from the Dutch-Belgian border. The numbering is shown in Figure 169 and Figure 170. The polygons are numbered from downstream (1) to upstream (75) and then the CRT areas and tributaries Durme and Rupel are given a number from upstream to downstream.

These polygons don't include the FCA areas, only the areas with CRT or that will be CRT by 2050.

The CRT areas included are:

76 = Ham

77 = Bergenmeersen

78 = Vlassenbroek 1

80 = Lippenbroek

81 = De Bunt

83 = Tielrodebroek

84 = Schousselbroek

86 = KBR

Number 79, Uiterdijk, is now FCA but will be de-embanked by 2050.

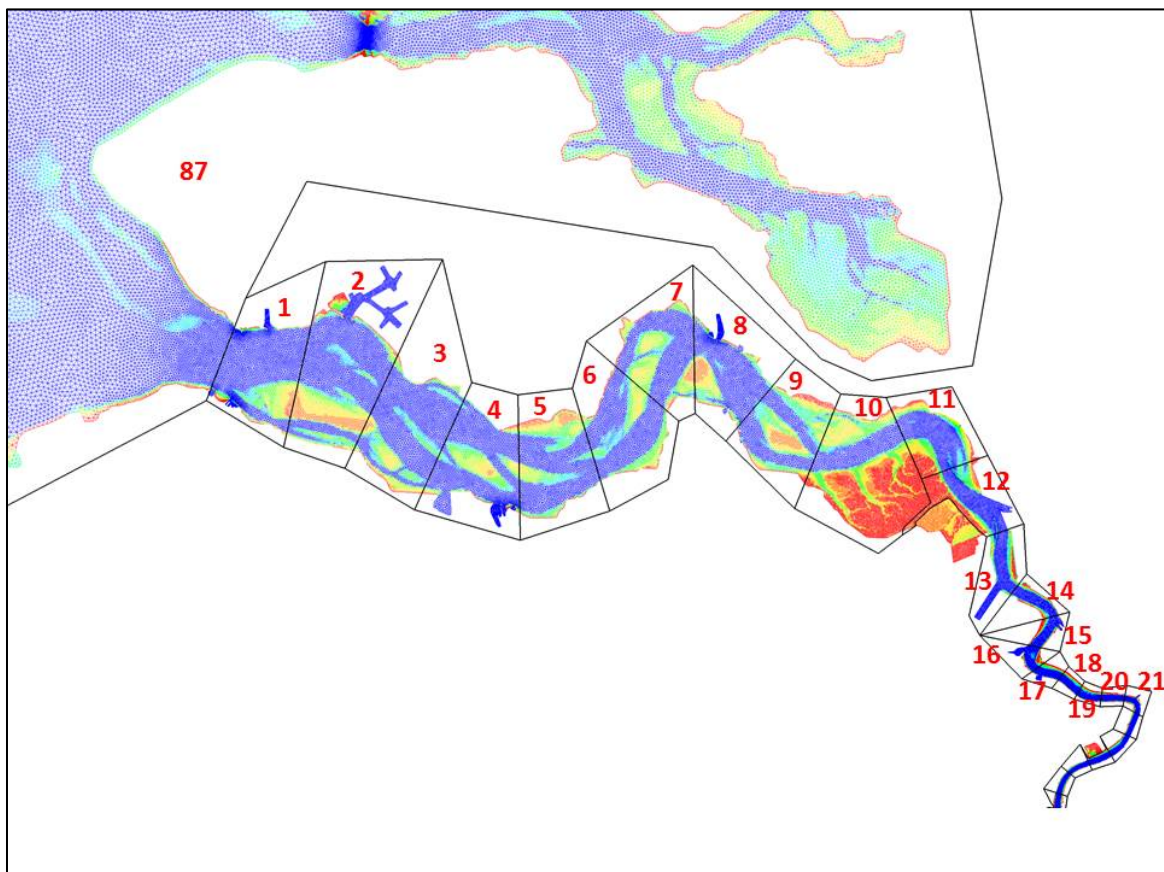


Figure 169 - Polygon numbering in Western Scheldt

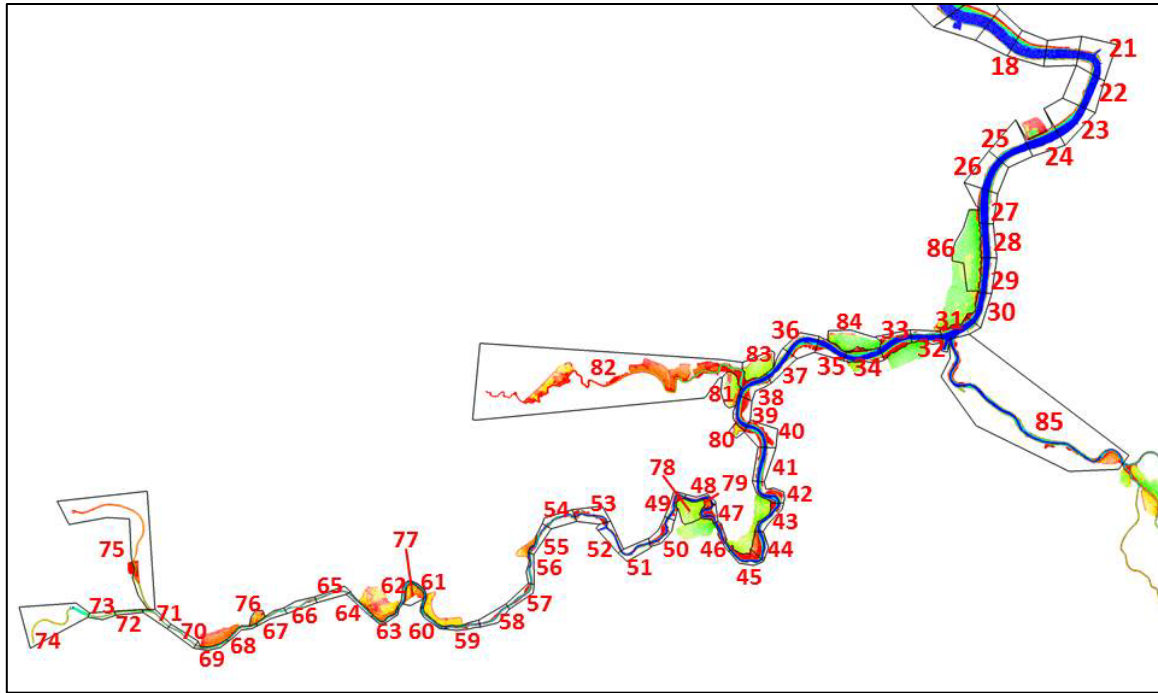


Figure 170 - Polygon numbering in Sea Scheldt.

13.5. Find mesh elements in polygon

The polygons are read by Matlab into a structured array P. A loop over all mesh nodes is launched and the presence of a certain node inside a polygon is checked with the function 'inpolygon'. As soon as a point is assigned to a certain polygon, the loop over all polygons is ended and the next node is assigned.

When all nodes are assigned to a certain polygon, the triangular elements, containing these nodes, are gathered for each polygon. In a next step, for each element or triangle the center of mass is calculated according to the following formula:

$$x = (x_1 + x_2 + x_3)/3$$

$$y = (y_1 + y_2 + y_3)/3$$

with x and y the coordinates of the center of mass and x_1, x_2, x_3 the x-coordinates and y_1, y_2, y_3 the y coordinates of nodes defining a certain element or triangle of the mesh.

A mesh element/ triangle is assigned to a polygon if it's center of mass lies inside this polygon!

So for all centers of mass their location inside the polygons is checked again with the matlab function 'inpolygon'. With help of Figure 171 we give an example: the center node in Figure 171 is assigned to polygon A. But this node is part of some triangles (1 to 4). For these triangles the center of mass is calculated (= light grey lines inside the triangles). For triangles 1 and 4 the center of mass lies inside polygon A, so these triangles are assigned to polygon A. The other two triangles, 2 and 3, have their center of mass inside polygon B and are thus assigned to polygon B. The boundary line separating the elements inside polygon A and B will not be a straight line (like the red line in Figure 171 defining the polygons), but will follow the triangles being part of the polygon.

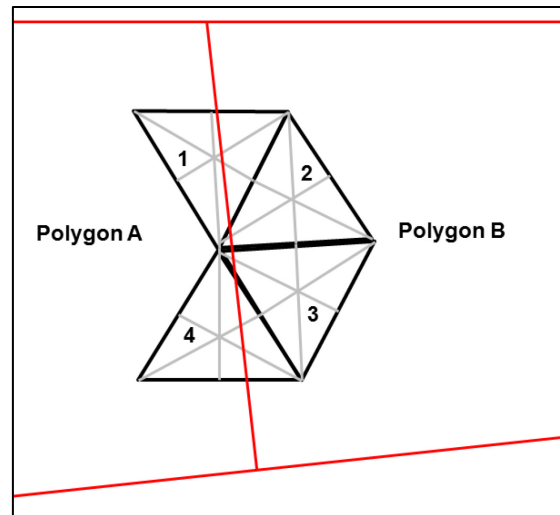


Figure 171 - assigning mesh elements to polygons based on the location of their center of mass

13.6. Assigning a tracer concentration

A tracer concentration of 1000 kg/m³ is assigned to all nodes of the elements belonging to polygons 3, 7, 11, 15, 19, 23, 27, 31, 35, 39, 43, 47, 51, 55, 59, 63, 67, 71, 75 (See Figure 172)

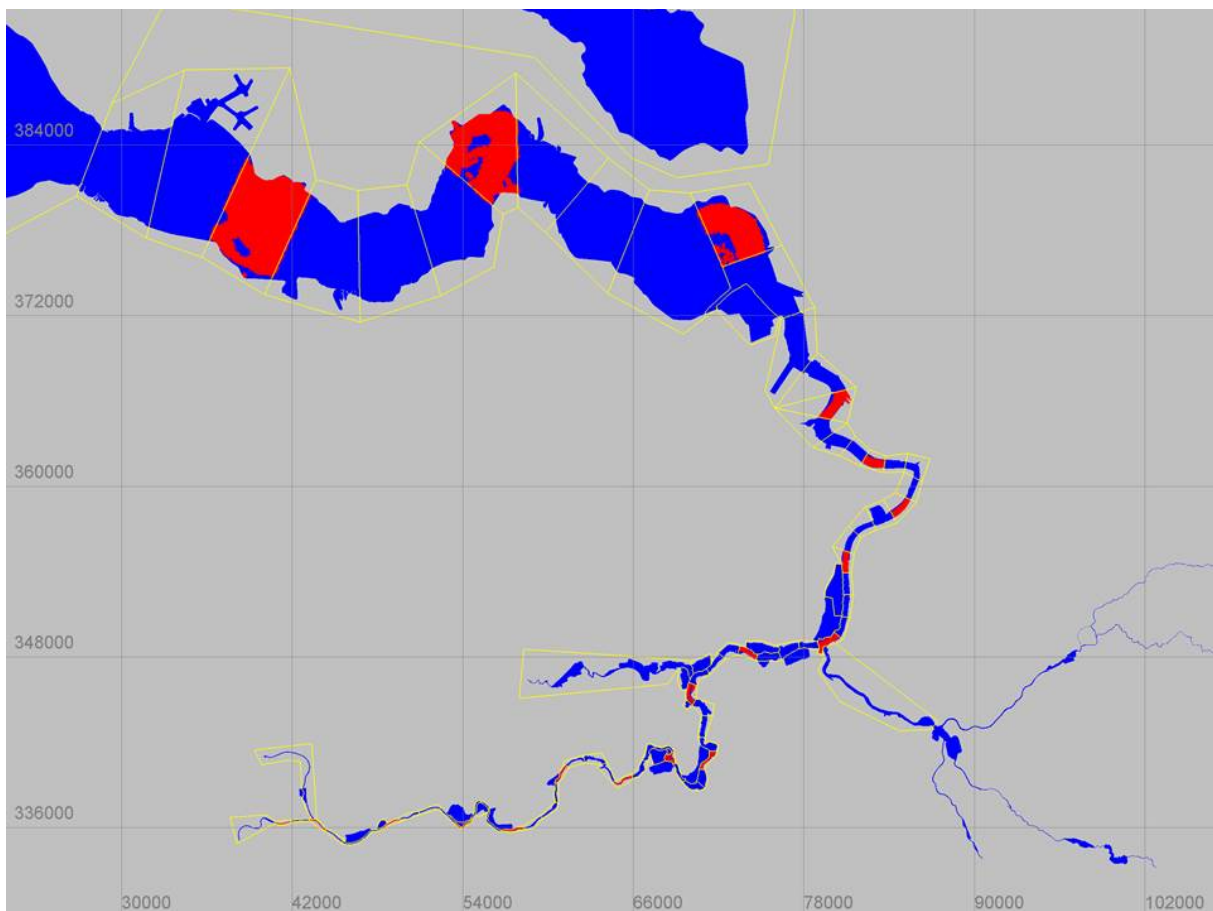


Figure 172 – Polygons representing the Scheldt estuary and some filled with a passive tracer (red color)

The tracer in polygon 3 is called TR2 (tracer 2, salinity is nr.1), the tracer in polygon 7 is called TR3, the tracer in polygon 15 is called TR4 and so on.

13.7. Surface area of triangles in polygon

In the previous section we ended with a structured array that will give us all triangles per polygon. The coordinates of their nodes are known and based on this information we can calculate the surface area of all triangles in a polygon separately using Heron's formula (for irregular triangles). For the total surface area per polygon we just have to summate over all triangles present in that polygon.

Heron's formula: (see Figure 173)

$$S = \frac{A + B + C}{2}$$

$$\text{Surface area} = \sqrt{S * (S - A) * (S - B) * (S - C)}$$

with A, B and C the lengths of the sides of the triangle according to Figure 173.

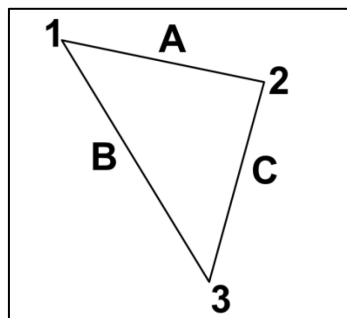


Figure 173 - Calculating surface area of an irregular triangle using Heron's formula

If we want to know the surface area of the water, we select only those nodes in a polygon that have a minimum depth of 0,02 m. The surface area of elements with one or two dry nodes is estimated with 2/3 or 1/3 of the elements total surface area.

13.8. Volume within polygon

For the total volume inside a polygon under the free surface of the water we calculate again the volume under each triangle and summate all to get the total volume.

We first make some assumptions:

- the free surface over a polygon is not necessarily flat or equal. Even within one triangle the different nodes can have a different value for the free surface.
- for elements near or on the shoreline/boundary: an element or triangle is taken into account if at least one of its three nodes has a water depth of 0,02 m.
- The bottom or bathymetry is taken into account for the volume calculation. So also on the bottom part of the prism under the triangle we take into account three different elevations for the three nodes.

The volume under each triangle is calculated in three steps. According to Figure 174 the irregular prism is divided into two irregular shapes on the top and bottom and one regular prism in the middle.

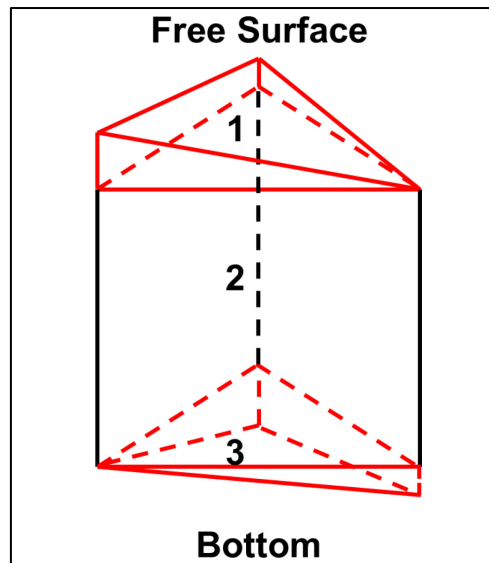


Figure 174 - Volume of irregular prism under surface triangle

1. **Volume of the regular prism.** The volume of the regular prism is calculated based on the surface area of the triangle times the height. The height is equal to the smallest free surface elevation of one of the three nodes minus the highest bottom elevation of one of the three nodes.
2. **Volume of the upper irregular shape.** If the difference in surface elevation between the three nodes is less than 0.01 m, this volume is neglected. If it is not, this volume is cut into two volumes, i.e. two irregular pyramids with a triangular ground surface (Figure 175).

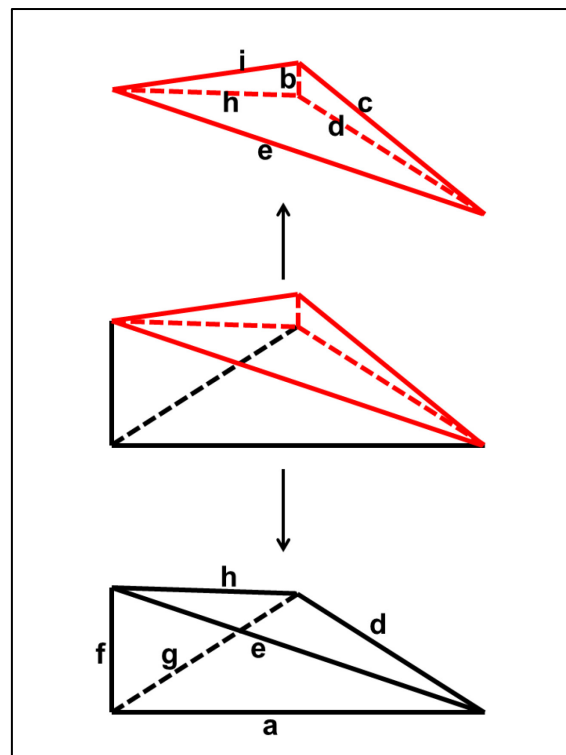


Figure 175 - Volume calculation of irregular shape under a triangle.

The volume of an irregular pyramid is given by the following formula:

$$Volume = \frac{\text{ground surface} * \text{height}}{3}$$

The volume of the lower pyramid (black lines) in Figure 175 is given by the ground surface (which is equal to the surface area of the triangle in the 2D mesh) times the height (= length f in Figure 175 and is equal to the difference between maximum and minimum surface elevations of the points of the triangle in the mesh) divided by three.

The calculation of the volume of the upper red irregular pyramid is more difficult as we need to calculate the ground surface, the height and the volume. This pyramid is enlarged in Figure 176 and the new height h is assigned. For the calculations of this volume we will work with the coordinates of the four points that determine this pyramid, i.e. A, B, C and D (Figure 176).

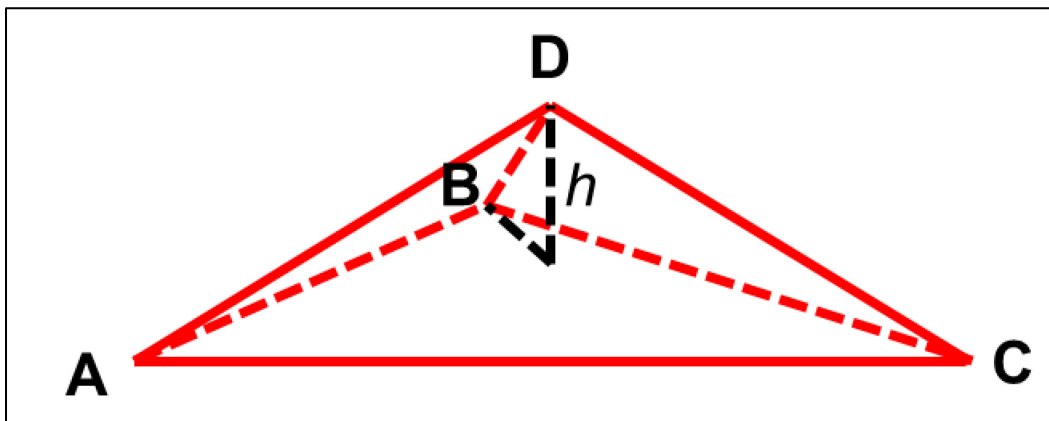


Figure 176 - Volume irregular triangular pyramid

The surface area of the ground triangle (ABC in Figure 176) can be calculated using Heron's formula, like explained in section 3.2. The height is calculated as the distance of point d to the plane determined by points A, B, C. A plane is also defined by two vectors, \overrightarrow{AB} and \overrightarrow{AC} . The formulas are given here below:

equation of a plane

$$\overrightarrow{AB} * \overrightarrow{AC} = ax + by + cz + d = 0$$

with

$$a = (y_b - y_a) * (z_c - z_a) - (z_b - z_a) * (y_c - y_a)$$

$$b = (z_b - z_a) * (x_c - x_a) - (x_b - x_a) * (z_c - z_a)$$

$$c = (x_b - x_a) * (y_c - y_a) - (y_b - y_a) * (x_c - x_a)$$

We can find d by filling in one point in the equation.

The distance (height h) from point D to the ground surface is given by the following formula:

$$h = \frac{ax + by + cz + d}{\sqrt{a^2 + b^2 + c^2}}$$

with x,y,z the coordinates of point D.

With the height h and the ground surface of the triangle ABC we can calculate the volume of this irregular pyramid with triangular ground surface.

3. **Volume of the lower irregular shape.** This volume is calculated analogue to the upper irregular shape. Instead of using the free surface levels, the bottom or bathymetry values are used.

The total volume under each triangle is the sum of the three steps above. The volume within a polygon is the summation of the volumes under all triangles inside this polygon.

13.9. Tracer concentration results

For every tracer the average concentrations in every polygon are calculated. Within a polygon only nodes with a minimum depth of 0,02 m are taken into account for the tracer concentration calculation.

The average tracer concentration per polygon is calculated based on the concentrations in the center of mass of every element weighted by the surface of every element.

A surface plot is made for every tracer. Its concentration in every polygon (in the figures only the polygons of the Scheldt river and not the tributaries or FCA/CRT areas) for 73 time steps of one hour is plotted. These 20 figures are given here below. The first one being the Salinity and the next ones are the other tracers (Tracers 2-20). Sometimes a part of the tracer got stuck in a part of the estuary and was not moved further up- or downstream by the tide. This can be seen in some of the figures.

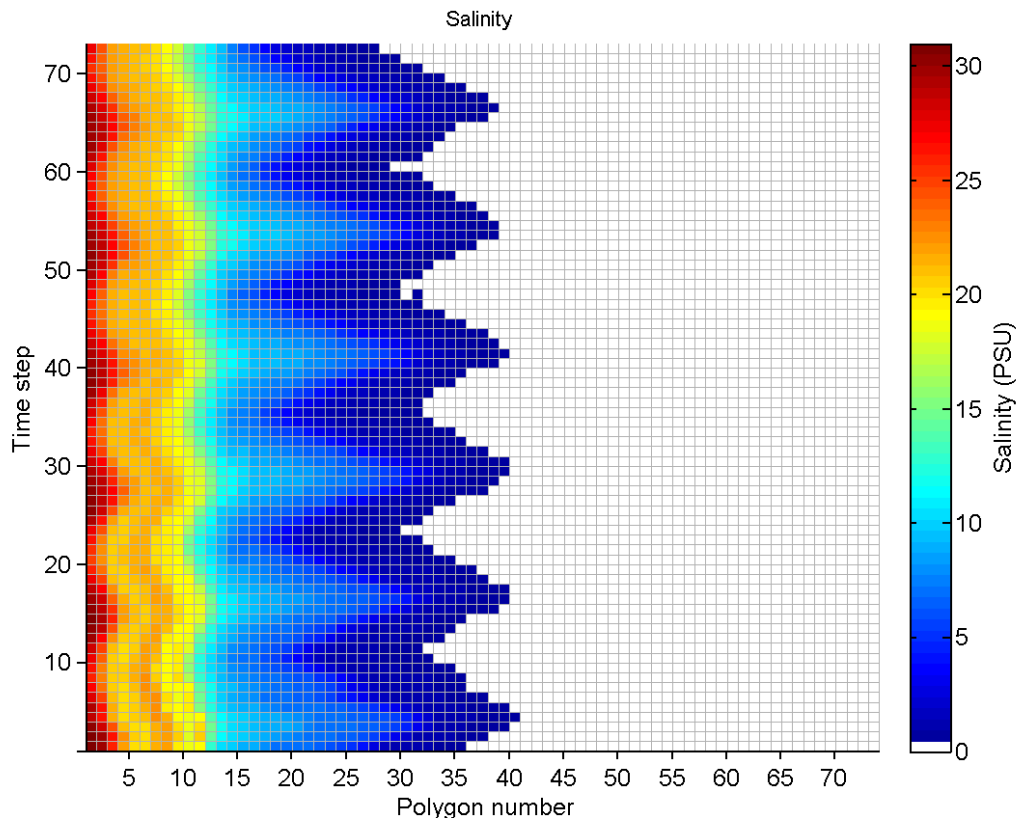


Figure 177 - Movement of average salinity concentrations in polygons over 73 time steps of one hour

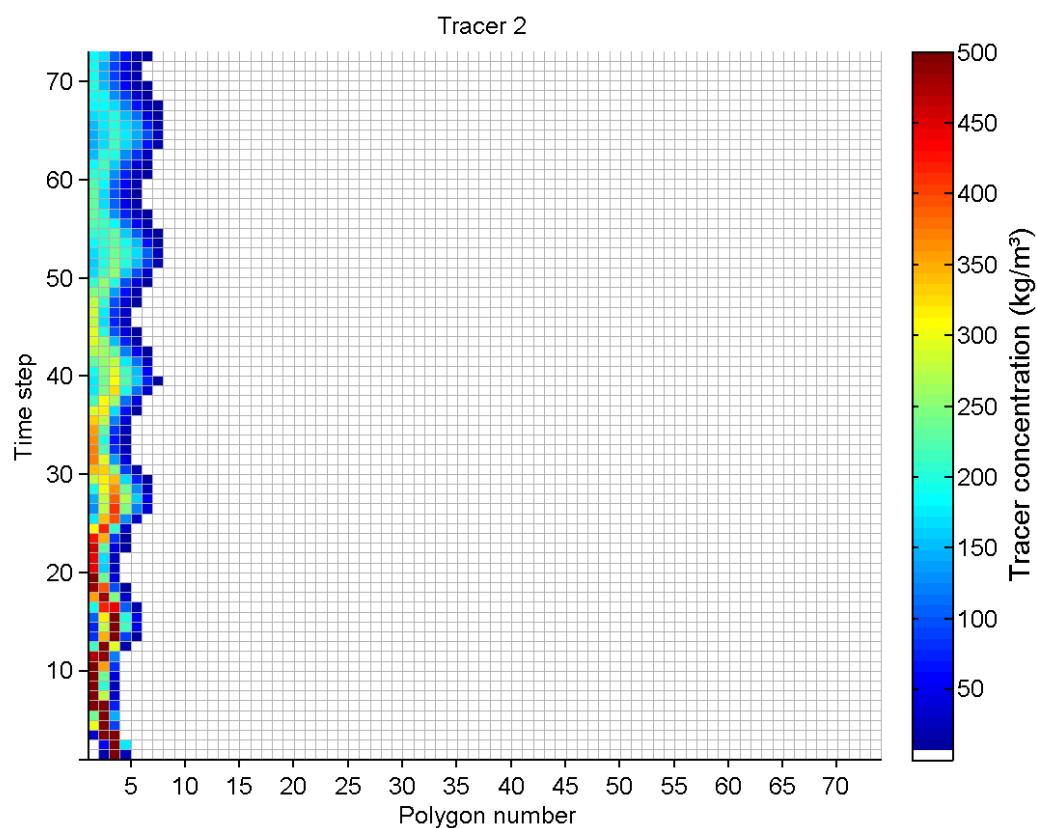


Figure 178 - Movement of tracer 2 concentrations in polygons over 73 time steps of one hour.

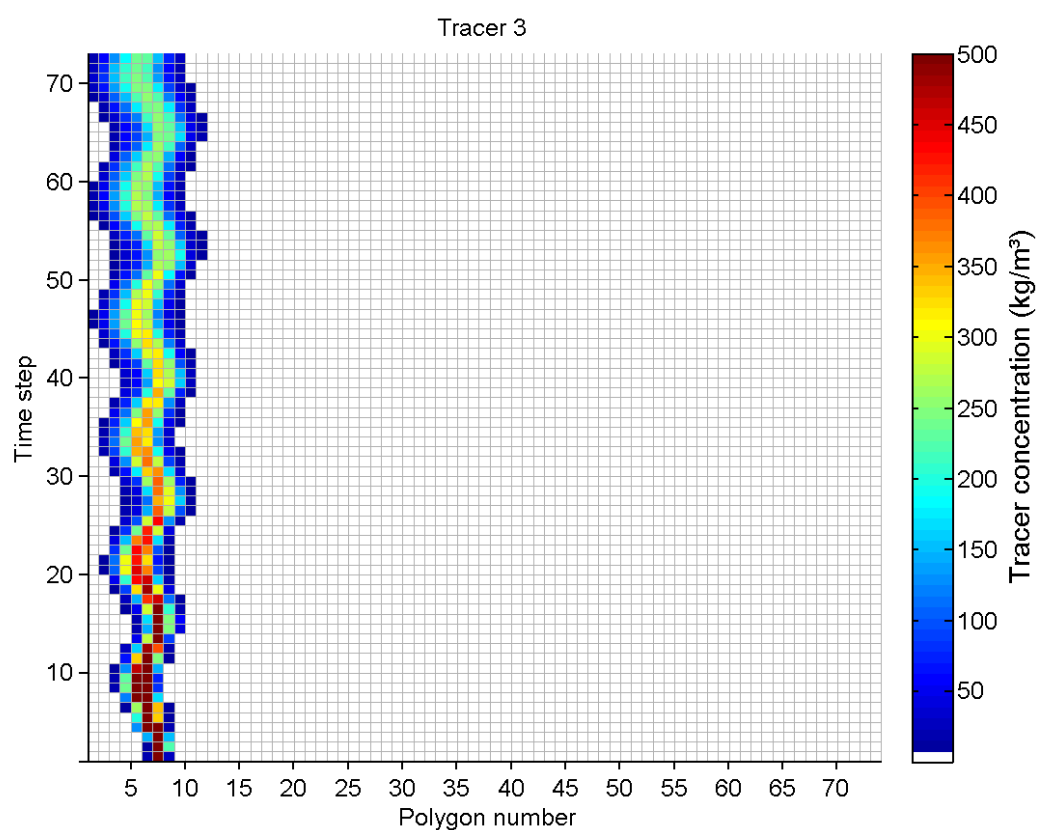


Figure 179 - Movement of tracer 3 concentrations in polygons over 73 time steps of one hour.

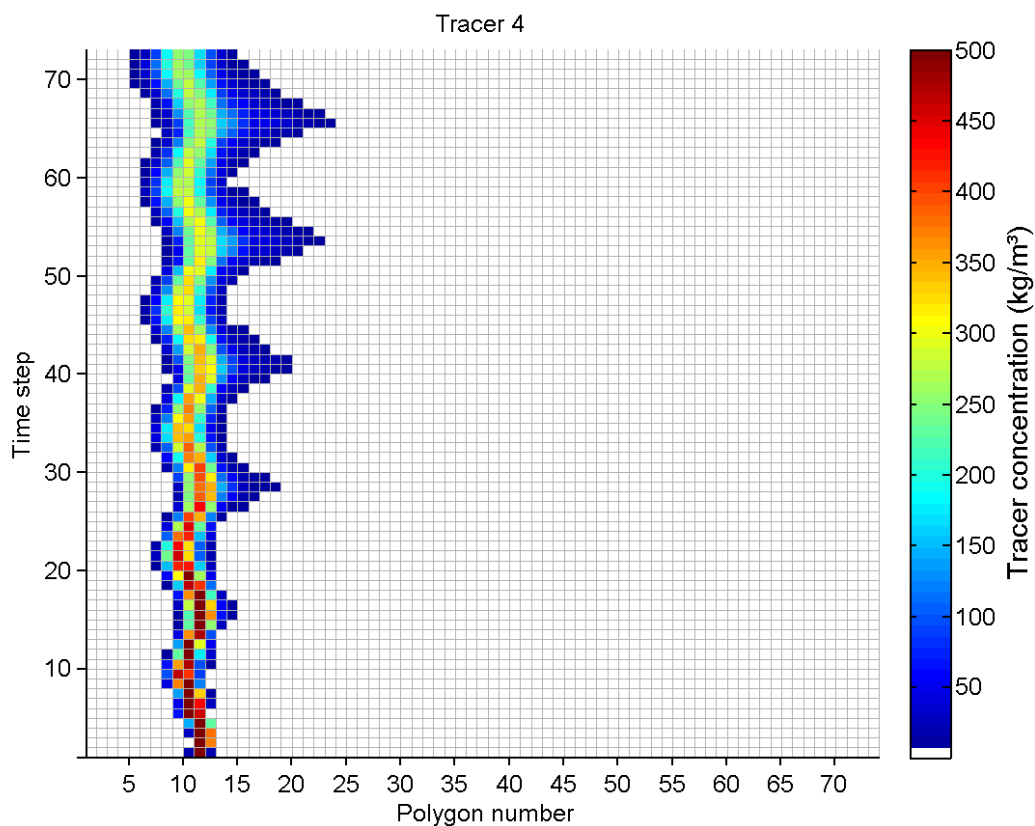


Figure 180 - Movement of tracer 4 concentrations in polygons over 73 time steps of one hour.

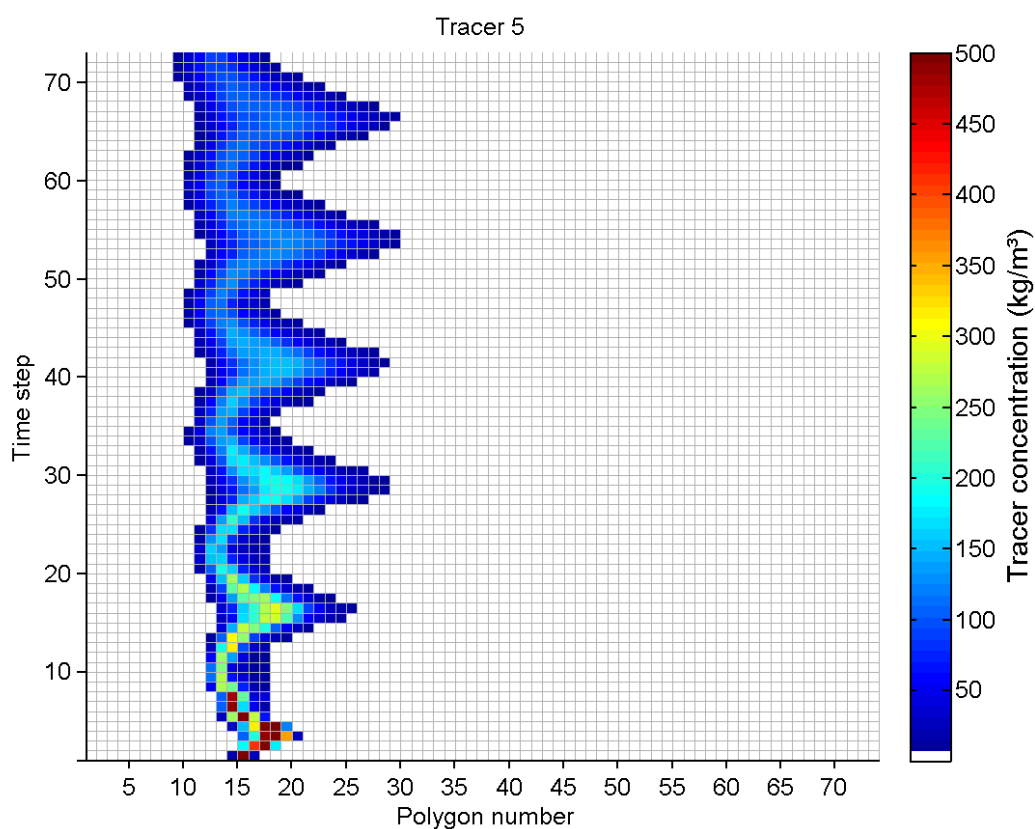


Figure 181 - Movement of tracer 5 concentrations in polygons over 73 time steps of one hour.

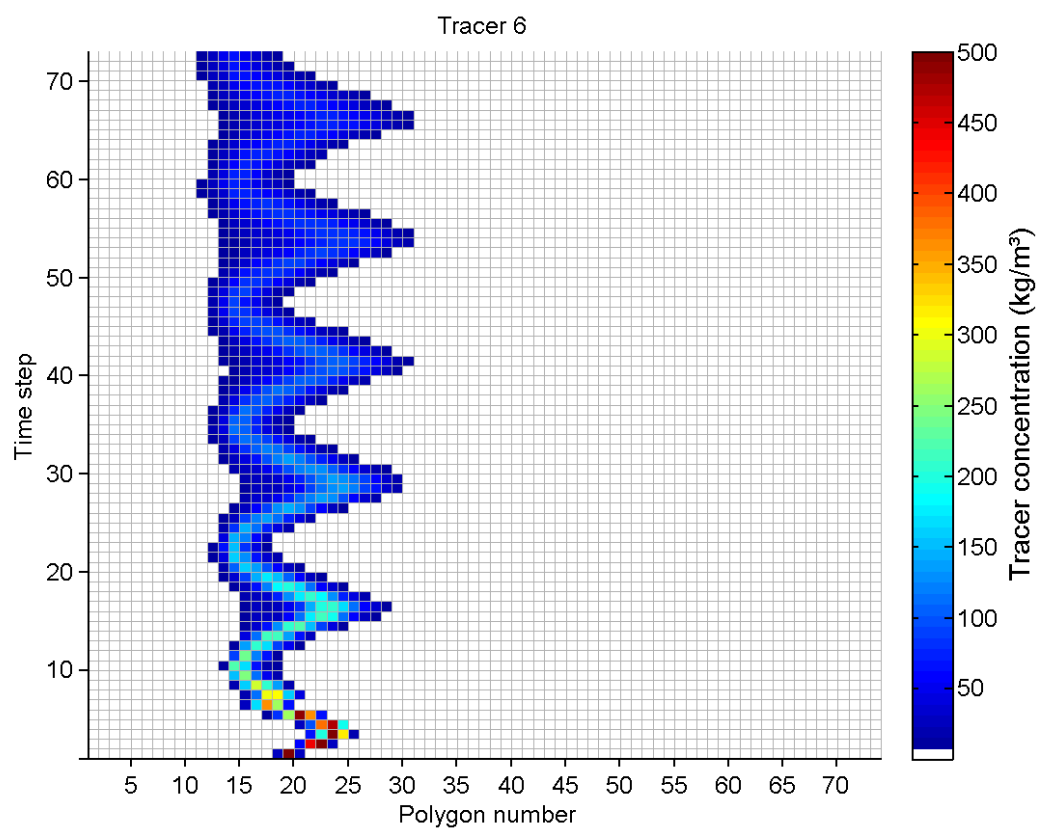


Figure 182 - Movement of tracer 6 concentrations in polygons over 73 time steps of one hour.

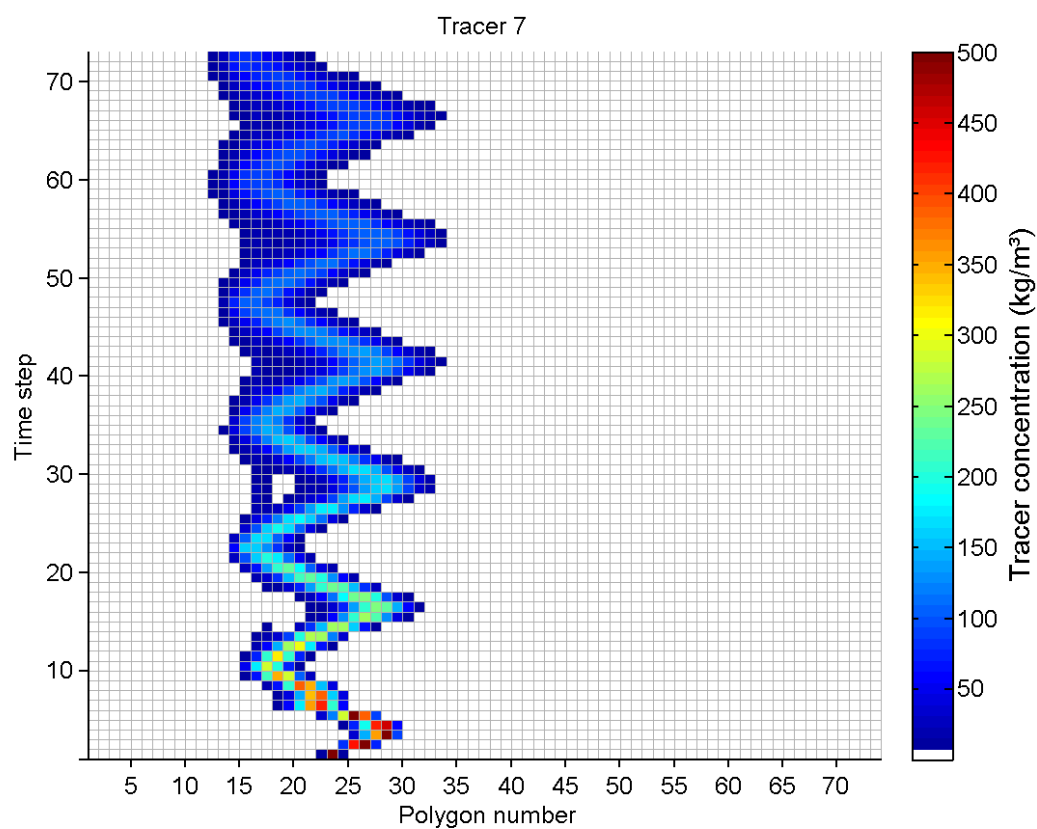


Figure 183 - Movement of tracer 7 concentrations in polygons over 73 time steps of one hour.

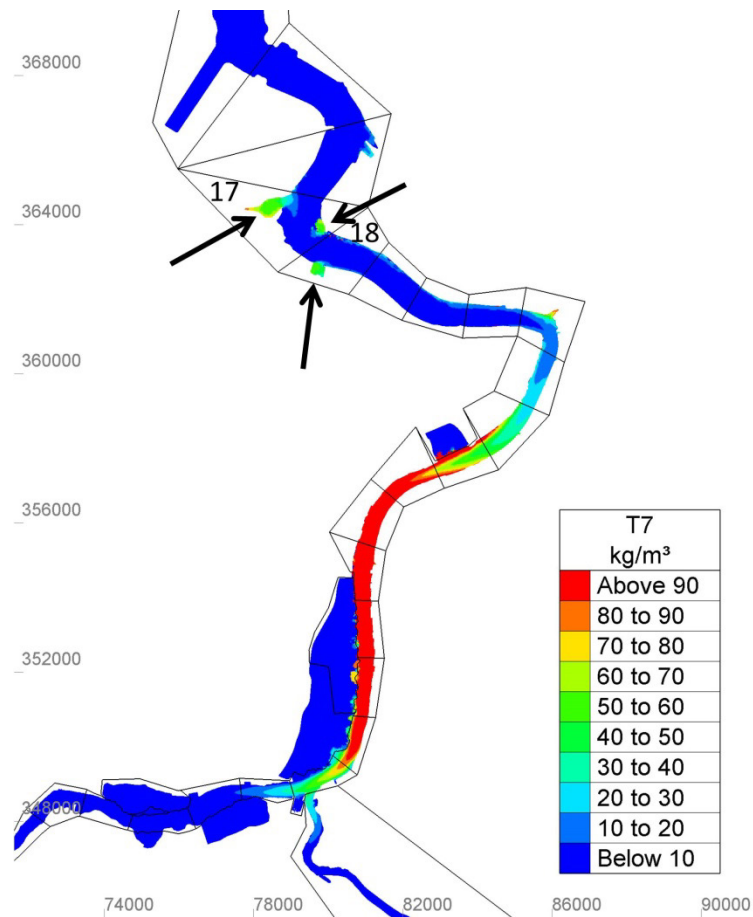


Figure 184 - tracer 7 remaining in some parts of the estuary

In Figure 183 it is noticed that at time step 27 and 28 tracer concentration is present. Figure 184 shows us the locations of where tracer 7 got left behind in the estuary compared to the bulk which is moving along with the tide. We can see that parts of tracer 7 got stuck at the sluices of Kallo and other small basins next to the estuary channel.

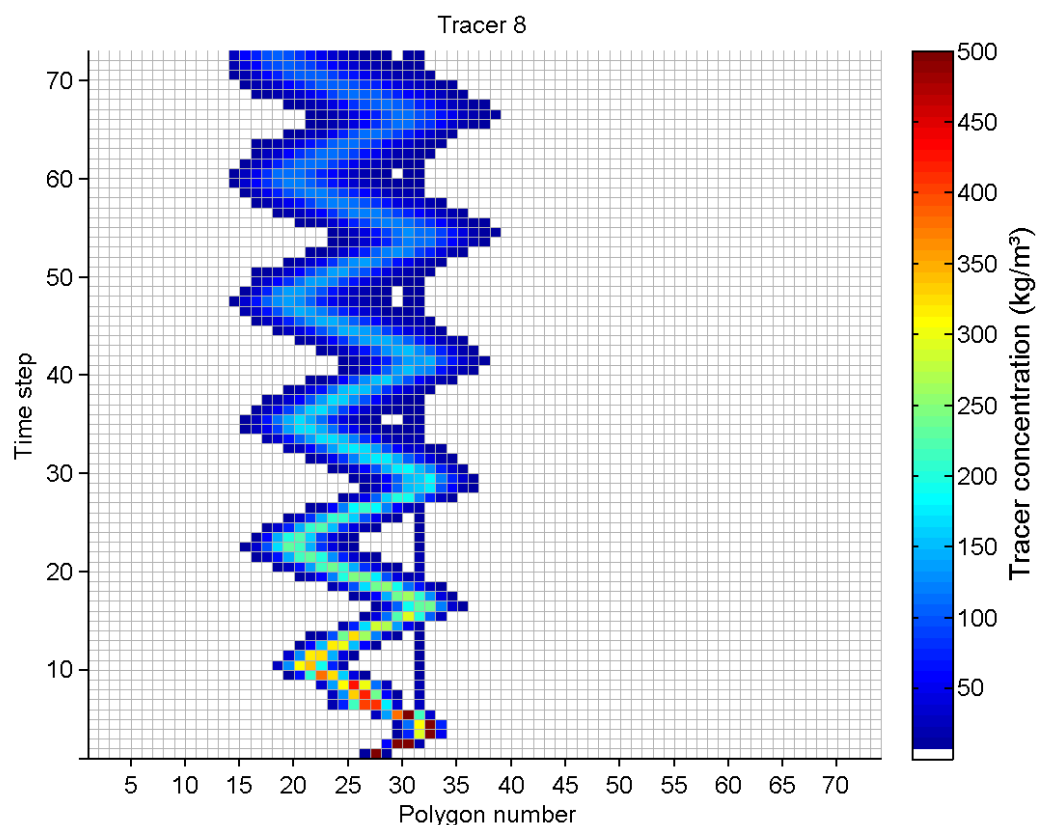


Figure 185 - Movement of tracer 8 concentrations in polygons over 73 time steps of one hour.

The tracer that is present in polygon 31 in time steps 6,7 and further got stuck on local marshes and in the small basin at the Wintam locks.

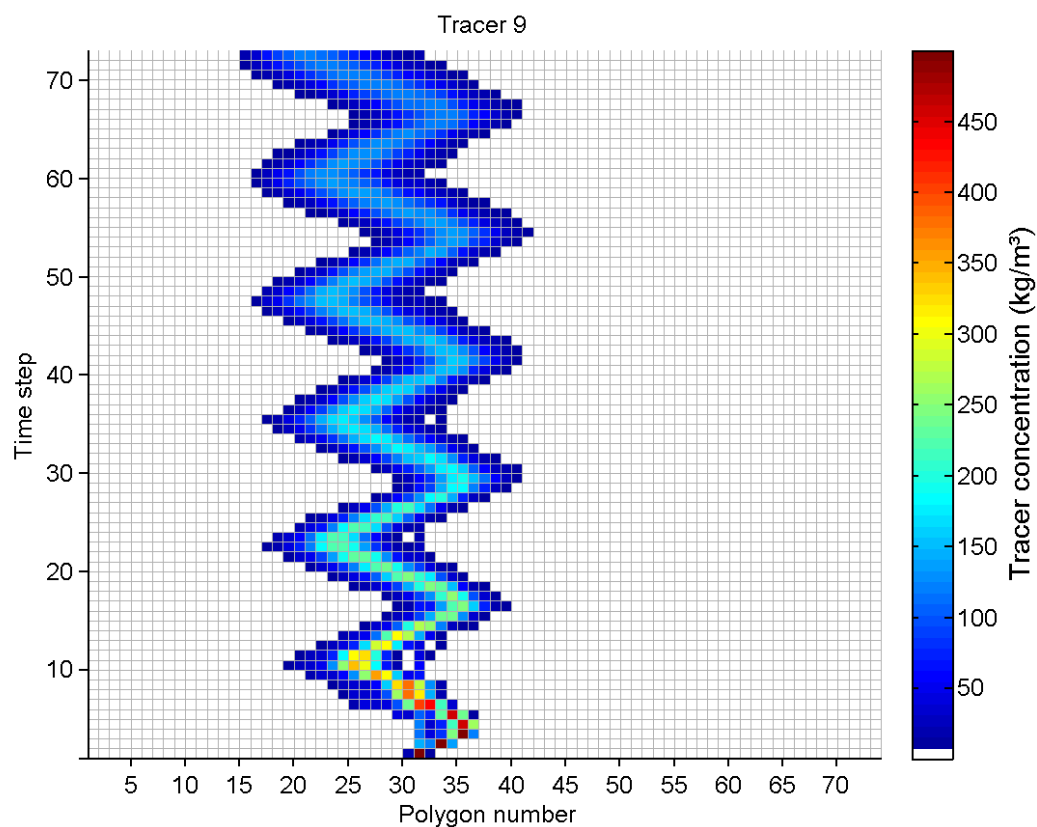


Figure 186 - Movement of tracer 9 concentrations in polygons over 73 time steps of one hour.

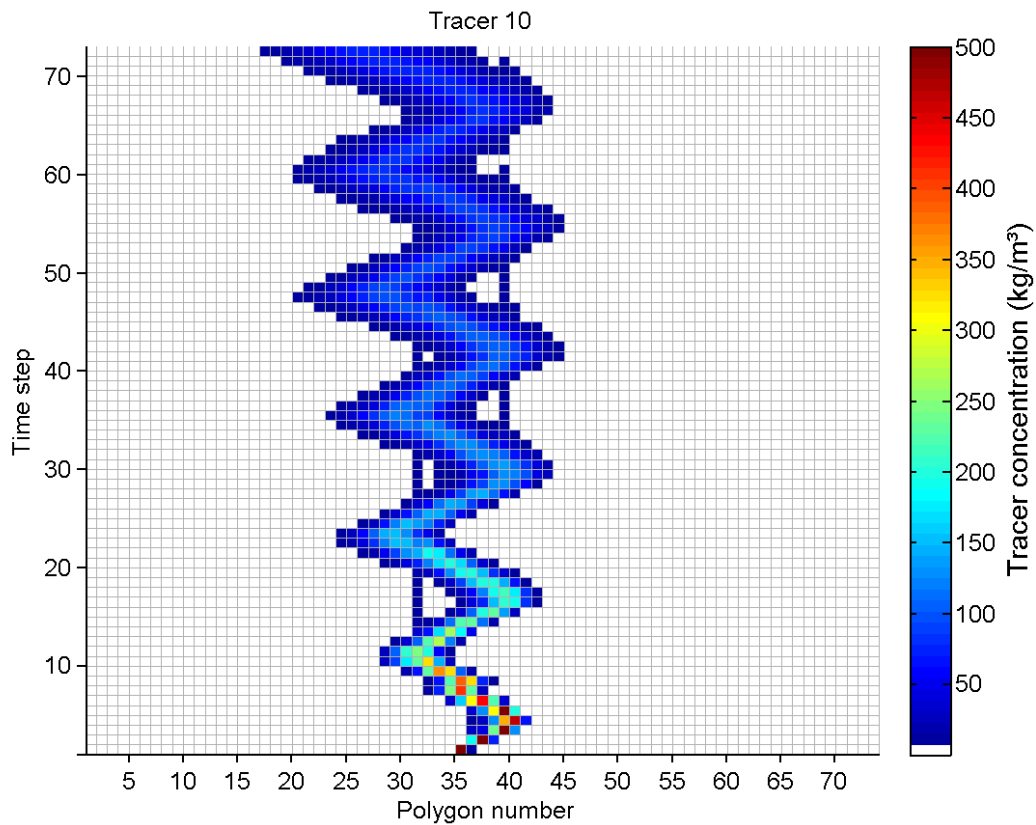


Figure 187 - Movement of tracer 10 concentrations in polygons over 73 time steps of one hour.

Tracer 10 remains like tracer 8 and 9 in the small basin at the Wintam lock (= polygon 31). The other artefact that can be seen in Figure 187 in polygon 39 is caused by tracer parts remaining at marsh areas.

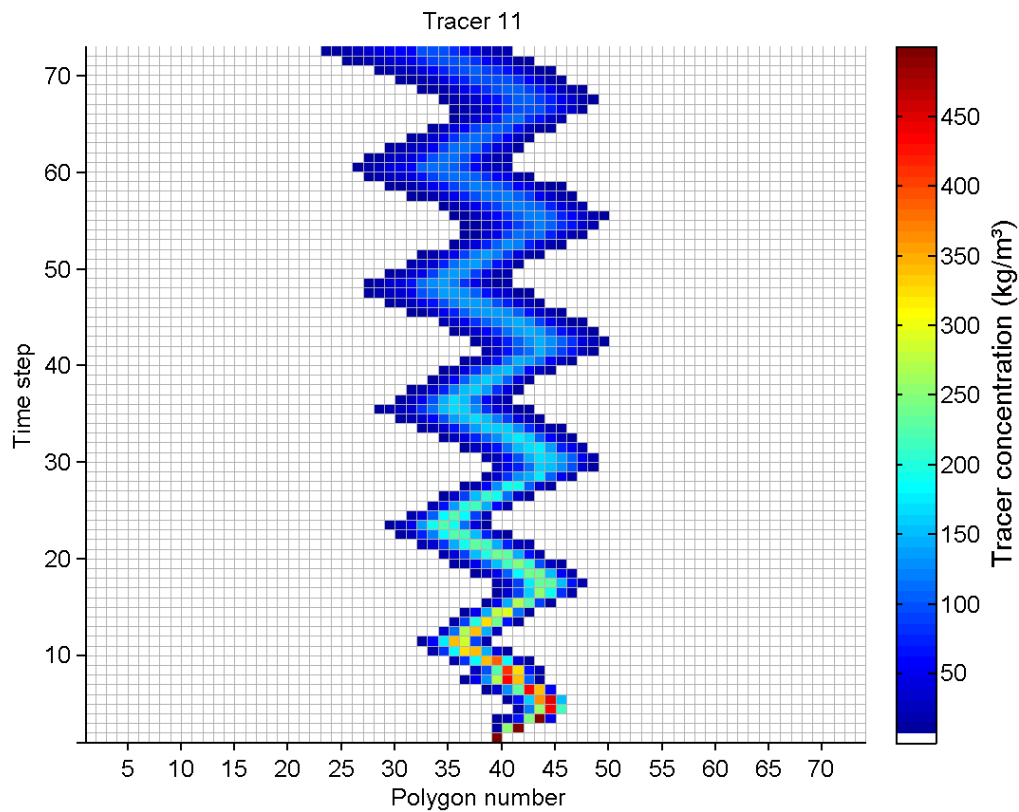


Figure 188 - Movement of tracer 11 concentrations in polygons over 73 time steps of one hour.

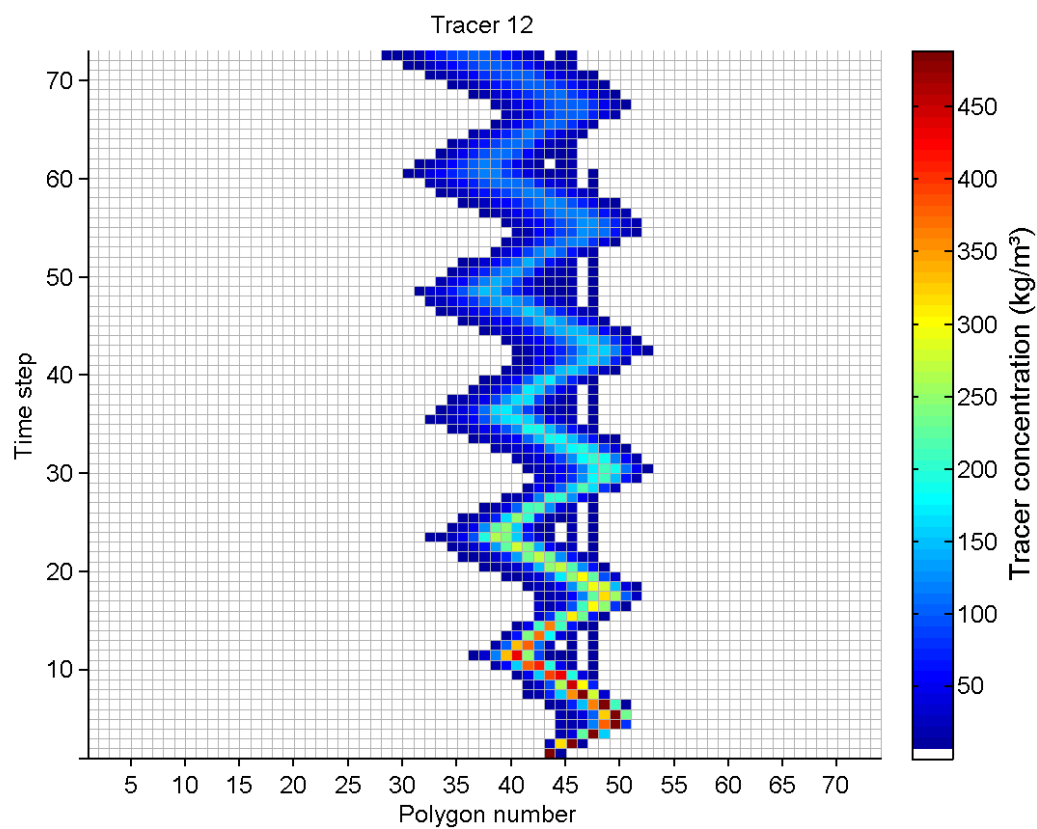


Figure 189 - Movement of tracer 12 concentrations in polygons over 73 time steps of one hour.

Tracer 12 left on marshes in polygon 45 and 47 explains the artefacts in Figure 189 and Figure 190.

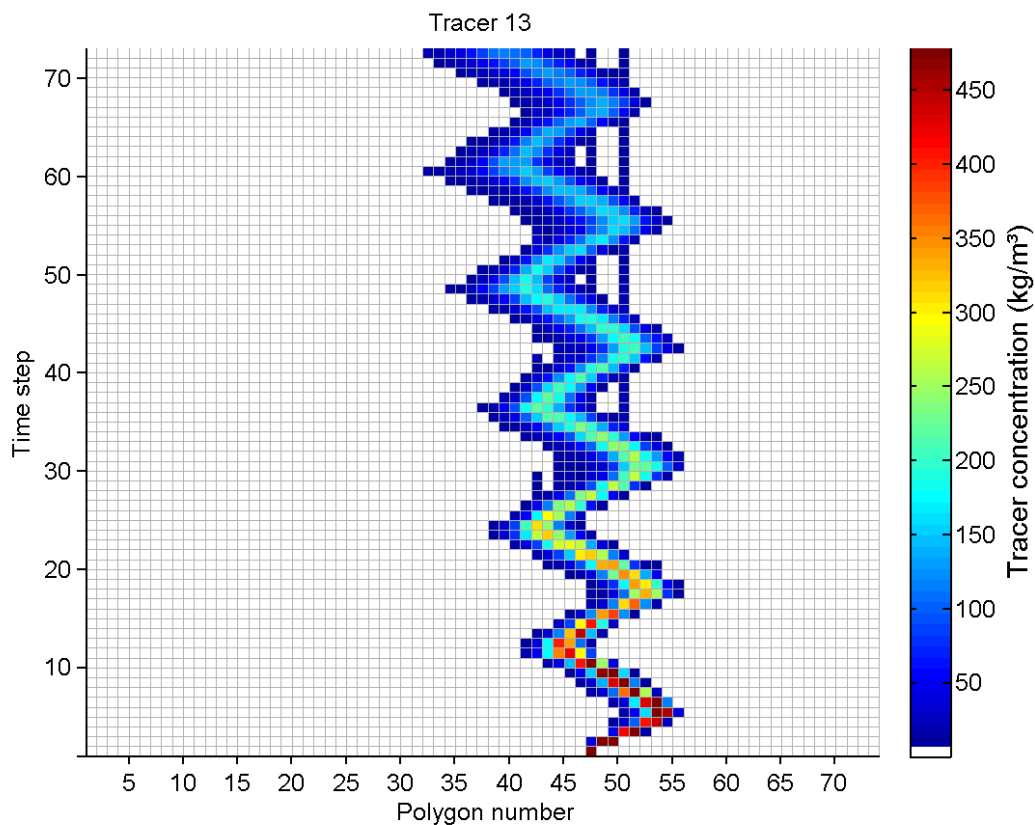


Figure 190 - Movement of tracer 13 concentrations in polygons over 73 time steps of one hour.

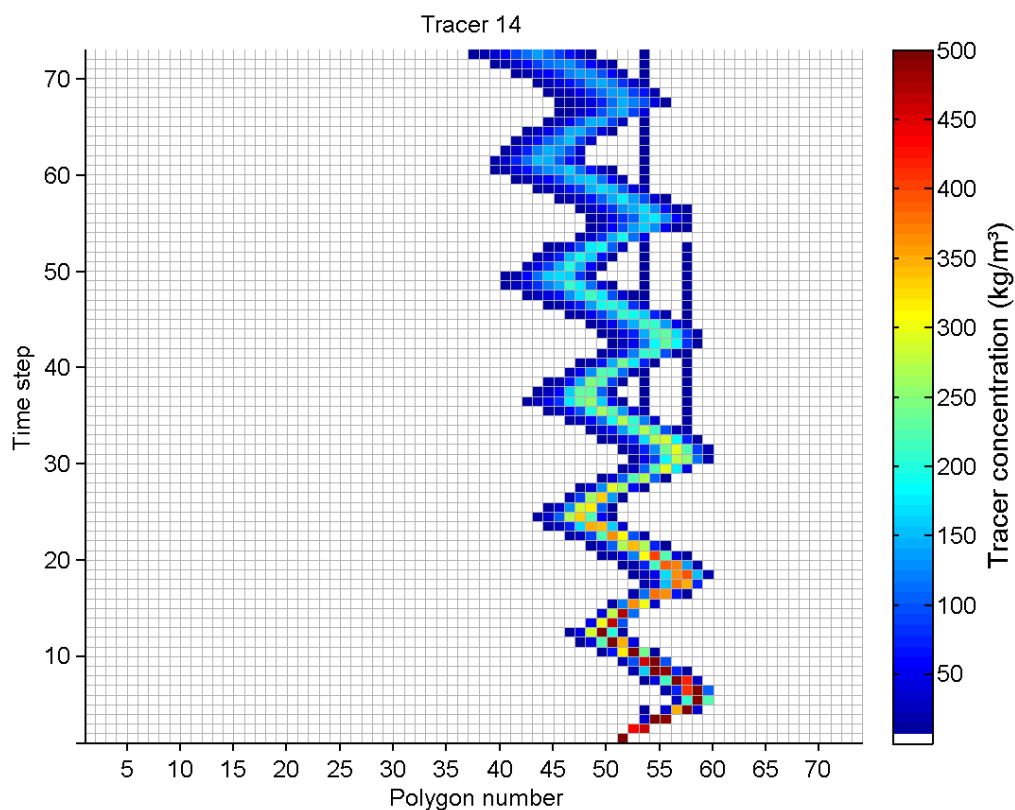


Figure 191 - Movement of tracer 14 concentrations in polygons over 73 time steps of one hour.

The artefacts in polygons 53 and 57 in Figure 191 can also be explained by tracer that is left behind on marshes.

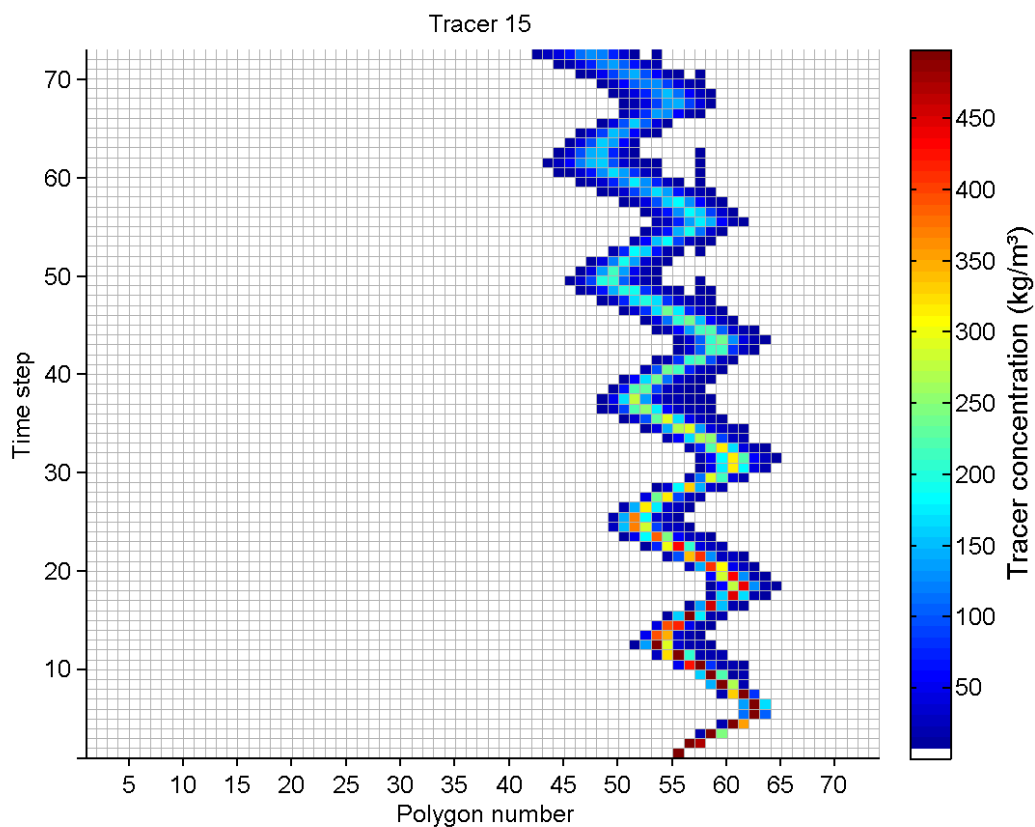


Figure 192 - Movement of tracer 15 concentrations in polygons over 73 time steps of one hour.

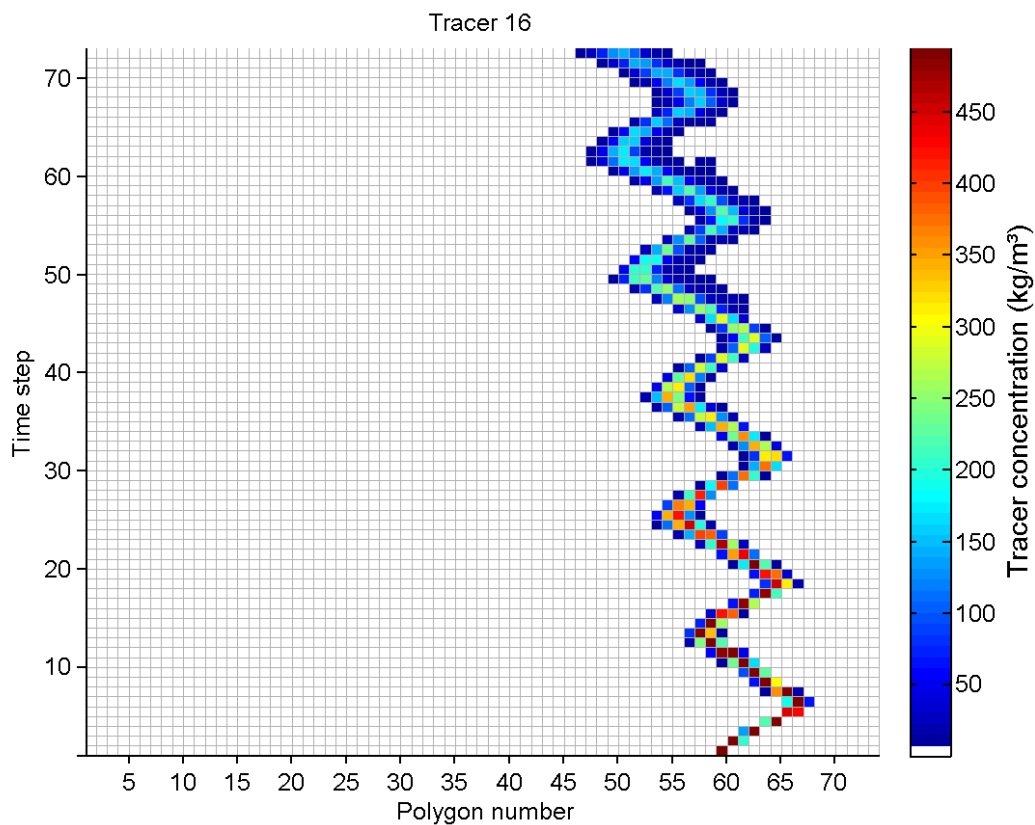


Figure 193 - Movement of tracer 16 concentrations in polygons over 73 time steps of one hour.

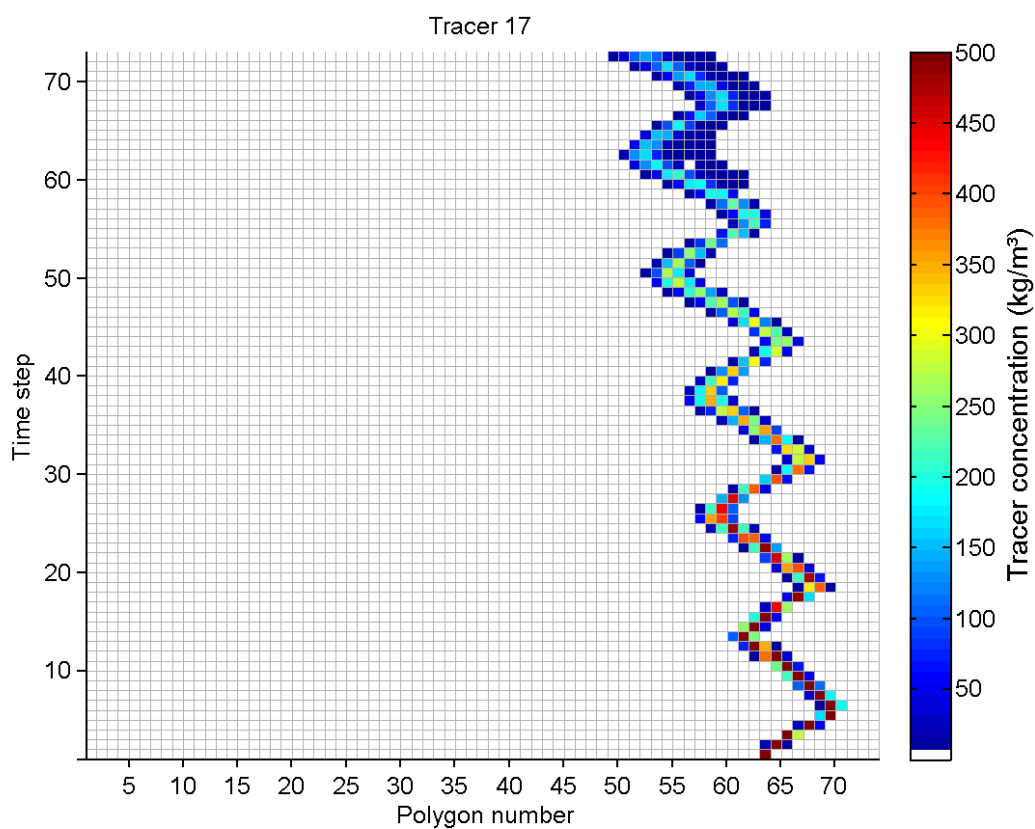


Figure 194 - Movement of tracer 17 concentrations in polygons over 73 time steps of one hour.

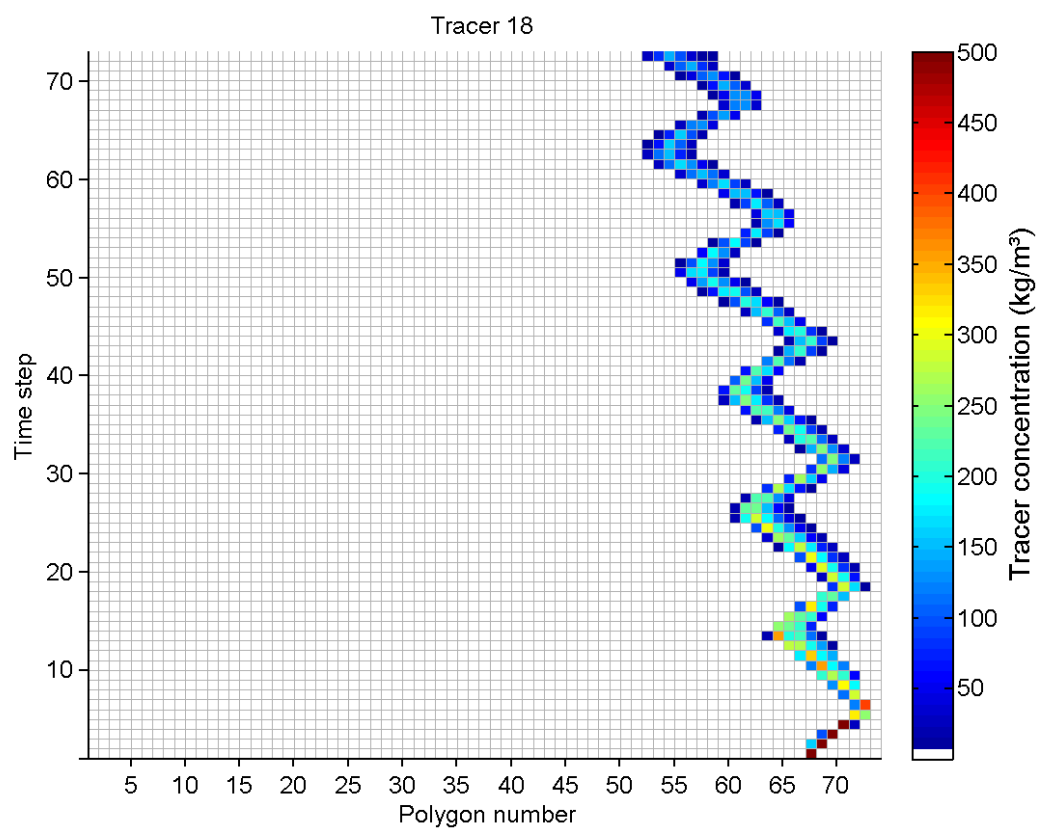


Figure 195 - Movement of tracer 18 concentrations in polygons over 73 time steps of one hour.

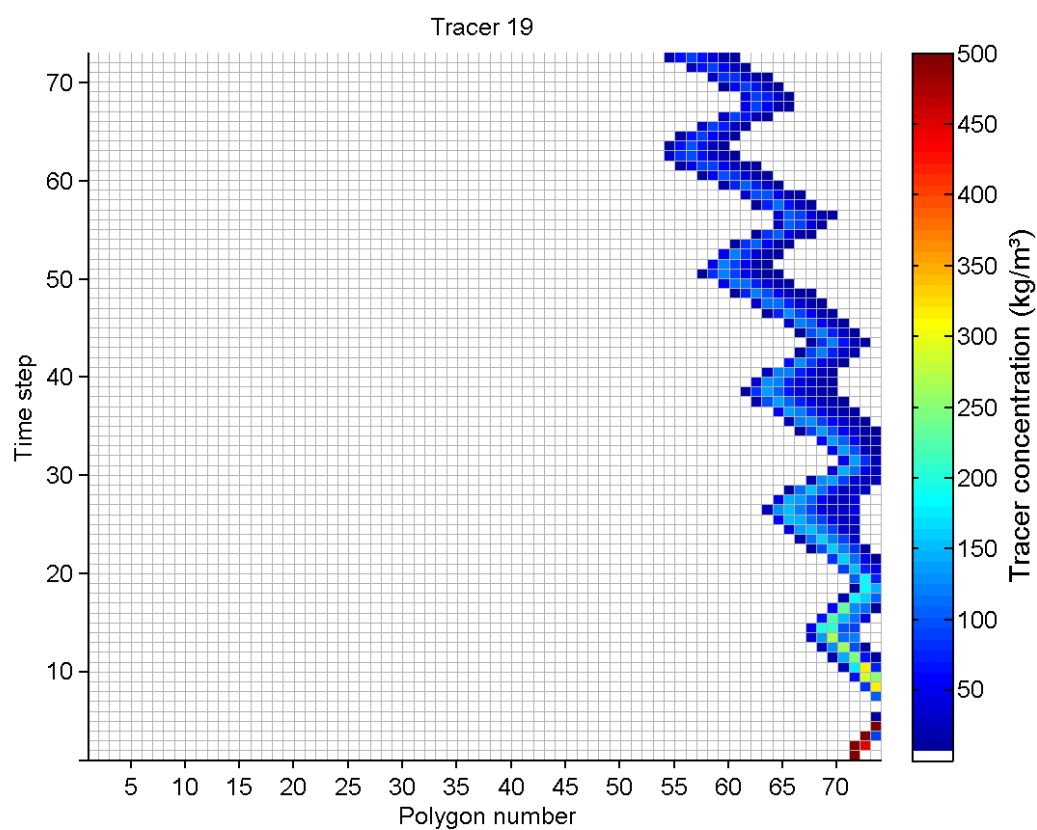


Figure 196 - Movement of tracer 19 concentrations in polygons over 73 time steps of one hour.

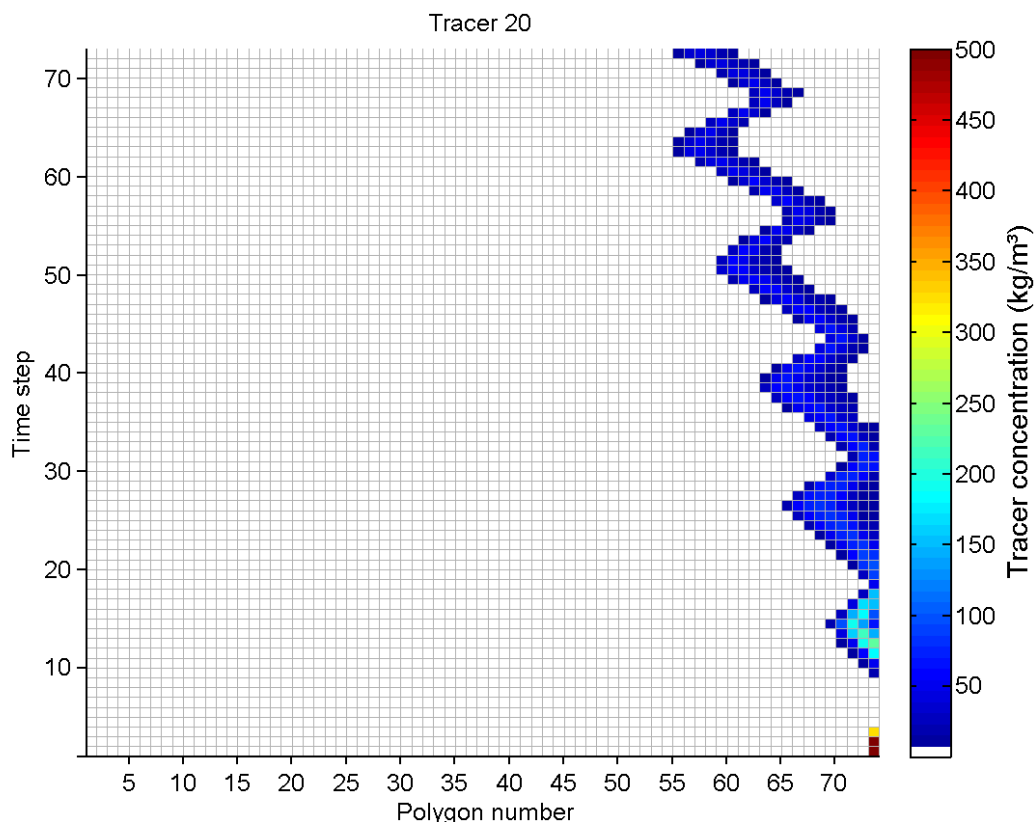


Figure 197 - Movement of tracer 20 concentrations in polygons over 73 time steps of one hour.

13.10. Tracer conservation

The Telemac software provides information about the conservation of mass in the simulation. For the tracer simulation the initial mass, the final mass, the mass leaving the domain through one of the boundaries and the mass loss are given for every tracer at the end of the simulation.

	initial mass	final mass	mass exiting	mass loss	mass loss %
Salinity	0.3541537E+13	0.3418275E+13	0.1232615E+12	100862.4	2.85E-6
Tracer 2	0.4824221E+12	0.4824997E+12	-0.8809083E+08	1.051742E+07	0.00218
Tracer 3	0.2709323E+12	0.2715648E+12	-0.6227712E+09	-9705164	0.00358
Tracer 4	0.1368699E+12	0.1375058E+12	-0.6340608E+09	-1835142	0.00134
Tracer 5	0.2683318E+11	0.2685079E+11	-0.2039947E+08	2784988	0.0104
Tracer 6	0.1032723E+11	0.1032673E+11	-1238655	1732855	0.0168
Tracer 7	0.8666256E+10	0.8666159E+10	-172736.9	269813.6	0.00311
Tracer 8	0.7240887E+10	0.7239982E+10	-117651.0	1022662	0.0141
Tracer 9	0.7025772E+10	0.7025857E+10	-526519.8	441847.0	0.00629
Tracer 10	0.3486410E+10	0.3494611E+10	-7713282	-487943.0	0.0140
Tracer 11	0.2490771E+10	0.2488959E+10	5772529	-3960557	0.159
Tracer 12	0.1782313E+10	0.1791471E+10	2491840	-0.1164998E+08	0.654

Tracer 13	0.1386700E+10	0.1388842E+10	668952.8	-2811229	0.203
Tracer 14	0.9187774E+09	0.9189328E+09	29216.6	-184588.8	0.0201
Tracer 15	0.6051280E+09	0.6036097E+09	1546226	-27992.57	0.00463
Tracer 16	0.4594948E+09	0.4603830E+09	-859664.4	-28527.21	0.00621
Tracer 17	0.3347757E+09	0.3348197E+09	-5747.2	-38220.47	0.0114
Tracer 18	0.2416671E+09	0.2415892E+09	95294.14	-17382.38	0.00719
Tracer 19	0.1682740E+09	0.1683521E+09	-78333.75	199.29	1.18E-4
Tracer 20	0.8623655E+08	0.8636378E+08	-74073.29	-53151.08	0.0616

14 Conclusions

This paper describes the calibration and validation of the 3D SCALDIS model. This model is developed for the tidal Scheldt in the TELEMAC software suite. The unstructured grid allows to combine a large model domain with a high resolution upstream.

A weighted dimensionless cost function is used to analyse the model results. The cost function attributes equal weight to the horizontal and vertical tide. The weights are given to different parameters based on the importance of these parameters for the model calibration.

The model sensitivity to different parameters is analyzed before the calibration. The model is calibrated against water levels, discharges and velocity measurements (sailed ADCP and stationary velocity measurements in shallow and deep areas). The model performance during a storm period is analyzed. The analysis of the model output shows that the model is accurate and can be used for the scenario analysis.

The total RMSE of high, low waters and complete water level time series is 7 to 10 cm in the North sea and Western Scheldt, around 10 cm in the Eastern Scheldt, 9 to 14 cm in the Lower Sea Scheldt and 12 to 14 cm in the Upper Sea Scheldt for most stations. In the North sea and Western Scheldt the difference in M2 amplitude is -2 to 5 cm; it is smaller than 2 cm at most stations. The difference is -1 to 2 cm in the Eastern Scheldt, -2 to 1 cm in the Lower Sea Scheldt and Upper Sea Scheldt. The difference in M2 phase is not significant at most stations (-3 to 3 degrees).

The RMSE of velocity magnitude varies between 12 cm/s and 21 cm/s for the locations with transverse ADCP measurements. For most transects it is smaller than 20 cm/s. The average RMSE of velocity magnitude is about 16 cm/s. The RMSE of velocities in the intertidal areas varies between 11 and 25 cm/s for most transects.

The RMSE of stationary velocity magnitude in the intertidal areas in the Western Scheldt varies between 5 and 20 cm/s. In the Sea Scheldt this value varies between 5 and 21 cm/s.

The shape of the discharges is well represented in the model for most cross sections. The RMSE of the discharge time series is 3 to 16% of the maximum discharge at a certain location.

The calibrated model will be used to analyze the effects of several scenarios and alternatives (different morphology of the Scheldt with different ranges of boundary conditions) within the framework of the Integrated Plan Upper Seascheldt project, and other projects as well.

15 List of references

- Breugem, W.A.; Decrop, B.; Da Silva, J.; Van Holland, G., 2013. Modelling the eddy pattern in the harbor of Zeebrugge, in: Kopmann, R. et al. (Ed.) (2013). Proceedings of the XXth TELEMAC-MASCARET User Conference, Karlsruhe, Germany, October 16–18, 2013. pp. 37 - 42
- Bruce E. Larock, Roland W. Jeppson, Gary Z. Watters, 2000. Hydraulics of Pipeline Systems, CRC Press
- Bodhaine, G.L., 1968. Measurement of peak discharge at culverts by indirect methods: U.S. Geological Survey, Techniques of Water-Resources Investigations, book 3, chapter A3 60p
- Bos, M.G., 1989. Discharge Measurement Structures, ILRI Publication 20, International Institute for Land Reclamation and Improvement, Wageningen, The Netherlands, 401 p. Bureau of Reclamation, Design of Small Dams, 3rd ed., Denver, CO
- Carrier, M., 1972. Hydraulique générale et appliquée, Paris, Eyrolles
- De Mulder, T.; Vercruysse, J.B.; Peeters, P.; Maris, T.; Meire, P., 2013. Inlet sluices for flood control areas with controlled reduced tide in the Scheldt estuary: an overview, in: Bung, D.B. et al. (Ed.). Proceedings of the international workshop on hydraulic design of low-head structures, Aachen, Germany, February, 20-22. pp. 43-53
- De Boeck, K.; Ferket, B.; Van Hoestenbergh, T.; Vanlierde, E.; Deschamps, M.; Verwaest, T.; Mostaert, F. (2014). Saliniteit – Chloriniteit – Chlorositeit: Relaties in gebruik in zeewater en in de Beneden-Zeeschedde. Versie 3.0. WL Rapporten, 12_076. Waterbouwkundig Laboratorium: Antwerpen, België
- EDF-R&D, (2013). 3D hydrodynamics TELEMAC-3D software. Release 6.2. Operating Manual
- French, R. H., J. Zselezsky and R. Margolies, eds., 1987. Open-Channel Hydraulics. McGraw-Hill, New York. 2nd edition. 318
- Hervouet, J.-M. (2007). Hydrodynamics of Free Surface Flows: Modelling with the Finite Element Method John Wiley & Sons, Ltd. ISBN: 978-0-470-03558-0
- IMDC Report 613_9_1_LPB, 2006 Debietscoefficienten_inuitwatering_v0
- Janna, W. S. (2010). Introduction to Fluid Mechanics, Fourth edition, CRC Press, Taylor & Francis Group, Boca Raton, USA. ISBN 978-1-4200-8524-2
- Kindsvater, C.E. and R.W.C. Carter, 1957. Discharge Characteristics of Rectangular Thin-Plate Weirs. Journal of the Hydraulics Division, Proceedings of the American Society of Civil Engineers, Vol. 83, No. HY6. Paper 1453.
- Lencastre, A., 1961. Manuel d'hydraulique générale, Paris, Eyrolles
- Maximova, T.; Vanlede, J.; Verwaest, T.; Mostaert, F. (2015). Vervolgonderzoek bevaarbaarheid Bovenzeeschedde: Subreport 4 – Modellentrein CSM – ZUNO: validatie 2013. WL Rapporten, 13_131. Flanders Hydraulics Research: Antwerp, Belgium
- Moulinec, C., Denis, C., Pham C.-T., Rougé, D., Hervouet, J.-M., Razafindrakoto, E., Barber, R.W., Emerson, D.R., Gu, X.-J. (2011). TELEMAC: An efficient hydrodynamics suite for massively parallel architectures. Computer & Fluids 51, 2011, 30-34.
- Pawlowicz, R., B. Beardsley, and S. Lentz, (2002). "Classical Tidal Harmonic Analysis Including Error Estimates in MATLAB using T_TIDE", Computers and Geosciences, 2002.
- Smolders, S. (2014 a). Sensitivity TELEMAC 3D parameters. WL2013M12_000_X
- Smolders, S. (2014 b). Integraal Plan Bovenzeeschedde : Rekenrooster en beschikbare bathymetrie data. WL2014M13_131_1

Smolders, S., (2015, in preparation). Morphological Management for the Scheldt estuary combining safety, port accessibility and ecology. Ph. D. thesis. University of Antwerp, Belgium

Soetaert K., Herman, P.M.J., (2009). A practical guide to ecological modelling: Using R as a simulation platform.

Sutherland, J., Walstra, D.J.R., Chesher, T.J., Van Rijn, L.C., Southgate, H.N., (2003) Evaluation of coastal area modelling systems at an estuary mouth. *Coastal Engineering*, 51 (2004), pp. 119 – 142

Teles, M. J. (2014). Culvert functionality. WL2014M13_131_2

Vanlede, J.; Delecluyse, K.; Primo, B.; Verheyen, B.; Leyssen, G.; Verwaest, T.; Mostaert, F. (2015, in preparation). Verbetering randvoorwaardenmodel: Deelrapport 7: Afregeling van het 3D Scheldemodel. WL Rapporten, 00_018. Flanders Hydraulics Research & IMDC: Antwerp, Belgium

Vos, R., Brummelhuis, P. G.J., Gerritsen (2000). Integrated data-modelling approach for suspended sediment transport on a regional scale. *Coastal Engineering*, 41, 177–200. Available from: <http://www.sciencedirect.com/science/article/pii/S0378383900000326> [Accessed 15/06/2015]

16 Tables

Table 56. Comparable tides for the ADCP measurements used for the calibration

ADCP measurements	Tref of comparable Tide	Tref of measured tide	RMSE
20110705 Everingen	24/09/2013 23:50	05/07/2011 11:20	0.1
20110706 R7 Terneuzen	23/09/2013 11:00	06/07/2011 12:00	0.12
20120508 R6 Middelgat	21/09/2013 22:30	08/05/2012 10:30	0.06
20120509 R6 GatVanOssenissee	22/09/2013 23:00	09/05/2012 11:10	0.12
20080407 dwarsraai Ossenissee	22/09/2013 04:40	07/04/2008 16:00	0.12
20060323 Waarde	28/09/2013 15:00	23/03/2006 14:20	0.15
20130424 R5 SchaarVanWaarde	24/09/2013 06:00	24/04/2013 14:00	0.06
20130425 R5 Zuidergat	24/09/2013 06:00	25/04/2013 14:50	0.1
20060912 Schaar van Ouden Doel	21/09/2013 10:50	12/09/2006 12:50	0.13
20050217 Zandvliet	27/09/2013 08:00	17/02/2005 09:10	0.1
20110902 Galgenschoor	22/09/2013 11:50	02/09/2011 13:00	0.11
20100318 langsraaiO	24/09/2013 06:00	18/03/2010 17:00	0.1
20080311 DGD K	18/09/2013 21:20	11/03/2008 12:30	0.22
20060323 DGD K	27/09/2013 14:40	23/03/2006 15:00	0.11
20050217 Liefkenshoek	27/09/2013 07:50	17/02/2005 09:00	0.11
20130625 Liefkenshoek	23/09/2013 00:10	25/06/2013 11:20	0.11
20140514 Liefkenshoek	23/09/2013 05:40	14/05/2014 15:10	0.1
20050218 Kallo	28/09/2013 21:50	18/02/2005 10:30	0.08
20090529 Oosterweel	25/09/2013 01:40	29/05/2009 14:00	0.18
20130627 Oosterweel	21/09/2013 11:20	27/06/2013 13:10	0.17
20140516 Oosterweel	24/09/2013 01:10	16/05/2014 11:30	0.1
20100414 Kruibeke	24/09/2013 01:20	14/04/2010 10:40	0.12
20130530 Kruibeke	23/09/2013 12:40	30/05/2013 14:20	0.19
20140702 Kruibeke	26/09/2013 02:00	02/07/2014 13:20	0.1
20060323 Schelle	27/09/2013 15:40	23/03/2006 16:00	0.12
20060928 Schelle	25/09/2013 14:20	28/09/2006 13:50	0.12
20130213 Wintam	22/09/2013 01:00	13/02/2013 13:40	0.27
20090610 Ballooi dwars	17/09/2013 08:50	10/06/2009 12:30	0.15
20090610 Notelaer langs	17/09/2013 08:50	10/06/2009 12:30	0.15
20130612 Driegoten	25/09/2013 15:00	12/06/2013 13:40	0.09
20140617 Driegoten	21/09/2013 11:30	17/06/2014 13:30	0.14
20110804 Branst	21/09/2013 13:10	04/08/2011 15:10	0.05
20110218 Kramp ebb	22/09/2013 01:40	18/02/2011 12:10	0.07
20110218 Kramp flood	21/09/2013 05:30	18/02/2011 16:40	0.07
20140417 Dendermonde	22/09/2013 00:10	17/04/2014 12:00	0.11
20110801 Appels downstream	24/09/2013 15:30	01/08/2011 13:40	0.07
20130527 Schoonaarde	21/09/2013 14:20	27/05/2013 14:50	0.08
20140703 Schoonaarde	26/09/2013 01:50	03/07/2014 13:40	0.11
20140415 Schellebelle	23/09/2013 00:30	15/04/2014 10:40	0.07
20100427 Boom	22/09/2013 01:10	27/04/2010 10:40	0.14
20130529 Terhagen	18/09/2013 10:30	29/05/2013 14:50	0.09
20140630 Terhagen	19/09/2013 10:10	30/06/2014 12:20	0.14

Table 57. Comparable tides for the ADCP measurements used for the validation

ADCP measurements	Tref of comparable Tide	Tref of measured tide	RMSE
20080604 Everingen	22/09/2013 22:50	04/06/2008 08:50	0.07
20080407 Ossensisse langsraai	22/09/2013 04:40	07/04/2008 16:00	0.11
20060928 Waarde	25/09/2013 12:40	28/09/2006 12:00	0.08
20100319 dwarsraai D	21/09/2013 23:40	19/03/2010 12:20	0.1
20060927 DGD K	26/09/2013 01:50	27/09/2006 12:30	0.13
20060322 DGD K	27/09/2013 02:00	22/03/2006 14:00	0.07
20060322 Liefkenshoek	27/09/2013 02:00	22/03/2006 14:00	0.07
20100430 Liefkenshoek	18/09/2013 21:20	30/04/2010 11:10	0.18
20100429 Oosterweel	19/09/2013 22:40	29/04/2010 11:00	0.14
20090526 Kruibeke	18/09/2013 21:40	26/05/2009 11:30	0.09
20050217 Schelle	27/09/2013 08:50	17/02/2005 10:00	0.09
20090611 Notelaer dwars	17/09/2013 08:50	11/06/2009 13:10	0.14
20100415 Driegoten	24/09/2013 02:30	15/04/2010 12:30	0.12
20110805 Branst	21/09/2013 13:10	05/08/2011 15:50	0.1
20110801 Appels upstream	24/09/2013 15:30	01/08/2011 13:40	0.07
20100414 Schoonaarde	24/09/2013 04:10	14/04/2010 13:40	0.1
20090622 Boom	24/09/2013 07:40	22/06/2009 16:10	0.15

Table 58. Comparable tides for the discharge measurements

ADCP measurements	Tref of comparable Tide	Tref of measured tide	RMSE
R12 Oostgat 20070618	19/09/2013 07:50	18/06/2007 10:20	0.13
R12 Deurloo 20070703	25/09/2013 23:50	03/07/2007 10:00	0.13
R12 Wielingen 20070619	25/09/2013 23:50	19/06/2007 11:10	0.13
R11 Wielingen 20060517	24/09/2013 23:20	17/05/2006 10:40	0.14
R11 Sardijneul 20060516	24/09/2013 17:20	16/05/2006 16:20	0.04
R10 Vaarwater langs hoofdplaat 20071011	24/09/2013 23:30	11/10/2007 08:20	0.1
R10 Honte schaar van spijker plaat 20071010	19/09/2013 14:10	10/10/2007 14:00	0.14
R9 Vaarwater langs hoofdplaat 20060913	24/09/2013 11:20	13/09/2006 12:10	0.12
R9 Honte schaar van spijker plaat 20060912	21/09/2013 09:20	12/09/2006 11:20	0.1
R7 Pas van Terneuzen 20080605	22/09/2013 22:40	05/06/2008 09:30	0.06
R7 Everingen 20080604	22/09/2013 22:50	04/06/2008 08:50	0.07
R6 Middelgat 20041013	24/09/2013 00:00	13/10/2004 08:40	0.1
R6 Gat van Ossensisse 20041013	24/09/2013 00:00	13/10/2004 08:40	0.1
R5 Zuidergat 20051130	26/09/2013 07:00	30/11/2005 14:00	0.15
R5 Schaar van Waarde 20051201	24/09/2013 05:50	01/12/2005 14:40	0.2
R3 Zimmermangeul 20070815	21/09/2013 10:30	15/08/2007 11:00	0.2
R3 Overloop van Valkenisse 20070814	23/09/2013 11:40	14/08/2007 10:30	0.07
R2 total 20120411	19/09/2013 09:30	11/04/2012 13:00	0.17
R2 Schaar van de Noord 20041028	21/09/2013 10:50	28/10/2004 09:40	0.11
R2 Nauw van Bath 20041028	21/09/2013 10:50	28/10/2004 09:40	0.11
R1 Ballastplaat 20100401	20/09/2013 03:30	01/04/2010 16:50	0.12

R1 Vaarwater boven Bath 20100330	19/09/2013 22:00	30/03/2010 10:00	0.11
R1 Vaarwater boven Bath 20061025	24/09/2013 12:40	25/10/2006 11:20	0.14
Liefkenshoek_20090527	19/09/2013 09:50	27/05/2009 12:00	0.17
Liefkenshoek_20100430	20/09/2013 10:30	30/04/2010 11:20	0.16
Liefkenshoek_20130625	23/09/2013 00:10	25/06/2013 11:20	0.11
Oosterweel_20090529	25/09/2013 01:40	29/05/2009 14:00	0.17
Oosterweel_20100429	19/09/2013 22:40	29/04/2010 11:00	0.15
Oosterweel_20130627	21/09/2013 11:20	27/06/2013 13:10	0.17
Kruikeke_20090526	18/09/2013 21:40	26/05/2009 11:30	0.09
Kruikeke_20100414	24/09/2013 01:10	14/04/2010 10:30	0.11
Kruikeke_20130530	23/09/2013 12:40	30/05/2013 14:20	0.19
Driegoten_20090623	25/09/2013 15:10	23/06/2009 12:00	0.1
Driegoten_20100415	24/09/2013 02:30	15/04/2010 12:30	0.12
Driegoten_20130612	25/09/2013 15:00	12/06/2013 13:40	0.09
Schoonaarde_20090625	21/09/2013 14:20	25/06/2009 15:10	0.07
Schoonaarde_20100414	24/09/2013 04:10	14/04/2010 13:40	0.1
Schoonaarde_20130527	21/09/2013 02:20	27/05/2013 13:50	0.11
Boom_20090622	24/09/2013 02:00	22/06/2009 10:30	0.15
Boom_20100427	22/09/2013 01:10	27/04/2010 10:40	0.14
Terhagen_20130529	18/09/2013 10:30	29/05/2013 14:50	0.09

Table 59. Statistical parameters for the water level time series (Scaldis_028_Q2 vs. Scaldis_028_Q1)

Station	Complete Time Series		
	BIAS TS	RMSE TS	RMSE_0 TS
	[m]	[m]	[m]
Schelle	0.00	0.01	0.01
Temse	0.00	0.01	0.01
Tielrode	0.00	0.01	0.01
StAmands	0.00	0.02	0.02
Dendermonde	0.00	0.05	0.05
Schoonaarde	0.00	0.10	0.10
Wetteren	0.01	0.17	0.17
Melle	0.01	0.23	0.23
Total	0.00	0.11	0.11

Table 60. Statistical parameters for high waters (Scaldis_028_Q2 vs. Scaldis_028_Q1)

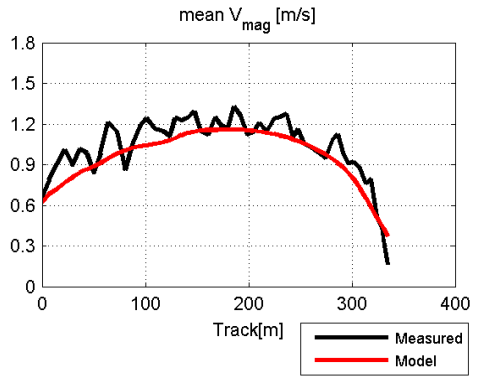
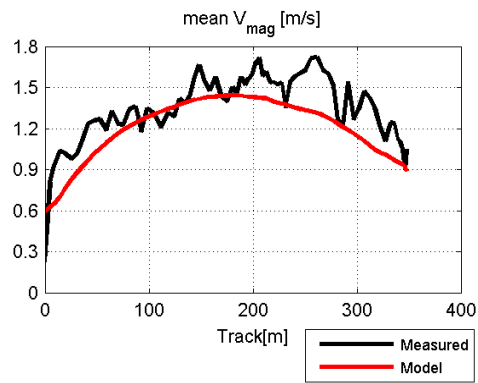
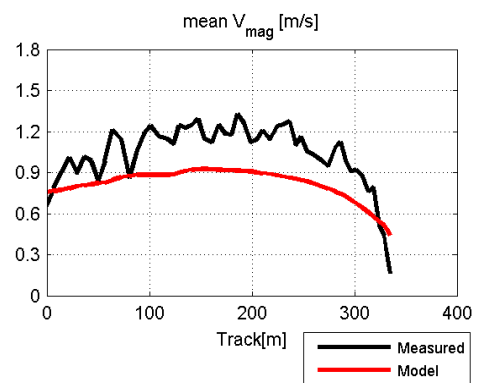
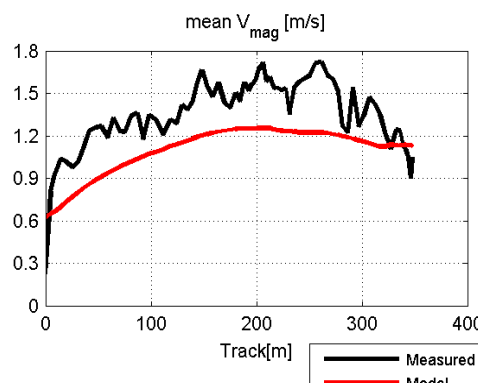
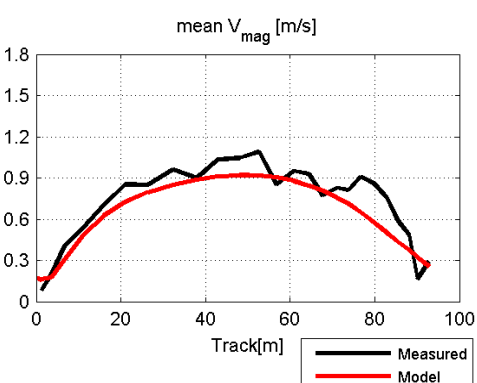
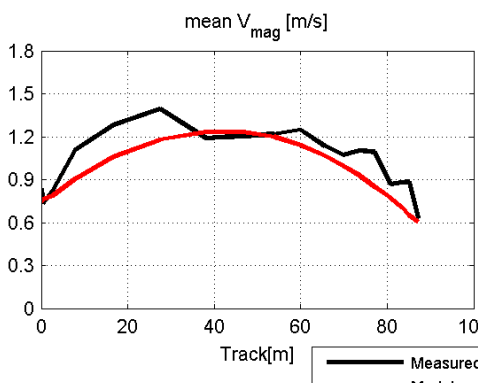
Station	HW					
	BIAS HW	RMSE HW	RMSE_0 HW	BIAS HW	RMSE HW	RMSE_0 HW
	[m]	[m]	[m]	[min]	[min]	[min]
Schelle	0.00	0.01	0.01	0	0	0
Temse	0.00	0.01	0.01	0	0	0
Tielrode	0.00	0.01	0.01	0	0	0
StAmands	0.00	0.01	0.01	0	2	2
Dendermonde	0.00	0.04	0.04	0	2	2
Schoonaarde	0.00	0.07	0.07	0	3	3
Wetteren	0.01	0.13	0.13	0	6	6
Melle	0.02	0.14	0.14	1	7	7
Total	0.00	0.07	0.07	0	4	4

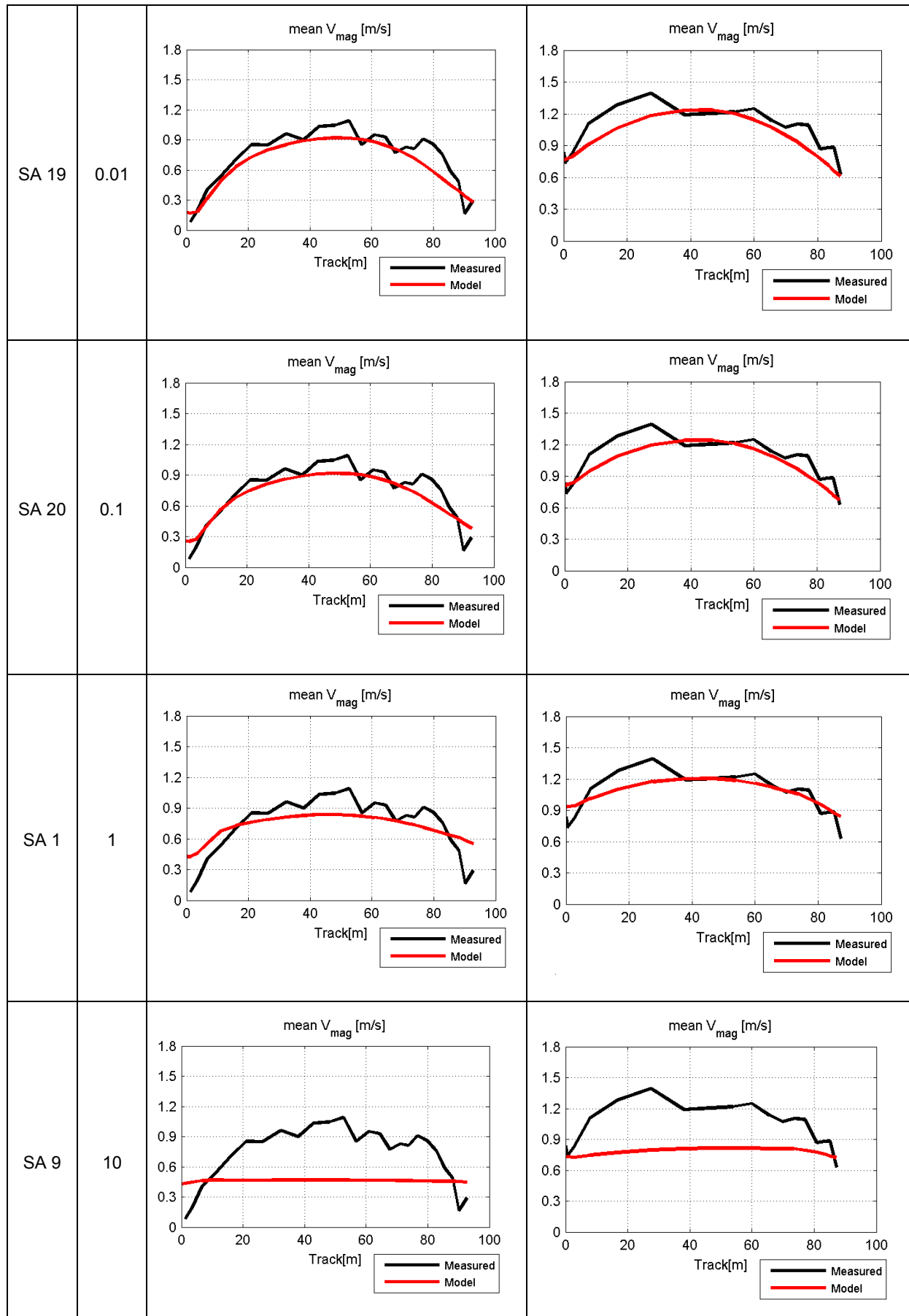
Table 61. Statistical parameters for low waters (Scaldis_028_Q2 vs. Scaldis_028_Q1)

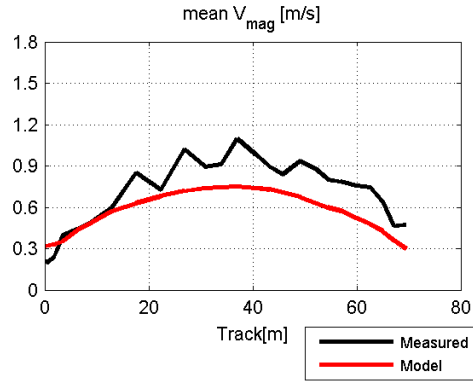
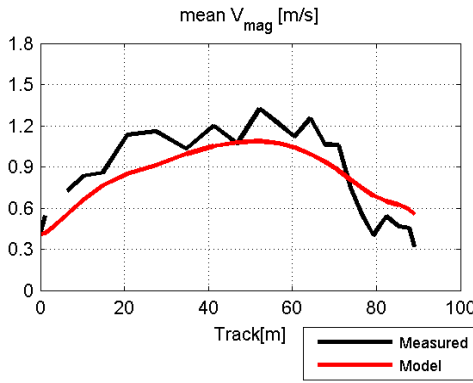
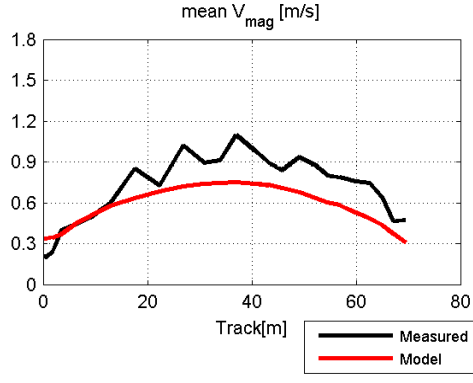
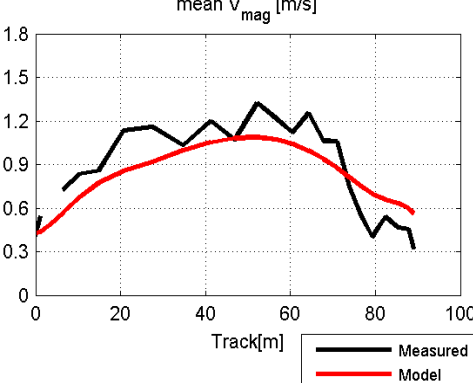
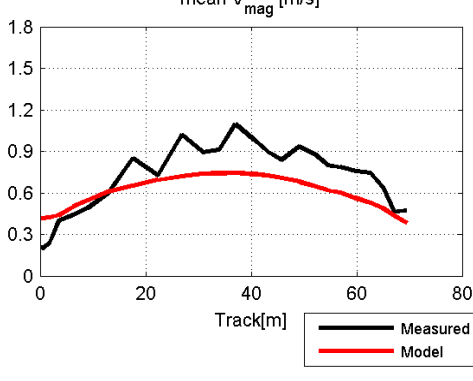
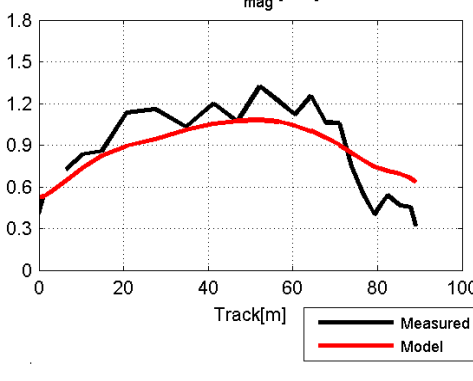
Station	LW					
	BIAS LW	RMSE LW	RMSE_0 LW	BIAS LW	RMSE LW	RMSE_0 LW
	[m]	[m]	[m]	[min]	[min]	[min]
Schelle	0.00	0.01	0.01	0	0	0
Temse	0.00	0.01	0.01	0	0	0
Tielrode	0.00	0.01	0.01	0	0	0
StAmands	0.00	0.03	0.03	0	0	0
Dendermonde	0.00	0.07	0.07	0	2	2
Schoonaarde	0.00	0.11	0.11	0	0	0
Wetteren	0.00	0.24	0.24	-2	7	6
Melle	0.04	0.32	0.32	-1	11	11
Total	0.00	0.15	0.15	0	5	5

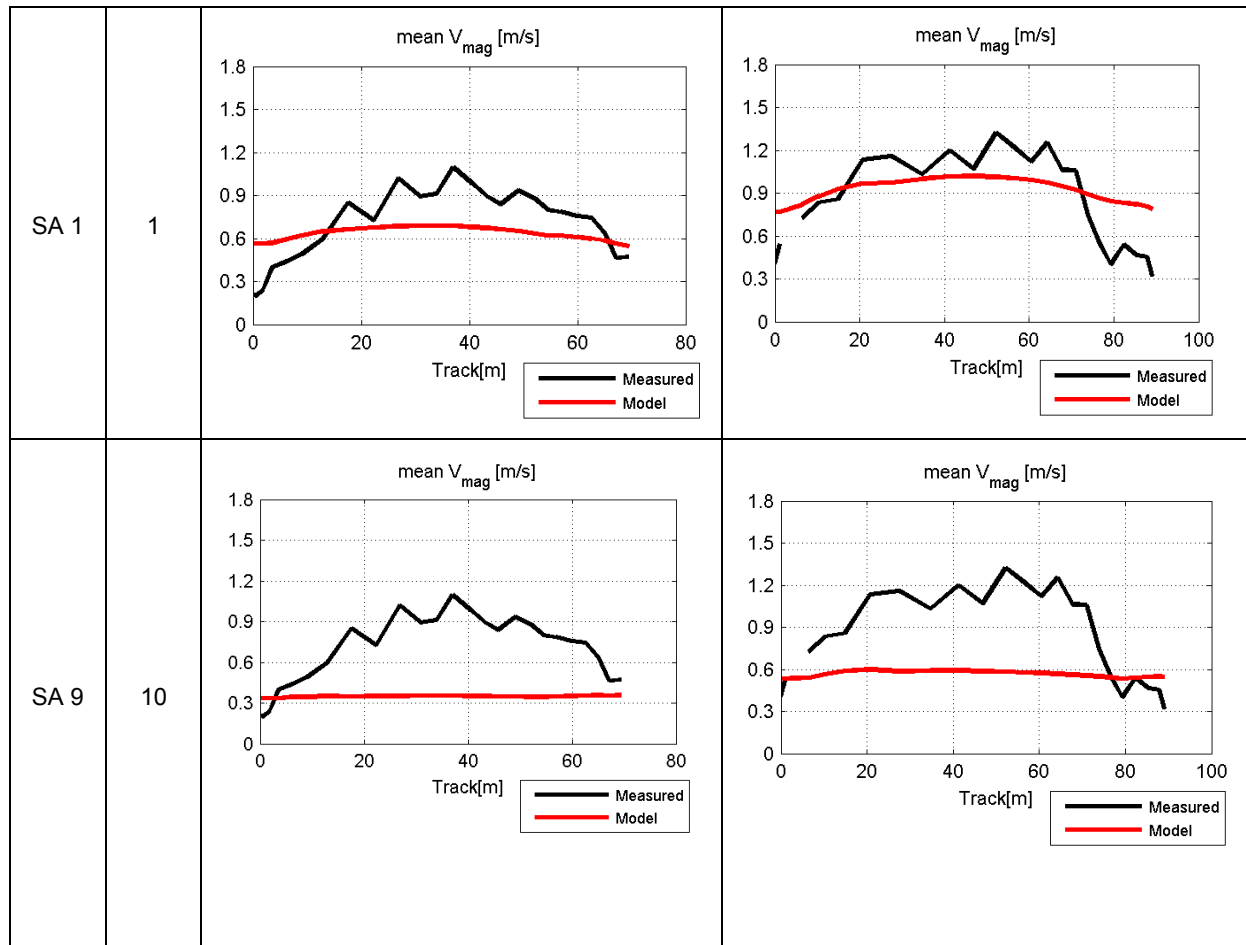
Table 62. Measured and modeled velocity at Kruibeke,
Dendermonde and Schoonaarde in runs with different diffusivity

20130530_Kruibeke			
Run	Diffusivity (m ² /s)	Max ebb	Max flood
SA 8	10 ⁻⁶		
SA 19	0.01		
SA 20	0.1		

SA 1	1		
SA 9	10		
20140417_Dendermonde			
Run	Diffusivity (m ² /s)	Max ebb	Max flood
SA 8	10 ⁻⁶		



20130527_Schoonaarde			
Run	Diffusivity (m ² /s)	Max ebb	Max flood
SA 8	10 ⁻⁶		
SA 19	0.01		
SA 20	0.1		



17 Figures

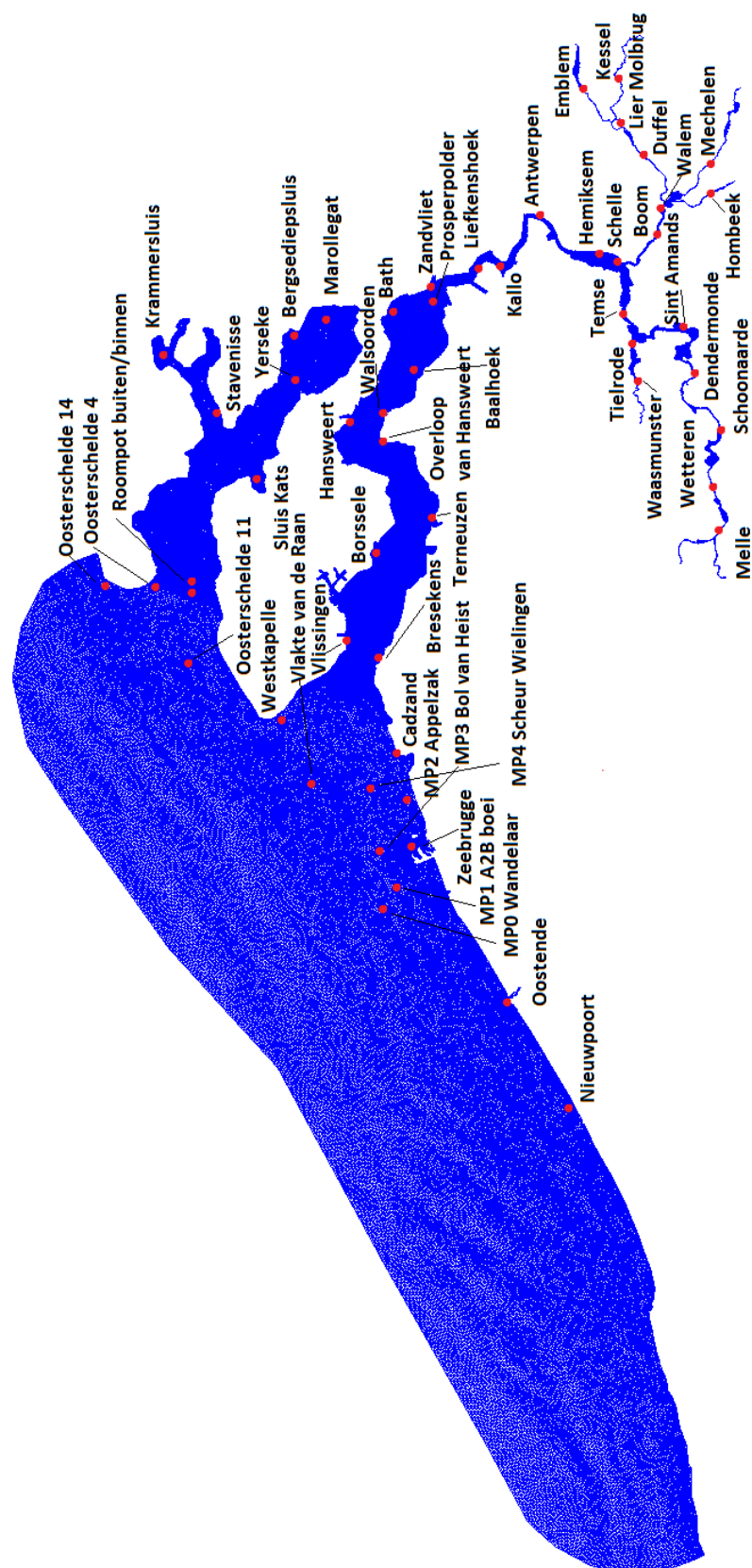


Figure 198 - Water level stations

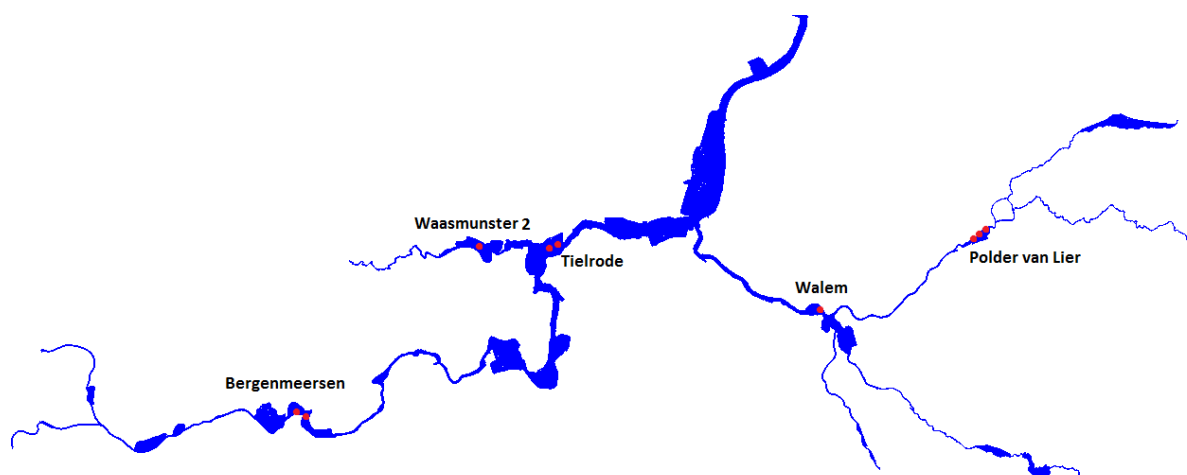


Figure 199 - Location of the available measurements for the Sinterklaasstorm



Figure 200 Measurement locations at Tielrode



Figure 201 - Measurement location at Waasmunster



Figure 202 - Measurement locations at Bergenmeersen



Figure 203 - Measurement location at Walem

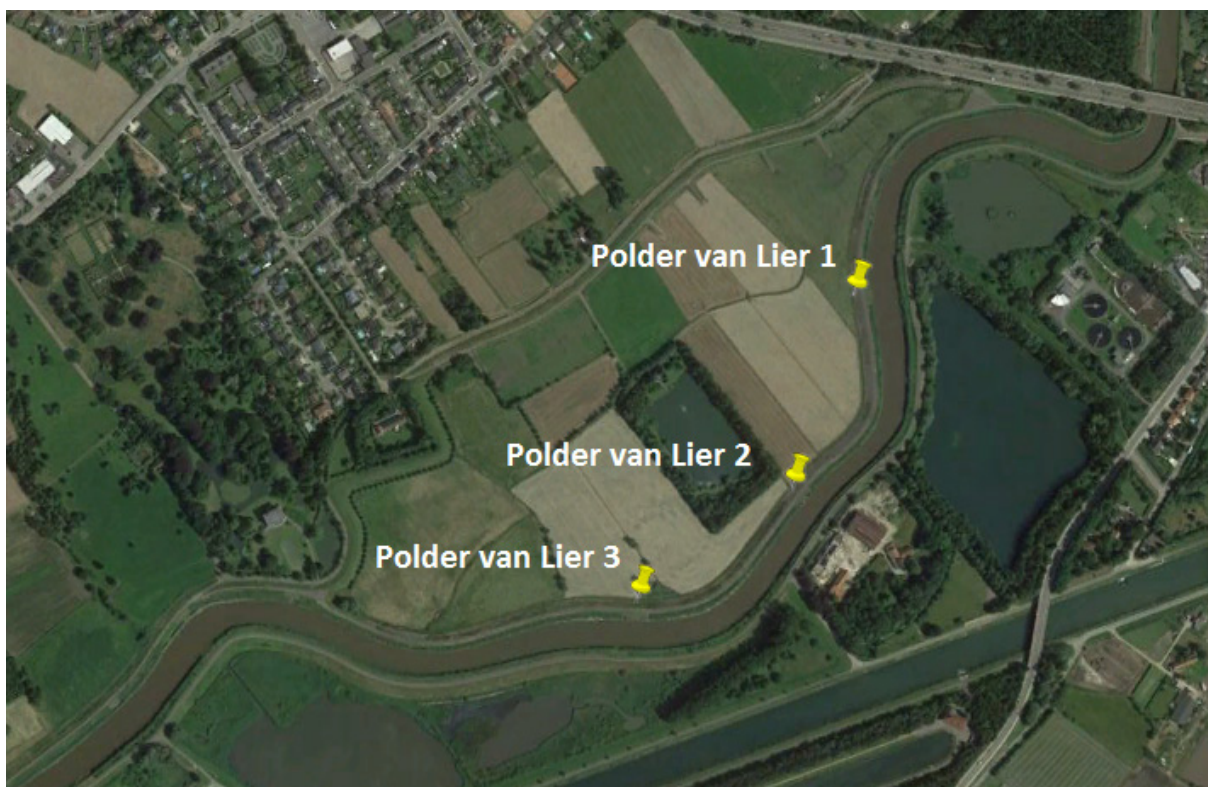


Figure 204 - Measurement locations at Lier

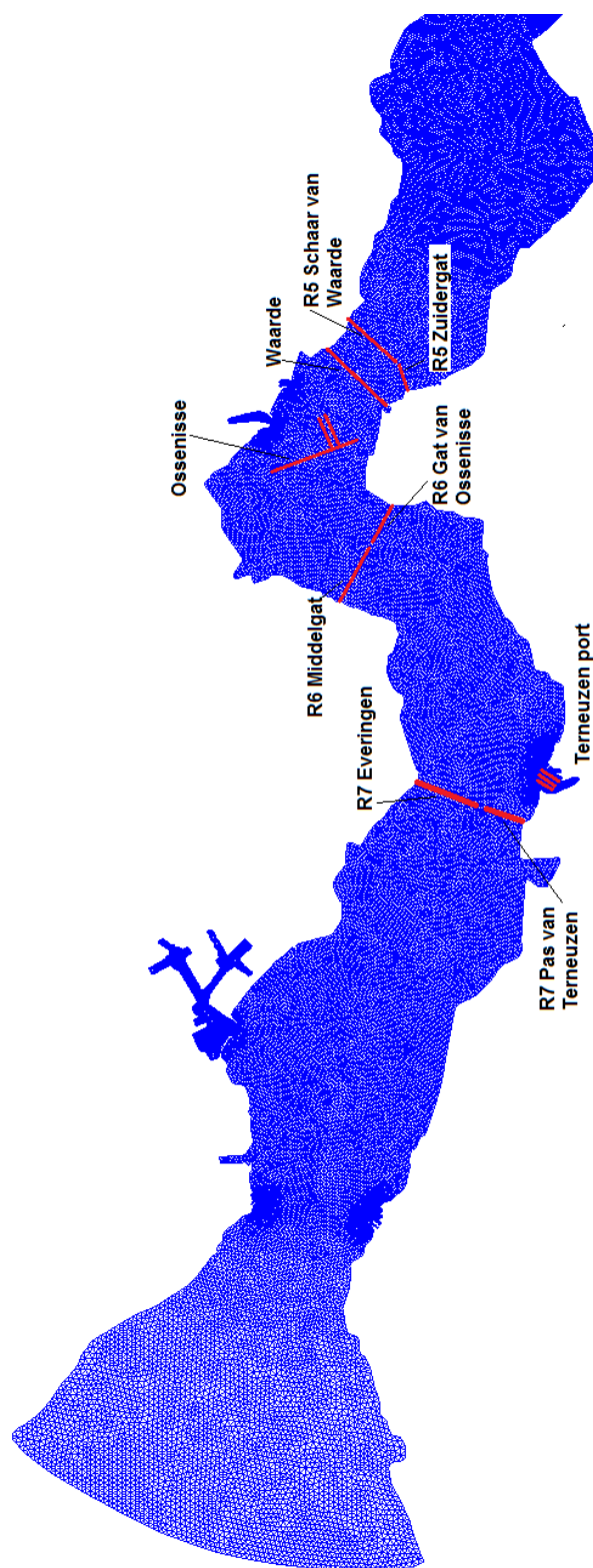


Figure 205. Available ADCP measurements in the Western Scheldt

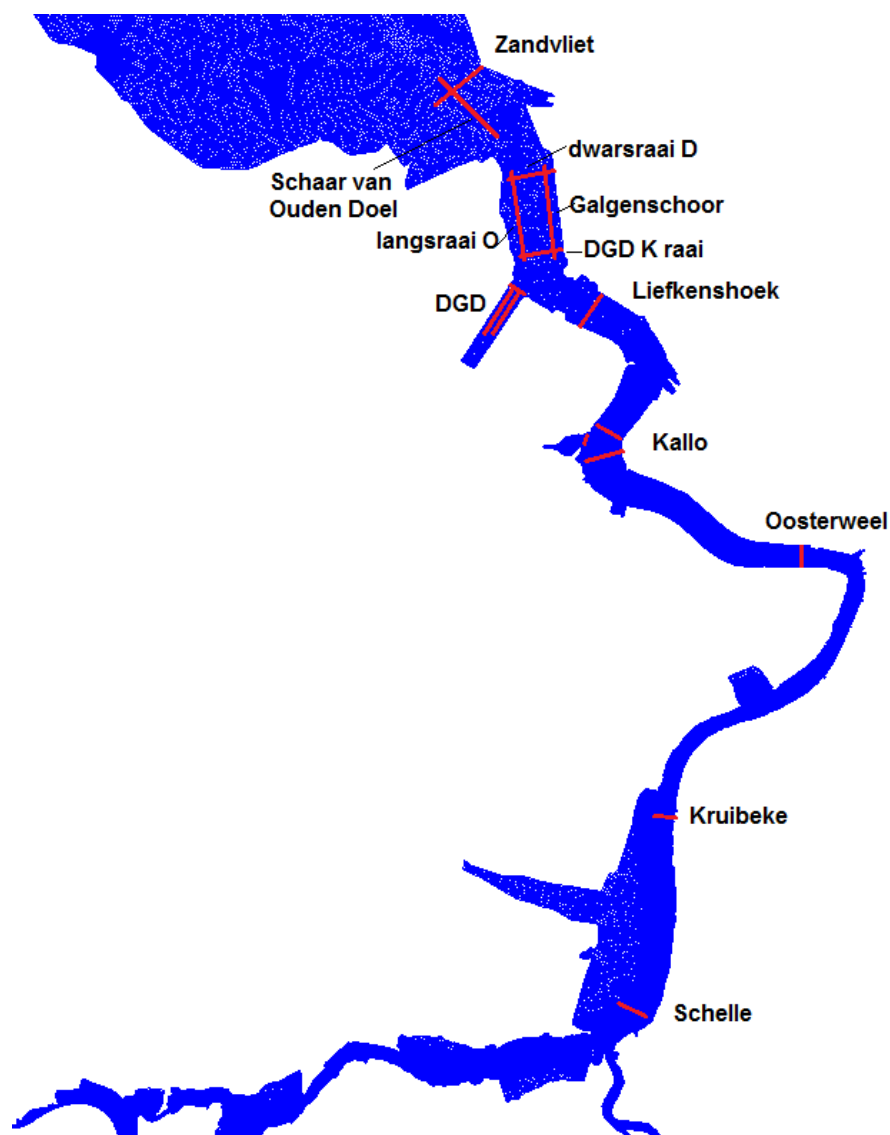


Figure 206 - Available ADCP measurements in the Lower Sea Scheldt

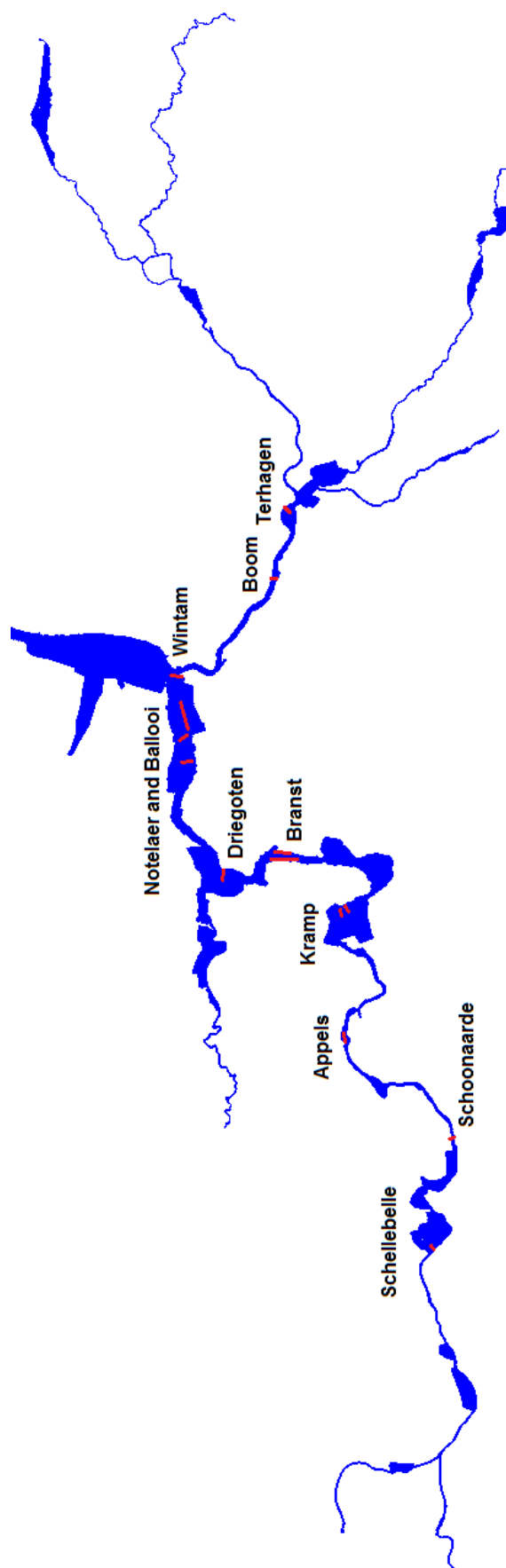


Figure 207 - Available ADCP measurements in the Upper Sea Scheldt and Rupel

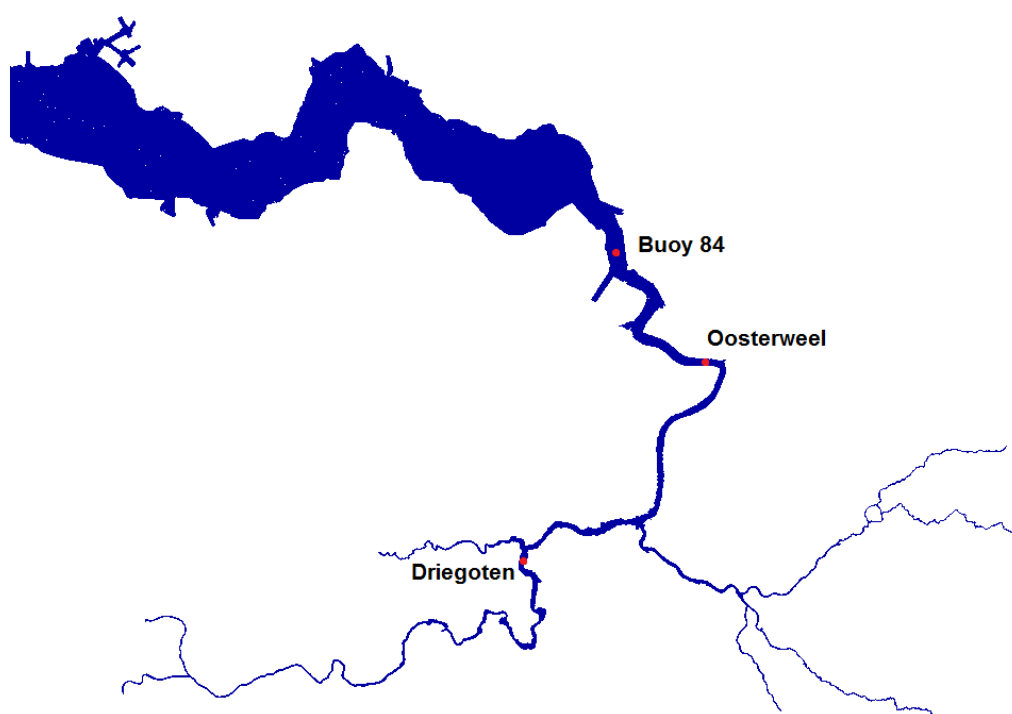


Figure 208 - Stationary velocity measurements in deep areas



Figure 209 - Location of stationary velocity measurements in shallow areas



Figure 210 - Stationary velocity measurements Hooge Platen West and Hooge Platen Noord

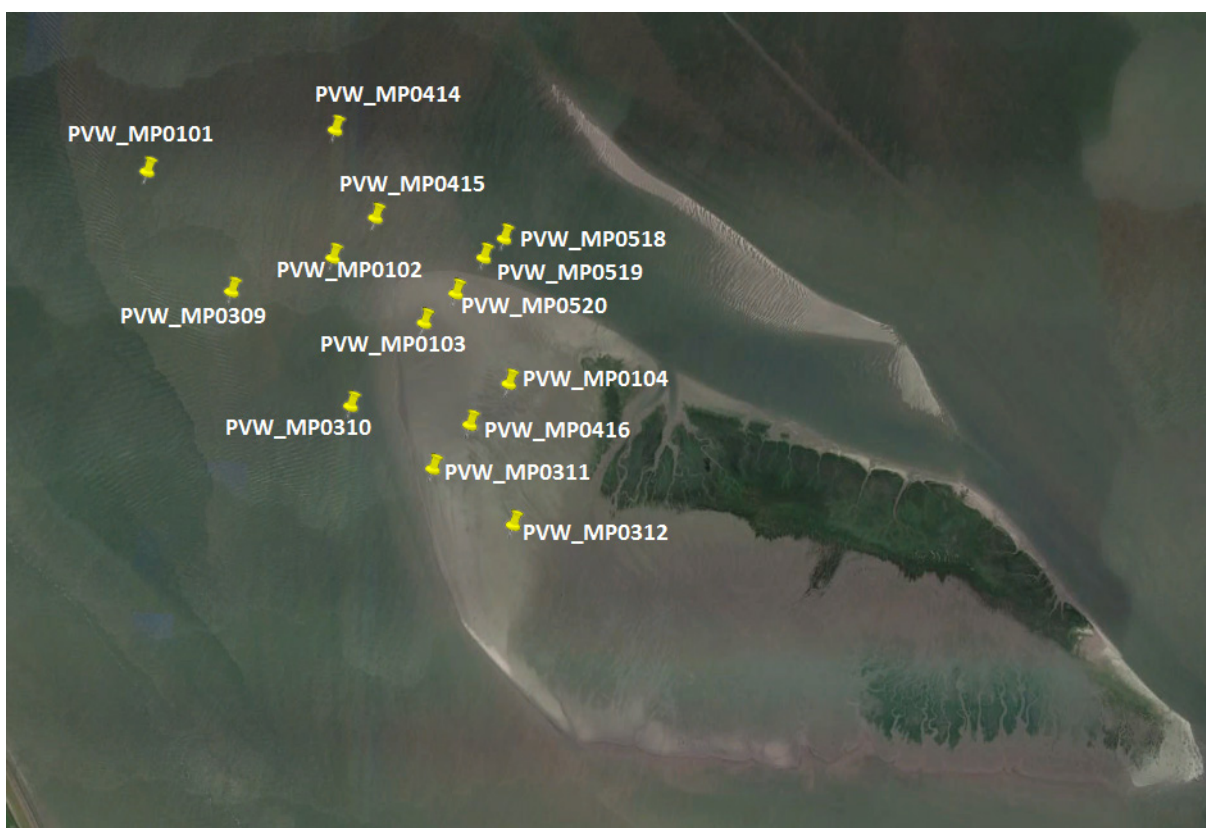


Figure 211 - Stationary velocity measurements Plaat van Walsoorden

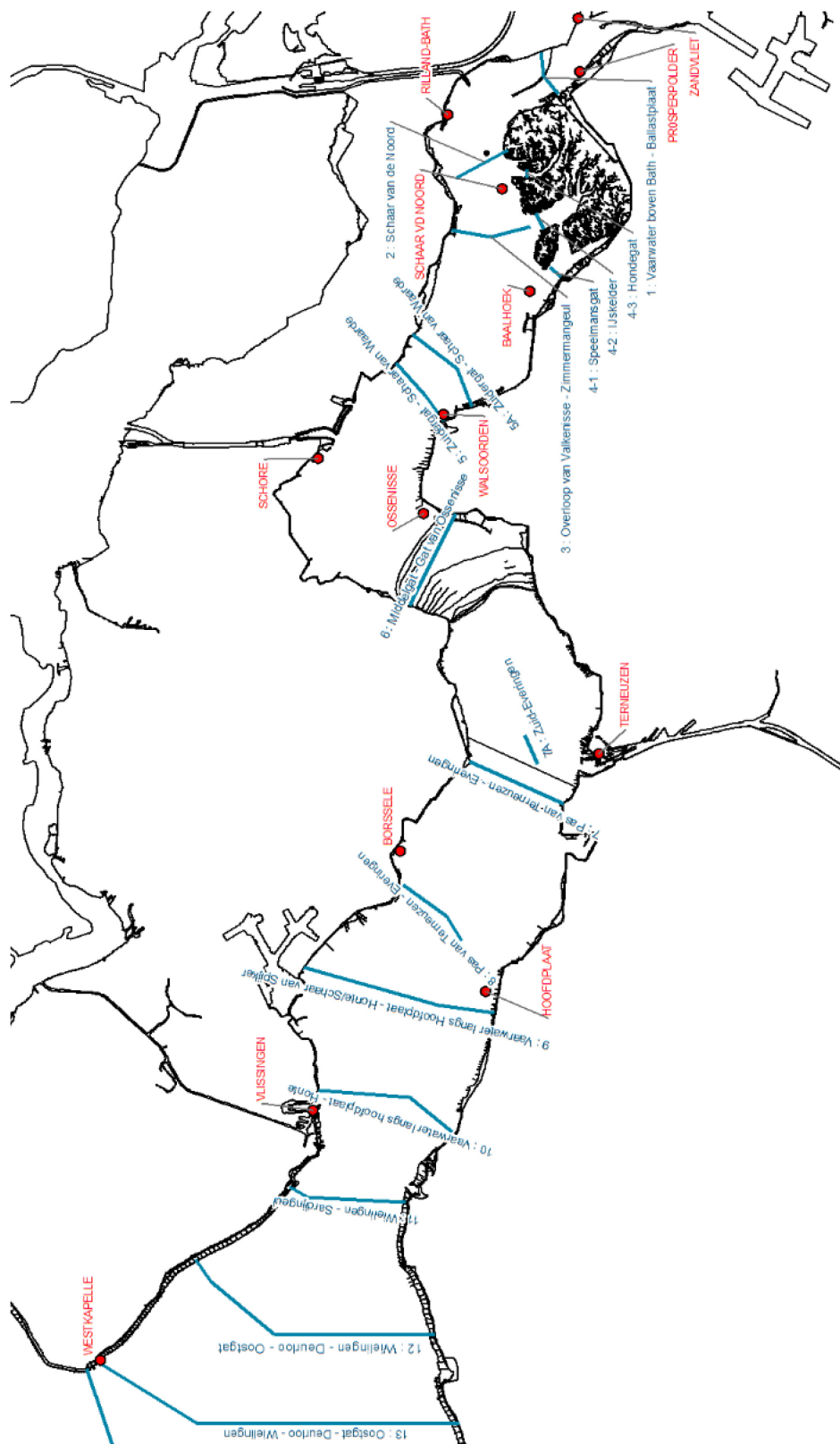


Figure 212 - Discharge cross sections in the Western Scheldt

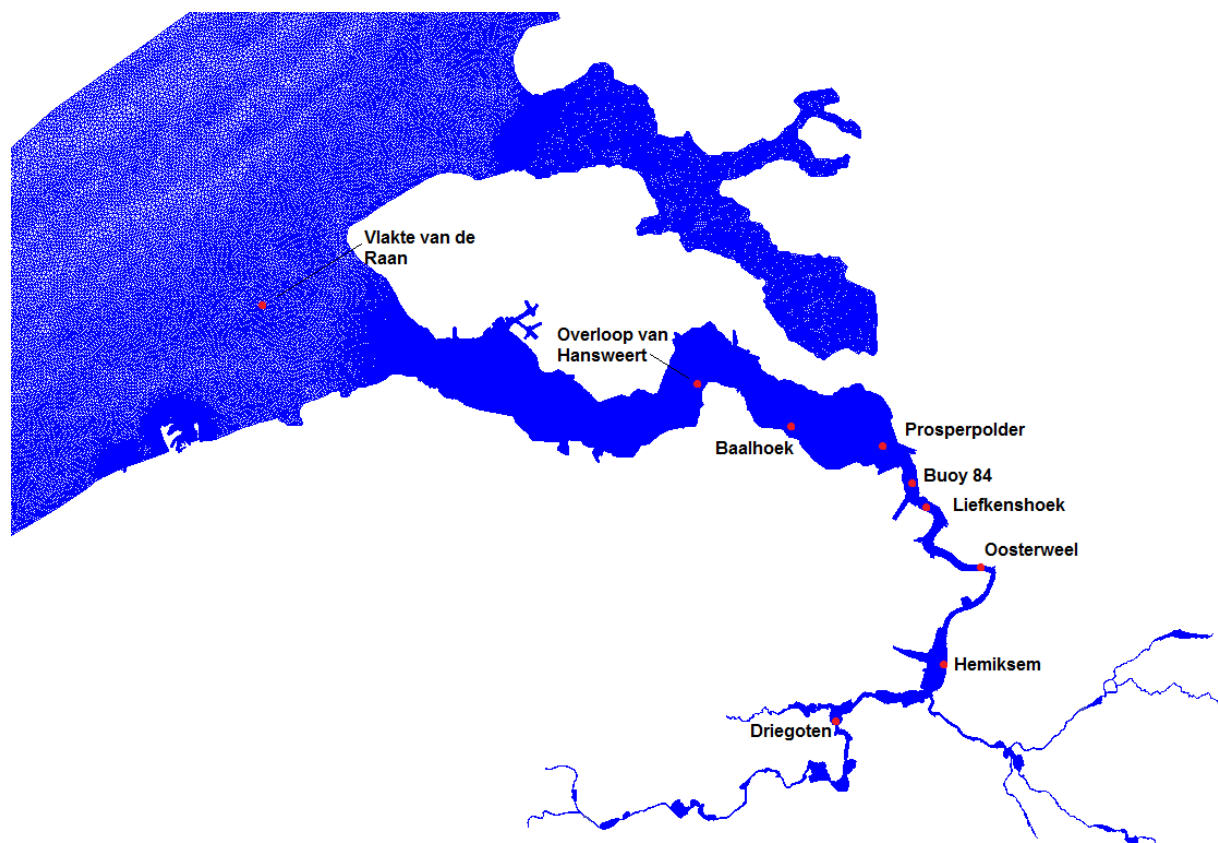


Figure 213 - Location of salinity measurements

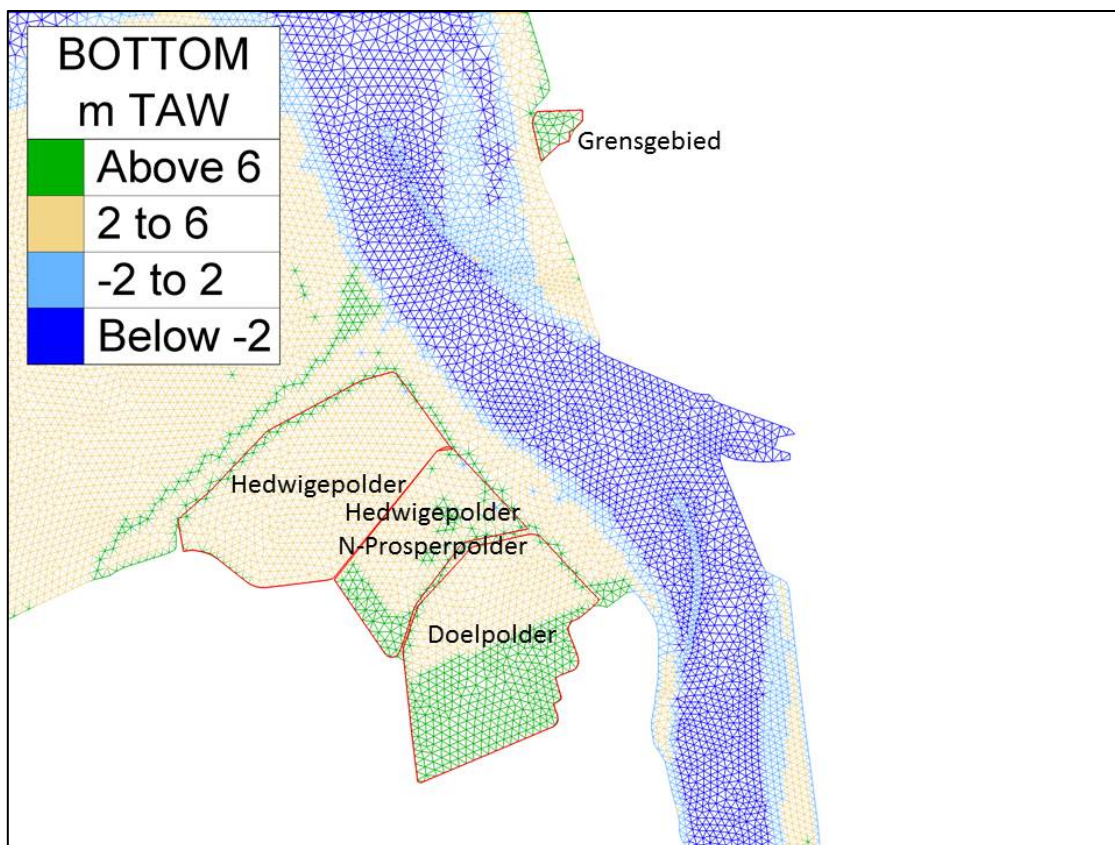


Figure 214 - Scaldis_v17_035 versus Sigma contour 04/2015: Grensgebied, Hedwigepolder en Doelpolder

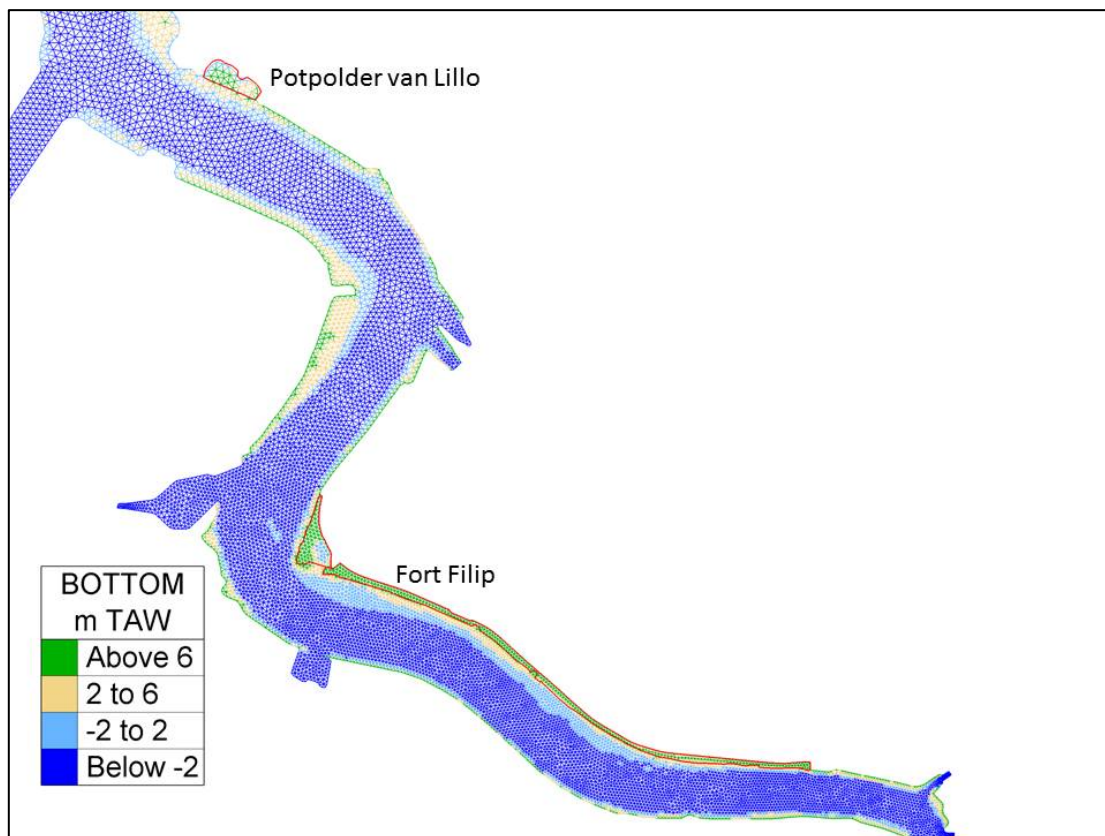


Figure 215 - Scaldis_v17_035 versus Sigma contour 04/2015: Potpolder van lillo en Fort Filip

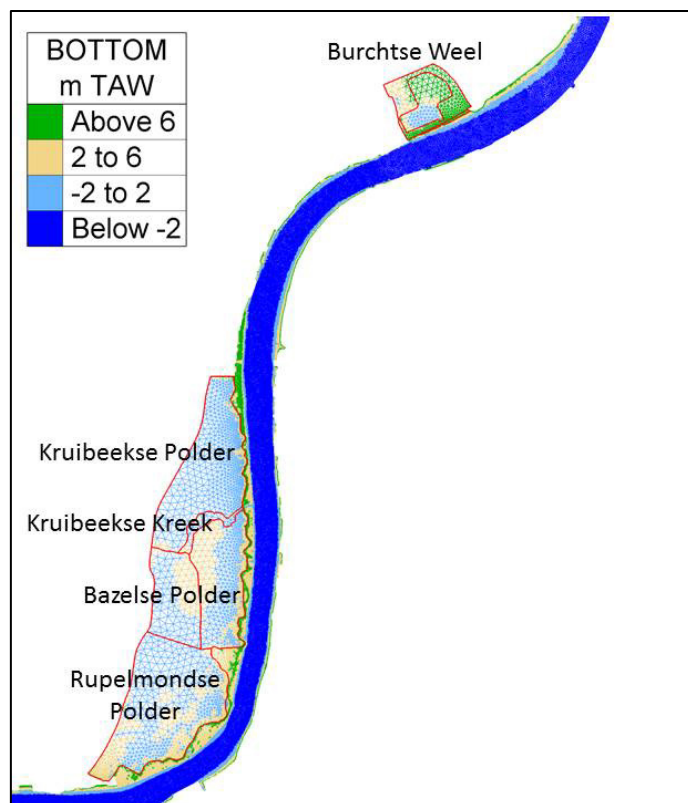


Figure 216 - Scaldis_v17_035 versus Sigma contour 04/2015: Burchtse Weel en KBR

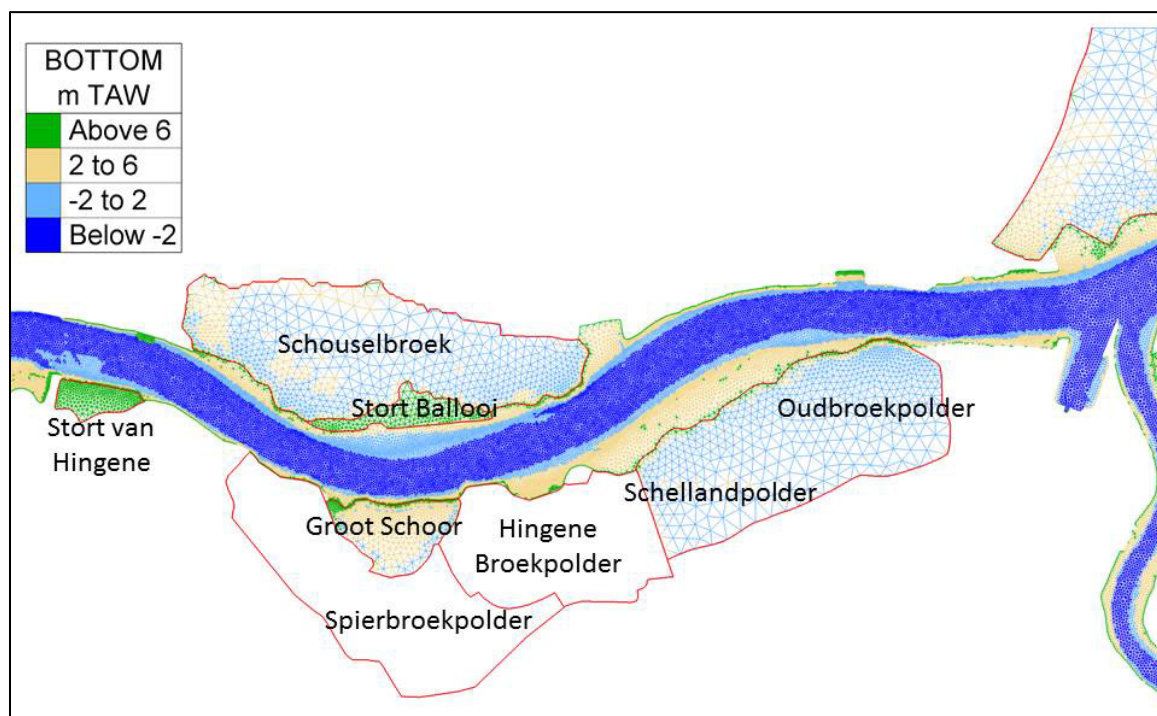


Figure 217 - Scaldis_v17_035 versus Sigma contour 04/2015: Oudbroekpolder, Schellandpolder, Hingene Broekpolder, Spierbroekpolder, Groot Schoor, Stort Hingene, Stort Ballooi en Schouselbroek

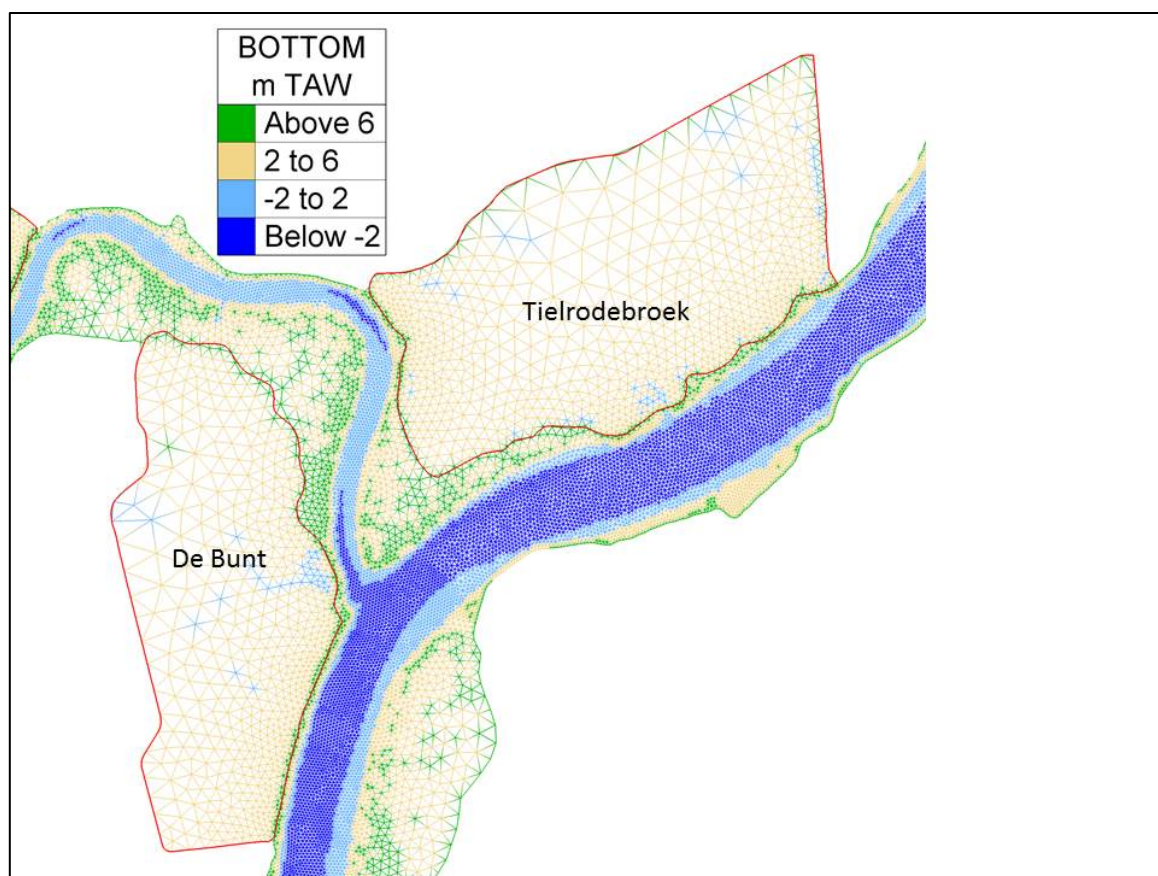


Figure 218 - Scaldis_v17_035 versus Sigma contour 04/2015: Tielrodebroek en De Bunt

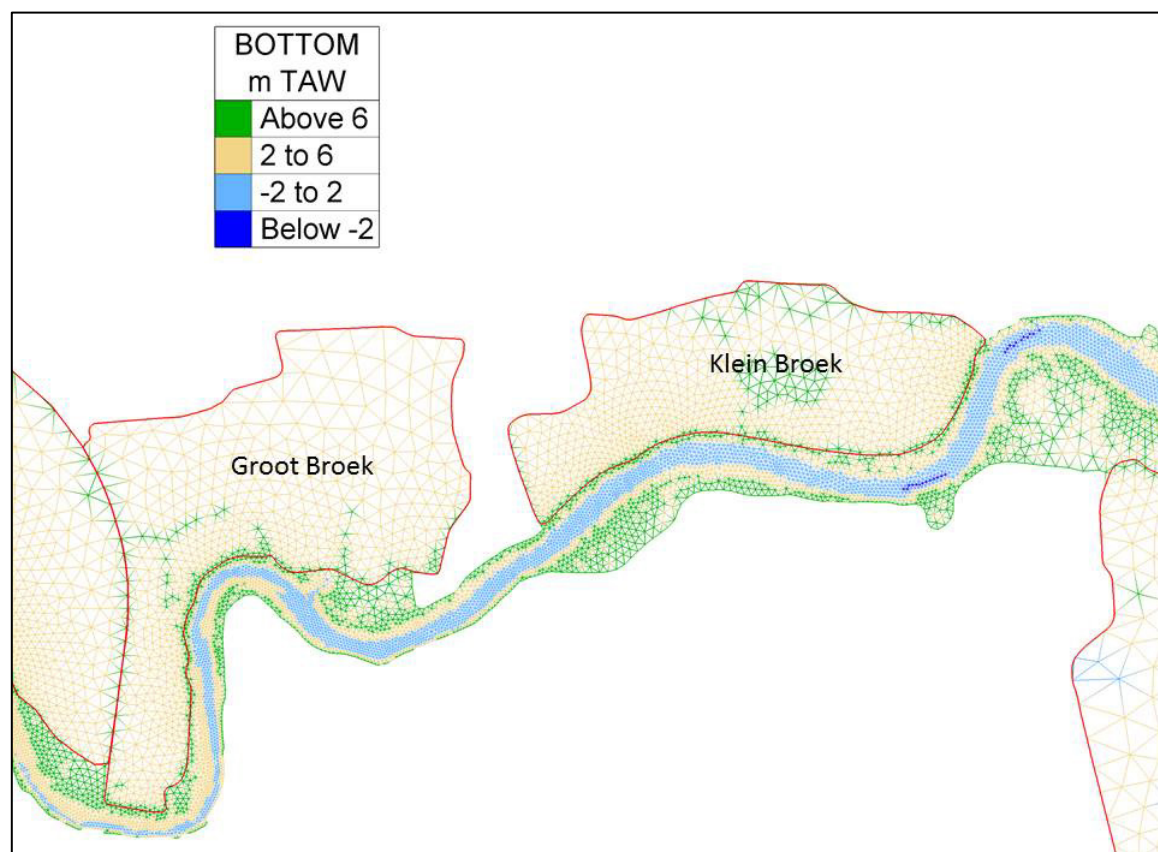


Figure 219 - Scaldis_v17_035 versus Sigma contour 04/2015: Klein Broek en Groot Broek

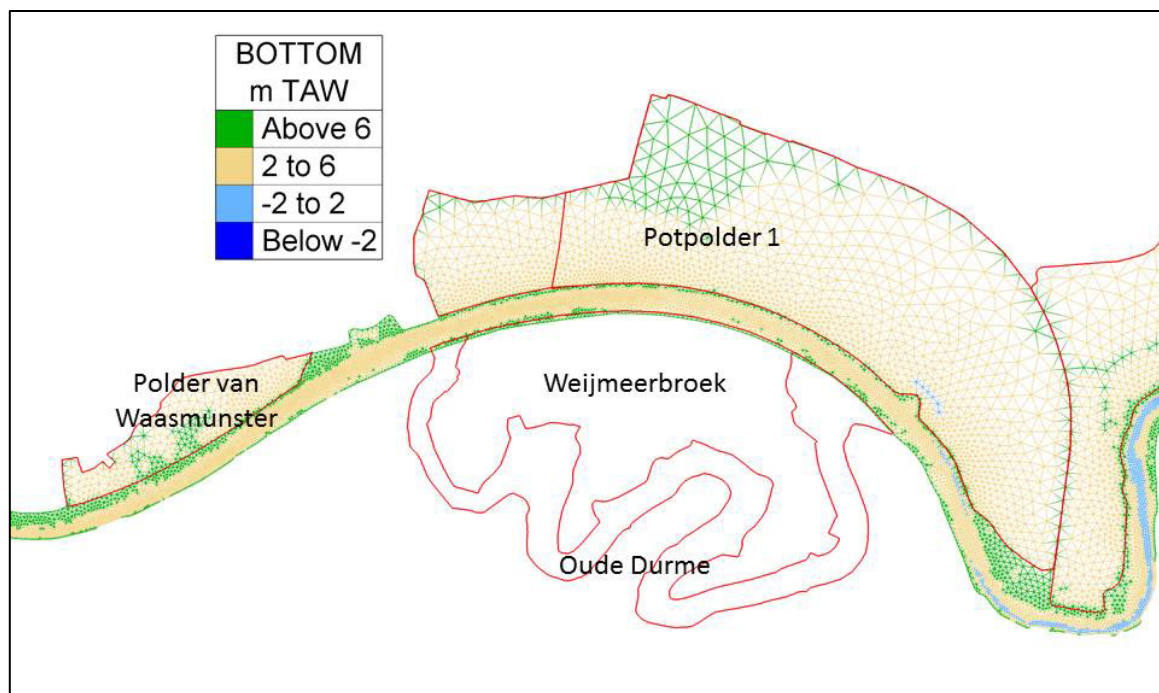


Figure 220 - Scaldis_v17_035 versus Sigma contour 04/2015: Potpolder I en Polder van Waasmunster

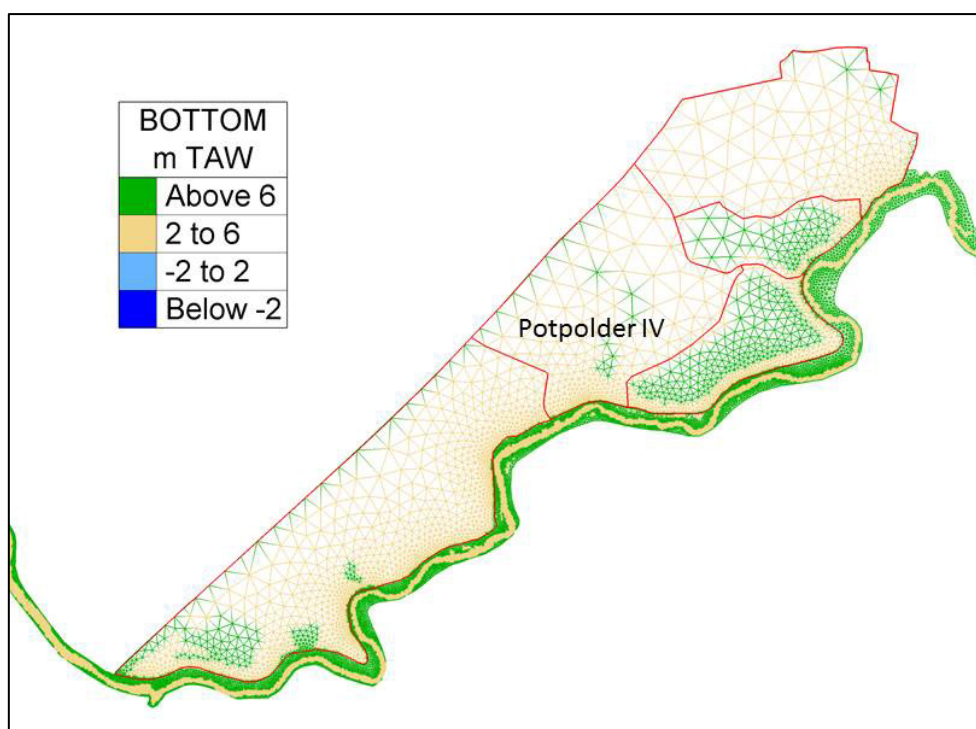


Figure 221 - Scaldis_v17_035 versus Sigma contour 04/2015: Potpolder IV

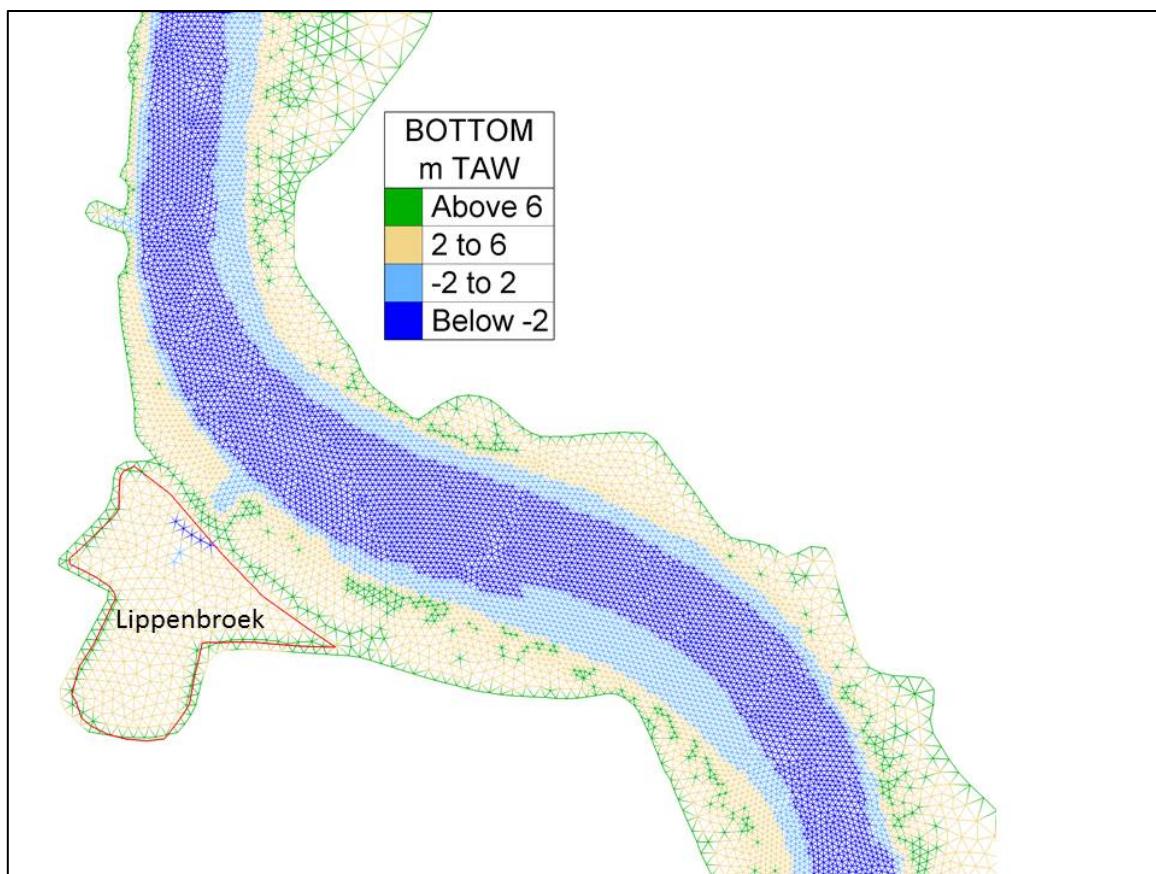


Figure 222 - Scaldis_v17_035 versus Sigma contour 04/2015: Lippenbroek

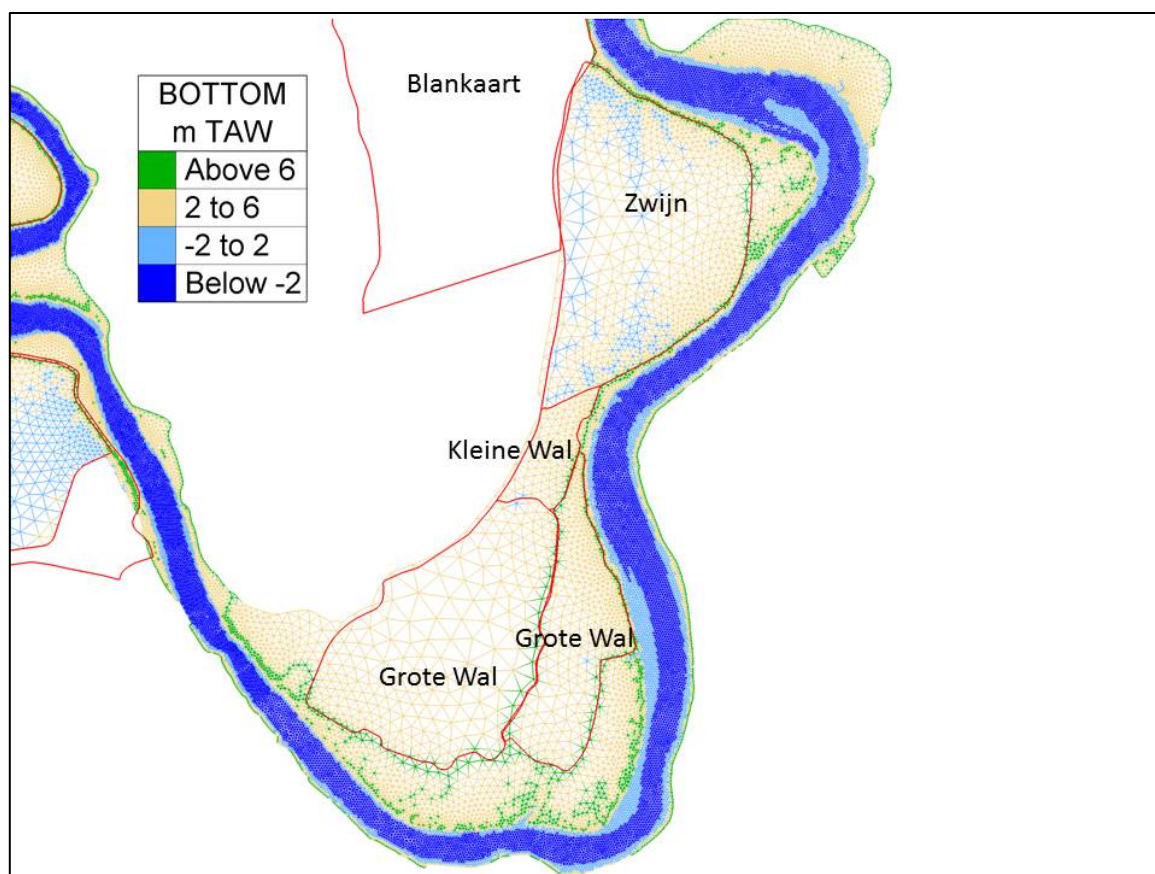


Figure 223 - Scaldis_v17_035 versus Sigma contour 04/2015: Blankaart, Zwijn, Grote Wal en Kleine Wal

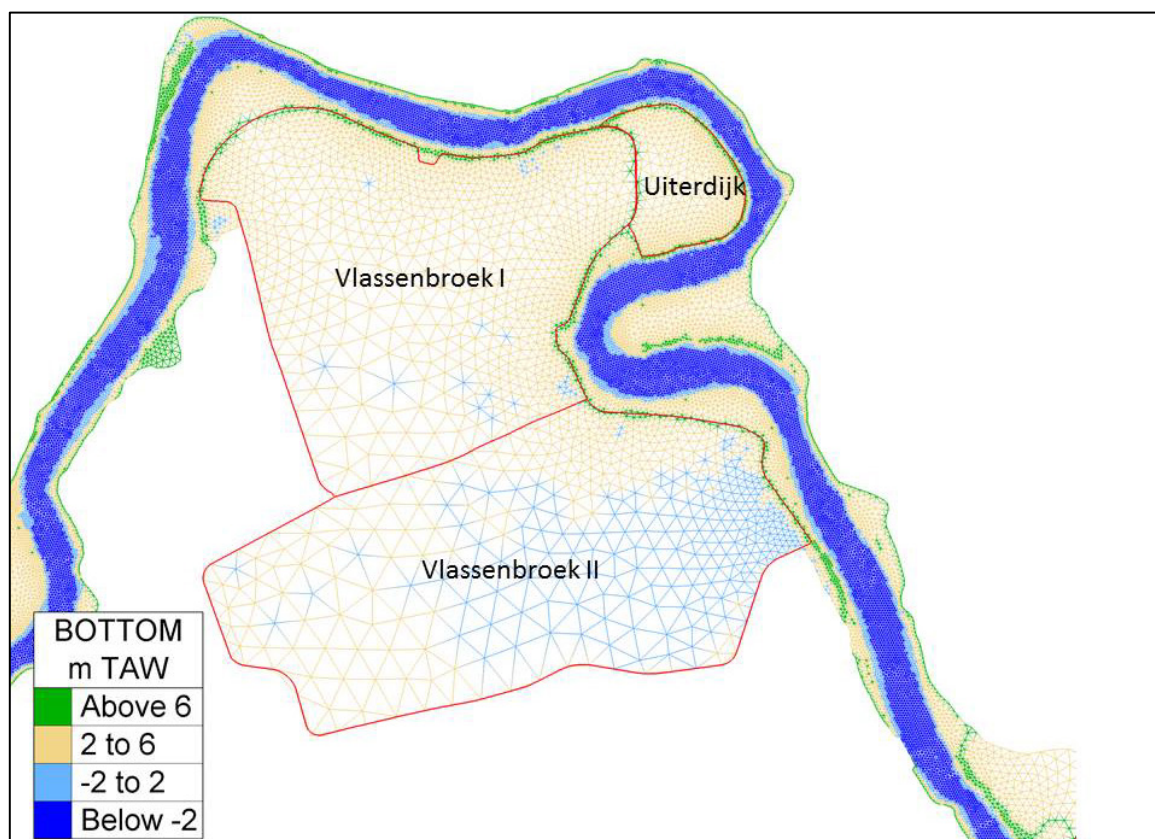


Figure 224 - Scaldis_v17_035 versus Sigma contour 04/2015: Uiterdijk, Vlassenbroek I en Vlassenbroek II

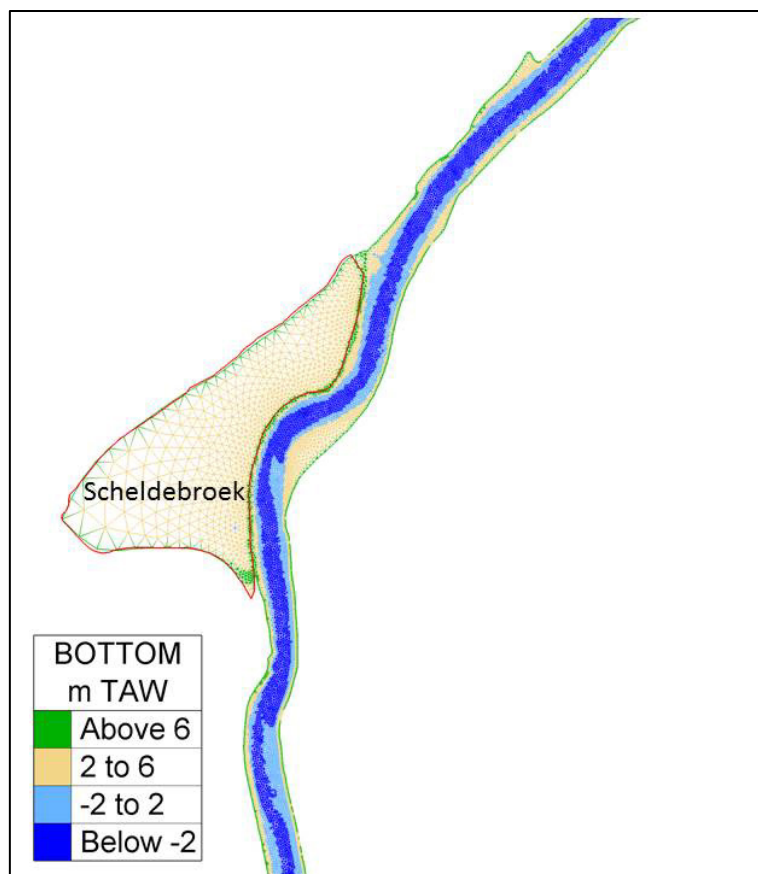


Figure 225 - Scaldis_v17_035 versus Sigma contour 04/2015: Scheldebroek

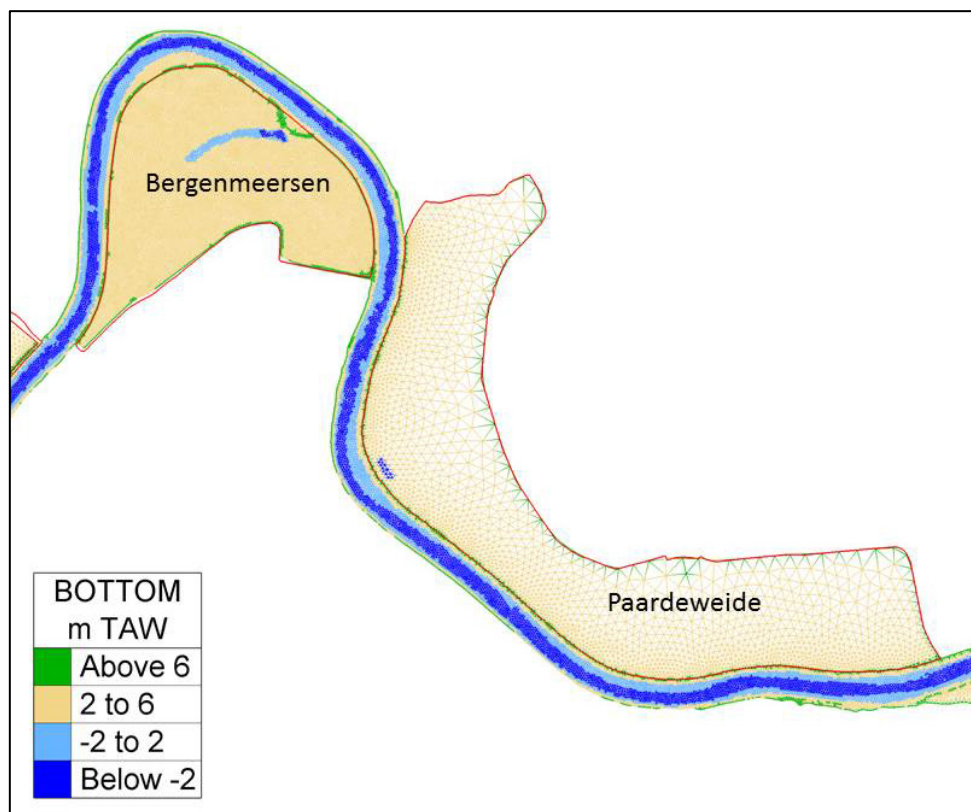


Figure 226 - Scaldis_v17_035 versus Sigma contour 04/2015: Paardeweide en Bergenmeersen

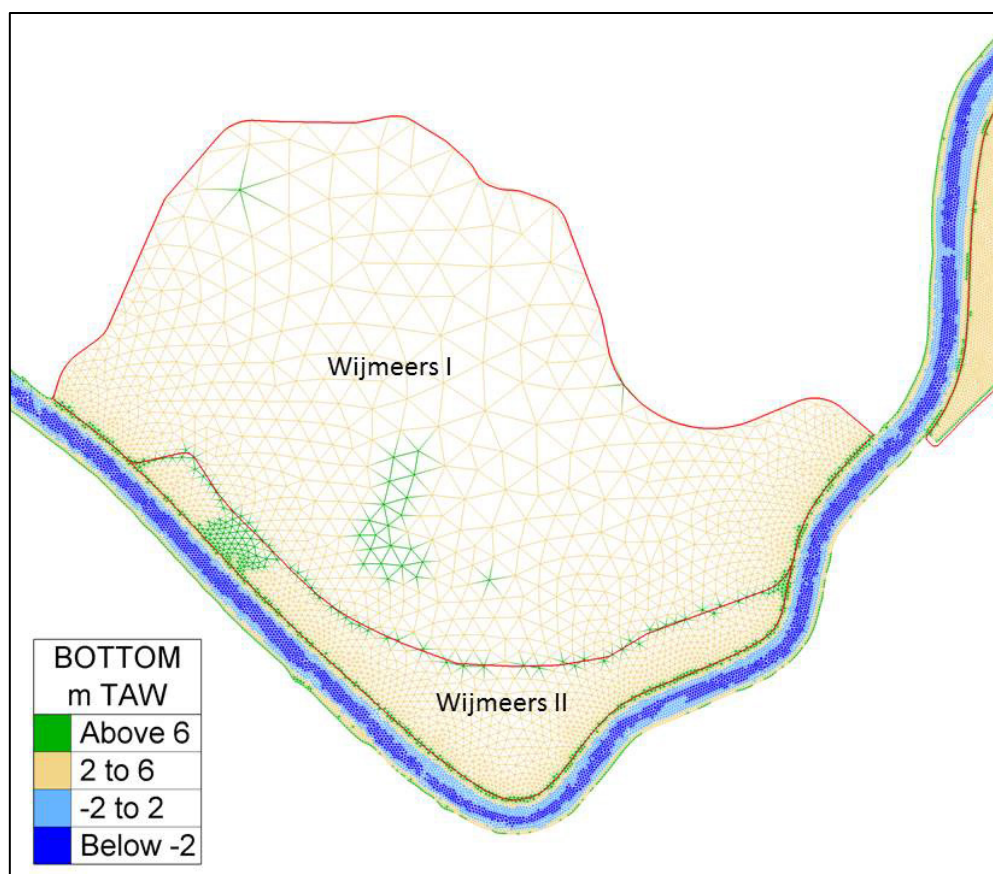


Figure 227 - Scaldis_v17_035 versus Sigma contour 04/2015: Wijmeers I en Wijmeers II

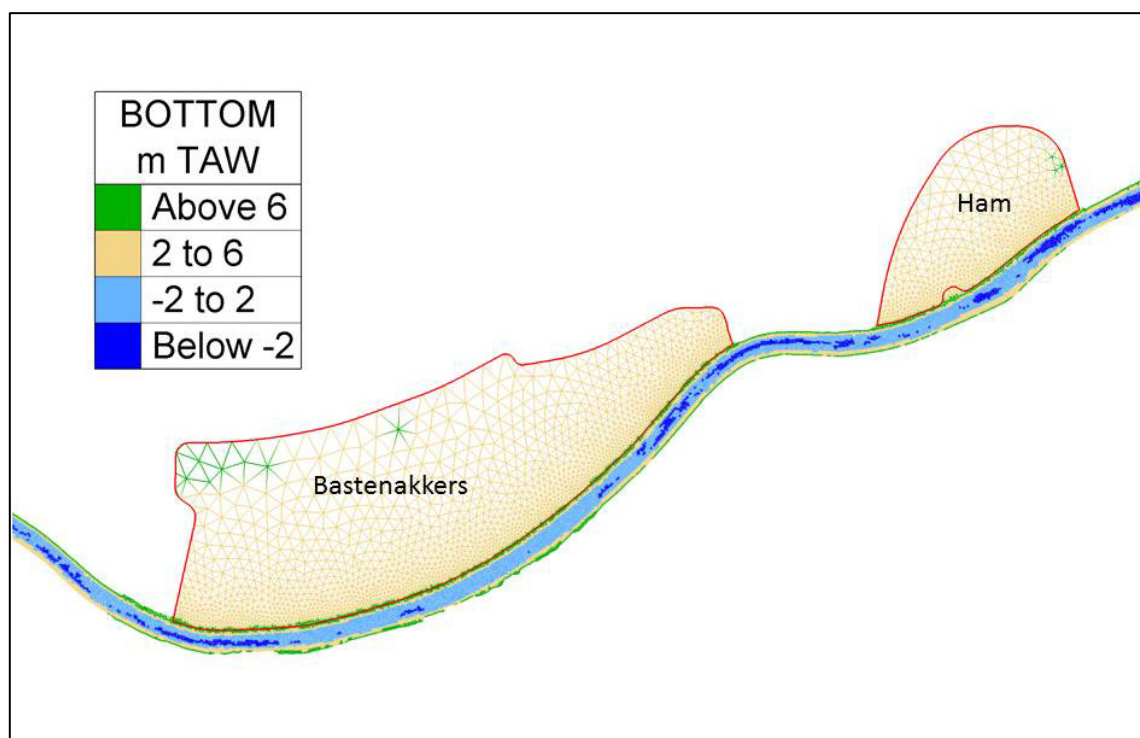


Figure 228 - Scaldis_v17_035 versus Sigma contour 04/2015: Bastenakkers en Ham

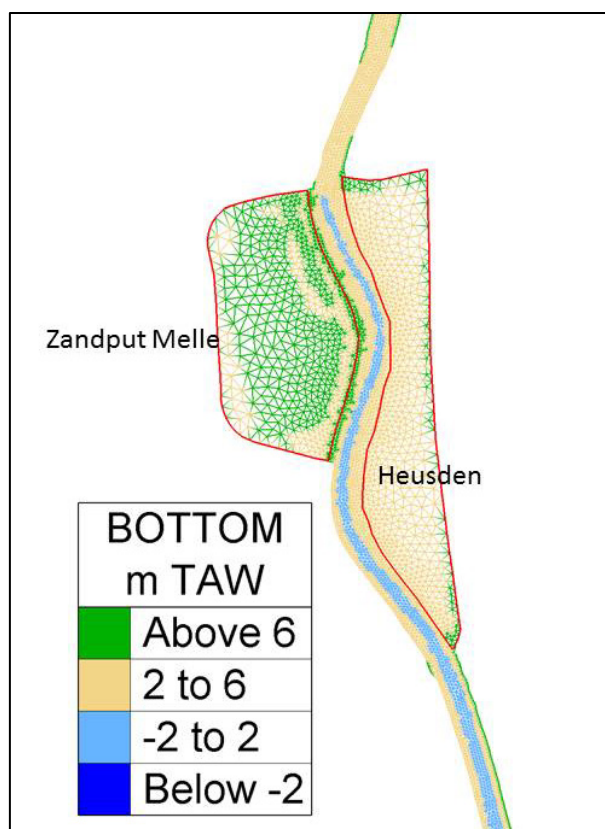


Figure 229 - Scaldis_v17_035 versus Sigma contour 04/2015: Zandput Melle en Heusden

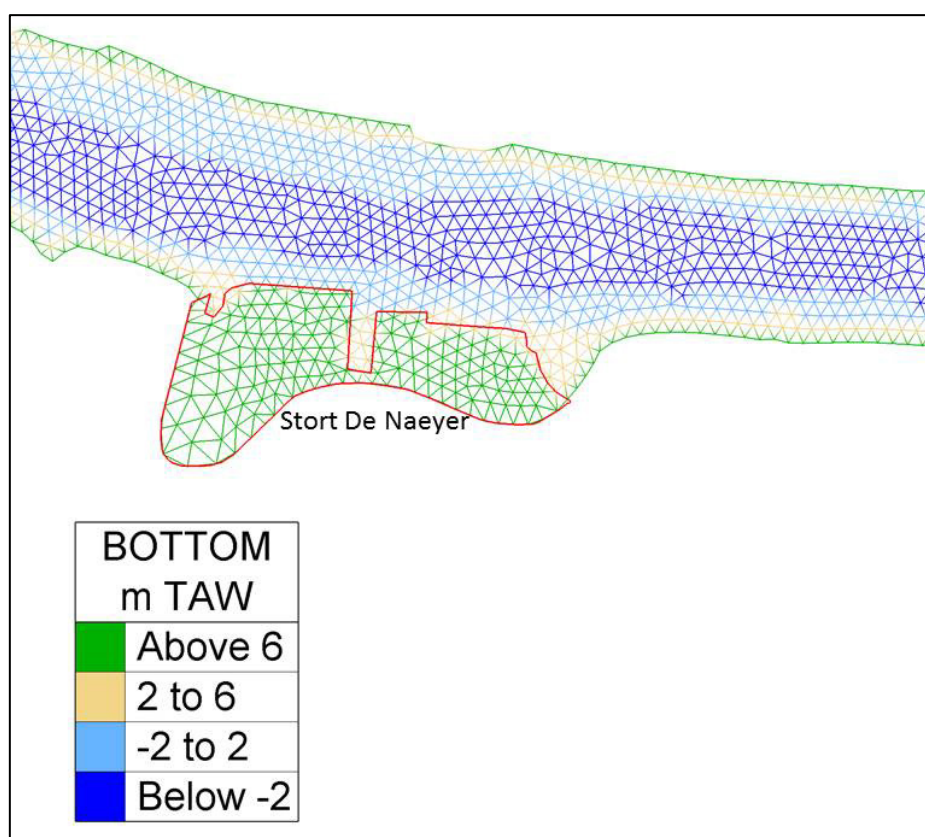


Figure 230 - Stort De Naeyer

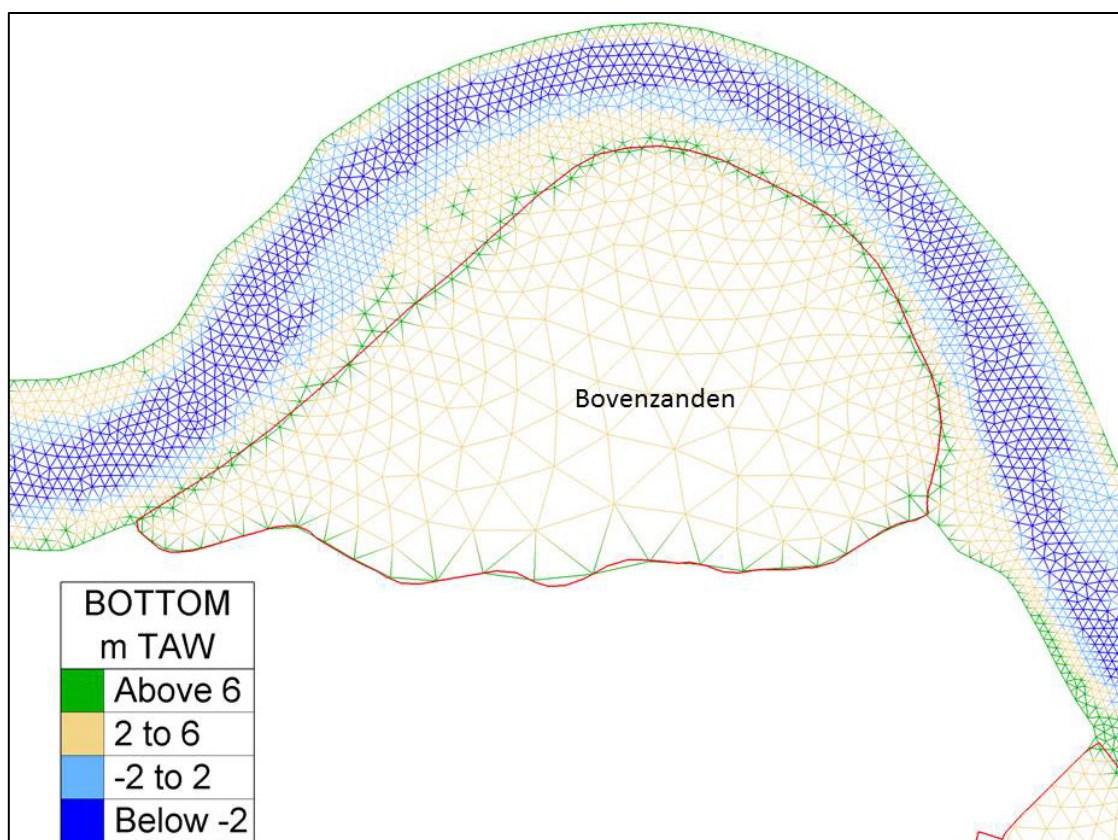


Figure 231 - Scaldis_v17_035 versus Sigma contour 04/2015: Bovenzanden

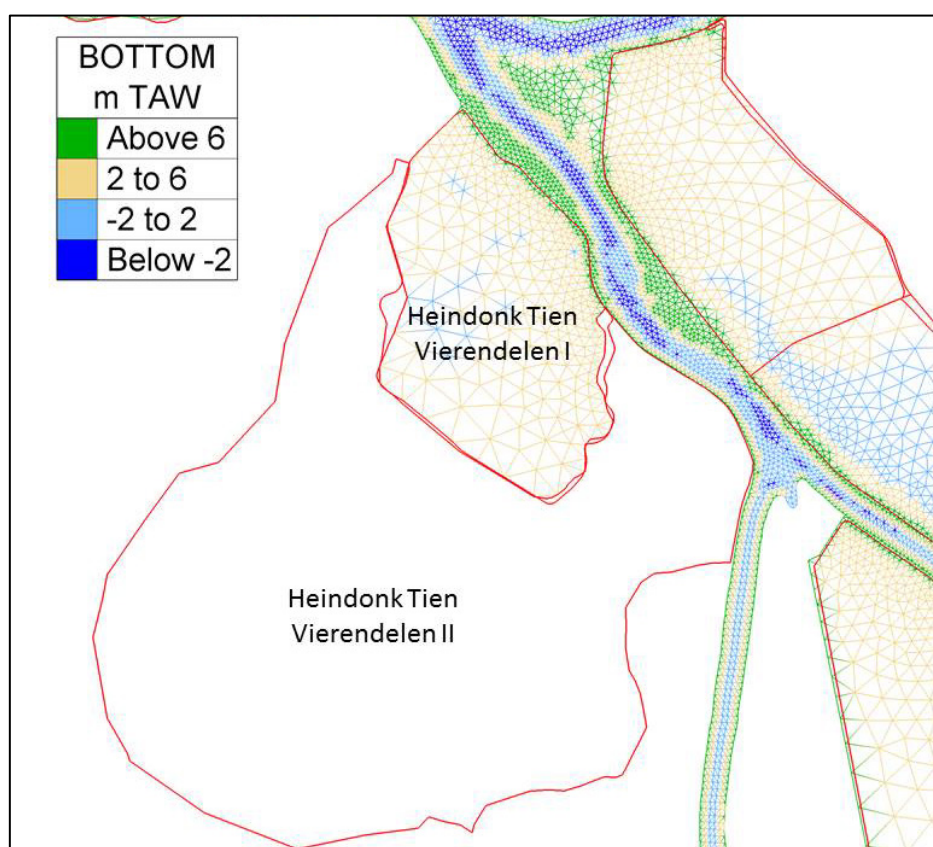


Figure 232 - Scaldis_v17_035 versus Sigma contour 04/2015: Heindonk Tien Vierendelen I en Heindonk Tien Vierendelen II

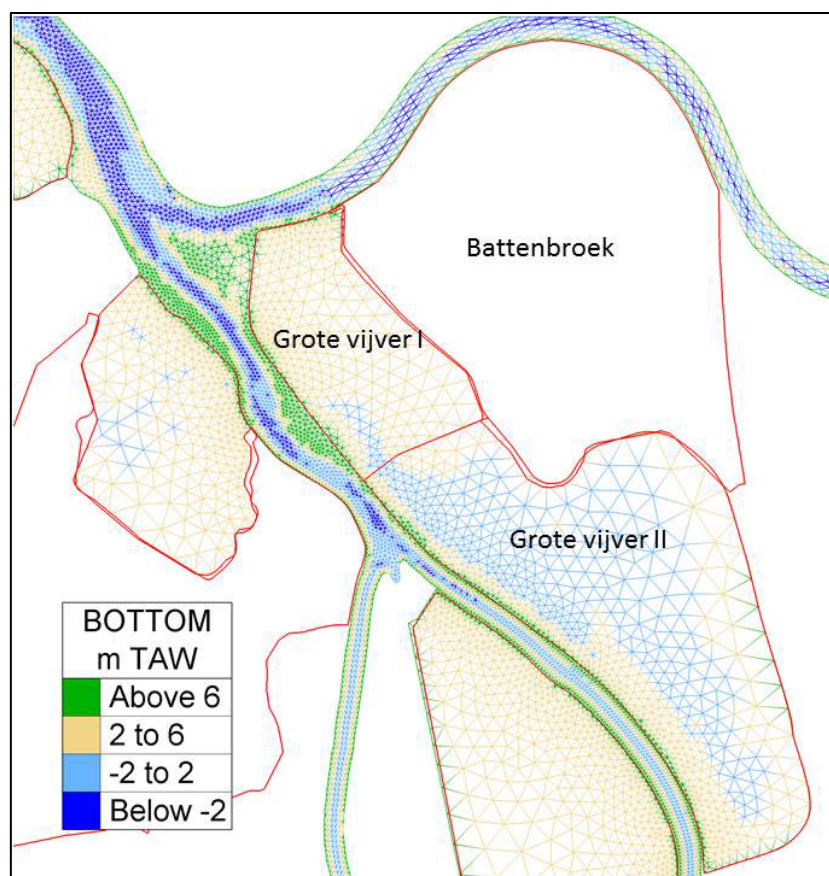


Figure 233 - Scaldis_v17_035 versus Sigma contour 04/2015: Grote Vijver I, Grote Vijver II en Battenbroek

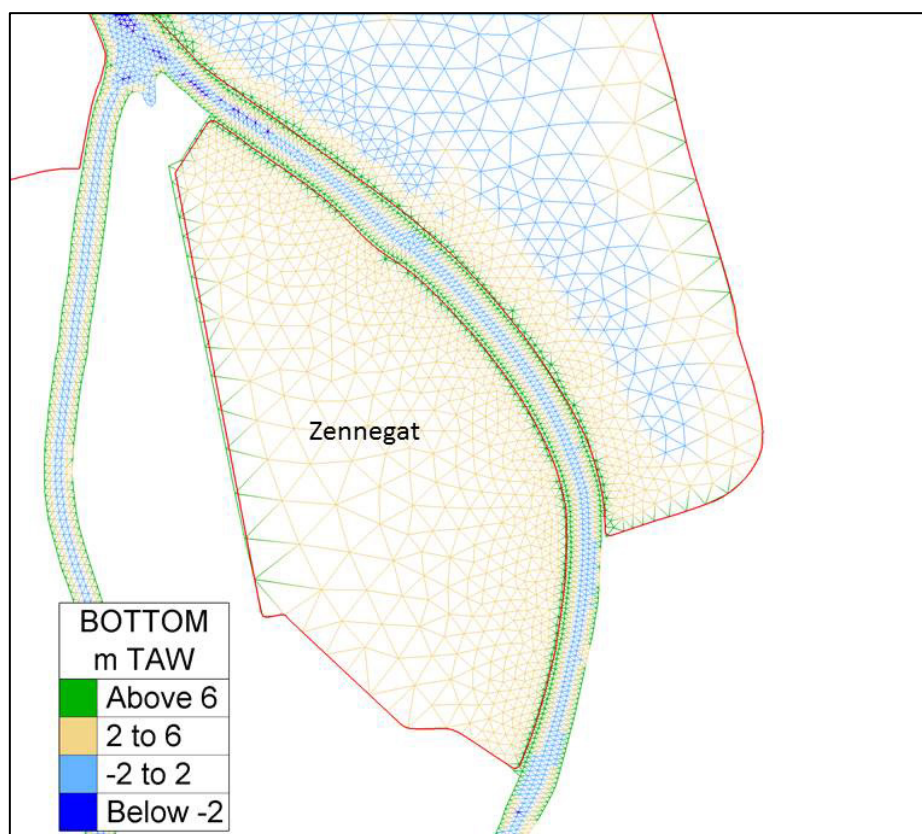


Figure 234 - Scaldis_v17_035 versus Sigma contour 04/2015: Zennegat

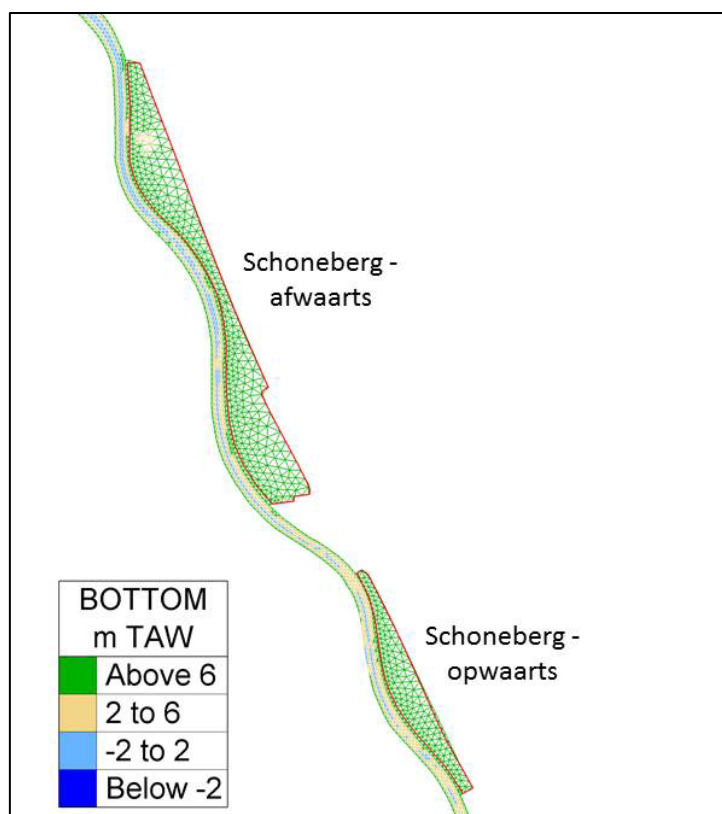


Figure 235 - Scaldis_v17_035 versus Sigma contour 04/2015: Schoneberg

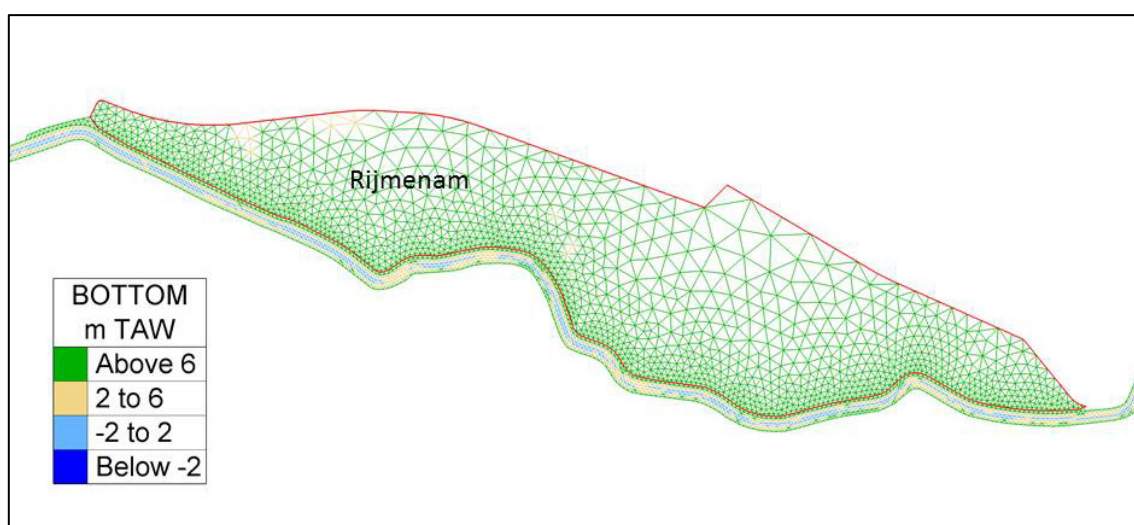


Figure 236 - Scaldis_v17_035 versus Sigma contour 04/2015: Rijmenam

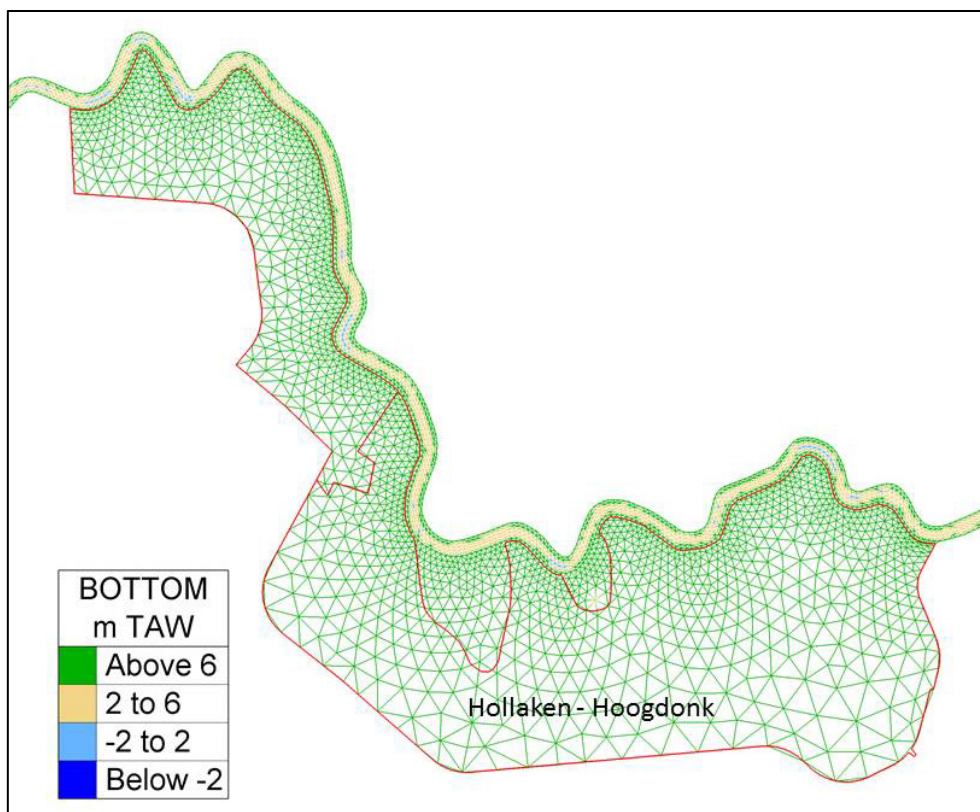


Figure 237 - Scaldis_v17_035 versus Sigma contour 04/2015: Hollaken-Hoogdonk

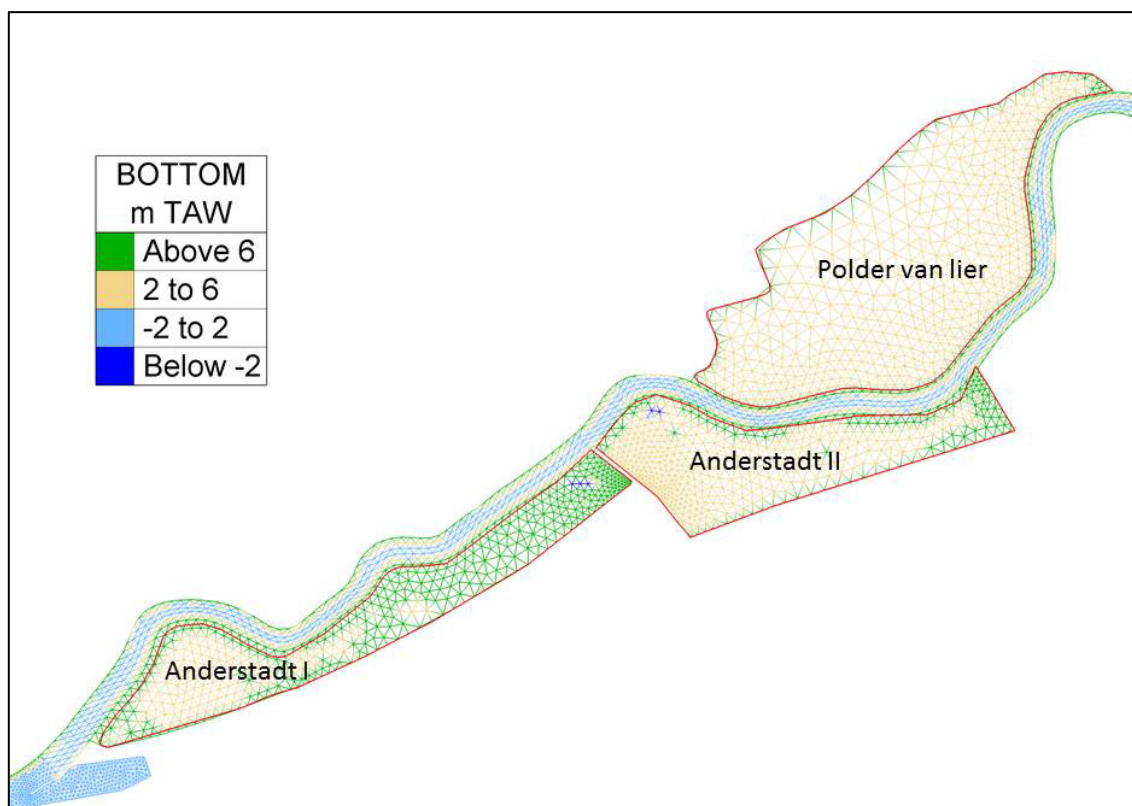


Figure 238 - Scaldis_v17_035 versus Sigma contour 04/2015: Polder van Lier, Anderstadt I en Anderstadt II

Appendix 1. Results of the model calibration

Water levels

Table 63. Statistical parameters for the water level time series (North sea and Western Scheldt)

Station	Complete Time Series		
	BIAS TS	RMSE TS	RMSE_0 TS
	[m]	[m]	[m]
Nieuwpoort	-0.01	0.09	0.09
Oostende	-0.04	0.10	0.09
Zeebrugge	-0.07	0.11	0.08
MP0 Wandelaar	0.00	0.08	0.08
MP1 A2B boei	-0.05	0.10	0.08
MP2 Appelzak	0.03	0.09	0.09
MP3 Bol van Heist	0.01	0.09	0.09
MP4 Scheur Wielingen	0.01	0.08	0.08
Vlakte van de Raan	0.00	0.08	0.08
Cadzand	0.04	0.10	0.09
Westkapelle	0.01	0.09	0.09
Vlissingen	0.01	0.09	0.09
Breskens	0.00	0.10	0.10
Borssele	0.02	0.11	0.10
Terneuzen	0.01	0.11	0.11
Overloop Hansweert	-0.01	0.10	0.10
Hansweert	0.00	0.10	0.10
Walsoorden	0.00	0.11	0.11
Baalhoek	0.01	0.12	0.11
Bath	0.04	0.12	0.11
Total*	0.00	0.10	0.10

*for the calculation of total bias, RMSE and RMSE_0 the number of data points at each station is taken into account

Table 64. Statistical parameters for the water level time series (Eastern Scheldt)

Station	Complete Time Series		
	BIAS TS	RMSE TS	RMSE_0 TS
	[m]	[m]	[m]
Oosterschelde 14	0.00	0.09	0.09
Oosterschelde 11	-0.01	0.09	0.09
Oosterschelde 4	0.01	0.09	0.09
Roompot buiten	0.02	0.10	0.09
Roompot binnen	0.03	0.09	0.08
Sluis Kats	0.04	0.08	0.07
Stavenisse	0.05	0.10	0.08
Krammersluis	0.05	0.11	0.10
Yerseke	0.02	0.09	0.08
Bergsediepsluis	0.05	0.10	0.09
Marollegat	0.05	0.11	0.10
Total	0.03	0.10	0.09

Table 65. Statistical parameters for the water level time series (Lower Sea Scheldt)

Station	Complete Time Series		
	BIAS TS	RMSE TS	RMSE_0 TS
	[m]	[m]	[m]
Zandvliet	0.07	0.14	0.12
Prosperpolder	0.05	0.12	0.12
Liefkenshoek	0.05	0.13	0.12
Kallosluis	0.05	0.13	0.12
Antwerpen	0.04	0.15	0.14
Hemiksem	0.08	0.15	0.13
Total	0.05	0.14	0.13

Table 66. Statistical parameters for the water level time series (Upper Sea Scheldt)

Station	Complete Time Series		
	BIAS TS	RMSE TS	RMSE_0 TS
	[m]	[m]	[m]
Schelle	0.01	0.15	0.15
Temse	0.01	0.13	0.13
Tielrode	0.05	0.14	0.13
StAmands	0.03	0.14	0.13
Dendermonde	-0.04	0.13	0.12
Schoonaarde	-0.05	0.12	0.11
Wetteren	-0.04	0.13	0.13
Melle	-0.10	0.18	0.15
Total	-0.02	0.14	0.13

Table 67. Statistical parameters for the water level time series (Rupel basin and Durme)

Station	Complete Time Series		
	BIAS TS	RMSE TS	RMSE_0 TS
	[m]	[m]	[m]
Boom	0.01	0.14	0.14
Walem	0.01	0.13	0.13
Duffel-sluis	0.00	0.14	0.14
Lier Molbrug	0.01	0.13	0.13
Lier Maasfort	-0.09	0.13	0.10
Emblem	-0.12	0.15	0.09
Kessel	-0.03	0.12	0.12
Mechelen lock	0.11	0.21	0.18
Hombeek	0.07	0.24	0.23
Waasmunster*			
Total	0.00	0.16	0.15

*low waters at Waasmunster are not accurate in the model probably because of differences between the measured and modeled bathymetry

Table 68. Statistical parameters for high waters (North sea and Western Scheldt)

Station	HW					
	BIAS HW	RMSE HW	RMSE_0 HW	BIAS HW	RMSE HW	RMSE_0 HW
	[m]	[m]	[m]	[min]	[min]	[min]
Nieuwpoort	-0.05	0.07	0.05	1	11	11
Oostende	-0.02	0.05	0.05	0	14	14
Zeebrugge	-0.11	0.12	0.05	-3	12	12
MP0 Wandelaar	-0.01	0.04	0.04	-3	9	9
MP1 A2B boei	-0.07	0.08	0.04	-4	11	11
MP2 Appelzak	-0.03	0.08	0.07	-3	10	10
MP3 Bol van Heist	-0.01	0.05	0.05	-7	11	9
MP4 Scheur Wielingen	-0.01	0.06	0.05	-4	8	7
Vlakte van de Raan	-0.04	0.07	0.06	-4	8	7
Cadzand	-0.03	0.09	0.08	-3	8	8
Westkapelle	-0.03	0.09	0.08	1	8	8
Vlissingen	-0.03	0.08	0.07	-3	8	7
Breskens	-0.05	0.09	0.07	-6	8	6
Borssele	-0.03	0.08	0.08	-6	11	8
Terneuzen	-0.02	0.08	0.07	-6	10	7
Overloop Hansweert	-0.05	0.10	0.08	-8	12	9
Hansweert	-0.02	0.09	0.09	-7	10	7
Walsoorden	-0.04	0.10	0.09	-6	9	6
Baalhoek	-0.02	0.09	0.09	-7	11	8
Bath	0.03	0.11	0.10	-6	10	8
Total	-0.03	0.08	0.07	-4	10	9

Table 69. Statistical parameters for high waters (Eastern Scheldt)

Station	HW					
	BIAS HW	RMSE HW	RMSE_0 HW	BIAS HW	RMSE HW	RMSE_0 HW
	[m]	[m]	[m]	[min]	[min]	[min]
Oosterschelde 14	-0.07	0.10	0.08	-2	9	9
Oosterschelde 11	-0.08	0.12	0.09	-8	11	7
Oosterschelde 4	-0.10	0.16	0.13	8	19	17
Roompot buiten	-0.01	0.09	0.09	-2	17	17
Roompot binnen	0.02	0.05	0.05	-2	7	7
Sluis Kats	0.02	0.06	0.06	-2	7	7
Stavenisse	0.05	0.08	0.06	1	9	9
Krammersluis	0.10	0.11	0.06	-4	14	13
Yerseke	-0.02	0.08	0.07	-5	9	7
Bergsediepsluis	0.02	0.08	0.08	-6	11	9
Marollegat	0.02	0.08	0.08	-6	10	7
Total	0.00	0.10	0.08	-3	12	10

Table 70. Statistical parameters for high waters (Lower Sea Scheldt)

Station	HW					
	BIAS HW	RMSE HW	RMSE_0 HW	BIAS HW	RMSE HW	RMSE_0 HW
	[m]	[m]	[m]	[min]	[min]	[min]
Zandvliet	0.09	0.13	0.10	-6	10	8
Prosperpolder	0.05	0.11	0.10	-7	11	8
Liefkenshoek	0.05	0.11	0.10	-6	12	10
Kallosluis	0.06	0.12	0.10	-6	12	11
Antwerpen	0.06	0.11	0.10	-7	13	11
Hemiksem	0.08	0.13	0.10	-10	13	9
Total	0.07	0.12	0.10	-7	12	9

Table 71. Statistical parameters for high waters (Upper Sea Scheldt)

Station	HW					
	BIAS HW	RMSE HW	RMSE_0 HW	BIAS HW	RMSE HW	RMSE_0 HW
	[m]	[m]	[m]	[min]	[min]	[min]
Schelle	0.04	0.11	0.11	-10	13	8
Temse	0.02	0.11	0.11	-9	12	8
Tielrode	0.05	0.12	0.11	-8	12	9
StAmands	0.05	0.11	0.10	-10	14	9
Dendermonde	-0.07	0.12	0.10	-9	11	6
Schoonaarde	-0.07	0.12	0.10	-8	10	6
Wetteren	-0.07	0.14	0.12	-5	8	7
Melle	-0.09	0.15	0.12	-4	7	6
Total	-0.02	0.12	0.11	-8	11	8

Table 72. Statistical parameters for high waters (Rupel basin and Durme)

Station	HW					
	BIAS HW	RMSE HW	RMSE_0 HW	BIAS HW	RMSE HW	RMSE_0 HW
	[m]	[m]	[m]	[min]	[min]	[min]
Boom	0.01	0.10	0.10	-10	14	9
Walem	0.01	0.11	0.11	-9	12	7
Duffel-sluis	0.08	0.12	0.09	-15	17	6
Lier Molbrug	-0.13	0.18	0.12	-12	13	5
Lier Maasfort	-0.17	0.21	0.13	-7	10	7
Emblem	-0.29	0.29	0.02	-3	6	5
Kessel	-0.19	0.20	0.04	-5	7	5
Mechelen lock	0.01	0.10	0.10	-5	9	8
Hombeek	0.08	0.12	0.09	4	8	7
Waasmunster	-0.08	0.22	0.21	-10	13	8
Total	-0.02	0.15	0.12	-8	12	7

Table 73. Statistical parameters for low waters (North sea and Western Scheldt)

Station	LW					
	BIAS LW	RMSE LW	RMSE_0 LW	BIAS LW	RMSE LW	RMSE_0 LW
	[m]	[m]	[m]	[min]	[min]	[min]
Nieuwpoort	0.01	0.05	0.05	-5	12	11
Oostende	-0.06	0.08	0.05	-2	12	12
Zeebrugge	-0.04	0.08	0.06	-2	10	9
MP0 Wandelaar	-0.01	0.06	0.06	-4	8	7
MP1 A2B boei	-0.04	0.07	0.06	-2	9	9
MP2 Appelzak	0.07	0.09	0.06	1	7	7
MP3 Bol van Heist	0.01	0.06	0.06	-1	9	9
MP4 Scheur Wielingen	0.01	0.06	0.06	-2	8	8
Vlakte van de Raan	-0.03	0.06	0.06	-3	8	7
Cadzand	0.05	0.08	0.06	0	7	7
Westkapelle	-0.02	0.07	0.06	4	11	10
Vlissingen	0.01	0.07	0.06	-5	9	8
Breskens	0.00	0.07	0.07	-6	9	7
Borssele	0.03	0.07	0.07	-5	8	6
Terneuzen	0.02	0.07	0.07	-5	11	10
Overloop Hansweert	-0.02	0.07	0.07	-3	7	6
Hansweert	0.01	0.07	0.07	-3	7	6
Walsoorden	0.01	0.07	0.07	-5	9	8
Baalhoek	0.00	0.08	0.08	-5	10	8
Bath	0.05	0.09	0.08	-4	8	7
Total	0.00	0.07	0.06	-3	9	8

Table 74. Statistical parameters for low waters (Eastern Scheldt)

Station	LW					
	BIAS LW	RMSE LW	RMSE_0 LW	BIAS LW	RMSE LW	RMSE_0 LW
	[m]	[m]	[m]	[min]	[min]	[min]
Oosterschelde 14	-0.01	0.07	0.07	-14	17	10
Oosterschelde 11	-0.01	0.07	0.07	-7	9	6
Oosterschelde 4	0.02	0.08	0.07	-5	10	9
Roompot buiten	0.01	0.07	0.07	-9	12	7
Roompot binnen	0.00	0.06	0.06	16	19	11
Sluis Kats	0.03	0.07	0.06	10	20	18
Stavenisse	0.05	0.09	0.07	13	19	13
Krammersluis	0.07	0.11	0.08	15	30	26
Yerseke	0.05	0.09	0.07	9	13	9
Bergsediepsluis	0.09	0.11	0.07	5	10	8
Marollegat	0.09	0.12	0.07	2	9	9
Total	0.04	0.09	0.07	3	16	13

Table 75. Statistical parameters for low waters (Lower Sea Scheldt)

Station	LW					
	BIAS LW	RMSE LW	RMSE_0 LW	BIAS LW	RMSE LW	RMSE_0 LW
	[m]	[m]	[m]	[min]	[min]	[min]
Zandvliet	0.06	0.09	0.07	-3	9	8
Prosperpolder	0.03	0.08	0.07	-2	9	8
Liefkenshoek	0.06	0.09	0.07	-2	9	8
Kallosluis	0.06	0.10	0.07	0	7	7
Antwerpen	0.05	0.09	0.08	-4	8	7
Hemiksem	0.08	0.11	0.07	-5	9	8
Total	0.06	0.09	0.07	-3	9	8

Table 76. Statistical parameters for low waters (Upper Sea Scheldt)

Station	LW					
	BIAS LW	RMSE LW	RMSE_0 LW	BIAS LW	RMSE LW	RMSE_0 LW
	[m]	[m]	[m]	[min]	[min]	[min]
Schelle	0.01	0.08	0.08	-8	11	7
Temse	0.01	0.07	0.07	-3	8	7
Tielrode	0.06	0.09	0.07	-2	8	8
StAmands	0.02	0.07	0.06	-4	9	8
Dendermonde	-0.06	0.10	0.08	-4	9	8
Schoonaarde	-0.08	0.12	0.09	-6	9	7
Wetteren	-0.03	0.15	0.14	-4	8	7
Melle	-0.11	0.19	0.16	-2	17	17
Total	-0.02	0.12	0.10	-4	10	9

Table 77. Statistical parameters for low waters (Rupel basin and Durme)

Station	LW					
	BIAS LW	RMSE LW	RMSE_0 LW	BIAS LW	RMSE LW	RMSE_0 LW
	[m]	[m]	[m]	[min]	[min]	[min]
Boom	-0.01	0.08	0.08	-7	11	9
Walem	-0.01	0.08	0.08	-5	9	7
Duffel-sluis	0.02	0.06	0.06	-2	8	8
Lier Molbrug	0.02	0.04	0.03	2	11	11
Lier Maasfort	-0.10	0.12	0.07	2	7	7
Emblem	-0.15	0.16	0.05	5	10	9
Kessel	0.02	0.07	0.07	19	21	9
Mechelen lock	0.33	0.34	0.08	7	9	6
Hombeek	0.00	0.09	0.09	59	67	33
Waasmunster*						
Total	0.01	0.14	0.07	7	22	12

*low waters at Waasmunster are not accurate in the model probably because of differences between the measured and modeled bathymetry

Table 78. Harmonic analysis: Amplitude M2 (North sea and Western Scheldt)

Amplitude M2	Measurement		Scaldis_039_0	
WL Station	Value	Error	Value	Error
Nieuwpoort	1.90	0.01	1.90	0.01
Oostende	1.76	0.01	1.80	0.01
Zeebrugge	1.64	0.01	1.65	0.01
MP0 Wandelaar	1.59	0.01	1.62	0.01
MP1 A2B boei	1.64	0.01	1.66	0.01
MP2 Appelzak	1.65	0.01	1.64	0.01
MP3 Bol van Heist	1.61	0.01	1.63	0.01
MP4 Scheur Wielingen	1.59	0.01	1.61	0.01
Vlakte van de Raan	1.47	0.01	1.49	0.01
Cadzand	1.66	0.01	1.65	0.01
Westkapelle	1.51	0.01	1.56	0.01
Vlissingen	1.71	0.01	1.72	0.01
Breskens	1.71	0.01	1.71	0.01
Borssele	1.80	0.01	1.79	0.01
Terneuzen	1.84	0.01	1.85	0.01
Overloop Hansweert	1.91	0.02	1.92	0.01
Hansweert	1.96	0.02	1.96	0.02
Walsoorden	2.00	0.02	1.99	0.02
Baalhoek	2.05	0.02	2.05	0.02
Bath	2.11	0.02	2.09	0.02

Table 79. Harmonic analysis: Amplitude M2 (Eastern Scheldt)

Amplitude M2	Measurement		Scaldis_039_0	
WL Station	Value	Error	Value	Error
Oosterschelde 14	1.18	0.01	1.19	0.01
Oosterschelde 11	1.29	0.01	1.31	0.01
Oosterschelde 4	1.29	0.01	1.30	0.01
Roompot buiten	1.33	0.01	1.36	0.01
Roompot binnen	1.16	0.01	1.17	0.01
Sluis Kats	1.33	0.01	1.34	0.01
Stavenisse	1.33	0.01	1.32	0.01
Krammersluis	1.37	0.01	1.36	0.01
Yerseke	1.42	0.01	1.42	0.01
Bergsediepsluis	1.45	0.01	1.45	0.01
Marollegat	1.47	0.01	1.47	0.01

Table 80. Harmonic analysis: Amplitude M2 (Lower Sea Scheldt)

Amplitude M2	Measurement		Scaldis_039_0	
WL Station	Value	Error	Value	Error
Zandvliet	2.13	0.02	2.13	0.02
Prosperpolder	2.12	0.02	2.12	0.02
Liefkenshoek	2.18	0.02	2.17	0.02
Kallosluis	2.22	0.02	2.20	0.02
Antwerpen	2.25	0.02	2.23	0.02
Hemiksem	2.28	0.02	2.26	0.02

Table 81. Harmonic analysis: Amplitude M2 (Upper Sea Scheldt)

Amplitude M2	Measurement		Scaldis_039_0	
WL Station	Value	Error	Value	Error
Schelle	2.26	0.02	2.25	0.02
Temse	2.23	0.02	2.22	0.02
Tielrode	2.23	0.02	2.20	0.02
StAmands	2.10	0.02	2.08	0.02
Dendermonde	1.69	0.02	1.66	0.02
Schoonaarde	1.32	0.02	1.33	0.02
Wetteren	1.15	0.02	1.15	0.02
Melle	1.11	0.02	1.12	0.02

Table 82. Harmonic analysis: Amplitude M2 (Rupel basin)

Amplitude M2	Measurement		Scaldis_039_0	
WL Station	Value	Error	Value	Error
Boom	2.22	0.02	2.20	0.02
Walem	2.12	0.02	2.11	0.02
Duffel-sluis	1.75	0.02	1.74	0.02
Lier Molbrug	1.15	0.02	1.07	0.01
Lier Maasfort	0.86	0.01	0.85	0.01
Emblem	0.71	0.01	0.71	0.01
Kessel	0.56	0.01	0.48	0.01
Mechelen lock	1.93	0.02	1.80	0.02
Hombeek	1.48	0.02	1.43	0.02

Table 83. Harmonic analysis: Phase M2 (North sea and Western Scheldt)

Phase M2	Measurement		Scaldis_039_0	
WL Station	Value	Error	Value	Error
Nieuwpoort	36	0	34	0
Oostende	40	0	39	0
Zeebrugge	49	0	47	0
MP0 Wandelaar	45	0	44	0
MP1 A2B boei	46	0	45	0
MP2 Appelzak	52	0	51	0
MP3 Bol van Heist	50	0	48	0
MP4 Scheur Wielingen	54	0	53	0
Vlakte van de Raan	52	0	50	0
Cadzand	55	0	54	0
Westkapelle	59	0	59	0
Vlissingen	66	0	65	0
Breskens	64	0	62	0
Borssele	72	0	71	0
Terneuzen	76	1	74	0
Overloop Hansweert	83	0	82	0
Hansweert	86	0	85	0
Walsoorden	89	0	88	0
Baalhoek	93	0	91	0
Bath	97	1	97	0

Table 84. Harmonic analysis: Phase M2 (Eastern Scheldt)

Phase M2	Measurement		Scaldis_039_0	
WL Station	Value	Error	Value	Error
Oosterschelde 14	71	0	68	0
Oosterschelde 11	63	0	61	0
Oosterschelde 4	71	1	72	0
Roompot buiten	70	0	68	0
Roompot binnen	92	1	95	1
Sluis Kats	99	1	100	1
Stavenisse	98	1	99	1
Krammersluis	99	1	100	1
Yerseke	101	1	102	1
Bergsediepsluis	102	0	103	1
Marollegat	103	0	105	1

Table 85. Harmonic analysis: Phase M2 (Lower Sea Scheldt)

Phase M2	Measurement		Scaldis_039_0	
WL Station	Value	Error	Value	Error
Zandvliet	100	1	99	0
Prosperpolder	99	1	98	0
Liefkenshoek	102	0	100	0
Kallosluis	104	1	103	0
Antwerpen	110	1	108	1
Hemiksem	120	1	118	1

Table 86. Harmonic analysis: Phase M2 (Upper Sea Scheldt)

Phase M2	Measurement		Scaldis_039_0	
WL Station	Value	Error	Value	Error
Schelle	123	1	121	1
Temse	129	1	127	1
Tielrode	132	1	131	1
StAmands	138	1	137	1
Dendermonde	158	1	157	1
Schoonaarde	182	1	181	1
Wetteren	208	1	208	1
Melle	221	1	220	1

Table 87. Harmonic analysis: Phase M2 (Rupel basin)

Phase M2	Measurement		Scaldis_039_0	
WL Station	Value	Error	Value	Error
Boom	131.25	0.56	129.09	0.55
Walem	137.95	0.62	136.42	0.55
Duffel-sluis	155.37	0.57	152.95	0.67
Lier Molbrug	171.07	0.85	174.08	0.82
Lier Maasfort	187.32	0.86	186.00	0.96
Emblem	199.77	1.11	200.40	0.91
Kessel	215.58	1.27	222.44	1.21
Mechelen lock	145.68	0.65	149.18	0.66
Hombeek	151.89	0.63	161.41	0.62

Table 88. Harmonic analysis: Amplitude M4 (North sea and Western Scheldt)

Amplitude M4	Measurement		Scaldis_039_0	
WL Station	Value	Error	Value	Error
Nieuwpoort	0.14	0.01	0.12	0.01
Oostende	0.10	0.01	0.11	0.01
Zeebrugge	0.09	0.01	0.10	0.01
MP0 Wandelaar	0.10	0.01	0.10	0.01
MP1 A2B boei	0.10	0.01	0.10	0.01
MP2 Appelzak	0.11	0.01	0.11	0.01
MP3 Bol van Heist	0.10	0.01	0.10	0.01
MP4 Scheur Wielingen	0.11	0.01	0.11	0.01
Vlakte van de Raan	0.13	0.01	0.11	0.01
Cadzand	0.12	0.01	0.11	0.01
Westkapelle	0.14	0.01	0.13	0.01
Vlissingen	0.13	0.01	0.12	0.01
Breskens	0.13	0.01	0.13	0.01
Borssele	0.12	0.01	0.11	0.01
Terneuzen	0.12	0.02	0.12	0.01
Overloop Hansweert	0.13	0.02	0.12	0.02
Hansweert	0.11	0.02	0.11	0.01
Walsoorden	0.12	0.02	0.12	0.02
Baalhoek	0.12	0.02	0.12	0.02
Bath	0.11	0.02	0.12	0.02

Table 89. Harmonic analysis: Amplitude M4 (Eastern Scheldt)

Amplitude M4	Measurement		Scaldis_039_0	
WL Station	Value	Error	Value	Error
Oosterschelde 14	0.14	0.01	0.14	0.01
Oosterschelde 11	0.14	0.01	0.12	0.01
Oosterschelde 4	0.14	0.01	0.13	0.01
Roompot buiten	0.13	0.01	0.13	0.01
Roompot binnen	0.05	0.01	0.04	0.01
Sluis Kats	0.07	0.01	0.07	0.01
Stavenisse	0.08	0.01	0.07	0.01
Krammersluis	0.09	0.01	0.08	0.01
Yerseke	0.11	0.01	0.10	0.01
Bergsediepsluis	0.11	0.01	0.10	0.01
Marollegat	0.11	0.01	0.10	0.01

Table 90. Harmonic analysis: Amplitude M4 (Lower Sea Scheldt)

Amplitude M4	Measurement		Scaldis_039_0	
WL Station	Value	Error	Value	Error
Zandvliet	0.11	0.02	0.12	0.02
Prosperpolder	0.12	0.02	0.12	0.02
Liefkenshoek	0.12	0.02	0.13	0.02
Kallosluis	0.12	0.02	0.13	0.02
Antwerpen	0.12	0.02	0.14	0.02
Hemiksem	0.14	0.02	0.14	0.02

Table 91. Harmonic analysis: Amplitude M4 (Upper Sea Scheldt)

Amplitude M4	Measurement		Scaldis_039_0	
WL Station	Value	Error	Value	Error
Schelle	0.13	0.02	0.14	0.02
Temse	0.17	0.02	0.18	0.02
Tielrode	0.19	0.02	0.21	0.02
StAmands	0.24	0.02	0.25	0.02
Dendermonde	0.25	0.02	0.24	0.02
Schoonaarde	0.23	0.02	0.23	0.02
Wetteren	0.20	0.02	0.19	0.02
Melle	0.22	0.02	0.21	0.02

Table 92. Harmonic analysis: Amplitude M4 (Rupel basin)

Amplitude M4	Measurement		Scaldis_039_0	
WL Station	Value	Error	Value	Error
Boom	0.19	0.02	0.18	0.02
Walem	0.22	0.02	0.21	0.02
Duffel-sluis	0.32	0.02	0.36	0.02
Lier Molbrug	0.33	0.02	0.32	0.02
Lier Maasfort	0.28	0.01	0.26	0.01
Emblem	0.24	0.01	0.24	0.01
Kessel	0.18	0.01	0.17	0.01
Mechelen lock	0.29	0.02	0.33	0.02
Hombeek	0.41	0.02	0.41	0.02

Table 93. Harmonic analysis: Phase M4 (North sea and Western Scheldt)

Phase M4	Measurement		Scaldis_039_0	
WL Station	Value	Error	Value	Error
Nieuwpoort	22	5	18	6
Oostende	43	6	41	7
Zeebrugge	96	7	89	7
MP0 Wandelaar	75	6	73	6
MP1 A2B boei	77	6	75	6
MP2 Appelzak	100	6	91	6
MP3 Bol van Heist	94	7	87	6
MP4 Scheur Wielingen	106	6	97	5
Vlakte van de Raan	105	4	99	6
Cadzand	105	6	94	6
Westkapelle	112	4	104	5
Vlissingen	133	7	128	5
Breskens	125	5	119	6
Borssele	144	7	141	7
Terneuzen	147	7	140	7
Overloop Hansweert	174	6	170	8
Hansweert	172	9	167	7
Walsoorden	180	7	177	7
Baalhoek	190	7	180	8
Bath	189	10	178	8

Table 94. Harmonic analysis: Phase M4 (Eastern Scheldt)

Phase M4	Measurement		Scaldis_039_0	
WL Station	Value	Error	Value	Error
Oosterschelde 14	135	5	132	4
Oosterschelde 11	132	4	124	5
Oosterschelde 4	142	4	137	5
Roompot buiten	143	5	133	5
Roompot binnen	171	13	160	15
Sluis Kats	210	10	194	9
Stavenisse	212	8	194	10
Krammersluis	213	9	200	8
Yerseke	225	7	207	8
Bergsediepsluis	229	7	208	8
Marollegat	234	7	209	9

Table 95. Harmonic analysis: Phase M4 (Lower Sea Scheldt)

Phase M4	Measurement		Scaldis_039_0	
WL Station	Value	Error	Value	Error
Zandvliet	193	10	179	9
Prosperpolder	193	9	179	8
Liefkenshoek	196	10	181	9
Kallosluis	198	8	184	9
Antwerpen	207	10	193	8
Hemiksem	216	8	207	7

Table 96. Harmonic analysis: Phase M4 (Upper Sea Scheldt)

Phase M4	Measurement		Scaldis_039_0	
WL Station	Value	Error	Value	Error
Schelle	219	8	210	9
Temse	221	7	214	7
Tielrode	225	7	218	6
StAmands	235	5	229	5
Dendermonde	261	5	255	5
Schoonaarde	297	5	293	4
Wetteren	347	5	347	5
Melle	16	5	13	4

Table 97. Harmonic analysis: Phase M4 (Rupel basin)

Phase M4	Measurement		Scaldis_039_0	
WL Station	Value	Error	Value	Error
Boom	223.67	6.72	215.02	7.01
Walem	231.44	4.85	227.46	5.20
Duffel-sluis	259.59	3.29	254.66	3.10
Lier Molbrug	294.77	2.75	288.46	2.69
Lier Maasfort	317.90	2.79	311.58	2.50
Emblem	342.70	3.47	341.60	2.56
Kessel	10.57	3.35	17.69	2.55
Mechelen lock	250.44	4.45	255.74	3.38
Hombeek	286.72	2.52	287.82	2.34

Table 98. Harmonic analysis: Amplitude M6 (North sea and Western Scheldt)

Amplitude M6	Measurement		Scaldis_039_0	
WL Station	Value	Error	Value	Error
Nieuwpoort	0.06	0.01	0.06	0.01
Oostende	0.07	0.01	0.08	0.01
Zeebrugge	0.10	0.01	0.10	0.01
MP0 Wandelaar	0.08	0.01	0.09	0.01
MP1 A2B boei	0.09	0.01	0.09	0.01
MP2 Appelzak	0.11	0.01	0.10	0.01
MP3 Bol van Heist	0.10	0.01	0.10	0.01
MP4 Scheur Wielingen	0.10	0.01	0.10	0.01
Vlakte van de Raan	0.09	0.01	0.09	0.01
Cadzand	0.11	0.01	0.11	0.01
Westkapelle	0.10	0.01	0.09	0.01
Vlissingen	0.09	0.01	0.09	0.01
Breskens	0.10	0.01	0.10	0.01
Borssele	0.10	0.01	0.09	0.01
Terneuzen	0.10	0.01	0.10	0.01
Overloop Hansweert	0.10	0.02	0.09	0.01
Hansweert	0.10	0.01	0.10	0.02
Walsoorden	0.11	0.01	0.10	0.02
Baalhoek	0.12	0.02	0.12	0.02
Bath	0.13	0.02	0.13	0.02

Table 99. Harmonic analysis: Amplitude M6 (Eastern Scheldt)

Amplitude M6	Measurement		Scaldis_039_0	
WL Station	Value	Error	Value	Error
Oosterschelde 14	0.08	0.01	0.08	0.01
Oosterschelde 11	0.09	0.01	0.09	0.01
Oosterschelde 4	0.07	0.01	0.07	0.01
Roompot buiten	0.07	0.01	0.08	0.01
Roompot binnen	0.03	0.01	0.02	0.01
Sluis Kats	0.04	0.01	0.03	0.01
Stavenisse	0.03	0.01	0.02	0.01
Krammersluis	0.04	0.01	0.03	0.01
Yerseke	0.08	0.01	0.07	0.01
Bergsediepsluis	0.09	0.01	0.08	0.01
Marollegat	0.11	0.01	0.09	0.01

Table 100. Harmonic analysis: Amplitude M6 (Lower Sea Scheldt)

Amplitude M6	Measurement		Scaldis_039_0	
WL Station	Value	Error	Value	Error
Zandvliet	0.15	0.02	0.14	0.02
Prosperpolder	0.15	0.02	0.14	0.02
Liefkenshoek	0.15	0.02	0.15	0.01
Kallosluis	0.16	0.02	0.15	0.02
Antwerpen	0.15	0.02	0.15	0.02
Hemiksem	0.16	0.02	0.15	0.02

Table 101. Harmonic analysis: Amplitude M6 (Upper Sea Scheldt)

Amplitude M6	Measurement		Scaldis_039_0	
WL Station	Value	Error	Value	Error
Schelle	0.16	0.02	0.15	0.02
Temse	0.16	0.02	0.15	0.02
Tielrode	0.17	0.02	0.15	0.02
StAmands	0.15	0.02	0.14	0.02
Dendermonde	0.11	0.02	0.10	0.02
Schoonaarde	0.08	0.02	0.07	0.02
Wetteren	0.05	0.02	0.05	0.02
Melle	0.05	0.02	0.05	0.01

Table 102. Harmonic analysis: Amplitude M6 (Rupel basin)

Amplitude M6	Measurement		Scaldis_039_0	
WL Station	Value	Error	Value	Error
Boom	0.14	0.02	0.14	0.02
Walem	0.13	0.02	0.12	0.02
Duffel-sluis	0.08	0.02	0.08	0.02
Lier Molbrug	0.08	0.01	0.08	0.01
Lier Maasfort	0.08	0.01	0.08	0.01
Emblem	0.08	0.01	0.08	0.01
Kessel	0.06	0.01	0.07	0.01
Mechelen lock	0.08	0.02	0.07	0.02
Hombeek	0.10	0.02	0.12	0.01

Table 103. Harmonic analysis: Phase M6 (North sea and Western Scheldt)

Phase M6	Measurement		Scaldis_039_0	
WL Station	Value	Error	Value	Error
Nieuwpoort	24	12	4	12
Oostende	44	9	26	8
Zeebrugge	76	6	59	7
MP0 Wandelaar	65	7	48	8
MP1 A2B boei	68	6	51	7
MP2 Appelzak	84	6	70	6
MP3 Bol van Heist	78	6	60	7
MP4 Scheur Wielingen	89	5	74	6
Vlakte van de Raan	85	6	65	8
Cadzand	92	5	79	6
Westkapelle	100	6	82	7
Vlissingen	128	6	112	8
Breskens	124	7	108	7
Borssele	151	8	136	8
Terneuzen	173	8	156	9
Overloop Hansweert	217	8	201	10
Hansweert	223	7	212	9
Walsoorden	242	8	231	9
Baalhoek	260	7	247	8
Bath	274	8	266	7

Table 104. Harmonic analysis: Phase M6 (Eastern Scheldt)

Phase M6	Measurement		Scaldis_039_0	
WL Station	Value	Error	Value	Error
Oosterschelde 14	116	7	92	8
Oosterschelde 11	105	6	80	7
Oosterschelde 4	111	9	86	10
Roompot buiten	105	10	85	8
Roompot binnen	143	18	116	26
Sluis Kats	262	17	254	28
Stavenisse	246	19	244	32
Krammersluis	249	17	251	23
Yerseke	283	10	273	11
Bergsediepsluis	286	9	276	10
Marollegat	291	7	280	9

Table 105. Harmonic analysis: Phase M6 (Lower Sea Scheldt)

Phase M6	Measurement		Scaldis_039_0	
WL Station	Value	Error	Value	Error
Zandvliet	290	7	278	7
Prosperpolder	287	6	275	7
Liefkenshoek	299	7	287	6
Kallosluis	309	7	297	8
Antwerpen	335	7	322	8
Hemiksem	14	7	2	8

Table 106. Harmonic analysis: Phase M6 (Upper Sea Scheldt)

Phase M6	Measurement		Scaldis_039_0	
WL Station	Value	Error	Value	Error
Schelle	25	7	10	9
Temse	41	7	30	9
Tielrode	53	7	42	8
StAmands	68	7	55	9
Dendermonde	108	10	99	10
Schoonaarde	142	12	132	14
Wetteren	193	23	195	21
Melle	238	26	230	20

Table 107. Harmonic analysis: Phase M6 (Rupel basin)

Phase M6	Measurement		Scaldis_039_0	
WL Station	Value	Error	Value	Error
Boom	45.41	8.77	33.77	9.01
Walem	62.47	9.21	51.80	9.40
Duffel-sluis	89.66	15.32	59.01	12.78
Lier Molbrug	73.83	11.06	57.22	8.93
Lier Maasfort	98.94	8.59	81.20	8.49
Emblem	127.19	8.97	121.19	8.49
Kessel	162.22	9.77	171.43	7.17
Mechelen lock	73.22	14.46	48.92	15.79
Hombeek	44.03	9.82	55.06	7.38

Table 108. Harmonic analysis: Amplitude S2 (North sea and Western Scheldt)

Amplitude S2	Measurement		Scaldis_039_0	
WL Station	Value	Error	Value	Error
Nieuwpoort	0.68	0.01	0.68	0.01
Oostende	0.63	0.01	0.64	0.01
Zeebrugge	0.58	0.01	0.56	0.01
MP0 Wandelaar	0.55	0.01	0.56	0.01
MP1 A2B boei	0.57	0.01	0.57	0.01
MP2 Appelzak	0.58	0.01	0.55	0.01
MP3 Bol van Heist	0.56	0.01	0.55	0.01
MP4 Scheur Wielingen	0.55	0.01	0.54	0.01
Vlakte van de Raan	0.51	0.01	0.50	0.01
Cadzand	0.57	0.01	0.55	0.01
Westkapelle	0.52	0.01	0.51	0.01
Vlissingen	0.57	0.01	0.56	0.01
Breskens	0.57	0.01	0.56	0.01
Borssele	0.59	0.01	0.57	0.01
Terneuzen	0.60	0.01	0.58	0.01
Overloop Hansweert	0.61	0.01	0.60	0.01
Hansweert	0.63	0.02	0.61	0.01
Walsoorden	0.63	0.02	0.62	0.02
Baalhoek	0.65	0.02	0.63	0.02
Bath	0.66	0.02	0.64	0.02

Table 109. Harmonic analysis: Amplitude S2 (Eastern Scheldt)

Amplitude S2	Measurement		Scaldis_039_0	
WL Station	Value	Error	Value	Error
Oosterschelde 14	0.38	0.01	0.36	0.01
Oosterschelde 11	0.43	0.01	0.41	0.01
Oosterschelde 4	0.42	0.01	0.39	0.01
Roompot buiten	0.43	0.01	0.42	0.01
Roompot binnen	0.35	0.01	0.34	0.01
Sluis Kats	0.41	0.01	0.39	0.01
Stavenisse	0.41	0.01	0.38	0.01
Krammersluis	0.42	0.01	0.40	0.01
Yerseke	0.43	0.01	0.41	0.01
Bergsediepsluis	0.44	0.01	0.42	0.01
Marollegat	0.45	0.02	0.43	0.01

Table 110. Harmonic analysis: Amplitude S2 (Lower Sea Scheldt)

Amplitude S2	Measurement		Scaldis_039_0	
WL Station	Value	Error	Value	Error
Zandvliet	0.67	0.02	0.65	0.02
Prosperpolder	0.66	0.02	0.65	0.02
Liefkenshoek	0.68	0.02	0.66	0.02
Kallosluis	0.69	0.02	0.67	0.02
Antwerpen	0.69	0.02	0.67	0.02
Hemiksem	0.68	0.02	0.66	0.02

Table 111. Harmonic analysis: Amplitude S2 (Upper Sea Scheldt)

Amplitude S2	Measurement		Scaldis_039_0	
WL Station	Value	Error	Value	Error
Schelle	0.68	0.02	0.66	0.02
Temse	0.66	0.02	0.64	0.02
Tielrode	0.65	0.02	0.63	0.02
StAmands	0.60	0.02	0.58	0.02
Dendermonde	0.46	0.02	0.44	0.02
Schoonaarde	0.35	0.02	0.33	0.02
Wetteren	0.30	0.02	0.28	0.02
Melle	0.28	0.02	0.27	0.02

Table 112. Harmonic analysis: Amplitude S2 (Rupel basin)

Amplitude S2	Measurement		Scaldis_039_0	
WL Station	Value	Error	Value	Error
Boom	0.65	0.02	0.63	0.02
Walem	0.61	0.02	0.59	0.02
Duffel-sluis	0.47	0.02	0.45	0.02
Lier Molbrug	0.30	0.02	0.26	0.01
Lier Maasfort	0.22	0.02	0.22	0.01
Emblem	0.19	0.01	0.18	0.01
Kessel	0.15	0.01	0.13	0.01
Mechelen lock	0.55	0.02	0.49	0.02
Hombeek	0.45	0.02	0.38	0.02

Table 113. Harmonic analysis: Phase S2 (North sea and Western Scheldt)

Phase S2	Measurement		Scaldis_039_0	
WL Station	Value	Error	Value	Error
Nieuwpoort	82	1	82	1
Oostende	86	1	87	1
Zeebrugge	95	1	96	1
MP0 Wandelaar	91	1	92	1
MP1 A2B boei	93	1	93	1
MP2 Appelzak	99	1	100	1
MP3 Bol van Heist	97	1	97	1
MP4 Scheur Wielingen	102	1	102	1
Vlakte van de Raan	98	1	98	1
Cadzand	102	1	104	1
Westkapelle	106	1	109	1
Vlissingen	114	1	116	1
Breskens	112	1	113	1
Borssele	122	1	123	2
Terneuzen	127	1	128	1
Overloop Hansweert	136	2	138	2
Hansweert	140	1	141	2
Walsoorden	143	1	144	2
Baalhoek	147	2	149	2
Bath	152	2	155	2

Table 114. Harmonic analysis: Phase S2 (Eastern Scheldt)

Phase S2	Measurement		Scaldis_039_0	
WL Station	Value	Error	Value	Error
Oosterschelde 14	118	2	117	2
Oosterschelde 11	109	1	110	1
Oosterschelde 4	119	2	122	2
Roompot buiten	117	1	118	2
Roompot binnen	145	2	150	2
Sluis Kats	155	2	157	2
Stavenisse	154	2	156	2
Krammersluis	154	2	158	2
Yerseke	157	2	160	2
Bergsediepsluis	159	2	161	2
Marollegat	160	2	163	2

Table 115. Harmonic analysis: Phase S2 (Lower Sea Scheldt)

Phase S2	Measurement		Scaldis_039_0	
WL Station	Value	Error	Value	Error
Zandvliet	156	2	158	2
Prosperpolder	155	2	157	2
Liefkenshoek	158	2	160	2
Kallosluis	160	2	162	2
Antwerpen	168	2	168	2
Hemiksem	179	2	180	2

Table 116. Harmonic analysis: Phase S2 (Upper Sea Scheldt)

Phase S2	Measurement		Scaldis_039_0	
WL Station	Value	Error	Value	Error
Schelle	183	2	183	2
Temse	189	2	191	2
Tielrode	193	2	195	2
StAmands	199	2	202	2
Dendermonde	221	2	224	3
Schoonaarde	247	3	249	4
Wetteren	274	4	279	3
Melle	287	4	292	4

Table 117. Harmonic analysis: Phase S2 (Rupel basin)

Phase S2	Measurement		Scaldis_039_0	
WL Station	Value	Error	Value	Error
Boom	192.33	1.72	193.18	2.30
Walem	200.53	1.91	201.81	2.32
Duffel-sluis	219.10	2.63	219.55	2.65
Lier Molbrug	233.08	2.76	241.50	3.85
Lier Maasfort	247.02	3.94	252.53	3.91
Emblem	259.30	3.85	265.34	3.62
Kessel	273.43	4.27	279.16	3.90
Mechelen lock	212.45	2.43	218.30	2.54
Hombeek	213.67	2.18	229.18	2.57

Table 118. Harmonic analysis: Amplitude K1 (North sea and Western Scheldt)

Amplitude K1	Measurement		Scaldis_039_0	
WL Station	Value	Error	Value	Error
Nieuwpoort	0.06	0.01	0.05	0.01
Oostende	0.07	0.01	0.06	0.01
Zeebrugge	0.07	0.01	0.07	0.01
MP0 Wandelaar	0.07	0.01	0.07	0.01
MP1 A2B boei	0.07	0.01	0.07	0.01
MP2 Appelzak	0.07	0.01	0.07	0.01
MP3 Bol van Heist	0.07	0.01	0.07	0.01
MP4 Scheur Wielingen	0.08	0.01	0.07	0.01
Vlakte van de Raan	0.08	0.01	0.07	0.01
Cadzand	0.08	0.01	0.07	0.01
Westkapelle	0.08	0.01	0.07	0.01
Vlissingen	0.08	0.01	0.07	0.01
Breskens	0.07	0.01	0.07	0.01
Borssele	0.08	0.02	0.07	0.01
Terneuzen	0.07	0.02	0.07	0.02
Overloop Hansweert	0.08	0.02	0.07	0.02
Hansweert	0.07	0.02	0.07	0.02
Walsoorden	0.07	0.02	0.07	0.02
Baalhoek	0.07	0.02	0.07	0.02
Bath	0.07	0.02	0.07	0.02

Table 119. Harmonic analysis: Amplitude K1 (Eastern Scheldt)

Amplitude K1	Measurement		Scaldis_039_0	
WL Station	Value	Error	Value	Error
Oosterschelde 14	0.08	0.01	0.08	0.01
Oosterschelde 11	0.08	0.01	0.07	0.01
Oosterschelde 4	0.08	0.01	0.07	0.01
Roompot buiten	0.08	0.01	0.07	0.02
Roompot binnen	0.07	0.01	0.07	0.01
Sluis Kats	0.07	0.01	0.07	0.01
Stavenisse	0.07	0.01	0.07	0.01
Krammersluis	0.07	0.02	0.07	0.01
Yerseke	0.07	0.02	0.07	0.01
Bergsediepsluis	0.08	0.02	0.07	0.02
Marollegat	0.07	0.02	0.07	0.02

Table 120. Harmonic analysis: Amplitude K1 (Lower Sea Scheldt)

Amplitude K1	Measurement		Scaldis_039_0	
WL Station	Value	Error	Value	Error
Zandvliet	0.07	0.02	0.06	0.02
Prosperpolder	0.07	0.02	0.06	0.02
Liefkenshoek	0.07	0.02	0.06	0.02
Kallosluis	0.07	0.02	0.06	0.02
Antwerpen	0.07	0.02	0.06	0.02
Hemiksem	0.07	0.02	0.06	0.02

Table 121. Harmonic analysis: Amplitude K1 (Upper Sea Scheldt)

Amplitude K1	Measurement		Scaldis_039_0	
WL Station	Value	Error	Value	Error
Schelle	0.07	0.02	0.06	0.02
Temse	0.06	0.02	0.06	0.02
Tielrode	0.06	0.02	0.06	0.02
StAmands	0.06	0.03	0.06	0.02
Dendermonde	0.05	0.02	0.05	0.02
Schoonaarde	0.04	0.02	0.04	0.02
Wetteren	0.05	0.02	0.04	0.02
Melle	0.06	0.02	0.04	0.02

Table 122. Harmonic analysis: Amplitude K1 (Rupel basin)

Amplitude K1	Measurement		Scaldis_039_0	
WL Station	Value	Error	Value	Error
Boom	0.06	0.02	0.06	0.02
Walem	0.05	0.02	0.06	0.02
Duffel-sluis	0.04	0.02	0.05	0.02
Lier Molbrug	0.02	0.02	0.04	0.02
Lier Maasfort	0.02	0.01	0.04	0.02
Emblem	0.02	0.02	0.03	0.01
Kessel	0.02	0.01	0.03	0.01
Mechelen lock	0.03	0.03	0.05	0.02
Hombeek	0.02	0.02	0.03	0.02

Table 123. Harmonic analysis: Phase K1 (North sea and Western Scheldt)

Phase K1	Measurement		Scaldis_039_0	
WL Station	Value	Error	Value	Error
Nieuwpoort	14	11	336	13
Oostende	13	11	335	14
Zeebrugge	13	10	337	11
MP0 Wandelaar	12	9	337	11
MP1 A2B boei	13	9	336	12
MP2 Appelzak	14	10	338	11
MP3 Bol van Heist	14	8	337	11
MP4 Scheur Wielingen	14	9	339	11
Vlakte van de Raan	12	9	337	11
Cadzand	14	10	338	11
Westkapelle	13	10	339	11
Vlissingen	21	12	343	11
Breskens	20	10	342	12
Borssele	24	10	346	14
Terneuzen	26	12	347	15
Overloop Hansweert	33	12	353	15
Hansweert	32	14	353	13
Walsoorden	35	13	355	17
Baalhoek	38	15	358	17
Bath	39	17	0	17

Table 124. Harmonic analysis: Phase K1 (Eastern Scheldt)

Phase K1	Measurement		Scaldis_039_0	
WL Station	Value	Error	Value	Error
Oosterschelde 14	13	9	340	9
Oosterschelde 11	13	8	339	11
Oosterschelde 4	15	9	342	10
Roompot buiten	15	9	340	10
Roompot binnen	30	11	353	11
Sluis Kats	34	11	355	13
Stavenisse	33	12	354	13
Krammersluis	33	14	354	11
Yerseke	37	12	356	14
Bergsediepsluis	38	12	356	13
Marollegat	39	13	358	13

Table 125. Harmonic analysis: Phase K1 (Lower Sea Scheldt)

Phase K1 WL Station	Measurement		Scaldis_039_0	
	Value	Error	Value	Error
Zandvliet	43	18	2	17
Prosperpolder	42	15	2	17
Liefkenshoek	44	17	4	21
Kallosluis	45	20	5	18
Antwerpen	51	17	9	23
Hemiksem	56	19	16	21

Table 126. Harmonic analysis: Phase K1 (Upper Sea Scheldt)

Phase K1 WL Station	Measurement		Scaldis_039_0	
	Value	Error	Value	Error
Schelle	57	19	17	24
Temse	62	20	19	22
Tielrode	66	26	21	23
StAmands	67	24	22	27
Dendermonde	75	30	29	25
Schoonaarde	83	26	34	25
Wetteren	87	24	46	33
Melle	80	24	53	32

Table 127. Harmonic analysis: Phase K1 (Rupel basin)

Phase K1 WL Station	Measurement		Scaldis_039_0	
	Value	Error	Value	Error
Boom	60.95	24.26	20.43	25.62
Walem	62.33	23.87	22.00	26.09
Duffel-sluis	63.11	26.92	20.23	27.03
Lier Molbrug	27.88	45.82	10.28	25.50
Lier Maasfort	17.74	36.63	7.90	22.34
Emblem	13.16	37.23	7.96	23.25
Kessel	7.09	42.57	11.76	19.24
Mechelen lock	55.49	38.86	10.00	27.77
Hombeek	329.88	64.13	349.98	37.72

Table 128. Harmonic analysis: Amplitude O1 (North sea and Western Scheldt)

Amplitude O1	Measurement		Scaldis_039_0	
WL Station	Value	Error	Value	Error
Nieuwpoort	0.12	0.01	0.12	0.01
Oostende	0.12	0.02	0.13	0.01
Zeebrugge	0.13	0.01	0.14	0.01
MP0 Wandelaar	0.13	0.01	0.14	0.01
MP1 A2B boei	0.13	0.01	0.14	0.01
MP2 Appelzak	0.14	0.01	0.14	0.01
MP3 Bol van Heist	0.13	0.01	0.14	0.01
MP4 Scheur Wielingen	0.14	0.01	0.14	0.01
Vlakte van de Raan	0.14	0.01	0.14	0.01
Cadzand	0.13	0.01	0.14	0.01
Westkapelle	0.13	0.01	0.14	0.02
Vlissingen	0.14	0.02	0.14	0.02
Breskens	0.14	0.01	0.14	0.02
Borssele	0.14	0.02	0.15	0.02
Terneuzen	0.14	0.02	0.15	0.02
Overloop Hansweert	0.14	0.02	0.15	0.02
Hansweert	0.14	0.02	0.15	0.02
Walsoorden	0.14	0.02	0.15	0.02
Baalhoek	0.14	0.02	0.16	0.02
Bath	0.15	0.02	0.16	0.02

Table 129. Harmonic analysis: Amplitude O1 (Eastern Scheldt)

Amplitude O1	Measurement		Scaldis_039_0	
WL Station	Value	Error	Value	Error
Oosterschelde 14	0.14	0.01	0.15	0.01
Oosterschelde 11	0.14	0.01	0.15	0.01
Oosterschelde 4	0.14	0.01	0.14	0.01
Roompot buiten	0.14	0.01	0.15	0.01
Roompot binnen	0.13	0.01	0.14	0.01
Sluis Kats	0.14	0.01	0.15	0.01
Stavenisse	0.14	0.01	0.14	0.02
Krammersluis	0.14	0.02	0.15	0.01
Yerseke	0.14	0.02	0.15	0.01
Bergsediepsluis	0.14	0.02	0.15	0.02
Marollegat	0.14	0.02	0.15	0.02

Table 130. Harmonic analysis: Amplitude O1 (Lower Sea Scheldt)

Amplitude O1 WL Station	Measurement		Scaldis_039_0	
	Value	Error	Value	Error
Zandvliet	0.15	0.02	0.16	0.02
Prosperpolder	0.15	0.02	0.16	0.02
Liefkenshoek	0.15	0.02	0.16	0.02
Kallosluis	0.15	0.03	0.16	0.02
Antwerpen	0.15	0.02	0.16	0.02
Hemiksem	0.15	0.03	0.16	0.02

Table 131. Harmonic analysis: Amplitude O1 (Upper Sea Scheldt)

Amplitude O1 WL Station	Measurement		Scaldis_039_0	
	Value	Error	Value	Error
Schelle	0.14	0.03	0.16	0.02
Temse	0.14	0.02	0.15	0.03
Tielrode	0.14	0.03	0.15	0.02
StAmands	0.13	0.03	0.14	0.02
Dendermonde	0.11	0.02	0.13	0.02
Schoonaarde	0.10	0.02	0.11	0.02
Wetteren	0.09	0.03	0.10	0.02
Melle	0.08	0.02	0.09	0.02

Table 132. Harmonic analysis: Amplitude O1 (Rupel basin)

Amplitude O1 WL Station	Measurement		Scaldis_039_0	
	Value	Error	Value	Error
Boom	0.14	0.03	0.15	0.02
Walem	0.13	0.03	0.15	0.02
Duffel-sluis	0.11	0.02	0.12	0.02
Lier Molbrug	0.08	0.02	0.09	0.02
Lier Maasfort	0.06	0.01	0.08	0.02
Emblem	0.06	0.02	0.06	0.01
Kessel	0.05	0.01	0.05	0.01
Mechelen lock	0.11	0.02	0.12	0.02
Hombeek	0.08	0.02	0.08	0.02

Table 133. Harmonic analysis: Phase O1 (North sea and Western Scheldt)

Phase O1	Measurement		Scaldis_039_0	
WL Station	Value	Error	Value	Error
Nieuwpoort	189	7	188	6
Oostende	190	7	189	6
Zeebrugge	194	6	193	6
MP0 Wandelaar	193	5	192	6
MP1 A2B boei	193	6	192	6
MP2 Appelzak	194	6	194	6
MP3 Bol van Heist	195	6	193	5
MP4 Scheur Wielingen	196	6	196	5
Vlakte van de Raan	195	6	195	6
Cadzand	195	6	196	6
Westkapelle	197	6	197	6
Vlissingen	202	6	201	6
Breskens	201	6	200	6
Borssele	205	6	204	6
Terneuzen	208	7	206	6
Overloop Hansweert	214	7	212	7
Hansweert	214	8	212	7
Walsoorden	216	8	214	7
Baalhoek	219	8	217	7
Bath	221	9	219	8

Table 134. Harmonic analysis: Phase O1 (Eastern Scheldt)

Phase O1	Measurement		Scaldis_039_0	
WL Station	Value	Error	Value	Error
Oosterschelde 14	201	5	200	4
Oosterschelde 11	199	5	198	5
Oosterschelde 4	202	5	202	5
Roompot buiten	202	5	201	5
Roompot binnen	217	6	216	5
Sluis Kats	221	6	219	6
Stavenisse	220	6	218	5
Krammersluis	220	6	219	6
Yerseke	222	6	220	6
Bergsediepsluis	222	7	221	6
Marollegat	224	6	222	6

Table 135. Harmonic analysis: Phase O1 (Lower Sea Scheldt)

Phase O1	Measurement		Scaldis_039_0	
WL Station	Value	Error	Value	Error
Zandvliet	224	9	221	9
Prosperpolder	223	9	221	8
Liefkenshoek	225	9	222	9
Kallosluis	226	8	223	8
Antwerpen	231	8	227	8
Hemiksem	237	11	233	9

Table 136. Harmonic analysis: Phase O1 (Upper Sea Scheldt)

Phase O1	Measurement		Scaldis_039_0	
WL Station	Value	Error	Value	Error
Schelle	238	10	235	9
Temse	242	10	239	9
Tielrode	243	10	241	10
StAmands	247	11	245	11
Dendermonde	258	11	258	11
Schoonaarde	271	14	270	11
Wetteren	283	15	285	10
Melle	292	16	292	12

Table 137. Harmonic analysis: Phase O1 (Rupel basin)

Phase O1	Measurement		Scaldis_039_0	
WL Station	Value	Error	Value	Error
Boom	242.98	9.33	239.71	9.65
Walem	245.84	10.60	243.83	10.27
Duffel-sluis	253.46	12.61	252.38	11.16
Lier Molbrug	256.00	14.43	257.68	12.52
Lier Maasfort	261.04	14.33	259.28	9.77
Emblem	265.04	16.76	261.26	12.02
Kessel	269.25	16.95	268.71	11.71
Mechelen lock	247.72	13.30	245.35	11.40
Hombeek	237.40	15.15	240.57	13.39

Table 138. Harmonic analysis : Z0 (North sea and Western Scheldt)

Z0	Measurement	Scaldis_039_0
WL Station	Value	Value
Nieuwpoort	2.32	2.31
Oostende	2.36	2.32
Zeebrugge	2.38	2.31
MP0 Wandelaar	2.31	2.31
MP1 A2B boei	2.37	2.32
MP2 Appelzak	2.29	2.32
MP3 Bol van Heist	2.30	2.31
MP4 Scheur Wielingen	2.30	2.31
Vlakte van de Raan	2.30	2.30
Cadzand	2.29	2.33
Westkapelle	2.30	2.31
Vlissingen	2.31	2.32
Breskens	2.32	2.33
Borssele	2.35	2.37
Terneuzen	2.39	2.40
Overloop Hansweert	2.41	2.40
Hansweert	2.44	2.44
Walsoorden	2.44	2.44
Baalhoek	2.44	2.45
Bath	2.45	2.50

Table 139. Harmonic analysis : Z0 (Eastern Scheldt)

Z0	Measurement	Scaldis_039_0
WL Station	Value	Value
Oosterschelde 14	2.30	2.30
Oosterschelde 11	2.31	2.29
Oosterschelde 4	2.30	2.31
Roompot buiten	2.29	2.31
Roompot binnen	2.31	2.35
Sluis Kats	2.33	2.37
Stavenisse	2.33	2.38
Krammersluis	2.34	2.39
Yerseke	2.35	2.37
Bergsediepsluis	2.34	2.39
Marollegat	2.33	2.38

Table 140. Harmonic analysis : Z0 (Lower Sea Scheldt)

Z0	Measurement	Scaldis_039_0
WL Station	Value	Value
Zandvliet	2.44	2.51
Prosperpolder	2.45	2.50
Liefkenshoek	2.46	2.51
Kallosluis	2.48	2.53
Antwerpen	2.50	2.54
Hemiksem	2.52	2.60

Table 141. Harmonic analysis : Z0 (Upper Sea Scheldt)

Z0	Measurement	Scaldis_039_0
WL Station	Value	Value
Schelle	2.60	2.62
Temse	2.67	2.68
Tielrode	2.65	2.70
StAmands	2.73	2.76
Dendermonde	2.96	2.92
Schoonaarde	3.12	3.08
Wetteren	3.20	3.16
Melle	3.31	3.20

Table 142. Harmonic analysis : Z0 (Rupel basin)

Z0	Measurement	Scaldis_039_0
WL Station	Value	Value
Boom	2.69	2.70
Walem	2.78	2.79
Duffel-sluis	3.05	3.05
Lier Molbrug	3.48	3.49
Lier Maasfort	3.72	3.63
Emblem	3.89	3.77
Kessel	3.95	3.92
Mechelen lock	2.98	3.09
Hombeek	3.28	3.35

Table 143. Vector differences of model results vs. measurements (North sea and Western Scheldt)

Vector differences of model results vs measurements	Scaldis_039_0
WL Station	Vector difference [m]
Nieuwpoort	0.15
Oostende	0.21
Zeebrugge	0.22
MP0 Wandelaar	0.12
MP1 A2B boei	0.19
MP2 Appelzak	0.18
MP3 Bol van Heist	0.16
MP4 Scheur Wielingen	0.16
Vlakte van de Raan	0.15
Cadzand	0.20
Westkapelle	0.18
Vlissingen	0.17
Breskens	0.18
Borssele	0.19
Terneuzen	0.21
Overloop Hansweert	0.17
Hansweert	0.15
Walsoorden	0.16
Baalhoek	0.19
Bath	0.21
Total vector difference of model results vs measurements	0.18

Table 144. Vector differences of model results vs. measurements (Eastern Scheldt)

Vector differences of model results vs measurements	Scaldis_039_0
WL Station	Vector difference [m]
Oosterschelde 14	0.17
Oosterschelde 11	0.19
Oosterschelde 4	0.15
Roompot buiten	0.19
Roompot binnen	0.21
Sluis Kats	0.16
Stavenisse	0.19
Krammersluis	0.21
Yerseke	0.18
Bergsediepsluis	0.23
Marollegat	0.25
Total vector difference of model results vs measurements	0.19

Table 145. Vector differences of model results vs. measurements (Lower Sea Scheldt)

Vector differences of model results vs measurements	Scaldis_039_0
WL Station	Vector difference [m]
Zandvliet	0.27
Prosperpolder	0.23
Liefkenshoek	0.25
Kallosluis	0.25
Antwerpen	0.28
Hemiksem	0.29
Total vector difference of model results vs measurements	0.26

Table 146. Vector differences of model results vs. measurements (Upper Sea Scheldt)

Vector differences of model results vs measurements	Scaldis_039_0
WL Station	Vector difference [m]
Schelle	0.26
Temse	0.21
Tielrode	0.25
StAmands	0.23
Dendermonde	0.19
Schoonaarde	0.16
Wetteren	0.12
Melle	0.21
Total vector difference of model results vs measurements	0.20

Table 147. Vector differences of model results vs. measurements (Rupel basin)

Vector differences of model results vs measurements	Scaldis_039_0
WL Station	Vector difference [m]
Boom	0.23
Walem	0.19
Duffel-sluis	0.24
Lier Molbrug	0.26
Lier Maasfort	0.21
Emblem	0.19
Kessel	0.21
Mechelen lock	0.48
Hombeek	0.52
Total vector difference of model results vs measurements	0.28

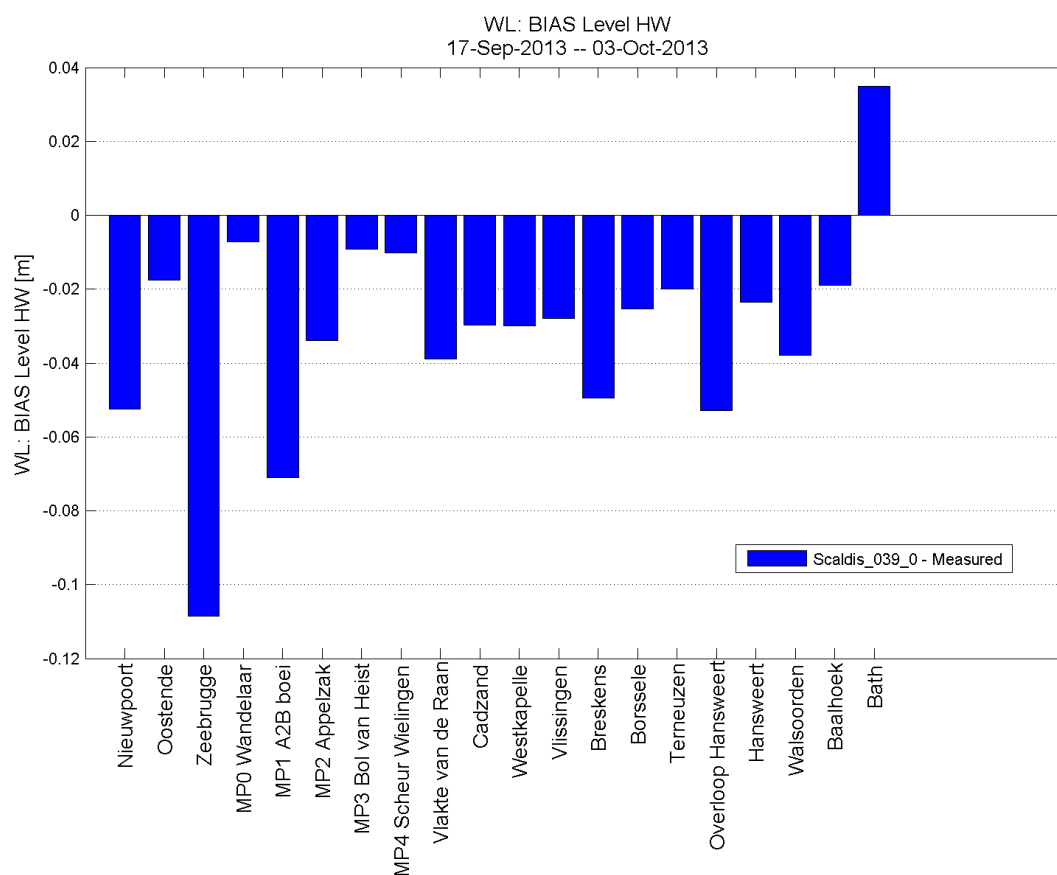


Figure 239 - Bias of high water magnitude (model – measurement) in the North sea and Western Scheldt

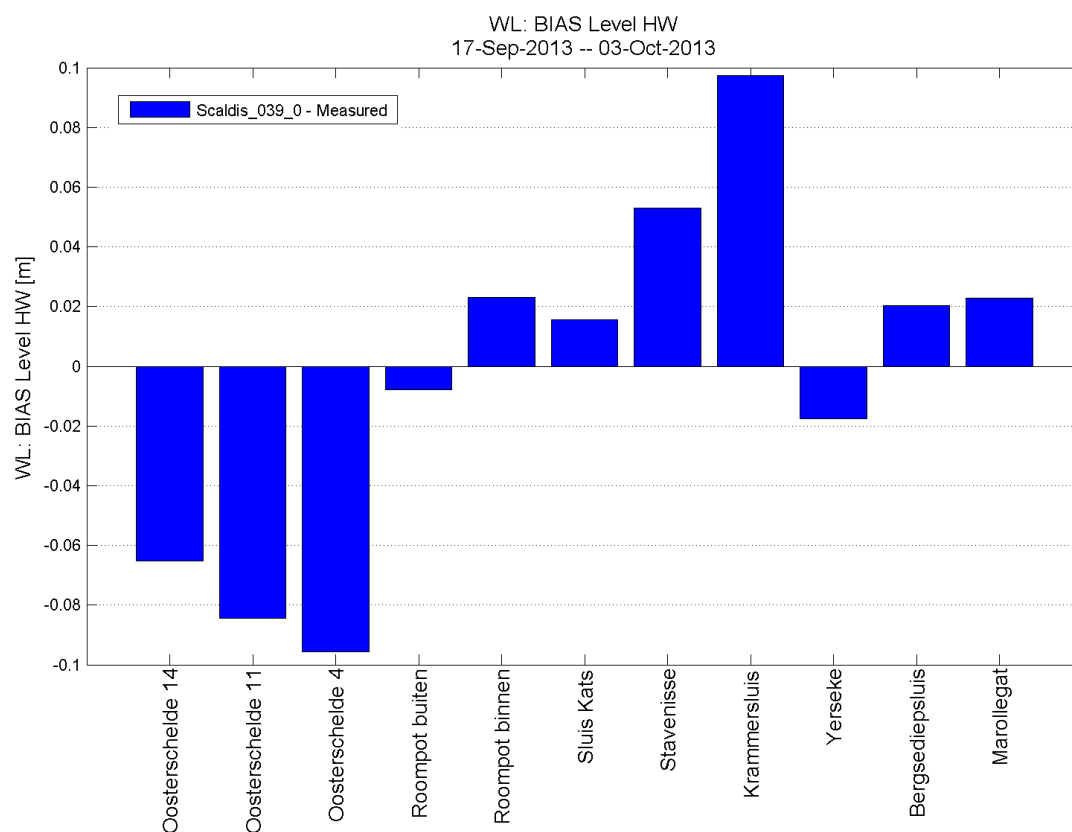


Figure 240 - Bias of high water magnitude (model – measurement) in the Eastern Scheldt

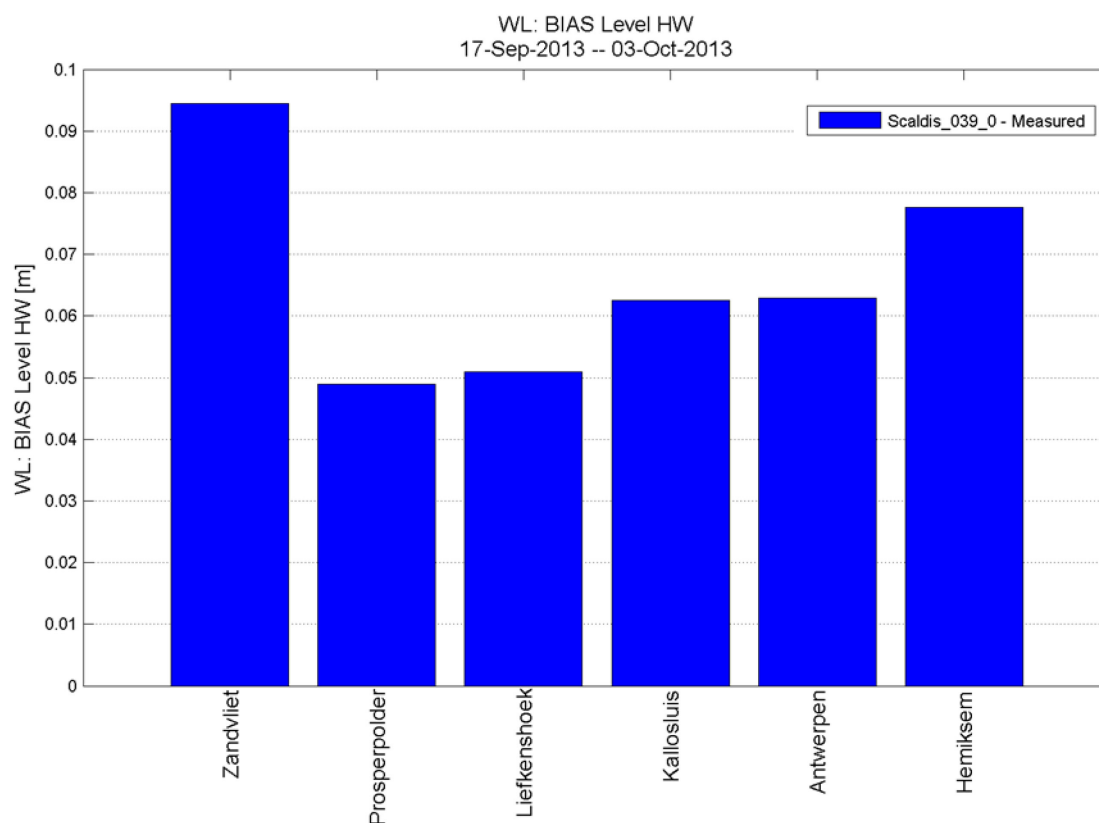


Figure 241 - Bias of high water magnitude (model – measurement) in the Lower Sea Scheldt

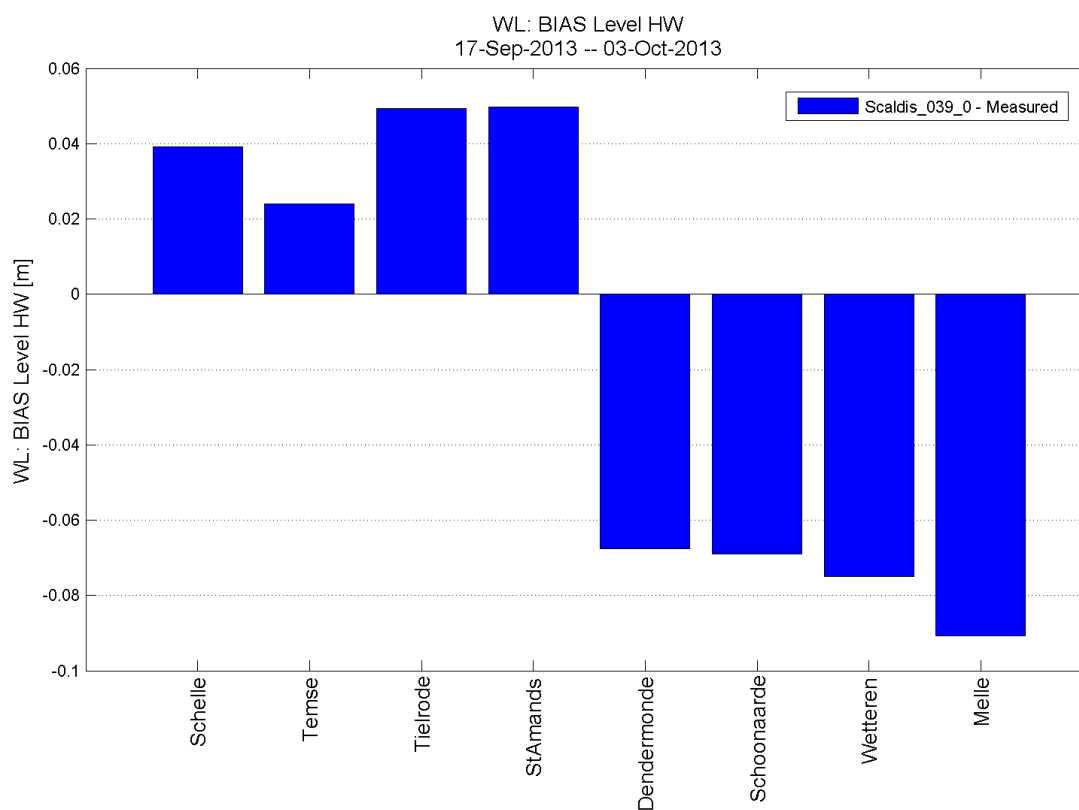


Figure 242 - Bias of high water magnitude (model – measurement) in the Upper Sea Scheldt

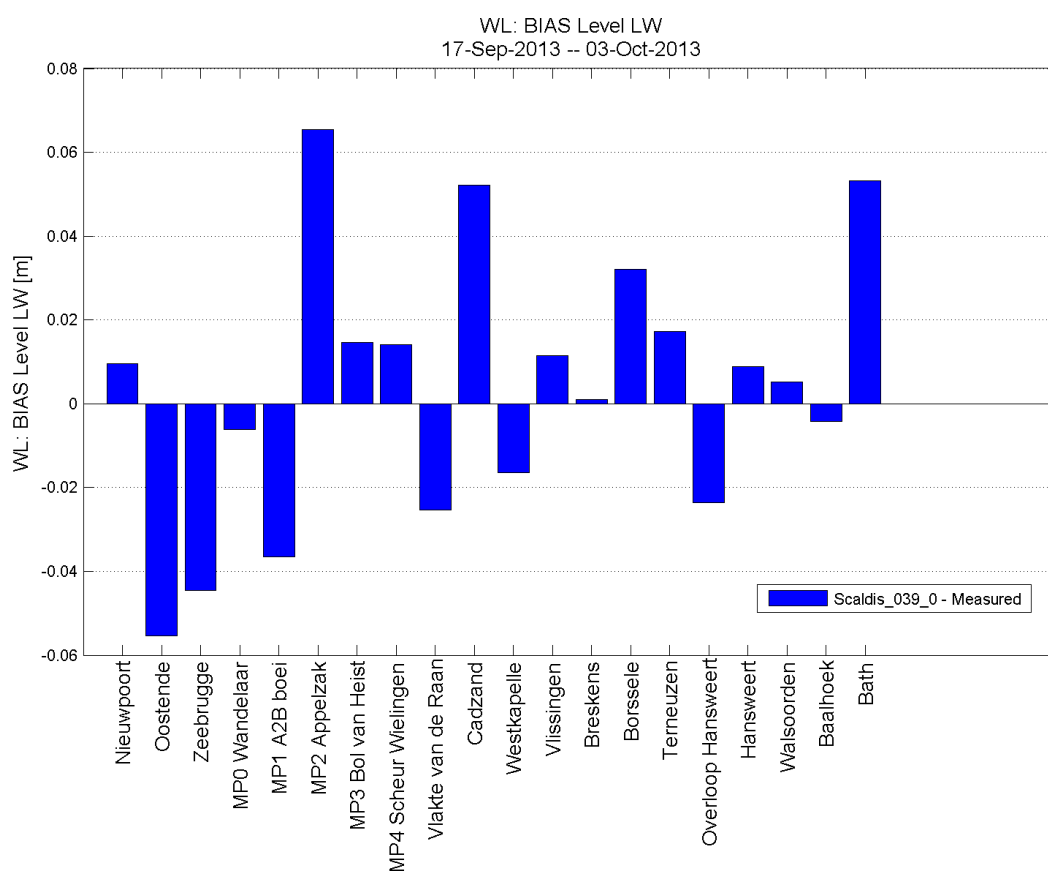


Figure 243 - Bias of low water magnitude (model – measurement) in the North sea and Western Scheldt

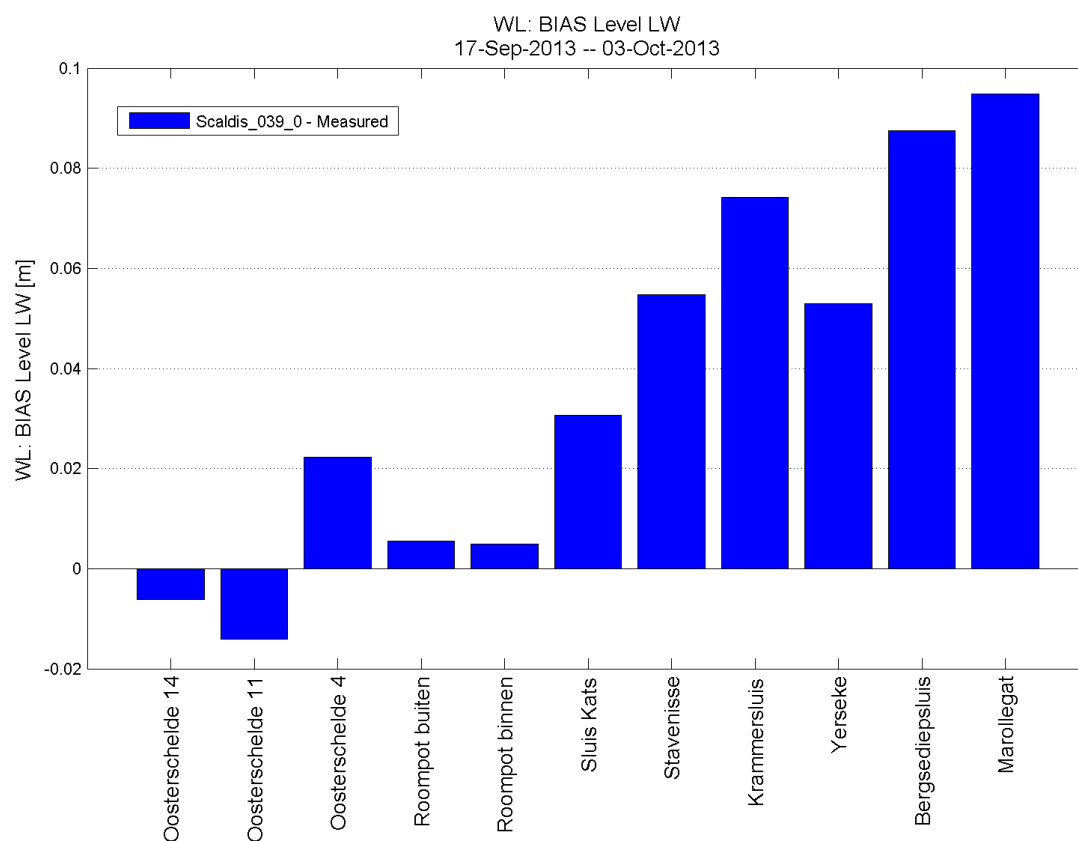


Figure 244 - Bias of low water magnitude (model – measurement) in the Eastern Scheldt

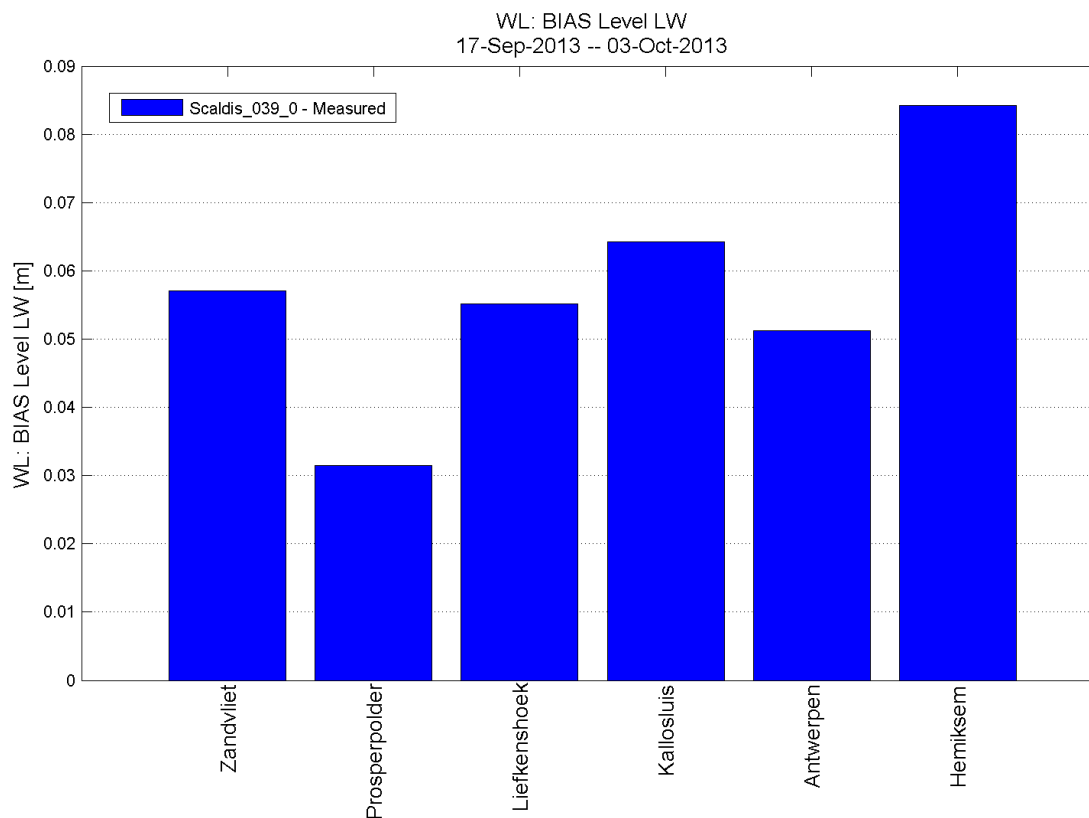


Figure 245 - Bias of low water magnitude (model – measurement) in the Lower Sea Scheldt

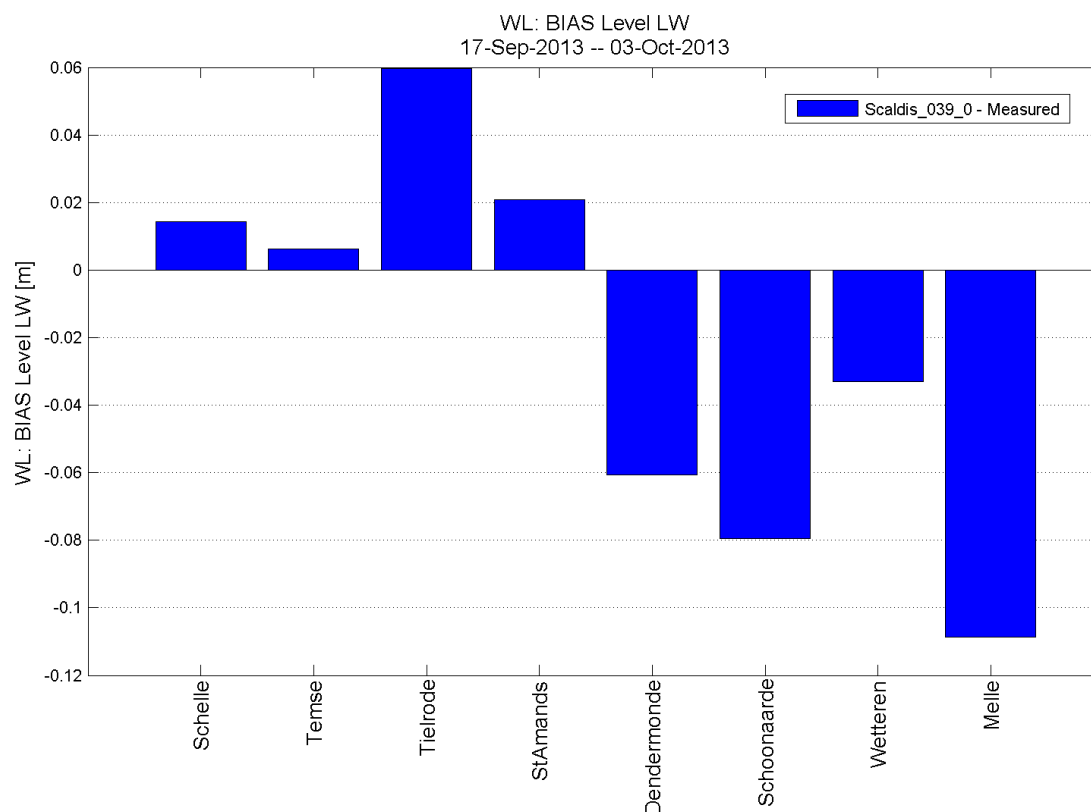


Figure 246 - Bias of low water magnitude (model – measurement) in the Upper Sea Scheldt

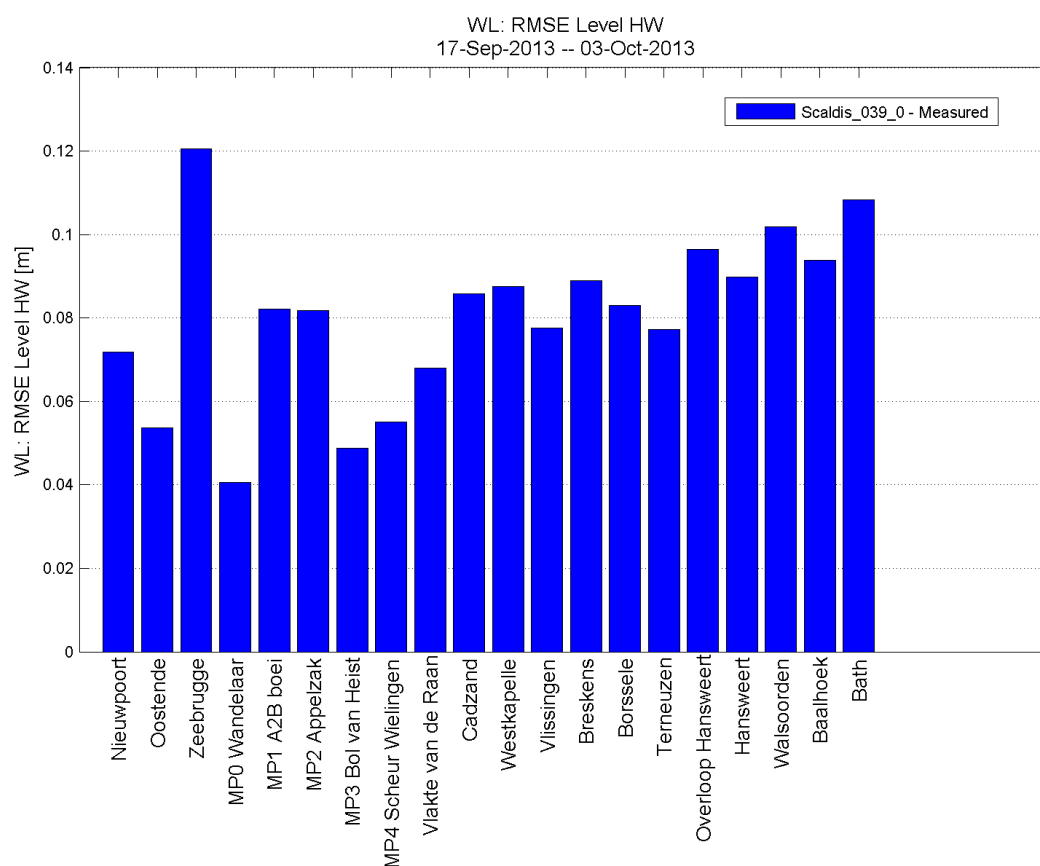


Figure 247 - RMSE of high water magnitude (model vs. measurement) in the North sea and Western Scheldt

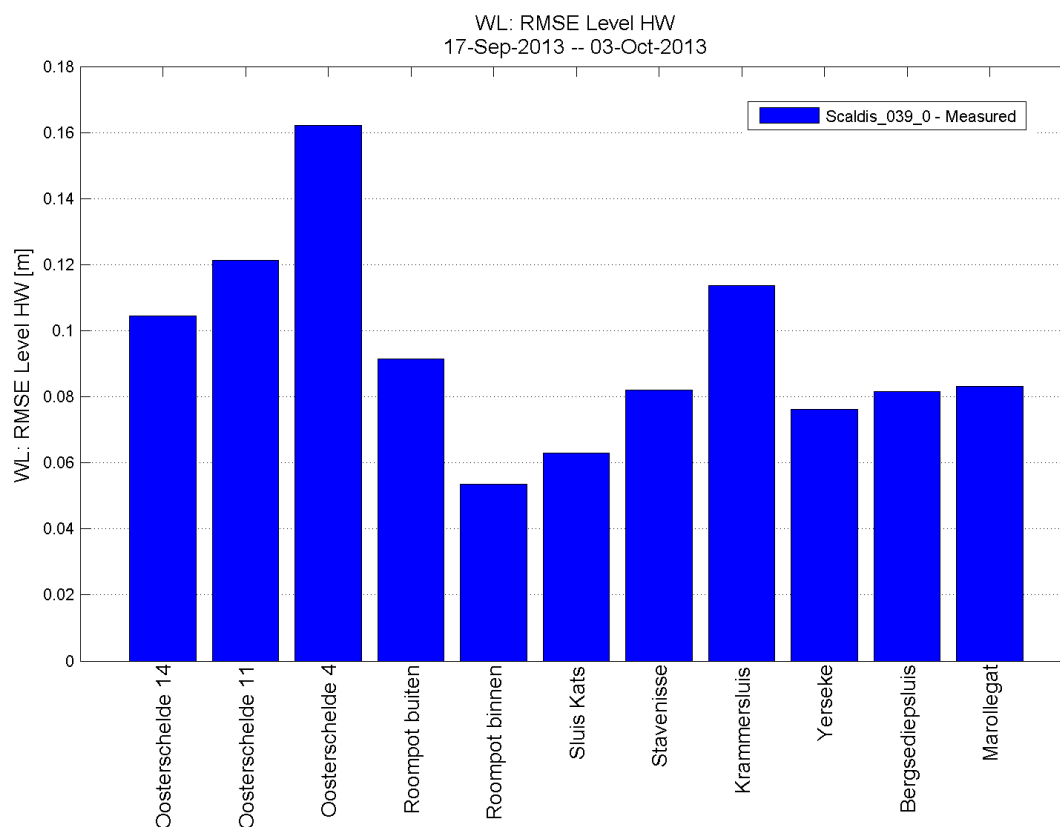


Figure 248 - RMSE of high water magnitude (model vs. measurement) in the Eastern Scheldt

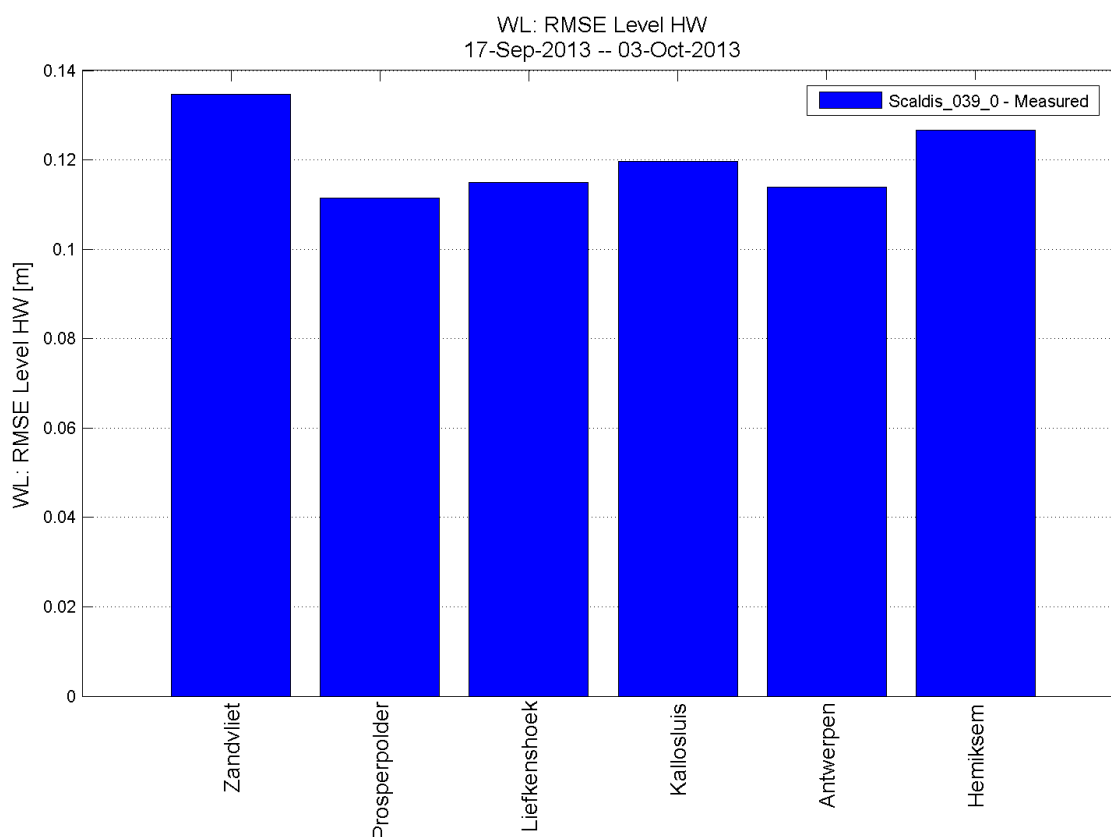


Figure 249 - RMSE of high water magnitude (model vs. measurement) in the Lower Sea Scheldt

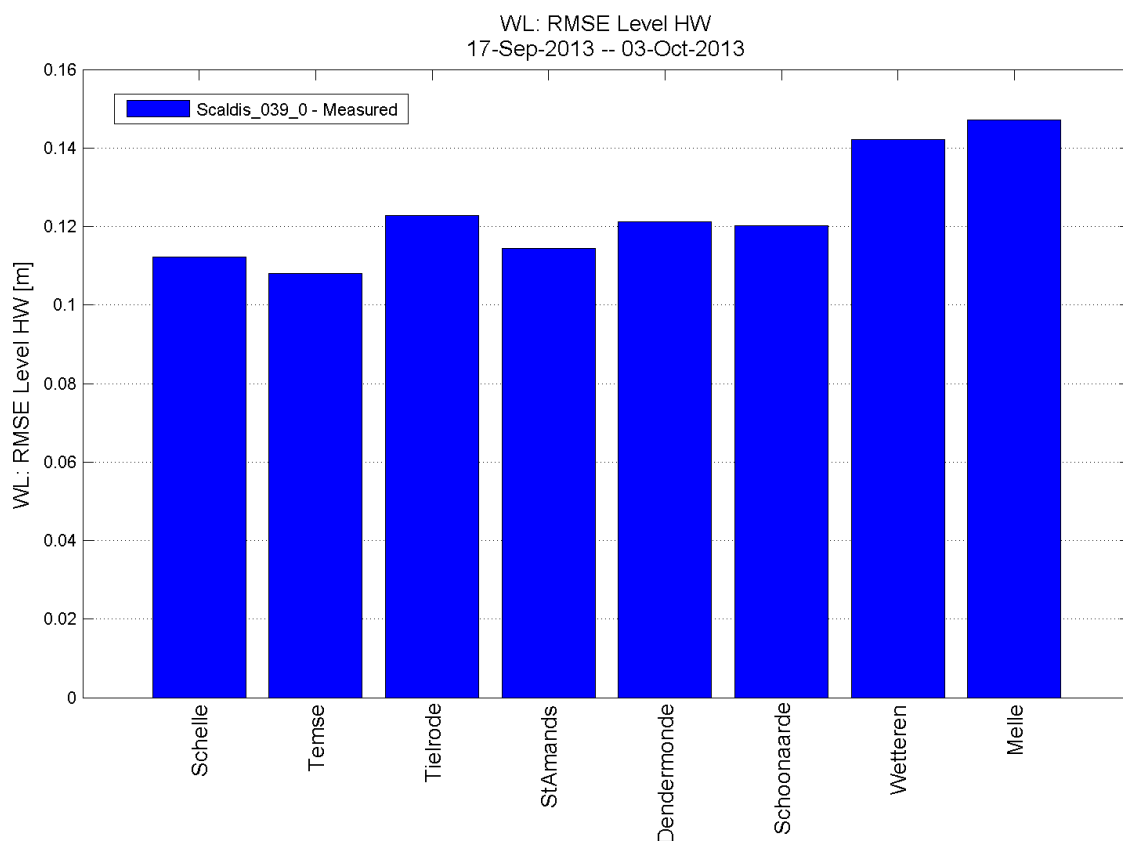


Figure 250 - RMSE of high water magnitude (model vs. measurement) in the Upper Sea Scheldt

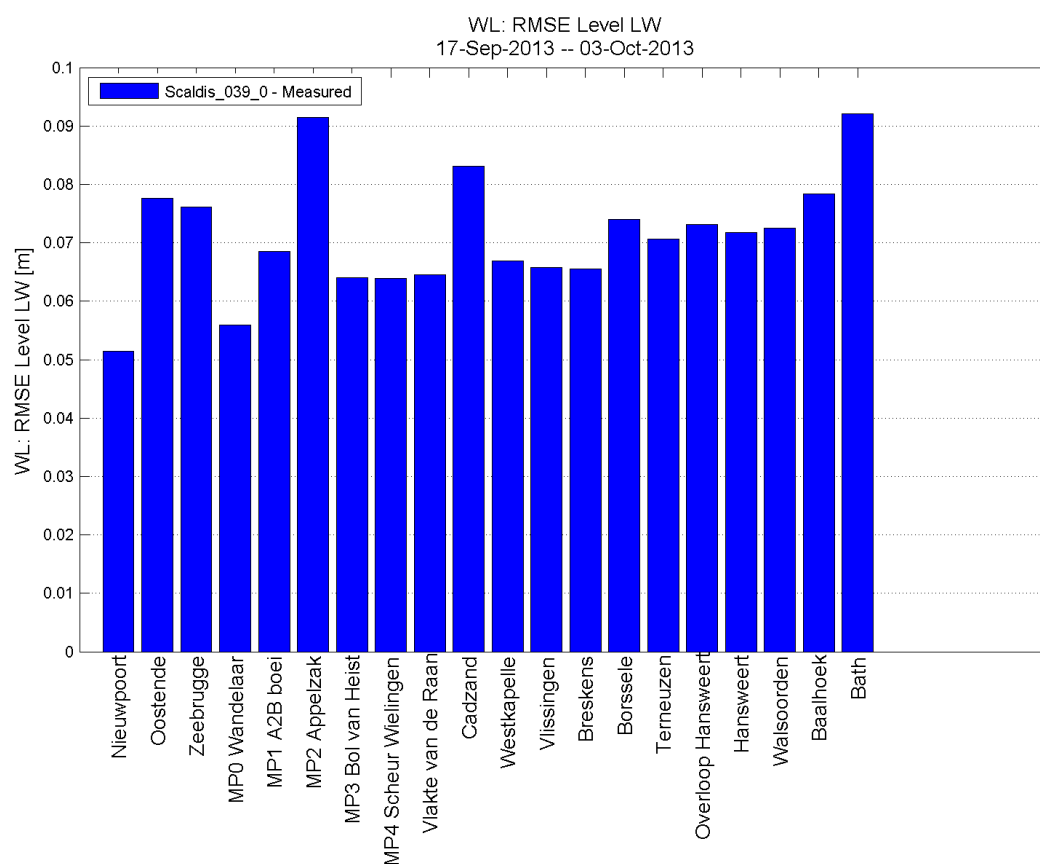


Figure 251 - RMSE of low water magnitude (model vs. measurement) in the North sea and Western Scheldt

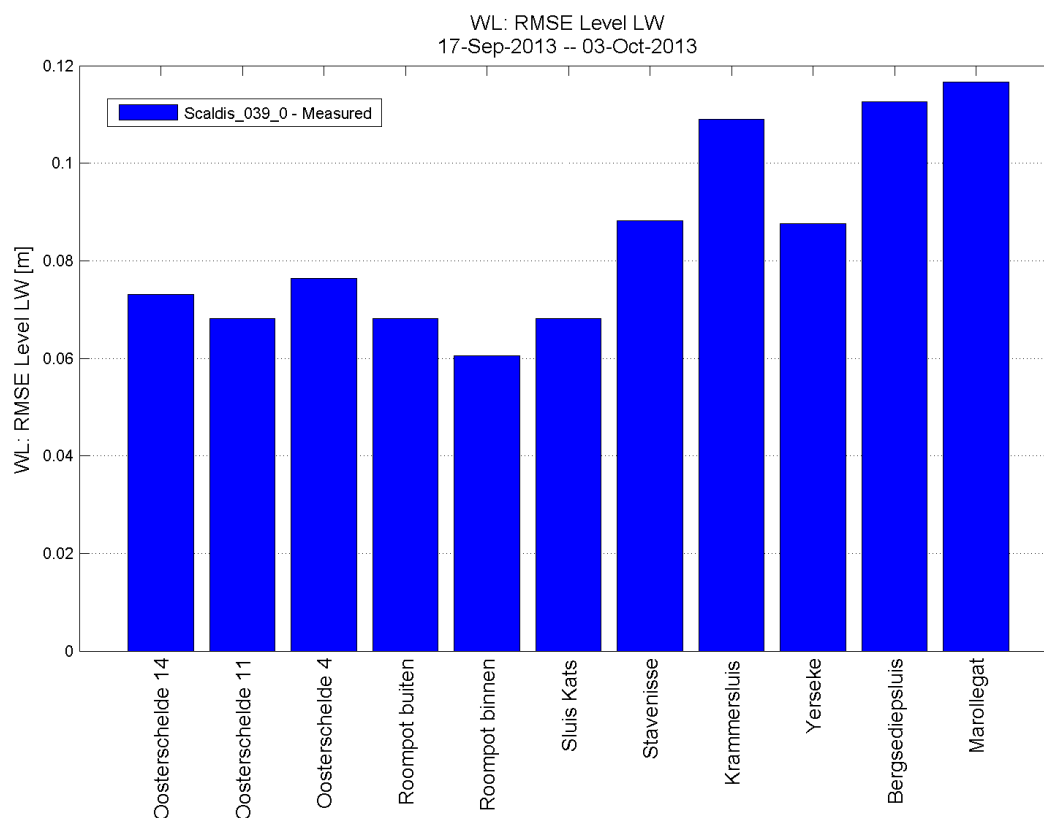


Figure 252 - RMSE of low water magnitude (model vs. measurement) in the Eastern Scheldt

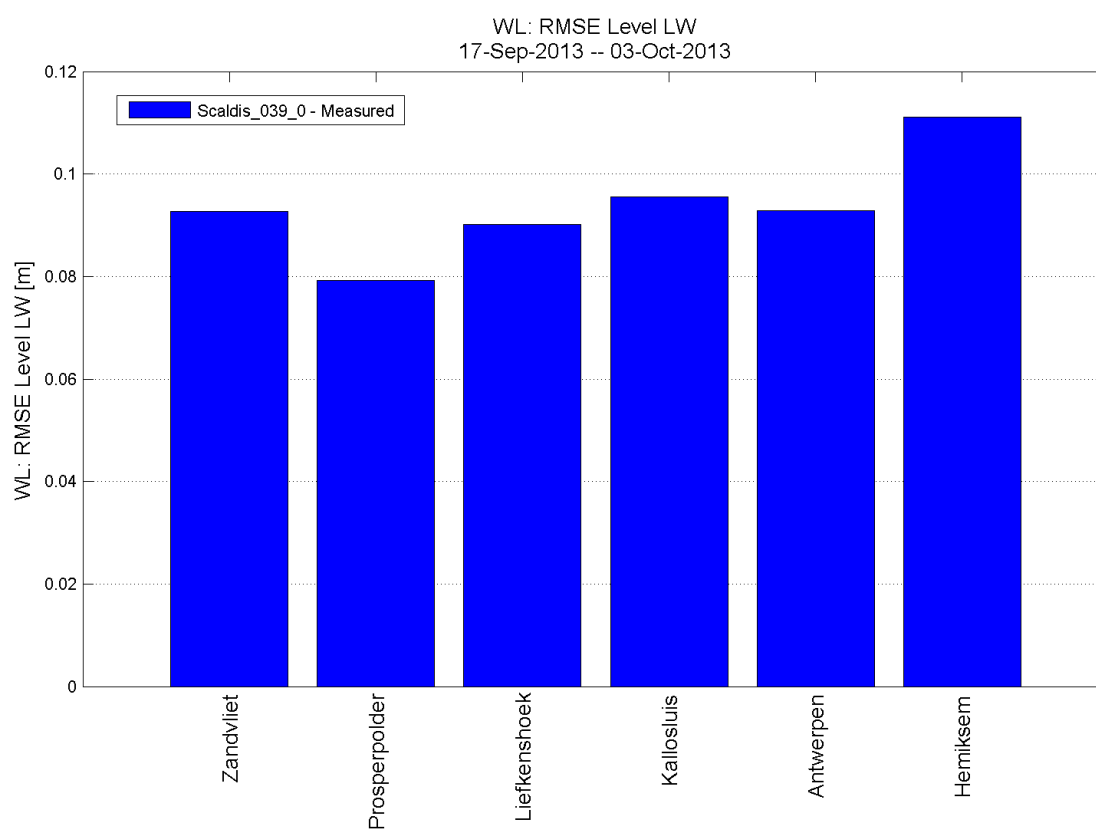


Figure 253 - RMSE of low water magnitude (model vs. measurement) in the Lower Sea Scheldt

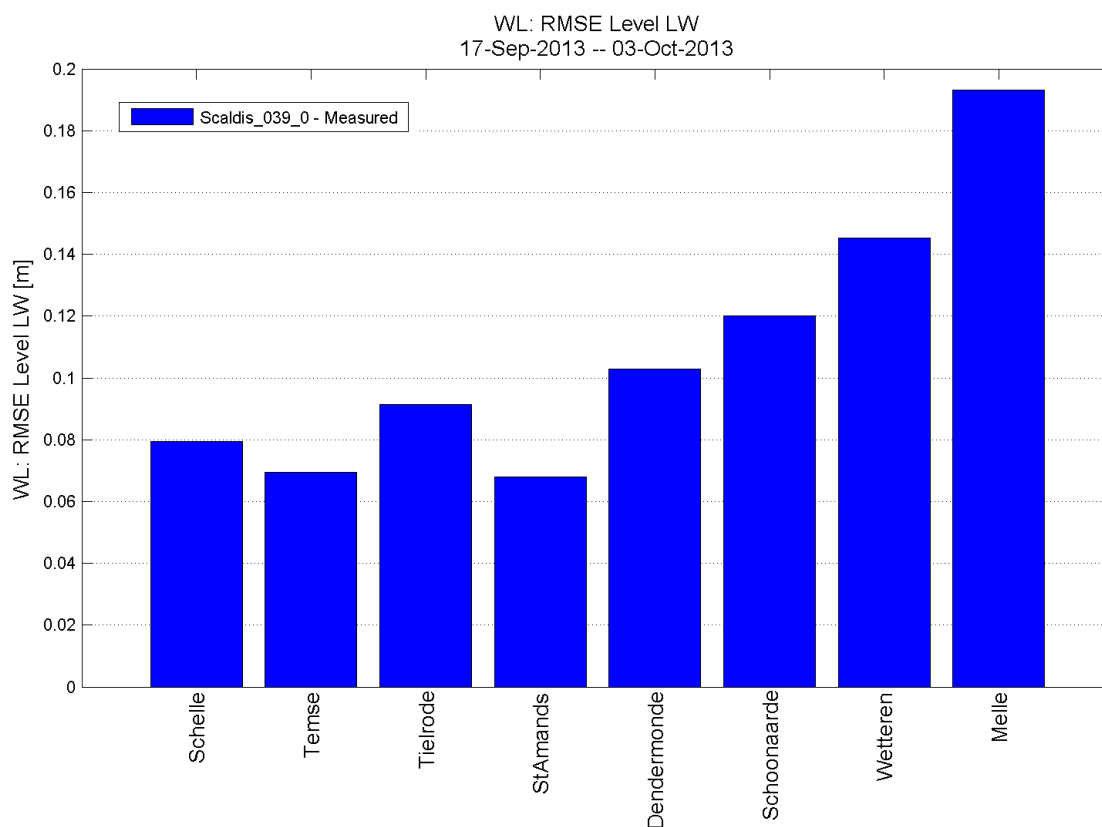


Figure 254 - RMSE of low water magnitude (model vs. measurement) in the Upper Sea Scheldt

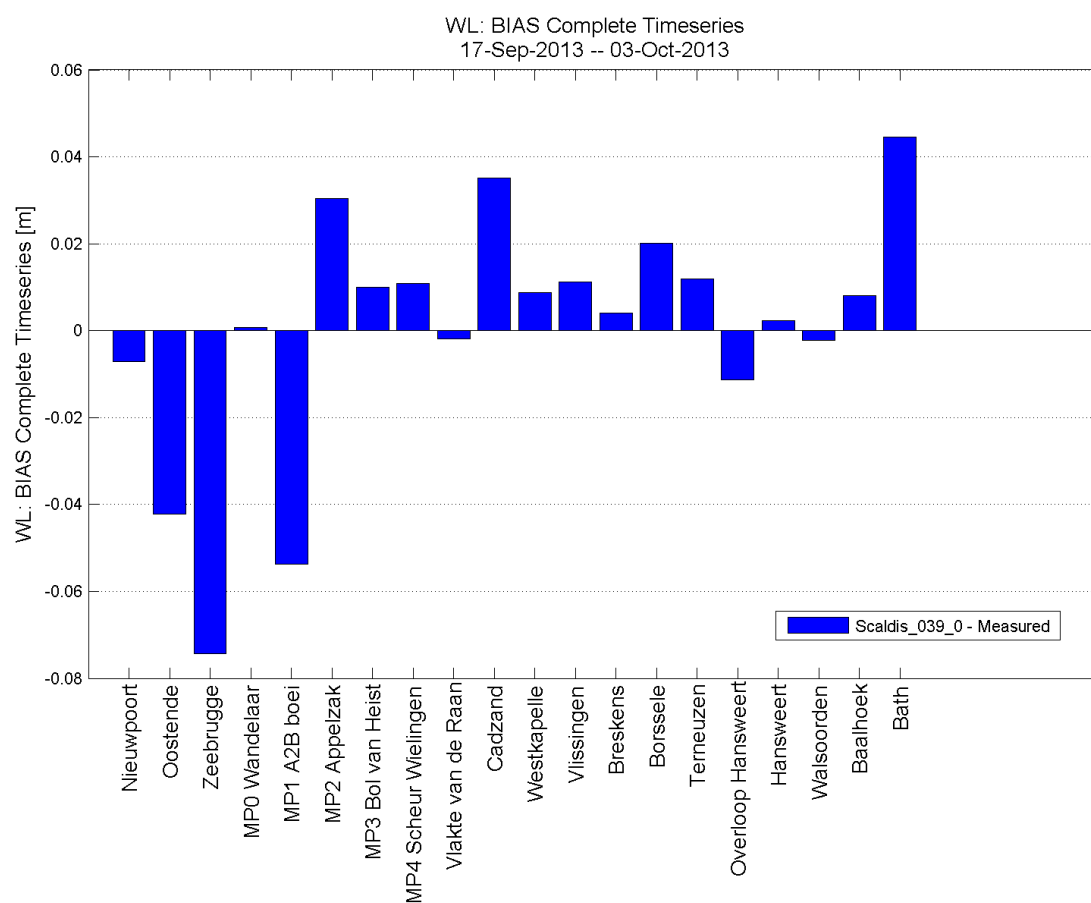


Figure 255 - Bias of the water level time series in the North sea and Western Scheldt

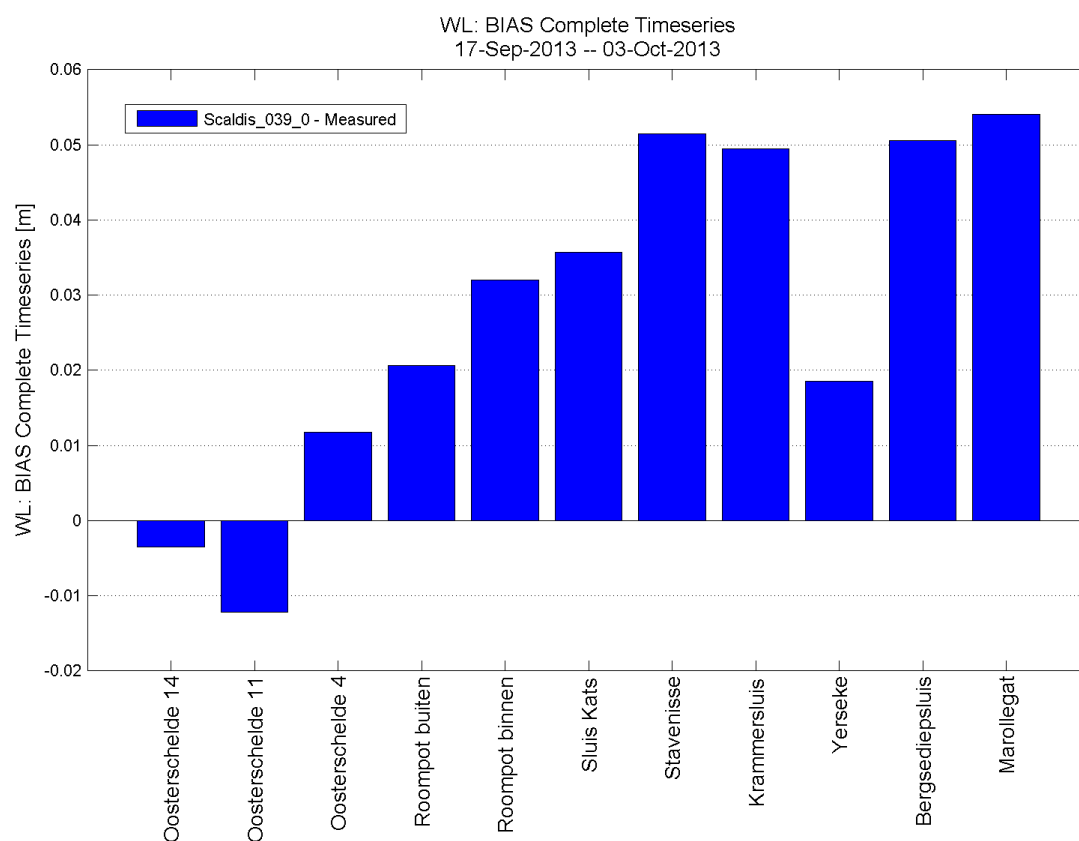


Figure 256 - Bias of the water level time series in the Eastern Scheldt

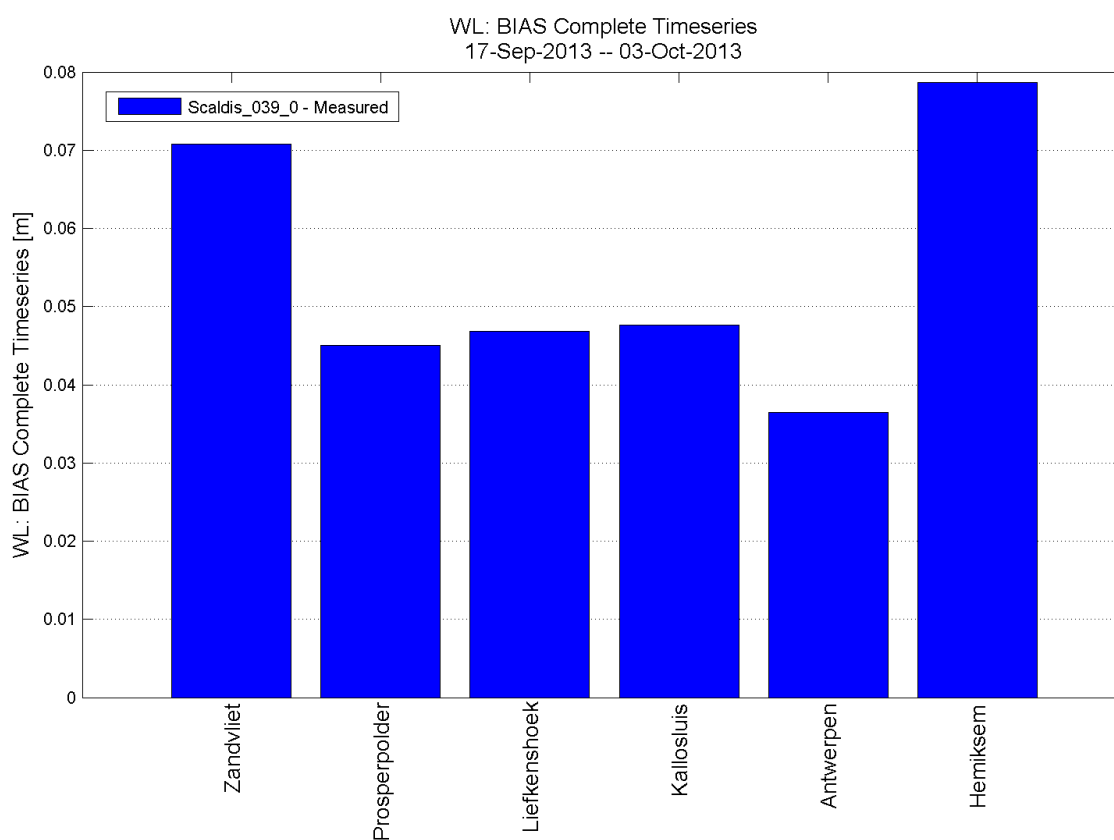


Figure 257 - Bias of the water level time series in the Lower Sea Scheldt

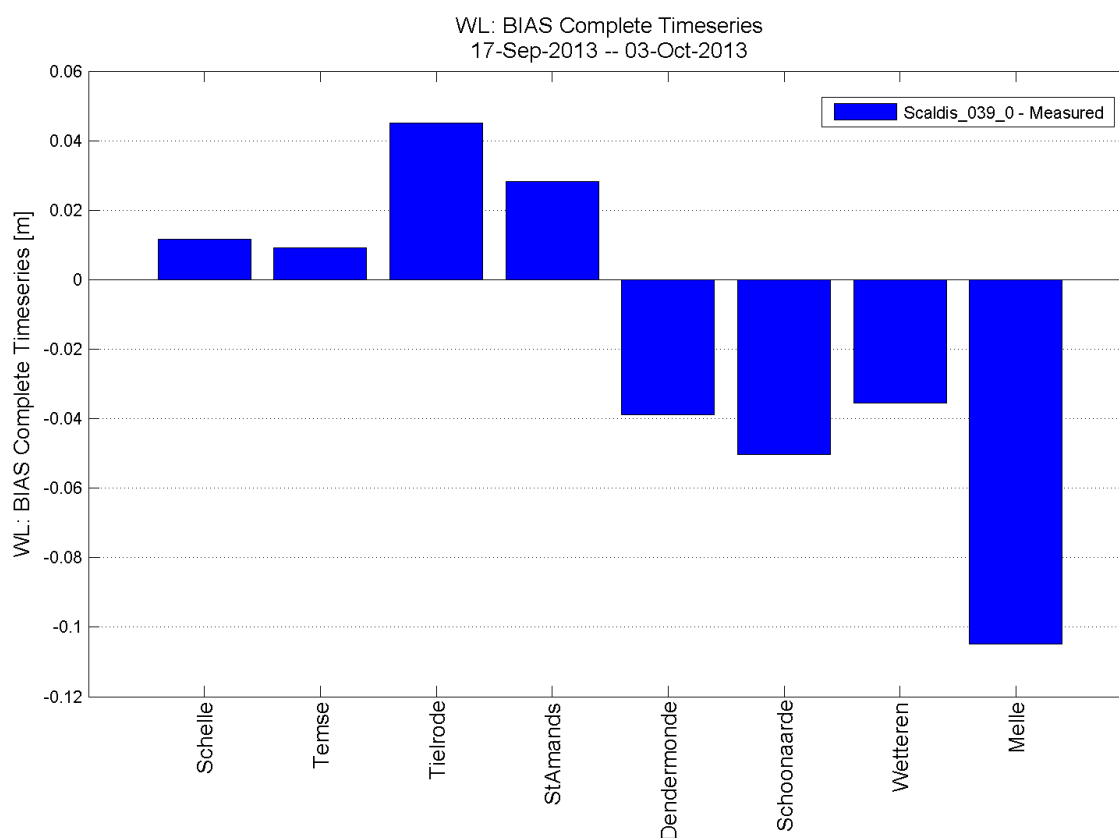


Figure 258 - Bias of the water level time series in the Upper Sea Scheldt

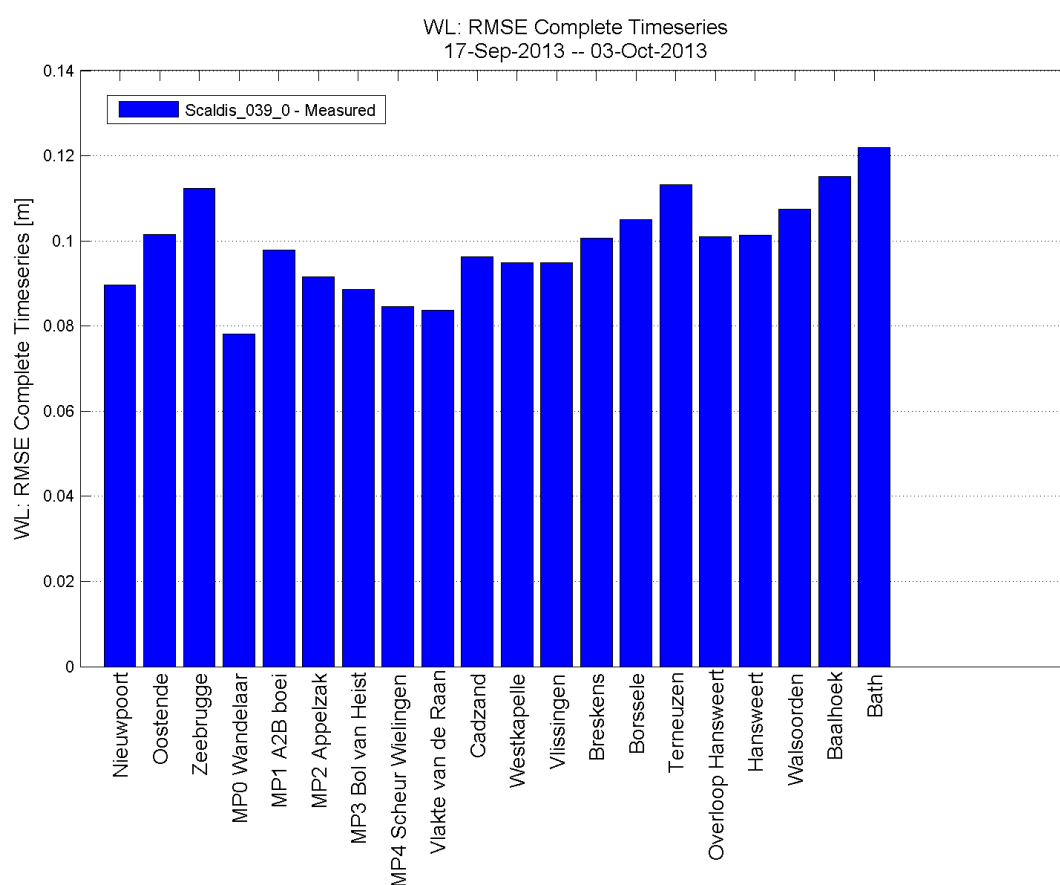


Figure 259 - RMSE of the water level time series in the North sea and Western Scheldt

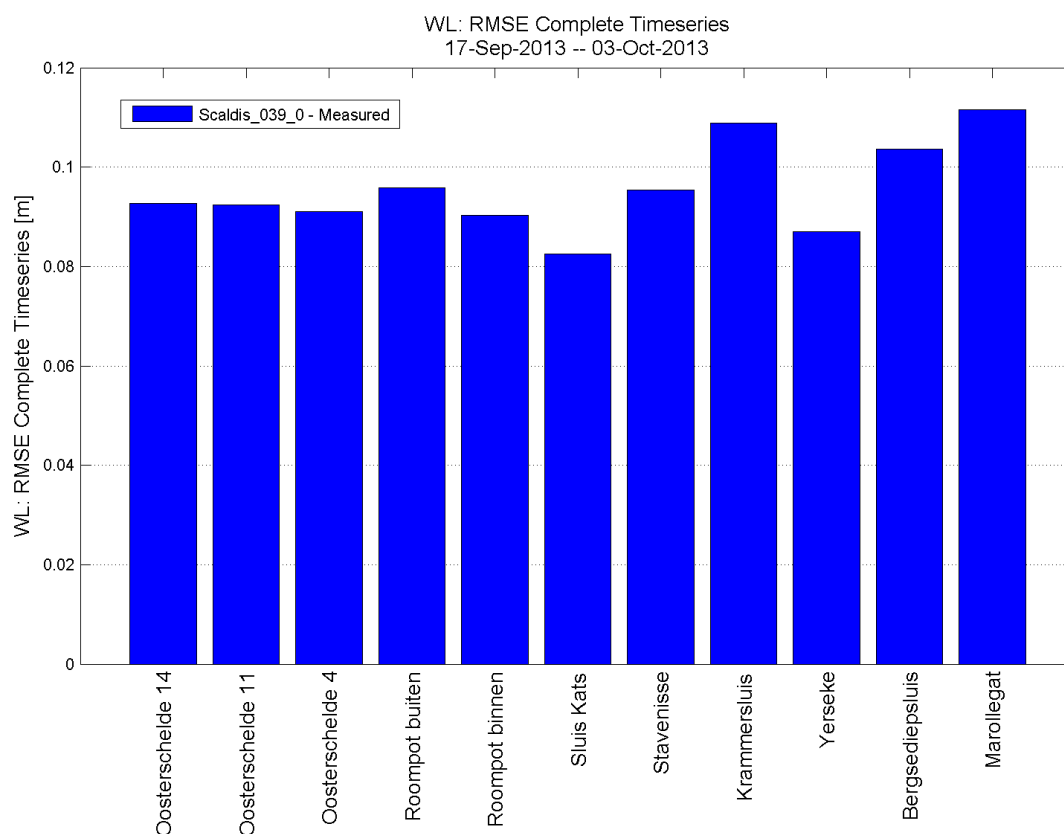


Figure 260 - RMSE of the water level time series in the Eastern Scheldt

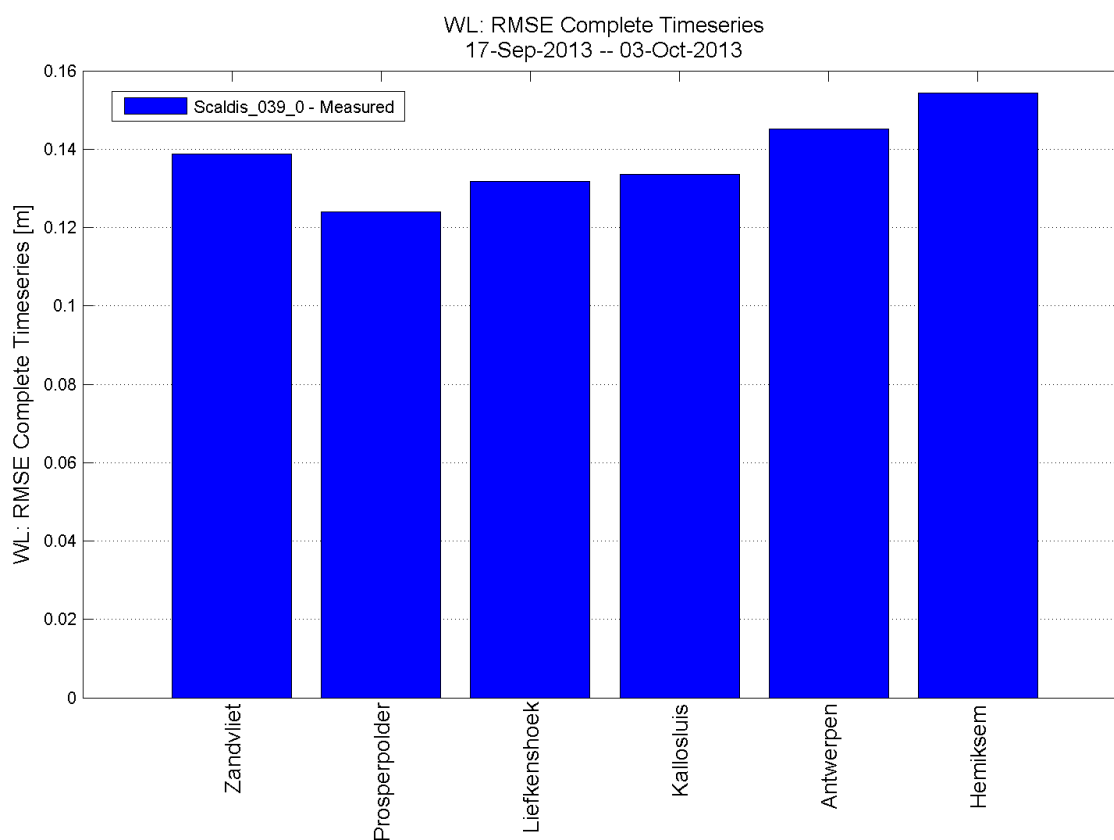


Figure 261 - RMSE of the water level time series in the Lower Sea Scheldt

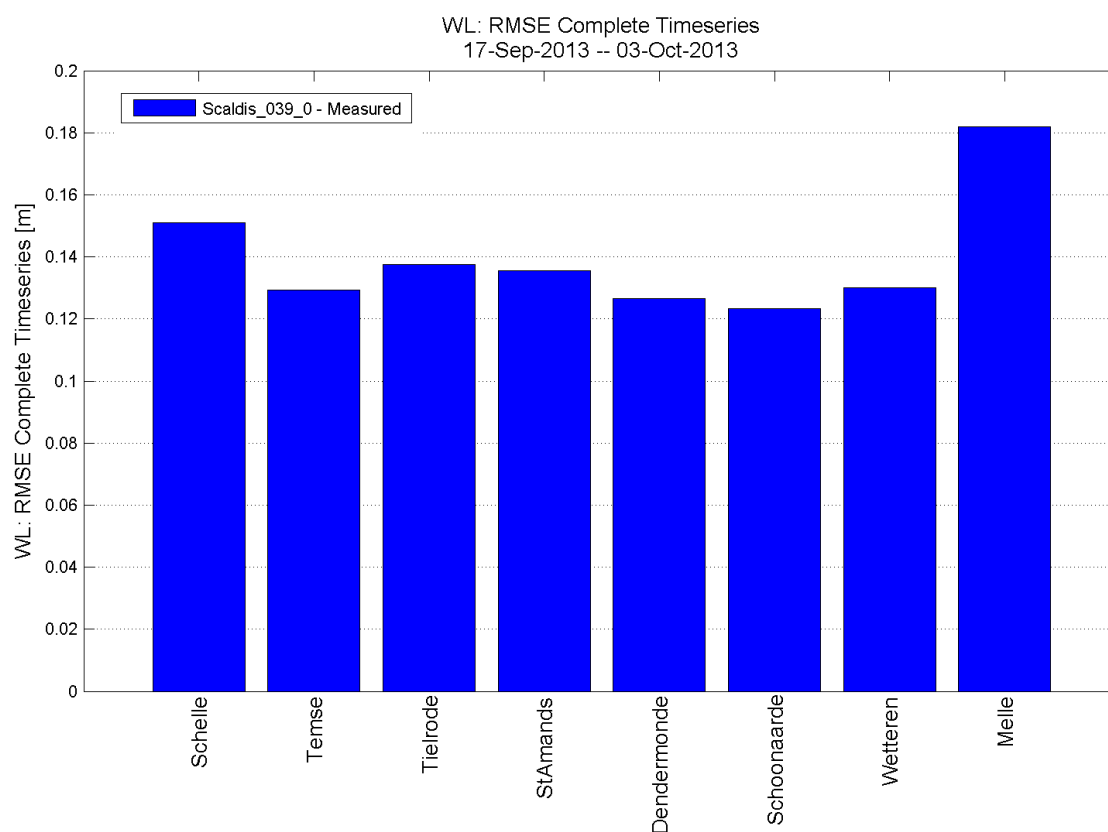


Figure 262 - RMSE of the water level time series in the Upper Sea Scheldt

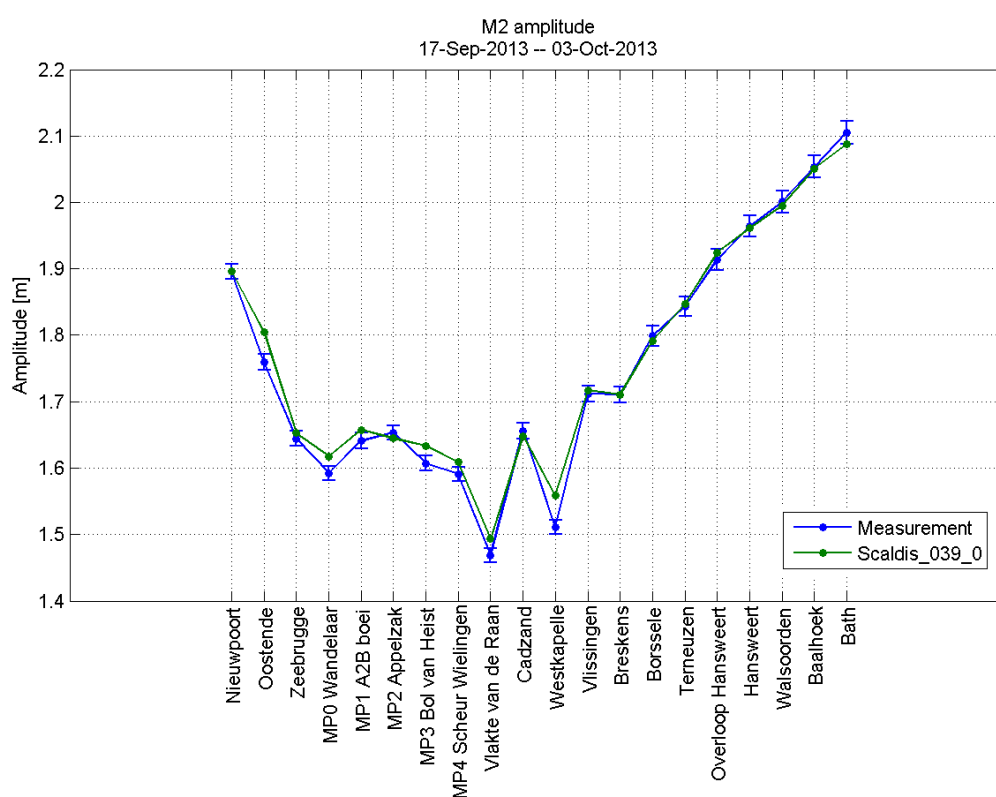


Figure 263 - M2 amplitude in the North sea and Western Scheldt

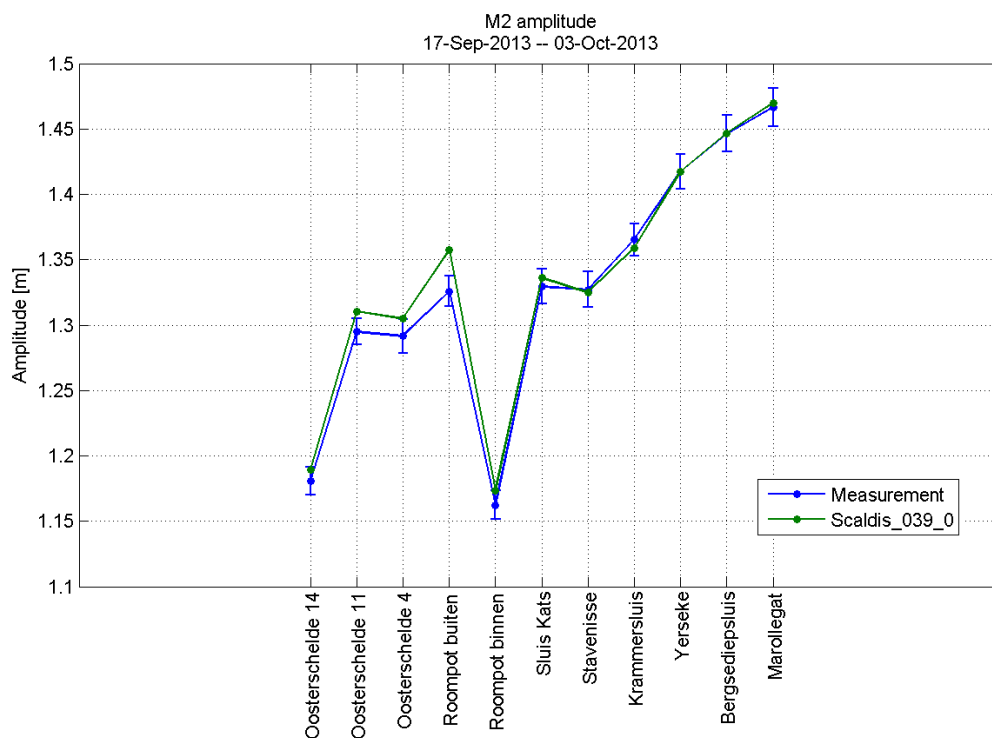


Figure 264 - M2 amplitude in the Eastern Scheldt

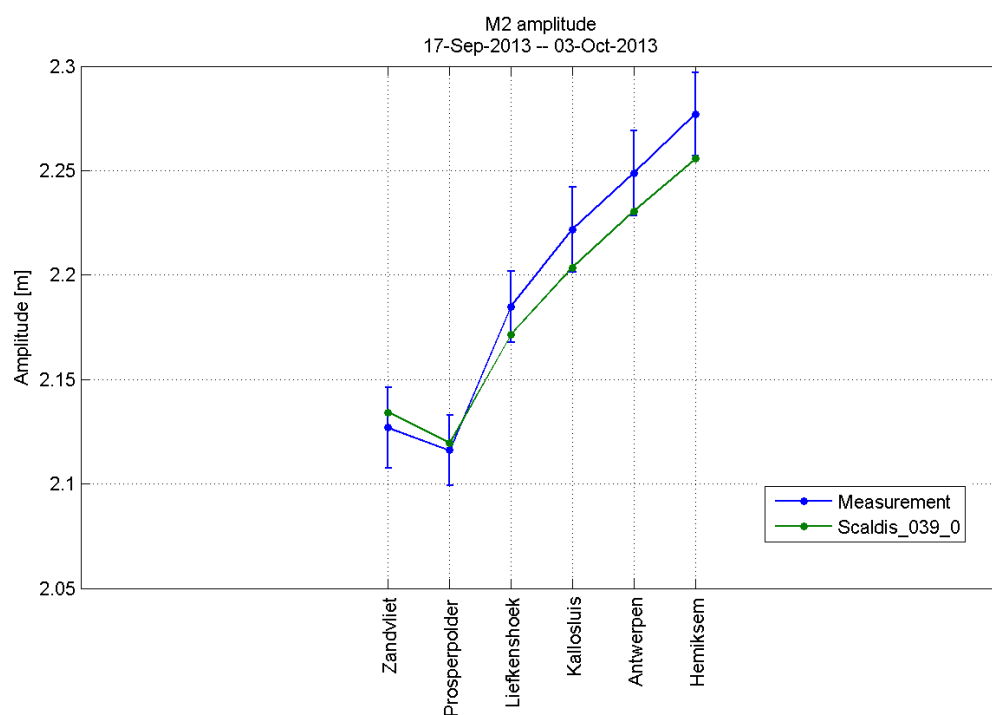


Figure 265 - M2 amplitude in the Lower Sea Scheldt

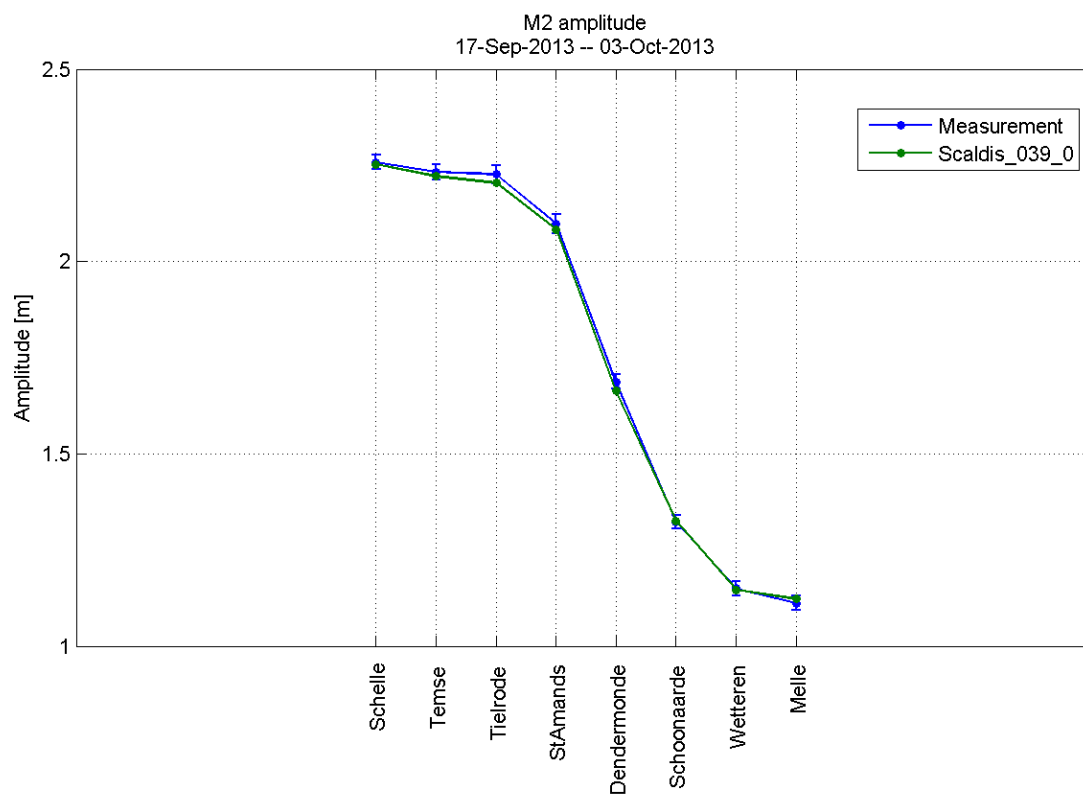


Figure 266 - M2 amplitude in the Upper Sea Scheldt

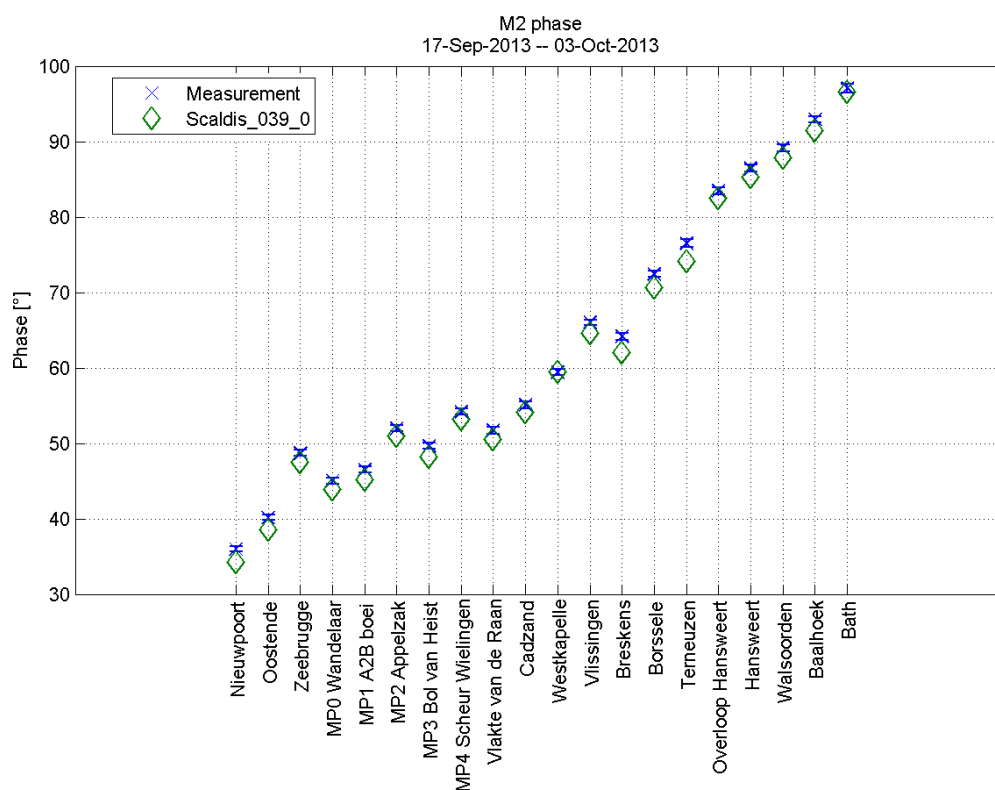


Figure 267 - M2 phase in the North sea and Western Scheldt

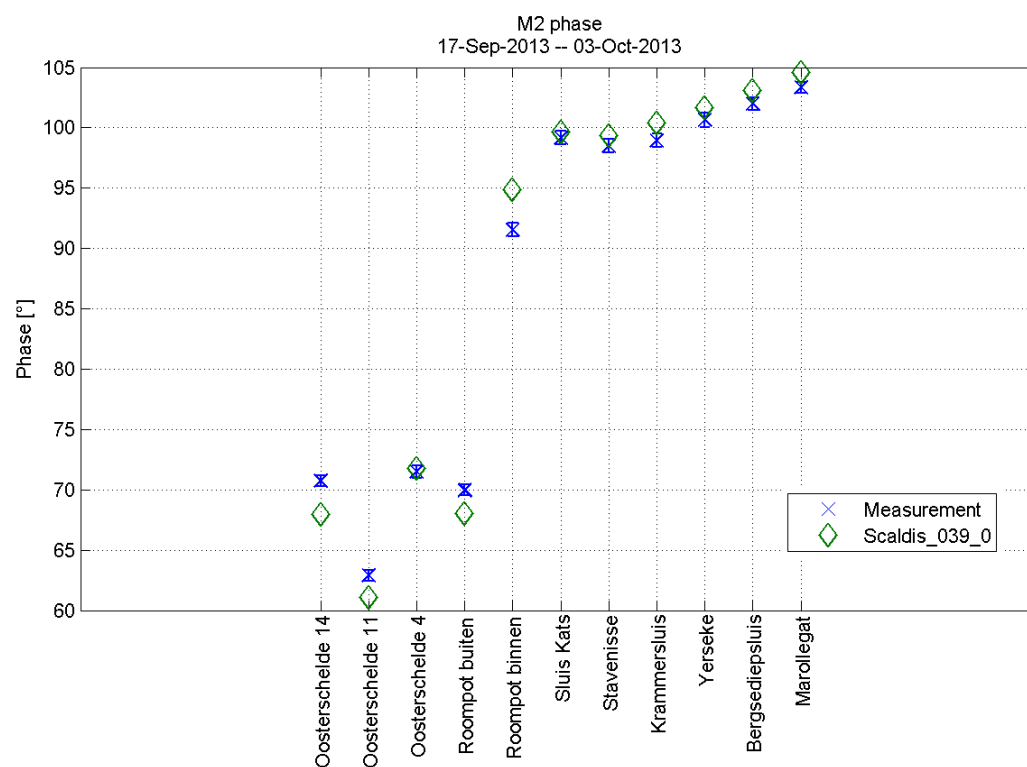


Figure 268 - M2 phase in the Eastern Scheldt

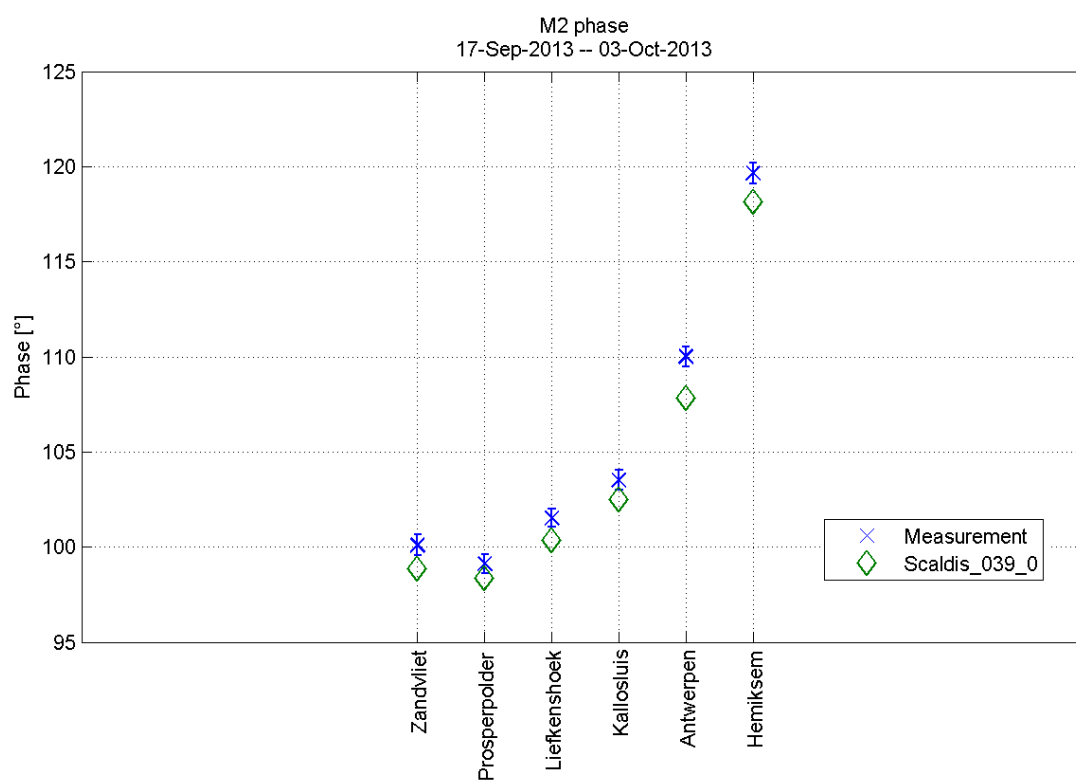


Figure 269 - M2 phase in the Lower Sea Scheldt

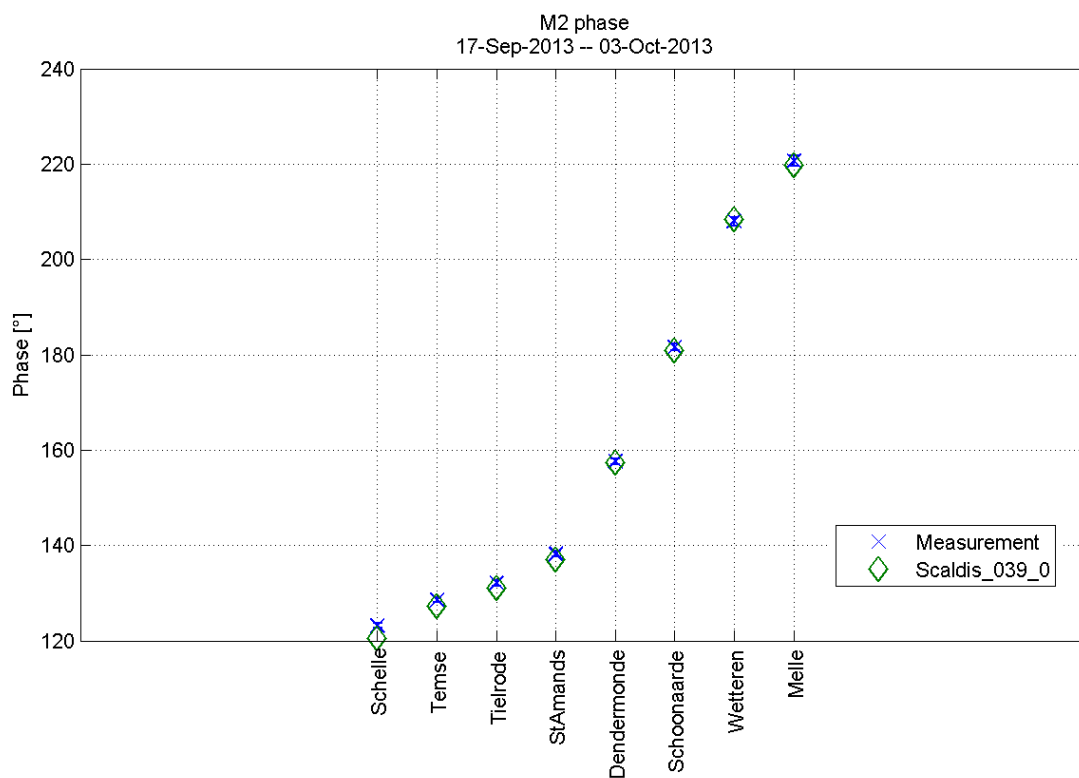


Figure 270 - M2 phase in the Upper Sea Scheldt

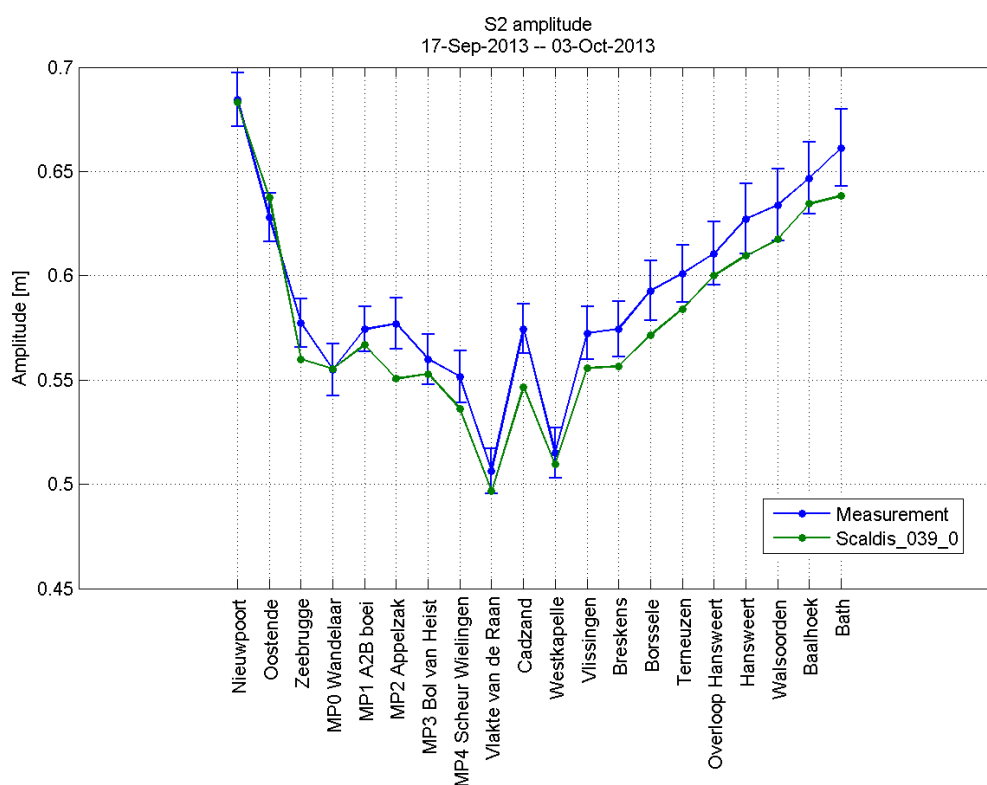


Figure 271 - S2 amplitude in the North sea and Western Scheldt

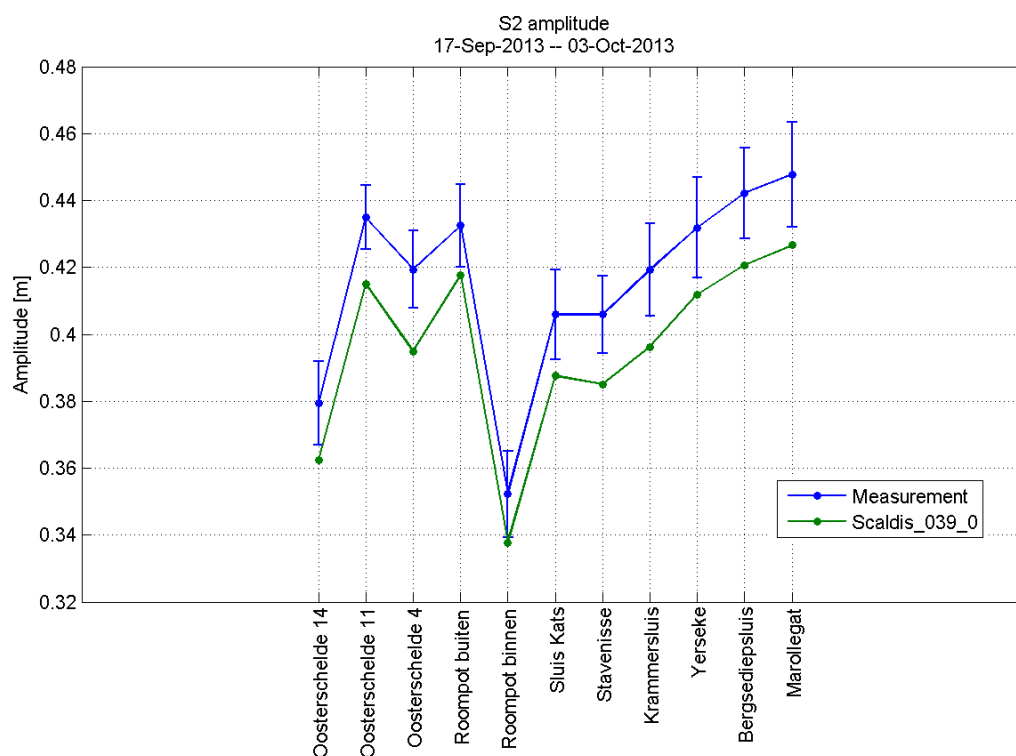


Figure 272 - S2 amplitude in the Eastern Scheldt

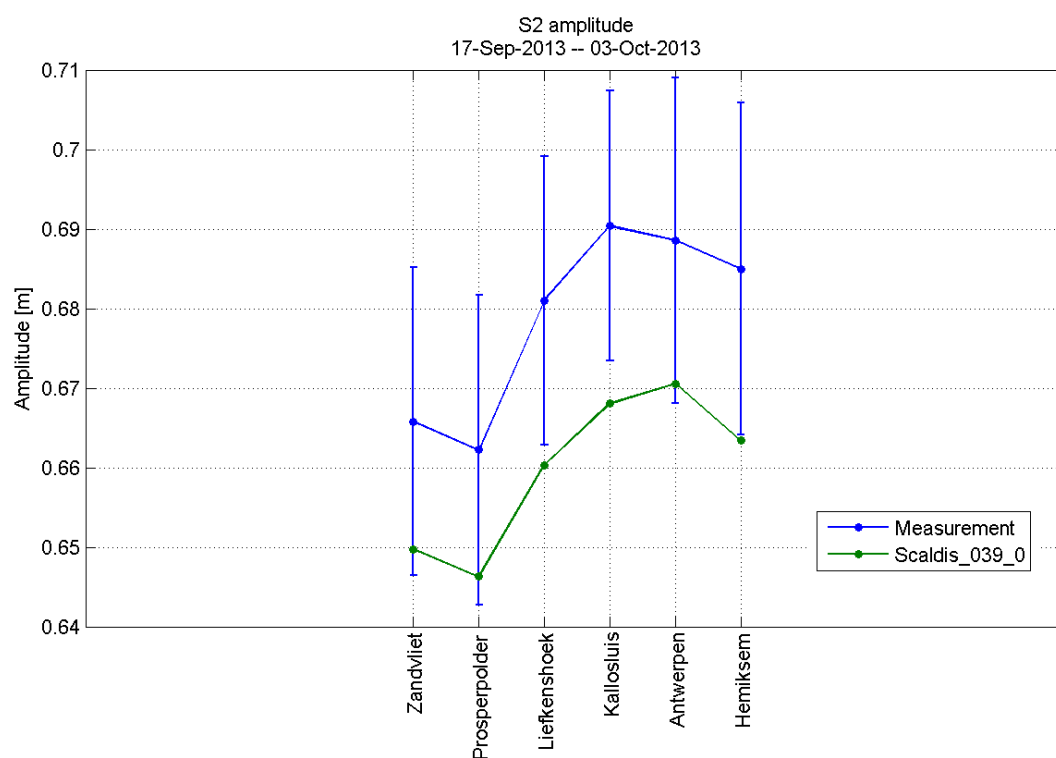


Figure 273 - S2 amplitude in the Lower Sea Scheldt

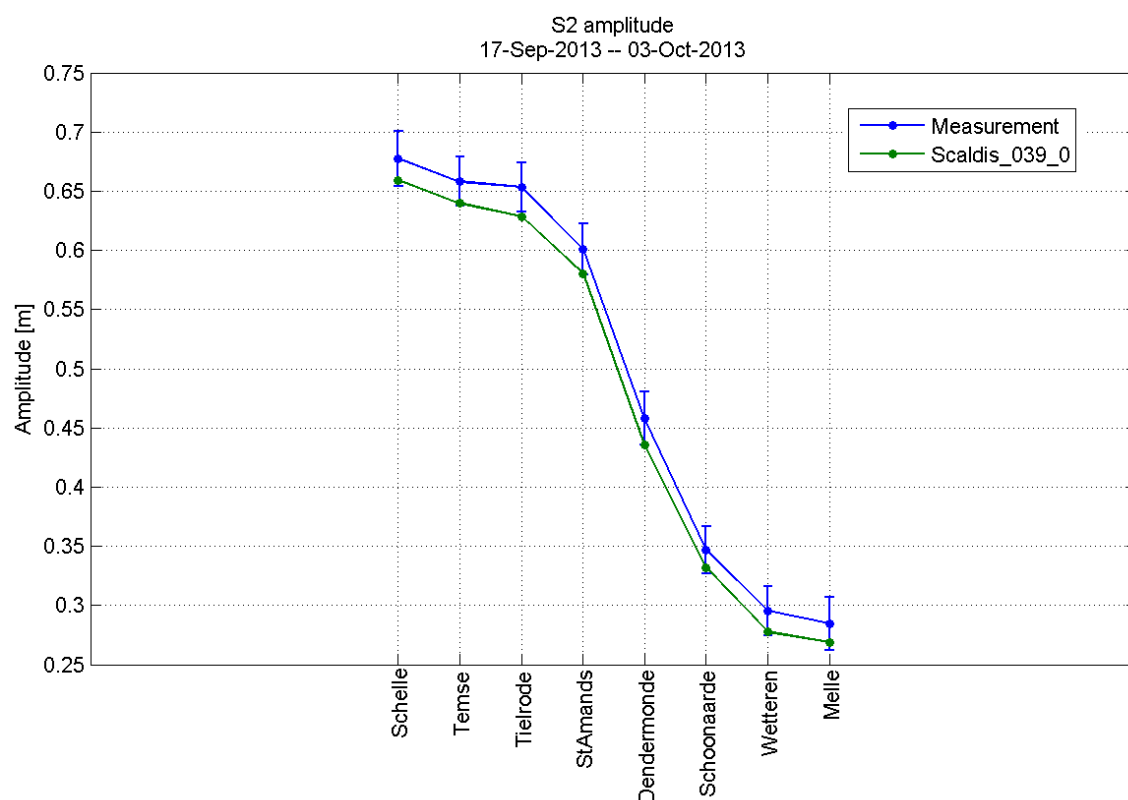


Figure 274 - S2 amplitude in the Upper Sea Scheldt

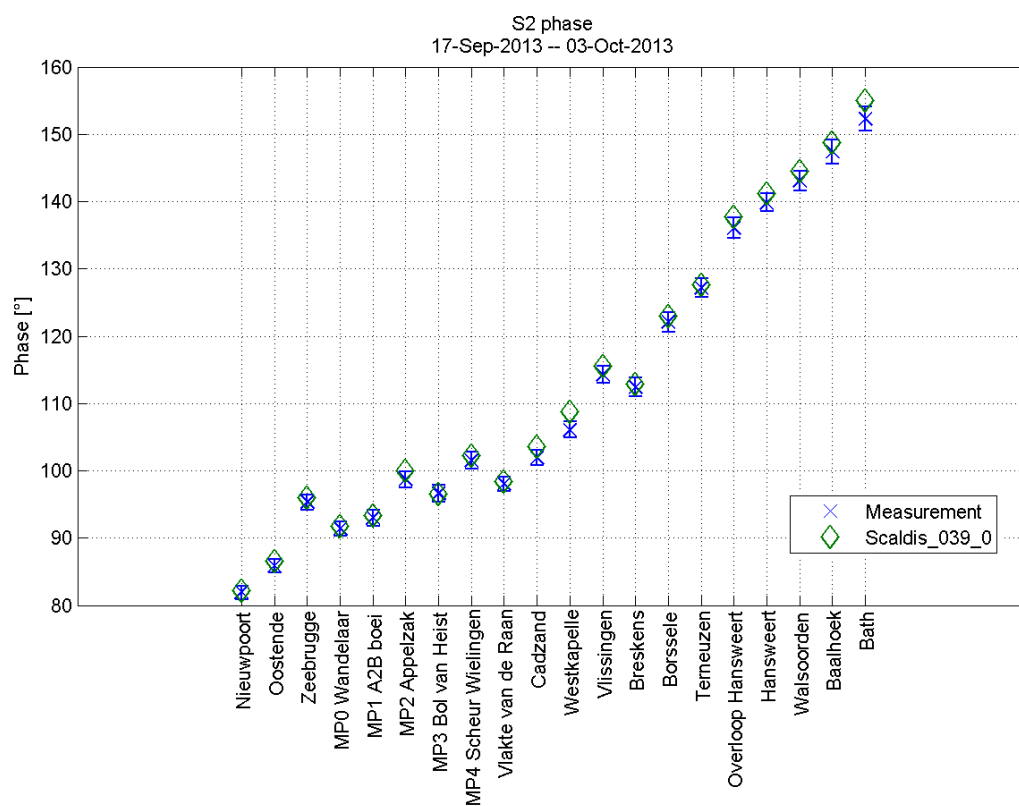


Figure 275 - S2 phase in the North sea and Western Scheldt

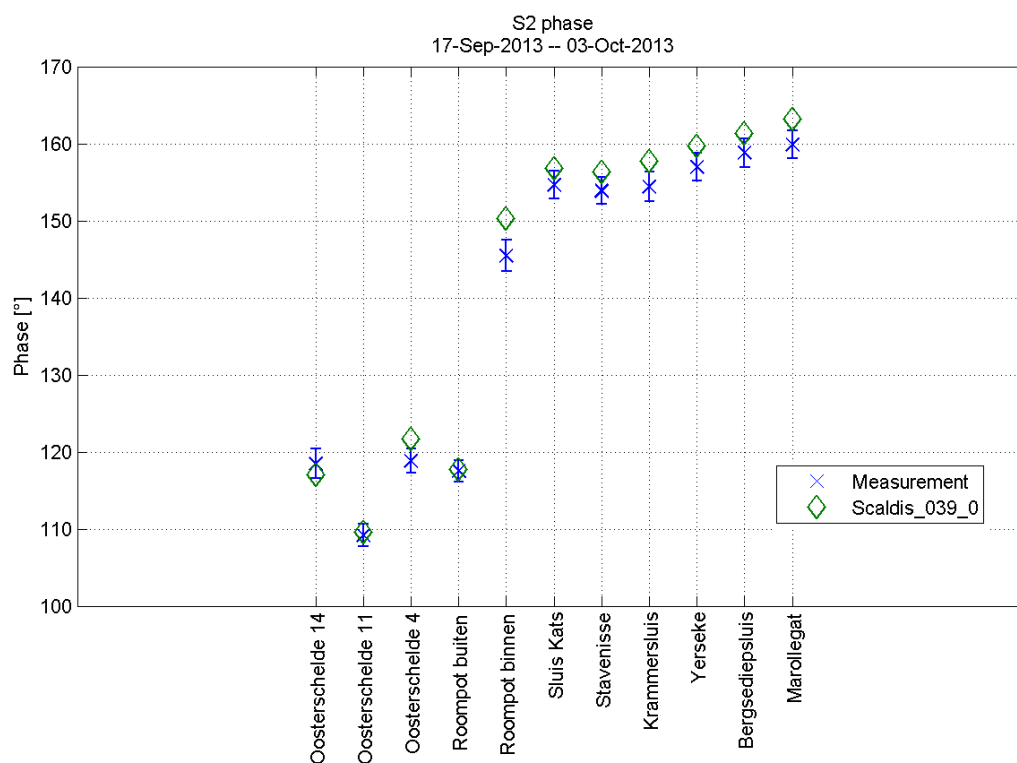


Figure 276 - S2 phase in the Eastern Scheldt

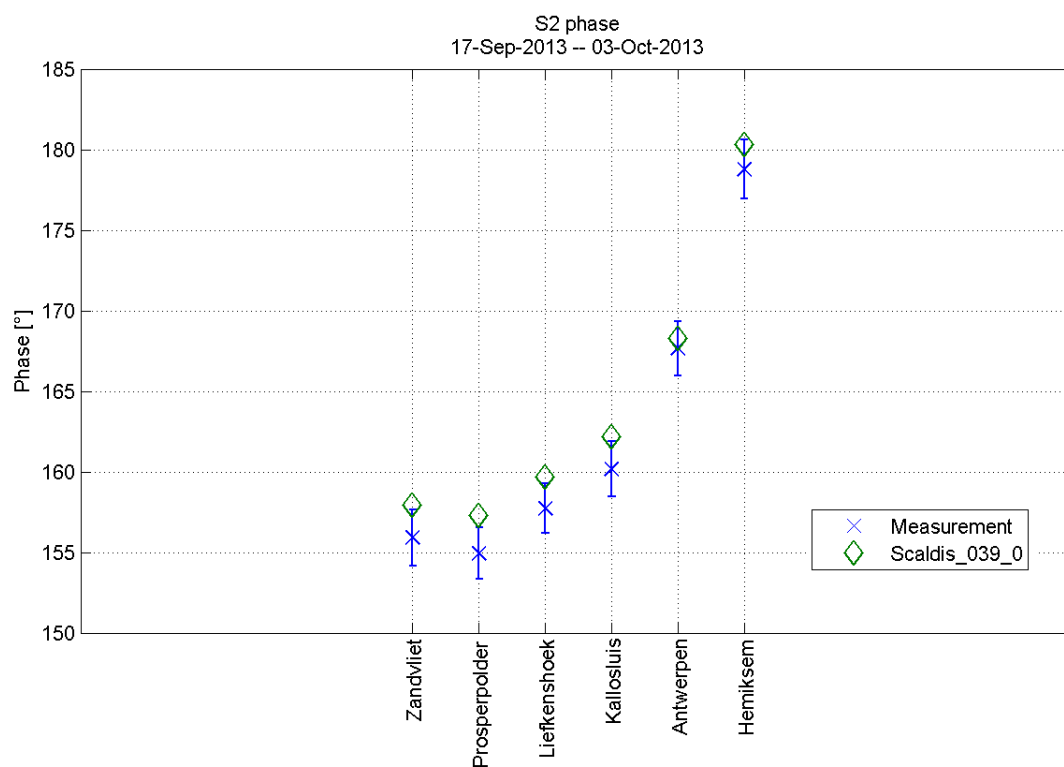


Figure 277 - S2 phase in the Lower Sea Scheldt

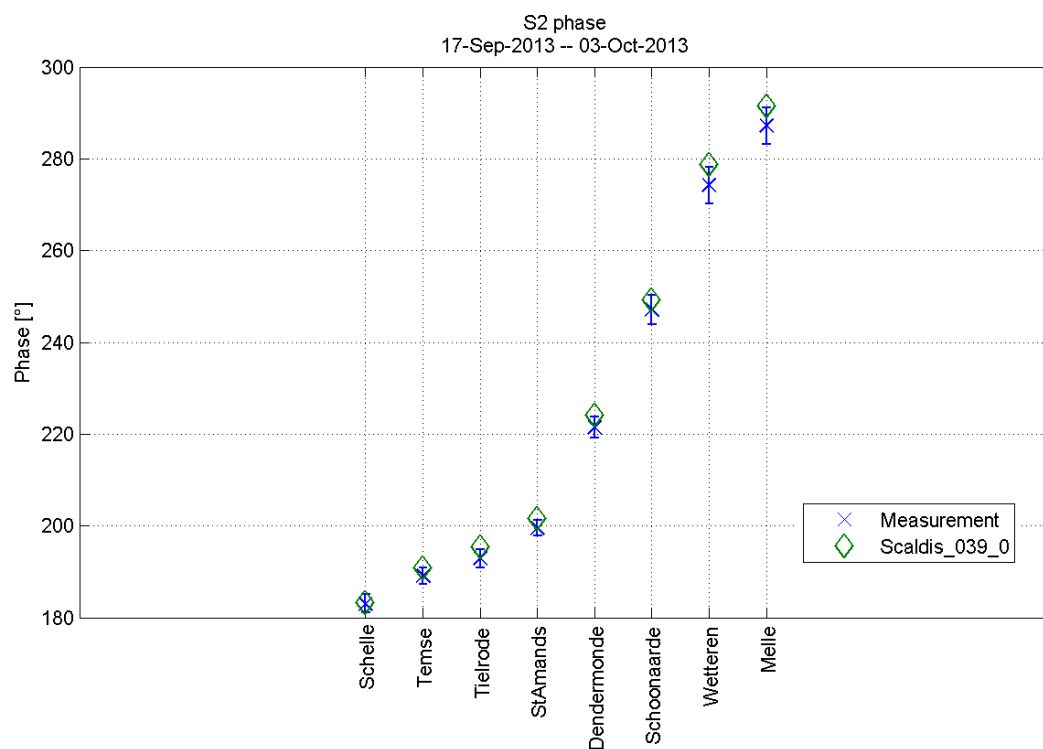


Figure 278 - S2 phase in the Upper Sea Scheldt

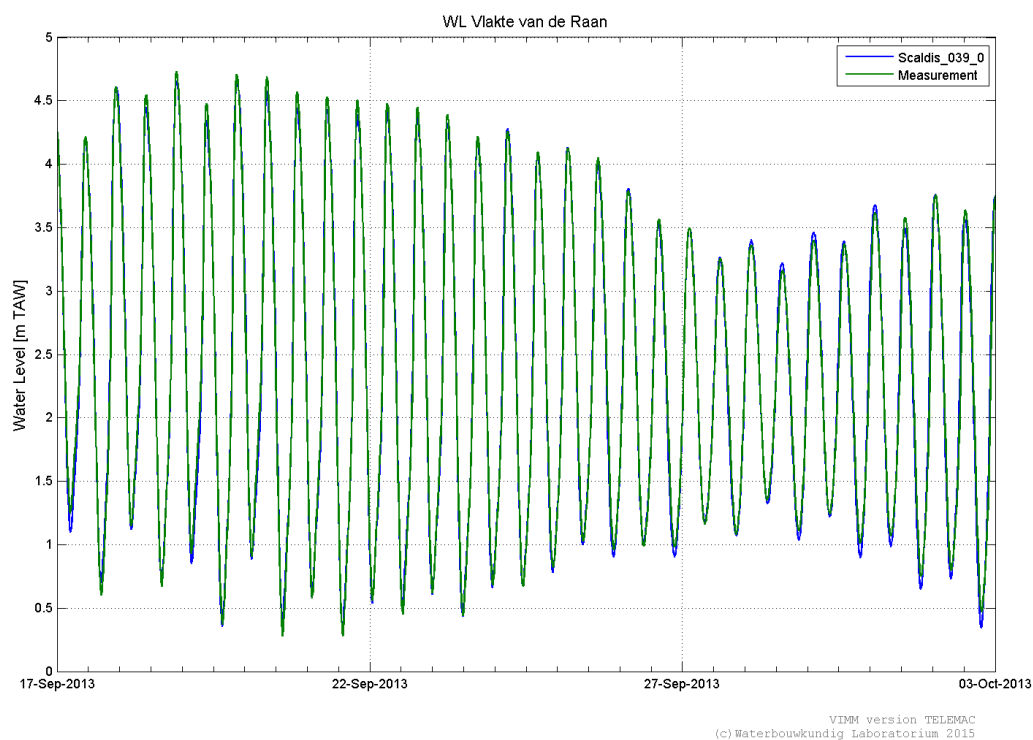


Figure 279 - Calculated and measured water levels at Vlakte van de Raan

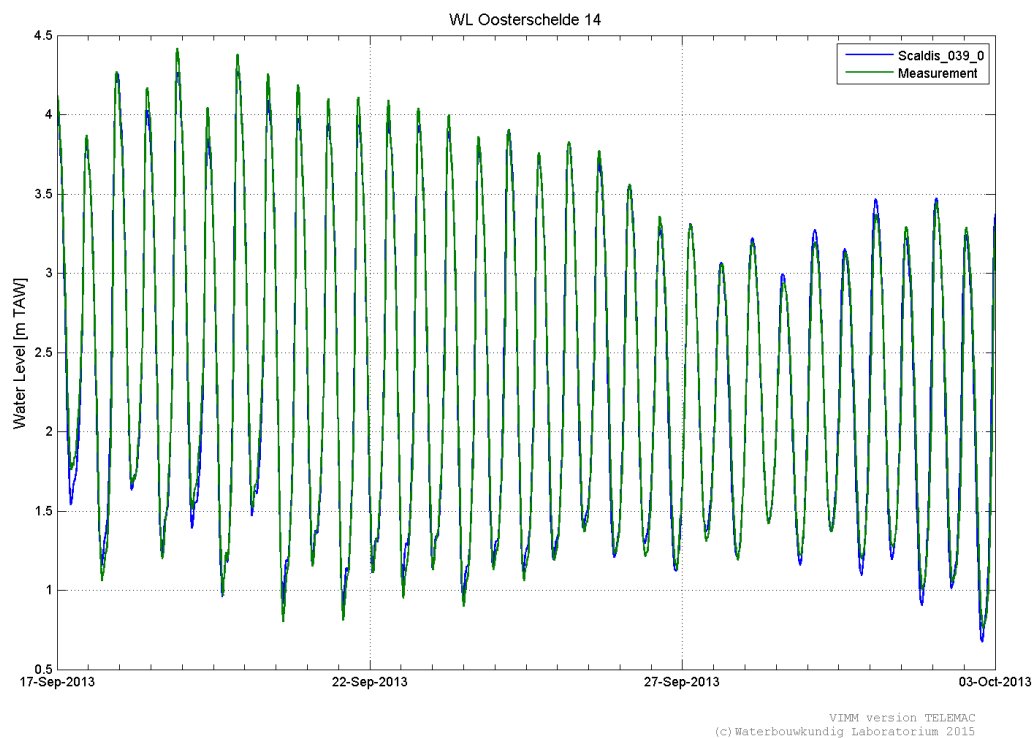


Figure 280 - Calculated and measured water levels at Oosterschelde 14

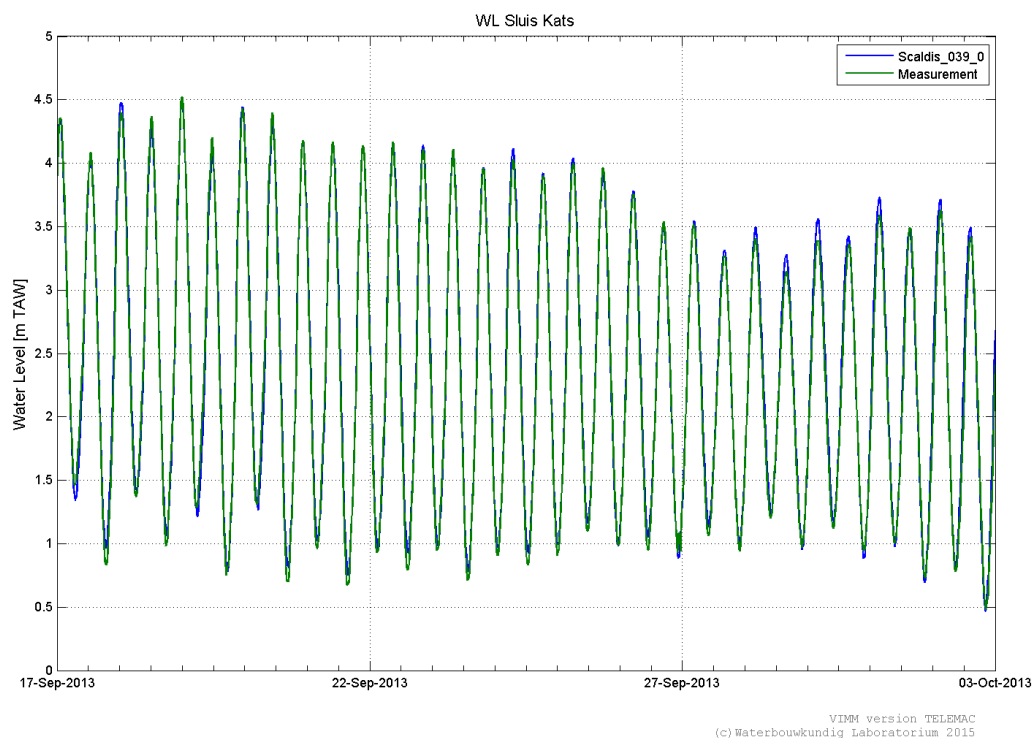


Figure 281 - Calculated and measured water levels at Sluis Kats

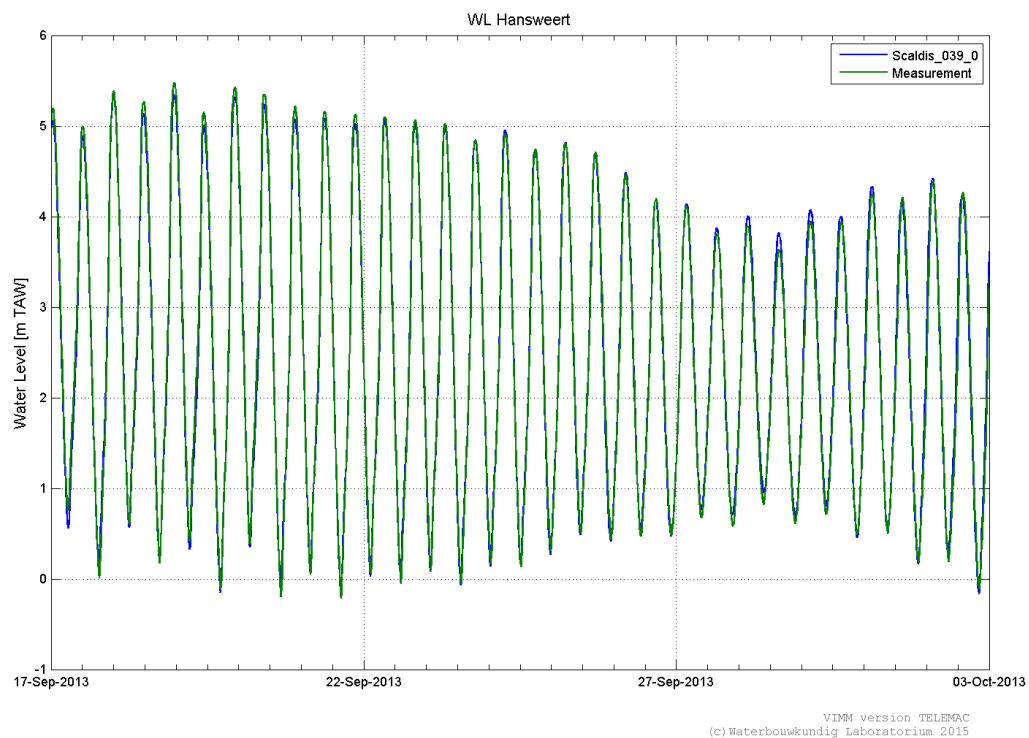


Figure 282 - Calculated and measured water levels at Hansweert

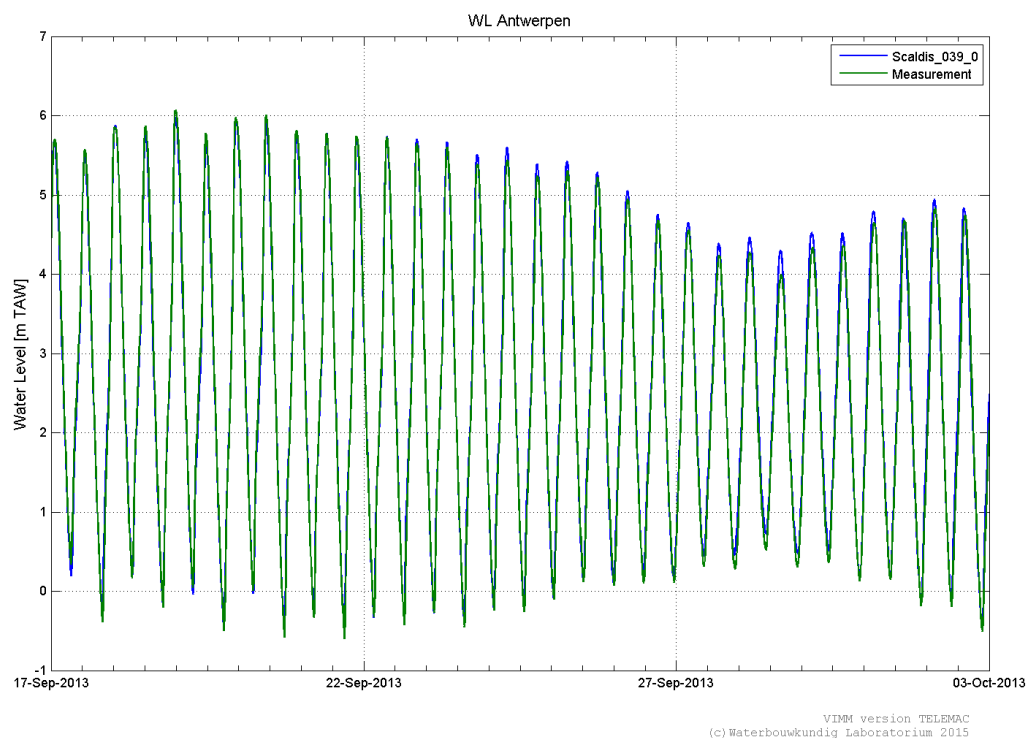


Figure 283 - Calculated and measured water levels at Antwerpen

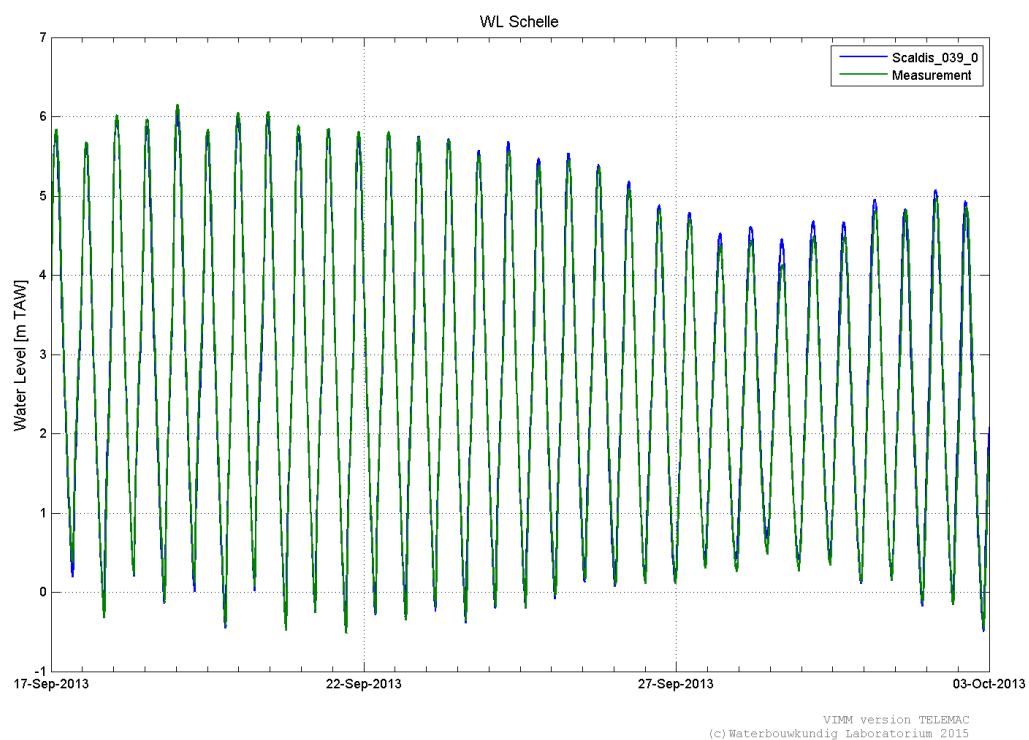


Figure 284 - Calculated and measured water levels at Schelle

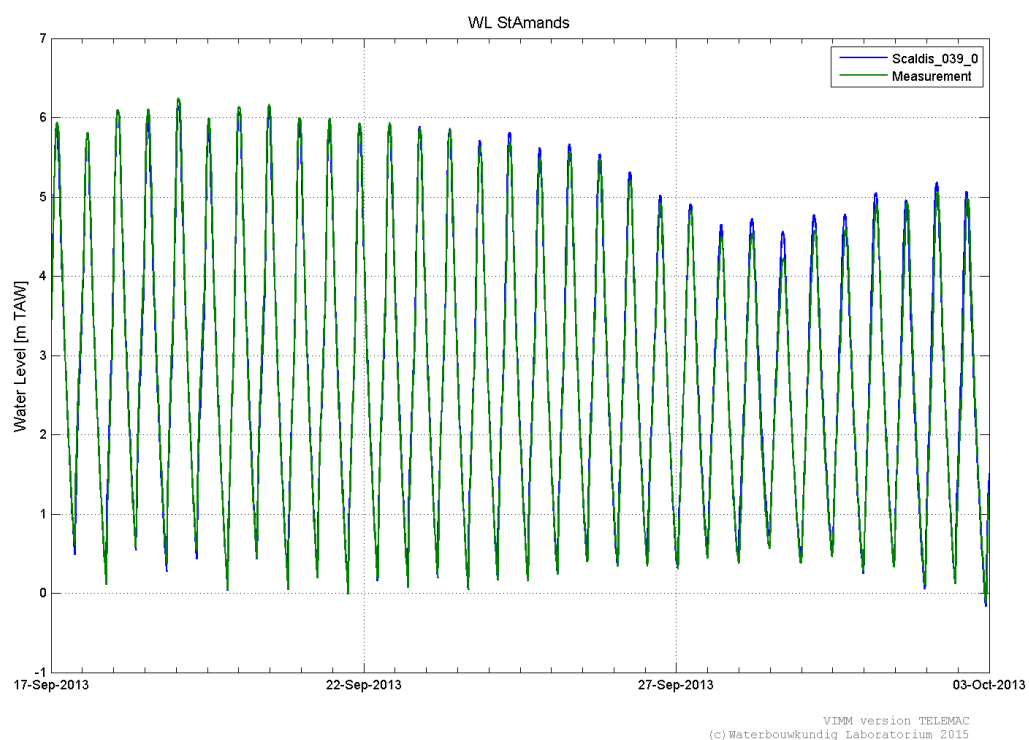


Figure 285 - Calculated and measured water levels at Sint Amands

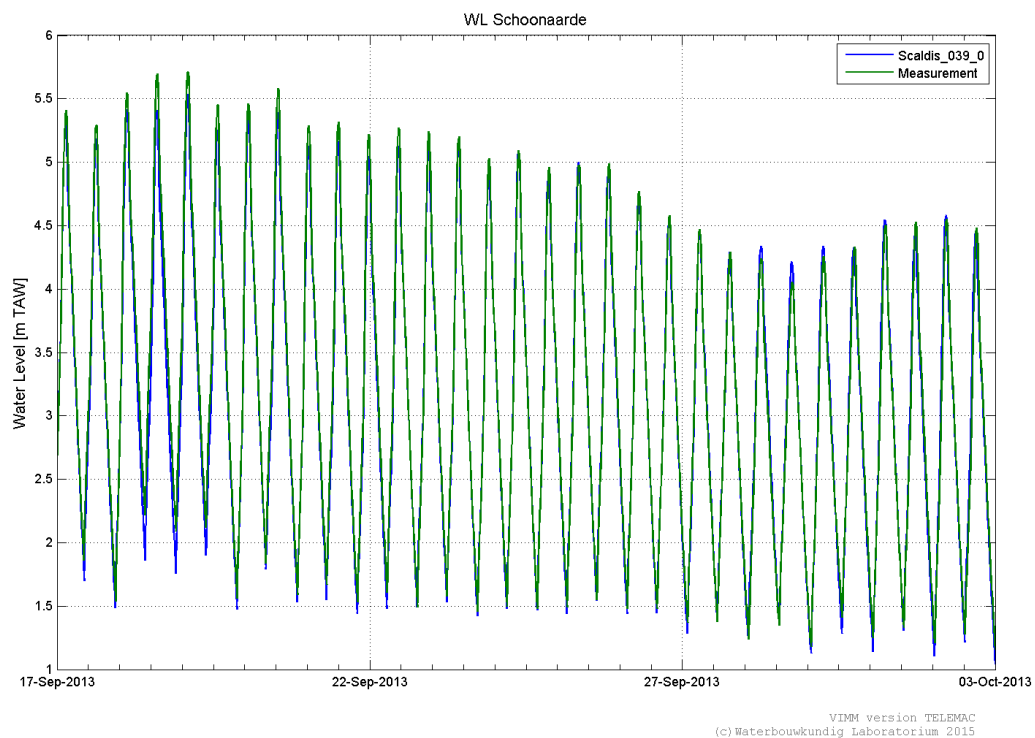


Figure 286 - Calculated and measured water levels at Schoonaarde

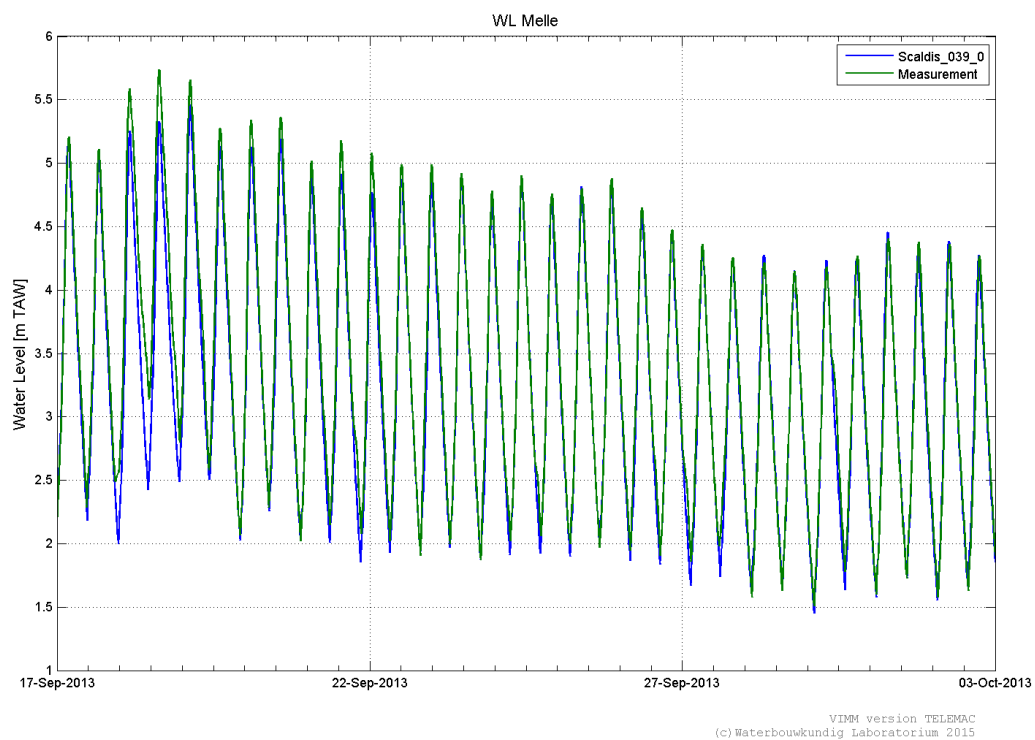


Figure 287 - Calculated and measured water levels at Melle

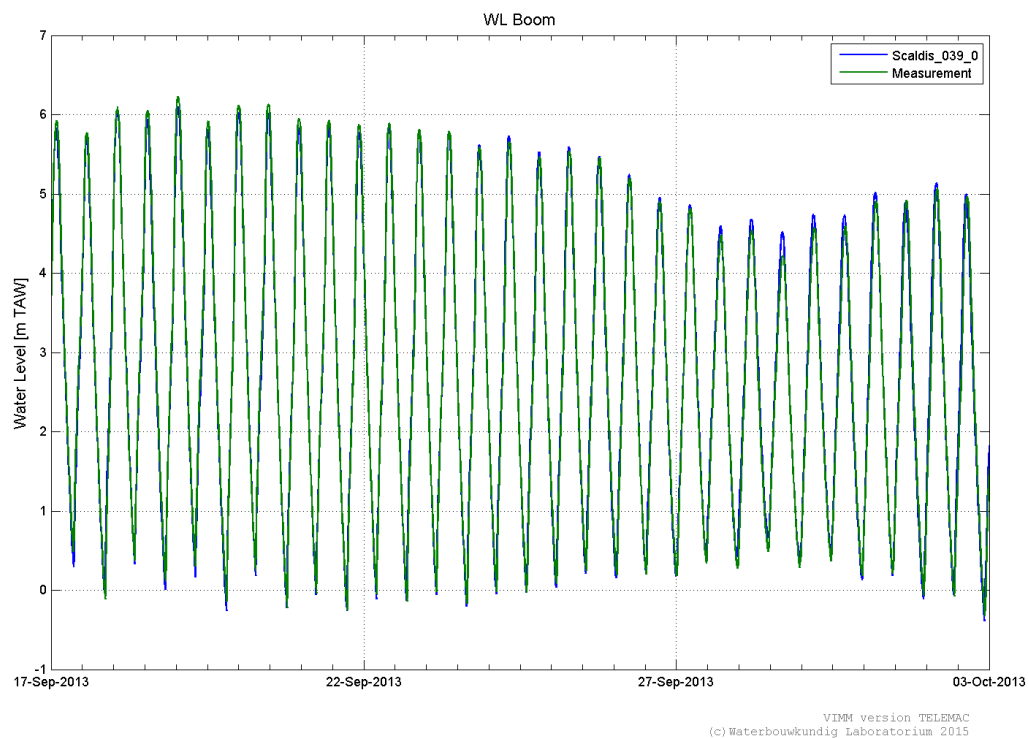


Figure 288 - Calculated and measured water levels at Boom

ADCP velocities

Table 148. Comparison of the model results and ADCP velocities for transverse transects

Scaldis_039_0	RMSE mag all (m/s)	RMSE dir all (degrees)	RMAE all
20110705 Everingen	0.14	24	0.31
20110706 R7 Terneuzen	0.17	37	0.34
20120508 R6 Middelgat	0.16	26	0.34
20120509 R6 GatVanOssenis	0.17	30	0.31
20080407 dwarsraai Ossenis	0.46	42	0.48
20060323 Waarde	0.14	27	0.28
20130424 R5 SchaarVanWaarde	0.17	26	0.34
20130425 R5 Zuidergat	0.17	29	0.36
20060912 Schaar van Ouden Doel	0.16	39	0.31
20050217 Zandvliet	0.12	43	0.33
20060323 DGD K	0.16	40	0.31
20080311 DGD K	0.20	29	0.28
20050217 Liefkenshoek	0.13	37	0.24
20130625 Liefkenshoek	0.15	31	0.26
20140514 Liefkenshoek	0.15	33	0.21
20050218 Kallo	0.12	41	0.27
20090529 Oosterweel	0.20	40	0.26
20130627 Oosterweel	0.17	18	0.25
20140516 Oosterweel	0.17	24	0.20
20100414 Kruike	0.16	32	0.19
20130530 Kruike	0.13	17	0.17
20140702 Kruike	0.12	32	0.16
20060323 Schelle	0.19	32	0.23
20060928 Schelle	0.16	21	0.17
20130213 Wintam	0.14	72	0.34
20090610 Ballooi dwars	0.13	16	0.20
20130612 Driegoten	0.19	43	0.34
20140617 Driegoten	0.17	23	0.24
20110218 Kramp ebb	0.17	35	0.23
20110218 Kramp flood	0.21	23	0.29
20140417 Dendermonde	0.15	20	0.20
20130527 Schoonaarde	0.16	17	0.26
20140703 Schoonaarde	0.17	31	0.27
20140415 Schellebelle	0.14	27	0.29
20100427 Boom	0.13	32	0.22
20130529 Terhagen	0.21	30	0.28
20140630 Terhagen	0.15	22	0.24

Table 149. Comparison of the model results and ADCP velocities for longitudinal transects

Scaldis_039_0	RMSE mag all (m/s)	RMSE dir all (degrees)	RMAE all
20110902 Galgenschoor	0.18	36	0.46
20100318 langsraai O	0.17	27	0.35
20090610 Notelaer langs	0.15	26	0.30
20110804 Branst	0.25	52	0.68
20110801 Appels downstream	0.15	62	0.66

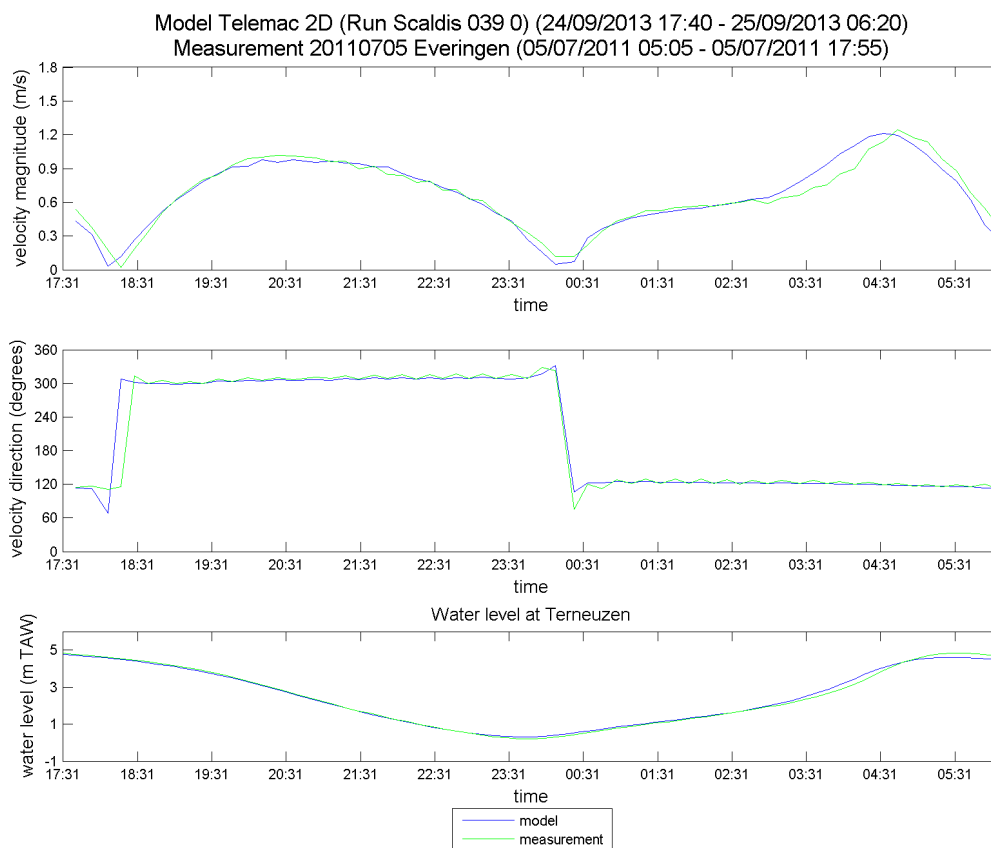


Figure 289 - Time series of the measured and modeled velocity magnitude and direction at 20110705 Everingen

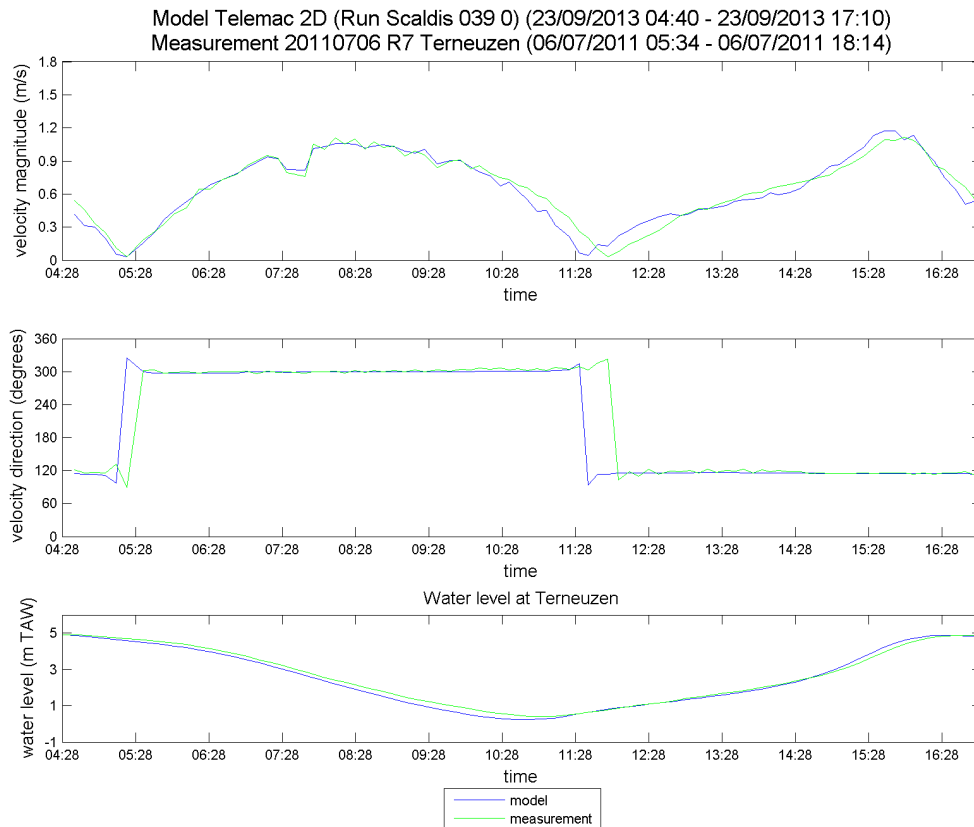


Figure 290 - Time series of the measured and modeled velocity magnitude and direction at 20110706 R7 Terneuzen

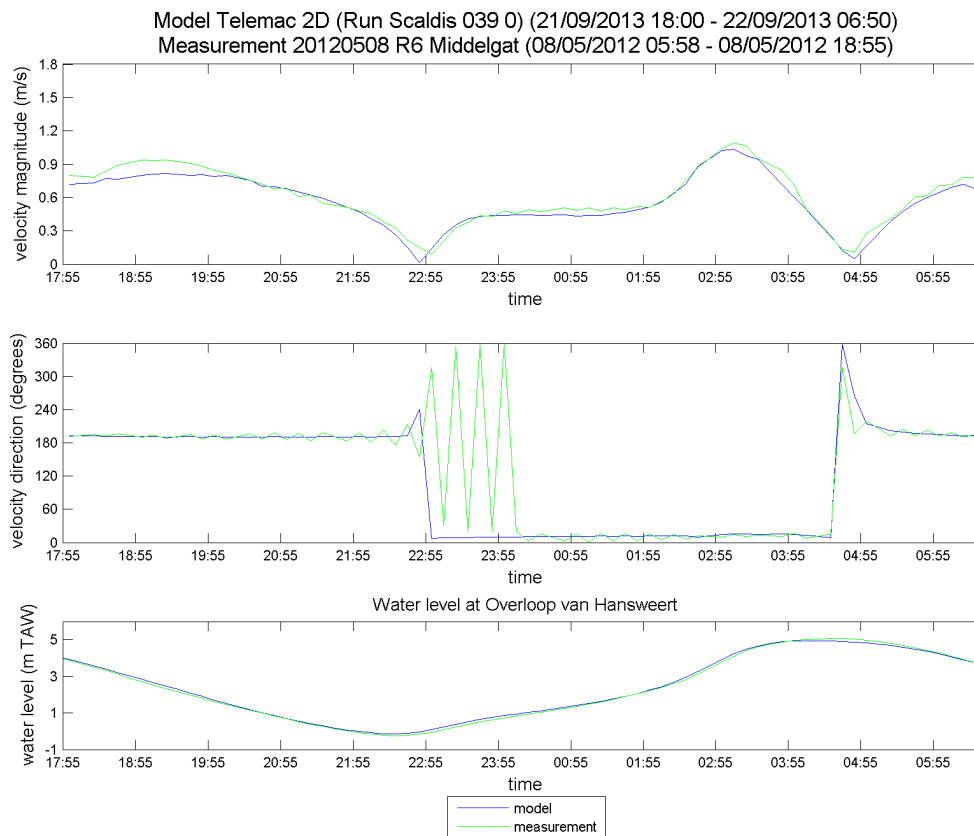


Figure 291 - Time series of the measured and modeled velocity magnitude and direction at 20120508 R6 Middelgat

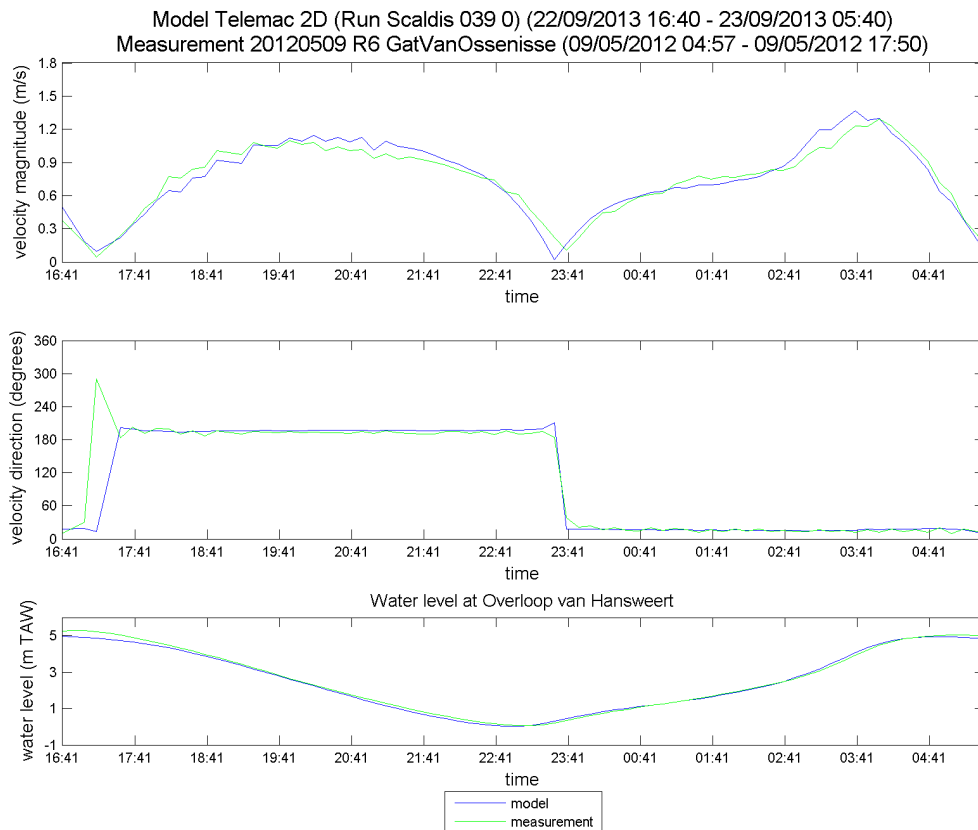


Figure 292 - Time series of the measured and modeled velocity magnitude and direction at 20120509 R6 GatVanOssenis

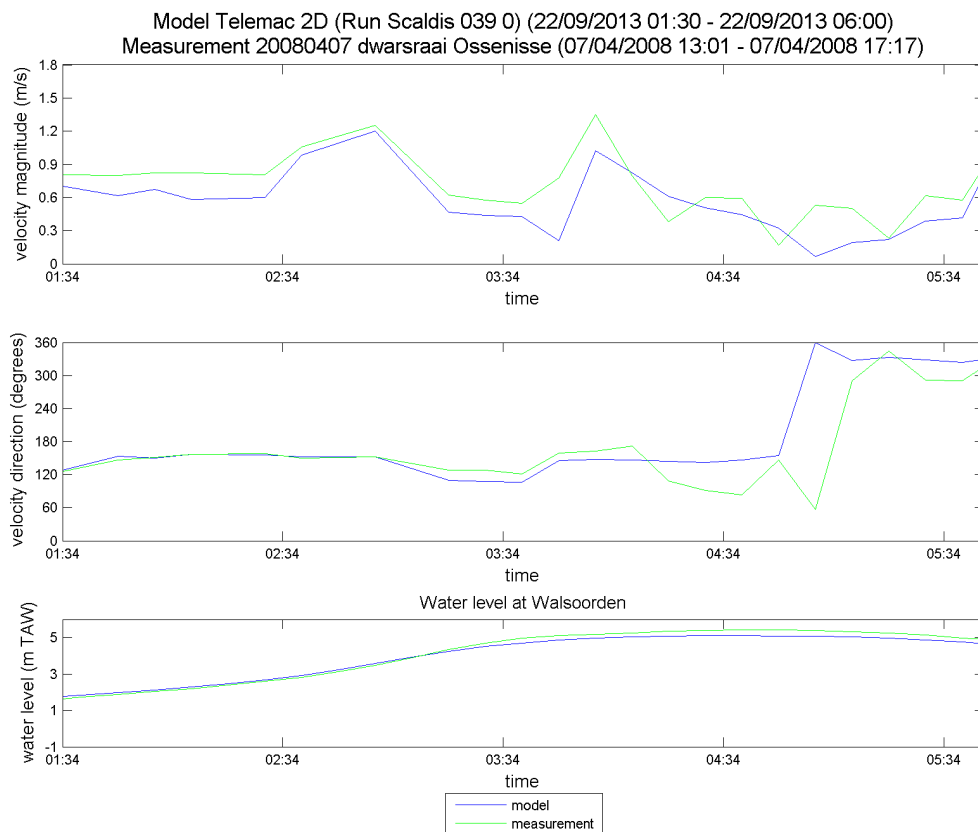


Figure 293 - Time series of the measured and modeled velocity magnitude and direction at 20080407 dwarsraai Ossenis

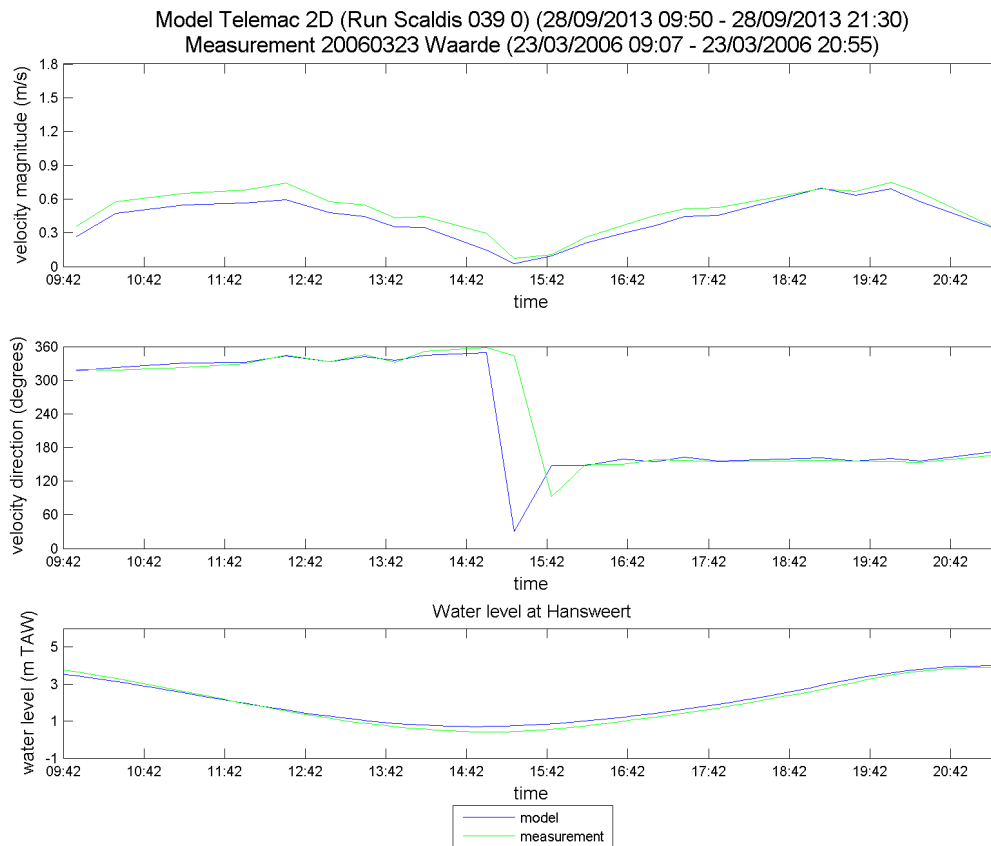


Figure 294 - Time series of the measured and modeled velocity magnitude and direction at 20060323 Waarde

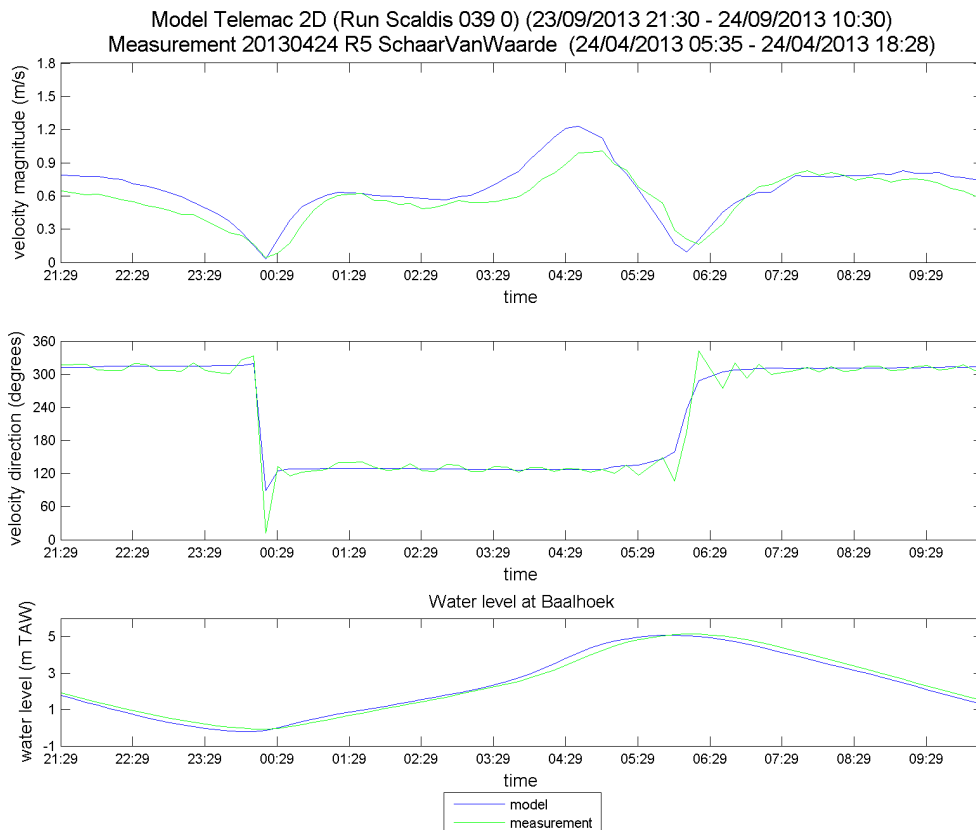


Figure 295 - Time series of the measured and modeled velocity magnitude and direction at 20130424 R5 SchaarVanWaarde

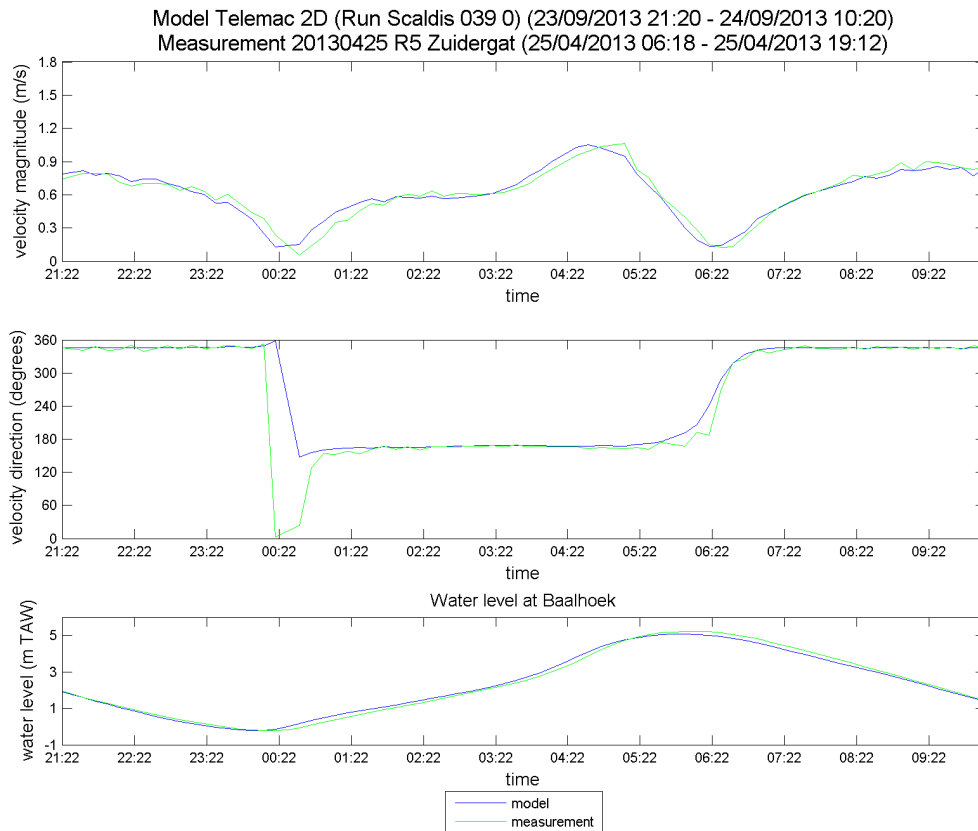


Figure 296 - Time series of the measured and modeled velocity magnitude and direction at 20130425 R5 Zuidergat

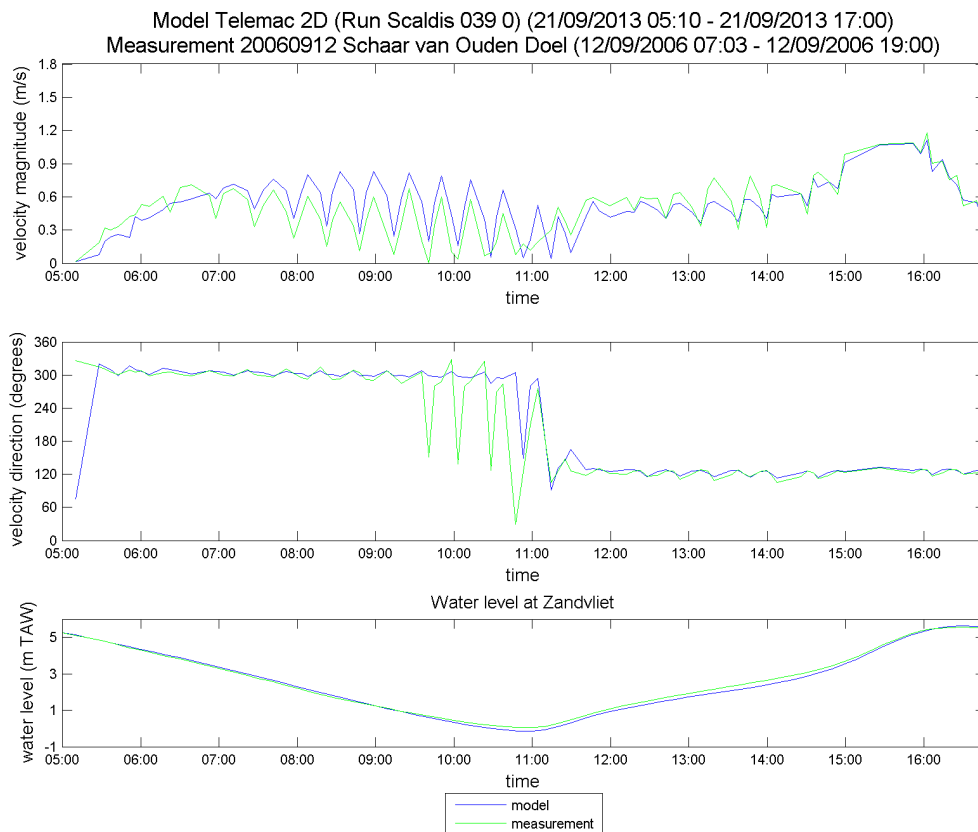


Figure 297 - Time series of the measured and modeled velocity magnitude and direction at 20060912 Schaar van Ouden Doel

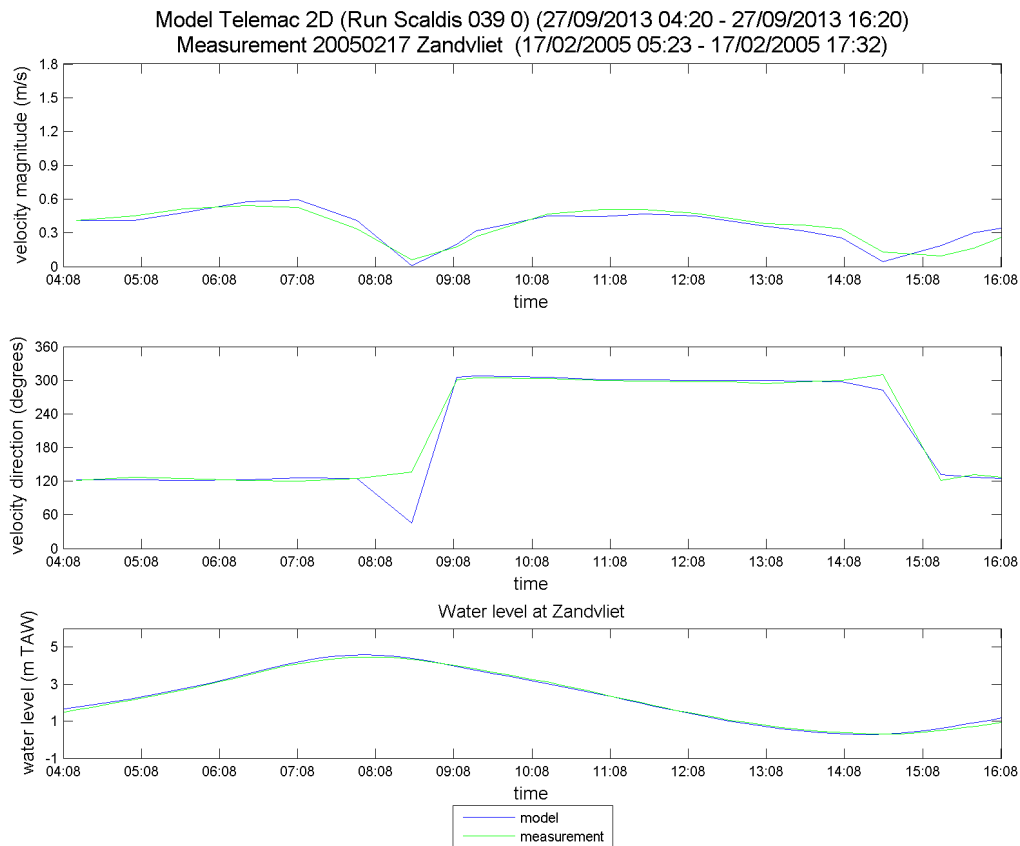


Figure 298 - Time series of the measured and modeled velocity magnitude and direction at 20050217 Zandvliet

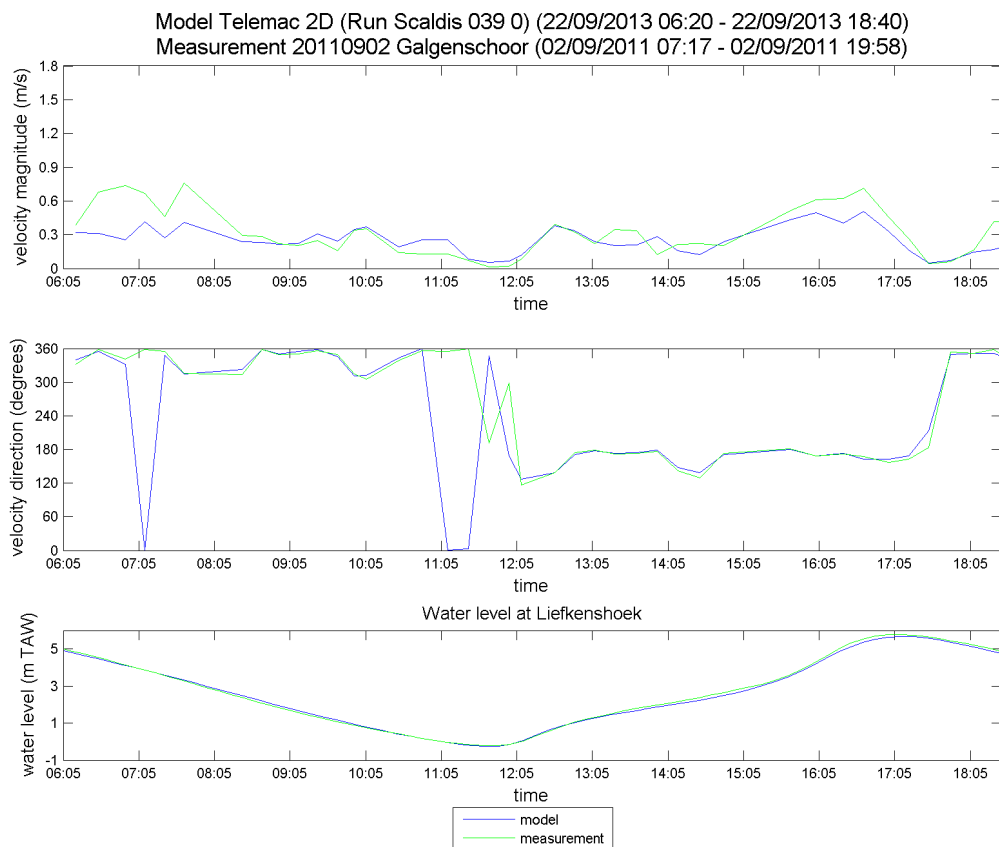


Figure 299 - Time series of the measured and modeled velocity magnitude and direction at 20110902 Galgenschoor

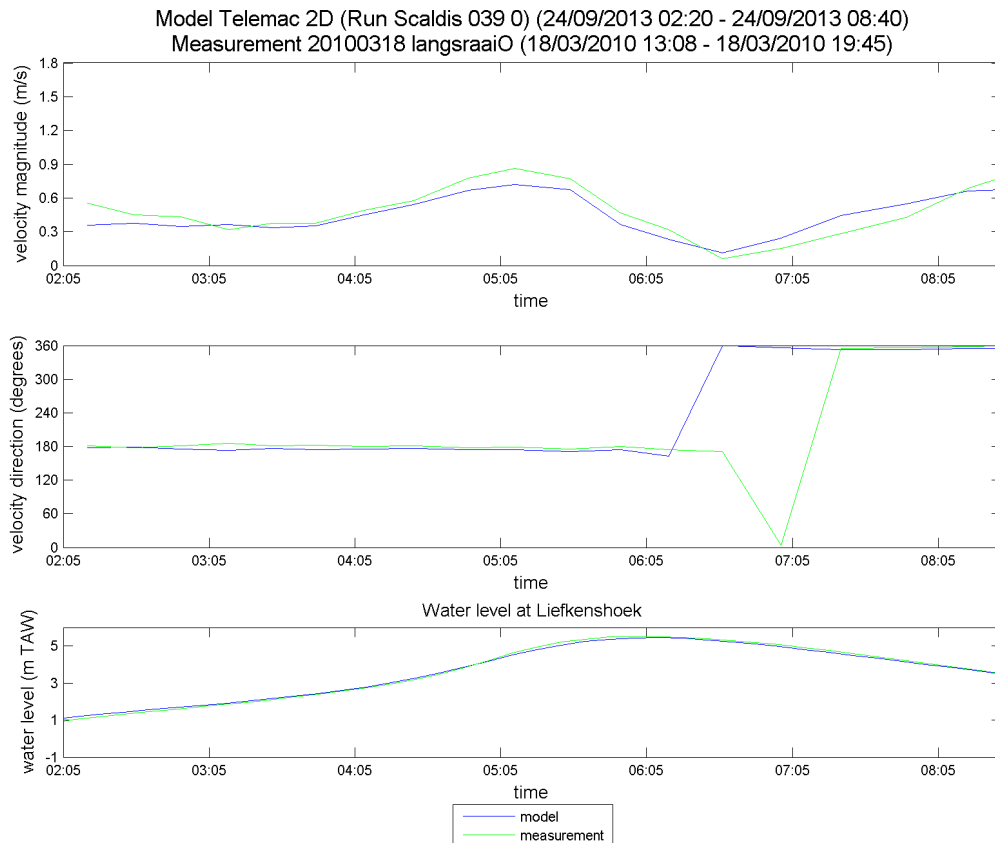


Figure 300 - Time series of the measured and modeled velocity magnitude and direction at 20100318 langsraai O

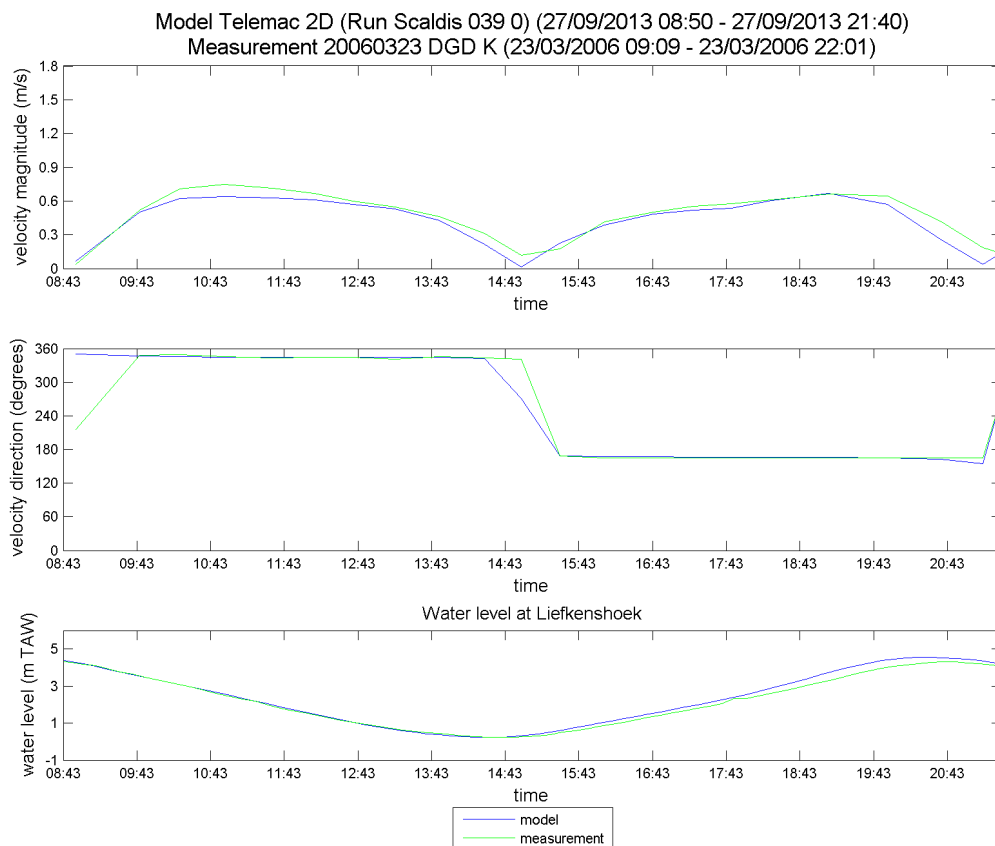


Figure 301 - Time series of the measured and modeled velocity magnitude and direction at 20060323 DGD K

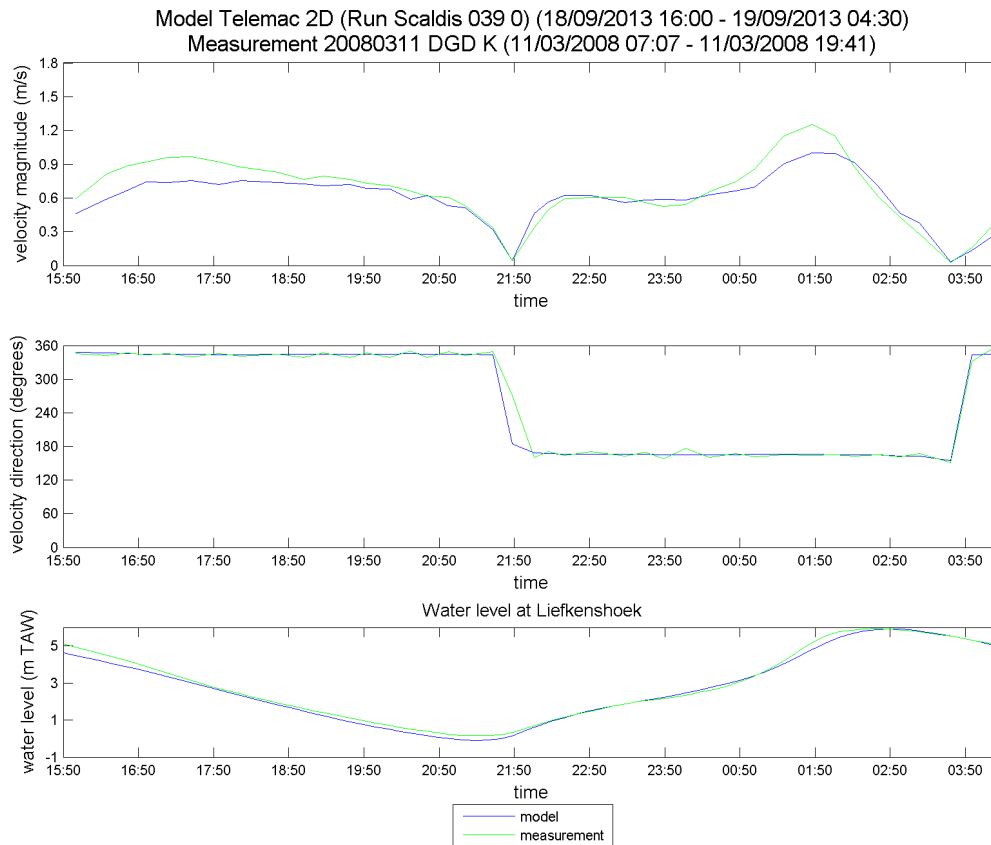


Figure 302 - Time series of the measured and modeled velocity magnitude and direction at 20080311 DGD K

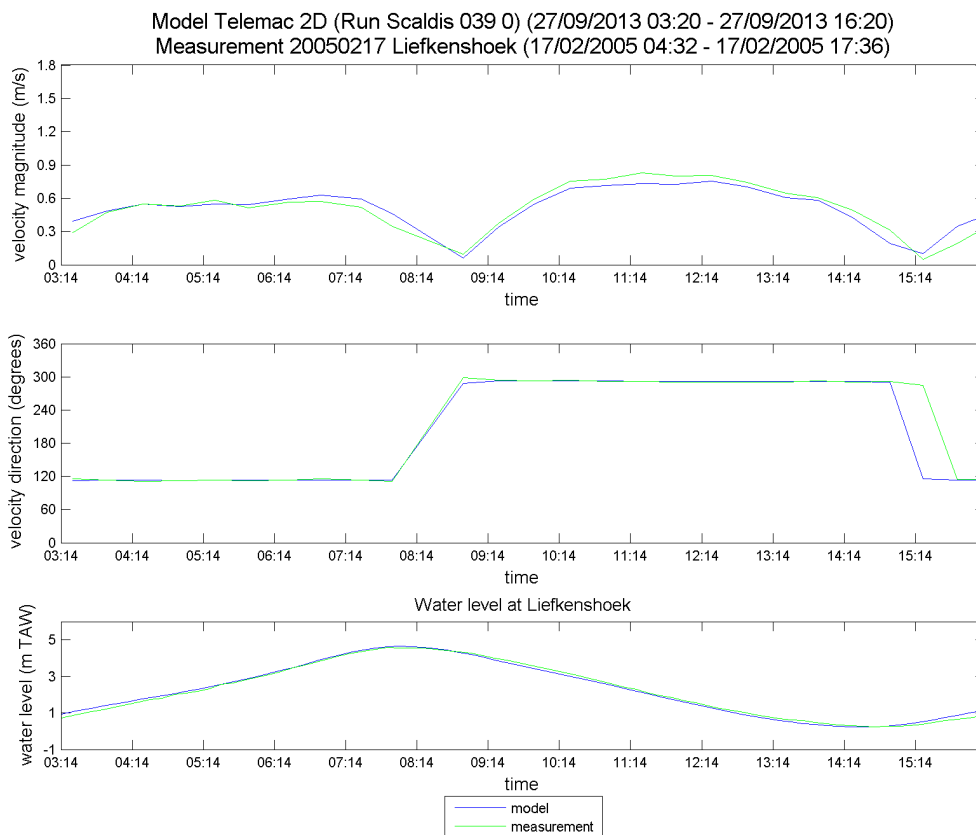


Figure 303 - Time series of the measured and modeled velocity magnitude and direction at 20050217 Liefkenshoek

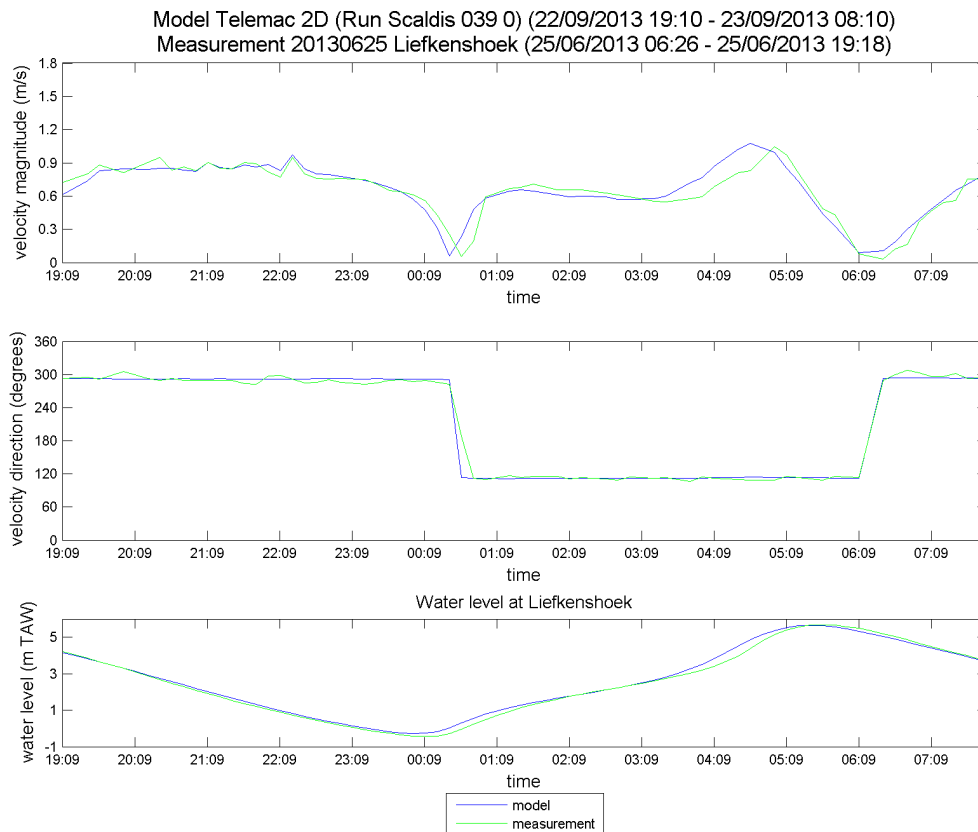


Figure 304 - Time series of the measured and modeled velocity magnitude and direction at 20130625 Liefkenshoek

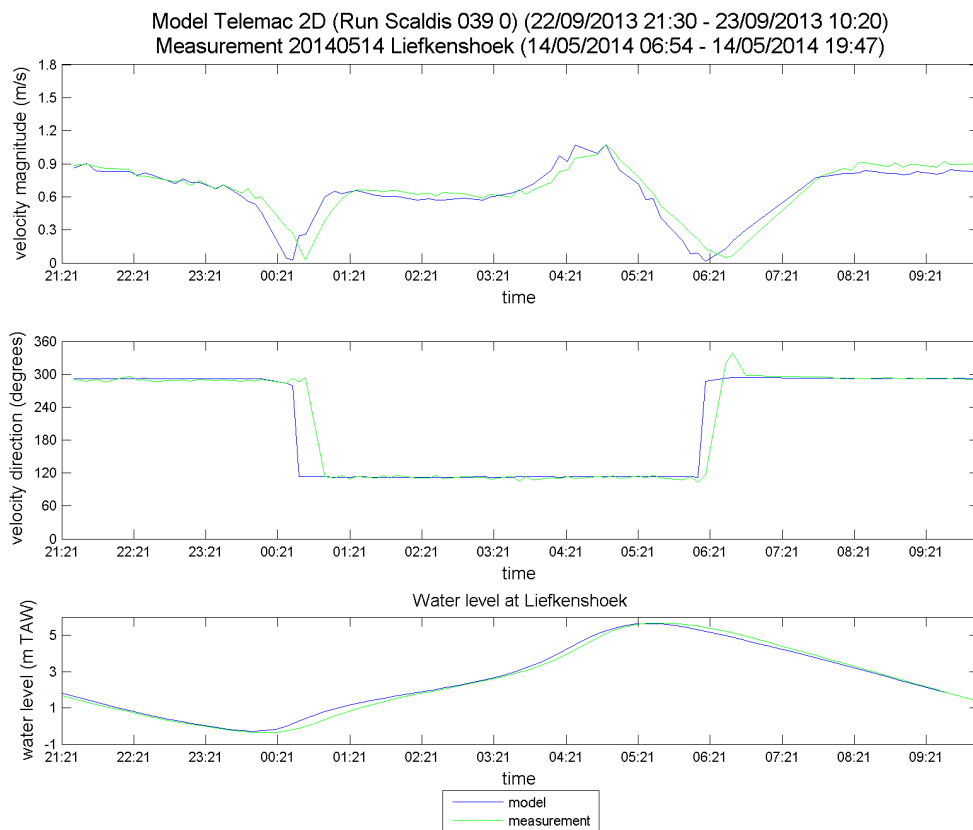


Figure 305 - Time series of the measured and modeled velocity magnitude and direction at 20140514 Liefkenshoek

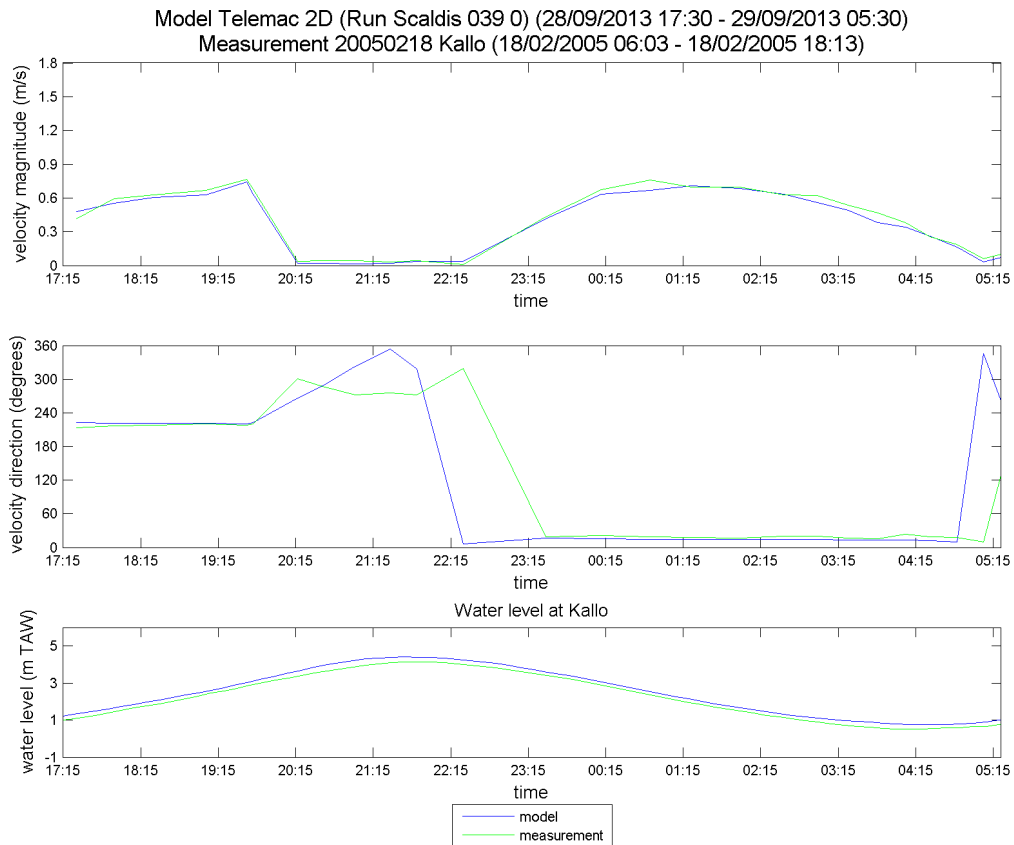


Figure 306 - Time series of the measured and modeled velocity magnitude and direction at 20050218 Kallo

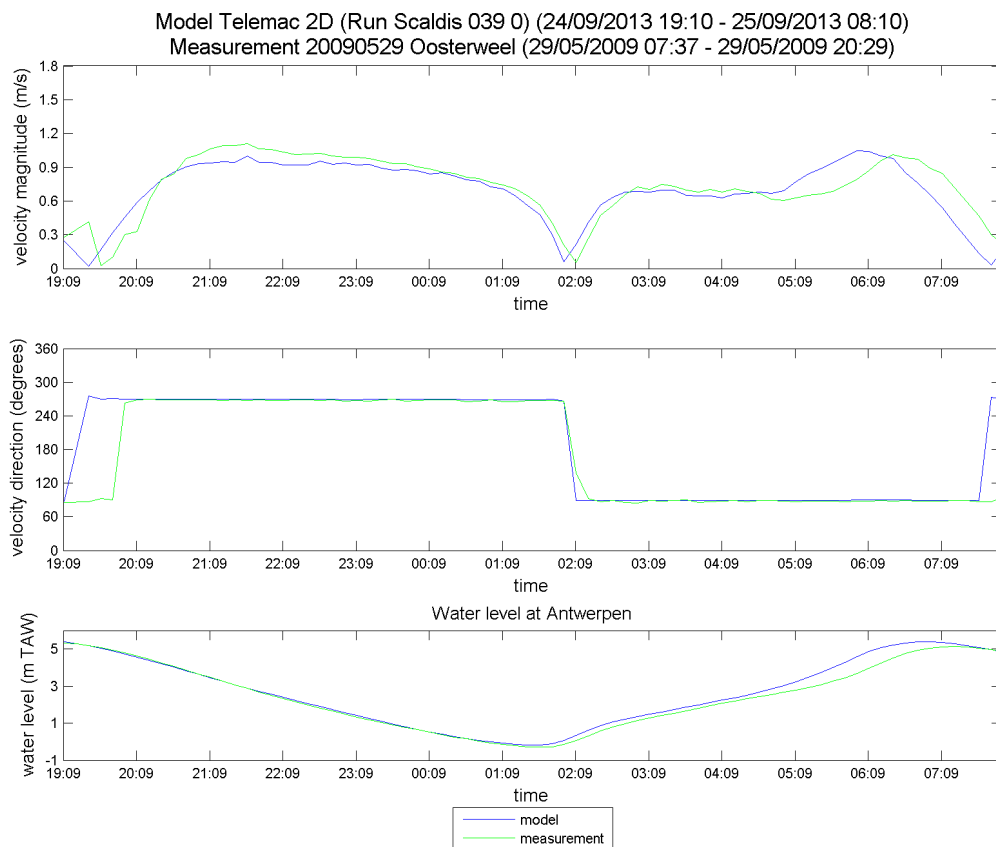


Figure 307 - Time series of the measured and modeled velocity magnitude and direction at 20090529 Oosterweel

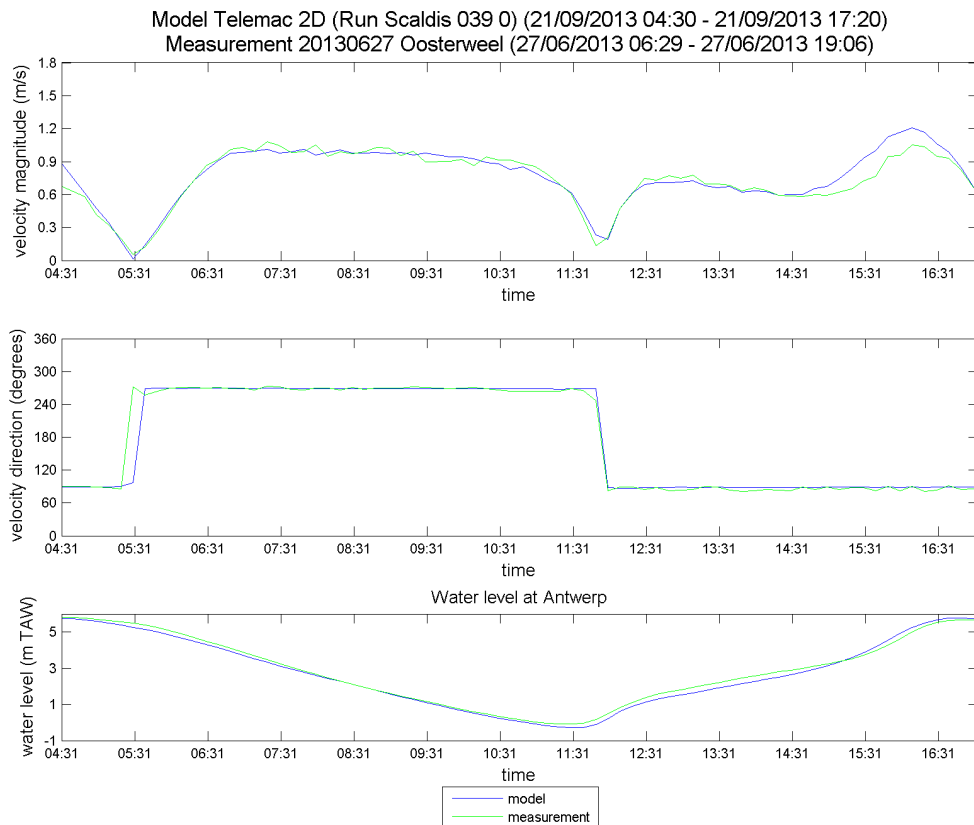


Figure 308 - Time series of the measured and modeled velocity magnitude and direction at 20130627 Oosterweel

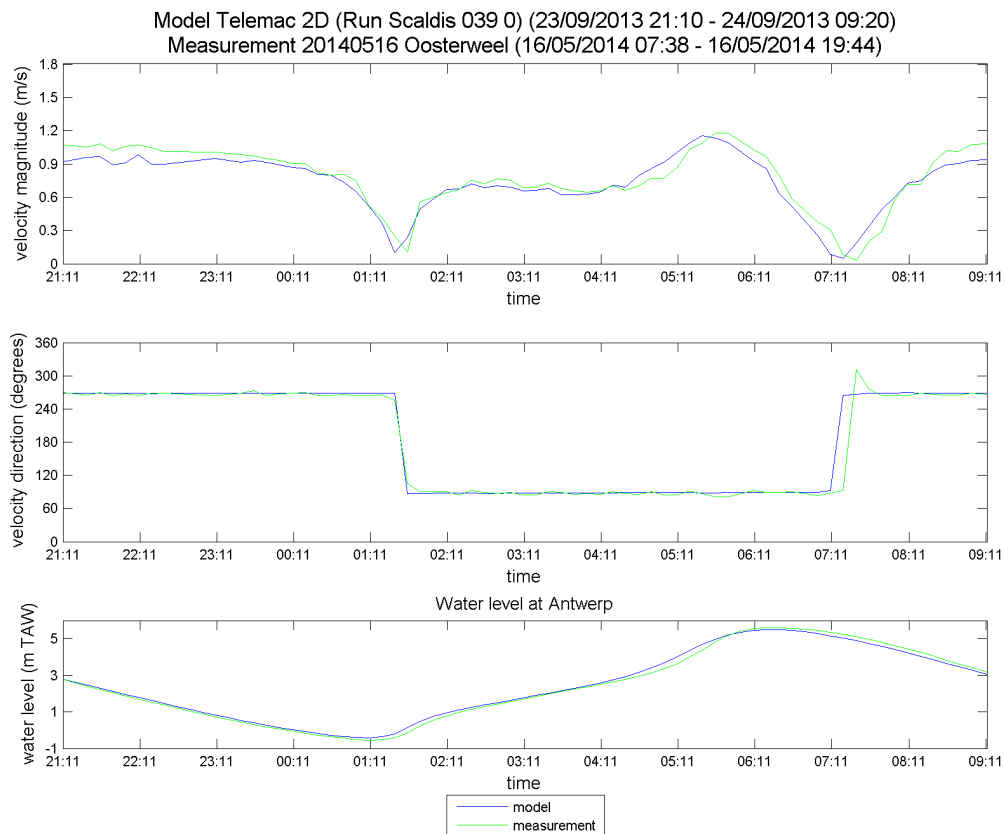


Figure 309 - Time series of the measured and modeled velocity magnitude and direction at 20140516 Oosterweel

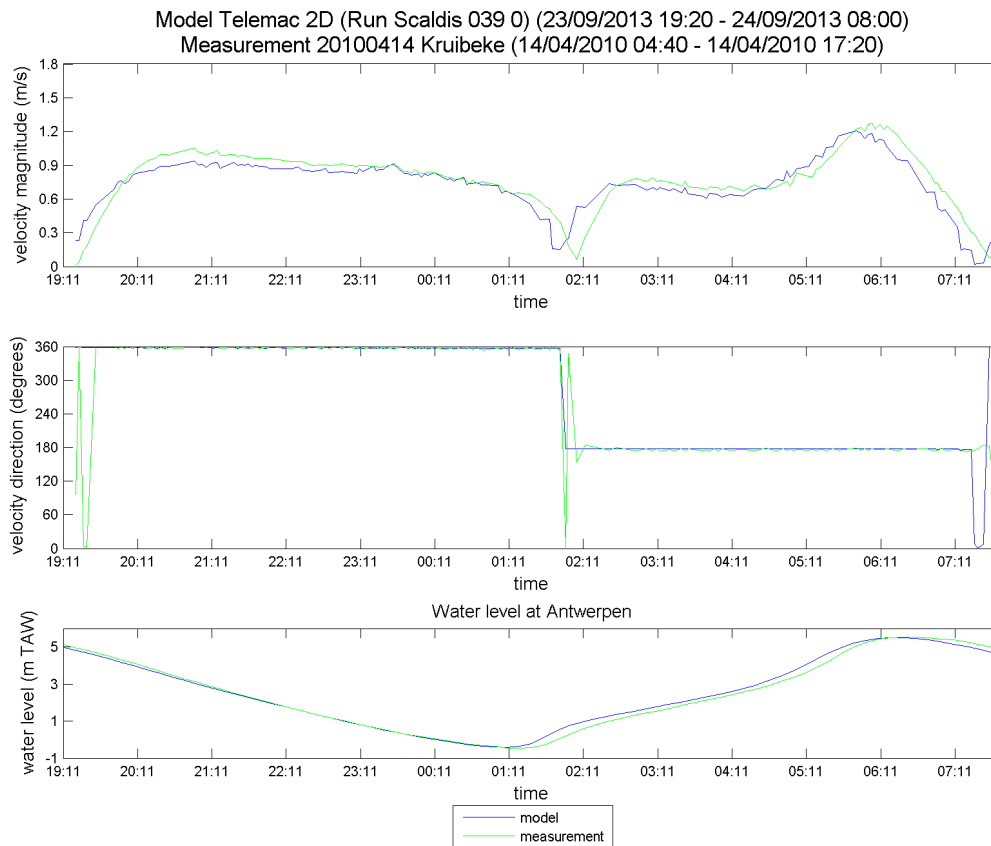


Figure 310 - Time series of the measured and modeled velocity magnitude and direction at 20100414 Kruibeke

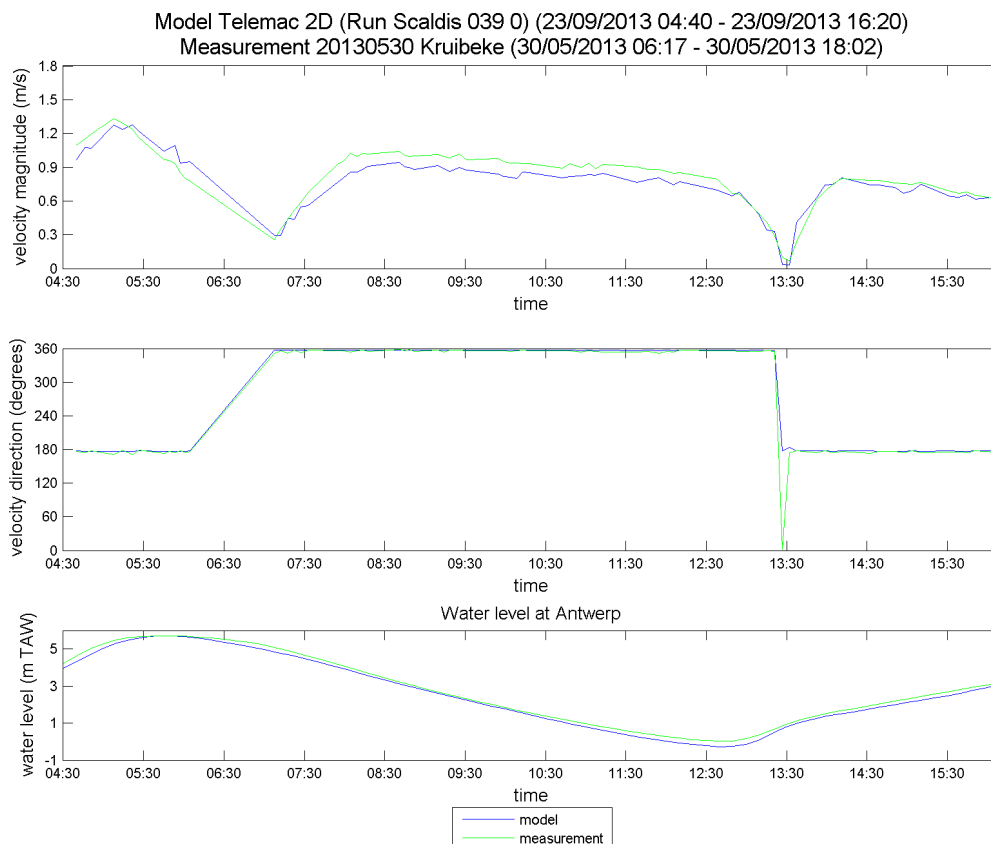


Figure 311 - Time series of the measured and modeled velocity magnitude and direction at 20130530 Kruibeke

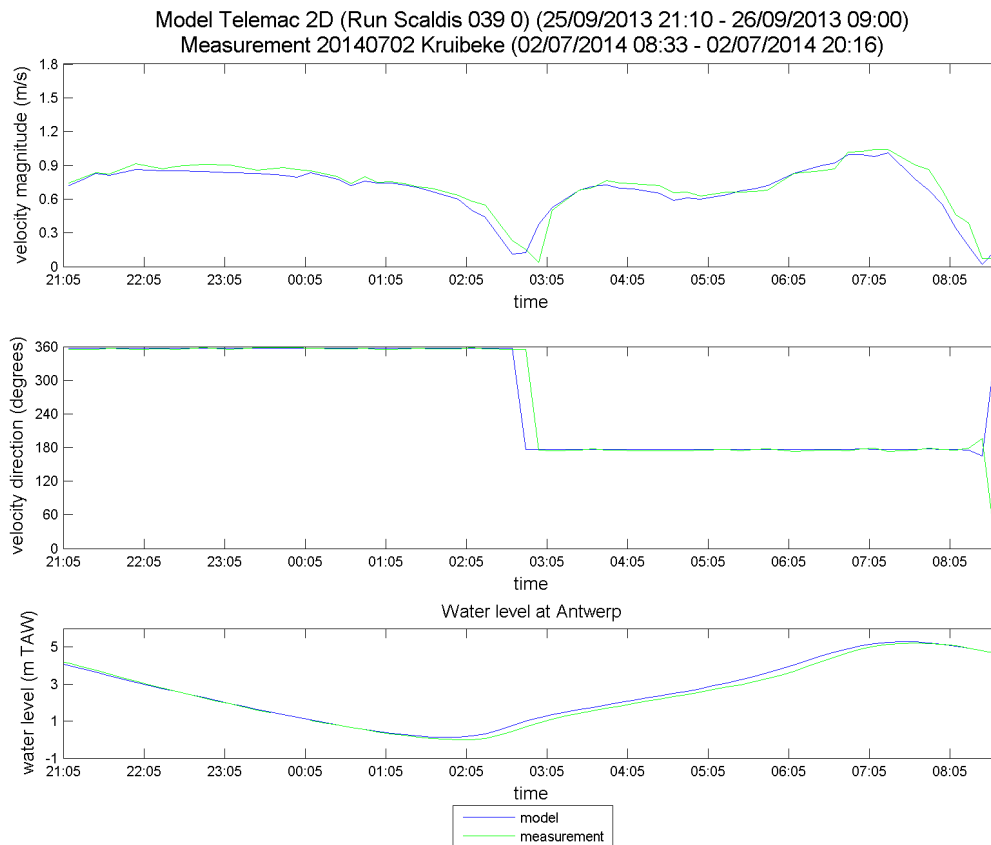


Figure 312 - Time series of the measured and modeled velocity magnitude and direction at 20140702 Kruibeke

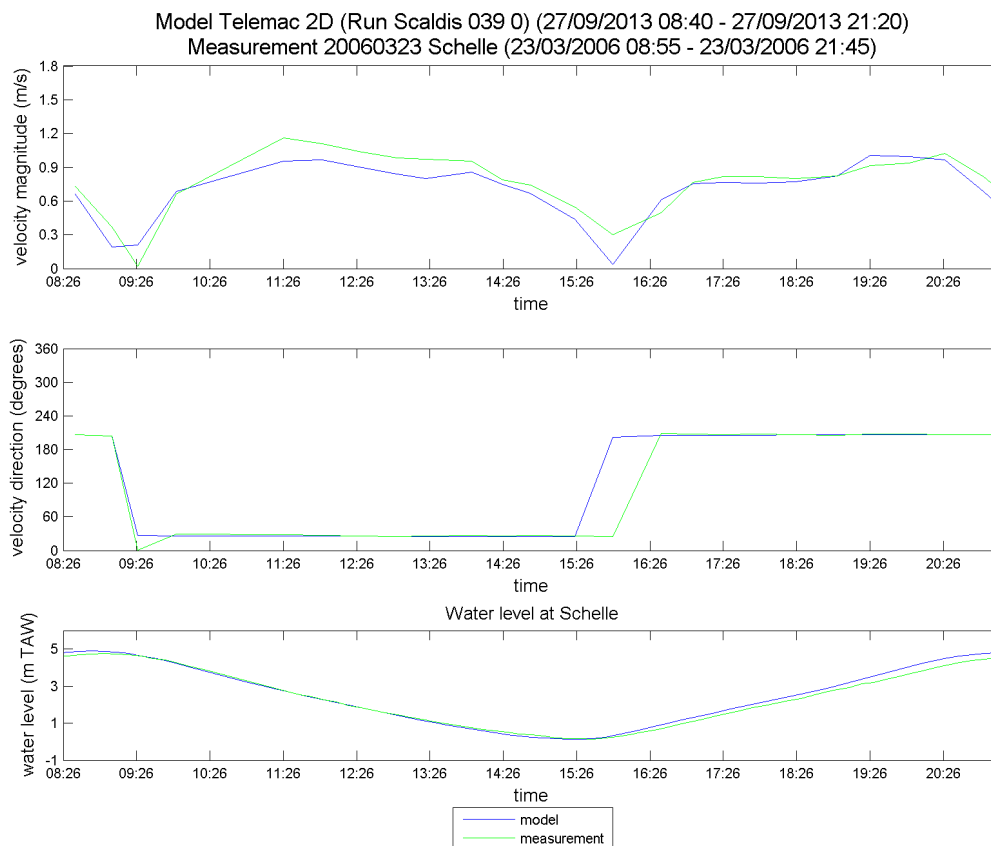


Figure 313 - Time series of the measured and modeled velocity magnitude and direction at 20060323 Schelle

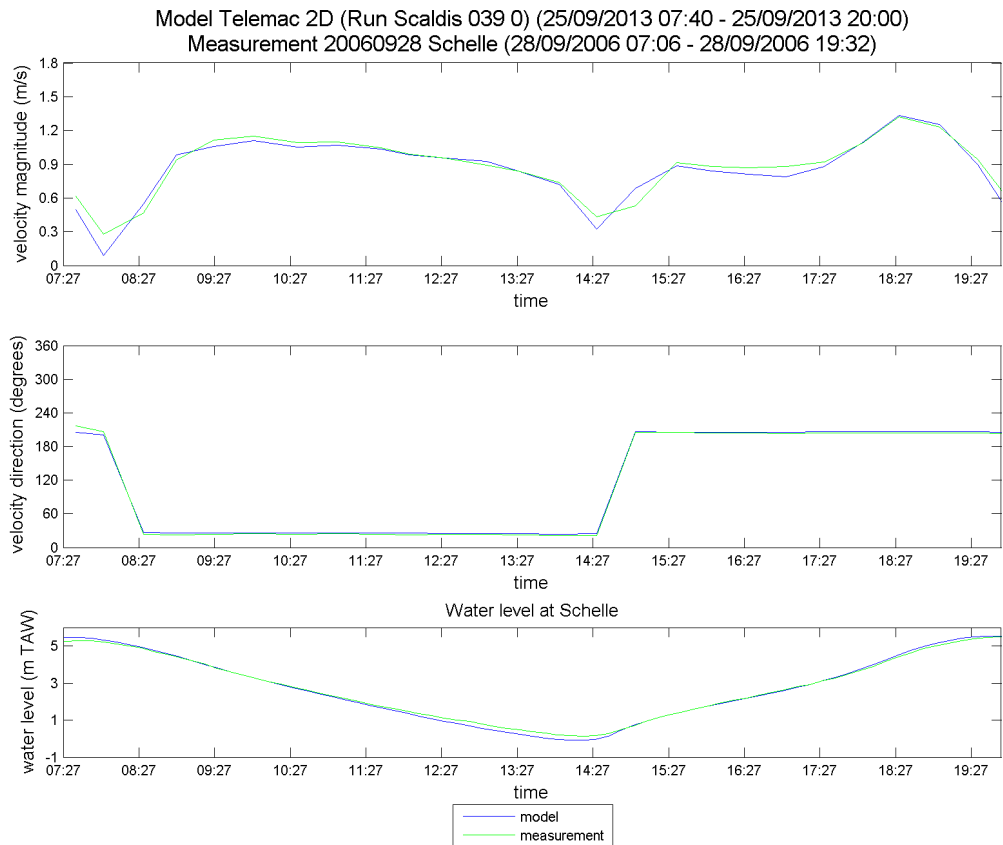


Figure 314 - Time series of the measured and modeled velocity magnitude and direction at 20060928 Schelle

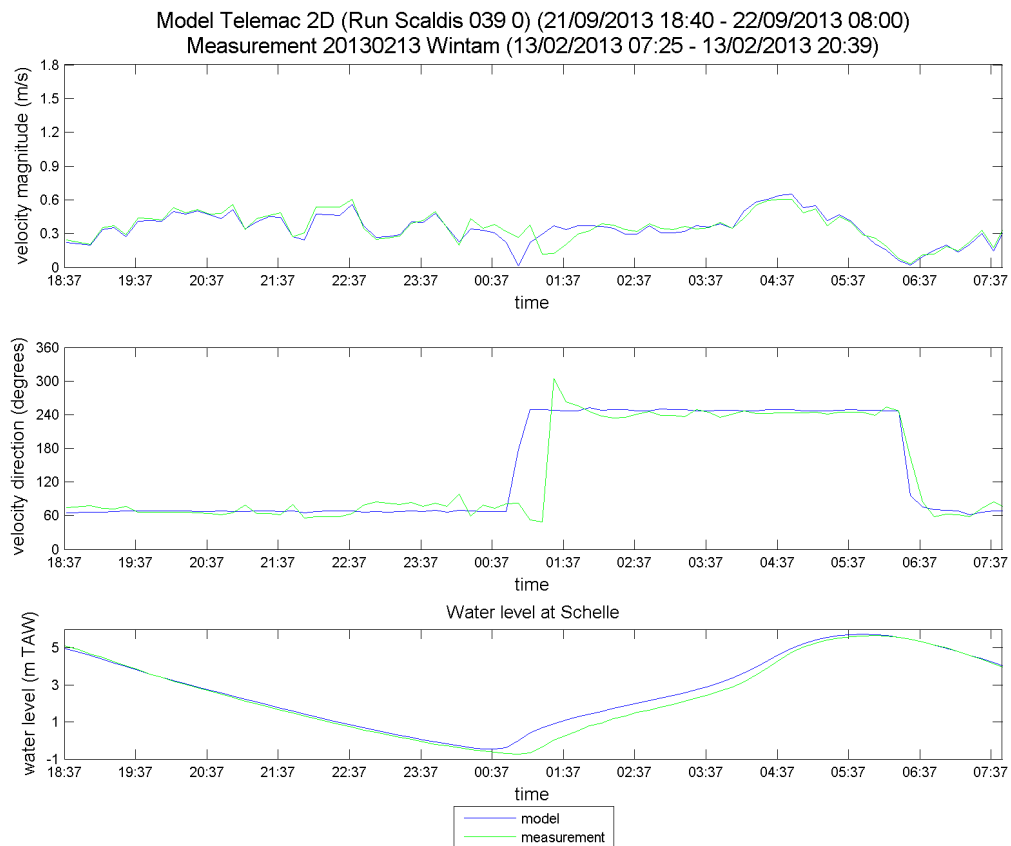


Figure 315 - Time series of the measured and modeled velocity magnitude and direction at 20130213 Wintam

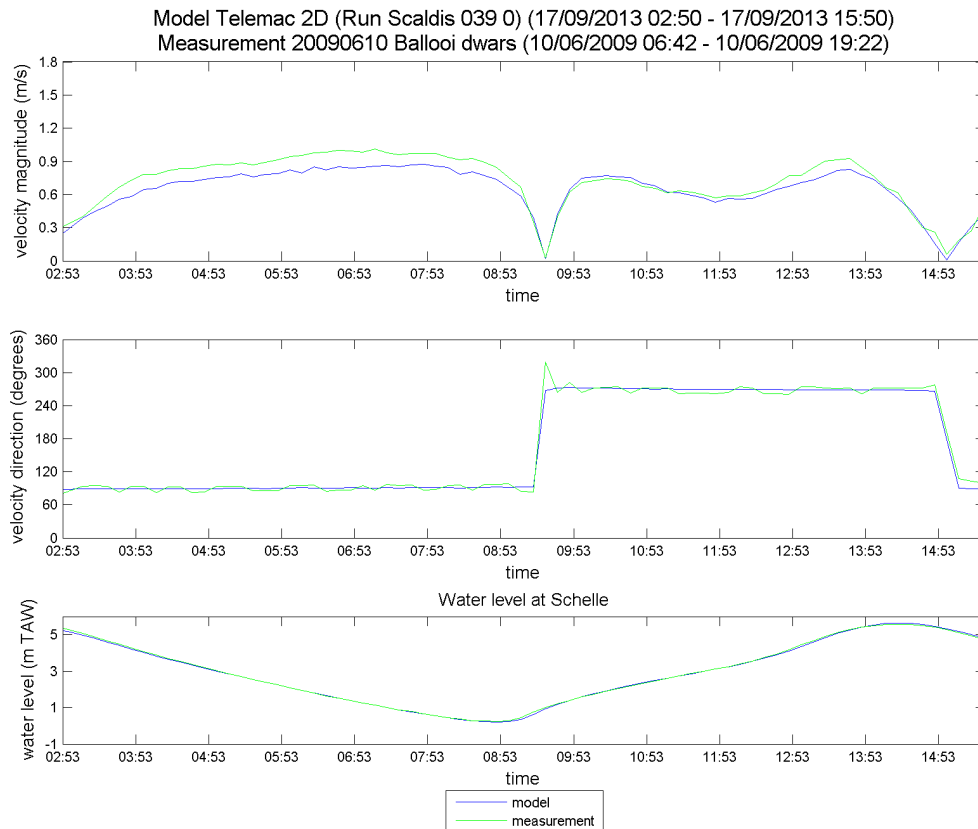


Figure 316 - Time series of the measured and modeled velocity magnitude and direction at 20090610 Ballooi dwars

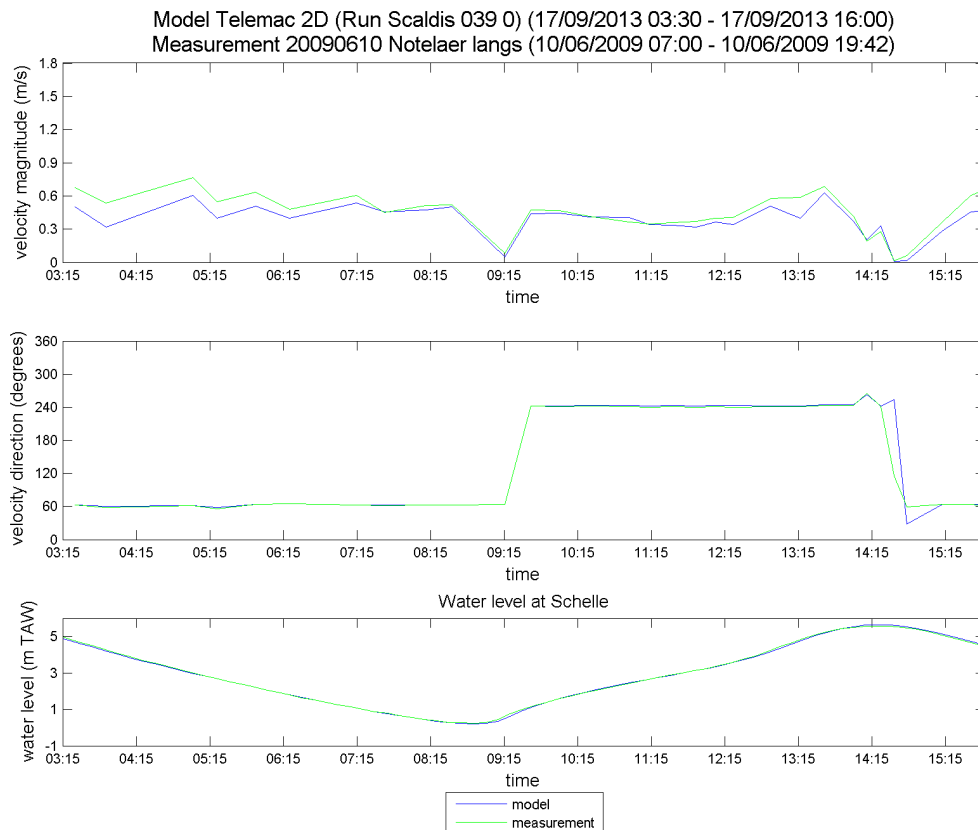


Figure 317 - Time series of the measured and modeled velocity magnitude and direction at 20090610 Notelaer langs

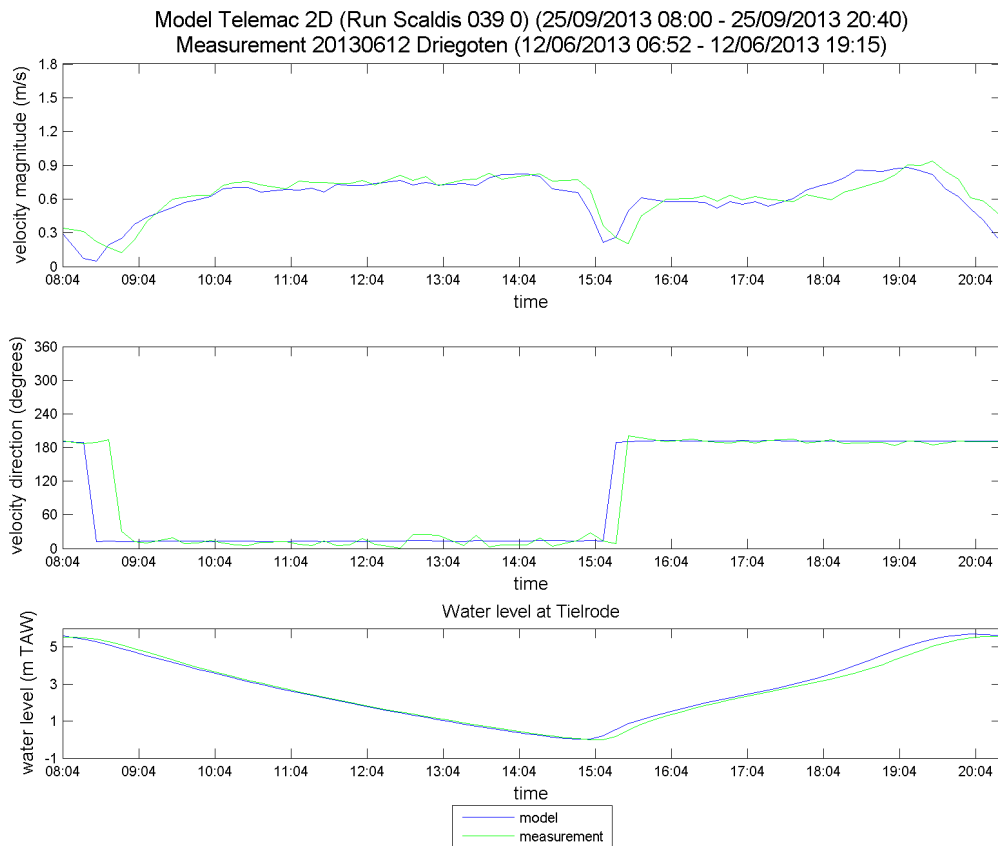


Figure 318 - Time series of the measured and modeled velocity magnitude and direction at 20130612 Driegoten

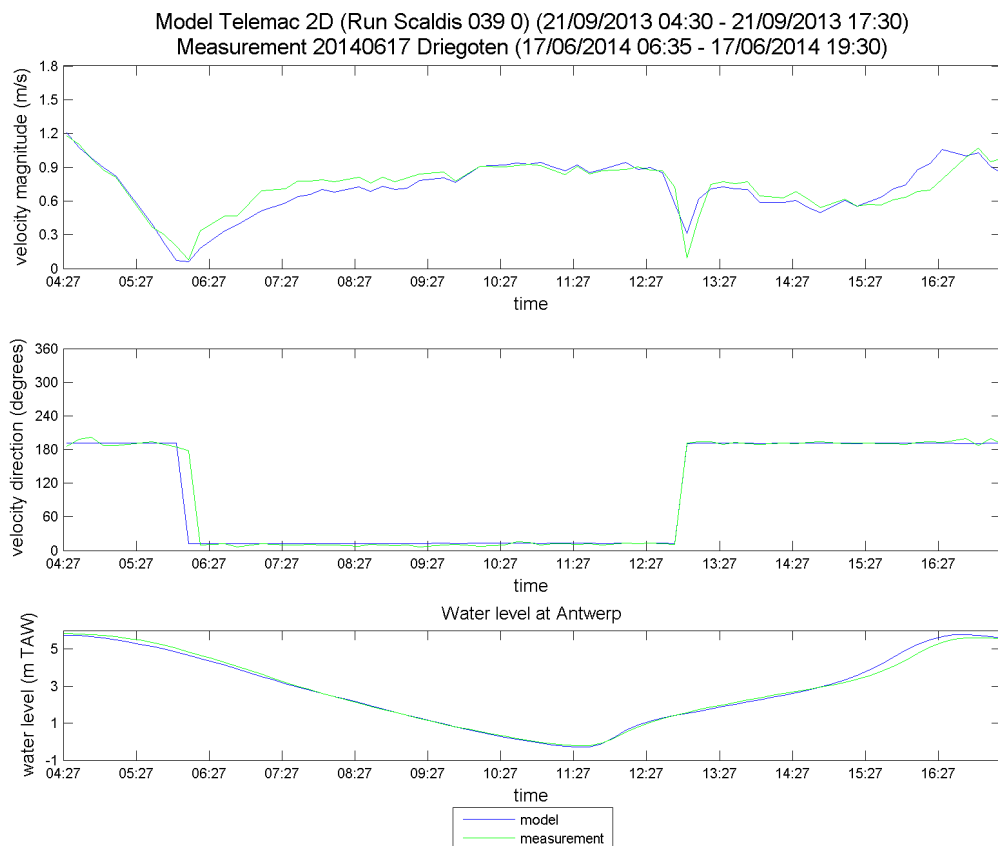


Figure 319 - Time series of the measured and modeled velocity magnitude and direction at 20140617 Driegoten

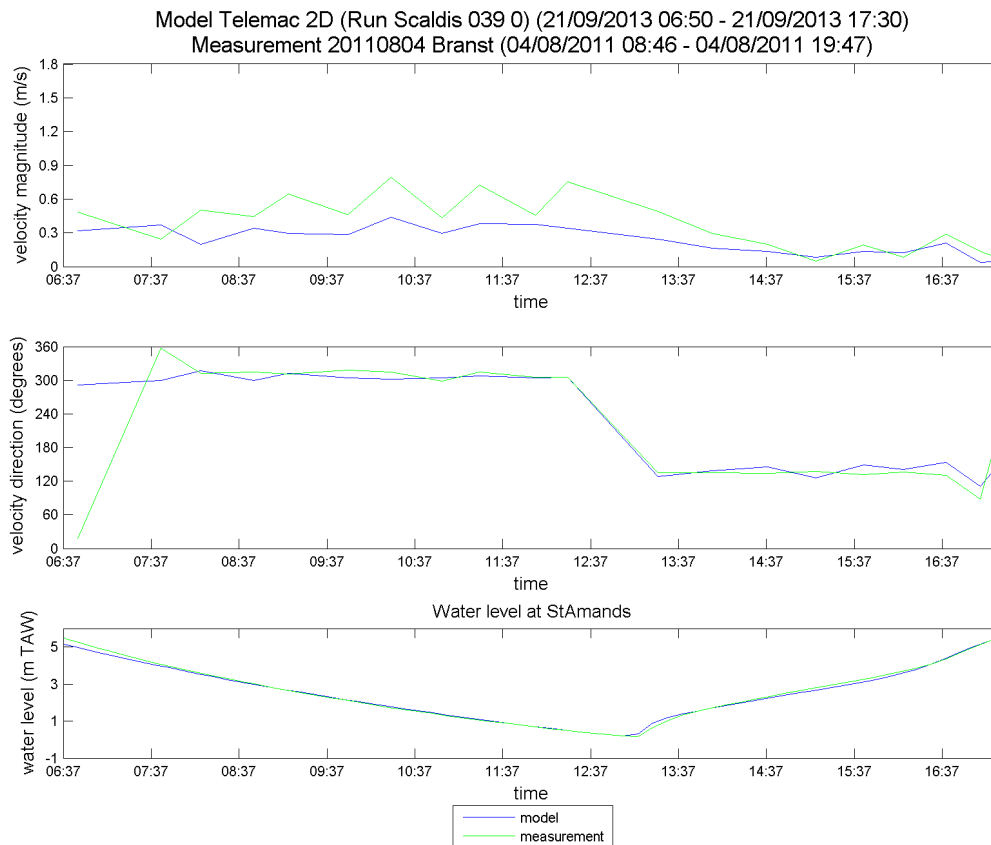


Figure 320 - Time series of the measured and modeled velocity magnitude and direction at 20110804 Branst

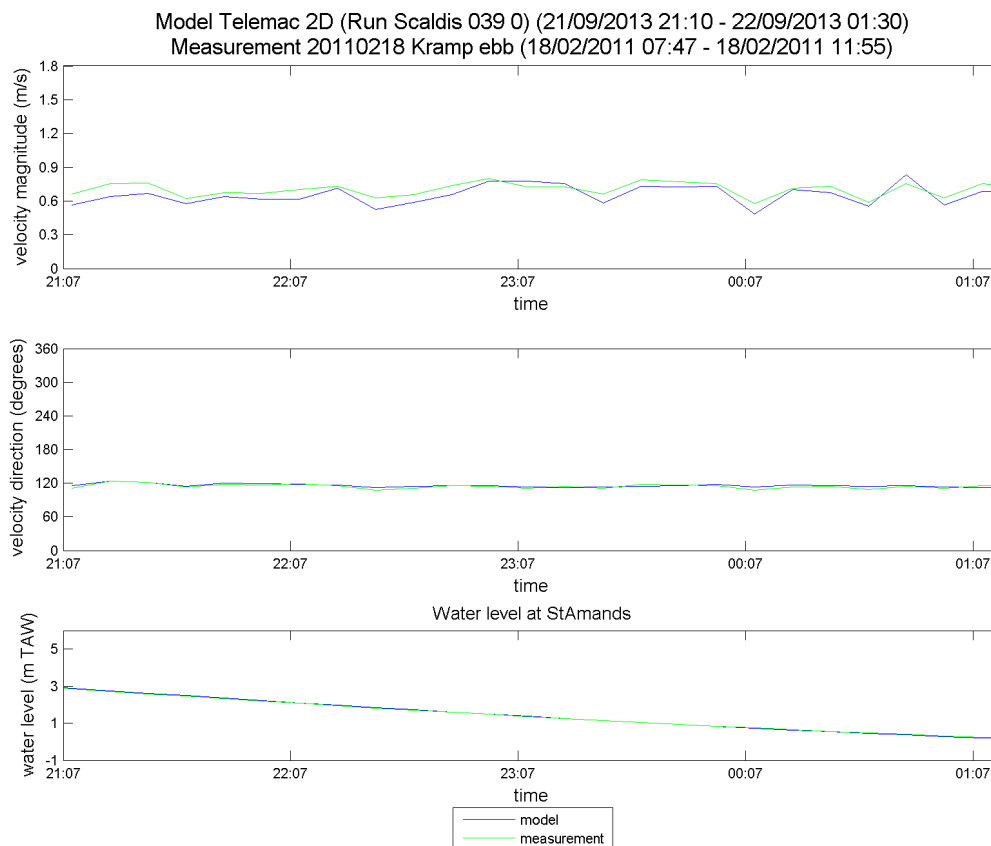


Figure 321 - Time series of the measured and modeled velocity magnitude and direction at 20110218 Kramp ebb

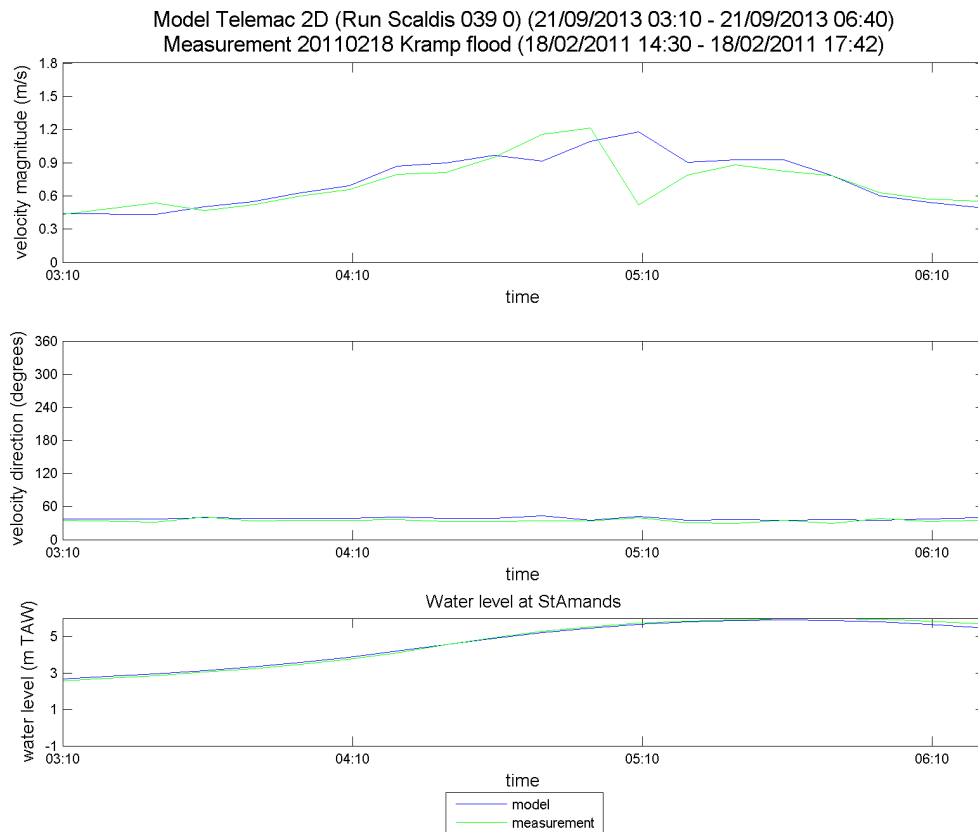


Figure 322 - Time series of the measured and modeled velocity magnitude and direction at 20110218 Kramp flood

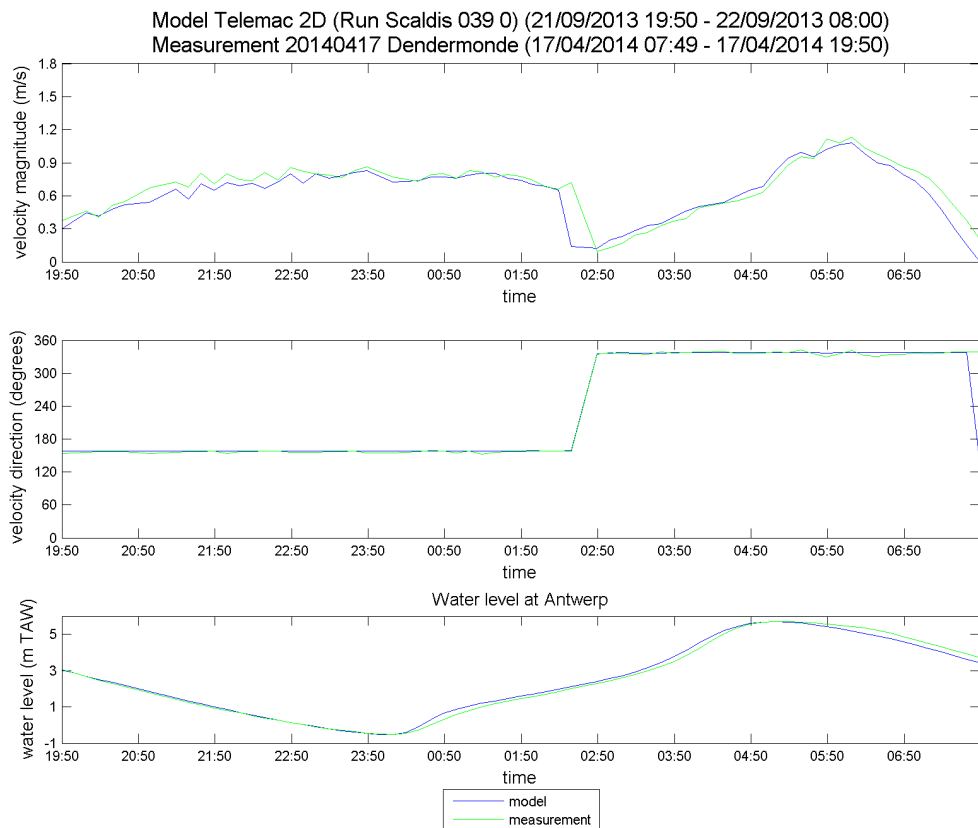


Figure 323 - Time series of the measured and modeled velocity magnitude and direction at 20140417 Dendermonde

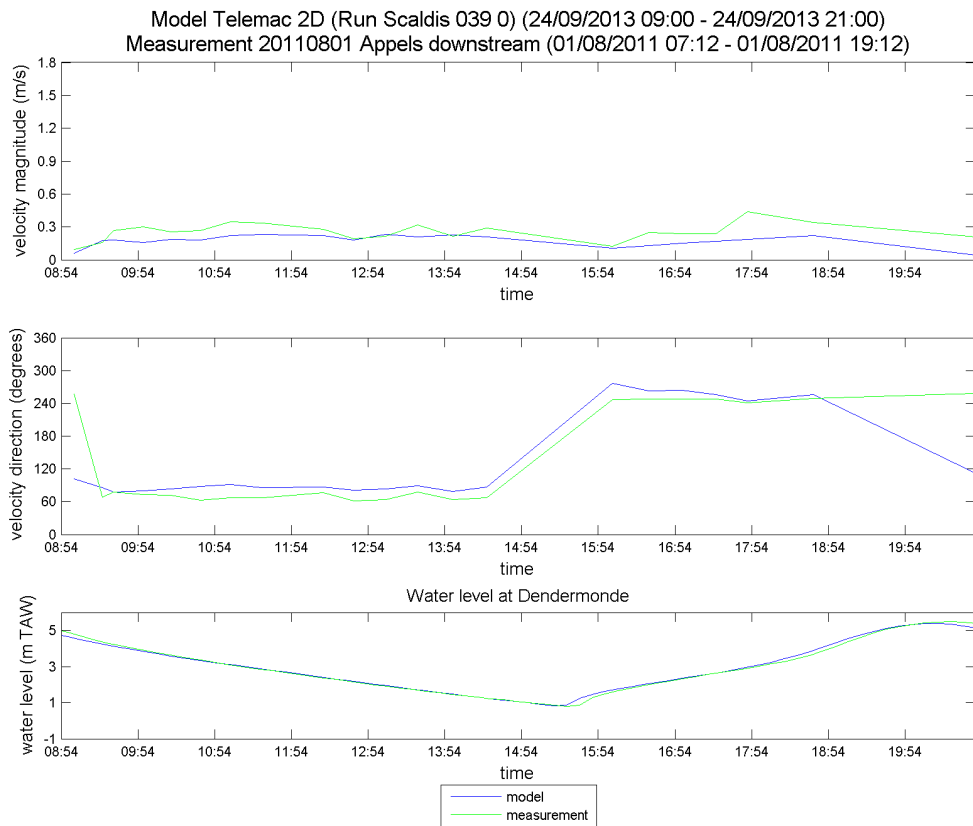


Figure 324 - Time series of the measured and modeled velocity magnitude and direction at 20110801 Appels downstream

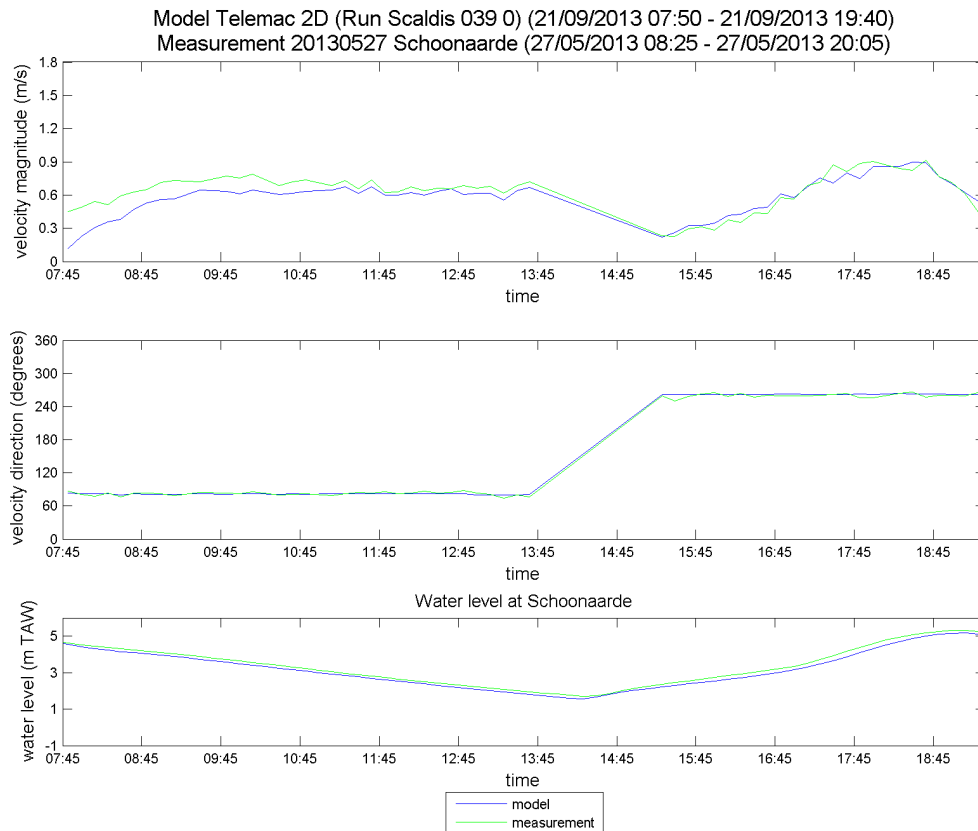


Figure 325 - Time series of the measured and modeled velocity magnitude and direction at 20130527 Schoonaarde

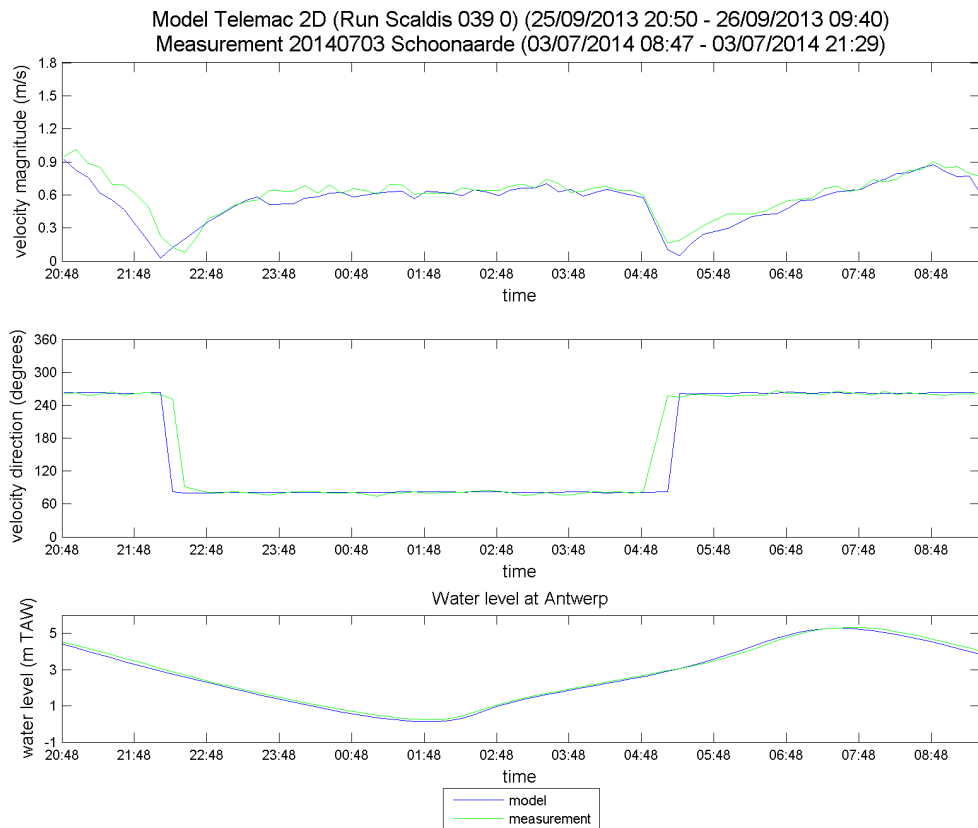


Figure 326 - Time series of the measured and modeled velocity magnitude and direction at 20140703 Schoonaarde

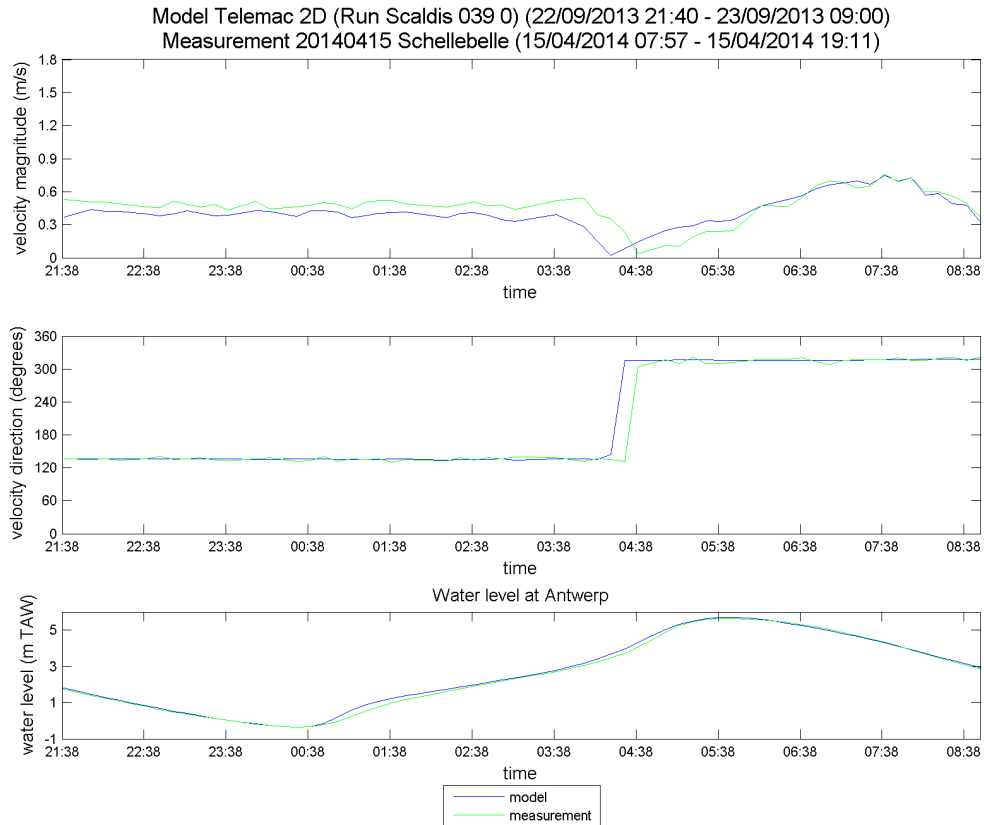


Figure 327 - Time series of the measured and modeled velocity magnitude and direction at 20140415 Schellebelle

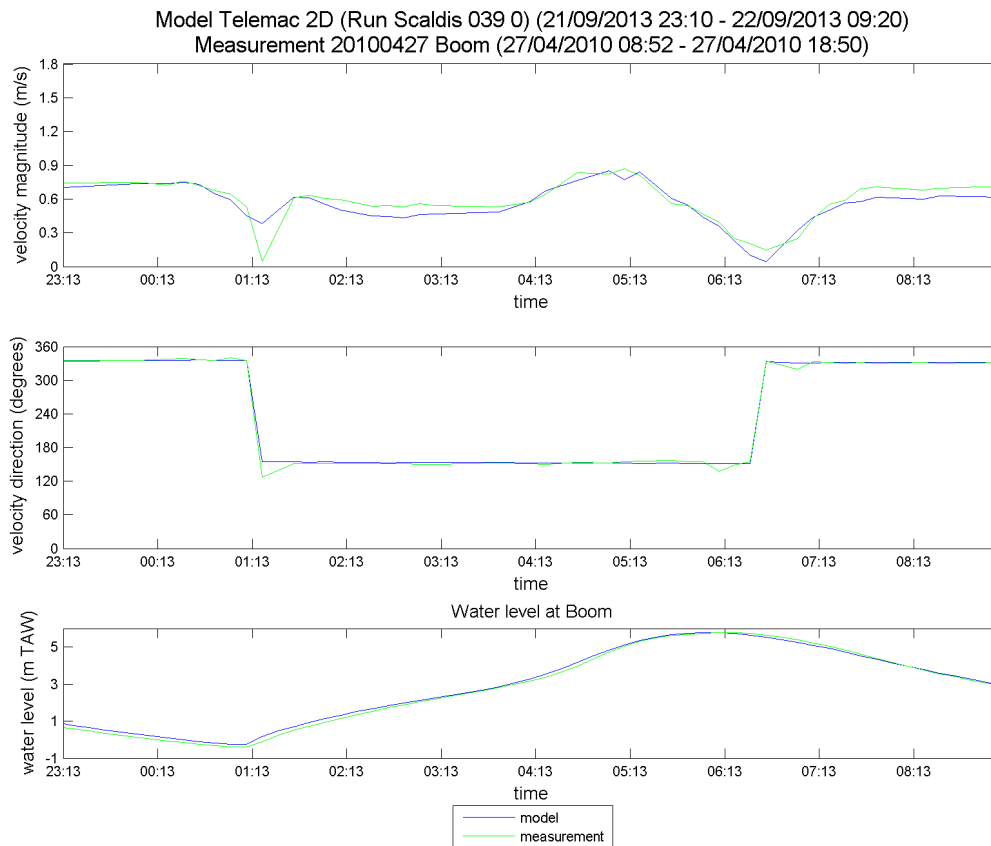


Figure 328 - Time series of the measured and modeled velocity magnitude and direction at 20100427 Boom

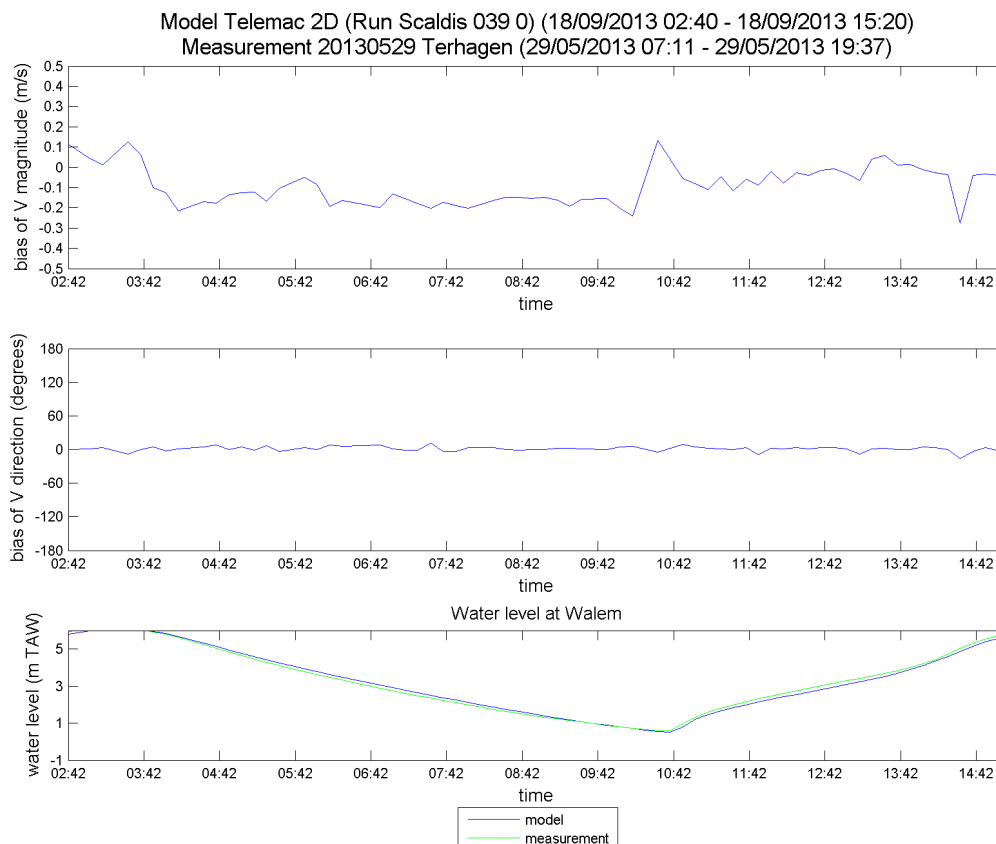


Figure 329 - Time series of the measured and modeled velocity magnitude and direction at 20130529 Terhagen

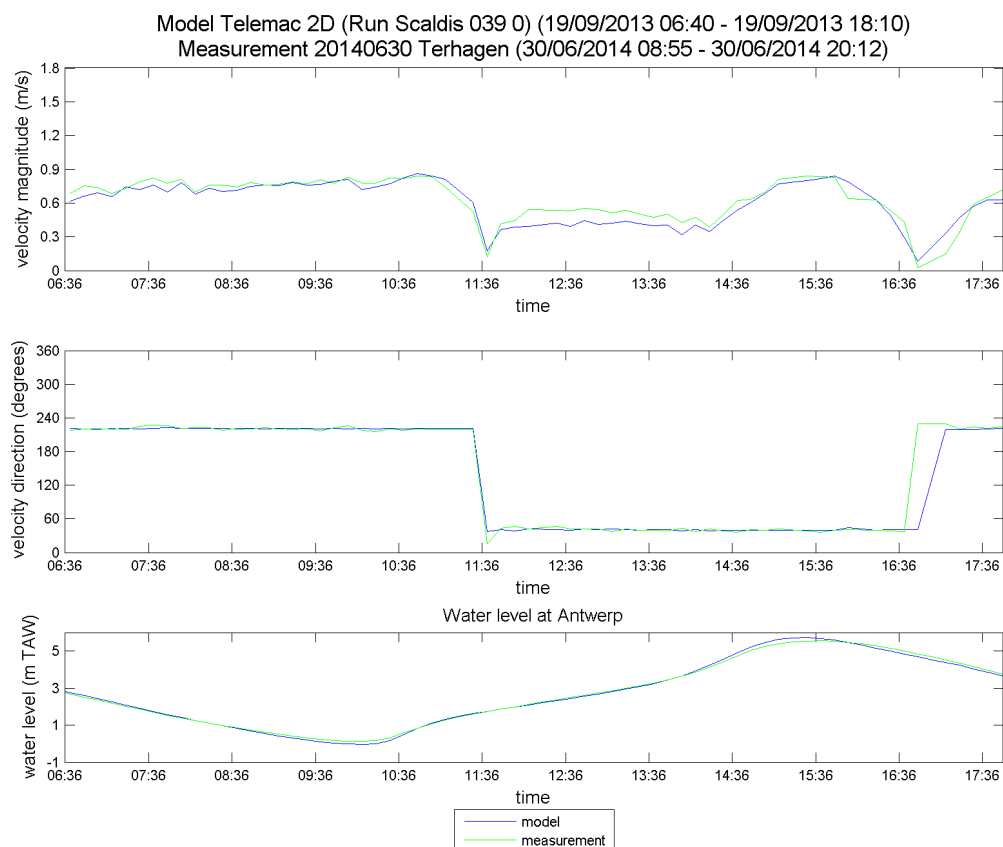


Figure 330 - Time series of the measured and modeled velocity magnitude and direction at 20140630 Terhagen

Model Telemac 2D (Run Scaldis 039 0) | Time= 22-Sep-2013 03:30:00
Measurement 20080407 dwarsraai Ossensisse | Time= 07-Apr-2008 14:51:16

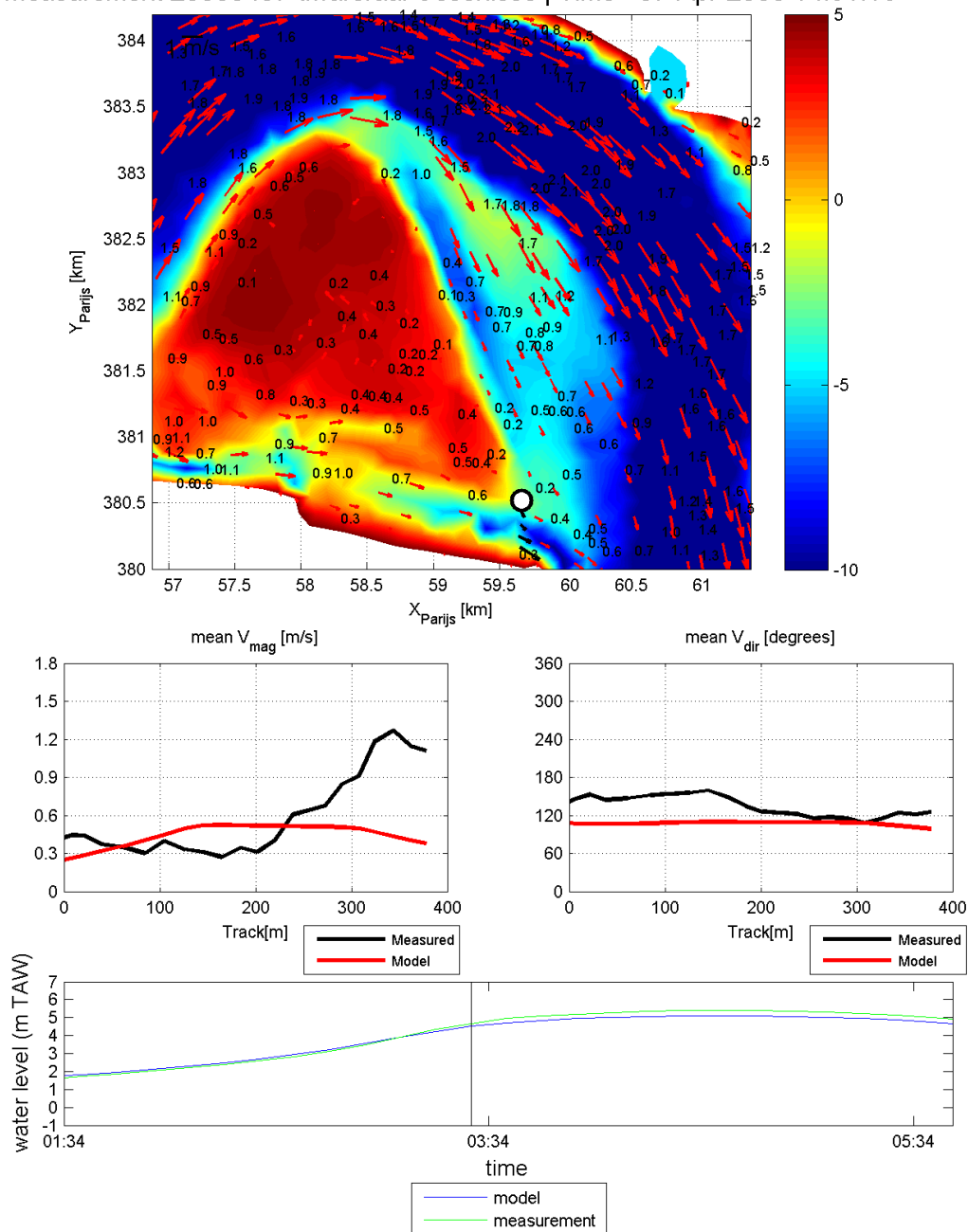


Figure 331 - Example of the modeled and measured velocity magnitude and direction for one of the transects at Ossensisse (transverse profile)*

*The white circle in the figure shows the location of the first measurement (0 m)

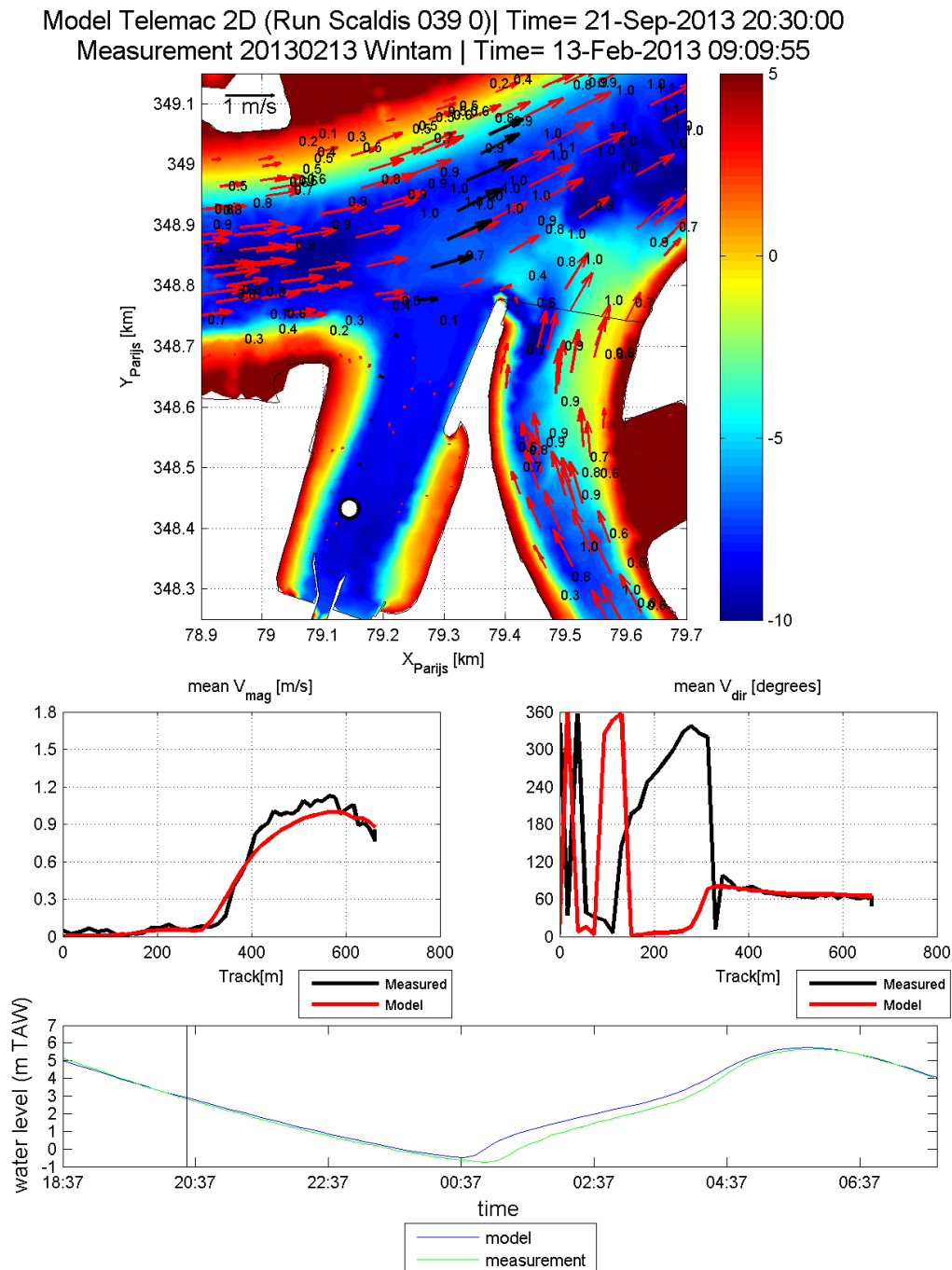


Figure 332 - Example of the modeled and measured velocity magnitude and direction for one of the transects at Wintam*

*The model accuracy for the velocity direction worsens in the locations where velocity magnitude is very small (the white circle in the figure shows the location of the first measurement (0 m))

Table 150. RMSE of velocity magnitude in the intertidal areas

Scaldis_039_0	RMSE mag all (m/s)
20110705 Everingen	no data in shallow areas
20110706 R7 Terneuzen	0.21
20120508 R6 Middelgat	0.28
20120509 R6 GatVanOssenis	0.25
20080407 dwarsraai Ossenis	no data in shallow areas
20060323 Waarde	no data in shallow areas
20130424 R5 SchaarVanWaarde	0.15
20130425 R5 Zuidergat	0.17
20060912 Schaar van Ouden Doel	no data in shallow areas
20050217 Zandvliet	0.24
20060323 DGD K	0.17
20080311 DGD K	0.16
20050217 Liefkenshoek	0.19
20130625 Liefkenshoek	0.17
20140514 Liefkenshoek	0.15
20050218 Kallo	no data in shallow areas
20090529 Oosterweel	0.30
20130627 Oosterweel	no data in shallow areas
20140516 Oosterweel	no data in shallow areas
20100414 Kruibeke	0.17
20130530 Kruibeke	0.18
20140702 Kruibeke	0.11
20060323 Schelle	0.34
20060928 Schelle	0.35
20130213 Wintam	no data in shallow areas
20090610 Ballooi dwars	0.17
20130612 Driegoten	0.22
20140617 Driegoten	0.22
20110218 Kramp ebb	not enough data in shallow areas
20110218 Kramp flood	not enough data in shallow areas
20140417 Dendermonde	0.12
20130527 Schoonaarde	0.24
20140703 Schoonaarde	0.30
20140415 Schellebelle	0.13
20100427 Boom	0.16
20130529 Terhagen	0.21
20140630 Terhagen	0.17

Scaldis_039_0	RMSE mag all (m/s)
20110902 Galgenschoor	0.21
20100318 langsraai O	not enough data in shallow areas
20090610 Notelaer langs	0.19
20110804 Branst	0.23
20110801 Appels downstream	0.20

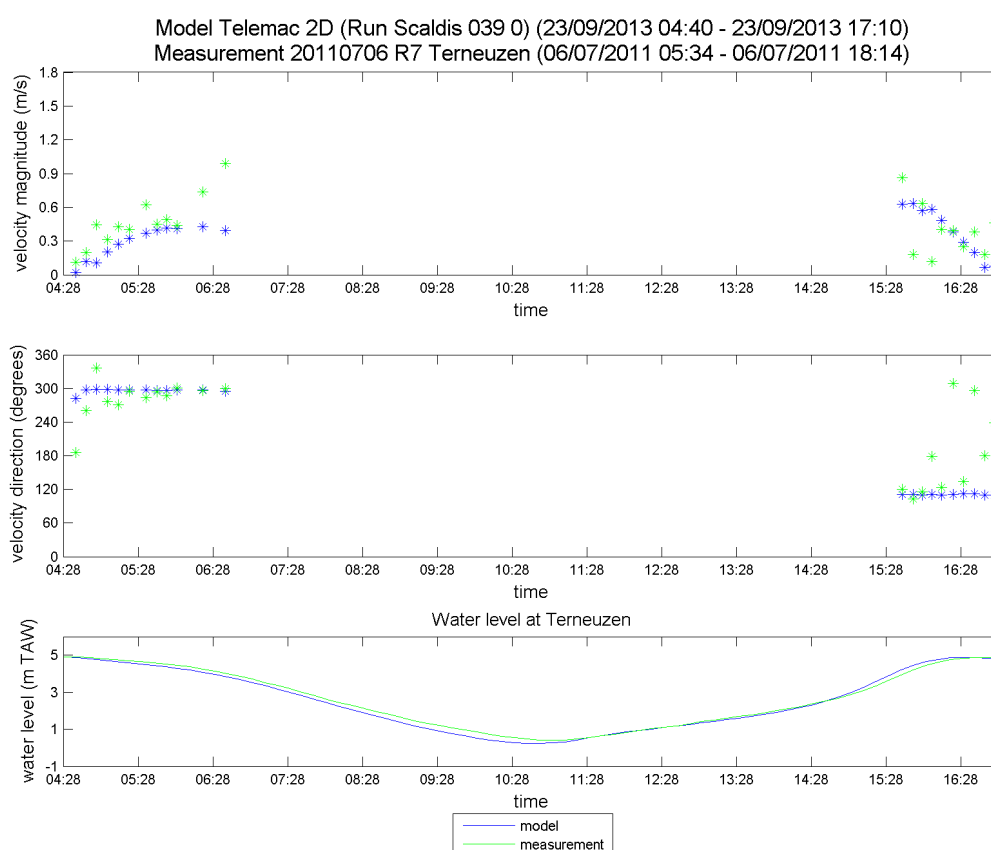


Figure 333 - Time series of the measured and modeled velocity magnitude and direction in the intertidal area at 20110706 R7 Terneuzen

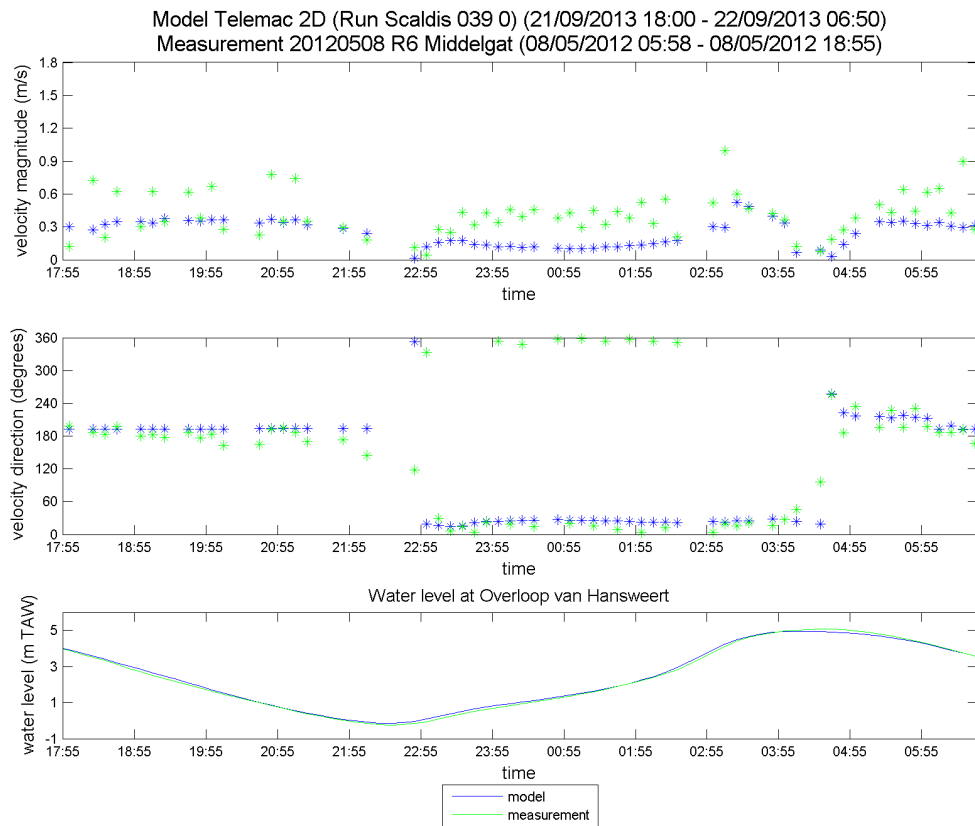


Figure 334 - Time series of the measured and modeled velocity magnitude and direction in the intertidal area at 20120508 R6 Middelgat

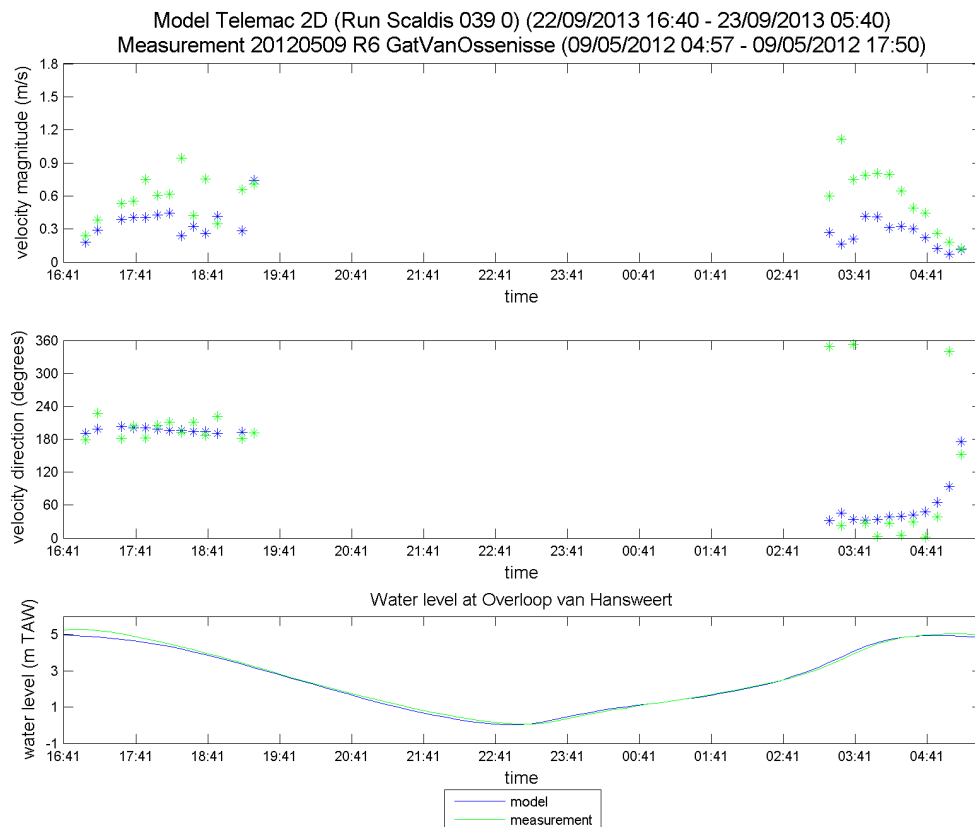


Figure 335 - Time series of the measured and modeled velocity magnitude and direction in the intertidal area at 20120509 R6 GatVanOssensisse

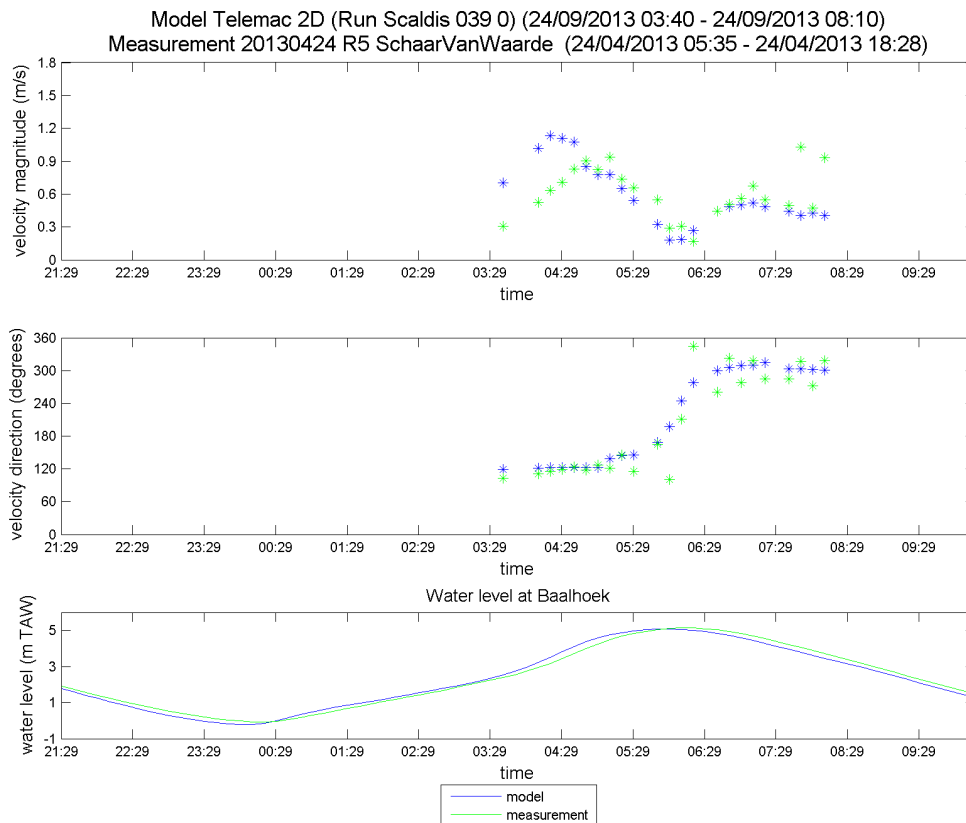


Figure 336 - Time series of the measured and modeled velocity magnitude and direction in the intertidal area at 20130424 R5 SchaarVanWaarde

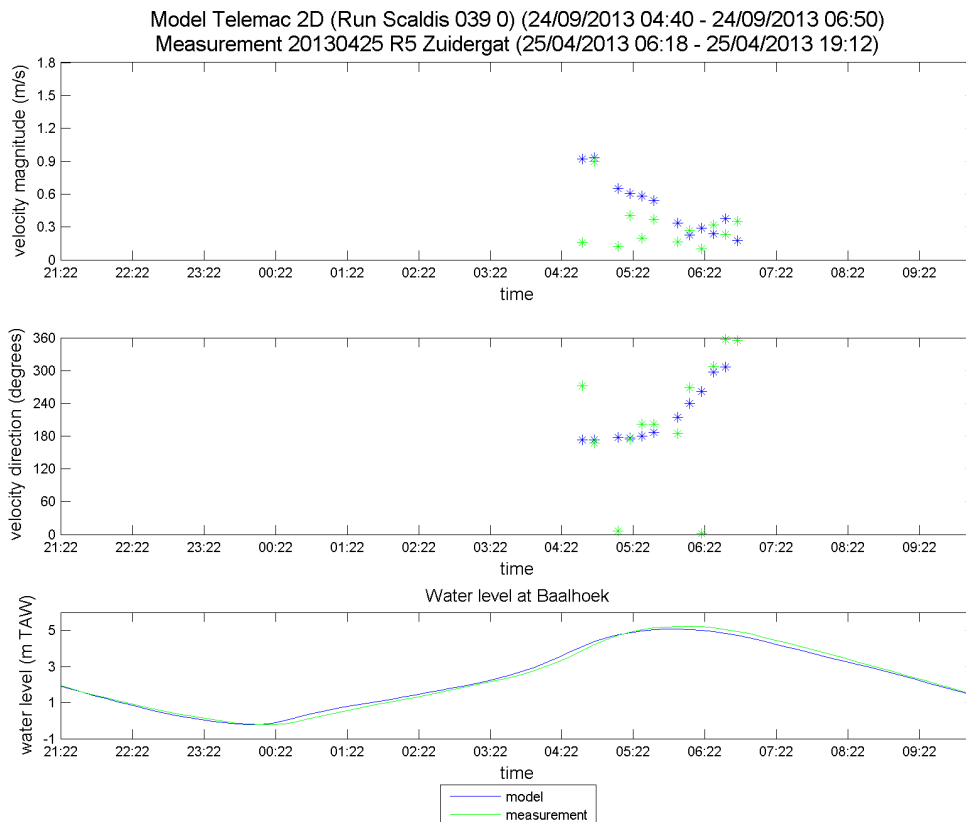


Figure 337 - Time series of the measured and modeled velocity magnitude and direction in the intertidal area at 20130425 R5 Zuidergat

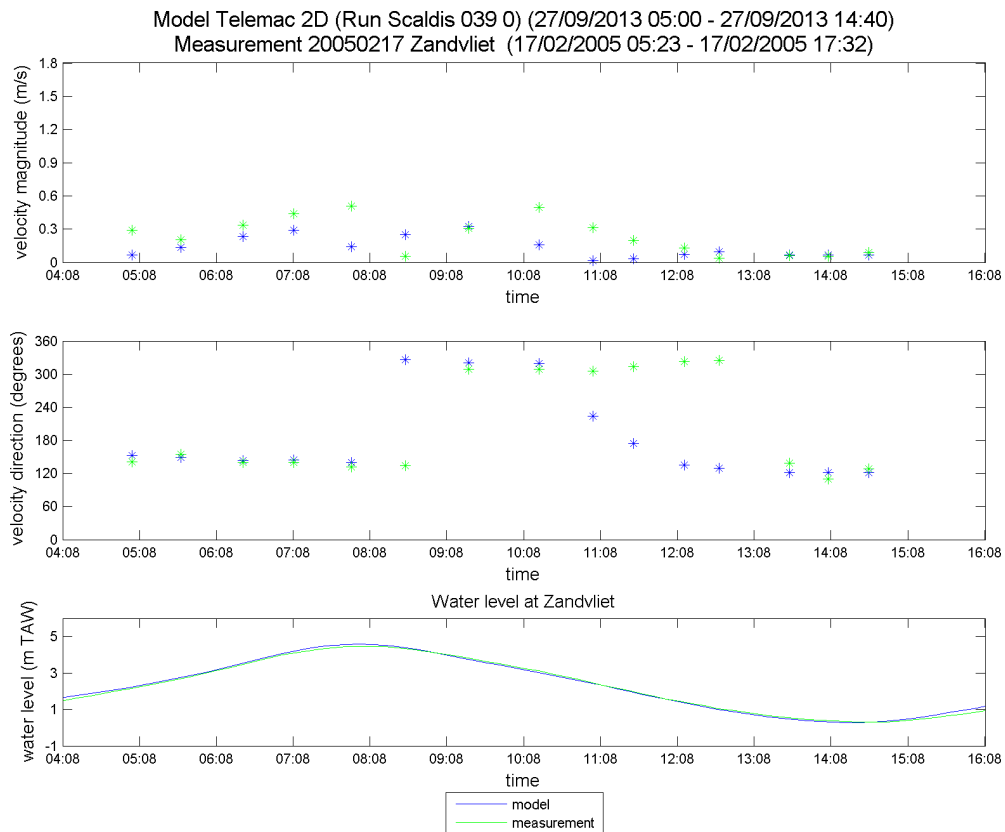


Figure 338 - Time series of the measured and modeled velocity magnitude and direction in the intertidal area at 20050217 Zandvliet

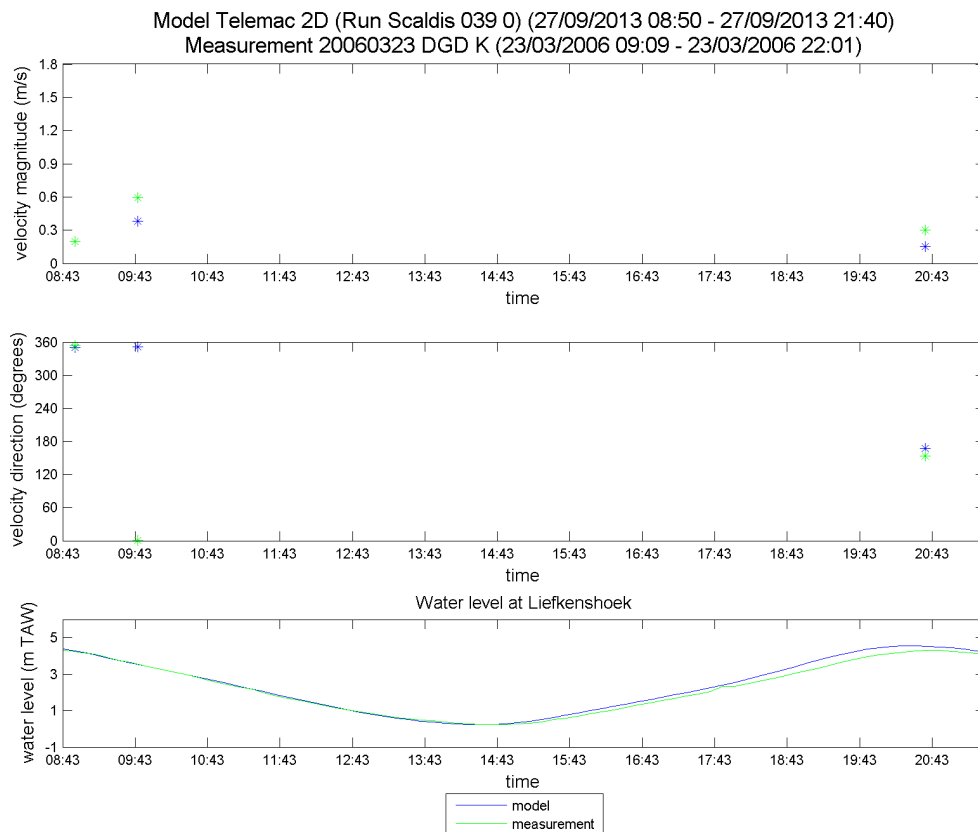


Figure 339 - Time series of the measured and modeled velocity magnitude and direction in the intertidal area at 20060323 DGD K

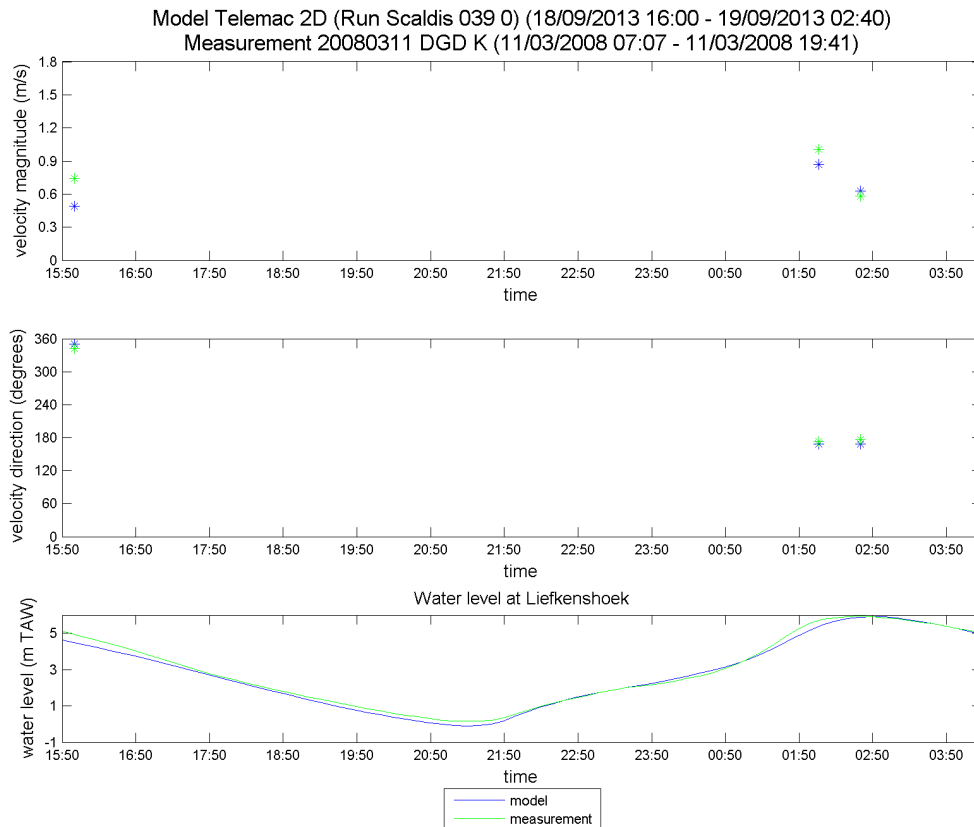


Figure 340 - Time series of the measured and modeled velocity magnitude and direction in the intertidal area at 20080311 DGD K

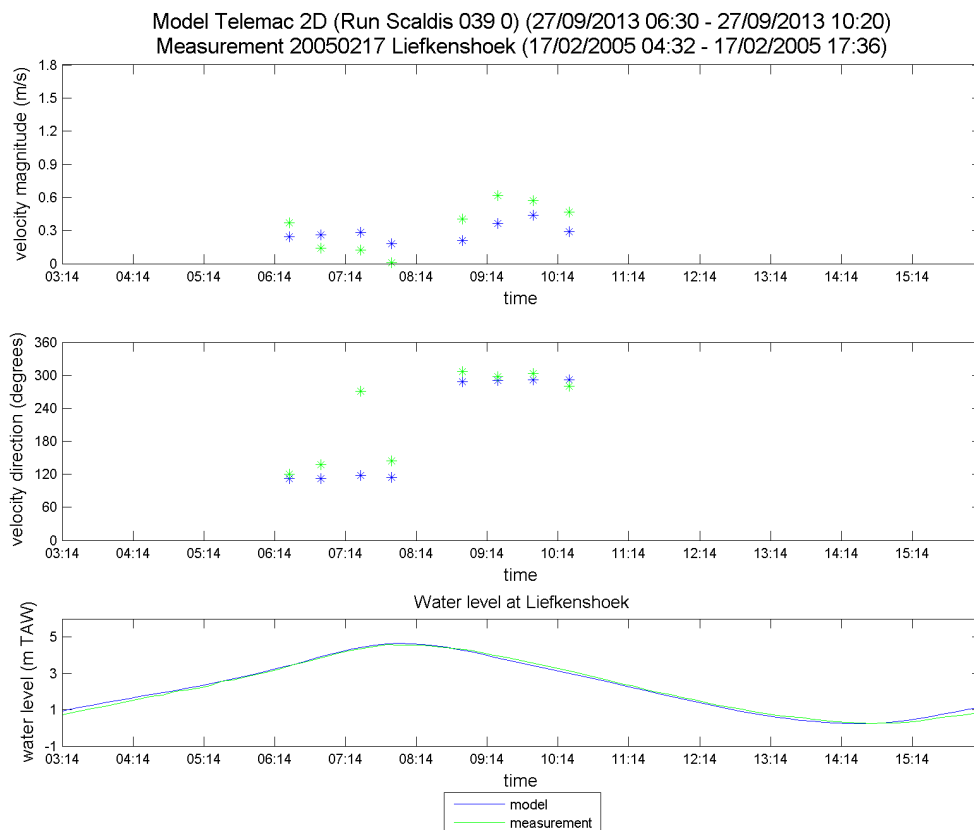


Figure 341 - Time series of the measured and modeled velocity magnitude and direction in the intertidal area at 20050217 Liefkenshoek

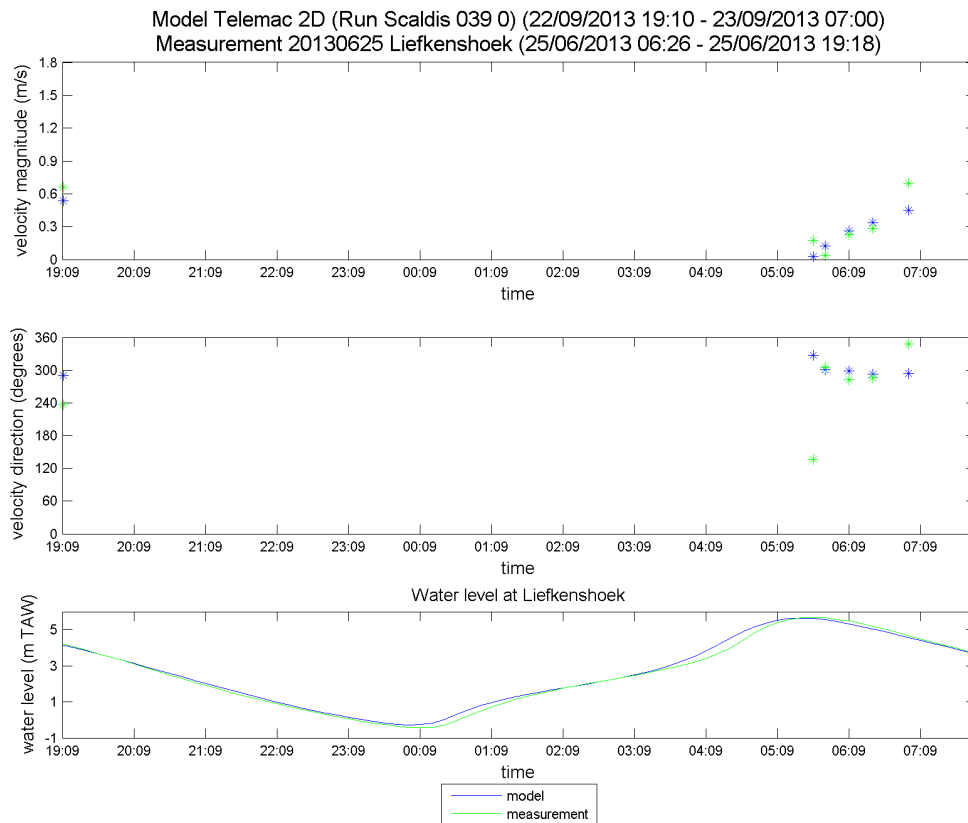


Figure 342 - Time series of the measured and modeled velocity magnitude and direction in the intertidal area at 20130625 Liefkenshoek

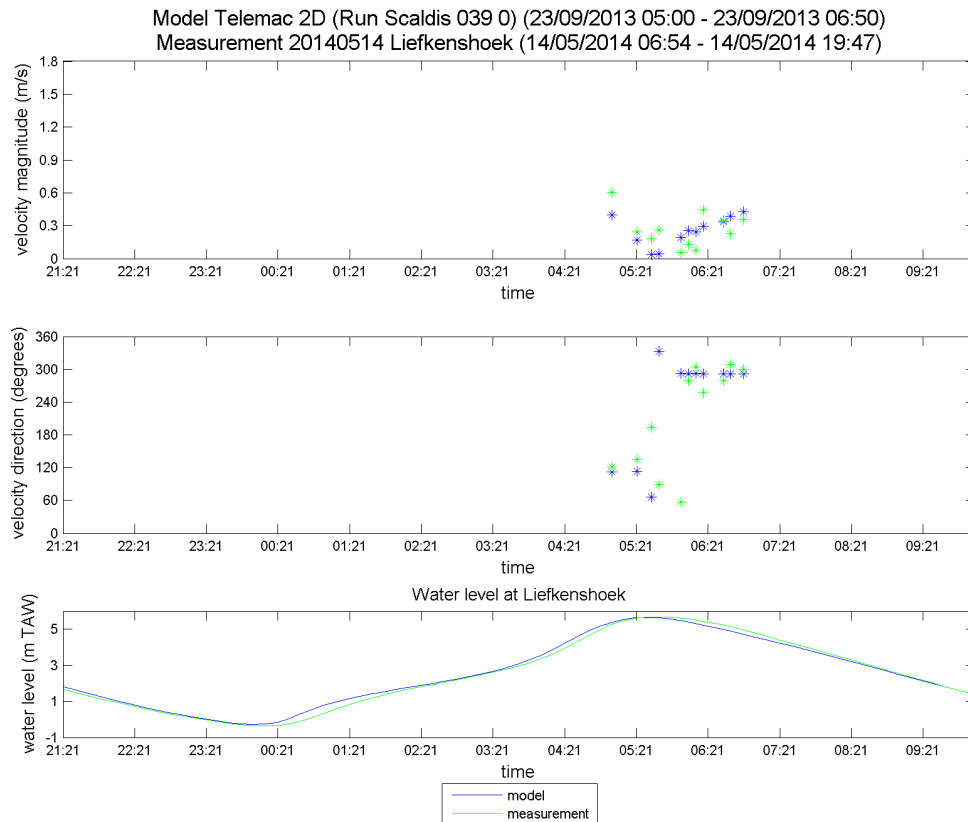


Figure 343 - Time series of the measured and modeled velocity magnitude and direction in the intertidal area at 20140514 Liefkenshoek

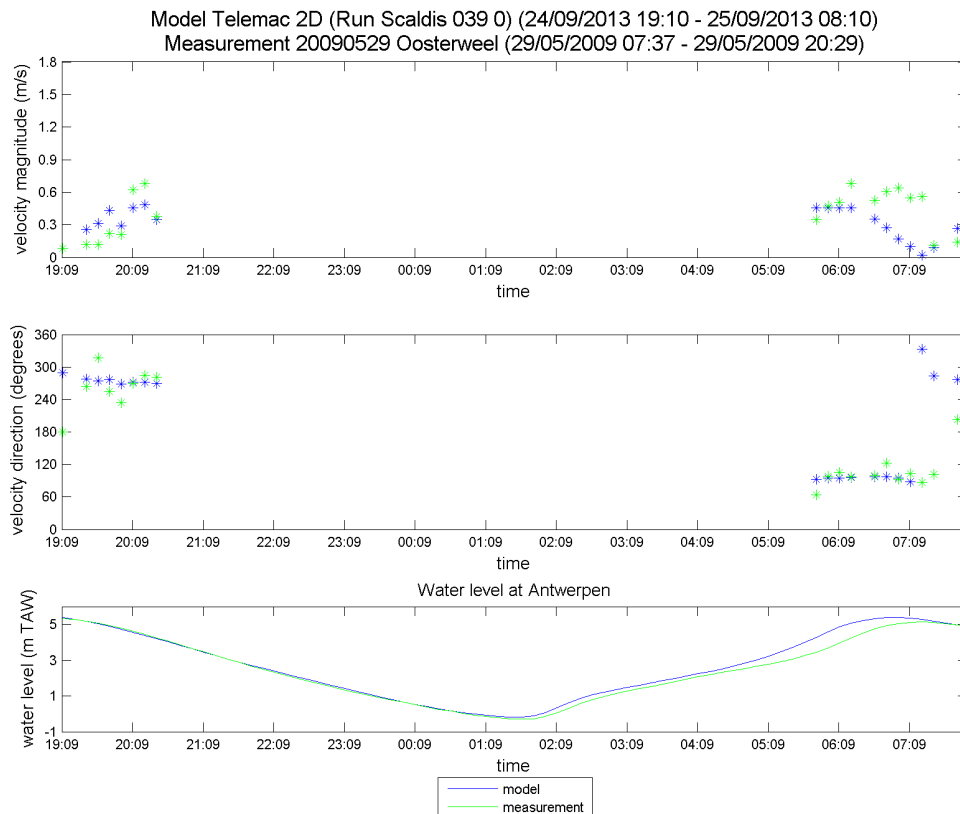


Figure 344 - Time series of the measured and modeled velocity magnitude and direction in the intertidal area at 20090529 Oosterweel

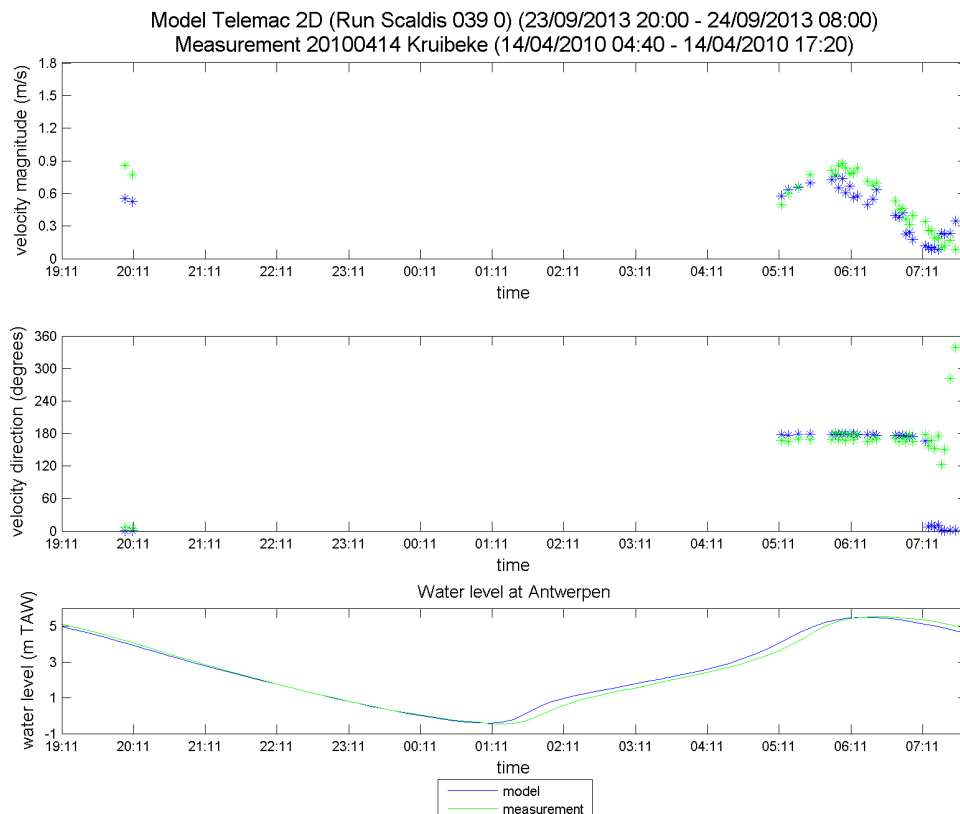


Figure 345 - Time series of the measured and modeled velocity magnitude and direction in the intertidal area at 20100414 Kruibeke

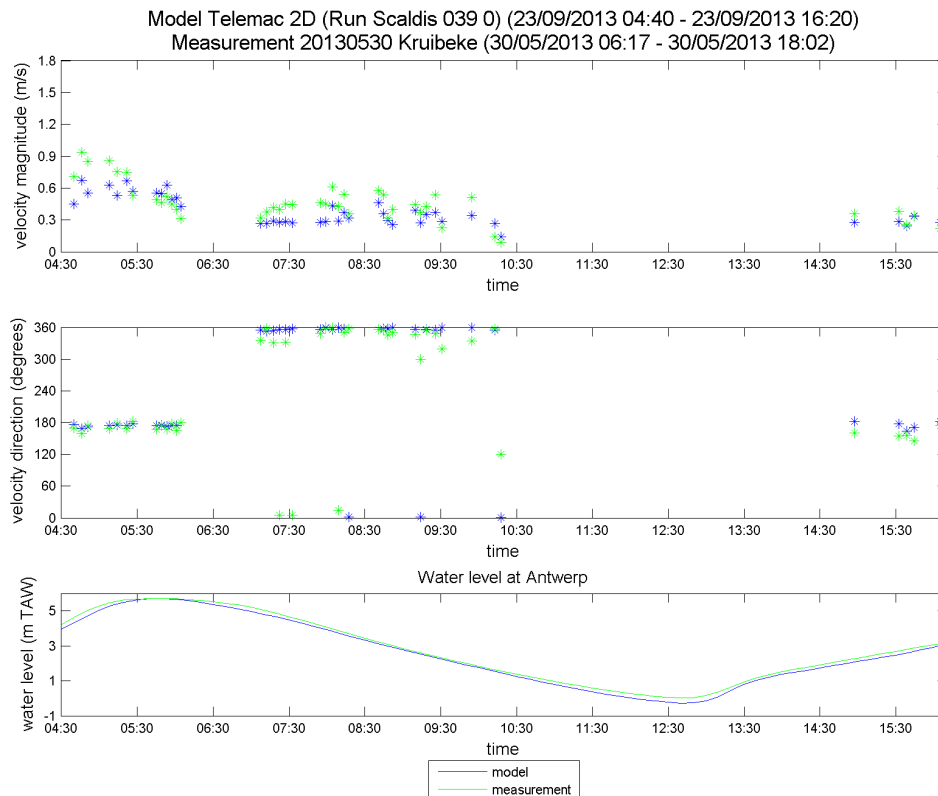


Figure 346 - Time series of the measured and modeled velocity magnitude and direction in the intertidal area at 20130530 Kruibeke

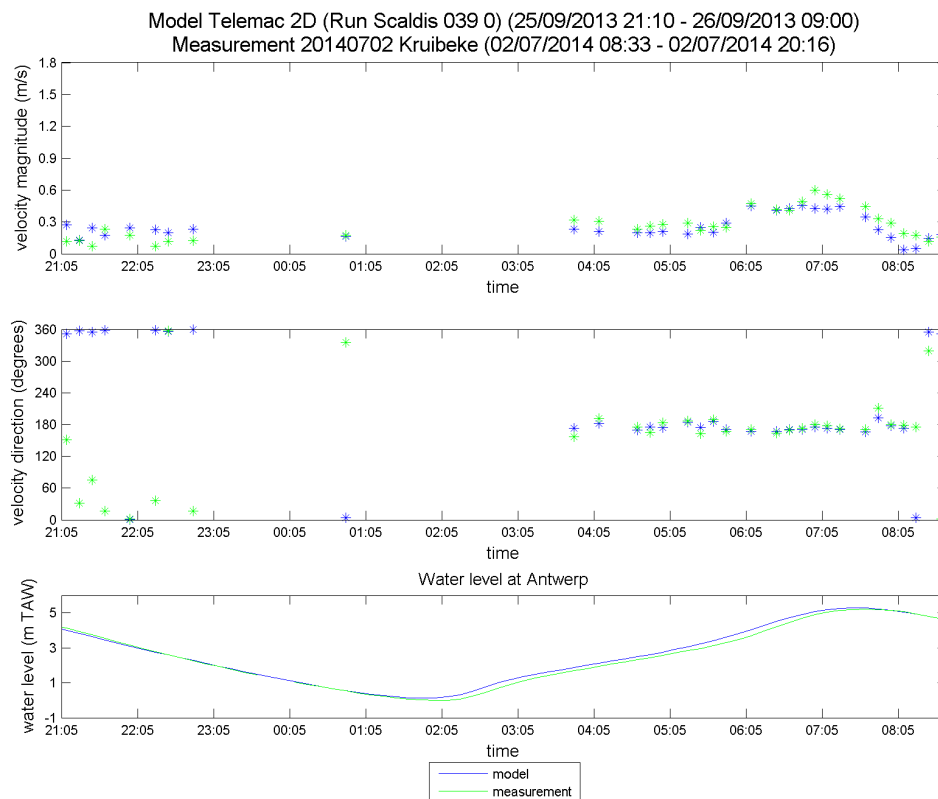


Figure 347 - Time series of the measured and modeled velocity magnitude and direction in the intertidal area at 20140702 Kruibeke

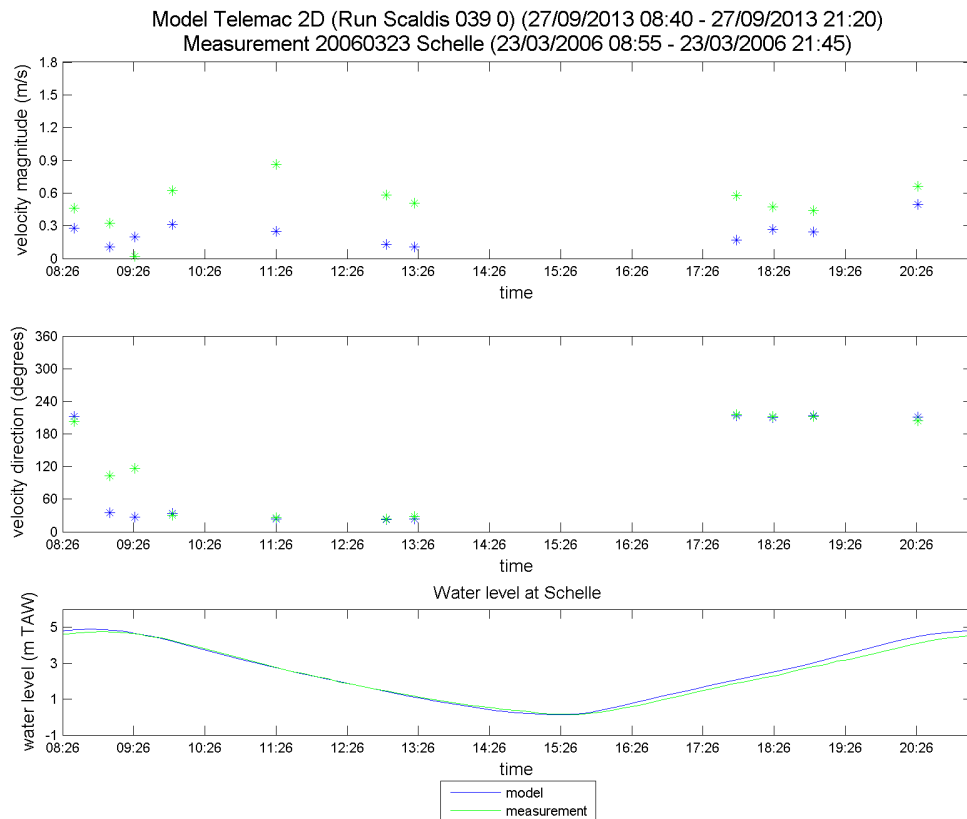


Figure 348 - Time series of the measured and modeled velocity magnitude and direction in the intertidal area at 20060323 Schelle

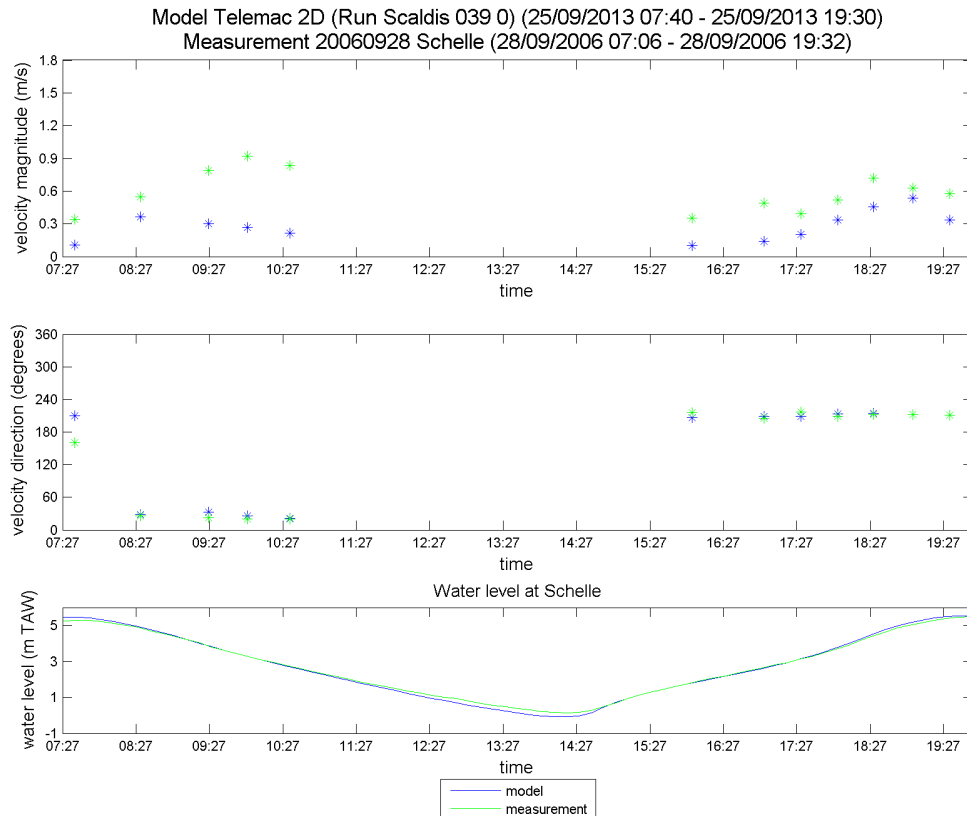


Figure 349 - Time series of the measured and modeled velocity magnitude and direction in the intertidal area at 20060928 Schelle

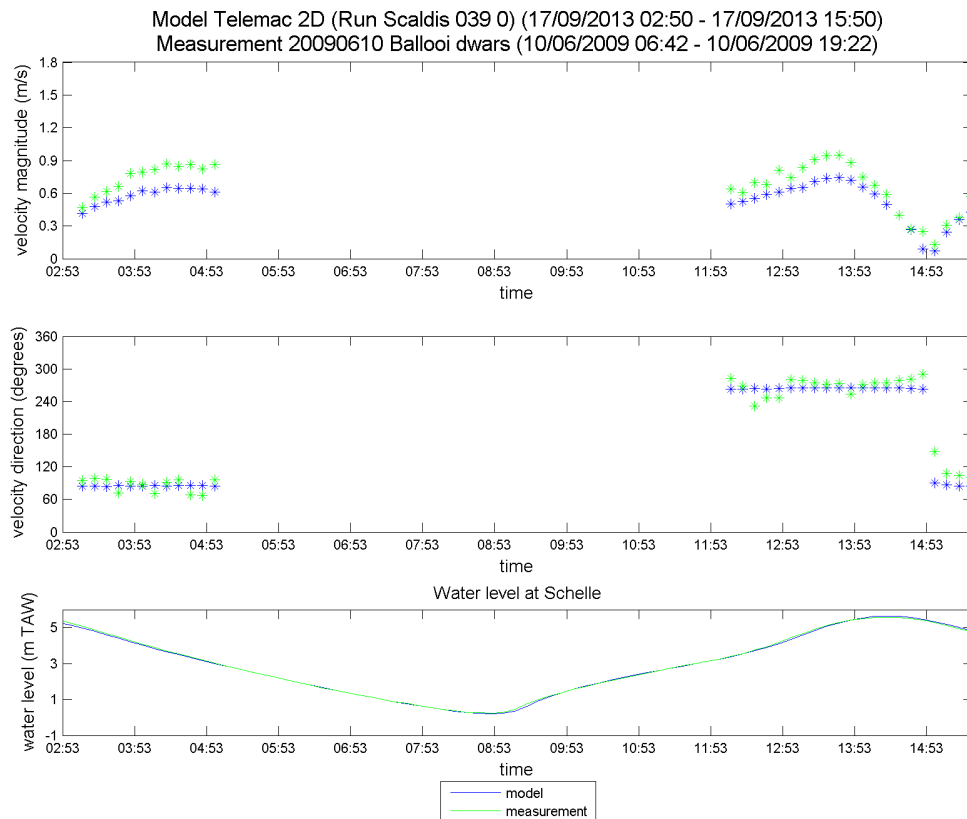


Figure 350 - Time series of the measured and modeled velocity magnitude and direction in the intertidal area at 20090610 Ballooi dwars

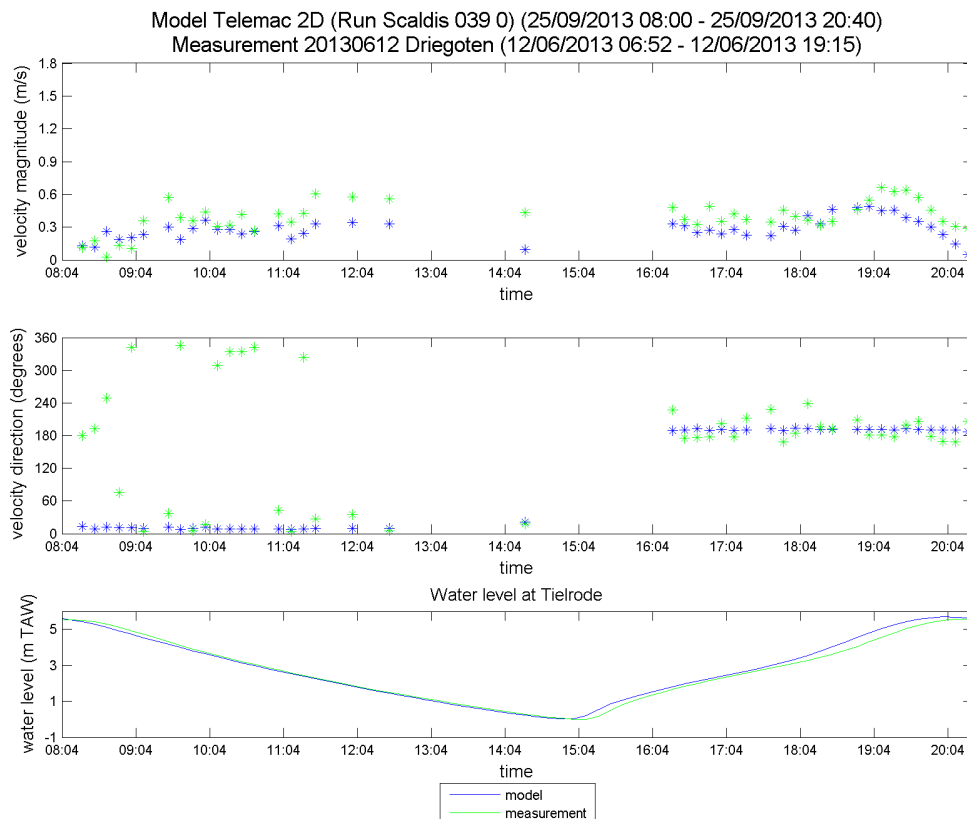


Figure 351 - Time series of the measured and modeled velocity magnitude and direction in the intertidal area at 20130612 Driegoten

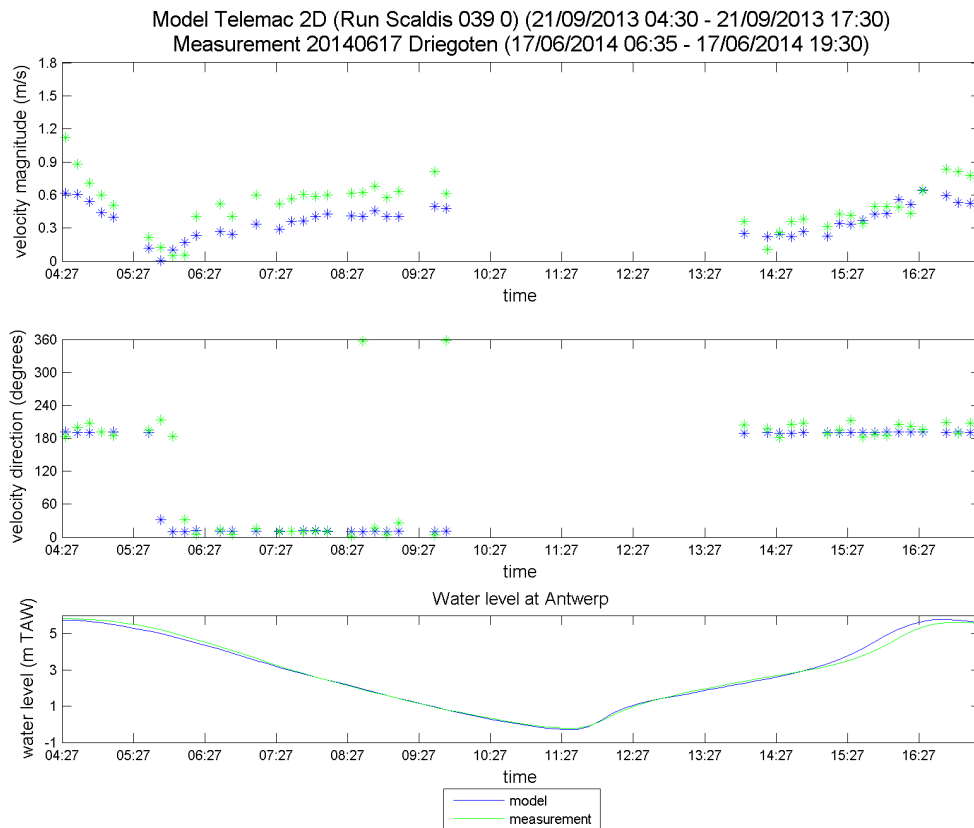


Figure 352 - Time series of the measured and modeled velocity magnitude and direction in the intertidal area at 20140617 Driegoten

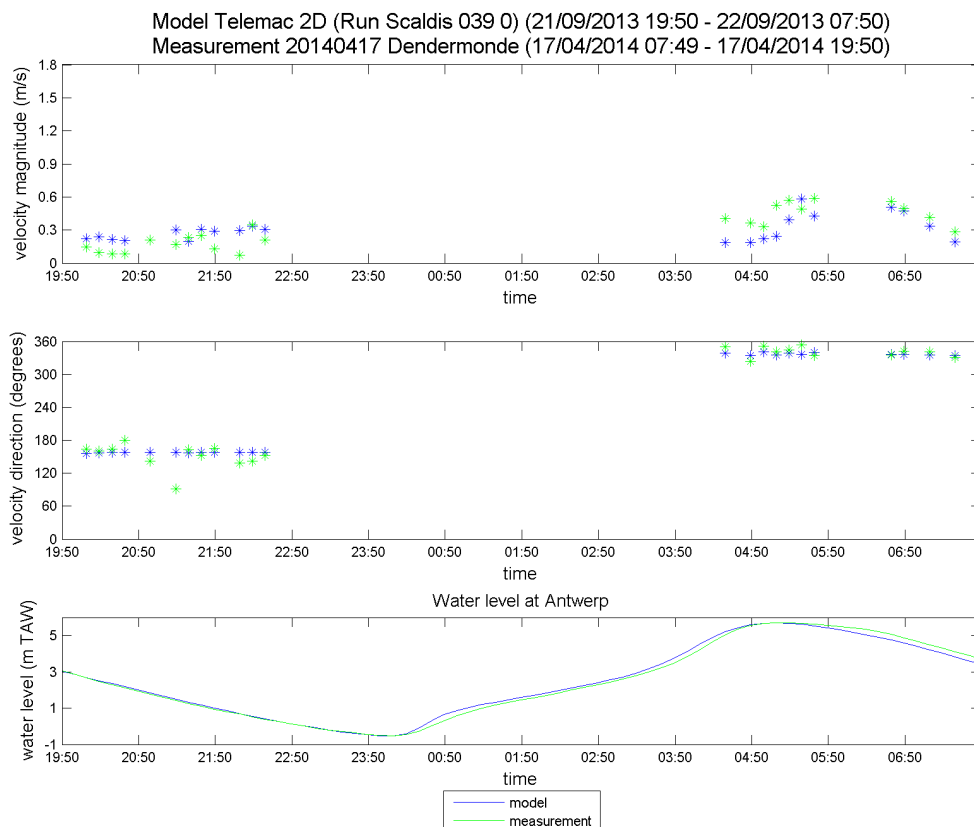


Figure 353 - Time series of the measured and modeled velocity magnitude and direction in the intertidal area at 20140417 Dendermonde

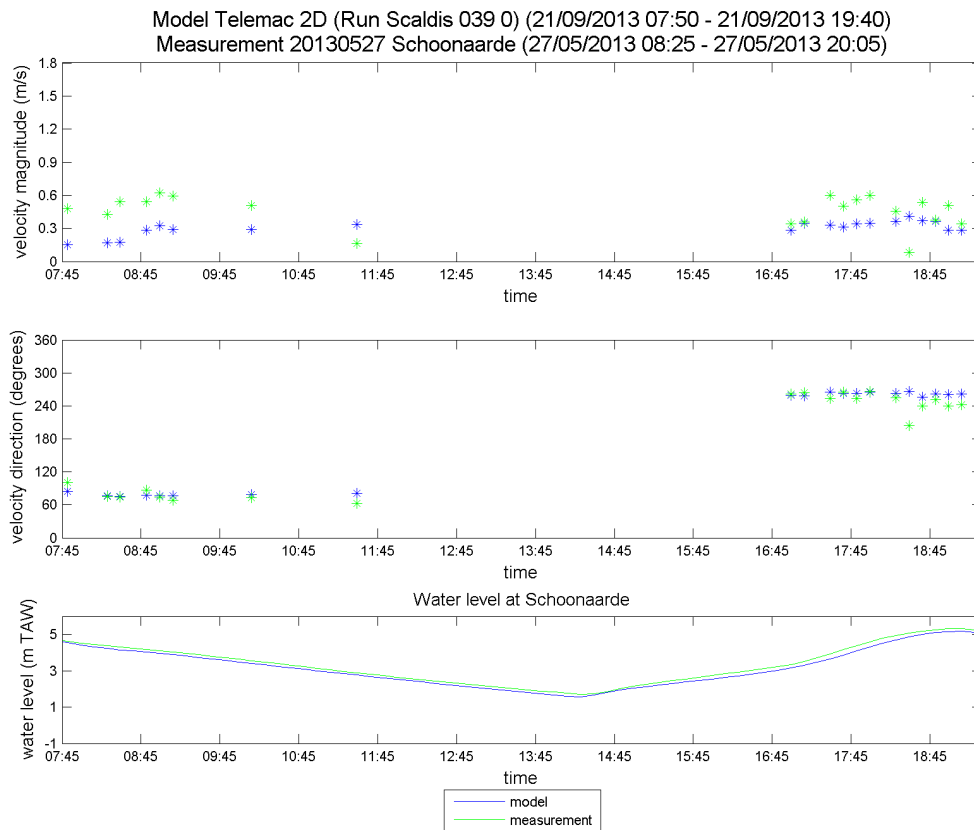


Figure 354 - Time series of the measured and modeled velocity magnitude and direction in the intertidal area at 20130527 Schoonaarde

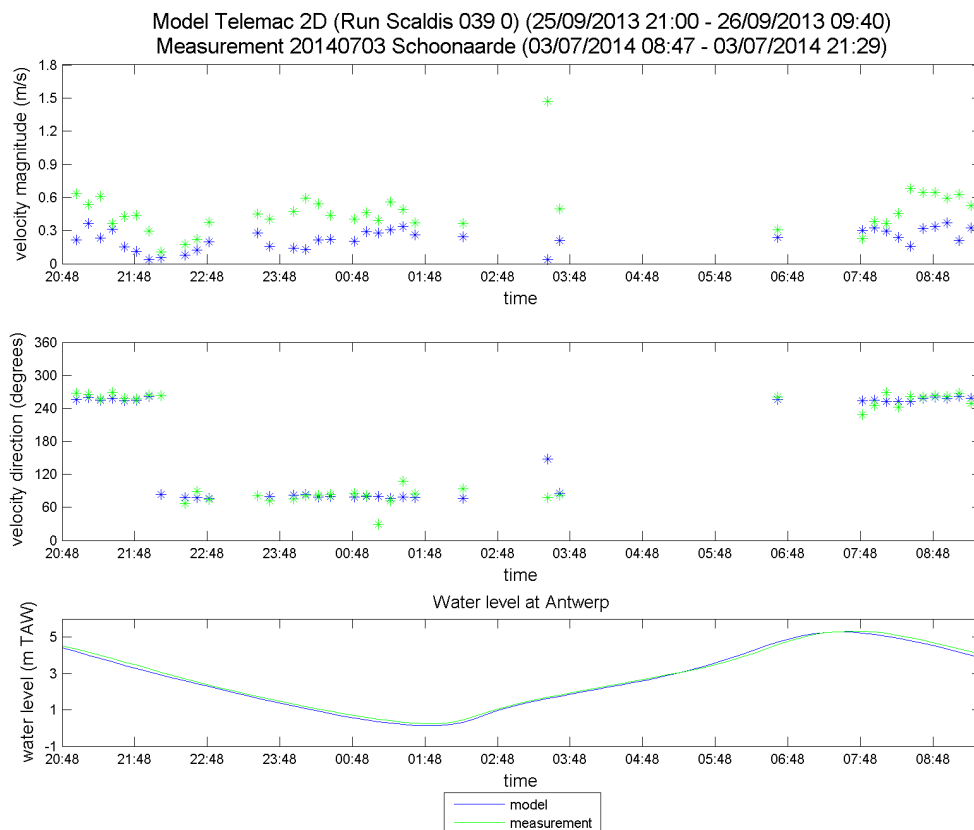


Figure 355 - Time series of the measured and modeled velocity magnitude and direction in the intertidal area at 20140703 Schoonaarde

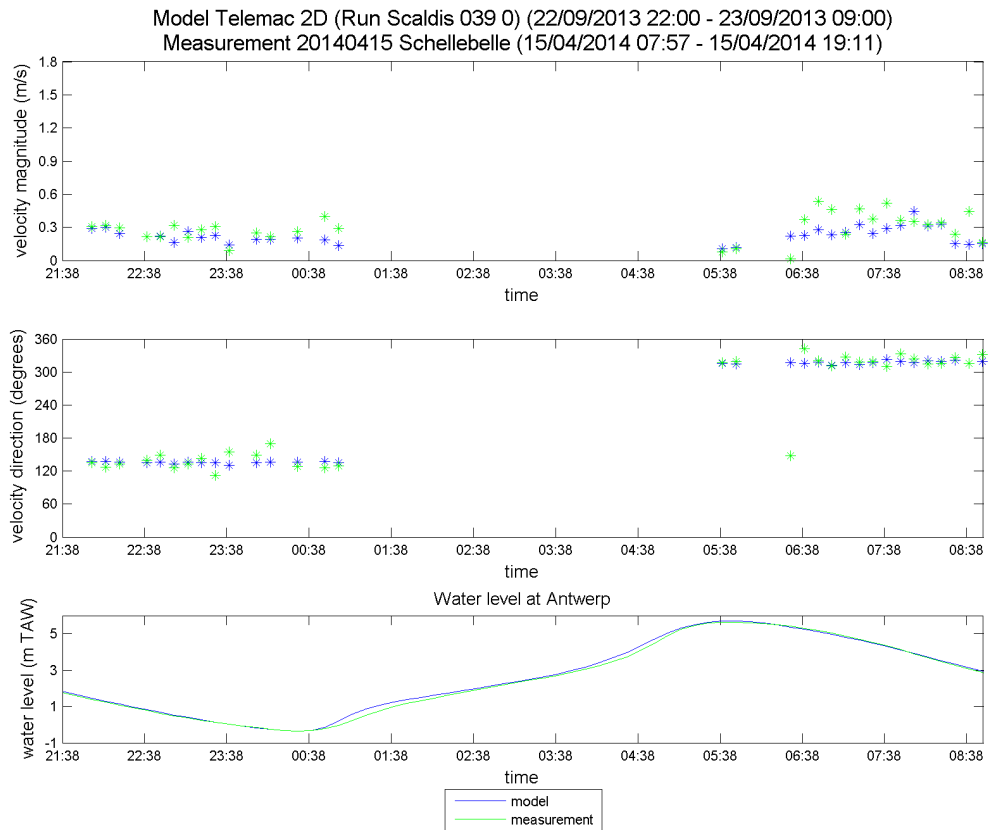


Figure 356 - Time series of the measured and modeled velocity magnitude and direction in the intertidal area at 20140415 Schellebelle

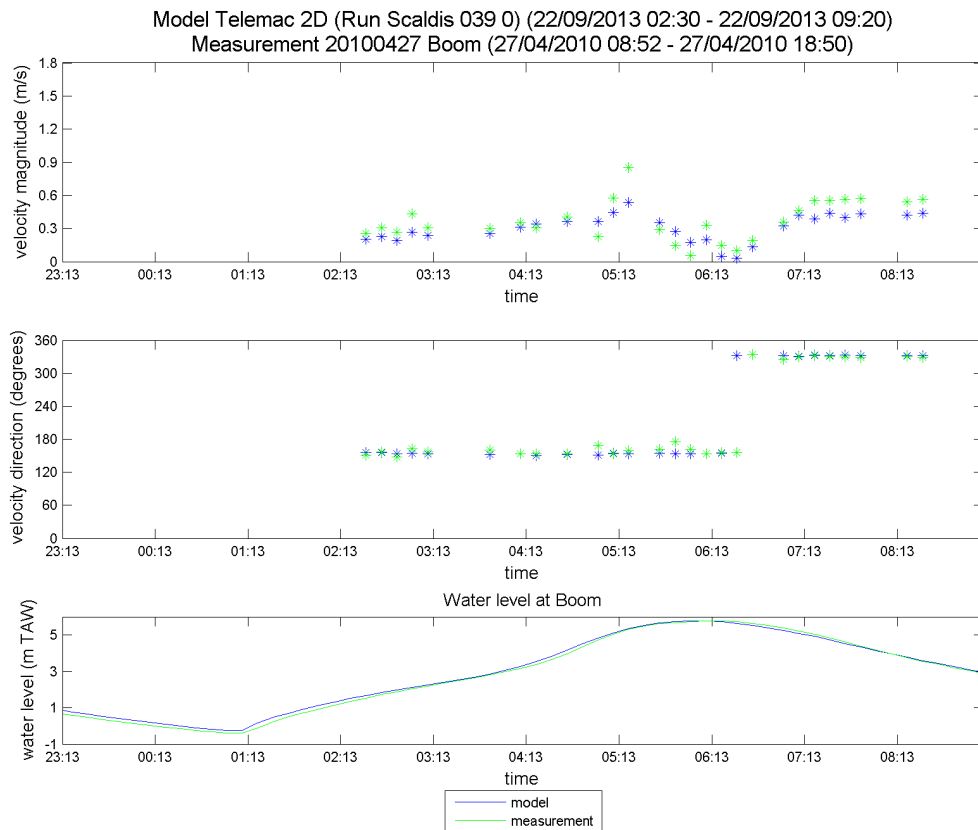


Figure 357 - Time series of the measured and modeled velocity magnitude and direction in the intertidal area at 20100427 Boom

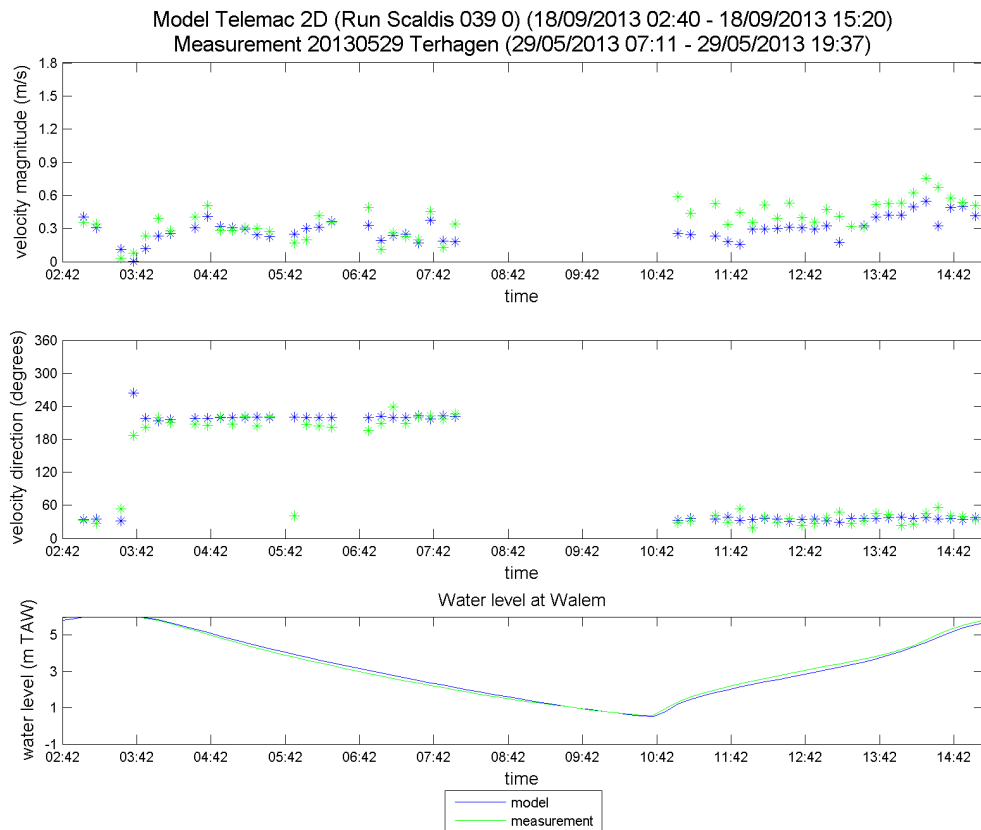


Figure 358 - Time series of the measured and modeled velocity magnitude and direction in the intertidal area at 20130529 Terhagen

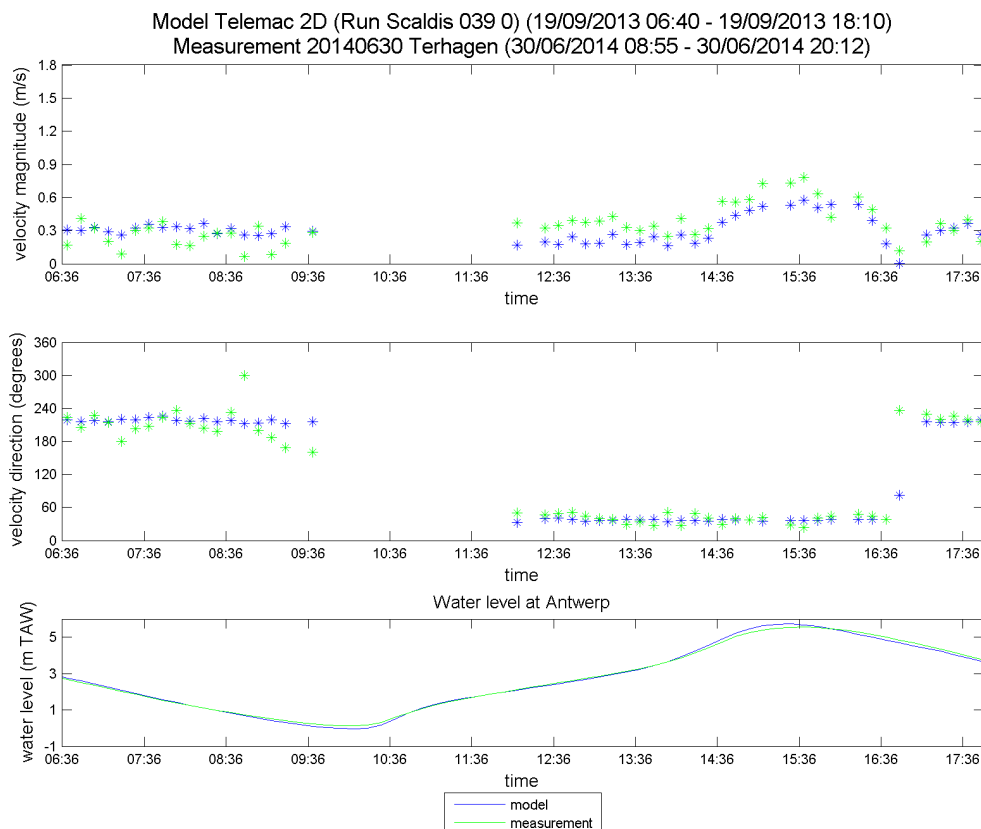


Figure 359 - Time series of the measured and modeled velocity magnitude and direction in the intertidal area at 20140630 Terhagen

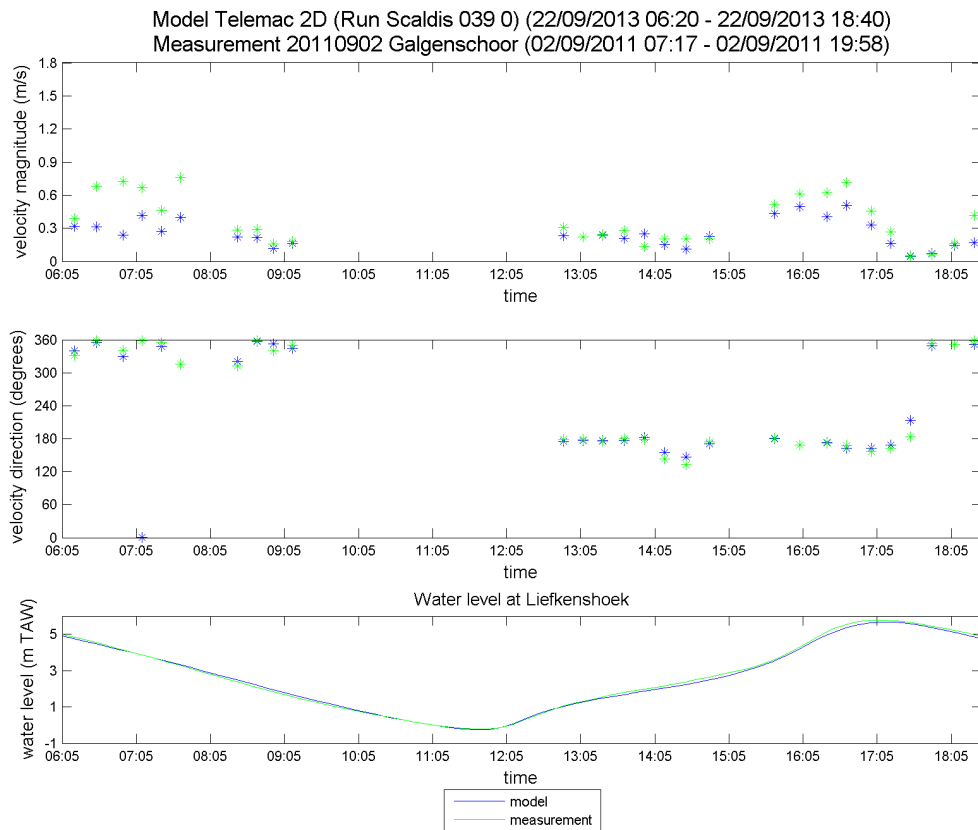


Figure 360 - Time series of the measured and modeled velocity magnitude and direction in the intertidal area at 20110902 Galgenschoor

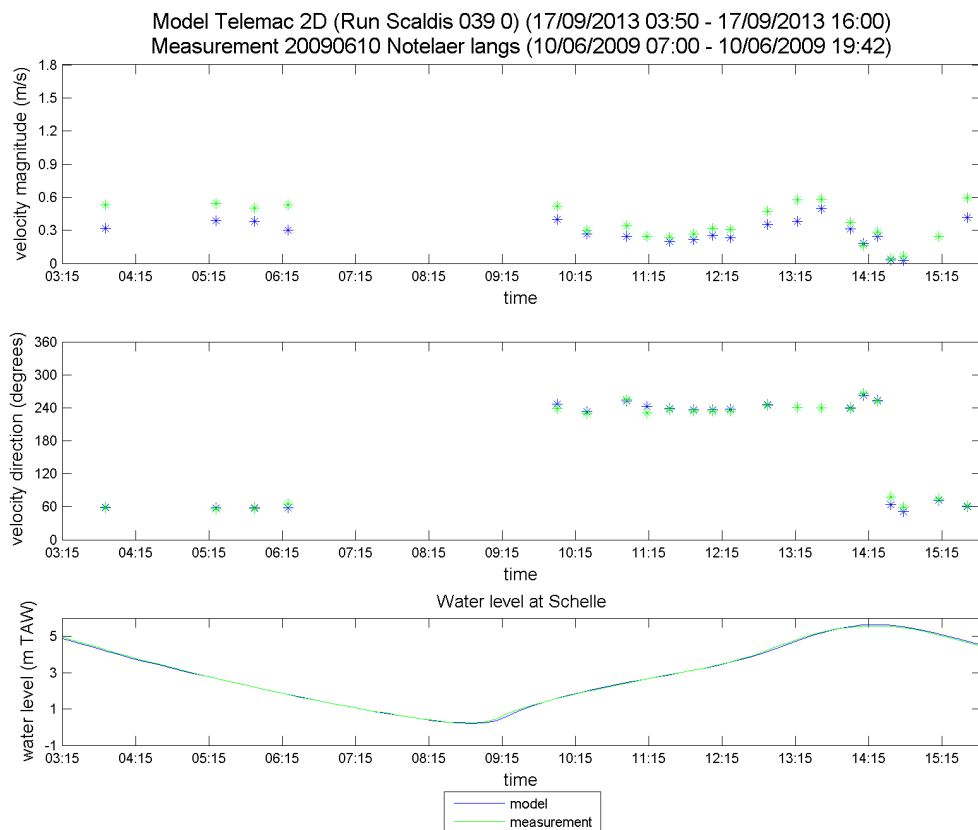


Figure 361 - Time series of the measured and modeled velocity magnitude and direction in the intertidal area at 20090610 Notelaer langs

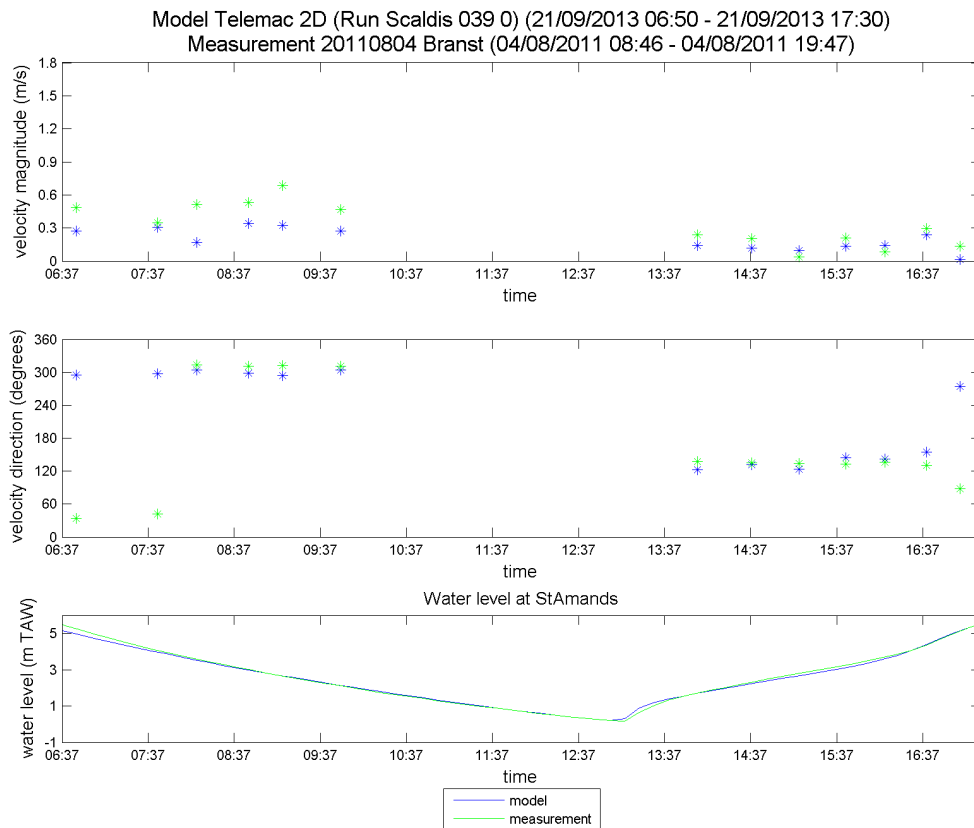


Figure 362 - Time series of the measured and modeled velocity magnitude and direction in the intertidal area at 20110804 Branst

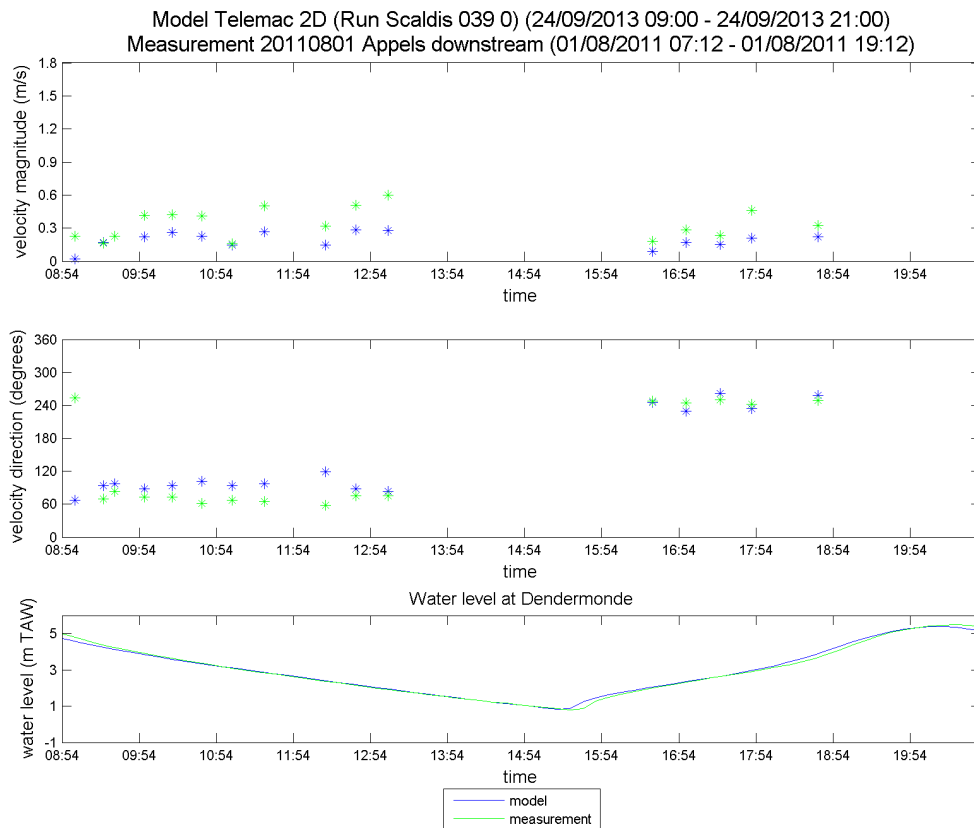


Figure 363 - Time series of the measured and modeled velocity magnitude and direction in the intertidal area at 20110801 Appels downstream

Discharges

Table 151. Statistical parameters for discharges (model vs. measurement) in the Western Scheldt

Location	BIAS TS	RMSE TS	RMSE TS	Max discharge (approx.)	RRMSE TS
	[m³/s]	[m³/s]	% of Qmax	[m³/s]	[-]
R12 Oostgat	-230	832	8	11000	0.11
R12 Deurloo	-144	1840	10	18000	0.18
R12 Wielingen	-603	3978	4	90000	0.08
R11 Wielingen	1706	4608	5	100000	0.08
R11 Sardijngeul	334	947	8	12000	0.15
R10 Vaarwater langs hoofdplaat	-647	1414	14	10000	0.25
R10 Honte schaar van spijker plaat	5465	7623	10	80000	0.15
R9 Honte schaar van spijker plaat	2659	5468	7	80000	0.12
R9 Vaarwater langs hoofdplaat	-564	1209	13	9000	0.26
R7 Everingen	970	2303	5	45000	0.1
R7 Pas van Terneuzen	-144	1707	5	33000	0.09
R6 Gat van Ossensisse	3873	4570	14	33000	0.26
R6 Middelgat	-1240	1694	9	18000	0.16
R5 Schaar van Waarde	322	1123	7	16000	0.16
R5 Zuidergat	-585	1728	8	22000	0.14
R3 Overloop van Valkenisse	1535	1963	8	25000	0.15
R3 Zimmermangeul	-134	293	15	2000	0.33
R2 Nauw van Bath	-261	1024	10	10000	0.15
R2 Schaar van de Noord	1400	1631	12	14000	0.27
R2 total	644	1535	7	23000	0.12
R1 Vaarwater boven Bath	443	1022	6	16000	0.12
R1 Vaarwater boven Bath	-432	1215	8	16000	0.12
R1 Ballastplaat	184	648	16	4000	0.35
Total	633	2848			0.18

Table 152. Statistical parameters for discharges (model vs. measurement) in the Lower Sea Scheldt

Location	BIAS TS	RMSE TS	RMSE TS	Max discharge	RRMSE TS
	[m³/s]	[m³/s]	% of Q max	[m³/s]	[-]
Liefkenshoek	-143	755	6	12000	0.11
Liefkenshoek	-229	771	6	12000	0.11
Liefkenshoek	524	1136	9	12000	0.18
Oosterweel	-20	939	13	7000	0.22
Oosterweel	-49	541	8	7000	0.11
Oosterweel	488	757	11	7000	0.19
Kruikeke	-117	291	4	7000	0.08
Kruikeke	-44	467	7	7000	0.14
Kruikeke	-33	426	6	7000	0.12
Total	42	723			0.15

Table 153. Statistical parameters for discharges (model vs. measurement) in the Upper Sea Scheldt

Location	BIAS TS	RMSE TS	RMSE TS	Max discharge	RRMSE TS
	[m³/s]	[m³/s]	% of Qmax	[m³/s]	[-]
Driegoten	-17	136	7	2000	0.13
Driegoten	-22	136	7	2000	0.13
Driegoten	9	166	8	2000	0.17
Schoonaarde	-1	20	4	450	0.08
Schoonaarde	-2	15	3	450	0.06
Schoonaarde	-9	26	6	450	0.1
Total	-7	105			0.12

Table 154. Statistical parameters for discharges (model vs. measurement) in the Rupel basin

Location	BIAS TS	RMSE TS	RMSE TS	Max discharge	RRMSE TS
	[m³/s]	[m³/s]	% of Qmax	[m³/s]	[-]
Boom	-14	106	9	1200	0.18
Boom	-22	66	5	1200	0.1
Terhagen	-22	54	7	800	0.12
Total	-20	79			0.14

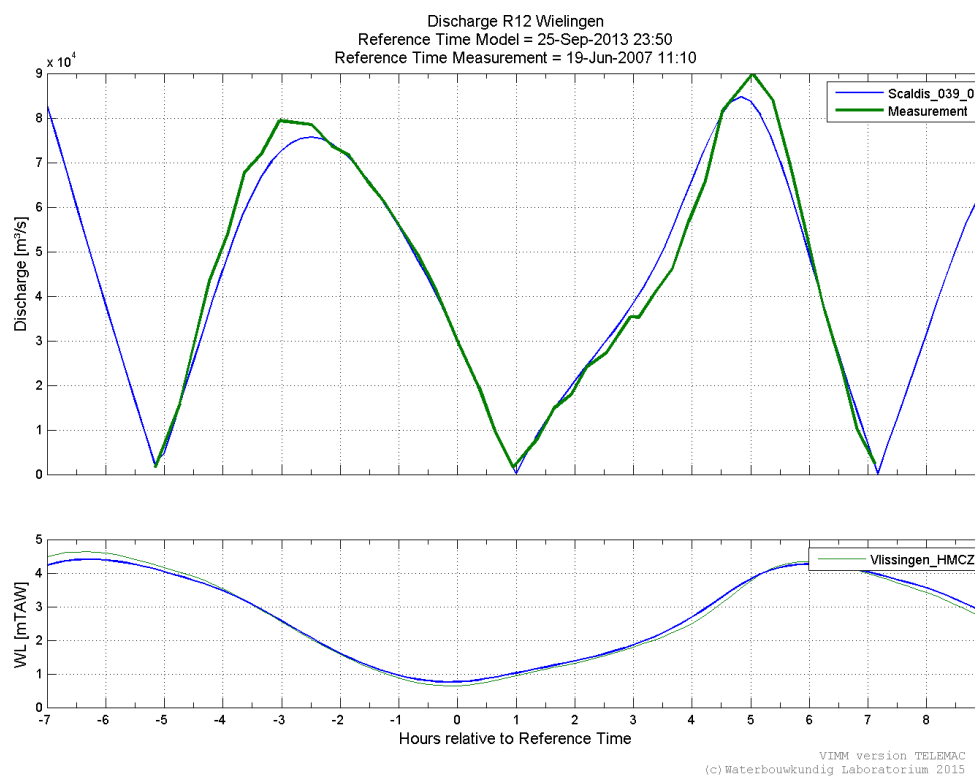


Figure 364 - Calculated and measured discharges at R12 Wielingen

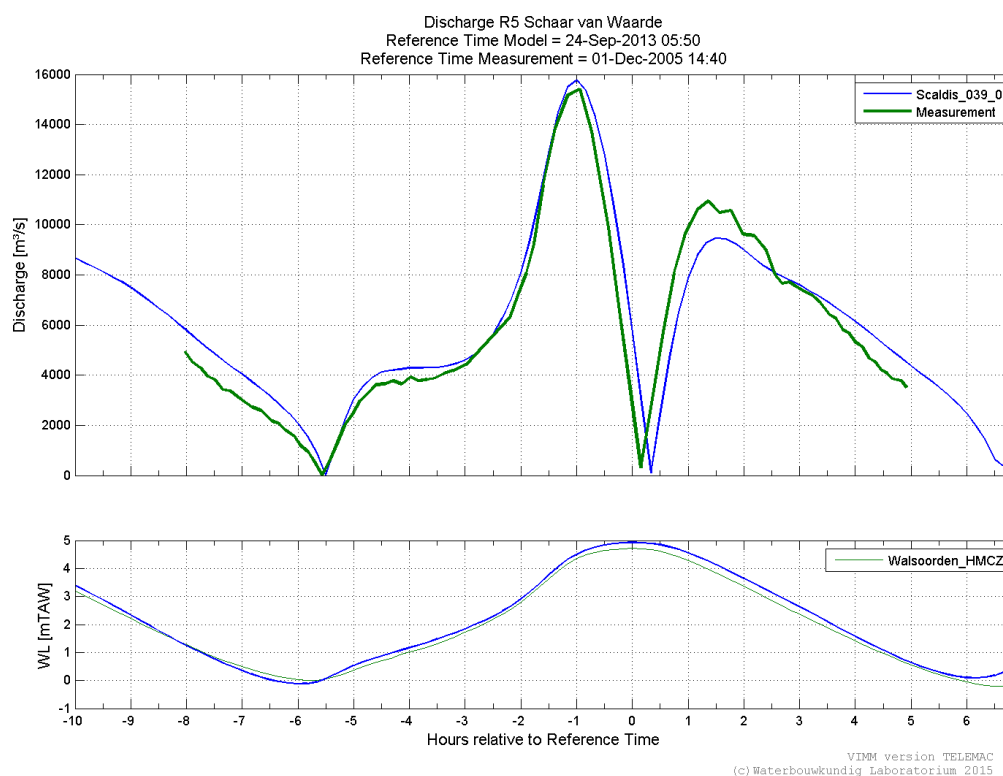


Figure 365 - Calculated and measured discharges at R5 Schaar van Waarde

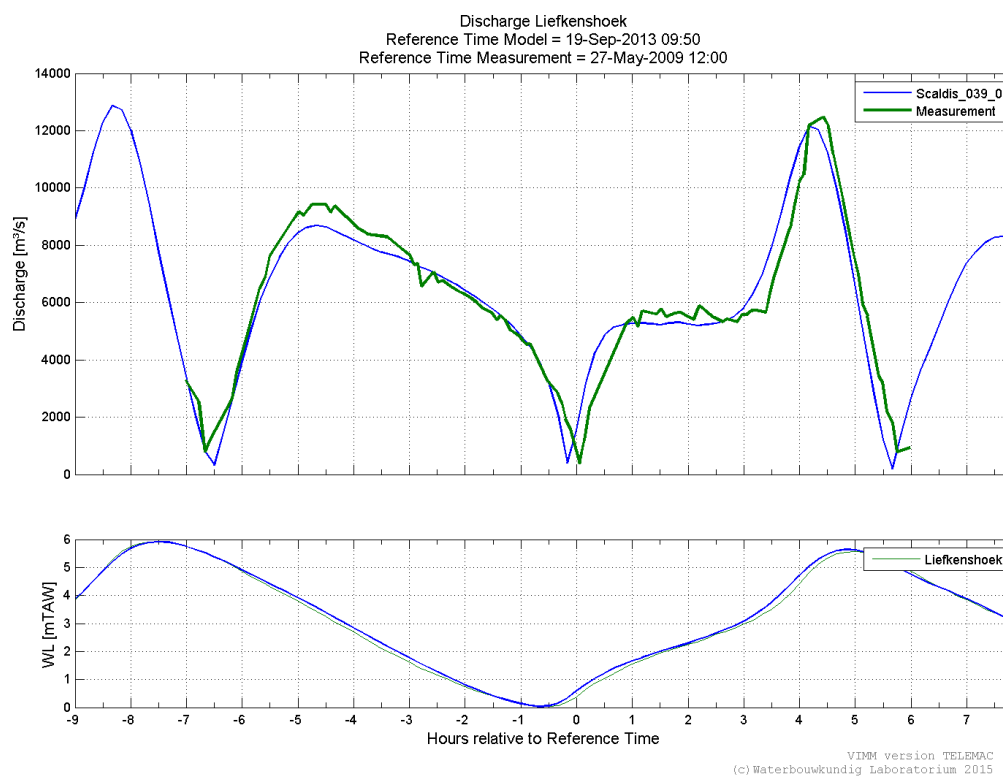


Figure 366 - Calculated and measured discharges at Liefkenshoek

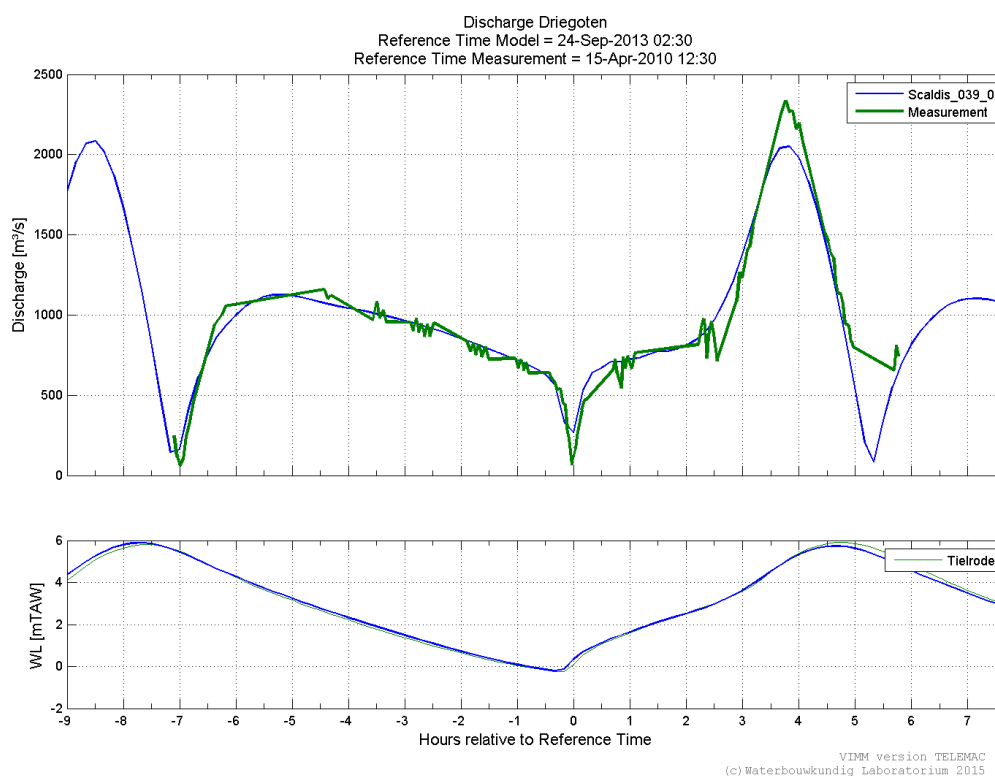


Figure 367 - Calculated and measured discharges at Driegoten

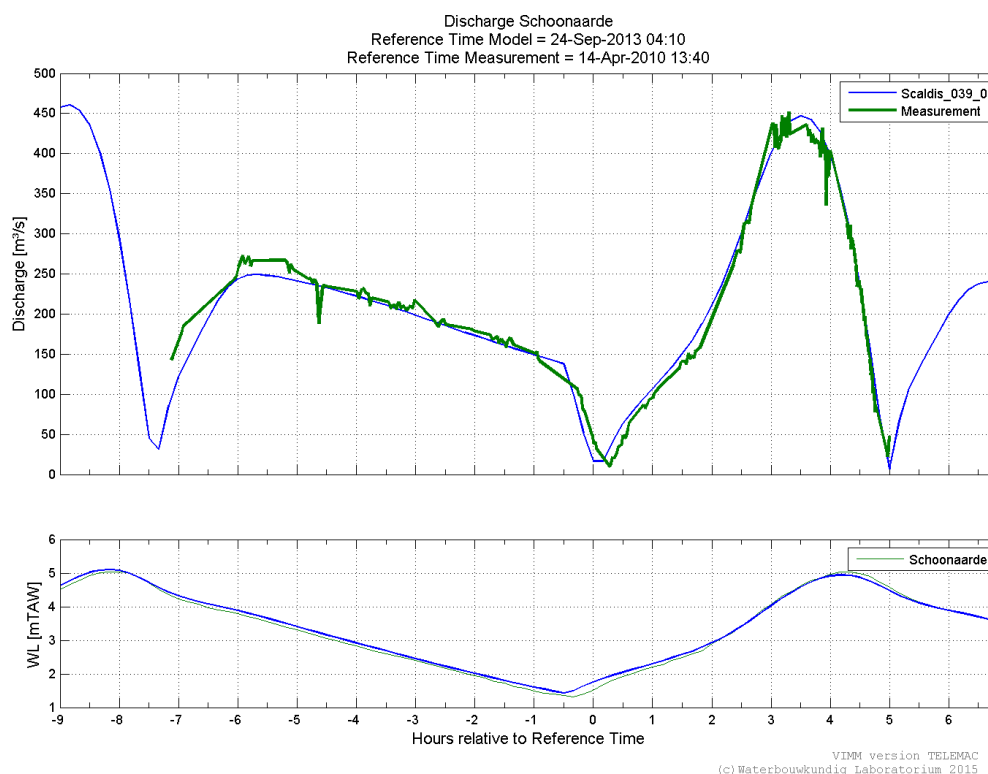


Figure 368 - Calculated and measured discharges at Schoonaarde

Stationary velocities

Table 155. Statistical parameters for the stationary velocities in deep zones

Location	Analysis vector		Magnitude		Direction	
	MAE TS	RMAE TS	BIAS TS	RMSE TS	BIAS TS	RMSE TS
	[m/s]	[-]	[m/s]	[m/s]	[°]	[°]
Buoy 84 bottom	0.13	0.29	0.05	0.13	1	22
Buoy 84 top	0.12	0.24	0.03	0.12	-2	22
Oosterweel bottom	0.10	0.20	0.02	0.10	4	23
Oosterweel top	0.14	0.22	-0.07	0.15	3	29
Driegoten (real)	0.15	0.33	0.03	0.16	-2	28
Driegoten (proxy1)	0.27	0.60	0.25	0.32	0	17
Totaal	0.15		0.03	0.18	0	25

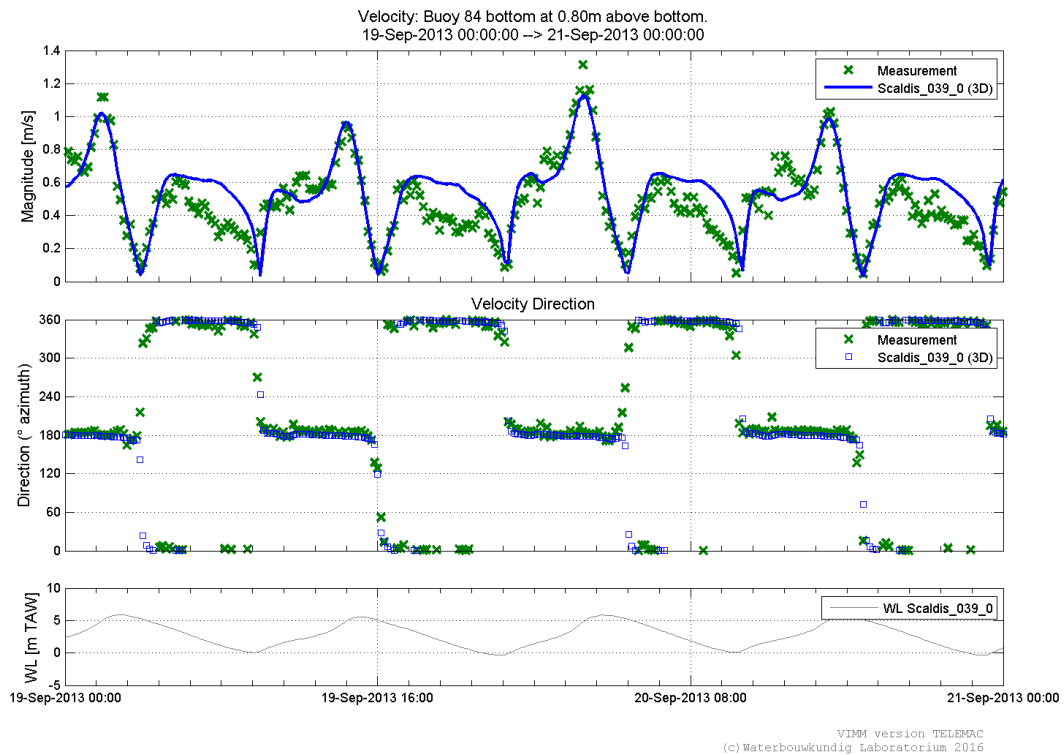


Figure 369 - Measured and modeled velocities at Buoy 84 (bottom)

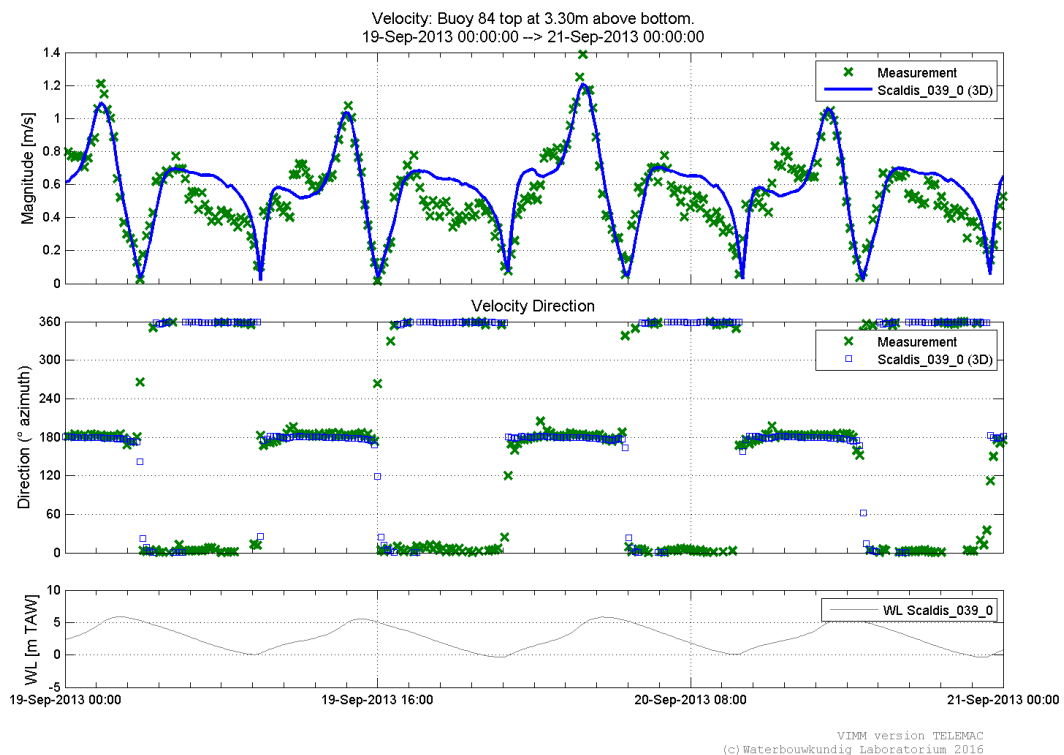


Figure 370 - Measured and modeled velocities at Buoy 84 (top)

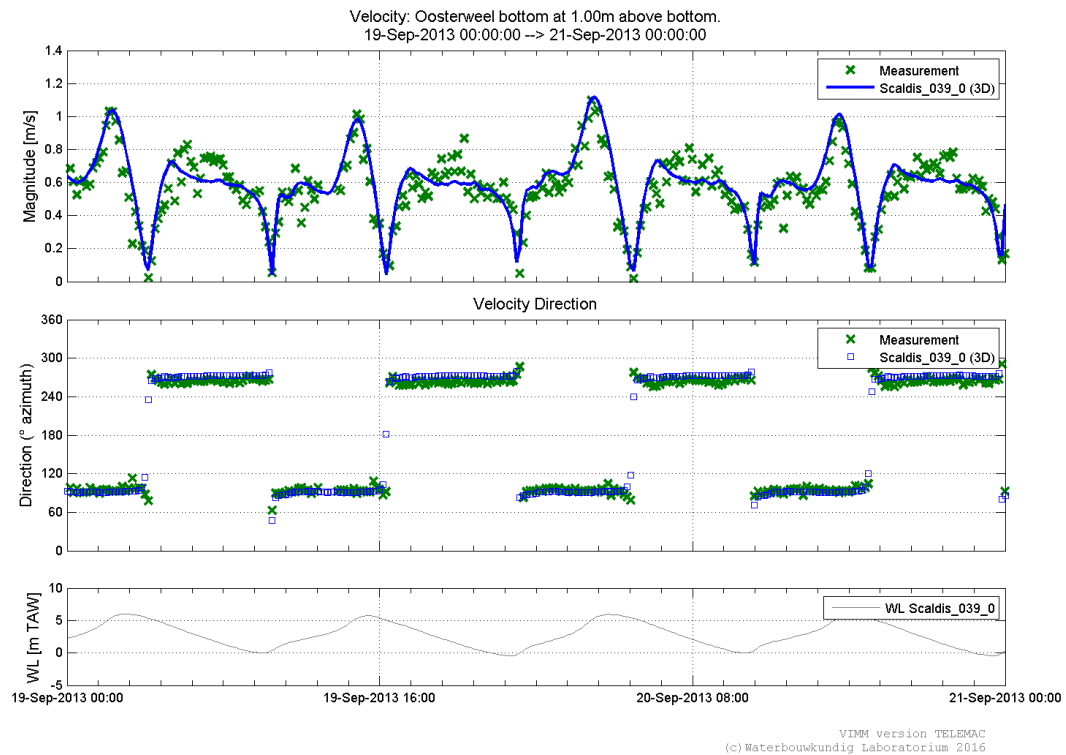


Figure 371 - Measured and modeled velocities at Oosterweel (bottom)

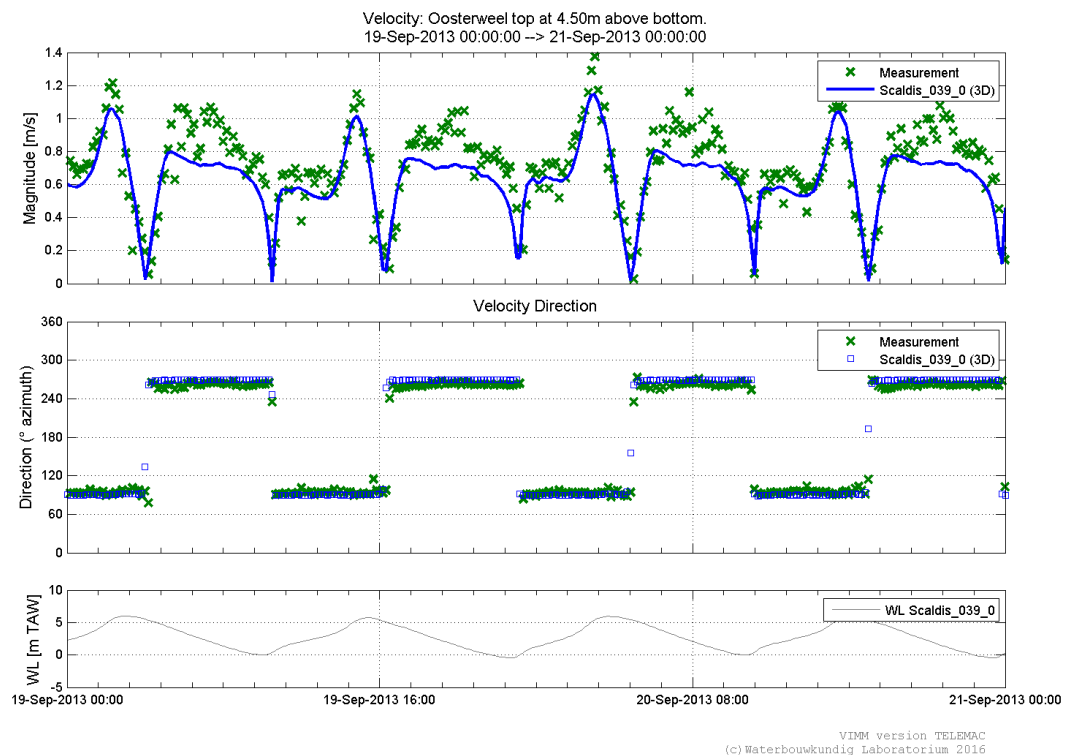


Figure 372 - Measured and modeled velocities at Oosterweel (top)

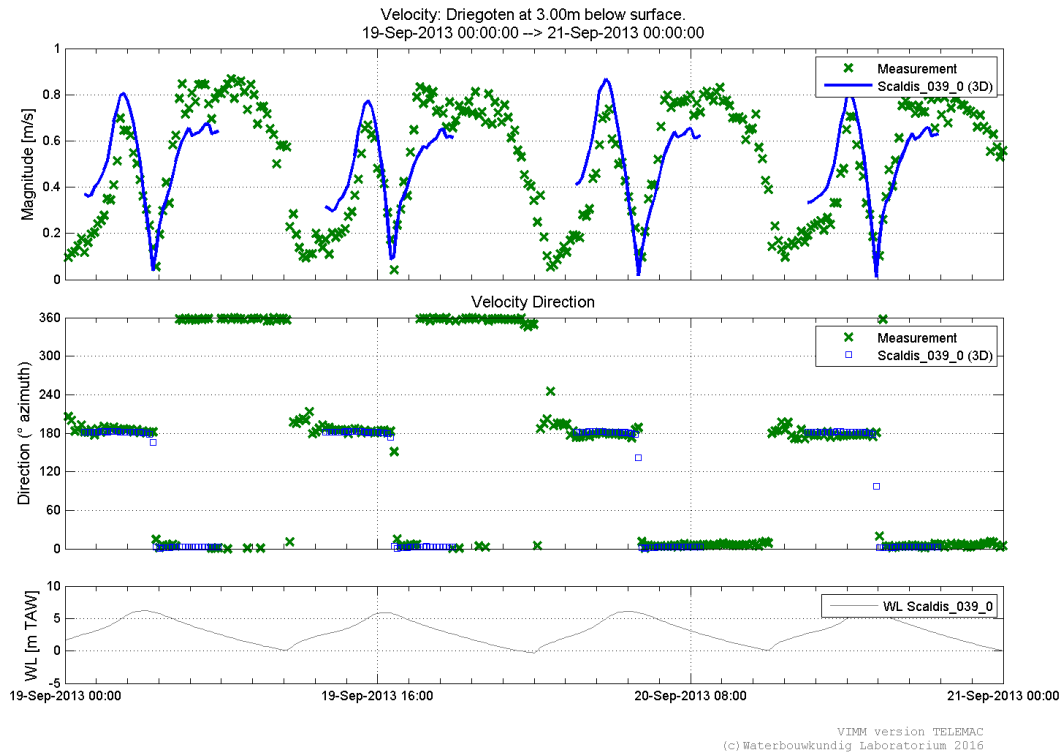


Figure 373 - Measured and modeled velocities at Driegoten (real)

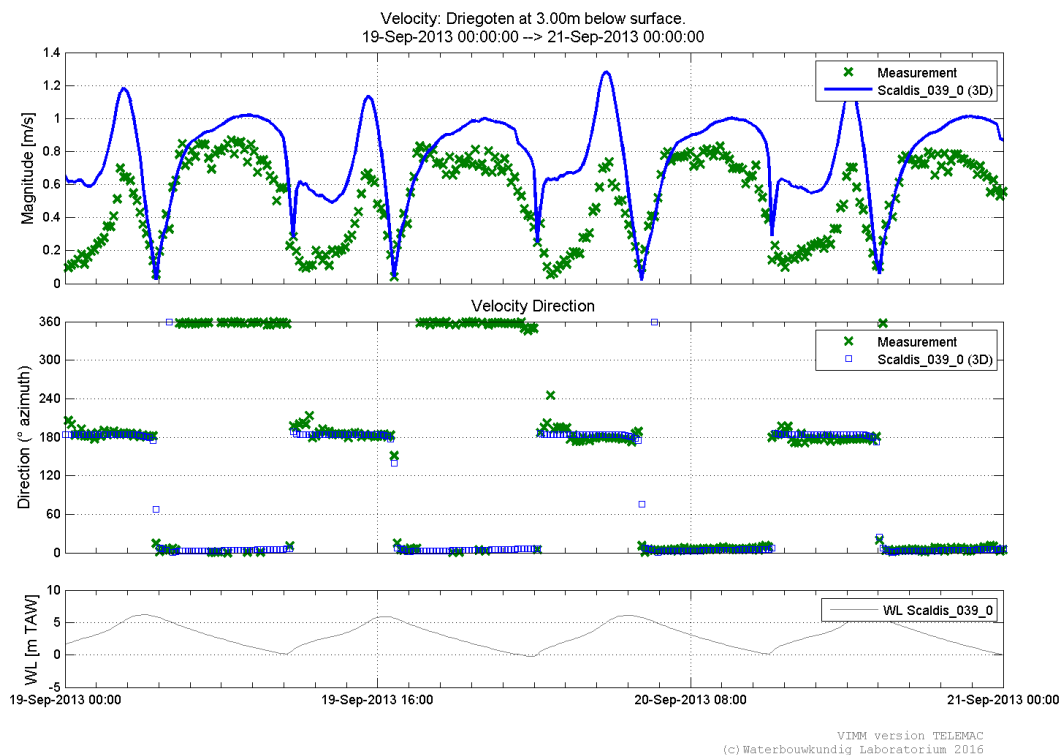


Figure 374 - Measured and modeled velocities at Driegoten (proxy1)

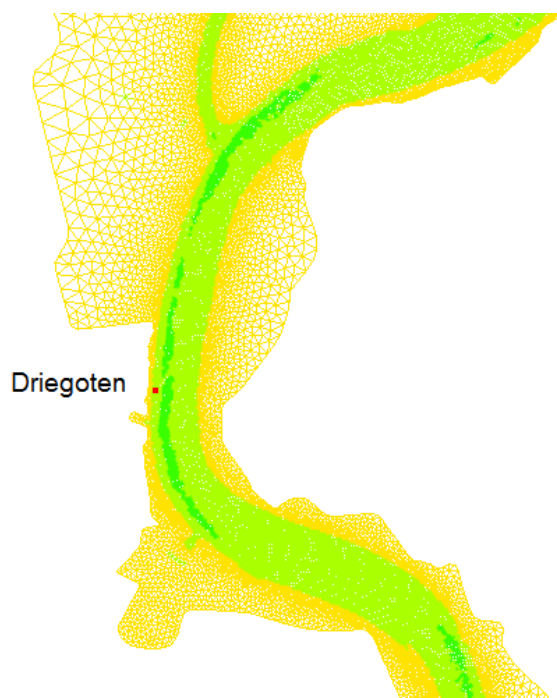


Figure 375 - Location of the measurement location Driegoten

Table 156. RMSE for the stationary velocities in shallow zones at INBO locations

Location*	Neap	Average	Spring	Total
Ballooi (INBO) real		0.05		0.05
Ballooi (INBO) real			0.07	0.07
Bergenmeersen (INBO) real		0.22	0.20	0.21
Branst (INBO) real			0.09	0.09
Branst (INBO) a			0.12	0.12
Brede Schoore (INBO) real			0.09	0.09
Dendermonde (INBO) real			0.08	0.08
Doel Kerncentrale (INBO) real			0.14	0.14
Doel Kerncentrale (INBO) a			0.11	0.11
Heusden (INBO) real			0.06	0.06
Lillo Polder (INBO) real			0.08	0.08
Nieuw schor van Appels (INBO) real		0.07		0.07
Notelaer (INBO) real			0.06	0.06
Notelaer (INBO) a			0.05	0.05
Paardenschor (INBO) real			0.15	0.15
Paardenschor (INBO) a			0.22	0.22
Plaat Driegoten (INBO) real			0.06	0.06
Weert_hoog_slik real (depth average)	0.23	0.23	0.23	0.23
Weert_laag_slik real (depth average)	0.26	0.24	0.27	0.26

*INBO velocities are measured at 5 cm above the bottom

Table 157. RMSE for the stationary depth average velocities in shallow zones in the Western Scheldt

Location (depth average velocities)	Neap	Average	Spring	Total
HPN_MP0102 real	0.08	0.06	0.05	0.07
HPN_MP0103 real	0.10	0.08	0.10	0.09
HPN_MP0103 a	0.09	0.07	0.09	0.08
HPN_MP0104 real	0.07	0.05	0.09	0.07
HPN_MP0206 real	0.06	0.05	0.04	0.05
HPN_MP0207 real	0.08	0.04	0.04	0.05
HPN_MP0208 real	0.09	0.08	0.08	0.08
HPN_MP0310 real	0.12	0.15	0.21	0.16
HPN_MP0310 a	0.12	0.15	0.21	0.16
HPN_MP0311 real	0.13	0.09	0.08	0.10
HPN_MP0311 a	0.11	0.07	0.06	0.08
HPN_MP0312 real	0.06	0.07	0.08	0.07
HPN_MP0312 a	0.06	0.07	0.08	0.07
HPN_MP0414 real	0.16	0.16	0.17	0.16
HPN_MP0415 real	0.13	0.12	0.17	0.15
HPN_MP0416 real	0.13	0.20	0.25	0.20
HPW_MP0102 real	0.12	0.20	0.07	0.14
HPW_MP0102 a	0.10	0.15	0.07	0.12
HPW_MP0103 real	0.05	0.05	0.07	0.05
HPW_MP0103 a	0.07	0.12	0.18	0.13
HPW_MP0104 real	0.05	0.04	0.08	0.06
HPW_MP0206 real	0.06	0.05	0.04	0.05
HPW_MP0206 a	0.07	0.09	0.08	0.08
HPW_MP0207 real	0.05	0.06	0.06	0.05
HPW_MP0208 real	0.06	0.05	0.07	0.06
HPW_MP0310 real	0.07	0.10	0.11	0.10
HPW_MP0311 real	0.08	0.11	0.09	0.10
HPW_MP0311 a	0.09	0.10	0.15	0.12
HPW_MP0312 real	0.06	0.08	0.14	0.10
HPW_MP0101 real	0.14	0.15	0.15	0.15
HPW_MP0205 real	0.17	0.14	0.12	0.15
PVW_MP0102 real	0.06	0.07	0.08	0.07
PVW_MP0103 real	0.06	0.06	0.09	0.07
PVW_MP0104 real	0.05	0.02	0.07	0.05
PVW_MP0310 real	0.07	0.07	0.09	0.08
PVW_MP0311 real	0.05	0.05	0.08	0.06
PVW_MP0311 a	0.05	0.09	0.14	0.10
PVW_MP0311 b	0.12	0.07	0.05	0.08
PVW_MP0312 real		0.03	0.09	0.07
PVW_MP0414 real	0.04	0.05	0.07	0.06
PVW_MP0415 real	0.07	0.08	0.09	0.08
PVW_MP0416 real	0.08	0.05	0.06	0.07
PVW_MP0416 a	0.05	0.03	0.08	0.06
PVW_MP0518 real	0.11	0.11	0.10	0.10
PVW_MP0519 real	0.09	0.08	0.08	0.08

PVW_MP0519 a	0.08	0.08	0.09	0.09
PVW_MP0520 real	0.06	0.08	0.10	0.09
PVW_MP0101 real	0.06	0.08	0.11	0.08
PVW_MP0309 real	0.07	0.07	0.09	0.08
PVW_MP0309 a	0.07	0.07	0.09	0.08

Table 158. RMSE for the stationary depth average velocities at Hooe Platen Noord

Location (velocities at different levels)	Neap	Average	Spring	Total
HPN_MP0102_level_-1.26	0.07	0.06	0.06	0.06
HPN_MP0102_level_-0.76	0.09	0.06	0.05	0.07
HPN_MP0102_level_-0.26	0.08	0.06	0.04	0.06
HPN_MP0102_level_0.24	0.09	0.04	0.04	0.06
HPN_MP0102_level_0.74	0.10	0.04	0.05	0.07
HPN_MP0102_level_1.24	0.07	0.05	0.06	0.06
HPN_MP0102_level_1.74		0.03	0.08	0.06
HPN_MP0102_level_2.24			0.16	0.16
HPN_MP0103_level_0.07	0.08	0.05	0.06	0.07
HPN_MP0103_level_0.57	0.11	0.09	0.10	0.10
HPN_MP0103_level_1.07	0.07	0.09	0.14	0.11
HPN_MP0103_level_1.57		0.07	0.17	0.14
HPN_MP0103_level_2.07			0.24	0.24
HPN_MP0103a_level_0.07	0.07	0.05	0.06	0.06
HPN_MP0103a_level_0.57	0.10	0.08	0.09	0.09
HPN_MP0103a_level_1.07	0.10	0.09	0.12	0.11
HPN_MP0103a_level_1.57	0.09	0.09	0.15	0.12
HPN_MP0103a_level_2.07		0.10	0.20	0.17
HPN_MP0104_level_0.81	0.05	0.05	0.07	0.06
HPN_MP0104_level_1.31	0.05	0.05	0.11	0.08
HPN_MP0104_level_1.81		0.03	0.16	0.13
HPN_MP0104_level_2.31			0.19	0.19
HPN_MP0206_level_-1.24	0.07	0.08	0.09	0.08
HPN_MP0206_level_-0.74	0.06	0.06	0.06	0.06
HPN_MP0206_level_-0.24	0.06	0.05	0.04	0.05
HPN_MP0206_level_0.26	0.06	0.04	0.03	0.04
HPN_MP0206_level_0.76	0.06	0.04	0.03	0.04
HPN_MP0206_level_1.26	0.06	0.06	0.06	0.06
HPN_MP0206_level_1.76		0.05	0.07	0.06
HPN_MP0206_level_2.26			0.12	0.12
HPN_MP0207_level_0.11	0.06	0.03	0.04	0.05
HPN_MP0207_level_0.61	0.08	0.05	0.03	0.06
HPN_MP0207_level_1.11	0.08	0.06	0.05	0.06
HPN_MP0207_level_1.61		0.04	0.07	0.06
HPN_MP0207_level_2.11		0.11	0.11	0.11
HPN_MP0208_level_0.88	0.07	0.07	0.07	0.07

HPN_MP0208_level_1.38	0.03	0.06	0.10	0.08
HPN_MP0208_level_1.88		0.06	0.12	0.11
HPN_MP0208_level_2.38			0.13	0.13
HPN_MP0310_level_-0.97	0.11	0.12	0.17	0.13
HPN_MP0310_level_-0.47	0.14	0.17	0.24	0.19
HPN_MP0310_level_0.03	0.18	0.22	0.26	0.22
HPN_MP0310_level_0.53	0.17	0.20	0.26	0.21
HPN_MP0310_level_1.03	0.19	0.18	0.25	0.21
HPN_MP0310_level_1.53	0.18	0.19	0.29	0.23
HPN_MP0310_level_2.03		0.25	0.31	0.29
HPN_MP0310a_level_-0.97	0.10	0.11	0.16	0.13
HPN_MP0310a_level_-0.47	0.13	0.16	0.23	0.18
HPN_MP0310a_level_0.03	0.15	0.20	0.25	0.20
HPN_MP0310a_level_0.53	0.15	0.19	0.24	0.20
HPN_MP0310a_level_1.03	0.15	0.18	0.25	0.20
HPN_MP0310a_level_1.53	0.17	0.15	0.29	0.23
HPN_MP0310a_level_2.03		0.21	0.34	0.32
HPN_MP0311_level_0.21	0.10	0.07	0.05	0.07
HPN_MP0311_level_0.71	0.11	0.08	0.07	0.09
HPN_MP0311_level_1.21	0.07	0.07	0.09	0.08
HPN_MP0311_level_1.71		0.03	0.12	0.10
HPN_MP0311_level_2.21			0.13	0.13
HPN_MP0311a_level_0.21	0.10	0.06	0.05	0.07
HPN_MP0311a_level_0.71	0.11	0.08	0.07	0.09
HPN_MP0311a_level_1.21	0.10	0.06	0.08	0.08
HPN_MP0311a_level_1.71		0.06	0.11	0.09
HPN_MP0311a_level_2.21			0.14	0.14
HPN_MP0312_level_1.23	0.05	0.06	0.07	0.06
HPN_MP0312_level_1.73		0.06	0.08	0.07
HPN_MP0312_level_2.23			0.11	0.11
HPN_MP0312a_level_1.23	0.05	0.06	0.07	0.07
HPN_MP0312a_level_1.73		0.06	0.08	0.07
HPN_MP0312a_level_2.23			0.11	0.11
HPN_MP0414_level_0.2	0.15	0.15	0.16	0.16
HPN_MP0414_level_0.7	0.18	0.18	0.17	0.18
HPN_MP0414_level_1.2	0.13	0.14	0.18	0.16
HPN_MP0414_level_1.7	0.01	0.11	0.11	0.10
HPN_MP0414_level_2.2			0.21	0.21
HPN_MP0415_level_1.63	0.08	0.12	0.16	0.14
HPN_MP0415_level_2.13		0.16	0.30	0.29
HPN_MP0416_level_-1.15	0.12	0.18	0.21	0.18
HPN_MP0416_level_-0.65	0.15	0.23	0.27	0.22
HPN_MP0416_level_-0.15	0.17	0.26	0.30	0.25
HPN_MP0416_level_0.35	0.15	0.26	0.32	0.27
HPN_MP0416_level_0.85		0.15	0.28	0.24
HPN_MP0416_level_1.35			0.14	0.14

Table 159. RMSE for the stationary depth average velocities at Hooge Platen West

Location (velocities at different levels)	Neap	Average	Spring	Total
HPW_MP0102_level_-0.83	0.09	0.17	0.05	0.12
HPW_MP0102_level_-0.33	0.11	0.15	0.06	0.12
HPW_MP0102_level_0.17	0.13	0.16	0.08	0.13
HPW_MP0102_level_0.67	0.15	0.17	0.10	0.14
HPW_MP0102_level_1.17	0.18	0.17	0.11	0.15
HPW_MP0102_level_1.67	0.23	0.19	0.12	0.18
HPW_MP0102_level_2.17		0.30	0.15	0.23
HPW_MP0102a_level_-0.83	0.07	0.13	0.06	0.09
HPW_MP0102a_level_-0.33	0.10	0.12	0.06	0.10
HPW_MP0102a_level_0.17	0.12	0.13	0.07	0.11
HPW_MP0102a_level_0.67	0.14	0.15	0.08	0.13
HPW_MP0102a_level_1.17	0.16	0.15	0.09	0.14
HPW_MP0102a_level_1.67	0.24	0.18	0.11	0.16
HPW_MP0102a_level_2.17		0.28	0.13	0.20
HPW_MP0103_level_0.16	0.02	0.04	0.09	0.06
HPW_MP0103_level_0.66	0.03	0.03	0.09	0.06
HPW_MP0103_level_1.16	0.04	0.05	0.09	0.07
HPW_MP0103_level_1.66		0.05	0.06	0.06
HPW_MP0103_level_2.16			0.06	0.06
HPW_MP0103a_level_0.16	0.08	0.13	0.18	0.14
HPW_MP0103a_level_0.66	0.06	0.12	0.19	0.14
HPW_MP0103a_level_1.16	0.08	0.11	0.17	0.13
HPW_MP0103a_level_1.66		0.10	0.15	0.13
HPW_MP0103a_level_2.16			0.15	0.15
HPW_MP0104_level_0.07	0.03	0.03	0.05	0.04
HPW_MP0104_level_0.57	0.05	0.04	0.08	0.06
HPW_MP0104_level_1.07	0.06	0.05	0.09	0.07
HPW_MP0104_level_1.57		0.03	0.11	0.09
HPW_MP0104_level_2.07		0.03	0.08	0.07
HPW_MP0206_level_-1.14	0.05	0.04	0.06	0.05
HPW_MP0206_level_-0.64	0.06	0.05	0.04	0.05
HPW_MP0206_level_-0.14	0.06	0.06	0.04	0.06
HPW_MP0206_level_0.36	0.08	0.08	0.05	0.07
HPW_MP0206_level_0.86	0.10	0.09	0.05	0.08
HPW_MP0206_level_1.36	0.16	0.11	0.06	0.12
HPW_MP0206_level_1.86		0.15	0.07	0.12
HPW_MP0206_level_2.36			0.09	0.09
HPW_MP0206a_level_-1.14	0.06	0.07	0.08	0.07
HPW_MP0206a_level_-0.64	0.07	0.08	0.06	0.07
HPW_MP0206a_level_-0.14	0.09	0.09	0.05	0.08
HPW_MP0206a_level_0.36	0.11	0.11	0.05	0.09
HPW_MP0206a_level_0.86	0.14	0.13	0.07	0.12
HPW_MP0206a_level_1.36	0.19	0.16	0.09	0.14

HPW_MP0206a_level_1.86		0.19	0.10	0.14
HPW_MP0206a_level_2.36			0.14	0.14
HPW_MP0207_level_-0.19	0.03	0.03	0.03	0.03
HPW_MP0207_level_0.31	0.05	0.05	0.05	0.05
HPW_MP0207_level_0.81	0.06	0.07	0.07	0.07
HPW_MP0207_level_1.31	0.10	0.09	0.09	0.09
HPW_MP0207_level_1.81		0.11	0.10	0.10
HPW_MP0207_level_2.31			0.11	0.11
HPW_MP0208_level_1	0.05	0.03	0.05	0.05
HPW_MP0208_level_1.5	0.09	0.06	0.09	0.08
HPW_MP0208_level_2		0.07	0.12	0.10
HPW_MP0310_level_-0.82	0.06	0.08	0.09	0.07
HPW_MP0310_level_-0.32	0.07	0.08	0.05	0.07
HPW_MP0310_level_0.18	0.08	0.09	0.06	0.08
HPW_MP0310_level_0.68	0.07	0.08	0.08	0.08
HPW_MP0310_level_1.18	0.05	0.04	0.08	0.06
HPW_MP0310_level_1.68	0.04	0.09	0.08	0.08
HPW_MP0310_level_2.18		0.10	0.10	0.10
HPW_MP0311_level_-0.65	0.07	0.10	0.07	0.08
HPW_MP0311_level_-0.15	0.10	0.14	0.10	0.12
HPW_MP0311_level_0.35	0.11	0.16	0.14	0.14
HPW_MP0311_level_0.85	0.11	0.15	0.14	0.14
HPW_MP0311_level_1.35	0.13	0.16	0.15	0.15
HPW_MP0311_level_1.85		0.24	0.14	0.20
HPW_MP0311_level_2.35		0.43	0.15	0.29
HPW_MP0311a_level_-0.65	0.10	0.11	0.16	0.13
HPW_MP0311a_level_-0.15	0.09	0.10	0.14	0.11
HPW_MP0311a_level_0.35	0.09	0.08	0.09	0.09
HPW_MP0311a_level_0.85	0.07	0.07	0.07	0.07
HPW_MP0311a_level_1.35	0.12	0.10	0.07	0.10
HPW_MP0311a_level_1.85		0.17	0.08	0.13
HPW_MP0311a_level_2.35		0.28	0.10	0.16
HPW_MP0312_level_0.24	0.05	0.06	0.10	0.07
HPW_MP0312_level_0.74	0.07	0.09	0.15	0.11
HPW_MP0312_level_1.24	0.09	0.12	0.20	0.15
HPW_MP0312_level_1.74		0.09	0.19	0.16
HPW_MP0312_level_2.24			0.16	0.16
HPW_MP0101_201309_level_-5.01	0.10	0.10	0.09	0.10
HPW_MP0101_201309_level_-4.01	0.12	0.13	0.11	0.12
HPW_MP0101_201309_level_-3.01	0.14	0.15	0.14	0.14
HPW_MP0101_201309_level_-2.01	0.16	0.18	0.17	0.17
HPW_MP0101_201309_level_-1.01	0.17	0.19	0.18	0.18
HPW_MP0101_201309_level_-0.01	0.18	0.21	0.23	0.20
HPW_MP0101_201309_level_0.99	0.25	0.21	0.25	0.24
HPW_MP0101_201309_level_1.99		0.25	0.29	0.28
HPW_MP0205_201309_level_-6.12	0.11	0.08	0.06	0.08

HPW_MP0205_201309_level_-5.12	0.14	0.11	0.09	0.11
HPW_MP0205_201309_level_-4.12	0.16	0.14	0.13	0.14
HPW_MP0205_201309_level_-3.12	0.18	0.16	0.16	0.17
HPW_MP0205_201309_level_-2.12	0.19	0.16	0.14	0.16
HPW_MP0205_201309_level_-1.12	0.20	0.16	0.12	0.16
HPW_MP0205_201309_level_-0.12	0.20	0.18	0.14	0.17
HPW_MP0205_201309_level_0.88	0.25	0.19	0.15	0.20
HPW_MP0205_201309_level_1.88		0.26	0.16	0.21

Table 160. RMSE for the stationary depth average velocities at Plaat van Walsoorden

Location (velocities at different levels)	Neap	Average	Spring	Total
PVW_MP0102_level_-0.52	0.05	0.07	0.08	0.07
PVW_MP0102_level_-0.02	0.06	0.08	0.09	0.08
PVW_MP0102_level_0.48	0.05	0.07	0.09	0.07
PVW_MP0102_level_0.98	0.06	0.07	0.09	0.08
PVW_MP0102_level_1.48	0.05	0.07	0.10	0.08
PVW_MP0102_level_1.98	0.08	0.09	0.10	0.10
PVW_MP0102_level_2.48		0.15	0.13	0.14
PVW_MP0102_level_2.98			0.19	0.19
PVW_MP0103_level_1.19	0.06	0.08	0.11	0.09
PVW_MP0103_level_1.69	0.07	0.08	0.09	0.08
PVW_MP0103_level_2.19		0.09	0.09	0.09
PVW_MP0103_level_2.69			0.11	0.11
PVW_MP0104_level_2.07		0.03	0.06	0.05
PVW_MP0104_level_2.57			0.05	0.05
PVW_MP0310_level_-1.67	0.06	0.09	0.11	0.09
PVW_MP0310_level_-1.17	0.05	0.07	0.10	0.08
PVW_MP0310_level_-0.67	0.05	0.06	0.08	0.07
PVW_MP0310_level_-0.17	0.06	0.06	0.08	0.07
PVW_MP0310_level_0.33	0.06	0.06	0.10	0.08
PVW_MP0310_level_0.83	0.06	0.07	0.10	0.08
PVW_MP0310_level_1.33	0.03	0.08	0.10	0.09
PVW_MP0310_level_1.83		0.11	0.11	0.11
PVW_MP0310_level_2.33			0.13	0.13
PVW_MP0311_level_1.16	0.04	0.05	0.09	0.06
PVW_MP0311_level_1.66	0.07	0.04	0.08	0.06
PVW_MP0311_level_2.16	0.08	0.05	0.09	0.07
PVW_MP0311_level_2.66		0.09	0.10	0.09
PVW_MP0311a_level_1.16	0.05	0.10	0.15	0.11
PVW_MP0311a_level_1.66	0.04	0.08	0.14	0.10
PVW_MP0311a_level_2.16	0.07	0.08	0.13	0.10
PVW_MP0311a_level_2.66		0.10	0.13	0.12
PVW_MP0311b_level_1.16	0.07	0.04	0.06	0.05
PVW_MP0311b_level_1.66		0.05	0.05	0.05

PVW_MP0311b_level_2.16			0.06	0.06
PVW_MP0312_level_2.33		0.04	0.06	0.06
PVW_MP0312_level_2.83			0.07	0.07
PVW_MP0414_level_-0.57	0.04	0.07	0.09	0.07
PVW_MP0414_level_-0.07	0.04	0.06	0.08	0.06
PVW_MP0414_level_0.43	0.05	0.05	0.08	0.06
PVW_MP0414_level_0.93	0.06	0.06	0.09	0.07
PVW_MP0414_level_1.43	0.07	0.07	0.09	0.08
PVW_MP0414_level_1.93	0.05	0.08	0.10	0.08
PVW_MP0414_level_2.43		0.12	0.13	0.12
PVW_MP0414_level_2.93			0.19	0.19
PVW_MP0415_level_0.19	0.08	0.10	0.11	0.10
PVW_MP0415_level_0.69	0.09	0.09	0.10	0.09
PVW_MP0415_level_1.19	0.08	0.09	0.10	0.09
PVW_MP0415_level_1.69	0.09	0.10	0.10	0.10
PVW_MP0415_level_2.19		0.10	0.12	0.11
PVW_MP0415_level_2.69		0.19	0.15	0.16
PVW_MP0416_level_1.86	0.07	0.05	0.07	0.06
PVW_MP0416_level_2.36	0.08	0.04	0.06	0.06
PVW_MP0416_level_2.86		0.08	0.09	0.09
PVW_MP0416a_level_1.86	0.04	0.05	0.09	0.07
PVW_MP0416a_level_2.36		0.06	0.08	0.07
PVW_MP0416a_level_2.86			0.11	0.11
PVW_MP0518_level_-1.59	0.07	0.06	0.07	0.07
PVW_MP0518_level_-1.09	0.11	0.10	0.10	0.10
PVW_MP0518_level_-0.59	0.12	0.12	0.11	0.12
PVW_MP0518_level_-0.09	0.11	0.12	0.11	0.11
PVW_MP0518_level_0.41	0.11	0.13	0.12	0.12
PVW_MP0518_level_0.91	0.12	0.14	0.15	0.14
PVW_MP0518_level_1.41	0.10	0.13	0.13	0.12
PVW_MP0518_level_1.91	0.09	0.12	0.13	0.12
PVW_MP0518_level_2.41		0.08	0.13	0.12
PVW_MP0518_level_2.91			0.03	0.03
PVW_MP0519_level_0.66	0.07	0.07	0.08	0.08
PVW_MP0519_level_1.16	0.08	0.08	0.08	0.08
PVW_MP0519_level_1.66	0.08	0.08	0.09	0.08
PVW_MP0519_level_2.16		0.10	0.10	0.10
PVW_MP0519_level_2.66			0.13	0.13
PVW_MP0519a_level_0.66	0.09	0.09	0.11	0.09
PVW_MP0519a_level_1.16	0.10	0.10	0.11	0.10
PVW_MP0519a_level_1.66	0.12	0.12	0.11	0.12
PVW_MP0519a_level_2.16		0.14	0.13	0.13
PVW_MP0519a_level_2.66			0.16	0.16
PVW_MP0520_level_1.28	0.08	0.09	0.12	0.10
PVW_MP0520_level_1.78	0.09	0.10	0.11	0.10
PVW_MP0520_level_2.28		0.10	0.12	0.11

PVW_MP0520_level_2.78			0.16	0.16
PVW_MP0101_201311_level_-5.38	0.09	0.12	0.13	0.12
PVW_MP0101_201311_level_-4.38	0.07	0.11	0.12	0.10
PVW_MP0101_201311_level_-3.38	0.07	0.10	0.11	0.09
PVW_MP0101_201311_level_-2.38	0.07	0.09	0.11	0.09
PVW_MP0101_201311_level_-1.38	0.08	0.09	0.13	0.10
PVW_MP0101_201311_level_-0.38	0.09	0.11	0.18	0.13
PVW_MP0101_201311_level_0.62	0.01	0.13	0.17	0.16
PVW_MP0101_201311_level_1.62			0.14	0.14
PVW_MP0309_201311_level_-5.44	0.07	0.08	0.09	0.08
PVW_MP0309_201311_level_-4.44	0.06	0.07	0.09	0.07
PVW_MP0309_201311_level_-3.44	0.07	0.08	0.10	0.08
PVW_MP0309_201311_level_-2.44	0.08	0.09	0.11	0.10
PVW_MP0309_201311_level_-1.44	0.12	0.12	0.10	0.11
PVW_MP0309_201311_level_-0.44	0.11	0.09	0.13	0.11
PVW_MP0309_201311_level_0.56	0.10	0.09	0.14	0.11
PVW_MP0309_201311_level_1.56	0.16	0.09	0.15	0.14
PVW_MP0309_201311_level_2.56	0.34	0.14	0.23	0.23
PVW_MP0309a_201311_level_-5.44	0.07	0.09	0.10	0.09
PVW_MP0309a_201311_level_-4.44	0.06	0.08	0.10	0.08
PVW_MP0309a_201311_level_-3.44	0.07	0.08	0.10	0.09
PVW_MP0309a_201311_level_-2.44	0.08	0.09	0.11	0.10
PVW_MP0309a_201311_level_-1.44	0.08	0.09	0.10	0.09
PVW_MP0309a_201311_level_-0.44	0.12	0.10	0.14	0.12
PVW_MP0309a_201311_level_0.56	0.11	0.10	0.16	0.13
PVW_MP0309a_201311_level_1.56	0.16	0.10	0.17	0.15
PVW_MP0309a_201311_level_2.56			0.17	0.17

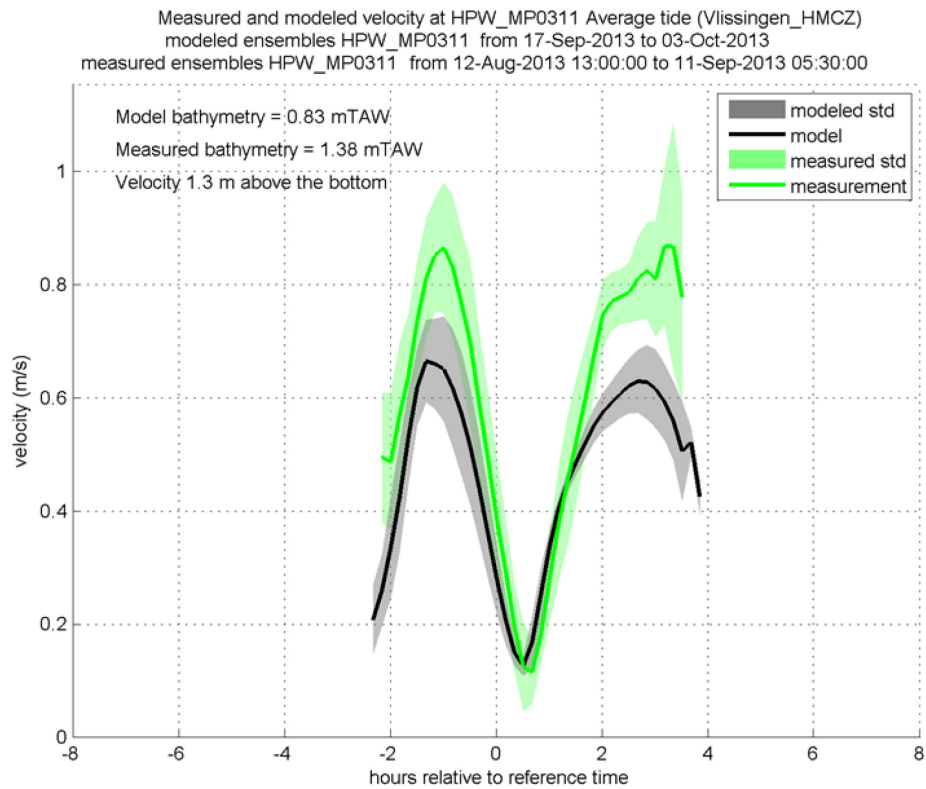


Figure 376 - Measured and modeled velocity at HPW_MP0311 (1.3 m above the bottom)

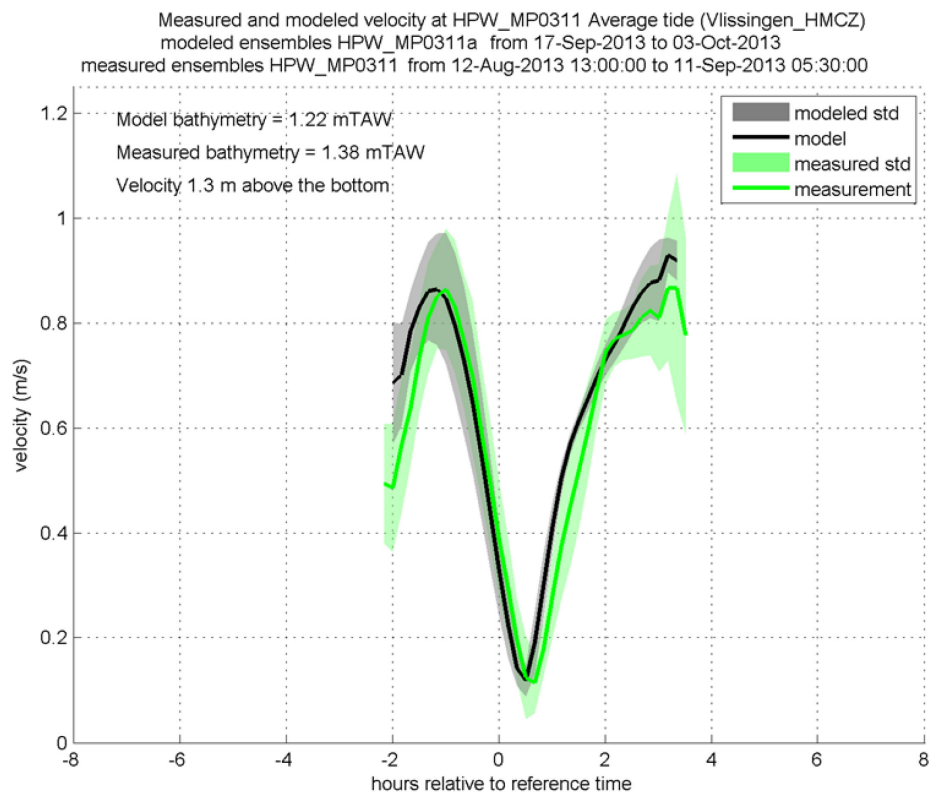


Figure 377 - Measured and modeled velocity at HPW_MP0311a (1.3 m above the bottom)

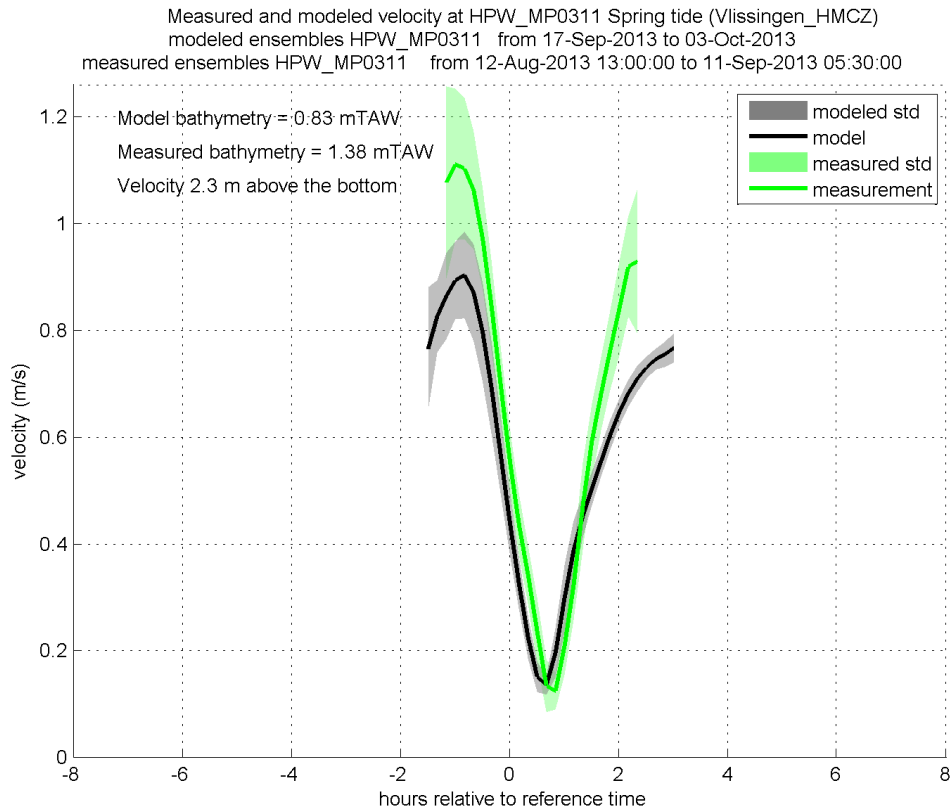


Figure 378 - Measured and modeled velocity at HPW_MP0311 (2.3 m above the bottom)

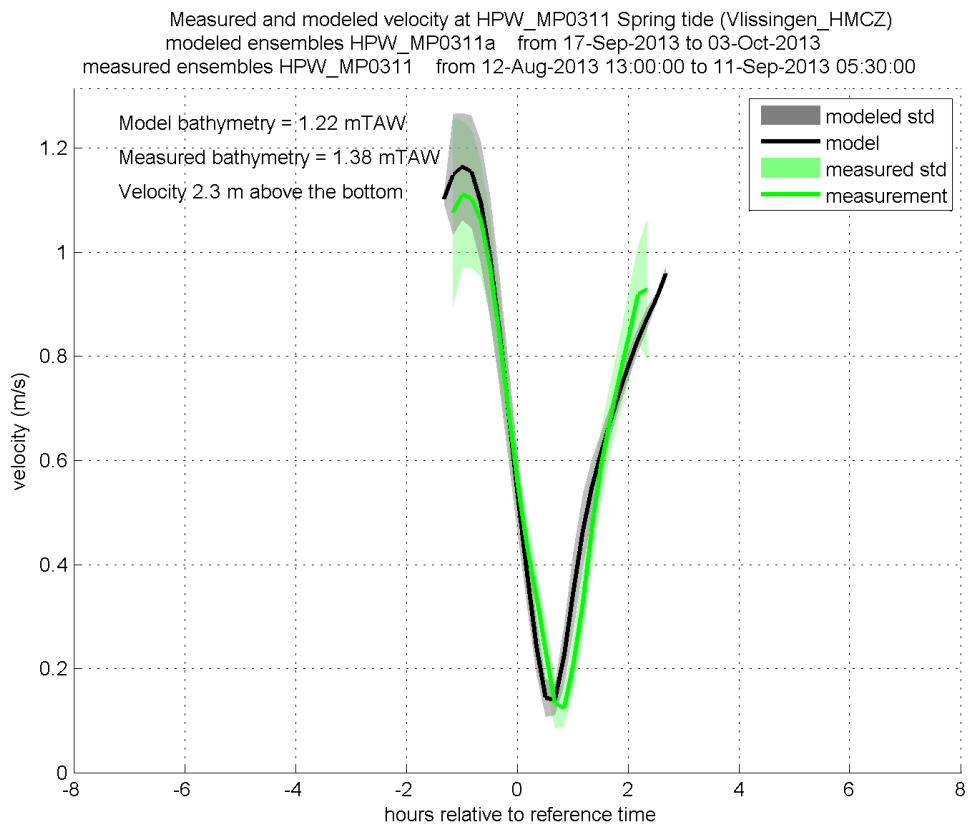


Figure 379 - Measured and modeled velocity at HPW_MP0311a (2.3 m above the bottom)

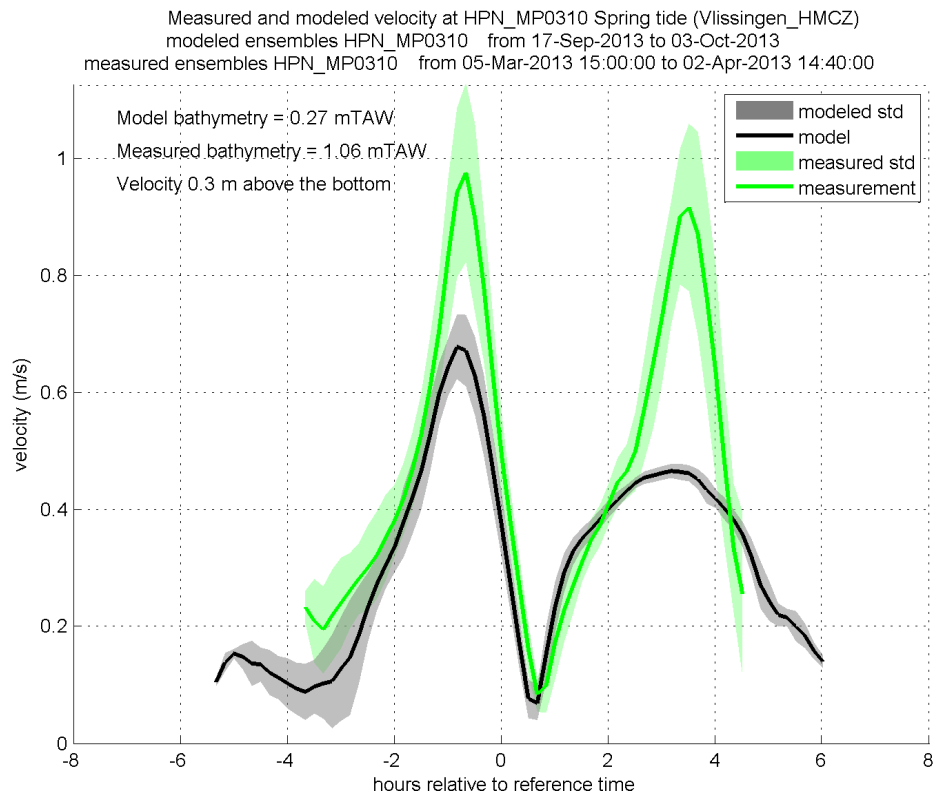


Figure 380 - Measured and modeled velocity at HPN_MP0310 (0.3 m above the bottom)

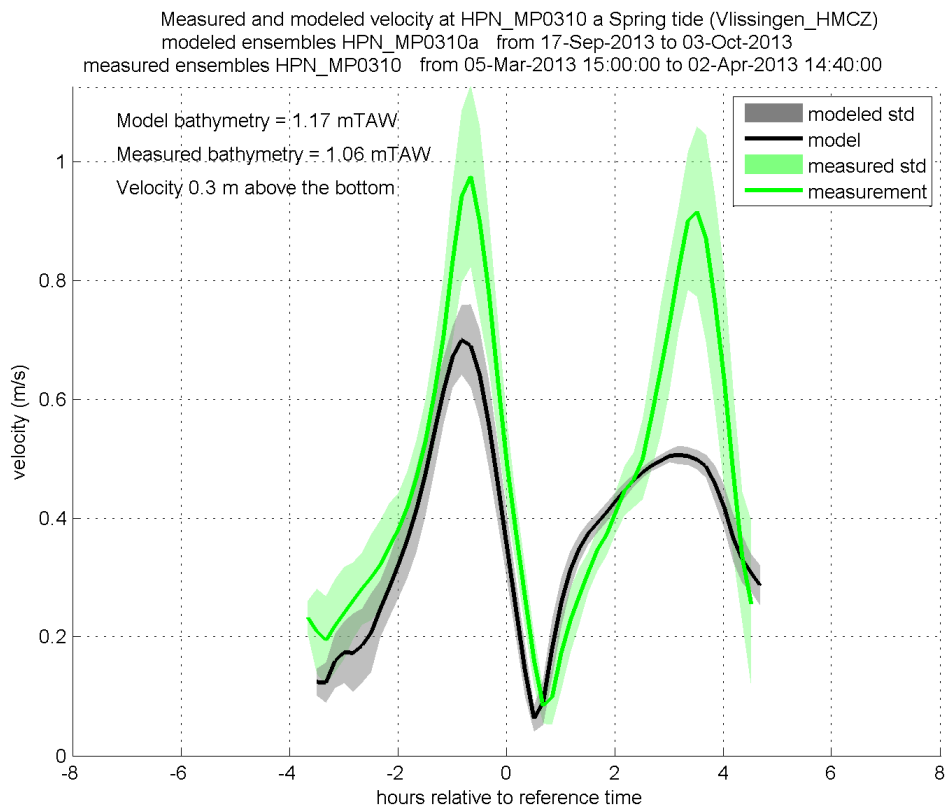


Figure 381 - Measured and modeled velocity at HPN_MP0310a (0.3 m above the bottom)

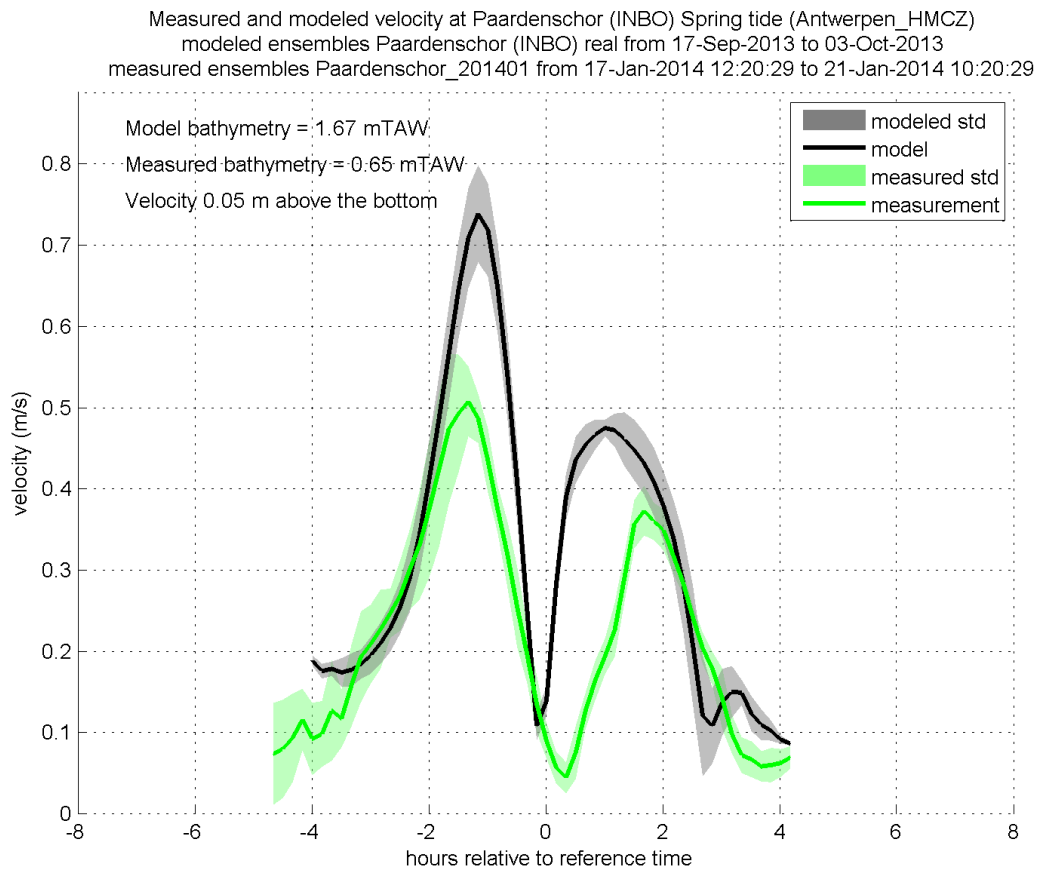


Figure 382 - Measured and modeled velocity at Paardenschor 0.05 m above the bottom (spring tide)

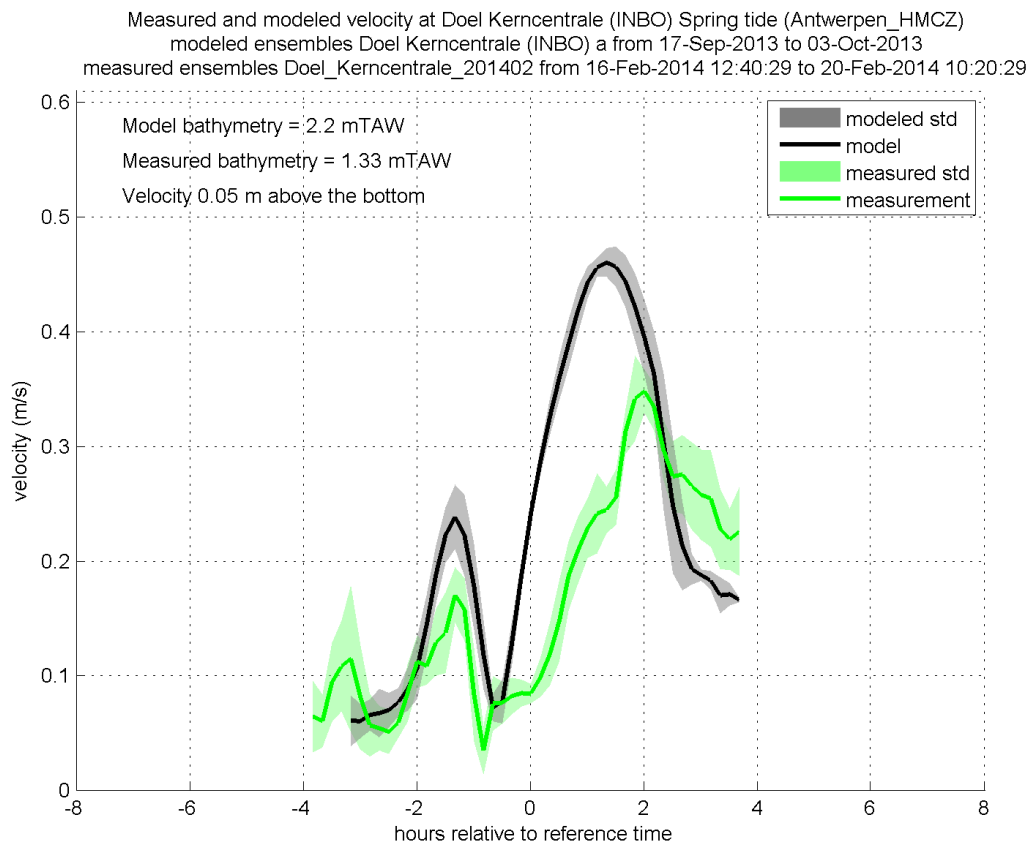


Figure 383 - Measured and modeled velocity at Doel Kerncentrale 0.05 m above the bottom (spring tide)

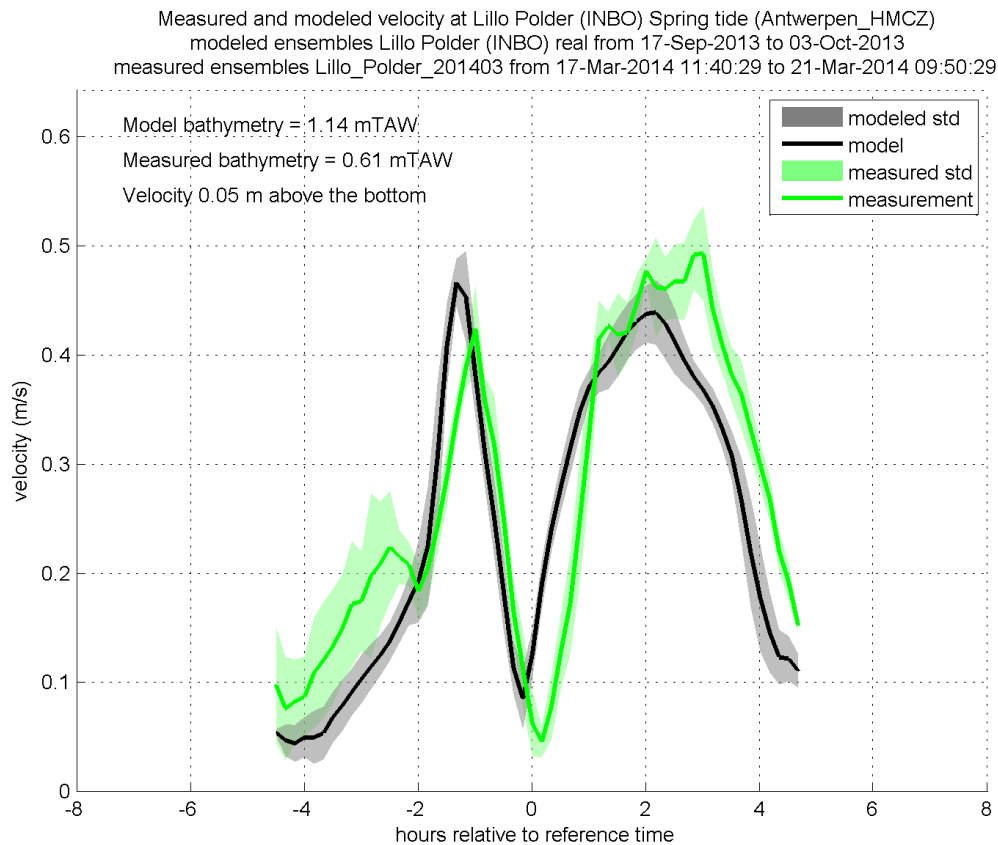


Figure 384 - Measured and modeled velocity at Lillo polder 0.05 m above the bottom (spring tide)

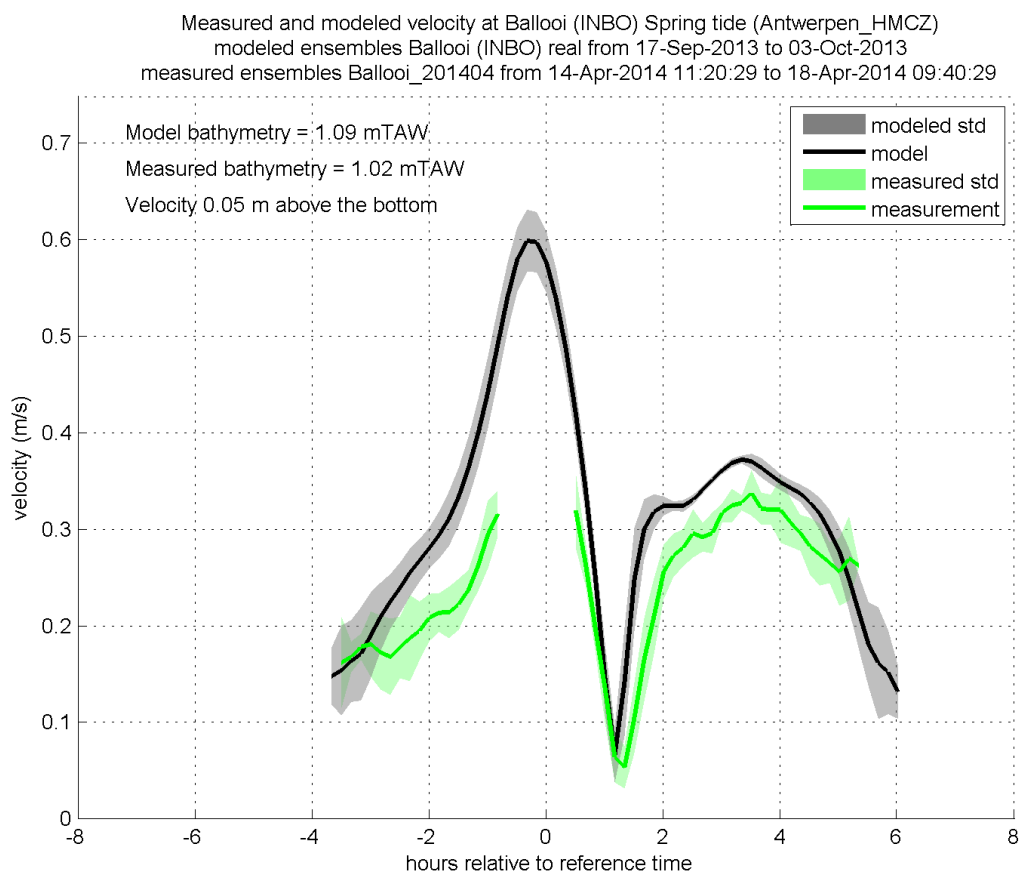


Figure 385 - Measured and modeled velocity at Ballooi 0.05 m above the bottom (spring tide)

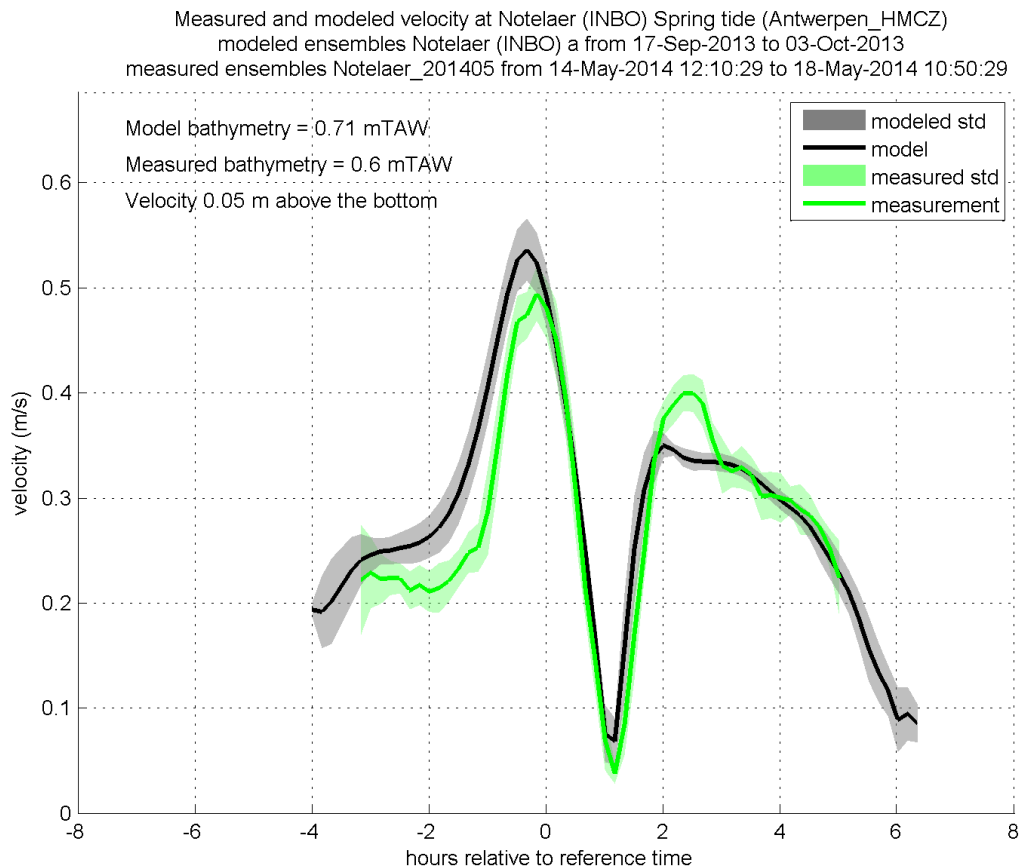


Figure 386 - Measured and modeled velocity at Notelaer 0.05 m above the bottom (spring tide)

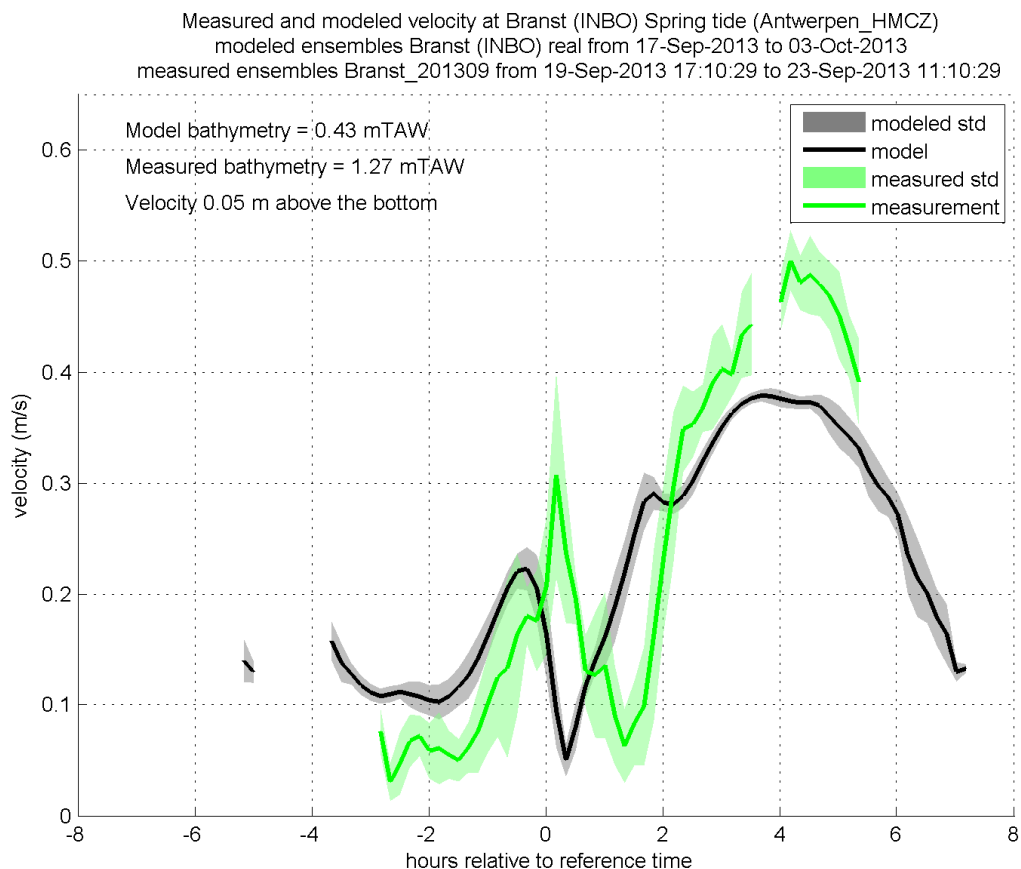


Figure 387 - Measured and modeled velocity at Branst 0.05 m above the bottom (spring tide)

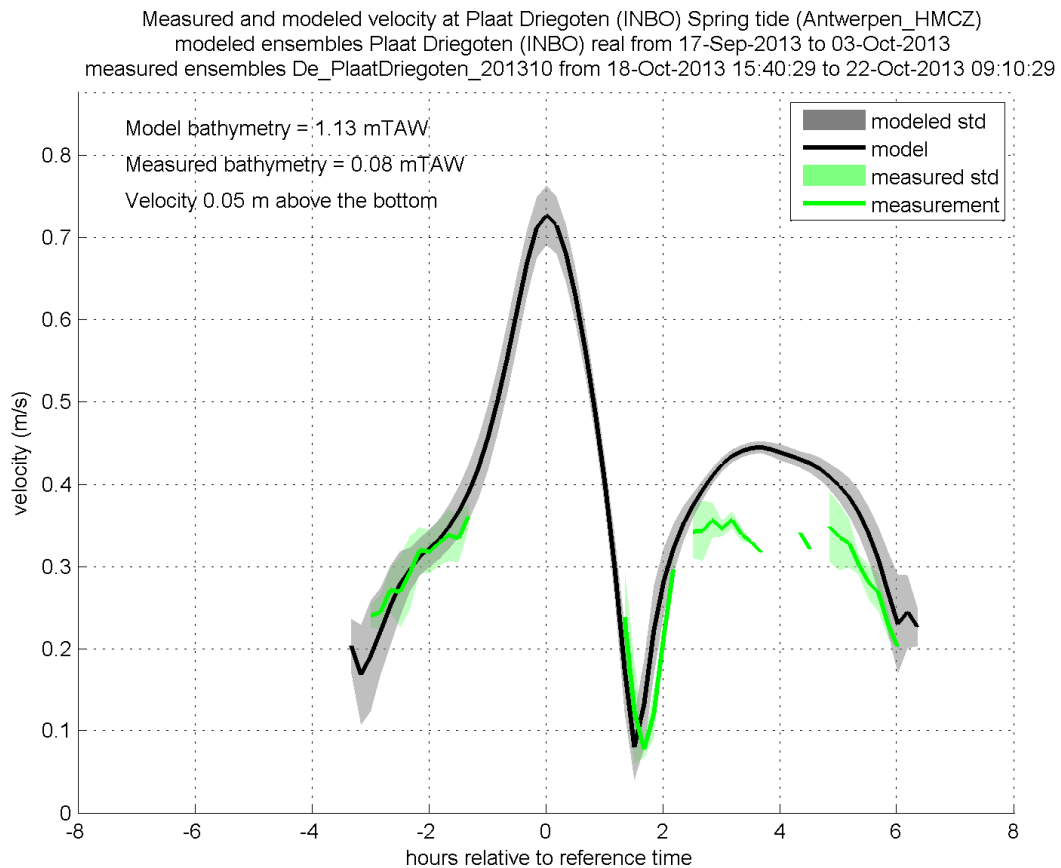


Figure 388 - Measured and modeled velocity at Plaat Driegoten 0.05 m above the bottom (spring tide)

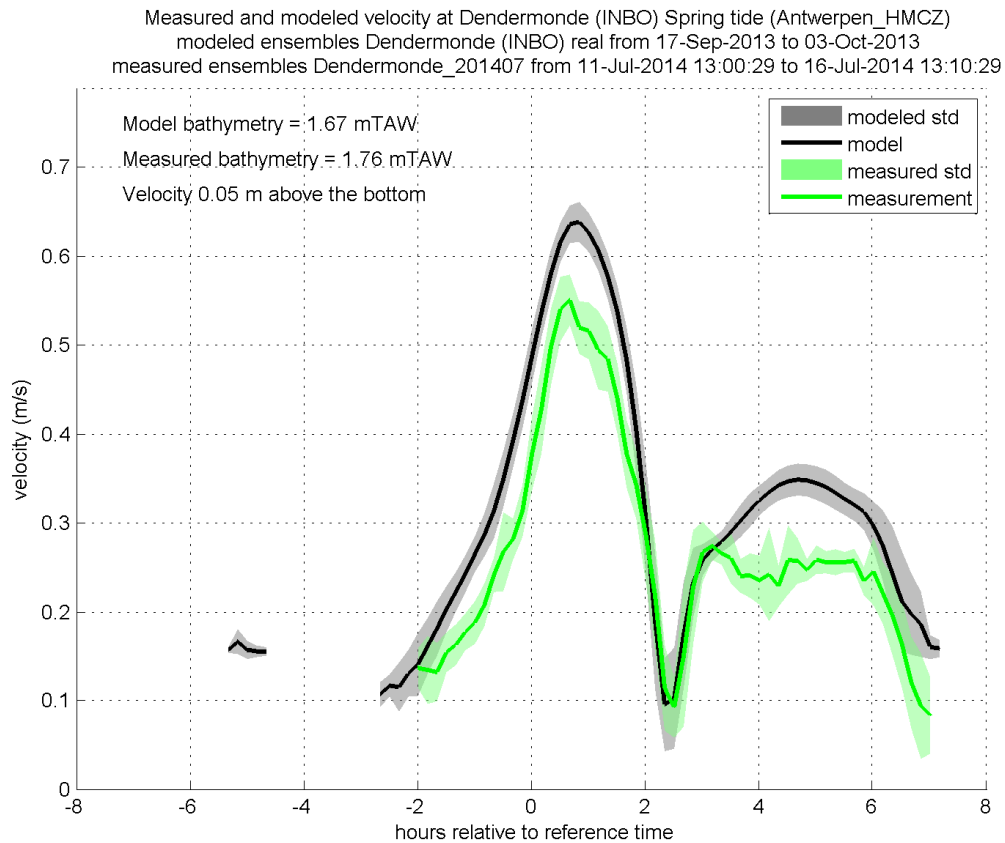


Figure 389 - Measured and modeled velocity at Dendermonde 0.05 m above the bottom (spring tide)

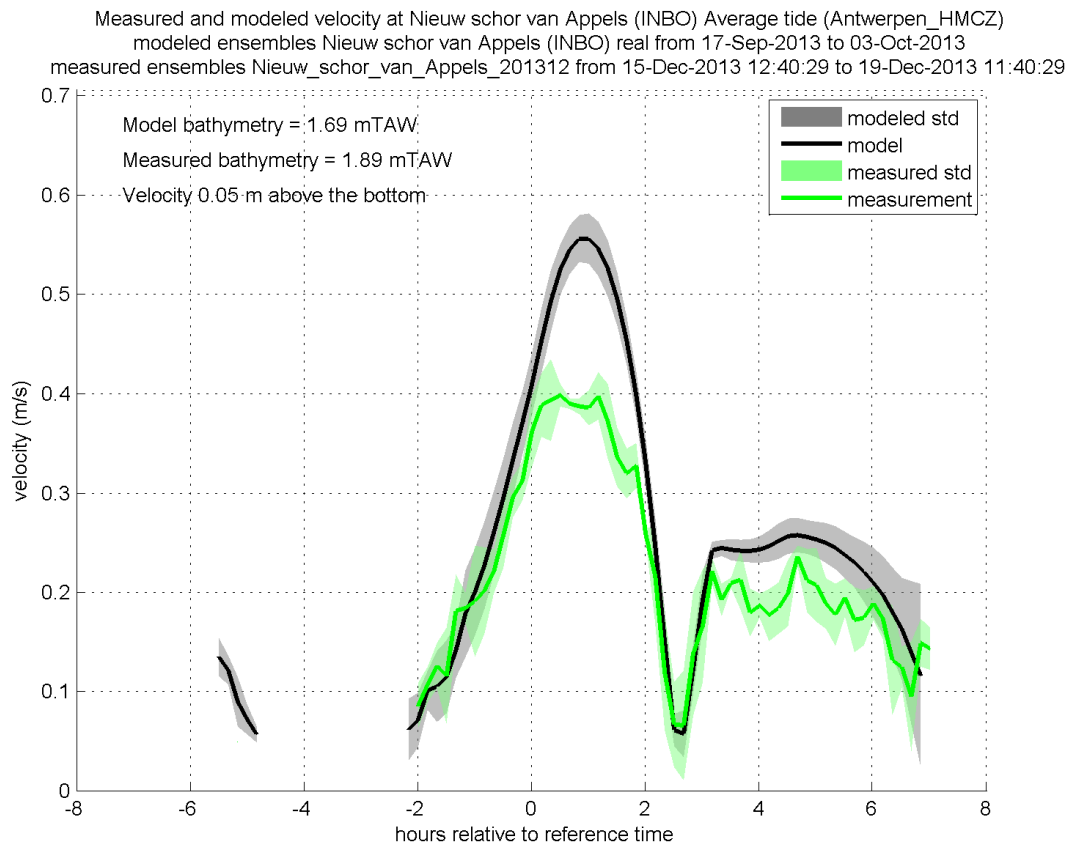


Figure 390 - Measured and modeled velocity at Nieuw schor van Appels 0.05 m above the bottom (average tide)

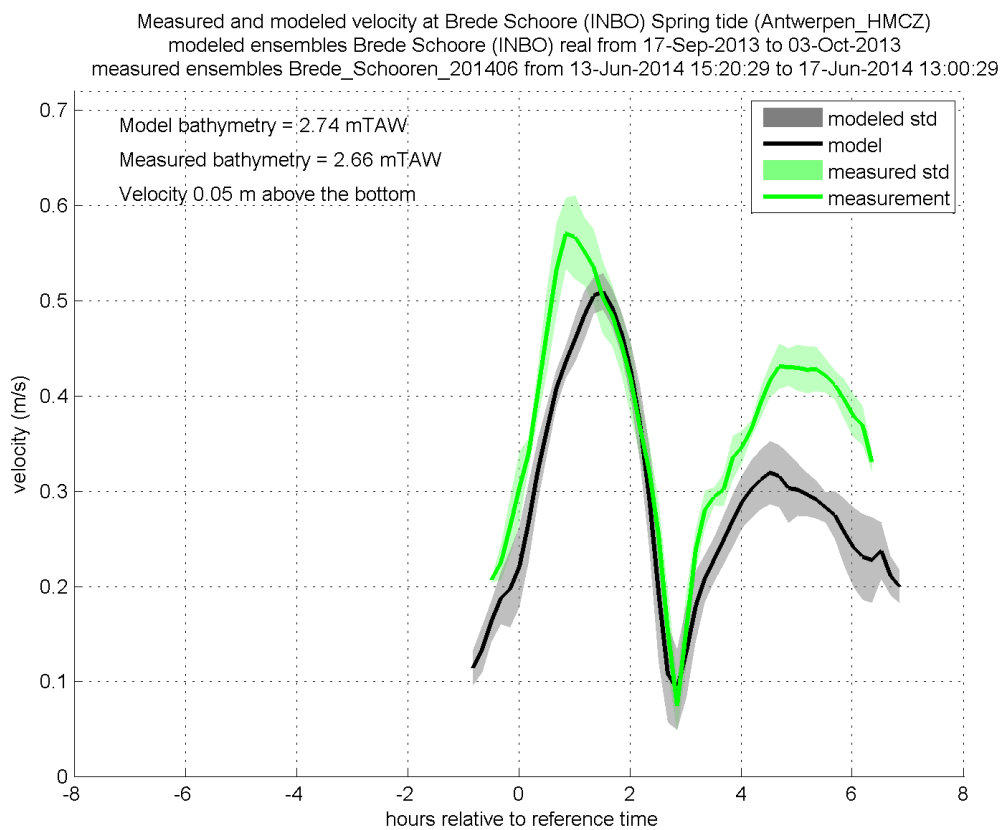


Figure 391 - Measured and modeled velocity at Brede Schooren 0.05 m above the bottom (spring tide)

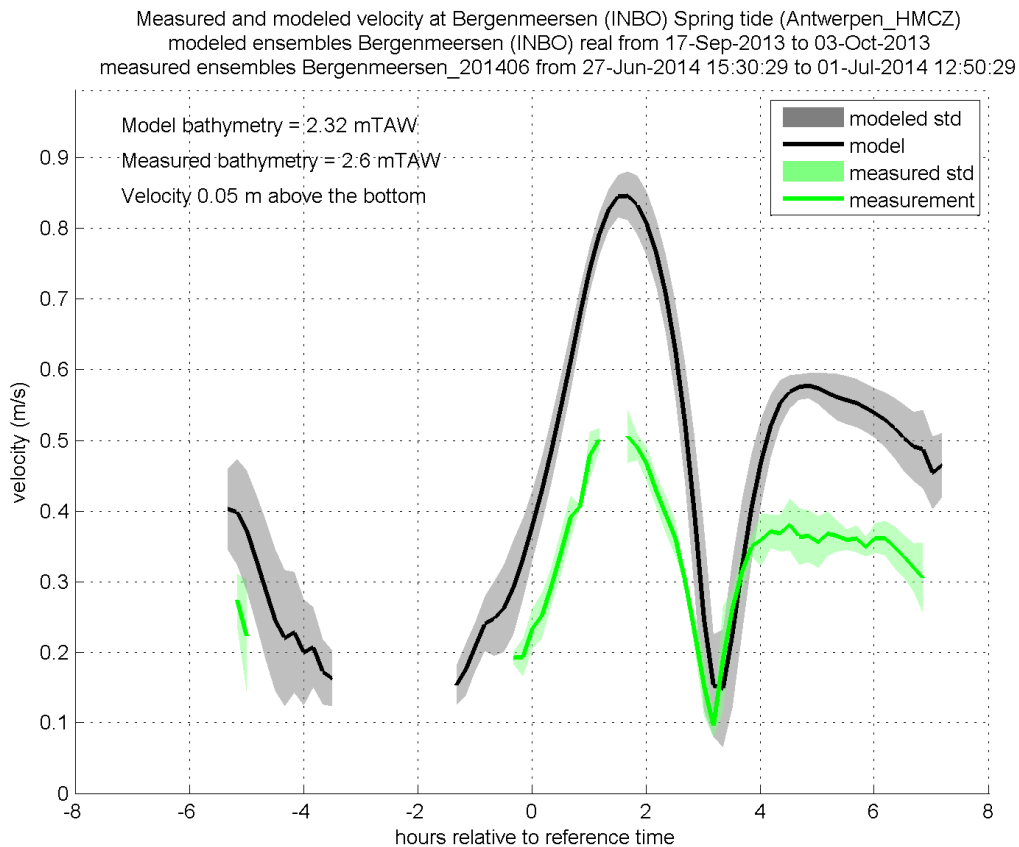


Figure 392 - Measured and modeled velocity at Bergenmeersen 0.05 m above the bottom (spring tide)

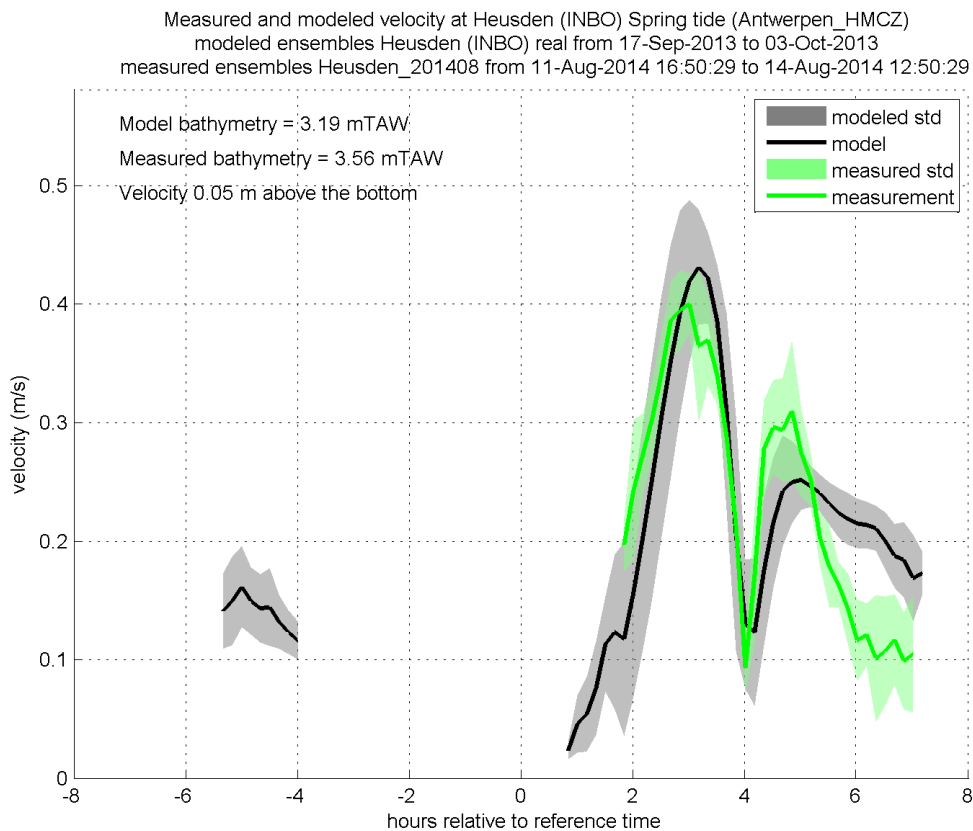


Figure 393 - Measured and modeled velocity at Heusden 0.05 m above the bottom (spring tide)

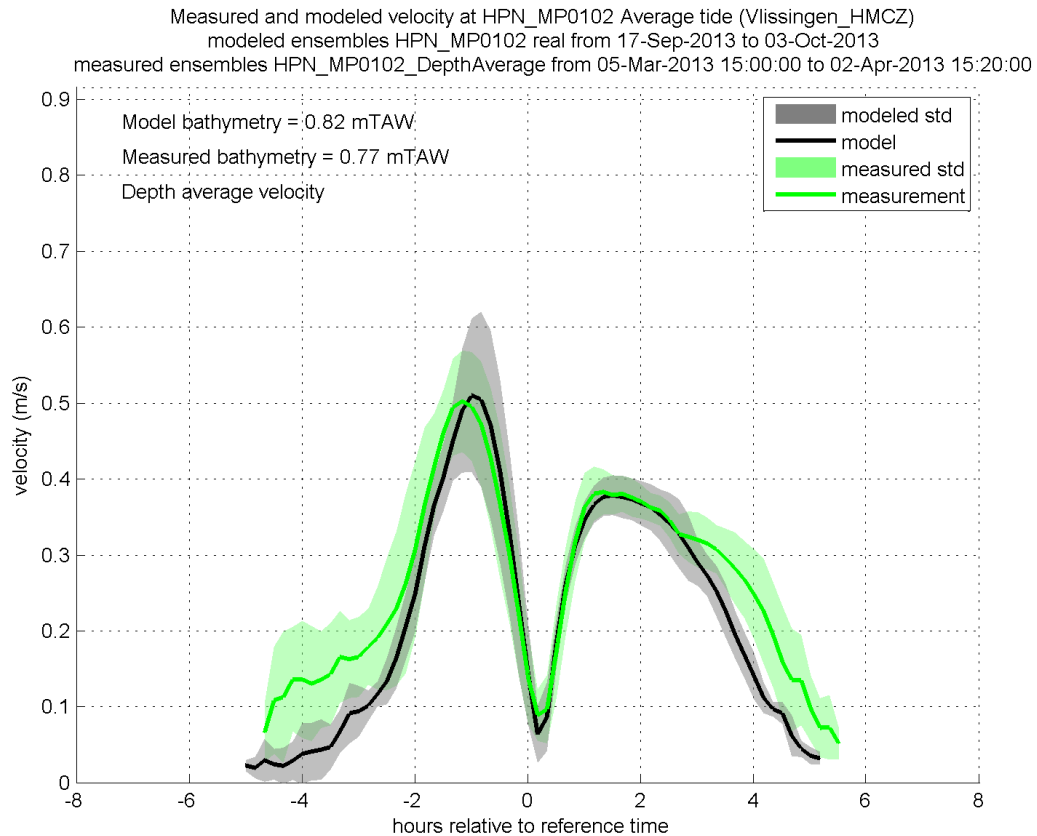


Figure 394 - Measured and modeled depth average velocity at Hooge Platen Noord MP0102 (average tide)

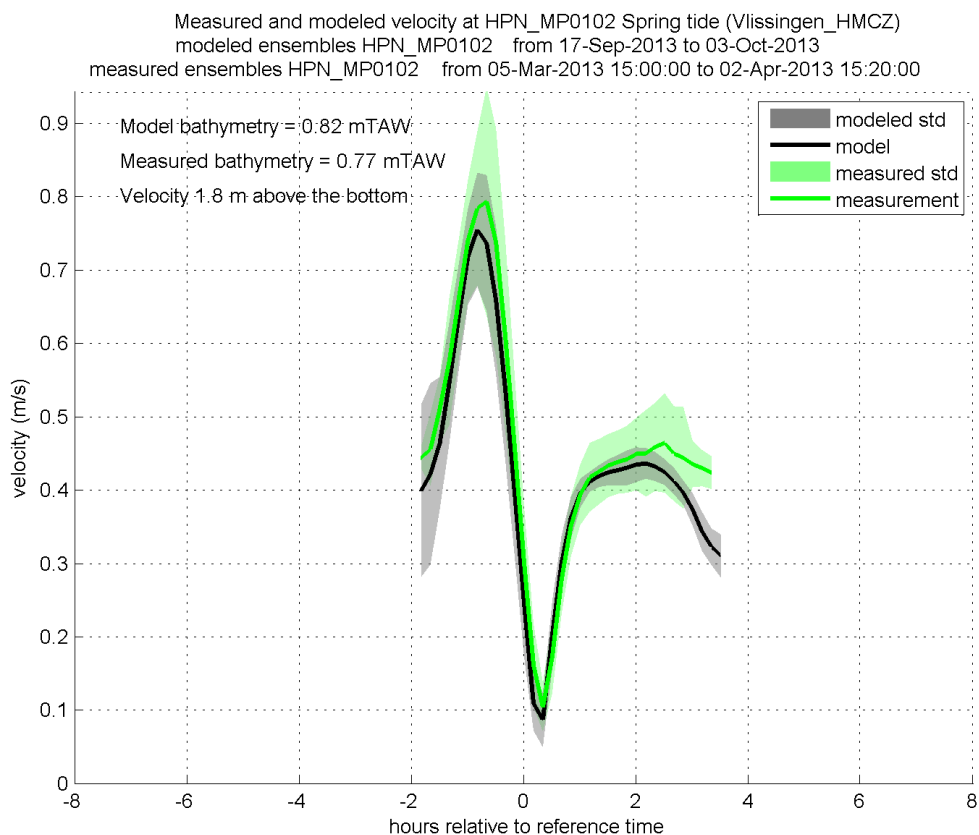


Figure 395 - Measured and modeled velocity at Hooge Platen Noord MP0102 1.8 m above the bottom (spring tide)

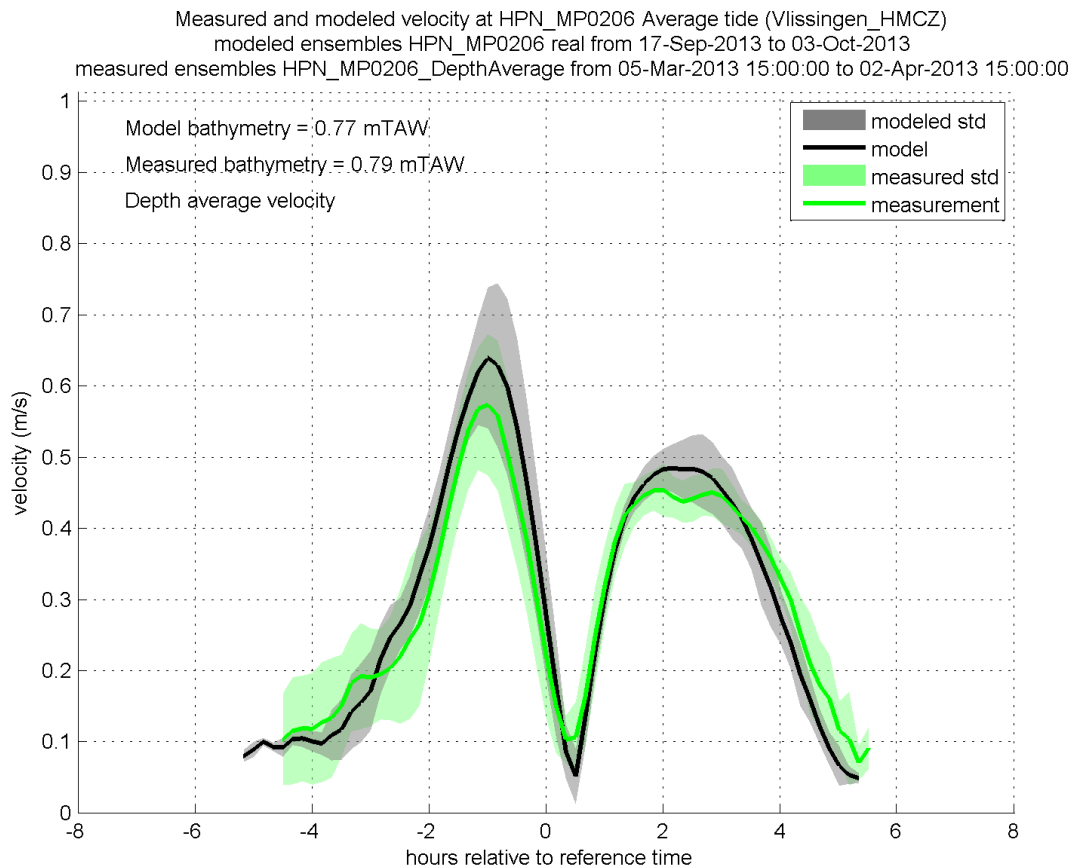


Figure 396 - Measured and modeled depth average velocity at Hooge Platen Noord MP0206 (average tide)

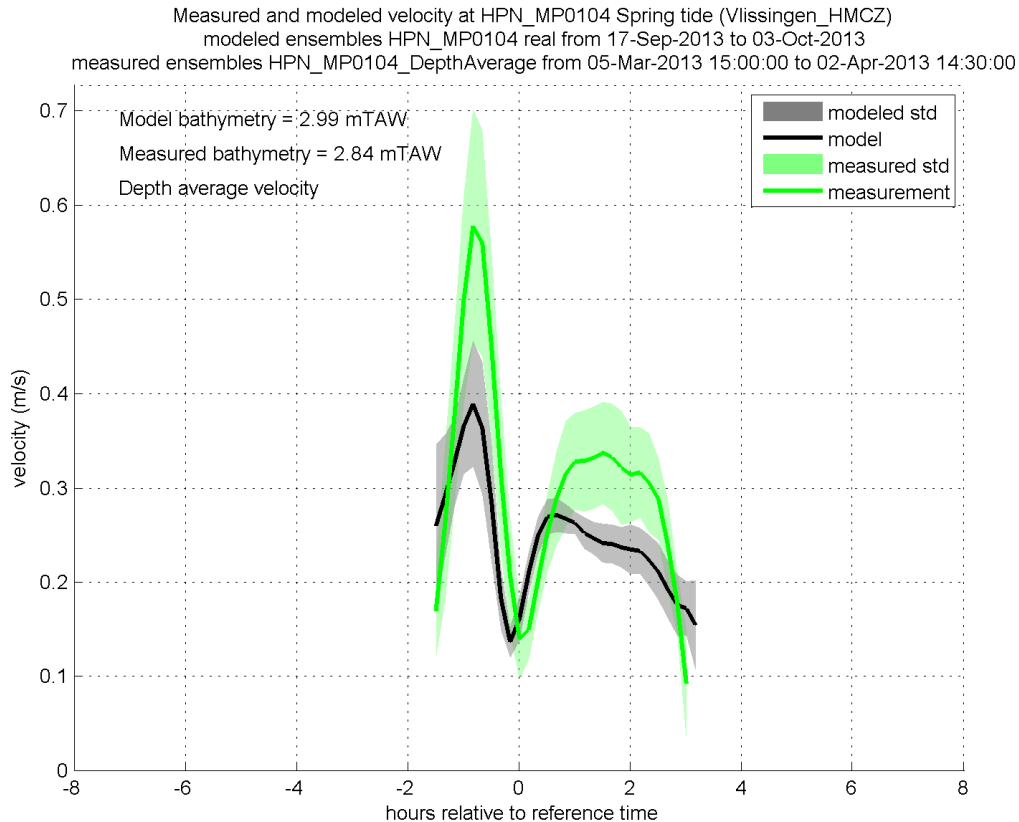


Figure 397 - Measured and modeled depth average velocity at Hooge Platen Noord MP0104 (spring tide)

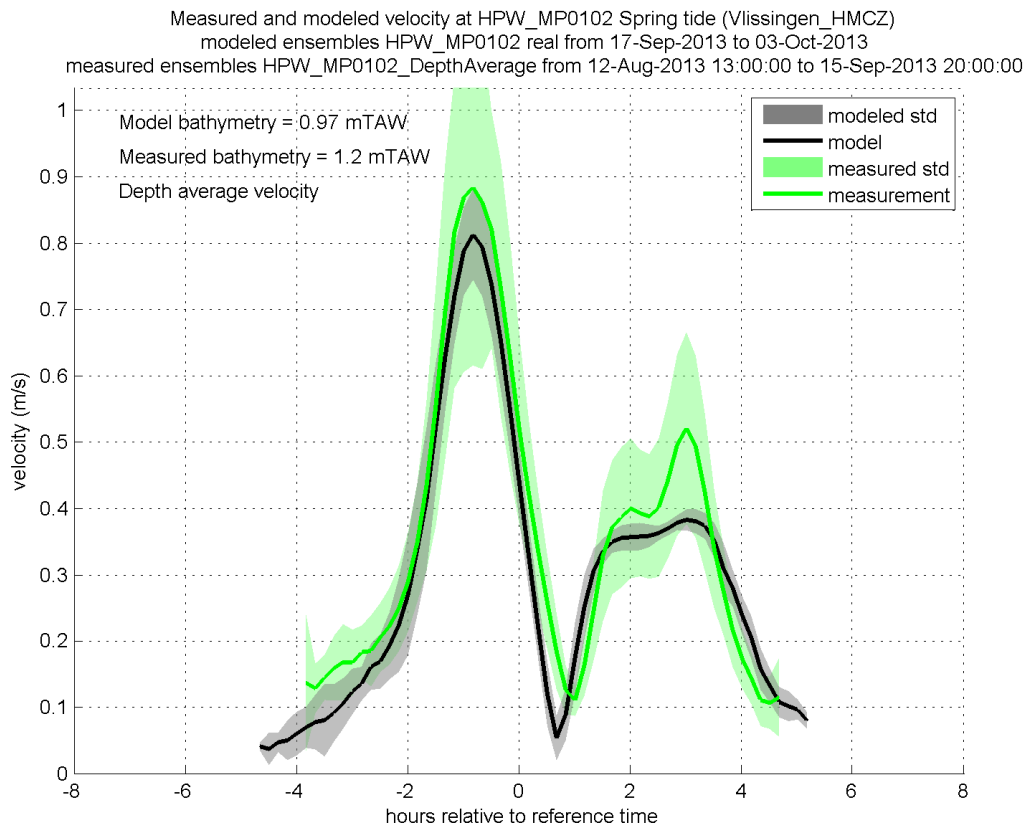


Figure 398 - Measured and modeled depth average velocity at Hooke Platen West MP0102 (spring tide)

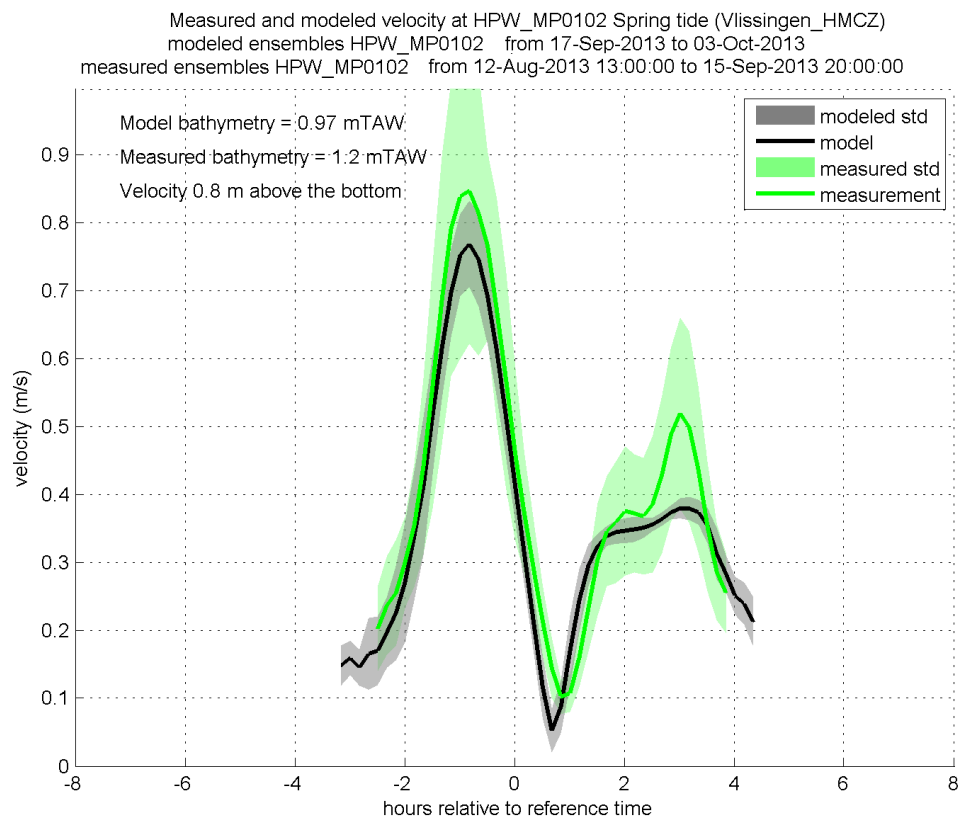


Figure 399 - Measured and modeled velocity at Hooke Platen West MP0102 0.8 m above the bottom (spring tide)

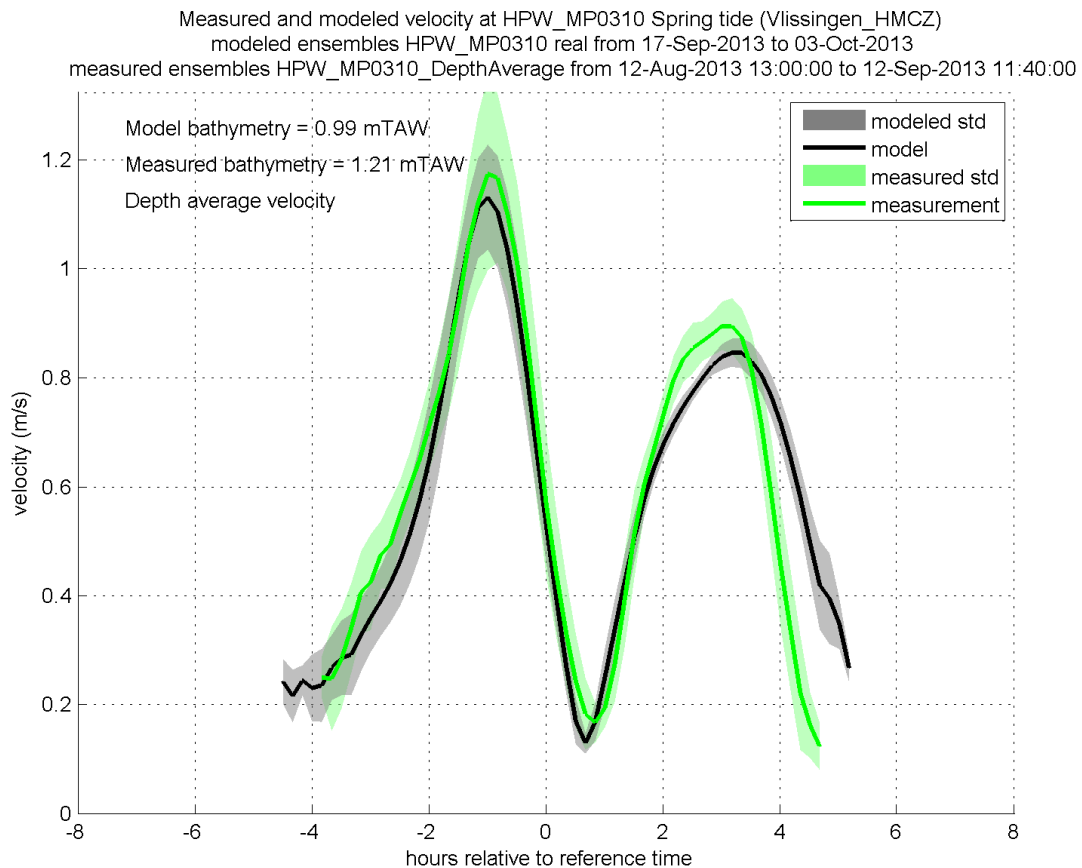


Figure 400 - Measured and modeled depth average velocity at Hooge Platen West MP0310 (spring tide)

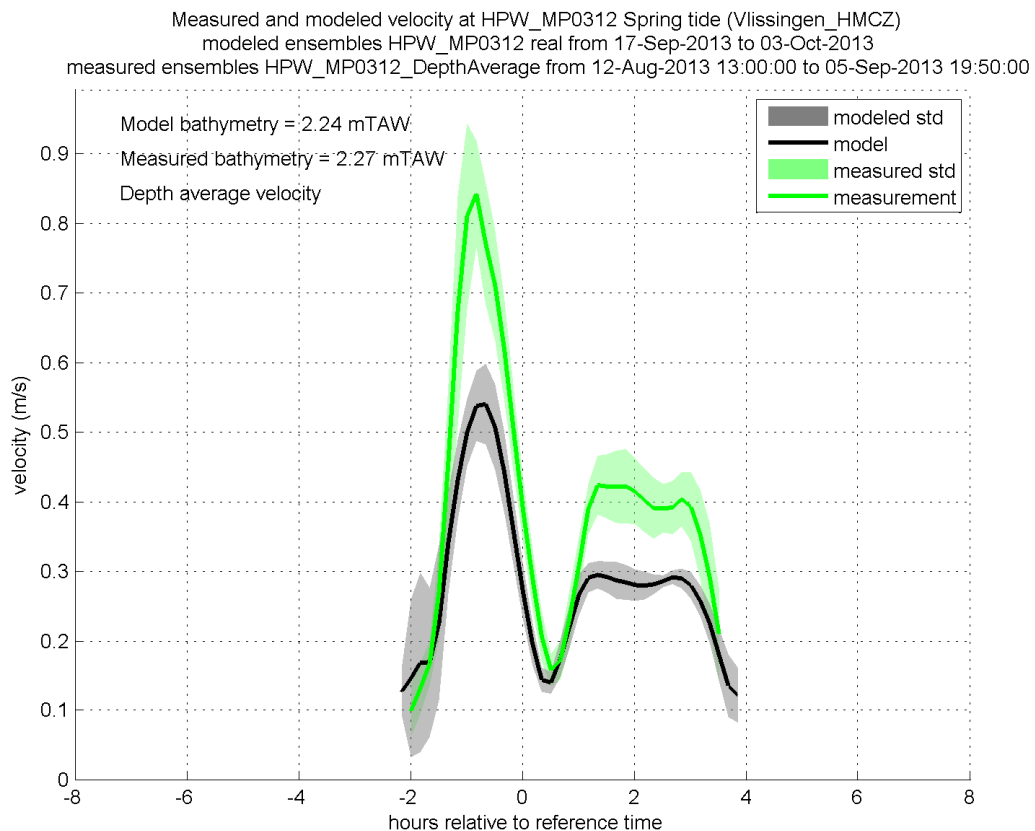


Figure 401 - Measured and modeled depth average velocity at Hooge Platen West MP0312 (spring tide)

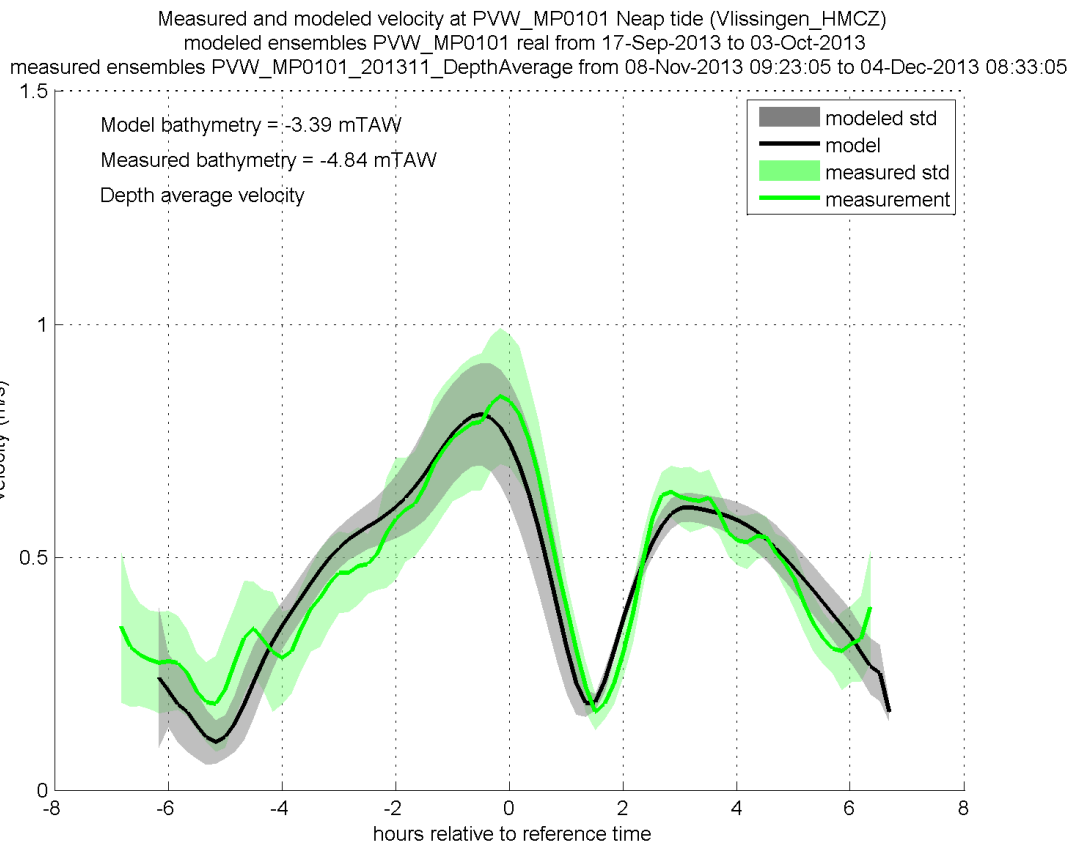


Figure 402 - Measured and modeled depth average velocity at Plaat van Walsoorden MP0101 (neap tide)

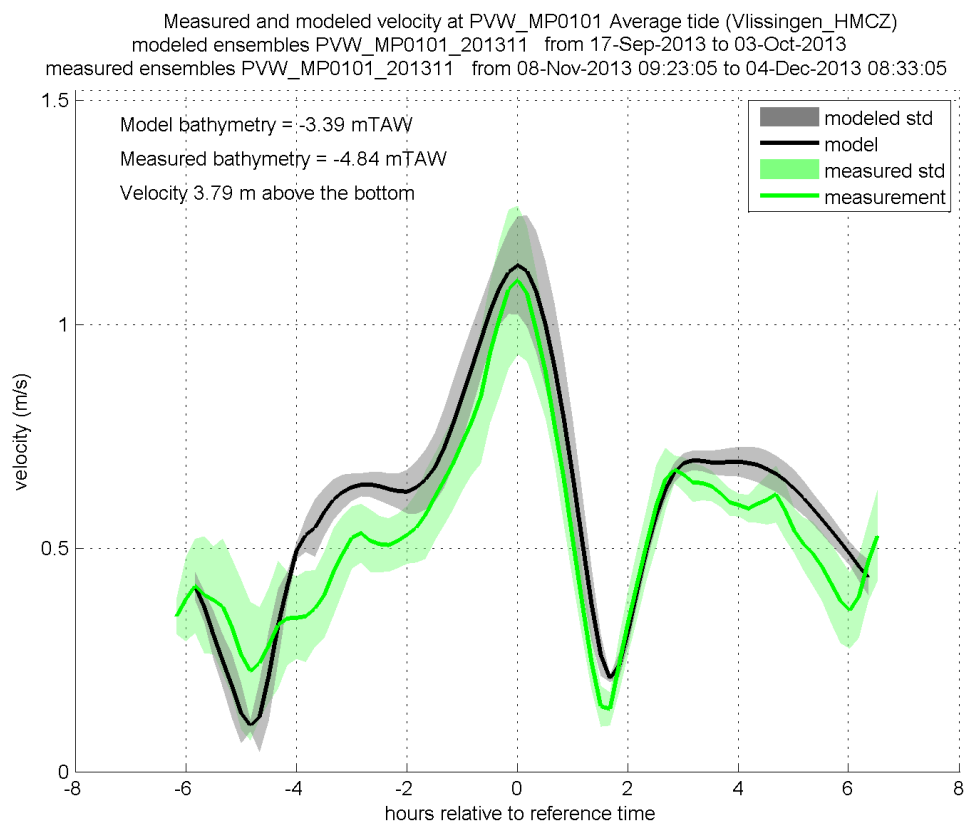


Figure 403 - Measured and modeled velocity at Plaat van Walsoorden MP0101 at 3.79 m above the bottom (average tide)

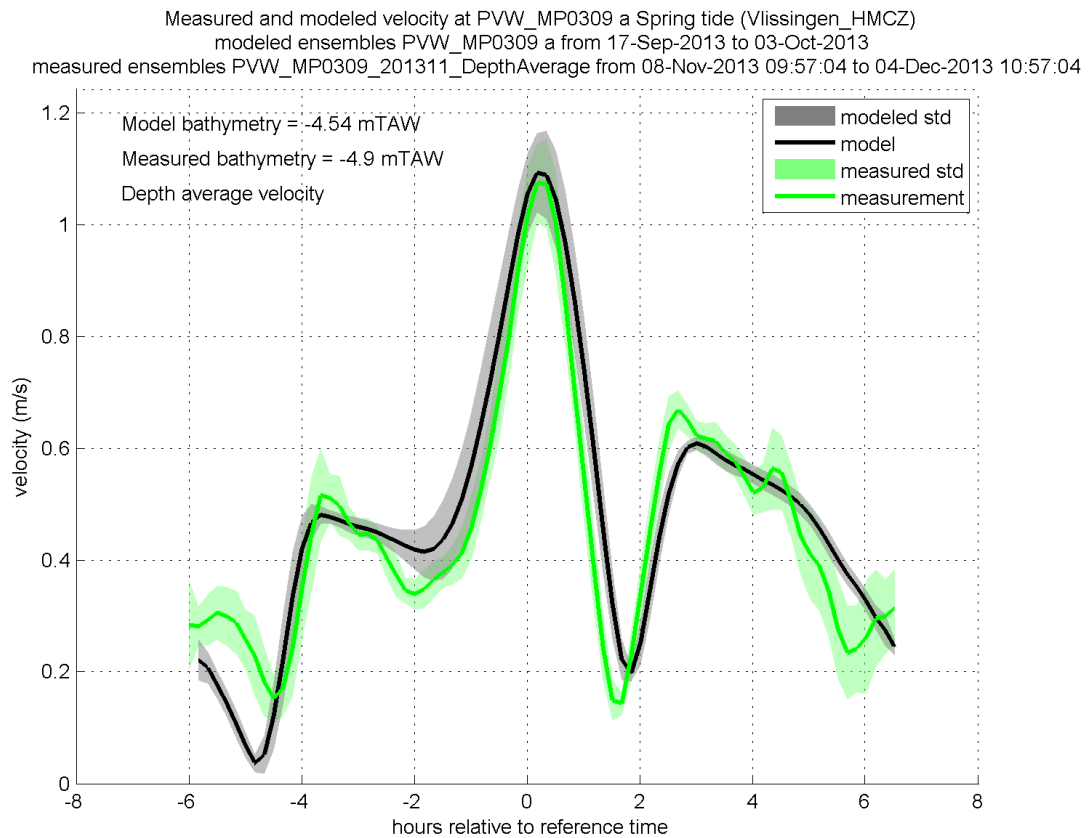


Figure 404 - Measured and modeled depth average velocity at Plaat van Walsoorden MP0309a (spring tide)

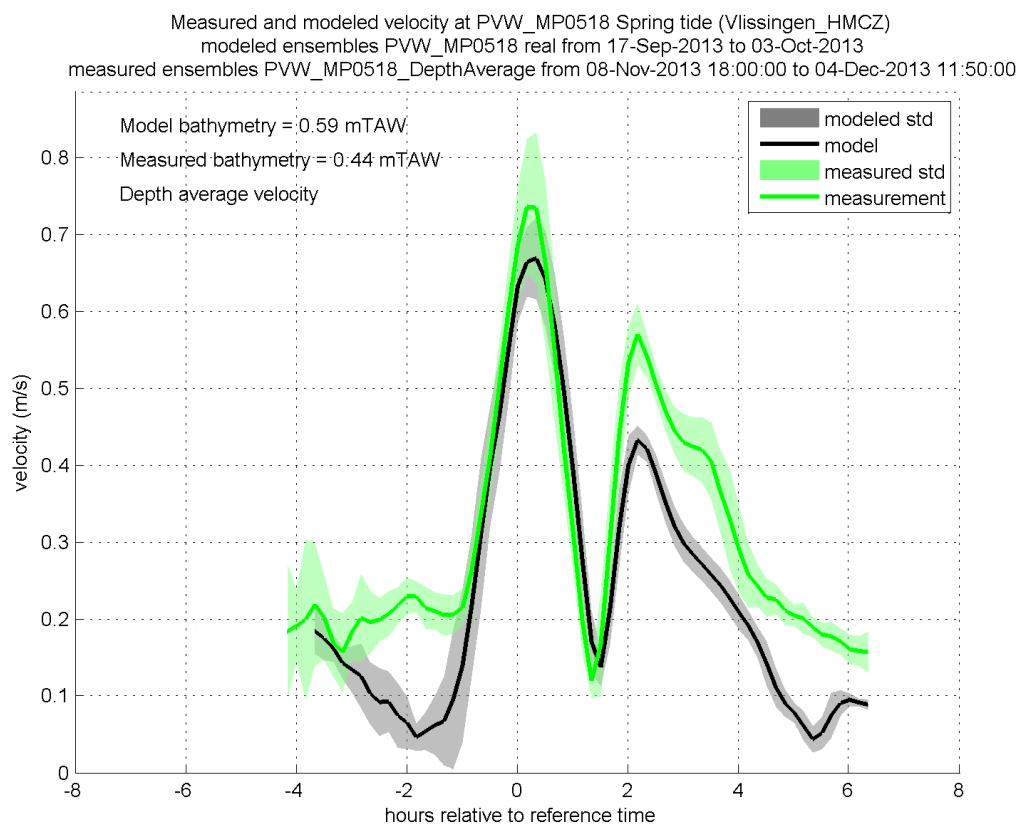


Figure 405 - Measured and modeled depth average velocity at Plaat van Walsoorden MP0518 (spring tide)

Salinity

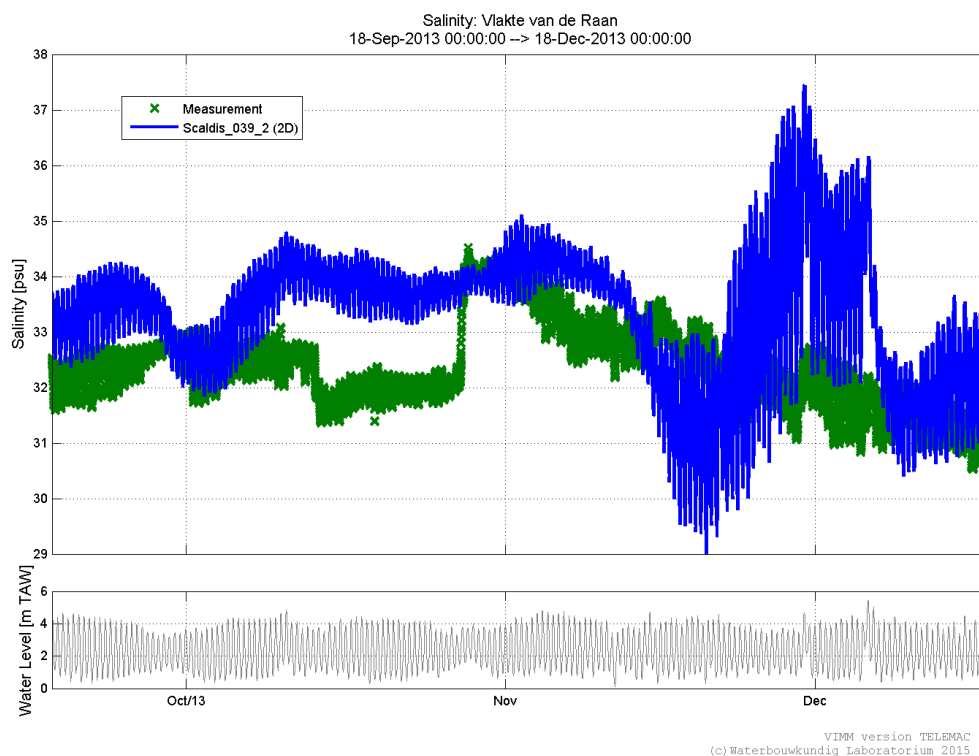


Figure 406 - Measured and modeled salinity at Vlake van de Raan in Scaldis_039_2

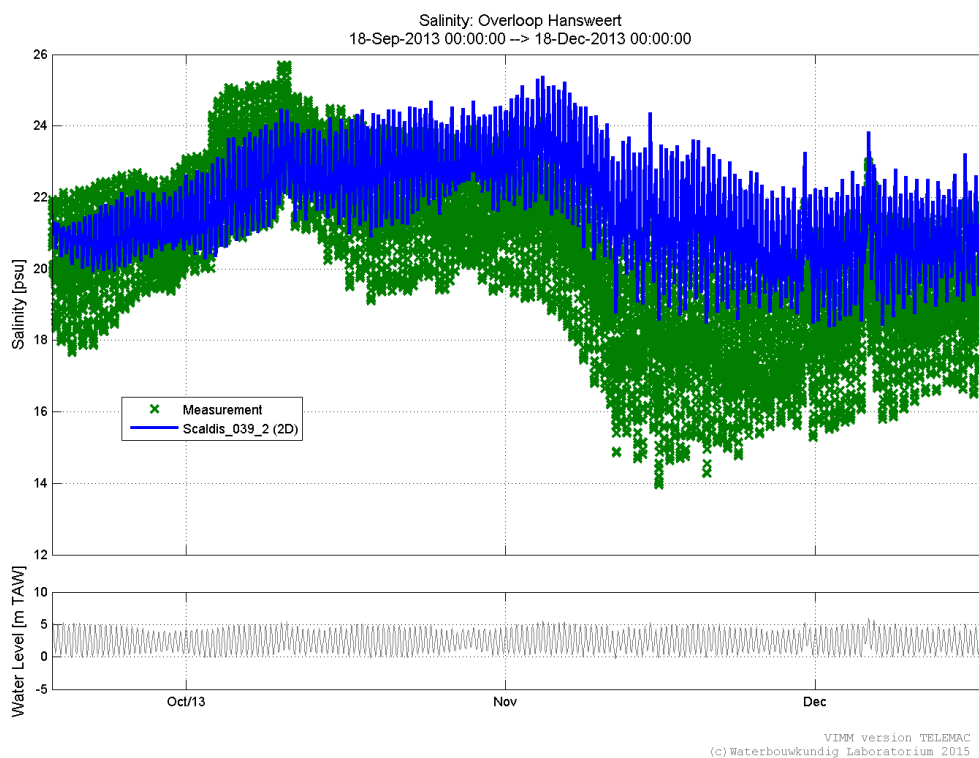


Figure 407 - Measured and modeled salinity at Overloop van Hansweert in Scaldis_039_2

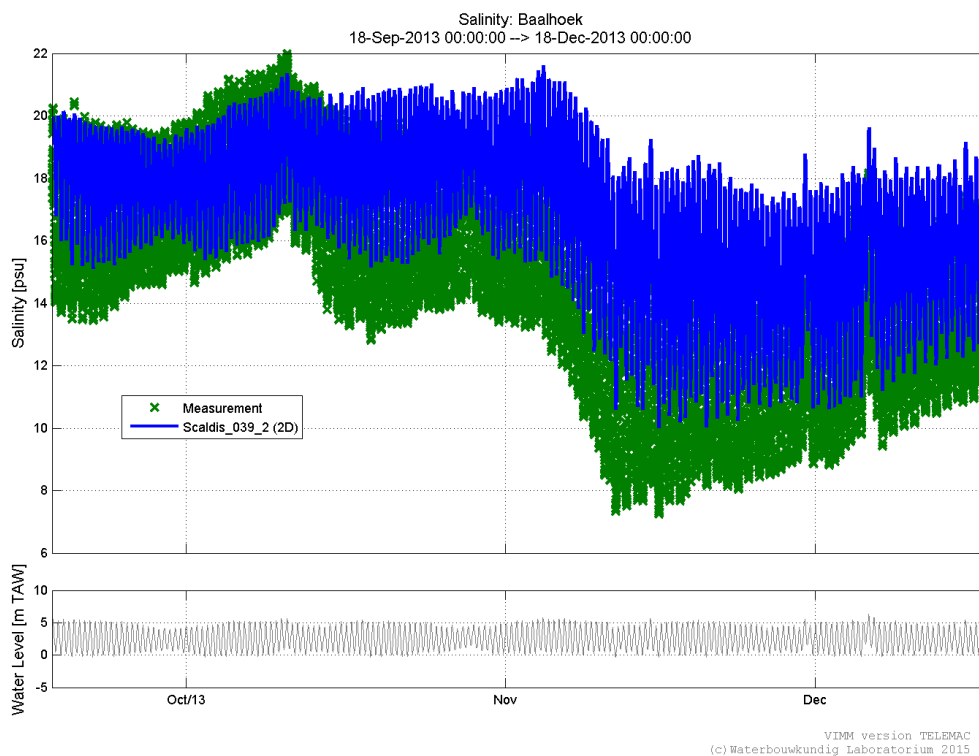


Figure 408 - Measured and modeled salinity at Baalhoek in Scaldis_039_2

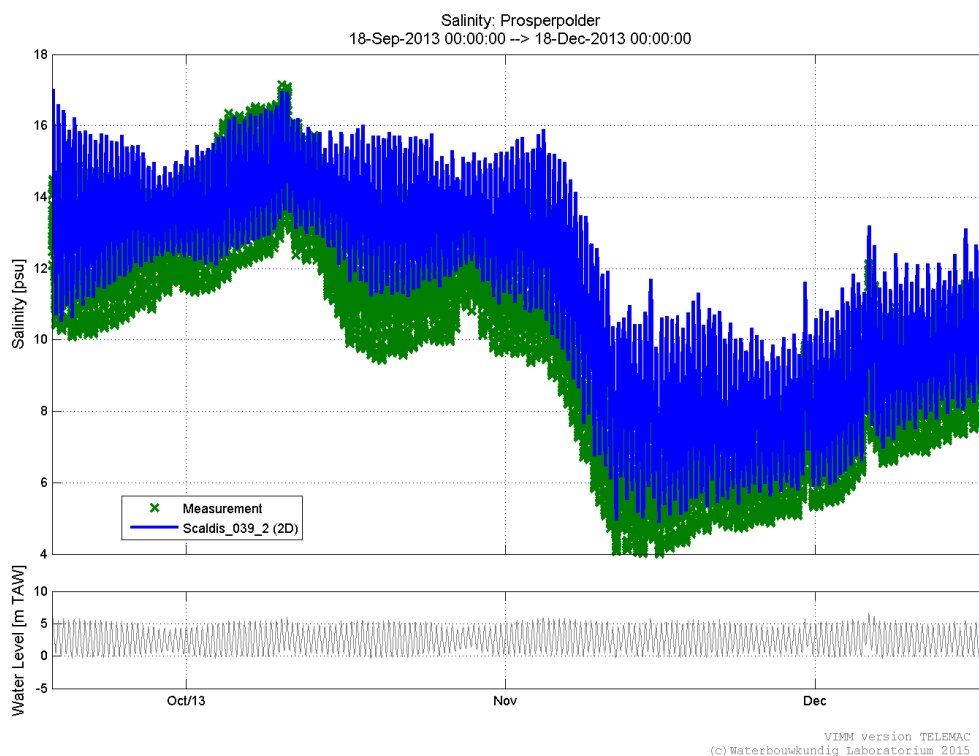


Figure 409 - Measured and modeled salinity at Prosperpolder in Scaldis_039_2

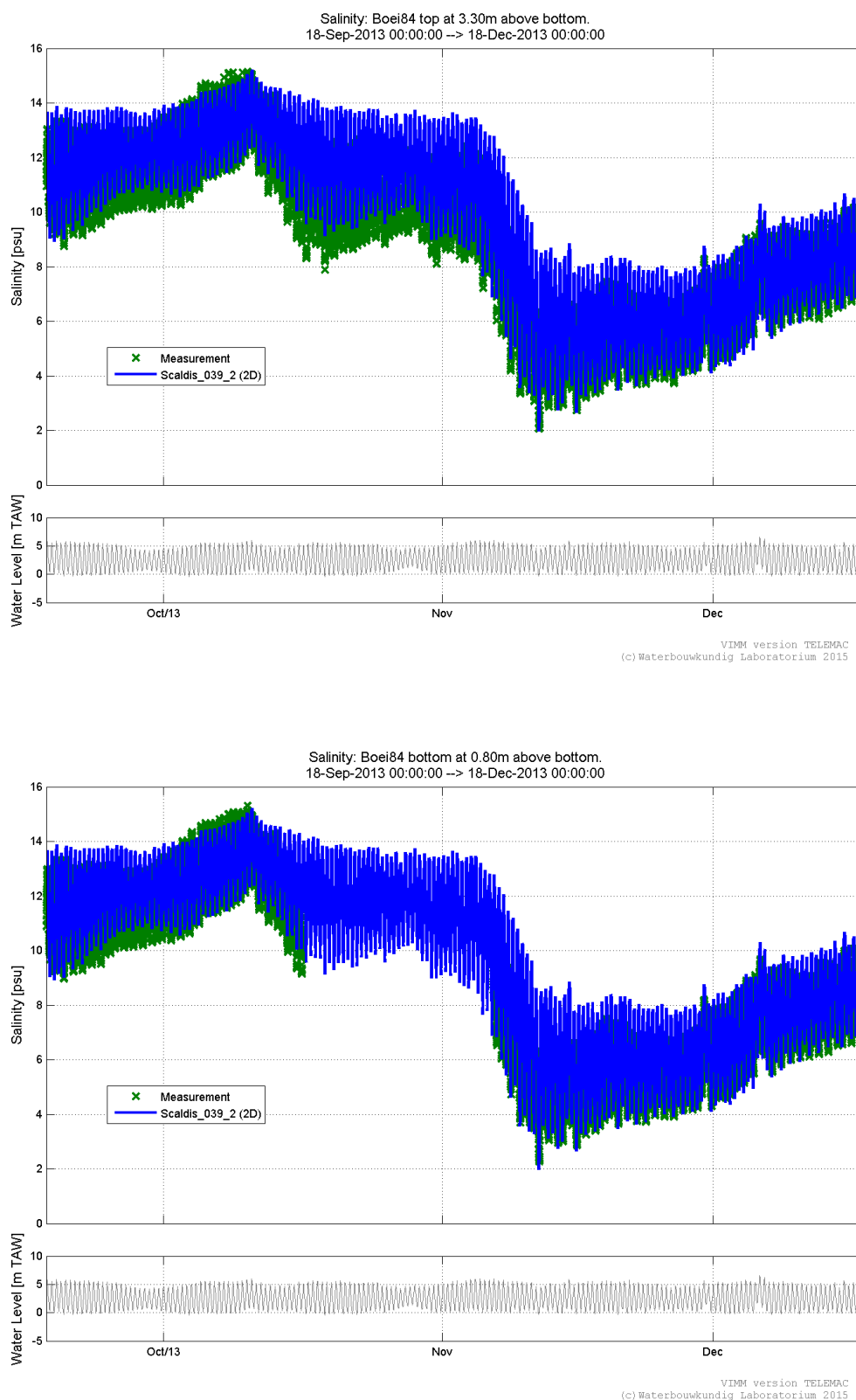


Figure 410 - Measured and modeled salinity at Buoy 84 in Scaldis_039_2

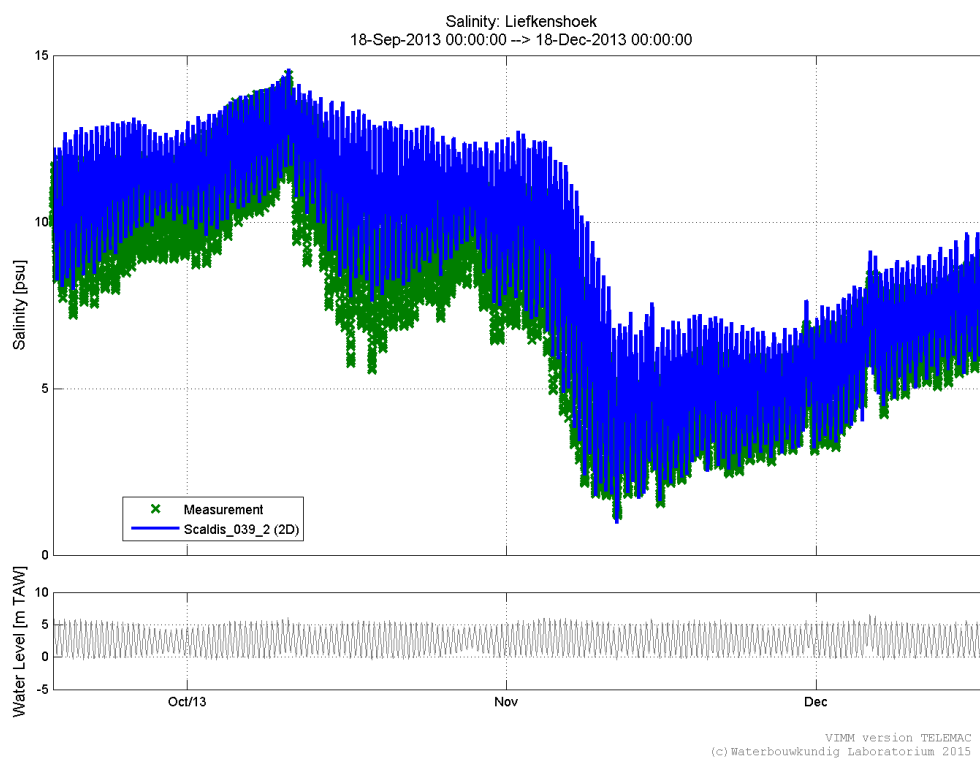


Figure 411 - Measured and modeled salinity at Liefkenshoek in Scaldis_039_2

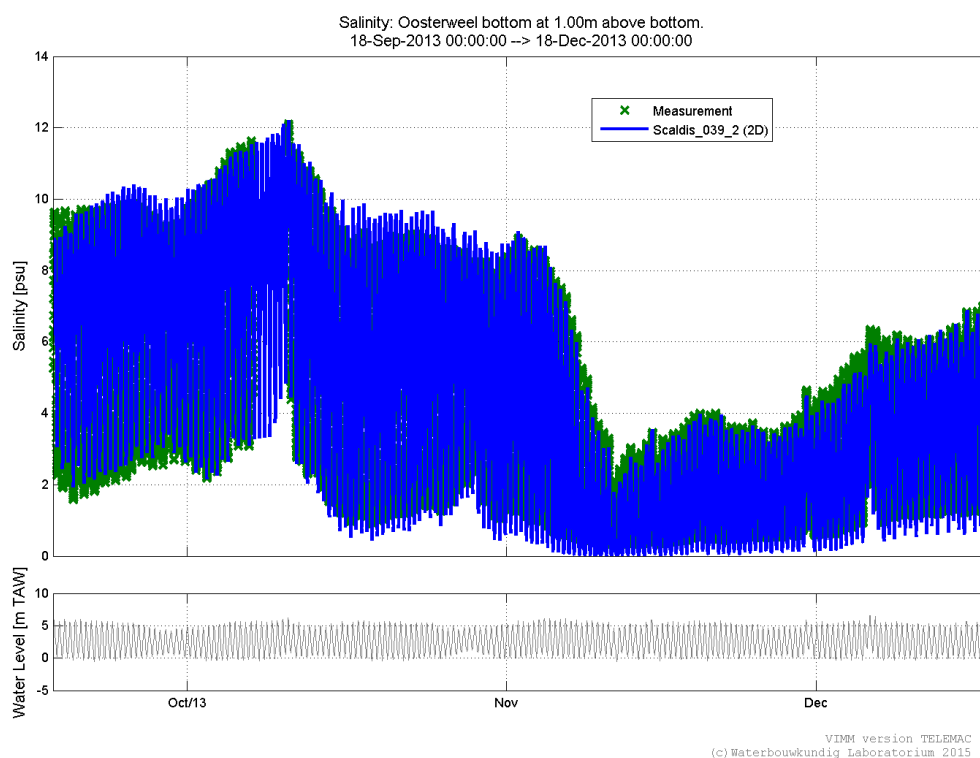
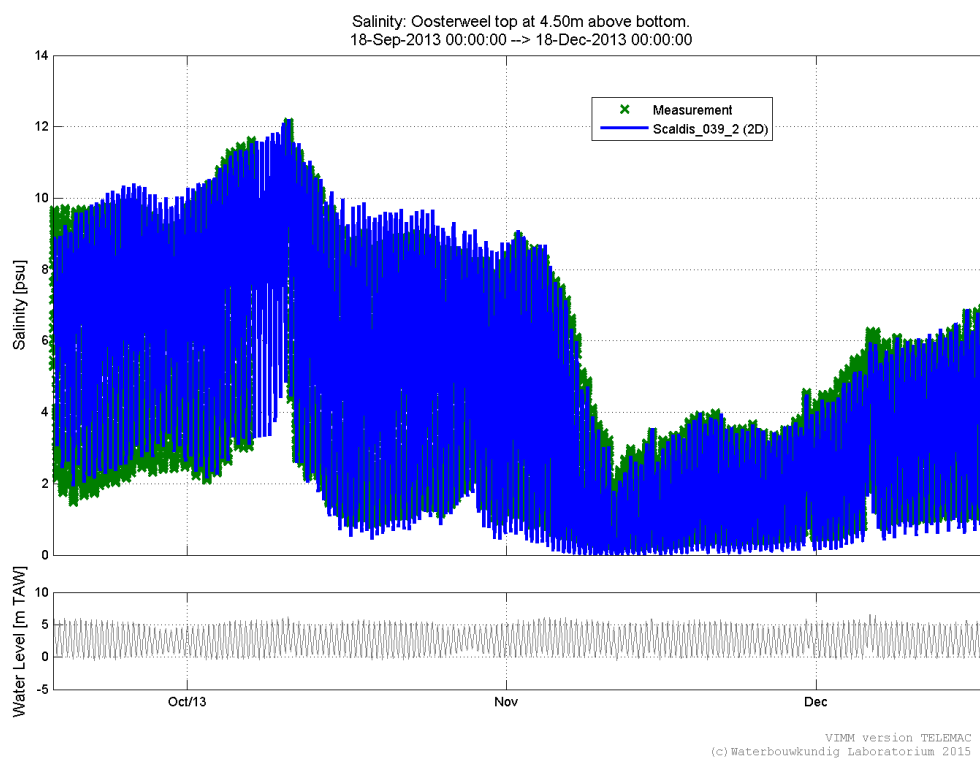


Figure 412 - Measured and modeled salinity at Oosterweel in Scaldis_039_2

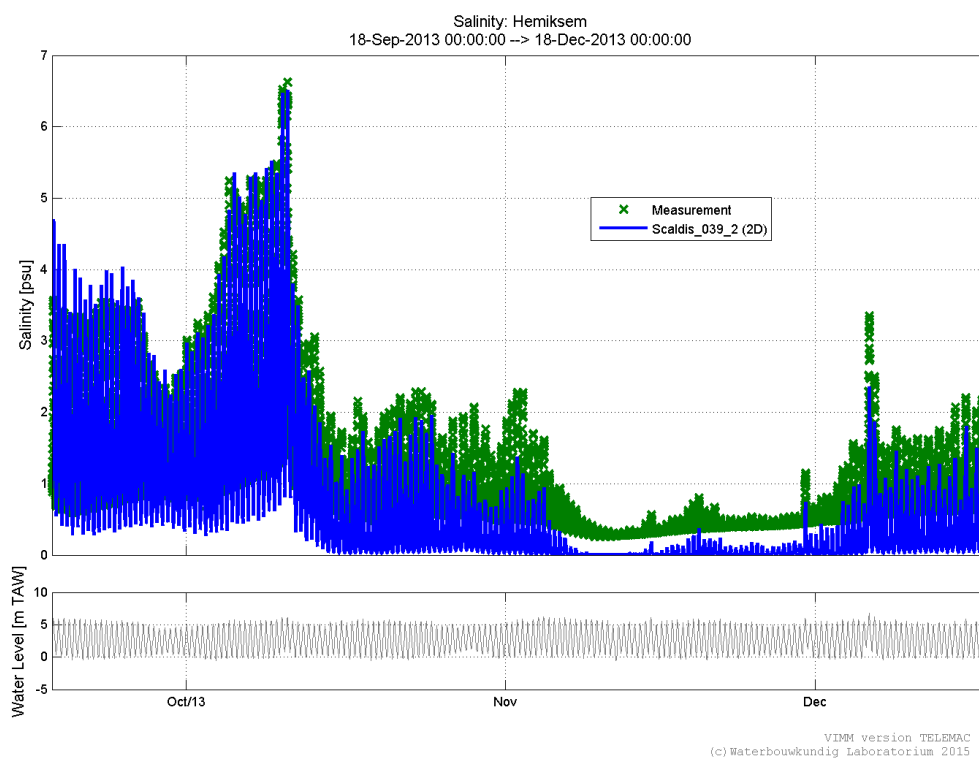


Figure 413 - Measured and modeled salinity at Hemiksem in Scaldis_039_2

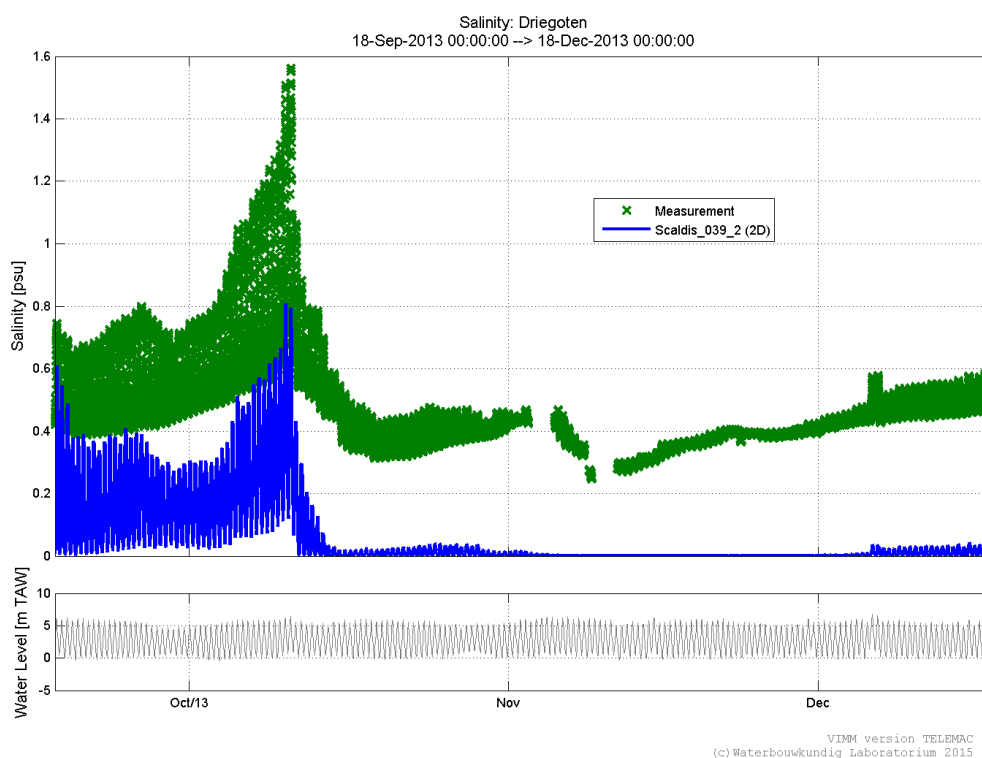


Figure 414 - Measured and modeled salinity at Driegoten in Scaldis_039_2

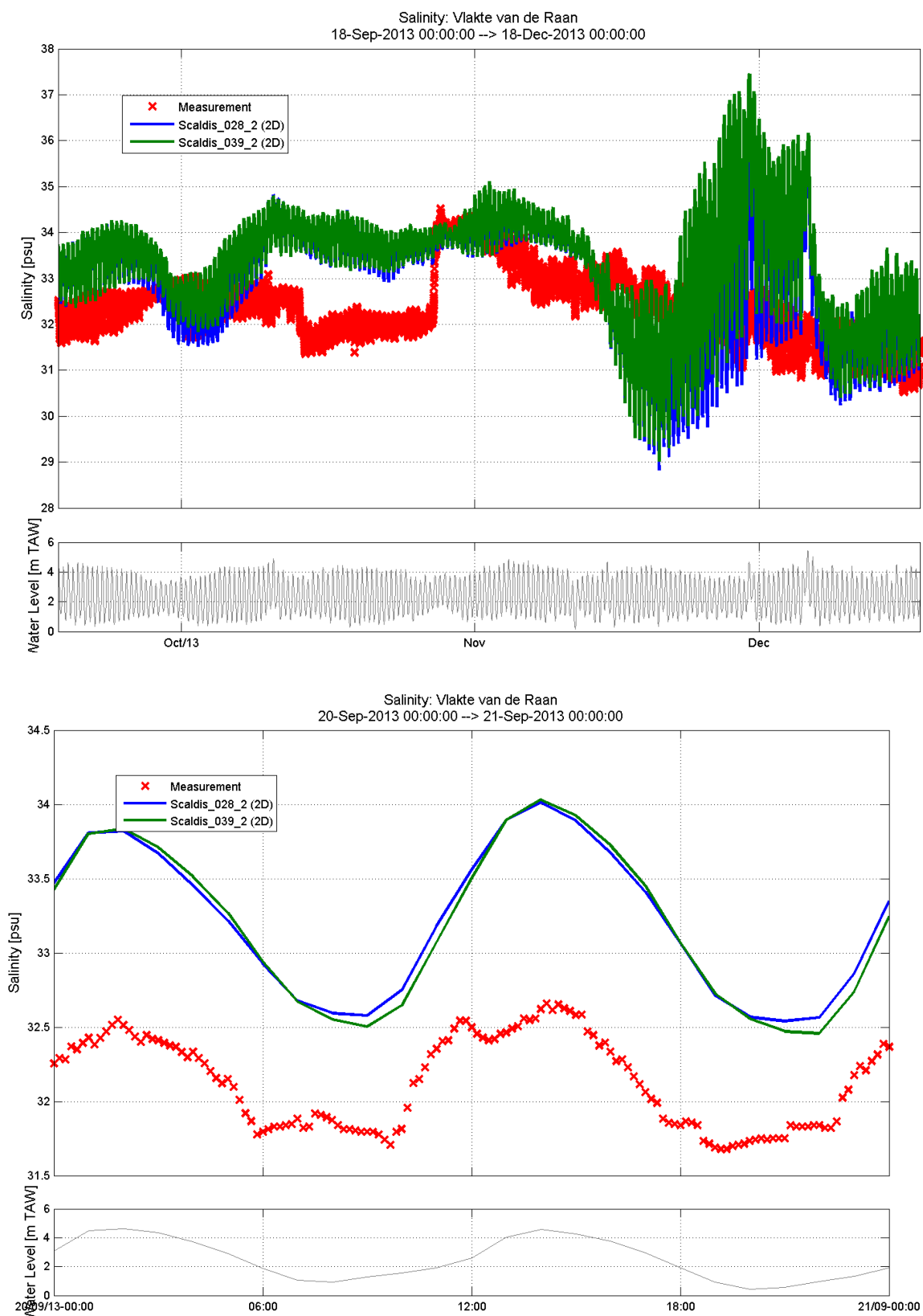


Figure 415 - Measured and modeled salinity at Vlakte van de Raan in Scaldis_028_2 and Scaldis_039_2

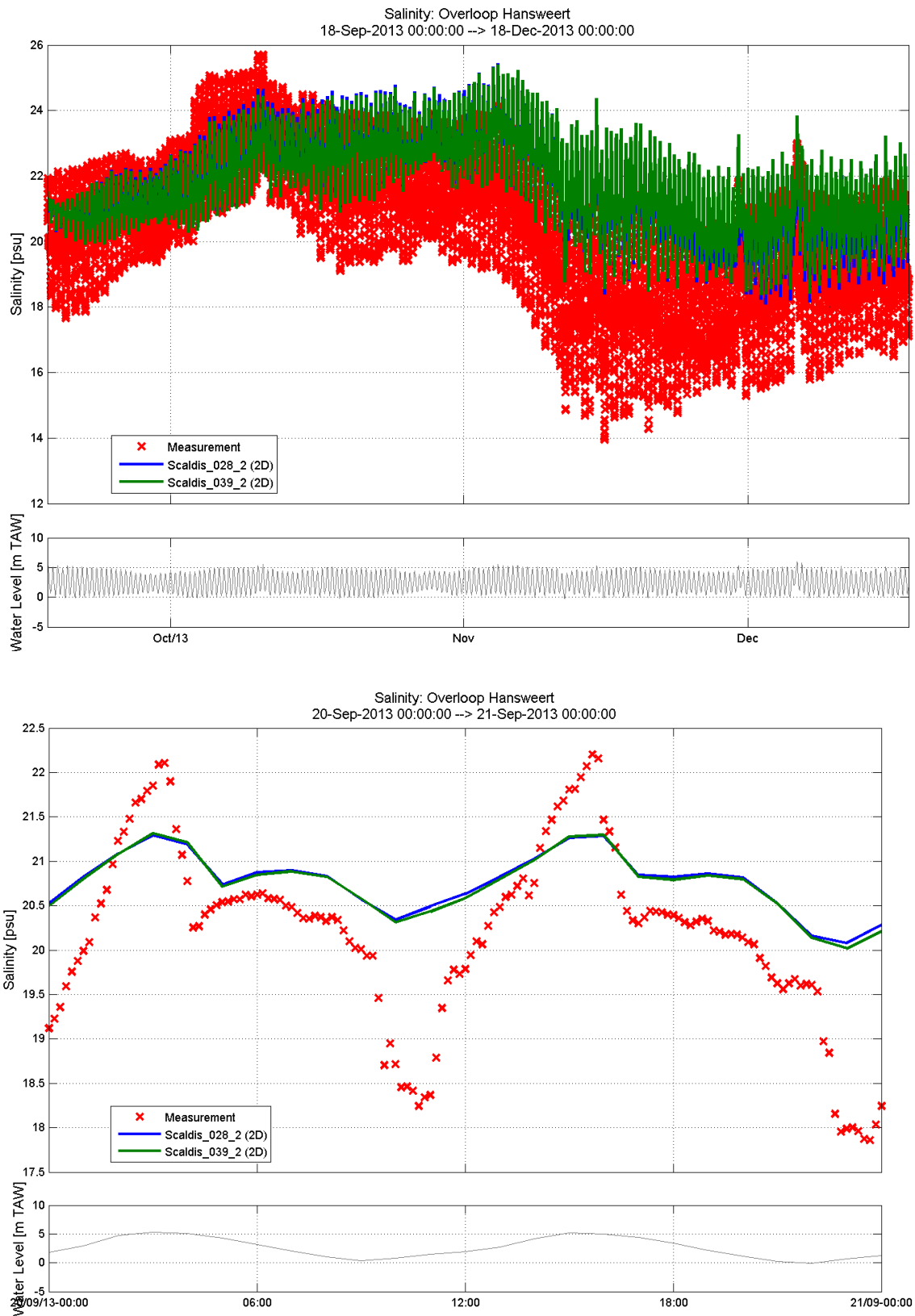


Figure 416 - Measured and modeled salinity at Overloop van Hansweert in Scaldis_028_2 and Scaldis_039_2

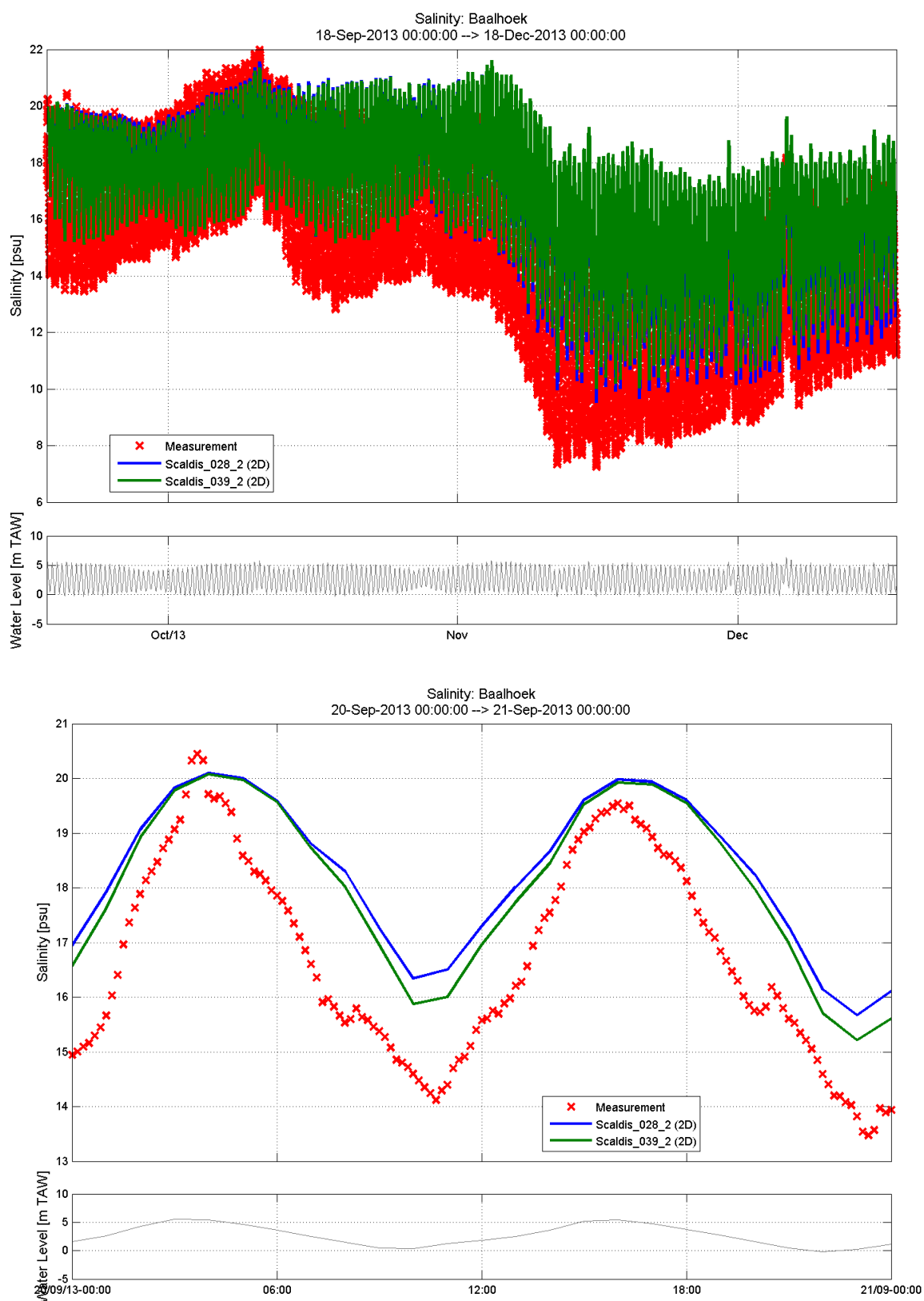


Figure 417 - Measured and modeled salinity at Baalhoek in Scaldis_028_2 and Scaldis_039_2

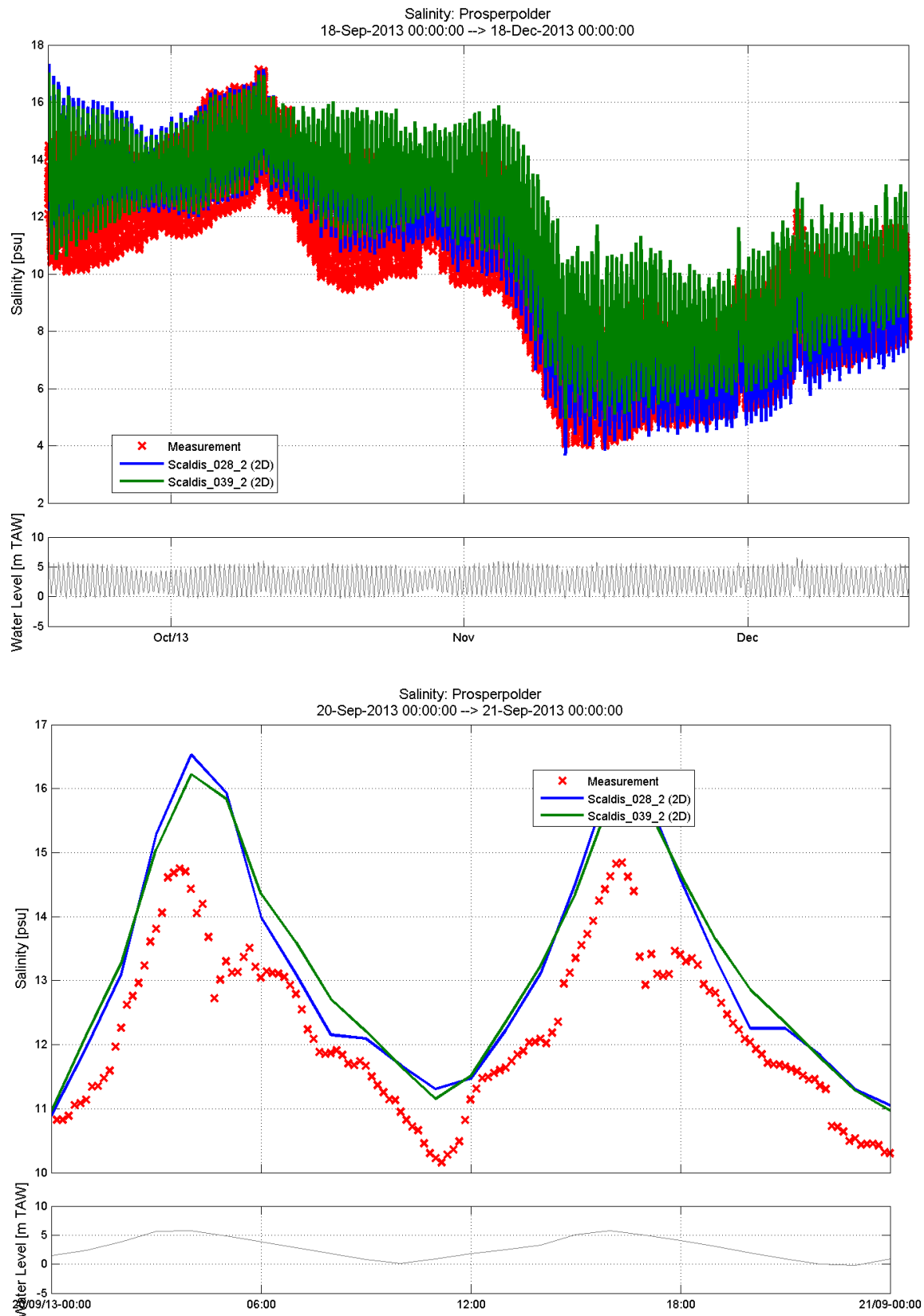


Figure 418 - Measured and modeled salinity at Prosperpolder in Scaldis_028_2 and Scaldis_039_2

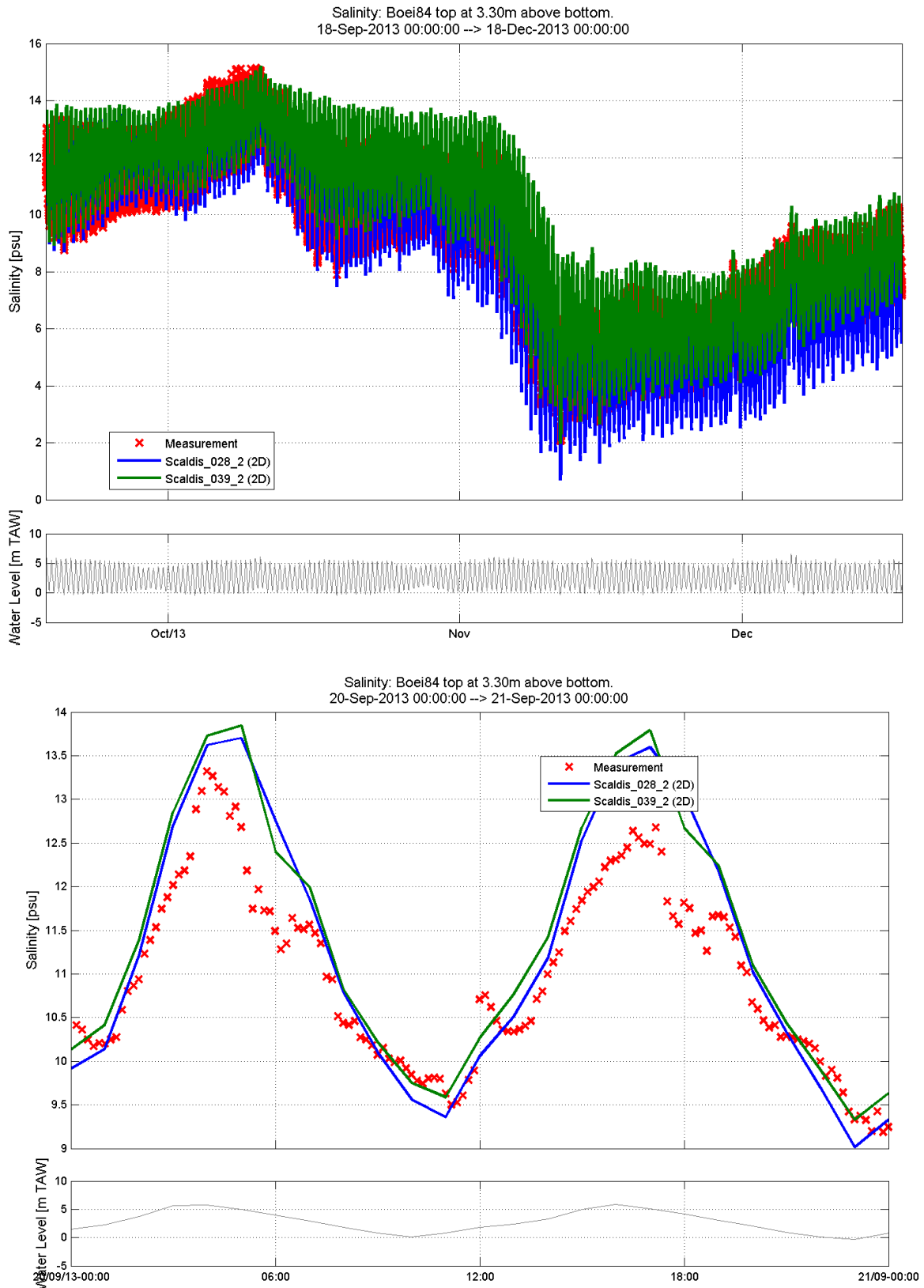


Figure 419 - Measured and modeled salinity at buoy 84 'top' in Scaldis_028_2 and Scaldis_039_2
(measurement at top vs 2D model result)

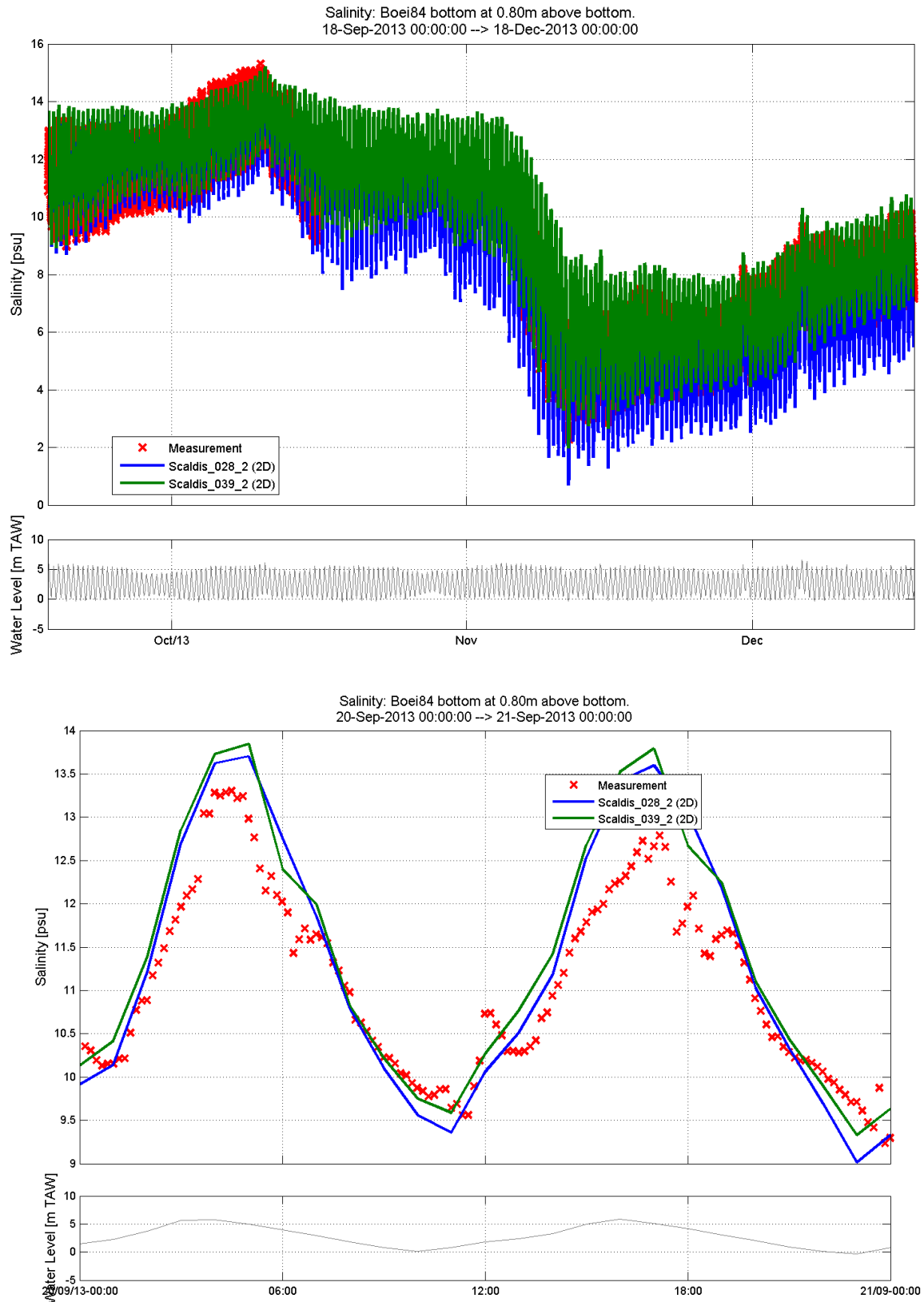


Figure 420 - Measured and modeled salinity at buoy 84 'bottom' in Scaldis_028_2 and Scaldis_039_2 (measurement at bottom vs 2D model result)

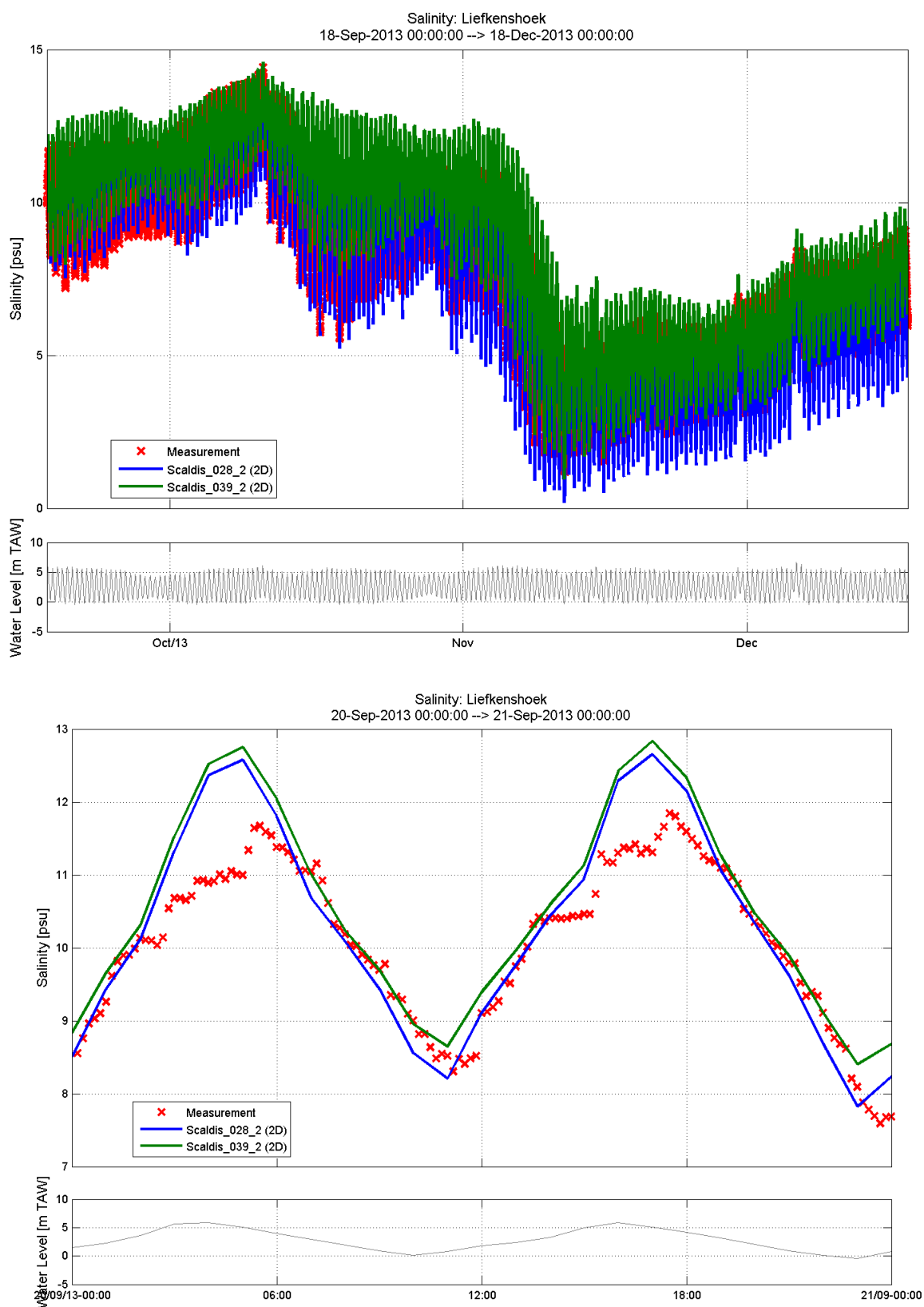


Figure 421 - Measured and modeled salinity at Liefkenshoek in Scaldis_028_2 and Scaldis_039_2

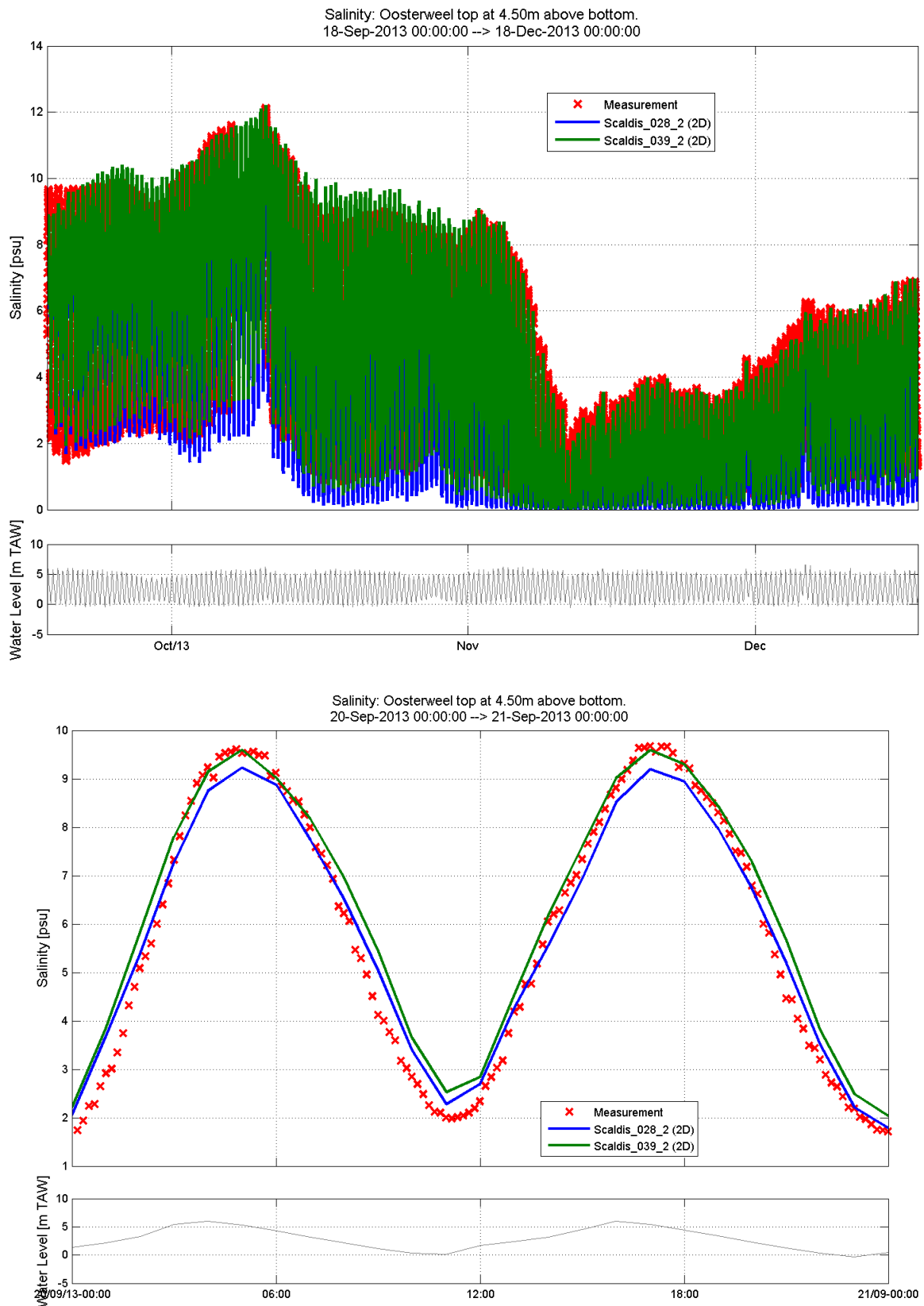


Figure 422 - Measured and modeled salinity at Oosterweel 'top' in Scaldis_028_2 and Scaldis_039_2
(measurement at top vs 2D model result)

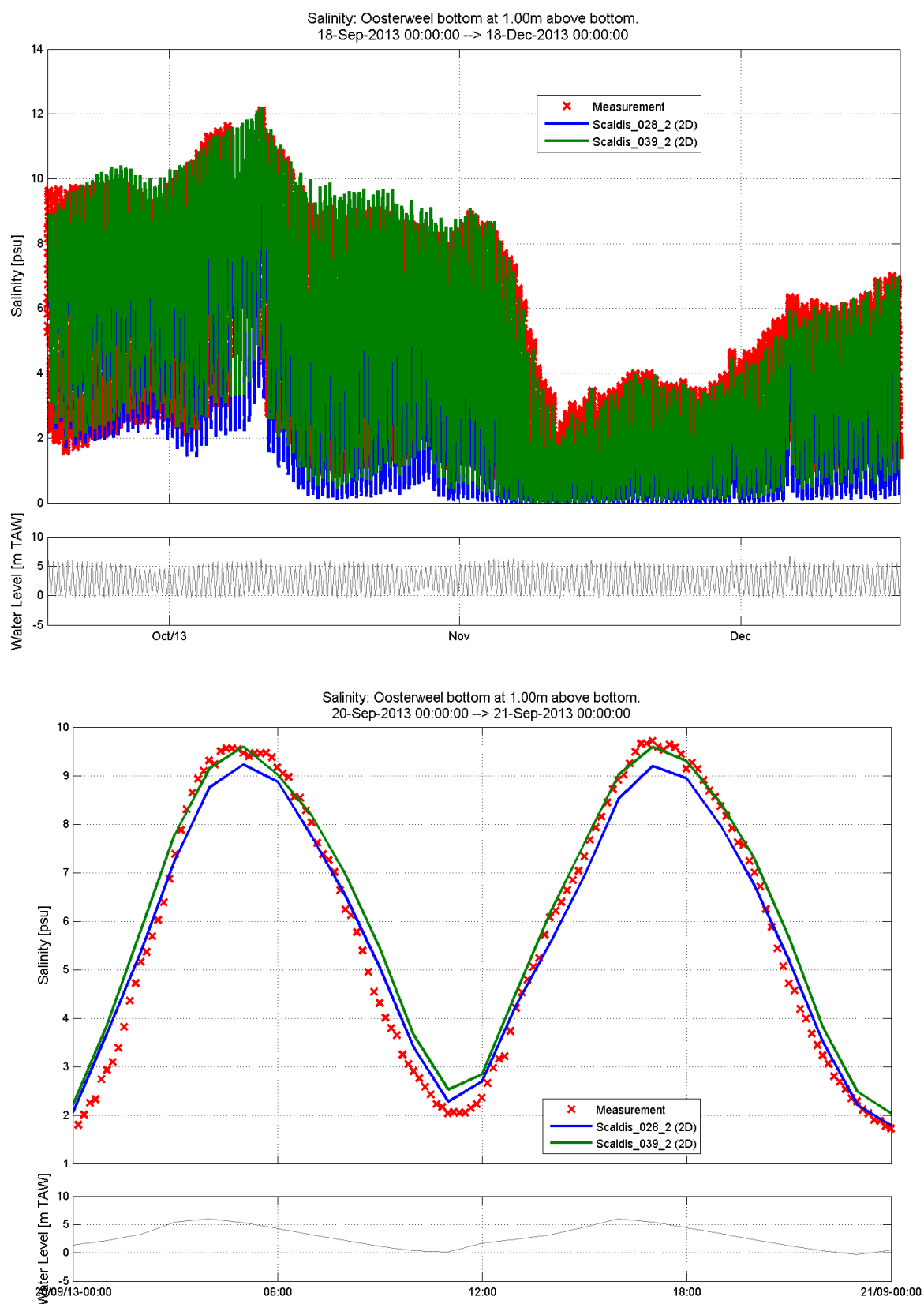


Figure 423 - Measured and modeled salinity at Oosterweel 'bottom' in Scaldis_028_2 and Scaldis_039_2 (measurement at bottom vs 2D model result)

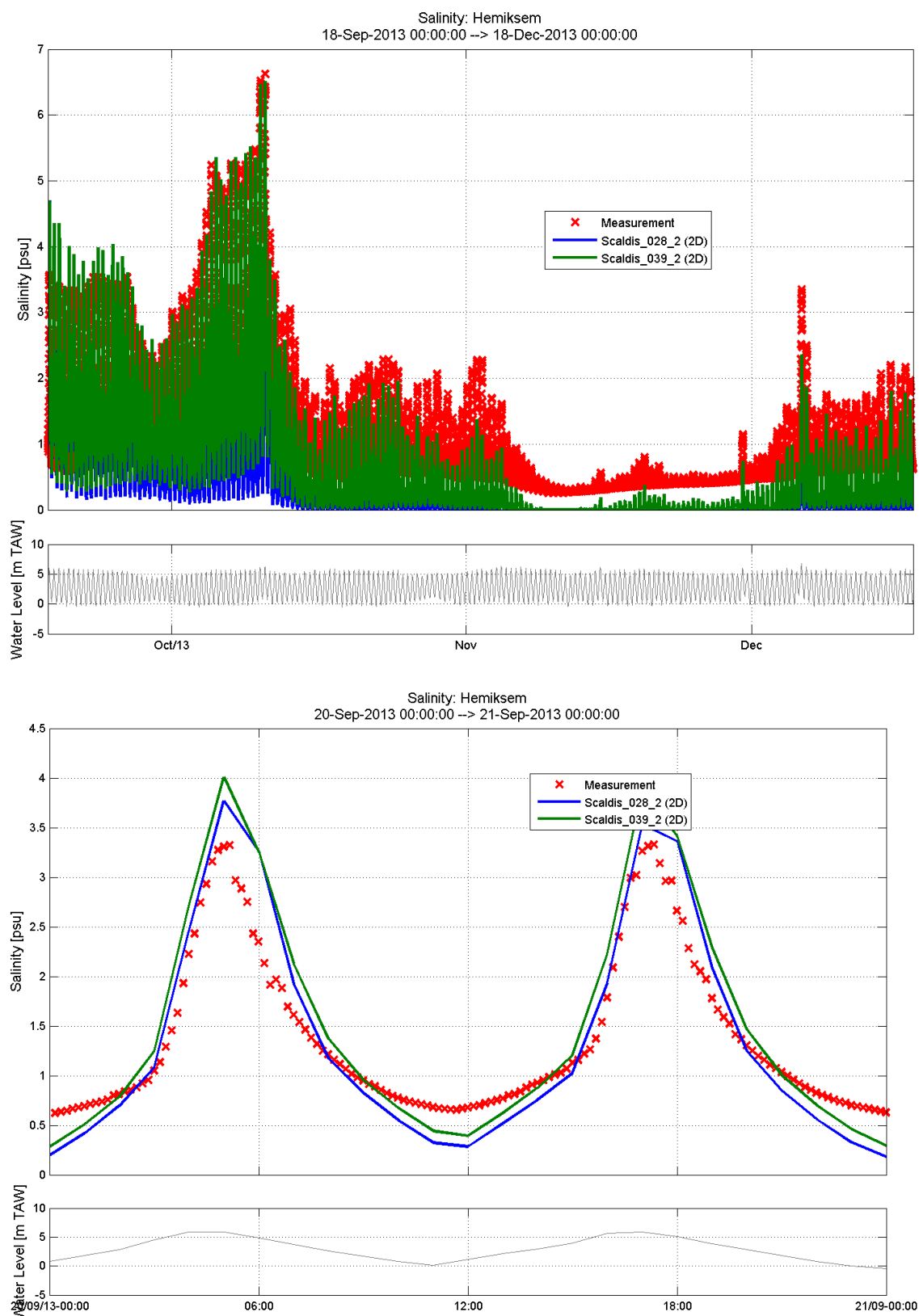


Figure 424 - Measured and modeled salinity at Hemiksem in Scaldis_028_2 and Scaldis_039_2

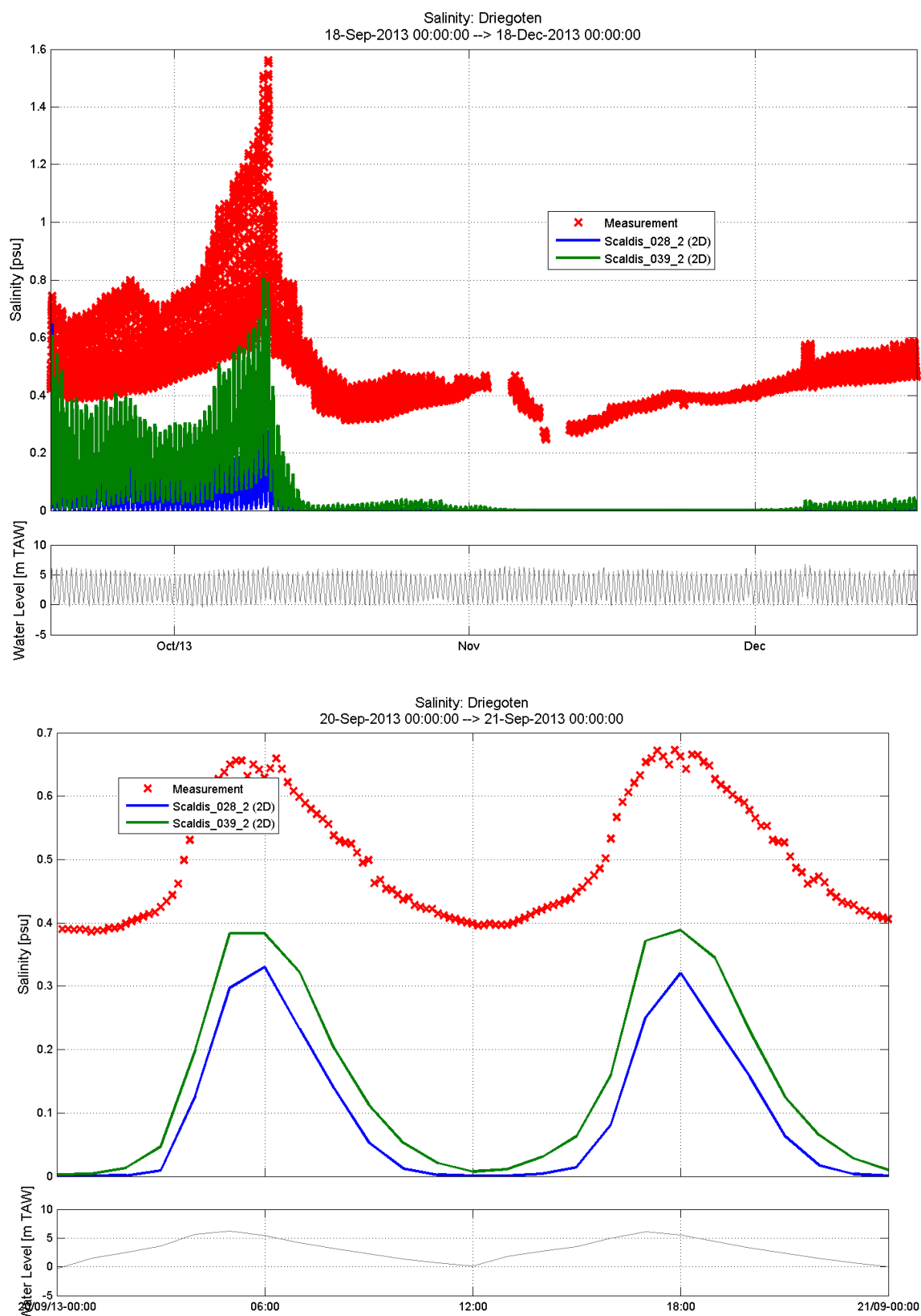


Figure 425 - Measured and modeled salinity at Driegoten in Scaldis_028_2 and Scaldis_039_2

Appendix 2. Model performance during storm

Scheldt estuary

Table 161. Statistical parameters for the water level time series during storm (North sea and Western Scheldt)

Station	Complete Time Series		
	BIAS TS	RMSE TS	RMSE_0 TS
	[m]	[m]	[m]
Nieuwpoort	0.18	0.24	0.15
Oostende	0.10	0.18	0.14
Zeebrugge	0.08	0.17	0.15
MP0 Wandelaar	0.16	0.21	0.13
MP1 A2B boei	0.10	0.17	0.14
MP2 Appelzak	0.16	0.23	0.16
MP3 Bol van Heist	0.15	0.21	0.15
MP4 Scheur Wielingen	0.14	0.20	0.14
Vlakte van de Raan	0.18	0.22	0.13
Cadzand	0.16	0.22	0.15
Westkapelle	0.13	0.20	0.15
Vlissingen	0.11	0.19	0.16
Breskens	0.10	0.19	0.17
Borssele	0.10	0.20	0.18
Terneuzen	0.09	0.20	0.18
Overloop Hansweert	0.05	0.19	0.18
Hansweert	0.05	0.19	0.19
Walsoorden	0.04	0.20	0.19
Baalhoek	0.05	0.21	0.20
Bath	0.08	0.22	0.21
Total	0.11	0.20	0.16

Table 162. Statistical parameters for the water level time series during storm (Eastern Scheldt)

Station	Complete Time Series		
	BIAS TS	RMSE TS	RMSE_0 TS
	[m]	[m]	[m]
Oosterschelde 14	0.13	0.21	0.16
Oosterschelde 11	0.18	0.23	0.14
Oosterschelde 4	0.12	0.21	0.17
Roompot buiten	0.14	0.21	0.16
Roompot binnen*	0.24	0.43	0.35
Sluis Kats*	0.22	0.43	0.37
Stavenisse*	0.21	0.42	0.36
Krammersluis*	0.20	0.44	0.39
Yerseke*	0.20	0.42	0.37
Bergsediepsluis*	0.22	0.46	0.40
Marollegat*	0.20	0.45	0.40
Total*	0.19	0.37	0.32

*big differences because the barrier in the Eastern Scheldt was closed during the Sinterklaasstorm but it is open in the model

Table 163. Statistical parameters for the water level time series during storm (Lower Sea Scheldt)

Station	Complete Time Series		
	BIAS TS	RMSE TS	RMSE_0 TS
	[m]	[m]	[m]
Zandvliet	0.11	0.24	0.21
Prosperpolder	0.08	0.23	0.21
Liefkenshoek	0.08	0.24	0.23
Kallosluis	0.08	0.25	0.23
Antwerpen	0.07	0.26	0.25
Hemiksem	0.12	0.27	0.24
Total	0.09	0.25	0.23

Table 164. Statistical parameters for the water level time series during storm (Upper Sea Scheldt)

Station	Complete Time Series		
	BIAS TS	RMSE TS	RMSE_0 TS
	[m]	[m]	[m]
Schelle	0.05	0.25	0.24
Temse	0.06	0.24	0.23
Tielrode	0.10	0.25	0.23
StAmands	0.08	0.24	0.23
Dendermonde	0.02	0.20	0.20
Schoonaarde	0.00	0.17	0.17
Wetteren	-0.04	0.19	0.19
Melle	-0.06	0.23	0.22
Total	0.03	0.22	0.21

Table 165. Statistical parameters for the water level time series during storm (Rupel basin and Durme)

Station	Complete Time Series		
	BIAS TS	RMSE TS	RMSE_0 TS
	[m]	[m]	[m]
Boom	0.06	0.25	0.24
Walem	0.05	0.23	0.23
Duffel-sluis	0.00	0.21	0.21
Lier Molbrug	0.02	0.17	0.17
Lier Maasfort	-0.11	0.17	0.13
Emblem	-0.08	0.14	0.12
Kessel	-0.11	0.16	0.12
Mechelen lock	0.10	0.24	0.22
Hombeek	0.11	0.27	0.24
Waasmunster*			
Total	0.00	0.21	0.19

*low waters at Waasmunster are not accurate in the model probably because of differences between the measured and modeled bathymetry

Table 166. Statistical parameters for high waters during storm (North sea and Western Scheldt)

Station	HW					
	BIAS HW	RMSE HW	RMSE_0 HW	BIAS HW	RMSE HW	RMSE_0 HW
	[m]	[m]	[m]	[min]	[min]	[min]
Nieuwpoort	0.05	0.13	0.12	8	23	21
Oostende	0.08	0.14	0.12	10	28	26
Zeebrugge	-0.02	0.10	0.10	-5	18	17
MP0 Wandelaar	0.11	0.14	0.08	-1	18	18
MP1 A2B boei	0.05	0.09	0.08	-3	19	19
MP2 Appelzak	0.03	0.11	0.11	0	18	18
MP3 Bol van Heist	0.08	0.13	0.10	-5	14	13
MP4 Scheur Wielingen	0.06	0.12	0.11	4	20	20
Vlakte van de Raan	0.07	0.12	0.10	0	9	9
Cadzand	0.02	0.11	0.11	6	21	20
Westkapelle	0.01	0.11	0.11	10	28	26
Vlissingen	-0.02	0.13	0.13	1	17	17
Breskens	-0.05	0.13	0.12	-1	14	14
Borssele	-0.04	0.14	0.14	2	14	14
Terneuzen	-0.03	0.15	0.15	2	19	18
Overloop Hansweert	-0.05	0.13	0.12	-7	16	14
Hansweert	-0.03	0.12	0.12	-4	14	13
Walsoorden	-0.07	0.13	0.12	-1	15	15
Baalhoek	-0.05	0.15	0.14	-1	12	12
Bath	-0.03	0.17	0.16	1	9	9
Total	0.01	0.13	0.12	1	18	17

Table 167. Statistical parameters for high waters during storm (Eastern Scheldt)

Station	HW					
	BIAS HW	RMSE HW	RMSE_0 HW	BIAS HW	RMSE HW	RMSE_0 HW
	[m]	[m]	[m]	[min]	[min]	[min]
Oosterschelde 14	-0.01	0.14	0.14	-2	25	25
Oosterschelde 11	0.01	0.12	0.12	6	24	23
Oosterschelde 4	-0.09	0.16	0.13	23	37	28
Roompot buiten	0.03	0.13	0.12	1	29	29
Roompot binnen*	0.30	0.65	0.57	-8	16	15
Sluis Kats*	0.34	0.78	0.71	-28	56	48
Stavenisse*	0.36	0.75	0.65	-15	43	41
Krammersluis*	0.41	0.76	0.64	-13	45	42
Yerseke*	0.08	0.13	0.10	1	11	11
Bergsediepsluis*	0.37	0.83	0.74	-12	37	35
Marollegat*	0.35	0.80	0.72	-15	38	34
Total*	0.19	0.57	0.50	-5	35	32

*big differences because the barrier in the Eastern Scheldt was closed during the Sinterklaasstorm but it is open in the model

Table 168. Statistical parameters for high waters during storm (Lower Sea Scheldt)

Station	HW					
	BIAS HW	RMSE HW	RMSE_0 HW	BIAS HW	RMSE HW	RMSE_0 HW
	[m]	[m]	[m]	[min]	[min]	[min]
Zandvliet	0.03	0.18	0.17	0	8	8
Prosperpolder	-0.02	0.17	0.17	-1	7	6
Liefkenshoek	-0.02	0.18	0.18	0	7	7
Kallosluis	-0.01	0.19	0.19	3	6	6
Antwerpen	0.01	0.19	0.19	7	10	8
Hemiksem	0.02	0.15	0.15	-6	8	5
Total	0.00	0.18	0.17	0	8	7

Table 169. Statistical parameters for high waters during storm (Upper Sea Scheldt)

Station	HW					
	BIAS HW	RMSE HW	RMSE_0 HW	BIAS HW	RMSE HW	RMSE_0 HW
	[m]	[m]	[m]	[min]	[min]	[min]
Schelle	-0.02	0.15	0.15	0	12	12
Temse	-0.02	0.14	0.14	-4	9	8
Tielrode	-0.02	0.15	0.14	-2	7	7
StAmands	0.00	0.14	0.14	-4	8	7
Dendermonde	-0.08	0.17	0.15	-4	8	7
Schoonaarde	-0.05	0.16	0.15	-7	12	9
Wetteren	-0.05	0.15	0.14	-6	14	13
Melle	-0.01	0.14	0.14	-4	12	11
Total	-0.03	0.15	0.15	-4	11	10

Table 170. Statistical parameters for high waters during storm (Rupel basin and Durme)

Station	HW					
	BIAS HW	RMSE HW	RMSE_0 HW	BIAS HW	RMSE HW	RMSE_0 HW
	[m]	[m]	[m]	[min]	[min]	[min]
Boom	-0.03	0.16	0.15	1	11	11
Walem	-0.02	0.15	0.15	0	9	9
Duffel-sluis	0.07	0.17	0.15	-13	14	7
Lier Molbrug	-0.17	0.20	0.12	-6	12	10
Lier Maasfort	-0.19	0.23	0.13	1	13	13
Emblem	-0.04	0.10	0.09	-4	9	8
Kessel	0.08	0.15	0.14	-5	7	5
Mechelen lock	0.00	0.14	0.14	3	8	7
Hombeek	0.11	0.19	0.15	-1	9	9
Waasmunster	-0.43	0.45	0.14	-9	18	15
Total	-0.06	0.21	0.14	-3	12	10

Table 171. Statistical parameters for low waters during storm (North sea and Western Scheldt)

Station	LW					
	BIAS LW	RMSE LW	RMSE_0 LW	BIAS LW	RMSE LW	RMSE_0 LW
	[m]	[m]	[m]	[min]	[min]	[min]
Nieuwpoort	0.27	0.30	0.13	-6	15	14
Oostende	0.19	0.24	0.15	-1	12	12
Zeebrugge	0.21	0.25	0.14	-4	8	7
MP0 Wandelaar	0.24	0.27	0.13	-9	16	14
MP1 A2B boei	0.20	0.24	0.13	-6	10	8
MP2 Appelzak	0.31	0.34	0.14	-2	9	9
MP3 Bol van Heist	0.26	0.29	0.13	-10	14	9
MP4 Scheur Wielingen	0.25	0.29	0.14	-6	10	8
Vlakte van de Raan	0.26	0.28	0.12	-7	14	12
Cadzand	0.30	0.33	0.13	-9	12	7
Westkapelle	0.22	0.25	0.13	-2	17	17
Vlissingen	0.21	0.26	0.14	-10	14	10
Breskens	0.21	0.25	0.14	-9	15	12
Borssele	0.22	0.26	0.14	-8	13	11
Terneuzen	0.21	0.25	0.15	-12	15	8
Overloop Hansweert	0.12	0.19	0.15	-8	12	9
Hansweert	0.16	0.22	0.15	-7	12	9
Walsoorden	0.14	0.20	0.14	-11	15	10
Baalhoek	0.13	0.20	0.15	-11	17	13
Bath	0.19	0.25	0.16	-9	15	12
Total	0.21	0.26	0.14	-7	13	11

Table 172. Statistical parameters for low waters during storm (Eastern Scheldt)

Station	LW					
	BIAS LW	RMSE LW	RMSE_0 LW	BIAS LW	RMSE LW	RMSE_0 LW
	[m]	[m]	[m]	[min]	[min]	[min]
Oosterschelde 14	0.26	0.29	0.14	-14	15	6
Oosterschelde 11	0.30	0.33	0.12	-11	15	11
Oosterschelde 4	0.22	0.28	0.18	9	32	30
Roompot buiten	0.23	0.28	0.15	-12	18	13
Roompot binnen	0.20	0.24	0.14	17	21	12
Sluis Kats	0.24	0.30	0.18	7	27	26
Stavenisse	0.25	0.30	0.16	19	30	23
Krammersluis	0.30	0.33	0.15	16	40	37
Yerseke	0.33	0.35	0.12	4	15	15
Bergsediepsluis	0.29	0.33	0.17	2	12	12
Marollegat	0.29	0.34	0.18	-3	14	13
Total	0.26	0.31	0.16	3	23	20

Table 173. Statistical parameters for low waters during storm (Lower Sea Scheldt)

Station	LW					
	BIAS LW	RMSE LW	RMSE_0 LW	BIAS LW	RMSE LW	RMSE_0 LW
	[m]	[m]	[m]	[min]	[min]	[min]
Zandvliet	0.18	0.24	0.16	-10	16	12
Prosperpolder	0.16	0.22	0.16	-9	14	11
Liefkenshoek	0.16	0.23	0.16	-8	13	9
Kallosluis	0.15	0.22	0.17	-7	11	8
Antwerpen	0.12	0.21	0.17	-8	11	7
Hemiksem	0.19	0.24	0.16	-11	14	9
Total	0.16	0.23	0.16	-9	13	10

Table 174. Statistical parameters for low waters during storm (Upper Sea Scheldt)

Station	LW					
	BIAS LW	RMSE LW	RMSE_0 LW	BIAS LW	RMSE LW	RMSE_0 LW
	[m]	[m]	[m]	[min]	[min]	[min]
Schelle	0.11	0.18	0.15	-14	17	11
Temse	0.10	0.17	0.14	-10	15	11
Tielrode	0.16	0.19	0.11	-7	14	12
StAmands	0.11	0.15	0.10	-10	14	9
Dendermonde	0.07	0.09	0.06	-11	14	9
Schoonaarde	0.04	0.07	0.06	-16	20	13
Wetteren	0.02	0.09	0.09	-13	21	16
Melle	-0.05	0.19	0.18	-10	29	27
Total	0.07	0.15	0.12	-11	19	15

Table 175. Statistical parameters for low waters during storm (Rupel basin and Durme)

Station	LW					
	BIAS LW	RMSE LW	RMSE_0 LW	BIAS LW	RMSE LW	RMSE_0 LW
	[m]	[m]	[m]	[min]	[min]	[min]
Boom	0.09	0.17	0.14	-10	14	10
Walem	0.05	0.13	0.12	-9	15	13
Duffel-sluis	0.00	0.12	0.12	-10	15	12
Lier Molbrug	0.08	0.10	0.06	-5	19	19
Lier Maasfort	-0.17	0.18	0.07	-8	19	17
Emblem	-0.13	0.15	0.06	-7	18	17
Kessel	-0.10	0.14	0.09	4	15	15
Mechelen lock	0.29	0.31	0.11	-3	13	12
Hombeek	0.15	0.16	0.05	36	50	35
Waasmunster*						
Total	0.02	0.17	0.10	-3	21	17

* low waters at Waasmunster are not accurate in the model probably because of differences between the measured and modeled bathymetry

Table 176. Harmonic analysis: Amplitude M2 during storm (North sea and Western Scheldt)

Amplitude M2	Measurement		Scaldis_039_1	
WL Station	Value	Error	Value	Error
Nieuwpoort	2.24	0.06	2.20	0.05
Oostende	2.06	0.06	2.06	0.06
Zeebrugge	1.89	0.06	1.84	0.06
MP0 Wandelaar	1.83	0.06	1.81	0.05
MP1 A2B boei	1.88	0.06	1.86	0.06
MP2 Appelzak	1.88	0.06	1.82	0.06
MP3 Bol van Heist	1.84	0.06	1.82	0.06
MP4 Scheur Wielingen	1.81	0.06	1.78	0.06
Vlakte van de Raan	1.67	0.06	1.65	0.06
Cadzand	1.89	0.07	1.82	0.06
Westkapelle	1.72	0.07	1.71	0.05
Vlissingen	1.94	0.07	1.88	0.06
Breskens	1.94	0.05	1.87	0.06
Borssele	2.03	0.06	1.95	0.06
Terneuzen	2.07	0.07	2.01	0.07
Overloop Hansweert	2.14	0.07	2.09	0.06
Hansweert	2.19	0.06	2.13	0.06
Walsoorden	2.23	0.08	2.16	0.06
Baalhoek	2.29	0.06	2.22	0.06
Bath	2.35	0.07	2.25	0.06

Table 177. Harmonic analysis: Amplitude M2 during storm (Eastern Scheldt)

Amplitude M2	Measurement		Scaldis_039_1	
WL Station	Value	Error	Value	Error
Oosterschelde 14	1.28	0.06	1.26	0.06
Oosterschelde 11	1.46	0.06	1.41	0.06
Oosterschelde 4	1.42	0.06	1.39	0.06
Roompot buiten	1.46	0.06	1.45	0.05
Roompot binnen	1.18	0.05	1.24	0.06
Sluis Kats	1.35	0.06	1.41	0.06
Stavenisse	1.35	0.05	1.40	0.06
Krammersluis	1.39	0.05	1.44	0.06
Yerseke	1.44	0.06	1.49	0.06
Bergsediepsluis	1.47	0.05	1.52	0.06
Marollegat	1.49	0.06	1.54	0.06

Table 178. Harmonic analysis: Amplitude M2 during storm (Lower Sea Scheldt)

Amplitude M2	Measurement		Scaldis_039_1	
WL Station	Value	Error	Value	Error
Zandvliet	2.37	0.08	2.30	0.06
Prosperpolder	2.36	0.08	2.28	0.06
Liefkenshoek	2.43	0.08	2.34	0.05
Kallosluis	2.42	0.07	2.37	0.06
Antwerpen	2.46	0.07	2.40	0.06
Hemiksem	2.50	0.07	2.41	0.07

Table 179. Harmonic analysis: Amplitude M2 during storm (Upper Sea Scheldt)

Amplitude M2	Measurement		Scaldis_039_1	
WL Station	Value	Error	Value	Error
Schelle	2.47	0.07	2.40	0.06
Temse	2.43	0.08	2.37	0.06
Tielrode	2.41	0.07	2.34	0.06
StAmands	2.27	0.07	2.22	0.06
Dendermonde	1.80	0.07	1.74	0.06
Schoonaarde	1.41	0.07	1.39	0.05
Wetteren	1.22	0.06	1.22	0.05
Melle	1.18	0.06	1.20	0.05

Table 180. Harmonic analysis: Amplitude M2 during storm (Rupel basin)

Amplitude M2	Measurement		Scaldis_039_1	
WL Station	Value	Error	Value	Error
Boom	2.42	0.08	2.35	0.06
Walem	2.29	0.08	2.24	0.06
Duffel-sluis	1.83	0.06	1.82	0.06
Lier Molbrug	1.23	0.05	1.14	0.05
Lier Maasfort	0.93	0.05	0.98	0.05
Emblem	0.79	0.05	0.85	0.04
Kessel	0.64	0.04	0.65	0.04
Mechelen lock	2.06	0.07	1.93	0.06
Hombeek	1.76	0.06	1.62	0.05

Table 181. Harmonic analysis: Phase M2 during storm (North sea and Western Scheldt)

Phase M2	Measurement		Scaldis_039_1	
WL Station	Value	Error	Value	Error
Nieuwpoort	22	1	23	1
Oostende	26	2	27	2
Zeebrugge	35	2	35	2
MP0 Wandelaar	31	2	31	2
MP1 A2B boei	33	2	33	2
MP2 Appelzak	38	2	39	2
MP3 Bol van Heist	36	2	36	2
MP4 Scheur Wielingen	41	2	41	2
Vlakte van de Raan	38	2	38	2
Cadzand	42	2	42	2
Westkapelle	46	2	47	2
Vlissingen	52	2	53	2
Breskens	50	2	50	2
Borssele	59	2	59	2
Terneuzen	64	2	63	1
Overloop Hansweert	71	2	71	2
Hansweert	74	2	74	1
Walsoorden	77	2	77	2
Baalhoek	81	2	80	2
Bath	86	2	86	2

Table 182. Harmonic analysis: Phase M2 during storm (Eastern Scheldt)

Phase M2	Measurement		Scaldis_039_1	
WL Station	Value	Error	Value	Error
Oosterschelde 14	56	3	56	3
Oosterschelde 11	49	2	49	3
Oosterschelde 4	57	3	60	2
Roompot buiten	56	3	56	3
Roompot binnen	82	2	83	3
Sluis Kats	90	2	88	2
Stavenisse	89	2	88	2
Krammersluis	90	2	89	2
Yerseke	92	2	91	2
Bergsediepsluis	93	2	92	2
Marollegat	95	2	93	2

Table 183. Harmonic analysis: Phase M2 during storm (Lower Sea Scheldt)

Phase M2	Measurement		Scaldis_039_1	
WL Station	Value	Error	Value	Error
Zandvliet	88	2	88	1
Prosperpolder	88	2	87	2
Liefkenshoek	90	2	89	2
Kallosluis	92	2	92	2
Antwerpen	99	2	97	1
Hemiksem	109	2	107	2

Table 184. Harmonic analysis: Phase M2 during storm (Upper Sea Scheldt)

Phase M2	Measurement		Scaldis_039_1	
WL Station	Value	Error	Value	Error
Schelle	113	2	110	2
Temse	118	2	116	2
Tielrode	122	2	120	2
StAmands	128	2	126	2
Dendermonde	148	2	146	2
Schoonaarde	171	2	169	2
Wetteren	198	3	195	3
Melle	211	3	206	3

Table 185. Harmonic analysis: Phase M2 during storm (Rupel basin)

Phase M2	Measurement		Scaldis_039_1	
WL Station	Value	Error	Value	Error
Boom	120.49	1.63	118.22	1.40
Walem	127.09	1.93	125.42	1.29
Duffel-sluis	144.27	2.37	140.25	1.94
Lier Molbrug	158.82	2.78	161.82	2.49
Lier Maasfort	172.54	3.06	173.96	3.00
Emblem	185.80	3.76	185.19	3.14
Kessel	199.51	4.09	200.13	3.06
Mechelen lock	135.67	1.86	137.54	1.55
Hombeek	140.56	1.81	146.21	1.91

Table 186. Harmonic analysis: Amplitude M4 during storm (North sea and Western Scheldt)

Amplitude M4	Measurement		Scaldis_039_1	
WL Station	Value	Error	Value	Error
Nieuwpoort	0.19	0.06	0.17	0.05
Oostende	0.15	0.06	0.17	0.05
Zeebrugge	0.17	0.07	0.20	0.05
MP0 Wandelaar	0.16	0.05	0.18	0.06
MP1 A2B boei	0.15	0.06	0.19	0.05
MP2 Appelzak	0.19	0.06	0.21	0.06
MP3 Bol van Heist	0.17	0.06	0.20	0.05
MP4 Scheur Wielingen	0.19	0.06	0.21	0.05
Vlakte van de Raan	0.21	0.05	0.21	0.06
Cadzand	0.20	0.06	0.21	0.05
Westkapelle	0.22	0.06	0.22	0.05
Vlissingen	0.22	0.07	0.23	0.06
Breskens	0.23	0.06	0.23	0.06
Borssele	0.20	0.06	0.22	0.06
Terneuzen	0.20	0.07	0.21	0.05
Overloop Hansweert	0.21	0.06	0.22	0.06
Hansweert	0.18	0.07	0.20	0.06
Walsoorden	0.20	0.07	0.21	0.06
Baalhoek	0.20	0.07	0.21	0.06
Bath	0.18	0.07	0.18	0.06

Table 187. Harmonic analysis: Amplitude M4 during storm (Eastern Scheldt)

Amplitude M4	Measurement		Scaldis_039_1	
WL Station	Value	Error	Value	Error
Oosterschelde 14	0.23	0.06	0.25	0.05
Oosterschelde 11	0.23	0.06	0.23	0.06
Oosterschelde 4	0.23	0.07	0.23	0.06
Roompot buiten	0.21	0.06	0.24	0.06
Roompot binnen	0.09	0.05	0.10	0.06
Sluis Kats	0.13	0.05	0.15	0.06
Stavenisse	0.13	0.05	0.15	0.06
Krammersluis	0.15	0.05	0.18	0.05
Yerseke	0.17	0.05	0.20	0.06
Bergsediepsluis	0.17	0.06	0.20	0.05
Marollegat	0.17	0.06	0.20	0.06

Table 188. Harmonic analysis: Amplitude M4 during storm (Lower Sea Scheldt)

Amplitude M4	Measurement		Scaldis_039_1	
WL Station	Value	Error	Value	Error
Zandvliet	0.18	0.07	0.18	0.06
Prosperpolder	0.19	0.07	0.18	0.06
Liefkenshoek	0.18	0.08	0.18	0.05
Kallosluis	0.20	0.07	0.18	0.06
Antwerpen	0.19	0.07	0.17	0.06
Hemiksem	0.18	0.08	0.15	0.07

Table 189. Harmonic analysis: Amplitude M4 during storm (Upper Sea Scheldt)

Amplitude M4	Measurement		Scaldis_039_1	
WL Station	Value	Error	Value	Error
Schelle	0.17	0.08	0.15	0.06
Temse	0.21	0.07	0.17	0.07
Tielrode	0.24	0.08	0.19	0.06
StAmands	0.29	0.07	0.24	0.06
Dendermonde	0.30	0.07	0.24	0.06
Schoonaarde	0.27	0.06	0.24	0.05
Wetteren	0.22	0.06	0.21	0.05
Melle	0.22	0.06	0.23	0.06

Table 190. Harmonic analysis: Amplitude M4 during storm (Rupel basin)

Amplitude M4	Measurement		Scaldis_039_1	
WL Station	Value	Error	Value	Error
Boom	0.22	0.07	0.17	0.07
Walem	0.26	0.07	0.20	0.06
Duffel-sluis	0.36	0.06	0.37	0.06
Lier Molbrug	0.37	0.05	0.34	0.04
Lier Maasfort	0.31	0.05	0.28	0.05
Emblem	0.27	0.04	0.26	0.04
Kessel	0.20	0.04	0.22	0.04
Mechelen lock	0.33	0.07	0.33	0.06
Hombeek	0.42	0.05	0.43	0.05

Table 191. Harmonic analysis: Phase M4 during storm (North sea and Western Scheldt)

Phase M4	Measurement		Scaldis_039_1	
WL Station	Value	Error	Value	Error
Nieuwpoort	14	17	25	17
Oostende	42	23	52	18
Zeebrugge	93	19	93	17
MP0 Wandelaar	74	22	80	18
MP1 A2B boei	76	20	82	16
MP2 Appelzak	96	19	95	13
MP3 Bol van Heist	93	20	92	17
MP4 Scheur Wielingen	101	17	100	15
Vlakte van de Raan	96	16	98	14
Cadzand	99	18	100	15
Westkapelle	101	17	103	14
Vlissingen	123	15	128	14
Breskens	116	14	120	15
Borsselle	136	19	144	15
Terneuzen	141	21	146	16
Overloop Hansweert	165	16	173	15
Hansweert	167	19	177	16
Walsoorden	175	17	185	14
Baalhoek	186	21	191	16
Bath	189	23	196	18

Table 192. Harmonic analysis: Phase M4 during storm (Eastern Scheldt)

Phase M4	Measurement		Scaldis_039_1	
WL Station	Value	Error	Value	Error
Oosterschelde 14	127	16	125	13
Oosterschelde 11	119	16	118	15
Oosterschelde 4	128	17	130	14
Roompot buiten	130	17	127	14
Roompot binnen	163	32	163	30
Sluis Kats	200	26	187	22
Stavenisse	199	25	186	20
Krammersluis	202	21	190	18
Yerseke	214	16	196	18
Bergsediepsluis	218	18	198	18
Marollegat	223	19	200	17

Table 193. Harmonic analysis: Phase M4 during storm (Lower Sea Scheldt)

Phase M4	Measurement		Scaldis_039_1	
WL Station	Value	Error	Value	Error
Zandvliet	192	21	198	17
Prosperpolder	191	23	197	19
Liefkenshoek	195	23	201	17
Kallosluis	194	21	204	19
Antwerpen	200	25	212	19
Hemiksem	211	24	223	21

Table 194. Harmonic analysis: Phase M4 during storm (Upper Sea Scheldt)

Phase M4	Measurement		Scaldis_039_1	
WL Station	Value	Error	Value	Error
Schelle	213	26	225	24
Temse	212	20	218	19
Tielrode	214	17	217	19
StAmands	221	13	221	15
Dendermonde	245	11	243	14
Schoonaarde	278	14	276	13
Wetteren	325	15	325	14
Melle	358	16	349	14

Table 195. Harmonic analysis: Phase M4 during storm (Rupel basin)

Phase M4	Measurement		Scaldis_039_1	
WL Station	Value	Error	Value	Error
Boom	211.90	20.30	215.63	22.85
Walem	218.03	16.50	220.60	15.47
Duffel-sluis	245.29	10.25	238.79	7.67
Lier Molbrug	276.76	8.07	270.41	8.05
Lier Maasfort	296.90	8.69	291.33	9.19
Emblem	320.85	9.30	315.07	10.06
Kessel	344.10	11.77	344.48	11.04
Mechelen lock	239.41	10.98	240.93	11.10
Hombeek	267.89	8.10	260.53	7.28

Table 196. Harmonic analysis: Amplitude M6 during storm (North sea and Western Scheldt)

Amplitude M6	Measurement		Scaldis_039_1	
WL Station	Value	Error	Value	Error
Nieuwpoort	0.13	0.05	0.13	0.04
Oostende	0.15	0.05	0.15	0.06
Zeebrugge	0.18	0.06	0.18	0.05
MP0 Wandelaar	0.16	0.05	0.16	0.05
MP1 A2B boei	0.17	0.06	0.17	0.05
MP2 Appelzak	0.20	0.06	0.19	0.05
MP3 Bol van Heist	0.18	0.06	0.18	0.06
MP4 Scheur Wielingen	0.19	0.06	0.18	0.05
Vlakte van de Raan	0.16	0.06	0.15	0.05
Cadzand	0.20	0.06	0.19	0.05
Westkapelle	0.18	0.06	0.16	0.05
Vlissingen	0.19	0.06	0.18	0.05
Breskens	0.19	0.06	0.18	0.05
Borssele	0.19	0.06	0.18	0.06
Terneuzen	0.20	0.06	0.19	0.05
Overloop Hansweert	0.19	0.06	0.18	0.06
Hansweert	0.20	0.06	0.19	0.06
Walsoorden	0.21	0.07	0.19	0.06
Baalhoek	0.22	0.06	0.22	0.06
Bath	0.25	0.07	0.25	0.06

Table 197. Harmonic analysis: Amplitude M6 during storm (Eastern Scheldt)

Amplitude M6	Measurement		Scaldis_039_1	
WL Station	Value	Error	Value	Error
Oosterschelde 14	0.13	0.07	0.11	0.05
Oosterschelde 11	0.15	0.06	0.13	0.05
Oosterschelde 4	0.13	0.06	0.10	0.05
Roompot buiten	0.13	0.06	0.12	0.05
Roompot binnen	0.06	0.05	0.04	0.05
Sluis Kats	0.06	0.05	0.05	0.05
Stavenisse	0.06	0.05	0.04	0.05
Krammersluis	0.07	0.05	0.06	0.05
Yerseke	0.11	0.05	0.11	0.05
Bergsediepsluis	0.13	0.05	0.12	0.05
Marollegat	0.15	0.06	0.15	0.06

Table 198. Harmonic analysis: Amplitude M6 during storm (Lower Sea Scheldt)

Amplitude M6	Measurement		Scaldis_039_1	
WL Station	Value	Error	Value	Error
Zandvliet	0.27	0.06	0.27	0.06
Prosperpolder	0.27	0.07	0.26	0.06
Liefkenshoek	0.28	0.07	0.28	0.06
Kallosluis	0.27	0.07	0.29	0.07
Antwerpen	0.26	0.08	0.28	0.05
Hemiksem	0.26	0.07	0.26	0.06

Table 199. Harmonic analysis: Amplitude M6 during storm (Upper Sea Scheldt)

Amplitude M6	Measurement		Scaldis_039_1	
WL Station	Value	Error	Value	Error
Schelle	0.26	0.07	0.27	0.06
Temse	0.26	0.08	0.27	0.05
Tielrode	0.27	0.07	0.27	0.07
StAmands	0.25	0.07	0.26	0.06
Dendermonde	0.18	0.06	0.19	0.06
Schoonaarde	0.13	0.07	0.13	0.06
Wetteren	0.06	0.05	0.07	0.05
Melle	0.06	0.06	0.07	0.05

Table 200. Harmonic analysis: Amplitude M6 during storm (Rupel basin)

Amplitude M6	Measurement		Scaldis_039_1	
WL Station	Value	Error	Value	Error
Boom	0.24	0.07	0.25	0.05
Walem	0.21	0.07	0.23	0.06
Duffel-sluis	0.14	0.06	0.15	0.06
Lier Molbrug	0.14	0.05	0.12	0.05
Lier Maasfort	0.13	0.04	0.11	0.04
Emblem	0.11	0.04	0.10	0.04
Kessel	0.09	0.04	0.09	0.04
Mechelen lock	0.14	0.06	0.13	0.05
Hombeek	0.19	0.05	0.18	0.05

Table 201. Harmonic analysis: Phase M6 during storm (North sea and Western Scheldt)

Phase M6	Measurement		Scaldis_039_1	
WL Station	Value	Error	Value	Error
Nieuwpoort	352	24	334	21
Oostende	9	22	353	19
Zeebrugge	39	17	23	18
MP0 Wandelaar	28	22	13	19
MP1 A2B boei	32	18	16	18
MP2 Appelzak	48	18	35	16
MP3 Bol van Heist	41	18	25	18
MP4 Scheur Wielingen	53	17	40	16
Vlakte van de Raan	51	17	32	21
Cadzand	57	18	45	17
Westkapelle	65	19	52	19
Vlissingen	91	19	78	18
Breskens	87	20	74	18
Borssele	112	19	101	17
Terneuzen	132	20	118	17
Overloop Hansweert	172	17	159	16
Hansweert	178	19	170	15
Walsoorden	196	19	188	17
Baalhoek	214	16	205	13
Bath	229	16	224	15

Table 202. Harmonic analysis: Phase M6 during storm (Eastern Scheldt)

Phase M6	Measurement		Scaldis_039_1	
WL Station	Value	Error	Value	Error
Oosterschelde 14	82	27	64	26
Oosterschelde 11	68	20	48	22
Oosterschelde 4	79	28	58	30
Roompot buiten	73	29	56	27
Roompot binnen	100	45	91	84
Sluis Kats	207	47	208	65
Stavenisse	193	56	195	72
Krammersluis	196	42	202	55
Yerseke	233	25	232	26
Bergsediepsluis	237	25	235	23
Marollegat	243	21	239	22

Table 203. Harmonic analysis: Phase M6 during storm (Lower Sea Scheldt)

Phase M6	Measurement		Scaldis_039_1	
WL Station	Value	Error	Value	Error
Zandvliet	243	15	236	13
Prosperpolder	241	16	234	13
Liefkenshoek	252	15	245	11
Kallosluis	260	15	254	11
Antwerpen	287	17	278	12
Hemiksem	329	16	320	12

Table 204. Harmonic analysis: Phase M6 during storm (Upper Sea Scheldt)

Phase M6	Measurement		Scaldis_039_1	
WL Station	Value	Error	Value	Error
Schelle	340	14	329	12
Temse	359	17	351	13
Tielrode	11	16	5	13
StAmands	27	15	20	13
Dendermonde	66	21	64	17
Schoonaarde	96	26	99	22
Wetteren	141	60	157	42
Melle	206	57	195	46

Table 205. Harmonic analysis: Phase M6 during storm (Rupel basin)

Phase M6	Measurement		Scaldis_039_1	
WL Station	Value	Error	Value	Error
Boom	2.12	15.48	354.04	12.75
Walem	19.66	16.76	14.10	14.47
Duffel-sluis	43.65	27.42	33.37	21.19
Lier Molbrug	41.55	26.69	31.43	23.14
Lier Maasfort	63.85	19.91	52.40	22.14
Emblem	94.48	21.86	84.44	21.50
Kessel	123.52	23.82	123.97	25.03
Mechelen lock	30.08	25.77	30.15	25.45
Hombeek	20.98	20.60	23.79	14.28

Table 206. Harmonic analysis: Amplitude K1 during storm (North sea and Western Scheldt)

Amplitude K1	Measurement		Scaldis_039_1	
WL Station	Value	Error	Value	Error
Nieuwpoort	0.25	0.06	0.25	0.06
Oostende	0.25	0.07	0.26	0.06
Zeebrugge	0.27	0.07	0.28	0.06
MP0 Wandelaar	0.27	0.06	0.28	0.06
MP1 A2B boei	0.26	0.08	0.28	0.06
MP2 Appelzak	0.27	0.07	0.28	0.06
MP3 Bol van Heist	0.27	0.07	0.28	0.07
MP4 Scheur Wielingen	0.26	0.07	0.28	0.06
Vlakte van de Raan	0.27	0.08	0.29	0.06
Cadzand	0.26	0.06	0.28	0.06
Westkapelle	0.24	0.07	0.28	0.07
Vlissingen	0.26	0.07	0.29	0.06
Breskens	0.26	0.07	0.29	0.07
Borssele	0.26	0.08	0.29	0.07
Terneuzen	0.26	0.08	0.29	0.07
Overloop Hansweert	0.26	0.08	0.30	0.07
Hansweert	0.25	0.08	0.30	0.06
Walsoorden	0.25	0.08	0.30	0.06
Baalhoek	0.25	0.07	0.30	0.07
Bath	0.25	0.09	0.30	0.07

Table 207. Harmonic analysis: Amplitude K1 during storm (Eastern Scheldt)

Amplitude K1	Measurement		Scaldis_039_1	
WL Station	Value	Error	Value	Error
Oosterschelde 14	0.26	0.08	0.28	0.06
Oosterschelde 11	0.26	0.07	0.28	0.06
Oosterschelde 4	0.26	0.07	0.28	0.07
Roompot buiten	0.27	0.08	0.28	0.06
Roompot binnen	0.23	0.06	0.26	0.07
Sluis Kats	0.24	0.06	0.27	0.07
Stavenisse	0.24	0.06	0.27	0.06
Krammersluis	0.24	0.06	0.27	0.06
Yerseke	0.25	0.06	0.28	0.07
Bergsediepsluis	0.25	0.06	0.28	0.07
Marollegat	0.25	0.07	0.28	0.07

Table 208. Harmonic analysis: Amplitude K1 during storm (Lower Sea Scheldt)

Amplitude K1 WL Station	Measurement		Scaldis_039_1	
	Value	Error	Value	Error
Zandvliet	0.25	0.09	0.30	0.07
Prosperpolder	0.25	0.09	0.30	0.06
Liefkenshoek	0.26	0.08	0.31	0.07
Kallosluis	0.29	0.08	0.31	0.06
Antwerpen	0.27	0.09	0.31	0.08
Hemiksem	0.25	0.08	0.30	0.08

Table 209. Harmonic analysis: Amplitude K1 during storm (Upper Sea Scheldt)

Amplitude K1 WL Station	Measurement		Scaldis_039_1	
	Value	Error	Value	Error
Schelle	0.25	0.09	0.30	0.07
Temse	0.24	0.07	0.29	0.08
Tielrode	0.23	0.08	0.29	0.07
StAmands	0.22	0.08	0.27	0.07
Dendermonde	0.18	0.08	0.23	0.07
Schoonaarde	0.14	0.08	0.20	0.06
Wetteren	0.11	0.07	0.21	0.07
Melle	0.11	0.07	0.21	0.07

Table 210. Harmonic analysis: Amplitude K1 during storm (Rupel basin)

Amplitude K1 WL Station	Measurement		Scaldis_039_1	
	Value	Error	Value	Error
Boom	0.24	0.08	0.29	0.08
Walem	0.22	0.07	0.27	0.07
Duffel-sluis	0.18	0.07	0.22	0.07
Lier Molbrug	0.11	0.06	0.15	0.05
Lier Maasfort	0.10	0.06	0.13	0.06
Emblem	0.09	0.05	0.12	0.05
Kessel	0.07	0.05	0.11	0.05
Mechelen lock	0.18	0.08	0.22	0.06
Hombeek	0.15	0.07	0.19	0.05

Table 211. Harmonic analysis: Phase K1 during storm (North sea and Western Scheldt)

Phase K1	Measurement		Scaldis_039_1	
WL Station	Value	Error	Value	Error
Nieuwpoort	340	17	329	15
Oostende	338	14	328	13
Zeebrugge	338	15	329	12
MP0 Wandelaar	339	15	328	14
MP1 A2B boei	339	14	328	12
MP2 Appelzak	337	13	330	12
MP3 Bol van Heist	339	16	329	13
MP4 Scheur Wielingen	338	15	331	12
Vlakte van de Raan	340	15	328	12
Cadzand	337	15	331	14
Westkapelle	337	17	332	12
Vlissingen	342	17	337	13
Breskens	341	18	336	14
Borssele	345	16	341	13
Terneuzen	347	17	344	14
Overloop Hansweert	353	16	350	13
Hansweert	354	18	351	14
Walsoorden	356	19	354	14
Baalhoek	359	18	356	11
Bath	0	19	360	13

Table 212. Harmonic analysis: Phase K1 during storm (Eastern Scheldt)

Phase K1	Measurement		Scaldis_039_1	
WL Station	Value	Error	Value	Error
Oosterschelde 14	335	16	327	14
Oosterschelde 11	338	16	329	13
Oosterschelde 4	337	14	333	12
Roompot buiten	338	16	332	12
Roompot binnen	313	14	351	14
Sluis Kats	319	13	355	13
Stavenisse	315	14	354	15
Krammersluis	313	15	355	15
Yerseke	317	15	356	16
Bergsediepsluis	315	15	357	14
Marollegat	317	14	358	14

Table 213. Harmonic analysis: Phase K1 during storm (Lower Sea Scheldt)

Phase K1	Measurement		Scaldis_039_1	
WL Station	Value	Error	Value	Error
Zandvliet	2	21	2	12
Prosperpolder	2	20	1	12
Liefkenshoek	4	22	3	13
Kallosluis	5	18	4	12
Antwerpen	10	20	9	14
Hemiksem	18	21	16	13

Table 214. Harmonic analysis: Phase K1 during storm (Upper Sea Scheldt)

Phase K1	Measurement		Scaldis_039_1	
WL Station	Value	Error	Value	Error
Schelle	20	19	18	12
Temse	25	19	24	14
Tielrode	29	22	28	15
StAmands	35	21	33	17
Dendermonde	50	22	51	16
Schoonaarde	67	29	68	17
Wetteren	94	36	85	17
Melle	114	37	91	16

Table 215. Harmonic analysis: Phase K1 during storm (Rupel basin)

Phase K1	Measurement		Scaldis_039_1	
WL Station	Value	Error	Value	Error
Boom	26.41	23.23	25.22	14.09
Walem	31.77	20.81	31.75	14.95
Duffel-sluis	47.70	22.31	46.42	13.98
Lier Molbrug	60.43	30.10	66.47	22.51
Lier Maasfort	70.21	35.44	76.34	22.66
Emblem	77.17	31.37	84.92	24.60
Kessel	88.81	36.66	97.01	24.75
Mechelen lock	39.23	22.12	43.47	16.38
Hombeek	42.31	27.02	54.11	20.65

Table 216. Harmonic analysis: Z0 during storm (North sea and Western Scheldt)

Z0	Measurement	Scaldis_039_1
WL Station	Value	Value
Nieuwpoort	2.58	2.76
Oostende	2.67	2.77
Zeebrugge	2.72	2.79
MP0 Wandelaar	2.63	2.79
MP1 A2B boei	2.70	2.80
MP2 Appelzak	2.65	2.81
MP3 Bol van Heist	2.64	2.80
MP4 Scheur Wielingen	2.67	2.81
Vlakte van de Raan	2.63	2.81
Cadzand	2.66	2.82
Westkapelle	2.68	2.81
Vlissingen	2.71	2.82
Breskens	2.73	2.83
Borssele	2.79	2.88
Terneuzen	2.84	2.93
Overloop Hansweert	2.87	2.93
Hansweert	2.92	2.97
Walsoorden	2.92	2.97
Baalhoek	2.93	2.99
Bath	2.96	3.04

Table 217. Harmonic analysis: Z0 during storm (Eastern Scheldt)

Z0	Measurement	Scaldis_039_1
WL Station	Value	Value
Oosterschelde 14	2.75	2.88
Oosterschelde 11	2.66	2.84
Oosterschelde 4	2.74	2.87
Roompot buiten	2.72	2.86
Roompot binnen	2.66	2.91
Sluis Kats	2.70	2.92
Stavenisse	2.72	2.93
Krammersluis	2.74	2.94
Yerseke	2.71	2.92
Bergsediepsluis	2.72	2.94
Marollegat	2.73	2.93

Table 218. Harmonic analysis: Z0 during storm (Lower Sea Scheldt)

Z0	Measurement	Scaldis_039_1
WL Station	Value	Value
Zandvliet	2.94	3.06
Prosperpolder	2.96	3.04
Liefkenshoek	2.97	3.06
Kallosluis	3.00	3.08
Antwerpen	3.02	3.09
Hemiksem	3.03	3.15

Table 219. Harmonic analysis: Z0 during storm (Upper Sea Scheldt)

Z0	Measurement	Scaldis_039_1
WL Station	Value	Value
Schelle	3.13	3.18
Temse	3.19	3.25
Tielrode	3.18	3.28
StAmands	3.26	3.34
Dendermonde	3.52	3.54
Schoonaarde	3.70	3.70
Wetteren	3.83	3.79
Melle	3.90	3.84

Table 220. Harmonic analysis: Z0 during storm (Rupel basin)

Z0	Measurement	Scaldis_039_1
WL Station	Value	Value
Boom	3.22	3.28
Walem	3.33	3.38
Duffel-sluis	3.67	3.67
Lier Molbrug	4.08	4.11
Lier Maasfort	4.33	4.22
Emblem	4.44	4.36
Kessel	4.56	4.45
Mechelen lock	3.59	3.69
Hombeek	3.76	3.88

Table 221. Vector differences of model results vs. measurements during storm (North sea and Western Scheldt)

Vector differences of model results vs measurements	Scaldis_039_1
WL Station	Vector difference [m]
Nieuwpoort	0.36
Oostende	0.23
Zeebrugge	0.25
MP0 Wandelaar	0.31
MP1 A2B boei	0.27
MP2 Appelzak	0.32
MP3 Bol van Heist	0.30
MP4 Scheur Wielingen	0.28
Vlakte van de Raan	0.33
Cadzand	0.31
Westkapelle	0.27
Vlissingen	0.27
Breskens	0.26
Borssele	0.29
Terneuzen	0.26
Overloop Hansweert	0.22
Hansweert	0.23
Walsoorden	0.23
Baalhoek	0.23
Bath	0.26
Total vector difference of model results vs measurements	0.27

Table 222. Vector differences of model results vs. measurements during storm (Eastern Scheldt)

Vector differences of model results vs measurements	Scaldis_039_1
WL Station	Vector difference [m]
Oosterschelde 14	0.26
Oosterschelde 11	0.34
Oosterschelde 4	0.29
Roompot buiten	0.25
Roompot binnen	0.49
Sluis Kats	0.50
Stavenisse	0.49
Krammersluis	0.49
Yerseke	0.53
Bergsediepsluis	0.54
Marollegat	0.54
Total vector difference of model results vs measurements	0.43

Table 223. Vector differences of model results vs. measurements during storm (Lower Sea Scheldt)

Vector differences of model results vs measurements	Scaldis_039_1
WL Station	Vector difference [m]
Zandvliet	0.29
Prosperpolder	0.26
Liefkenshoek	0.29
Kallosluis	0.22
Antwerpen	0.29
Hemiksem	0.37
Total vector difference of model results vs measurements	0.29

Table 224. Vector differences of model results vs. measurements during storm (Upper Sea Scheldt)

Vector differences of model results vs measurements	Scaldis_039_1
WL Station	Vector difference [m]
Schelle	0.34
Temse	0.30
Tielrode	0.34
StAmands	0.32
Dendermonde	0.22
Schoonaarde	0.17
Wetteren	0.23
Melle	0.35
Total vector difference of model results vs measurements	0.28

Table 225. Vector differences of model results vs. measurements during storm (Rupel basin)

Vector differences of model results vs measurements	Scaldis_039_1
WL Station	Vector difference [m]
Boom	0.33
Walem	0.28
Duffel-sluis	0.25
Lier Molbrug	0.24
Lier Maasfort	0.28
Emblem	0.23
Kessel	0.17
Mechelen lock	0.31
Hombeek	0.46
Total vector difference of model results vs measurements	0.28

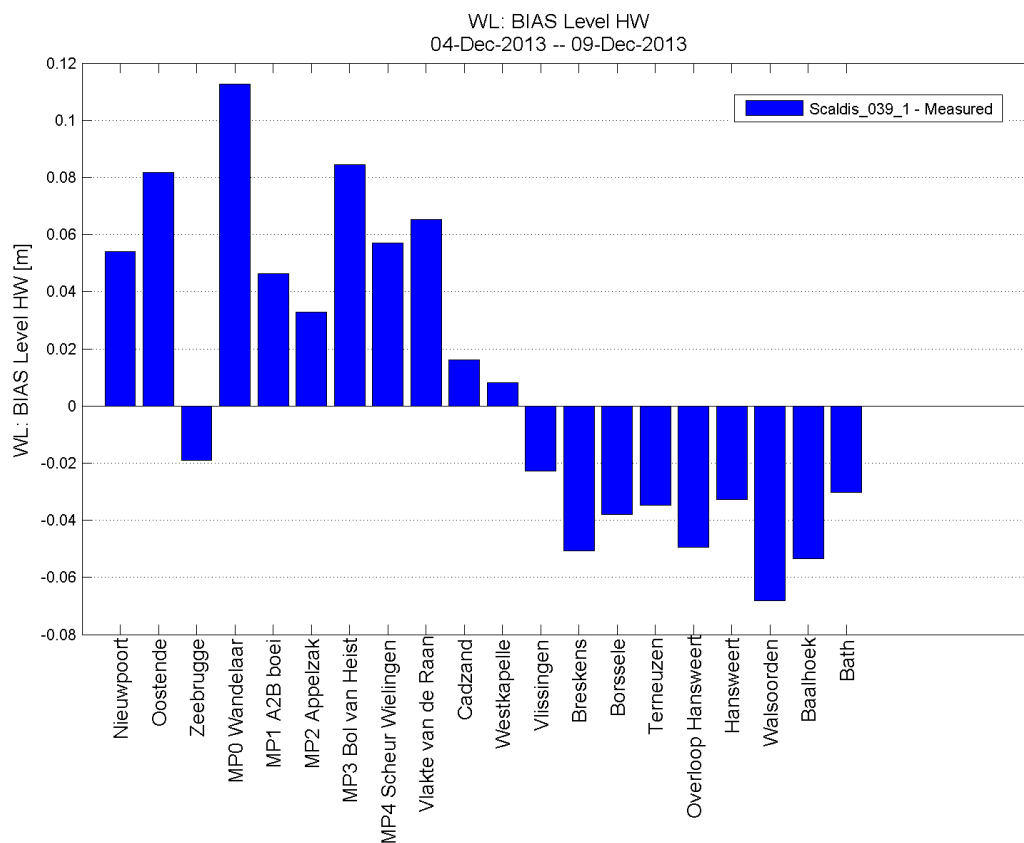


Figure 426 - Bias of high water magnitude (model – measurement) during storm in the North sea and Western Scheldt

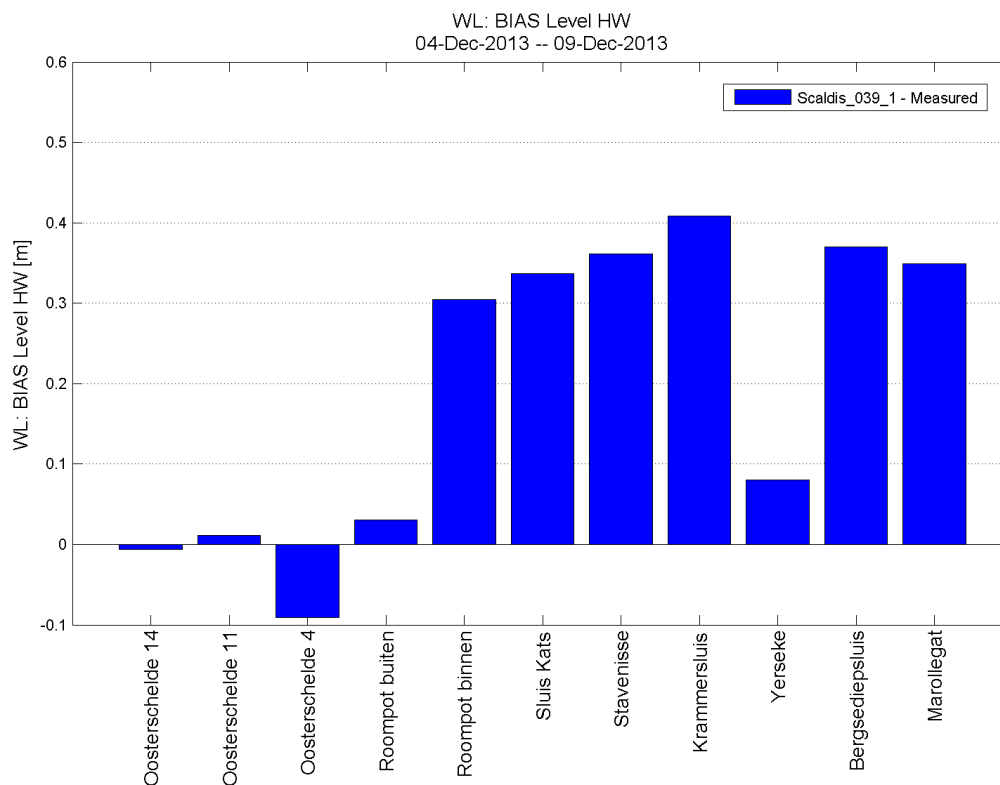


Figure 427 - Bias of high water magnitude (model – measurement) during storm in the Eastern Scheldt

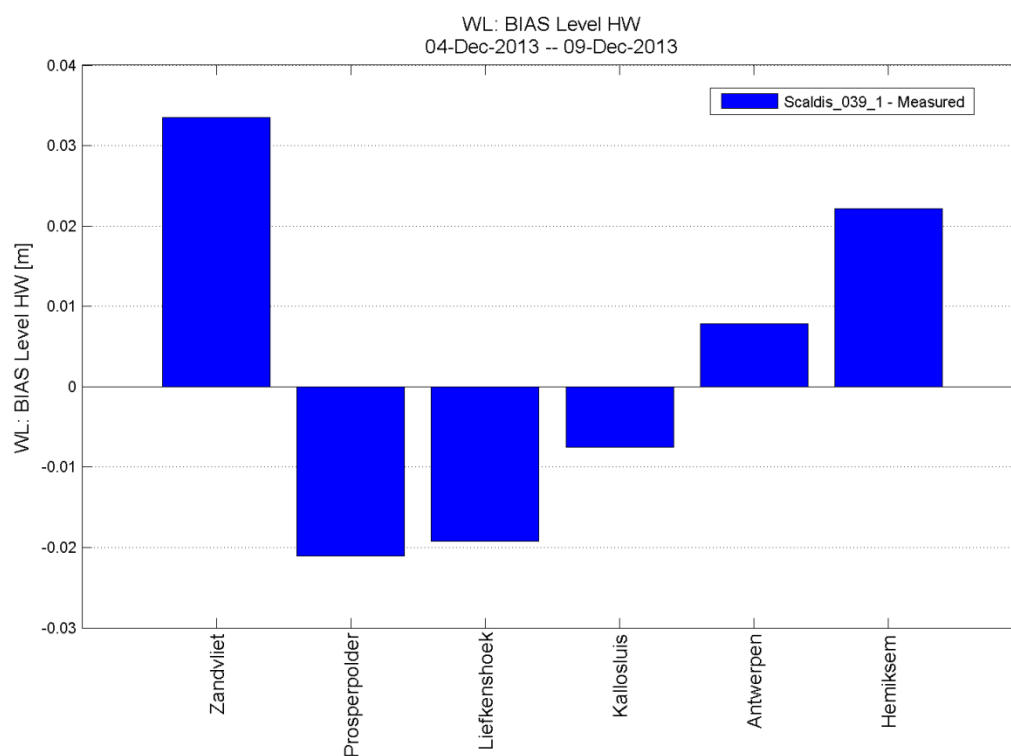


Figure 428 - Bias of high water magnitude (model – measurement) during storm in the Lower Sea Scheldt

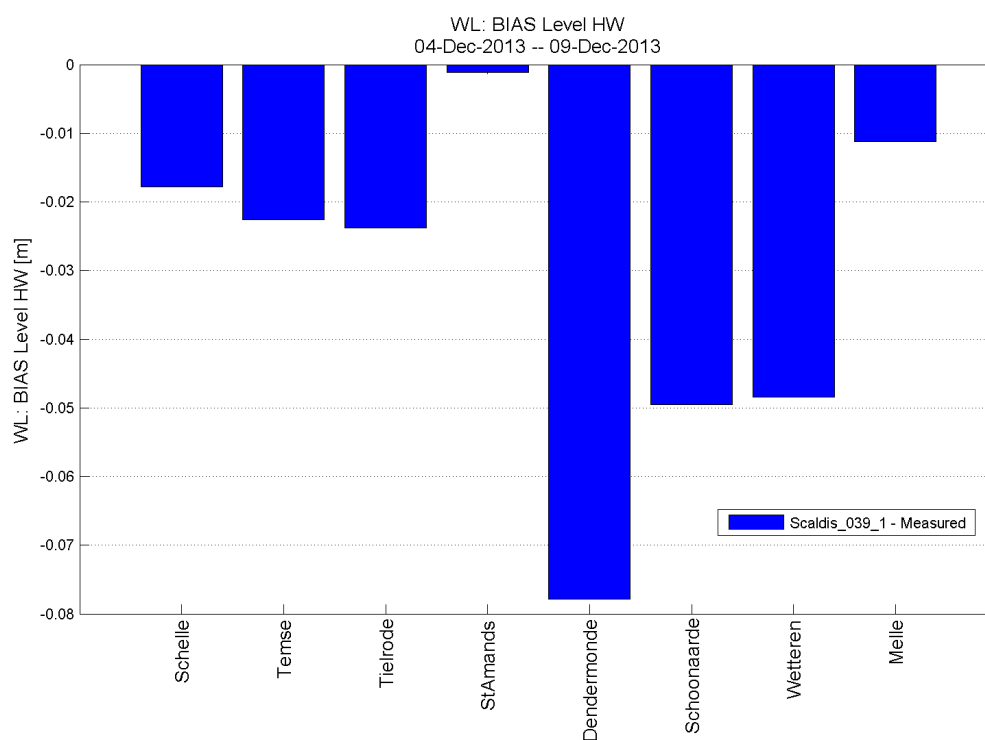


Figure 429 - Bias of high water magnitude (model – measurement) during storm in the Upper Sea Scheldt

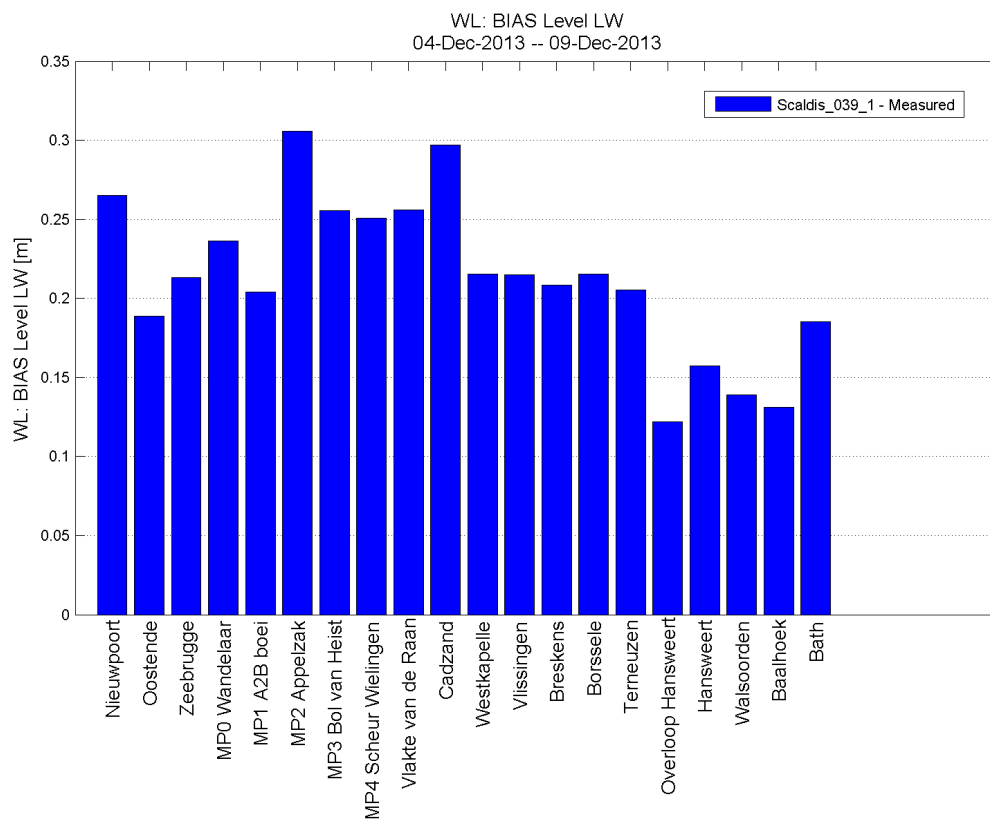


Figure 430 - Bias of low water magnitude (model – measurement) during storm in the North sea and Western Scheldt

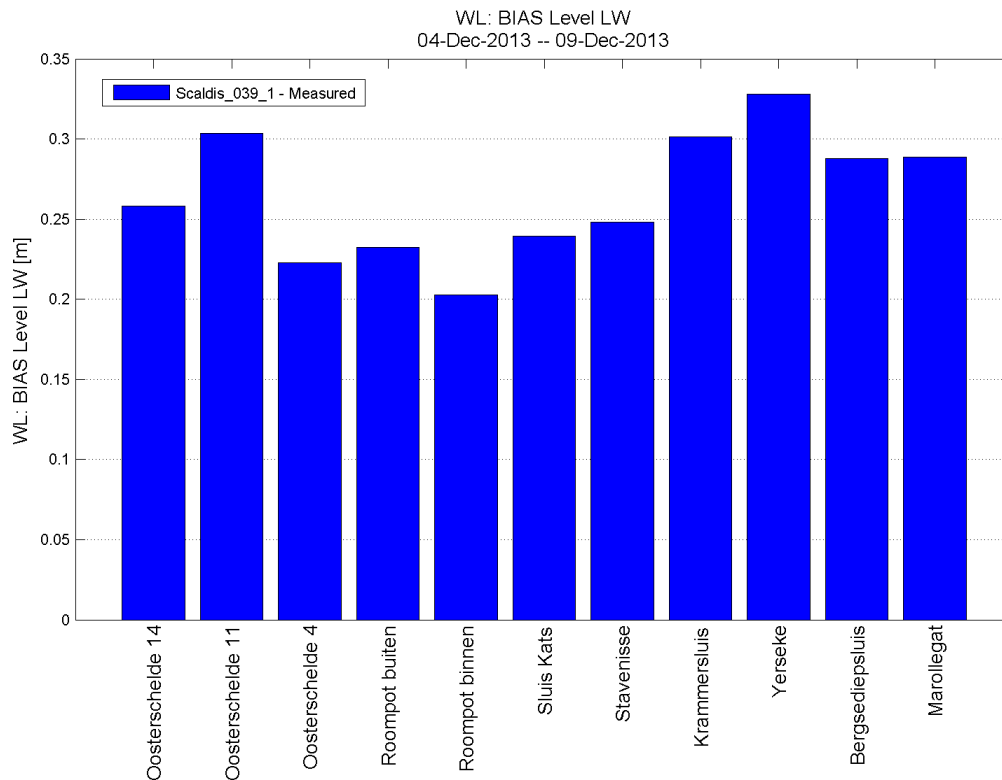


Figure 431 - Bias of low water magnitude (model – measurement) during storm in the Eastern Scheldt

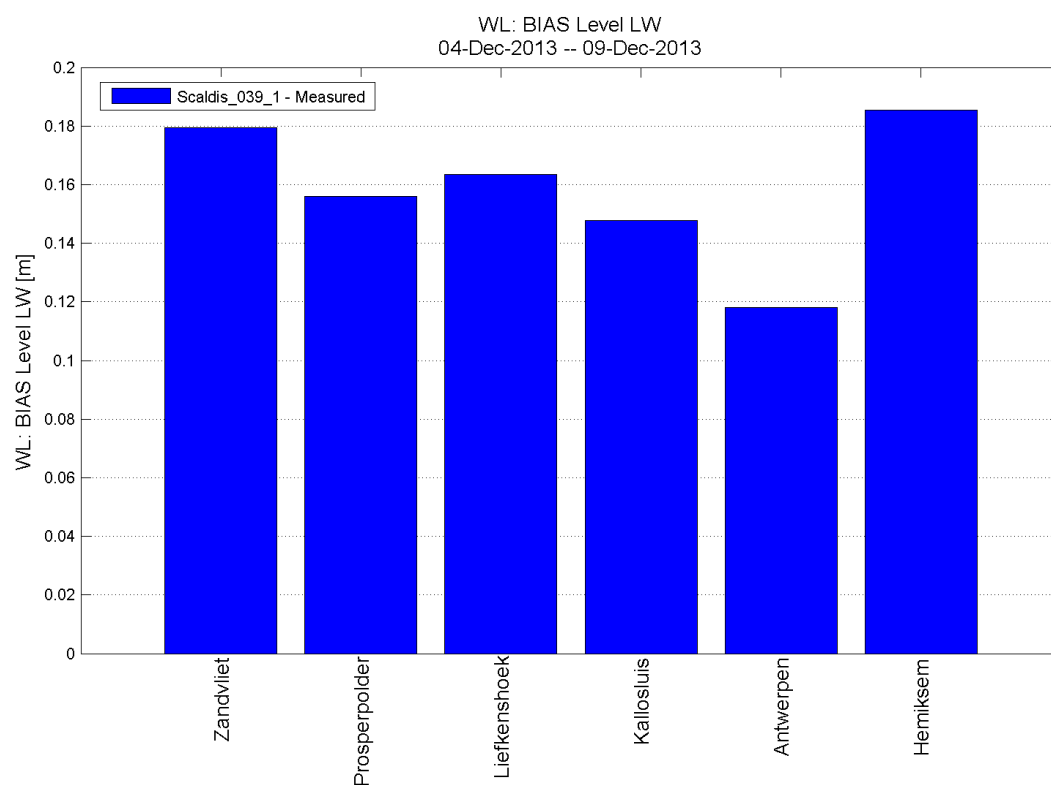


Figure 432 - Bias of low water magnitude (model – measurement) during storm in the Lower Sea Scheldt

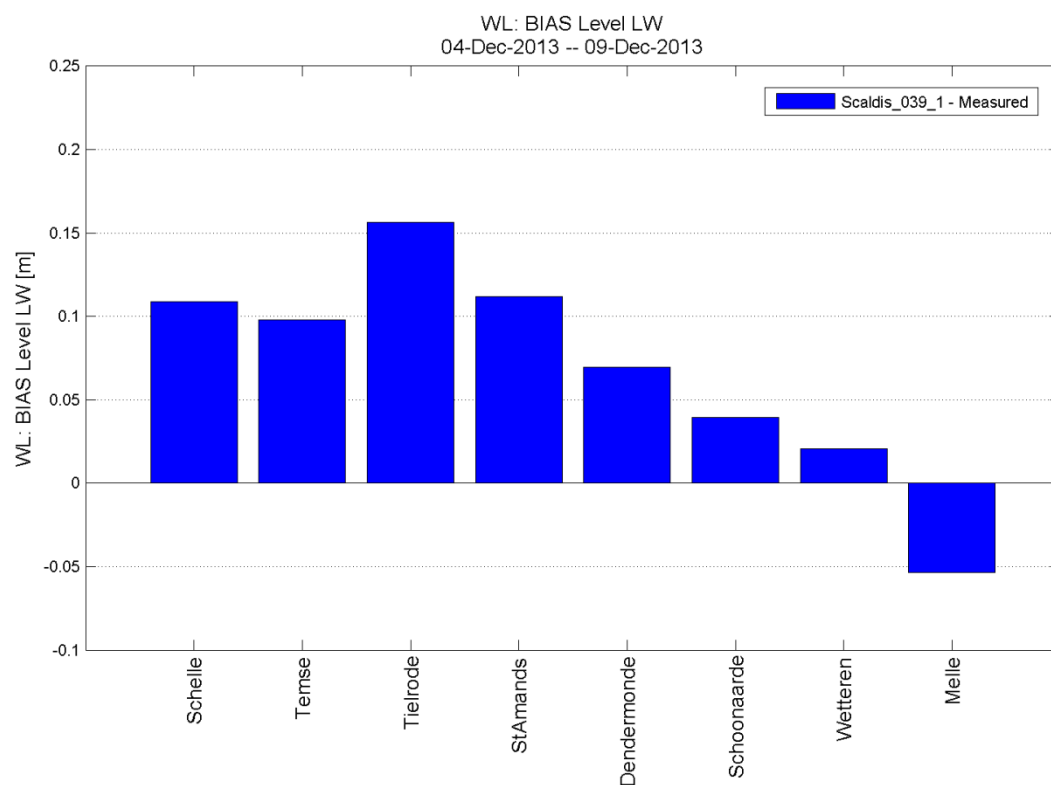


Figure 433 - Bias of low water magnitude (model – measurement) during storm in the Upper Sea Scheldt

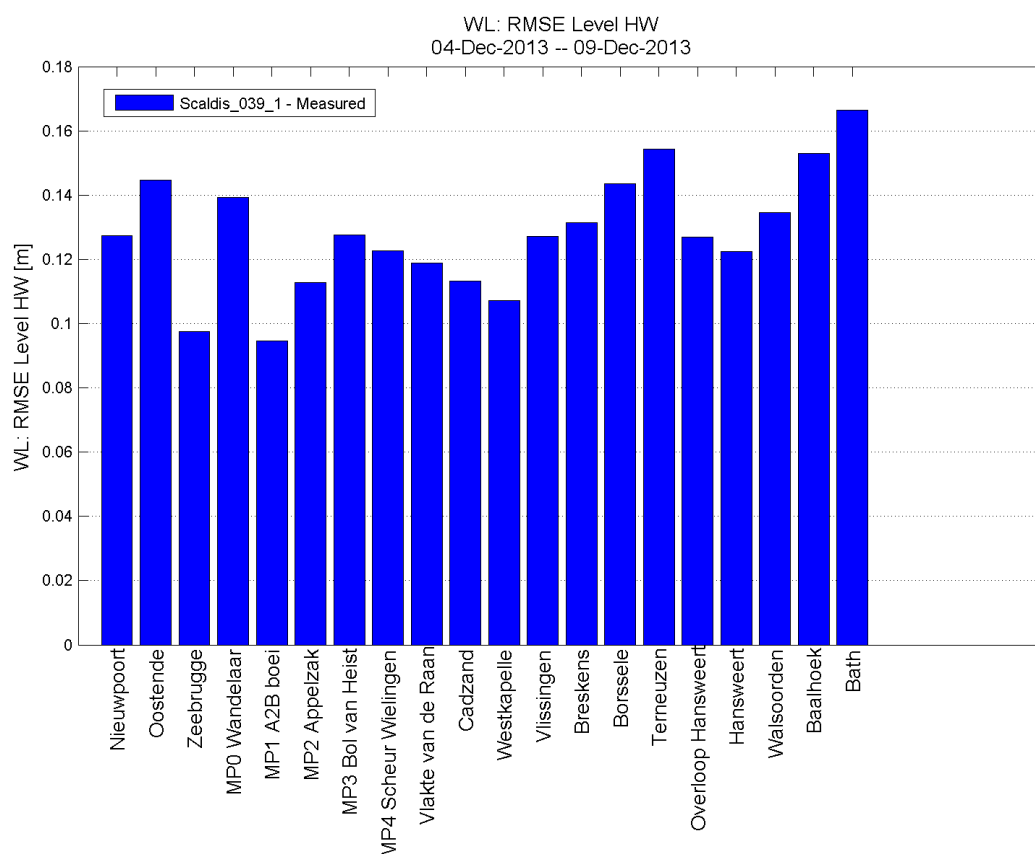


Figure 434 - RMSE of high water magnitude (model vs. measurement) during storm in the North sea and Western Scheldt

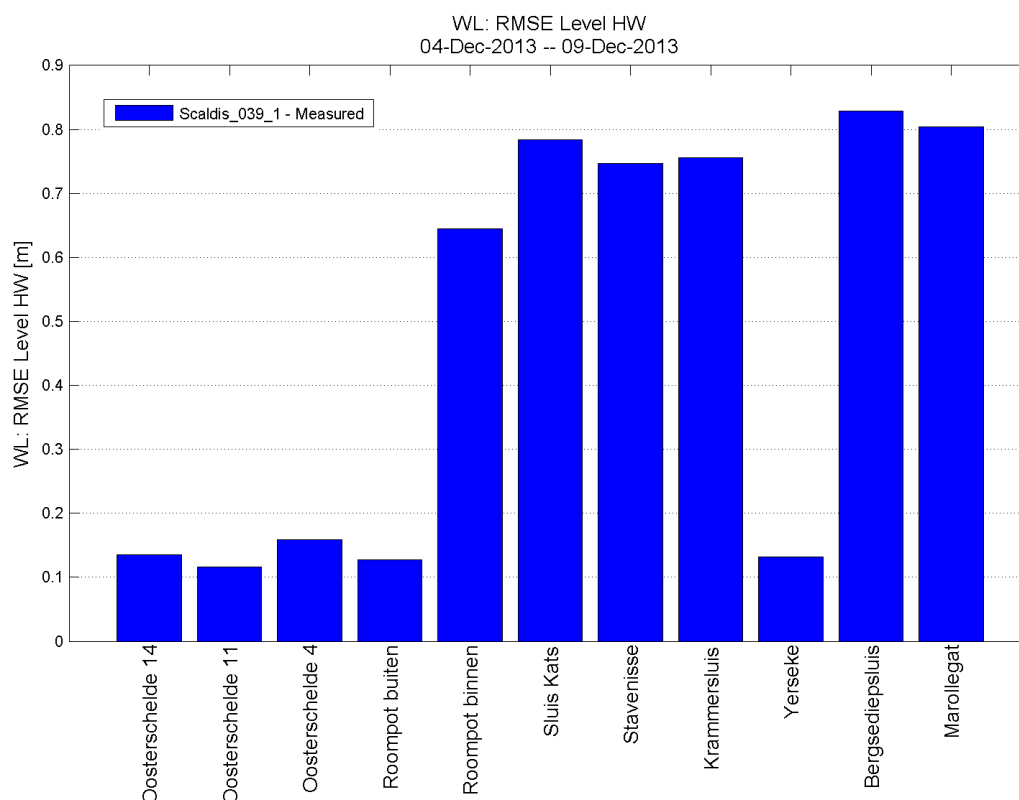


Figure 435 - RMSE of high water magnitude (model vs. measurement) during storm in the Eastern Scheldt

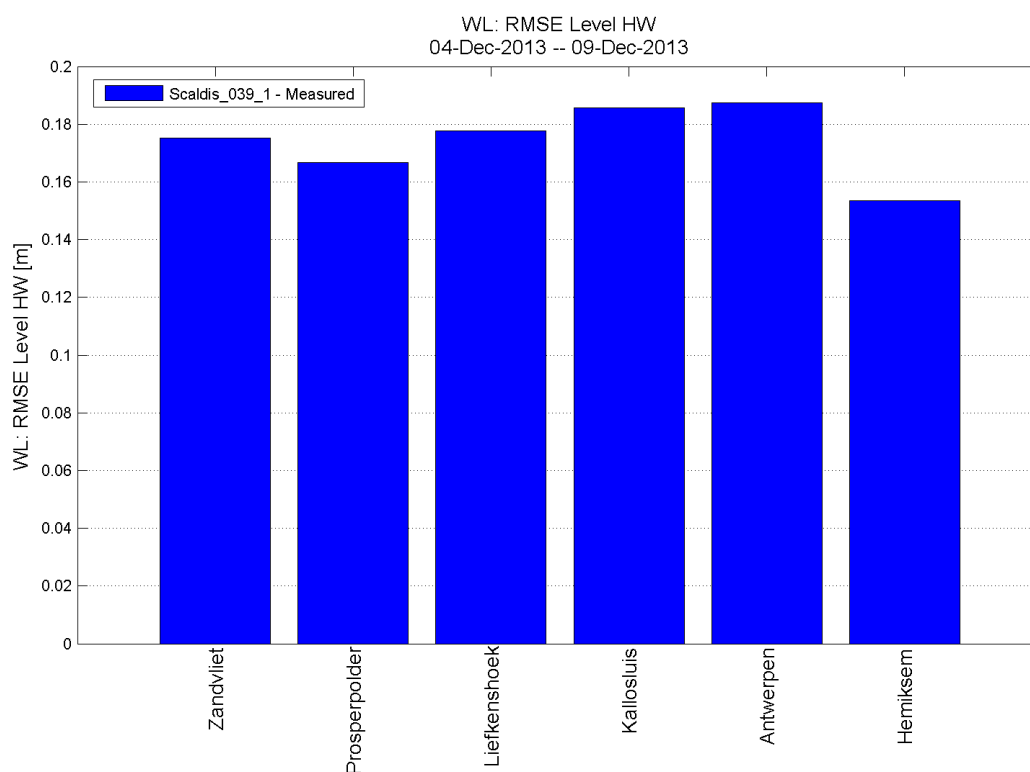


Figure 436 - RMSE of high water magnitude (model vs. measurement) during storm in the Lower Sea Scheldt

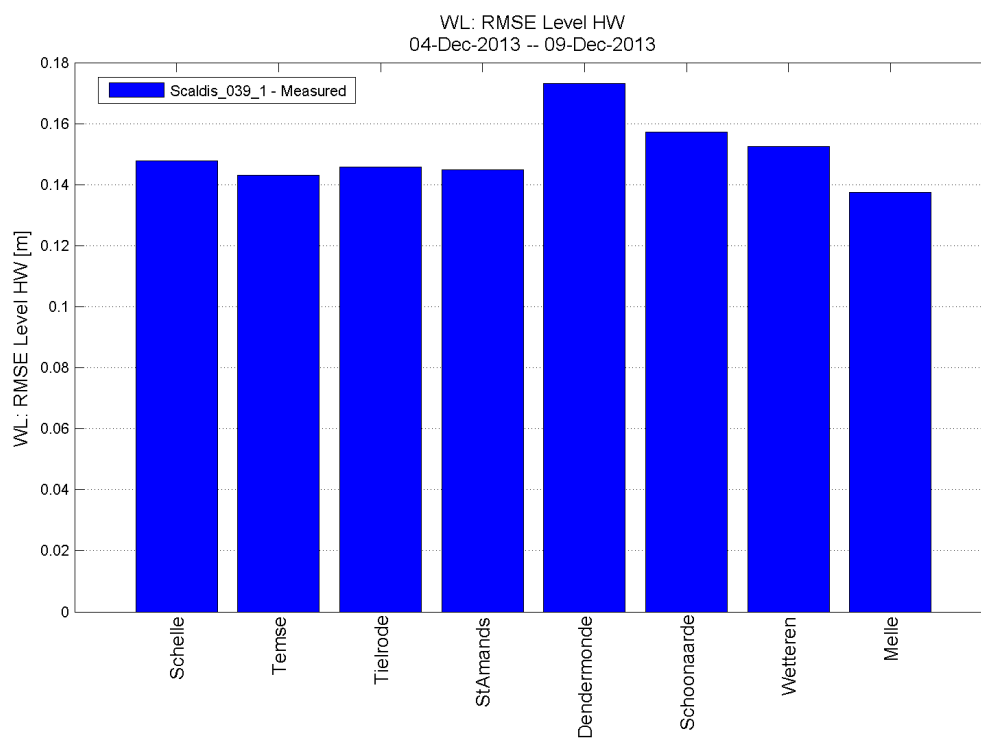


Figure 437 - RMSE of high water magnitude (model vs. measurement) during storm in the Upper Sea Scheldt

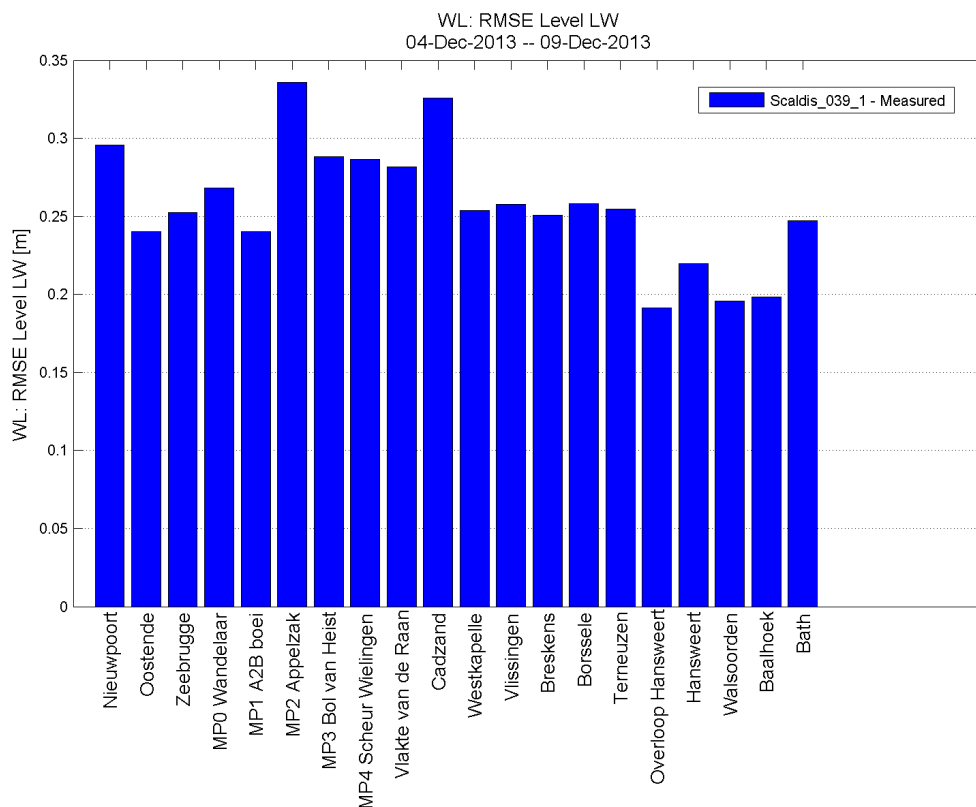


Figure 438 - RMSE of low water magnitude (model vs. measurement) during storm in the North sea and Western Scheldt

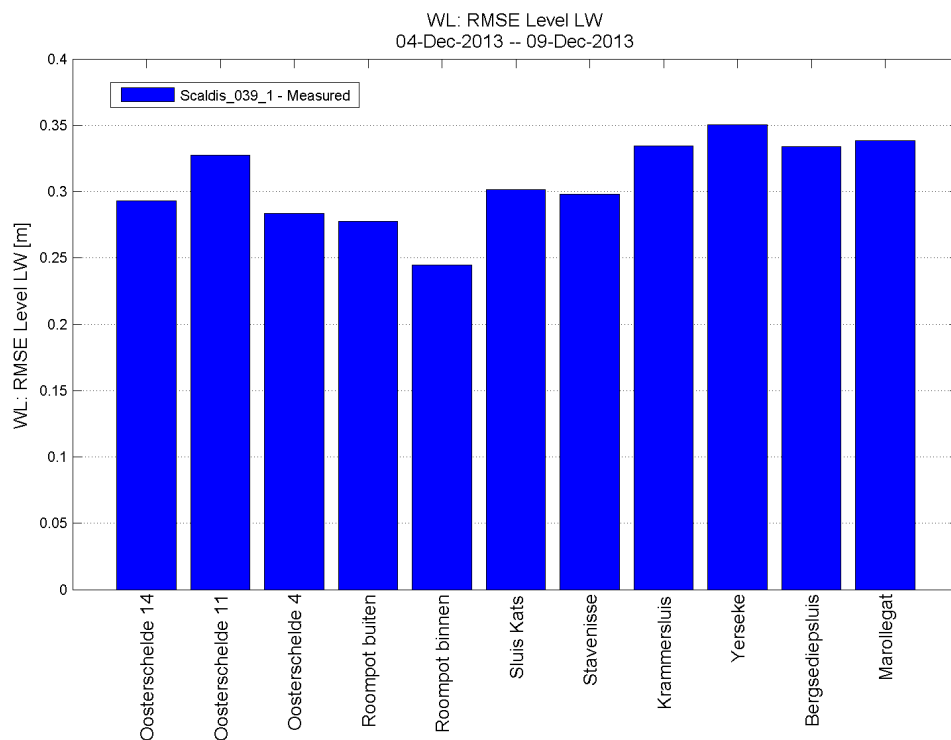


Figure 439 - RMSE of low water magnitude (model vs. measurement) during storm in the Eastern Scheldt

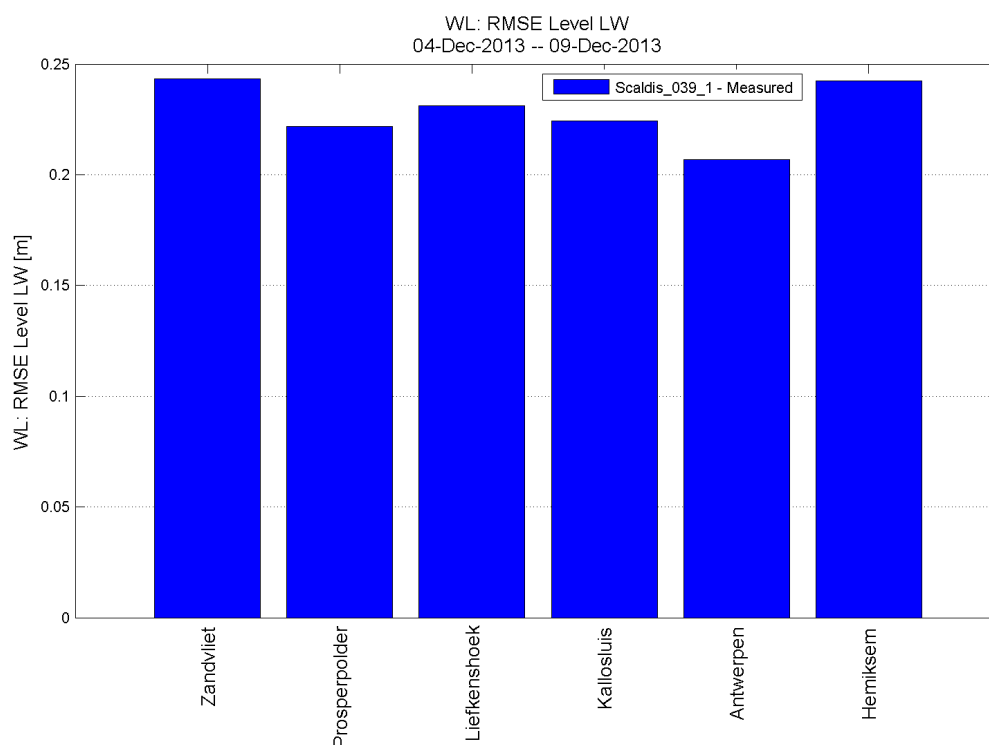


Figure 440 - RMSE of low water magnitude (model vs. measurement) during storm in the Lower Sea Scheldt

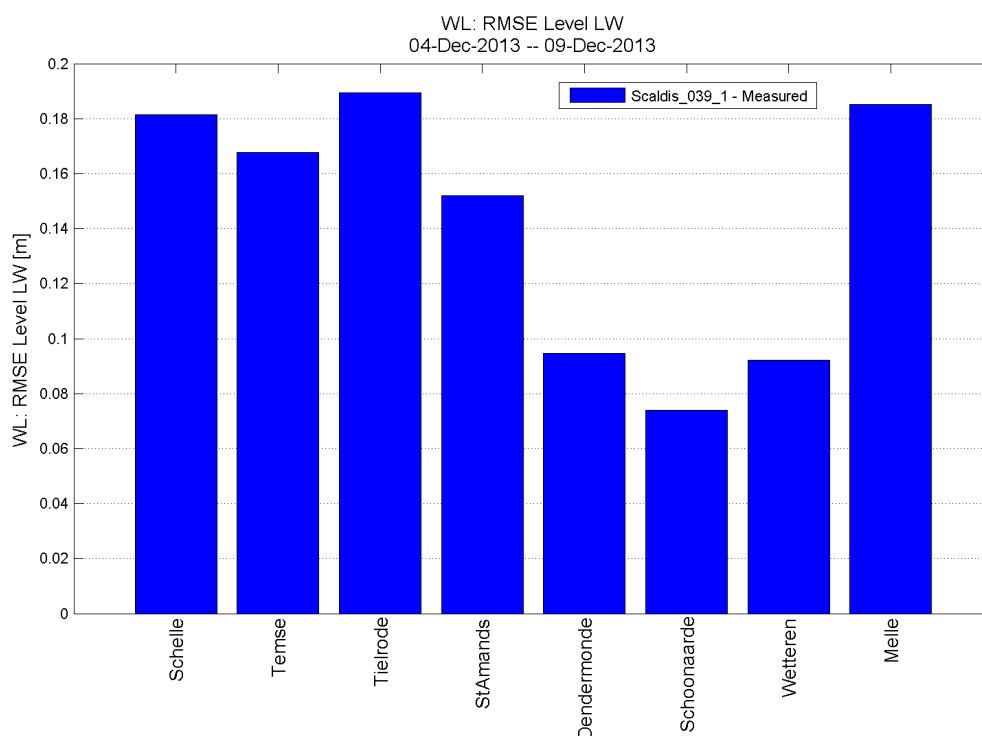


Figure 441 - RMSE of low water magnitude (model vs. measurement) during storm in the Upper Sea Scheldt

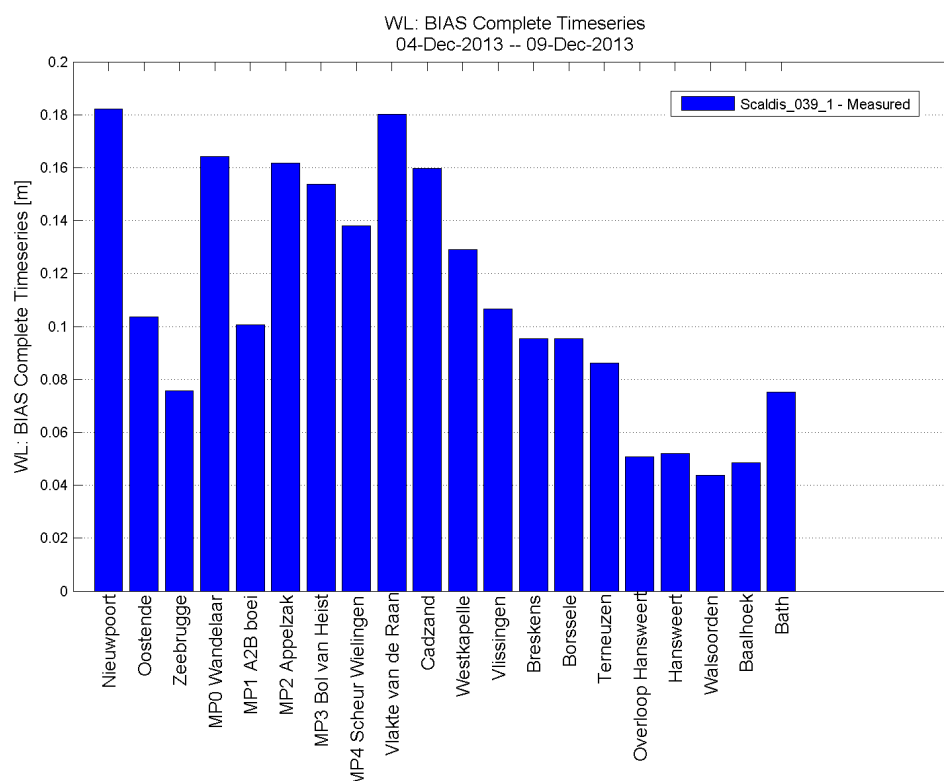


Figure 442 - Bias of the water level time series during storm in the North sea and Western Scheldt

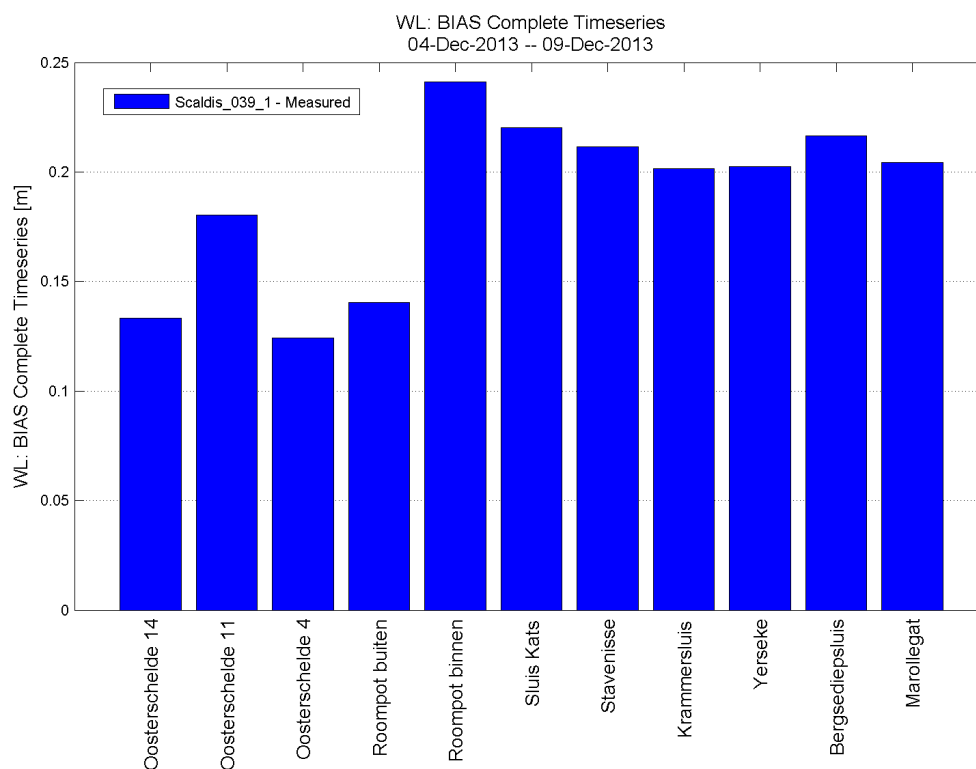


Figure 443 - Bias of the water level time series during storm in the Eastern Scheldt

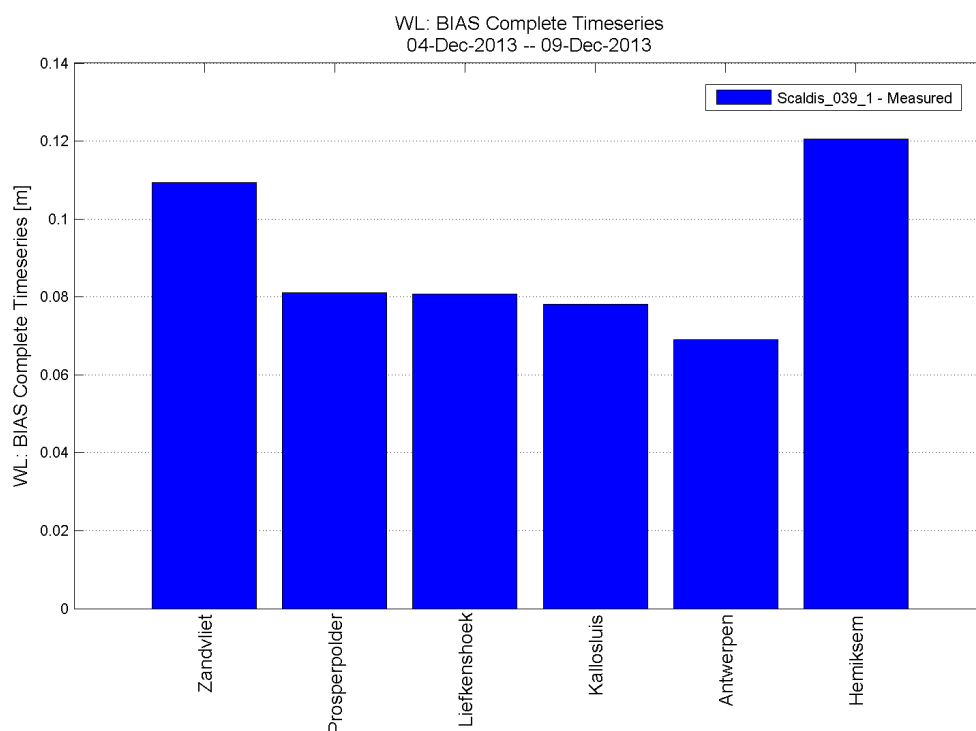


Figure 444 - Bias of the water level time series during storm in the Lower Sea Scheldt

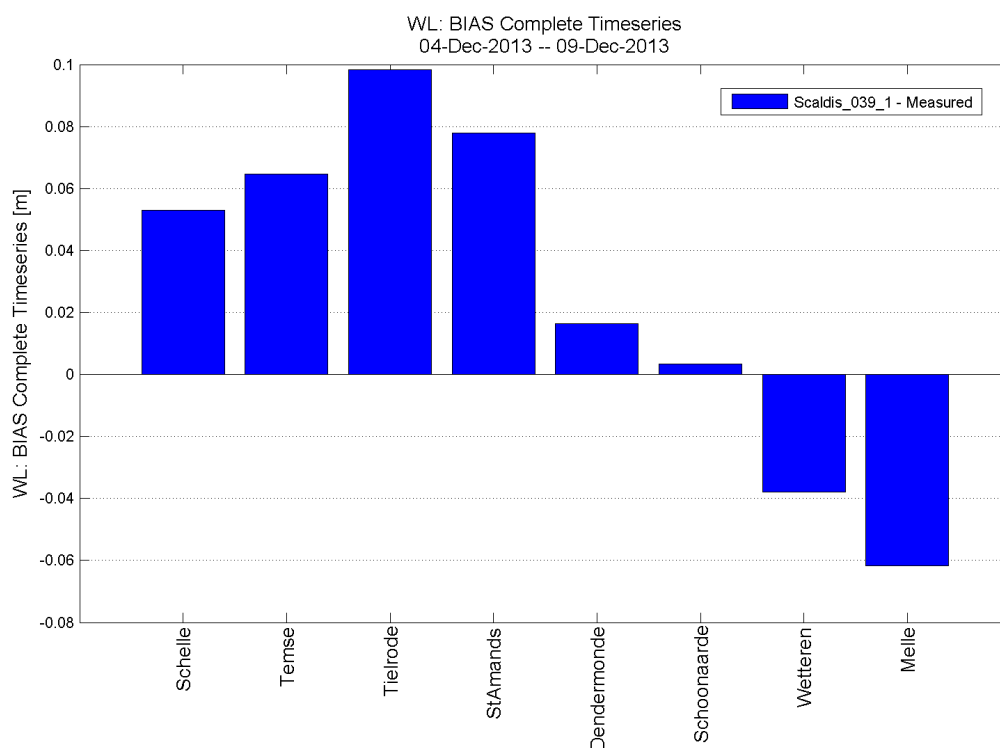


Figure 445 - Bias of the water level time series during storm in the Upper Sea Scheldt

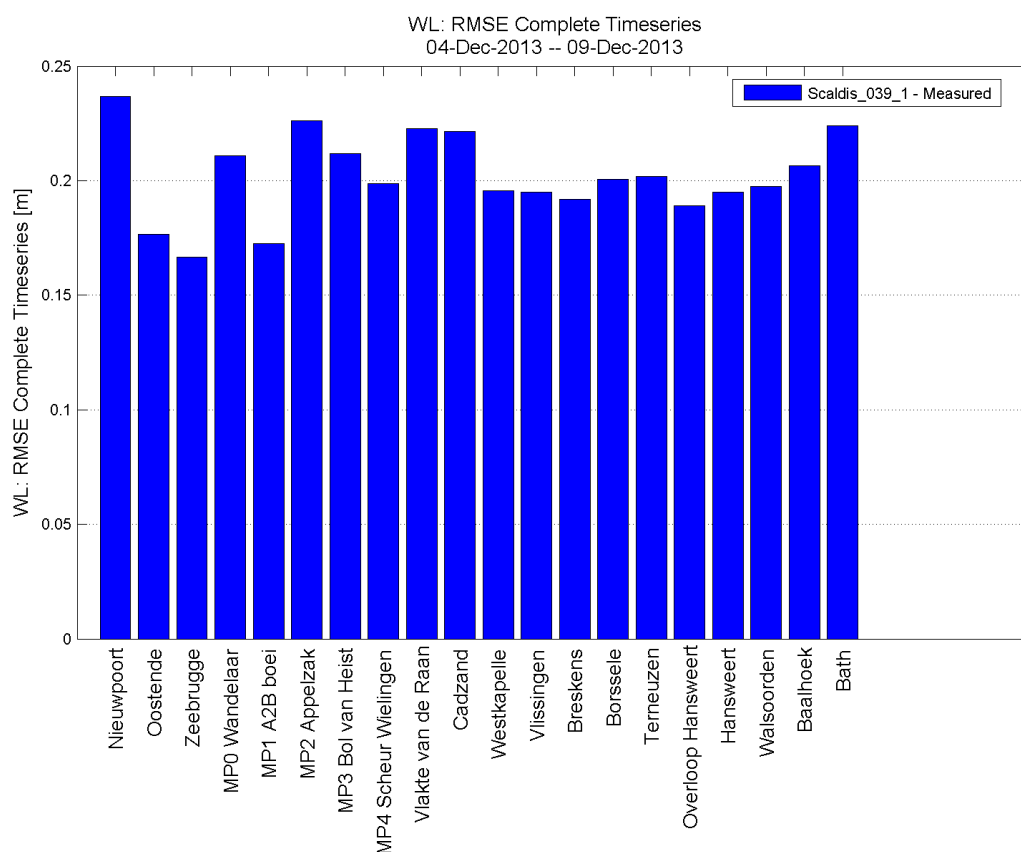


Figure 446 - RMSE of the water level time series during storm in the North sea and Western Scheldt

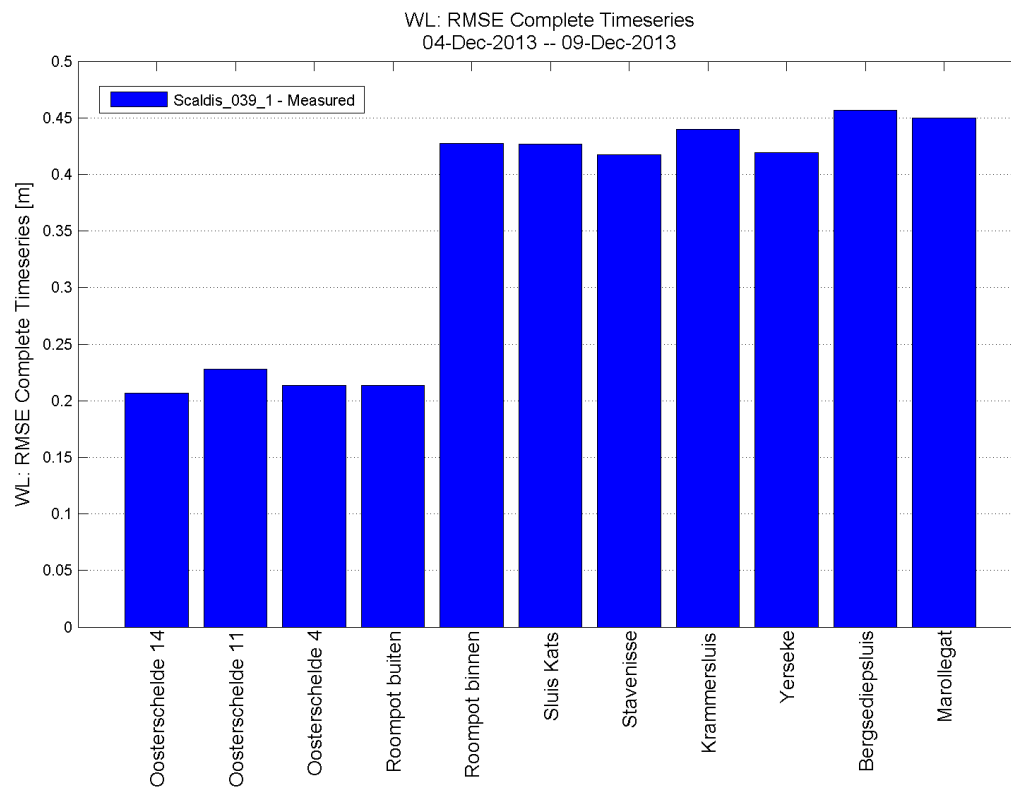


Figure 447 - RMSE of the water level time series during storm in the Eastern Scheldt

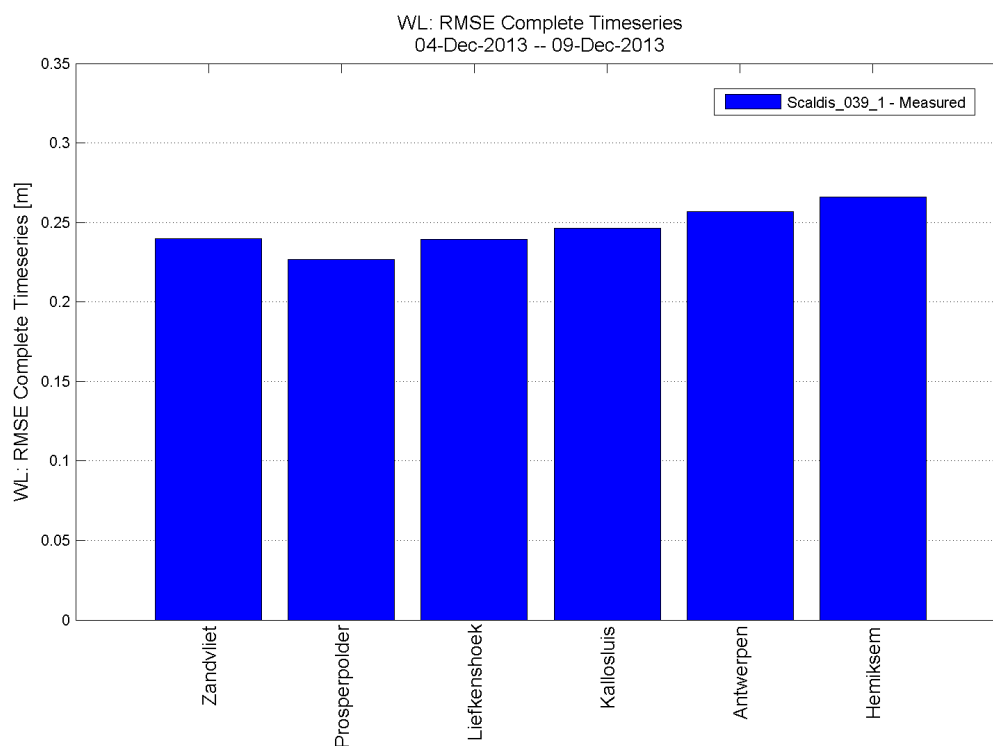


Figure 448 - RMSE of the water level time series during storm in the Lower Sea Scheldt

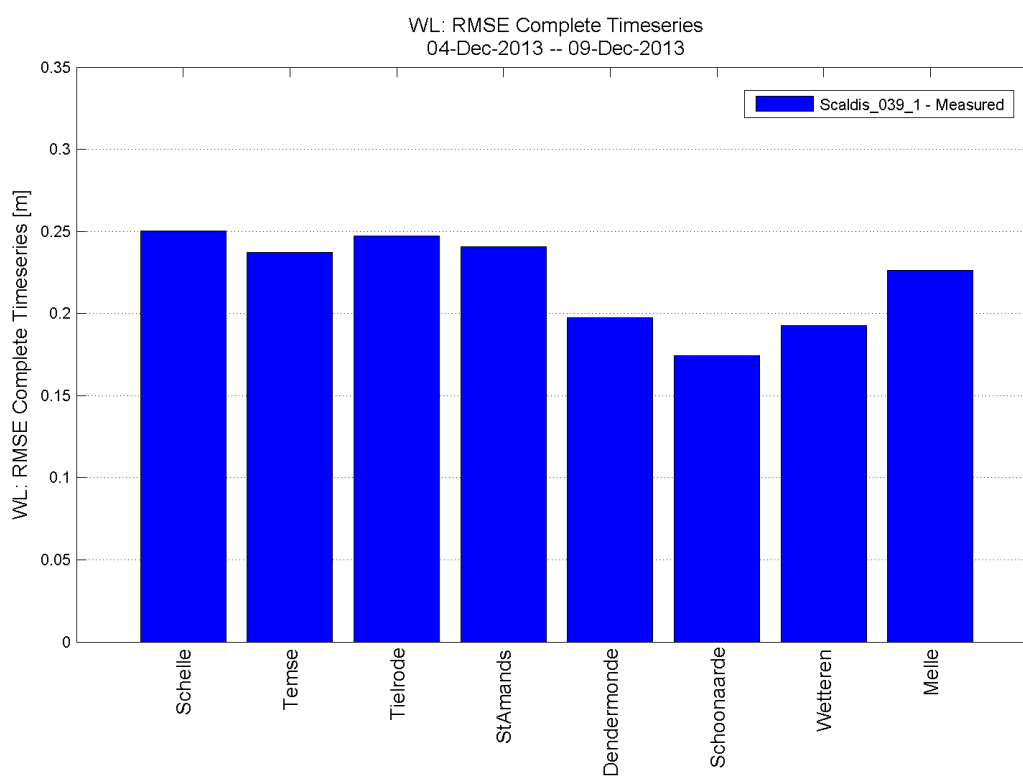


Figure 449 - RMSE of the water level time series during storm in the Upper Sea Scheldt

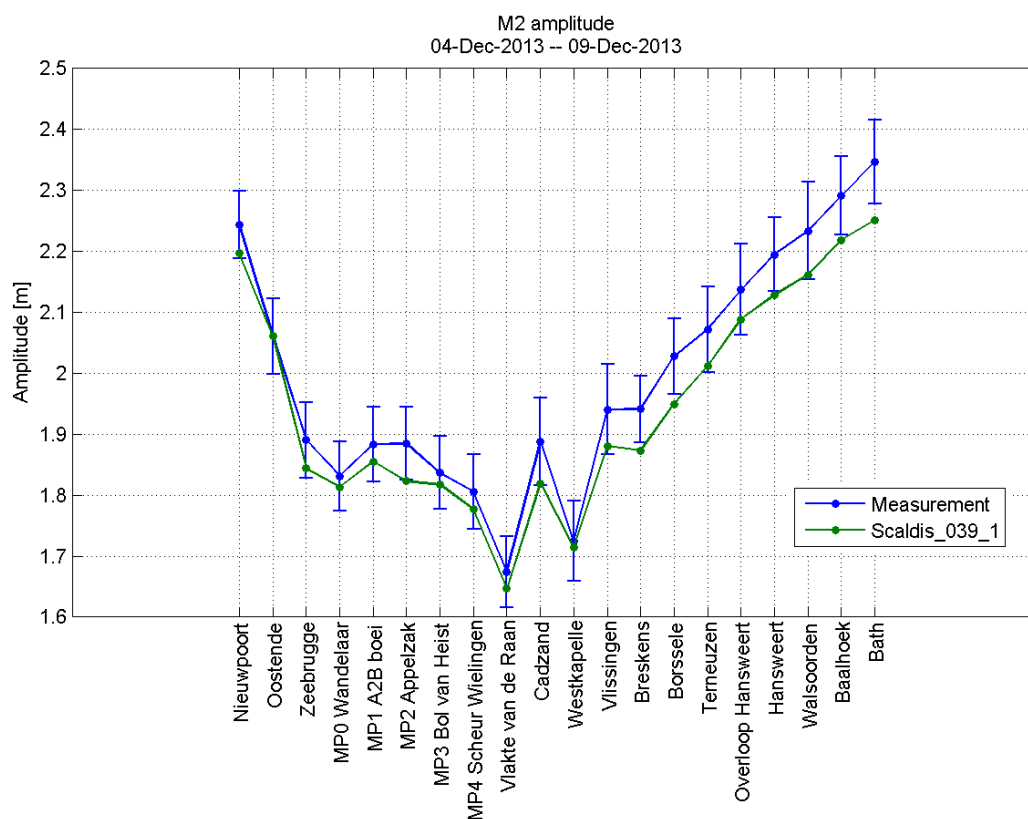


Figure 450 - M2 amplitude during storm in the North sea and Western Scheldt

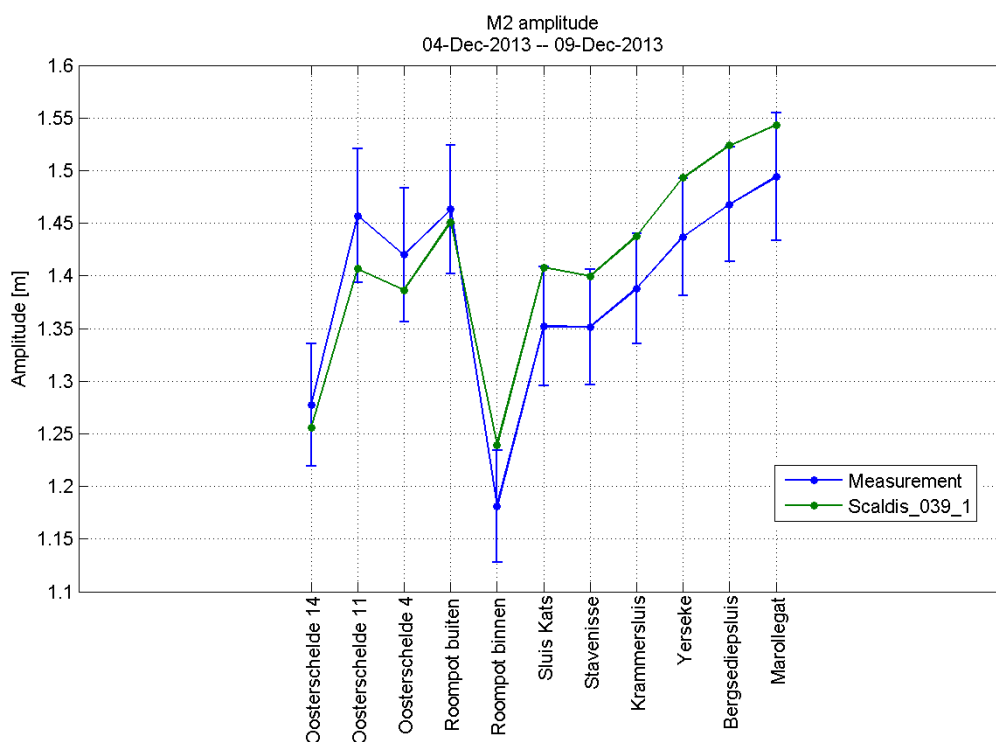


Figure 451 - M2 amplitude during storm in the Eastern Scheldt

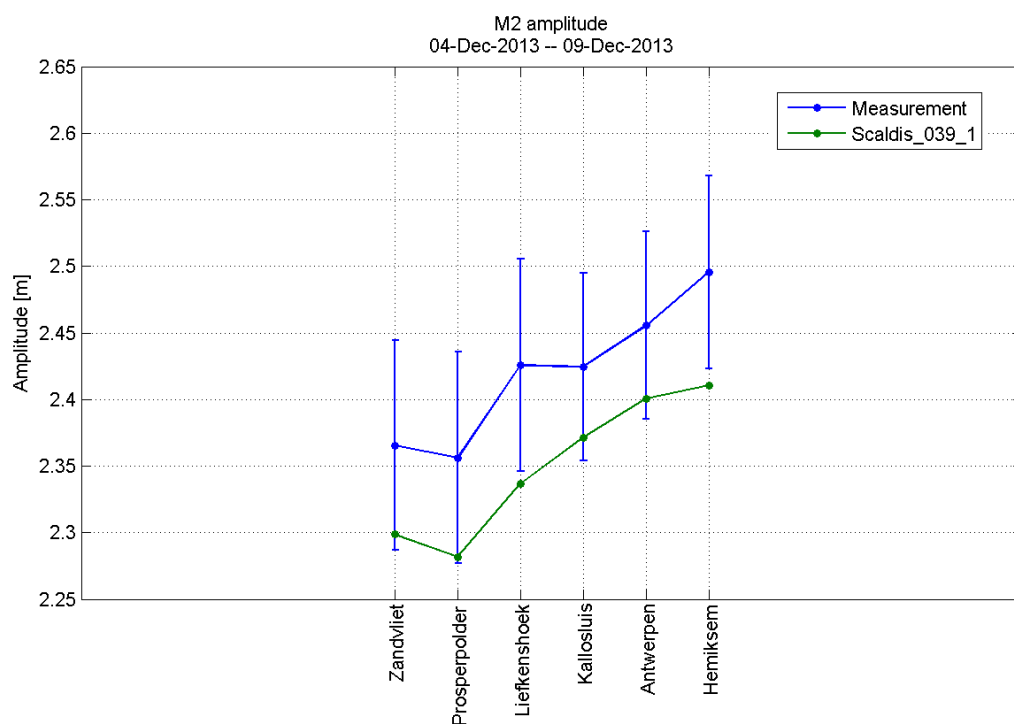


Figure 452 - M2 amplitude during storm in the Lower Sea Scheldt

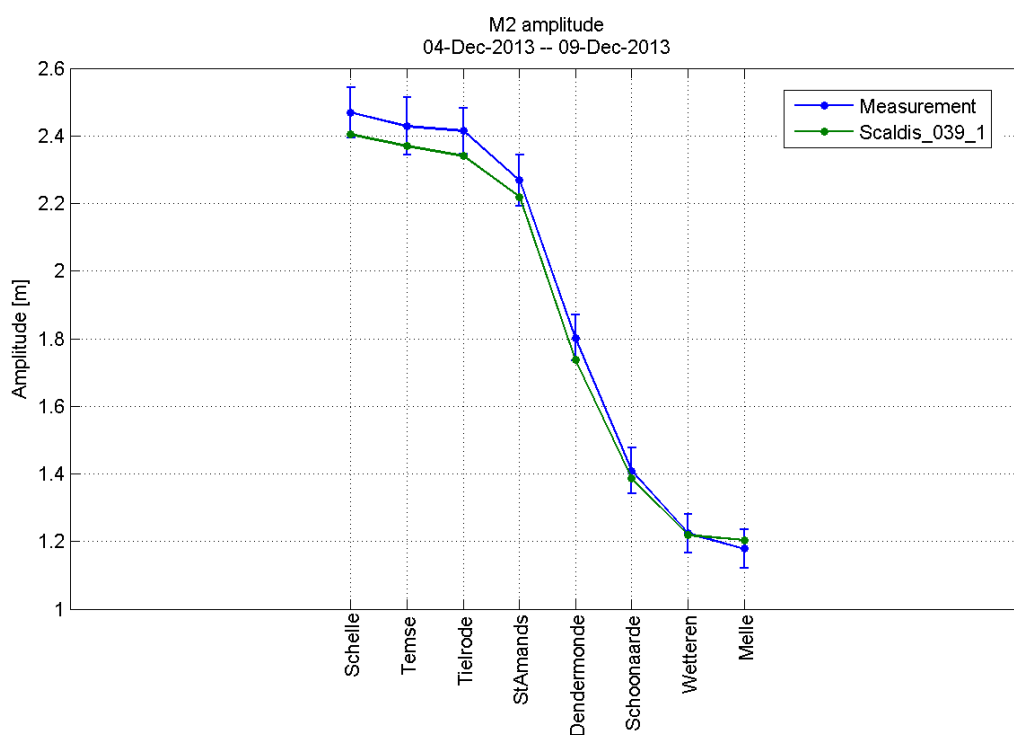


Figure 453 - M2 amplitude during storm in the Upper Sea Scheldt

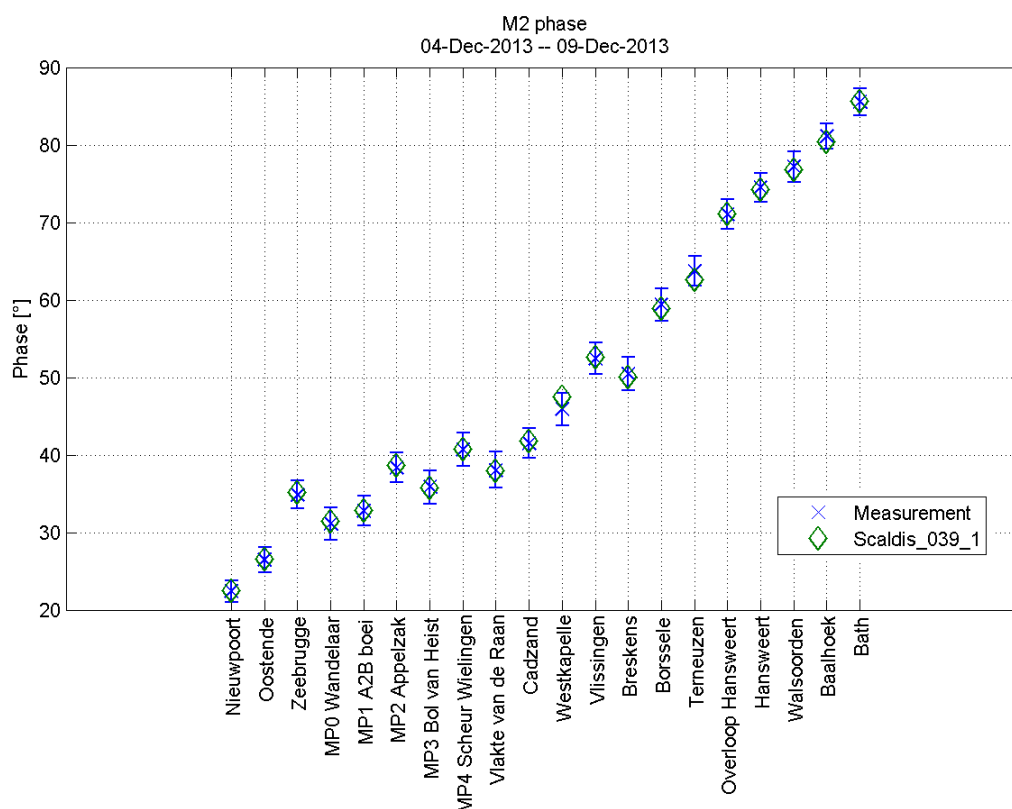


Figure 454 - M2 phase during storm in the North sea and Western Scheldt

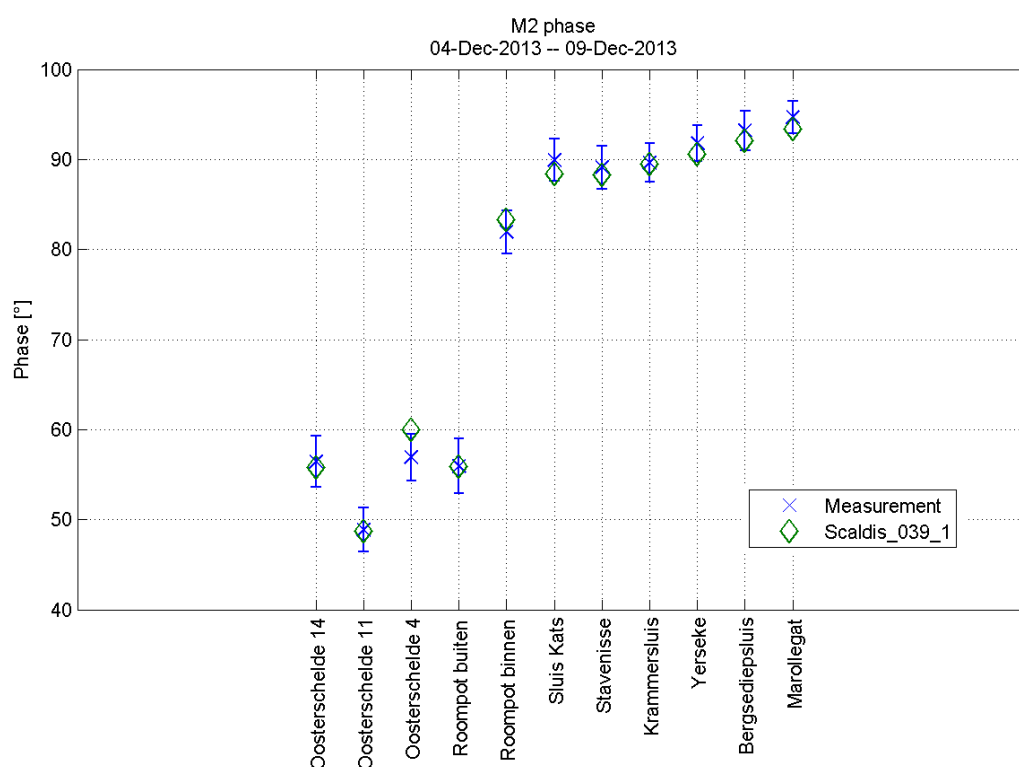


Figure 455 - M2 phase during storm in the Eastern Scheldt

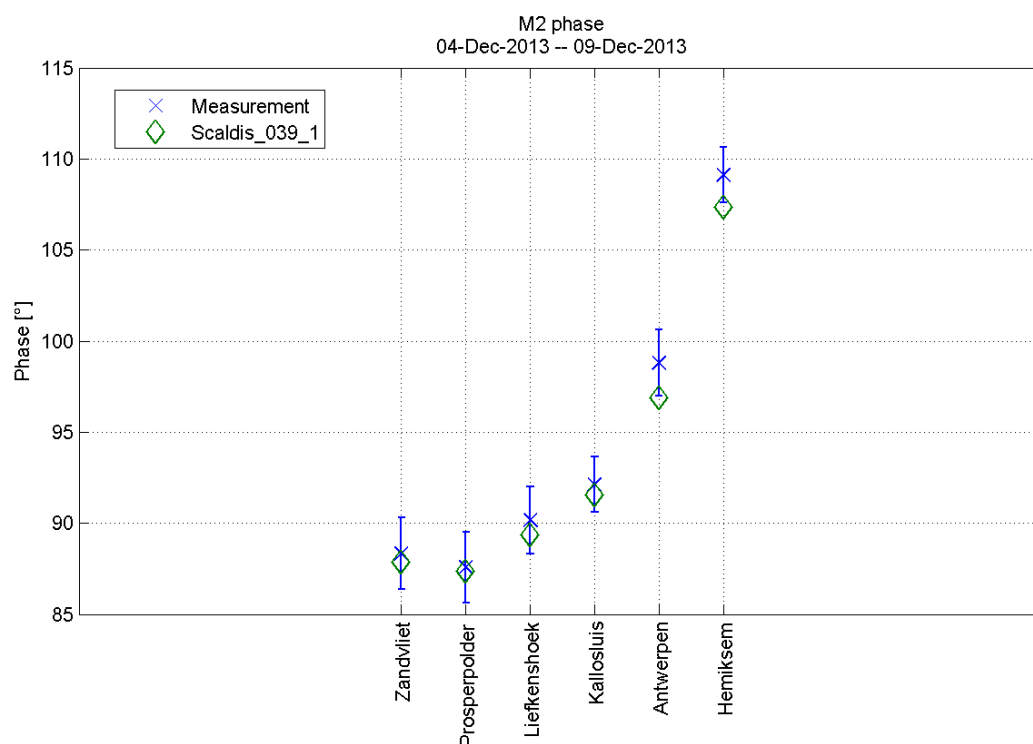


Figure 456 - M2 phase during storm in the Lower Sea Scheldt

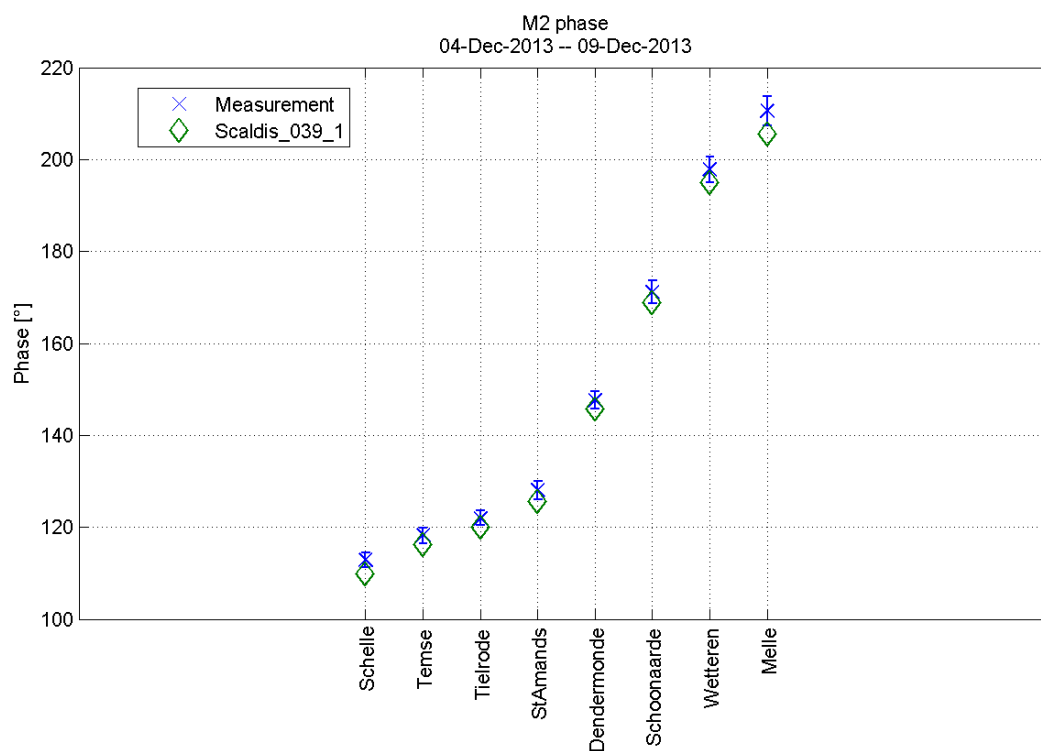


Figure 457 - M2 phase during storm in the Upper Sea Scheldt

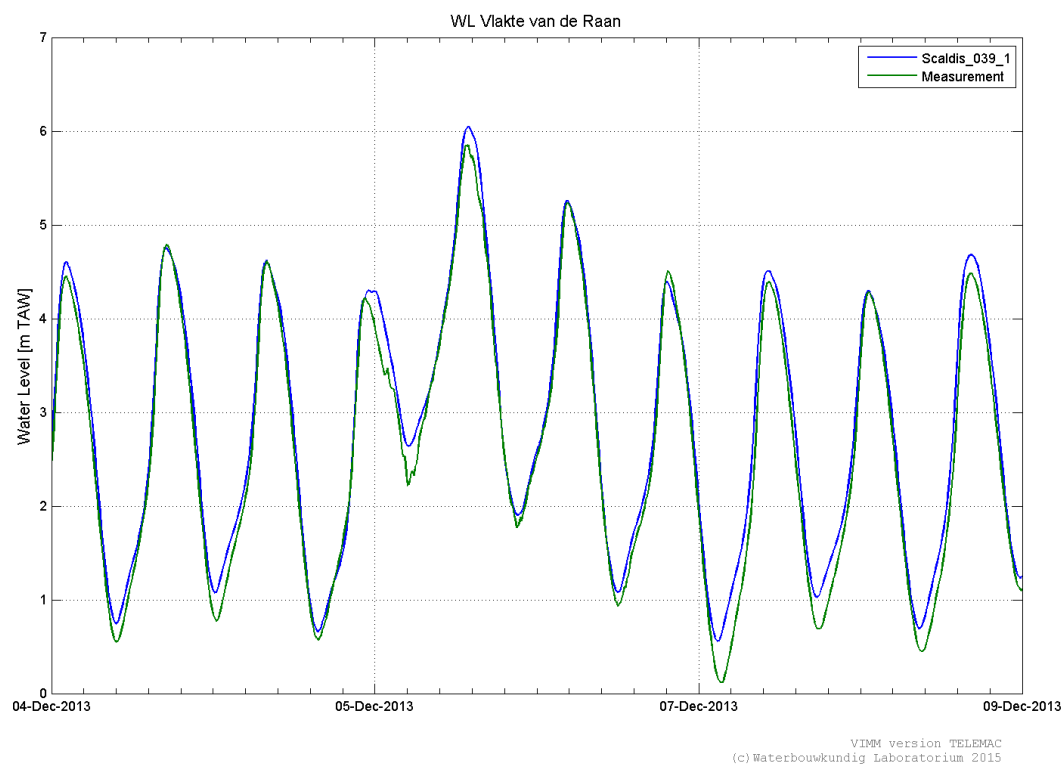


Figure 458 - Calculated and measured water levels at Vlake van de Raan during storm

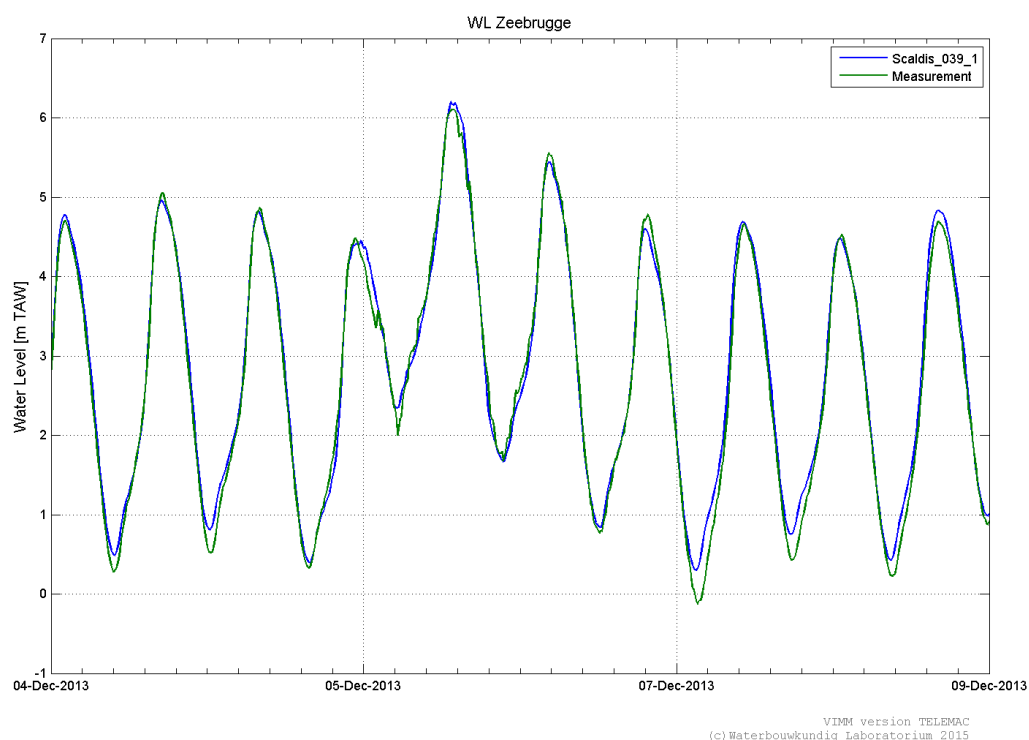


Figure 459 - Calculated and measured water levels at Zeebrugge during storm

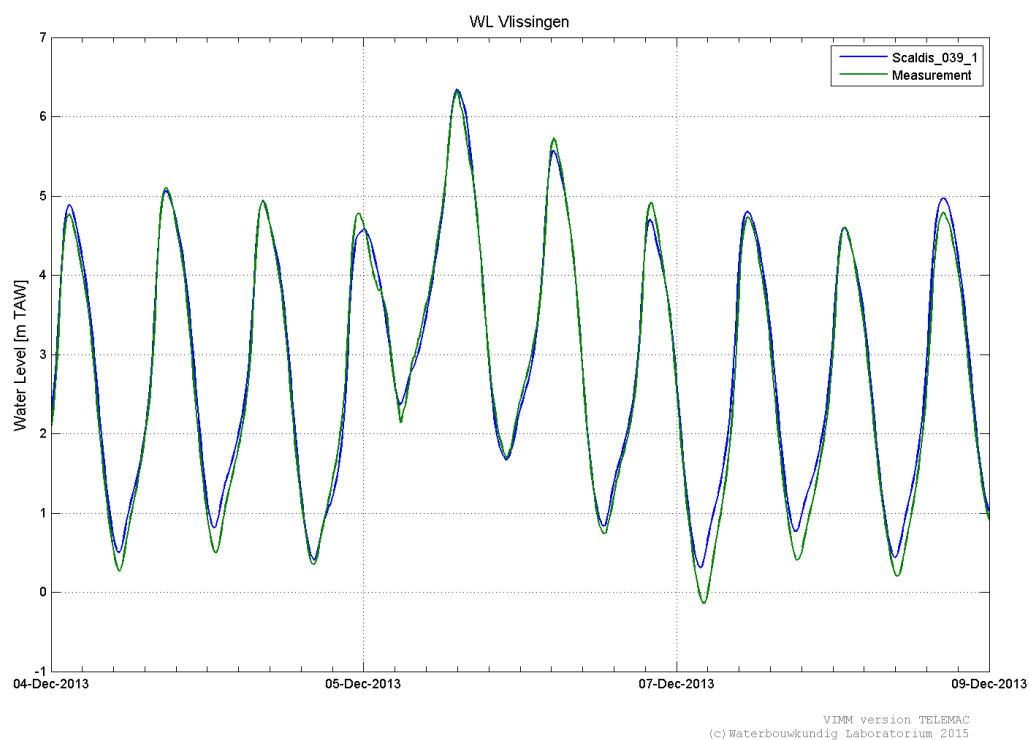


Figure 460 - Calculated and measured water levels at Vlissingen during storm

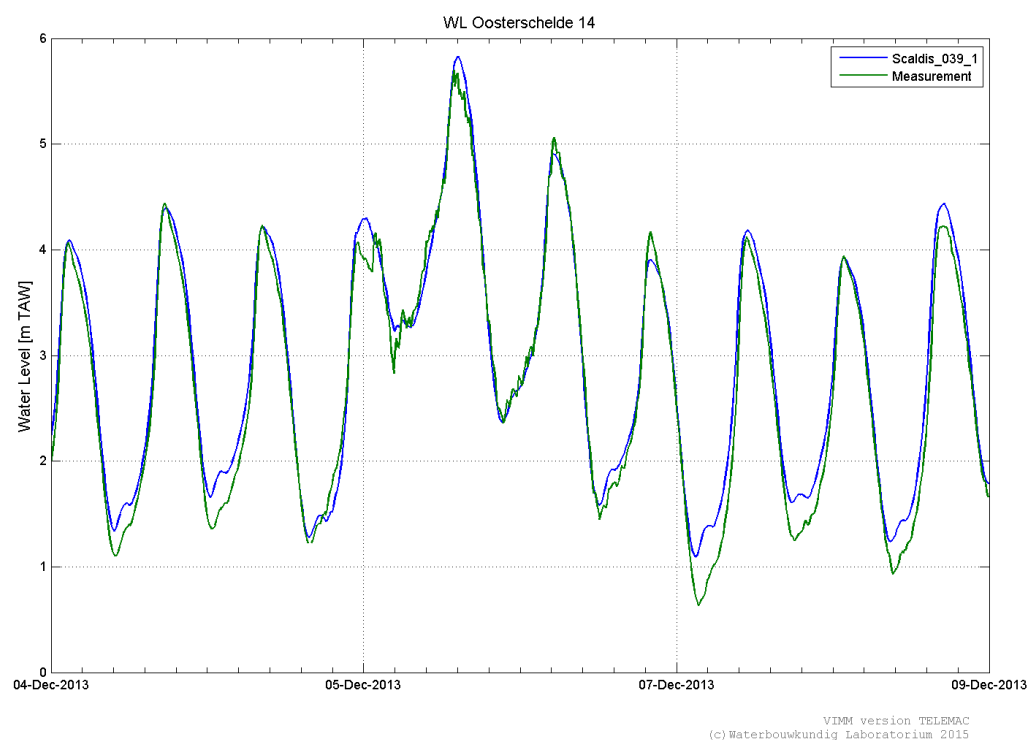


Figure 461 - Calculated and measured water levels at Oosterschelde 14 during storm

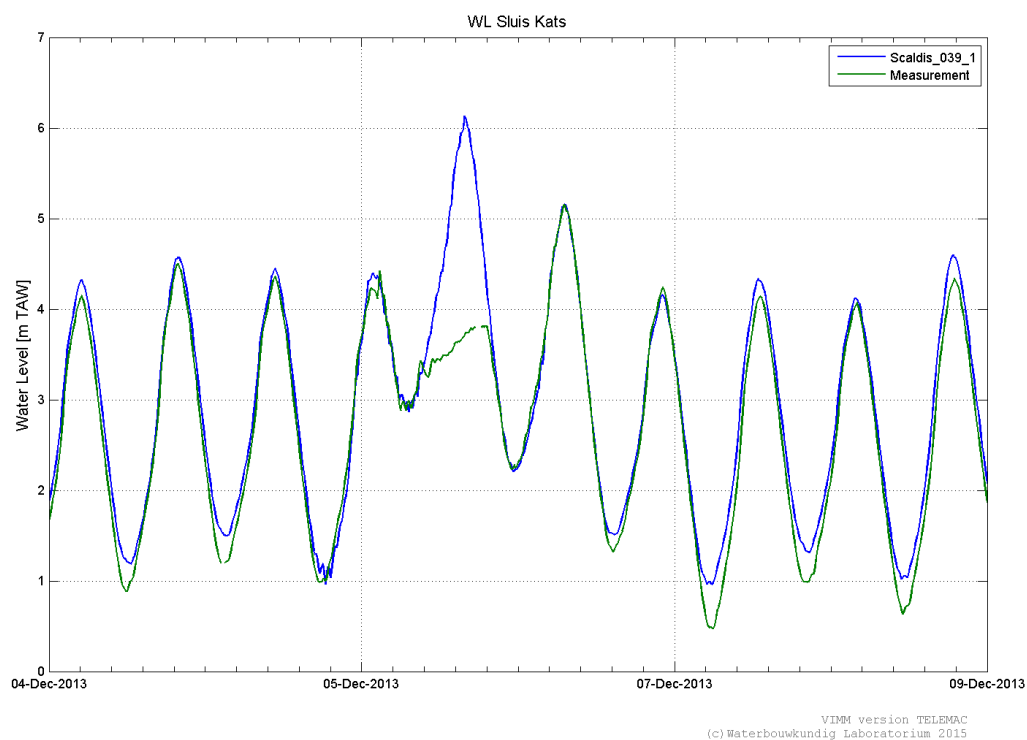


Figure 462 - Calculated and measured water levels at Sluis Kats during storm

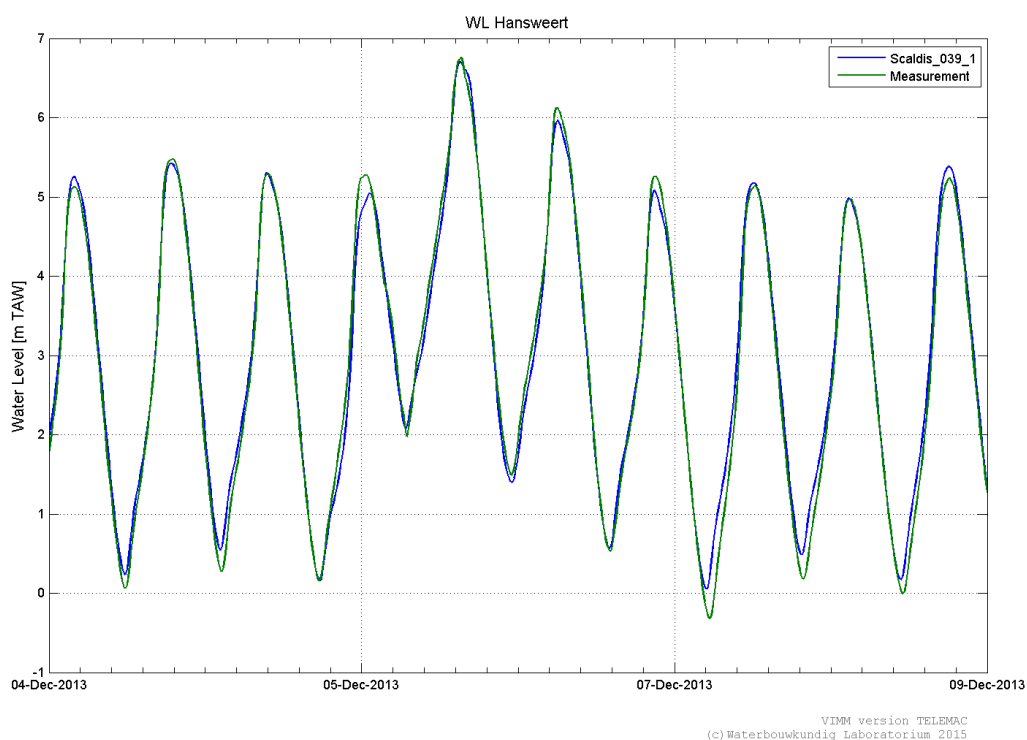


Figure 463 - Calculated and measured water levels at Hansweert during storm

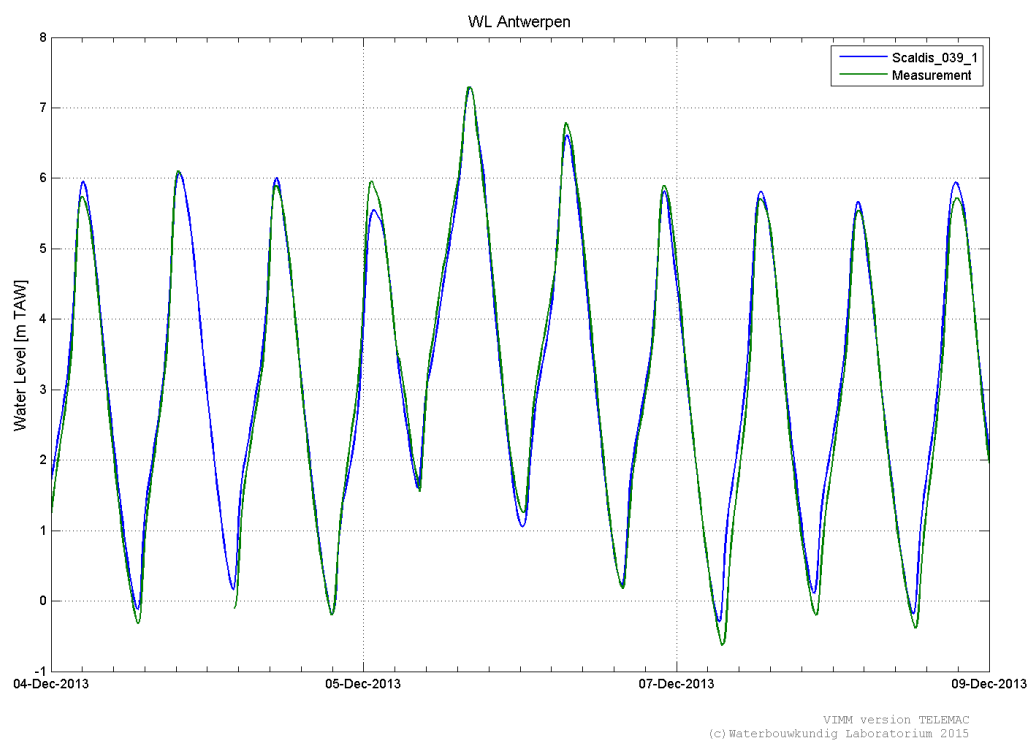


Figure 464 - Calculated and measured water levels at Antwerpen during storm

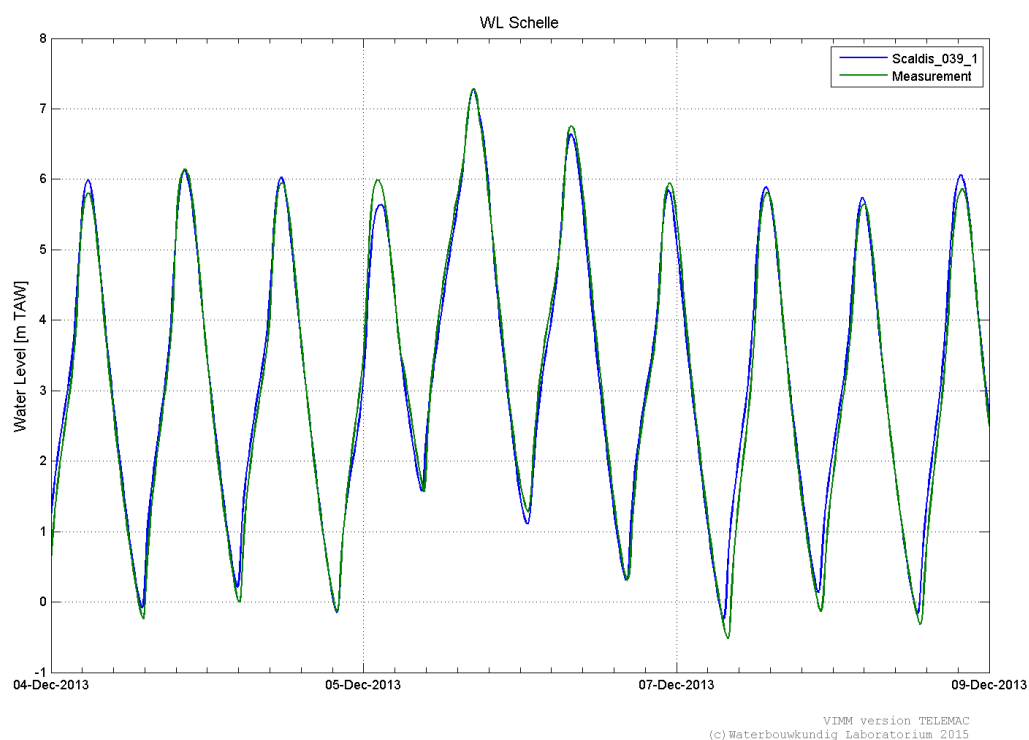


Figure 465 - Calculated and measured water levels at Schelle during storm

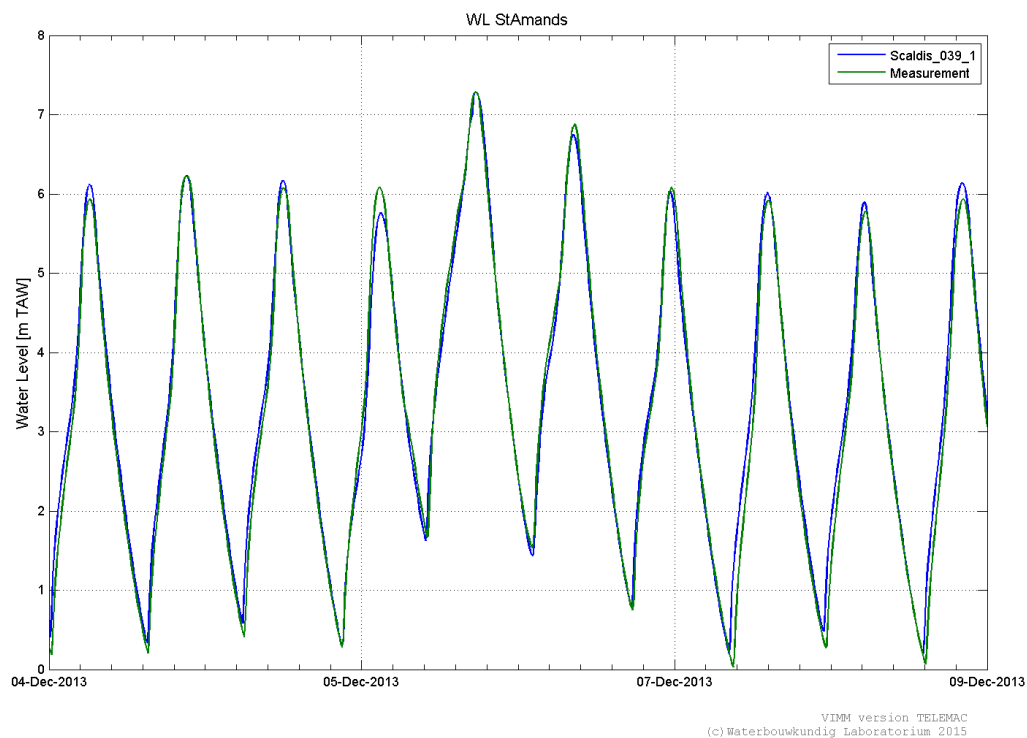


Figure 466 - Calculated and measured water levels at Sint Amands during storm

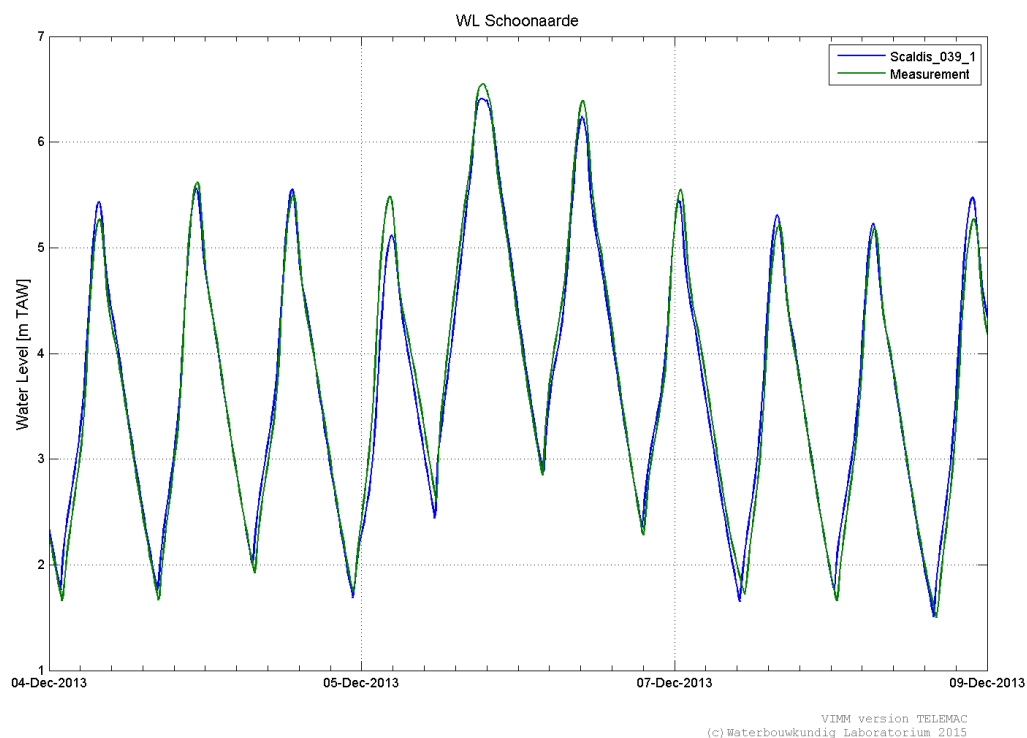


Figure 467 - Calculated and measured water levels at Schoonaarde during storm

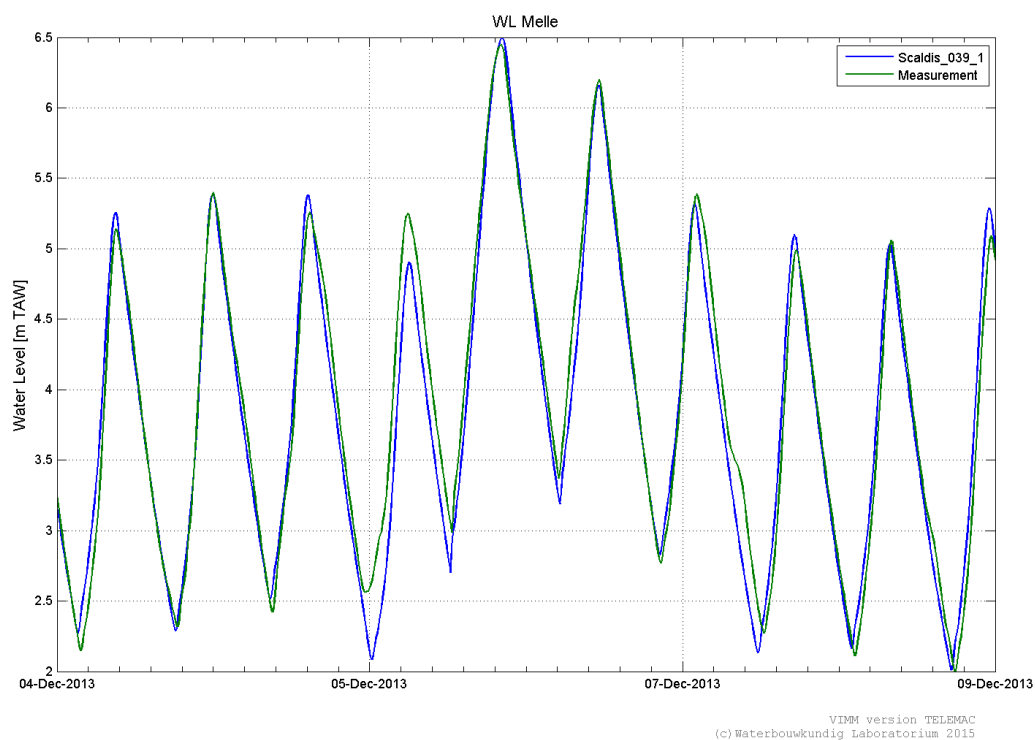


Figure 468 - Calculated and measured water levels at Melle during storm

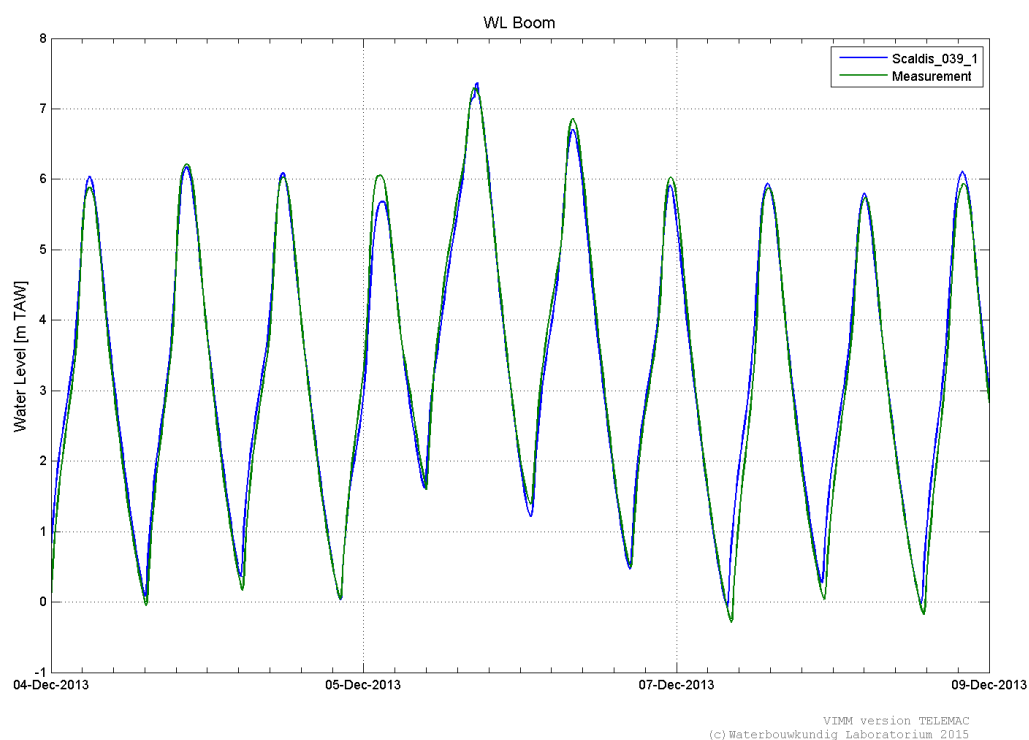


Figure 469 - Calculated and measured water levels at Boom during storm

Flood areas

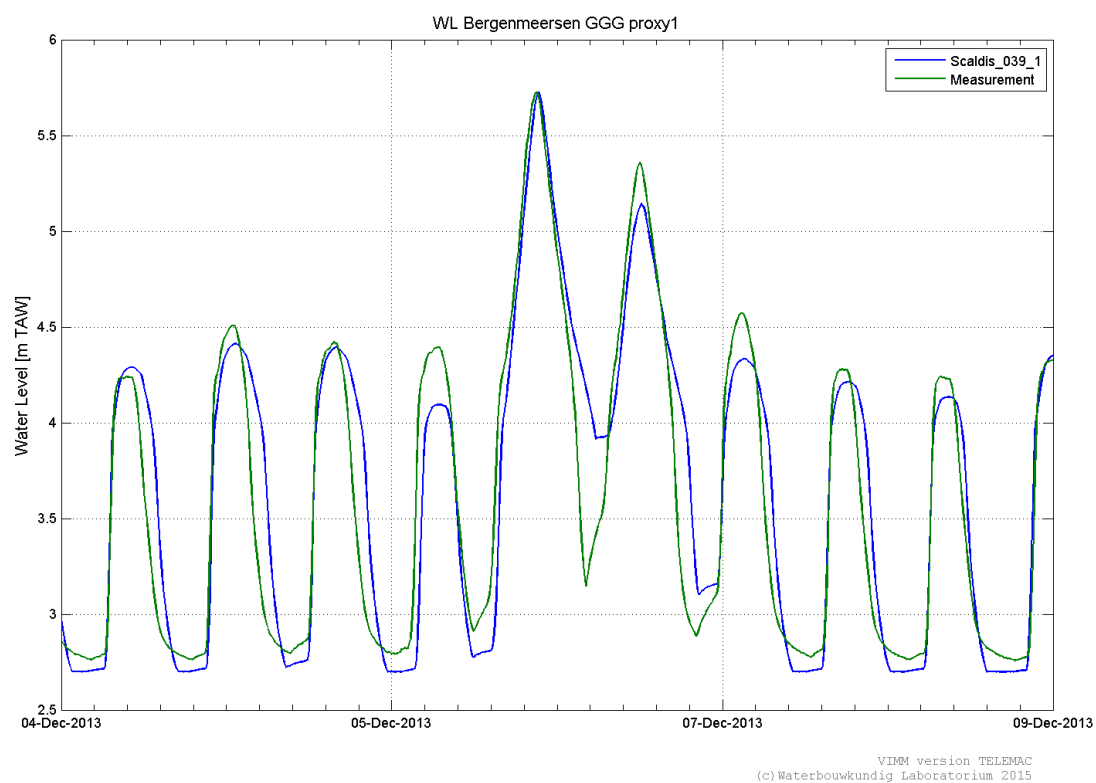


Figure 470 - Calculated and measured water levels at Bergenmeersen CRT

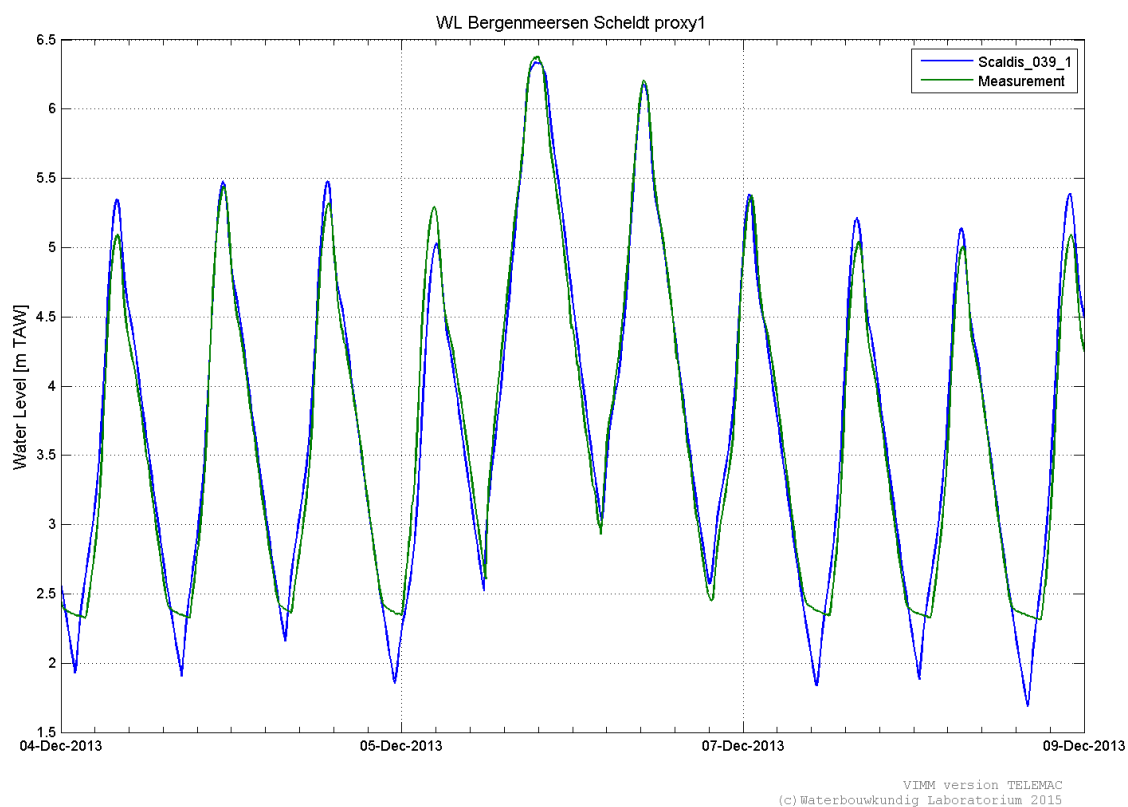


Figure 471 - Calculated and measured water levels at Bergenmeersen (Scheldt)



Figure 472 - Calculated and measured water levels at Bergenmeersen CRT2 (Scheldt)

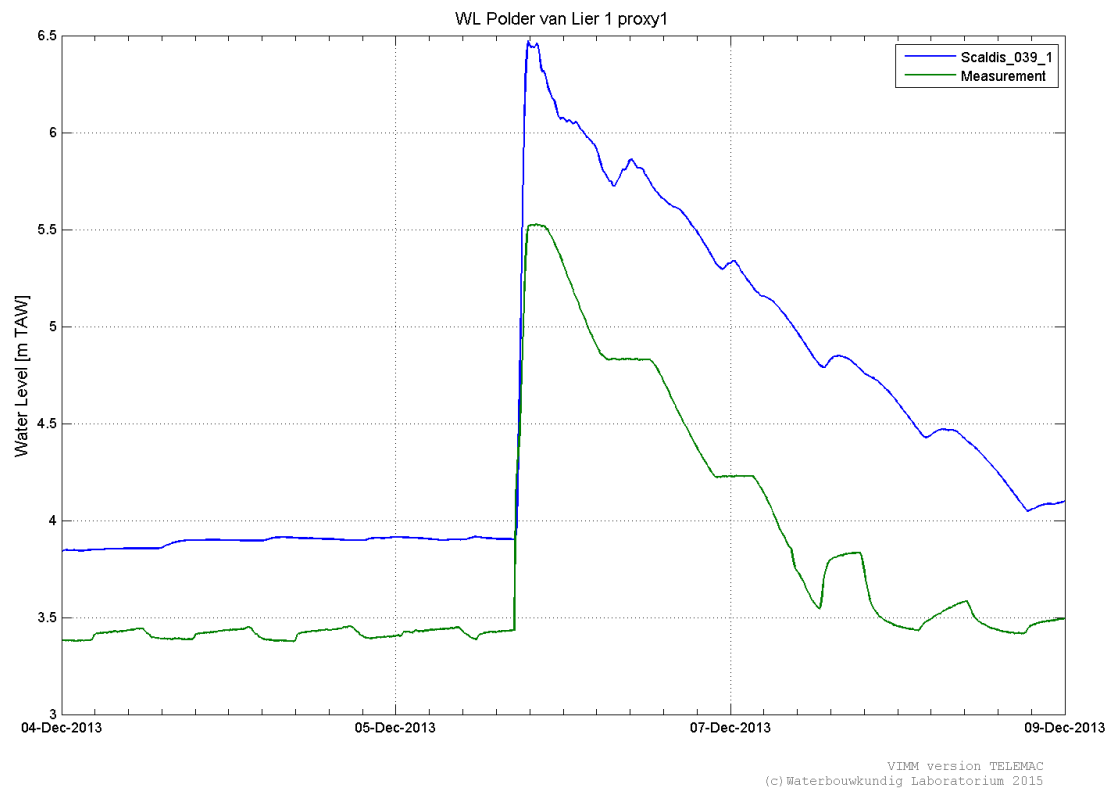


Figure 473 - Calculated and measured water levels at Polder van Lier 1

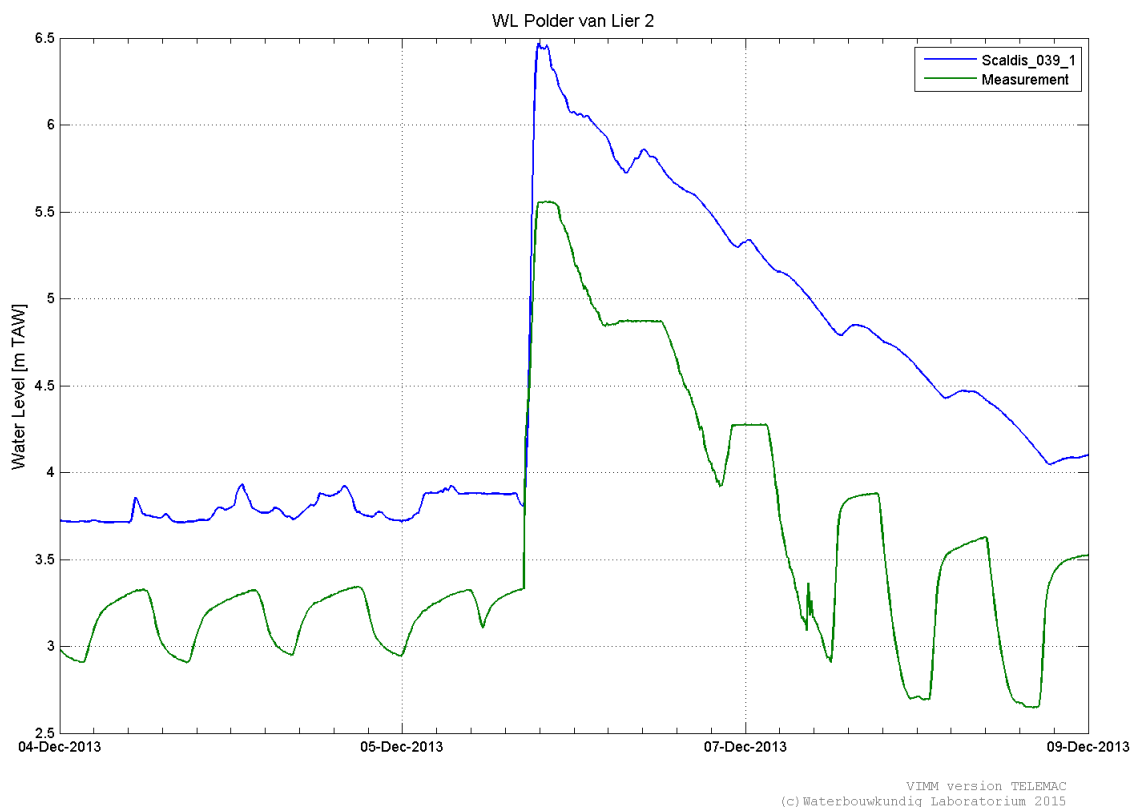


Figure 474 - Calculated and measured water levels at Polder van Lier 2

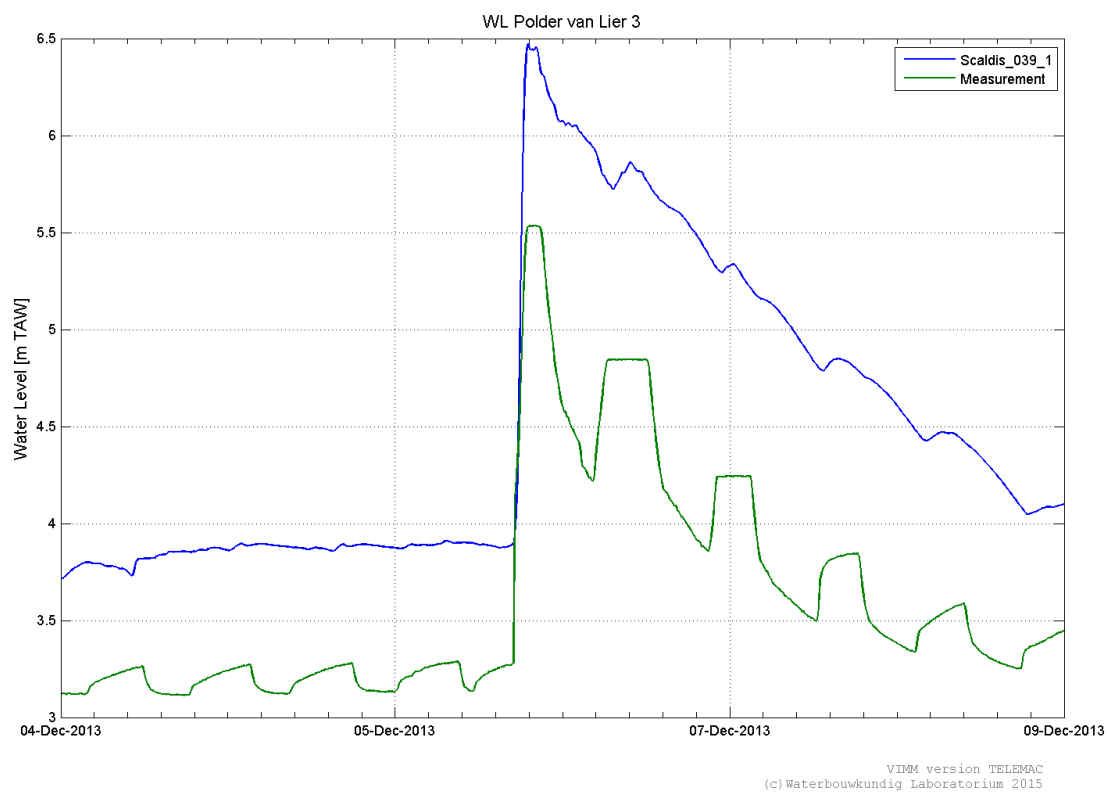


Figure 475 - Calculated and measured water levels at Polder van Lier 3

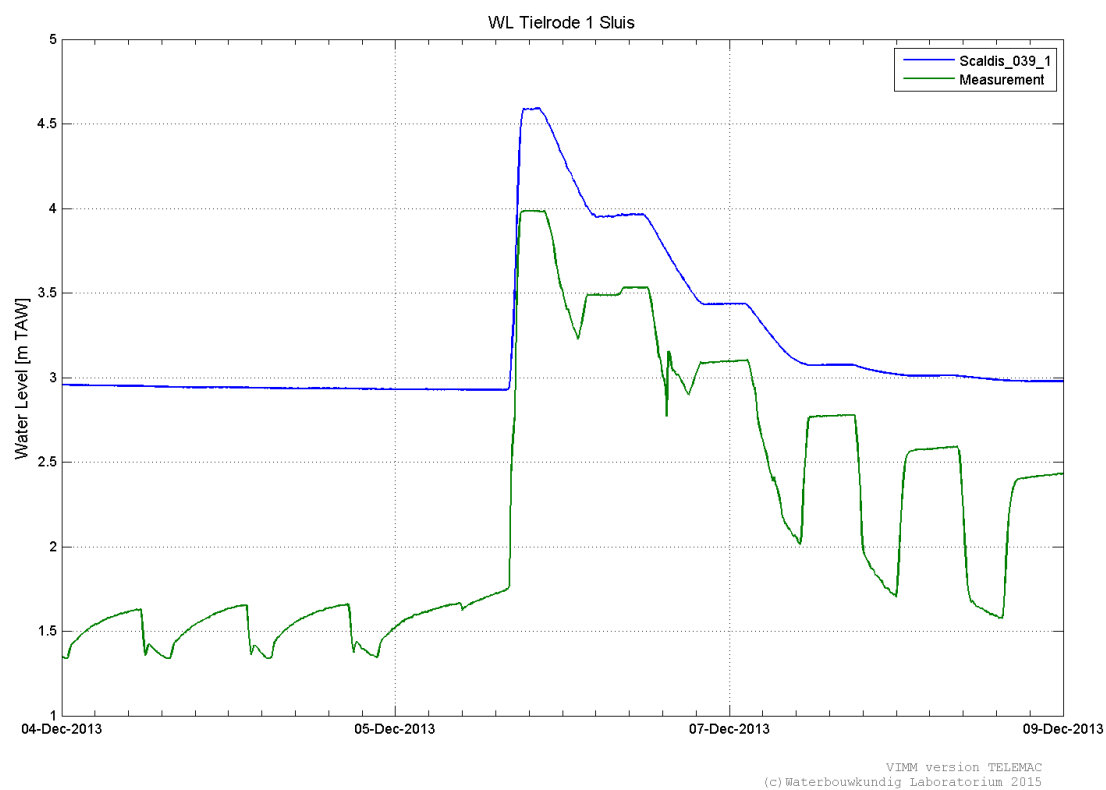


Figure 476 - Calculated and measured water levels at Tielrode 1

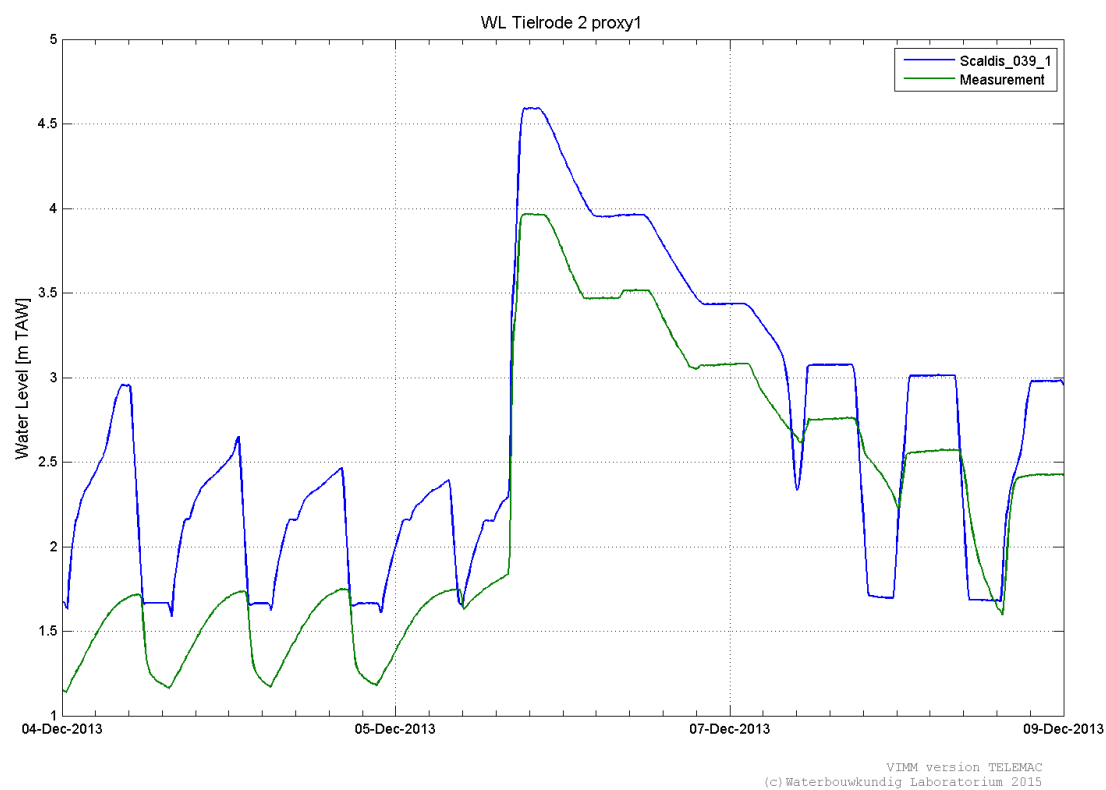


Figure 477 - Calculated and measured water levels at Tielrode 2

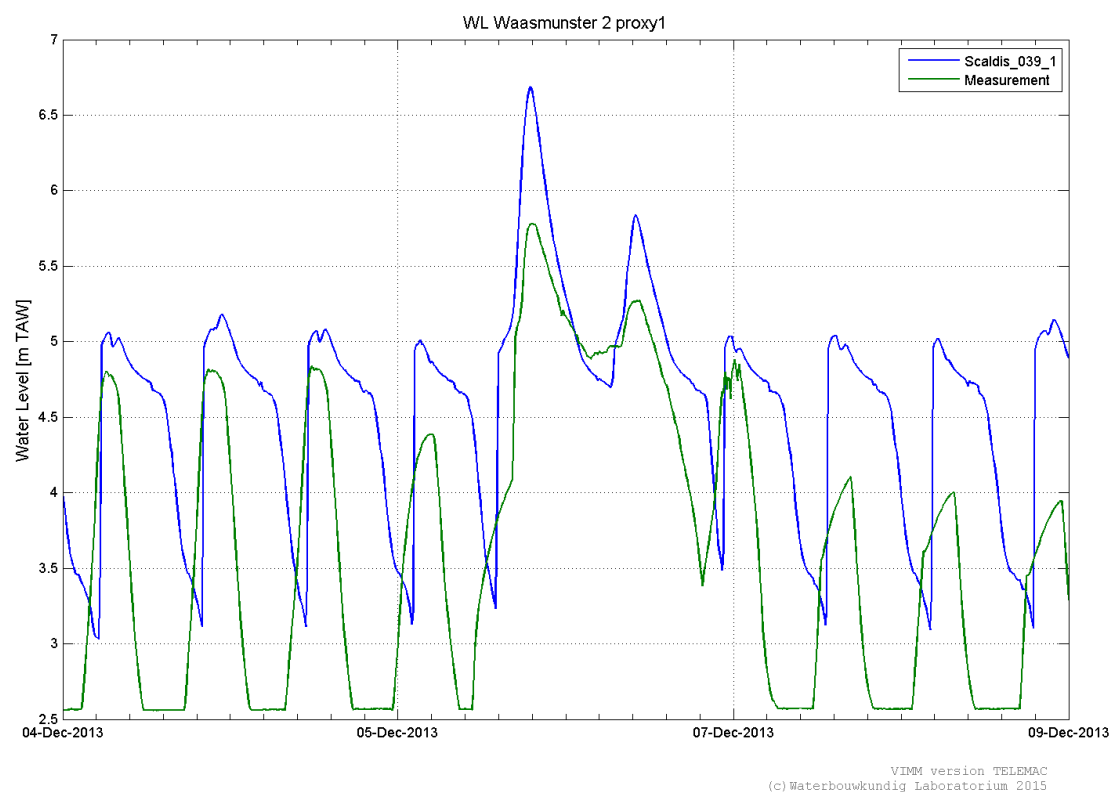


Figure 478 - Calculated and measured water levels at Waasmunster 2

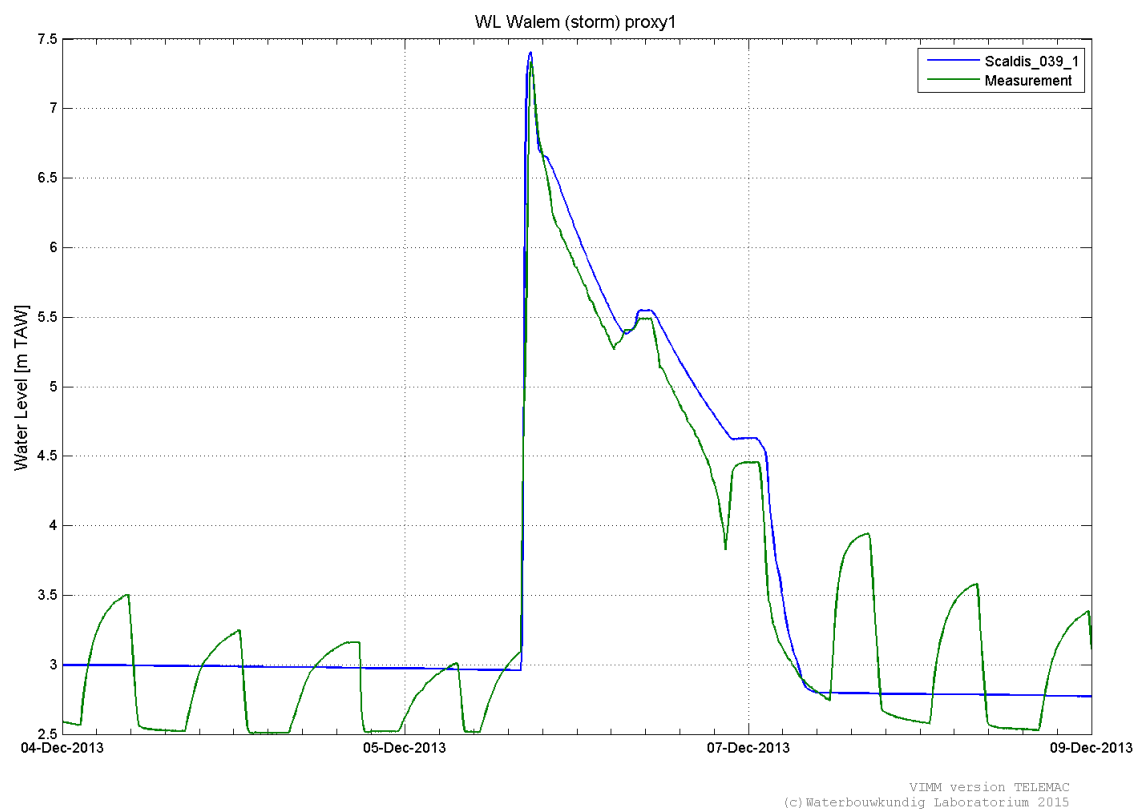


Figure 479 - Calculated and measured water levels at Walem

Appendix 3. Results of the model validation

Table 226. Comparison of the model results and ADCP velocities for the model validation

Scaldis_039_0	RMSE mag all (m/s)	RMSE dir all (degrees)	RMAE all
20080604 Everingen	0.17	25	0.19
20080407 Ossensisse langsraai	0.36	40	0.56
20060928 Waarde	0.13	36	0.42
20100319 dwarsraai D	0.21	24	0.29
20060322 DGD K	0.18	39	0.36
20060927 DGD K	0.19	37	0.31
20060322 Liefkenshoek	0.13	37	0.20
20100430 Liefkenshoek	0.14	25	0.18
20100429 Oosterweel	0.16	20	0.18
20090526 Kruibeke	0.15	26	0.19
20050217 Schelle	0.23	23	0.26
20090611 Notelaer dwars	0.13	21	0.21
20100415 Driegoten	0.16	26	0.19
20110805 Branst	0.18	60	0.83
20110801 Appels upstream	0.18	58	0.55
20100414 Schoonaarde	0.09	28	0.17
20090622 Boom	0.13	46	0.25

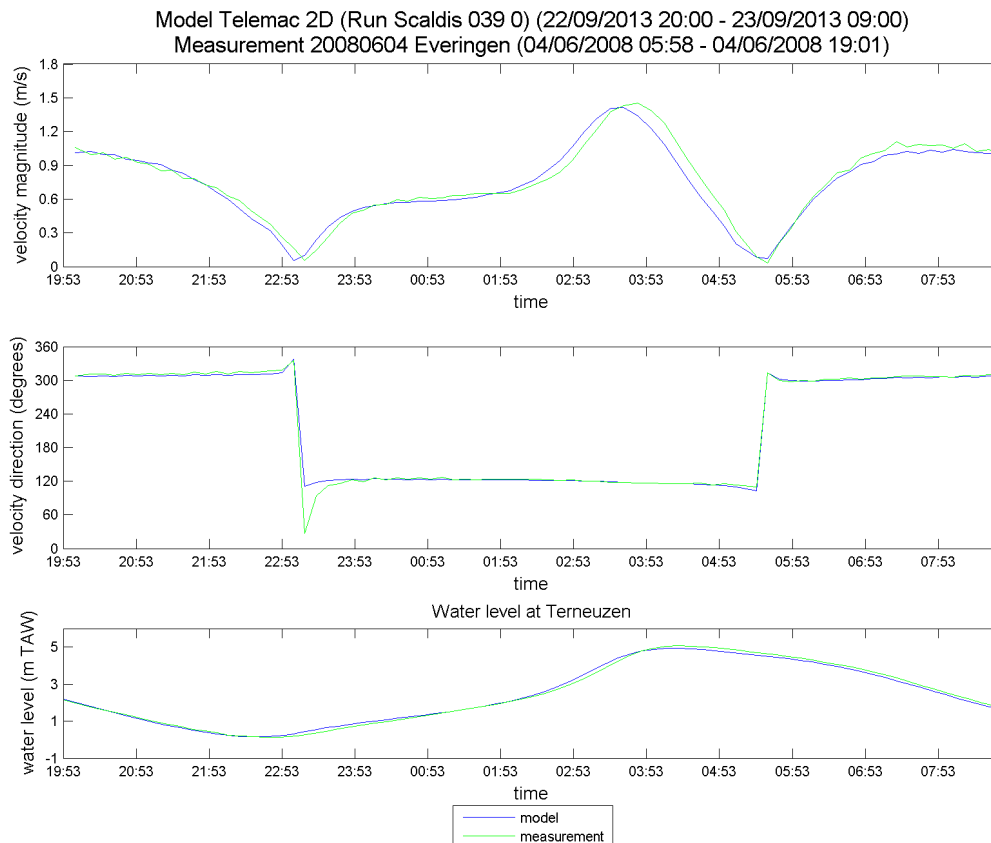


Figure 480 - Time series of the measured and modeled velocity magnitude and direction at 20080604 Everingen

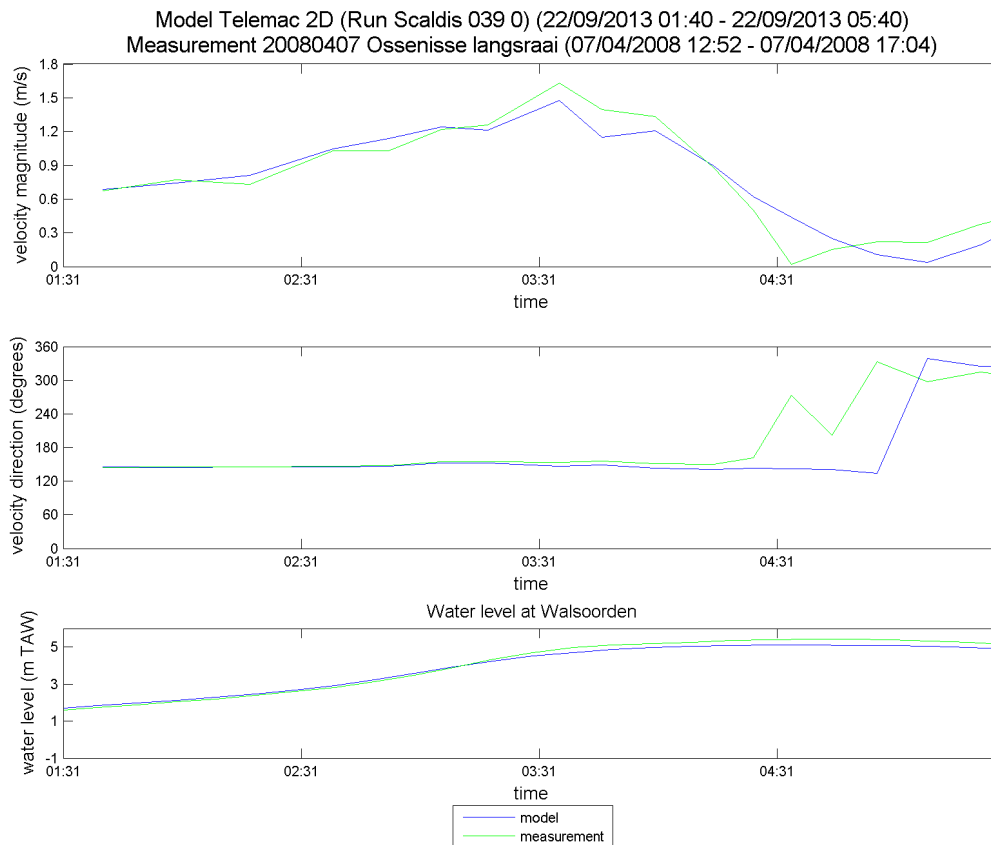


Figure 481 - Time series of the measured and modeled velocity magnitude and direction at 20080407 Ossenisse langsraai

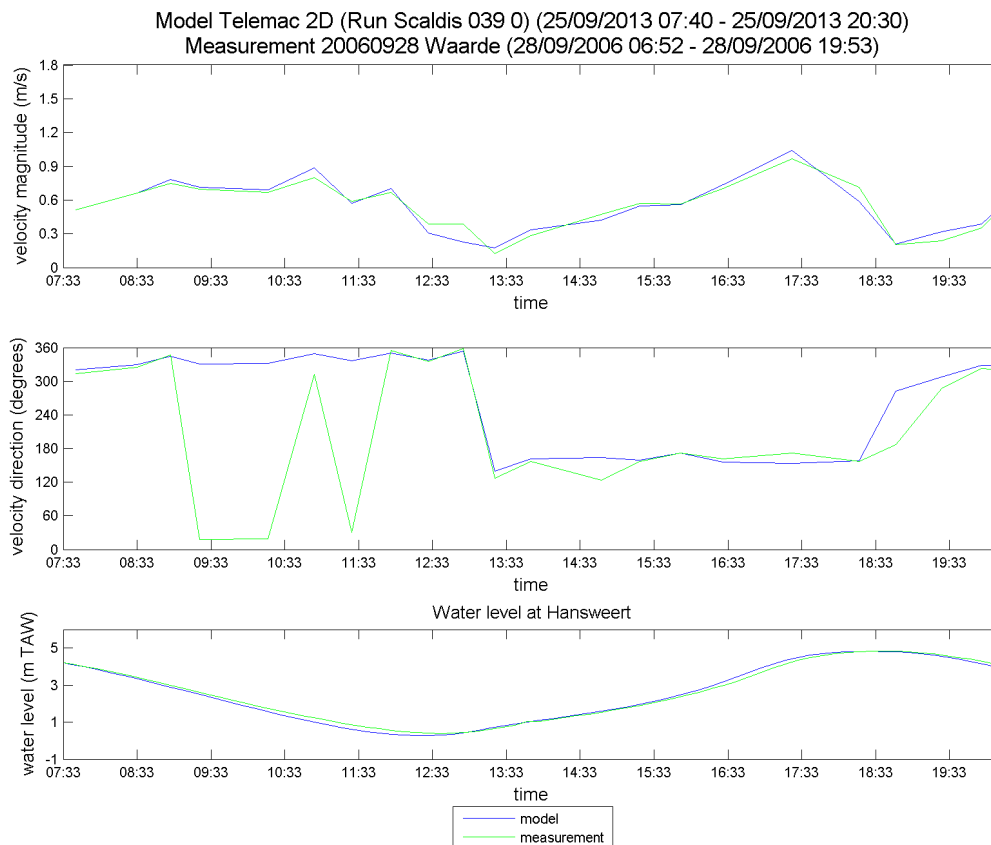


Figure 482 - Time series of the measured and modeled velocity magnitude and direction at 20060928 Waarde

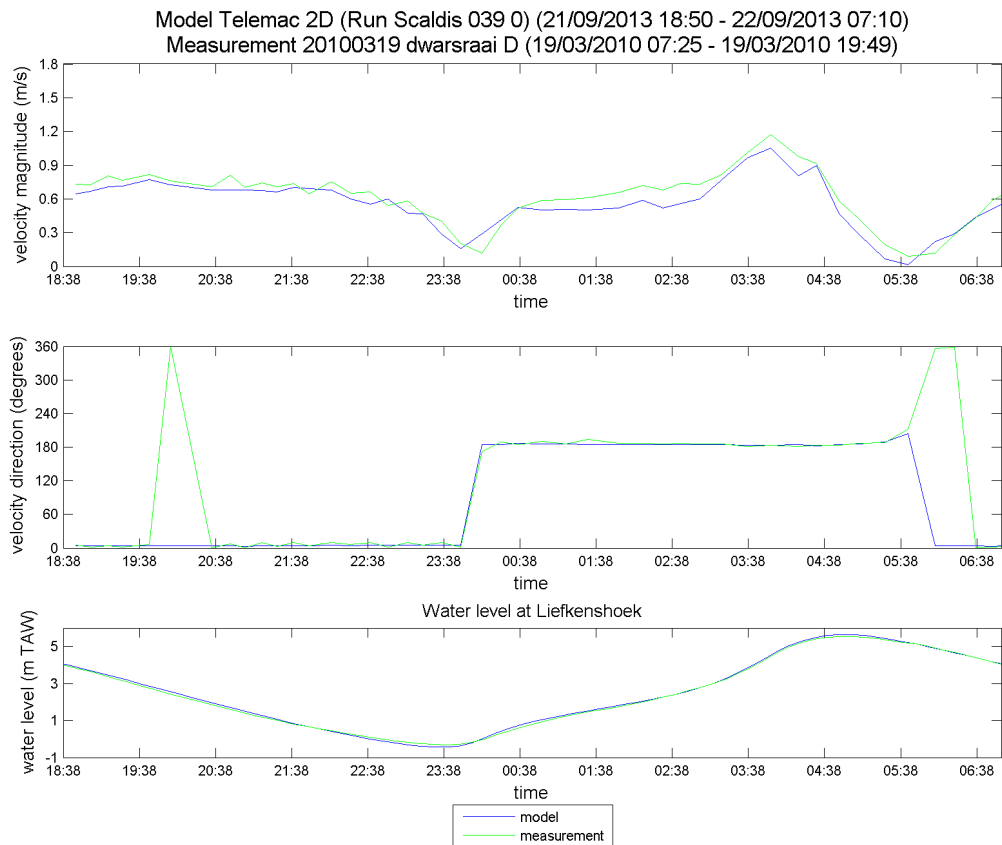


Figure 483 - Time series of the measured and modeled velocity magnitude and direction at 20100319 dwarsraaiD

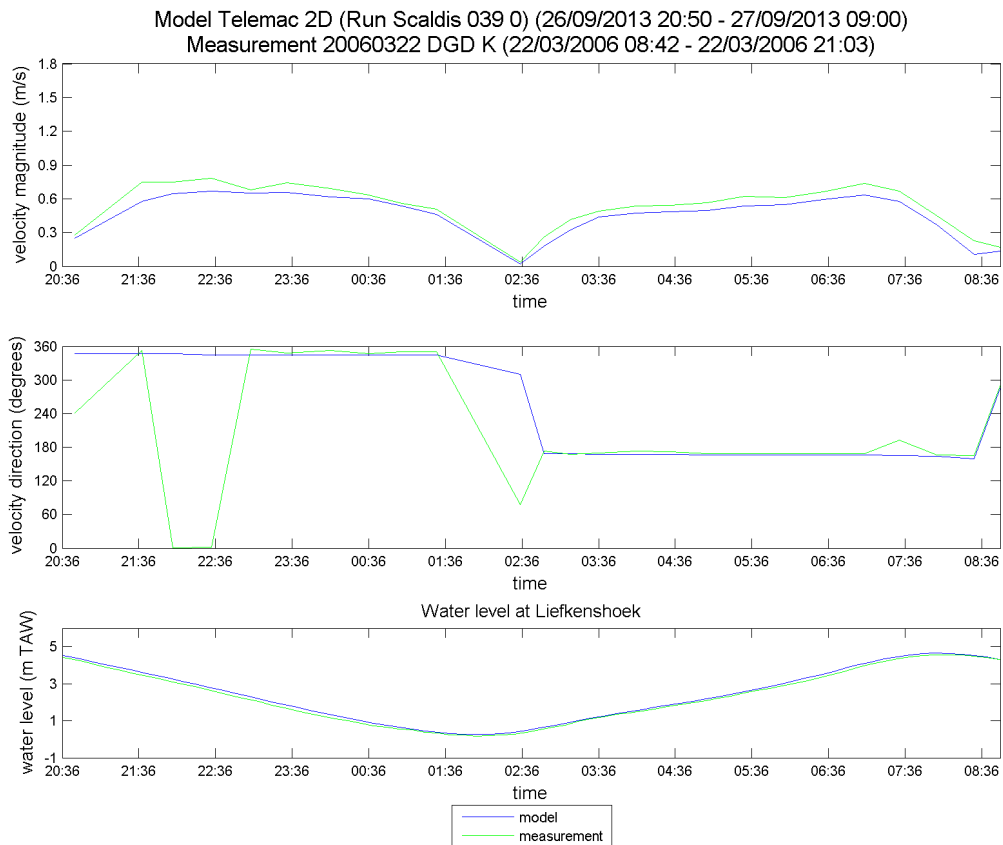


Figure 484 - Time series of the measured and modeled velocity magnitude and direction at 20060322 DGD K

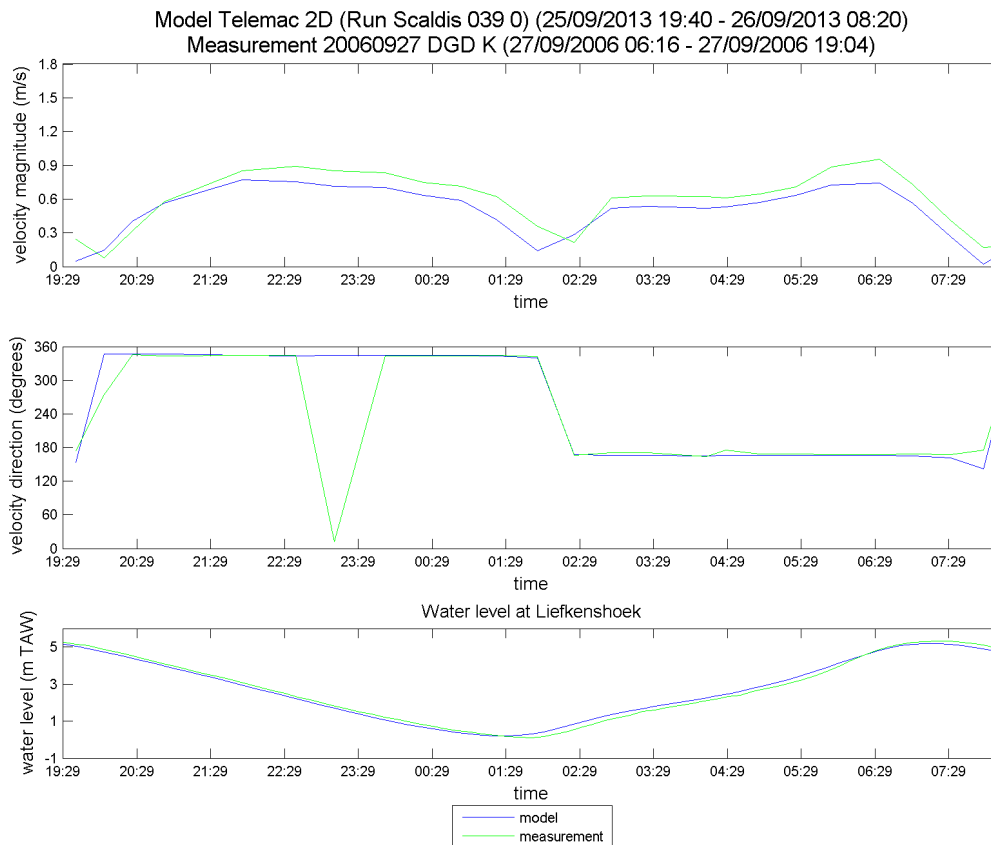


Figure 485 - Time series of the measured and modeled velocity magnitude and direction at 20060927 DGD K

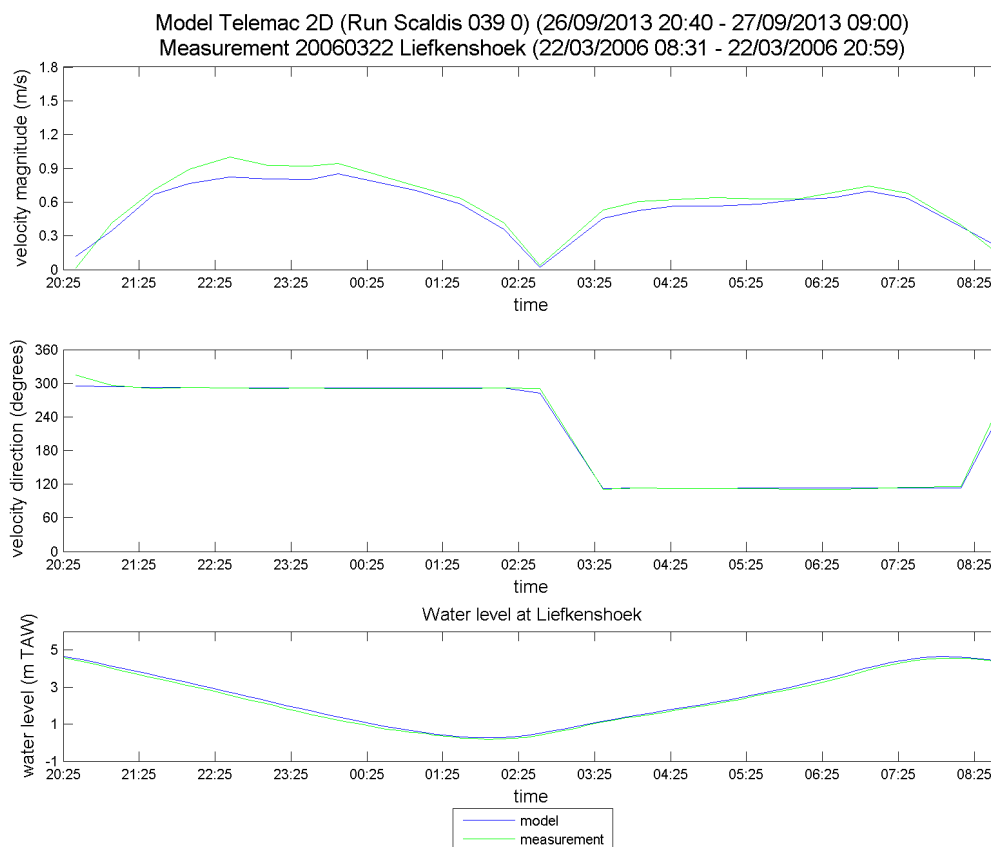


Figure 486 - Time series of the measured and modeled velocity magnitude and direction at 20060322 Liefkenshoek

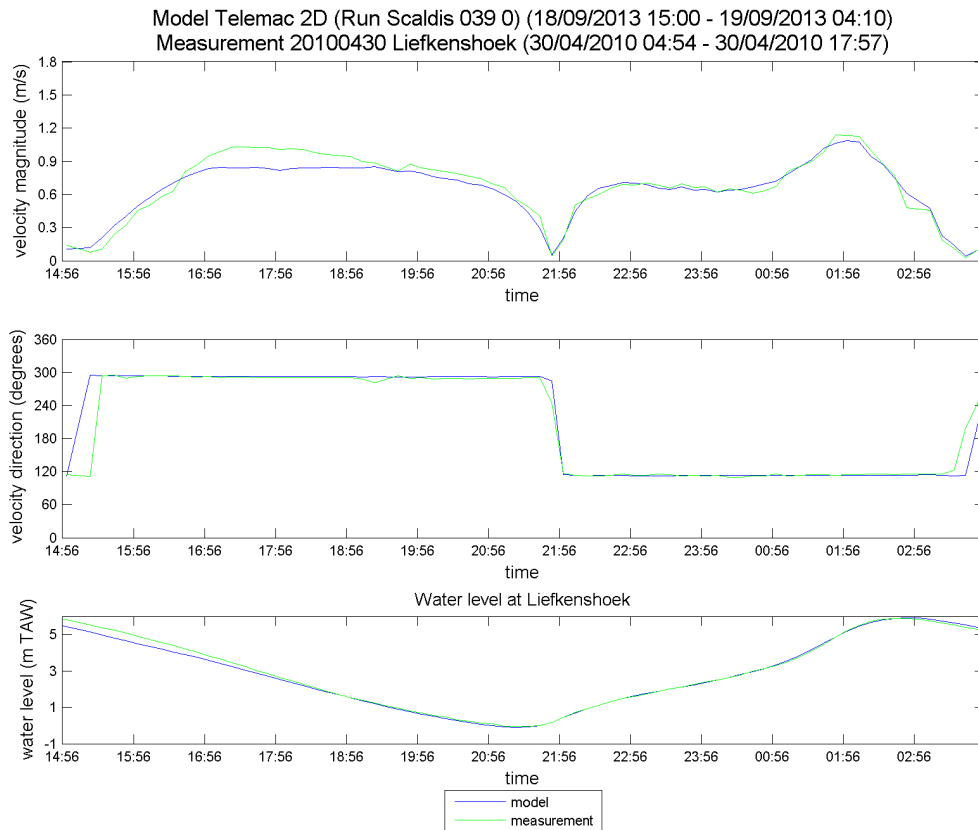


Figure 487 - Time series of the measured and modeled velocity magnitude and direction at 20100430 Liefkenshoek

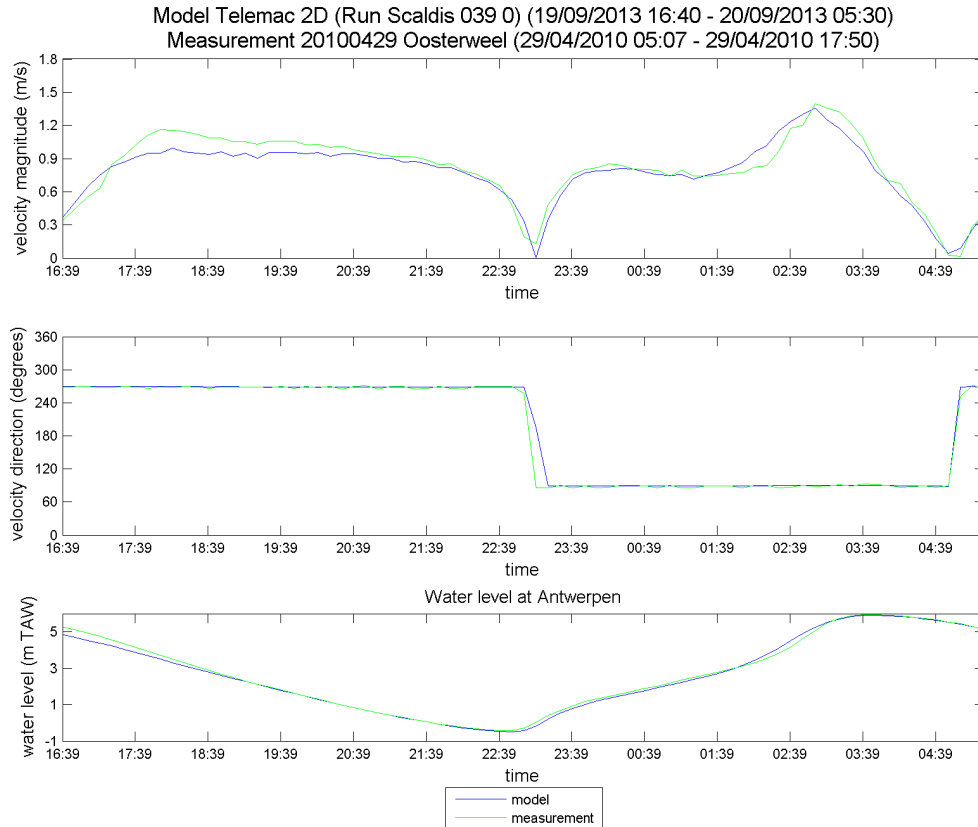


Figure 488 - Time series of the measured and modeled velocity magnitude and direction at 20100429 Oosterweel

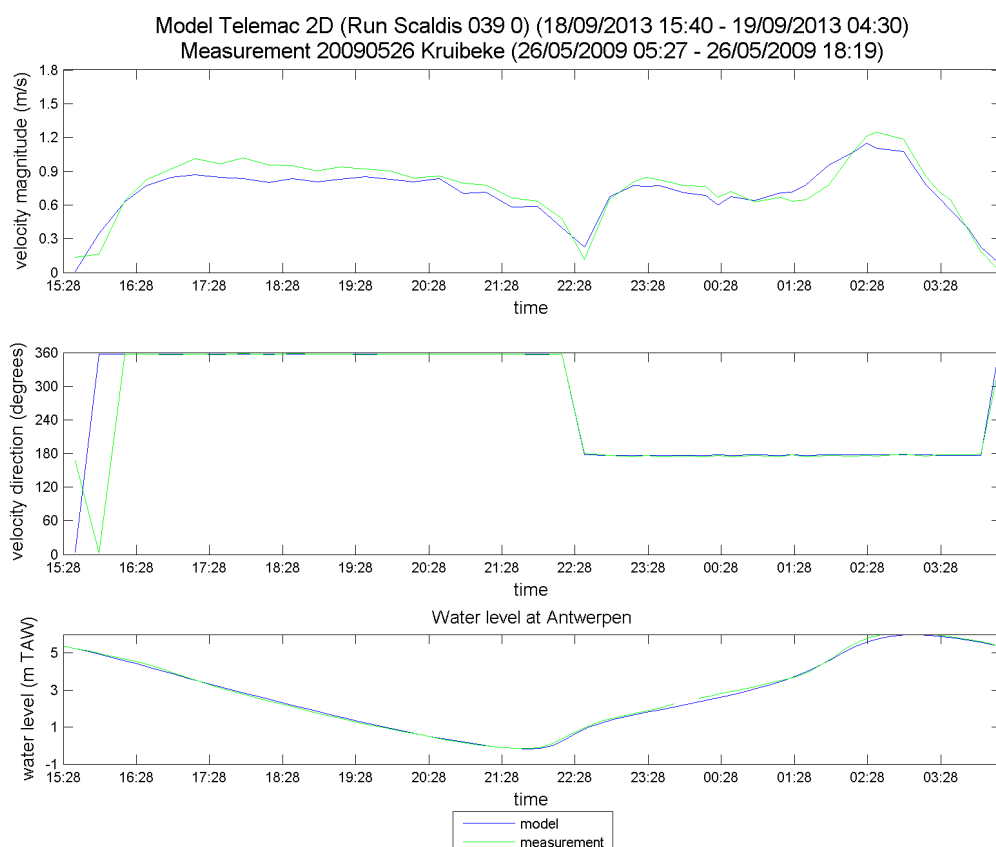


Figure 489 - Time series of the measured and modeled velocity magnitude and direction at 20090526 Kruibeke

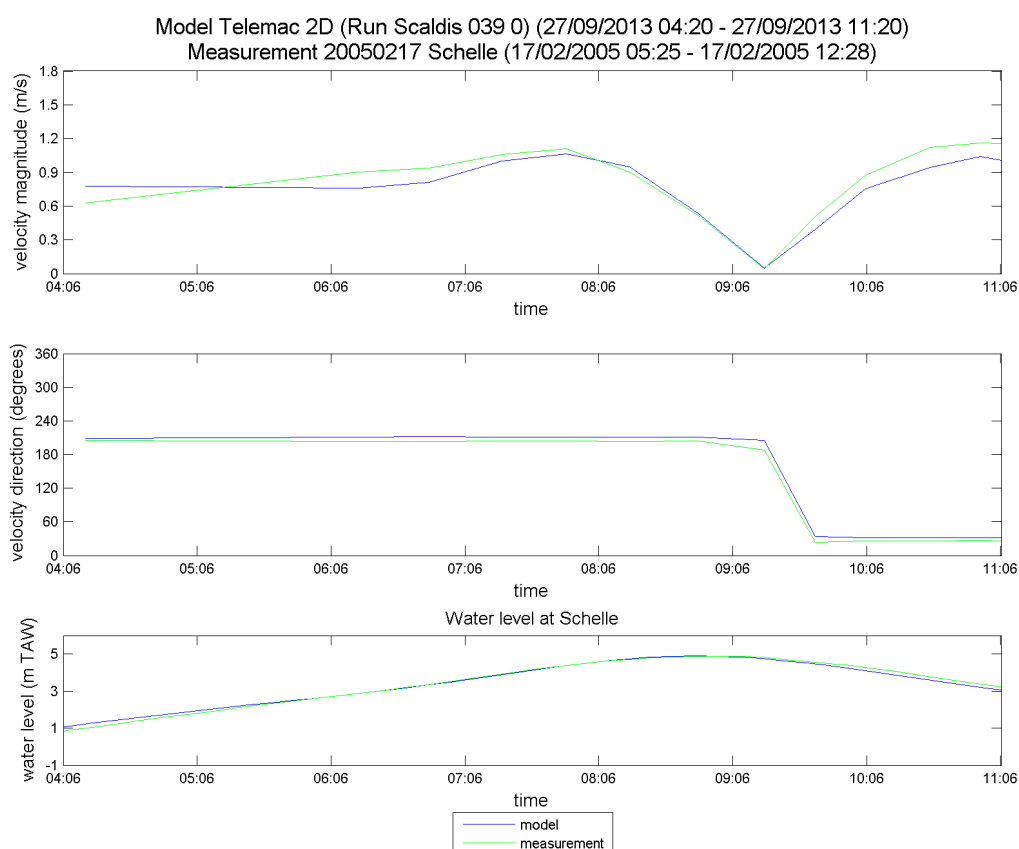


Figure 490 - Time series of the measured and modeled velocity magnitude and direction at 20050217 Schelle

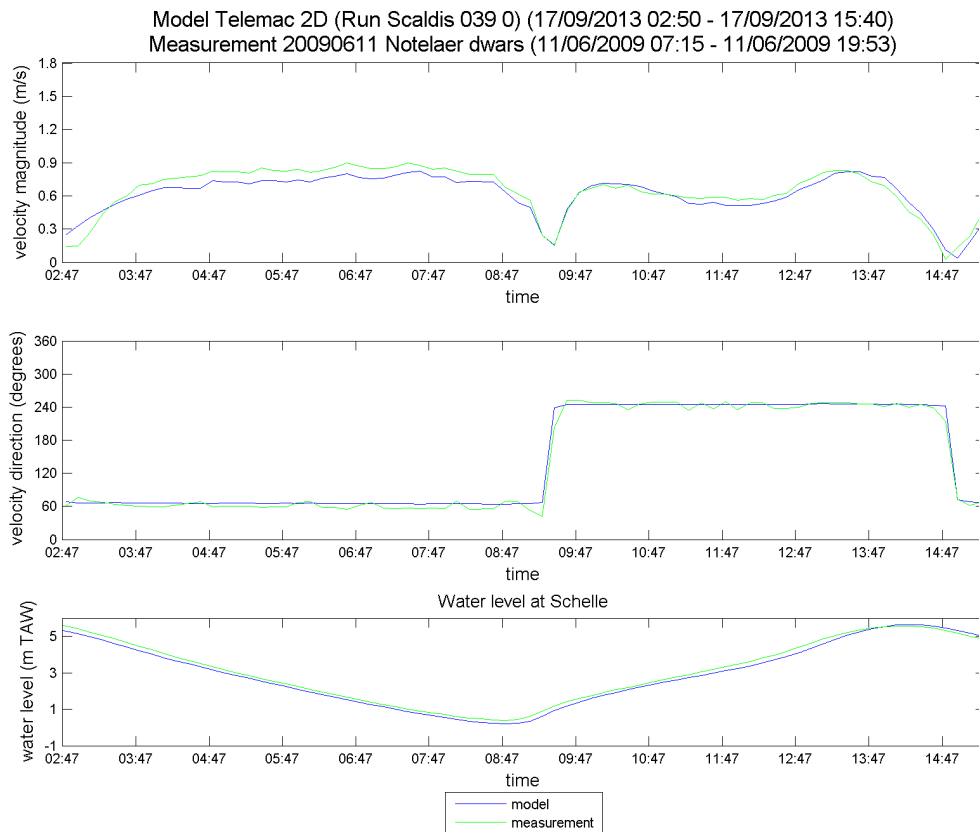


Figure 491 - Time series of the measured and modeled velocity magnitude and direction at 20090611 Notelaer dwars

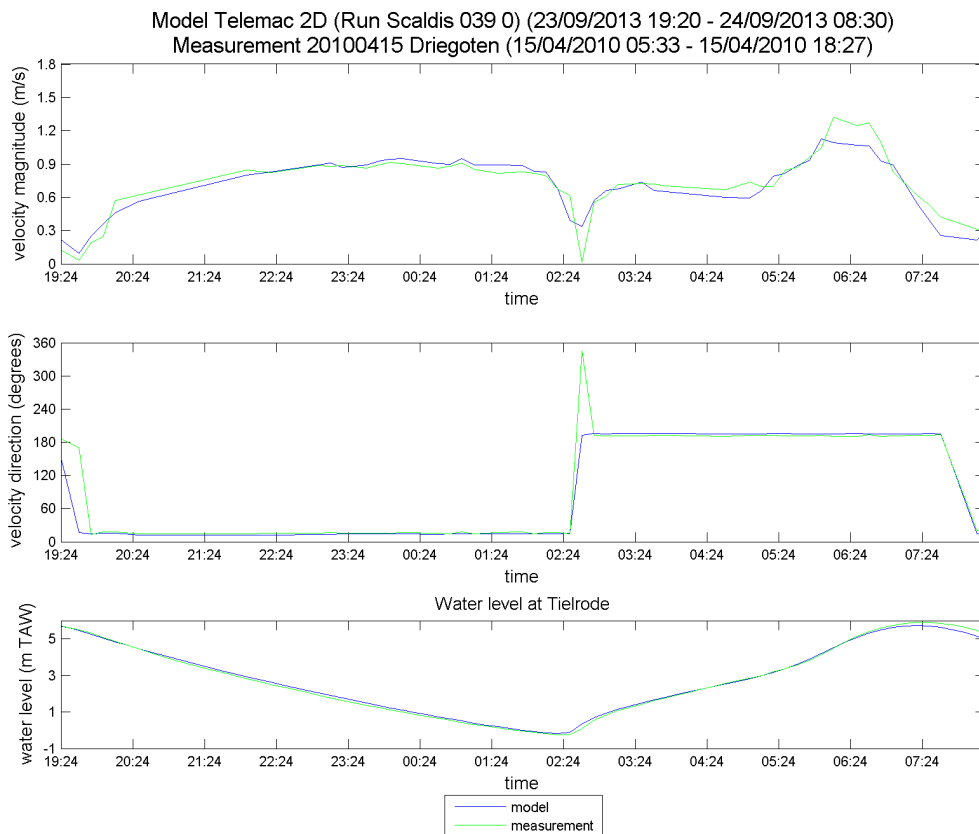


Figure 492 - Time series of the measured and modeled velocity magnitude and direction at 20100415 Driegoten

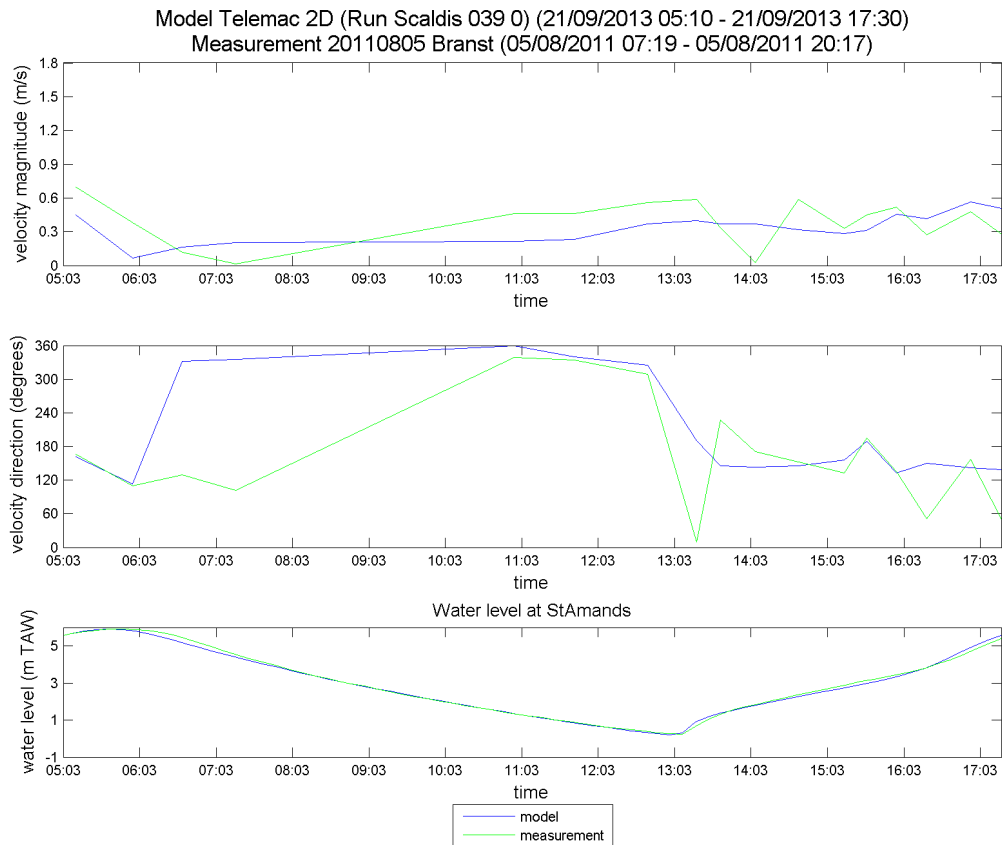


Figure 493 - Time series of the measured and modeled velocity magnitude and direction at 20110805 Branst

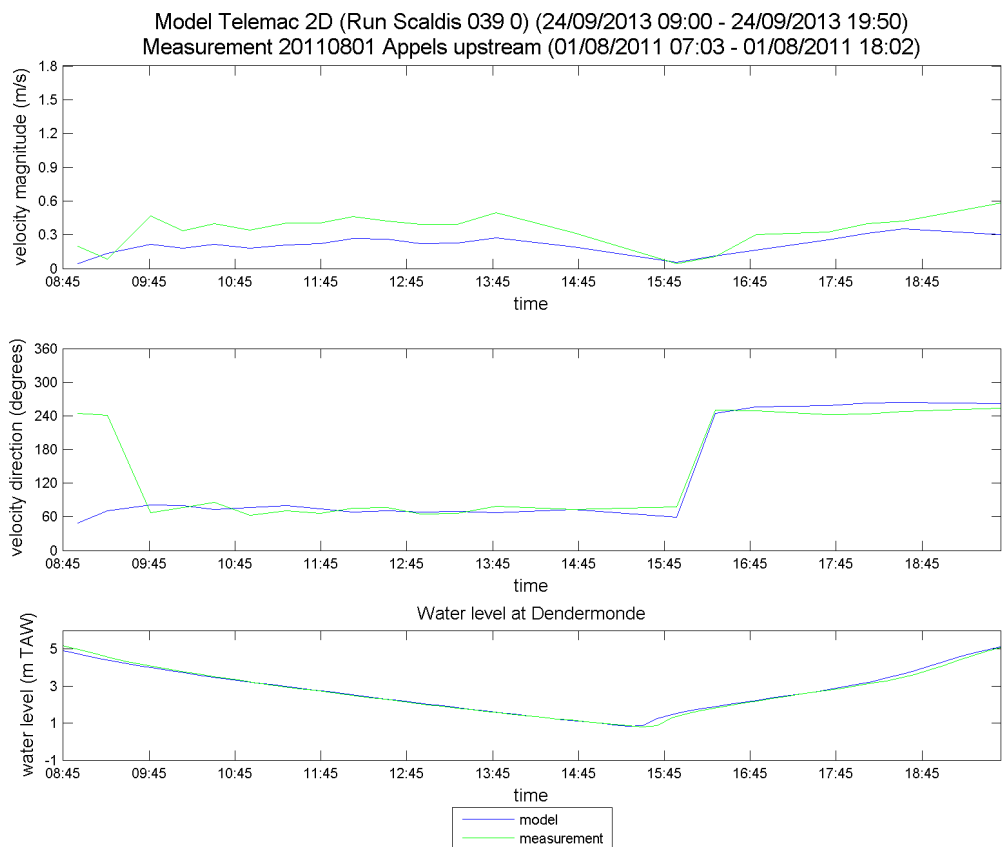


Figure 494 - Time series of the measured and modeled velocity magnitude and direction at 20110801 Appels upstream

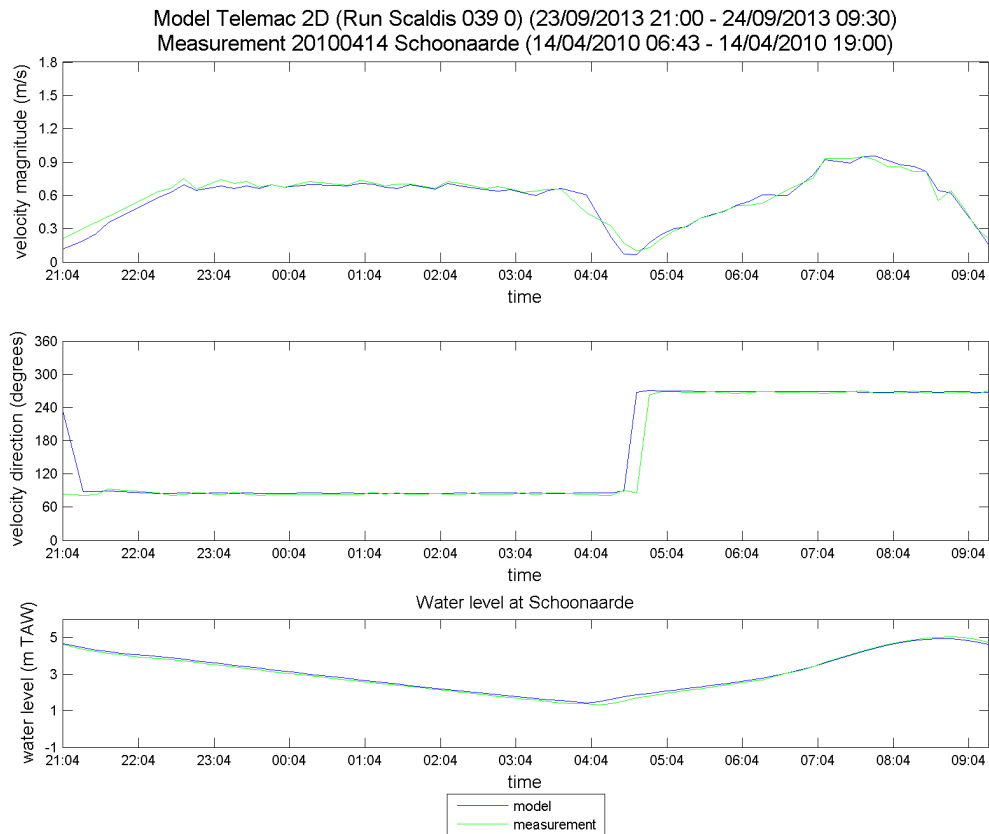


Figure 495 - Time series of the measured and modeled velocity magnitude and direction at 20100414 Schoonaarde

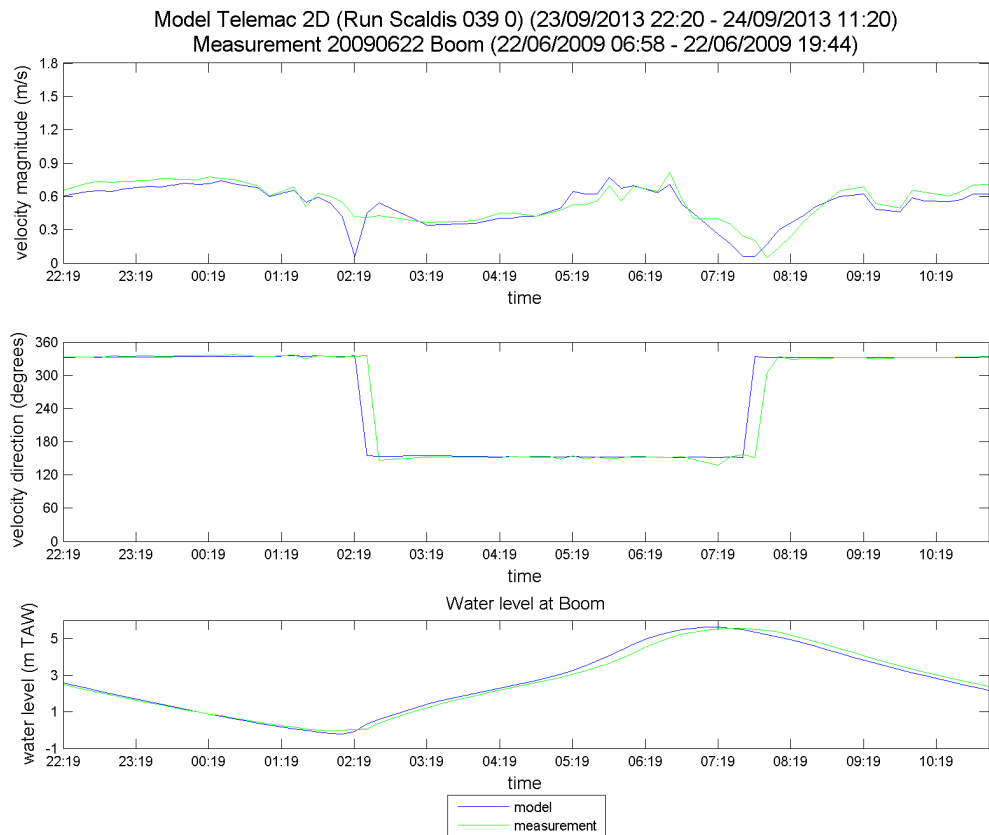


Figure 496 - Time series of the measured and modeled velocity magnitude and direction at 20090622 Boom

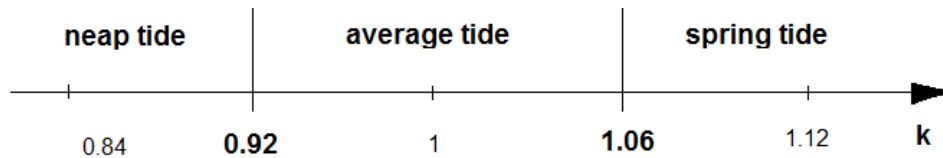
Appendix 4. Tidal coefficients

A tidal coefficient is calculated as a ratio of the tidal amplitude during the analyzed period to the amplitude of the average tide for the period from 1991 to 2000. Tidal coefficients are calculated for all analysed tides based on the measured water levels at Antwerp.

Table 227 shows the typical values of the tidal coefficients corresponding to the neap, average and spring tides. Tides with coefficients higher than 1.06 are considered to be spring tides; tides with coefficients lower than 0.92 are neap.

Table 227. Typical values of the tidal coefficients for neap, average and spring tides

Tide	Amplitude at Antwerp (m)	k
Neap	4.43	0.84
Average	5.29	1
Spring	5.95	1.12



Appendix 5. Statistical parameters

Time series of water levels, velocities and discharges

Straight setup (Figure 497) is defined as the instantaneous difference between two time series. It gives an overall idea of the bias between the measured and modelled complete time series. The $RMSE_0$ (unbiased Root Mean Square Error) shows the variation of the error between modelled and measured data.

Oblique setup (Figure 497) only takes into account the high and low waters. This way, the level and the timing of those events can be studied separately. Bias and $RMSE_0$ are calculated separately for level and timing of high and low waters.

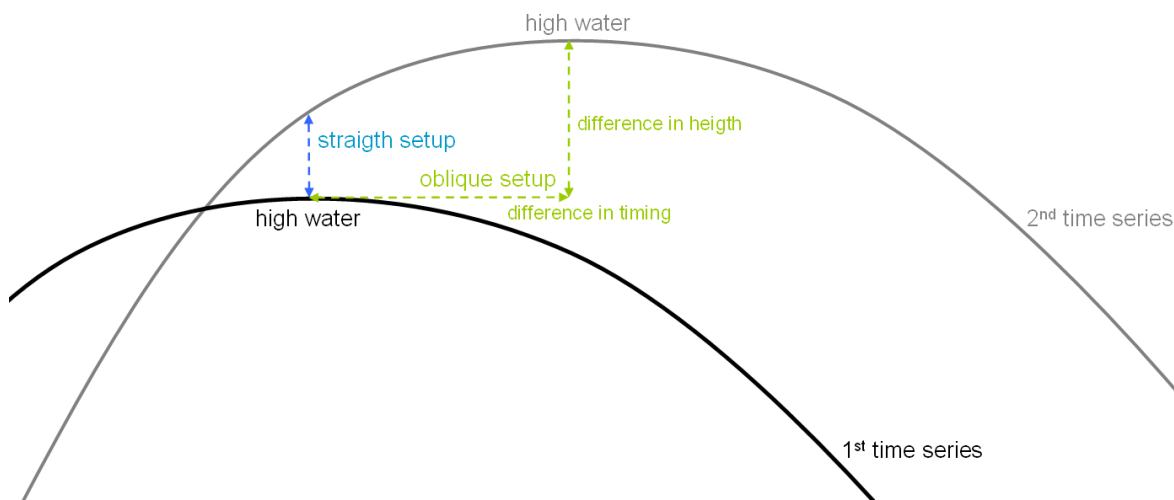


Figure 497 - Definition of straight and oblique setup (after Adema, 2006).

For both straight and oblique setup the statistical parameters bias, RMSE (root mean square error) and unbiased RMSE ($RMSE_0$) can be calculated. A positive bias value means that (in the case of water level or velocity magnitude) the modelled time series are an overestimation of the observed time series or (in the case of difference in timing) that the modelled time series lags behind the observed time series. A negative bias value means that (in the case of water level or velocity magnitude) the modelled time series are an underestimation of the observed time series or (in the case of difference in timing) that the modelled time series proceeds on the observed time series.

Hereafter, the reference time series will be presented as x and the time series that is subject to the test as y .

The **mean** values of the time series are represented by \bar{x} (reference) and \bar{y} (subject to test).

$$\bar{x} = \frac{1}{N} \sum_{i=1}^N x_i$$

where N is the length of the time series.

$$\bar{y} = \frac{1}{N} \sum_{i=1}^N y_i$$

The **bias** is the difference between the mean of the tested and the reference time series. The closer the bias is to zero, the better both time series correspond.

$$bias = \bar{y} - \bar{x}$$

The **root mean square error** (RMSE) is defined as:

$$RMSE = \sqrt{\frac{\sum_{i=1}^N (x_i - y_i)^2}{N}}$$

Corresponding time series will result in RMSE values close to zero. An important, extra source of information is the **unbiased root mean square error** or **RMSE₀**. If the tested time series shows apart from a constant offset (bias) to the reference time series no other differences in its signal, the RMSE₀ will be zero, while both bias and RMSE will be non zero. If \bar{x} and \bar{y} are time series of a tidal signal (water level, current), an RMSE₀ value of zero means that both signals are equal in phasing and amplitude. This does not imply there is no constant bias between both.

$$RMSE_0 = \sqrt{\frac{\sum_{i=1}^N [(x_i - y_i) - (\bar{x} - \bar{y})]^2}{N}}$$

The **relative error** or **Scatter Index** of the tested time series is given by the quotient of the RMSE and the mean value of the reference time series.

$$S.I. = \frac{RMSE}{\bar{x}}$$

The correlation between both signals is given by **Pearson's correlation coefficient**, defined as:

$$r = \frac{\sum_{i=1}^N (x_i - \bar{x})(y_i - \bar{y})}{\sqrt{\sum_{i=1}^N (x_i - \bar{x})^2} \sqrt{\sum_{i=1}^N (y_i - \bar{y})^2}}$$

Harmonic analysis

A parameter combining the evaluation of both the amplitude and the phase between the observed and modeled tidal components is the vector difference.

The vector difference can be calculated over one tidal station for the different considered tidal components or different tidal stations can be considered. The first summation takes all the errors of the different considered harmonic constituents in account in a certain station. Then the errors in all stations are summed and averaged (*de Brye et al.*, 2010).

$$e_s = \sum_{i=1}^{N_c} \sqrt{[A_{c,i} \cos(\varphi_{c,i}) - A_{m,i} \cos(\varphi_{o,i})]^2 + [A_{c,i} \sin(\varphi_{c,i}) - A_{m,i} \sin(\varphi_{o,i})]^2}$$

$$e = \frac{1}{N_s} \sum_{s=1}^{N_s} e_s$$

The error e_s is the vector difference for a specific station with $A_{c,i}$ and $\varphi_{c,i}$ (the calculated amplitude and phase of harmonic constituent i) and $A_{o,i}$ and $\varphi_{o,i}$ (the observed amplitude and phase of harmonic constituent i). The total error over all specified stations is e .

Stationary velocities

Sutherland et al., (2003) proposed a method to evaluate the combined effect of magnitude and direction of the current. The MAE (mean absolute error) is calculated based on the calculated (Y_1, Y_2) and observed

(X_1, X_2) components of the current. A relative mean absolute error is derived (RMAE) to identify the order of magnitude of the error compared to the observed velocities. A table was proposed in which the RMAE was used to identify the model quality to represent the current.

$$MAE = \left\langle \left\| \vec{Y} - \vec{X} \right\| \right\rangle = \frac{1}{N} \sum_{n=1}^N \sqrt{(Y_{1,n} - X_{1,n})^2 + (Y_{2,n} - X_{2,n})^2}$$

$$RMAE = \frac{\left\langle \left\| \vec{Y} - \vec{X} \right\| \right\rangle}{\left\langle \left\| \vec{X} \right\| \right\rangle} = \frac{MAE}{\left\langle \left\| \vec{X} \right\| \right\rangle}$$

Table 228. Model qualification based on (Sutherland et al., 2003)

Model qualification	RMAE
Excellent	<0.2
Good	0.2-0.4
Reasonable/fair	0.4-0.7
Poor	0.7-1.0
Bad	>1.0

Furthermore a statistical analysis can be performed on the magnitude and direction of currents as represented below.

$$BIAS_{mag} = \frac{1}{N} \sum_{n=1}^N (MAG_{Y,n} - MAG_{X,n})$$

$$MAE_{mag} = \frac{1}{N} \sum_{n=1}^N \|MAG_{Y,n} - MAG_{X,n}\|$$

$$RMSE_{mag} = \sqrt{\frac{1}{N} \sum_{n=1}^N (MAG_{Y,n} - MAG_{X,n})^2}$$

$$\Delta DIR_n = \begin{cases} DIR_{Y,n} - DIR_{X,n} & \dots \text{if } -180 \leq DIR_{Y,n} - DIR_{X,n} \leq 180 \\ DIR_{Y,n} - DIR_{X,n} + 360 & \dots \text{if } DIR_{Y,n} - DIR_{X,n} < -180 \\ DIR_{Y,n} - DIR_{X,n} - 360 & \dots \text{if } DIR_{Y,n} - DIR_{X,n} > +180 \end{cases}$$

$$BIAS_{dir} = \frac{1}{N} \sum_{n=1}^N \Delta DIR_n$$

$$MAE_{dir} = \frac{1}{N} \sum_{n=1}^N \|\Delta DIR_n\|$$

$$RMSE_{dir} = \sqrt{\frac{1}{N} \sum_{n=1}^N (\Delta DIR_n)^2}$$

ADCP velocities

Average velocity magnitude and direction for each transect are calculated as the magnitude and direction of the average vector (based on the average U and V components), (average means the combination of the depth average and average over the transect). This means that both magnitude and direction of velocities are taken into account. For example, a direction of the velocity with a higher magnitude has more weight in the calculation of an average direction than a direction of the velocity with a smaller magnitude.

$$\vec{V}_{met}(x, z, t) = \vec{e}_x U_{met}(x, z, t) + \vec{e}_y V_{met}(x, z, t)$$

$$\vec{V}_{mod}(x, z, t) = \vec{e}_x U_{mod}(x, z, t) + \vec{e}_y V_{mod}(x, z, t)$$

where $\vec{V}_{met}(x, z, t)$ is the vector of the measured velocity;

$\vec{V}_{mod}(x, z, t)$ is the vector of the modeled velocity.

Average velocity magnitude and direction:

$$MAG_{met}(t) = \left\| \frac{\sum_x \langle \vec{V}_{met} \rangle}{n} \right\| \quad DIR_{met}(t) = dir \left(\frac{\sum_x \langle \vec{V}_{met} \rangle}{n} \right)$$

$$MAG_{mod}(t) = \left\| \frac{\sum_x \langle \vec{V}_{mod} \rangle}{n} \right\| \quad DIR_{mod}(t) = dir \left(\frac{\sum_x \langle \vec{V}_{mod} \rangle}{n} \right)$$

where $\langle \vec{V}_{mod} \rangle(x, t)$ and $\langle \vec{V}_{met} \rangle(x, t)$ are depth average modeled and measured velocities.

The **bias of magnitude and direction** is calculated as the difference between the calculated and measured average velocity magnitude and direction.

$$BIAS_{mag}(t) = MAG_{mod} - MAG_{met}$$

$$BIAS_{dir}(t) = DIR_{mod} - DIR_{met}$$

The **RMSE of velocity magnitude and direction** is calculated based on the depth average velocity magnitude and direction for each point along the transect. Magnitude is not taken into account for the calculation of the RMSE of velocity direction and vice-versa. Therefore, the RMSE plots show more variation between the model and measurements than the plots of average velocity magnitude and direction for all transects.

$$RMSE_{mag}(t) = \sqrt{\frac{\sum_x \left(\left\| \langle \vec{V}_{mod} \rangle \right\| - \left\| \langle \vec{V}_{met} \rangle \right\| \right)^2}{n}}$$

$$RMSE_{dir}(t) = \sqrt{\frac{\sum_x \left(dir\left(\langle \overrightarrow{V}_{mod} \rangle\right) - dir\left(\langle \overrightarrow{V}_{met} \rangle\right) \right)^2}{n}}$$

Appendix 6. Fortran code culvert functionality for Telemac 3D

```
! *****  
  
      SUBROUTINE T3D_CULVERT2  
  
! *****  
  
      & ( HAUS , LRGS , HAUS2 , CLP , C556 , CES1 , CES2 , CSS1 , CSS2 ,  
      &  CV , NM , C115 , CV5 , CTRASH , LENGT , Q_CULVERT )  
  
!  
! ~~~~~  
!  
! DISCE      |-->| ARRAY OF DISCHARGES OF SOURCES.  
!  
!          | | READ IN THE PARAMETER FILE.  
!  
!          | | NAME OF DISCE IS QSCE IN TELEMAC-3D.  
!  
! I          |-->| NUMBER OF THE SOURCE  
!  
! TIME      |-->| TIME  
!  
! ~~~~~  
  
      USE BIEF  
  
      USE DECLARATIONS_TELEMAC3D  
  
      IMPLICIT NONE  
  
      INTEGER LNG,LU  
  
      COMMON/INFO/LNG,LU  
  
! +-----+  
  
      INTEGER :: I,I1,I2,N  
  
      DOUBLE PRECISION,INTENT(INOUT), DIMENSION(NSCE) :: Q_CULVERT  
  
  
      DOUBLE PRECISION,INTENT(IN),DIMENSION(NSCE) :: HAUS,LRGS  
      DOUBLE PRECISION,INTENT(IN),DIMENSION(NSCE) :: CLP,C556  
      DOUBLE PRECISION,INTENT(IN),DIMENSION(NSCE) :: CES1,CES2  
      DOUBLE PRECISION,INTENT(IN),DIMENSION(NSCE) :: CSS1,CSS2  
      DOUBLE PRECISION,INTENT(IN),DIMENSION(NSCE) :: CV,NM  
      DOUBLE PRECISION,INTENT(IN),DIMENSION(NSCE) :: CV5,CTRASH  
      DOUBLE PRECISION,INTENT(IN),DIMENSION(NSCE) :: LENGT,HAUS2  
      DOUBLE PRECISION,INTENT(IN),DIMENSION(NSCE) :: C115  
      DOUBLE PRECISION :: S1,S2,Q,RELAXB,L,HAST,RAYON  
  
      INTRINSIC SQRT  
  
      DOUBLE PRECISION :: QMAX1,QMAX2  
  
      DOUBLE PRECISION P_DMAX,P_DMIN  
  
      EXTERNAL      P_DMAX,P_DMIN  
  
! +-----+
```

```

! we make a loop over all culverts. NSCE is number of sources. For every culvert there are 2 sources
! We progress in this loop with an increase of 2 --> I=1,3,5,7,...

DO I=1,NSCE,2

!POINT NUMBER FROM THE BEGINNING TO THE END OF THE TUBE corresponding to one source and on sink term

! I1 is always the channel side and I2 is always the flood control area side

    I1=ISCE(I)
    I2=ISCE(I+1)

! LOADS, TAKEN AS FREE SURFACE ELEVATION = depth (H) + bottom elevation (ZF)

    S1=H%R(I1)+ZF%R(I1)
    QMAX1=0.9D0*H%R(I1)*V2DPA%R(I1)/DT
    S2=H%R(I2)+ZF%R(I2)
    QMAX2=0.9D0*H%R(I2)*V2DPA%R(I2)/DT ! maximum discharge is equal to 90% of water in cell

! Safety when ISCE does not find the nodes

    IF(I1.EQ.0.OR.I2.EQ.0) THEN

        S1=0.D0
        QMAX1=0.D0
        S2=0.D0
        QMAX2=0.D0

! WRITE(LU,*) 'ISCE does not find nodes = ',I2

    ENDIF

! CASE WHERE ONE OF THE ENDS IS NOT IN THE SUB-DOMAIN

! So with P_DMAX and P_DMIN we find the values over all subdomains

    IF(NCSIZE.GT.1) THEN

        S1=P_DMAX(S1)+P_DMIN(S1)
        S2=P_DMAX(S2)+P_DMIN(S2)
        QMAX1=P_DMAX(QMAX1)+P_DMIN(QMAX1)
        QMAX2=P_DMAX(QMAX2)+P_DMIN(QMAX2)

    ENDIF

!Calculation of discharges based on water levels S1 and S2

!EQUATIONS BASED ON BODHAINE (1968) + CARLIER (1976)

    IF(S1.GE.S2) THEN !WL channel higher than WL FCA; only inflow possible!

        IF(S1.GT.ZSCE(I).AND.S1.GT.ZSCE(I+1)) THEN ! If WL channel is greater than bottom of culvert then ...

!

!FREE SURFACE FLOW

        IF((S1-ZSCE(I)).LT.1.5d0*HAUS(I).AND.S2.LE.(ZSCE(I+1)+
& HAUS2(I))) THEN

!SUBMERGED WEIR - FLOW TYPE 3

        IF(S2.GT.(0.666666667D0*(S1-((ZSCE(I+1)+ZSCE(I))/2.d0))

```

& +((ZSCE(I+1)+ZSCE(I))/2.d0))) THEN

HAST=0.5d0*(S1-((ZSCE(I+1)+ZSCE(I))/2.d0))+0.5d0*

& (S2-((ZSCE(I+1)+ZSCE(I))/2.d0))

RAYON=(HAST*LRGS(I))/(2.d0*HAST+LRGS(I))

L=(2.d0*9.81d0*LENGT(I)*NM(I)**2.d0)/(RAYON**

& 1.33333333d0)

Q=LRGS(I)*SQRT(2.D0*GRAV*(S1-S2)/(CES1(I)+L+CSS2(I)+

& CTRASH(I)))*(S2-((ZSCE(I+1)+ZSCE(I))/2.d0))

!UNSUBMERGED WEIR - FLOW TYPE 2

ELSEIF(S2.LE.(0.666666667D0*(S1-((ZSCE(I+1)+ZSCE(I))/

& 2.d0))+((ZSCE(I+1)+ZSCE(I))/2.d0))) THEN

HAST=0.5d0*(0.666666667D0*(S1-((ZSCE(I+1)+ZSCE(I))/2.d0)))

& +0.5d0*(S1-((ZSCE(I+1)+ZSCE(I))/2.d0))

RAYON=(HAST*LRGS(I))/(2.d0*HAST+LRGS(I))

L=(2.d0*9.81d0*LENGT(I)*NM(I)**2.d0)/(RAYON**1.33333333d0)

Q=LRGS(I)*SQRT(2.D0*GRAV*(S1-(((ZSCE(I+1)+ZSCE(I))/

& 2.d0)+0.666666667D0*(S1-((ZSCE(I+1)+ZSCE(I))/2.d0))))/

& (CES1(I)+L+CSS2(I)+CTRASH(I)))*(0.666666667D0*(S1-((ZSCE

& (I+1)+ZSCE(I))/2.d0)))

ENDIF

!PRESSURE FLOW --> ORIFICE LAW

ELSEIF((S1-ZSCE(I)).GE.1.5d0*HAUS(I).AND.S2.LE.(ZSCE(I+1)+

& HAUS2(I))) THEN

!FLOW TYPE 6

IF(LENGT(I).GE.C556(I)*HAUS(I)) THEN

HAST=HAUS(I)

RAYON=(HAST*LRGS(I))/(2.d0*HAST+2.d0*LRGS(I))

L=(2.d0*9.81d0*LENGT(I)*NM(I)**2.d0)/

& (RAYON**1.33333333d0)

```

Q=LRGS(I)*HAUS(I)*SQRT(2.D0*GRAV*(S1-((ZSCE(I+1)+
&      ZSCE(I))/2.d0)+HAUS2(I)))/(CES1(I)+L+CSS2(I)+CTRASH(I)))

```

!FLOW TYPE 5

```

ELSEIF(LENGT(I).LT.C556(I)*HAUS(I)) THEN

HAST=HAUS(I)
RAYON=(HAST*LRGS(I))/(2.d0*HAST+2.d0*LRGS(I))
L=(2.d0*9.81d0*LENGT(I)*NM(I)**2.d0)/
&      (RAYON**1.33333333d0)

Q=LRGS(I)*HAUS(I)*SQRT(2.D0*GRAV*(S1-((ZSCE(I+1)+
&      ZSCE(I))/2.d0))/(C115(I)*CES1(I)+CTRASH(I)))

ENDIF

```

!FLOW TYPE 4 SUBMERGED OUTLET

```

ELSEIF (S1.GT.(ZSCE(I)+HAUS(I)).AND.S2.GT.(ZSCE(I+1)+
&      HAUS2(I))) THEN

HAST=HAUS(I)
RAYON=(HAST*LRGS(I))/(2.d0*HAST+2.d0*LRGS(I))
L=(2.d0*9.81d0*LENGT(I)*NM(I)**2.d0)/
&      (RAYON**1.33333333d0)

Q=LRGS(I)*HAUS(I)*SQRT(2.D0*GRAV*(S1-S2)/(CES1(I)+L+
&      CSS2(I)+CTRASH(I)))

ENDIF

ELSE ! IF WL on both sides is lower than the culvert

Q=0.D0

ENDIF

```

!

ELSE ! IF S1 is smaller than S2; so only outlet flow

```

IF(S2.GT.ZSCE(I).AND.S2.GT.ZSCE(I+1)) THEN

```

!FREE SURFACE FLOW

```

IF((S2-ZSCE(I+1)).LT.1.5d0*HAUS2(I).AND.S1.LE.(ZSCE(I)+
&      HAUS(I))) THEN

```

ISUBMERGED WEIR - FLOW TYPE 3

```

IF(S1.GT.(0.666666667D0*(S2-((ZSCE(I+1)+ZSCE(I))/2.d0))
&      +((ZSCE(I+1)+ZSCE(I))/2.d0))) THEN

HAST=0.5d0*(S2-((ZSCE(I+1)+ZSCE(I))/2.d0))+0.5d0*(S1-
&      ((ZSCE(I+1)+ZSCE(I))/2.d0))
RAYON=(HAST*LRGS(I))/(2.d0*HAST+LRGS(I))
L=(2.d0*9.81d0*LENGT(I)*NM(I)**2.d0)
&      /(RAYON**1.33333333d0)

Q=-LRGS(I)*SQRT(2.D0*GRAV*(S2-S1)/(CES2(I)+L+CV(I)+
&      CSS1(I)+CTRASH(I)))*(S1-((ZSCE(I+1)+ZSCE(I))/2.d0))

```

!UNSUBMERGED WEIR - FLOW TYPE 2

```

ELSEIF(S1.LE.(0.666666667D0*(S2-((ZSCE(I+1)+ZSCE(I))/
&      2.d0))+((ZSCE(I+1)+ZSCE(I))/2.d0))) THEN

HAST=0.5d0*(0.666666667D0*(S2-((ZSCE(I+1)+ZSCE(I))/
&      2.d0))+0.5d0*(S2-((ZSCE(I+1)+ZSCE(I))/2.d0))
RAYON=(HAST*LRGS(I))/(2.d0*HAST+LRGS(I))
L=(2.d0*9.81d0*LENGT(I)*NM(I)**2.d0)
&      /(RAYON**1.33333333d0)

Q=-LRGS(I)*SQRT(2.D0*GRAV*(S2-(((ZSCE(I+1)+ZSCE(I))/
&      2.d0)+0.666666667D0*(S2-((ZSCE(I+1)+ZSCE(I))/2.d0))))
&      /(CES2(I)+CV(I)+L+CSS1(I)+CTRASH(I)))
&      *(0.666666667D0*(S2-((ZSCE(I+1)+ZSCE(I))/2.d0)))
ENDIF

```

!PRESSURE FLOW --> ORIFICE LAW

```

ELSEIF((S2-ZSCE(I+1)).GE.1.5d0*HAUS2(I).AND.S1.LE.(ZSCE(I)+
&      HAUS(I))) THEN

```

!FLOW TYPE 6

```

IF(LENGT(I).GE.C556(I)*HAUS2(I)) THEN

HAST=HAUS2(I)

RAYON=(HAST*LRGS(I))/(2.d0*HAST+2.d0*LRGS(I))

L=(2.d0*9.81d0*LENGT(I)*NM(I)**2.d0)

&      /(RAYON**1.33333333d0)

```

```

Q = -LRGS(I)*HAUS2(I)*SQRT( 2.D0*GRAV*(S2-(((ZSCE(I+1)+
&      ZSCE(I))/2.d0)+HAUS(I)))/(CES2(I)+CV(I)+L+CSS1(I)+
&      CTRASH(I)))

```

!FLOW TYPE 5

```

      ELSEIF(LENGT(I).LT.C556(I)*HAUS2(I)) THEN
        HAST=HAUS2(I)
        RAYON=(HAST*LRGS(I))/(2.d0*HAST+2.d0*LRGS(I))
        L=(2.d0*9.81d0*LENGT(I)*NM(I)**2.d0)
&      /(RAYON**1.3333333d0)

        Q = -LRGS(I)*HAUS2(I)*SQRT(2.D0*GRAV*(S2-((ZSCE(I+1)+
&      ZSCE(I))/2.d0))/(C115(I)*CES2(I)+CV5(I)*CV(I)+
&      CTRASH(I)))

      ENDIF

```

!FLOW TYPE 4 SUBMERGED OUTLET

```

      ELSEIF (S2.GT.(ZSCE(I+1)+HAUS2(I)).AND.S1.GT.(ZSCE(I)+
&      HAUS(I))) THEN

        HAST=HAUS2(I)

        RAYON=(HAST*LRGS(I))/(2.d0*HAST+2.d0*LRGS(I))
        L=(2.d0*9.81d0*LENGT(I)*NM(I)**2.d0)
&      /(RAYON**1.3333333d0)

        Q=-LRGS(I)*HAUS2(I)*SQRT(2.D0*GRAV*(S2-S1)
&      /(CES2(I)+CV(I)+L+CSS1(I)+CTRASH(I)))

      ENDIF

      ELSE ! IF the water does not reach high enough to enter the culvert

        Q=0.D0

      ENDIF

    ENDIF

```

! EXTRA SAFETY: NOTHING HAPPENS IF THE LOADS AT THE 2 ENDS ARE LOWER THAN

! THE ELEVATION OF THE NOZZLES

IF(S1.LT.ZSCE(I).AND.S2.LT.ZSCE(I+1)) Q=0.D0 ! the water is not reaching the culvert level

IF(HAUS(I).EQ.0.d0.OR.HAUS2(I).EQ.0.d0) THEN

```
      Q=0.D0 ! the culvert is closed

      WRITE(LU,*) 'Culvert ',I,' has no height'

      ENDIF

! SLUICE VALVE TREATMENT

      IF ((CLP(I).EQ.1.AND.S2.GT.S1).OR.
& (CLP(I).EQ.2.AND.S1.GT.S2).OR.
& (CLP(I).EQ.3))
& Q=0.D0

! ASSIGNING Q TO QSCE(I) (=ARRAY WITH FIXED DISCHARGES FOR SOURCES)

      QSCE(I)=Q*1.D0

! LIMITATION WITH AVAILABLE WATER

      IF(QSCE(I).GT.0.D0) THEN

          IF (QSCE(I).GT.QMAX1) THEN

!              WRITE(LU,*) 'Q greater than Qmax1 Q= ',QSCE(I)
!              WRITE(LU,*) 'Qmax1= ',QMAX1
!              WRITE(LU,*) 'for source nr I= ',I

          ENDIF

          QSCE(I)=MIN(QMAX1,QSCE(I))

      ELSE

          IF (QSCE(I).LT.-QMAX2) THEN

!              WRITE(LU,*) 'Q smaller than -Qmax2 Q= ',QSCE(I)
!              WRITE(LU,*) 'Qmax2= ',QMAX2
!              WRITE(LU,*) 'for source nr I= ',I

          ENDIF

          QSCE(I)=MAX(-QMAX2,QSCE(I))

      ENDIF

!Q_CULVERT(I) is negative when the flow goes from the river to the flood control area: a sink term is imposed in the river with a
correspondent source term in the fca

! therefore the sign for I is negative.

      Q_CULVERT(I+1)=QSCE(I)
      Q_CULVERT(I)=-QSCE(I)

      END DO

      RETURN

      END SUBROUTINE
```

DEPARTEMENT MOBILITY AND PUBLIC WORKS

Flanders Hydraulics Research

Berchemlei 115, 2140 Antwerpen

T +32 (0)3 224 60 35

F +32 (0)3 224 60 36

waterbouwkundiglabo@vlaanderen.be

mow.vlaanderen.be

waterbouwkundiglaboratorium.be

//



DEPARTMENT **MOBILITY & PUBLIC WORKS**
Flanders hydraulics Research

Berchemlei 115, 2140 Antwerp

T +32 (0)3 224 60 35

F +32 (0)3 224 60 36

waterbouwkundiglabo@vlaanderen.be

www.flandershydraulicsresearch.be